HOST AND PATHOGEN MECHANISMS UNDERPINNING VIRAL ECOLOGY AND EMERGING INFECTIONS

EDITED BY: Declan C. Schroeder, Jim L. Van Etten, Ian M. Jones, Janusz Tadeusz Paweska, Zhengli Shi and Ahmed Sayed Abdel-Moneim

PUBLISHED IN: Frontiers in Microbiology

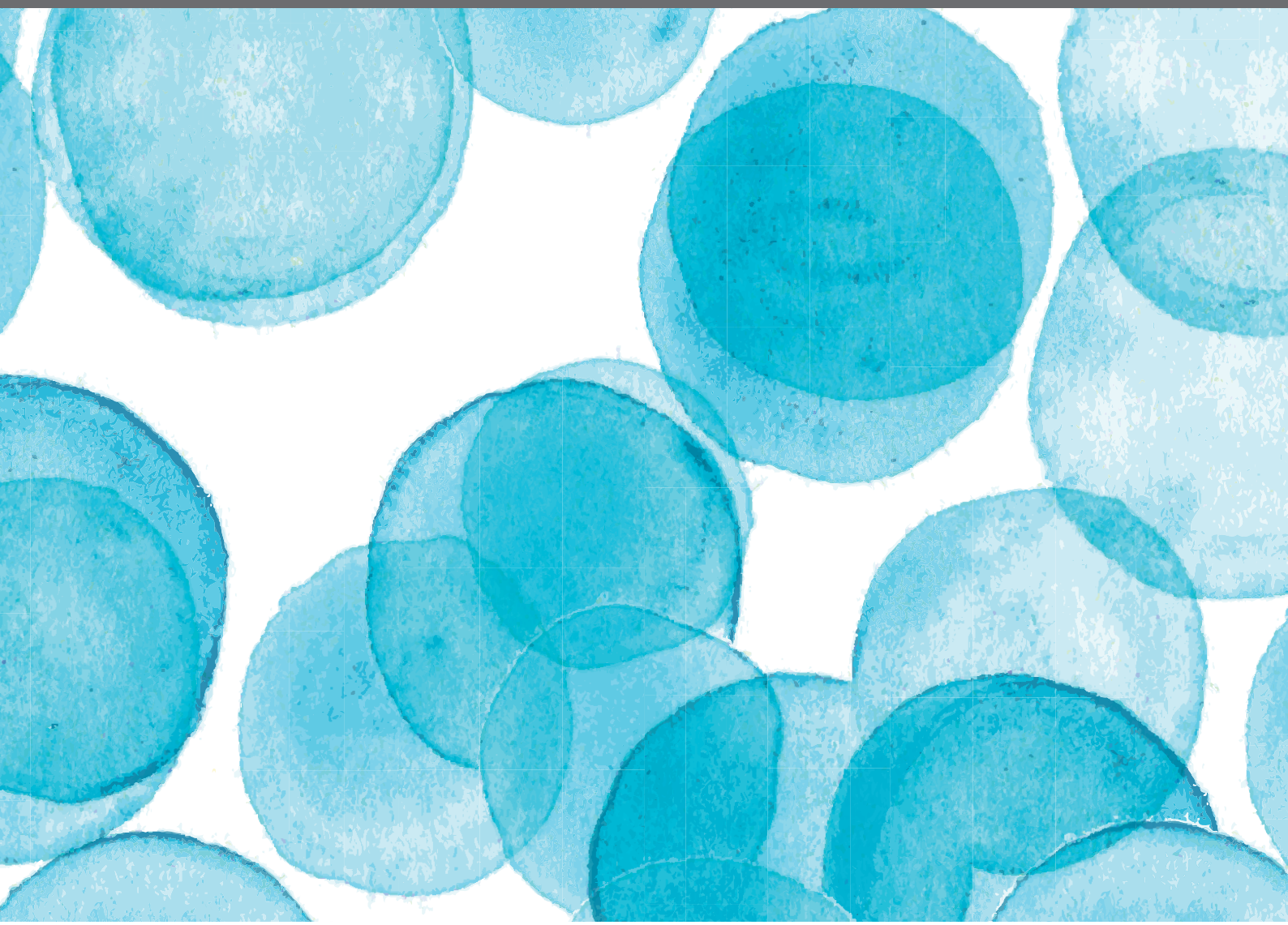

frontiers Research Topics

frontiers

Frontiers eBook Copyright Statement

The copyright in the text of individual articles in this eBook is the property of their respective authors or their respective institutions or funders. The copyright in graphics and images within each article may be subject to copyright of other parties. In both cases this is subject to a license granted to Frontiers.

The compilation of articles constituting this eBook is the property of Frontiers.

Each article within this eBook, and the eBook itself, are published under the most recent version of the Creative Commons CC-BY licence. The version current at the date of publication of this eBook is CC-BY 4.0. If the CC-BY licence is updated, the licence granted by Frontiers is automatically updated to the new version.

When exercising any right under the CC-BY licence, Frontiers must be attributed as the original publisher of the article or eBook, as applicable.

Authors have the responsibility of ensuring that any graphics or other materials which are the property of others may be included in the CC-BY licence, but this should be checked before relying on the CC-BY licence to reproduce those materials. Any copyright notices relating to those materials must be complied with.

Copyright and source acknowledgement notices may not be removed and must be displayed in any copy, derivative work or partial copy which includes the elements in question.

All copyright, and all rights therein, are protected by national and international copyright laws. The above represents a summary only. For further information please read Frontiers' Conditions for Website Use and Copyright Statement, and the applicable CC-BY licence.

ISSN 1664-8714
ISBN 978-2-88966-506-8
DOI 10.3389/978-2-88966-506-8

About Frontiers

Frontiers is more than just an open-access publisher of scholarly articles: it is a pioneering approach to the world of academia, radically improving the way scholarly research is managed. The grand vision of Frontiers is a world where all people have an equal opportunity to seek, share and generate knowledge. Frontiers provides immediate and permanent online open access to all its publications, but this alone is not enough to realize our grand goals.

Frontiers Journal Series

The Frontiers Journal Series is a multi-tier and interdisciplinary set of open-access, online journals, promising a paradigm shift from the current review, selection and dissemination processes in academic publishing. All Frontiers journals are driven by researchers for researchers; therefore, they constitute a service to the scholarly community. At the same time, the Frontiers Journal Series operates on a revolutionary invention, the tiered publishing system, initially addressing specific communities of scholars, and gradually climbing up to broader public understanding, thus serving the interests of the lay society, too.

Dedication to Quality

Each Frontiers article is a landmark of the highest quality, thanks to genuinely collaborative interactions between authors and review editors, who include some of the world's best academicians. Research must be certified by peers before entering a stream of knowledge that may eventually reach the public - and shape society; therefore, Frontiers only applies the most rigorous and unbiased reviews.
Frontiers revolutionizes research publishing by freely delivering the most outstanding research, evaluated with no bias from both the academic and social point of view. By applying the most advanced information technologies, Frontiers is catapulting scholarly publishing into a new generation.

What are Frontiers Research Topics?

Frontiers Research Topics are very popular trademarks of the Frontiers Journals Series: they are collections of at least ten articles, all centered on a particular subject. With their unique mix of varied contributions from Original Research to Review Articles, Frontiers Research Topics unify the most influential researchers, the latest key findings and historical advances in a hot research area! Find out more on how to host your own Frontiers Research Topic or contribute to one as an author by contacting the Frontiers Editorial Office: frontiersin.org/about/contact

HOST AND PATHOGEN MECHANISMS UNDERPINNING VIRAL ECOLOGY AND EMERGING INFECTIONS

Topic Editors:
Declan C. Schroeder, University of Minnesota, United States
Jim L. Van Etten, University of Nebraska-Lincoln, United States
Ian M. Jones, University of Reading, United Kingdom
Janusz Tadeusz Paweska, National Institute of Communicable Diseases (NICD), South Africa
Zhengli Shi, Chinese Academy of Sciences, China
Ahmed Sayed Abdel-Moneim, Taif University, Saudi Arabia

Citation: Schroeder, D. C., Etten, J. L. V., Jones, I. M., Paweska, J. T., Shi, Z., Abdel-Moneim, A. S., eds. (2021). Host And Pathogen Mechanisms Underpinning Viral Ecology And Emerging Infections. Lausanne: Frontiers Media SA.
doi: 10.3389/978-2-88966-506-8

Table of Contents

06 ***Gga-miR-19b-3p Inhibits Newcastle Disease Virus Replication by Suppressing Inflammatory Response via Targeting RNF11 and ZMYND11***
Yu Chen, Wen Liu, Haixu Xu, Jingjing Liu, Yonghuan Deng, Hao Cheng, Tiansong Zhan, Xiaolong Lu, Tianxing Liao, Lili Guo, Shanshan Zhu, Yuru Pei, Jiao Hu, Zenglei Hu, Xiaowen Liu, Xiaoquan Wang, Min Gu, Shunlin Hu and Xiufan Liu

19 ***Origin of Canine Distemper Virus: Consolidating Evidence to Understand Potential Zoonoses***
Carolina Quintero-Gil, Santiago Rendon-Marin, Marlen Martinez-Gutierrez and Julian Ruiz-Saenz

24 ***Factors Affecting the Tissue Damaging Consequences of Viral Infections***
Deepak Sumbria, Engin Berber and Barry T. Rouse

37 ***Isolation and Identification of Porcine Epidemic Diarrhea Virus and Its Effect on Host Natural Immune Response***
Shaoju Qian, Weida Zhang, Xiangchao Jia, Zhijian Sun, Yang Zhang, Yuncai Xiao and Zili Li

49 ***Temporal Dynamics of Co-circulating Lineages of Porcine Reproductive and Respiratory Syndrome Virus***
Igor Adolfo Dexheimer Paploski, Cesar Corzo, Albert Rovira, Michael P. Murtaugh, Juan Manuel Sanhueza, Carles Vilalta, Declan C. Schroeder and Kimberly VanderWaal

62 ***Molecular Detection and Genetic Characterization of Novel RNA Viruses in Wild and Synanthropic Rodents and Shrews in Kenya***
Samson Omondi Onyuok, Ben Hu, Bei Li, Yi Fan, Kelvin Kering, Griphin Ochieng Ochola, Xiao-Shuang Zheng, Vincent Obanda, Sheila Ommeh, Xing-Lou Yang, Bernard Agwanda and Zheng-Li Shi

73 ***Dengue Virus Infection Activates Interleukin-1β to Induce Tissue Injury and Vascular Leakage***
Pan Pan, Qi Zhang, Weiyong Liu, Wenbiao Wang, Zhenyang Yu, Zizhao Lao, Wei Zhang, Miaomiao Shen, Pin Wan, Feng Xiao, Muhammad Adnan Shereen, Wen Zhang, Qiuping Tan, Yuntao Liu, Xiaohong Liu, Kailang Wu, Yingle Liu, Geng Li and Jianguo Wu

87 ***Insulin-Like Growth Factor 1 Regulates Acute Inflammatory Lung Injury Mediated by Influenza Virus Infection***
Guiping Li, Lijuan Zhou, Can Zhang, Yun Shi, Derong Dong, Miao Bai, Rong Wang and Chuanfu Zhang

99 ***Estimating Transmission Potential of H5N1 Viruses Among Humans in Egypt Using Phylogeny, Genetic Distance and Sampling Time Interval***
Wessam Mohamed, Kimihito Ito and Ryosuke Omori

109 ***Neglected Australian Arboviruses Associated With Undifferentiated Febrile Illnesses***
Narayan Gyawali, Andrew W. Taylor-Robinson, Richard S. Bradbury, Wayne Pederick, Helen M. Faddy and John G. Aaskov

120 ***The Host Heat Shock Protein MRJ/DNAJB6 Modulates Virus Infection***
Shih-Han Ko, Li-Min Huang and Woan-Yuh Tarn

129 ***Epstein-Barr Virus Nuclear Antigen 1 Recruits Cyclophilin A to Facilitate the Replication of Viral DNA Genome***
Shuyu Xin, Shujuan Du, Lingzhi Liu, Yan Xie, Lielian Zuo, Jing Yang, Jingjin Hu, Wenxing Yue, Jing Zhang, Pengfei Cao, Fanxiu Zhu and Jianhong Lu

143 ***Host Gene SEL1L Involved in Endoplasmic Reticulum-Associated Degradation Pathway Could Inhibit Hepatitis B Virus at RNA, DNA, and Protein Levels***
Jinyu Wang, Jing Li, Jingwen Wu, Minhui Dong, Zhongliang Shen, Yong Lin, Fahong Li, Yongmei Zhang, Richeng Mao, Mengji Lu and Jiming Zhang

153 ***Comparative Pathogenicity and Transmissibility of Pandemic H1N1, Avian H5N1, and Human H7N9 Influenza Viruses in Tree Shrews***
Shuai Xu, Xuyong Li, Jiayun Yang, Zhengxiang Wang, Yane Jia, Lu Han, Liang Wang and Qiyun Zhu

168 ***Dual NDP52 Function in Persistent CSFV Infection***
Shuangqi Fan, Keke Wu, Chaowei Luo, Xin Li, Mengpo Zhao, Dan Song, Shengming Ma, Erpeng Zhu, Yuming Chen, Hongxing Ding, Lin Yi, Jun Li, Mingqiu Zhao and Jinding Chen

181 ***Transmissible Gastroenteritis Virus Infection Up-Regulates FcRn Expression via Nucleocapsid Protein and Secretion of TGF-β in Porcine Intestinal Epithelial Cells***
Shaoju Qian, Zitong Gao, Rui Cao, Kang Yang, Yijie Cui, Shaowen Li, Xianrong Meng, Qigai He and Zili Li

193 ***Coxsackievirus A6 Induces Necroptosis for Viral Production***
Shuxia Zhang, Xiaoyan Yu, Xiangling Meng, Wenbo Huo, Ying Su, Jinming Liu, Yumeng Liu, Jun Zhang, Shaohua Wang and Jinghua Yu

205 ***Transcriptome Analysis Reveals New Insight of Fowl Adenovirus Serotype 4 Infection***
Yuan Chen, Ruiling Huang, Guishu Qu, Yaoshun Peng, Lihui Xu, Changkang Wang, Cuiqin Huang and Quanxi Wang

217 ***A Long Non-coding RNA IVRPIE Promotes Host Antiviral Immune Responses Through Regulating Interferon β1 and ISG Expression***
Lingna Zhao, Min Xia, Keyu Wang, Chengcai Lai, Hongxia Fan, Hongjing Gu, Penghui Yang and Xiliang Wang

228 ***MiR-10a-5p-Mediated Syndecan 1 Suppression Restricts Porcine Hemagglutinating Encephalomyelitis Virus Replication***
Shiyu Hu, Zi Li, Yungang Lan, Jiyu Guan, Kui Zhao, Dianfeng Chu, Gencheng Fan, Yuguang Guo, Feng Gao and Wenqi He

238 ***Phylogeographic Dynamics of Influenza A(H9N2) Virus Crossing Egypt***
Ruiyun Li, Amany Adel, Jon Bohlin, Åke Lundkvist, Björn Olsen, John H.-O. Pettersson and Mahmoud M. Naguib

246 ***Accumulation and Competition Amongst Deformed Wing Virus Genotypes in Naïve Australian Honeybees Provides Insight Into the Increasing Global Prevalence of Genotype B***
Amanda M. Norton, Emily J. Remnant, Gabriele Buchmann and Madeleine Beekman

260 ***Friend or Enemy: A Dual Role of Autophagy in Plant Virus Infection***
Xiuqin Huang, Siping Chen, Xiaorong Yang, Xin Yang, Tong Zhang and Guohui Zhou

269 ***Interactions Between Thiamethoxam and* Deformed Wing Virus *Can Drastically Impair Flight Behavior of Honey Bees***
Marianne Coulon, Anne Dalmon, Gennaro Di Prisco, Alberto Prado, Florine Arban, Eric Dubois, Magali Ribière-Chabert, Cedric Alaux, Richard Thiéry and Yves Le Conte

281 ***Cleavage of Desmosomal Cadherins Promotes γ-Catenin Degradation and Benefits Wnt Signaling in Coxsackievirus B3-Induced Destruction of Cardiomyocytes***
Guangze Zhao, Huifang M. Zhang, Ye Qiu, Xin Ye and Decheng Yang

300 ***Distinct Cell Transcriptomic Landscapes Upon Henipavirus Infections***
Mingyue Chen, Mary Tachedjian, Glenn A. Marsh, Jie Cui and Lin-Fa Wang

310 ***Canine Distemper Virus (CDV) Transit Through the Americas: Need to Assess the Impact of CDV Infection on Species Conservation***
Santiago Rendon-Marin, Marlen Martinez-Gutierrez, José Antonio Suarez and Julian Ruiz-Saenz

314 ***The Coronavirus PEDV Evades Type III Interferon Response Through the miR-30c-5p/SOCS1 Axis***
Changlin Wang, Lingling Shan, Shuxin Qu, Mei Xue, Keliang Wang, Fang Fu, Lu Wang, Ziqi Wang, Li Feng, Wanhai Xu and Pinghuang Liu

324 ***Bee Viruses: Routes of Infection in Hymenoptera***
Orlando Yañez, Niels Piot, Anne Dalmon, Joachim R. de Miranda, Panuwan Chantawannakul, Delphine Panziera, Esmaeil Amiri, Guy Smagghe, Declan Schroeder and Nor Chejanovsky

346 ***Modulation of Gut Microbiota, Short-Chain Fatty Acid Production, and Inflammatory Cytokine Expression in the Cecum of Porcine Deltacoronavirus-Infected Chicks***
Hai-yan Li, Hong-lei Zhang, Fu-jie zhao, Shi-qiong Wang, Zhi-xiang Wang and Zhan-yong Wei

358 ***Temperature Dramatically Shapes Mosquito Gene Expression With Consequences for Mosquito–Zika Virus Interactions***
Priscila Gonçalves Ferreira, Blanka Tesla, Elvira Cynthia Alves Horácio, Laila Alves Nahum, Melinda Ann Brindley, Tiago Antônio de Oliveira Mendes and Courtney Cuinn Murdock

380 ***Chikungunya Virus: An Emergent Arbovirus to the South American Continent and a Continuous Threat to the World***
Marcela S. Cunha, Pedro A. G. Costa, Isadora Alonso Correa, Marcos R. M. de Souza, Pedro Teles Calil, Gustavo P. Duarte da Silva, Sara Mesquita Costa, Vinícius Wakoff P. Fonseca and Luciana J. da Costa

400 ***Sequencing the Genome of Indian Flying Fox, Natural Reservoir of Nipah Virus, Using Hybrid Assembly and Conservative Secondary Scaffolding***
Julien Fouret, Frédéric G. Brunet, Martin Binet, Noémie Aurine, Francois Enchéry, Séverine Croze, Marie Guinier, Abdelghafar Goumaidi, Doris Preininger, Jean-Nicolas Volff, Marc Bailly-Bechet, Joël Lachuer, Branka Horvat and Catherine Legras-Lachuer

414 ***Screening and Validation of Reference Genes for RT-qPCR Under Different Honey Bee Viral Infections and dsRNA Treatment***
Yanchun Deng, Hongxia Zhao, Sa Yang, Li Zhang, Lina Zhang and Chunsheng Hou

frontiers in Microbiology

ORIGINAL RESEARCH
published: 27 August 2019
doi: 10.3389/fmicb.2019.02006

Gga-miR-19b-3p Inhibits Newcastle Disease Virus Replication by Suppressing Inflammatory Response via Targeting RNF11 and ZMYND11

*Yu Chen[1], Wen Liu[1], Haixu Xu[1], Jingjing Liu[1], Yonghuan Deng[1], Hao Cheng[1], Tiansong Zhan[1], Xiaolong Lu[1], Tianxing Liao[1], Lili Guo[1], Shanshan Zhu[1], Yuru Pei[1], Jiao Hu[1,2], Zenglei Hu[1], Xiaowen Liu[1,2], Xiaoquan Wang[1], Min Gu[1,3], Shunlin Hu[1] and Xiufan Liu[1,2,3]**

[1] Animal Infectious Disease Laboratory, College of Veterinary Medicine, Yangzhou University, Yangzhou, China, [2] Jiangsu Co-innovation Center for Prevention and Control of Important Animal Infections Diseases and Zoonoses, Yangzhou University, Yangzhou, China, [3] Jiangsu Key Laboratory of Zoonosis, Yangzhou University, Yangzhou, China

OPEN ACCESS

Edited by:
Declan C. Schroeder,
University of Minnesota, Twin Cities, United States

Reviewed by:
Qingmei Xie,
South China Agricultural University, China
Shijun Zheng,
China Agricultural University (CAU), China

***Correspondence:**
Xiufan Liu
xfliu@yzu.edu.cn

Specialty section:
This article was submitted to Virology, a section of the journal Frontiers in Microbiology

Received: 23 May 2019
Accepted: 15 August 2019
Published: 27 August 2019

Citation:
Chen Y, Liu W, Xu H, Liu J, Deng Y, Cheng H, Zhan T, Lu X, Liao T, Guo L, Zhu S, Pei Y, Hu J, Hu Z, Liu X, Wang X, Gu M, Hu S and Liu X (2019) Gga-miR-19b-3p Inhibits Newcastle Disease Virus Replication by Suppressing Inflammatory Response via Targeting RNF11 and ZMYND11. Front. Microbiol. 10:2006. doi: 10.3389/fmicb.2019.02006

Newcastle disease (ND), an acute and highly contagious avian disease caused by virulent Newcastle disease virus (NDV), often results in severe economic losses worldwide every year. Although it is clear that microRNAs (miRNAs) are implicated in modulating innate immune response to invading microbial pathogens, their role in host defense against NDV infection remains largely unknown. Our prior study indicates that gga-miR-19b-3p is up-regulated in NDV-infected DF-1 cells (a chicken embryo fibroblast cell line) and functions to suppress NDV replication. Here we report that overexpression of gga-miR-19b-3p promoted the production of NDV-induced inflammatory cytokines and suppressed NDV replication, whereas inhibition of endogenous gga-miR-19b-3p expression had an opposite effect. Dual-luciferase and gene expression array analyses revealed that gga-miR-19b-3p directly targets the mRNAs of ring finger protein 11 (RNF11) and zinc-finger protein, MYND-type containing 11 (ZMYND11), two negative regulators of nuclear factor kappa B (NF-κB) signaling, in DF-1 cells. RNF11 and ZMYND11 silencing by small interfering RNA (siRNA) induced NF-κB activity and inflammatory cytokine production, and suppressed NDV replication; whereas ectopic expression of these two proteins exhibited an opposite effect. Our study provides evidence that gga-miR-19b-3p activates NF-κB signaling by targeting RNF11 and ZMYND11, and that enhanced inflammatory cytokine production is likely responsible for the suppression of NDV replication.

Keywords: NDV, gga-miR-19b-3p, DF-1 cells, RNF11, ZMYND11, inflammatory cytokine, NF-κB signaling

INTRODUCTION

Newcastle disease virus (NDV) was first described in the early 1900s as the contagious agent of the fatal avian disease known as chicken pest (Dimitrov et al., 2016, 2017). It is classified as an avian paramyxovirus-1 (APMV-1) in the Avulavirus genus of the family Paramyxoviridae (Cheng et al., 2016). The viral particles have a negative-sense, single-stranded RNA genome of about 15 kb that

contains six genes in the order of 3′-NP-P-M-F-HN-L-5′, encoding six proteins: nucleoprotein (NP), phosphor protein (P), matrix protein (M), fusion protein (F), hemagglutinin-neuraminidase (HN), and large protein (L), respectively. As one of the most devastating pathogens for poultry industry, NDV has a wide host range and can naturally or experimentally infect more than 250 bird species (Ganar et al., 2014). Although all NDV isolates belong to a single serotype, they have a high genetic diversity and evolve rapidly. According to recent epidemiological investigations, sub-genotype VIId has become the dominant genotype in many Asian and African countries since the late 1990s (Qin et al., 2008; Wu et al., 2011; Munir et al., 2012). Currently, vaccination is the main way to prevent and control NDV prevalence. However, due to the wide range of host and high genetic diversity, the failure of Newcastle disease (ND) vaccine immunization and reduction of vaccine efficiency often occur in cultivation industry worldwide (Miller et al., 2009, 2013).

During NDV infection, a variety of the host pattern recognition receptors (PRRs) are activated such as toll-like receptor 3 (TLR-3) (Cheng et al., 2014), retinoic-acidinducible gene I (RIG-I) (Kato et al., 2006; Sun et al., 2013), melanoma differentiation associated gene 5 (MDA5) (Rue et al., 2011), and protein kinase R (PKR) (Liao et al., 2016) by recognizing virus double-stranded RNA. These PRRs subsequently activate downstream transcription factors such as interferon regulatory factor 7 (IRF7) (Wang et al., 2014) and NF-κB (Rajmani et al., 2016), leading to inflammatory cytokine production. For NF-κB activation, PRRs initiate a signaling cascade resulting in the IκB kinase (IKK) phosphorylation, which subsequently phosphorylates and ubiquitinates IκB-α bound to NF-κB in resting cells, and results in IκB-α proteasomal degradation, thereby allowing NF-κB nuclear translocation to transcriptionally activate its gene targets (Woronicz et al., 1997). However, to maintain cellular homeostasis, activation of NF-κB signaling pathway is tightly controlled with multiple tiers of regulation (Ruland, 2011), such as RNF11 (Shembade et al., 2009; Dalal et al., 2012; Pranski et al., 2012) and ZMYND11 (Ikeda et al., 2009, 2010). These two proteins negatively regulate NK-κB activity and greatly impact the replication of certain viruses such as Hendra virus (HeV) (Stewart et al., 2013), Japanese encephalitis virus (JEV) (Ashraf et al., 2016), and Epstein-Barr virus (EBV) (Ikeda et al., 2009).

miRNAs are small non-coding RNAs that are usually composed of 21–23 nucleotides. miRNAs negatively regulate the expression of half protein-coding genes involving in cell growth, proliferation, apoptosis, and signal transduction through post-transcriptional mechanisms (Bartel, 2004). Accumulating evidence suggests that virus infection profoundly impacts miRNA expression, and that altered miRNA expression can enhance or suppress anti-viral responses (Trobaugh and Klimstra, 2017). Recent studies have shown that NDV infection alters the levels of several miRNAs. For example, NDV infection induces hsa-miR-485 expression in human embryonic kidney (HEK) 293T cells, which in turn suppresses antiviral response and enhances NDV replication by targeting RIG-I mRNA (Ingle et al., 2015). In contrast, NDV infection down-regulates gga-miR-203a expression in chicken embryos, overexpression of gga-miR-203a effectively increases NDV replication both *in vivo* and *in vitro* via targeting transglutaminase 2 (TGM2) (Jia et al., 2018). Up-regulated gga-miR-375 in NDV-infected DF-1 cells suppresses NDV replication via targeting viral M gene or cellular embryonic lethal, abnormal vision, Drosophila-like RNA binding protein 4 (ELAVL4) gene (Wang et al., 2019). These observations collectively suggest that miRNAs play a critical role in NDV infection and replication. Identification of host-dysregulated miRNAs and understanding of their roles in virus replication may shed light on NDV pathogenesis and provide better strategies for the control of NDV infection.

Our present study focuses on the effect of gga-miR-19b-3p on NDV replication and the underlying molecular mechanisms. Here we report that RNF11 and ZMYND11 are two targets of gga-miR-19b-3p in DF-1 cells, and that up-regulation of gga-miR-19b-3p and the subsequent down-regulation of RNF11 and ZMYND11 expression enhance NDV-induced NF-κB activation, leading to increased inflammatory cytokine production and suppression of virus replication. Data presented herein improve our understanding of the role of host miRNAs in regulating NDV replication.

MATERIALS AND METHODS

Cells and Viruses

DF-1 cells obtained from ATCC (CRL-12203) were cultured in Dulbecco's modified Eagle's medium (DMEM) (Life Technologies, United States) supplemented with 10% fetal bovine serum (FBS) (Life Technologies, United States), 100 U/mL penicillin and 100 μg/mL streptomycin at 37℃ under 5% CO_2 atmosphere. Velogenic genotype VII NDV strain JS5/05 (Accession Number: JN631747) was propagated in chicken embryos and the biological characteristics of the virus were determined previously (Hu et al., 2011). Velogenic genotype IV Herts/33 (Accession Number: AY741404) was obtained from Dr. D. J. Alexander (Animal Health and Veterinary Laboratories Agency, United Kingdom) and avirulent genotype II NDV strain La Sota (Accession Number: AF077761) was isolated and maintained in our laboratory.

MiRNA Mimic and Inhibitor

Gga-miR-19b-3p mimic was chemically modified double-stranded oligonucleotides for overexpression of gga-miR-19b-3p and gga-miR-19b-3p inhibitor was single-stranded oligonucleotides for inhibition of gga-miR-19b-3p. All RNA oligonucleotides were designed and synthesized by GenePharma, China. For miRNA transfection, DF-1 cells were transfected with gga-miR-19b-3p mimic and inhibitor and mimic negative control (mimic-NC) and inhibitor negative control (inh-NC) at a final concentration of 100 nM using EL Transfection Reagent (Transgen Biotech, China) following the manufacturer's instructions.

Knockdown of RNF11 and ZMYND11

siRNAs (double-stranded RNA oligonucleotides) (Genepharma, China) were used to knockdown the expressions of RNF11 and ZMYND11 in DF-1 cells and the sequences were shown in **Table 1**. siRNA duplexes were transfected into DF-1 cells at a final concentration of 50 nM using EL Transfection Reagent (Transgen Biotech, China). The interference efficiency was detected by qRT-PCR and Western blot as described below.

Determination of Viral Titers

DF-1 cells (2×10^5 cells/mL) were seeded on 12-well plates and cultured for 24 h before transfection with indicated RNA oligonucleotides or plasmids. Eighteen hours after transfection, DF-1 cells were infected with JS5/05 strain at a multiplicity of infection (MOI) of 0.1. The culture supernatants were collected and replaced with an equal volume of fresh media at different time points (12, 24, 36, 48, and 60 h) after infection. The viral contents in the supernatants were quantified by 50% tissue culture infective doses ($TCID_{50}$) on DF-1 cells (Reed and Muench, 1938).

Plasmids Construction

DNA sequences of gga-miR-19b-3p promoter were cloned from genomic DNA of DF-1 cells using specific primers and sub-cloned into *Kpn*I/*Xho*I restriction sites in the pGL-6 reporter vector (Beyotime, China) to generate the pGL-6-miR-19b-3p reporter vector. Target sequences of gga-miR-19b-3p in RNF11 and ZMYND11 were amplified by polymerase chain reaction (PCR) using a cDNA template synthesized from total RNA of DF-1 cells. Subsequently, both PCR products were sub-cloned into *Xho*I/*Not*I restriction sites in the pmiR-RB-reporter™ vector (Ribobio, China), which can express firefly luciferase and renilla luciferase in one plasmid, to generate pmiR-RNF11-3′UTR-wild and pmiR-ZMYND11-3′UTR-wild plasmids. To generate gga-miR-19b-3p target-mutated reporter vector, pmiR-RNF11-3′UTR-mut and pmiR-ZMYND11-3′UTR-mut were achieved by changing the gga-miR-19b-3p binding seed sequences using Fast Mutagenesis System kit (Transgen Biotech, China) according to manufacturer's instructions. The coding sequences of RNF11 (Accession No. NM001006540) and ZMYND11 (Accession No. XM025148320) were amplified and subsequently cloned into pCMV-blank overexpression vector (Beyotime, China) to generate pCMV-RNF11 and pCMV-ZMYND11 plasmids. All the primers for plasmids construction (shown in **Table 2**) were synthesized by Sangon Company, China. All the fragments were amplified by PCR using TransStart Fast Pfu Fly DNA Polymerase (Transgen Biotech, China).

miRNA Target Prediction and Dual-Luciferase Reporter Gene Assays

Gga-miR-19b-3p targets in host cells were predicted by two online softwares: TargetScan[1] and miRDB[2]. GO Ontology (GO) analysis was conducted to screen the genes on the Database for Annotation, Visualization and Integrated Discovery (DAVID) platform. Luciferase activity was measured using Dual-GLO®Luciferase Assay System Kits (Promega, United States) following the manufacturer's instructions. For targets verification, DF-1 cells were seeded on 24-well plates with a density of 1×10^5 cells/mL per well. After 24 h, the cells were co-transfected with indicated plasmids and RNA oligonucleotides using EL Transfection Reagent. Forty-eight hours after transfection, luciferase assays were performed with a Fluorescence/Multi-Detection Microplate Reader (Biotek, United States). Renilla luciferase activities were normalized on the basis of firefly luciferase activities. For the detection of promoter activity, DF-1 cells were transfected with pGL-6 or pGL-6-miR-19b-3p plasmid using EL Transfection Reagent. To normalize transfection efficiency, pRL-TK renilla luciferase reporter plasmid (Promega, United States) was also transfected into the cells as an internal control. Then the cells were infected with JS 5/05 at different MOIs at 48h post transfection. Twelve hours post infection (hpi), the dual-luciferase activity was detected and firefly luciferase activities were normalized to

[1]http://www.targetscan.org/

[2]http://www.mirdb.org/

TABLE 1 | siRNA sequences.

siRNAs	Sense (5′-3′)	Anti-sense (5′-3′)
SiRNA-ZMYND 11-1	GCACAUACCUGCGGUUCAUTT	AUGAACCGCAGGUAUGUGCTT
SiRNA-ZMYND 11-2	GCUAUCCUUGUAUACCUAATT	UUAGGUAUACAAGGAUAGCTT
SiRNA-ZMYND 11-3	GCUGUUGAUGUUCCUACUATT	UAGUAGGAACAUCAACAGCTT
SiRNA-RNF11-1	GCCAGAAAUUAGGAAUUAATT	UUAAUUCCUAAUUUCUGGCTT
SiRNA-RNF11-2	CCUACCGAAGGGAGUCUAUTT	AUAGACUCCCUUCGGUAGGTT
SiRNA-RNF11-3	CCACCUGGACUGUAUAGAUTT	AUCUAUACAGUCCAGGUGGTT
SiRNA-NC	UUCUCCGAACGUGUCACGUTT	ACGUGACACGUUCGGAGAATT

TABLE 2 | Primers used for plasmids construction.

Gene	Forward primers (5′-3′)	Reverse primer (5′-3′)
19b-3p promoter	GGTACCGCCGGGAGG GTCTGCC	CTCGAGTTCAATTTAAC AACAAATTGCAAA
RNF11-3′UTR-wild	CTCGAGGCCAGGGTTTCTC CGTGAAC	GCGGCCGCCAAGAGATG CGGTATCCTTTGC
ZMYND11-3′UTR-wild	CTCGAGGAGCCATTCCTCCG CTAGAACA	GCGGCCGCCTCGGTCTA AGACCAGCCTCTG
RNF11-3′UTR-mut	ATAGTTTTAAGCTTGTGCAC GTAGTTCTTTT	ACGTGCACAAGCTTAAAAC TATTTCTTTGT
ZMYND11-3′UTR-mut	TTCCCATTAAGGTGCAGCCT TTAAACA	GCACCTTAATGGGAAGC AAATTCTAAACA
RNF11 CDS	ACTAGTATGGGGAACTGCCTC AAGTCC	GGGCCCTCAGTTAGTCTCG TATGATGAAAG
ZMYND11 CDS	ACTAGTATGGCACGCTTA ACGAAGAGACG	GGGCCCTCATCTTTTTCTG CGGCAGGTACG

renilla luciferase activities. To measure the activity of NF-κB, pNF-κB-luc (Beyotime, China) plasmid and indicated siRNAs or plasmids were transfected into DF-1 cells together with the internal control plasmid pRL-TK (Promega, United States). Eighteen hours after transfection, the cells were infected with JS 5/05 strain at an MOI of 0.1 and dual-luciferase assays were performed as described above at 18 hpi.

miRNA and Total RNA Extraction and Quantitative Real-Time PCR (qRT-PCR) Analysis

To measure the dynamic expression pattern of gga-miR-19b-3p after NDV infection, DF-1 cells seeded in 12-well plates were infected with JS5/05 strain at different MOIs for 12 h and then miRNAs were extracted using a miRNA Extraction Kit according to manufacturer's instructions. cDNA synthesis was carried out with a tagged polyT primer according to the protocol of One Step miRNA cDNA Synthesis Kit. Quantification of gga-miR-19b-3p was performed by HG miRNA SYBR Green PCR Kit with a pair of specific primers. Gga-miR-19b-3p expression level was normalized to 5s rRNA levels using the $2^{-\Delta\Delta Ct}$ model. All kits used for miRNA extraction, cDNA synthesis and qRT-PCR were purchased from HaiGene Corporation, China.

For the detection of inflammatory cytokines and IκB-α, DF-1 cells were transfected with indicated RNA oligonucleotides for 18 h before infected with JS 5/05 at an MOI of 0.1. Then the total RNAs were extracted from the cells at 18 hpi using TRIzol (TransGen Biotech, China) following the manufacturer's instructions. The cDNA synthesis and qRT-PCR reaction were performed using TransScript Green One-Step qRT-PCR Super Mix (TransGen Biotech, China) according to the manufacturer's instructions. To detect RNF11 and ZMYND11 mRNA expression levels, DF-1 cells were transfected with indicated RNA oligonucleotides or infected with JS 5/05 or Herts/33 or La Sota strain at an MOI of 0.1. Eighteen hours post transfection or infection, qRT-PCR were performed as described above using RNF11 and ZMYND11 specific primers. The relative expressions of inflammatory cytokines, IκB-α, RNF11, and ZMYND11 were all normalized with glyceraldehyde phosphate dehydrogenase (GAPDH) and calculated using the $2^{-\Delta\Delta CT}$ method. All qRT-PCR experiments were preformed in LightCycler 480 (Roche, Switzerland) and primers used were shown in **Table 3**.

Enzyme-Linked Immunosorbent Assay (ELISA)

DF-1 cells in 6-well plates were transfected with indicated RNA oligonucleotides or plasmids and were incubated for 18 h and then either left uninfected or infected with JS 5/05 at an MOI of 0.1 for 18 h. The protein levels of IFN-β, TNF-α, IL-1β, IL-6, and IL-8 in cell cultures were determined by ELISA kits according to the manufacturer's instructions. The IFN-β (cat. no. CH50022), TNF-α (cat. no. CH50032), IL-1β (cat. no. CH50020), IL-6 (cat. no. CH50016), and IL-8 ELISA kits (cat. no. CH50027) were purchased from Bio-Swamp, China.

TABLE 3 | Primers used for qRT-PCR.

Gene	Forward primers (5′-3′)	Reverse primer (5′-3′)
gga-miR-19b-3p	AGTGTGCAAATCCATGCAA	GGTCCAGTTTTTTTTTTTT TTTCAGT
IFN-β	TGCACAGCATCCTACTG CTCTTG	GTTGGCATCCTGGTGACGAA
TNF-α	GGACAGCCTATGCCAACAAG	ACACGACAGCCAAGTCAACG
IL-1β	ACCCGCTTCATCTTCTACCG	TCAGCGCCCACTTAGCTT
IL-6	GGCATTCTCATTTCCTTCT	CTGGCTGCTGGACATTTT
IL-8	CCAAGCACACCTCTCTTCCA	GCAAGGTAGGACGCTGGTAA
IκB-α	CTGGACTCCATGAAGGA GGAGG	TCGTGAATGATCGCCA AGTGGAG
RNF11	GCCTTGACCCACCATTGTCTTT	CCTTGACCCAAATGCCAGGAC
ZMYND11	GGCGATCCAACATCTTTGGGC	GCCTTTGACCCTTTACACCCCA
5s RNA	AACGCCCGATCTCGTCTGAT	AGTCTCCCATCCAAGTA CTAACCG
GAPDH	GAGGGTAGTGAAGGCTGCTG	CACAACACGGTTGCTGTATC

For the detection of phosphorylation of IκB-α protein, DF-1 cells seeded on 12-well plates were transfection with indicated RNA oligonucleotides or plasmids for 18 h. Then the cells were infected with JS5/05 strain at an MOI of 0.1 for 18 h. The phosphorylation of IκB-α protein was measured by ELISA kit (SbjBio, China, cat. no. SBJ-C134) according to the manufacturer's instructions.

Western Blot Analysis

To measure the expression levels of RNF11 and ZMYND11 proteins, DF-1 cells were transfected with indicated RNA oligonucleotides or plasmids or infected with different NDV strains at an MOI of 0.1. Eighteen hours post transfection, the cells were lysed and 20 μg protein samples of each group were used for electrophoresis on 12% sodium dodecylsulfate-polyacrylamide gel electrophoresis (SDS-PAGE) gels, and resolved proteins were transferred onto polyvinylidene difluoride (PVDF) membranes using electro-transfer (Bio-Rad, United States). After blocking with 5% skimmed milk for 1 h at room temperature, the membranes were incubated with the appropriate primary antibodies, including rabbit polyclonal anti-RNF11 (LSBio, United States), rabbit polyclonal anti-ZMYND11 (LSBio, United States) and mouse monoclonal anti-β-actin (Transgene, China) followed by incubation with goat anti-rabbit and goat anti-mouse HRP-conjugated secondary antibodies (Beyotime, China). The proteins on the membranes were detected using an ECL^{TM} detection system (Bio-Rad, United States).

To measure the translocation of NF-κB from the cytoplasm to the nucleus, DF-1 cells transfected with indicated RNA oligonucleotides or plasmids were infected with JS 5/05 at an MOI of 0.1 for 18 h. Then cytoplasmic and nuclear proteins of the cells were prepared using nuclear and cytoplasmic protein extraction kit (Beyotime, China) according to the manufacturer's instructions. Western blot assays were performed as described above using NF-kB p65 rabbit monoclonal antibody (Beyotime, China). Monoclonal rabbit anti-tubulin β and anti-histone H3 antibody (Beyotime, China) were used as control

of cytoplasmic and nuclear proteins, respectively. The relative protein quantification was analyzed by Image J software (Bethesda, United States).

Statistical Analysis

All data are the averages of triplicates and are representative of results from at least three independent experiments. The statistical analysis were analyzed using one-way analysis of variance (ANOVA) following Bonferroni's multiple comparison tests for $TCID_{50}$, miRNA, Western blot and mRNA detections and two-way ANOVA using a Bonferroni's multiple comparison tests for viral growth curve using GraphPad Prism 5 (GraphPad Software, San Diego, United States). $P < 0.05$ was considered as a significant difference.

RESULTS

Gga-miR-19b-3p Is Upregulated During NDV Infection and Inhibits NDV Replication in DF-1 Cells

We first conducted qRT-PCR to determine if NDV infection regulated gga-miR-19b-3p expression in DF-1 cells. As shown in **Figure 1A**, gga-miR-19b-3p was up-regulated in NDV-infected DF-1 cells in a dose-dependent manner. Consistently, NDV infection also increased the gga-miR-19b-3p promoter-driven luciferase reporter gene expression in a dose-dependent manner (**Figure 1B**).

We next evaluated the effect of gga-miR-19b-3p on NDV replication. DF-1 cells were transfected with gga-miR-19b-3p

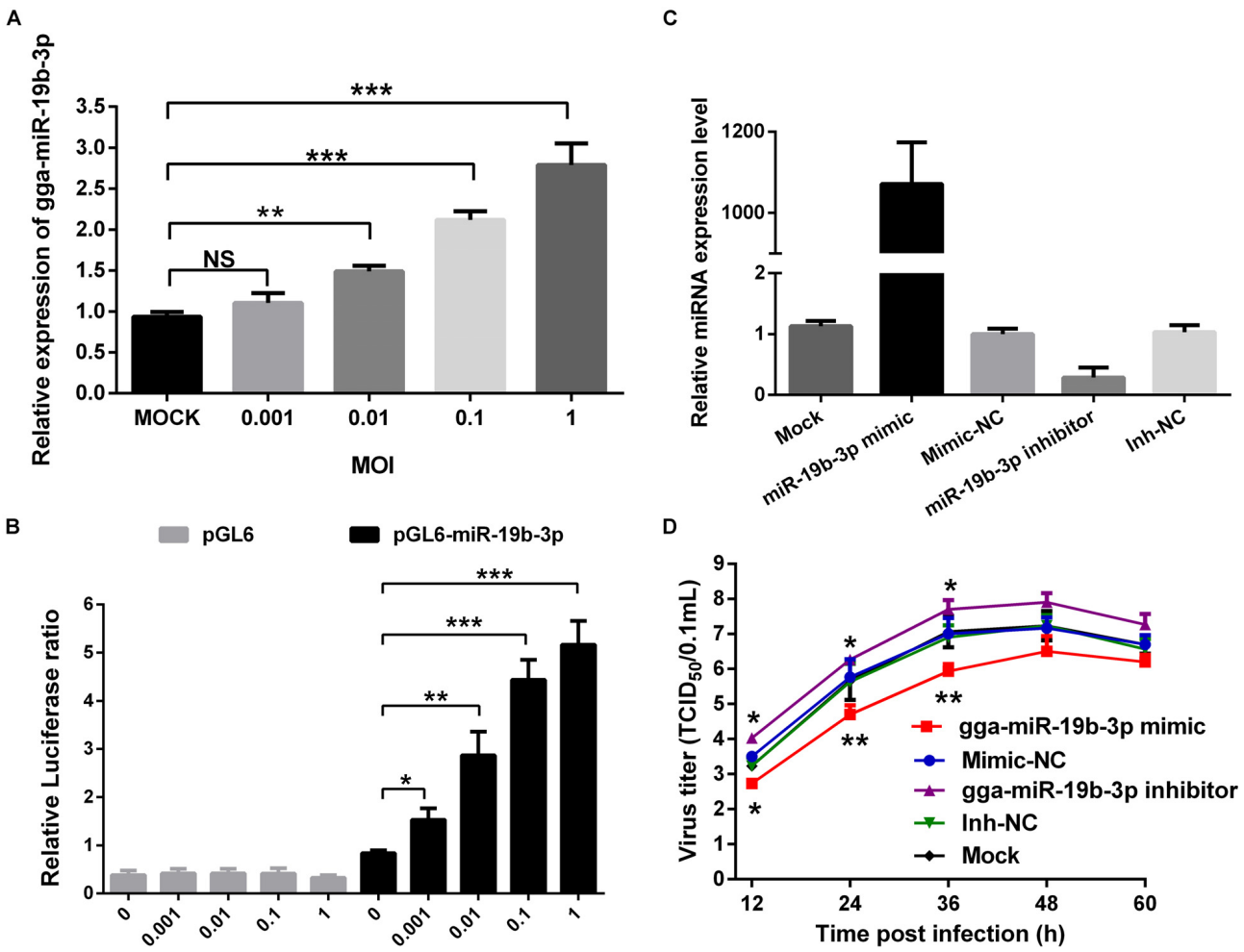

FIGURE 1 | Newcastle disease virus-induced gga-miR-19b-3p inhibits NDV replication in DF-1 cells. **(A)** DF-1 cells were infected with JS 5/05 strain at indicated MOIs for 12 h, and then the expression of gga-miR-19b-3p was detected by qRT-PCR. **(B)** The pGL-6-miR-19b-3p or pGL-6 plasmid was transfected into DF-1 cells together with pRL-TK renilla luciferase reporter plasmid as an internal control. Forty-eight hours post transfection, the cells were infected with JS 5/05 strain at different MOIs for 12 h, and then the dual-luciferase activity was detected and firefly luciferase activities were normalized to firefly renilla luciferase activities. **(C,D)** DF-1 cells were transfected with gga-miR-19b-3p mimic or inhibitor or mimic-NC or inh-NC at a final concentration of 100 nM or left untreated. The gga-miR-19b-3p expression was measured by qRT-PCR at 18 h post transfection **(C)**. Eighteen hours after transfection, DF-1 cells were infected with JS5/05 strain at an MOI of 0.1. The viral road in the supernatants collected at different time points were quantified by $TCID_{50}$ on DF-1 cells **(D)**. Results are representative of three independent experiments and presented as means ± SD. $^{*}p < 0.05$, $^{**}p < 0.01$, $^{***}p < 0.001$.

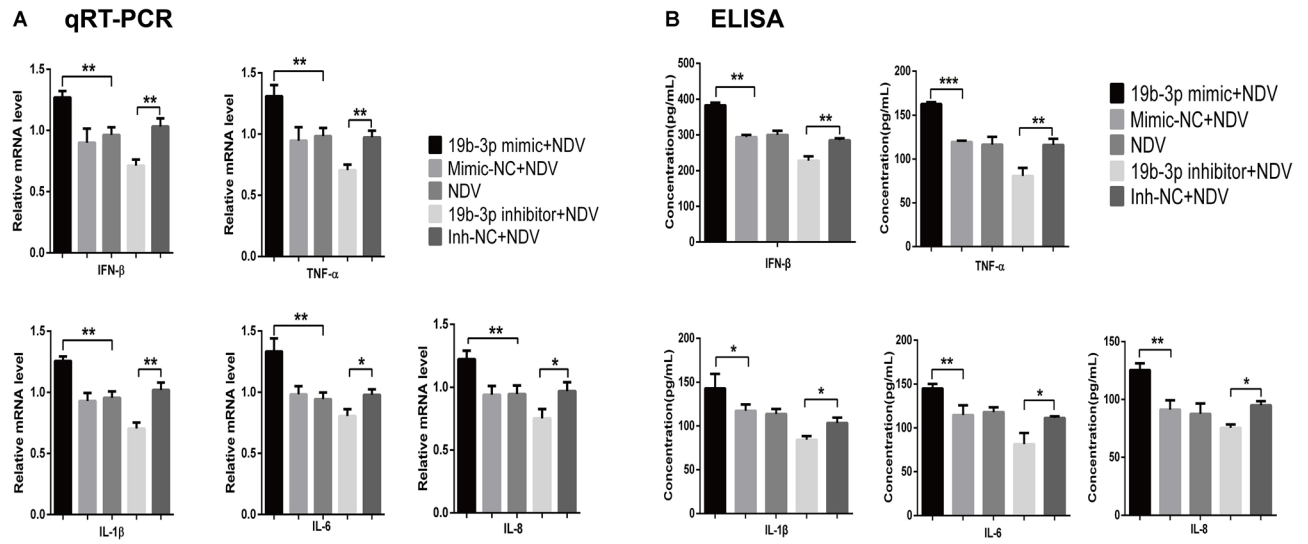

FIGURE 2 | Gga-miR-19b-3p promotes NDV-induced expression of inflammatory cytokines. DF-1 cells were transfected with indicated RNA oligonucleotides at a final concentration of 100 nM for 18 h or left untreated before infected with JS 5/05 at an MOI of 0.1. The expression levels of IFN-β, TNF-α, IL-1β, IL-6, and IL-8 were measured by qRT-PCR **(A)** and ELISA **(B)** at 18 hpi. Results are representative of three independent experiments and presented as means ± SD. $^{*}p < 0.05$, $^{**}p < 0.01$, $^{***}p < 0.001$.

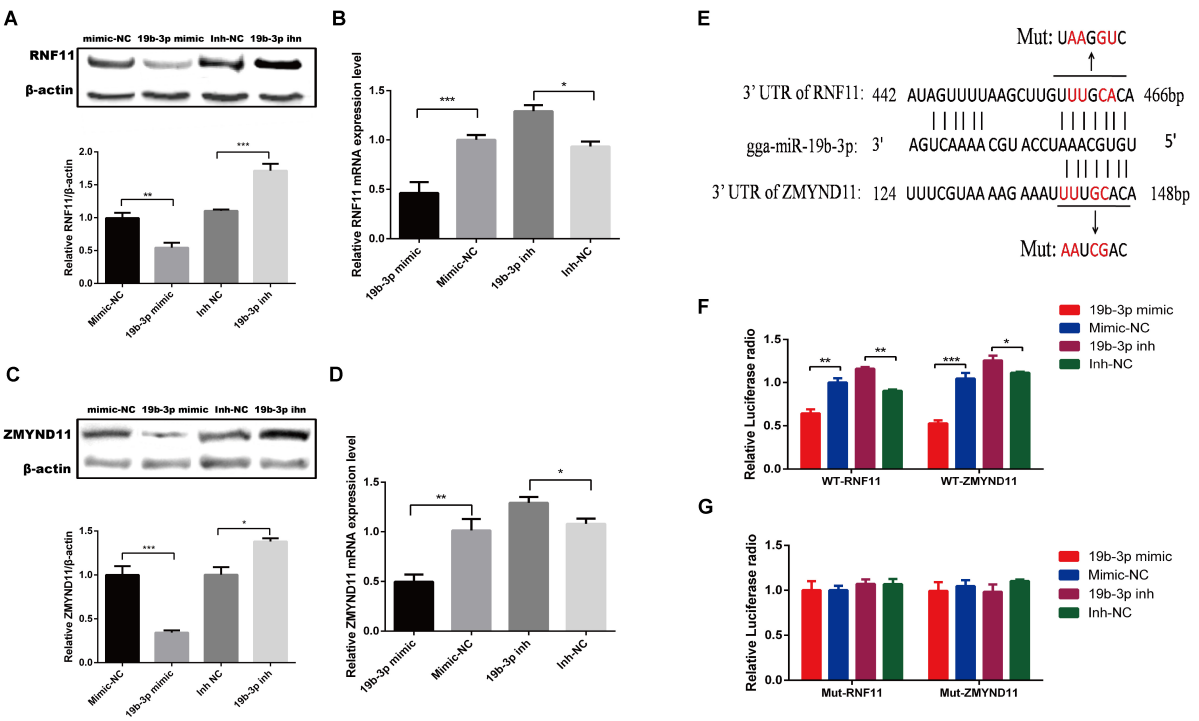

FIGURE 3 | Gga-miR-19b-3p directly targets RNF11 and ZMYND11 in DF-1 cells. DF-1 cells were transfected with indicated RNA oligonucleotides at a final concentration of 100 nM for 18 h. Then the expression of RNF11 and ZMYND11 were detected by Western blot **(A,C)** and qRT-PCR **(B,D)** assays. The relative levels of RNF11 and ZMYND11 proteins were calculated as follows: band density of RNF11 or ZMYND11/band density of β-actin in the same sample and showed in the below of **(A,C)**. Diagram of the predicted target sites for gga-miR-19b-3p in RNF11 and ZMYND11 were shown in **(E)**. DF-1 cells were co-transfected with indicated RNA oligonucleotides and wild type **(F)** or mutant luciferase reporter gene vectors **(G)** before luciferase reporter gene assay was performed. The relative level of renilla luciferase activities was calculated normalized on the basis of firefly luciferase activities. Data are representative of three independent experiments and presented as means ± SD. $^{*}p < 0.05$, $^{**}p < 0.01$, $^{***}p < 0.001$.

mimic or its inhibitor, followed by infection with NDV (JS 5/05 strain, 0.1 MOI). As shown in **Figure 1C**, gga-miR-19b-3p mimic increased gga-miR-19b-3p expression about 1000-fold in DF-1 cells, whereas gga-miR-19b-3p antagonist decreased its expression by >70%. Overexpression of gga-miR-19b-3p mimic significantly suppressed NDV replication, whereas gga-miR-19b-3p inhibitor increased NDV replication (**Figure 1D**).

Gga-miR-19b-3p Positively Regulates NDV-Induced Expression of Inflammatory Cytokines

We next determined if gga-miR-19b-3p affected virus replication by regulating the inflammatory cytokine production. As shown in **Figures 2A,B**, gga-miR-19b-3p mimic significantly increased both mRNA and protein levels of IFN-β, TNF-α, IL-1β, IL-6, and IL-8 in NDV-infected DF-1 cells. In contrast, gga-miR-19b-3p inhibitor significantly decreased the levels of IFN-β, TNF-α, IL-1β, IL-6, and IL-8 mRNA and protein.

Gga-miR-19b-3p Directly Targets RNF11 and ZMYND11 in DF-1 Cells

We then investigated the targets of gga-miR-19b-3p that might be involved in regulating NDV-induced inflammatory cytokine production. A total of 571 and 547 targets were predicted by TargetScan and miRDB, respectively. Two hundred and twenty-one common target genes were used to do GO analysis on the DAVID platform. After enrichment by GO analysis, we found that two potential target genes RNF11 and ZMYND11were

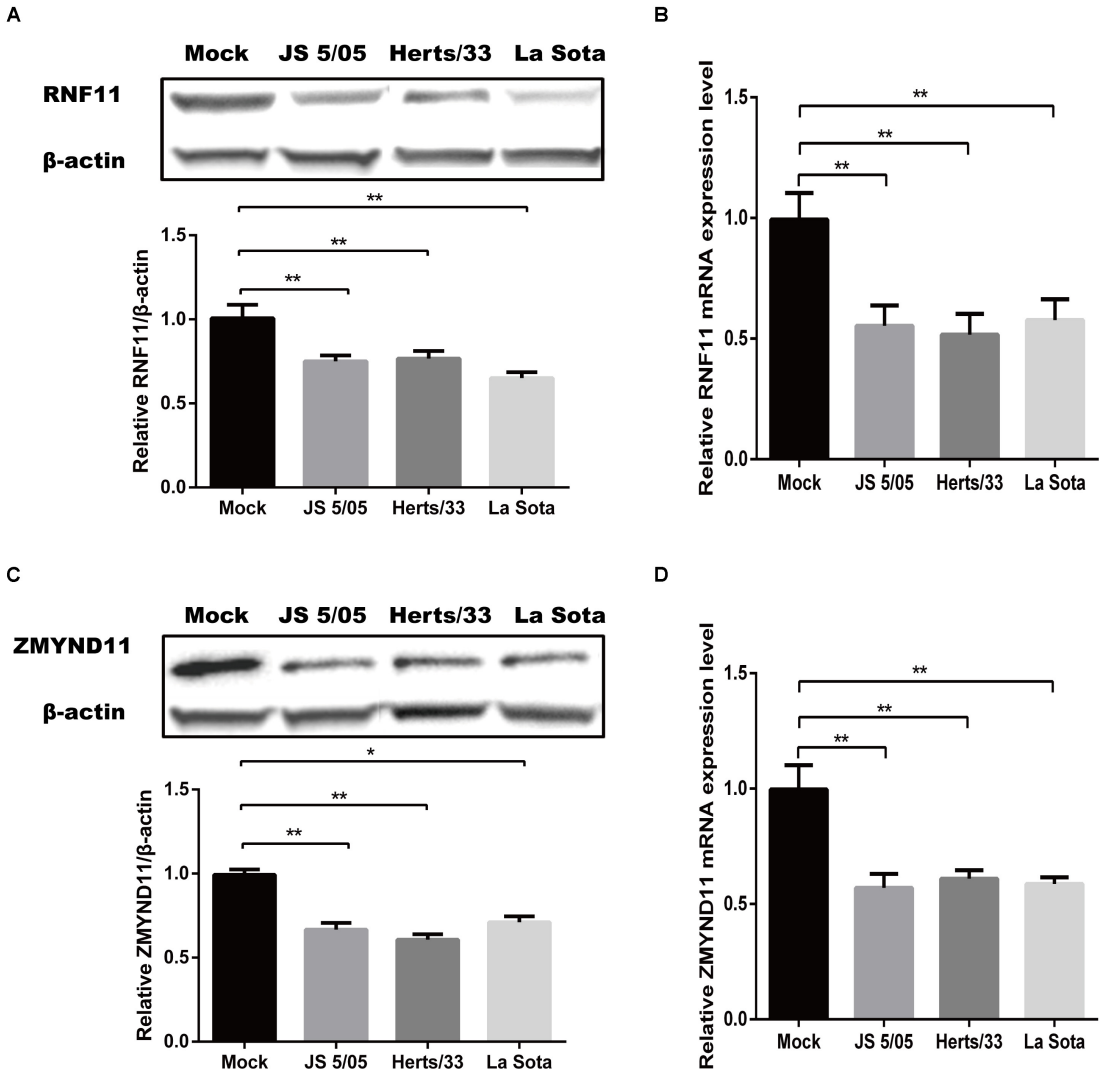

FIGURE 4 | Newcastle disease virus infection inhibits the expressions of RNF11 and ZMYND11. DF-1 cells were infected with different NDV strains (JS 5/05, Herts/33, and La Sota) at an MOI of 0.1 for 18 h. The expressions of RNF11 and ZMYND11 were detected by Western blot **(A,C)** and qRT-PCR **(B,D)** assays. The relative levels of RNF11 and ZMYND11 proteins were calculated as described above and showed in the below of **(A,C)**. Data are representative of three independent experiments and presented as means ± SD. $*p < 0.05$, $**p < 0.01$.

clustered on immune system process. Moreover, both of them were reported as negatively regulators of NK-κB activity. Finally, RNF11 and ZMYND11 were screened for validation given the GO analysis results and previous study.

To examine whether gga-miR-19b-3p directly targets RNF11 and ZMYND11, We first detected whether gga-miR-19b-3p regulates the RNF11 and ZMYND11 expression. qRT-PCR and Western blot revealed that transfection of DF-1 cells with gga-miR-19b-3p mimic led to decreased RNF11 (**Figures 3A,B**) and ZMYND11 (**Figures 3C,D**) expression at both protein and mRNA levels, compared to that transfected with mimic-NC or inh-NC. We then constructed luciferase reporter plasmids containing the wild-type or mutant 3′-UTR of the RNF11 and ZMYND11 genes. Predicted target sequences for gga-miR-19b-3p in the 3′-UTR of RNF11 and ZMYND11 are illustrated in **Figure 3E**. DF-1 cells were co-transfected with indicated RNA oligonucleotides plus wild-type or mutated-type luciferase reporter plasmids. Forty eight hours after transfection, dual-luciferase reporter assays were performed. gga-miR-19b-3p mimic significantly decreased the ratio of Renilla/Firefly in pmiR-RNF11-3′UTR-wild and pmiR-ZMYND11-3′UTR-wild transfected DF-1 cells, but not in pmiR-RNF11-3′UTR-mut and pmiR-ZMYND11-3′UTR-mut cells (**Figures 3F,G**). As expected, inhibition of gga-miR-19b-3p exhibited a significant promotion of the luciferase radio in pmiR-RNF11-3′UTR-wild and pmiR-ZMYND11-3′UTR-wild DF-1 cells, whereas no changes in pmiR-RNF11-3′UTR-mut and pmiR-ZMYND11-3′UTR-mut cells (**Figures 3F,G**). Combined with these results, we demonstrated that RNF11 and ZMYND11 are directly targeted by gga-miR-19b-3p in DF-1 cells.

NDV Infection Inhibits the Expressions of RNF11 and ZMYND11

Given that gga-miR-19b-3p directly targeted RNF11 and ZMYND11 mRNAs, we tested if NDV infection indeed affected the expression of these two proteins. qRT-PCR and Western blot revealed that the protein and mRNA levels of RNF11 (**Figures 4A,B**) and ZMYND11 (**Figures 4C,D**) were significantly down-regulated in DF-1 cells infected with three different NDV strains, including JS 5/05, Herts/33 and La Sota.

RNF11 and ZMYND11 Modulate NDV Replication via Suppressing NDV-Induced Inflammatory Cytokines

We next determined if RNF11 and ZMYND11 indeed regulated inflammatory production and virus replication. Firstly, we detected the interference and overexpression efficiency of siRNAs and overexpression plasmids by Western blot and qRT-PCR assays. As shown in **Figures 5A–D**, the levels of RNF11 or ZMYND11 were increased by 4.5 or 7-fold in DF-1 cells transfected with pCMV-RNF11 and pCMV-ZMYND11, respectively. siRNA-RNF11-2 (hereafter called siRNA-RNF11) and siRNA-ZMYND11-3 (hereafter called siRNA-ZMYND11) down-regulated the expression of ZMYND and RNF11 by about 70%. RNF11 or ZMYND11 knockdown in DF-1 cells markedly enhanced the expressions of NDV-induced inflammatory cytokines and suppressed NDV replication, whereas RNF11 or ZMYND11 overexpression blocked NDV-induced inflammatory cytokine expression and promoted NDV replication (**Figures 5E–G**). Simultaneous knockdown or overexpression of these two proteins showed synergistic

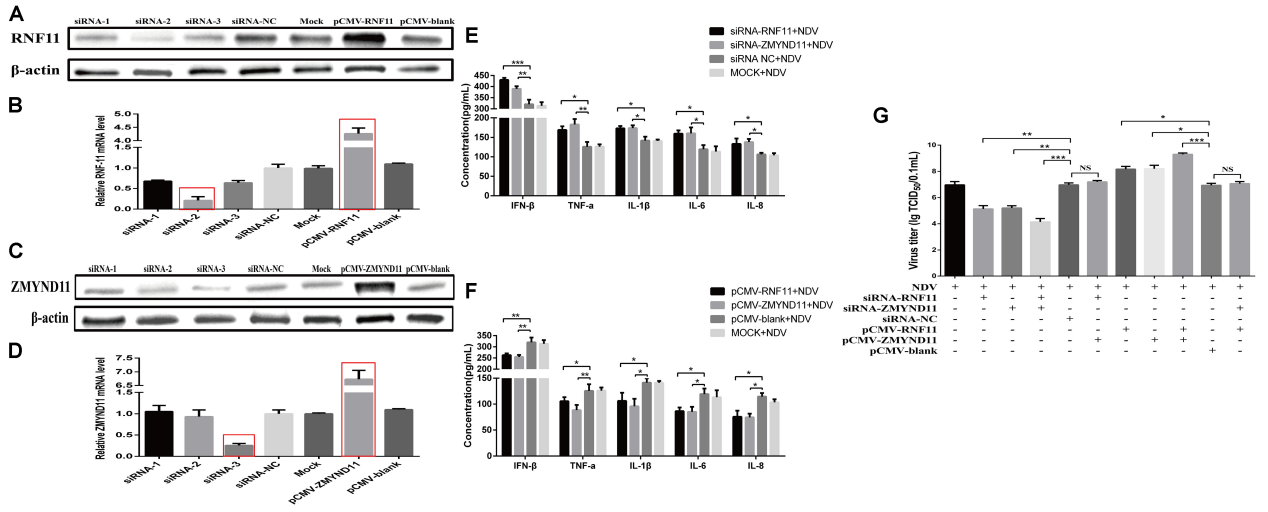

FIGURE 5 | RNF11 and ZMYND11 inhibit NDV-induced inflammatory cytokines and promote NDV replication in DF-1 cells. DF-1 cells were transfected with indicated siRNAs or siRNA-NC or overexpression plasmids or pCMV-blank. The efficiencies of interference and overexpression in transfected DF-1 cells were measured by Western blot **(A,C)** and qRT-PCR **(B,D)** at 18 h post transfection. DF-1 cells transfected with indicated siRNAs or siRNA-NC or overexpression plasmids or pCMV-blank or left untreated were infected with JS 5/05 at an MOI of 0.1 for 18 h. The expression levels of IFN-β, TNF-α, IL-1β, IL-6, and IL-8 were measured by ELISA assay **(E,F)**. DF-1 cells transfected with indicated siRNAs or siRNA-NC or overexpression plasmids or pCMV-blank were infected with JS 5/05 at an MOI of 0.1. After 36 h, viral titers in infected DF-1 cells were measured by $TCID_{50}$ as described above **(G)**. Data are representative of three independent experiments and presented as means ± SD. $^{*}p < 0.05$, $^{**}p < 0.01$, $^{***}p < 0.001$.

effects on viral replication. However, overexpression of ZMYND11 and knockdown of RNF-11, or overexpression of RNF-11 and knockdown of ZMYND11 showed no effect on viral replication.

RNF11 and ZMYND11 Suppress NF-κB Activity

Previous studies demonstrated that RNF11 and ZMYND11 negatively regulate the NF-κB signaling pathway in human cell lines (Ikeda et al., 2010; Dalal et al., 2012). In order to explore the mechanism by which RNF11 and ZMYND11 suppress NDV-induced inflammatory cytokines, we detected NF-κB activity in siRNAs or overexpression plasmids transfected DF-1 cells after NDV infection using a pNF-κB-luc plasmid which containing multiple binding motifs of NF-κB (GGGAATTTCC). We found that knockdown of RNF11 or ZMYND11 in DF-1 cells significantly increased NF-κB activity, while overexpression of them had completely opposite effects (**Figure 6A**). For further understand the underlying mechanism of the suppression effect on NF-κB activity by RNF11 and ZMYND11, we then detected the changes of p-IκB-α, IκB-α, and p65 nuclear translocation in siRNAs or overexpression plasmids transfected DF-1 cells after NDV infection. As shown in **Figures 6B,C**, knockdown of RNF11 or ZMYND11 in DF-1 cells significantly promoted p-IκB-α expression and inhibited IκB-α expression, while overexpression of them had completely opposite effects. Similarly, simultaneous knockdown or overexpression of these two proteins also showed synergistic effects on NF-κB activity, p-IκB-α and IκB-α expression. However, overexpression of ZMYND11 and knockdown of RNF-11, or overexpression of RNF-11 and knockdown of ZMYND11 showed no effect. In expectation, transfection of siRNA-RNF11 or siRNA-ZMYND11 increased the translocation of p65, an active subunit of NF-κB with transcriptional activity (Vermeulen et al., 2002),

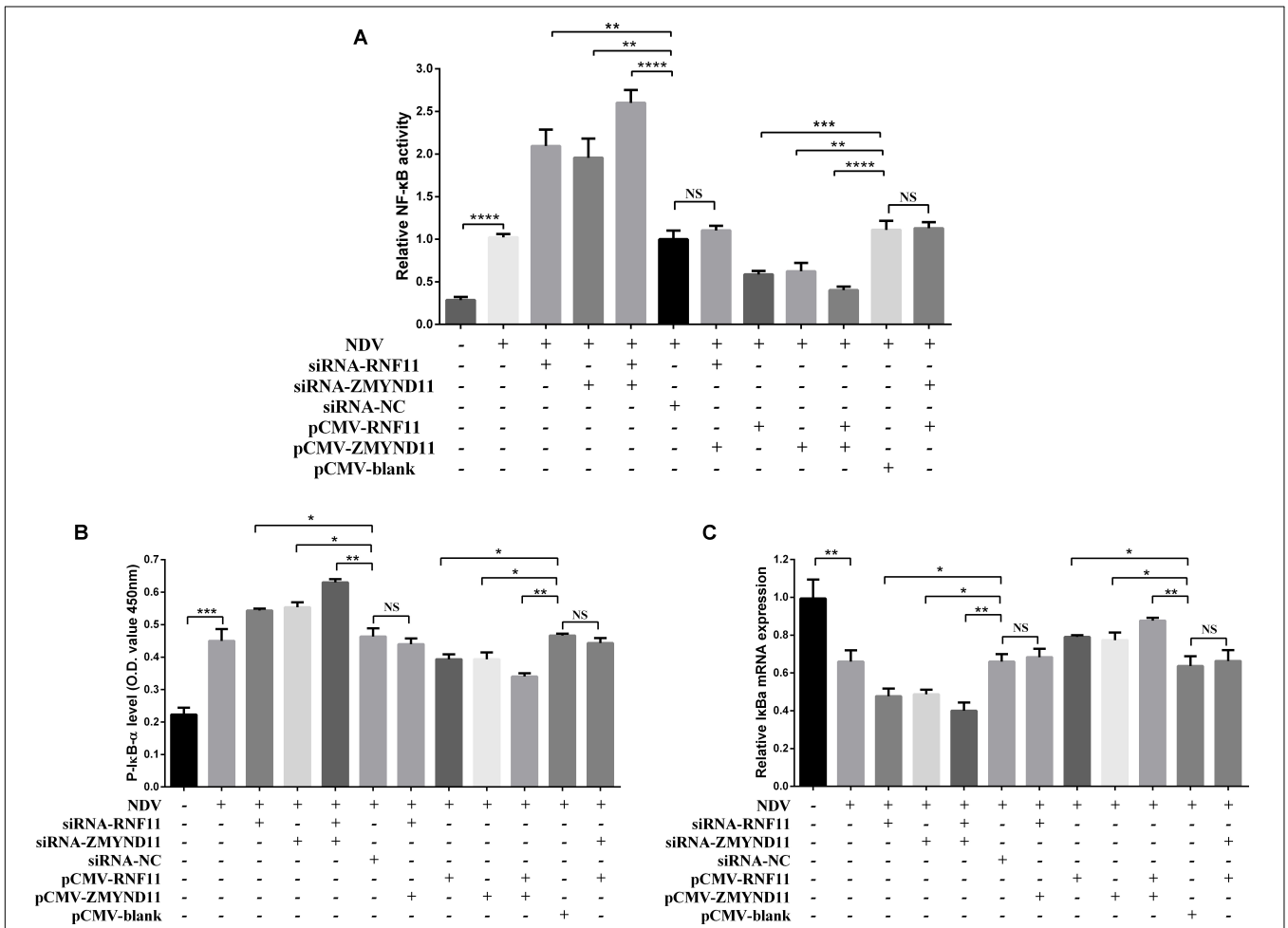

FIGURE 6 | RNF11 and ZMYND11 suppress NF-κB activity. pNF-κB-luc plasmid and indicated siRNAs or siRNA-NC or overexpression plasmids or pCMV-blank were co-transfected into DF-1 cells together with the internal control plasmid pRL-TK. Eighteen hours after transfection, the cells were infected with JS 5/05 strain at an MOI of 0.1 or left uninfected, dual-luciferase **(A)**, ELISA **(B)**, and qRT-PCR **(C)** assays were performed as described above at 18 hpi. NF-κB activities were indicated by the ratio of firefly luciferase activities to renilla luciferase activities. The relative expression of IκB-α was normalized with GAPDH and calculated using the $2^{-\Delta\Delta CT}$ method. Data are representative of three independent experiments and presented as means ± SD. *$p < 0.05$, **$p < 0.01$, ***$p < 0.001$, ****$p < 0.0001$.

from the cytoplasm to the nucleus (**Figures 7A,D**). In contrast, treatment of cells with pCMV-RNF11 or pCMV-ZMYND11 significantly inhibited the nuclear translocation of p65 in NDV-infected DF-1 cells (**Figures 7A,D**). The relative p65 expression in cytoplasm or nucleus was calculated normalized on the basis of tubulin β or histone H3, respectively (**Figures 7B,C,E,F**).

DISCUSSION

miRNAs are post-transcriptional regulators that mediate translational repression and/or mRNA degradation by complementary binding to the 3′ UTRs in target mRNAs. Mounting evidence suggest that cellular miRNAs can coordinate host defense against viral infections by direct binding to virus genome or through virus-mediated changes in the host transcriptome (Trobaugh and Klimstra, 2017). For some paramyxoviruses, such as respiratory syncytial virus (RSV) (Bakre et al., 2012; Thornburg et al., 2012), HeV (Stewart et al., 2013), and Nipah virus (NiV) (Foo et al., 2016), critical roles of cellular miRNAs in host defense against virus replication have already been well characterized. Even so, little is known about miRNAs roles in NDV replication until now.

Our previous deep sequencing results showed that the expression of gga-miR-19b-3p is significantly increased in NDV-infected DF-1 cells. Further study suggests that this up-regulated miRNAs might function as an anti-viral factor and play a role in NDV-infected DF-1 cells. Our present study focuses on the mechanism by which gga-miR-19b-3p inhibits NDV replication. We found that NDV infection increased the expression and promoter activity of gga-miR-19b-3p. miR-19b-3p has been shown to play an important role in regulating the replication of other viruses. For example, up-regulated miR-19b enhances $CD8^+$ T cell function via targeting the phosphatase and tensin homolog (PTEN) and inhibits viral production of human immunodeficiency virus (HIV) in T cells (Yin et al., 2018). Our study showed that transfection of gga-miR-19b-3p mimic significantly promoted NDV-induced inflammatory cytokines and inhibited NDV replication in DF-1 cells, suggesting that gga-miR-19b-3p might play an anti-viral role during NDV infection.

Like other paramyxoviruses, NDV infection can be sensed by host innate immune system via PRRs in the cytosol. Activated PRRs lead to activation of the innate immune response and the production of inflammatory cytokines that establishes an antiviral state (Schoggins and Rice, 2011). NF-κB plays a crucial role in the production of inflammatory cytokines (i.e., TNF-α, IL-6), apoptotic factors, and oxidative stress (Deng et al., 2018). A growing body of research suggests that miRNAs can regulate viral replication via influencing NF-κB activity. For example, has-miR-215 directly targets the tripartite motif 22 (TRIM22) to block the NF-κB signaling pathway, and exerts a positively regulatory role on (hepatitis C virus) HCV replication (Tian and He, 2018). Up-regulated miR-221-5p inhibits porcine epidemic diarrhea virus (PEDV) replication by targeting the 3′ UTR of the viral genome and activating the NF-κB-signaling pathway (Zheng et al., 2018). In addition, during HIV infection, the down-regulation of miR-16 results in the activation of the

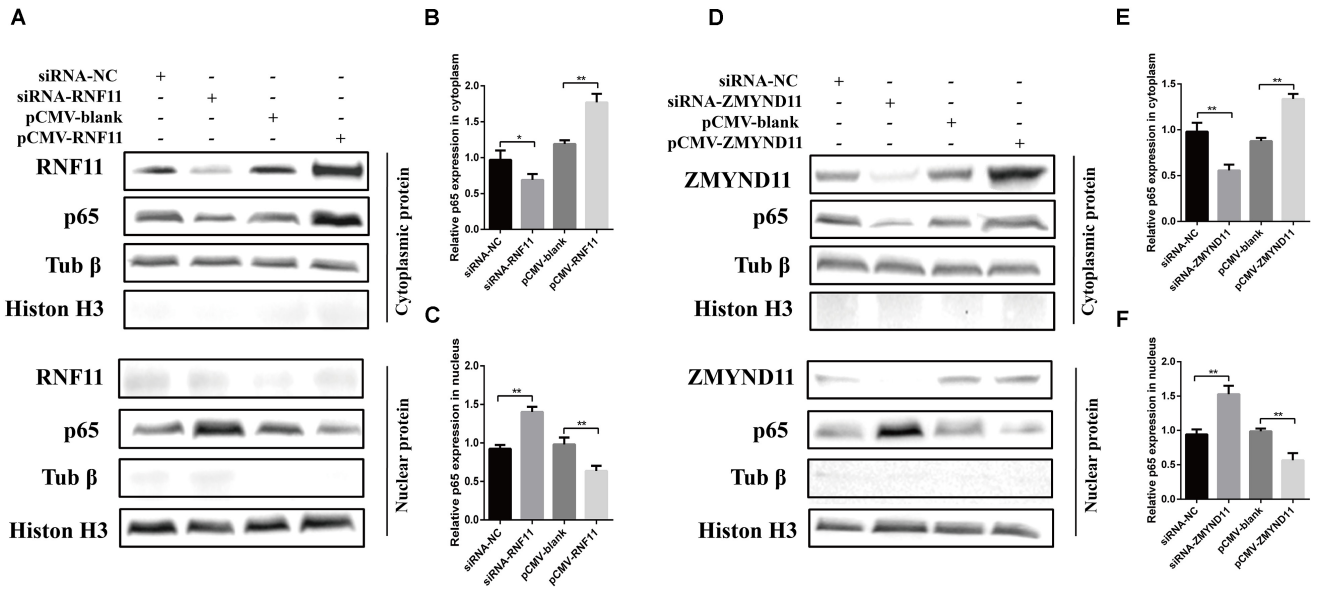

FIGURE 7 | RNF11 and ZMYND11 inhibit the nucleus translocation of p65. DF-1 cells were transfected with indicated siRNAs or siRNA-NC or overexpression plasmids or pCMV-blank for 18 h. Then JS 5/05 strain were used to infect the cells at an MOI of 0.1. Eighteen hours post infection, the cytoplasmic and nuclear proteins of the cells were prepared as described above. Western blot was used to detect the translocation of p65 from cytoplasm to the nucleus **(A,D)**. The relative p65 expression in cytoplasm **(B,E)** or nucleus **(C,F)** was analyzed by Image J software and calculated normalized on the basis of tubulin β or histone H3, respectively. Data are representative of three independent experiments and presented as means ± SD. $^*p < 0.05$, $^{**}p < 0.01$.

NF-κB signaling pathway, thus inhibiting HIV replication (Li et al., 2010).

RNF11 is an evolutionarily conserved 154 amino acid protein that acts as a negative regulator of NF-κB signaling pathway through its associations with the A20 ubiquitin-editing protein complex (Pranski et al., 2012). Earlier studies have shown that ZMYND11 or BS69, a multidomain cellular protein, can directly interact with tumor necrosis factor receptor associated factor 3 (TRAF3) to negatively regulated Epstein–Barr virus latent membrane protein 1-mediated NF-κB activation and then enhanced IL-6 expression (Ikeda et al., 2010). Moreover, recent studies demonstrated that ZMYND11 could negatively regulate the NF-κB signaling pathway in mycoplasma gallisepticum-infected chicken embryos and DF-1 cells (Hu et al., 2016). In our present study, we found that RNF11 and ZMYND11were directly targets of gga-miR-19b-3p in DF-1 cells. Since gga-miR-19b-3p enhanced NDV-induced inflammatory response, it was imperative to evaluate effect of RNF11 and ZMYND11 on inflammatory cytokines production in NDV-infected DF-1 cells. We found that knockdown of RNF11 and ZMYND11 increased NDV-induced inflammatory cytokines and inhibited NDV replication, similar to the effect of gga-miR-19b-3p. However, overexpression of RNF11 and ZMYND11 showed an opposite effect. These results suggested that gga-miR-19b-3p enhances NDV-induced inflammatory response via targeting RNF11 and ZMYND11. Moreover, different virulence NDV strains infection resulted in a similar suppression of these two proteins expression, indicated that a virulence-independent regulation of RNF11 and ZMYND11 during NDV infection *in vitro*.

Further research of mechanism by which RNF11 and ZMYND11 influence NDV-induced inflammatory response, we found that silencing of these two proteins by siRNAs promotes NDV-induced NF-κB activity indicated that these two proteins negatively regulate NF-κB signaling pathway in avian cells. It has been well established that phosphorylation and subsequent proteasomal degradation of IκB-α and translocation of NF-κB from the cytoplasm to the nucleus are key determinants of NF-κB activation (Woronicz et al., 1997; Zhu et al., 2015). Therefore, we also determined the effect of RNF11 and ZMYND11 on the expression of p-IκB-α and IκB-α and nucleus translocation of NF-κB after NDV infection in DF-1 cells. We found that treatment of DF-1 cells with siRNA-RNF11 and siRNA-ZMYND11 enhanced the expression of p-IκB-α and nucleus translocation of p65 and inhibited IκB-α expression, whereas its overexpression prevented the expression of p-IκB-α and p65 nuclear translocation and increased IκB-α expression. All these results strongly indicate that RNF11 and ZMYND11can negatively regulate NF-κB activity in DF-1 cells after NDV infection and their down-regulation after NDV infection may be responsible for gga-miR-19b-3p stimulative role on NDV-induced inflammatory cytokines expression. However, the molecular mechanism by which RNF11 and ZMYND11 negatively regulate NF-κB activity in DF-1 cells remains to be further investigated.

To further elucidate the association of the regulated roles of RNF11 and ZMYND11, we knocked down or overexpressed of both proteins concurrently or knocked down one of them while overexpressed the other one before NDV infection. We found that simultaneous knockdown or overexpression of both proteins showed synergistic effects on viral replication and NF-κB activity. However, overexpression of ZMYND11 and knockdown of RNF-11, or overexpression of RNF-11 and knockdown of ZMYND11 showed no effect on viral replication and NF-κB activity. However, we believe that these results do not indicate that RNF11 and ZMYND11 have similar abilities in regulating NDV replication and NF-κB activity. Since the interference efficiency of both genes is approximately 30%, while the overexpression efficiency of both genes is approximately five to sevenfold. Moreover, the expression levels of endogenous RNF11 and ZMYND11 are also different in DF-1 cells. Therefore, further precise experiments are needed to confirm which protein plays more critical role on NDV replication.

In summary, our results indicate that NDV-induced gga-miR-19b-3p inhibits the expressions of RNF11 and ZMYND11 by directly binding them, thereby enhancing NF-κB activity and increasing inflammatory cytokines production, which finally leads to the inhibition of NDV replication in DF-1 cells. However, the study of gga-miR-19b-3p *in vivo* is more complicated than that in DF-1 cells, further studies are needed to elucidate the role of gga-miR-19b-3p in host response to NDV infection.

DATA AVAILABILITY

All datasets generated for this study are included in the manuscript and/or the supplementary files.

AUTHOR CONTRIBUTIONS

YC was responsible for experiment design, data analysis, and writing the manuscript. WL, HX, YD, HC, TZ, XLL, TL, LG, SZ, and YP were responsible for performing the experiments. JL, JH, XW, MG, and XWL were responsible for suggestion during the experiments performance. ZH, SH, and XFL were responsible for revising the manuscript. All authors read and approved the final manuscript.

FUNDING

This work was supported by grants from the National Key Research and Development Program of China (2017YFD0500101), the National Key Technology R&D Program of China (2015BAD12B03). The Earmarked Fund For China Agriculture Research System (CARS-40), the National Key Research and Development Program of China (2017YFD500101 and 2017YFD0500702), and a project funded by the Priority Academic Program Development of Jiangsu Higher Education Institutions.

REFERENCES

Ashraf, U., Zhu, B., Ye, J., Wan, S., Nie, Y., Chen, Z., et al. (2016). MicroRNA-19b-3p modulates japanese encephalitis virus-mediated inflammation via targeting RNF11. *J. Virol.* 90, 4780–4795. doi: 10.1128/jvi.02586-15

Bakre, A., Mitchell, P., Coleman, J. K., Jones, L. P., Saavedra, G., Teng, M., et al. (2012). Respiratory syncytial virus modifies microRNAs regulating host genes that affect virus replication. *J. Gen. Virol.* 93(Pt 11), 2346–2356. doi: 10.1099/vir.0.044255-0

Bartel, D. P. (2004). MicroRNAs: genomics, biogenesis, mechanism, and function. *Cell* 116, 281–297.

Cheng, J., Sun, Y., Zhang, X., Zhang, F., Zhang, S., Yu, S., et al. (2014). Toll-like receptor 3 inhibits newcastle disease virus replication through activation of pro-inflammatory cytokines and the type-1 interferon pathway. *Arch. Virol.* 159, 2937–2948. doi: 10.1007/s00705-014-2148-6

Cheng, X., Wang, W., Xu, Q., Harper, J., Carroll, D., Galinski, M. S., et al. (2016). Genetic modification of oncolytic newcastle disease virus for cancer therapy. *J. Virol.* 90, 5343–5352. doi: 10.1128/jvi.00136-16

Dalal, N. V., Pranski, E. L., Tansey, M. G., Lah, J. J., Levey, A. I., and Betarbet, R. S. (2012). RNF11 modulates microglia activation through NF-kappaB signalling cascade. *Neurosci. Lett.* 528, 174–179. doi: 10.1016/j.neulet.2012.08.060

Deng, L., Zeng, Q., Wang, M., Cheng, A., Jia, R., Chen, S., et al. (2018). Suppression of NF-kappaB activity: a viral immune evasion mechanism. *Viruses* 10:409. doi: 10.3390/v10080409

Dimitrov, K. M., Afonso, C. L., Yu, Q., and Miller, P. J. (2017). Newcastle disease vaccines-A solved problem or a continuous challenge? *Vet. Microbiol.* 206, 126–136. doi: 10.1016/j.vetmic.2016.12.019

Dimitrov, K. M., Ramey, A. M., Qiu, X., Bahl, J., and Afonso, C. L. (2016). Temporal, geographic, and host distribution of avian paramyxovirus 1 (Newcastle disease virus). *Infect. Genet. Evol.* 39, 22–34. doi: 10.1016/j.meegid.2016.01.008

Foo, C. H., Rootes, C. L., Cowley, K., Marsh, G. A., Gould, C. M., Deffrasnes, C., et al. (2016). Dual microRNA Screens reveal that the immune-responsive miR-181 Promotes henipavirus entry and cell-cell fusion. *PLoS Pathog.* 12:e1005974. doi: 10.1371/journal.ppat.1005974

Ganar, K., Das, M., Sinha, S., and Kumar, S. (2014). Newcastle disease virus: current status and our understanding. *Virus Res.* 184, 71–81. doi: 10.1016/j.virusres.2014.02.016

Hu, Q., Zhao, Y., Wang, Z., Hou, Y., Bi, D., Sun, J., et al. (2016). Chicken gga-miR-19a targets ZMYND11 and plays an important role in host defense against *Mycoplasma gallisepticum* (HS Strain) infection. *Front. Cell Infect. Microbiol.* 6:102. doi: 10.3389/fcimb.2016.00102

Hu, Z., Hu, S., Meng, C., Wang, X., Zhu, J., and Liu, X. (2011). Generation of a genotype VII Newcastle disease virus vaccine candidate with high yield in embryonated chicken eggs. *Avian. Dis.* 55, 391–397. doi: 10.1637/9633-122410-Reg.1

Ikeda, O., Miyasaka, Y., Yoshida, R., Mizushima, A., Oritani, K., Sekine, Y., et al. (2010). BS69 cooperates with TRAF3 in the regulation of Epstein-Barr virus-derived LMP1/CTAR1-induced NF-kappaB activation. *FEBS Lett.* 584, 865–872. doi: 10.1016/j.febslet.2010.01.060

Ikeda, O., Sekine, Y., Mizushima, A., Oritani, K., Yasui, T., Fujimuro, M., et al. (2009). BS69 negatively regulates the canonical NF-kappaB activation induced by Epstein-Barr virus-derived LMP1. *FEBS Lett.* 583, 1567–1574. doi: 10.1016/j.febslet.2009.04.022

Ingle, H., Kumar, S., Raut, A. A., Mishra, A., Kulkarni, D. D., Kameyama, T., et al. (2015). The microRNA miR-485 targets host and influenza virus transcripts to regulate antiviral immunity and restrict viral replication. *Sci. Signal.* 8:ra126. doi: 10.1126/scisignal.aab3183

Jia, Y. Q., Wang, X. L., Wang, X. W., Yan, C. Q., Lv, C. J., Li, X. Q., et al. (2018). Common microRNA(-)mRNA interactions in different newcastle disease virus-infected chicken embryonic visceral tissues. *Int. J. Mol. Sci.* 19:E1291. doi: 10.3390/ijms19051291

Kato, H., Takeuchi, O., and Akira, S. (2006). [Cell type specific involvement of RIG-I in antiviral responses]. *Nihon Rinsho* 64, 1244–1247.

Li, T., Morgan, M. J., Choksi, S., Zhang, Y., Kim, Y. S., and Liu, Z. G. (2010). MicroRNAs modulate the noncanonical transcription factor NF-kappaB pathway by regulating expression of the kinase IKKalpha during macrophage differentiation. *Nat. Immunol.* 11, 799–805. doi: 10.1038/ni.1918

Liao, Y., Gu, F., Mao, X., Niu, Q., Wang, H., Sun, Y., et al. (2016). Regulation of de novo translation of host cells by manipulation of PERK/PKR and GADD34-PP1 activity during Newcastle disease virus infection. *J. Gen. Virol.* 97, 867–879. doi: 10.1099/jgv.0.000426

Miller, P. J., Afonso, C. L., El Attrache, J., Dorsey, K. M., Courtney, S. C., Guo, Z., et al. (2013). Effects of Newcastle disease virus vaccine antibodies on the shedding and transmission of challenge viruses. *Dev. Comp. Immunol.* 41, 505–513. doi: 10.1016/j.dci.2013.06.007

Miller, P. J., Estevez, C., Yu, Q., Suarez, D. L., and King, D. J. (2009). Comparison of viral shedding following vaccination with inactivated and live Newcastle disease vaccines formulated with wild-type and recombinant viruses. *Avian. Dis.* 53, 39–49. doi: 10.1637/8407-071208-Reg.1

Munir, M., Abbas, M., Khan, M. T., Zohari, S., and Berg, M. (2012). Genomic and biological characterization of a velogenic Newcastle disease virus isolated from a healthy backyard poultry flock in 2010. *Virol. J.* 9:46. doi: 10.1186/1743-422x-9-46

Pranski, E. L., Dalal, N. V., Herskowitz, J. H., Orr, A. L., Roesch, L. A., Fritz, J. J., et al. (2012). Neuronal RING finger protein 11 (RNF11) regulates canonical NF-kappaB signaling. *J. Neuroinflamm.* 9:67. doi: 10.1186/1742-2094-9-67

Qin, Z. M., Tan, L. T., Xu, H. Y., Ma, B. C., Wang, Y. L., Yuan, X. Y., et al. (2008). Pathotypical characterization and molecular epidemiology of Newcastle disease virus isolates from different hosts in China from 1996 to 2005. *J. Clin. Microbiol.* 46, 601–611. doi: 10.1128/jcm.01356-7

Rajmani, R. S., Gupta, S. K., Singh, P. K., Gandham, R. K., Sahoo, A. P., Chaturvedi, U., et al. (2016). HN protein of Newcastle disease virus sensitizes HeLa cells to TNF-alpha-induced apoptosis by downregulating NF-kappaB expression. *Arch. Virol.* 161, 2395–2405. doi: 10.1007/s00705-016-2923-7

Reed, L. J., and Muench, H. (1938). A simple method of estimating fifty per cent endpoints12. *Am. J. Epidemiol.* 27, 493–497. doi: 10.1093/oxfordjournals.aje.a118408

Rue, C. A., Susta, L., Cornax, I., Brown, C. C., Kapczynski, D. R., Suarez, D. L., et al. (2011). Virulent Newcastle disease virus elicits a strong innate immune response in chickens. *J. Gen. Virol.* 92, 931–939. doi: 10.1099/vir.0.025486-0

Ruland, J. (2011). Return to homeostasis: downregulation of NF-kappaB responses. *Nat. Immunol.* 12, 709–714. doi: 10.1038/ni.2055

Schoggins, J. W., and Rice, C. M. (2011). Interferon-stimulated genes and their antiviral effector functions. *Curr. Opin. Virol.* 1, 519–525. doi: 10.1016/j.coviro.2011.10.008

Shembade, N., Parvatiyar, K., Harhaj, N. S., and Harhaj, E. W. (2009). The ubiquitin-editing enzyme A20 requires RNF11 to downregulate NF-kappaB signalling. *EMBO J.* 28, 513–522. doi: 10.1038/emboj.2008.285

Stewart, C. R., Marsh, G. A., Jenkins, K. A., Gantier, M. P., Tizard, M. L., Middleton, D., et al. (2013). Promotion of Hendra virus replication by microRNA 146a. *J. Virol.* 87, 3782–3791. doi: 10.1128/jvi.01342-12

Sun, Y., Ding, N., Ding, S. S., Yu, S., Meng, C., Chen, H., et al. (2013). Goose RIG-I functions in innate immunity against Newcastle disease virus infections. *Mol. Immunol.* 53, 321–327. doi: 10.1016/j.molimm.2012.08.022

Thornburg, N. J., Hayward, S. L., and Crowe, J. E. Jr. (2012). Respiratory syncytial virus regulates human microRNAs by using mechanisms involving beta interferon and NF-kappaB. *mBio* 3:e00220-12. doi: 10.1128/mBio.00220-12

Tian, H., and He, Z. (2018). miR-215 enhances HCV replication by targeting TRIM22 and inactivating NF-kappaB signaling. *Yonsei Med. J.* 59, 511–518. doi: 10.3349/ymj.2018.59.4.511

Trobaugh, D. W., and Klimstra, W. B. (2017). MicroRNA regulation of RNA virus replication and pathogenesis. *Trends Mol. Med.* 23, 80–93. doi: 10.1016/j.molmed.2016.11.003

Vermeulen, L., De Wilde, G., Notebaert, S., Vanden Berghe, W., and Haegeman, G. (2002). Regulation of the transcriptional activity of the nuclear factor-kappaB p65 subunit. *Biochem. Pharmacol.* 64, 963–970. doi: 10.1016/s0006-2952(02)01161-9

Wang, X., Jia, Y., Wang, X., Wang, C., Lv, C., Li, X., et al. (2019). MiR-375 has contrasting effects on Newcastle disease virus growth depending on the target gene. *Int. J. Biol. Sci.* 15, 44–57. doi: 10.7150/ijbs.25106

Wang, Z., Ning, Z., Sun, M., Gao, S., Kang, Y., Xie, P., et al. (2014). Interferon regulatory factor 7- (IRF7-) mediated immune response affects Newcastle disease virus replication in chicken embryo fibroblasts. *Acta Vet. Hung.* 62, 500–511. doi: 10.1556/AVet.2014.023

Woronicz, J. D., Gao, X., Cao, Z., Rothe, M., and Goeddel, D. V. (1997). IkappaB kinase-beta: NF-kappaB activation and complex formation with IkappaB kinase-alpha and NIK. *Science* 278, 866–869. doi: 10.1126/science.278.5339.866

Wu, S., Wang, W., Yao, C., Wang, X., Hu, S., Cao, J., et al. (2011). Genetic diversity of Newcastle disease viruses isolated from domestic poultry species in Eastern China during 2005-2008. *Arch. Virol.* 156, 253–261. doi: 10.1007/s00705-010-0851-5

Yin, L. B., Song, C. B., Zheng, J. F., Fu, Y. J., Qian, S., Jiang, Y. J., et al. (2018). Elevated expression of miR-19b enhances CD8(+) T Cell function by targeting PTEN in HIV infected long term non-progressors with sustained viral suppression. *Front. Immunol.* 9:3140. doi: 10.3389/fimmu.2018.03140

Zheng, H., Xu, L., Liu, Y., Li, C., Zhang, L., Wang, T., et al. (2018). MicroRNA-221-5p inhibits porcine epidemic diarrhea virus replication by targeting genomic viral RNA and activating the NF-kappaB pathway. *Int. J. Mol. Sci.* 19:E3381. doi: 10.3390/ijms19113381

Zhu, B., Ye, J., Nie, Y., Ashraf, U., Zohaib, A., Duan, X., et al. (2015). MicroRNA-15b modulates Japanese encephalitis virus-mediated inflammation via targeting RNF125. *J. Immunol.* 195, 2251–2262. doi: 10.4049/jimmunol.1500370

Conflict of Interest Statement: The authors declare that the research was conducted in the absence of any commercial or financial relationships that could be construed as a potential conflict of interest.

Copyright © 2019 Chen, Liu, Xu, Liu, Deng, Cheng, Zhan, Lu, Liao, Guo, Zhu, Pei, Hu, Hu, Liu, Wang, Gu, Hu and Liu. This is an open-access article distributed under the terms of the Creative Commons Attribution License (CC BY). The use, distribution or reproduction in other forums is permitted, provided the original author(s) and the copyright owner(s) are credited and that the original publication in this journal is cited, in accordance with accepted academic practice. No use, distribution or reproduction is permitted which does not comply with these terms.

frontiers in Microbiology

OPINION
published: 28 August 2019
doi: 10.3389/fmicb.2019.01982

Origin of Canine Distemper Virus: Consolidating Evidence to Understand Potential Zoonoses

Carolina Quintero-Gil[1], *Santiago Rendon-Marin*[1], *Marlen Martinez-Gutierrez*[1,2] *and Julian Ruiz-Saenz*[1,3*†]

[1] Grupo de Investigación en Ciencias Animales–GRICA, Universidad Cooperativa de Colombia, Bucaramanga, Colombia, [2] Infettare, Facultad de Medicina, Universidad Cooperativa de Colombia, Medellín, Colombia, [3] Asociación Colombiana de Virología, Bogotá, Colombia

Keywords: distemper, evolution, morbillivirus, measles, zoonotic disease

OPEN ACCESS

Edited by:
Ahmed Sayed Abdel-Moneim, Taif University, Saudi Arabia

Reviewed by:
Sara Louise Cosby, Agri-Food and Biosciences Institute (AFBI), United Kingdom
Edward J. Dubovi, Cornell University, United States

****Correspondence:***
Julian Ruiz-Saenz
julianruizsaenz@gmail.com;
julian.ruizs@campusucc.edu.co

†ORCID:
Julian Ruiz-Saenz
orcid.org/0000-0002-1447-1458

Specialty section:
This article was submitted to Virology, a section of the journal Frontiers in Microbiology

Received: *15 May 2019*
Accepted: *12 August 2019*
Published: *28 August 2019*

Citation:
Quintero-Gil C, Rendon-Marin S, Martinez-Gutierrez M and Ruiz-Saenz J (2019) Origin of Canine Distemper Virus: Consolidating Evidence to Understand Potential Zoonoses. Front. Microbiol. 10:1982. doi: 10.3389/fmicb.2019.01982

Morbilliviruses are highly contagious pathogens and are responsible for various outbreaks in unexposed populations (Pfeffermann et al., 2018). They belong to the order Mononegavirales and family *Paramyxoviridae* and are characterized by a non-segmented, linear, negative-stranded RNA genome (Lamb and Parks, 2013). Morbilliviruses are distinguished for causing moderate-to-severe respiratory, gastrointestinal, immunosuppression, and/or neurological diseases in a wide range of hosts, including humans (measles virus), carnivores (canine morbillivirus formerly canine distemper virus), cattle (rinderpest virus), dolphins and porpoises, and other wildlife-endangered species (Lamb and Parks, 2013; Martinez-Gutierrez and Ruiz-Saenz, 2016).

Measles virus (MeV) and canine morbillivirus (CDV) are considered the most contagious viruses among this family (De Vries et al., 2015), and due to the high transmission potential of CDV as well as its cross-species transmission potential, the global health, and conservationist authorities are greatly concerned about role of CDV on endangered species conservation and the possible "jump" from animals to humans (Terio and Craft, 2013; Ohishi et al., 2014). Domestic dogs are the main host for CDV and could also be considered as a reservoir for other mammals (Suzuki et al., 2015; Duque-valencia et al., 2019); however, based on the biology of CDV, humans could also turn into a potential target (Cosby and Weir, 2018; Rendon-Marin et al., 2019).

Trying to understand the potential risk of transmission of CDV to humans, it is necessary to gather all the existing evidence; and the study of the origin and dissemination of this agent in the canine population could present an important key to understanding this process. Recently, a paper published in the *International Journal of Paleopathology* invited to a discussion on the evolutionary origin of CDV. It concludes that CDV originated as a pandemic pathogen in South America following the infection and adaptation of MeV to dogs during the South American colonization period. This result was obtained via an interdisciplinary approach adopted by synthesizing a paleopathological analysis of 96 pre-Columbian dogs (750–1470 CE) from the Weyanoke Old Town, Virginia site, with historical reports, molecular analysis, and morbilliviral epidemiology (Uhl et al., 2019).

Notably, native dog populations from America almost disappeared after the colonization period, and European and Eurasian dogs were introduced to the continent, leaving little genetic background of its American predecessors (Ni Leathlobhair et al., 2018). Another important factor worth considering is that "unknown" diseases could have also been introduced, making it harder to track the origin of new pathogens. Moreover, artificial selection pressure over domestic dogs and even human populations, particularly during the colonization period, could have enhanced disease incidence, thereby limiting genetic variation (Ostrander et al., 2017), which in turn could mean less effective response against pathogens.

Among these "new" pathogens/diseases, CDV was first described by Antonio de Ulloa y de la Torre-Giral in 1746 as a disease affecting dogs in the Quito region and the other parts of

South America, and it was reported soon afterward in Europe. CDV was recorded in Spain in 1760, with 900 deaths occurring in a single day in Madrid, and 3 years later, i.e., by 1764 and 1770, it had reached Great Britain and Italy, respectively (Blancou, 2004). Virus transmissibility and greater susceptibility of puppies compared with adult dogs were later reported by Edward Jenner in the early 1800s. He compared their transmissibility with that of MeV and discovered that survivors were protected from subsequent infection (Jenner, 1809; Nambulli et al., 2016).

Briefly, after the arrival of European pioneers in the fifteenth century, novel infectious diseases arguably became the most devastating consequence of colonization because the indigenous American populations had no prior exposure to pathogens that had become common in Europe (Walker et al., 2015). Multiple measles epidemics, therefore, devastated the indigenous American populations (Walker et al., 2015; Nambulli et al., 2016). Uhl et al. via a mixed approach of paleopathological, historical, molecular, and epidemiological evidence, reported that severe MeV epidemics in the indigenous American populations facilitated the jump of MeV to large domestic dog populations of urban environments in South America and the adaptation of the virus as endemic CDV (Uhl et al., 2019). Also, historical records could prove that few years after that adaptation to South American dogs, CDV was transported to Europe in 1760, where it initially induced widespread epidemics with high mortality before becoming endemic (Jenner, 1809).

However, molecular phylogeography related to evolutionary predictions and the time to the most recent common ancestor (tMRCA) were calculated for the CDV origin in the United States in the 1880s (95% highest posterior density, 1858–1913) (Panzera et al., 2015), which clearly contradicts the description of the virus in Europe in the eighteenth century. Sequence analyses that led to this hypothesis must be carefully examined because of the bias and the limited availability of sequences that were used in this molecular phylogeography reconstruction. Moreover, many original ancestral sequences have been lost due to the lability of the viral RNA genome of the CDV and other morbilliviruses. These factors have given rise to the questioning of the utility of current tMRCA calculations for RNA viruses (Sharp and Simmonds, 2011; Nambulli et al., 2016).

According to Uhl et al., morbillivirus could have originated from cattle around 376 BC in the "old continent" (**Figure 1**), and animal domestication may have had a significant influence on cross-species events, probably tracing a starting point in MeV emergence to approximately 900 AC (Uhl et al., 2019). Contrary to the current CDV phylogenetic reconstructions, MeV divergence is strongly supported by the relaxed clock Bayesian phylogenetic analysis. The divergence time between MeV and the rinderpest virus had been shown to have occurred in approximately the eleventh to twelfth centuries (Furuse et al., 2010). Other molecular data, such as the presence of a new morbillivirus (closely related to CDV and PDV) circulating in bats from Brazil (DrMV), allows the speculation that CDV and DrMV might share a common South American ancestor (Drexler et al., 2012), thereby indirectly supporting the idea of the early South American Origin of CDV.

Beyond the epistemological and/or scientific meaning of the geographical origin and date of CDV divergence, there are important clues that must be clarified to better understand the current impact of CDVs on interspecies transmission, animal conservation, and zoonotic potential (**Figure 1**). It

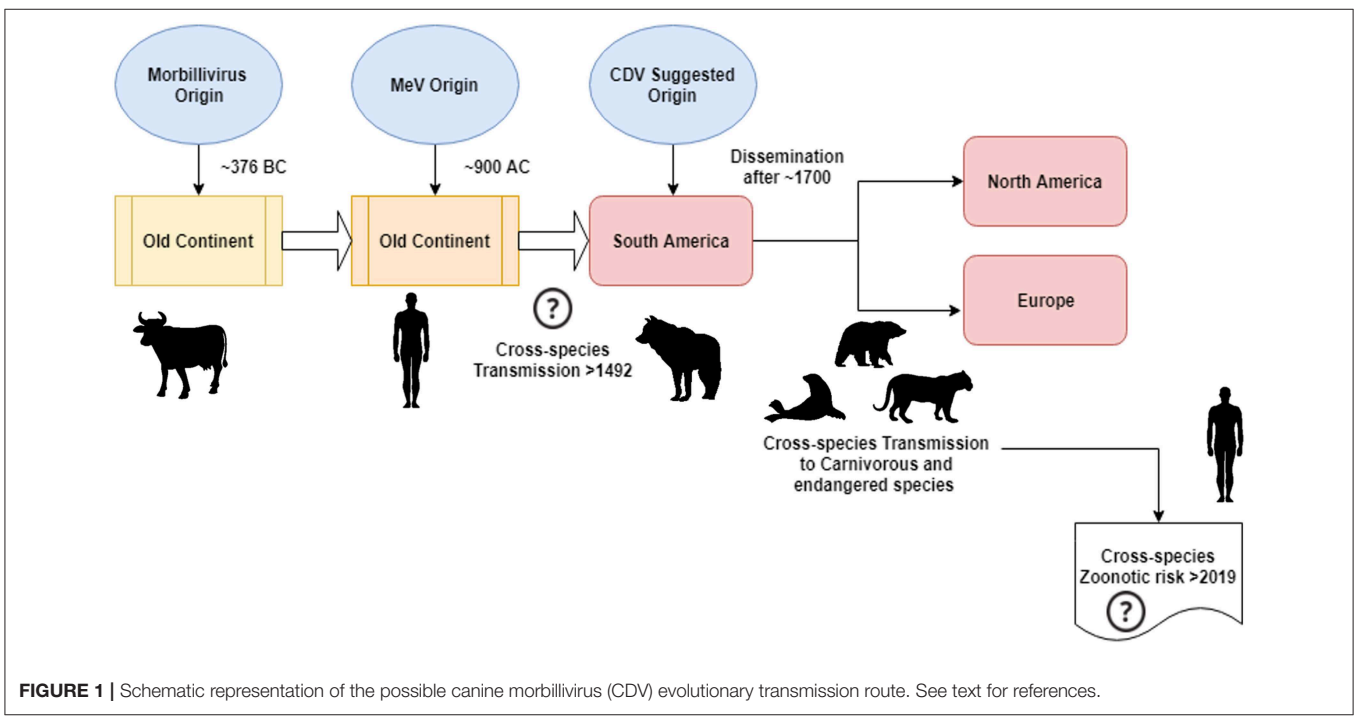

FIGURE 1 | Schematic representation of the possible canine morbillivirus (CDV) evolutionary transmission route. See text for references.

is clear that unlike the MeV infection, which is maintained by a single host (humans), CDV has been widely proved to be a promiscuous pathogen-causing infection/disease in a vast array of carnivorous and non-carnivorous species (Martinez-Gutierrez and Ruiz-Saenz, 2016). This promiscuity has been attributed to not only the capacity of the CDV hemagglutinin (H) to interact with host cellular receptors, such as SLAM in mononuclear cells and nectin-4 in epithelial cells, but also the similarity among species sequences of the receptors mentioned above (Rendon-Marin et al., 2019). The amino acid similarity among mammal SLAM receptors, including marine mammals, is >80% (Ohishi et al., 2014), thereby supporting the results of cross-species transmission. In addition, there is a lack of species-related variation in the nectin-4 sequences among humans, mice, and dogs because human nectin-4 could function as an *in vitro* receptor for CDV (Noyce et al., 2011).

Natural CDV outbreaks in different non-human primates have raised a concern regarding the possible transmission of CDV to humans (Yoshikawa et al., 1989; Sun et al., 2010; Qiu et al., 2011; Sakai et al., 2013a). There are reports that CDV monkey strains have the intrinsic ability to use human nectin-4 for virus entry and that those monkey CDVs easily adapt to use the human CD150 (SLAM) receptor following minimal amino acid changes to the viral H protein (Bieringer et al., 2013; Sakai et al., 2013b). However, based on the *in vivo* experimental CDV infection of Cynomolgus macaques (*Macaca fascicularis*) in the presence of MeV immunity, macaques were partially cross protected from the CDV challenge (De Vries et al., 2014). This suggests that although CDV can readily infect primates, MeV immunity is protective and that CDV infection could be self-limiting. Transferring this result to humans, there is a potential risk of CDV infection in people who lack cross-protective MeV immunity due to non-vaccination and vaccine failures (Haralambieva et al., 2015) or due to the absence of vaccination in the possible post-eradication era (Holzmann et al., 2016).

"Emerging viruses" could reportedly arise via the cross-species transmission of viruses from animals into humans (Wolfe et al., 2007). Novel studies, both structural and bioinformatic, suggest that just a single amino acid change in a protein sequence could be enough to overcome the restriction in using cellular receptors among two different hosts, such as humans and ruminants (Abdullah et al., 2018). A unique mutation in the CDV H protein *in vitro* enables this pathogen to infect cells expressing the human SLAM receptor (Otsuki et al., 2013). Moreover, if we embrace the hypothesis that CDV evolved from MeV, it could be possible that a CDV descendant could be able to re-infect humans because of the continuous evolution of both the virus and humans, as has been previously suggested in other models even though the ancestral "jumper virus" had disappeared from earth time ago (Emerman and Malik, 2010).

Furthermore, one of the most interesting results presented by Uhl et al. is the optimization of both the CDV and MeV genes to human codon usage bias (CUB), suggesting that CDV codon usage is closer to human CUB than canine CUB because the virus or its progenitor, most likely MeV, was initially adapted to humans (Uhl et al., 2019). CUB refers to the phenomenon wherein some synonymous codons are used more often than others and how this preference varies within and among species (Behura and Severson, 2013). In RNA viruses, codon usage is under selection because the viruses are completely dependent on host tRNAs and the bias results from viruses matching the codon usage of their hosts (Jenkins and Holmes, 2003). Evolution can sometimes favor viruses that match their host codon usage to promote the replication speed and adaptation to the host as has been reported in other RNA viruses (Goni et al., 2012; Lauring et al., 2012; Di Paola et al., 2018; Freire et al., 2018).

Finally, we would like to argue that some other factors must be considered in the possible zoonotic scenario of CDV. Cross neutralization between MeV and CDV has been recognized since many years (Brown and Mccarthy, 1974), and this premise has existed for more than half a century when the MeV vaccine was used to protect pups against CDV at an age when passive maternal immunity often interfered with CDV vaccination (Baker et al., 1966; Brown et al., 1972). Nevertheless, the use of a commercial dual CDV/MeV vaccine is still recommended for vaccination in the presence of maternal immunity, and the vaccine has been useful against clinical measles disease in non-human primates (Christe et al., 2019). Hence, one may speculate that MeV herd immunity avoids CDV jump and possible readaptation to humans via transmission through dogs or wildlife animals.

CONCLUDING REMARKS

The evolution and origin of viral pathogens cannot be easily studied; hereafter, a multidisciplinary approach is necessary to understand and perhaps predict new possible viral threats to humans. Due to their peculiar biology, viral pathogens such as CDV represent a unique model for understanding interspecies jumping and zoonotic potential of viral agents very close to the human population. Besides the traditional molecular phylogenetic studies and the paleopathology works, researchers must adopt different approaches to study CDV origin and current viral and host requirements for interspecies jumping. The introduction of computational methods, such as structural bioinformatics and paleovirology studies, could help in the prediction and prevention or at least provide a better understanding of this emerging, and perhaps, zoonotic disease from a different perspective considering not only sequencing data but also structures and functions as key information to this aim.

AUTHOR CONTRIBUTIONS

All authors listed have made a substantial, direct and intellectual contribution to the work, and approved it for publication.

FUNDING

This work was financially supported by the Departamento Administrativo de Ciencia, Tecnología e Innovación–COLCIENCIAS Grant No. 123171249669 to JR-S.

REFERENCES

Abdullah, N., Kelly, J. T., Graham, S. C., Birch, J., Goncalves-Carneiro, D., Mitchell, T., et al. (2018). Structure-guided identification of a nonhuman morbillivirus with zoonotic potential. *J. Virol.* 92:e01248-18. doi: 10.1128/JVI.01248-18

Baker, J. A., Sheffy, B. E., Robson, D. S., and Gilmartin, J. (1966). Response to measles virus by puppies with maternally transferred distemper antibodies. *Cornell Vet.* 56:588.

Behura, S. K., and Severson, D. W. (2013). Codon usage bias: causative factors, quantification methods and genome-wide patterns: with emphasis on insect genomes. *Biol. Rev.* 88, 49–61. doi: 10.1111/j.1469-185X.2012.00242.x

Bieringer, M., Han, J. W., Kendl, S., Khosravi, M., Plattet, P., and Schneider-Schaulies, J. (2013). Experimental adaptation of wild-type canine distemper virus (CDV) to the human entry receptor CD150. *PLoS ONE* 8:e57488. doi: 10.1371/journal.pone.0057488

Blancou, J. (2004). Dog distemper: imported into Europe from South America? *Hist. Med. Vet.* 29, 35—41.

Brown, A. L., and Mccarthy, R. E. (1974). Relationship between measles and canine distemper viruses determined by delayed type hypersensitivity reactions in dogs. *Nature* 248, 344–345. doi: 10.1038/248344a0

Brown, A. L., Vitamvas, J. A., Merry, D. L., and Beckenhauer, W. H. (1972). Immune response of pups to modified live-virus canine distemper-measles vaccine. *Am. J. Vet. Res.* 33, 1447–1456.

Christe, K. L., Salyards, G. W., Houghton, S. D., Ardeshir, A., and Yee, J. L. (2019). Modified dose efficacy trial of a canine distemper-measles vaccine for use in Rhesus Macaques (*Macaca mulatta*). *J. Am. Assoc. Lab. Anim. Sci.* 58, 397–405. doi: 10.30802/AALAS-JAALAS-18-000091

Cosby, S. L., and Weir, L. (2018). Measles vaccination: threat from related veterinary viruses and need for continued vaccination post measles eradication. *Hum. Vaccin. Immunother.* 14, 229–233. doi: 10.1080/21645515.2017.1403677

De Vries, R. D., Duprex, W. P., and De Swart, R. L. (2015). Morbillivirus infections: an introduction. *Viruses* 7, 699–706. doi: 10.3390/v7020699

De Vries, R. D., Ludlow, M., Verburgh, R. J., Van Amerongen, G., Yuksel, S., Nguyen, D. T., et al. (2014). Measles vaccination of nonhuman primates provides partial protection against infection with canine distemper virus. *J. Virol.* 88, 4423–4433. doi: 10.1128/JVI.03676-13

Di Paola, N., De Melo Freire, C. C., and De Andrade Zanotto, P. M. (2018). Does adaptation to vertebrate codon usage relate to flavivirus emergence potential? *PLoS ONE* 13:e0191652. doi: 10.1371/journal.pone.0191652

Drexler, J. F., Corman, V. M., Muller, M. A., Maganga, G. D., Vallo, P., Binger, T., et al. (2012). Bats host major mammalian paramyxoviruses. *Nat. Commun.* 3:796. doi: 10.1038/ncomms1796

Duque-valencia, J., Sarute, N., Olarte-Castillo, X. A., and Ruíz-Sáenz, J. (2019). Evolution and interspecies transmission of canine distemper virus-an outlook of the diverse evolutionary landscapes of a multi-host virus. *Viruses* 11:E582. doi: 10.3390/v11070582

Emerman, M., and Malik, H. S. (2010). Paleovirology–modern consequences of ancient viruses. *PLoS Biol.* 8:e1000301. doi: 10.1371/journal.pbio.1000301

Freire, C. C. M., Palmisano, G., Braconi, C. T., Cugola, F. R., Russo, F. B., Beltrão-Braga, P. C., et al. (2018). NS1 codon usage adaptation to humans in pandemic Zika virus. *Mem. Inst. Oswaldo Cruz* 113:e170385. doi: 10.1590/0074-02760170385

Furuse, Y., Suzuki, A., and Oshitani, H. (2010). Origin of measles virus: divergence from rinderpest virus between the 11th and 12th centuries. *Virol. J.* 7:52. doi: 10.1186/1743-422X-7-52

Goni, N., Iriarte, A., Comas, V., Sonora, M., Moreno, P., Moratorio, G., et al. (2012). Pandemic influenza A virus codon usage revisited: biases, adaptation and implications for vaccine strain development. *Virol. J.* 9:263. doi: 10.1186/1743-422X-9-263

Haralambieva, I. H., Kennedy, R. B., Ovsyannikova, I. G., Whitaker, J. A., and Poland, G. A. (2015). Variability in humoral immunity to measles vaccine: new developments. *Trends Mol. Med.* 21, 789–801. doi: 10.1016/j.molmed.2015.10.005

Holzmann, H., Hengel, H., Tenbusch, M., and Doerr, H. W. (2016). Eradication of measles: remaining challenges. *Med. Microbiol. Immunol.* 205, 201–208. doi: 10.1007/s00430-016-0451-4

Jenkins, G. M., and Holmes, E. C. (2003). The extent of codon usage bias in human RNA viruses and its evolutionary origin. *Virus Res.* 92, 1–7. doi: 10.1016/S0168-1702(02)00309-X

Jenner, E. (1809). Observations on the distemper in dogs. *Med. Chir. Trans.* 1, 265–270. doi: 10.1177/095952870900100119

Lamb, R. A., and Parks, G. D. (2013). "Paramyxoviridae: the viruses and their replication," in *Fields Virology: Sixth Edition,* eds B. N. Fields, D. M. Knipe, and P. M. Howley (Philadelphia, PA: Lippincott, Williams, and Wilkins), 957–995.

Lauring, A. S., Acevedo, A., Cooper, S. B., and Andino, R. (2012). Codon usage determines the mutational robustness, evolutionary capacity, and virulence of an RNA virus. *Cell Host Microbe* 12, 623–632. doi: 10.1016/j.chom.2012.10.008

Martinez-Gutierrez, M., and Ruiz-Saenz, J. (2016). Diversity of susceptible hosts in canine distemper virus infection: a systematic review and data synthesis. *BMC Vet. Res.* 12:78. doi: 10.1186/s12917-016-0702-z

Nambulli, S., Sharp, C. R., Acciardo, A. S., Drexler, J. F., and Duprex, W. P. (2016). Mapping the evolutionary trajectories of morbilliviruses: what, where and whither. *Curr. Opin. Virol.* 16, 95–105. doi: 10.1016/j.coviro.2016.01.019

Ni Leathlobhair, M., Perri, A. R., Irving-Pease, E. K., Witt, K. E., Linderholm, A., Haile, J., et al. (2018). The evolutionary history of dogs in the Americas. *Science* 361, 81–85. doi: 10.1126/science.aao4776

Noyce, R. S., Bondre, D. G., Ha, M. N., Lin, L.-T., Sisson, G., Tsao, M.-S., et al. (2011). Tumor cell marker PVRL4 (nectin 4) is an epithelial cell receptor for measles virus. *PLoS Pathog.* 7:e1002240. doi: 10.1371/journal.ppat.1002240

Ohishi, K., Suzuki, R., Maeda, T., Tsuda, M., Abe, E., Yoshida, T., et al. (2014). Recent host range expansion of canine distemper virus and variation in its receptor, the signaling lymphocyte activation molecule, in carnivores. *J. Wildl. Dis.* 50, 596–606. doi: 10.7589/2013-09-228

Ostrander, E. A., Wayne, R. K., Freedman, A. H., and Davis, B. W. (2017). Demographic history, selection and functional diversity of the canine genome. *Nat. Rev. Genet.* 18, 705–720. doi: 10.1038/nrg.2017.67

Otsuki, N., Nakatsu, Y., Kubota, T., Sekizuka, T., Seki, F., Sakai, K., et al. (2013). The V protein of canine distemper virus is required for virus replication in human epithelial cells. *PLoS ONE* 8:e82343. doi: 10.1371/journal.pone.0082343

Panzera, Y., Sarute, N., Iraola, G., Hernandez, M., and Perez, R. (2015). Molecular phylogeography of canine distemper virus: geographic origin and global spreading. *Mol. Phylogenet. Evol.* 92, 147–154. doi: 10.1016/j.ympev.2015.06.015

Pfeffermann, K., Dorr, M., Zirkel, F., and Von Messling, V. (2018). Morbillivirus pathogenesis and virus-host interactions. *Adv. Virus Res.* 100, 75–98. doi: 10.1016/bs.aivir.2017.12.003

Qiu, W., Zheng, Y., Zhang, S., Fan, Q., Liu, H., Zhang, F., et al. (2011). Canine distemper outbreak in rhesus monkeys, China. *Emerging Infect. Dis.* 17, 1541–1543. doi: 10.3201/eid1708.101153

Rendon-Marin, S., Da Fontoura Budaszewski, R., Canal, C. W., and Ruiz-Saenz, J. (2019). Tropism and molecular pathogenesis of canine distemper virus. *Virol. J.* 16:30. doi: 10.1186/s12985-019-1136-6

Sakai, K., Nagata, N., Ami, Y., Seki, F., Suzaki, Y., Iwata-Yoshikawa, N., et al. (2013a). Lethal canine distemper virus outbreak in cynomolgus monkeys in Japan in 2008. *J. Virol.* 87, 1105–1114. doi: 10.1128/JVI.02419-12

Sakai, K., Yoshikawa, T., Seki, F., Fukushi, S., Tahara, M., Nagata, N., et al. (2013b). Canine distemper virus associated with a lethal outbreak in monkeys can readily adapt to use human receptors. *J. Virol.* 87, 7170–7175. doi: 10.1128/JVI.03479-12

Sharp, P. M., and Simmonds, P. (2011). Evaluating the evidence for virus/host co-evolution. *Curr. Opin. Virol.* 1, 436–441. doi: 10.1016/j.coviro.2011.10.018

Sun, Z., Li, A., Ye, H., Shi, Y., Hu, Z., and Zeng, L. (2010). Natural infection with canine distemper virus in hand-feeding Rhesus monkeys in China. *Vet. Microbiol.* 141, 374–378. doi: 10.1016/j.vetmic.2009.09.024

Suzuki, J., Nishio, Y., Kameo, Y., Terada, Y., Kuwata, R., Shimoda, H., et al. (2015). Canine distemper virus infection among wildlife before and after the epidemic. *J. Vet. Med. Sci.* 77, 1457–1463. doi: 10.1292/jvms.15-0237

Terio, K. A., and Craft, M. E. (2013). Canine distemper virus (CDV) in another big cat: should CDV be renamed carnivore distemper virus? *MBio* 4, e00702–00713. doi: 10.1128/mBio.00702-13

Uhl, E. W., Kelderhouse, C., Buikstra, J., Blick, J. P., Bolon, B., and Hogan, R. J. (2019). New world origin of canine distemper: interdisciplinary insights. *Int. J. Paleopathol.* 24, 266–278. doi: 10.1016/j.ijpp.2018.12.007

Walker, R. S., Sattenspiel, L., and Hill, K. R. (2015). Mortality from contact-related epidemics among indigenous populations in Greater Amazonia. *Sci. Rep.* 5:14032. doi: 10.1038/srep 14032

Wolfe, N. D., Dunavan, C. P., and Diamond, J. (2007). Origins of major human infectious diseases. *Nature* 447, 279–283. doi: 10.1038/nature 05775

Yoshikawa, Y., Ochikubo, F., Matsubara, Y., Tsuruoka, H., Ishii, M., Shirota, K., et al. (1989). Natural infection with canine distemper virus in a Japanese monkey (*Macaca fuscata*). *Vet. Microbiol.* 20, 193–205. doi: 10.1016/0378-1135(89)90043-6

Conflict of Interest Statement: The authors declare that the research was conducted in the absence of any commercial or financial relationships that could be construed as a potential conflict of interest.

Copyright © 2019 Quintero-Gil, Rendon-Marin, Martinez-Gutierrez and Ruiz-Saenz. This is an open-access article distributed under the terms of the Creative Commons Attribution License (CC BY). The use, distribution or reproduction in other forums is permitted, provided the original author(s) and the copyright owner(s) are credited and that the original publication in this journal is cited, in accordance with accepted academic practice. No use, distribution or reproduction is permitted which does not comply with these terms.

frontiers in Microbiology

REVIEW
published: 04 October 2019
doi: 10.3389/fmicb.2019.02314

Factors Affecting the Tissue Damaging Consequences of Viral Infections

*Deepak Sumbria, Engin Berber and Barry T. Rouse**

Department of Biomedical and Diagnostic Sciences, College of Veterinary Medicine, The University of Tennessee, Knoxville, Knoxville, TN, United States

Humans and animals are infected by multiple endogenous and exogenous viruses but few agents cause overt tissue damage. We review the circumstances which favor overt disease expression. These can include intrinsic virulence of the agent, new agents acquired from heterologous species, the circumstances of infection such as dose and route, current infection with other agents which includes the composition of the microbiome at mucosal and other sites, past history of exposure to other infections as well as the immune status of the host. We also briefly discuss promising therapeutic strategies that can expand immune response patterns that minimize tissue damaging responses to viral infections.

Keywords: viral infection, immunopathology, outcome of past and concomitant infections, influence of microbiome and virome, therapeutic management of infections

OPEN ACCESS

Edited by:
Ian M. Jones,
University of Reading,
United Kingdom

Reviewed by:
Ryan Troyer,
University of Western Ontario, Canada
Alexander Freiberg,
The University of Texas Medical Branch at Galveston, United States

***Correspondence:**
Barry T. Rouse
btr@utk.edu

Specialty section:
This article was submitted to Virology, a section of the journal Frontiers in Microbiology

Received: *29 July 2019*
Accepted: *23 September 2019*
Published: *04 October 2019*

Citation:
Sumbria D, Berber E and Rouse BT (2019) Factors Affecting the Tissue Damaging Consequences of Viral Infections. Front. Microbiol. 10:2314. doi: 10.3389/fmicb.2019.02314

INTRODUCTION

Humans are perpetually infected with multiple endogenous and exogenous viral agents and estimates suggest that some of us generate up to 10^{12} new virus particles per day (Virgin et al., 2009). Moreover, thanks to astonishing advances in technology we are constantly discovering new viruses that are present somewhere on or in our bodies. However, few exogenous viruses cause overt disease and when this does occur usually only a minority of individuals are affected. Since viruses are obligate intracellular parasites that require host cells to replicate and assemble infectious progeny, the question arises as to the nature of factors which impact on whether or not infections are unobserved or develop into some form of overt cell and tissue damage. Some viruses do have high intrinsic levels of pathogenicity and mediate notable, often lethal, tissue damage in a high proportion of infected individuals. Smallpox was the poster child of this situation in mankind. These days, Ebola virus and some other viruses that cause hemorrhagic fevers have high intrinsic pathogenicity causing dramatic effects that include death in most infected persons (Feldmann and Geisbert, 2011).

In animal populations, highly virulent viruses also occur from time to time. For example, when it first occurred in the 1950s, myxomatosis killed more than 95% of the rabbit population in parts of Europe and Australia (Kerr, 2012). Every so often new virulent strains of influenza (Flu) appear after reformulation usually in birds or swine. These variants can be devastating to humans, as happened in 1918–1919 and often occurs with concentrated poultry flocks (Taubenberger and Morens, 2006; Peiris et al., 2007). This has occurred a few times in southern China and was of great

concern when strain H5N1 came onto the scene since spread to humans was anticipated (Peiris et al., 2007). The likelihood that any virus infection can cause disease is increased if the host has a clear-cut defect in one or more components responsible for immune protection, but this situation is uncommon. A more common cause of tissue damage is that the circumstances of infection result in an imbalanced host response with one or more components that are proinflammatory dominating over regulatory activities. In these situations, the host response to the infection, which in many instances is persistent and difficult to remove, is the main cause of tissue damage. Most commonly the main cellular orchestrators of such lesions are certain subsets of T cells with antigen non-specific inflammatory cells and various mediators causing the actual tissue damage (Rouse and Sehrawat, 2010).

EXOTIC INFECTIONS CAN BE HIGHLY TISSUE DAMAGING

Several circumstances during a viral infection can set the stage for tissue damage (Belkaid and Rouse, 2005; Rouse and Sehrawat, 2010). Foremost of these is infection by an exotic agent invariably derived from another species where the virus may be an asymptomatic natural infection. Indeed, we believe that many of our common virus infections were originally introduced at the time when human populations came to live more closely together and along with animals. This happened when many humans became agriculturalists rather than being more solitary hunters and gatherers. Several infections were acquired from their newly domesticated livestock such as measles, likely derived from rinderpest infected cattle and sheep (Pearce-Duvet, 2006). However, it is surmised that most human virus pathogens were acquired from rodents (>60) and about the same number from bats (Luis et al., 2013). We are still acquiring exotic infections particularly from other primates, and when this occurs they are often clinically severe and sometimes lethal. Most famous of these exotic infections was the occurrence of AIDS in the early 1980s now known to be caused by human immunodeficiency virus (HIV) derived from a non-human primate (Sharp and Hahn, 2011). More recently primate derived Ebola and Zika viruses have been a cause for concern and bat derived Nipah virus is a frequent problem in Bangladesh (Faria et al., 2016; Malvy et al., 2019; Nikolay et al., 2019). The dog communities received a pathogenic gift from cats-parvovirus which caused major clinical problems worldwide, but now well controlled by vaccines (Parrish et al., 1985). The aforementioned myxomatosis virus which killed so many European rabbits was originally a natural well tolerated pathogen in Brazilian wild rabbits (Arthur and Louzis, 1988). The current devastating epidemic of African swine fever virus in Chinese pigs is an inapparent infection in its original host-warthogs and bush pigs in Africa (Meng et al., 2009).

Whereas exotic infections can cause severe clinical consequences when they first emerge, in most instances the virus-host relationship undergoes genetic changes on both sides and the interaction evolves to become less tissue damaging. This happened remarkably quickly with myxomatosis in the fast breeding rabbit population. Adaptation also occurs successfully if the exotic agent induces protective immunity as happened with the flaviviruses Zika and yellow fever. In contrast, adaptation is prolonged with agents that induce inferior immunity such as with the flavivirus hepatitis C virus (HCV). Exotic virus infections which fail to induce protective immunity and at the same time may be immunosuppressive, such as HIV, are proving difficult to control with vaccines.

INFECTION BY VIRUSES THAT BLUNT COMPONENTS OF IMMUNITY

Another situation which sets the stage for tissue damage is when the virus has properties that blunt the efficacy of one or more components of host defense. This immune blunting property, more commonly referred to as immune evasion, may also impact on the response to heterologous infections as is discussed in a subsequence section (the influence of previous and concomitant infections). The topic of immune evasion has received intense study and has received many excellent reviews (Ploegh, 1998; Alcami and Koszinowski, 2000). Blunting the efficacy of protective immunity is particularly consequential with HIV, but all members of the herpesvirus family possess strategies that interfere with effective host immunity (Kumar et al., 2018). In their natural hosts, herpesviruses usually persist, resist immune removal and usually cause minimal disturbance in immunocompetent hosts (Ploegh, 1998; Sehrawat et al., 2018). The most genetically complex of all herpesviruses, human cytomegalovirus (HCMV), has an abundance of immune blunting activities and seldom causes relevant tissue damage in immunocompetent hosts (Nolan et al., 2017; Picarda and Benedict, 2018). Like all herpesviruses, HCMV can establish an alternative replication pattern called latency where the virus can persist for prolonged times and may make them invisible to the immune system (Picarda and Benedict, 2018). This is the state of affairs with herpes simplex virus (HSV), but with this herpesvirus periodic recurrences often result in tissue damaging episodes which can be more of consequence when the immune system is dysfunctional or unbalanced (Van de Perre et al., 2008). In part because of the many ways by which herpesviruses avoid and manage host immune responses, we have few effective vaccines and antivirals against these agents.

INFLUENCE OF AGE AT TIME OF INFECTION

Whether or not a virus infection causes significant tissue damage often depends on the age at which the infection occurs. Generally speaking, young children and elderly people are more susceptible to the tissue damaging consequences of virus infection than healthy adults. For instance, several respiratory viral infections such as Flu and respiratory syncytial virus (RSV) and some gastrointestinal infections cause more severe disease in young persons, particularly infants (Collins and Graham, 2008). Old individuals can also suffer more severe problems

with Flu as well as with RSV, especially if they reside in community centers. Some infections are particularly damaging if they infect the fetus especially in those species that transfer minimal or no maternal antibody across the placenta during pregnancy. Thus, *in utero* infection of non-antibody protected calves with bovine diarrhea virus or bovine herpesvirus can either result in abortion or congenital abnormalities (Baker, 1995). A similar outcome can occur in foals when infected *in utero* with equine herpes virus and lambs infected *in utero* with bluetongue virus (Clarke and Osburn, 1978; Walter et al., 2013). The recent global concern that happened when Zika virus first appeared in Brazil causing congenital and other problems has now receded (Faria et al., 2016). Thus, Zika has become endemic and many women are infected and develop protective immunity before they become pregnant. Moreover, other flaviviruses also cross-react with Zika and these may also confer cross-protection or potentially could increase pathogenicity (Stettler et al., 2016).

The situation with Zika recalls the past consequences of maternal infection with rubella in the pre-vaccination era. Thus, if seronegative women were infected with rubella during pregnancy their children could have a range of congenital lesions that often involved the nervous system (Bouthry et al., 2014). Today HCMV infection remains a problem if infection occurs *in utero* or around the time of birth. Children can develop congenital CMV, a syndrome that mainly affects the nervous system. The most common problem is hearing loss, but problems with vision and cognition also occur (Schleiss, 2018). A small minority develop microcephaly the major sign noticed when Zika first occurred. Curiously, infants can develop congenital CMV when born to seropositive mothers (Britt, 2018) since adaptive immunity does not preclude herpesvirus infection–bad news for vaccinologists.

The observation that young animals infected with some viruses can develop more tissue damaging responses than do adults can have multiple explanations. For instance, several aspects of the immune system are not fully functional *in utero* and even after birth. For example, the type-I interferon response and the activity of some subsets of dendritic cells (DC) are less active, the specific immune repertoire may be lacking some reactivities, the immune reactivity pattern lacks regulatory components and many signaling pathways may be not fully functional. This topic has been reviewed by others (Samuel, 2001; García-Sastre, 2002; Katze et al., 2002). Older animals too may develop more severe responses to virus infections because of senescence changes to the immune system. This subject will not be further discussed but is under intense investigation with many excellent reviews available (Nikolich-Žugich, 2008; Maue et al., 2009).

Finally, of some interest is that some virus infections that persist and cause no tissue damage for decades may suddenly become very consequential. This may happen with varicella zoster virus (VZV) which years after causing chicken pox in children (or even vaccination against chickenpox) persons may develop distressing and painful dermal lesions called shingles (John and Canaday, 2017). This represents reactivation from VZV latency and it usually occurs in only one or a few ganglia of the far greater number of ganglia that are latently infected. The lesions represent T cell-mediated immunopathological reactions, and ultimately the recurrent infection is controlled by the immune system. Among the unsolved mysteries of shingles are explaining the circumstances of its occurrence, why only a minority of the many infected ganglia reactivate and why a vaccine that largely induces only antibody-mediated immunity appears to be so efficacious to prevent shingles.

THE INFLUENCE OF DOSE AND ROUTE OF INFECTION

Several additional circumstances during viral infection can influence the outcome in terms of being subclinical or tissue damaging. Exposure dose and route of infection are relevant variables. In fact, it is likely that the majority of persons who escape clinical infections during Flu outbreaks could in part be explained by a lifestyle that limits the level of infection. Those of us who have few close interactions with others, and especially if we adopt a non-affectionate behavior pattern, are less likely to receive high dose infections. However, quantitative effects of infection can only be assessed by control studies in experimental animals. Influenza virus infections in mice have been used for this purpose (Legge and Braciale, 2005). In such studies, animals given a high dose all developed disease and this could be lethal. The deaths seemed to be the consequence of the otherwise protective CD8 T cell response being suppressed. The suppression was explained by plasmacytoid DC, which express Fas-ligand upon Flu infection, making contact with Fas-expressing CD8 effector T cells causing these otherwise protective cells to undergo apoptosis. A similar form of plasmacytoid DC/leucocyte interaction could explain the lymphopenia which occurs with virulent H5N1 flu infection (Langlois and Legge, 2010). At lower doses of flu infection, other types of DC were preferentially infected but these cells fail to express Fas-ligand permitting protective T cells to survive. At even lower doses of virus one can assume the virus is fully controlled by innate defenses and adaptive aspects of immunity may not be induced.

A few years back when infection experiments in chimpanzees were still permitted, some remarkable observations on the infection dose effects was reported by the Chisari group (Asabe et al., 2009). They showed that when animals were infected with between 10^4 to 10^8 virions of hepatitis B virus, animals developed mild hepatitis and readily controlled the disease. However, infection at a higher dose resulted in damaging chronic active hepatitis thought to be an immuno-pathological response to the infection. Surprisingly, infecting chimpanzees with a minimal dose which could be as low as 100 virions gave the same outcome as those infected with greater than 10^8 virions. Explanations for these observations were not at hand but it could have related to the virus avoiding contact and elimination by some aspect of innate immunity, but still able to present antigens to induce an unbalanced T cell response that mediated tissue damage.

Apart from dose effects of infection, the route of exposure can also be critical. With HIV, for example, infection is more likely to occur when virus infects the rectal compared to the vaginal epithelium (Tebit et al., 2012). With experimental HSV infections

in mice, route critically influences consequences. Thus, if animals are infected subcutaneously or intramuscularly, the outcome is usually subclinical and a full range of adaptive immune responses are induced. However, intradermal infection on the flank gives rise to a so-called zosteriform reaction in the whole dermatome which innervates the site of infection (Simmons and Nash, 1984). These lesions resemble those which occur in human shingles. The skin lesions represent host immunopathological reactions to virus reemerging at nerve endings after first replicating in the innervating nerve ganglion. Similar immunopathological lesions occur in the eye when virus gains access to the cornea. This lesion is referred to as stromal keratitis and it is a common cause of vision impairment in humans (Pepose et al., 1996). Curiously, if HSV is delivered to the anterior chamber of the eye some aspects of adaptive immunity are induced but not others. The consequences of anterior chamber administration may be retinitis which occurs in the contralateral but not in the ipsilateral retina which is thought to be protected by an interferon response (Vann and Atherton, 1991).

Infection by the mucosal route often results in minimal tissue damage, in part because infection by this route preferentially induces regulatory T cells and cytokine responses such as IL-10 producing macrophages (Rezende and Weiner, 2017). This induction of oral or nasal tolerance is usually accomplished using soluble antigens at a critical dose level and although viruses when given orally were suspected to induce a form of tolerance but because most infections induce an inflamed environment the idea is no longer in favor (Rezende and Weiner, 2017). Some enteric virus infections, however, can terminate oral tolerance induced against autoantigens and allergens likely by establishing a more inflammatory less regulatory immune environment (Rezende and Weiner, 2017).

INFLUENCE OF HOST GENETICS

The outcome of a virus infection can be profoundly influenced by host genetics especially by genes that encode major innate or adaptive components of immunity. Thus, animals lacking the ability to generate T lymphocytes become highly susceptible to many virus infections (Dropulic and Cohen, 2011). Some infections that are usually inconsequential can be severe or even lethal in those with T cell defects. Infections by herpesviruses illustrate this scenario (Ruffner et al., 2017). By way of contrast, genetic defects which affect antibody production usually result in more clinical problems with bacterial than viral infections (Carneiro-Sampaio and Coutinho, 2007). Humans have approximately 23,000 genes and many of these can influence the efficacy of virus control. However, usually the deletion or changed function of a single gene product has only a partial effect on responses and then only under certain circumstances of infection. For example, the phenotype of the chemokine receptor gene CCR-5 may be associated with greater resistance to HIV infection, but this resistance is readily overcome at higher doses of HIV exposure (Wilkin and Gulick, 2012). Curiously, the same phenotype of CCR-5 that increases resistance to HIV renders persons more susceptible to West Nile virus (Glass et al., 2006).

In addition to CCR-5, many other genes that influence innate immune function can impact on the severity of virus infections. For example, several genes that affect interferon or interferon receptor functions can also result in more severe responses to several virus infections. Well studied examples are defects in genes such as toll like receptor (TLR) 3 and UNC93B (Casrouge et al., 2006). Both defects result in defective cytokine production especially interferon alpha and beta in response to infection. If babies with the defects are infected with HSV they can readily develop herpes simplex encephalitis (Casrouge et al., 2006). Defects in natural killer (NK) cell function may also result in more severe herpesvirus infections in humans (Biron et al., 1989; Orange, 2002). Countless functional defects in innate as well as adaptive immune activity have been produced in mouse models and many have been studied for effects on susceptibility to a wide range of viral infections. For example, studies on the pathogenesis and immunology of dengue and Zika virus in mice only became possible using mice when the interferon receptor was knocked out (IFN-$R^{-/-}$) making them susceptible to infection (Lazear et al., 2016).

INFLUENCE OF THE MICROBIOME

Whereas dysfunctions or deletions of host genes can affect the efficacy of antiviral defense, the far more abundant genetic material present in the form of microbes acting as passengers within or on the body surfaces may also influence the outcome of infection by a pathogen. The focus of attention has been on the microbiome of the gut and skin whose combined genetic material can exceed 10^{13} gene and hence far exceeds the number of host genes (Bik et al., 2006). The microbiome, particularly of the gut, impacts on the disease pattern of numerous syndromes. Many excellent reviews have been written and we shall comment only briefly emphasizing effects of the microbiome on responses to virus infections (Honda and Littman, 2012; Belkaid and Harrison, 2017). The microbiome consists of several families of bacteria (10^{11} per gram/contents), fungi, viruses, eukaryotes such as the protozoan Blastocystis as well as helminths. The actual composition of the microbiome differs during development and is strongly influenced by diet, previous exposure to infections and other factors (Honda and Littman, 2012; Thomas et al., 2017). Evidence accumulates to show that the composition of the microbiome can markedly affect how the host responds to exogenous viral pathogens. Most studies have measured the effects of the bacterial microbiome. If this is diminished by treatment with broad spectrum antibiotics, or removed by germ free procedures, responses to several viral infections are changed. Overall, the manipulated animals generate more tissue damaging responses to several infections compared to controls. One of the first to be studied was lymphocytic choriomeningitis virus (LCMV) which becomes more severe or prolonged in antibiotic purged mice (Abt et al., 2012). The outcome was explained by a reduced antibody and CD8 T cell response in treated mice perhaps associated with diminished TLR induced cytokine and chemokine responses involved in immune induction (Abt et al., 2012). Influenza virus infections can also be more severe in

antibiotic treated animals because of increased viral replication in lungs perhaps mainly a consequence of a reduced inflammasome response in treated animals which led in turn to reduced T cell priming (Ichinohe et al., 2011). Experimental flavivirus infections in IFN-$R^{-/-}$ mice may also be more severe in antibiotic treated mice, an effect explained also by a reduced innate and adaptive response to the infection (Thackray et al., 2018).

Antibiotic purging can also cause some virus infections to become less tissue damaging. This pattern of events can occur with mouse rotavirus and norovirus infection (Uchiyama et al., 2014; Baldridge et al., 2015). The subject is currently of high interest since it has become evident that the resident microbiome may influence how many viruses are controlled and how well persons respond to vaccines. For example, the lesser effectiveness of rotavirus vaccines in some developing countries could be explained by the composition of their microbiome.

The mechanisms by which the resident microbiome could influence the outcome of other disease syndromes is under intense investigation. Ideas include effects on the expression or access of cell receptors required for viral entry, the production of microbial products that bind to viruses and influence their infectability and, perhaps of most relevance, the effect the microbiome has on the pattern of immune responsiveness to both mucosal and systemic infections. As regards effects on viral receptors one study showed that the bacterial product flagellin affected susceptibility to rotavirus and to a lesser extent reovirus infection (Uchiyama et al., 2014). The flagellin was shown to act via TLR5 and nucleotide oligomerization domain (NOD)-like receptor 4 engagement to induce IL-22 and IL-18 which likely caused apoptosis of the target cells that normally support virus replication. Thus, pre-exposure of mice to flagellin could prevent rotavirus infection and even accelerate cure of established infections. Additionally, the observation that the presence of *Staphylococcus aureus* in the lungs of mice prior to Flu infection resulted in reduced mortality was explained by changing TLR2 induced recruitment of inflammatory cells which inhibited the Flu infection (Wang et al., 2013; Zhang et al., 2014).

An example of the effect of a microbial product on the efficiency of infection by a virus was observed with poliovirus where optimal infectivity was observed to depend on the virus binding to bacterial surface polysaccharides and peptidoglycans (Kuss et al., 2011; Robinson et al., 2014). The bound virus was also more stable which facilitated transmission. Human norovirus infections also become more infectious when bound to bacterial surface glycans (Norman et al., 2014). Another example is vertical infection with mouse mammary tumor virus. Here the binding of bacterial lipopolysaccharides (LPS) to the maternal-derived virus caused the production of immunosuppressive IL-10 in the pups and this facilitated their infection (Kane et al., 2011). The microbiome might also play a role in dengue virus (DENV) infection. Here too LPS can enhance disease acting by increasing the production of platelet activating factor (PAF), TNF-alpha and IL-6 from DENV infected monocyte derived macrophages which worsened disease expression (Kamaladasa et al., 2016; Malavige and Ogg, 2017). The outcome occurred in part by PAF mediating increased vascular leakage, a significant component of dengue lesions (Kamaladasa et al., 2016).

Products from the microbiome can also help protect against the pathogenic effects of virus infections. For example, factors released from the microbiome residents *Lactobacillus casei* and *Bacteroides thetaiotaomicron* can bind to cell surface glycans and preclude infection by rotaviruses (Varyukhina et al., 2012). Indeed, rotavirus-associated diarrhea can be reduced by feeding Lactobacillus (Guandalini et al., 2000). Another recently reported example where microbiome-derived products decreased viral susceptibility was with herpes simplex encephalitis where a polysaccharide derived from the gut resident *Bacteroides fragilis* induced IL-10 producing protective B and T cells (Ramakrishna et al., 2019).

It is likely that the most common mechanistic explanation for the influence of the microbiome on the outcome of virus infections involve effects on the induction and activity of both innate and adaptive immune responses. The balance of microbiome constituents is in turn affected by many factors which include diet, stage of development and antibiotic use (Belkaid and Harrison, 2017). It is also curious to note that the gut microbiome of children born by natural delivery compared to caesarian section can show marked differences and this could influence their responses to viral infections (Mueller et al., 2015). With regard to dietary effects, a diet rich in fiber causes the production of short-chain fatty acids (SCFA) such as acetate, butyrate and propionate which favors the expansion of regulatory T cells in the mucosa and as well as systemically (Smith et al., 2013). This would provide an anti-inflammatory environment. On the contrary, diets low in fiber, such as we prefer in the United States, favor the expansion of segmented filamentous bacteria such as Clostridia species. These bacteria set the scene for a proinflammatory T cell responses, especially induction of the Th17 subset (Atarashi et al., 2011; Honda and Littman, 2012). The effect of diet on the outcome in terms of susceptibility to virus infection is under active investigation. Studies have revealed that Flu susceptibility can be affected by diet, although it is not clear if such effects proceed by affecting the composition of the microbiota. For example, mice fed a high fat diet led to a change in the balance of several immune parameters to favor inflammatory components (Milner et al., 2015). High fat recipients suffered more lung epithelial cell damage because of increased inflammatory cytokine (TNF-a, IL-6, INF-gamma, and IL-1 beta) responses and reduced regulatory T cells, M2 macrophages as well as decreased numbers of NK cells. Moreover, death rates were higher than animals fed a normal chow diet (Honce and Schultz-Cherry, 2019). High fat diets can result in obesity and there is also some epidemiological evidence that obesity could increase human susceptibility to Flu although the mechanisms involved are poorly understood (Gill et al., 2010). Conceivably, the observation that obese individuals had reduced ability to activate and perform functional CD4 and CD8 T cell responses as compared to healthy individuals could be one explanation (Paich et al., 2013).

Another way to evaluate microbiome effects on susceptibility to virus infection is to manipulate the diet in some way. This approach has received minimal study in humans and livestock and when any effects were observed they were not related to microbiota changes. The topic is certainly well worth further

investigation. Thus, it would be curious to explain why the high consumption of fruits and vegetables seems to reduce the risk of upper respiratory viral infections in pregnant women (Li and Werler, 2010) and how feeding high levels of soya beans to pigs lowers their susceptibility to the important disease reproductive and respiratory porcine viral syndrome (Rochell et al., 2015). More diet manipulation studies have been done in experimental animals such as mice. For example, in a recent study a diet rich in the fermentable fiber inulin protected against Flu-induced pathology (Trompette et al., 2018). The mechanism proposed involved *Bacteroidetes* present in the gut which fermented the dietary inulin to produce SCFA. These SCFA were advocated to enhance protective CD8 T cell effectors and to reduce lung inflammatory effects by favoring M2 macrophages and reducing neutrophils (Trompette et al., 2018).

The bacterial microbiome is not the only component that can affect the outcome of virus infections. Thus enteric helminths infection can increase susceptibility to norovirus infection acting by inhibiting the protective CD8 T cell response (Osborne et al., 2014). Moreover, helminths are well known to influence patterns of immune responsiveness toward the Th2 pattern (Reese et al., 2014). This likely explains how helminth infection via inducing IL-4 and IL-13 can causes the breakdown of latency with some herpesviruses (Reese et al., 2014). Helminth infection might also impact on the severity of childhood RSV infection when the tissue damage is associated with a type II inflammatory response (McFarlane et al., 2017).

INFLUENCE OF THE VIROME

There is mounting evidence that other viruses which constitute the so-called virome also influence the consequences of pathogenic virus infections. Thanks to advances in sequencing and analysis of meta-genomic data many new viruses have been discovered especially in the intestinal tract. The great majority of these viruses are DNA bacteriophages and these may reach 10^{15} in number (Carding et al., 2017). Many of the rest are RNA containing plant viruses and about 1% are many types of passenger animal viruses that belong mainly to the anellovirus, parvovirus, adenovirus and papilloma virus groups (Neil and Cadwell, 2018). Added to the virome are the endogenous retroviruses which can account for up to 8% of the human genome as well as several DNA and RNA viruses in the body which act as chronic, but usually non-disease causing infections. Several of these latter agents belong to the herpesvirus family all of which can persist in the host in a non-replicating state referred to as latency.

It is strongly suspected that many components of the virome could influence the nature of the host response made to infection by an exogenous potential pathogen. For example, persistent infection with a non-pathogenic norovirus can reduce the extent of CD8 T cell responses which acts as major defense mechanisms against several viruses (Tomov et al., 2013). In homozygous twins discordantly infected with HCMV, those infected with the herpesvirus suffer more severe reactions to Flu infection (Brodin et al., 2015; Picarda and Benedict, 2018). There is gathering evidence that persistent infection with HCMV can impact on immune system function (Picarda and Benedict, 2018). Thus, the virus possesses numerous proteins that blunt immune response to infected cells and some of these activities could have general paracrine effects. Several additional resident viruses present in normal animals could also impact on the outcome pathogenic virus infections. So far the effects of the virome have mainly focused on their influence on the outcome of non-viral pathogens. For instance, an early report from the Virgin group noted that that mice latently infected with the herpesvirus HV68 or MCMV were more resistant to bacterial infection with *Listeria monocytogenes* and *Yersinia pestis* (Barton et al., 2007). These protective effects were attributed to systemically activated macrophages and upregulation of cytokines such as interferon-gamma. Additionally, mouse norovirus infection may increase the survival of mice challenged in the respiratory tract with *Pseudomonas aeruginosa*, an effect caused by a reduced IL-6 and TNF-alpha response to infection (Thépaut et al., 2015).

It is also curious to note that mice raised in pet stores (often referred to as a dirty environment) rather than in vivariums are infected with several viruses and other microbes and had antibodies to more agents than laboratory-raised animals (Beura et al., 2016; Masopust et al., 2017). The pet store mice also had more abundant naïve and memory T cells in lymphoid and non-lymphoid tissues (Beura et al., 2016; Masopust et al., 2017). Particularly striking was the high levels of tissue-resident memory cells in the tissues of dirty compared to lab-raised mice. Of interest, mice raised in the dirty state had immune cell response patterns that more resembled the human situation than occurred with laboratory-raised animals (Reese et al., 2016). Thus when performing pathogenesis and immune protection studies in mice using human viruses, perhaps we should be using pet store rather than laboratory-raised animals for such studies. In support of this idea, the Masopust group compared the response pattern to yellow fever virus vaccination in normal laboratory mice with those subjected to sequential infection with unrelated pathogens such as herpesviruses Flu and intestinal helminths. The dirty/co-infected mice compared to laboratory mice had enhanced baseline and vaccination responses measured by several assays and by metagenomic analysis had a response pattern resembling that observed in human adults frequently exposed to infections.

THE INFLUENCE OF PREVIOUS AND CONCOMITANT INFECTIONS

The impact of a virus infection can be markedly affected by past or ongoing infection. The subject is a complex and the story is still unfolding. When different infections occur closely together the pattern of innate immune responsiveness to one or both agents critically affect the outcome. However, when infections are separated by several days, the response pattern of the adaptive immune response to the first infection also plays a crucial role. Older studies by the McKanass group in the early 1960s had observed that infection with one intracellular pathogen provided resistance for a few days to infection by an unrelated agent.

The effect was attributed at that time when cellular immunology was still in its infancy, to non-specific protective effects of activated macrophages (Mackaness, 1962). More recently, the Chisari group showed that infection with LCMV caused reduced liver immunopathology caused by hepatitis B virus infection an effect also attributed to enhanced responses of innate aspects of immunity (Cavanaugh et al., 1998). With regard to the outcome of sequential infections with different viruses, the subject has been carefully studied for many years in mice models by the Selin and Welsh group (Welsh et al., 2010). Their studies have identified mechanistic circumstances which result in the second infection either being effectively controlled or to result in a tissue damaging immunopathological reaction that is more severe than would occur in a naïve infected animal. We shall discuss the highlights of their results later.

Closely spaced infections with different agents most commonly involve viral with non-viral infections. This happens, for example, with Flu which is usually accompanied by respiratory bacterial infections. When Flu becomes a severe clinical problem with even lethal results, secondary bacterial infections usually contribute to the severe tissue damage (Goka et al., 2015). Indeed, patients with severe Flu are normally treated with antibiotics and one assumes that this therapy is valuable. When coinfections with different viruses occurs, the outcome is affected by interference phenomena. The most common mechanisms of interference involve several types of interferon proteins which act to make infected cells antiviral and to influence the function of other cells, especially cells involved in immune reactions (Kumar et al., 2018). The functional effects include activation of immune cells, changes of signaling pathways and modulation of function via the induction of a large number of interferon-stimulated gene products. This topic has received many reviews (Dianzani, 1975; Otto, 2015). In instances where different viruses happen to infect the same cells, additional mechanisms of interference come into play. These so-called intrinsic interference phenomena, which was first studied with Newcastle disease virus (Marcus and Carver, 1967), include defective interfering particles, *trans*-acting proteases, non-specific double-stranded RNA and some others were recently reviewed in depth by Kumar et al. (2018). This review also lists many examples of co-infections along with their outcomes. One of the more notable consequences of two virus strains infecting the same cell is the production of viral recombinants which may have enhanced pathogenicity. This mechanism is at play when antigenic shift variants occur with influenza virus infection. The shift variants are often responsible for major Flu pandemics. Genetic reassortments also occur with other infections (Becher et al., 2001).

One major example from the veterinary world occurs when cows are persistently infected with bovine virus diarrhea (BVD) virus. This virus can recombine with other BVD strains, including vaccine strains, to generate highly lethal recombinants which causes a lethal mucosal disease in cattle (Becher et al., 2001). Intrinsic interference can also occur between unrelated viruses which may explain how enterovirus infection can inhibit the effectiveness of poliovirus vaccination (Becher et al., 2001).

The best studied examples where prior infections affect the outcome of a subsequent virus infection involves changes imposed on the adaptive immune responsive pattern that resulted from the first infection. This is often referred to as heterologous immunity (Welsh et al., 2010). In human disease situations, there are a few notable examples although actual mechanistic understanding is less forthcoming than is available from experimental situations with mouse models. A current relevant example involves the flaviviruses dengue and Zika. In dengue, where there are 4 major viral serotypes, some infected persons, usually children, develop a severe inflammatory reaction. This represents a cytokine storm and is called dengue hemorrhagic fever/dengue shock syndrome (DHF/DSS) (Halstead, 2007). The often lethal syndrome involves fever, hypotension, vascular leakage, thrombocytopenia and damage to several organs. Most of the time (but there are exceptions) DHF/DSS occurs in young persons who had already been infected with a different strain of dengue than the current infection. Some time ago Scott Halstead hypothesized that DHF/DSS represented the consequence of non-neutralizing antibody facilitated infection of inflammatory cells such as macrophages which mediate the pronounced inflammatory reaction (Halstead and O'Rourke, 1977). This was called antibody-induced enhancement (ADE). ADE still holds sway but other explanations have been advocated. These include the involvement of low avidity CD8 T cells which act to mediate immunopathology rather than controlling the infection (Mathew and Rothman, 2008).

More recently interest has focused on the relevance of heterologous immunity with the cross reactive flaviviruses dengue and Zika (Langerak et al., 2019). *In vitro* studies have provided evidence for ADE *in vitro* in both directions (Littaua et al., 1990; Bardina et al., 2017). However, the situation *in vivo* remains in debate although more convincing results show that pre-infection with Zika makes subsequent responses to dengue more consequential than the obverse situation where data are inconsistent (Langerak et al., 2019). Persons seropositive for dengue may be more likely to transmit Zika virus across the placenta to infect the fetus especially in late trimesters when placental transfer does not usually occur (Langerak et al., 2019). Prior infection with Zika can result in more severe lesions in persons subsequently infected with dengue, but this is by no means a regular occurrence and overt DHF/DSS is unusual (Langerak et al., 2019). The main relevance of unraveling whether or not heterologous severe responses occurs with double infections impacts on vaccine use. Thus, already a vaccine against the 4 strains of dengue has been withdrawn because of the increased incidence of DHF/DSS in some vaccines who were seronegative when vaccinated (Aguiar et al., 2016; Plotkin, 2019). A vaccine against Zika might also have adverse effects in some persons subsequently exposed to dengue. Similarly, dengue vaccines might cause more severe reactions when exposed to Zika as well as to some other cross-reacting flaviviruses such as West Nile virus (Bardina et al., 2017). A particular concern is that dengue vaccines could make Zika infected women more likely to transmit virus to the fetus.

Heterologous damaging immune reactions have been reported with other human viral diseases. One such example could be

infectious mononucleosis (IM) occurring in young adults upon primary infection with the gamma herpesvirus Epstein Barr virus (EBV) (Aslan et al., 2017). Thus in HLA2 positive persons cross reactivity of CD8 T cells occurs between T cells that recognize epitopes from a Flu virus matrix protein and the protein BMLF1280 of EBV. The cross reactive T cells generated in response to Flu, which can be shown by *in vitro* studies to react with EBV, were proposed to be inadequate to control EBV infection, but instead contributed to inflammatory reactions upon EBV infection (Aslan et al., 2017). This concept of one virus inducing non-protective T cell responses that are expanded by the second infection which then mediate tissue damaging reactions was carefully studied by Selin and Welsh in mice using the cross-reacting arenaviruses LCMV and Pichinde virus and an unrelated virus Vaccinia (Selin et al., 1998). They focused on the numbers, specificity and avidity characteristics of the memory T cell repertoire induced by primary and secondary infection. Of interest, the nature of the memory response to the first infection impacted on the type of response made to the subsequent cross reacting pathogen. The T cell repertoire responding to the first infection consisted of multiple different specificities and binding efficiencies. Exposure to the heterologous second infection served to expand only the cross-reactive cells, many of which had low avidity and produced minimal protective cytokines such as interferon-gamma. Consequently, the second infection was not promptly controlled. However, these non-protective T cells could help orchestrate a tissue damaging inflammatory reaction.

Other interpretations for the untoward outcome of heterologous infections includes effects on the balance of several immune components preferentially expanded by the second infection. Thus, if the response is non-inflammatory, it could be explained by the dominance of regulatory aspects of immunity expanded by the second infection. These include regulatory T cells and anti-inflammatory cytokines such as IL-10 and TGF-beta. Inflammatory responses would accrue from the preferential expansion of Th1 and Th17 cells, M1 macrophages and cells producing IL-6, TGF-beta, and other inflammatory molecules. This concept has been discussed in detail in other reviews (Gil et al., 2015; Souquette and Thomas, 2018).

In this current world where measles has re-emerged as a problem infection and we still suffer the onslaughts of HIV infection, it is pertinent to point out that some virus infections are highly suppressive to the immune system such that multiple infections, including several viruses that in normal persons are well controlled become significant pathogens. Measles virus is one of the most immunosuppressive of all infections and persons with clinical measles readily suffer problems with other infections, some of which can be lethal (Griffin et al., 2012). HIV infection is always persistent and it takes many months in untreated persons for them to become markedly immune suppressed. Once this happens, normally non-troubling infections by herpesviruses and other agents become problematic. For example, the normally inapparent HCMV infection can cause a blinding retinitis (Alan, 1988; Salzberger et al., 2005). In addition, the usually silent Kaposi sarcoma herpesvirus infection can cause Kaposi sarcomas and primary or reactivation of HSV can result in severe dermal lesions which can disseminate to the brain and cause encephalitis (Sepkowitz, 2001; Rezaee et al., 2006). This topic has received several reviews including one by our own group (Sehrawat et al., 2018).

HOW CAN WE RESET IMMUNE RESPONSE PATTERNS TO MINIMIZE TISSUE DAMAGING RESPONSES TO VIRUS INFECTIONS?

We have argued that in many instances where a viral infection causes overt tissue damage rather than being controlled without notice happens because of some defect or imbalance in the host response to the infection. Accordingly, controlling such events would require immune replacement or rebalance of the immune response pattern. The traditional approach to control virus induced lesions is to combine specific antiviral drugs or monoclonal antibodies (few viruses can be controlled in this way) along with counteracting the inflammatory response. The latter is commonly achieved with steroids, non-steroidal anti-inflammatory drugs and occasionally other approaches such as immunosuppressants, specialized pro-resolving mediators, and some other novel approaches (Spite et al., 2014; Bhela and Rouse, 2018). There is a need for additional approaches particularly to control inflammatory lesions associated with persistent viral infections. We shall briefly discuss three approaches we consider to be promising.

The general approach that currently enjoys the most attention is checkpoint blockade. The strategy is being widely used to improve immunity to several cancers (O'Sullivan and Pearce, 2015). Its success depends on using mAb that engage and inhibit costimulatory molecules expressed at the surface of T cells which when bound to their normal ligand act to inhibit the protective function of T cells. The popular parlance is to describe the inhibited T cells is exhaustion (Roy et al., 2018). Such exhausted T cells were first noted in the chronic virus infection LCMV (Barber et al., 2006), but the phenomenon has now been observed in several other infections (Wherry, 2011). Indeed, there is a tendency to exaggerate the relevance of exhaustion as explaining the failure to control chronic tissue damaging infections. In the best studied system, which remains LCMV, exhaustion appears real and when it is reversed, as can be done with mAb against several molecules that include PD1, PDL1, TIM3, CTLA4, LAG-3, and perhaps others the course of inflammatory events can be inhibited and the virus better controlled (Barber et al., 2006; Roy et al., 2018). Many entertain the idea that reversing exhaustion could be useful to help control HIV, HSV, HCV, and hepatitis B virus (Saeidi et al., 2018). For instance, reversing the function of putative exhausted T cells was shown to reduce the severity of lesions following herpesvirus recurrences (Allen et al., 2011). Moreover, the approach was advocated as a potential means to facilitate the efficacy of therapeutic vaccines against HSV, HIV as well as a way to prevent human papilloma induced cancers in already infected persons (Palefsky, 2009). The value of the approach was recently reported to protect against recurrent ocular HSV lesions (Roy et al., 2018). The use of checkpoint

blockade to control chronic virus disease and potentiate vaccine merits further evaluation paying attention to side effect than might occur such as increasing the consequences of some inflammatory diseases (Johnson et al., 2018).

A second viable approach that might prove useful to change the course of tissue damaging virus infections is to manipulate miRNA expression. Thus several reports indicate that the expression of either host or viral miRNA can influence aspects of viral pathogenesis (Gottwein and Cullen, 2008; Ressel et al., 2019). For example, in a HSV model of immunopathology mice that lacked the expression of miR155, because of gene knockout, had markedly reduced lesions of herpetic stromal keratitis (SK) (Bhela et al., 2014). Similarly, inhibition of miR155 using an antagomer approach also reduced lesion severity. The effects occurred because miR155 is necessary for the function of proinflammatory Th1 and Th17 T cells that orchestrate the ocular lesions. A similar outcome was also observed in a model of inflammatory encephalitis caused by Japanese encephalitis virus (JEV) (Thounaojam et al., 2014). In this JEV model, knockdown of miR155 with antagomers resulted in less encephalitis (Thounaojam et al., 2014). Modulation of other miRNA such as miR-15b and 19-3b, both involved in inflammatory responses, were also studied in the JEV system. In such studies therapy with antagomers diminished lesions and levels of the inflammatory mediators IL-1β, IL-6, and CCL2 were decreased apparently a consequence of reduced RIG-1 signaling (Zhu et al., 2015; Ashraf et al., 2016).

Other miRNA whose modulated expression could impact on viral lesions include those critical for angiogenesis such as miR132 (Mulik et al., 2012), those such as miR-10a, miR-146a, and miR-17 which might act by enhancing T_{reg} function, as well as those that can promote the resolution of inflammation by regulating specialized pro-resolving mediators (Mulik et al., 2013). miRNAs can also control the production of pro and anti-inflammatory cytokines from innate immune cells (Tahamtan et al., 2018). In this regard our own unpublished data indicates that miR-142 acts as an anti-inflammatory miRNA by potentially targeting proinflammatory cytokine IL-6, thereby preventing an early onset of SK.

With some viruses their replication and consequent tissue damage is facilitated by host miRNA species. This is true for HCV which uses host miR122 to facilitate its replication (Janssen et al., 2013). In fact, drugs which target miR122 such as the antagomer miravirsen which inhibits HCV replication are currently in clinical trials.

We can surmise that manipulating disease associated miRNAs hold promise but there are many problems to solve. These include targeting to appropriate sites and realizing that each miRNA may have additional functions giving rise to unwanted off-target effects.

A so far poorly explored, but potentially valuable approach to make responses to virus infections less tissue damaging is to take advantage of the fact that cells of the immune system differ in their metabolism. Thus, as lucidly reviewed by O'Neill et al. (2016), cells of the immune system employ 6 major metabolic pathways to support their functions, but these are used differentially by cells that participate in immune processes. Accordingly, drugs that target metabolic pathways to increase or decrease their activity should act differentially on the various cells involved in immune defense or tissue damage. Using drugs that target metabolic pathways was pioneered in the cancer field exploiting the fact that cells involved in reacting to tumors rely on different pathways to support their energy and other metabolic requirements (Pearce et al., 2013). For example, pro-inflammatory T cell subsets (Th1, Th17), inflammatory M1 macrophages, activated neutrophils (Loftus and Finlay, 2016) rely mainly on aerobic glycolysis (Warburg Effect) and the pentose phosphate pathway to provide their energy. In contrast, the counter inflammatory components such as T_{reg} and M2 macrophages obtain their energy using oxidative phosphorylation and fatty acid oxidation (O'Neill and Hardie, 2013; Galván-Peña and O'Neill, 2014). Limited studies have so far been done using metabolic pathway inhibitor drugs to modulate viral pathogenesis. However, one study showed that if oxidative glycolysis was inhibited using 2-Deoxy-D-glucose (2DG) in a model of viral immunopathology then lesions were markedly diminished (Varanasi et al., 2017). The outcome was explained by a selective inhibitory effect on proinflammatory CD4 T cells permitting uninhibited regulatory T cells to remain active (Varanasi et al., 2017). The effects of 2DG has also been studied in a rhinovirus model of lung damage. Here too 2DG resulted in reduced lesions (Gualdoni et al., 2018).

Using 2DG during a viral infection can result in untoward effects especially in situations where virus replication in non-immune cells is the primary cause of pathology. For example, in the HSV model in mice, therapy with 2DG in the acute phase of infection resulted in suppression of the protective aspects of defense. This allowed the virus to spread to the brain to cause lethal encephalitis (Varanasi et al., 2017). In an influenza model too, 2DG therapy in the early phases of infection resulted in higher levels of mortality (Wang et al., 2016).

Additional metabolic pathways such as amino acid metabolism are beginning to be studied for effects on the outcome of viral infections. In Sindbis virus infected mice, for example, treatment of mice with the drug 6-Diazo-5-oxo-L-norleucine (DON), which inhibits glutamine metabolism, diminished the immunoinflammatory lesions in the brain and spinal cord which result in paralysis and mortality (Manivannan et al., 2016; Baxter et al., 2017). Changing the fatty acid synthesis metabolic pathway as can be done using the drug PF-05175157 has also led to reduced viral immunoinflammatory lesions caused by West Nile virus infection (Jiménez de Oya et al., 2019). Modulating different metabolic pathways could also turn out to be a viable approach to influence the expression of some persistent infections such as herpesvirus latency. Examples include suppressing viral reactivation by manipulating glutamine availability (Wang et al., 2017) and modulating fatty acid oxidation which can influence the breakdown of latency *in vitro*.

CONCLUSION

We are constantly exposed to viruses but few of them have the intrinsic pathogenicity to cause significant damage to normal

hosts. We have reviewed the circumstances of infection and the status of the host which does favor tissue damage. Understanding the details of virus-host interaction which leads to disease is expected to result in developing novel approaches to prevent the untoward effects of infections.

AUTHOR CONTRIBUTIONS

BR conceptualized the manuscript. BR, DS, and EB wrote the manuscript.

FUNDING

This work was supported by the NIH Grant R01 EY 005093.

ACKNOWLEDGMENTS

We appreciate the input of Kevin Legge, Lbachir BenMohamed, and Mehul Suthar for their information and constructive criticism.

REFERENCES

Abt, M. C., Osborne, L. C., Monticelli, L. A., Doering, T. A., Alenghat, T., Sonnenberg, G. F., et al. (2012). Commensal bacteria calibrate the activation threshold of innate antiviral immunity. *Immunity* 37, 158–170. doi: 10.1016/j.immuni.2012.04.011

Aguiar, M., Stollenwerk, N., and Halstead, S. B. (2016). The risks behind dengvaxia recommendation. *Lancet Infect. Dis.* 16, 882–883. doi: 10.1016/S1473-3099(16)30168-2

Alan, G. P. (1988). Clinical aspects of cytomegalovirus retinitis. *Rev. Infect. Dis.* 10, S515–S521. doi: 10.1093/clinids/10.Supplement_3.S515

Alcami, A., and Koszinowski, U. H. (2000). Viral mechanisms of immune evasion. *Trends Microbiol.* 8, 410–418. doi: 10.1016/S0966-842X(00)01830-8

Allen, S. J., Hamrah, P., Gate, D., Mott, K. R., Mantopoulos, D., Zheng, L., et al. (2011). The role of LAT in increased CD8+ T cell exhaustion in trigeminal ganglia of mice latently infected with herpes simplex virus 1. *J. Virol.* 85, 4184–4197. doi: 10.1128/jvi.02290-10

Arthur, C., and Louzis, C. (1988). A review of myxomatosis among rabbits in France. *Rev. sci. Tech. Off. Int. Epiz* 65, 937–976. doi: 10.20506/rst.7.4.385

Asabe, S., Wieland, S. F., Chattopadhyay, P. K., Roederer, M., Engle, R. E., Purcell, R. H., et al. (2009). The size of the viral inoculum contributes to the outcome of hepatitis B virus infection. *J. Virol.* 83, 9652–9662. doi: 10.1128/jvi.00867-09

Ashraf, U., Zhu, B., Ye, J., Wan, S., Nie, Y., Chen, Z., et al. (2016). MicroRNA-19b-3p modulates japanese encephalitis virus-mediated inflammation via targeting RNF11. *J. Virol.* 90, 4780–4795. doi: 10.1128/jvi.02586-15

Aslan, N., Watkin, L. B., Gil, A., Mishra, R., Clark, F. G., Welsh, R. M., et al. (2017). Severity of Acute infectious mononucleosis correlates with cross-reactive influenza CD8 T-Cell receptor repertoires. *MBio* 8:e1841-17. doi: 10.1128/mBio.01841-17

Atarashi, K., Tanoue, T., Shima, T., Imaoka, A., Kuwahara, T., Momose, Y., et al. (2011). Induction of colonic regulatory T cells by indigenous Clostridium species. *Science* 331, 337–341. doi: 10.1126/science.1198469

Baker, J. C. (1995). The clinical manifestations of bovine viral diarrhea infection. *Vet. Clin. North Am. Food Anim. Pract.* 11, 425–445. doi: 10.1016/S0749-0720(15)30460-6

Baldridge, M. T., Nice, T. J., McCune, B. T., Yokoyama, C. C., Kambal, A., Wheadon, M., et al. (2015). Commensal microbes and interferon-λ determine persistence of enteric murine norovirus infection. *Science* 347, 266–269. doi: 10.1126/science.1258025

Barber, D. L., Wherry, E. J., Masopust, D., Zhu, B., Allison, J. P., Sharpe, A. H., et al. (2006). Restoring function in exhausted CD8 T cells during chronic viral infection. *Nature* 439, 682–687. doi: 10.1038/nature04444

Bardina, S. V., Bunduc, P., Tripathi, S., Duehr, J., Frere, J. J., Brown, J. A., et al. (2017). Enhancement of Zika virus pathogenesis by preexisting antiflavivirus immunity. *Science* 356, 175–180. doi: 10.1126/science.aal4365

Barton, E. S., White, D. W., Cathelyn, J. S., Brett-McClellan, K. A., Engle, M., Diamond, M. S., et al. (2007). Herpesvirus latency confers symbiotic protection from bacterial infection. *Nature* 447, 326–329. doi: 10.1038/nature05762

Baxter, V. K., Glowinski, R., Braxton, A. M., Potter, M. C., Slusher, B. S., and Griffin, D. E. (2017). Glutamine antagonist-mediated immune suppression decreases pathology but delays virus clearance in mice during nonfatal alphavirus encephalomyelitis. *Virology* 508, 134–149. doi: 10.1016/j.virol.2017.05.013

Becher, P., Orlich, M., and Thiel, H.-J. (2001). RNA recombination between persisting pestivirus and a vaccine strain: generation of Cytopathogenic Virus and induction of lethal disease. *J. Virol.* 75, 6256–6264. doi: 10.1128/jvi.75.14.6256-6264.2001

Belkaid, Y., and Harrison, O. J. (2017). Homeostatic immunity and the microbiota. *Immunity* 46, 562–576. doi: 10.1016/j.immuni.2017.04.008

Belkaid, Y., and Rouse, B. T. (2005). Natural regulatory T cells in infectious disease. *Nat. Immunol.* 6, 353–360. doi: 10.1038/ni1181

Beura, L. K., Hamilton, S. E., Bi, K., Schenkel, J. M., Odumade, O. A., Casey, K. A., et al. (2016). Normalizing the environment recapitulates adult human immune traits in laboratory mice. *Nature* 532, 512–516. doi: 10.1038/nature17655

Bhela, S., Mulik, S., Reddy, P. B. J., Richardson, R. L., Gimenez, F., Rajasagi, N. K., et al. (2014). Critical role of microRNA-155 in herpes simplex encephalitis. *J. Immunol.* 192, 2734–2743. doi: 10.4049/jimmunol.1302326

Bhela, S., and Rouse, B. T. (2018). Are miRNAs critical determinants in herpes simplex virus pathogenesis? *Microbes Infect.* 20, 461–465. doi: 10.1016/j.micinf.2017.12.007

Bik, E. M., Eckburg, P. B., Gill, S. R., Nelson, K. E., Purdom, E. A., Francois, F., et al. (2006). Molecular analysis of the bacterial microbiota in the human stomach. *Proc. Natl. Acad. Sci. U.S.A.* 103, 732–737. doi: 10.1073/pnas.0506655103

Biron, C. A., Byron, K. S., and Sullivan, J. L. (1989). Severe herpesvirus infections in an adolescent without natural killer cells. *N. Engl. J. Med.* 320, 1731–1735. doi: 10.1056/NEJM198906293202605

Bouthry, E., Picone, O., Hamdi, G., Grangeot-Keros, L., Ayoubi, J. M., and Vauloup-Fellous, C. (2014). Rubella and pregnancy: diagnosis, management and outcomes. *Prenat. Diagn.* 34, 1246–1253. doi: 10.1002/pd.4467

Britt, W. J. (2018). Maternal immunity and the natural history of congenital human cytomegalovirus infection. *Viruses* 10:E405. doi: 10.3390/v10080405

Brodin, P., Jojic, V., Gao, T., Bhattacharya, S., Angel, C. J., Furman, D., et al. (2015). Variation in the human immune system is largely driven by non-heritable influences. *Cell* 160, 37–47. doi: 10.1016/j.cell.2014.12.020

Carding, S. R., Davis, N., and Hoyles, L. (2017). Review article: the human intestinal virome in health and disease. *Aliment. Pharmacol. Ther.* 46, 800–815. doi: 10.1111/apt.14280

Carneiro-Sampaio, M., and Coutinho, A. (2007). Immunity to microbes: lessons from primary immunodeficiencies. *Infec. Immun.* 75, 1545–1555. doi: 10.1128/iai.00787-06

Casrouge, A., Zhang, S.-Y., Eidenschenk, C., Jouanguy, E., Puel, A., Yang, K., et al. (2006). Herpes simplex virus encephalitis in human UNC-93B deficiency. *Science* 314, 308–312. doi: 10.1126/science.1128346

Cavanaugh, V. J., Guidotti, L. G., and Chisari, F. V. (1998). Inhibition of Hepatitis B virus replication during adenovirus and cytomegalovirus infections in transgenic mice. *J. Virol.* 72, 2630–2637.

Clarke, G. L., and Osburn, B. I. (1978). Transmissible congenital demyelinating encephalopathy of lambs. *Vet. Pathol.* 15, 68–82. doi: 10.1177/030098587801500109

Collins, P. L., and Graham, B. S. (2008). Viral and host factors in human respiratory syncytial virus pathogenesis. *J. Virol.* 82, 2040–2055. doi: 10.1128/jvi.01625-07

Dianzani, F. (1975). Viral interference and interferon. *Ric. Clin. Lab.* 5, 196–213.

Dropulic, L. K., and Cohen, J. I. (2011). Severe viral infections and primary immunodeficiencies. *Clin. Infect. Dis.* 53, 897–909. doi: 10.1093/cid/cir610

Faria, N. R., Azevedo, R., Kraemer, M. U. G., Souza, R., Cunha, M. S., Hill, S. C., et al. (2016). Zika virus in the Americas: early epidemiological and genetic findings. *Science* 352, 345–349. doi: 10.1126/science.aaf5036

Feldmann, H., and Geisbert, T. W. (2011). Ebola haemorrhagic fever. *Lancet* 377, 849–862. doi: 10.1016/S0140-6736(10)60667-8

Galván-Peña, S., and O'Neill, L. A. J. (2014). Metabolic reprograming in macrophage polarization. *Front. Immunol.* 5:420. doi: 10.3389/fimmu.2014.00420

García-Sastre, A. (2002). Mechanisms of inhibition of the host interferon α/β-mediated antiviral responses by viruses. *Microbes. Infect.* 4, 647–655. doi: 10.1016/S1286-4579(02)01583-6

Gil, A., Kenney, L. L., Mishra, R., Watkin, L. B., Aslan, N., and Selin, L. K. (2015). Vaccination and heterologous immunity: educating the immune system. *Trans R Soc. Trop. Med. Hyg.* 109, 62–69. doi: 10.1093/trstmh/tru198

Gill, J. R., Sheng, Z. M., Ely, S. F., Guinee, D. G., Beasley, M. B., Suh, J., et al. (2010). Pulmonary pathologic findings of fatal 2009 pandemic influenza A/H1N1 viral infections. *Arch. Pathol. Lab. Med.* 134, 235–243. doi: 10.1043/1543-2165-134.2.235

Glass, W. G., McDermott, D. H., Lim, J. K., Lekhong, S., Yu, S. F., Frank, W. A., et al. (2006). CCR5 deficiency increases risk of symptomatic West Nile virus infection. *J. Exp. Med.* 203, 35–40. doi: 10.1084/jem.20051970

Goka, E. A., Vallely, P. J., Mutton, K. J., and Klapper, P. E. (2015). Single, dual and multiple respiratory virus infections and risk of hospitalization and mortality. *Epidemiol. Infect.* 143, 37–47. doi: 10.1017/S0950268814000302

Gottwein, E., and Cullen, B. R. (2008). Viral and cellular microRNAs as determinants of viral pathogenesis and immunity. *Cell Host Microbe* 3, 375–387. doi: 10.1016/j.chom.2008.05.002

Griffin, D. E., Lin, W.-H., and Pan, C.-H. (2012). Measles virus, immune control, and persistence. *FEMS Microbiol. Rev.* 36, 649–662. doi: 10.1111/j.1574-6976.2012.00330.x

Gualdoni, G. A., Mayer, K. A., Kapsch, A.-M., Kreuzberg, K., Puck, A., Kienzl, P., et al. (2018). Rhinovirus induces an anabolic reprogramming in host cell metabolism essential for viral replication. *Proc. Natl. Acad. Sci. U.S.A.* 115, E7158–E7165. doi: 10.1073/pnas.1800525115

Guandalini, S., Pensabene, L., Zikri, M. A., Dias, J. A., Casali, L. G., Hoekstra, H., et al. (2000). Lactobacillus GG administered in oral rehydration solution to children with acute diarrhea: a multicenter European trial. *J. Pediatr. Gastroenterol. Nutr.* 30, 54–60. doi: 10.1097/00005176-200001000-00018

Halstead, S. B. (2007). Dengue. *Lancet* 370, 1644–1652. doi: 10.1016/S0140-6736(07)61687-0

Halstead, S. B., and O'Rourke, E. J. (1977). Antibody-enhanced dengue virus infection in primate leukocytes. *Nature* 265, 739–741. doi: 10.1038/265739a0

Honce, R. R., and Schultz-Cherry, S. (2019). Impact of obesity on influenza A virus pathogenesis, immune response, and evolution. *Front. Immunol.* 10:1071. doi: 10.3389/fimmu.2019.01071

Honda, K., and Littman, D. R. (2012). The microbiome in infectious disease and inflammation. *Annu. Rev. Immunol.* 30, 759–795. doi: 10.1146/annurev-immunol-020711-074937

Ichinohe, T., Pang, I. K., Kumamoto, Y., Peaper, D. R., Ho, J. H., Murray, T. S., et al. (2011). Microbiota regulates immune defense against respiratory tract influenza A virus infection. *Proc. Natl. Acad. Sci. U.S.A.* 108, 5354–5359. doi: 10.1073/pnas.1019378108

Janssen, H. L. A., Reesink, H. W., Lawitz, E. J., Zeuzem, S., Rodriguez-Torres, M., Patel, K., et al. (2013). Treatment of HCV Infection by Targeting MicroRNA. *N. Engl. J. Med.* 368, 1685–1694. doi: 10.1056/NEJMoa1209026

Jiménez de Oya, N., Esler, W. P., Huard, K., El-Kattan, A. F., Karamanlidis, G., Blázquez, A.-B., et al. (2019). Targeting host metabolism by inhibition of acetyl-Coenzyme A carboxylase reduces flavivirus infection in mouse models. *Emerg. Microbes. Infect.* 8, 624–636. doi: 10.1080/22221751.2019.1604084

John, A. R., and Canaday, D. H. (2017). Herpes zoster in the older adult. *Infect. Dis. Clin. North Am.* 31, 811–826. doi: 10.1016/j.idc.2017.07.016

Johnson, D. B., Chandra, S., and Sosman, J. A. (2018). Immune checkpoint inhibitor toxicity in 2018. *JAMA* 320, 1702–1703. doi: 10.1001/jama.2018.13995

Kamaladasa, A., Gomes, L., Jeewandara, C., Shyamali, N. L. A., Ogg, G. S., and Malavige, G. N. (2016). Lipopolysaccharide acts synergistically with the dengue virus to induce monocyte production of platelet activating factor and other inflammatory mediators. *Antiviral. Res.* 133, 183–190. doi: 10.1016/j.antiviral.2016.07.016

Kane, M., Case, L. K., Kopaskie, K., Kozlova, A., MacDearmid, C., Chervonsky, A. V., et al. (2011). Successful transmission of a retrovirus depends on the commensal microbiota. *Science* 334, 245–249. doi: 10.1126/science.1210718

Katze, M. G., He, Y., and Gale, M. (2002). Viruses and interferon: a fight for supremacy. *Nat. Rev. Immunol.* 2, 675–687. doi: 10.1038/nri888

Kerr, P. J. (2012). Myxomatosis in Australia and Europe: a model for emerging infectious diseases. *Antiviral. Res.* 93, 387–415. doi: 10.1016/j.antiviral.2012.01.009

Kumar, N., Sharma, S., Barua, S., Tripathi, B. N., and Rouse, B. T. (2018). Virological and immunological outcomes of coinfections. *Clin. Microbiol. Rev.* 31, e00111–e00117. doi: 10.1128/cmr.00111-17

Kuss, S. K., Best, G. T., Etheredge, C. A., Pruijssers, A. J., Frierson, J. M., Hooper, L. V., et al. (2011). Intestinal microbiota promote enteric virus replication and systemic pathogenesis. *Science* 334, 249–252. doi: 10.1126/science.1211057

Langerak, T., Mumtaz, N., Tolk, V. I., van Gorp, E. C. M., Martina, B. E., Rockx, B., et al. (2019). The possible role of cross-reactive dengue virus antibodies in Zika virus pathogenesis. *PLoS Pathog.* 15:e1007640. doi: 10.1371/journal.ppat.1007640

Langlois, R. A., and Legge, K. L. (2010). Plasmacytoid dendritic cells enhance mortality during lethal influenza infections by eliminating virus-specific CD8 T cells. *J. Immunol.* 184, 4440–4446. doi: 10.4049/jimmunol.0902984

Lazear, H. M., Govero, J., Smith, A. M., Platt, D. J., Fernandez, E., Miner, J. J., et al. (2016). A mouse model of Zika virus pathogenesis. *Cell Host Microbe* 19, 720–730. doi: 10.1016/j.chom.2016.03.010

Legge, K. L., and Braciale, T. J. (2005). Lymph node dendritic cells control CD8+ T Cell Responses through regulated FasL expression. *Immunity* 23, 649–659. doi: 10.1016/j.immuni.2005.11.006

Li, L., and Werler, M. M. (2010). Fruit and vegetable intake and risk of upper respiratory tract infection in pregnant women. *Public Health Nutr.* 13, 276–282. doi: 10.1017/S1368980009990590

Littaua, R., Kurane, I., and Ennis, F. A. (1990). Human IgG Fc receptor II mediates antibody-dependent enhancement of dengue virus infection. *J. Immunol.* 144, 3183–3186.

Loftus, R. M., and Finlay, D. K. (2016). Immunometabolism: cellular metabolism turns immune regulator. *J. Biol. Chem.* 291, 1–10. doi: 10.1074/jbc.R115.693903

Luis, A. D., Hayman, D. T., O'Shea, T. J., Cryan, P. M., Gilbert, A. T., Pulliam, J. R., et al. (2013). A comparison of bats and rodents as reservoirs of zoonotic viruses: are bats special? *Proc. Biol. Sci.* 280:20122753. doi: 10.1098/rspb.2012.2753

Mackaness, G. B. (1962). Cellular resistance to infection. *J. Exp. Med.* 116, 381–406. doi: 10.1084/jem.116.3.381

Malavige, G. N., and Ogg, G. S. (2017). Pathogenesis of vascular leak in dengue virus infection. *Immunology* 151, 261–269. doi: 10.1111/imm.12748

Malvy, D., McElroy, A. K., de Clerck, H., Gunther, S., and van Griensven, J. (2019). Ebola virus disease. *Lancet* 393, 936–948. doi: 10.1016/s0140-6736(18)33132-5

Manivannan, S., Baxter, V. K., Schultz, K. L. W., Slusher, B. S., and Griffin, D. E. (2016). protective effects of glutamine antagonist 6-Diazo-5-Oxo-l-norleucine in mice with alphavirus encephalomyelitis. *J. Virol.* 90, 9251–9262. doi: 10.1128/jvi.01045-16

Marcus, P. I., and Carver, D. H. (1967). Intrinsic interference: a new type of viral interference. *J. Virol.* 1, 334–343.

Masopust, D., Sivula, C. P., and Jameson, S. C. (2017). Of mice, dirty mice, and men: using mice to understand human immunology. *J. Immunol.* 199, 383–388. doi: 10.4049/jimmunol.1700453

Mathew, A., and Rothman, A. L. (2008). Understanding the contribution of cellular immunity to dengue disease pathogenesis. *Immunol. Rev.* 225, 300–313. doi: 10.1111/j.1600-065X.2008.00678.x

Maue, A. C., Yager, E. J., Swain, S. L., Woodland, D. L., Blackman, M. A., and Haynes, L. (2009). T-cell immunosenescence: lessons learned from mouse models of aging. *Trends Immunol.* 30, 301–305. doi: 10.1016/j.it.2009.04.007

McFarlane, A. J., McSorley, H. J., Davidson, D. J., Fitch, P. M., Errington, C., Mackenzie, K. J., et al. (2017). Enteric helminth-induced type I interferon signaling protects against pulmonary virus infection through interaction with the microbiota. *J. Allergy. Clin. Immunol.* 140, 1068.e6–1078.e6. doi: 10.1016/j.jaci.2017.01.016

Meng, X. J., Lindsay, D. S., and Sriranganathan, N. (2009). Wild boars as sources for infectious diseases in livestock and humans. *Philos. Trans. R Soc. Lond. B Biol. Sci.* 364, 2697–2707. doi: 10.1098/rstb.2009.0086

Milner, J. J., Rebeles, J., Dhungana, S., Stewart, D. A., Sumner, S. C., Meyers, M. H., et al. (2015). Obesity increases mortality and modulates the lung metabolome during pandemic H1N1 influenza virus infection in mice. *J. Immunol.* 194, 4846–4859. doi: 10.4049/jimmunol.1402295

Mueller, N. T., Bakacs, E., Combellick, J., Grigoryan, Z., and Dominguez-Bello, M. G. (2015). The infant microbiome development: mom matters. *Trends Mol. Med.* 21, 109–117. doi: 10.1016/j.molmed.2014.12.002

Mulik, S., Bhela, S., and Rouse, B. T. (2013). Potential Function of miRNAs in herpetic stromal keratitis potential function of miRNAs in herpetic stromal keratitis. *Invest. Ophthalmol. Vis. Sci.* 54, 563–573. doi: 10.1167/iovs.12-11094

Mulik, S., Xu, J., Reddy, P. B. J., Rajasagi, N. K., Gimenez, F., Sharma, S., et al. (2012). Role of miR-132 in angiogenesis after ocular infection with herpes simplex virus. *Am. J. Pathol.* 181, 525–534. doi: 10.1016/j.ajpath.2012.04.014

Neil, J. A., and Cadwell, K. (2018). The intestinal virome and immunity. *J. Immunol.* 201, 1615–1624. doi: 10.4049/jimmunol.1800631

Nikolay, B., Salje, H., Hossain, M. J., Khan, A., Sazzad, H. M. S., Rahman, M., et al. (2019). Transmission of Nipah Virus - 14 Years of investigations in bangladesh. *N. Engl. J. Med.* 380, 1804–1814. doi: 10.1056/NEJMoa1805376

Nikolich-Žugich, J. (2008). Ageing and life-long maintenance of T-cell subsets in the face of latent persistent infections. *Nat. Rev. Immunol.* 8, 512–522. doi: 10.1038/nri2318

Nolan, N., Halai, U.-A., Regunath, H., Smith, L., Rojas-Moreno, C., and Salzer, W. (2017). Primary cytomegalovirus infection in immunocompetent adults in the United States–A case series. *IDCases* 10, 123–126. doi: 10.1016/j.idcr.2017.10.008

Norman, J. M., Handley, S. A., and Virgin, H. W. (2014). Kingdom-agnostic metagenomics and the importance of complete characterization of enteric microbial communities. *Gastroenterology* 146, 1459–1469. doi: 10.1053/j.gastro.2014.02.001

O'Neill, L. A., Kishton, R. J., and Rathmell, J. (2016). A guide to immunometabolism for immunologists. *Nat. Rev. Immunol.* 16, 553–565. doi: 10.1038/nri.2016.70

O'Neill, L. A. J., and Hardie, D. G. (2013). Metabolism of inflammation limited by AMPK and pseudo-starvation. *Nature* 493, 346–355. doi: 10.1038/nature11862

Orange, J. S. (2002). Human natural killer cell deficiencies and susceptibility to infection. *Microbes Infect.* 4, 1545–1558. doi: 10.1016/S1286-4579(02)00038-2

Osborne, L. C., Monticelli, L. A., Nice, T. J., Sutherland, T. E., Siracusa, M. C., Hepworth, M. R., et al. (2014). Virus-helminth coinfection reveals a microbiota-independent mechanism of immunomodulation. *Science* 345, 578–582. doi: 10.1126/science.1256942

O'Sullivan, D., and Pearce, E. L. (2015). Targeting T cell metabolism for therapy. *Trends Immunol.* 36, 71–80. doi: 10.1016/j.it.2014.12.004

Otto, H. (2015). Jean Lindenmann: from viral interference to interferon and beyond (1924–2015). *J. Interferon. Cytokine Res.* 35, 239–241. doi: 10.1089/jir.2015.1500

Paich, H. A., Sheridan, P. A., Handy, J., Karlsson, E. A., Schultz-Cherry, S., Hudgens, M. G., et al. (2013). Overweight and obese adult humans have a defective cellular immune response to pandemic H1N1 influenza A virus. *Obesity* 21, 2377–2386. doi: 10.1002/oby.20383

Palefsky, J. (2009). Human papillomavirus-related disease in people with HIV. *Curr. Opin. HIV AIDS* 4, 52–56. doi: 10.1097/COH.0b013e32831a7246

Parrish, C. R., O'Connell, P. H., Evermann, J. F., and Carmichael, L. E. (1985). Natural variation of canine parvovirus. *Science* 230, 1046–1048. doi: 10.1126/science.4059921

Pearce, E. L., Poffenberger, M. C., Chang, C.-H., and Jones, R. G. (2013). Fueling immunity: insights into metabolism and lymphocyte function. *Science* 342:1242454. doi: 10.1126/science.1242454

Pearce-Duvet, J. M. (2006). The origin of human pathogens: evaluating the role of agriculture and domestic animals in the evolution of human disease. *Biol. Rev. Camb. Philos. Soc.* 81, 369–382. doi: 10.1017/S1464793106007020

Peiris, J. S., de Jong, M. D., and Guan, Y. (2007). Avian influenza virus (H5N1): a threat to human health. *Clin. Microbiol. Rev.* 20, 243–267. doi: 10.1128/CMR.00037-06

Pepose, J., Leib, D., Stuart, P., Easty, D., Pepose, J. S., Holland, G. N., et al. (1996). "Herpes simplex virus diseases: anterior segment of the eye," in *Ocular Infection and Immunity*, (St. Louis, MO: Mosby), 905–932.

Picarda, G., and Benedict, C. A. (2018). Cytomegalovirus: shape-Shifting the Immune System. *J. Immunol.* 200, 3881–3889. doi: 10.4049/jimmunol.1800171

Ploegh, H. L. (1998). Viral Strategies of Immune Evasion. *Science* 280, 248–253. doi: 10.1126/science.280.5361.248

Plotkin, S. A. (2019). Dengue Vaccine, A Double-Edged Sword. *J. Pediatric Infect. Dis. Soc.* doi: 10.1093/jpids/piy140 [Epub ahead of print].

Ramakrishna, C., Kujawski, M., Chu, H., Li, L., Mazmanian, S. K., and Cantin, E. M. (2019). *Bacteroides* fragilis polysaccharide A induces IL-10 secreting B and T cells that prevent viral encephalitis. *Nat. Commun.* 10:2153. doi: 10.1038/s41467-019-09884-6

Reese, T. A., Bi, K., Kambal, A., Filali-Mouhim, A., Beura, L. K., Burger, M. C., et al. (2016). Sequential Infection with common pathogens promotes human-like immune gene expression and altered vaccine response. *Cell Host Microbe* 19, 713–719. doi: 10.1016/j.chom.2016.04.003

Reese, T. A., Wakeman, B. S., Choi, H. S., Hufford, M. M., Huang, S. C., Zhang, X., et al. (2014). Helminth infection reactivates latent γ-herpesvirus via cytokine competition at a viral promoter. *Science* 345, 573–577. doi: 10.1126/science.1254517

Ressel, S., Rosca, A., Gordon, K., and Buck, A. H. (2019). Extracellular RNA in viral-host interactions: thinking outside the cell. *Wiley Interdiscip. Rev. RNA* 10, e1535. doi: 10.1002/wrna.1535

Rezaee, S. A. R., Cunningham, C., Davison, A. J., and Blackbourn, D. J. (2006). Kaposi's sarcoma-associated herpesvirus immune modulation: an overview. *J. Gen. Virol.* 87, 1781–1804. doi: 10.1099/vir.0.81919-0

Rezende, R. M., and Weiner, H. L. (2017). History and mechanisms of oral tolerance. *Semin. Immunol.* 30, 3–11. doi: 10.1016/j.smim.2017.07.004

Robinson, C. M., Jesudhasan, P. R., and Pfeiffer, J. K. (2014). Bacterial lipopolysaccharide binding enhances virion stability and promotes environmental fitness of an enteric virus. *Cell Host Microbe* 15, 36–46. doi: 10.1016/j.chom.2013.12.004

Rochell, S., Alexander, L., Rocha, G., Van Alstine, W., Boyd, R., Pettigrew, J., et al. (2015). Effects of dietary soybean meal concentration on growth and immune response of pigs infected with porcine reproductive and respiratory syndrome virus. *J. Anim. Sci.* 93, 2987–2997. doi: 10.2527/jas.2014-8462

Rouse, B. T., and Sehrawat, S. (2010). Immunity and immunopathology to viruses: what decides the outcome? *Nat. Rev. Immunol.* 10, 514–526. doi: 10.1038/nri2802

Roy, S., Coulon, P.-G., Srivastava, R., Vahed, H., Kim, G. J., Walia, S. S., et al. (2018). Blockade of LAG-3 immune checkpoint combined with therapeutic vaccination restore the function of tissue-resident anti-viral CD8+ T Cells and protect against recurrent ocular herpes simplex infection and disease. *Front. Immunol.* 9:2922. doi: 10.3389/fimmu.2018.02922

Ruffner, M. A., Sullivan, K. E., and Henrickson, S. E. (2017). Recurrent and sustained viral infections in primary immunodeficiencies. *Front. Immunol.* 8:665. doi: 10.3389/fimmu.2017.00665

Saeidi, A., Zandi, K., Cheok, Y. Y., Saeidi, H., Wong, W. F., Lee, C. Y. Q., et al. (2018). T-Cell exhaustion in chronic infections: reversing the state of exhaustion and reinvigorating optimal protective immune responses. *Front. Immunol.* 9:2569. doi: 10.3389/fimmu.2018.02569

Salzberger, B., Hartmann, P., Hanses, F., Uyanik, B., Cornely, O. A., Wöhrmann, A., et al. (2005). Incidence and prognosis of CMV Disease in HIV–Infected patients before and after introduction of combination antiretroviral therapy. *Infection* 33, 345–349. doi: 10.1007/s15010-005-5050-z

Samuel, C. E. (2001). Antiviral actions of interferons. *Clin. Microbiol. Rev.* 14, 778–809. doi: 10.1128/cmr.14.4.778-809.2001

Schleiss, M. R. (2018). Congenital cytomegalovirus: impact on child health. *Contemp. Pediatr.* 35, 16–24.

Sehrawat, S., Kumar, D., and Rouse, B. T. (2018). Herpesviruses: harmonious pathogens but relevant cofactors in other diseases? *Front. Cell Infect. Microbiol.* 8:177. doi: 10.3389/fcimb.2018.00177

Selin, L. K., Varga, S. M., Wong, I. C., and Welsh, R. M. (1998). Protective heterologous antiviral immunity and enhanced immunopathogenesis mediated by memory T cell populations. *J. Exp. Med.* 188, 1705–1715. doi: 10.1084/jem.188.9.1705

Sepkowitz, K. A. (2001). AIDS–the first 20 years. *N. Engl. J. Med.* 344, 1764–1772. doi: 10.1056/nejm200106073442306

Sharp, P. M., and Hahn, B. H. (2011). Origins of HIV and the AIDS pandemic. *Cold Spring Harb. Perspect. Med.* 1, a006841–a006841. doi: 10.1101/cshperspect.a006841

Simmons, A., and Nash, A. A. (1984). Zosteriform spread of herpes simplex virus as a model of recrudescence and its use to investigate the role of immune cells in prevention of recurrent disease. *J. Virol.* 52, 816–821.

Smith, P. M., Howitt, M. R., Panikov, N., Michaud, M., Gallini, C. A., Bohlooly-y, M., et al. (2013). The microbial metabolites, short-chain fatty acids, regulate colonic Treg cell homeostasis. *Science* 341, 569–573. doi: 10.1126/science.1241165

Souquette, A., and Thomas, P. G. (2018). Past Life and future effects-how heterologous infections alter immunity to influenza viruses. *Front. Immunol.* 9:1071. doi: 10.3389/fimmu.2018.01071

Spite, M., Clària, J., and Serhan, C. N. (2014). Resolvins, Specialized Proresolving Lipid Mediators, and Their Potential Roles in Metabolic Diseases. *Cell Metab.* 19, 21–36. doi: 10.1016/j.cmet.2013.10.006

Stettler, K., Beltramello, M., Espinosa, D. A., Graham, V., Cassotta, A., Bianchi, S., et al. (2016). Specificity, cross-reactivity, and function of antibodies elicited by Zika virus infection. *Science* 353, 823–826. doi: 10.1126/science.aaf8505

Tahamtan, A., Teymoori-Rad, M., Nakstad, B., and Salimi, V. (2018). Anti-inflammatory MicroRNAs and their potential for inflammatory diseases treatment. *Front. Immunol.* 9:1377. doi: 10.3389/fimmu.2018.01377

Taubenberger, J. K., and Morens, D. M. (2006). 1918 influenza: the mother of all pandemics. *Emerg. Infect. Dis.* 12, 15–22. doi: 10.3201/eid1201.050979

Tebit, D. M., Ndembi, N., Weinberg, A., and Quiñones-Mateu, M. E. (2012). Mucosal transmission of human immunodeficiency virus. *Curr. HIV Res.* 10, 3–8. doi: 10.2174/157016212799304689

Thackray, L. B., Handley, S. A., Gorman, M. J., Poddar, S., Bagadia, P., Briseño, C. G., et al. (2018). Oral antibiotic treatment of mice exacerbates the disease severity of multiple flavivirus infections. *Cell Rep.* 22, 3440.e6–3453.e6. doi: 10.1016/j.celrep.2018.03.001

Thépaut, M., Grandjean, T., Hober, D., Lobert, P.-E., Bortolotti, P., Faure, K., et al. (2015). Protective role of murine norovirus against *Pseudomonas aeruginosa* acute pneumonia. *Vet. Res.* 46:91. doi: 10.1186/s13567-015-0239-3

Thomas, S., Izard, J., Walsh, E., Batich, K., Chongsathidkiet, P., Clarke, G., et al. (2017). The host microbiome regulates and maintains human health: a primer and perspective for non-microbiologists. *Cancer Res.* 77, 1783–1812. doi: 10.1158/0008-5472.can-16-2929

Thounaojam, M. C., Kundu, K., Kaushik, D. K., Swaroop, S., Mahadevan, A., Shankar, S. K., et al. (2014). MicroRNA 155 regulates Japanese encephalitis virus-induced inflammatory response by targeting src homology 2-containing inositol phosphatase 1. *J. Virol.* 88, 4798–4810. doi: 10.1128/jvi.02979-13

Tomov, V. T., Osborne, L. C., Dolfi, D. V., Sonnenberg, G. F., Monticelli, L. A., Mansfield, K., et al. (2013). Persistent enteric murine norovirus infection is associated with functionally suboptimal virus-specific CD8 T cell responses. *J. Virol.* 87, 7015–7031. doi: 10.1128/jvi.03389-12

Trompette, A., Gollwitzer, E. S., Pattaroni, C., Lopez-Mejia, I. C., Riva, E., Pernot, J., et al. (2018). Dietary fiber confers protection against flu by shaping Ly6c-patrolling monocyte hematopoiesis and CD8+ T cell metabolism. *Immunity* 48, 992.e8–1005.e8. doi: 10.1016/j.immuni.2018.04.022

Uchiyama, R., Chassaing, B., Zhang, B., and Gewirtz, A. T. (2014). Antibiotic treatment suppresses rotavirus infection and enhances specific humoral immunity. *J. Infect. Dis.* 210, 171–182. doi: 10.1093/infdis/jiu037

Van de Perre, P., Segondy, M., Foulongne, V., Ouedraogo, A., Konate, I., Huraux, J. M., et al. (2008). Herpes simplex virus and HIV-1: deciphering viral synergy. *Lancet Infect. Dis.* 8, 490–497. doi: 10.1016/s1473-3099(08)70181-6

Vann, V. R., and Atherton, S. S. (1991). Neural spread of herpes simplex virus after anterior chamber inoculation. *Invest. Ophthalmol. Vis. Sci.* 32, 2462–2472.

Varanasi, S. K., Donohoe, D., Jaggi, U., and Rouse, B. T. (2017). Manipulating glucose metabolism during different stages of viral pathogenesis can have either detrimental or beneficial effects. *J. Immunol.* 199, 1748–1761. doi: 10.4049/jimmunol.1700472

Varyukhina, S., Freitas, M., Bardin, S., Robillard, E., Tavan, E., Sapin, C., et al. (2012). Glycan-modifying bacteria-derived soluble factors from *Bacteroides* thetaiotaomicron and Lactobacillus casei inhibit rotavirus infection in human intestinal cells. *Microbes Infect.* 14, 273–278. doi: 10.1016/j.micinf.2011.10.007

Virgin, H. W., Wherry, E. J., and Ahmed, R. (2009). Redefining chronic viral infection. *Cell* 138, 30–50. doi: 10.1016/j.cell.2009.06.036

Walter, J., Seeh, C., Fey, K., Bleul, U., and Osterrieder, N. (2013). Clinical observations and management of a severe equine herpesvirus type 1 outbreak with abortion and encephalomyelitis. *Acta Vet. Scand.* 55:19. doi: 10.1186/1751-0147-55-19

Wang, A., Huen, S. C., Luan, H. H., Yu, S., Zhang, C., Gallezot, J. D., et al. (2016). Opposing effects of fasting metabolism on tissue tolerance in bacterial and viral inflammation. *Cell* 151:e1512. doi: 10.1016/j.cell.2016.07.026

Wang, J., Li, F., Sun, R., Gao, X., Wei, H., Li, L. J., et al. (2013). Bacterial colonization dampens influenza-mediated acute lung injury via induction of M2 alveolar macrophages. *Nat. Commun.* 4:2106. doi: 10.1038/ncomms3106

Wang, K., Hoshino, Y., Dowdell, K., Bosch-Marce, M., Myers, T. G., Sarmiento, M., et al. (2017). Glutamine supplementation suppresses herpes simplex virus reactivation. *J. Clin. Invest.* 127, 2626–2630. doi: 10.1172/jci88990

Welsh, R. M., Che, J. W., Brehm, M. A., and Selin, L. K. (2010). Heterologous immunity between viruses. *Immunol. Rev.* 235, 244–266. doi: 10.1111/j.0105-2896.2010.00897.x

Wherry, E. J. (2011). T cell exhaustion. *Nat. Immunol.* 12, 492–499. doi: 10.1038/ni.2035

Wilkin, T. J., and Gulick, R. M. (2012). CCR5 antagonism in HIV infection: current concepts and future opportunities. *Annu. Rev. Med.* 63, 81–93. doi: 10.1146/annurev-med-052010-145454

Zhang, B., Chassaing, B., Shi, Z., Uchiyama, R., Zhang, Z., Denning, T. L., et al. (2014). Prevention and cure of rotavirus infection via TLR5/NLRC4–mediated production of IL-22 and IL-18. *Science* 346, 861–865. doi: 10.1126/science.1256999

Zhu, B., Ye, J., Nie, Y., Ashraf, U., Zohaib, A., Duan, X., et al. (2015). MicroRNA-15b modulates japanese encephalitis virus–mediated inflammation via targeting RNF125. *J. Immunol.* 195, 2251–2262. doi: 10.4049/jimmunol.1500370

Conflict of Interest: The authors declare that the research was conducted in the absence of any commercial or financial relationships that could be construed as a potential conflict of interest.

Copyright © 2019 Sumbria, Berber and Rouse. This is an open-access article distributed under the terms of the Creative Commons Attribution License (CC BY). The use, distribution or reproduction in other forums is permitted, provided the original author(s) and the copyright owner(s) are credited and that the original publication in this journal is cited, in accordance with accepted academic practice. No use, distribution or reproduction is permitted which does not comply with these terms.

frontiers in Microbiology

ORIGINAL RESEARCH
published: 04 October 2019
doi: 10.3389/fmicb.2019.02272

Isolation and Identification of Porcine Epidemic Diarrhea Virus and Its Effect on Host Natural Immune Response

*Shaoju Qian[1], Weida Zhang[1], Xiangchao Jia[1], Zhijian Sun[1], Yang Zhang[1], Yuncai Xiao[1,2,3] and Zili Li[1,2,3]**

[1]State Key Laboratory of Agricultural Microbiology, Department of Preventive Veterinary Medicine, College of Veterinary Medicine, Huazhong Agricultural University, Wuhan, China, [2]Key Laboratory of Preventive Veterinary Medicine in Hubei Province, The Cooperative Innovation Center for Sustainable Pig Production, Wuhan, China, [3]Key Laboratory of Development of Veterinary Diagnostic Products, Ministry of Agriculture of the People's Republic of China, Wuhan, China

Porcine epidemic diarrhea (PED) is a highly infectious intestinal disease caused by porcine epidemic diarrhea virus (PEDV). A PEDV strain was isolated from the piglet intestinal tract in Vero cells in Jiangsu Province, designated as the JS-A strain. PEDV was identified as the isolated virus by cytopathology, immunofluorescence assay, western blotting, transmission electron microscopy, and sequence analysis. The full-length genome of the JS-A isolate and the S gene were systematically analyzed, indicating that PEDV JS-A belongs to the G2a subtype, which is closely related to the prevalent PEDV in many countries and different from many current vaccines. Animal regression tests showed that piglets that are orally infected with the virus continue to develop diarrhea with yellowish and unpleasant odors. Further, piglets showed reduced food consumption and weight loss in the challenged group, while there were no abnormalities in the control group. In addition, Toll-like receptors (TLRs), RIG-I, and the downstream medium gene in the intestinal mucosa of newborn pigs infected with PEDV JS-A strain were studied. The neonatal Fc receptor (FcRn) was the only IgG transport receptor and protected IgG from degradation. Therefore, PEDV JS-A infection might inhibit FcRn expression by down-regulating TLRs and downstream signaling molecules. Taken together, isolation of the JS-A variant contributes to evolutionary analysis of the diarrhea virus. Further, the experimental infection model lays a foundation for further research related to vaccine development and the antiviral natural immune response of infected piglets, which helps us to better understand PEDV pathogenesis and immune mechanism.

Keywords: porcine epidemic diarrhea virus, neonatal fc receptor, Toll-like receptor, NF-κB, neutralizing antibody

OPEN ACCESS

Edited by:
Zhengli Shi,
Chinese Academy of Sciences, China

Reviewed by:
Yulan Liu,
Wuhan Polytechnic University, China
Daniel C. Pevear,
VenatoRx Pharmaceuticals, United States

****Correspondence:***
Zili Li
lizili@mail.hzau.edu.cn

Specialty section:
This article was submitted to Virology, a section of the journal Frontiers in Microbiology

Received: *28 June 2019*
Accepted: *18 September 2019*
Published: *04 October 2019*

Citation:
Qian S, Zhang W, Jia X, Sun Z, Zhang Y, Xiao Y and Li Z (2019) Isolation and Identification of Porcine Epidemic Diarrhea Virus and Its Effect on Host Natural Immune Response. Front. Microbiol. 10:2272. doi: 10.3389/fmicb.2019.02272

INTRODUCTION

Porcine epidemic diarrhea virus (PEDV) causes severe enteritis, watery diarrhea, vomiting, dehydration, and even death in suckling piglets. In the 1970s, the first PEDV outbreak occurred in Europe (Wood, 1977). Subsequently, the virus affected many countries such as the Czech Republic, Belgium, Hungary, South Korea, Italy, and Thailand (Song and Park, 2012). Since 2010, a

large-scale outbreak of PEDV has occurred in swine herds around China. Then, the emergence of PEDV occurred in Ohio in the United States in 2013, which spread throughout the United States (Huang et al., 2013). Currently, due to lack of effective vaccines, isolation and identification of new PEDV strains to develop appropriate vaccines for prevention and control of the disease have garnered great interest.

PEDV belongs to the genus Alphacoronavirus within the Coronaviridae family (Brian and Baric, 2005). Its genome size is about 28 kb, and it possesses at least seven open reading frames (ORF): ORF1a, ORF1b, spike (S), ORF3, envelope (E), membrane (M), and nucleocapsid (N). PEDV S protein plays a critical role in inducing neutralization antibodies, specific receptor binding, and membrane fusion. In addition, the S gene has shown a high degree of genetic variability. Therefore, it is often used to analyze PEDV genetic variation. According to phylogenetic analysis of S genes, PEDV strains have been divided into two clusters: genome I subtype and genome II subtype (Lee et al., 2010; Li et al., 2013; Chen et al., 2014). Further, several variant PEDV strains have been identified, which were characterized by insertion and deletion (INDEL) in labeled (S) genes named S-INDEL PEDV. The pathogenesis of PEDV is strain specific. Studies on its pathogenesis in piglets suggest that the PEDV non-S-INDEL strain has stronger pathogenicity compared to the PEDV S-INDEL strain (Chen et al., 2014; Yamamoto et al., 2015; Wang et al., 2016). PEDV JS-A belongs to the non-S-INDEL strain.

Upon viral infection, the host innate immune response is the first line of defense (Moynagh, 2005). NF-κB regulates expression of numerous components of the immune system, which is thought to be the hallmark of most infection, including coronaviruses (DeDiego et al., 2014). RNA viruses interact with pattern-recognition receptors (PRRs), including Toll-like receptors (TLRs) and RIG-I-like receptors (RLRs). Several *in vitro* studies have been conducted to clarify the role of PEDV in innate immune responses at the cellular level. Several other studies have determined that PEDV nucleocapsid protein (N) inhibits the production of type I and III interferons (IFNs) (Ding et al., 2014; Cao et al., 2015a; Shan et al., 2018). PEDV non-S-INDEL infection inhibits the induction of proinflammatory cytokines and IFN-I by down-regulating TLRs and downstream signaling molecules (Temeeyasen et al., 2018).

Neonatal Fc receptor (FcRn) has been fully characterized to transfer maternal IgG to the fetus or newborn and protect IgG from degradation. In addition to IgG, FcRn binds to albumin, which regulates liver damage (Pyzik et al., 2017). Transmissible gastroenteritis virus (TGEV) infection up-regulates pFcRn expression and activates the NF-κB signaling pathway in IPEC-J2 cells (Guo et al., 2016a). In our study, the pathogenicity of JS-A in 5-day-old piglets was studied by clinical evaluation, quantitative analysis of virus copy number in the feces, histology, and immunohistochemistry. We also studied the gene regulation of TLRs, RIG-I, and downstream signaling pathways in the intestinal mucosa of pigs newly infected with JS-A. The purpose of this study was to investigate the genomic characteristics and pathogenicity of JS-A and the expression of TLRs, RIG-I, NF-κB, and FcRn in the intestinal mucosa of infected piglets.

MATERIALS AND METHODS

Clinical Samples and Virus Isolation

Fecal samples and intestinal contents from piglets suffering from severe watery diarrhea were collected in a pig farm from Jiangsu Province. PEDV-positive samples were detected by real-time polymerase chain reaction (RT-PCR), based on the N gene, as previously described (Lee et al., 2015). Clinical samples were homogenized in DMEM (HyClone, Logan, UT, USA), centrifuged at 4,000 rpm/min, and filtered through a 0.22-μm filter (Millipore, MA).

Vero (ATCC, CCL-81) cells were obtained from the China Center for Type Culture Collection (Wuhan, China) and were cultured in DMEM containing 10% fetal bovine serum (FBS, Gibco, Waltham, MA, USA). Vero cells were incubated with 1 mL of filtered inoculum for 2 h. After virus adsorption, cells were maintained in DMEM containing 8 μg/mL trypsin (Gibco, USA) and antibiotics. After 2 h, the cells were maintained in DMEM containing 8 μg/mL trypsin at 37°C in 5% CO_2 until a cytopathic effect became visible. The supernatant was collected after the cytopathic effect was observed. The virus was cloned and purified by plaque purification three times and tested by $TCID_{50}$.

Immunofluorescence Assay

At 24 h post-infection, cells were fixed with 4% paraformaldehyde in PBS for 15 min and permeabilized with 0.1% Triton X-100 for 10 min. Subsequently, cells were incubated with PBST containing 5% skim milk for 1 h, followed by primary (PEDV polyclonal antibody; prepared in our laboratory) and secondary [fluorescein isothiocyanate (FITC)-labeled goat anti-rabbit IgG; ABclonal, China] antibodies for 1 h. Finally, the samples were stained with DAPI for 15 min and examined using a fluorescence microscope (Olympus IX73, Japan).

Western Blot

At 24 h post-infection, cells lysates were prepared for 12% SDS-PAGE, and proteins were electroblotted onto a polyvinylidene difluoride membrane (Bio-Rad, USA). PEDV-N polyclonal antibody (prepared in our laboratory) was used as a primary antibody, followed by HRP-conjugated goat anti-rabbit IgG or anti-mouse IgG (ABclonal, China) as secondary antibodies. Proteins were visualized as described previously (Guo et al., 2016b).

Electron Microscopy

PEDV-infected Vero cells were examined by electron microscopy (EM), following previously described procedures (Chen et al., 2014). These samples were negatively stained with 2% sodium phosphotungstic acid (pH 6.8) and examined using a Hitachi Model H-7650 TEM (Hitachi H-7000FA, Japan).

Phylogenetic Analysis

Total RNAs were extracted using TRIzol® reagent (Invitrogen, Carlsbad, CA, USA), and total RNA was reverse transcribed into cDNA using reverse transcriptase (TaKaRa, Osaka, Japan). The whole genome of JS-A was sequenced using 25 pairs of primers previously reported in **Table 1** by Chen (Chen et al., 2012).

Phylogenetic trees with 25 strains (**Table 2**) full-length genome and S-nucleotide sequences were generated using the distance-based adjacency method in MEGA7.

Inoculation of Piglets With Porcine Epidemic Diarrhea Virus Strain JS-A

This study was implemented according to the Guide of the Scientific Ethics Committee of Huazhong Agricultural University (HZAUSW-2018-011). Twelve 5-day-old piglets were purchased from a commercial pig farm, both PEDV RNA and antibody negative, and were randomly divided into two groups (6 piglets/group) in two separate rooms. Piglets were fed a mixture of liquid milk replacer and had free access to water. After 1 day of adaptation, piglets in the challenged group received 3×10^5 $TCID_{50}$ PEDV JS-A orally, while piglets in the control group received 3 mL maintenance medium orally. The piglets were observed daily for signs of vomiting, diarrhea, lethargy, weight, and body temperature until the end of the experiment. Intestinal segments, including the jejunum and ileum, were collected after euthanasia of three of six piglets in each group, selected at random, at 4 dpi for histopathological and immunohistochemical examinations using the method described previously (Lee et al., 2010). At the end of the experiment (21 dpi), the remaining piglets were euthanized. Expressions of mRNA for TLRs, NF-κB

TABLE 1 | Primers for amplifications of the PEDV genomic fragments by RT-PCR.

Name	Sequence (5′ to 3′)	Position in PEDV genome	Size (bp)
PP1F	GTGGAATTTCATTAGGTTTG	123-142	1,380
PP1R	AAGCTTACGTATGAACCAAG	1502-1483	
PP2F	TGCTGGTCATGTTGTTGTTG	1421-1440	1,488
PP2R	TAGAAAGCGAAGCCATCAAC	2908-2889	
PP3F	ATTGAAACTTCTTTTGTGGA	2817-2836	1,451
PP3R	TTCTCATTTGCAGCATTAAC	4267-4248	
PP4F	CTGCTCTCTCCTTGGATTCT	3940-3959	1,478
PP4R	AGTATGGTCTAGCATGTGGA	5417-5398	
PP5F	TGTCACAGACAACAAACCTG	5300-5319	1,487
PP5R	CATCACCAAAGACATCAAAA	6786-6767	
PP6F	ATTGGTAATGTGATGCCTTT	6609-6628	1,323
PP6R	AAAGCTTAGTGCAAAGAAAG	7931-7912	
PP7F	TTTCAAAGGTTAAGAAATTCT	7861-7881	1,408
PP7R	CTCACAGTGGGTGGTGTGTAT	9268-9248	
PP8F	CGTTATACACACCACCCACT	9244-9263	1,304
PP8R	GGTAACAACAAAGCACACAA	10547-10528	
PP9F	CAGAGCATTTTGATTACCAT	10465-10484	1,470
PP9R	CAACTATGCCATCTCCTTCT	11934-11915	
PP10F	GGTGTGAGCGTATTGTTAAG	11842-11861	1,266
PP10R	AATGCATAGACACGATGAAT	13107-13088	
PP11F	TTTGATTAAGGTAGGTGCTT	13012-13031	1,397
PP11R	CAACACCATCAATAAGGTTC	14408-14389	
PP12F	TATGGTGGTTGGGACAATAT	14363-14382	946
PP12R	CTTCCAAAAGTGTGACAGAA	15308-15289	
PP13F	ATTGCTTGAACGTTATGTGT	15142-15161	1,676
PP13R	CATTACCCTTGCAAAAGATC	16817-16798	
PP14F	TTAAGCCTGATGTCTTCTTG	16674-16693	1,691
PP14R	CCTACAGCGAGTATCAAAAC	18364-18345	
PP15F	TGGACATGTATCCAGAATTT	18312-18331	1,455
PP15R	GCATGGAATAACCACACTTC	19766-19747	
PP16F	AAAATGTGGAGGTGGATGTT	19670-19689	1,362
PP16R	GGCCCAATGTTTTATTATCG	21031-21012	
S-1F	TAAGTTGCTAGTGCGTAAT	20572-20590	1,692
S-1R	GTCAACACAGAAAGAACTA	22263-22245	
S-2F	TGAGTCATGAACAGCCAA	22003-22020	1,511
S-2R	CTGGTTGCGCTGTAGAA	23513-23497	
S-3F	GCGTCTCTCATAGGTGGT	23491-23508	1,310
S-3R	GTCCAAGAAACATCACTG	24801-24784	
ORF3-EF	CGTGCAGTGATGTTTCTTGGAC	24780-24801	895
ORF3-ER	TTATACGTCAATAACAGTACT	25674-25654	
EMF	CTTCACTTGTCACCGGTTGT	25557-25576	1,097
EMR	CCTCAGTACGAGTCCTATAAC	26549-26529	
MF	GGCGAATTCAATATGTCTAACGGTTC	25670-25695	675
MR	CGCGTCGACCCATAAAGTTTCTGTT	26368-26362	
NF	GGATCCATGGCTTCTGTCAGCTTT	26107-26218	1,332
NR	GACGTCACATTGTTTAATTTCCTGTACC		
3F	GGAAAAGAAGAACAAGCGT	27355-27373	580
3R	ATCGGTCACCAGTATTTTTTTTTTTTTT		

and FcRn on piglet intestinal mucosa in each group were detected by RT-qPCR at 4 and 21 dpi.

Real-Time Polymerase Chain Reaction

Viral RNA of PEDV in piglet feces or intestinal mucosa was detected as previously described (Subramaniam et al., 2018). The specific porcine primers are referenced in previous publications in **Table 3** (Guo et al., 2016a; Temeeyasen et al., 2018) were synthesized by the GenScript Company (Nanjing, China). The N gene amplified from the PEDV JS-A strain was cloned into pMD18-T (Takara, Dalian). The known plasmid concentrations were serially diluted 10-fold to generate a standard

TABLE 2 | Comparison of nucleotide sequences of the JS-A isolate with other strains.

Strains	Countries	Accession	Strains	Countries	Accession
JS-A	China	MH748550	MEX/124/2014	USA	KJ645700
LZC	China	EF185992	MN	USA	KF468752
AJ1102	China	JX188454	PC21A	USA	KR078299
AH2012	China	KC210145	USA/Colorado/2013	USA	KF272920
GD-B	China	JX088695	CH/JX-2/2013	China	KJ526096
CH-S	China	JN547228	CH/JX-1/2013	China	KF760557
IA2	USA	KF468754	CH/HNAY/2015	China	KR809885
SM98	Korea	GU937797	LC	China	JX489155
Attenuated DR13	Korea	JQ023162	FL2013	China	KP765609
CV777	Switzerland	AF353511	DR13	Korea	JQ023162
YN144	China	KT021232	JS2008	China	KC109141
JS-HZ2012	China	KC210147	Belgorod/dom/2008	Russia	MF577027
GD-1	China	JX647847			

TABLE 3 | Primers used for RT-qPCR analysis of genes expression of pig intestinal mucosa.

Gene name	Primer sequence (5′–3′)	Amplicon length (bp)	Accession number
GAPDH-F	GGAAAGGCCATCACCATCTT	85	XM_021091114.1
GAPDH-R	CATGGTCGTGAAGACACCAG		
FcRn-F	GGCGACGAGCACCACTACTG	88	HQ026019.1
FcRn-R	AGCCGACCATGATTCCAACC		
TLR2-F	GAGTCTGCCACAACTCAAAGA	68	XM_005653576.3
TLR2-R	CAGAACTGACAACATGGGTAGAA		
TLR3-F	GCGGTCCTGTTCAGTTTCT	72	KT735340.1
TLR3-R	AAGGCATCTGCTGGGATTT		
TLR4-F	AACTGCAGGTGCTGGATTTAT	74	AB078418.1
TLR4-R	CCGTCAGTATCAAGGTGGAAAG		
TLR7-F	CCCAGGTCCTCGAATCATTAC	77	DQ647699.2
TLR7-R	CATTAAGAGGCAAGGAGGAAGA		
TLR8-F	CTTTGATGATGACGCTGCTTTC	77	KF019635.1
TLR8-R	GGTGTGTCACTCCTGCTATTC		
TLR9-F	CCTCACACATCTCTCACTCAAG	82	KC860785.1
TLR9-R	GGTGACAATGTGGTTGTAGGA		
RIG-I-F	GAGCCCTTGTGGATGCTTTA	91	KC011279.1
RIG-I-R	GGGTCATCCCTATGTTCTGATTC		
TRIF-F	CTCCGGTGCAGTCAAACA	91	KC969185.1
TRIF-R	GGTAGTGTGTGCTGGTTTCT		
MyD88A-F	GGCAGCTGGAACAGACCAA	41	EU056736.1
MyD88A-R	GGCAGGACATCTCGGTCAGA		
MyD88B-F	TGCAGGTGCCCATCAGAAG	64	EU056737.1
MyD88B-R	TGATGAACCGCAGGATGCT		
NF-κB1(p105)-F	GAGGTGCATCTGACGTATTC	118	NM_001048232.1
NF-κB1(p105)-R	CACATCTCCTGTCACTGCAT		
NF-κB1(p50)-F	AAGCACGGAACTGTAGACAC	107	KC316024.1
NF-κB1(p50)-R	TCTGTGGTTTCTGTGACTTTCC		
RELA-F	ACATGGACTTCTCAGCCCTTCTGA	285	CN155798.1
RELA-R	CCGAAGACATCACCCAAAGATGCT		
TRAF6-F	GGGAACGATACGCCTTACAA	156	NM_001105286.1
TRAF6-R	CTCTGTCTTAGGGCGTCC		

curve in each plate. The amount of PEDV viral RNA in the test sample was calculated based on the cycle curve threshold (Ct) value of the standard curve. Expression levels of genes were calculated relative to the expression of GAPDH using the delta-delta cycles to threshold ($2^{-\Delta\Delta Ct}$) method.

IgG/IgA Enzyme-Linked Immunosorbent Assay and Neutralization Assay

The PEDV-specific IgG/IgA antibodies were measured in serum samples by ELISA as previously described (Subramaniam et al., 2018). Polystyrene 96-well microplates were coated with purified PEDV N diluted in PBS containing Tween-20 (PBST) and incubated overnight at 4°C, followed by the removal of the coating solution. The plates were blocked with 100 μL 5% skimmed milk in PBST and incubated at 37°C for 30 min. After which, 100 μL of serum samples (diluted 1:200) per well was added and incubated at 37°C for 1 h, respectively. After washing the plates, HRP-conjugated goat anti-swine IgG or goat anti-swine IgA was incubated for 1 h. The plates were washed and incubated with TMB solution (Sigma-Aldrich) for 10 min. The absorbance was measured at 450 nm with a termination solution (2 M H_2SO_4).

PEDV isolate JS-A was used to determine the presence of neutralization (PEDV nucleocapsid protein) in serum samples as previously described (Oh et al., 2014). Vero cells were grown to 90% confluence in the 96-well plates. Further, 200 $TCID_{50}$ of JS-A virus was diluted in DMEM in a 50 μL volume. Subsequently, 50 μL of 2-fold serial dilutions of inactivated serum samples was added to the diluted virus and incubated at 37°C for 1 h. The mixture was inoculated into Vero cells and incubated at 37°C for 1 h. After removing the mixture and washing the plates, the virus in the maintenance medium was incubated in a 37°C and 5% CO_2 incubator for 2 days. The neutralization titer was calculated as the reciprocal of the highest serum dilution that neutralizes PEDV infection.

Statistical Analysis

Data were analyzed as mean ± SEM. Differences among groups were performed by one-way ANOVA using GraphPad Prism software. The significance level for all analyses was set as $^{*}p < 0.05$, $^{**}p < 0.01$ and $^{***}p < 0.001$.

RESULTS

Virus Isolation and Characterization

The treated samples were inoculated onto Vero cells. Cytopathic effects, including cell fusion, syncytium, and detachment, were observed at 36 h post-infection (hpi). No cytopathic effects were observed in the control wells (**Figure 1A**). To confirm the occurrence of virus multiplication, the infectivity of the JS-A strain (purified by plaque in Vero cells) was assessed by western blot (WB) and IFA using the PEDV N protein polyclonal antibody. IFA results demonstrated a green signal in infected Vero cells, but not in the mock-infected cells (**Figure 1A**). Western blot analysis also detected N protein in PEDV-infected Vero cells (**Figure 1B**). According to the structural analysis of the infected cells by transmission electron microscopy, PEDV virus particles were round and showed obvious radial protrusion (**Figure 1C**), which is typical of coronaviruses. The plaque-purified virus was titrated to $10^{5.625}$ $TCID_{50}$/mL.

Phylogenetic Tree Analysis of JS-A Genomic Sequence

The JS-A genome was sequenced and deposited in GenBank (MH748550). To further understand the evolutionary relationship between JS-A and other PEDV strains, a phylogenetic tree was constructed based on its genome and the S gene sequence (**Figure 2**). These two phylogenetic trees all indicated that PEDV was mainly divided into two groups: group I consists mainly of classical strains and vaccine strains, while group II consists mainly of variant strains of China and mutant strains of the United States and South Korea. PEDV JS-A shared homology with the GD-1 strain of 99.9%, belong to non-S INDEL strain. Homology with the classic strain CV777, LZC, and SM98 was 96.8, 96.5, and 96.6%, respectively. The results showed that the S gene had 15 base insertions at 20806–20817 nt and 21,046–21,048 nt, and nine base deletions at 21,114–21,119 nt and 24,225–24,227 nt. It is currently a prevalent species compared to the classical strain CV777.

Clinical Observations in Pigs Challenged With JS-A

To explore the pathogenicity of PEDV JS-A in piglets, we observed their clinical symptoms. All piglets from the control group were in great health throughout the study without observation of clinical symptoms. However, three of six piglets in the challenged group developed diarrhea at 1 dpi, and the additional three piglets developed various degrees of diarrhea, vomiting, lethargy, and anorexia at 2–6 dpi. Drowsiness, anorexia, and watery diarrhea developed most severely at 3–6 dpi, and piglets gradually recovered thereafter (**Figure 3A**). No significant temperature change was observed between the two groups (**Figure 3B**). The infected group showed significant weight loss, while the uninfected piglets experienced weight gain (**Figure 3C**). Despite watery diarrhea with vomiting, drowsiness, and anorexia, no deaths occurred during the study period. These results indicate that JS-A is pathogenic to newborn pigs.

Fecal Shedding, Virus Distribution, and Neutralizing Antibody Against JS-A

To determine the fecal viral shedding, we attempted to detect viral RNA in rectal swab samples from 1 to 21 dpi by RT-PCR. Viral RNA was detected in 6/6 rectal swab samples collected from 1 to 14 dpi in the challenged group. PEDV RNA copies reached the peak of 10^4–10^7 copies/mL in the homogenate rectal swab supernatant at 2–7 dpi, and the PEDV RNA was detected up to 14 dpi (**Figure 4A**). Notably, PEDV RNA was not detected in piglet samples from negative controls throughout the study.

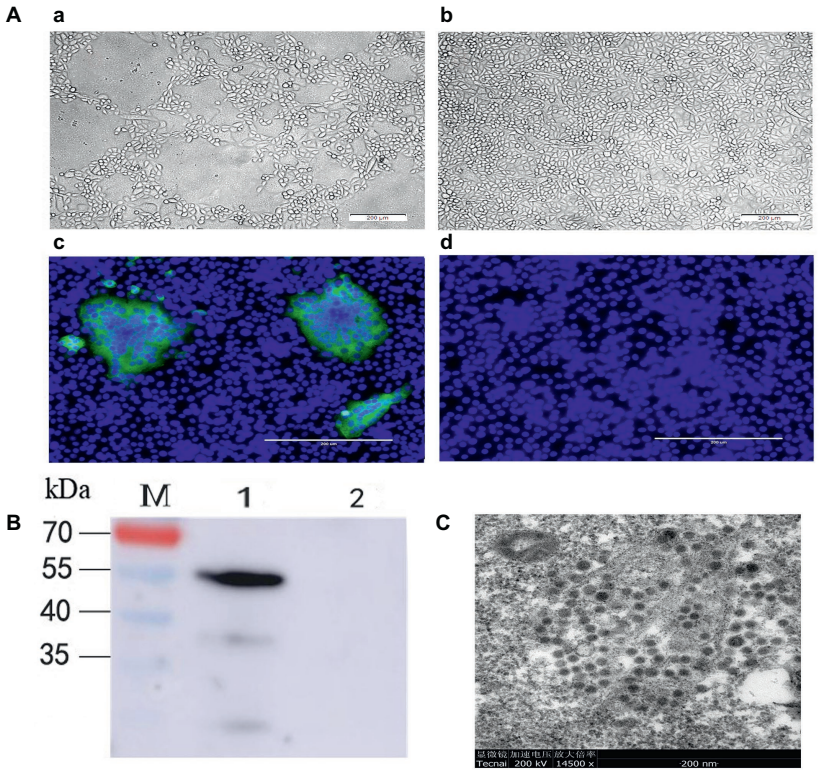

FIGURE 1 | The isolated PEDV strain JS-A was identified. **(A)** Simulated infected Vero cells of 24 hpi **(a)** and negative control Vero cells at 24 hpi **(b)**. PEDV-infected **(c)** or negative control Vero cells **(d)** were examined by IFA at 24 hpi using polyclonal antibodies against PEDV N protein. **(B)** PEDV-infected or negative control Vero cells were subjected to analysis at 24 hpi with polyclonal antibodies against PEDV N protein by western blot; **(C)** electron microscopic images of purified PEDV particles were analyzed.

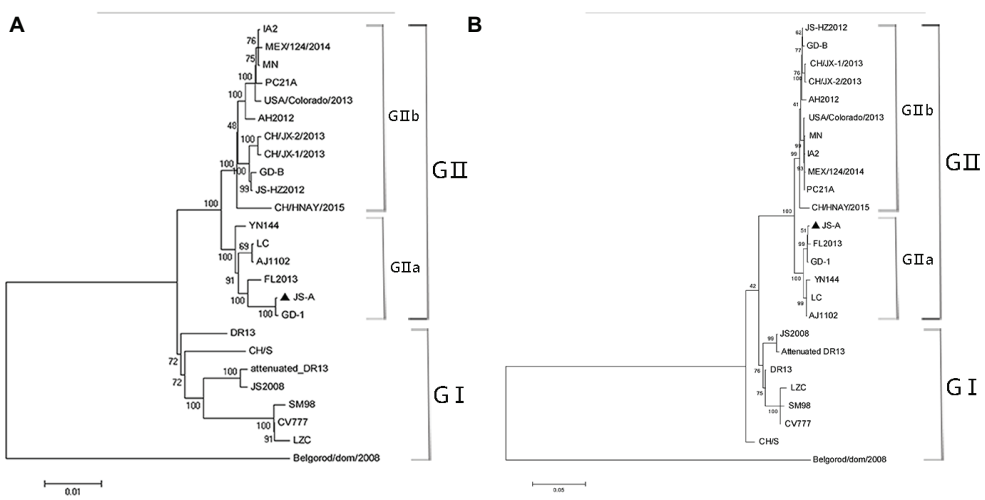

FIGURE 2 | Phylogenetic analysis was performed using the nucleotide sequences of the complete genome **(A)** and S genes **(B)** of the PEDV strain from the GenBank database. JS-A is represented by a triangle. The phylogenetic tree was constructed by the adjacency method in MEGA 7 (http://www.megasoftware.net). Bootstrap analysis was performed using 1,000 iterations and the bootstrap value was indicated on each branch. Scale bar indicates nucleotide substitution at each site.

To determine when PEDV IgG, IgA, and neutralizing antibodies were detected in infected piglets, PEDV IgG, IgA, and neutralizing antibodies were measured in serum samples collected at 7, 14, and 21 dpi. The OD values of serum IgG and IgA in piglets inoculated with PEDV gradually increased at 7, 14, and 21 dpi, and the antibody titer gradually increased and peaked at

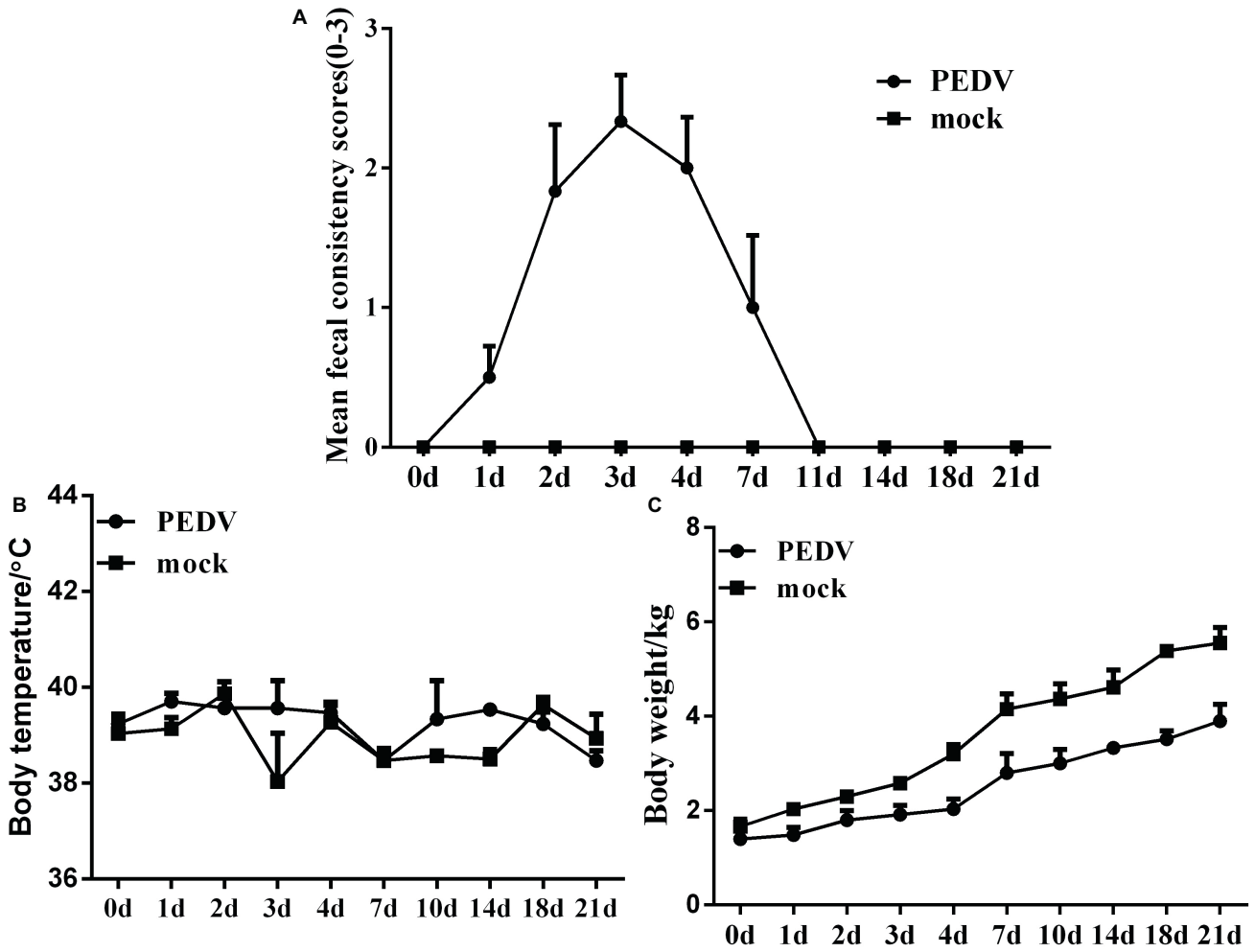

FIGURE 3 | Pathogenicity analysis of PEDV JS-A. **(A)** Diarrhea of piglets in different groups. The severity of diarrhea was scored based on visual examination; 0 = normal and no diarrhea; 1 = mild and fluidic diarrhea; 2 = severe watery diarrhea; with scores of 1 or more considered diarrheic. **(B)** The average body temperature changes in each group. **(C)** The changes in average body weight of each group.

21 dpi (**Figures 4B,C**). Neutralizing antibodies in collected serum samples were detected, and it was found that the antibody titer gradually increased and reached a peak at 21 dpi, as high 1:255 (**Figure 4D**). PEDV IgG, IgA, and neutralizing antibodies were not observed in the serum of control piglets.

Gross Pathology and Histopathology

In order to ascertain changes in piglets infected with JS-A about the overall histology and pathology, three of six piglets in each group were randomly selected for autopsy at 4 dpi. The typical gross lesion seen in infected pigs is the accumulation of large amounts of yellow watery contents in the small intestine, resulting in thin and transparent intestinal wall and gas expansion due to atrophy of intestinal villi (**Figure 5A**). No other injuries were observed in any organs of the control pigs (**Figure 5B**). Histopathological examination showed necrosis of small intestinal epithelial cells, atrophy of intestinal villi and vacuolation in infected pigs compared with the control group (**Figures 5C,D**), but the intestines of the negative control were normal (**Figures 5E,F**). Consistent with histopathological findings, PEDV antigen was found in the cytoplasm of infected atrophic intestinal villous epithelial cells (**Figures 5G,H**), and no PEDV IHC antigen was found in uninfected piglets (**Figures 5I,J**).

Porcine Epidemic Diarrhea Virus JS-A Infection Suppresses Neonatal Fc Receptor Expression Through Down-Regulation of Toll-Like Receptors and Downstream Signaling Molecules

At 3 dpi, PEDV JS-A infection downregulated TLR3, TLR4, TLR7, TLR8, and TLR9 expression, as compared to the control group. Further, the corresponding downstream molecules TRIF, MyD88 (subunits A and B), and TRAF6 were significantly downregulated, eventually leading to down-regulation of the NF-κB pathway ($p < 0.05$) (**Figures 6A,B**). However, at 21 dpi, TLR4, TLR7, and corresponding downstream MyD88 (subunits A and B) were up-regulated, further up-regulating NF-κB. We found that FcRn expression was down-regulated

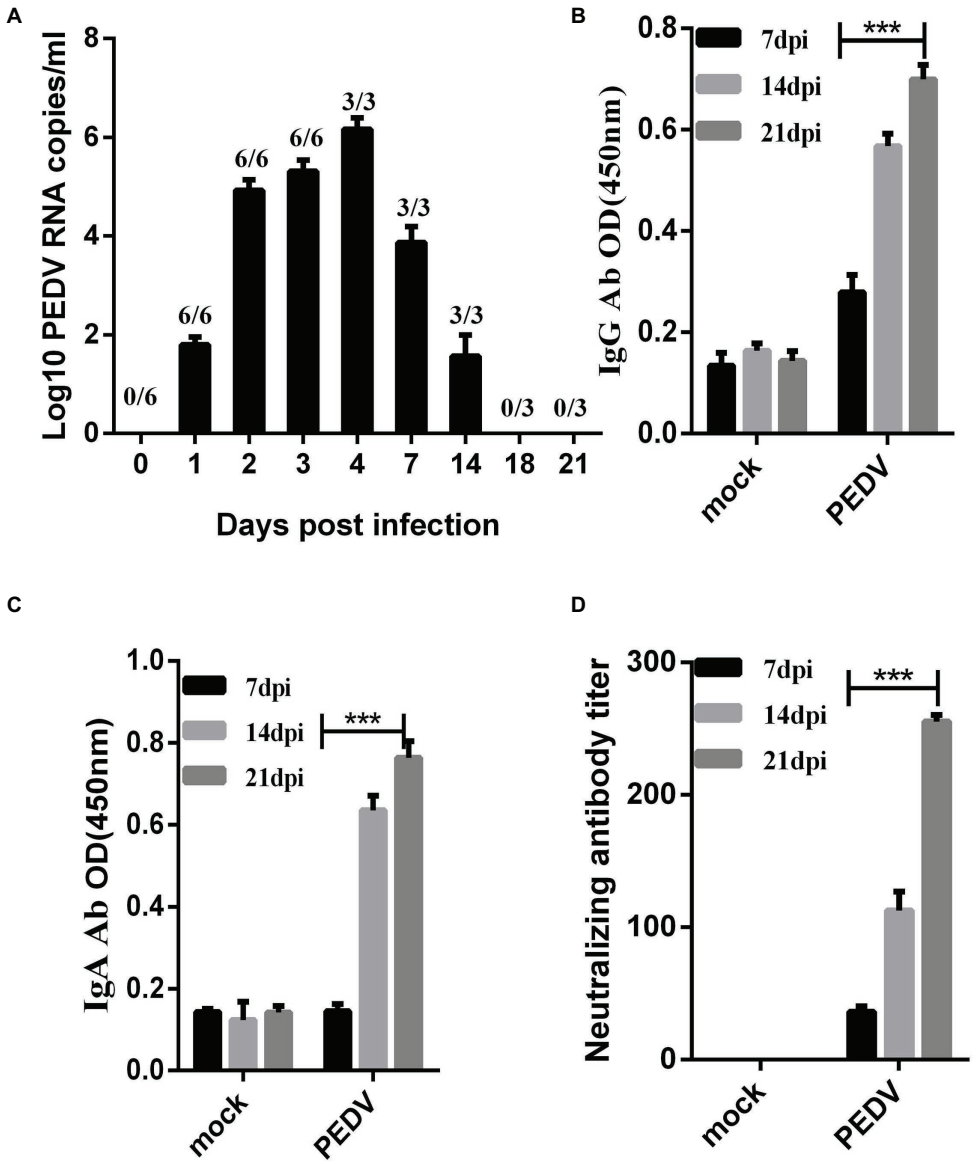

FIGURE 4 | Fecal detoxification and humoral immune response in piglets challenged with PEDV-JS-A. **(A)** Fecal virus shedding in PEDV-challenged piglets. **(B)** Detection of PEDV IgG in serum samples from PEDV-challenged piglets. **(C)** PEDV IgA detection in serum samples from PEDV-challenged piglets. **(D)** Detection of neutralizing antibodies in serum samples of immunized piglets. (Data were analyzed as mean ± SEM) (n = 3 for the JS-A group, and statistically significant for the unchallenged group by Student's t test. $^{***}p < 0.001$).

at 4 dpi, yet up-regulated at 21 dpi, and the regulation of FcRn was closely related to regulation of NF-κB (**Figures 6C,D**).

DISCUSSION

Despite the use of commercially inactivated vaccines, the characteristics of PED infection and its epidemiology are highly significant, with morbidity and mortality rates approaching 100% in piglets (Pan et al., 2012). In 2013, a sudden PED outbreak occurred in the United States and spread quickly throughout the country, as well as Canada and Mexico, resulting in high mortality of newborn piglets and serious financial problems (Mole, 2013; Stevenson et al., 2013; Vlasova et al., 2014).

In this study, the isolated JS-A strain was more similar to the PEDV GD-1 strain, which was distant from classical strains such as CV777, LZC, and SM98, suggesting that PEDV is continuously evolving, with variation in the epidemiological process. Therefore, vaccines made from classical strains cannot provide effective protection, which is consistent with current findings. The PEDV S gene evolutionary tree and homology

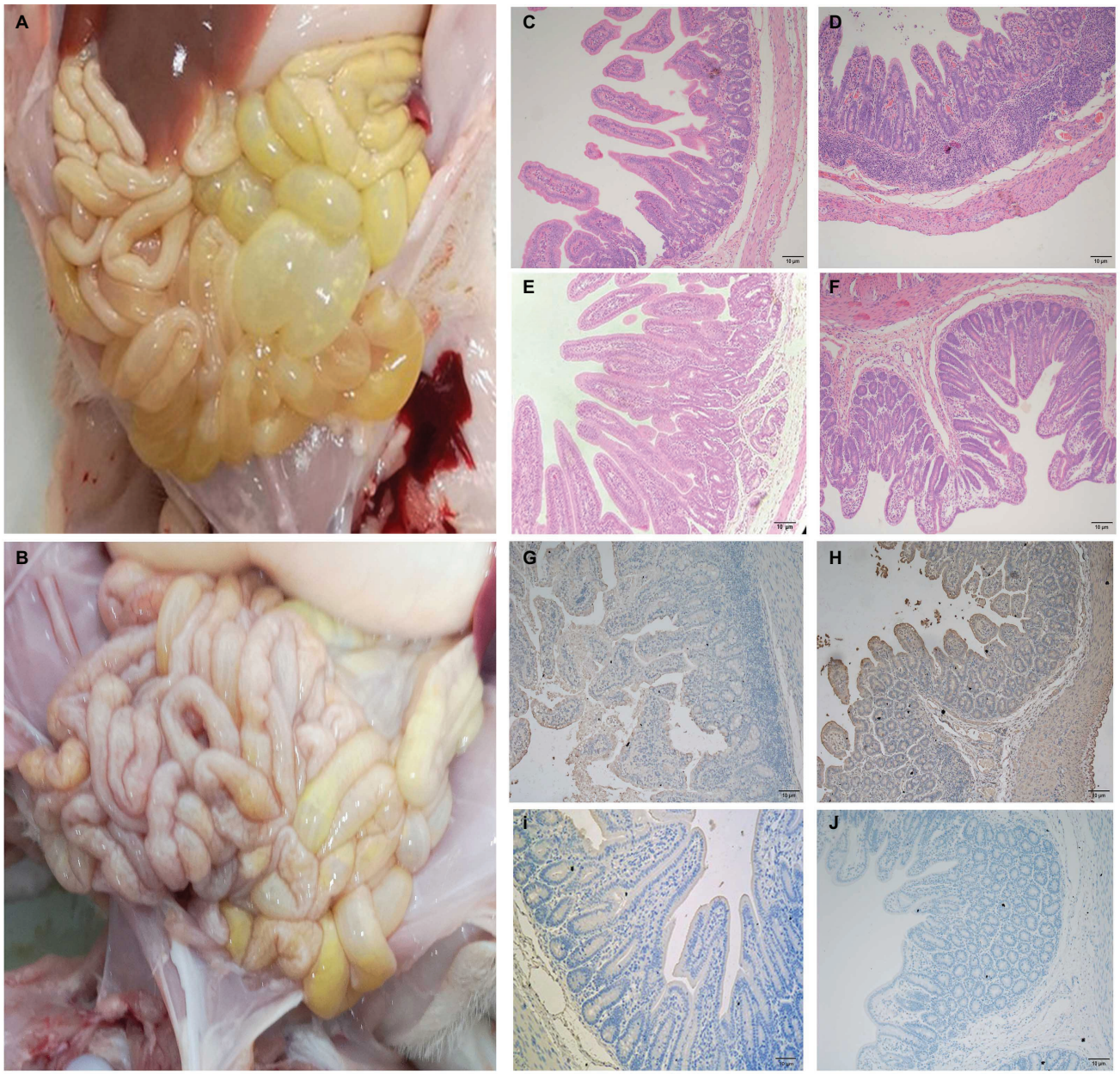

FIGURE 5 | The intestinal microscopic lesions of piglets. **(A)** Macroscopic damage of piglets challenged with PEDV at 4 dpi. **(B)** Macroscopic view of 4 dpi negative control piglets. **(C,D)** H&E stained jejunal **(C)** and ileal **(D)** tissue sections of piglets challenged with PEDV. **(E,F)** H&E stained jejunal **(E)** and ileal **(F)** tissue sections of negative control pigs. **(G,H)** PEDV challenge immunohistochemical staining of jejunal **(G)** and ileal **(H)** tissue sections of piglets. Immunohistochemically stained jejunal **(I)** and ileal **(J)** tissue sections of **(I,J)** negative control pigs.

were further analyzed. The phylogenetic tree was divided into two evolutionary branches, namely G1 and G2 groups. The G1 group contained classic strains such as CV777, DR13, and SM98. The G2 group has been the most prevalent strain since 2010. JS-A, which has been separated this time, also belongs to G2a. This shows that JS-A is indeed the dominant strain in current pig farms. Induced stronger primary and anamnestic immune responses. The JS-A strain belongs to the non-S-INDEL, which is highly pathogenic.

To study the pathogenicity of PEDV JS-A, 5-day-old piglets were inoculated orally. As expected, vomiting and severe diarrhea were observed in piglets from 1 to 6 dpi, indicating that JS-A was pathogenic to newborn piglets. Fecal swabs were collected from piglets infected with PEDV, and viral fecal shedding was detected by real-time PCR. PEDV RNA was detected from 1 to 14 dpi, suggesting that PEDV infection *via* fecal-oral contamination may be the main transmission route of piglet diarrhea in pig farms. Previously, it has been reported that coronavirus HKU15

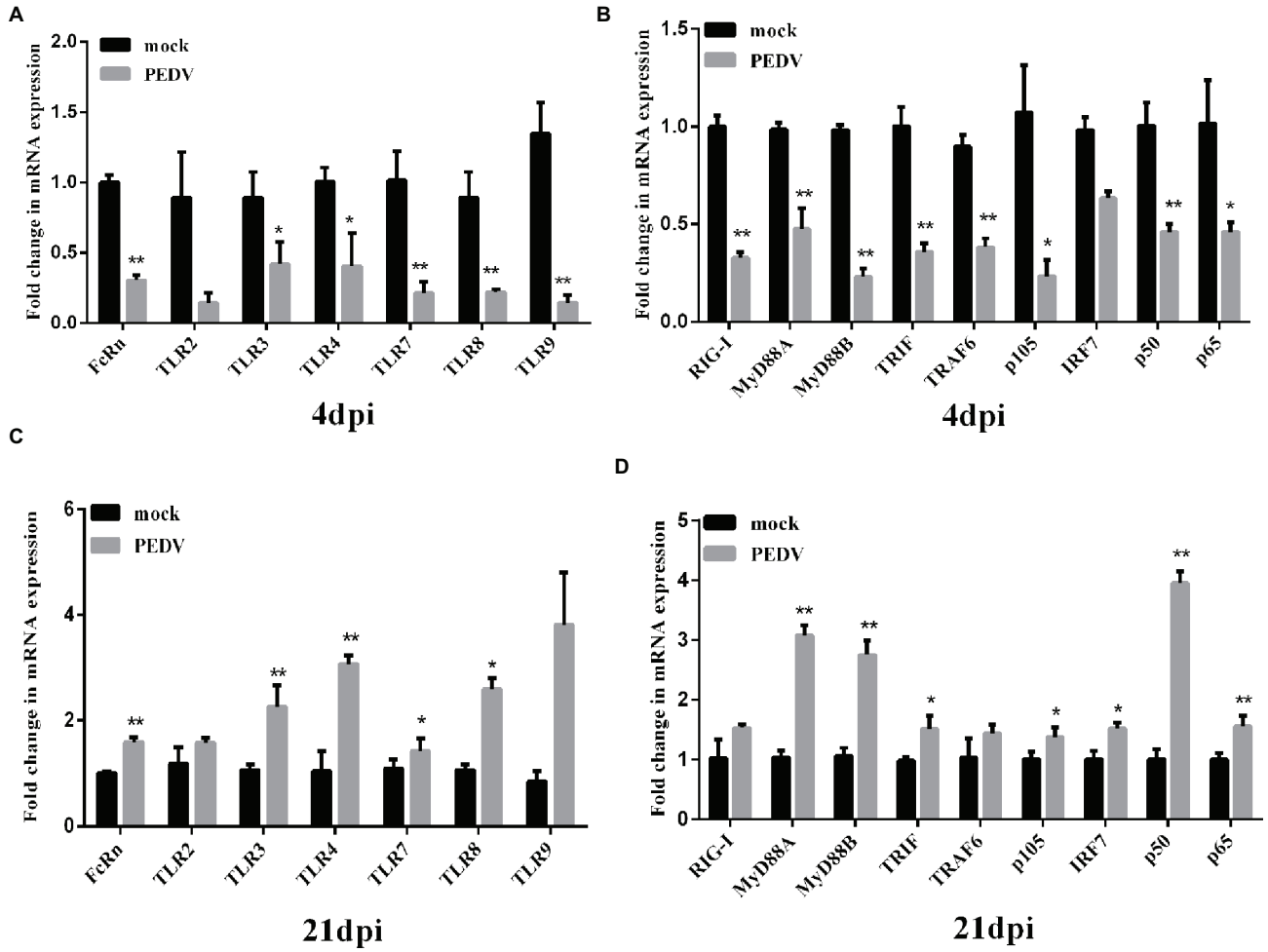

FIGURE 6 | Changes in FcRn, TLRs and its downstream-signaling molecules mRNA expression on intestinal mucosa of piglets induced by PEDV JS-A at 4 and 21 dpi. **(A,C)** The mRNA expressions of FcRn, TLR2, TLR3, TLR4, TLR7, TLR8, TLR9 at the intestinal mucosa from piglets after infection with JS-A at 4dpi **(A)** and 21dpi **(C)** by RT-qPCR. **(B,D)** The mRNA expressions of RIG-I, TRIF, MyD88A, MyD88B, IRF7, TRAF6, NF-kB1 (p105), NF-kB1 (p50), RelA (p65) at the intestinal mucosa from piglets after infection with JS-A at 4dpi **(B)** and 21dpi **(D)** by RT-qPCR. All samples were tested in triplicate and the results are expressed as fold changes relative to the control animals Data are presented as means ± SEM. Significant difference between PEDV JS-A and control group are expressed with their p. $^{*}p < 0.05$; $^{**}p < 0.01$.

may be transmitted *via* the respiratory route, in addition to fecal–oral transmission (Woo et al., 2017; Li et al., 2018). Notably, we only observed microlesions in the jejunum and ileum of piglets infected with JS-A, but PEDV infection did not cause death of newborn piglets, despite drowsiness, anorexia, and watery diarrhea in these animals. These results suggest that PEDV JS-A has a milder toxicity and may be a weak strain. At the same time, there were slight differences in body weight and no significant differences in body temperature during infection.

We also tested the serum-specific IgG, IgA, and neutralizing antibody levels in piglets at 7, 14, and 21 dpi and found that the antibody levels of IgG and IgA gradually increased with time. Further, the serum IgA level was higher than that of IgG. PEDV-challenged protection during the first infection was positively correlated with IgA and IgG antibodies in intestinal-associated lymphoid tissues and blood (de Arriba et al., 2002), indicating that VN antibody can be detected in piglets inoculated with PEDV JS-A, and the titer of VN antibody gradually increases and remains high at the end of the experiment (Chen et al., 2016). In our study, PEDV VN antibody was detected as early as 7 dpi in piglets infected with PEDV. The antibody titer of VN increased and remained high up to 21 dpi, at which point all pigs in the challenged group recovered completely.

In vitro studies have proven to be highly dependent on strains, and cell types cannot be used to assess innate immune responses against low virulence strains (Kint et al., 2015). PEDV has been reported to induce innate immune responses *in vivo*. However, few studies have been reported. Therefore, in this study, *in vivo* models were used to further observe the natural TLRs and signaling pathway homeostasis regulated by the gut microbiota. Natural immunity is the first line of host defense against a variety of pathogenic infections (Li et al., 2013).

Furthermore, *in vitro* PEDV N and E protein mediated NF-κB activation and had effects on cell growth and ER stress, upregulating IL-8 expression (Xu et al., 2013; Cao et al., 2015b). However, PEDV non-S-INDEL N and nsp1 protein inhibited NF-κB activation (Ding et al., 2014; Zhang et al., 2017). MyD88 is an essential component of the innate immune response to SARS-CoV infection in mice *in vivo* (Totura et al., 2015). The pathogenesis of PEDV is strain specific. The lack of TRAF6 leads to enhanced viral replication and a significant reduction in the production of type I IFN after infection with RNA virus. *In vivo*, PEDV non-S-INDEL down-regulates the NF-κB signaling pathway through negative regulation of TLR4, TLR7, TLR8, and TLR9, resulting in the final attenuation of MyD88, TRIF, and TRAF6 gene expression (Temeeyasen et al., 2018).

The IgA plays a major role in the mucosal anti-PEDV infection immunity. However, recent studies have found that IgG also plays an important role against pathogen infection in mucosal sites, while the neonatal Fc receptor (FcRn) is the only IgG transport receptor (Tsuruta et al., 2012). Down-regulation of FcRn and pIgR has been shown in the tracheal mucosa of SHIV/SIV-infected rhesus macaques (Wang and Yang, 2016; Li et al., 2017). Further, transmissible gastroenteritis virus infection up-regulates FcRn through TLR3 and RIG-I in porcine intestinal epithelial cells (unpublished results). PEDV JS-A can down-regulate NF-κB signaling pathway by inhibiting mRNA expression of TLR3, TLR4, TLR7, TLR8, and TLR9 at 4 dpi, resulting in the final attenuation of FcRn gene expression. In contrast, FcRn expression was up-regulated through TLR3, TLR4, TLR8 at 21 dpi.

In conclusion, we successfully isolated the PEDV JS-A strain, and phylogenetic analysis indicated that the major parent of JS-A strain was identified as strain FL2013 or GD-1. The study results showed that JS-A was a variant PEDV strain with weak pathology to piglets, compared to other emerging strains. High levels of serum IgG, IgA, and VN antibodies were also detected in the sera of infected piglets at 21 dpi. In addition, inoculation of piglets with JS-A suppressed FcRn expression *via* TLR, RIG-I, and NF-κB mRNA expressions at 4 dpi, yet induced FcRn expression at 21 dpi in infected intestinal mucosa. All results showed that innate immunity was suppressed at 4 dpi and that innate immunity might have been activated by the virus at 21 dpi. The down-regulated expression of FcRn resulted in its incapacity to transport antibodies, providing another insight into the immune escape strategy of PEDV.

DATA AVAILABILITY STATEMENT

The datasets generated for this study can be found in the PEDV JS-A (GenBank: MH748550.1).

ETHICS STATEMENT

The animal study was reviewed and approved by the Scientific Ethic Committee of Huazhong Agricultural University; Huazhong Agricultural University. Written informed consent was obtained from the owners for the participation of their animals in this study.

AUTHOR CONTRIBUTIONS

SQ and ZL wrote the paper and conceived and initiated the study. SQ, WZ, and XJ extracted the data set. SQ, WZ, XJ, ZS, YZ, and YX performed the analysis. All authors reviewed the manuscript.

FUNDING

This work was supported by the National Natural Science Foundation of China (31572500 to ZL).

REFERENCES

Brian, D. A., and Baric, R. S. (2005). Coronavirus genome structure and replication. *Curr. Top. Microbiol. Immunol.* 287, 1–30. doi: 10.1007/3-540-26765-4_1

Cao, L., Ge, X., Gao, Y., Herrler, G., Ren, Y., Ren, X., et al. (2015b). Porcine epidemic diarrhea virus inhibits dsRNA-induced interferon-β production in porcine intestinal epithelial cells by blockade of the RIG-I-mediated pathway. *Virol. J.* 12:127. doi: 10.1186/s12985-015-0345-x

Cao, L., Ge, X., Gao, Y., Ren, Y., Ren, X., and Li, G. (2015a). Porcine epidemic diarrhea virus infection induces NF-kappaB activation through the TLR2, TLR3 and TLR9 pathways in porcine intestinal epithelial cells. *J. Gen. Virol.* 96, 1757–1767. doi: 10.1099/vir.0.000133

Chen, Q., Li, G., Stasko, J., Thomas, J. T., Stensland, W. R., Pillatzki, A. E., et al. (2014). Isolation and characterization of porcine epidemic diarrhea viruses associated with the 2013 disease outbreak among swine in the United States. *J. Clin. Microbiol.* 52, 234–243. doi: 10.1128/JCM.02820-13

Chen, J., Liu, X., Shi, D., Shi, H., Zhang, X., and Feng, L. (2012). Complete genome sequence of a porcine epidemic diarrhea virus variant. *J. Virol.* 86:3408. doi: 10.1128/JVI.07150-11

Chen, Q., Thomas, J. T., Gimenez-Lirola, L. G., Hardham, J. M., Gao, Q., Gerber, P. F., et al. (2016). Evaluation of serological cross-reactivity and cross-neutralization between the United States porcine epidemic diarrhea virus prototype and S-INDEL-variant strains. *BMC Vet. Res.* 12:70. doi: 10.1186/s12917-016-0697-5

de Arriba, M. L., Carvajal, A., Pozo, J., and Rubio, P. (2002). Isotype-specific antibody-secreting cells in systemic and mucosal associated lymphoid tissues and antibody responses in serum of conventional pigs inoculated with PEDV. *Vet. Immunol. Immunopathol.* 84, 1–16. doi: 10.1016/S0165-2427(01)00386-5

DeDiego, M. L., Nieto-Torres, J. L., Regla-Nava, J. A., Jimenez-Guardeno, J. M., Fernandez-Delgado, R., Fett, C., et al. (2014). Inhibition of NF-kappaB-mediated inflammation in severe acute respiratory syndrome coronavirus-infected mice increases survival. *J. Virol.* 88, 913–924. doi: 10.1128/JVI.02576-13

Ding, Z., Fang, L., Jing, H., Zeng, S., Wang, D., Liu, L., et al. (2014). Porcine epidemic diarrhea virus nucleocapsid protein antagonizes beta interferon production by sequestering the interaction between IRF3 and TBK1. *J. Virol.* 88, 8936–8945. doi: 10.1128/JVI.00700-14

Guo, J., Li, F., He, Q., Jin, H., Liu, M., Li, S., et al. (2016b). Neonatal fc receptor-mediated IgG transport across porcine intestinal epithelial cells: potentially provide the mucosal protection. *DNA Cell Biol.* 35, 301–309. doi: 10.1089/dna.2015.3165

Guo, J., Li, F., Qian, S., Bi, D., He, Q., Jin, H., et al. (2016a). TGEV infection up-regulates FcRn expression via activation of NF-kappaB signaling. *Sci. Rep.* 6:32154. doi: 10.1038/srep32154

Huang, Y. W., Dickerman, A. W., Pineyro, P., Li, L., Fang, L., Kiehne, R., et al. (2013). Origin, evolution, and genotyping of emergent porcine epidemic diarrhea virus strains in the United States. *MBio* 4, e00737–e00713. doi: 10.1128/mBio.00737-13

Kint, J., Fernandez-Gutierrez, M., Maier, H. J., Britton, P., Langereis, M. A., Koumans, J., et al. (2015). Activation of the chicken type I interferon response by infectious bronchitis coronavirus. *J. Virol.* 89, 1156–1167. doi: 10.1128/JVI.02671-14

Lee, S., Kim, Y., and Lee, C. (2015). Isolation and characterization of a Korean porcine epidemic diarrhea virus strain KNU-141112. *Virus Res.* 208, 215–224. doi: 10.1016/j.virusres.2015.07.010

Lee, D. K., Park, C. K., Kim, S. H., and Lee, C. (2010). Heterogeneity in spike protein genes of porcine epidemic diarrhea viruses isolated in Korea. *Virus Res.* 149, 175–182. doi: 10.1016/j.virusres.2010.01.015

Li, B., Liu, H., He, K., Guo, R., Ni, Y., Du, L., et al. (2013). Complete genome sequence of a recombinant porcine epidemic diarrhea virus strain from eastern China. *Genome Announc.* 1:e0010513. doi: 10.1128/genomeA.00105-13

Li, D., Wang, F. J., Yu, L., Yao, W. R., Cui, Y. F., and Yang, G. B. (2017). Expression of pIgR in the tracheal mucosa of SHIV/SIV-infected rhesus macaques. *Zool. Res.* 38, 44–48. doi: 10.13918/j.issn.2095-8137.2017.007

Li, Y., Wu, Q., Huang, L., Yuan, C., Wang, J., and Yang, Q. (2018). An alternative pathway of enteric PEDV dissemination from nasal cavity to intestinal mucosa in swine. *Nat. Commun.* 9:3811. doi: 10.1038/s41467-018-06056-w

Mole, B. (2013). Deadly pig virus slips through US borders. *Nature* 499:388. doi: 10.1038/499388a

Moynagh, P. N. (2005). The NF-kappaB pathway. *J. Cell Sci.* 118, 4589–4592. doi: 10.1242/jcs.02579

Oh, J., Lee, K. W., Choi, H. W., and Lee, C. (2014). Immunogenicity and protective efficacy of recombinant S1 domain of the porcine epidemic diarrhea virus spike protein. *Arch. Virol.* 159, 2977–2987. doi: 10.1007/s00705-014-2163-7

Pan, Y., Tian, X., Li, W., Zhou, Q., Wang, D., Bi, Y., et al. (2012). Isolation and characterization of a variant porcine epidemic diarrhea virus in China. *Virol. J.* 9:195. doi: 10.1186/1743-422X-9-195

Pyzik, M., Rath, T., Kuo, T. T., Win, S., Baker, K., Hubbard, J. J., et al. (2017). Hepatic FcRn regulates albumin homeostasis and susceptibility to liver injury. *Proc. Natl. Acad. Sci. USA* 114, E2862–E2871. doi: 10.1073/pnas.1618291114

Shan, Y., Liu, Z. Q., Li, G. W., Chen, C., Luo, H., Liu, Y. J., et al. (2018). Nucleocapsid protein from porcine epidemic diarrhea virus isolates can antagonize interferon-lambda production by blocking the nuclear factor-kappaB nuclear translocation. *J. Zhejiang Univ. Sci. B* 19, 570–580. doi: 10.1631/jzus.B1700283

Song, D., and Park, B. (2012). Porcine epidemic diarrhoea virus: a comprehensive review of molecular epidemiology, diagnosis, and vaccines. *Virus Genes* 44, 167–175. doi: 10.1007/s11262-012-0713-1

Stevenson, G. W., Hoang, H., Schwartz, K. J., Burrough, E. R., Sun, D., Madson, D., et al. (2013). Emergence of porcine epidemic diarrhea virus in the United States: clinical signs, lesions, and viral genomic sequences. *J. Vet. Diagn. Investig.* 25, 649–654. doi: 10.1177/1040638713501675

Subramaniam, S., Yugo, D. M., Heffron, C. L., Rogers, A. J., Sooryanarain, H., LeRoith, T., et al. (2018). Vaccination of sows with a dendritic cell-targeted porcine epidemic diarrhea virus S1 protein-based candidate vaccine reduced viral shedding but exacerbated gross pathological lesions in suckling neonatal piglets. *J. Gen. Virol.* 99, 230–239. doi: 10.1099/jgv.0.001001

Temeeyasen, G., Sinha, A., Gimenez-Lirola, L. G., Zhang, J. Q., and Piñeyro, P. E. (2018). Differential gene modulation of pattern-recognition receptor TLR and RIG-I-like and downstream mediators on intestinal mucosa of pigs infected with PEDV non S-INDEL and PEDV S-INDEL strains. *Virology* 517, 188–198. doi: 10.1016/j.virol.2017.11.024

Totura, A. L., Whitmore, A., Agnihothram, S., Schäfer, A., Katze, M. G., Heise, M. T., et al. (2015). Toll-like receptor 3 signaling via TRIF contributes to a protective innate immune response to severe acute respiratory syndrome coronavirus infection. *MBio* 6, e00638–e00615. doi: 10.1128/mBio.00638-15

Tsuruta, T., Inoue, R., Tsukahara, T., Nakamoto, M., Hara, H., Ushida, K., et al. (2012). Commensal bacteria coated by secretory immunoglobulin A and immunoglobulin G in the gastrointestinal tract of pigs and calves. *Anim. Sci. J.* 83, 799–804. doi: 10.1111/j.1740-0929.2012.01026.x

Vlasova, A. N., Marthaler, D., Wang, Q., Culhane, M. R., Rossow, K. D., Rovira, A., et al. (2014). Distinct characteristics and complex evolution of PEDV strains, North America, May 2013-February 2014. *Emerg. Infect. Dis.* 20, 1620–1628. doi: 10.3201/eid2010.140491

Wang, L., Hayes, J., Byrum, B., and Zhang, Y. (2016). US variant porcine epidemic diarrhea virus: histological lesions and genetic characterization. *Virus Genes* 52, 578–581. doi: 10.1007/s11262-016-1334-x

Wang, Y., and Yang, G. B. (2016). Alteration of polymeric immunoglobulin receptor and neonatal fc receptor expression in the gut mucosa of immunodeficiency virus-infected rhesus macaques. *Scand. J. Immunol.* 83, 235–243. doi: 10.1111/sji.12416

Woo, P. C., Lau, S. K., Tsang, C. C., Lau, C. C., Wong, P. C., Chow, F. W., et al. (2017). Coronavirus HKU15 in respiratory tract of pigs and first discovery of coronavirus quasispecies in 5′-untranslated region. *Emerg. Microbes Infect.* 6:e53. doi: 10.1038/emi.2017.37

Wood, E. N. (1977). An apparently new syndrome of porcine epidemic diarrhoea. *Vet. Rec.* 100, 243–244. doi: 10.1136/vr.100.12.243

Xu, X., Zhang, H., Zhang, Q., Dong, J., Liang, Y., Huang, Y., et al. (2013). Porcine epidemic diarrhea virus E protein causes endoplasmic reticulum stress and up-regulates interleukin-8 expression. *Virol. J.* 10:26. doi: 10.1186/1743-422X-10-26

Yamamoto, R., Soma, J., Nakanishi, M., Yamaguchi, R., and Niinuma, S. (2015). Isolation and experimental inoculation of an S INDEL strain of porcine epidemic diarrhea virus in Japan. *Res. Vet. Sci.* 103, 103–106. doi: 10.1016/j.rvsc.2015.09.024

Zhang, Q., Liu, X., Fang, Y., Zhou, P., Wang, Y., and Zhang, Y. (2017). Detection and phylogenetic analyses of spike genes in porcine epidemic diarrhea virus strains circulating in China in 2016-2017. *Virol. J.* 14:194. doi: 10.1186/s12985-017-0860-z

Conflict of Interest: The authors declare that the research was conducted in the absence of any commercial or financial relationships that could be construed as a potential conflict of interest.

Copyright © 2019 Qian, Zhang, Jia, Sun, Zhang, Xiao and Li. This is an open-access article distributed under the terms of the Creative Commons Attribution License (CC BY). The use, distribution or reproduction in other forums is permitted, provided the original author(s) and the copyright owner(s) are credited and that the original publication in this journal is cited, in accordance with accepted academic practice. No use, distribution or reproduction is permitted which does not comply with these terms.

frontiers in Microbiology

ORIGINAL RESEARCH
published: 01 November 2019
doi: 10.3389/fmicb.2019.02486

Temporal Dynamics of Co-circulating Lineages of Porcine Reproductive and Respiratory Syndrome Virus

*Igor Adolfo Dexheimer Paploski[1], Cesar Corzo[1], Albert Rovira[1], Michael P. Murtaugh[2†], Juan Manuel Sanhueza[1], Carles Vilalta[1], Declan C. Schroeder[1,3] and Kimberly VanderWaal[1]**

[1] Department of Veterinary Population Medicine, University of Minnesota, Saint Paul, MN, United States, [2] Department of Veterinary and Biomedical Sciences, University of Minnesota, Saint Paul, MN, United States, [3] School of Biological Sciences, University of Reading, Reading, United Kingdom

OPEN ACCESS

Edited by:
Akio Adachi,
Kansai Medical University, Japan

Reviewed by:
Enric M. Mateu,
Autonomous University of Barcelona, Spain
Raymond Rowland,
Kansas State University, United States
Yijun Du,
Shandong Academy of Agricultural Sciences, China
Hanchun Yang,
China Agricultural University (CAU), China

***Correspondence:**
Kimberly VanderWaal
kvw@umn.edu

[†] *Deceased*

Specialty section:
This article was submitted to Virology, a section of the journal Frontiers in Microbiology

Received: *29 July 2019*
Accepted: *15 October 2019*
Published: *01 November 2019*

Citation:
Paploski IAD, Corzo C, Rovira A, Murtaugh MP, Sanhueza JM, Vilalta C, Schroeder DC and VanderWaal K (2019) Temporal Dynamics of Co-circulating Lineages of Porcine Reproductive and Respiratory Syndrome Virus. Front. Microbiol. 10:2486. doi: 10.3389/fmicb.2019.02486

Porcine Reproductive and Respiratory Syndrome Virus (PRRSV) is the most important endemic pathogen in the U.S. swine industry. Despite control efforts involving improved biosecurity and different vaccination protocols, the virus continues to circulate and evolve. One of the foremost challenges in its control is high levels of genetic and antigenic diversity. Here, we quantify the co-circulation, emergence and sequential turnover of multiple PRRSV lineages in a single swine-producing region in the United States over a span of 9 years (2009–2017). By classifying over 4,000 PRRSV sequences (open-reading frame 5) into phylogenetic lineages and sub-lineages, we document the ongoing diversification and temporal dynamics of the PRRSV population, including the rapid emergence of a novel sub-lineage that appeared to be absent globally pre-2008. In addition, lineage 9 was the most prevalent lineage from 2009 to 2010, but its occurrence fell to 0.5% of all sequences identified per year after 2014, coinciding with the emergence or re-emergence of lineage 1 as the dominant lineage. The sequential dominance of different lineages, as well as three different sub-lineages within lineage 1, is consistent with the immune-mediated selection hypothesis for the sequential turnover in the dominant lineage. As host populations build immunity through natural infection or vaccination toward the most common variant, this dominant (sub-) lineage may be replaced by an emerging variant to which the population is more susceptible. An analysis of patterns of non- synonymous and synonymous mutations revealed evidence of positive selection on immunologically important regions of the genome, further supporting the potential that immune-mediated selection shapes the evolutionary and epidemiological dynamics for this virus. This has important implications for patterns of emergence and re-emergence of genetic variants of PRRSV that have negative impacts on the swine industry. Constant surveillance on PRRSV occurrence is crucial to a better understanding of the epidemiological and evolutionary dynamics of co-circulating viral lineages. Further studies utilizing whole genome sequencing and exploring the extent of cross-immunity between heterologous PRRS viruses could shed further light on PRRSV immunological response and aid in developing strategies that might be able to diminish disease impact.

Keywords: PRRSV, epidemiology, ecology, evolution, multi-strain dynamics, emergence, outbreak

INTRODUCTION

Porcine reproductive and respiratory syndrome virus (PRRSV), the etiological agent of PRRS, is one of the most important endemic viruses affecting the swine industry in the United States (Holtkamp et al., 2013) and globally (Stadejek et al., 2013; VanderWaal and Deen, 2018). The economic impact of the disease in the United States has been estimated at $664 million annually (Holtkamp et al., 2013). Clinical signs in affected farms vary by viral variant and according to the farm's production stage (e.g., breeding or growing herd), herd management, immune status, and other factors (Goldberg et al., 2000). Premature farrowing can occur in 5–30% of sows in an affected farm, and up to 35% of piglets are stillborn during an outbreak (Christianson and Joo, 1994). Piglets may be born with low weight and can present with lethargy and anorexia, which can lead to a mortality of more than 70% among piglets (Pejsak et al., 1997). PRRSV-infected pigs are also susceptible to secondary infections leading to poor average daily gain and feed conversion, further increasing production loss (Solano et al., 1997; Xu et al., 2010). Up to 40% of United States breeding herds experience outbreaks annually (Tousignant et al., 2015a) and control of the disease in the United States, Europe, and globally is challenging due to high levels of antigenic variability and its rapidly expanding genetic diversity (Frossard et al., 2013; Brar et al., 2015; Guo et al., 2018; Smith et al., 2018).

Porcine reproductive and respiratory syndrome virus was first recognized almost simultaneously in Europe (Wensvoort et al., 1991) and North America (Collins et al., 1992) in the late 1980s and early 1990s, but genetic differences suggested a much earlier evolutionary divergence between the North American and European viral types. Thus, PRRSV is divided into two major phylogenetic clades, PRRSV Type 1 (more prevalent in Europe) and Type 2 (more prevalent in North America) (Shi et al., 2010a,b; Stadejek et al., 2013). Within each clade, high levels of genetic and antigenic diversity exist and cross-protection is only partial (Roberts, 2003; Kim et al., 2013; Correas et al., 2017). Genetic similarities between PRRSV isolates have been used as a tool to understand disease transmission and epidemiology (Kapur et al., 1996; Wesley et al., 1998), and several different strategies have been used for classifying isolates of PRRSV into epidemiologically meaningful groups. For PRRSV Type 2, the most commonly used classification system is based on restriction fragment length polymorphisms (RFLP) and sequencing, both of which are typically based on the open reading frame 5 (*ORF5*) portion of its genome (Kapur et al., 1996; Wesley et al., 1998). The *ORF5* gene encodes for the major envelope protein (GP5), which plays a role in inducing virus neutralizing antibodies and cross-protection among PRRSV variants (Dea et al., 2000; Kim et al., 2013). RFLPs have been broadly adopted by the U.S. swine industry despite shortcomings, such as the fact that the genetic relationship between different RFLP types is unclear, the potential for two distantly related viruses to share the same RFLP type, and the instability of RFLP-typing when assessing isolates related to each other by as few as 10 animal passages (Cha et al., 2004). In 2010, a classification system based on the phylogenetic relatedness of the *ORF5* portion of the virus's genome was proposed (Shi et al., 2010a,b). This classification system aggregates isolates into phylogenetic lineages based on the ancestral relationships and genetic distance among isolates. Using this system, nine different lineages were described within PRRSV Type 2, each of which was estimated to have diverged between 1980 and 1992 (Shi et al., 2010b). Phylogeny-based classification of organisms is seen as the most powerful and robust instrument for distinguishing between variants of a viral population (Hungnes et al., 2000) and has been used in the study of other viral diseases (Liu et al., 2009). Phylogeny-based classification of PRRSV, rather than RFLP profiling, is expected to provide fewer ambiguities and more insight into the evolutionary relatedness amongst different variants. While the existence of PRRSV lineages is well established, the dynamics of their co-circulation within a given region has not been well documented.

Vaccination is often used as a tool to mitigate clinical impact and viral shedding (Holtkamp et al., 2011). Although specific practices vary across farms, gilts are typically vaccinated before entering the herd, and sometimes the sow herd is mass vaccinated during the year. Most commercial PRRSV vaccines currently sold in the United States are considered "modified live vaccines" (MLV), which means that the vaccine is an attenuated live virus. Vaccines against PRRSV show different degrees of protection against homologous and heterologous challenges (Cano et al., 2007; Díaz et al., 2012; Geldhof et al., 2012); the exact definition of what constitutes a homologous or heterologous challenge is often not clear, especially taking into consideration the genetic diversity existing within PRRSV Type 2 (Shi et al., 2010b). Five major PRRSV vaccines are commercialized in the United States, each developed using a different wild PRRSV isolate (lineages 1, 5, 7, and 8, with the lineage 5 vaccine being the most widely used historically).

Porcine reproductive and respiratory syndrome virus is known to possess a high mutation rate (Hanada et al., 2005; Brar et al., 2014). Genetic mutations for PRRSV are thought to result from RNA polymerase errors (Murtaugh et al., 2010) and from the lack of proofreading (Kappes and Faaberg, 2015). Coupled to that, genetic recombination events can contribute to PRRSV diversity (Forsberg et al., 2002). Thus, the emergence of new variants of PRRSV is expected to occur potentially through both mutation and recombination. Viral variants can quickly emerge in animals (Goldberg et al., 2003) even after inoculation with a single variant (Chang et al., 2002). Thus, the viral population within an animal can be referred to as a viral cloud or swarm (Lauring and Andino, 2010), which suggests that mutation has a considerable impact in virus diversification even on short time scales. In addition, it is assumed that the immune response removes genetic variants of the virus that it recognizes with high specificity, potentially creating selection pressure favoring antigenically divergent PRRSV variants (Murtaugh et al., 2010). Hypervariable portions of the viral genome may be subject to immune selective pressure (Chen et al., 2016); variation in proteins coded by those sites may play a role in evasion of host immune defenses (Ansari et al., 2006; Darwich et al., 2011). PRRSV vaccines are known to diminish the severity of clinical signs once an infection occurs, but not to prevent an infection from occurring (Lyoo, 2015). At the population scale, it can be

expected that most animals have some level of immunity because of the high prevalence of natural infection and widespread use of vaccine. This creates the potential for immune-mediated selection to be a driver of PRRSV diversification and evolution (Murtaugh et al., 2010).

The identification of point mutations that are undergoing positive selective pressure is often interpreted as evidence of increased evolutionary fitness (Kryazhimskiy and Plotkin, 2008). One way to identify such sites is to evaluate dN/dS ratios, which measure the rate at which substitutions at non-synonymous sites (dN) occur relative to substitutions in synonymous sites (dS). Substitutions in synonymous sites are thought to be mostly neutral, but a higher occurrence of substitutions in non-synonymous sites can be interpreted as evidence of selective processes that favor changes in the protein sequence (Kosakovsky Pond and Frost, 2005). Positive selective pressure in sites that code for epitopes recognized by the host immune system are of special interest, because they suggest that the origin of such selective pressure, if present, could be driven by the host immune response.

The rapid evolution of PRRSV coupled with the periodic emergence of new and sometimes more virulent viral variants creates a need to continually update our knowledge on circulating PRRSV variants. Reports that show the waxing and waning of different viral types in the whole North America (Shi et al., 2010b) are helpful when understanding continent-wide status of PRRSV lineages. However, understanding viral dynamics on a regional scale could provide important insights into local evolutionary and ecological dynamics of PRRSV, including an improved understanding of how often new variants emerge or re-emerge within the region. Here, we describe the temporal dynamics of PRRSV occurrence in a swine-dense region of the United States, characterizing these patterns according to *ORF5* genetic lineages and sub-lineages. We quantify the contemporary occurrence of each lineage, investigate the temporal dynamics and turnover of lineages, identify emerging sub-lineages, and examine evolutionary patterns for evidence of positive selective pressures.

MATERIALS AND METHODS

Sequences available through the Morrison Swine Health Monitoring Project (MSHMP) were used for this analysis. Briefly, MSHMP is an ongoing voluntary producer-driven nation-wide monitoring program for endemic swine diseases that affect the U.S. swine industry. Based at the University of Minnesota (UMN), this program collects weekly reports on the infection status of sow farms from participating swine-producing companies, veterinary practices, and regional control programs, which serves to capture the occurrence of infectious diseases in the country (Tousignant et al., 2015a,b; Perez et al., 2016). Infection status data classifies farms into the following categories (Holtkamp et al., 2011): Status 1: positive-unstable, Status 2: positive-stable, either through use of live virus inoculation (2lvi) or use of vaccines (2vx); Status 3: provisional negative; and Status 4: negative. The main difference between positive-unstable (Status 1) and positive-stable (Status 2vx or 2lvi) is that unstable herds have an active clinical outbreak and are weaning PRRSV RT-PCR positive piglets. In contrast, PRRSV may be still present in positive-stable herds (through use of field virus inoculation or modified live vaccine) but clinical disease is controlled and piglets weaned from such farms are PRRSV-negative as a result of herd immunity, decreased shedding, and maternal antibodies (Holtkamp et al., 2011). MSHMP collects farm-level data from approximately 3.2 million sows, which represents approximately 50.5% of the United States breeding herd population (National Agricultural Statistics Service [NASS], Agricultural Statistics Board, and United States Deparment of Agriculture [USDA], 2018). Specific production systems (companies involved in pig production) participating in the project also share the *ORF5* PRRSV sequences identified on their farms as part of routine veterinary management. For example, samples may be submitted by veterinary practitioners to determine if circulating PRRSV on the farm is the same or different from the vaccine virus or a previous variant present on the farm.

For this analysis, we analyzed 4,390 sequences reported between 2009 and 2017 from MSHMP participants located in a relatively isolated swine-dense region in the United States with an approximate area of 250 thousand square kilometers. Production systems operating in this region account for ∼12% of the United States sow population. Approximately 90% of farms within this region participate in MSHMP and in this project in particular. Sequences used in this study came mostly from sow (64.9% of sequences), nursery (16.8%) and finisher farms (14.7%), followed by boar stud farms (0.3%) and sequences without a description of their origin (3.3%). Sequences shared with us by project participants were sequenced according to standardized protocols adopted by laboratories at SDSU (Animal Disease Research and Diagnostic Laboratory et al., 2017), ISU (Zhang et al., 2017) and Eurofins Genomics. Of the *ORF5* gene sequences used in this analysis, seven had fewer than 550 nucleotides. These were deemed incomplete and were excluded from further analysis. We also included 841 *ORF5* gene sequences previously classified into nine different genetic lineages (Shi et al., 2010a,b) and added these to the collection of MSHMP sequences. These sequences, assembled from a database of sequences that spanned from 1989 to 2008, were used as guides to classify the MSHMP sequences into the previously described genetic lineages, and will be referred to here as "anchor" sequences. We also obtained the *ORF5* gene sequences for five vaccines (Ingelvac PRRSV ATP – GenBank ID DQ988080.1, Ingelvac PRRSV MLV – GenBank ID AF066183.4 (both from Boehringer Ingelheim), Fostera PRRSV from Zoetis – GenBank ID KP300938.1, Prime Pac PRRSV RR from Merck – GenBank ID DQ779791.1, and Prevacent, from Elanco – GenBank ID KU131568.1). The Ingelvac PRRSV ATP and Fostera vaccines use isolates belonging to lineage 8, while Ingelvac PRRSV MLV uses a lineage 5 isolate, Prime Pac a lineage 7 isolate and Prevacent a lineage 1 isolate. We also obtained two PRRSV prototypes (Lelystad – GenBank ID NC_043487.1, and VR2332 – GenBank ID EF536003.1, which represent the prototypical European Type 1 and North American Type 2 viruses, respectively). The sequence dataset used here is

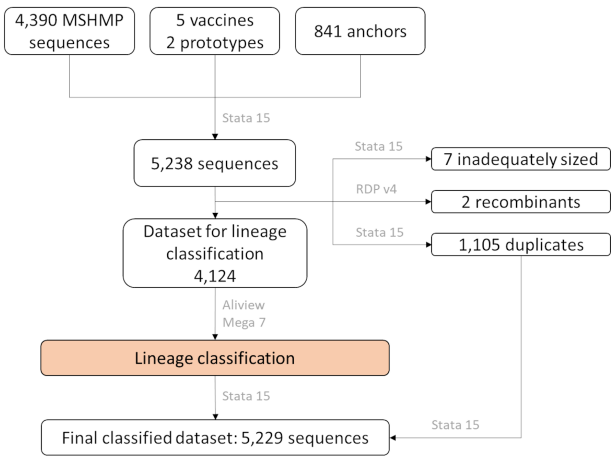

FIGURE 1 | Number of *ORF5* sequences according to their source and how they were treated in the lineage classification process. In gray, name of software used in each step.

available in Genbank under the accession numbers MN498289 – MN502669.

Sequences were aligned using the MUSCLE algorithm implemented in AliView (Larsson, 2014) using default settings. The alignment was then examined for the presence of recombinants using the Recombinant Detection Program version 4 (Martin et al., 2015), followed by removal of potential recombinants. In addition, duplicated sequences (with 100% nucleotide similarity) were identified and set aside for the allocation of sequences into lineages. The aligned and cleaned dataset was imported into Mega 7 (Kumar et al., 2016), where the genetic pairwise distance was measured as a percentage nucleotide difference. Using Stata 15 (StataCorp, 2017), each of the MSHMP sequences were assigned to the lineage that had the smallest genetic distance to an anchor. After sequences were classified into lineages, the duplicated sequences were allocated to their respective lineage group according to the sequence with 100% similarity that was kept in the lineage classification process. A flow-chart of these steps can be seen in **Figure 1**.

A maximum likelihood phylogenetic tree illustrating genetic relatedness of sequences was constructed based on 1,000 bootstraps, adopting the Tamura-Nei model for substitution of amino acids (Tamura and Nei, 1993; Kumar et al., 2016). ClusterPicker software was used to further stratify the most abundant lineage into sub-lineages (Ragonnet-Cronin et al., 2013), in a matter that seemed consistent with the tree main branches while still returning epidemiological meaningful sub-lineages. The phylogenetic tree was then colored according to the lineage classification and source of sequences (anchor versus MSHMP) using Microreact (Argimón et al., 2016). Traditional bootstrap support is estimated based on resampling and replication, which tends to yield low support particularly on deep branches and in large trees with hundreds or thousands of sequences (Lemoine et al., 2018). Branch support on the phylogenetic tree thus was evaluated using the bootstrap support by the transfer method (Lemoine et al., 2018). This method circumvents issues of traditional bootstrapping by assigning a gradual "transfer" index to each clade within the tree rather than a binary presence/absence index for the presence of a clade in each bootstrap (i.e., a clade is considered absent in the bootstrap replicate if the sequences found within the clade is different by even a single member). Temporal changes in the frequency of different lineages was tabulated by quarter of the year. Graphs representing the relative frequency of PRRSV lineages over time were constructed using Stata 15. The frequency with which each lineage occurred over different years was compared using trend analysis for proportions (using the *ptrend* command) in Stata 15 (StataCorp, 2017). For this test only, lineages with fewer than 10 sequences overall were grouped.

The ratio of synonymous to non-synonymous mutations (dN/dS) for all sites in the *ORF5* gene region was calculated using the Single-Likelihood Ancestor Counting protocol (Kosakovsky Pond and Frost, 2005), implemented on the Datamonkey webserver (Pond and Frost, 2005). Because the analysis can only be performed on 500 sequences at a time, the analysis was repeated on ten random subsets of 500 sequences (after removal of 100% identical sequences). Sites were considered under positive selective pressure if the *p*-value associated with a higher rate of non-synonymous versus synonymous mutations was smaller than 0.05. The dN/dS (re-scaled for branch length) of all sites from different runs were averaged and the percentage of runs in which each codon was identified as under significant positive selection was calculated.

RESULTS

Lineage Classification

After removal of the seven inadequately sized and two recombinant sequences from the MSHMP data, the remaining 4,381 MSHMP sequences were classified in five different lineages. 70.9% (3,110 sequences) were classified as lineage 1, 10.0% (436) as lineage 5, 0.2% (9) as lineage 7, 2.2% (94) as lineage 8, and 9.2% (404) as lineage 9. A group of 7.5% (328) of the MSHMP sequences were genetically closer to the European Prototype (Lelystad) reference, and were thus classified as Type 1 PRRSV sequences. Lineage 1 was further separated into five sub-lineages (A to E). Out of the total 3,110 sequences in lineage 1, 48.7% (1515) were classified in lineage 1A, 13.9% (433) in lineage 1B, 37.2% (1157) in lineage 1C, 0.03% (1) in lineage 1D and 0.1% (4) in lineage 1E. The phylogenetic tree with all sequences used in the analysis can be seen on **Figure 2**. Using the Booster method (Lemoine et al., 2018), branch support on main branches (lineages and sub-lineages) was above 90%. The within- and between-lineage nucleotide pairwise genetic distance is shown in **Table 1**. In general, between lineage/sub-lineage distances are higher than within lineage variation. The distances between sub-lineages of lineage 1 seem to be smaller between them than between other lineages. Broad tree topology was similar when the tree was constructed using nucleotides or amino acids alignment (**Supplementary Figure S2**).

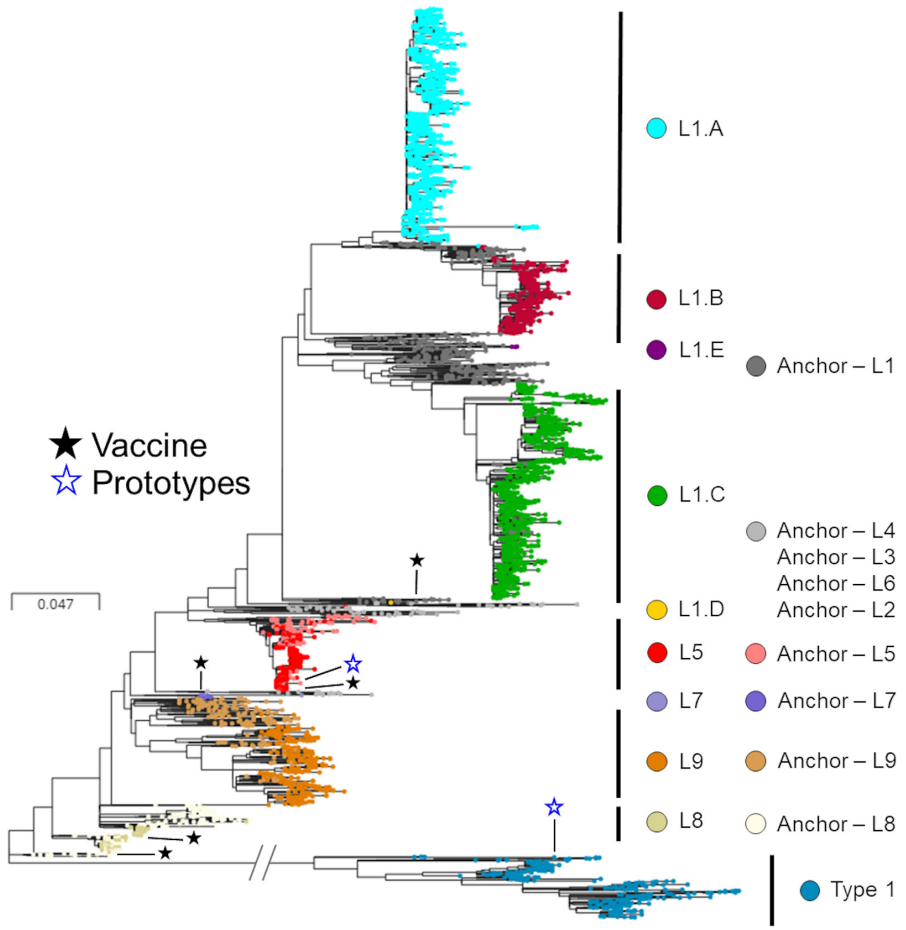

FIGURE 2 | Phylogenetic tree of *ORF5* sequences stratified according to lineages. Colors represent different lineages or sub-lineages, and differences in hues within a color represent anchor versus MSHMP sequences. Prototypes (North American – VR2332; European – Lelystad) and vaccines are highlighted using hollow blue stars and solid dark stars, respectively.

TABLE 1 | Mean *ORF5* genetic distance as percentage difference in nucleotides within- (gray cells) and between-lineages (white cells).

Lineage	L1A *n* = 1515	L1B *n* = 433	L1C *n* = 1157	L5 *n* = 436	L8 *n* = 94	L9 *n* = 404	Others* *n* = 14	Type1 *n* = 328
L1A	2.3							
L1B	8.3	3.8						
L1C	9.7	11	5					
L5	12.4	13.7	13.4	0.7				
L8	11.6	12.6	11.7	7.5	4.5			
L9	12.3	12.3	10.9	8.4	4.7	8.6		
Others	8.4	10.1	8.4	7	4.8	5	9.5	
Type1	62.6	60.8	60.9	58.6	57.7	55.2	58.6	10.2

**Represent the sum of uncommon lineages/sub-lineages, namely sub-lineages 1D (n =1), 1E (n =4) and lineage 7 (n =9).*

Temporal Dynamics of Lineage Occurrence

On average, the total number of sequences reported to MSHMP increased by 46 each year (**Supplementary Table S1**), and there was a clear seasonal pattern (**Figure 3B**). The first quarter of each year (January – March) was the one with highest number of sequences reported in all but 1 year. The relative frequency of each lineage changed through time (**Figure 3A** and **Supplementary Table S1**), and specific patterns are noteworthy. First, the absolute and relative occurrence of lineage 9 decreased over time from 68.4% (149 sequences) in 2009 to <1% (5 sequences) in the years 2014–2017. As lineage 9 occurrence

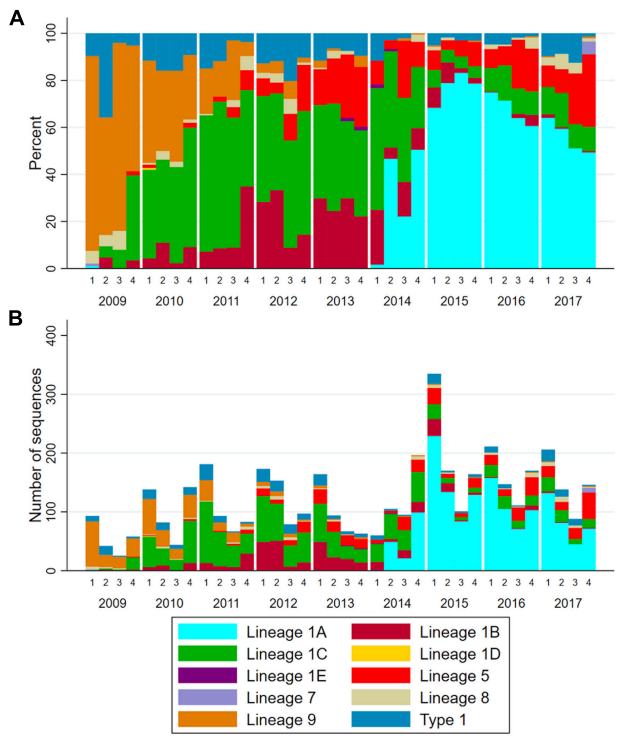

FIGURE 3 | (A) Stacked bar chart of the relative frequency and **(B)** number of *ORF5* sequences according to lineages over years and quarters.

declined, lineage 1 occurrence increased until it represented >60% of sequences reported in the period spanning 2011–2017. Within lineage 1, turnover in the dominant sub-lineages is apparent as the relative frequency of lineage 1C between 2009 and 2011 rose from 11.5% to 55.2%, then subsequently declined to approximately 10% of the sequences reported in years 2014–2017. Somewhat concurrently to the emergence of sub-lineage 1C, sub-lineage 1B increased from 1.8% to 27.4% in 2013, then subsequently declined to <2% of sequences reported in 2016 and 2017. Concomitant with the decrease in occurrence of lineage 1C and 1B was a sharp increase in the occurrence of lineage 1A. A single sequence of lineage 1A was observed in 2009, after which this sub-lineage was not detected in any subsequent years until 2014, at which point it was responsible for 37.3% of the sequences. By 2015, almost 75% of sequences belonged to this sub-lineage. Since then, the frequency in which this lineage has occurred decreased (68.4 and 57.3% of the sequences from 2016 and 2017, respectively).

To determine whether changes in sampling effort across time impacted general patterns observed here, we repeated the analysis five times, each time randomly sampling 50 *ORF5* sequences per quarter. General patterns of lineage occurrence did not change, suggesting that patterns of lineage occurrence were not affected by sampling effort in each quarter (**Supplementary Figure S1**).

The visual patterns and turnover of lineages apparent in **Figure 3A** were shown to be statistically significant. The increase in the frequency of lineages 1A, 5, 9, and type 1 ($p < 0.001$) was significant, and changes in the grouped frequency of other lineages (a sum of lineages 1D, 1E, and 7, $p = 0.0472$) was also significant, but with a difficult interpretation since this is an aggregate of several uncommon lineages. Lineages 1B and 1C increased in frequency and then decreased ($p < 0.001$). Lineage 9 frequency decreased over time (p-value < 0.001), while lineage 8 occurrence remained unchanged (p-value = 0.958).

Evidence for Positive Selective Pressure

A total of 26 sites were identified as under positive selection in at least one Single-Likelihood Ancestor Counting run (**Figure 4**). Some sites were identified as under positive selection in all 10 runs, while others were only identified in some runs. Those identified in all runs (with the largest p-value across all runs), were sites 14 (p-value = 0.045), 30 (p-value = 0.012), 32 (p-value < 0.001), 33 (p-value < 0.001), 34 (p-value < 0.001), 35 (p-value < 0.001), 58 (p-value = 0.005), and 104 (p-value = 0.029). A list of all sites identified as under positive selection in at least one run can be found in the caption of **Figure 4**. Most of the sites positively selected were located in the first third of the PRRSV ORF5.

The infection status of farms part of MSHMP in the studied area over the study time span is shown in **Figure 5**. This data show two periods in which vaccine usage increased, the first one in mid-2012, and a second in approximately mid-2014. Not all farms that reported its status to MSHMP contributed to sequences to this analysis.

DISCUSSION

We documented the circulation, emergence and sequential turnover of multiple PRRSV lineages in a single United States swine-producing region over a span of 9 years (2009–2017). By classifying over 4,000 PRRSV *ORF5* contemporary sequences into phylogenetic lineages based on pre-2008 data (Shi et al., 2010a,b), we illustrated the continual diversification and temporal dynamics of the PRRSV population. Through further stratifying lineage 1 into three main sub-lineages, we also describe the rapid emergence of a sub-lineage (1A), which was absent in the pre-2008 analysis even though that dataset was based on >8000 sequences from across the world (including the region in which we collected our samples) (Shi et al., 2010b). We also identified sites within PRRSV *ORF5* gene and resultant ORF5 protein that showed evidence of positive selective pressure, indicating that non-synonymous mutations that lead to amino acid changes in the protein at these sites are favored.

From 2009 to 2010, lineage 9 was the most prevalent genetic group observed in our dataset. Shi et al., 2010a,b showed that lineage 9 was rapidly increasing in genetic diversity, which is a proxy for the effective population size of the virus, from 1992 to 2008, and reached a peak from 2004 to 2008. Our data suggests that, at least for our study region, the occurrence of lineage 9 peaked pre-2009, after which it rapidly declined and was replaced mostly by lineage 1 variants. From 2011 to 2017, three different major sub-lineages within lineage 1 emerged, two of those being the most prevalent lineage in certain years (1C

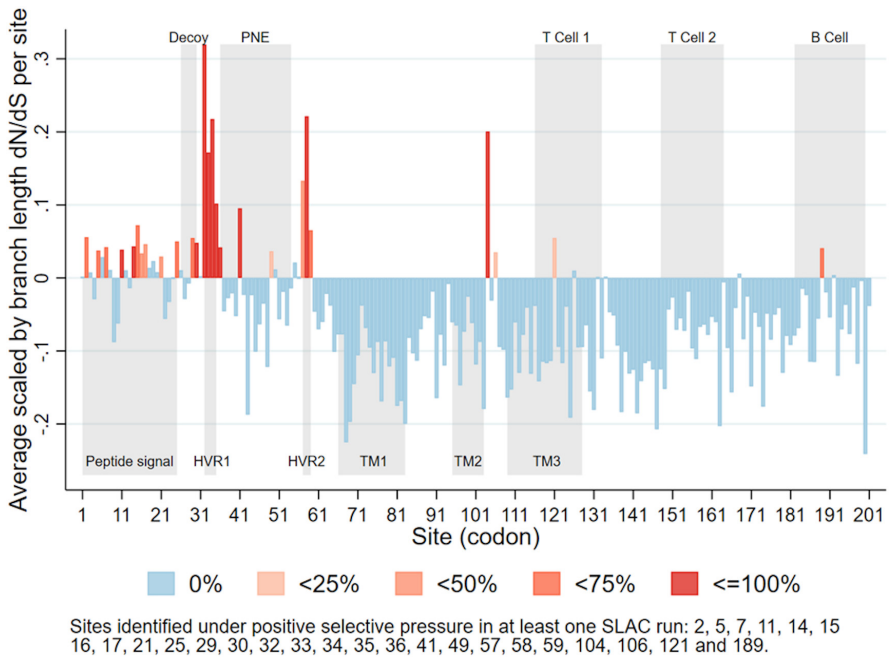

FIGURE 4 | Average scaled by branch length dN/dS for each site in PRRSV ORF5, categorized according to percentage of runs (n = 10) in which each site was identified as under positive selective pressure. Upper gray rectangles show antigenic regions (PNE – principal neutralizing epitope), lower gray rectangles show biologically significant regions (HVR – hypervariable region; TM – transmembrane region) (Delisle et al., 2012).

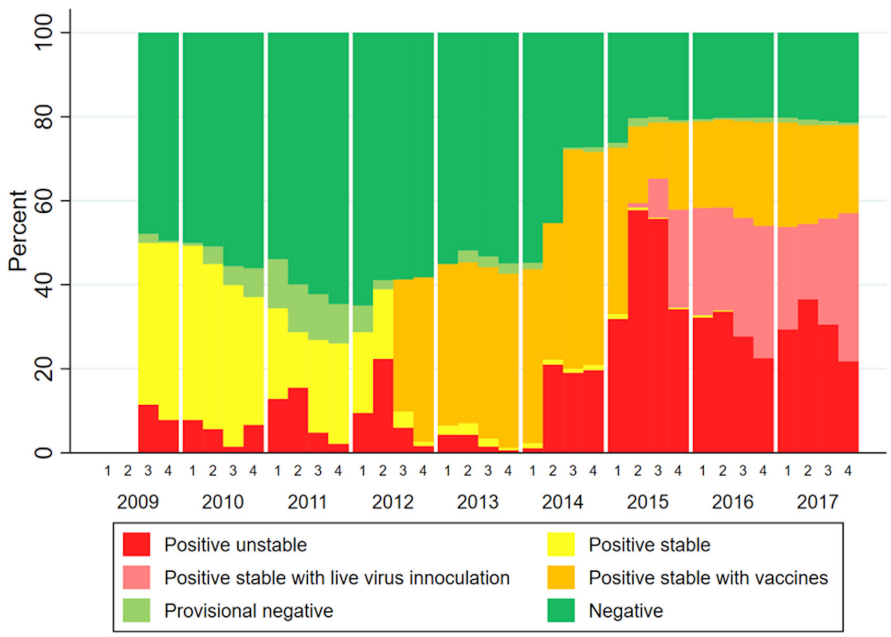

FIGURE 5 | Infection status of farms in the study area over time (quarters and years).

from 2011 to 2014, 1A from 2015 to 2017). The emergence of sub-lineage 1A, beginning in 2014 and peaking in 2015 was perceived by veterinarians in the studied area as being a noteworthy event coinciding with the spread of the 1-7-4 RFLP-type. In our dataset, 70.7% of the sequences belonging to the 1A sub-lineage were RFLP-typed as 1-7-4 (followed by 9.4% of sequences with RFLP 1-6-4 and less than 5% of 1-21-4, 1-7-3, 1-4-4, 1-7-2 and several others with less than 1% – see **Supplementary Table S2**).

While the failure to achieve consistent and reliable PRRSV control and prevention through vaccination demonstrates gaps

in our understanding of PRRSV immunology (Murtaugh, 2004), based on current understanding, PRRSV vaccines are expected to better protect against wild viral variants that have a higher degree of similarity to the original parental isolate used for vaccine development (Cano et al., 2007; Díaz et al., 2012; Geldhof et al., 2012). Despite our limited understanding of heterologous cross-protection for PRRSV, the emergence and sequential dominance of different variants leading to lineages and sub-lineages is consistent with the theory of multi-strain dynamics (Gupta et al., 1998; Kucharski et al., 2016). Immune responses, whether originating from human interventions or accumulation of immunity toward wild variants, can exert selective pressure that can ultimately lead to the emergence of new pathogen sub-populations (Gupta et al., 1998). As a virus evolves, immune responses generated against a past variant are expected to become less effective, resulting in a highly complex system, with different lineages interacting through the partial cross-immunity that they generate in the host population (Gupta et al., 1998; Kucharski et al., 2016). Theory predicts that due to frequency-dependent selection amongst co-circulating viral variants, rare antigenic variants are expected to spread more widely in the host population but then subsequently decline as herd immunity rises. Such dynamics have been more thoroughly understood for Influenza A (Webster et al., 1992; McCullers et al., 1999; Ferguson et al., 2003; Nelson et al., 2008) and HIV (McMichael et al., 2010).

For PRRSV, recent research demonstrates that antibodies can exert a strong selective pressure to viral pathogens by targeting specific viral sub-populations, while allowing for the establishment of other sub-populations (Wang, 2016). When comparing PRRSV genetic diversity before and after vaccine adoption in South Korea, PRRSV vaccination was suggested to increase viral genetic heterogeneity and the emergence of new glycosylation sites in viral populations (Kwon et al., 2019). However, the extent in which PRRSV immunity, whether from natural infection or vaccination, can potentially drive the evolution of the virus in the field remains largely unanswered. Our data does show a dominance of non-vaccine related lineages over time, which leads to speculation that these lineages have partially escaped the immunity induced by commercial vaccines or natural infection by variants in other lineages. PRRSV vaccines do not protect against infection (Scortti et al., 2006), but diminish clinical signs and improve animal performance (Cano et al., 2007). Since our project did not evaluate clinical signs of animals, it is difficult to assess the effects of vaccination in that regard. However, despite high region-wide vaccine usage from 2012 onward (**Figure 5**), Lineage 1A spread widely in the studied region, suggesting that vaccination and other biosecurity measures were insufficient to limit the transmission of lineage 1A.

Lineages shown (**Figure 2**) and discussed here and elsewhere are based on phylogenetic relationships in the ORF5 region, and might not be predictive of cross-protection and immunological responses developed by hosts when faced with viruses belonging to different lineages. Despite that, the lineage classification protocol used in this study did reveal temporal patterns consistent with what is expected based on epidemiological theory related to the spread of disease in immunologically naive populations. For example, epidemic-shaped curves of occurrence of different PRRSV populations were seen, a pattern consistent with the spread of new pathogens (or subtypes) within a naive population. New (sub-) lineages may potentially be able to become the dominant PRRSV in the population if they are sufficiently immunologically distinct to overcome herd immunity, and herds with different levels of immunity induced by pre-exposure protocols or natural infections might create selective pressure that changes how fast a new viral variant is selected in that population. For PRRSV, it is apparent that protection against homologous PRRSV is more robust than against heterologous variants, though the definition of what constitutes a heterologous virus is highly variable (Cano et al., 2007; Díaz et al., 2012; Geldhof et al., 2012). At the same time, genetic distance has not been shown to correlate with cross-protection, perhaps because pairwise nucleotide identity fails to capture key mutations that impact cross-protection. Studies that further explore the immunological cross-reactivity among PRRSV lineages are needed.

With the data available in this study, it was not possible to investigate the occurrence of specific lineages with vaccination use and more precisely to which vaccine each farm/system used or to which virus was circulating previously on a specific farm. MSHMP data of farms from systems that contributed sequences to this paper (**Figure 5**) show two periods in which vaccine usage increased. The first increase in mid-2012, and a second in approximately mid-2014. The second spike in vaccine usage coincided with when lineage 1A began spreading in the study area. It is possible that this second spike in vaccine usage was a reaction to the shift in circulating lineages (more specifically, to the emergence of lineage 1A PRRSV). It is also possible that the increased use of vaccines 2012 onward (shown on **Figure 5**) and the occurrence of lineages 1B and 1C (shown on **Figure 3**) immunologically selected sequences in a manner that allowed for the emergence of lineage 1A in 2014. By mid-2015, a proportion of farms began using live virus inoculation (lvi). This strategy refers to the use of controlled exposure in gilts through inoculation with live virus isolated from recent clinical outbreak(s) at the farm (Desrosiers and Boutin, 2002). The rationale is that by exposing gilts to virus found in a farm, gilts will mount "homologous" immunity to that specific wild-type virus and contribute to herd immunity and thus stability. According to veterinarians in the area, the increased use of lvi was due to the circulating virus being "different enough" from the viruses used in commercial vaccines. The practice of lvi in the systems here reported began primarily in 2015 (**Figure 5**). It is difficult to assess the impact that lvi might have on immunologically selecting for specific viral populations within specific lineages, especially with the aggregated data used in this analysis. While the inability of vaccination to control the spread of PRRSV lends credence to immunological selection as a driver of PRRSV diversification (Murtaugh et al., 2010), the impacts that immune-driven selection could have on long term PRRSV evolution remain unknown. Recording exposure procedures (lvi or vaccine use) within farms is crucial when trying to interpret longitudinal patterns of occurrence of PRRSV. In future research aimed at more robustly testing hypotheses about immunity as

a driver of evolutionary change, this crucial information would allow for investigation of frequencies in which specific lineages occur in farms pre- and post-vaccine/lvi adoption.

Within ORF5, we found sites under positive selective pressure within or near two hypervariable regions (**Figure 4**; Hanada et al., 2005; Delisle et al., 2012) located near the principal neutralizing epitope (PNE). The PNE is located between amino acids 36–52 and forms an ectodomain which triggers antibodies development during PRRSV infection (Plagemann et al., 2002; Hanada et al., 2005). The flanking hypervariable regions can be linked to the development of an immune response that block accessibility of antibodies to the PNE (Popescu et al., 2017), including N-linked glycosylation sites such as N34, N44, and N51 (Ansari et al., 2006). In general terms, glycosylation may modulate protein-protein interactions, whether these proteins involve the humoral or cellular immune response of the host (Lisowska, 2002). In PRRSV, there is evidence that these glycosylation sites play a role in glycan shielding, which is an important mechanism by which the virus evades neutralizing immune responses (Vu et al., 2011). While our findings do not explicitly explain the change in lineage, it does raise one hypothesis of the mechanism behind such change. Further studies on how specific portions for the genome, both within ORF5 and the whole genome, modulate immune recognition and possibly selective pressure are needed.

We also consistently identified positive selective pressure within the PNE region, specifically for amino acid 41. The identification of positive selective pressure in this region suggests that viral variants with different amino acid composition in that region may experience higher fitness and thus are favored. Since this region seems to be the primary binding site of neutralizing antibodies developed during PRRSV infection (Plagemann et al., 2002; Kim et al., 2013), this suggests that the reason for such selective pressure could be immune in nature. Such a scenario has been considered as a possible explanation for long-term evolution of RNA viruses (Domingo et al., 1996; Pérez-Sautu et al., 2011). Additional *in vitro* research is necessary to further clarify the immunological importance of sites identified in our analysis. However, our results suggest the plausibility of a scenario where PRRSV variants with mutations in key immunological regions are able to evade immune responses and thus persist and spread within host populations with partial immunity (**Figure 6**). Further studies to investigate the role of an incomplete immunity on the evolution of PRRSV are required.

Other mechanisms that might change the ability of the virus to infect hosts have also been proposed. Non-muscle myosin heavy chain 9 (MYH9) is a molecule that has been shown to be an essential host factor for PRRSV infection (Gao et al., 2016). MYH9 interacts with PRRSV glycoprotein 5 (coded for by ORF5), changing cell susceptibility to infection. Further studies that investigate the contribution that molecules such as MYH9 have on the infection of different ORF5 PRRSV variants are needed. Additionally, non-neutralizing antibodies can delay the induction of neutralizing antibodies (Ostrowski et al., 2002) in PRRSV infection. Indeed, the mean level and duration of viremia in pigs was greater among animal injected with sub-neutralizing PRRSV-specific IgG antibodies (Yoon et al., 1996), suggesting the existence of an antibody-dependent enhancement (ADE) effect in PRRSV. The extent in which prior exposures to the virus can elicit such effect, and how this may relate to emergence of new viral variants, also remains uncertain.

As an epidemiologic study relying on secondary data generated at the population level, this study has several limitations. Our sequence data were generated by different production systems that differ in number of farms, number of samples submitted, management practices, and health monitoring protocols. Because of that, information may be incomplete and interpretation of data might not always be straightforward. For example, the reason for sample collection (clinical outbreak or routine monitoring), sample composition (single versus pool of animals) and type of sample (serum or tissues) is not always clear. The lack of a denominator (total amount of animals sampled in a farm, total number of farms tested) does not allow for the calculation of risk indicators for disease occurrence. Data contribution by each system also varies with time. However, restricting the data to only the periods in which all systems contributed to the dataset would limit our ability to visualize long-term trends. Additionally, the production system that was responsible for 79% of all sequences was present in the study for the entire study period. Therefore, we believe that biases introduced by this issue were likely small and would not have changed the conclusions of our work. In this United States region, systems that participate in the MSHMP represent approximately 90% of the swine farms. The remaining 10% of farms belong to smaller systems in the area or independent farmers. By having data from systems that represent the vast majority of farms in this region, we expect our data to be reasonably representative of PRRSV occurrence in the region as a whole. Additionally, despite the shortcomings mentioned above, the usage of MSHMP data allows us to work with data directly from the systems, which might suffer less bias toward diseased animals than usual veterinary diagnostics laboratories data do.

Another limitation of this analysis involves the data generation process for the sequences analyzed here. Production systems usually collect samples and send them to different diagnostic laboratories. Laboratory details on quality of sequence reads were not available. These sequences most likely represent a consensus of viral sub-populations present within the host (Goldberg et al., 2003; Lauring and Andino, 2010), but further information that could help in assessing the quality of the read and the variability of sub-populations is not available. The sequences used here are from the *ORF5* gene alone and may not fully represent evolutionary dynamics elsewhere in the genome, since the *ORF5* gene represents approximately 4% of the whole genome of PRRSV. Studies that further explore whole genome sequencing as a tool to understand PRRSV epidemiological and evolutionary patterns are required.

Factors affecting PRRSV dynamics in specific farms are not clearly understood. We show overall temporal dynamics of PRRSV in a swine-producing region of the United States, however, we have limited farm-level information. Thus, we have limited ability to track turnover of viral variants within farms, though we expect this to be influenced by management practices, such as the vaccination protocol adopted by farms, the movement

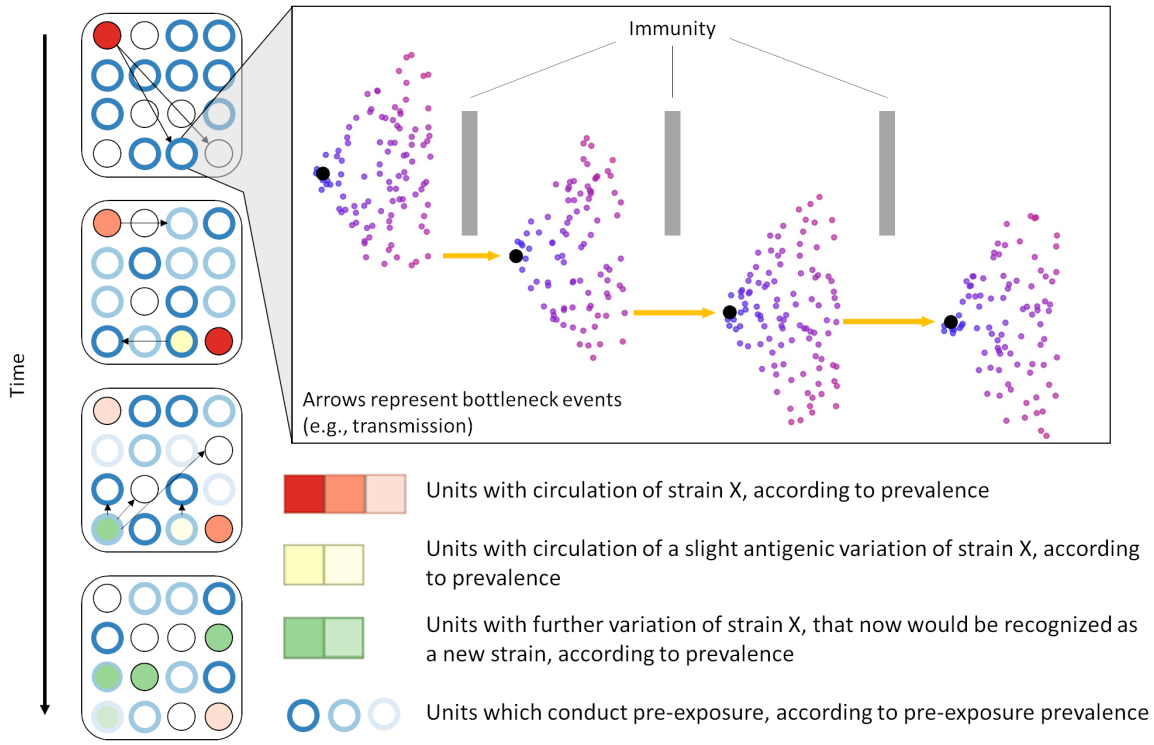

FIGURE 6 | We hypothesize that PRRSV evolution is partially driven by immune-mediated selective pressure. Immune-mediated pressure (either within an animal or during transmission between animals/farms) selects for escapee viral variants (inset). Over time, the selection of escapees may allow for emergence of a heterologous viral populations (i.e., strains, genetic groups, or lineages) which are able to spread within the host population. In scenarios in which some method of pre-exposure is adopted, prevalence of immunity against specific types of PRRSV is high (often artificially through vaccination or live virus inoculation) despite high population turnover, possibly favoring the occurrence of immune-mediated selection.

of animals and personnel to and between farms, the proximity to other swine producing farms, how neighboring farms manage their animals, etc. Pig production in the U.S. swine industry is characterized by multi-site pig production, which refers to segregating the breeding herd from the growing herd such that animals in each stage of production are housed at separate locations. Multi-site production results in the movement of animals between different production sites, which can be located in different states within the United States (Valdes-Donoso et al., 2017; VanderWaal et al., 2018; Kinsley et al., 2019). The role of animal movement in shaping the temporal dynamics of PRRSV lineages is outside the scope of this study, but is an area of active research. In addition, the commingling of animals from different sources, which might have been previously exposed to different viral populations, may allow for the introduction of viral types prevalent in other parts of the country and also exacerbate the potential for recombination of viral populations. Still, in our dataset we found evidence for recombination in only two MSHMP sequences.

Future Research

Immune interaction between infections of differing PRRSV isolates remains poorly understood in swine. The vast adoption of control protocols that rely on imperfect immune response aimed mostly at reducing severity of upcoming infections (such as pre-exposure protocols with commercial vaccines or with lvi) suggests that a better understanding of the cross-immunity generated by infection with different isolates of the virus would be valuable to the industry as a whole. Prospective studies that obtain sera from sow farms under different pre-exposure regimens and follow the farms through time recording PRRSV occurrence would provide valuable information of potential cross-immunity in field conditions. Of interest also is the better understanding of how the spread different lineages/sub-lineages are related to epidemiological data, for example, animal movement data and farm proximity. This might allow for a better comprehension of drivers for PRRSV transmission while allowing for the evaluation of the effectiveness of practices aimed at reducing PRRSV risk (dead animals disposal, manure composting, filtering the air of farms, to name a few).

This study reflects data from a single United States region, which possibly does not reflect PRRSV diversity and temporal dynamics of the whole swine industry in the country (Shi et al., 2010b). That being said, the data presented here reflects a substantial portion of the U.S. swine industry in a region that is relatively spatially discontinuous from other swine producing regions in the United States. In addition, the general pattern of emergence and turnover of different lineages over time observed here describe an evolutionary phenomenon that is expected to also occur in other United States regions. A better understanding

of the natural history of PRRSV can provide insights that can potentially aid in mitigating the impact of the emergence of new viral variants as well as serving as a basis for further work exploring the evolution of PRRSV and the effect this has on disease control, management and impact on the industry.

CONCLUSION

Here, we describe the occurrence of PRRSV over 9 years in a single United States region. We identified the emergence and turnover of different lineages and sub-lineages in the commercial pig population. Such rapid turnover in the dominant lineage through time suggests that temporal patterns of PRRSV occurrence are characterized by multi-strain dynamics, where different PRRSV variants potentially interact through immune-mediated competition or selection. However, cross-immunity between different PRRSV lineages elicited by natural or intentional infection is not fully understood, which hinders the effectiveness of disease control. More research is needed on drivers of evolution and emergence of new sub-lineages in order for the industry to be able to predict, prevent, and mitigate the impacts of PRRSV. Ongoing surveillance for PRRSV using molecular epidemiological methods is invaluable to characterize the evolution of the virus but also to identify recent and historical trends that help understanding the natural history of PRRSV in the United States.

DATA AVAILABILITY STATEMENT

The sequence dataset used here is available in GenBank under the accessions numbers MN498289–MN502669.

AUTHOR CONTRIBUTIONS

IP and KV analyzed, conceptualized, and designed the study. CC, JS, CV, and KV contributed to acquisition of the data. IP, CC, AR, JS, CV, DS, and KV interpreted the data. MM aided in early interpretation of data. All authors but MM were involved in drafting the manuscript and revising it critically for intellectual content and have given final approval of the version to be published.

FUNDING

This project was supported by the Agriculture and Food Research Initiative Competitive grant no. 2018-68008-27890 from the USDA National Institute of Food and Agriculture and by the joint NIFA-NSF-NIH Ecology and Evolution of Infectious Disease award 2019-67015-29918.

ACKNOWLEDGMENTS

We gratefully thank the contributions that Emily Smith and Andres Perez made on early stages of the project. We would like to acknowledge the industry partners who contributed to data for this analysis and to SHIC and MSHMP in general, especially to Emily Geary, involved in the MSHMP data curation.

SUPPLEMENTARY MATERIAL

The Supplementary Material for this article can be found online at: https://www.frontiersin.org/articles/10.3389/fmicb.2019.02486/full#supplementary-material

REFERENCES

Animal Disease Research and Diagnostic Laboratory, and South Dakota State Univeristy, (2017). *DNA Sequencing of PRRSV using ORF 5 PCR - MOL.SOP.0007.08*. Brookings, SD: South Dakota State Univeristy.

Ansari, I. H., Kwon, B., Osorio, F. A., and Pattnaik, A. K. (2006). Influence of N-linked glycosylation of porcine reproductive and respiratory syndrome virus GP5 on virus infectivity, antigenicity, and ability to induce neutralizing antibodies. *J. Virol.* 80, 3994–4004. doi: 10.1128/jvi.80.8.3994-4004.2006

Argimón, S., Abudahab, K., Goater, R. J. E., Fedosejev, A., Bhai, J., Glasner, C., et al. (2016). Microreact: visualizing and sharing data for genomic epidemiology and phylogeography. *Microb. Genom.* 2:e000093. doi: 10.1099/mgen.0.000093

Brar, M. S., Shi, M., Hui, R. K.-H., and Leung, F. C.-C. (2014). Genomic evolution of porcine reproductive and respiratory syndrome virus (PRRSV) isolates revealed by deep sequencing. *PLoS One* 9:e88807. doi: 10.1371/journal.pone.0088807

Brar, M. S., Shi, M., Murtaugh, M. P., and Leung, F. C. (2015). Evolutionary diversification of type 2 porcine reproductive and respiratory syndrome virus. *J. Gen. Virol.* 96(Pt 7), 1570–1580. doi: 10.1099/vir.0.000104

Cano, J. P., Dee, S. A., Murtaugh, M. P., Trincado, C. A., and Pijoan, C. B. (2007). Effect of vaccination with a modified-live porcine reproductive and respiratory syndrome virus vaccine on dynamics of homologous viral infection in pigs. *Am. J. Vet. Res.* 68, 565–571. doi: 10.2460/ajvr.68.5.565

Cha, S.-H., Chang, C.-C., and Yoon, K.-J. (2004). Instability of the restriction fragment length polymorphism pattern of open reading frame 5 of porcine reproductive and respiratory syndrome virus during sequential pig-to-pig passages. *J. Clin. Microbiol.* 42, 4462–4467. doi: 10.1128/jcm.42.10.4462-4467.2004

Chang, C.-C., Yoon, K.-J., Zimmerman, J. J., Harmon, K. M., Dixon, P. M., Dvorak, C. M. T., et al. (2002). Evolution of porcine reproductive and respiratory syndrome virus during sequential passages in pigs. *J. Virol.* 76, 4750–4763. doi: 10.1128/jvi.76.10.4750-4763.2002

Chen, N., Trible, B. R., Kerrigan, M. A., Tian, K., and Rowland, R. R. R. (2016). ORF5 of porcine reproductive and respiratory syndrome virus (PRRSV) is a target of diversifying selection as infection progresses from acute infection to virus rebound. *Infect. Genet. Evol.* 40, 167–175. doi: 10.1016/j.meegid.2016.03.002

Christianson, W. T., and Joo, H. S. (1994). Porcine reproductive and respiratory syndrome: a review. *Swine Health Prod.* 2, 10–28.

Collins, J. E., Benfield, D. A., Christianson, W. T., Harris, L., Hennings, J. C., Shaw, D. P., et al. (1992). Isolation of swine infertility and respiratory syndrome virus (isolate ATCC VR-2332) in north america and experimental reproduction of the disease in gnotobiotic pigs. *J. Vet. Diagn. Investig.* 4, 117–126. doi: 10.1177/104063879200400201

Correas, I., Osorio, F. A., Steffen, D., Pattnaik, A. K., and Vu, H. L. X. (2017). Cross reactivity of immune responses to porcine reproductive and respiratory syndrome virus infection. *Vaccine* 35, 782–788. doi: 10.1016/j.vaccine.2016.12.040

Darwich, L., Gimeno, M., Sibila, M., Diaz, I., de la Torre, E., Dotti, S., et al. (2011). Genetic and immunobiological diversities of porcine reproductive

and respiratory syndrome genotype I strains. *Vet. Microbiol.* 150, 49–62. doi: 10.1016/j.vetmic.2011.01.008

Dea, S., Gagnon, C. A., Mardassi, H., Pirzadeh, B., and Rogan, D. (2000). Current knowledge on the structural proteins of porcine reproductive and respiratory syndrome (PRRS) virus: comparison of the North American and European isolates. *Arch. Virol.* 145, 659–688. doi: 10.1007/s007050050662

Delisle, B., Gagnon, C. A., Lambert M-È, D., and Allaire, S. (2012). Porcine reproductive and respiratory syndrome virus diversity of Eastern Canada swine herds in a large sequence dataset reveals two hypervariable regions under positive selection. *Infect. Genet. Evol.* 12, 1111–1119. doi: 10.1016/j.meegid.2012.03.015

Desrosiers, R., and Boutin, M. (2002). An attempt to eradicate porcine reproductive and respiratory syndrome virus (PRRSV) after an outbreak in a breeding herd: eradication strategy and persistence of antibody titers in sows. *J. Swine Health Prod.* 10, 23–25.

Díaz, I., Gimeno, M., Darwich, L., Navarro, N., Kuzemtseva, L., López, S., et al. (2012). Characterization of homologous and heterologous adaptive immune responses in porcine reproductive and respiratory syndrome virus infection. *Vet. Res.* 43:30. doi: 10.1186/1297-9716-43-30

Domingo, E., Escarmís, C., Sevilla, N., Moya, A., Elena, S. F., Quer, J., et al. (1996). Basic concepts in RNA virus evolution. *FASEB J.* 10, 859–864.

Ferguson, N. M., Galvani, A. P., and Bush, R. M. (2003). Ecological and immunological determinants of influenza evolution. *Nature* 422, 428–433. doi: 10.1038/nature01509

Forsberg, R., Storgaard, T., Nielsen, H. S., Oleksiewicz, M. B., Cordioli, P., Sala, G., et al. (2002). The genetic diversity of european type PRRSV is similar to that of the North American type but is geographically skewed within Europe. *Virology* 299, 38–47. doi: 10.1006/viro.2002.1450

Frossard, J.-P., Hughes, G. J., Westcott, D. G., Naidu, B., Williamson, S., Woodger, N. G. A., et al. (2013). Porcine reproductive and respiratory syndrome virus: genetic diversity of recent British isolates. *Vet. Microbiol.* 162, 507–518. doi: 10.1016/j.vetmic.2012.11.011

Gao, J., Xiao, S., Xiao, Y., Wang, X., Zhang, C., Zhao, Q., et al. (2016). MYH9 is an essential factor for porcine reproductive and respiratory syndrome virus infection. *Sci. Rep.* 6:25120. doi: 10.1038/srep25120

Geldhof, M. F., Vanhee, M., Van Breedam, W., Van Doorsselaere, J., Karniychuk, U. U., and Nauwynck, H. J. (2012). Comparison of the efficacy of autogenous inactivated porcine reproductive and respiratory syndrome virus (PRRSV) vaccines with that of commercial vaccines against homologous and heterologous challenges. *BMC Vet. Res.* 8:182. doi: 10.1186/1746-6148-8-182

Goldberg, T. L., Lowe, J. F., Milburn, S. M., and Firkins, L. D. (2003). Quasispecies variation of porcine reproductive and respiratory syndrome virus during natural infection. *Virology* 317, 197–207. doi: 10.1016/j.virol.2003.07.009

Goldberg, T. L., Weigel, R. M., Hahn, E. C., and Scherba, G. (2000). Associations between genetics, farm characteristics and clinical disease in field outbreaks of porcine reproductive and respiratory syndrome virus. *Prev. Vet. Med.* 43, 293–302. doi: 10.1016/s0167-5877(99)00104-x

Guo, Z., Chen, X.-X., Li, R., Qiao, S., and Zhang, G. (2018). The prevalent status and genetic diversity of porcine reproductive and respiratory syndrome virus in China: a molecular epidemiological perspective. *Virol. J.* 15:2. doi: 10.1186/s12985-017-0910-6

Gupta, S., Ferguson, N., and Anderson, R. (1998). Chaos, persistence, and evolution of strain structure in antigenically diverse infectious agents. *Science* 280, 912–915. doi: 10.1126/science.280.5365.912

Hanada, K., Suzuki, Y., Nakane, T., Hirose, O., and Gojobori, T. (2005). The origin and evolution of porcine reproductive and respiratory syndrome viruses. *Mol. Biol. Evol.* 22, 1024–1031. doi: 10.1093/molbev/msi089

Holtkamp, D. J., Kliebenstein, J. B., Neumann, E. J., Zimmerman, J. J., Rotto, H. F., Yoder, T. K., et al. (2013). Assessment of the economic impact of porcine reproductive and respiratory syndrome virus on United States pork producers. *J. Swine Health Prod.* 21, 72–84.

Holtkamp, D. J., Polson, D. D., Torremorell, M., Morrison, B., Classen, D. M., Becton, L., et al. (2011). Terminology for classifying the porcine reproductive and respiratory syndrome virus (PRRSV) status of swine herds. *Tierarztl. Prax. Ausg. G Grosstiere Nutztiere* 39, 101–112.

Hungnes, O., Jonassen, T. O., Jonassen, C. M., and Grinde, B. (2000). Molecular epidemiology of viral infections. How sequence information helps us understand the evolution and dissemination of viruses. review article. *APMIS* 108, 81–97. doi: 10.1034/j.1600-0463.2000.d01-31.x

Kappes, M. A., and Faaberg, K. S. (2015). PRRSV structure, replication and recombination: origin of phenotype and genotype diversity. *Virology* 479–480, 475–486. doi: 10.1016/j.virol.2015.02.012

Kapur, V., Elam, M. R., Pawlovich, T. M., and Murtaugh, M. P. (1996). Genetic variation in porcine reproductive and respiratory syndrome virus isolates in the midwestern United States. *J. Gen. Virol.* 77, 1271–1276. doi: 10.1099/0022-1317-77-6-1271

Kim, W.-I., Kim, J.-J., Cha, S.-H., Wu, W.-H., Cooper, V., Evans, R., et al. (2013). Significance of genetic variation of PRRSV ORF5 in virus neutralization and molecular determinants corresponding to cross neutralization among PRRS viruses. *Vet. Microbiol.* 162, 10–22. doi: 10.1016/j.vetmic.2012.08.005

Kinsley, A. C., Perez, A. M., Craft, M. E., and Vanderwaal, K. L. (2019). Characterization of swine movements in the United States and implications for disease control. *Prev. Vet. Med.* 164, 1–9. doi: 10.1016/j.prevetmed.2019.01.001

Kosakovsky Pond, S. L., and Frost, S. D. W. (2005). Not so different after all: a comparison of methods for detecting amino acid sites under selection. *Mol. Biol. Evol.* 22, 1208–1222. doi: 10.1093/molbev/msi105

Kryazhimskiy, S., and Plotkin, J. B. (2008). The population genetics of dN/dS. *PLoS Genet.* 4:e1000304. doi: 10.1371/journal.pgen.1000304

Kucharski, A. J., Andreasen, V., and Gog, J. R. (2016). Capturing the dynamics of pathogens with many strains. *J. Math. Biol.* 72, 1–24. doi: 10.1007/s00285-015-0873-4

Kumar, S., Stecher, G., and Tamura, K. (2016). MEGA7: molecular evolutionary genetics analysis version 7.0 for bigger datasets. *Mol. Biol. Evol.* 33, 1870–1874. doi: 10.1093/molbev/msw054

Kwon, T., Yoo, S. J., Lee, D.-U., Sunwoo, S. Y., Je, S. H., Park, J. W., et al. (2019). Differential evolution of antigenic regions of porcine reproductive and respiratory syndrome virus 1 before and after vaccine introduction. *Virus Res.* 260, 12–19. doi: 10.1016/j.virusres.2018.11.004

Larsson, A. (2014). AliView: a fast and lightweight alignment viewer and editor for large datasets. *Bioinformatics* 30, 3276–3278. doi: 10.1093/bioinformatics/btu531

Lauring, A. S., and Andino, R. (2010). Quasispecies theory and the behavior of RNA viruses. *PLoS Pathog.* 6:e1001005. doi: 10.1371/journal.ppat.1001005

Lemoine, F., Domelevo Entfellner, J.-B., Wilkinson, E., Correia, D., Dávila Felipe, M., De Oliveira, T., et al. (2018). Renewing Felsenstein's phylogenetic bootstrap in the era of big data. *Nature* 556, 452–456. doi: 10.1038/s41586-018-0043-0

Lisowska, E. (2002). The role of glycosylation in protein antigenic properties. *Cell Mol. Life Sci.* 59, 445–455. doi: 10.1007/s00018-002-8437-3

Liu, S., Ji, K., Chen, J., Tai, D., Jiang, W., Hou, G., et al. (2009). Panorama Phylogenetic Diversity and Distribution of Type A Influenza Virus. *PLoS One* 4:e5022. doi: 10.1371/journal.pone.0005022

Lyoo, Y. S. (2015). Porcine reproductive and respiratory syndrome virus vaccine does not fit in classical vaccinology. *Clin. Exp. Vaccine Res.* 4, 159–165.

Martin, D. P., Murrell, B., Golden, M., Khoosal, A., and Muhire, B. (2015). RDP4: detection and analysis of recombination patterns in virus genomes. *Virus Evol.* 1:vev003.

McCullers, J. A., Wang, G. C., He, S., and Webster, R. G. (1999). Reassortment and insertion-deletion are strategies for the evolution of influenza B viruses in nature. *J. Virol.* 73, 7343–7348.

McMichael, A. J., Borrow, P., Tomaras, G. D., Goonetilleke, N., and Haynes, B. F. (2010). The immune response during acute HIV-1 infection: clues for vaccine development. *Nat. Rev. Immunol.* 10, 11–23. doi: 10.1038/nri2674

Murtaugh, M. P. (2004). *What We Know About the Primary Immune Response to PRRSV*. Available at: https://www.prrs.com/en/publications/articles/Murtaugh/ (accessed November 20, 2018).

Murtaugh, M. P., Stadejek, T., Abrahante, J. E., Lam, T. T. Y., and Leung, F. C.-C. (2010). The ever-expanding diversity of porcine reproductive and respiratory syndrome virus. *Virus Res.* 154, 18–30. doi: 10.1016/j.virusres.2010.08.015

National Agricultural Statistics Service [NASS], Agricultural Statistics Board and United States Deparment of Agriculture [USDA] (2018). *Quarterly Hogs and Pigs*. Available at: http://usda.mannlib.cornell.edu/usda/current/HogsPigs/HogsPigs-09-27-2018.pdf (accessed November 20, 2018).

Nelson, M. I., Viboud, C., Simonsen, L., Bennett, R. T., Griesemer, S. B., St George, K., et al. (2008). Multiple reassortment events in the evolutionary history of

h1n1 influenza a virus since 1918. *PLoS Pathog.* 4:e1000012. doi: 10.1371/journal.ppat.1000012

Ostrowski, M., Galeota, J. A., Jar, A. M., Platt, K. B., Osorio, F. A., and Lopez, O. J. (2002). Identification of neutralizing and nonneutralizing epitopes in the porcine reproductive and respiratory syndrome virus GP5 ectodomain. *J. Virol.* 76, 4241–4250. doi: 10.1128/jvi.76.9.4241-4250.2002

Pejsak, Z., Stadejek, T., and Markowska-Daniel, I. (1997). Clinical signs and economic losses caused by porcine reproductive and respiratory syndrome virus in a large breeding farm. *Vet. Microbiol.* 55, 317–322. doi: 10.1016/s0378-1135(96)01326-0

Perez, A. M., Alba, A., Goede, D., McCluskey, B., and Morrison, R. (2016). Monitoring the spread of swine enteric coronavirus diseases in the United States in the absence of a regulatory framework. *Front. Vet. Sci.* 3:18. doi: 10.3389/fvets.2016.00018

Pérez-Sautu, U., Costafreda, M. I., Caylà, J., Tortajada, C., Lite, J., Bosch, A., et al. (2011). Hepatitis a virus vaccine escape variants and potential new serotype emergence. *Emerg. Infect. Dis.* 17, 734–737. doi: 10.3201/eid1704.101169

Plagemann, P. G. W., Rowland, R. R. R., and Faaberg, K. S. (2002). The primary neutralization epitope of porcine respiratory and reproductive syndrome virus strain VR-2332 is located in the middle of the GP5 ectodomain. *Arch. Virol.* 147, 2327–2347. doi: 10.1007/s00705-002-0887-2

Pond, S. L. K., and Frost, S. D. W. (2005). Datamonkey: rapid detection of selective pressure on individual sites of codon alignments. *Bioinformatics* 21, 2531–2533. doi: 10.1093/bioinformatics/bti320

Popescu, L. N., Trible, B. R., Chen, N., and Rowland, R. R. R. (2017). GP5 of porcine reproductive and respiratory syndrome virus (PRRSV) as a target for homologous and broadly neutralizing antibodies. *Vet. Microbiol.* 209, 90–96. doi: 10.1016/j.vetmic.2017.04.016

Ragonnet-Cronin, M., Hodcroft, E., Hué, S., Fearnhill, E., Delpech, V., Brown, A. J. L., et al. (2013). Automated analysis of phylogenetic clusters. *BMC Bioinformatics* 6:317. doi: 10.1186/1471-2105-14-317

Roberts, J. (2003). "Using "DNA finger printing" to monitor the PRRS viruses infecting a sow herd," in *PRRS compendium: A Comprehensive Reference on Porcine Reproductive and Respiratory Syndrome for Pork Producers, Veterinary Practitioners, and Researchers*, 2nd Edn, eds J. J. Zimmerman, and K.-J. Yoon, (Des Moines: National Pork Board), 71–75.

Scortti, M., Prieto, C., Simarro, I., and Castro, J. M. (2006). Reproductive performance of gilts following vaccination and subsequent heterologous challenge with European strains of porcine reproductive and respiratory syndrome virus. *Theriogenology* 66, 1884–1893. doi: 10.1016/j.theriogenology.2006.04.043

Shi, M., Lam, T. T.-Y., Hon, C.-C., Hui, R. K.-H., Faaberg, K. S., Wennblom, T., et al. (2010a). Molecular epidemiology of PRRSV: a phylogenetic perspective. *Virus Res.* 154, 7–17. doi: 10.1016/j.virusres.2010.08.014

Shi, M., Lam, T. T.-Y., Hon, C.-C., Murtaugh, M. P., Davies, P. R., Hui, R. K.-H., et al. (2010b). Phylogeny-based evolutionary, demographical, and geographical dissection of north american type 2 porcine reproductive and respiratory syndrome viruses. *J. Virol.* 84, 8700–8711. doi: 10.1128/JVI.02551-09

Smith, N., Power, U. F., and McKillen, J. (2018). Phylogenetic analysis of porcine reproductive and respiratory syndrome virus isolates from Northern Ireland. *Arch. Virol.* 63, 2799–2804. doi: 10.1007/s00705-018-3886-7

Solano, G. I., Segalés, J., Collins, J. E., Molitor, T. W., and Pijoan, C. (1997). Porcine reproductive and respiratory syndrome virus (PRRSv) interaction with Haemophilus parasuis. *Vet. Microbiol.* 55, 247–257. doi: 10.1016/s0378-1135(96)01325-9

Stadejek, T., Stankevicius, A., Murtaugh, M. P., and Oleksiewicz, M. B. (2013). Molecular evolution of PRRSV in Europe: current state of play. *Vet. Microbiol.* 165, 21–28. doi: 10.1016/j.vetmic.2013.02.029

StataCorp. (2017). *Stata Statistical Software: Release 15*. College Station, TX: StataCorp LLC.

Tamura, K., and Nei, M. (1993). Estimation of the number of nucleotide substitutions in the control region of mitochondrial DNA in humans and chimpanzees. *Mol. Biol. Evol.* 10, 512–526.

Tousignant, S. J. P., Perez, A., and Morrison, R. (2015a). Comparison between the 2013-2014 and 2009-2012 annual porcine reproductive and respiratory syndrome virus epidemics in a cohort of sow herds in the United States. *Can. Vet. J.* 56, 1087–1089.

Tousignant, S. J. P., Perez, A. M., Lowe, J. F., Yeske, P. E., and Morrison, R. B. (2015b). Temporal and spatial dynamics of porcine reproductive and respiratory syndrome virus infection in the United States. *Am. J. Vet. Res.* 76, 70–76. doi: 10.2460/ajvr.76.1.70

Valdes-Donoso, P., VanderWaal, K., Jarvis, L. S., Wayne, S. R., and Perez, A. M. (2017). Using machine learning to predict swine movements within a regional program to improve control of infectious diseases in the US. *Front. Vet. Sci.* 4:2. doi: 10.3389/fvets.2017.00002/full

VanderWaal, K., and Deen, J. (2018). Global trends in infectious diseases of swine. *Proc. Natl. Acad. Sci.* 115, 11495–11500. doi: 10.1073/pnas.1806068115

VanderWaal, K., Perez, A., Torremorrell, M., Morrison, R. M., and Craft, M. (2018). Role of animal movement and indirect contact among farms in transmission of porcine epidemic diarrhea virus. *Epidemics* 24, 67–75. doi: 10.1016/j.epidem.2018.04.001

Vu, H. L. X., Kwon, B., Yoon, K.-J., Laegreid, W. W., Pattnaik, A. K., and Osorio, F. A. (2011). Immune Evasion of Porcine Reproductive and Respiratory Syndrome Virus through Glycan Shielding Involves both Glycoprotein 5 as Well as Glycoprotein 3. *J. Virol.* 85, 5555–5564. doi: 10.1128/JVI.00189-11

Wang, X. (2016). *Immunological Selection as a Driver of Porcine Reproductive and Respiratory Syndrome Virus (PRRSV) Evolution*. Minneapolis: University of Minnesota.

Webster, R. G., Bean, W. J., Gorman, O. T., Chambers, T. M., and Kawaoka, Y. (1992). Evolution and ecology of influenza A viruses. *Microbiol. Rev.* 56, 152–179.

Wensvoort, G., Terpstra, C., Pol, J. M., ter Laak, E. A., Bloemraad, M., de Kluyver, E. P., et al. (1991). Mystery swine disease in the Netherlands: the isolation of Lelystad virus. *Vet. Q.* 13, 121–130. doi: 10.1080/01652176.1991.9694296

Wesley, R. D., Mengeling, W. L., Lager, K. M., Clouser, D. F., Landgraf, J. G., and Frey, M. L. (1998). Differentiation of a porcine reproductive and respiratory syndrome virus vaccine strain from North American field strains by restriction fragment length polymorphism analysis of ORF 5. *J. Vet. Diagn. Invest.* 10, 140–144. doi: 10.1177/104063879801000204

Xu, M., Wang, S., Li, L., Lei, L., Liu, Y., Shi, W., et al. (2010). Secondary infection with *Streptococcus* suis serotype 7 increases the virulence of highly pathogenic porcine reproductive and respiratory syndrome virus in pigs. *Virol. J.* 7, 1–9. doi: 10.1186/1743-422X-7-184

Yoon, K. J., Wu, L. L., Zimmerman, J. J., Hill, H. T., and Platt, K. B. (1996). Antibody-dependent enhancement (ADE) of porcine reproductive and respiratory syndrome virus (PRRSV) infection in pigs. *Viral Immunol.* 9, 51–63. doi: 10.1089/vim.1996.9.51

Zhang, J., Zheng, Y., Xia, X.-Q., Chen, Q., Bade, S. A., Yoon, K.-J., et al. (2017). High-throughput whole genome sequencing of porcine reproductive and respiratory syndrome virus from cell culture materials and clinical specimens using next-generation sequencing technology. *J. Vet. Diagn. Invest.* 29, 41–50. doi: 10.1177/1040638716673404

Conflict of Interest: The authors declare that the research was conducted in the absence of any commercial or financial relationships that could be construed as a potential conflict of interest.

Copyright © 2019 Paploski, Corzo, Rovira, Murtaugh, Sanhueza, Vilalta, Schroeder and VanderWaal. This is an open-access article distributed under the terms of the Creative Commons Attribution License (CC BY). The use, distribution or reproduction in other forums is permitted, provided the original author(s) and the copyright owner(s) are credited and that the original publication in this journal is cited, in accordance with accepted academic practice. No use, distribution or reproduction is permitted which does not comply with these terms.

frontiers in Microbiology

ORIGINAL RESEARCH
published: 21 November 2019
doi: 10.3389/fmicb.2019.02696

Molecular Detection and Genetic Characterization of Novel RNA Viruses in Wild and Synanthropic Rodents and Shrews in Kenya

Samson Omondi Onyuok[1,2,3,4†], Ben Hu[1,2,4†], Bei Li[1], Yi Fan[1], Kelvin Kering[1,4], Griphin Ochieng Ochola[1,2,3,4], Xiao-Shuang Zheng[1], Vincent Obanda[5], Sheila Ommeh[6], Xing-Lou Yang[1,2,4], Bernard Agwanda[3] and Zheng-Li Shi[1,2,4]**

[1] CAS Key Laboratory of Special Pathogens and Biosafety, Wuhan Institute of Virology, Chinese Academy of Sciences, Wuhan, China, [2] Sino-Africa Joint Research Center, Chinese Academy of Sciences, Wuhan, China, [3] Mammalogy Section, National Museums of Kenya, Nairobi, Kenya, [4] University of Chinese Academy of Sciences, Beijing, China, [5] Veterinary Services Department, Kenya Wildlife Service, Nairobi, Kenya, [6] Institute of Biotechnology Research, Jomo Kenyatta University of Science and Technology, Nairobi, Kenya

OPEN ACCESS

Edited by:
Erna Geessien Kroon, Federal University of Minas Gerais, Brazil

Reviewed by:
Marta Canuti, Memorial University of Newfoundland, Canada
Jane Megid, São Paulo State University, Brazil

***Correspondence:**
Bernard Agwanda
benrisky@gmail.com
Zheng-Li Shi
zlshi@wh.iov.cn

† These authors have contributed equally to this work

Specialty section:
This article was submitted to Virology, a section of the journal Frontiers in Microbiology

Received: *05 August 2019*
Accepted: *06 November 2019*
Published: *21 November 2019*

Citation:
Onyuok SO, Hu B, Li B, Fan Y, Kering K, Ochola GO, Zheng X-S, Obanda V, Ommeh S, Yang X-L, Agwanda B and Shi Z-L (2019) Molecular Detection and Genetic Characterization of Novel RNA Viruses in Wild and Synanthropic Rodents and Shrews in Kenya. Front. Microbiol. 10:2696. doi: 10.3389/fmicb.2019.02696

The majority of emerging and reemerging zoonotic viral pathogens are RNA viruses. Pathogen discovery programs of emerging infectious diseases (EIDs) in wildlife have implicated rodents and shrews as hosts of diverse human pathogens, such as hantaviruses, arenaviruses, paramyxoviruses, etc. Despite these threats, little is known about the diversity of viruses circulating among rodents and shrews in Kenya, meaning the risk of infectious disease outbreak from these small mammals could be oblivious. This study reports the first surveillance toward understanding the diversity of RNA viruses carried by rodents and shrews in areas of high-potential contact with humans in Kenya through molecular detection. A total of 617 samples comprising fecal, urine, and tissues from 138 rodents and 5 shrews were screened for eight different families of viruses using RT-PCR assays. The results highlight the presence of diverse astroviruses, paramyxoviruses, hepeviruses, and arenavirus, circulating in both wild and synanthropic Kenyan rodents and shrews. Most of the viruses detected in this study are novel strains and some belong to the families that contain important human viral pathogens. Notably, a novel arenavirus was detected in *Grammomys macmillani*, a rodent species newly identified to harbor arenavirus, and it potentially represent a novel arenavirus species. Our findings demonstrate the need for continued pathogen surveillance among these small mammals as well as among the vulnerable and exposed livestock and humans. This would help in development and implementation of effective preventive and control strategies on EIDs in countries with rich wildlife biodiversity like Kenya.

Keywords: Kenya, RNA viruses, zoonotic pathogens, rodents, shrews, arenavirus

INTRODUCTION

More than half of the documented human pathogens are zoonotic, and emerging infectious diseases (EIDs) are more likely to be caused by pathogens of zoonotic origin (Woolhouse and Gowtage-Sequeria, 2005; Jones et al., 2008). In most instances, high impact outbreaks of the past decades and present pandemics have resulted from pathogens of wildlife origin, which usually cause little or no clinical signs of infection in their natural hosts (Wu et al., 2018), but with devastating global health and economic effects when they spill over into humans and livestock (Allen et al., 2017). The present global upsurge in outbreaks of emerging and re-emerging infectious diseases has necessitated the search for reservoirs of zoonoses of public health importance in order to develop resilient response strategies.

RNA viruses account for a large part of the known zoonotic pathogens owing to their often high rates of mutation and capacity to infect and adapt in a wide range of hosts (Woolhouse and Gowtage-Sequeria, 2005; Jones et al., 2008; Meheretu et al., 2012). Surveillance and discovery programs of EIDs in wildlife have identified rodents and shrews as natural reservoirs of diverse RNA viruses such as hantaviruses, arenaviruses, astroviruses, picornaviruses, paramyxoviruses, etc. (Klempa et al., 2006; Meheretu et al., 2012; Firth et al., 2014; Hu et al., 2014; Sasaki et al., 2014; Gryseels et al., 2015; Gouy de Bellocq et al., 2016; Těšíková et al., 2017; Wang et al., 2017). It is believed that these viruses establish themselves in their hosts through co-evolution and are maintained in nature by both vertical and horizontal transmissions (Streicker, 2013). Spillover events into humans and livestock result from encounters with these small mammals whose presence around human dwellings is on the rise either as pests or as food (Bonwitt et al., 2016). Evidently this poses a potential threat to public health and it is imperative that pathogen surveillance and discovery programs are implemented on high risk wildlife groups including rodents and shrews.

Kenya is a country rich in wildlife diversity, with a nationwide distribution of about 106 rodent and 36 shrew species (Musila et al., 2019). Expansion in agricultural activities among other anthropogenic factors encourages encroachment into wildlife habitats and amplifies the frequency of human contacts with these animals and pathogens carried by them (Young et al., 2017). However, there is currently no documentation of viruses harbored by rodents and shrews in Kenya yet they have been sighted and trapped around human dwellings. Also, there could be a possibility of misdiagnosis and underreporting of human infections with rodent-borne viruses in the country. These gaps justify the need to investigate and characterize the diversity of viruses in rodents and shrews and quantify the possible impact of these viruses on public health in Kenya. It was against this backdrop that we carried out this study, in which both wild and peridomestic species of these animals around and within agro-ecological zones near human habitations were sampled and screened for a variety of RNA viral families. This work thus constitutes the first virus surveillance study in Kenyan rodents and shrews, and provides baseline data for understanding the distribution, genetic diversity, as well as potential spillover risk of RNA viruses circulating in small mammals in Kenya.

MATERIALS AND METHODS

Study Area and Sample Collection

Field component of this research was conducted in Kenya, a country rich in wildlife, with a varied climate ranging from the tropical climate in the coastal region, hot dry lowlands, and temperate highlands. Three specific locations were selected for this study: (a) Mtwapa, in the Coast at 0 m above sea level (m.a.s.l), (b) Nakuru, in the Rift Valley at 1500 m.a.s.l., and (c) Kitale, in Western at 2000 m.a.s.l. (**Figure 1**). Each location provides unique ecotype in a high human density neighborhood with intensive large and small scale farming practices indicating high probability of human contacts with rodents and shrews. Line transects were established in homes (compound, kitchens, and stores), farms, and natural habitats (bushes and forests) between August and September, 2016. In every transect, a combination of peanut butter with oat meal as well as fish was used as bait in 20–50 Sherman and Museum Special traps.

Captured animals were sedated via intramuscular injection with ketamine and knocked off by cervical dislocation. Individuals were taxonomically identified using the field guide (Kingdom et al., 2013), and their morphometrics were taken. The animals were necropsied and the following tissues were aseptically collected in cryotubes: lung, liver, kidney, and spleen. Fecal pellets and urine were collected only when available, in both RNALater and VTM. All samples were kept in liquid nitrogen and shipped to Wuhan Institute of Virology, China, for storage at −80°C and for analysis.

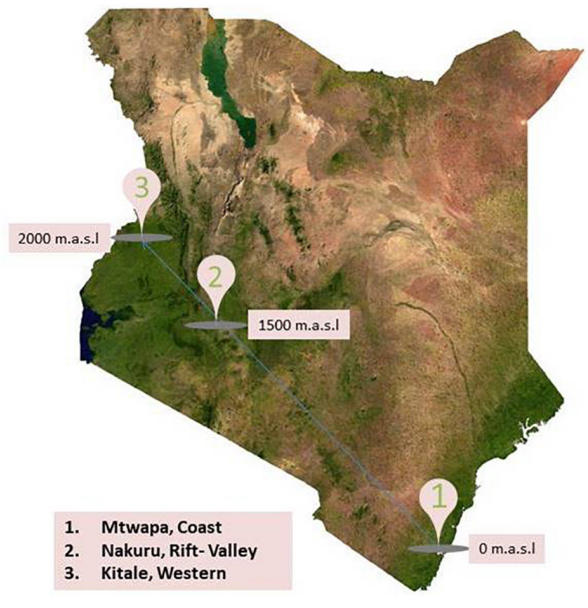

FIGURE 1 | Map of Kenya showing rodent and shrew sampling sites between August and September, 2016.

Molecular Detection of Viruses and Phylogenetic Analysis

RNA was extracted using a viral RNA extraction kit (Roche, Germany) according to the manufacturer's instructions. The first strand cDNA was synthesized with superscript III reverse transcriptase (Invitrogen) and random hexamers. PCR assays utilizing the Platinum Taq DNA polymerase kit (Invitrogen) were applied to screen the presence of following RNA viruses: hantaviruses (Klempa et al., 2006), arenaviruses (Li et al., 2015), coronaviruses (Watanabe et al., 2010), paramyxoviruses (Tong et al., 2008), astroviruses (Chu et al., 2008), hepeviruses (Drexler et al., 2012), picornaviruses (Lau et al., 2011), and flaviviruses (Moureau et al., 2007). The information of primers used in PCR testing of different viral families are presented in **Table 1**. Hantaviruses, arenaviruses, and flaviviruses were screened using kidney, liver, lung, and spleen tissues. Feces were tested for astroviruses, coronaviruses, paramyxoviruses, and picornaviruses which are known to infect gastrointestinal tract. Liver tissues were tested for hepeviruses as liver is the major target tissue for hepatitis E virus infection. Since paramyxoviruses can be secreted in urine, we also screened kidney and the nine urine samples for paramyxovirus RNA. Identities of positive host species were confirmed by sequencing of mitochondrial *Cyt b* gene, recommended for species identification (Bowen et al., 1997). Nucleotide sequences of products with expected amplicon sizes were determined by Sanger sequencing. Sequences were aligned with representative members of relevant family using ClustalW. Phylogenetic inference of each alignment was done in MEGA version 7.0, using the maximum-likelihood (ML) approach and the Tamura–Nei model with a bootstrap of 1000 replicates (Hall, 2013).

Genomic Characterization of the Novel Arenavirus

Isolation of arenavirus was attempted with spleen sample. Vero cells were inoculated with the spleen homogenate and observed daily for cytopathic effect. For next-generation sequencing (NGS), library was constructed using Illumina Truseq Stranded mRNA Sample Preparation Kit (Illumina, San Diego, CA, United States) following the manufacturer's instructions and sequencing was performed on an HiSeq 3000 sequencer (Illumina, San Diego, CA, United States). *De novo* assembly of NGS data was performed using Trinity version r2011-08-20 (Grabherr et al., 2011) and the resulting contigs were aligned to the non-redundant nucleotide database on NCBI. Contigs mapping significantly to the reference sequences were then retrieved and re-mapped to the full genome reference to generate a consensus sequence. The genome end sequence was amplified through the SMARTer® RACE 5′/3′ Kit (Takara). The recovered genome sequence was used for ORF prediction and aligned with those of representative members of mammarenavirus using ClustalW. Pairwise sequence similarities of the L/S segments and

TABLE 1 | Sequences of primers used for RT-PCR screening.

Virus	Primer name	Primer sequence (5′–3′)	Region	Amplicon size
Arenavirus	Arena-F1	AYNGGNACNCCRTTNGC	L gene	Round 1 938 bp
	Arena-R1	TCHTAYAARGARCARGTDGGDGG		
	Arena-F2	GGNACYTCHTCHCCCCANAC		Round 2 610 bp
	Arena-R2	AGYAARTGGGGNCCNAYKATG		
Astrovirus	AstroFWD1	GARTTYGATTGGRCKCGKTAYGA	RdRp	Round 1 436 bp
	AstroFWD2	GARTTYGATTGGRCKAGGTAYGA		
	AstroRVS1	GGYTTKACCCACATNCCRAA		
	AstroFWD3	CGKTAYGATGGKACKATHCC		Round 2 421 bp
	AstroFWD4	AGGTAYGATGGKACKATHCC		
Coronavirus	CoV-FWD3	GGTTGGGAYTAYCCHAARTGTGA	RdRp	Round 1 440 bp
	CoV-RVS3	CCATCATCASWYRAATCATCATA		
	CoV-FWD4	GAYTAYCCHAARTGTGAUMGWGC		Round 2 434 bp
Flavirirus	Flavi-FWD	TGYRBTTAYAACATGATGGG	NS5 gene	270 bp
	Flavi-RVS	GTGTCCCAICCNGCNGTRTC		
Hantavirus	HAN-L-F1	ATGTAYGTBAGTGCWGATGC	L gene	Round 1 453 bp
	HAN-L-R1	AACCADTCWGTYCCRTCATC		
	HAN-L-F2	TGCWGATGCHACIAARTGGTC		Round 2 385 bp
	HAN-L-R2	GCRTCRTCWGARTGRTGDGCAA		
Hepevirus	DE-F4228	ACYTTYTGTGCYYTITTTGGTCCITGGTT	RdRp	Round 1 371 bp
	DE-R4598	CCGGGTTCRCCIGAGTGTTTCTTCCA		
	DE-R4565	GCCATGTTCCAGAYGGTGTTCCA		Round 2 338 bp
Paramyxovirus	PAR-F1	GAAGGITATTGTCAIAARNTNTGGAC	*pol* gene	Round 1 639 bp
	PAR-R	GCTGAAGTTACIGGITCICCDATRTTNC		
	PAR-F2	GTTGCTTCAATGGTTCARGGNGAYAA		Round 2 561 bp
Picornavirus	Picorna-F	CYTATHTRAARGATGAGCTKAGA	$3D^{pol}$	571 bp
	Picorna-R	GCAATNACRTCATCKCCRTA		

ORFs of the novel arenavirus to other mammarenaviruses were calculated using DNAstar. Phylogenetic inference of the aligned homologs of the four ORFs was done in MEGA version 7.0, using the ML approach and the Tamura–Nei model with a bootstrap of 1000 replicates.

RESULTS

Rodents and Shrew Samples

A total of 617 tissue and fecal samples from 143 individual small mammals of 18 species (17 rodent species and 1 shrew species) were collected between August and September, 2016 from the three distinct sampling localities in Kenya (Mtwapa, Nakuru, and Kitale). The samples comprised 138 lungs, 142 livers, 138 kidneys, 134 spleens, 56 fecal samples, and 9 urine samples (**Table 2**).

Virus Detection

Viruses of four families, astroviruses, paramyxoviruses, hepevirus, and arenaviruses, were detected in 17 out of 143 animals, among which eight were from Nakuru and nine were from Kitale. The positive rates ranged from 0.7 (1/142, arenavirus) to 12.5% (7/56, astrovirus) (**Table 3**). However, none of these small mammals tested positive for hantavirus, coronavirus, picornavirus, or flavivirus. There was no detection of viruses from any of the samples from Mtwapa, possibly due to a biased small sample size (**Tables 2**, **3**).

Astrovirus

Fifty-six fecal samples were screened for astroviruses by nested PCR targeting the RNA-dependent RNA polymerase (RdRp) gene of all known mammalian astroviruses. Astroviruses were detected in seven rodents from three species (**Table 3**). The prevalence rate in *Mastomys natalensis* and *Rattus rattus* was 23.5 (4/17) and 20.0% (2/10), respectively. The only one *Cricetomys gambianus* sampled in this study was also found to harbor astrovirus. Phylogenetic tree of the partial RdRp gene showed that astroviruses detected in Kenyan rodents could be divided into three host-specific groups (**Figure 2**). The *R. rattus* astroviruses and *M. natalensis* astroviruses were clustered with previously reported rodent astroviruses, but these two novel clades from Kenya were distinct from the existing strains, sharing lower than 86% nucleotide sequence identity. The single astrovirus detected in *C. gambianus* was exceptionally interesting, as it was closely related to feline astroviruses, sharing 93–99% nt sequence identities to strains from domestic cats and cheetah (**Figure 2**), which implied the possibility of cross-species transmission between rodents and cats.

Paramyxovirus

A total of 138 kidney samples, 56 fecal samples, and 9 urine samples were tested for paramyxovirus RNA. Seven samples tested positive, including six kidney tissues and one urine from four rodent species (**Table 3**). Among the six individuals of *Lophuromys aquilus*, paramyxovirus was discovered in two animals (33.3%), with one positive in kidney and the other positive in urine. *Mus triton* had an equivalent prevalence rate, in which three out of nine animals were positive (**Table 3**).

The seven newly identified Kenyan rodent paramyxoviruses showed <82% nt sequence identities to known paramyxoviruses. In the phylogenetic tree, they fell into the large clade of

TABLE 2 | Numbers of individual animals and numbers of each type of sample per species collected in this study.

Species	Number of individual animals				Number of each type of sample					
	Mtwapa	Nakuru	Kitale	Total	Kidney	Liver	Spleen	Lung	Feces	Urine
Aethomys kaiseri	0	10	0	10	10	10	10	10	4	1
Arvicanthis niloticus	0	7	4	11	11	11	11	11	5	–
Aterelix albiventrix	1	0	0	1	1	1	1	1	1	1
Cricetomys gambianus	0	1	0	1	1	1	1	1	1	1
Crocidura Olivieri	0	3	2	5	4	5	5	4	–	–
Gerbilliscus robustus	5	0	0	5	4	5	4	4	3	–
Grammomys macmillani	0	0	2	2	2	2	2	2	1	–
Graphiurus murinus	0	0	2	2	2	2	2	2	2	1
Lemniscomys striatus	0	5	2	7	7	7	5	7	–	–
Lophuromys aquilus	0	0	6	6	6	6	6	6	5	3
Mastomys natalensis	0	37	14	51	50	51	50	50	17	1
Mus minutoides	0	10	2	12	11	11	9	11	3	–
Mus triton	0	5	4	9	9	9	7	9	1	–
Oenomys hypoxanthus	0	0	1	1	1	1	1	1	1	–
Otomys tropicalis	0	1	0	1	1	1	1	1	–	–
Paraxerus ochraceus	2	0	0	2	2	2	2	2	–	–
Rattus rattus	2	3	10	15	14	15	14	14	10	1
Tachyoryctes splendens	0	2	0	2	2	2	2	2	2	–
Total	10	84	49	143	138	142	134	138	56	9

TABLE 3 | Individual animals and sample types positive for four viral families.

		Number of positives/number of tested individuals				Number of positives/number of tested samples					
Virus	**Positive species**	**MT**	**NK**	**KT**	**Total**	**Feces**	**Lung**	**Liver**	**Kidney**	**Spleen**	**Urine**
Astrovirus	*C. gambianus*	–	1/1	–	1/1	1/1	–	–	–	–	–
	M. natalensis	–	4/7	0/10	4/17	4/17	–	–	–	–	–
	R. rattus	0/1	0/2	2/7	2/10	2/10	–	–	–	–	–
Paramyxovirus	*L. aquilus*	–	–	2/6	2/6	0/5	–	–	1/6	–	1/3
	M. natalensis	–	0/37	1/14	1/51	0/17	–	–	1/50	–	0/1
	M. minutoides	–	1/10	0/2	1/12	0/3	–	–	1/11	–	–
	M. triton	–	2/5	1/4	3/9	0/1	–	–	3/9	–	–
Hepevirus	*C. olivieri*	–	0/3	1/2	1/5	–	–	1/5	–	–	–
	R. rattus	0/2	0/3	1/10	1/15	–	–	1/15	–	–	–
Arenavirus	*G. macmillani*	–	–	1/2	1/2	–	1/2	1/2	1/2	1/2	–

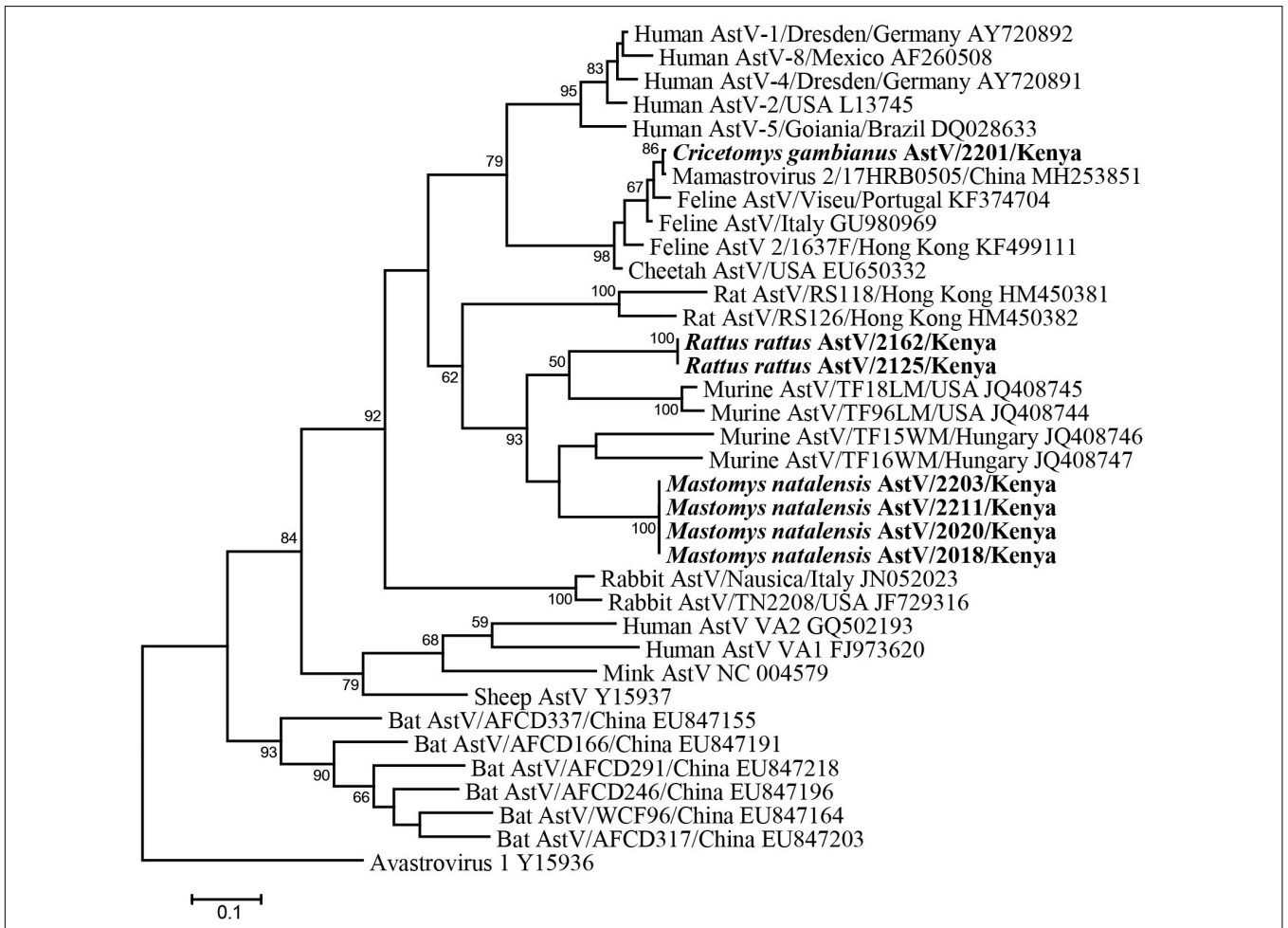

FIGURE 2 | ML tree based on 315-nt partial RdRp gene of astroviruses (corresponding to human astrovirus 1 genome nt 3619-3933, AY720892). Strains detected in this study are indicated in bold.

the newly recognized genus *Jeilongvirus*. The Kenyan rodent paramyxoviruses were genetically diverse and formed four distinct clusters, most of which exhibited host species specificity (**Figure 3**). Three strains from *M. triton* and *Mus minutoides* were phylogenetically related to J virus. The paramyxoviruses discovered in *M. natalensis* and *L. aquilus* from Kenya were most closely related to strains previously found in these two species, respectively, from other African countries (**Figure 3**).

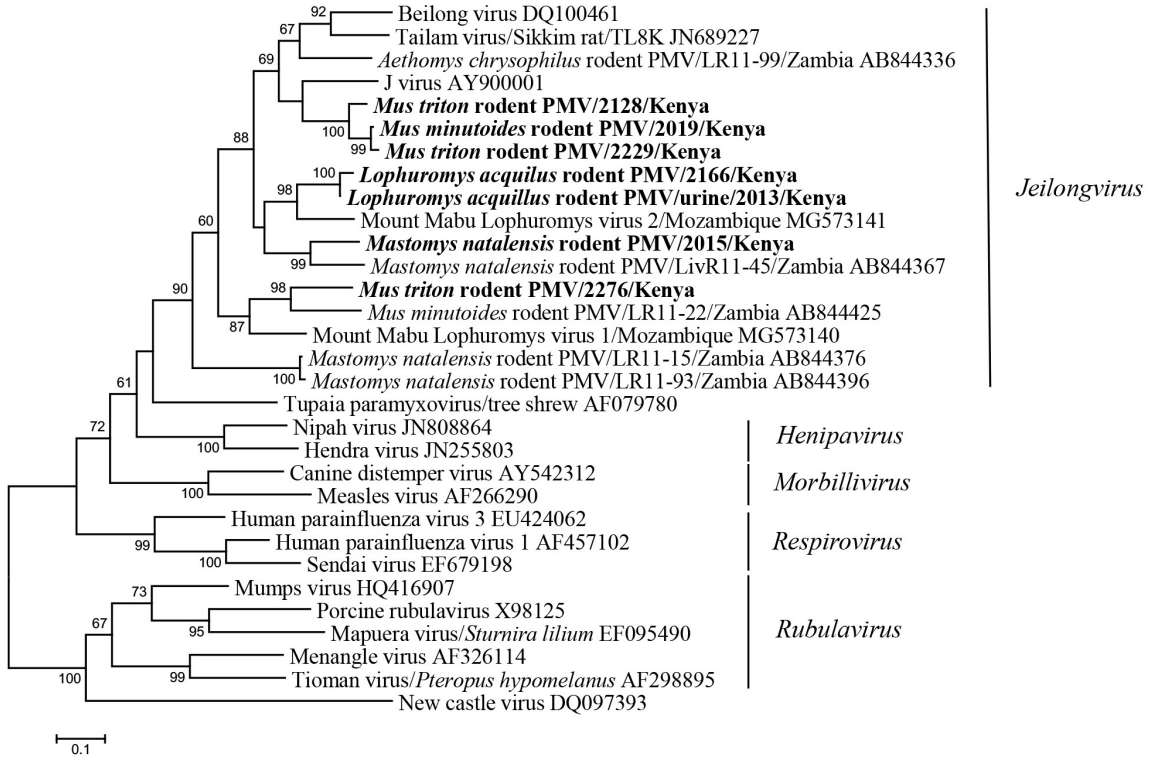

FIGURE 3 | ML tree based on 506-nt partial L gene of paramyxoviruses (corresponding to Beilong virus genome nt 14889-15394, DQ100461). Strains detected in this study are indicated in bold.

Hepevirus

Hemi-nested RT-PCR was applied to screen a total of 142 liver tissues, and hepevirus RNA was found in two specimens. One positive sample originated from *R. rattus*, with the detection rate of 6.67% (1/15) (**Table 3**). The Kenyan rat hepevirus shared <87% nt sequence identity with rat hepeviruses reported in Europe and Asia in the partial RdRp gene. It was placed phylogenetically in the clade consisting of rodent-specific hepeviruses, and can be identified as a novel variant within the *Orthohepevirus C* species (**Figure 4**).

In addition to rodents, novel shrew hepevirus sequence was detected in one of the five samples from *Crocidura olivieri* (**Table 3**). The amino acid sequence identities of partial RdRp between the shrew hepevirus and known hepeviruses were no >76%. Phylogenetic analysis revealed that the shrew hepevirus was divergent from rodent hepevirus and formed a separate monophyletic branch (**Figure 4**).

Genomic Characterization of a Novel Arenavirus

Kidney, liver, lung, and spleen tissues from 143 rodent and shrews were screened for presence of arenavirus RNA by RT-PCR targeting partial L gene. One out of the two *Grammomys macmillani* individuals was arenavirus PCR positive, and the virus was detected in all four types of tissue (**Table 3**). The animal infected with arenavirus was trapped in a bush on the outskirts of Kitale town in western Kenya. The newly identified arenavirus was thus designated as Kitale virus under the name of its geographical origin.

The viral RNA extracted from the positive spleen sample was used for NGS to determine genome sequence of Kitale virus. Assembly allowed reconstruction of complete coding sequences of its S and L segments. Each of the two segments of Kitale virus genome has the typical two open-reading frames (ORFs) in ambisense orientation, separated by the stem–loop structures. The S segment contains genes for glycoprotein precursor (GPC, 493 aa) and nucleoprotein (NP, 566 aa), while the L segment encodes the RdRp, also known as the L protein (2225 aa), and matrix Z protein (96 aa). In the L ORF of Kitale virus, the endonuclease motif (P_{88}, D_{89}, E_{102}, and K_{115}) is well conserved like other arenaviruses (Vieth et al., 2004). The two late domains PTAP and PPPY are also contained in the Z protein as in most arenaviruses including Lassa virus (LASV).

We compared the nucleotide and deduced amino acid (aa) sequences of the four ORFs of Kitale virus and other representative Old-World arenaviruses (OWA) (**Table 4**). In both of the two genomic segments and all four genes, Kitale virus shared the highest sequence identity with Ippy virus, which infected *Arvicanthis* in Central Africa Republic. The nucleotide/aa sequence identities between Kitale virus and Ippy virus were 71.4/80.5 and 69.5/78.1% for GPC and NP genes, respectively. Sequence identities in the L segment were substantially lower, with 61.5/62.2% (L) and 55.7/61.1% (Z).

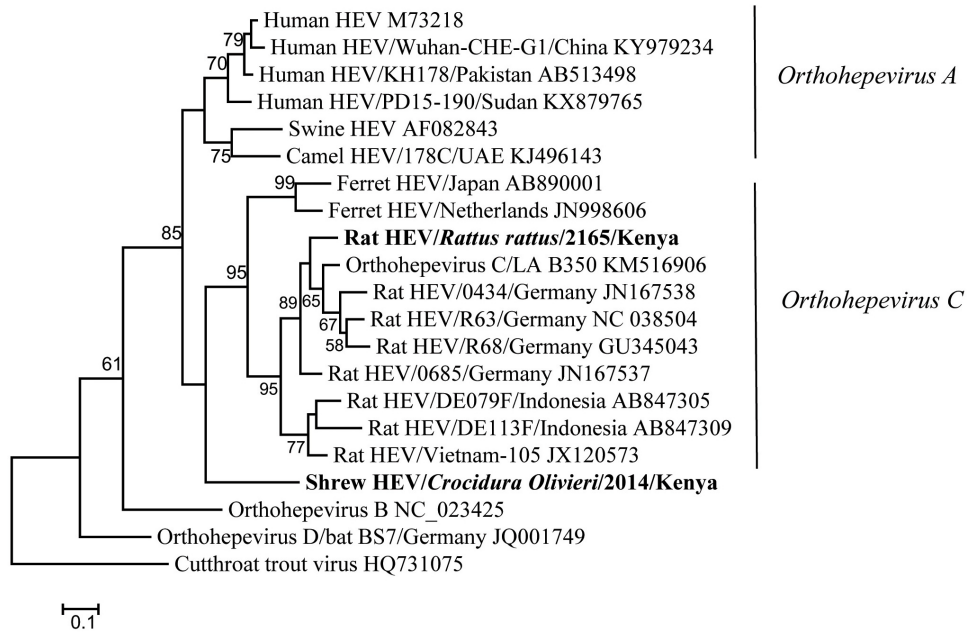

FIGURE 4 | ML tree based on 254-nt partial RdRp gene of hepeviruses (corresponding to Orthohepevirus C strain LA-B350 genome nt 4145-4398, KM516906). Strains detected in this study are indicated in bold.

None of the other known OWAs has >60% sequence identity with Kitale virus in the L protein (**Table 4**). Furthermore, analysis using the PAirwise Sequence Comparison (PASC) tool revealed that the closest hits for both S and L segments of Kitale virus were Ippy virus. The pairwise sequence identities between Kitale virus and Ippy virus were 69.27 and 60% for S and L segments, respectively, which are below the cut-off values (80 and 76%) recommended by the International Committee on Taxonomy of Viruses (ICTV) for arenavirus species demarcation, justifying the recognition of Kitale virus as a new species in the genus *Mammarenavirus* (Radoshitzky et al., 2015; Blasdell et al., 2016).

TABLE 4 | Sequence comparison of the four ORFs of Kitale virus and selected mammarenaviruses.

Mammarenavirus species*	nt/aa sequence identities			
	Z	L	GPC	NP
Ippy virus	55.7/61.1	61.5/62.2	71.4/80.5	69.5/78.1
Mariental virus	50.2/55.9	57.5/52.6	66.8/73.6	67.6/73.5
Loie River virus	54.7/56.5	57.0/56.3	65.2/69.5	66.4/71.1
Lassa virus	54.3/57.0	58.5/55.3	67.0/72.4	65.1/70.6
Wenzhou virus	53.0/51.6	57.1/55.1	63.0/67.2	67.3/73.7
Luna virus	57.7/57.6	56.7/54.3	69.0/73.7	64.7/68.0
Merino Walk virus	48.5/51.7	56.0/53.6	62.3/68.3	64.8/67.6
Gairo virus	63.1/54.8	57.2/54.7	66.8/71.1	64.4/69.9
Mopeia virus	55.7/57.9	56.8/54.7	66.6/71.7	65.9/69.6
LCMV	47.3/50.0	51.9/47.3	61.8/61.2	62.3/63.8
Lujo virus	46.1/47.2	50.4/43.5	52.8/42.3	59.3/58.4
Mobala virus	56.5/60.0	56.8/54.9	67.5/72.0	65.4/69.8

**The GenBank accession numbers of the reference mammarenavirus genome sequences are as following: Ippy virus (NC_007905, NC_007906), Mariental virus (NC_027134, NC_027136), Loie River virus (KC669692, KC669697), Lassa virus (KF478762, KF478765), Wenzhou virus (NC_026018, NC_026019), Luna virus (NC_016152, NC_016153), Merino Walk virus (NC_023763, NC_023764), Gairo virus (NC_026246, NC_026247), Mopeia virus (DQ328874, DQ328875), LCMV (FJ607025, FJ607036), Lujo virus (NC_012776, NC_012777), and Mobala virus (NC_007903, NC_007904).*

Phylogenetic trees from the entire L, GCP, and NP genes placed Kitale virus with Ippy virus in a monophyletic clade (**Figure 5**). The phylogeny of GPC gene revealed that African arenaviruses, including Kitale virus, were divergent from Asian arenaviruses. However, in the phylogenetic tree of the L gene, Kitale virus and Ippy virus were more related to the cluster of Wenzhou-like viruses found in Asia than to other African arenaviruses (**Figure 5**).

DISCUSSION

Rodents, bats, and shrews constitute the three largest groups of mammalian species. They have been characterized as reservoir hosts of a variety of viruses including emerging viruses that cause human diseases (Meerburg et al., 2009; Shi, 2013). East Africa is a tropical region inhabited by rich diversity of these small mammals. A large number of viruses from various families were detected in Kenyan bats in a country-wide bat virus surveillance (Waruhiu et al., 2017). Novel rodent viruses have also been described from Tanzania and Ethiopia (Meheretu et al., 2012; Gryseels et al., 2015). However, little is known about diversity and spillover potential of the viruses carried by rodents in Kenya. We hereby report the first virus surveillance research targeting Kenyan rodent and shrew populations. In our study, novel RNA

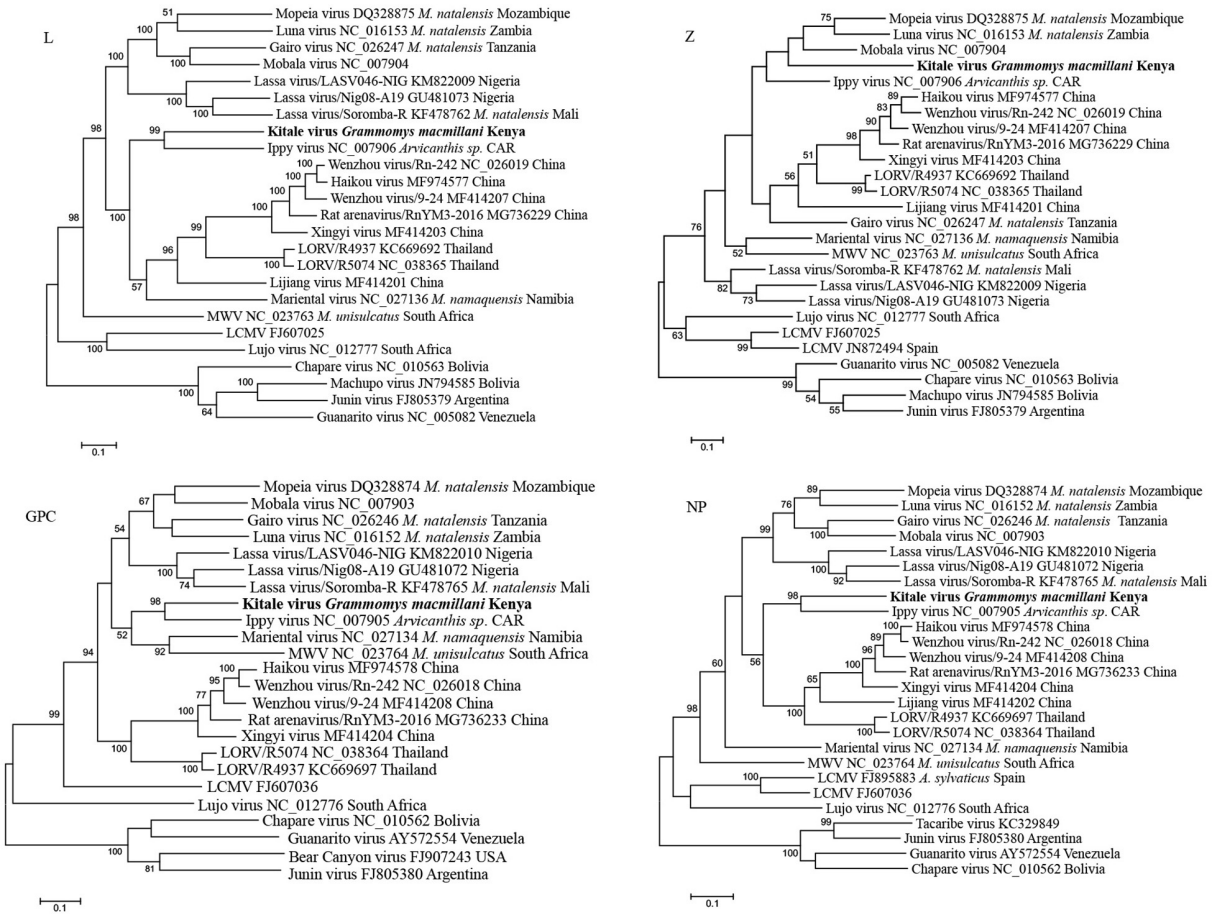

FIGURE 5 | Phylogenetic analysis of complete L, Z, GPC, and NP genes of mammarenaviruses. The novel *Grammomys macmillani* arenavirus identified in this study is indicated in bold. MWV, Merino Walk virus; LORV, Loie River virus; LCMV, Lymphocytic choriomeningitis virus. *M. natalensis*, *Mastomys natalensis*; *M. namaquensis*, *Micaelamys namaquensis*; *M. unisulcatus*, *Myotomys unisulcatus*. CAR, Central African Republic.

viruses belonging to four families, *Astroviridae*, *Paramyxoviridae*, *Hepeviridae*, and *Arenaviridae*, have been found circulating among rodent and shrew communities within areas of intensive agricultural activities and human settlements in Kenya.

Astroviruses, which cause mild to severe gastroenteritis in humans and animals, infect a broad range of host species, and thus pose a potential zoonotic risk for human populations especially in regions with poor hygiene condition. In recent years, an increasing number of astroviruses have been discovered in urban and wild rodents globally (Chu et al., 2010; Farkas et al., 2012; Hu et al., 2014). Although with large diversity, the phylogeny of mammalian astroviruses shows grouping with host restriction, in which most of rodent astroviruses fall into one big clade and are further clustered by rat, mice, and vole host species (Mombo et al., 2019). In this study, we detected two different novel astroviruses in fecal samples from Kenya corresponding to two different species *R. rattus* and *M. natalensis*, which tend to be species specific. They are clustered within the murine astroviruses, but more information about the full-length capsid gene is required to determine whether they can be considered novel genotype or species.

Interestingly, this study describes for the first time a rodent infected by feline astrovirus. This finding indicates the potential cross-species infection of astroviruses between cats and rodents. Feline astrovirus infects felids including domestic cats and cheetahs, and has been worldwide reported (Atkins et al., 2009). However, viruses detected in different geographical locations and in different felid species are closely related, suggesting that feline astrovirus has existed and evolved in cats for long history. Hence, the infection of feline astrovirus in *C. gamnianus* from Kenya was more likely to result from the cross-species transmission from cats to rodents. The *C. gambianus* individual in this study was captured in a farm store where this rodent has a high likelihood of interactions with domestic cats. However, as the virus was detected in feces of the rodent, there also existed the possibility that the *C. gambianus* ingested foods contaminated by domestic cats. The virus passed intact through its gastrointestinal tract, but did not actually infect the rodent.

In the past decades, a growing number of new paramyxoviruses have been discovered from rodents. These include J-virus from mice (Jack et al., 2005), Beilong virus from rat-derived cell line (Li et al., 2006), Tailam virus from

Sikkim rats (Woo et al., 2011), Mossman virus from wild rats in Australia (Miller et al., 2003), Nariva virus from the Trinidadian rat (Lambeth et al., 2009), and groups of novel paramyxoviruses reported more recently from various rodent species in Africa (Sasaki et al., 2014; Vanmechelen et al., 2018). Owing to their similar rodent hosts and close phylogenetic relationship, according to the latest ICTV taxonomy release, these viruses compose a new paramyxovirus genus named *Jeilongvirus* (Rima et al., 2018). In this study, we present diverse novel paramyxoviruses found in rodents from Kenya, all of which cluster within the genus *Jeilongvirus*. Within these large clade, the phylogenetic clustering of most Kenyan paramyxoviruses showed host specificity, as different viruses are grouped separately with those from the same rodent species or genus described in other African countries. For example, two viruses from *L. aquilus* constitute a lineage with another *Lophuromys* paramyxovirus from Mozambique. Five viruses from four rodent species in Kenya detected in our study showed distinction from each other, as well as from previously reported ones, further expanding the genetic diversity of jeilongviruses. The results provide additional support for recognition of rodents as the important natural reservoir of this paramyxovirus genus.

Members of *Hepeviridae*, also known as hepatitis E viruses (HEVs), infect a wide range of mammalian and avian species as well as trout. Hepeviruses which infect humans can cause self-limiting acute hepatitis in immune competent individuals (Smith et al., 2014). All mammalian and avian HEV isolates belong to the genus *Orthohepevirus*, and can be divided into four species. The species *Orthohepevirus A* consists of HEV variants detected in human populations worldwide and those from pigs, wild boars, camels, some of which can be transmitted to humans and cause zoonotic diseases. The species *Orthohepevirus C* is composed of two genotypes with host restriction. All HEVs identified from rodent hosts are designated genotype C1, while genotype C2 includes isolates derived from ferrets (Smith et al., 2014). We discovered a novel HEV within genotype C1 from a *R. rattus* in Kenya, further suggesting the global distribution of *Orthohepevirus C* variants. Previous studies revealed that HEVs detected in Asian musk shrew (*Suncus murinus*) from different regions of China were closely related to rat HEVs and fell within HEV-C1 genotype. As those shrews always share the same environment with wild rats, they may carry rat HEVs as a result of the cross species transmission from the wild rat reservoirs (Guan et al., 2013; He et al., 2018). In this study, we detected a distinct HEV in *C. olivieri*, a shrew species native in Africa, which is phylogenetically distant from rat HEVs. Full-length genome sequence of the new shrew HEV needs to be obtained to judge whether it can be classified as a novel species or it remains within *Orthohepevirus C* as a new genotype, following the demarcation criteria for *Orthohepevirus* species by the ICTV. In order to better understand the evolutionary position of shrew HEVs in Hepeviridae family, virus sequences from a greater diversity of shrew host species and geographic origin need to be determined. The zoonotic potential of rodent and shrew HEVs is also yet to be characterized.

The genus *Mammarenavirus* consists of two main groups corresponding to Old-World and New-World mammarenaviruses, which are the causative agents of a variety of human hemorrhagic fever diseases in Africa and America, respectively (Radoshitzky et al., 2015). Rodents are the primary natural reservoir of mammarenaviruses and have been the major target wildlife for surveillance of this category of viruses in nature. Among Old-World mammarenaviruses, besides the worldwide spread Lymphocytic choriomeningitis virus (LCMV) and Wenzhou-related viruses which have recently been widely reported in China and southeast Asia (Wang et al., 2019), all other viruses have been exclusively found in Africa, with each virus hosted by a specific host species or group of species (Charrel and de Lamballerie, 2010). These include LASV, Gbagroube virus, and Menekre viruses in West Africa; Ippy and Luna viruses in Central Africa; Morogoro, Gairo, and Mobala viruses in East Africa; Mopeia, Mariental, and Merino walk virus (MWV) in Southern Africa (Ishii et al., 2012; Gryseels et al., 2015). In Kenya, regardless of its large rodent diversity and the prevalent populations of *M. natalensis*, one of the most important host species of arenavirus, there are no records of arenavirus in rodents up to date. In this study, we characterized an arenavirus from rodents in Kenya for the first time. The novel virus from *G. macmillani* termed Kitale virus shows significant sequence distinction from all previously known arenaviruses in both of the two genomic segments, as well as in the four ORFs. Our results not only report the first arenavirus detection in Kenya, but also present the discovery of a new mammarenavirus species from a novel species of rodent host.

A number of OWA are associated with human diseases. LASV causes Lassa hemorrhagic fever with 5,000–10,000 cases of death per year in West Africa (Fichet-Calvet and Rogers, 2009). Another pathogenic arenavirus in Africa, Lujo virus, was discovered in South Africa following a nosocomial infection occasioned by a patient who traveled from Zambia (Ishii et al., 2012). In Asia, a genetic variant of Wenzhou virus was reported to have been associated with influenza-like human respiratory illness in Cambodia (Blasdell et al., 2016). The pathogenicity of other OWA remains unclear. However, Ippy virus, to which Kitale virus is most closely related, was found to be antigenically a member of the Lassa fever complex of arenaviruses via cross-immunofluorescence test (Swanepoel et al., 1985). While the pathogenic potential of Kitale virus requires further studies, the spillover risk of this novel rodent arenavirus should not be neglected. Additionally, the detection of Kitale virus in all tested tissues of the infected animal suggests its wide tissue tropism in the natural host. This may increase the potential of being transmitted to humans by enabling viral shedding into the environment through numerous routes such as saliva, urine, and feces.

As increased disturbance of natural habitats has brought rodents and shrews in closer contact with people, these small mammals are likely to be the next source of zoonotic disease outbreak in Kenya. Therefore, identification of known and novel viruses in rodents and shrews is of public health significance. In this study, diverse novel RNA viruses of different families were discovered in rodents and shrews from regions of intensive agricultural activities, including a novel arenavirus related to those known to infect humans. The findings extend

our knowledge on the host range, ecological distribution, and evolution of these RNA viral families. It also highlights the need for continued pathogen surveillance and disease monitoring not only in risk wildlife but also in livestock and humans in Kenya to prevent the occurrence of future zoonotic diseases.

DATA AVAILABILITY STATEMENT

All sequences generated by this study were deposited in the GenBank under accession numbers MK935152–MK9345169.

ETHICS STATEMENT

The study was approved by the Research and Ethics Committee of the Kenya Wildlife Service, with research permit KWS/BRM/5001. All Institutional and National guidelines for care and handling use of animals were followed.

AUTHOR CONTRIBUTIONS

Z-LS, BA, BH, and SOO conceptualized and designed the study. Z-LS, BA, BH, SO, and VO coordinated the study and the field work. BA, SO, VO, and SOO participated in the field work. Z-LS and BA supervised the study. BA, SOO, BH, and X-LY designed and coordinated the experiments. SOO and GO managed the storage and retrieval of specimen. BL and BH coordinated the laboratory skills training. BA and VO were responsible for application and acquisition of ethics permit. SOO performed the experiments, and analyzed and interpreted the data. KK, YF, and X-SZ assisted with data analysis. SOO and BH drafted the manuscript.

FUNDING

The study was supported by the Sino-Africa Joint Research Center, Chinese Academy of Sciences (SAJC201605) and the National Science and Technology Major Project (2018ZX0101004) and External Cooperation Program of CAS (153211KYSB20160001).

ACKNOWLEDGMENTS

We thank the Kenya Wildlife Service, National Museums of Kenya, and the State Office of Director of Veterinary Services for their logistic support without which this research could not have been accomplished. This study would not be a success without the cooperation of local authorities in the sampling localities.

REFERENCES

Allen, T., Murray, K. A., Zambrana-Torrelio, C., Morse, S. S., Rondinini, C., Di Marco, M., et al. (2017). Global hotspots and correlates of emerging zoonotic diseases. *Nat. Commun.* 8:1124. doi: 10.1038/s41467-017-00923-8

Atkins, A., Wellehan, J. F. Jr., Childress, A. L., Archer, L. L., Fraser, W. A., and Citino, S. B. (2009). Characterization of an outbreak of astroviral diarrhea in a group of cheetahs (*Acinonyx jubatus*). *Vet. Microbiol.* 136, 160–165. doi: 10.1016/j.vetmic.2008.10.035

Blasdell, K. R., Duong, V., Eloit, M., Chretien, F., Ly, S., Hul, V., et al. (2016). Evidence of human infection by a new mammarenavirus endemic to Southeastern Asia. *eLife* 5:e13135. doi: 10.7554/eLife.13135

Bonwitt, J., Kelly, A. H., Ansumana, R., Agbla, S., Sahr, F., Saez, A. M., et al. (2016). Rat-atouille: a mixed method study to characterize rodent hunting and consumption in the context of lassa fever. *Ecohealth* 13, 234–247. doi: 10.1007/s10393-016-1098-8

Bowen, M. D., Peters, C. J., and Nichol, S. T. (1997). Phylogenetic analysis of the *arenaviridae*: patterns of virus evolution and evidence for cospeciation between arenaviruses and their rodent hosts. *Mol. Phylogenet. Evol.* 8, 301–316. doi: 10.1006/mpev.1997.0436

Charrel, R. N., and de Lamballerie, X. (2010). Zoonotic aspects of arenavirus infections. *Vet. Microbiol.* 140, 213–220. doi: 10.1016/j.vetmic.2009.08.027

Chu, D. K., Poon, L. L., Guan, Y., and Peiris, J. S. (2008). Novel astroviruses in insectivorous bats. *J. Virol.* 82, 9107–9114. doi: 10.1128/JVI.00857-08

Chu, D. K., Chin, A. W., Smith, G. J., Chan, K. H., Guan, Y., Peiris, J. S., et al. (2010). Detection of novel astroviruses in urban brown rats and previously known astroviruses in humans. *J. Gen. Virol.* 91, 2457–2462. doi: 10.1099/vir.0.022764-0

Drexler, J. F., Seelen, A., Corman, V. M., Fumie Tateno, A., Cottontail, V., Melim Zerbinati, R., et al. (2012). Bats worldwide carry hepatitis e virus-related viruses that form a putative novel genus within the family hepeviridae. *J. Virol.* 86, 9134–9147. doi: 10.1128/JVI.00800-12

Farkas, T., Fey, B., Keller, G., Martella, V., and Egyed, L. (2012). Molecular detection of novel astroviruses in wild and laboratory mice. *Virus Genes* 45, 518–525. doi: 10.1007/s11262-012-0803-0

Fichet-Calvet, E., and Rogers, D. J. (2009). Risk maps of lassa fever in west Africa. *PLoS Negl. Trop. Dis.* 3:e388. doi: 10.1371/journal.pntd.0000388

Firth, C., Bhat, M., Firth, M. A., Williams, S. H., Frye, M. J., Simmonds, P., et al. (2014). Detection of zoonotic pathogens and characterization of novel viruses carried by commensal *Rattus norvegicus* in New York City. *mBio* 5:e1933-14. doi: 10.1128/mBio.01933-14

Gouy, de Bellocq, J., Tesikova, J., Meheretu, Y., Cizkova, D., Bryjova, A., et al. (2016). Complete genome characterisation and phylogenetic position of Tigray hantavirus from the Ethiopian white-footed mouse *Stenocephalemys albipes*. *Infect. Genet. Evol.* 45, 242–245. doi: 10.1016/j.meegid.2016.09.009

Grabherr, M. G., Haas, B. J., Yassour, M., Levin, J. Z., Thompson, D. A., Amit, I., et al. (2011). Full-length transcriptome assembly from RNA-Seq data without a reference genome. *Nat. Biotechnol.* 29, 644–652. doi: 10.1038/nbt.1883

Gryseels, S., Rieger, T., Oestereich, L., Cuypers, B., Borremans, B., Makundi, R., et al. (2015). Gairo virus, a novel arenavirus of the widespread mastomys natalensis: genetically divergent, but ecologically similar to lassa and morogoro viruses. *Virology* 476, 249–256. doi: 10.1016/j.virol.2014.12.011

Guan, D., Li, W., Su, J., Fang, L., Takeda, N., Wakita, T., et al. (2013). Asian musk shrew as a reservoir of rat hepatitis E virus. *China Emerg. Infect. Dis.* 19, 1341–1343. doi: 10.3201/eid1908.130069

Hall, G. B. (2013). Building phylogenetic trees from molecular data with MEGA. *Mol. Biol. Evol.* 30, 1229–1235. doi: 10.1093/molbev/mst012

He, W., Wen, Y., Xiong, Y., Zhang, M., Cheng, M., and Chen, Q. (2018). The prevalence and genomic characteristics of hepatitis E virus in murine rodents and house shrews from several regions in China. *BMC Vet. Res.* 14:414. doi: 10.1186/s12917-018-1746-z

Hu, B., Chmura, A. A., Li, J., Zhu, G., Desmond, J. S., Zhang, Y., et al. (2014). Detection of diverse novel astroviruses from small mammals in China. *J. Gen. Virol.* 95, 2442–2449. doi: 10.1099/vir.0.067686-0

Ishii, A., Thomas, Y., Moonga, L., Nakamura, I., Ohnuma, A., Hang'ombe, B. M., et al. (2012). Molecular surveillance and phylogenetic analysis of Old World arenaviruses in Zambia. *J. Gen. Virol.* 93, 2247–2251. doi: 10.1099/vir.0.044099-0

Jack, P. J., Boyle, D. B., Eaton, B. T., and Wang, L. F. (2005). The complete genome sequence of J virus reveals a unique genome structure in the family

Paramyxoviridae. *J. Virol.* 79, 10690–10700. doi: 10.1128/jvi.79.16.10690-10700.2005

Jones, K. E., Patel, N. G., Levy, M. A., Storeygard, A., Balk, D., Gittleman, J. L., et al. (2008). Global trends in emerging infectious diseases. *Nature* 451, 990–993. doi: 10.1038/nature06536

Kingdom, J., Happold, D., Butynski, T., Hoffmann, M., Happold, M., and Kalina, J. (2013). *Mammals of Africa*. London: Bloomsbury Publishing.

Klempa, B., Fichet-Calvet, E., Lecompte, E., Auste, B., Aniskin, V., Meisel, H., et al. (2006). Hantavirus in African wood mouse Guinea. *Emerg. Infect. Dis.* 12, 838–840. doi: 10.3201/eid1205.051487

Lambeth, L. S., Yu, M., Anderson, D. E., Crameri, G., Eaton, B. T., and Wang, L. F. (2009). Complete genome sequence of Nariva virus, a rodent paramyxovirus. *Arch. Virol.* 154, 199–207. doi: 10.1007/s00705-008-0287-3

Lau, S. K., Woo, P. C., Lai, K. K., Huang, Y., Yip, C. C., Shek, C. T., et al. (2011). Complete genome analysis of three novel picornaviruses from diverse bat species. *J. Virol.* 85, 8819–8828. doi: 10.1128/JVI.02364-10

Li, K., Lin, X. D., Wang, W., Shi, M., Guo, W. P., Zhang, X. H., et al. (2015). Isolation and characterization of a novel arenavirus harbored by rodents and shrews in Zhejiang province China. *Virology* 476, 37–42. doi: 10.1016/j.virol.2014.11.026

Li, Z., Yu, M., Zhang, H., Magoffin, D. E., Jack, P. J., Hyatt, A., et al. (2006). Beilong virus, a novel paramyxovirus with the largest genome of non-segmented negative-stranded RNA viruses. *Virology* 346, 219–228. doi: 10.1016/j.virol.2005.10.039

Meerburg, B. G., Singleton, G. R., and Kijlstra, A. (2009). Rodent-borne diseases and their risks for public health. *Crit. Rev. Microbiol.* 35, 221–270. doi: 10.1080/10408410902989837

Meheretu, Y., Cizkova, D., Tesikova, J., Welegerima, K., Tomas, Z., Kidane, D., et al. (2012). High diversity of RNA viruses in rodents Ethiopia. *Emerg. Infect. Dis.* 18, 2047–2050. doi: 10.3201/eid1812.120596

Miller, P. J., Boyle, D. B., Eaton, B. T., and Wang, L. F. (2003). Full-length genome sequence of Mossman virus, a novel paramyxovirus isolated from rodents in Australia. *Virology* 317, 330–344. doi: 10.1016/j.virol.2003.08.013

Mombo, I. M., Suquet, E., Boundenga, L., Mveang-Nzoghe, A., Maganga-Mboga, C., Arnathau, C., et al. (2019). Detection of novel astroviruses among rodents of Gabon Central Africa. *Infect. Genet. Evol.* 68, 43–46. doi: 10.1016/j.meegid.2018.12.003

Moureau, G., Temmam, S., Gonzalez, J. P., Charrel, R. N., Grard, G., and de Lamballerie, X. (2007). A real-time RT-PCR method for the universal detection and identification of flaviviruses. *Vector Borne Zoonotic Dis.* 7, 467–477.

Musila, S., Monadjem, A., Webala, P., Patterson, B., Hutterer, R., De Jong, Y., et al. (2019). An annotated checklist of mammals of Kenya. *Zool. Res.* 40, 3–52. doi: 10.24272/j.issn.2095-8137.2018.059

Radoshitzky, S. R., Bao, Y., Buchmeier, M. J., Charrel, R. N., Clawson, A. N., Clegg, C. S., et al. (2015). Past, present, and future of arenavirus taxonomy. *Arch. Virol.* 160, 1851–1874. doi: 10.1007/s00705-015-2418-y

Rima, B., Collins, P., Easton, A., Fouchier, R., Kurath, G., Lamb, R. A., et al. (2018). Problems of classification in the family *Paramyxoviridae*. *Arch. Virol.* 163, 1395–1404. doi: 10.1007/s00705-018-3720-2

Sasaki, M., Muleya, W., Ishii, A., Orba, Y., Hang'ombe, B. M., Mweene, A. S., et al. (2014). Molecular epidemiology of paramyxoviruses in Zambian wild rodents and shrews. *J. Gen. Virol.* 95, 325–330. doi: 10.1099/vir.0.058404-0

Shi, Z. (2013). Emerging infectious diseases associated with bat viruses. *Sci. China Life Sci.* 56, 678–682. doi: 10.1007/s11427-013-4517-x

Smith, D. B., Simmonds, P., International Committee on Taxonomy of Viruses Hepeviridae Study Group, Jameel, S., Emerson, S. U., Harrison, T. J., et al. (2014). Consensus proposals for classification of the family *Hepeviridae*. *J. Gen. Virol.* 95, 2223–2232. doi: 10.1099/vir.0.068429-0

Streicker, D. G. (2013). From persistence to cross-species emergence of a viral zoonosis. *Science* 342, 1185–1186. doi: 10.1126/science.1247566

Swanepoel, R., Leman, P. A., Shepherd, A. J., Shepherd, S. P., Kiley, M. P., and McCormick, J. B. (1985). Identification of Ippy as a lassa-fever-related virus. *Lancet* 1:639. doi: 10.1016/s0140-6736(85)92175-0

Těšíková, J., Bryjová, A., Bryja, J., Lavrenchenko, L. A., Goüy, and de Bellocq, J. (2017). Hantavirus strains in East Africa related to western african hantaviruses. *Vector Borne Zoonotic Dis.* 17, 278–280. doi: 10.1089/vbz.2016.2022

Tong, S., Chern, S. W., Li, Y., Pallansch, M. A., and Anderson, L. J. (2008). Sensitive and broadly reactive reverse transcription-PCR assays to detect novel paramyxoviruses. *J. Clin. Microbiol.* 46, 2652–2658. doi: 10.1128/JCM.00192-08

Vanmechelen, B., Bletsa, M., Laenen, L., Lopes, A. R., Vergote, V., Beller, L., et al. (2018). Discovery and genome characterization of three new Jeilongviruses, a lineage of paramyxoviruses characterized by their unique membrane proteins. *BMC Genomics* 19:617. doi: 10.1186/s12864-018-4995-0

Vieth, S., Torda, A. E., Asper, M., Schmitz, H., and Günther, S. (2004). Sequence analysis of L RNA of lassa virus. *Virology* 318, 153–168. doi: 10.1016/j.virol.2003.09.009

Wang, B., Cai, C. L., Li, B., Zhang, W., Zhu, Y., Chen, W. H., et al. (2017). Detection and characterization of three zoonotic viruses in wild rodents and shrews from shenzhen city China. *Virol. Sin.* 32, 290–297. doi: 10.1007/s12250-017-3973-z

Wang, J., Yang, X., Liu, H., Wang, L., Zhou, J., Han, X., et al. (2019). Prevalence of Wēnzhōu virus in small mammals in yunnan province China. *PLoS Negl. Trop. Dis.* 13:e0007049. doi: 10.1371/journal.pntd.0007049

Waruhiu, C., Ommeh, S., Obanda, V., Agwanda, B., Gakuya, F., Ge, X. Y., et al. (2017). Molecular detection of viruses in Kenyan bats and discovery of novel astroviruses, caliciviruses and rotaviruses. *Virol. Sin.* 32, 101–114. doi: 10.1007/s12250-016-3930-2

Watanabe, S., Masangkay, J. S., Nagata, N., Morikawa, S., Mizutani, T., Fukushi, S., et al. (2010). Bat coronaviruses and experimental infection of bats, the Philippines. *Emerg. Infect. Dis.* 16, 1217–1223. doi: 10.3201/eid1608.100208

Woo, P. C., Lau, S. K., Wong, B. H., Wong, A. Y., Poon, R. W., and Yuen, K. Y. (2011). Complete genome sequence of a novel paramyxovirus, Tailam virus, discovered in Sikkim rats. *J. Virol.* 85, 13473–13474. doi: 10.1128/JVI.06356-11

Woolhouse, M. E., and Gowtage-Sequeria, S. (2005). Host range and emerging and reemerging pathogens. *Emerg. Infect. Dis.* 11, 1842–1847. doi: 10.3201/eid1112.050997

Wu, Z., Lu, L., Du, J., Yang, L., Ren, X., Liu, B., et al. (2018). Comparative analysis of rodent and small mammal viromes to better understand the wildlife origin of emerging infectious diseases. *Microbiome* 6:178. doi: 10.1186/s40168-018-0554-9

Young, H. S., McCauley, D. J., Dirzo, R., Nunn, C. L., Campana, M. G., Agwanda, B., et al. (2017). Interacting effects of land use and climate on rodent-borne pathogens in central Kenya. *Philos. Trans. R. Soc. Lond. B Biol. Sci.* 372:20160116. doi: 10.1098/rstb.2016.0116

Conflict of Interest: The authors declare that the research was conducted in the absence of any commercial or financial relationships that could be construed as a potential conflict of interest.

Copyright © 2019 Onyuok, Hu, Li, Fan, Kering, Ochola, Zheng, Obanda, Ommeh, Yang, Agwanda and Shi. This is an open-access article distributed under the terms of the Creative Commons Attribution License (CC BY). The use, distribution or reproduction in other forums is permitted, provided the original author(s) and the copyright owner(s) are credited and that the original publication in this journal is cited, in accordance with accepted academic practice. No use, distribution or reproduction is permitted which does not comply with these terms.

frontiers in Microbiology

ORIGINAL RESEARCH
published: 22 November 2019
doi: 10.3389/fmicb.2019.02637

Dengue Virus Infection Activates Interleukin-1β to Induce Tissue Injury and Vascular Leakage

Pan Pan[1†], Qi Zhang[1†], Weiyong Liu[1†], Wenbiao Wang[2], Zhenyang Yu[1], Zizhao Lao[3], Wei Zhang[3], Miaomiao Shen[1], Pin Wan[1], Feng Xiao[1], Muhammad Adnan Shereen[1], Wen Zhang[4], Qiuping Tan[4], Yuntao Liu[5], Xiaohong Liu[3], Kailang Wu[1], Yingle Liu[1,2], Geng Li[3]* and Jianguo Wu[1,2]**

[1] State Key Laboratory of Virology, College of Life Sciences, Wuhan University, Wuhan, China, [2] Key Laboratory of Virology of Guangzhou, Institute of Medical Microbiology, Jinan University, Guangzhou, China, [3] Center for Animal Experiment, Guangzhou University of Chinese Medicine, Guangzhou, China, [4] Guangdong LongFan Biological Science and Technology, Foshan, China, [5] Guangdong Provincial Hospital of Traditional Chinese Medicine, Guangzhou, China

Dengue virus (DENV) infection causes several diseases ranging from dengue fever to life-threatening dengue hemorrhagic fever and dengue shock syndrome characterized by endothelial dysfunction, vascular leakage, and shock. Here, we identify a potential mechanism by which DENV induces tissue injury and vascular leakage by promoting the activation of interleukin (IL)-1β. DENV facilitates IL-1β secretion in infected patients, mice, human peripheral blood mononuclear cells (PBMCs), mouse bone marrow-derived macrophages (BMDMs), and monocyte-differentiated macrophages (THP-1) *via* activating the NLRP3 inflammasome. The accumulated data suggest that IL-1β probably induces vascular leakage and tissue injury in interferon-alpha/beta receptor 1 deficient C57BL/6 mice (*IFNAR*$^{-/-}$ C57BL/6), whereas IL-1 receptor antagonist (IL-1RA) alleviates these effects of IL-1β. Finally, administration of recombinant IL-1β protein results in vascular leakage and tissue injury in C57BL/6 mice. Together, the accumulated results demonstrate that IL-1β contributes to DENV-associated pathology and suggest that IL-1RA acts as a potential agent for the treatment of DENV-associated diseases.

Keywords: dengue virus, inflammatory response, IL-1RA, IL-1β, NLRP3 inflammasome, vascular leakage

OPEN ACCESS

Edited by:
Janusz Tadeusz Paweska, National Institute for Communicable Diseases (NICD), South Africa

Reviewed by:
Guruprasad R. Medigeshi, Translational Health Science and Technology Institute (THSTI), India
Svetlana Khaiboullina, University of Nevada, Reno, United States

***Correspondence:**
Yingle Liu
mvlwu@whu.edu.cn
Geng Li
lg@gzucm.edu.cn
Jianguo Wu
jwu@whu.edu.cn

[†] These authors have contributed equally to this work

Specialty section:
This article was submitted to Virology, a section of the journal Frontiers in Microbiology

Received: *27 June 2019*
Accepted: *30 October 2019*
Published: *22 November 2019*

Citation:
Pan P, Zhang Q, Liu W, Wang W, Yu Z, Lao Z, Zhang W, Shen M, Wan P, Xiao F, Shereen MA, Zhang W, Tan Q, Liu Y, Liu X, Wu K, Liu Y, Li G and Wu J (2019) Dengue Virus Infection Activates Interleukin-1β to Induce Tissue Injury and Vascular Leakage. Front. Microbiol. 10:2637. doi: 10.3389/fmicb.2019.02637

INTRODUCTION

The proinflammatory cytokine interleukin (IL)-1β is a regulator of systemic inflammatory response and functions as a fever-inducing pyrogen (Dinarello, 1997). IL-1β is activated by two distinct pathways. The nuclear factor (NF)-κB pathway facilitates the transcription of pro-IL-1β mRNA, whereas the second pathway involves the assembly of a multiprotein complex termed inflammasome that mediates pro-IL-1β maturation (Martinon et al., 2009). The inflammasome regulates the cleavage of inactive pro-IL-1β by activated caspase-1, a process that yields mature IL-1β (Kostura et al., 1989; Martinon et al., 2002; Allen et al., 2009; Rathinam and Fitzgerald, 2016). The best-characterized inflammasome, the pyrin domain-containing 3 (NLRP3), belongs to the Nod-like receptor family. As an essential part of the innate immune system, the inflammasome has a critical role in recognizing viral infection (Allen et al., 2009; Wang et al., 2018; Negash et al., 2019). Upon activation, NLRP3 recruits the apoptosis-associated speck-like protein, which contains a caspase recruitment domain (ASC), and procaspase-1 to form the inflammasome complex. Within the complex, caspase-1

is activated by autocatalytic cleavage to catalyze the conversion of pro-IL-1β into active IL-1β (Yan et al., 2015).

The particles of the dengue virus (DENV) are spherical, possess an envelope, and contain a single-stranded RNA genome of approximately 11 kb (Kuhn et al., 2002). The virus invades host cells by receptor-mediated endocytosis, and its RNA is translated into a polyprotein, which is then cleaved in three structural and seven non-structural proteins (Modis et al., 2004; Yu et al., 2008). Worldwide, DENV causes 390 million infections; 58.4 million of them are symptomatic, resulting in 13,586 deaths (Bhatt et al., 2013; Shepard et al., 2016). DENV infection causes several diseases, ranging from dengue fever to life-threatening dengue hemorrhagic fever and dengue shock syndrome (Guzman et al., 2010). Massive cytokine secretion (cytokine storm), heterotypic secondary infection, host genetics, and antibody-dependent enhancement (ADE) may contribute to DENV pathogenesis (Pang et al., 2007; Katzelnick et al., 2017). Despite the fact that dengue pathogenesis remains subtle, among them, the cytokine storm is believed to be one of the primary contributing factors (Hatch et al., 2011; Rothman, 2011). It has been demonstrated that DENV infection induces synthesis of IL-1β (Chang and Shaio, 1994; Hottz et al., 2013; Tan and Chu, 2013; Callaway et al., 2015), a cytokine typically generated at sites of injury or immunological challenge to coordinate cellular recruitment to the affected location (Puhlmann et al., 2005; Dinarello, 2010; Hakanpaa et al., 2018). However, the direct contribution of IL-1β to tissue injury in dengue disease remains elusive.

The present study documents that DENV induces tissue injury and vascular leakage by activating the NLRP3 inflammasome to release of IL-1β. In addition to previous findings, DENV was found to induce IL-1β activation in blood samples of infected patients, human peripheral blood mononuclear cells (PBMCs) and macrophages, C57BL/6 mice, and mouse bone marrow-derived macrophages (BMDMs). Moreover, DENV induces vascular leakage and tissue injury in mice most likely by activating IL-1β, whereas IL-1 receptor antagonist (IL-1RA) protects from this damage. Interestingly, recombinant IL-1β protein may directly induce vascular leakage and tissue injury in mice. Thus, the obtained results reveal the mechanism of DENV pathogenesis and provide evidence of a link between IL-1β and vascular leakage, thereby improving our understanding of the role of IL-1β in DENV pathogenesis.

MATERIALS AND METHODS

Clinical Sample Analysis

All blood samples were provided by The First Affiliated Hospital of Guangzhou University of Chinese Medicine and Guangdong Province Traditional Chinese Medicine Hospital. Fifteen adult patients (eight males and seven females, median age 33 years) diagnosed with DENV infection were recruited in this study. The presence of DENV was confirmed by anti-dengue IgM and IgG enzyme-linked immunosorbent assay (ELISA) and qRT-PCR; the patients were negative for other pathogens. In addition, platelet count, hematological parameters (including hematocrit, hemoglobin, lymphocyte count, and monocyte count), and biochemical parameters (including aspartate aminotransferase, alanine aminotransferase, and alkaline phosphatase) were determined. Control samples were obtained from randomly selected 20 healthy individuals (10 males and 10 females, median age 35 years) with no history of DENV infection. Informed consent was obtained from each person (**Supplementary Table 1**). PBMCs were isolated by centrifugation in Histopaque (Haoyang Biotech) density gradient using fresh peripheral venous blood samples diluted 1:1 in pyrogen-free PBS. Separated PBMCs were washed twice with phosphate buffer saline (PBS) and resuspended in RPMI 1640 medium supplemented with 10% FBS, penicillin (100 U/ml), and streptomycin (100 μg/ml).

Animal Studies

Wild-type (WT) C57BL/6 mice were purchased from the Hubei Research Center of Laboratory Animals (Wuhan, China). *IFNAR*$^{-/-}$ C57BL/6 mice were provided by Prof. Jincun Zhao of Guangzhou Medical University, China. Both strains of mice were bred and maintained under specific pathogen-free conditions at Wuhan University. All protocols of animal experiments were reviewed and approved by the Institutional Animal Care and Use Committee of Wuhan University.

In all studies, age- and sex-matched mice were randomly assigned to experimental groups. For DENV2 infection assays, 6-week-old *IFNAR*$^{-/-}$ C57BL/6 mice were tail vein injected with PBS (mock infection), pretreated with 300 μl PBS containing 2 μg mice IL-1RA by intraperitoneal injection for 90 min, treated with DENV2 (1×10^6 PFU/mouse), and treated with IL-1RA (2 μg/mice) at 4 days postinfection again (DENV + IL-1RA infection) or infected with 300 μl containing 1×10^6 PFU/mouse of DENV2 (DENV infection). One week after the DENV2 injection, mice were sacrificed, and tissues were collected for immunohistochemical and histopathological analyses.

BMDMs were isolated from 6–8-week-old male C57BL/6 mice. Cells were cultured for 6 days in RPMI 1640 medium supplemented with 10% fetal bovine serum (FBS) and 10% granulocyte-macrophage colony stimulating factor (GM-CSF)-conditioned medium collected from L929 cells.

Ethics Statement

All human subjects used in this study were adults. The study was conducted according to the principles of the Declaration of Helsinki and approved by the institutional review board (IRB) of the College of Life Sciences, Wuhan University, in accordance with its guidelines for the protection of human subjects (IRB approval number AF/04-05.0/10.0). The collection of blood samples was conducted in accordance with the guidelines for the protection of human subjects. Written informed consent was obtained from each participant.

All animal studies were performed in accordance with the principles described by the Animal Welfare Act and the National Institutes of Health Guidelines for the care and use of laboratory animals in biomedical research. All experimental protocols involving mice were reviewed and approved by the Institutional Animal Care and Use Committee (IACUC) of the College of Life Sciences, Wuhan University (IACUC approval number WDSKY0201901). All of the mice that needed to be sacrificed used the method of euthanasia.

Cell Lines and Cultures

Human monocytic cell line THP-1, *Aedes albopictus* gut cells (C6/36), and African green monkey kidney cells (Vero) were purchased from the American Type Culture Collection (ATCC). Human umbilical vein endothelial cells (HUVEC) were purchased from Obio Technology (Shanghai, China).

THP-1 cells were grown in RPMI 1640 medium supplemented with 10% FCS, 100 U/ml penicillin, and 100 μg/ml streptomycin sulfate. HUVEC, C6/36, and Vero cells were grown in dulbecco's modified eagle medium (DMEM) with 10% FCS, 100 U/ml penicillin, and 100 μg/ml streptomycin sulfate. Cell cultures were kept at 37°C in a 5% CO_2 incubator except for C6/36, which was maintained at 30°C.

THP-1 cells were stimulated with phorbol-12-myristate-13-acetate (PMA) for 12 h to induce differentiation into macrophages. The cells were stimulated with DENV, nigericin, lipopolysaccharide (LPS), and adenosine triphosphate (ATP). Supernatants were collected for the measurement of mature IL-1β (p17) and caspase-1(p20), while the cells were harvested for real time-polymerase chain reaction (RT-PCR) and immunoblot analyses.

Viruses

The NGC strain of DENV2 (GenBank accession number KM204118.1) was kindly provided by Dr. Xulin Chen of Wuhan Institute of Virology, Chinese Academy of Sciences. The TSV01 strain of DENV2 (GenBank accession number AY037116.1) was kindly provided by Dr. Wenxin Li of College of Life Sciences, Wuhan University, China. To generate large stocks of the DENV, C6/36 cells or Vero cells were incubated with DENV2 at multiplicity of infection (MOI) of 0.5 for 2 h, and then the unbound DENV was washed away. Infected cells were cultured sequentially in a fresh medium with 2% FBS for 7 days. The supernatant was harvested and centrifuged at 4,000 rpm for 10 min to remove cellular debris and then filtered through a 0.22-μm membrane. The suspension of DENV was aliquoted and frozen at −70°C. The virus titer was determined by the plaque assay. For animal infection experiments, DENV was concentrated by centrifugation at 30,000 *g* for 2 h at 4°C and purified by centrifugation in a 20% sucrose solution at 80,000 *g* overnight at 4°C.

Reagents and Antibodies

Phorbol-12-myristate-13-acetate (PMA), LPS, nigericin, ATP, and dansylsarcosine piperidinium salt (DSS) were purchased from Sigma-Aldrich. Caspase-1 inhibitor (VX-765) was purchased from Selleck. Recombinant human IL-1β protein (200-01B) and human IL-1RA (200-01RA) were obtained from Peprotech. Recombinant mouse IL-1β protein (401-ML/CF) and recombinant mouse IL-1RA (480-RM/CF) were purchased from R&D Systems. Trizol reagent was from Invitrogen, and Lipofectamine 2000 was from Invitrogen. The human IL-1β ELISA kit was purchased from BD Biosciences, the mouse IL-1β and tumor necrosis factor (TNF)-α ELISA kits were purchased from R&D Systems, and the LPS ELISA kit was purchased from Expandbio (Beijing, China).

Antibodies against NLRP3 (D4d8T), caspase-1 (D7F10), and IL-1β (D3U3E and 3A6) were purchased from Cell Signaling Technology. Antibody against DENV-NS3 (GTX124252) and DENV-Prm (GTX128092) were purchased from Genetex. Anti-β-actin antibody (66009) was purchased from Proteintech. Antibody against ASC (sc-271054) was purchased from Santa Cruz Biotechnology. Anti-mouse IgG Dylight 649, anti-mouse IgG Dylight 488, anti-rabbit IgG Dylight 649, and anti-rabbit IgG fluorescein isothiocyanate (FITC) were purchased from Abbkine.

RNA Extraction and Quantitative RT-PCR

Total cellular RNA was extracted using the Trizol reagent (Invitrogen, Carlsbad, CA, United States) according to the manufacturer's protocol. RNA (1 μg) was reverse-transcribed into cDNA by incubation with 0.5 μl of oligo(dT) and 0.5 μl of random primers, first at 37°C for 60 min and then at 72°C for 10 min. The resulting cDNA was used as the template for real-time PCR, performed in a LightCycler 480 thermal cycler (Roche). The thermocycling protocol included activation of polymerase at 95°C for 5 min, 45 cycles of 95°C for 15 s, 58°C for 15 s, and 72°C for 30 s; the fluorescence was measured and analyzed at the 72°C step. A final melting curve step from 50 to 95°C was applied to test the specificity of the primer. The primers used are listed in **Supplementary Table 2**.

Enzyme-Linked Immunosorbent Assay (ELISA)

The concentration of culture supernatants and serum of IL-1β were measured by IL-1β ELISA Kit (BD Biosciences-CA, for human and R&D systems, Minneapolis, MN, United States, for mice), and the concentration of culture supernatants of LPS was measured by LPS ELISA Kit (EXPANDBIO) according to manufacturer's instructions.

Western Blotting

THP-1 cells induced to differentiate by PMA were washed twice with PBS and dissolved in lysis buffer (50 mM Tris–HCl, 150 mM NaCl, 0.1% Non-idet P-40, 5 mM EDTA, and 10% glycerol, pH 7.4). Protein concentration was measured using the Bradford assay kit (Bio-Rad, Richmond, CA, United States). The protein lysates, 50 μg, were electrophoresed in an 8–12% SDS-polyacrylamide gel and transferred to nitrocellulose membranes (Amersham, Piscataway, NJ, United States). Non-specific binding was blocked by incubating the membranes in 5% skim milk for 2 h. Subsequently, the membranes were then washed three times with PBS containing 0.1% Tween (PBST) and incubated with the antibody. Protein bands were visualized using a Luminescent Image Analyzer (Fujifilm LAS-4000).

Immunofluorescence

THP-1 cells induced to differentiate by PMA were grown on sterile coverslips and infected with DENV2 (NGC) (MOI = 5) for 48 h. Subsequently, the cells were fixed with 4% paraformaldehyde for 15 min, washed three times with ice-cold wash buffer (PBS with 0.1% BSA), permeabilized with PBS containing 0.2% Triton X-100 for 5 min, and washed three times with the wash buffer. The cells were then blocked with

5% BSA for 30 min and incubated overnight with anti-ASC antibody and anti-DENV-Prm antibody (1:200 in wash buffer). Bound primary antibodies were visualized by staining for 1 h with FITC-conjugated donkey anti-mouse IgG and Daylight 649-conjugated donkey anti-rabbit IgG secondary antibody (1:100 in wash buffer). Nuclei were counterstained with DAPI for 5 min, and the cells were washed three times with the wash buffer. The immunostaining was examined by confocal microscopy (Fluo View FV1000; Olympus, Tokyo, Japan).

ASC Oligomerization Analysis

THP-1 cells induced to differentiate by PMA were lysed in the lysis buffer. The lysates were gently agitated at 4°C for 30 min and centrifuged at 6,000 rpm at 4°C for 15 min. The pellets were washed three times with PBS and resuspended in 500 μl of PBS, and 2 mM disuccinimidyl suberate (DSS) (Sigma) was added. After cross-linking at 37°C for 30 min, the samples were centrifuged at 6,000 rpm for 10 min, and the cross-linked pellets were resuspended in 50 μl of 2 × SDS loading buffer. The suspension was boiled for 10 min and analyzed by Western blotting.

Quantization of Vascular Leakage *in vivo*

One week after the infection with DENV2, the mice were injected intravenously with 300 μl of 0.5% Evans blue. The dye was allowed to circulate for 2 h, and the mice were euthanized and extensively perfused with PBS. Tissues were collected, weighed, and incubated in 1 ml formamide and 37°C for 24 h. The concentration of Evans blue concentration was measured as OD_{610} and calculated from the standard curve. Data were expressed as (ng Evans blue)/(mg tissue weight).

Trans-Endothelial Electrical Resistance

Human umbilical vein endothelial cells monolayers were grown on a Transwell polycarbonate membrane system (Corning Inc.) and treated with recombinant human IL-1β or preincubated with IL-1RA for 24 h. Half of the medium contained in the upper and lower chambers was replaced by fresh endothelial cell medium. Untreated HUVECs were used as a negative control, and medium alone was used as a blank control. Endothelial permeability was evaluated by measuring *trans*-endothelial electrical resistance (TEER) at 2-h intervals using the EVOM2 epithelial Voltohmmeter (World Precision Instruments). Relative TEER was expressed as follows: [(resistance in experimental group) – (resistance in medium alone)]/[(resistance in untreated HUVECs) – (resistance in medium alone)]; resistance was expressed in ohms.

Statistical Analysis

All experiments were repeated at least three times with similar results. All results were expressed as the mean ± the standard error of mean (SEM). Statistical significance of the difference between two groups was calculated using the *t*-test and among multiple groups by one-way ANOVA. GraphPad Prism5 software was used to perform statistical analyses. *P*-values of less than 0.05 were considered statistically significant.

RESULTS

DENV Infection Activates IL-1β in Humans and Mice

To determine whether DENV infection affects the level of circulating IL-1β, blood samples of DENV-infected patients (n = 15) and healthy individuals (n = 20) were analyzed (**Supplementary Tables 1,3**). Serum level of IL-1β was significantly higher in dengue patients than in healthy individuals (24.44 ± 0.68 pg/ml vs. 19.48 ± 0.42 pg/ml, $P < 0.0001$) (**Figure 1A**). Infection of human PBMCs by DENV2(NGC) (Liu et al., 2014; Zhu et al., 2017) increased the expression of IL-1β at the mRNA and protein levels (**Figure 1B**). DENV2(NGC) *E* mRNA and infectious DENV2 (NGC) were confirmed by qRT-PCR and plaque assays, suggesting that DENV successfully infected PBMCs (**Supplementary Figures 1A,B**). The effect of DENV2(NGC) infection on the secretion of IL-1β was then evaluated in $IFNAR^{-/-}$ C57BL/6 mice deficient in IFN-α/β receptor (Beatty et al., 2015). IL-1β mRNA in blood cells and IL-1β protein in the sera were higher in DENV2(NGC)-infected mice (n = 8) than in mock-infected mice (n = 6) (**Figure 1C**). The presence of DENV2(NGC) *E* mRNA in the blood cells of mice was verified, suggesting that DENV successfully infected DENV2(NGC)-infected mice (**Supplementary Figure 1C**). The level of IL-1β mRNA and IL-1β protein in BMDMs of C57BL/6 mice was increased after DENV2(NGC) infection (**Figure 1D**). Infected BMDMs produced DENV2(NGC) *E* mRNA and infectious DENV(NGC), suggesting that DENV successfully infected BMDMs (**Supplementary Figures 1D,E**). In all above-described experiments, LPS or LPS + ATP-stimulated cells (**Figures 1B,D**) were used as positive controls. Collectively, these results demonstrate that DENV induces IL-1β activation in infected patients and human PBMCs, as well as in $IFNAR^{-/-}$ C57BL/6 mice and BMDMs isolated from these animals. These findings expand the conclusions of previous reports (Hottz et al., 2013; Wu et al., 2013).

Different Strains of DENV Activate IL-1β in THP-1 Macrophages

Whether different strains of DENV2 affect the synthesis and secretion of IL-1β was evaluated in macrophages generated by PMA-induced differentiation of THP-1 cells (Park et al., 2007). Infection by DENV2(NGC) resulted in the activation of IL-1β secretion, Casp-1 p20 maturation, IL-1β p17 processing, and DENV2 NS3 production (**Figures 2A,B**). The increase in the level of pro-IL-1β in cell lysates raised the possibility that DENV infection could activate the NF-κB signaling pathway, upregulating the expression of IL-1β mRNA. This mechanism is supported by data shown in **Figures 2C,D**. The level of procaspase-1 in cell lysates remained essentially unchanged, and the significant increase in IL-1β and caspase-1 in the supernatant resulted from the activation of NLRP3 inflammasome by DENV infection (**Figure 3**). The NLRP3 inflammasome can cleave procaspase-1 to generate active caspase-1, which, in turn, can convert pro-IL-1β into active IL-1β. DENV2 (NGC) *E* mRNA and the infectious virus were detected in infected cells

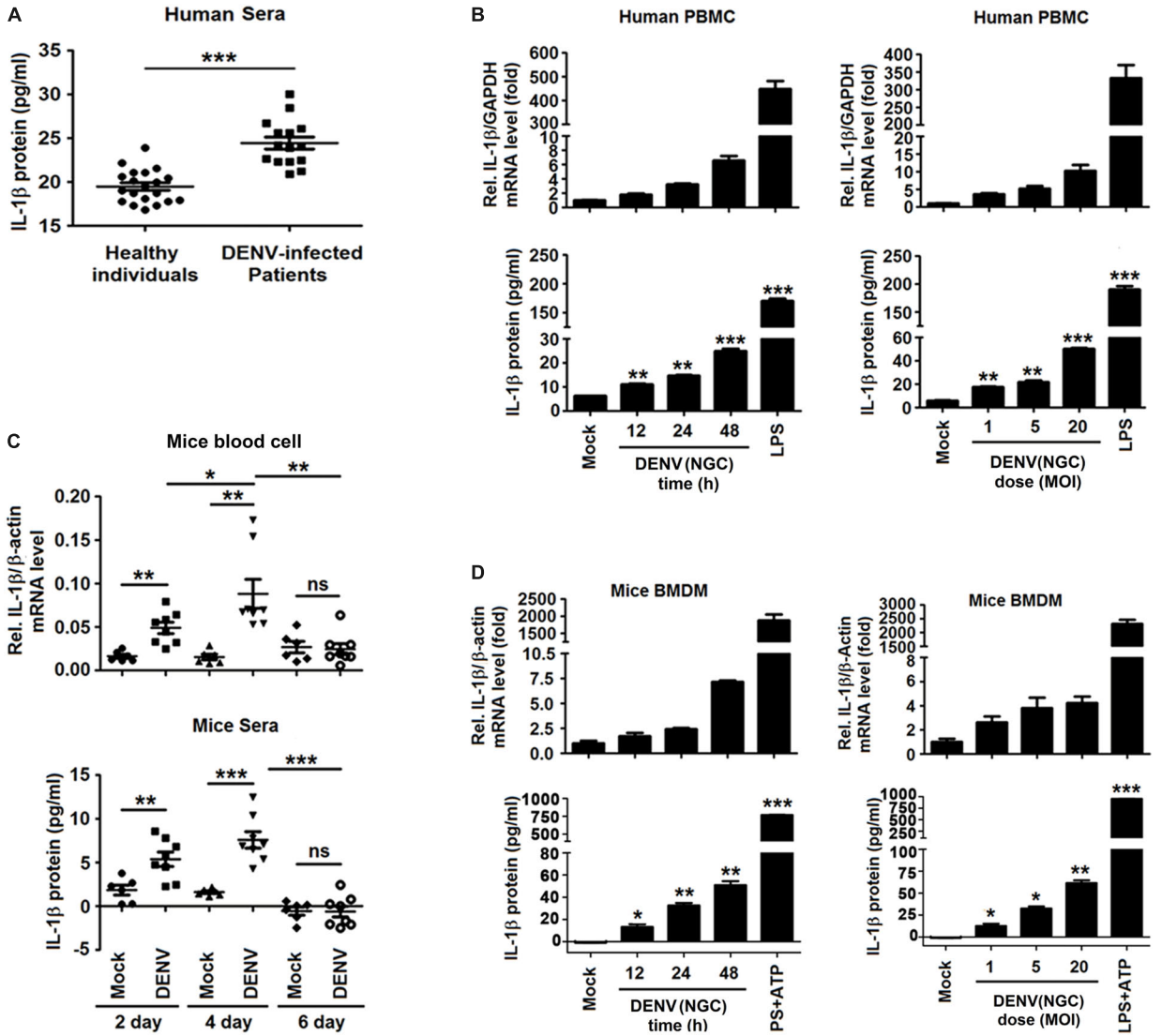

FIGURE 1 | Dengue virus (DENV) infection activated interleukin (IL)-1β in patients and mice. **(A)** Blood samples were obtained from 15 DENV-infected patients and 20 healthy individuals. The serum level of IL-1β was measured by ELISA. Points represent the IL-1β value in each serum sample. **(B)** Human PBMCs were infected with DENV2(NGC) for 12, 24, and 48 h (left), different concentrations of the virus (MOI = 1, 5, and 20) for 24 h (right), or treated with LPS (1 μg/ml) for 6 h. The intracellular level of IL-1β mRNA was determined by qRT-PCR analysis (top), and IL-1β protein in cell culture supernatant was measured by ELISA (bottom). **(C)** *IFNAR*$^{-/-}$ mice were infected with DENV2(NGC) (n = 8) or mock-infected (n = 6), and blood samples were collected at 2, 4, and 6 days later. IL-1β mRNA in blood cells was determined by qRT-PCR (top), and the serum level of IL-1β protein was measured by ELISA (bottom). Points represent the individual IL-1β value in each serum sample. **(D)** Mouse BMDMs differentiated by GM-GSF were infected with DENV2(NGC) for 12, 24, and 48 h at MOI = 5 (left) or at different MOI (MOI = 1, 5, and 20) for 24 h (right), treated with LPS (1 μg/ml) for 6 h, or stimulated with ATP (10 mM) for 20 min. IL-1β mRNA was determined by qRT-PCR (top), and IL-1β protein was measured by ELISA (bottom). Mock: PBS or supernatant of C6/36 cells without DENV2 infection. The number of replicates equals 2 **(A,C)** or 3 **(B,D)**. Values are mean ± SEM; ns, not significant; *, **, *** indicate P-values less than 0.05, 0.01, and 0.001, respectively.

(**Supplementary Figures 2A,B**). IL-1β mRNA and IL-1β protein were also induced upon infection by the TSV01 strain of DENV2 (Grant et al., 2011; **Figures 2C,D**). DENV2 (TSV01) *E* mRNA and infectious virus were detected in infected cells (**Supplementary Figures 2C,D**). Importantly, LPS (Chen and Wang, 2002) was not detected in mock solution and stocks of DENV2(NGC) and DENV2(TSV01) (**Supplementary Figure 2E**), excluding the possibility that the observed effects could be caused by LPS contamination. Together, the results demonstrated that both DENV2(NGC) and DENV2(TSV01) activate synthesis, maturation, and secretion of IL-1β.

DENV Induces IL-1β Release *via* Activating the NLRP3 Inflammasome

IL-1β activation is regulated at two levels: the transcription of pro-IL-1β mRNA and the processing of IL-1β protein (Martinon et al., 2002), and the maturation and release of IL-1β are

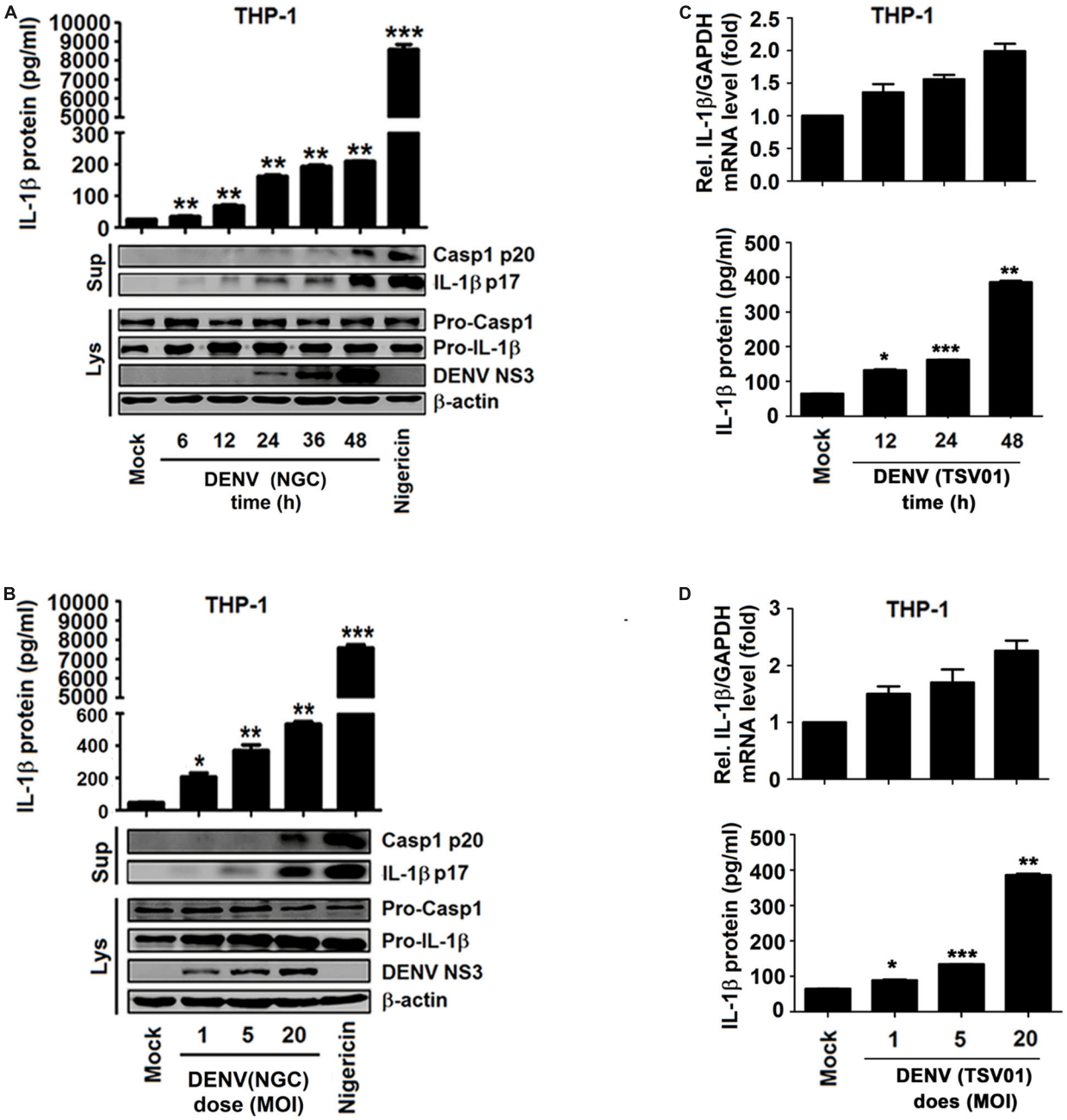

FIGURE 2 | Different strains of dengue virus (DENV) activate interleukin (IL)-1β in THP-1 macrophages. **(A,B)** Macrophages differentiated from THP-1 cells by phorbol-12-myristate-13-acetate (PMA) were infected with DENV2(NGC) for 6, 12, 24, 36, and 48 h at MOI = 5 **(A)** or at different MOI (MOI = 1, 5, and 20) for 24 h **(B)** or treated with 2 μM nigericin for 90 min. The secreted IL-1β was measured in cell supernatant by ELISA (top), and intracellular proteins (LYS) were analyzed by Western blotting (WB) (bottom). **(C,D)** Macrophages differentiated from THP-1 cells by PMA were infected with DENV2 (TSV01) for 12, 24, and 48 h at MOI = 5 **(C)** or at different MOI (1, 5, and 20) for 24 h **(D)**. IL-1β mRNA was determined by qRT-PCR (top), and IL-1β protein was measured by ELISA (bottom). Mock: supernatant of C6/36 cells without DENV2 infection. *N* = 3 in all experiments. Values are mean ± SEM. *, **, *** indicate *P*-values less than 0.05, 0.01, and 0.001, respectively.

controlled by inflammasomes (Swanson et al., 2019). Therefore, experiments were performed to determine whether the NLRP3 inflammasome is involved in DENV-induced activation of IL-1β. For this purpose, THP-1 cells stably expressing short hairpin RNAs (shRNAs) attenuating the mRNAs of NLRP3 inflammasome components NLRP3, Casp-1, and ASC were generated (Wang et al., 2017) (**Supplementary Figures 3A–C**). The cells were then differentiated into macrophages and stimulated with nigericin, an inducer of Casp-1 maturation and IL-1β release, or infected with DENV2(NGC) (Ito et al., 2012). Both types of stimulation increased IL-1β secretion, IL-1β p17 processing, and Casp-1 p20 maturation, but these

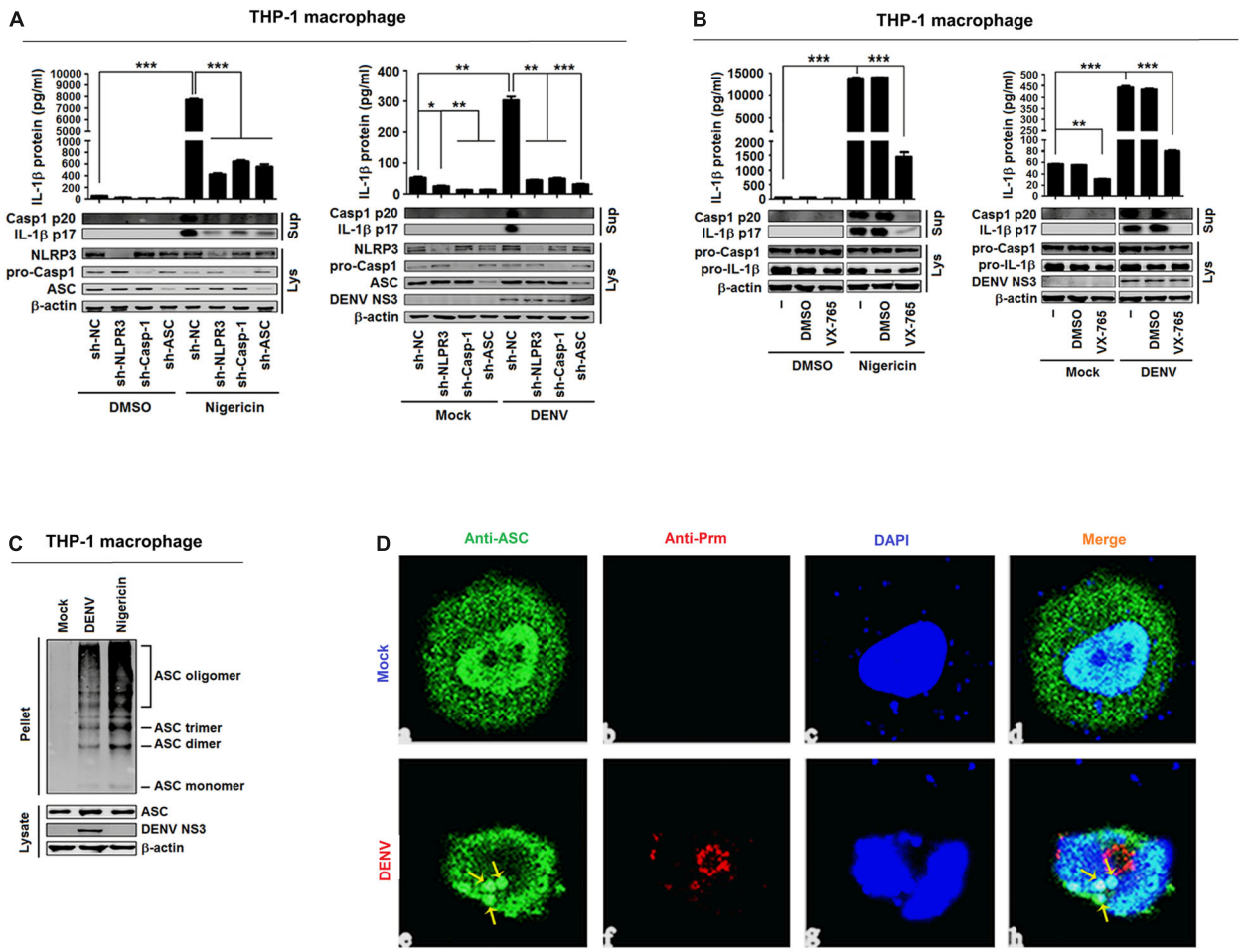

FIGURE 3 | Dengue virus (DENV) infection induces interleukin (IL)-1β release by activating the NLRP3 inflammasome. **(A)** Macrophages differentiated from THP-1 cells by phorbol-12-myristate-13-acetate (PMA) stably expressing sh-RNAs, sh-*NLRP3*, sh-*ASC*, sh-*Casp-1*, or sh-NC were stimulated by 2 μM nigericin for 2 h (left) or infected with DENV2 at MOI = 5 for 24 h (right). IL-1β protein in cell supernatant was measured by ELISA (top), and intracellular proteins (LYS) were analyzed by Western blotting (bottom). **(B)** Macrophages differentiated from THP-1 cells by PMA were stimulated by 2 μM nigericin for 2 h. IL-1β protein in cell supernatant was measured by ELISA (top), and intracellular proteins (LYS) were analyzed by Western blotting (bottom). **(C)** Macrophages differentiated from THP-1 cells by PMA were stimulated by 2 μM nigericin for 2 h (left) or infected with DENV2 at MOI = 5 for 24 h (right). ASC oligomerization in cytosolic pellets cross-linked with disuccinimidyl suberate (DSS) was analyzed by immunoblotting. **(D)** Macrophages differentiated from THP-1 cells by PMA were infected with DENV2 at MOI = 5 for 24 h. The subcellular localization of ASC (green) and DENV2 (red) was visualized with confocal microscopy. sh-NC: negative control vector containing scrambled shRNA. Mock: macrophages treated with the supernatant of C6/36 cells without DENV2 infection. *N* = 3 in all experiments. Values are mean ± SEM. *, **, *** indicate *P*-values less than 0.05, 0.01, and 0.001, respectively.

effects were attenuated by stable expression of sh-NLRP3, sh-Casp-1, and sh-ASC (**Figure 3A**). These findings indicate that knockdown of NLRP3 inflammasome components attenuates nigericin- and DENV2-induced IL-1β activation and caspase-1 maturation. Next, macrophages were derived from THP-1 cells with VX-765, a specific inhibitor of caspase-1 (Stack et al., 2005), and stimulated with nigericin or infected with DENV2(NGC). Nigericin- and DENV2(NGC)-induced IL-1β secretion, IL-1β (p17) processing, and caspase-1 (p20) maturation were all inhibited by VX-765 (**Figure 3B**), indicating that caspase-1 has a critical function in the DENV-induced processing of IL-1β. NLRP3 recruits ASC to participate in the maturation of caspase-1, and ASC oligomerization indicates the activation of inflammasome (Swanson et al., 2019). As illustrated in **Figure 3C**, nigericin and DENV2(NGC) induced oligomerization of ASC. ASC was diffusely distributed in mock-infected macrophages but formed small specks, indicative of oligomerization, in DENV-infected macrophages (**Figure 3D**). Therefore, the possibility can be raised that DENV2 activates NLRP3 inflammasome to induce IL-1β processing. These findings are consistent with an earlier report (Hottz et al., 2013).

DENV Promotes IL-1β Release in *IFNAR*$^{-/-}$ C57BL/6 Mice

To determine whether a cause-and-effect relationship exists between the activation of IL-1β and vascular leakage *in vivo*, an *IFNAR*$^{-/-}$ C57BL/6 mouse model was generated, and the

animals were infected with DENV(NGC). These experiments were performed since previous studies reported vascular leakage in AG129 or *STAT1*$^{-/-}$ mice infected with the DENV2(NGC) strain (Johnson and Roehrig, 1999; Chen et al., 2008; Sung et al., 2019) and in *IFNAR*$^{-/-}$ mice infected with the DENV2 (PL046) strain (Beatty et al., 2015), but the effects of infection of *IFNAR*$^{-/-}$ C57BL/6 mice with the DEV2(NGC) strain were not studied. In the present experiments, *IFNAR*$^{-/-}$ C57BL/6 mice were treated with PBS (n = 6), infected with DENV2(NGC) (n = 6), or injected intravenously with IL-1RA (Collison, 2019) and then infected with DENV2(NGC) (n = 6). While the body weight of mock-infected mice gradually increased, DENV2(NGC)-infected mice lost weight from 1 to 6 days postinfection, and the body weight of DENV2(NGC)-infected mice treated with IL-1RA increased from 1 to 3 days postinfection and gradually decreased during the infection (**Figure 4A**). The body weight of DENV2-infected mice treated with IL-1RA was significantly higher than in the absence of IL-1RA treatment (**Figure 4A**), suggesting that IL-1RA may compensate for the loss of body weight induced by DENV2. High levels of DENV2 *E* mRNA (**Supplementary Figures 4A,B**), NS5 mRNA (**Supplementary Figures 4C,D**), and viral copies (**Supplementary Figures 4E,F**) were detected in DENV2-infected mice serum and tissues, including heart, liver, spleen, lung, kidney, large intestine, and small intestine, but were not identified in mock-infected mice. These data indicate that the virus successfully infected the host organism. Interestingly, the levels of DENV *E* mRNA, NS5 mRNA, and viral copies were lower in DENV2-infected mice treated with IL-1RA than in untreated infected mice (**Supplementary Figures 4A–F**), suggesting that IL-1RA may inhibit DENV2 infection. At 4 days after the infection with DENV, blood level of IL-1β and TNF-α mRNA and protein was increased (**Figures 4B,C**) in DENV2-infected mice and DENV2-infected mice treated with IL-1RA but not in mock-infected mice. Moreover, IL-1β was upregulated in the heart, liver, spleen, lung, large intestine, and small intestine of DENV2-infected mice but not in the organs of mock-infected mice or DENV2-infected mice treated with IL-1RA (**Figure 4D**). Together, these results demonstrate that DENV activates the synthesis and secretion of IL-1β and TNF-α in *IFNAR*$^{-/-}$ C57BL/6 mice.

DENV Induces Tissue Injury and Vascular Leakage in Mice

In agreement with the above results, inflammatory cell infiltration and tissue injury were present in organs of DENV2-infected C57BL/6 mice but not in organs of mock-infected mice (**Figure 5A**). Notably, in the spleen of DENV2-infected mice, but not in the spleen of infected mice treated with IL-1RA, the boundaries between the red and the white pulp were disrupted, and the number of lymphatic nodules and pulping cells was increased, resulting in a significant infiltration of lymphocytes into the red pulp region (**Figure 5A**). The spleen weight and size in infected mice were significantly higher than in mock-infected mice or infected mice treated with IL-1RA (**Figures 5B,C**). Given the major function of the spleen in the immune system (Mebius and Kraal, 2005), DENV2-induced surge of inflammatory cytokines might have generated considerable damage to the spleen. Thus, the results appear to indicate that DENV2 induces IL-1β secretion and inflammatory responses in mice and may contribute to inflammatory cell infiltration and tissue injury after DENV infection in mice. Additionally, the intensity of Evans blue dye in the liver, spleen, lung, kidney, large intestine, and small intestine of DENV2-infected mice was significantly higher than in mock-infected mice or DENV2-infected mice treated with IL-1RA (**Figure 5D**). These results probably suggest that DENV2 infection in mice induces inflammatory response and vascular leakage by an IL-1β-dependent mechanism.

Recombinant IL-1β Protein Induces Vascular Leakage in Mice

Finally, the effect of IL-1β on endothelial cell permeability was examined *in vitro* to demonstrate whether IL-1β can directly induce vascular leakage. For this purpose, HUVECs were treated with recombinant human IL-1β protein or preincubated with human IL-1RA (Descamps et al., 2012), and the endothelial permeability was determined by the measurement of TEER. The magnitude of TEER level was reduced by the treatment of cells with IL-1β, but this decrease was reversed in the presence of IL-1RA (**Figure 6A**). Thus, IL-1β induces endothelial hyperpermeability in HUVECs. However, it should be noted that these *in vitro* experiments utilized concentrations of IL-1β higher than those measured in DENV2-infected mice. Recombinant IL-1β was intravenously injected into the caudal region of C57BL/6 mice or preincubated with mouse IL-1RA through intraperitoneal injection (Itani et al., 2016). The injection of IL-1β or IL-1RA + IL-1β resulted in a significant increase in circulating IL-1β mRNA and IL-1β protein in comparison with PBS-treated mice (**Supplementary Figures 5A,B**), indicating that IL-1β was successfully delivered. IL-1β-injected mice exhibited higher tissue levels of IL-1β, barely detectable in the tissues of IL-1β + IL-1RA-treated mice (**Figure 6B**). Similarly, infiltration by inflammatory cells and tissue injury were present in the tissues of IL-1β-treated mice but not in IL-1RA + IL-1β-treated mice (**Figure 6C**). The vascular leakage assay demonstrated that the intensity of Evans blue was significantly higher in the tissues of IL-1β-treated mice but relatively unaltered in the tissues of IL-1RA + IL-1β-treated animals (**Figure 6D**), supporting the notion that IL-1β induces vascular leakage in mice. Taken together, these results demonstrate that IL-1β plays an important role in the induction of inflammatory response and vascular leakage (**Figure 7**).

DISCUSSION

Immune dysfunction during DENV infection may cause life-threatening hypovolemic shock resulting from the leakage of vascular fluids, and the ensuing cytokine storm is thought to contribute to the pathogenesis of DENV (Culshaw et al., 2017). While this process has been partially characterized, the specific mechanisms governing cytokine regulation upon DENV infection remain largely unknown. The current work provides

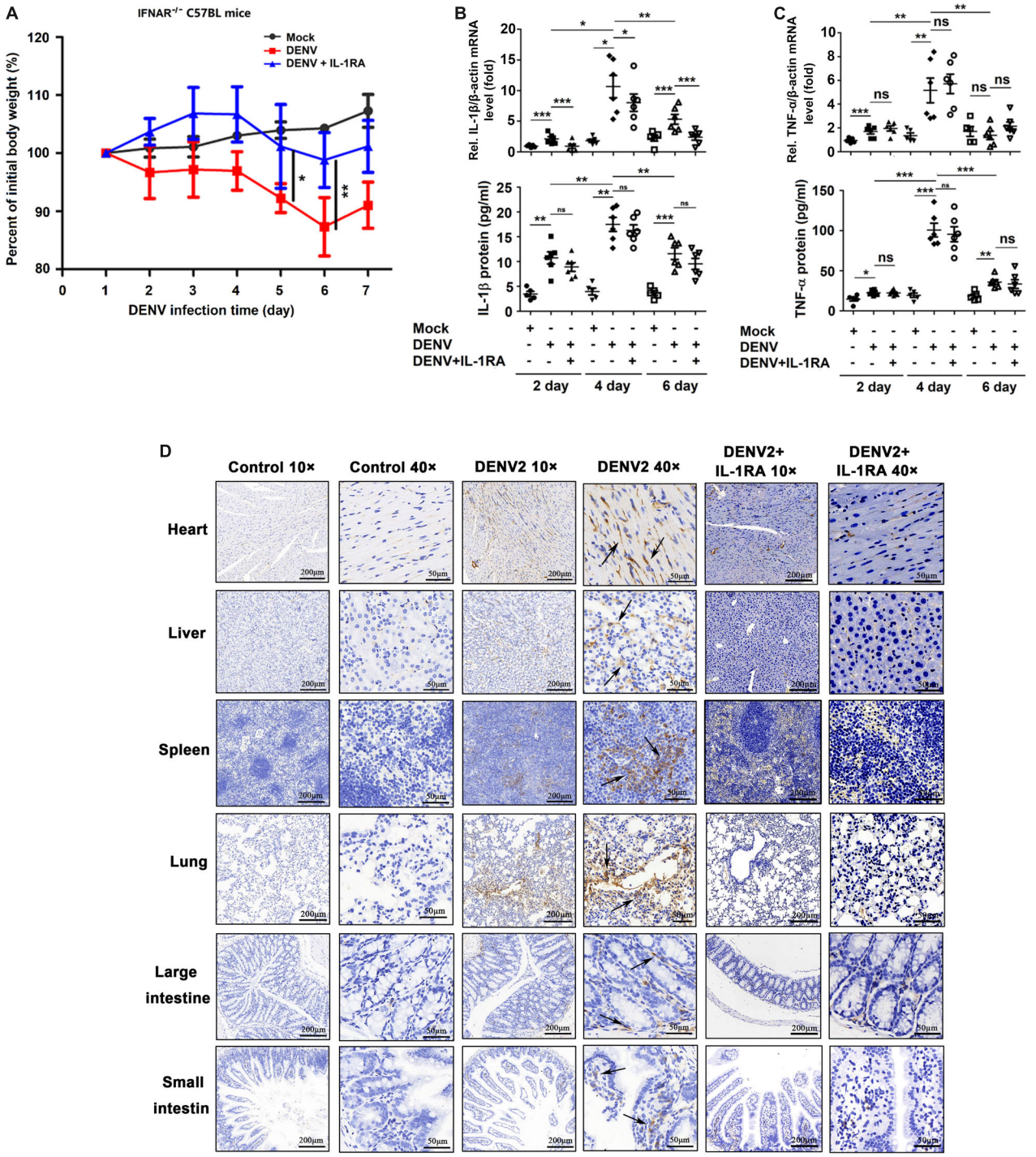

FIGURE 4 | Dengue virus (DENV) promotes interleukin (IL)-1β release in *IFNAR*$^{-/-}$ C57BL/6 mice. **(A–D)** *IFNAR*$^{-/-}$ C57BL/6 mice were intravenously injected with 300 μl of DENV2(NGC) suspension at a dose of 1 × 10^6 PFU/mouse (n = 6), pretreated with intraperitoneal injection of 300 μl of PBS containing 2 μg of mouse IL-1RA at 90 min before the infection with DENV2(NGC) (1 × 10^6 PFU/mouse) with the IL-1RA treatment repeated 4 days after the infection (n = 6) or injected with 300 μl of PBS only (control group, n = 6). Mice were euthanized 7 days after infection or PBS injection, and the tissues were collected. **(A)** Mice were weighed daily; body weight is expressed as the percentage of the initial weight. **(B)** Blood samples were collected at 2, 4, and 6 days postinfection. IL-1β mRNA in blood cells was determined by qRT-PCR (top), and IL-1β protein in the serum was measured by ELISA (bottom). Individual points represent the IL-1β value in each sample. **(C)** Blood samples were collected at 2, 4, and 6 days postinfection. TNF-α mRNA in blood cells was determined by qRT-PCR (top), and TNF-α protein in the serum was measured by ELISA (bottom). Individual points represent the TNF-α value in each sample. **(D)** Detection of IL-1β by immunohistochemistry in the heart, liver, spleen, lung, large intestine, and small intestine after DENV infection. Black arrows indicated the immunostaining of IL-1β. Mock: injection of the same volume of PBS. Data represent two independent experiments. Values are mean ± SEM; ns, not significant; *, **, *** indicate P-values less than 0.05, 0.01, and 0.001, respectively.

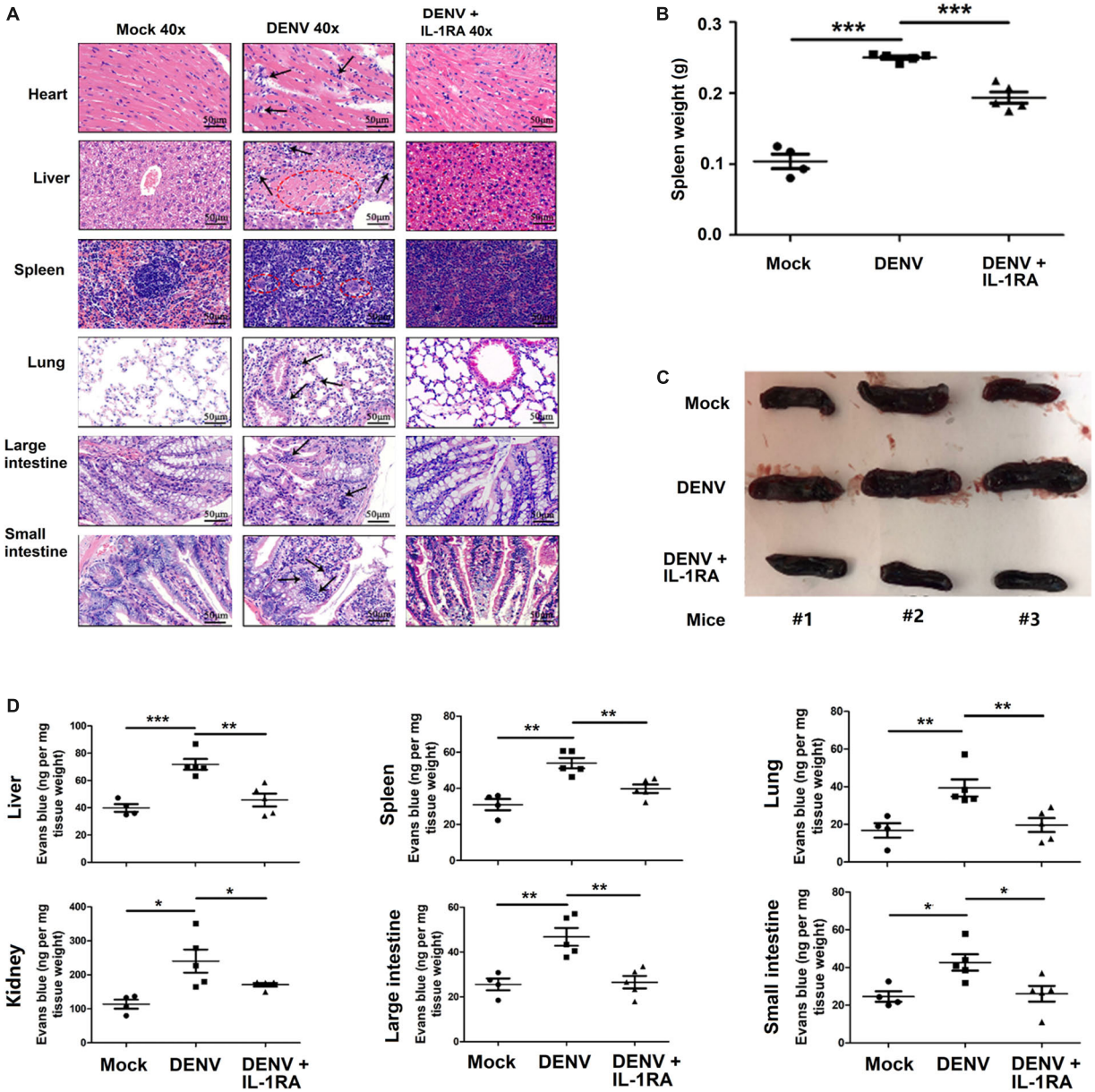

FIGURE 5 | Dengue virus (DENV) induces tissue injury and vascular leakage in mice. **(A–D)** *IFNAR*$^{-/-}$ C57BL/6 mice were intravenously injected with 300 μl of DENV2 suspension at a dose of 1 × 10^6 PFU/mouse (n = 6), pretreated with intraperitoneal injection of 300 μl of PBS containing 2 μg interleukin (IL)-1RA at 90 min before injection of DENV2(NGC) (1 × 10^6 PFU/mouse); the IL-1RA treatment was repeated 4 days after the viral infection (n = 6) or injected with 300 μl of PBS (control group, n = 6). Mice were euthanized 7 days after infection, and histopathologic analysis of the heart, liver, spleen, lung, large intestine, and small intestine was performed. Black arrows indicate the infiltrated inflammatory cells; the red circle indicates the aberrant cells **(A)**. Weight changes **(B)** and anatomy **(C)** of the spleen in the three groups of mice. Mice were intravenously injected with Evans blue 7 days after infection. DENV-infected group, n = 5; DENV + IL-1RA group, n = 5; control group, n = 4. Mice were euthanized after the dye was circulating for 2 h, and the concentration of Evans blue was measured at OD_{610} in the liver, spleen, lung, kidney, large intestine, and small intestine **(D)**. Data represent two independent experiments. Values are mean ± SEM; *, **, *** indicate P-values less than 0.05, 0.01, and 0.001, respectively.

experimental evidence of the activation of IL-1β synthesis and secretion during vascular leakage in DENV-associated infection and identifies IL-1RA as a potential agent for the prevention and treatment of this infectious disease. Although it was previously shown that DENV infection induces the production of IL-1β (Hottz et al., 2013; Wu et al., 2013), the present findings strengthen this conclusion by using samples from DENV patients and a mouse model of DENV infection, primary cells isolated from infected mice, PBMCs isolated from healthy individuals, and *in vitro* cultures of human macrophages infected by two different strains of DENV. Moreover, the obtained results show that DENV increases the serum concentration of IL-1β in both

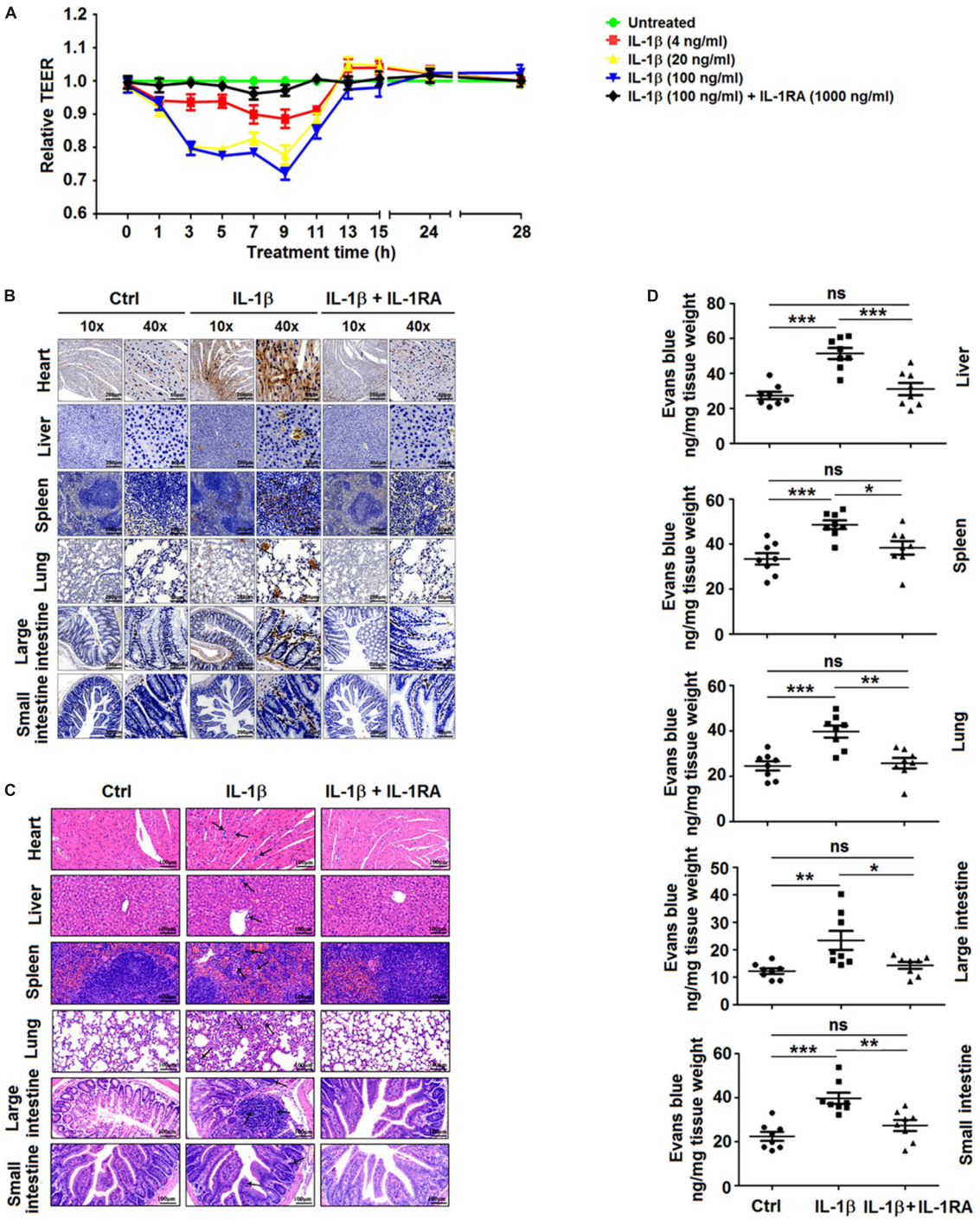

FIGURE 6 | Recombinant interleukin (IL)-1β induces vascular leakage in mice. **(A)** Confluent monolayers of human umbilical vein endothelial cells (HUVEC) were grown on polycarbonate membrane system and treated with different concentrations of recombinant human IL-1β protein for 48 h or preincubated with IL-1RA (1,000 ng/ml) for 1 h. Endothelial permeability was evaluated by the measurement of *trans*-endothelial electrical resistance. **(B–D)** C57BL/6 mice received tail vein injection of 300 μl PBS (control group, $n = 8$) or injection of 300 μl of PBS containing 0.2 μg of recombinant mouse IL-1β protein (IL-1β group $n = 8$) or were pretreated with intraperitoneal injection of 300 μl of PBS containing 2 μg of human IL-1RA at 90 min before the tail vein injection of 300 μl of PBS containing 0.2 μg of recombinant mouse IL-1β protein (IL-1RA + IL-1β group, $n = 8$). At 9 h postinjection with IL-1β, mice were euthanized, and the distribution of IL-1β in the heart, liver, spleen, lung, large intestine, and small intestine was analyzed by immunohistochemistry. Black arrows indicate the immunostaining of IL-1β **(B)**. Histopathologic analysis of the heart, liver, spleen, lung, large intestine, and small intestine. Black arrows indicate infiltrating inflammatory cells **(C)**. At 9 h after the administration of IL-1β, mice were intravenously injected with Evans blue. The dye was allowed to circulate for 2 h before mice were euthanized, and liver, spleen, lung, large intestine, and small intestine were collected. The concentration of Evans blue was measured at OD_{610} **(D)**. Data represent two independent experiments. Values are mean ± SEM; *, **, *** indicate *P*-values less than 0.05, 0.01, and 0.001, respectively.

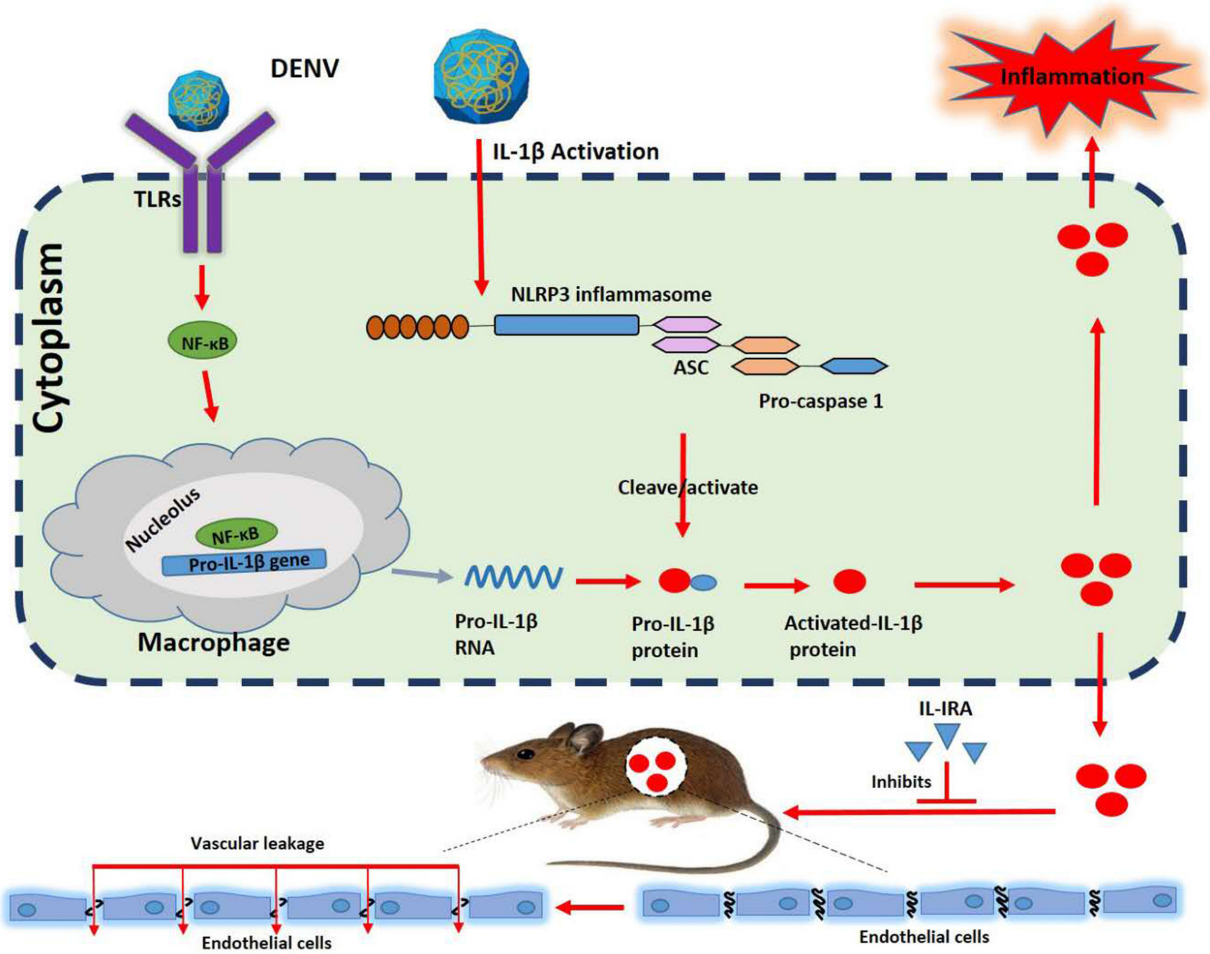

FIGURE 7 | A distinct mechanism by which dengue virus (DENV) activates interleukin (IL)-1β to induce tissue injury and vascular leakage. Upon DENV infection, the DENV promotes ASC oligomerization and inflammasome assembly. The inflammasome facilitates the synthesis and secretion of IL-1β, inflammation, and vascular leakage. The present study highlights the major contribution of IL-1β to DENV-associated pathology.

patients and mice, strongly suggesting that DENV activates IL-1β *in vivo*.

IL-1β is an essential proinflammatory cytokine acting as a fever-inducing pyrogen in the host (Kugelberg, 2016; Leake, 2019). *In vivo*, the NLRP3 inflammasome is required for IL-1β processing, with caspase -1 and ASC oligomerization mediating IL-1β maturation and secretion. As a crucial element of the innate immune system, the NLRP3 inflammasome is not only an important component in host defense against pathogens (Allen et al., 2009; Wang et al., 2018; Negash et al., 2019) but is also involved in the progression of several inflammatory human diseases, such as gout and type 2 diabetes (So and Martinon, 2017; Wu et al., 2018). Additionally, DENV infection triggers the assembly of the NLRP3 inflammasome in platelets, further contributing to increased vascular permeability by synthesis and release of IL-1β (Hottz et al., 2013). However, the mechanism underlying the relationship between enhanced inflammatory response and loss of vascular barrier integrity has not been addressed *in vivo*. The current work utilized the *IFNAR*$^{-/-}$ C57BL/6 mouse model of DENV infection, and documented high serum levels of inflammatory factors IL-1β and TNF-α were abundantly expressed in sera. IL-1β was also highly expressed in different organs, including heart, liver, spleen, lung, large intestine, and small intestine. These alterations in the expression and distribution of cytokines were accompanied by a significant change in vascular permeability. Importantly, IL-1RA alleviated the damage produced by inflammatory factors, demonstrating that IL-1β may have an important role in the pathogenesis of the dengue disease in a TNF-α-independent manner. The obtained results provided also evidence of the induction of vascular leakage in human HUVEC and C57BL/6 mice by recombinant IL-1β. Conversely, competitive binding of IL-1β receptor by IL-1RA ameliorated IL-1β-induced damages.

In conclusion, during DENV infection, the virus promotes the oligomerization of ASC and the assembly of inflammasome, facilitating the synthesis and secretion of IL-1β, and, thereby, activating inflammation, which may lead to vascular leakage. Thus, the presented investigation identified the contribution

of IL-1β to DENV-associated pathology and established a possible direct link between IL-1β and vascular leakage. These findings suggest that IL-1β is an essential part of the complex immunopathological nature of severe dengue, and targeting this cytokine may be used in the prevention and treatment of DENV-associated diseases.

DATA AVAILABILITY STATEMENT

All datasets generated for this study are included in the article/**Supplementary Material**.

ETHICS STATEMENT

The studies involving human participants were reviewed and approved by the Institutional Review Board of the College of Life Sciences, Wuhan University. The patients/participants provided their written informed consent to participate in this study. The animal study was reviewed and approved by the Institutional Review Board of the College of Life Sciences, Wuhan University.

AUTHOR CONTRIBUTIONS

PP, QZ, WL, WW, QT, KW, YiL, GL, and JW contributed to the design of the experiments. PP, QZ, WL, WW, ZY, ZL, WIZ, MS, PW, FX, and MS contributed to the conduction of the experiments. PP, QZ, WL, WW, ZY, ZL, WIZ, MS, PW, FX, MS, WNZ, and QT contributed to the reagents. PP, QZ, WL, WW, ZY, ZL, WIZ, MS, PW, FX, MS, and WNZ, and QT contributed to the analyses of the data. PP, QZ, WL, YiL, GL, and JW contributed to the writing of the manuscript. PP and JW contributed to the editing of the manuscript.

FUNDING

This work was supported by the National Natural Science Foundation of China (Grant Numbers 81730061, 31800147, 81803813, and 81973549), the National Health and Family Planning Commission of the People's Republic of China, National Mega Project on Major Infectious Disease Prevention (Grant Numbers 2017ZX10103005 and 2017ZX10202201), Guangdong Province "Pearl River Talent Plan" Innovation and Entrepreneurship Team Project (Grant Number 2017ZT07Y580), GZUCM First-Class Universities and Top Disciplines Projects (2019KYTD102 and A1-AFD018191A17), Science and Technology Planning Project of Guangzhou (No. 201804010029), and Innovative Program of State Key Laboratory of Virology (No. 2016KF001).

ACKNOWLEDGMENTS

We thank Dr. Jincun Zhao of the First Affiliated Hospital of Guangzhou Medical University, Guangzhou, China, for the gift of *IFNAR*$^{-/-}$ C57BL/6 mice deficient in IFN-α/β receptors, Dr. Xulin Chen of Wuhan Institute of Virology, Chinese Academy of Sciences, for the gift of DENV-2 strain NGC (GenBank accession number KM204118.1), and Dr. Wenxin Li of College of Life Sciences, Wuhan University, Wuhan, China, for DENV2 strain TSV01.

SUPPLEMENTARY MATERIAL

The Supplementary Material for this article can be found online at: https://www.frontiersin.org/articles/10.3389/fmicb.2019.02637/full#supplementary-material

REFERENCES

Allen, I. C., Scull, M. A., Moore, C. B., Holl, E. K., McElvania-TeKippe, E., Taxman, D. J., et al. (2009). The NLRP3 inflammasome mediates in vivo innate immunity to influenza a virus through recognition of viral RNA. *Immunity* 30, 556–565. doi: 10.1016/j.immuni.2009.02.005

Beatty, P. R., Puerta-Guardo, H., Killingbeck, S. S., Glasner, D. R., Hopkins, K., and Harris, E. (2015). Dengue virus NS1 triggers endothelial permeability and vascular leak that is prevented by NS1 vaccination. *Sci. Transl. Med.* 7:304ra141. doi: 10.1126/scitranslmed.aaa3787

Bhatt, S., Gething, P. W., Brady, O. J., Messina, J. P., Farlow, A. W., Moyes, C. L., et al. (2013). The global distribution and burden of dengue. *Nature* 496, 504–507. doi: 10.1038/nature12060

Callaway, J. B., Smith, S. A., McKinnon, K. P., de Silva, A. M., Crowe, J. J., and Ting, J. P. (2015). Spleen tyrosine kinase (Syk) mediates IL-1beta induction by primary human monocytes during antibody-enhanced dengue virus infection. *J. Biol. Chem.* 290, 17306–17320. doi: 10.1074/jbc.M115.664136

Chang, D. M., and Shaio, M. F. (1994). Production of interleukin-1 (IL-1) and IL-1 inhibitor by human monocytes exposed to dengue virus. *J. Infect. Dis.* 170, 811–817. doi: 10.1093/infdis/170.4.811

Chen, S. T., Lin, Y. L., Huang, M. T., Wu, M. F., Cheng, S. C., Lei, H. Y., et al. (2008). CLEC5A is critical for dengue-virus-induced lethal disease. *Nature* 453, 672–676. doi: 10.1038/nature07013

Chen, Y.-C., and Wang, S. Y. (2002). Activation of terminally differentiated human monocytes/macrophages by dengue virus: productive infection, hierarchical production of innate cytokines and chemokines, and the synergistic effect of lipopolysaccharide. *J. Virol.* 76, 9877–9887. doi: 10.1128/jvi.76.19.9877-9887.2002

Collison, J. (2019). Recombinant IL-1Ra as first-line therapy in sJIA. *Nat. Rev. Rheumatol.* 15:250. doi: 10.1038/s41584-019-0208-8

Culshaw, A., Mongkolsapaya, J., and Screaton, G. R. (2017). The immunopathology of dengue and Zika virus infections. *Curr. Opin. Immunol.* 48, 1–6. doi: 10.1016/j.coi.2017.07.001

Descamps, D., Le Gars, M., Balloy, V., Barbier, D., Maschalidi, S., Tohme, M., et al. (2012). Toll-like receptor 5 (TLR5). *Proc. Natl. Acad. Sci. U.S.A.* 109, 1619–1624.

Dinarello, C. A. (1997). Interleukin-1. *Cytokine Growth Factor Rev.* 8, 253–265.

Dinarello, C. A. (2010). How interleukin-1beta induces gouty arthritis. *Arthritis. Rheum.* 62, 3140–3144. doi: 10.1002/art.27663

Grant, D., Tan, G. K., Qing, M., Ng, J. K., Yip, A., Zou, G., et al. (2011). A single amino acid in nonstructural protein NS4B confers virulence to dengue virus in AG129 mice through enhancement of viral RNA synthesis. *J. Virol.* 85, 7775–7787. doi: 10.1128/JVI.00665-11

Guzman, M. G., Halstead, S. B., Artsob, H., Buchy, P., Farrar, J., Gubler, D. J., et al. (2010). Dengue: a continuing global threat. *Nat. Rev. Microbiol.* 8, S7–S16. doi: 10.1038/nrmicro2460

Hakanpaa, L., Kiss, E. A., Jacquemet, G., Miinalainen, I., Lerche, M., Guzman, C., et al. (2018). Targeting beta1-integrin inhibits vascular leakage in endotoxemia. *Proc. Natl. Acad. Sci. U.S.A.* 115, E6467–E6476. doi: 10.1073/pnas.1722317115

Hatch, S., Endy, T. P., Thomas, S., Mathew, A., Potts, J., Pazoles, P., et al. (2011). Intracellular cytokine production by dengue virus-specific T cells correlates with subclinical secondary infection. *J. Infect. Dis.* 203, 1282–1291. doi: 10.1093/infdis/jir012

Hottz, E. D., Lopes, J. F., Freitas, C., Valls-de-Souza, R., Oliveira, M. F., Bozza, M. T., et al. (2013). Platelets mediate increased endothelium permeability in dengue through NLRP3-inflammasome activation. *Blood* 122, 3405–3414. doi: 10.1182/blood-2013-05-504449

Itani, S., Watanabe, T., Nadatani, Y., Sugimura, N., Shimada, S., Takeda, S., et al. (2016). NLRP3 inflammasome has a protective effect against oxazolone-induced colitis: a possible role in ulcerative colitis. *Sci. Rep.* 6:39075. doi: 10.1038/srep39075

Ito, M., Yanagi, Y., and Ichinohe, T. (2012). Encephalomyocarditis virus viroporin 2B activates NLRP3 inflammasome. *PLoS Pathog* 8:e1002857. doi: 10.1371/journal.ppat.1002857

Johnson, A. J., and Roehrig, J. T. (1999). New mouse model for dengue virus vaccine testing. *J. Virol.* 73, 783–786.

Katzelnick, L. C., Gresh, L., Halloran, M. E., Mercado, J. C., Kuan, G., Gordon, A., et al. (2017). Antibody-dependent enhancement of severe dengue disease in humans. *Science* 358, 929–932. doi: 10.1126/science.aan6836

Kostura, M. J., Tocci, M. J., Limjuco, G., Chin, J., Cameron, P., Hillman, A. G., et al. (1989). Identification of a monocyte specific pre-interleukin 1 beta convertase activity. *Proc. Natl. Acad. Sci. U.S.A.* 86, 5227–5231. doi: 10.1073/pnas.86.14.5227

Kugelberg, E. (2016). Innate immunity: IL-1beta activation under scrutiny. *Nat. Rev. Immunol.* 16, 594–595. doi: 10.1038/nri.2016.102

Kuhn, R. J., Zhang, W., Rossmann, M. G., Pletnev, S. V., Corver, J., Lenches, E., et al. (2002). Structure of dengue virus: implications for flavivirus organization, maturation, and fusion. *Cell* 108, 717–725.

Leake, I. (2019). Choline uptake is vital for IL-1beta-driven inflammation. *Nat. Rev. Rheumatol.* 15:320. doi: 10.1038/s41584-019-0228-4

Liu, Y., Zhang, F., Liu, J., Xiao, X., Zhang, S., Qin, C., et al. (2014). Transmission-blocking antibodies against mosquito C-type lectins for dengue prevention. *PLoS Pathog.* 10:e1003931. doi: 10.1371/journal.ppat.1003931

Martinon, F., Burns, K., and Tschopp, J. (2002). The inflammasome: a molecular platform triggering activation of inflammatory caspases and processing of proIL-beta. *Mol. Cell* 10, 417–426.

Martinon, F., Mayor, A., and Tschopp, J. (2009). The inflammasomes: guardians of the body. *Annu. Rev. Immunol.* 27, 229–265. doi: 10.1146/annurev.immunol.021908.132715

Mebius, R. E., and Kraal, G. (2005). Structure and function of the spleen. *Nat. Rev. Immunol.* 5, 606–616. doi: 10.1038/nri1669

Modis, Y., Ogata, S., Clements, D., and Harrison, S. C. (2004). Structure of the dengue virus envelope protein after membrane fusion. *Nature* 427, 313–319. doi: 10.1038/nature02165

Negash, A. A., Olson, R. M., Griffin, S., and Gale, M. J. (2019). Modulation of calcium signaling pathway by hepatitis C virus core protein stimulates NLRP3 inflammasome activation. *PLoS Pathog.* 15:e1007593. doi: 10.1371/journal.ppat.1007593

Pang, T., Cardosa, M. J., and Guzman, M. G. (2007). Of cascades and perfect storms: the immunopathogenesis of dengue haemorrhagic fever-dengue shock syndrome (DHF/DSS). *Immunol. Cell Biol.* 85, 43–45. doi: 10.1038/sj.icb.7100008

Park, E. K., Jung, H. S., Yang, H. I., Yoo, M. C., Kim, C., and Kim, K. S. (2007). Optimized THP-1 differentiation is required for the detection of responses to weak stimuli. *Inflamm. Res.* 56, 45–50. doi: 10.1007/s00011-007-6115-5

Puhlmann, M., Weinreich, D. M., Farma, J. M., Carroll, N. M., Turner, E. M., and Alexander, H. J. (2005). Interleukin-1beta induced vascular permeability is dependent on induction of endothelial tissue factor (TF) activity. *J. Transl. Med.* 3:37.

Rathinam, V. A., and Fitzgerald, K. A. (2016). Inflammasome complexes: emerging mechanisms and effector functions. *Cell* 165, 792–800. doi: 10.1016/j.cell.2016.03.046

Rothman, A. L. (2011). Immunity to dengue virus: a tale of original antigenic sin and tropical cytokine storms. *Nat. Rev. Immunol.* 11, 532–543. doi: 10.1038/nri3014

Shepard, D. S., Undurraga, E. A., Halasa, Y. A., and Stanaway, J. D. (2016). The global economic burden of dengue: a systematic analysis. *Lancet. Infect. Dis.* 16, 935–941. doi: 10.1016/S1473-3099(16)00146-8

So, A. K., and Martinon, F. (2017). Inflammation in gout: mechanisms and therapeutic targets. *Nat. Rev. Rheumatol.* 13, 639–647. doi: 10.1038/nrrheum.2017.155

Stack, J. H., Beaumont, K., Larsen, P. D., Straley, K. S., Henkel, G. W., Randle, J. C., et al. (2005). IL-converting enzyme/caspase-1 inhibitor VX-765 blocks the hypersensitive response to an inflammatory stimulus in monocytes from familial cold autoinflammatory syndrome patients. *J. Immunol.* 175, 2630–2634. doi: 10.4049/jimmunol.175.4.2630

Sung, P. S., Huang, T. F., and Hsieh, S. L. (2019). Extracellular vesicles from CLEC2-activated platelets enhance dengue virus-induced lethality via CLEC5A/TLR2. *Nat. Commun.* 10:2402. doi: 10.1038/s41467-019-10360-4

Swanson, K. V., Deng, M., and Ting, J. P. (2019). The NLRP3 inflammasome: molecular activation and regulation to therapeutics. *Nat. Rev. Immunol.* 19, 477–489. doi: 10.1038/s41577-019-0165-0

Tan, T. Y., and Chu, J. J. (2013). Dengue virus-infected human monocytes trigger late activation of caspase-1, which mediates pro-inflammatory IL-1beta secretion and pyroptosis. *J. Gen. Virol.* 94(Pt 10), 2215–2220. doi: 10.1099/vir.0.055277-0

Wang, W., Li, G., De, W., Luo, Z., Pan, P., Tian, M., et al. (2018). Zika virus infection induces host inflammatory responses by facilitating NLRP3 inflammasome assembly and interleukin-1beta secretion. *Nat. Commun.* 9:106. doi: 10.1038/s41467-017-02645-3

Wang, W., Xiao, F., Wan, P., Pan, P., Zhang, Y., Liu, F., et al. (2017). EV71 3D protein binds with NLRP3 and enhances the assembly of inflammasome complex. *PLoS Pathog.* 13:e1006123. doi: 10.1371/journal.ppat.1006123

Wu, D., Yan, Z. B., Cheng, Y. G., Zhong, M. W., Liu, S. Z., Zhang, G. Y., et al. (2018). Deactivation of the NLRP3 inflammasome in infiltrating macrophages by duodenal-jejunal bypass surgery mediates improvement of beta cell function in type 2 diabetes. *Metabolism* 81, 1–12. doi: 10.1016/j.metabol.2017.10.015

Wu, M. F., Chen, S. T., Yang, A. H., Lin, W. W., Lin, Y. L., Chen, N. J., et al. (2013). CLEC5A is critical for dengue virus-induced inflammasome activation in human macrophages. *Blood* 121, 95–106. doi: 10.1182/blood-2012-05-430090

Yan, Y., Jiang, W., Liu, L., Wang, X., Ding, C., Tian, Z., et al. (2015). Dopamine controls systemic inflammation through inhibition of NLRP3 inflammasome. *Cell* 160, 62–73. doi: 10.1016/j.cell.2014.11.047

Yu, I. M., Zhang, W., Holdaway, H. A., Li, L., Kostyuchenko, V. A., Chipman, P. R., et al. (2008). Structure of the immature dengue virus at low pH primes proteolytic maturation. *Science* 319, 1834–1837. doi: 10.1126/science.1153264

Zhu, Y., Zhang, R., Zhang, B., Zhao, T., Wang, P., Liang, G., et al. (2017). Blood meal acquisition enhances arbovirus replication in mosquitoes through activation of the GABAergic system. *Nat. Commun.* 8:1262. doi: 10.1038/s41467-017-01244-6

Conflict of Interest: The authors declare that the research was conducted in the absence of any commercial or financial relationships that could be construed as a potential conflict of interest.

Copyright © 2019 Pan, Zhang, Liu, Wang, Yu, Lao, Zhang, Shen, Wan, Xiao, Shereen, Zhang, Tan, Liu, Liu, Wu, Liu, Li and Wu. This is an open-access article distributed under the terms of the Creative Commons Attribution License (CC BY). The use, distribution or reproduction in other forums is permitted, provided the original author(s) and the copyright owner(s) are credited and that the original publication in this journal is cited, in accordance with accepted academic practice. No use, distribution or reproduction is permitted which does not comply with these terms.

frontiers in Microbiology

ORIGINAL RESEARCH
published: 26 November 2019
doi: 10.3389/fmicb.2019.02541

Insulin-Like Growth Factor 1 Regulates Acute Inflammatory Lung Injury Mediated by Influenza Virus Infection

Guiping Li[1,2†], Lijuan Zhou[1,2†], Can Zhang[1], Yun Shi[1], Derong Dong[1], Miao Bai[1], Rong Wang[3] and Chuanfu Zhang[1*]*

[1]Center for Hygienic Assessment and Research, Center for Disease Control and Prevention of Chinese PLA, Beijing, China, [2]College of Life Science, Huaibei Normal University, Huaibei, China, [3]Laboratory of Protein Engineering, Beijing Institute of Biotechnology, Beijing, China

OPEN ACCESS

Edited by:
Ian M. Jones,
University of Reading,
United Kingdom

Reviewed by:
Julie McAuley,
The University of Melbourne,
Australia
Wei Zou,
University of Michigan,
United States

***Correspondence:**
Rong Wang
wangrong_8312@163.com
Chuanfu Zhang
hnzcf@126.com

†These authors have contributed equally to this work

Specialty section:
This article was submitted to Virology, a section of the journal Frontiers in Microbiology

Received: *12 August 2019*
Accepted: *21 October 2019*
Published: *26 November 2019*

Citation:
Li G, Zhou L, Zhang C, Shi Y, Dong D, Bai M, Wang R and Zhang C (2019) Insulin-Like Growth Factor 1 Regulates Acute Inflammatory Lung Injury Mediated by Influenza Virus Infection. Front. Microbiol. 10:2541. doi: 10.3389/fmicb.2019.02541

The acute inflammatory lung injury is an important cause of death due to influenza A virus (IAV) infection. Insulin-like growth factor 1 (IGF1) played an important role in the regulation of inflammation in the immune system. To investigate the role of IGF1 in IAV-mediated acute inflammatory lung injury, the expression of IGF1 and inflammatory cytokines was tested after IAV A/Puerto Rico/8/1934 (H1N1; abbreviated as PR8) infection in A549 cells. Then, a BALB/c mouse model of PR8 infection was established. On days 3, 5, 7, and 9 post-infection, the mice lung tissue was collected to detect the expression changes in IGF1 mRNA and protein. The mice were divided into four groups: (1) PBS (abbreviation of phosphate buffered saline); (2) PR8 + PBS; (3) PR8 + IGF1; and (4) PR8 + PPP (abbreviation of picropodophyllin, the IGF1 receptor inhibitor). The body weight and survival rate of the mice were monitored daily, and the clinical symptoms of the mice were recorded. On day 5 post-infection, the mice were sacrificed to obtain the serum and lung tissues. The expression of inflammatory cytokines in the serum was detected by enzyme linked immunosorbent assay; lung injury was observed by hematoxylin-eosin staining; the viral proliferation in the lung was detected by real-time quantitative PCR; and the protein expression of the main molecules in the phosphatidylinositol-3-kinases/protein kinase B (PI3K/AKT) and mitogen-activated protein kinase (MAPK) signaling pathways was detected by Western blot. It was found that IGF1 expression is upregulated in A549 cells and BALB/c mice infected with PR8, whereas IGF1 regulated the expression of inflammatory cytokines induced by PR8 infection. Overexpression of IGF1 aggravated the IAV-mediated inflammatory response, whereas the inhibition of IGF1 receptor reduced such inflammatory response. The phosphorylation of IGF1 receptor triggered the PI3K/AKT and MAPK signaling pathways to induce an inflammatory response after IAV infection. Therefore, IGF1 plays an important immune function in IAV-mediated acute inflammatory lung injury. IGF1 may provide a therapeutic target for humans in response to an influenza outbreak, and inhibition of IGF1 or IGF1 receptor may represent a novel approach to influenza treatment.

Keywords: influenza virus, IGF1, acute inflammatory lung injury, PI3K/AKT, MAPK

INTRODUCTION

Influenza is an acute infectious disease caused by influenza virus infection, which is primarily characterized by respiratory damage. Moreover, it is associated with serious features (e.g., acute onset, wide spread, strong contagiousness, and great harm), which seriously threatens human health. Studies have shown that a series of symptoms and consequences caused by the influenza virus are not caused by the direct action of the influenza virus itself but are rather due to the inflammatory injury caused by the excessive activation of the immune response induced by an influenza virus infection (Oda et al., 1989; Taubenberger and Morens, 2006; Basler and Aguilar, 2008; Li and Cao, 2017). During the process of an IAV infection, there are different cytokine waves from the initial early responses of monocyte chemotactic protein-1 (MCP-1), interleukin-8 (IL-8), and interferon-alpha/beta/kappa (IFN-α/β/κ) to the later responses of IL-1α/β, IL-6, IL-18, tumor necrosis factor-alpha (TNF-α), IFN type I, macrophage inflammatory protein-1 alpha/beta (MIP-1α/β), MIP-3α, MCP-3, and interferon-inducible protein-10 (IP-10), which are mainly secreted by infected macrophages in the lower respiratory tract (Julkunen et al., 2001; Xagorari and Chlichlia, 2008; Jewell et al., 2010; Gu et al., 2019). The modest cytokine response contributes to the induction of antiviral and Th1-type immune responses in the body; however, excessive inflammatory responses can be harmful. For example, the main reason for the high pathogenicity of the H5N1 avian influenza virus is the exaggerated generation and secretion of excessively high levels of pro-inflammatory cytokines, known as a "cytokine storm" (Kobasa et al., 2007; Allen et al., 2009). In 1918, the "Spanish flu" also caused fatal inflammatory damage to the lung tissue by triggering an overreaction of the human immune response (Ocana-Macchi et al., 2009). This inflammatory injury to the lung tissue is both an important cause of death due to influenza virus infection and a major cause of lung infections caused by severe acute respiratory syndrome (SARS), sepsis, and aspiration pneumonia (Imai et al., 2005; Nicholls and Peiris, 2005). Currently, immunosuppressive agents (e.g., glucocorticoids) are often used in clinical practice to inhibit inflammatory cytokine responses, thereby blocking disease progression and improving the clinical therapeutic effect. The literature reports that 51–69% of patients with severe H1N1 influenza are treated with glucocorticoids, which have a specific therapeutic effect (Aikawa et al., 2012); however, glucocorticoids systemically inhibit the immune function of the infected individual. Moreover, the long-term treatment with such medication can induce or aggravate the infection, causing a variety of complications and serious side effects (e.g., femoral head necrosis). Therefore, it is imperative to develop a deep understanding of the pathogenesis of influenza virus and to identify new strategies of treating influenza more safely and effectively.

Insulin-like growth factor 1 (IGF1) belongs to the insulin-like growth factor family, which also includes growth hormone (GH), insulin-like growth factor II (IGF2), insulin-like growth factor 1 receptor (IGF1R), insulin-like growth factor II receptor (IGF2R), and insulin-like growth factor binding protein 1–6 (IGFBP1–6; Jogie-Brahim et al., 2009). This family plays an extremely important role in the process of cell growth, differentiation, and apoptosis (Stewart and Rotwein, 1996; Granata et al., 2004). IGF1 mainly functions by binding to IGF1R, a transmembrane protein composed of two α domains and two β domains (Siddle et al., 2001). The α domain binds to IGF1 to activate the β domain (Siddle et al., 2001). Since the β domain has tyrosine kinase activity, it can promote the phosphorylation of the substrate hepatocyte growth factor (HGF), docking protein insulin receptor substrate (IRS), vascular endothelial growth factor (VEGF), and growth factor receptor binding protein 2 (Grb2; Wilden et al., 1992; Hubbard, 1997). Some phosphorylated substrates activate the downstream phosphatidylinositol-3-kinases/protein kinase B (PI3K/AKT) and mitogen-activated protein kinase (MAPK) signaling pathways to regulate a range of biological responses (Myers et al., 1992; Egan et al., 1993).

Recent studies have found that IGF1 plays an important role in the regulation of inflammation in the immune system. IGF1 mRNA expression in the bronchial cells of asthmatic patients was significantly higher than that of normal people and was significantly associated with fibrosis in epithelial cells (Hoshino et al., 1998). The associated mechanism is that IGF1 binds to the receptor and activates the PI3K/AKT signaling pathway and induces Akt activation, which further activates the downstream IL-17-mediated inflammatory pathway (Lee et al., 2014). In addition, the levels of serum IGF1 protein in patients with type 2 diabetes are significantly higher than those in healthy people. Obesity is closely related to the pathogenesis of type 2 diabetes, as long-term obesity will lead to IL-6 and IL-17-mediated chronic inflammation (Cohen and LeRoith, 2012; Ge et al., 2013). In non-autoimmune inflammatory contact dermatitis, IGF1 relieves the inflammatory response by recruiting regulatory T cells to release the anti-inflammatory cytokine, IL-10 (Johannesson et al., 2014). In the nervous system, IGF1 recruits anti-inflammatory proteins to protect nerve cells from degeneration (Arroba et al., 2016). Other studies have shown that IGF1 plays an important role in regulating the function of lactating buffalo oocytes and preventing inflammation induced by post-partum genital tract infections. A concentration of 50 ng/ml IGF1 acts on lipopolysaccharides (LPS; 1 μg/ml)-infected buffalo granulosa cells, reducing the expression of the inflammatory cytokines, IL-6, TNF-α, and IL-1β, as well as decreasing Akt phosphorylation in PI3K/AKT signaling pathway and extracellular-regulated kinase 1/2 (ERK1/2) phosphorylation in the MAPK signaling pathway (Onnureddy et al., 2015).

However, whether IGF1 plays a significant role in mediating inflammation and pathology during influenza infection and its associated mechanism remains unknown. In this study, we found that IGF1 mRNA and protein increased after influenza virus infection. Overexpression of IGF1 aggravated cytokine expression during infection by influenza, while blocking of IGF1 production in mice treated with IGF1R inhibitor, decreased immunopathology. The phosphorylation level of IGF1R was elevated after influenza virus infection, triggering the PI3K/AKT and MAPK signaling pathways to induce an inflammatory response. Thus, IGF1 could regulate influenza virus-mediated acute inflammatory lung injury, which may provide a therapeutic target for humans in response to an influenza outbreak.

MATERIALS AND METHODS

Cell Lines, Viruses, and Animals

The human alveolar epithelial cell line A549 is particularly sensitive to influenza virus infection and has been widely used as a good *in vitro* model to study influenza virus for nearly 20 years. The cell line A549 was purchased from the American Type Culture Collection (ATCC, USA) and propagated in Dulbecco's Modified Eagle's Medium (DMEM; Life Technologies, USA) supplemented with 10% fetal bovine serum (FBS; HyClone, USA) at 37°C in a 5% CO_2 incubator.

The mouse adapted Influenza A virus (IAV) A/Puerto Rico/8/1934 (H1N1; abbreviated as PR8) was kindly provided by Prof. Shihui Sun (Beijing Institute of Microbiology and Epidemiology) and propagated in 9- to 11-day-old SPF chicken embryos. The allantoic fluid was collected and titrated to determine the 50% tissue culture infection dose ($TCID_{50}$) in A549 cells and the median lethal dose (LD_{50}) in mice following the Reed-Muench method (Reed and Muench, 1938).

Specific pathogen free (SPF) grade female BALB/c mice aged 6–8 weeks (body weight: 18–20 g) were purchased from the Experimental Animal Center of the Military Medical Research Institute.

Construction of a Cellular Model for the Overexpression/Inhibition of IGF1

Amplification of human IGF1 open reading frame (ORF; Guangzhou GeneCopoeia Biotechnology Co., Ltd.) using primers containing Xba I and Xho I restriction sites (Forward: 5′-TGCTCTAGAATGGGAAAAATCAGCAGTCT-3′; Reverse: 5′-CCGCTCGAGCTACATCCTGTAGTTCTTGT-3′) ligated into a pcDNA3.1 expression vector, constructing pcDNA3.1-IGF1. The pcDNA3.1-IGF1 vector was transfected into A549 cells with LiPO2000. The cell line overexpressing IGF1 was screened with G418 (500 μg/ml). The human IGF1 shRNA lentiviral particles (sc-37193-V) were purchased from Santa Cruz Company.

mRNA Levels Detected by Real-Time Quantitative PCR

The total cellular RNA was extracted using TRIZOL (Invitrogen, Cat: 15596-026). The cDNA was synthesized by reverse transcription using a TIANscript RT Kit (TIANGEN, Cat: KR104), followed by quantitative PCR (qPCR) using SYBR Premix Ex Taq II (TAKARA, Cat: RR820A). The primer sequences that were used are presented in **Table 1**. When detecting the viral proliferation in the lungs of mice, a real-time fluorescent quantitative PCR probe method was used, and the probe sequence was FAM-TGCAGTCCTCGCTCAC TGGGCACG-BHQ1. The primer sequence of matrix protein 1 (M1) was Forward: 5′-GACCRATCCTGTCACCTCTGAC-3′; Reverse: 5′-GGGCATTYTGGACAAAKCGTCTACG-3′. GAPDH was selected as the internal reference, and the results were analyzed using the $2^{-\triangle\triangle Ct}$ method. The reaction conditions were set as follows: step 1: 95°C for 30 s; step 2: 95°C for 5 s, 60°C for 30 s, 40 cycles; and step 3: dissolution curve analysis.

TABLE 1 | Quantitative PCR primer sequences for inflammatory cytokines.

Gene	Primer 5′-3′
GAPDH-F	AACGGGAAGCTCACTGGCATG
GAPDH-R	TCCACCACTGTTGCTGTAG
IGF1-F	TAAGGAGGCTGGAGATGTAT
IGF1-R	CTCTACTTGCGTTCTTCA
IL-6-F	AGCCCTGAGAAAGGAGACATG
IL-6-R	GCAAGTCTCCTCATTGAATCCAG
IL-8-F	TGTGGAGAAGTTTTTGAAGAGGG
IL-8-R	CCCTACAACAGACCCACACAATAC
IL-10-F	ACCTGCCTAACATGCTTCGAG
IL-10-R	CTGGGTCTTGGTTCTCAGCTT
TNF-α-F	TGGAGAAGGGTGACCGACTCAG
TNF-α-R	GTTTGGGAAGGTTGGATGTTCG
IL-1β-F	CCCAGAGAGTCCTGTGCTGAATG
IL-1β-R	GAGAGCTGACTGTCCTGGCTGAT
CCL2-F	GCTCGCTCAGCCAGATGCAATC
CCL2-R	GCTTCTTTGGGACACTTGCTGC

Western Blot Detection of the Level of Protein Expression

For the cultured cells, the total cellular protein was extracted using the Whole Cell Lysate (Beijing ComWin, Cat: CW0074) containing a protease inhibitor cocktail (Roche, Germany). The protein was quantified using a bicinchoninic acid (BCA) Protein Assay Kit (Beijing ComWin, Cat: CW0014), and a 30 μg protein sample was obtained for polyacrylamide gel electrophoresis (PAGE). The lung tissues from six mice of each group were mixed and ground in liquid nitrogen, and then the total cellular protein was extracted using the Whole Cell Lysate (Beijing ComWin, Cat: CW0074) containing a protease inhibitor cocktail (Roche, Germany). Protein was quantified using a BCA Protein Assay Kit (Beijing ComWin, Cat: CW0014). A 50 μg protein sample was obtained for PAGE and subsequently transferred to a polyvinylidene fluoride (PVDF) membrane. The primary antibodies of rabbit anti-glyceraldehyde phosphate dehydrogenase (GAPDH) and goat anti-IGF1 (Abcam) were diluted to 1:2,000. The secondary antibodies of horseradish peroxidase (HRP)-goat anti-rabbit immunoglobulin G (IgG) and HRP-rabbit anti-goat IgG (ZSGB-BIO) were diluted to 1:5,000. The signals were detected using a Western HPR Substrate Peroxide solution (Millipore). The quantification of Western blot analysis was performed by using Image J software, and the protein expression levels were normalized to GAPDH levels.

Level of Cytokine Expression Detection

The level of cytokine expression was detected using mouse IGF1 ELISA Kit, IL-6 ELISA Kit, TNF-α ELISA Kit, IFN-γ ELISA Kit, and IL-1β ELISA Kit (all purchased from R&D systems).

Viral Infection of A549

For viral infection, A549 cells were washed with phosphate buffered saline (PBS) and subsequently infected with PR8 at the multiplicity of infection (MOI) of 0.5 or 1.0 in infection medium, which was DMEM supplemented 0.5 mg/ml N-p-tosyl-phenylalanine

chloromethyl ketone (TPCK)-treated trypsin (Sigma, USA) and 0.3% bovine serum albumin (BSA; Sangon, China). After 1 h, cells were incubated with fresh infection medium at 37°C for the indicated times.

Infection, Monitoring, and Sampling of Mice

BALB/c mice were intraperitoneally injected with sodium pentobarbital (50 mg/kg), and the mice were induced into a deep anesthetic state and administered a nasal inhalation of phosphate buffered saline (PBS) or PR8 (diluted 10-fold, 30 μl/mouse, $50LD_{50}$). In the PR8 + IGF1 group, IGF1 (20 μg/kg, Peprotech) was intraperitoneally injected 6 h before infection, and after infection, IGF1 was intraperitoneally injected every 24 h. The PR8 + PPP group was intraperitoneally injected with the IGF1 receptor inhibitor, and picropodophyllin (PPP, 20 mg/kg, Selleck) 6 h before infection and after infection PPP was intraperitoneally injected every 12 h. After the continuous administration for 14 days, changes in the clinical symptoms of mice were observed daily, and changes in the body weight and survival were recorded. On days 3, 5, 7, and 9 after PR8 infection, six mice of each group were sacrificed every time. The blood was taken by excising the eyeballs, and the lung tissues were collected. The blood was kept at room temperature for 1 h and centrifuged at 11,000 *g* for 15 min. The serum was collected and aliquoted and stored at −80°C for later use.

All animal experimental procedures were approved by the Animal Care and Use Committee of the Academy of Military Medical Sciences (AMMS; ID: SYXK2012-05) and were carried out in strict accordance with the guidelines. All experiments involving the live virus were performed in an approved biosafety level 2 facility.

Lung Injury Conditions and Lung Index

After removing the whole lung tissue of the mice, damage to the lung tissue was observed. The degree of lung injury visible to the naked eye was dark red due to edema. The area ratio of lung injury to the total lung tissue was estimated. Each sample was estimated by at least three different individuals, and the average was obtained. Finally, the lung injury area of six mice in each group was counted. The wet weight of the lung tissue was weighed. Lung index = lung wet weight/body mass.

Data Analysis

All experiments were repeated at least three times. Data were expressed as means ± standard deviation (SD). The graphical representation of the data was performed using GraphPad Prism 5 software. The grayscale analysis of the Western blot images was performed using Image J software by comparing the integrated density of the IGF1 band with the control GAPDH. The statistical analyses were performed using SPSS 20.0 statistical software with two-tailed Student's *t* test for two comparisons, $^{*}p < 0.05$; $^{**}p < 0.01$; and $^{***}p < 0.001$. A p below 0.05 was considered statistically significant.

RESULTS

IGF1 Expression Is Upregulated in A549 Cells Infected With Influenza A Virus PR8

To detect the regulation of IGF1 by IAV, A549 cells were infected with PR8 ($10^{4.58}$ $TCID_{50}$/ml) at different multiplicity of infection (MOI) of 0.1, 0.5, or 1.0, and the level of IGF1 mRNA and protein expression was detected at 12, 24, 48, and 72 h post-infection. As shown in **Figure 1A**, compared with the Mock-infected controls, the level of IGF1 mRNA expression in A549 cells increased gradually at 12, 24, and 48 h after PR8 infection at a MOI of 0.5. The level of IGF1 mRNA expression peaked at 48 h post-infection, which was 6.35 ± 0.30 times higher than that of the Mock controls. The level of IGF1 mRNA expression decreased slightly at 72 h post-infection but still reached 4.23 ± 0.18 times that of the Mock group. As shown in **Figure 1B**, in A549 cells infected with different MOIs of PR8, the level of IGF1 mRNA expression increased following the increasing of MOI at 48 h post-infection. At a MOI of 1.0, the level of IGF1 mRNA increased to 7.49 ± 0.38 times that of the Mock group.

The level of IGF1 protein expression was also upregulated at 12, 24, 48, and 72 h post-infection of PR8 (**Figure 1C**) and following the increasing of MOI at 48 h post-infection in A549 cells (**Figure 1D**). To compare the trend in IGF1 variability more intuitively, the grayscale analysis of **Figures 1C,D** was performed and plotted according to the ratio of the integrated density of IGF1/GAPDH. **Figures 1E,F** show that the level of IGF1 protein expression in the A549 cells following PR8 infection was consistent with the level of IGF1 mRNA; however, such upregulation times were lower than the level of mRNA. Compared with the Mock group, the level of IGF1 protein expression peaked 1.82 times at 48 h after PR8 infection at a MOI of 0.5 (**Figure 1E**). The level of IGF1 protein expression was also increased following the increasing of MOI. At a MOI of 1.0, the level of IGF1 protein expression reached 2.26 times that of the Mock group at 48 h post-infection (**Figure 1F**). The above results indicate that IGF1expression is upregulated in PR8-infected A549 cells.

IGF1 Regulates the Expression of Inflammatory Cytokines in Response to PR8 Infection

To investigate the role of IGF1 in the inflammatory response to influenza virus infection, we established two stable A549 cell lines, in which IGF1 is overexpressed or inhibited. Using pcDNA3.1-IGF1 to overexpress IGF1, **Figure 2A** showed that the level of IGF1 mRNA was increased 15.28 ± 1.84 times that of the control group. The expression of IGF1 in the cells was inhibited by lentiviral packaged shRNA (Lenti + shIGF1), after which the level of IGF1 mRNA was reduced to 0.21 ± 0.087 times that of the control group (**Figure 2A**). As shown in **Figure 2B**, the level of IGF1 protein was also increased in stable A549 cell line with pcDNA3.1-IGF1 and inhibited in stable A549 cell line with Lenti + shIGF1. The stably transfected A549 cell lines were infected with PR8 at a MOI of 0.5. After 24 h, real-time quantitative PCR (qPCR) was used to detect

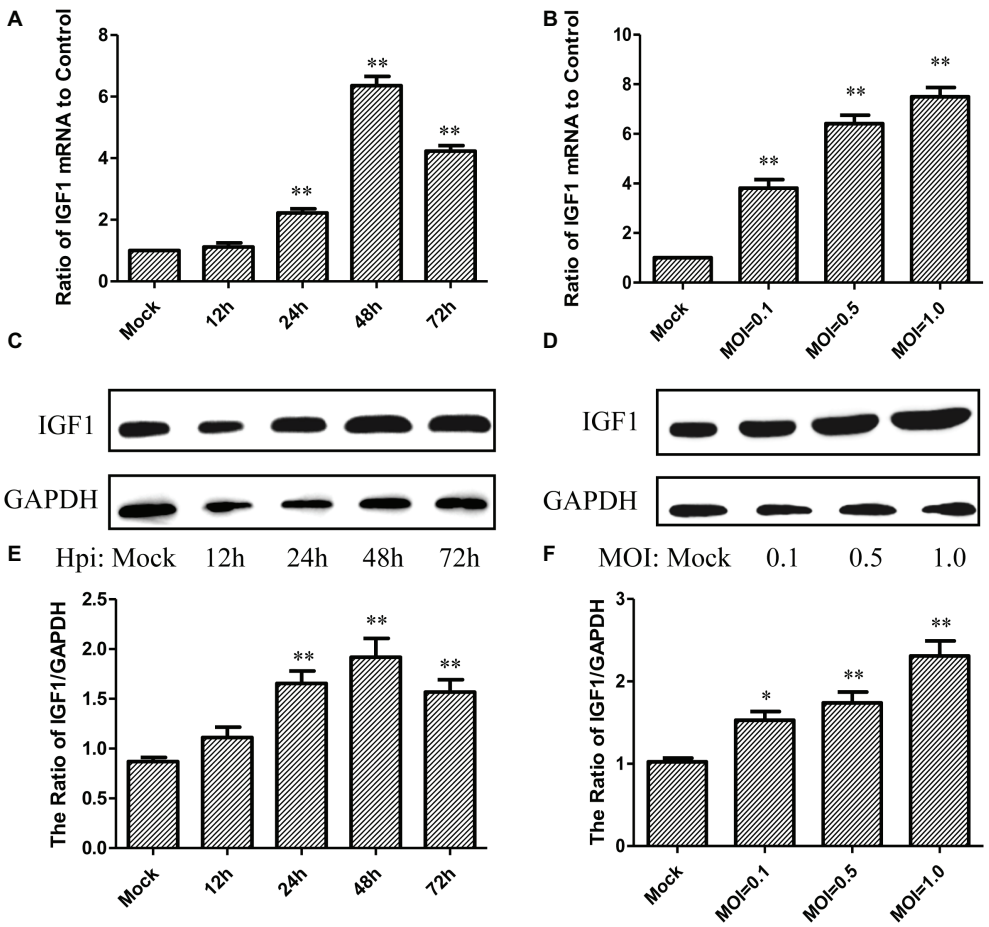

FIGURE 1 | IGF1 expression was upregulated in A549 cells infected with influenza A virus (IAV) PR8. **(A)** Changes in the level of IGF1 mRNA over time in PR8-infected A549 cells (MOI = 0.5); **(B)** changes in the level of IGF1 mRNA over MOI in PR8-infected A549 cells at 48 h post-infection; **(C)** changes in the level of IGF1 protein expression over time in PR8-infected A549 cells (MOI = 0.5); GAPDH was used as loading control, and figures were representative of three independent experiments; **(D)** changes in the level of IGF1 protein expression over MOI in PR8-infected A549 cells at 48 h post-infection; GAPDH was used as loading control, and figures were representative of three independent experiments; **(E)** grayscale analysis of Figure 1C, and plotted as the ratio of the integrated density of IGF1/GAPDH; **(F)** grayscale analysis of Figure 1D, and plotted as the ratio of the integrated density of IGF1/GAPDH. Data were the means ± SD from three independent experiments. $^{**}p < 0.01$ vs. Mock by *t* test.

the changes in cytokine expressions [IL-6, IL-8, IL-10, monocyte chemotactic protein-1 (MCP-1, or CCL2), TNF-α, and IL-1β], which were related to the inflammatory response. The results in **Figure 2C** showed that compared with the Mock controls, the cytokine levels were significantly increased following PR8 infection in control cells (PR8 + pcDNA3.1-con group and PR8 + Lenti + con group). IGF1 overexpression further increased the level of cytokine mRNA expression, whereas the levels of cytokine expression in the PR8-infected cells with IGF1 knocked down (PR8 + Lenti + shIGF1) were significantly decreased far lower than the PR8-infected control cell (PR8 + Lenti + con group), as well as the uninfected Mock group. Especially the lowest CCL2 and TNF-α mRNA of PR8 + Lenti + shIGF1 group were downregulated to less than half that of the Mock group. These results indicate that the overexpression of IGF1 aggravated the inflammatory response induced by influenza virus infection, whereas the inhibition of IGF1 expression can alleviate this inflammatory response.

IGF1 Expression Is Upregulated in Mice Infected With IAV PR8

To detect whether influenza virus can also regulate IGF1expression *in vivo*, IAV PR8 (diluted 10-fold, 30 μl/mouse, $50LD_{50}$) was intranasally inoculated into BALB/c mice. Mice were sacrificed on days 3, 5, 7, and 9 post-infection to obtain mice lung tissue and serum, and the samples of six mice in every group were mixed. The level of IGF1 mRNA expression in the lung tissue of mice was detected by qPCR. As shown in **Figure 3A**, the level of IGF1 mRNA expression in the lung tissue gradually increased at days 3, 5, and 7 after PR8 infection. On day 7 post-infection, IGF1 mRNA increased to 5.81 ± 0.623 times that of the control group and decreased slightly on day 9 post-infection. A Western blot was used to detect changes in IGF1 protein expression in the lung tissue following PR8 infection (**Figure 3B**). The grayscale analysis by comparing the integrated density of the IGF1 band with the control GAPDH showed that the trend in the level of IGF1 protein expression was

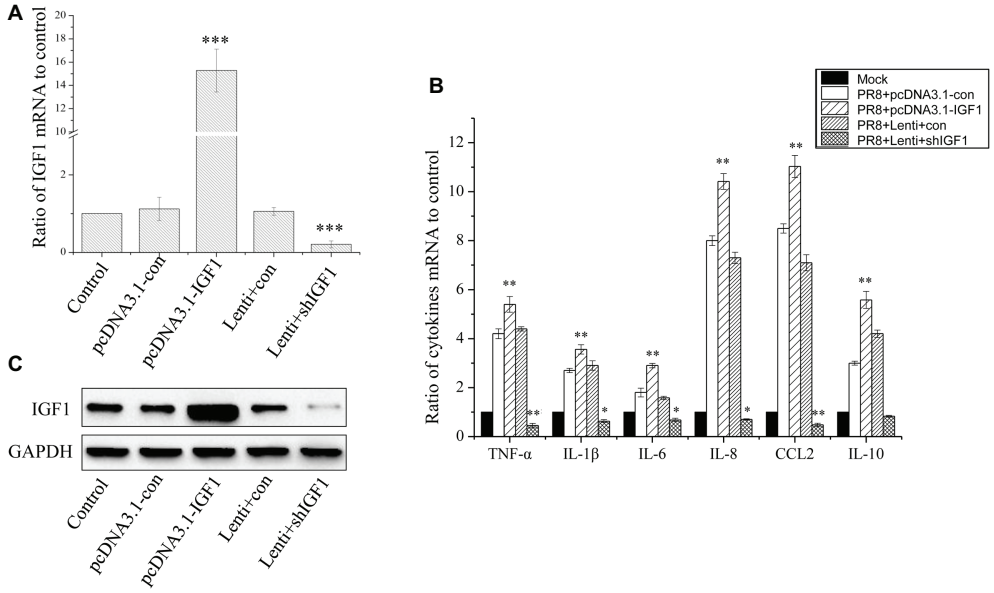

FIGURE 2 | IGF1 regulates the expression of inflammatory cytokines in response to PR8 infection. **(A)** Q-PCR detection of IGF1 mRNA overexpression and inhibition in stably transfected A549 cells; **(B)** Western blot detection of IGF1 overexpression and inhibition in stably transfected A549 cells; GAPDH was used as loading control, and figures were representative of three independent experiments; **(C)** regulation of the intracellular inflammatory cytokines expression following PR8 infection (MOI = 0.5) after overexpression or inhibition of IGF1. Data were the means ± SD from three independent experiments. $^{*}p < 0.05$; $^{**}p < 0.01$; $^{***}p < 0.001$ vs. Mock by *t* test.

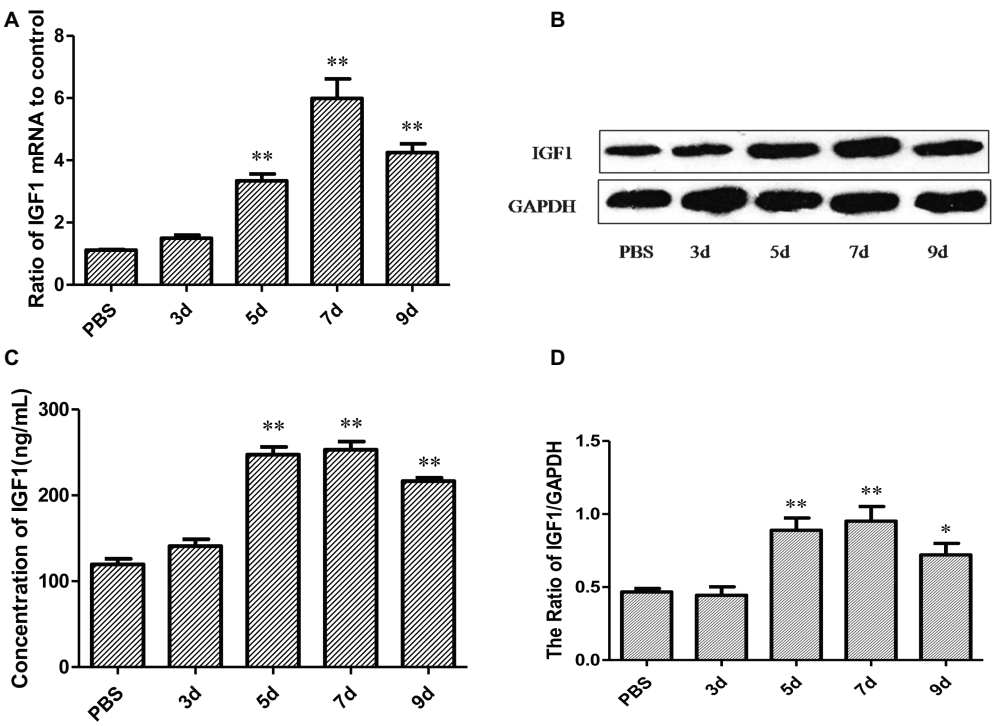

FIGURE 3 | IGF1 expression is upregulated in BALB/c mice infected with IAV PR8. **(A)** Changes in the level of IGF1 mRNA over time in the lung tissue of BALB/c mice infected with PR8 ($50LD_{50}$); **(B)** changes in the level of IGF1 protein over time in the lung tissue of BALB/c mice infected with PR8 ($50LD_{50}$); **(C)** grayscale analysis of Figure 3B, and plotted as the ratio of the integrated density of IGF1/GAPDH; and **(D)** changes in the level of IGF1 mRNA expression over time in the serum of BALB/c mice infected with PR8 ($50LD_{50}$). The lung and serum sample were mixed from six mice in the group. Data were the means ± SD from three independent experiments. $^{**}p < 0.01$ vs. PBS group by *t* test.

consistent with that of the mRNA data (**Figure 3C**). The content of IGF1 in the serum of mice was detected by enzyme linked immunosorbent assay (ELISA). As shown in **Figure 3D**, compared with the PBS control group, the content of IGF1 protein in serum increased significantly on day 5 post-infection of PR8 and decreased on day 9. These results were also consistent with the qPCR and Western blot findings.

IGF1 Regulates Acute Inflammatory Lung Injury in PR8-Infected Mice

To detect whether IGF1 regulates acute inflammatory lung injury in PR8 infection, BALB/c mice were tested as follow. BALB/c mice were randomly divided into four groups: (1) PBS; (2) PR8 + IGF1; (3) PR8+ PPP; and (4) PR8 + PBS. The PBS group was intranasally inoculated with 30 μl PBS, whereas the other three groups were intranasally inoculated with 30 μl influenza virus PR8 ($50LD_{50}$). From 6 h before the inoculation to day 14 post-infection, the mice in the PR8 + IGF1 group were intraperitoneally injected with IGF1 protein (20 μg/kg/24 h); PR8 + PPP mice were injected intraperitoneally with an IGF1 receptor inhibitor, picropodophyllin (PPP, 20 mg/kg/12 h); and the PR8 + PBS group was injected with PBS (30 μl/24 h). The clinical symptoms of the mice were observed daily for 14 days, and changes in body weight and survival were recorded. Six mice of each group were sacrificed at day 5 post infection of PR8, and the serum and lung tissues of each group were collected and mixed. The extent of lung injury and inflammatory cell infiltration of the mice in each group was observed by histologically. Changes in the level of serum cytokines were detected by ELISA. A western blot was used to detect the changes in the expression of major proteins in the IGF1/IGF1R-related signaling pathways.

There was no change in the general appearance of the PBS control group mice. In the PR8 + PBS group, flu-like symptoms began to appear on day 3 after PR8 inoculation, such as reduced activity, ruffled fur, and slight weight loss. On day 5 post-infection, these conditions worsened with 20% weight loss, canthus secretion, hunched back. The symptoms of the PR8 + IGF1 group were more severe than those of the PR8 + PBS group, whereas the PR8 + PPP group displayed milder clinical symptoms than that of the PR8 + PBS group (**Figure 4A**).

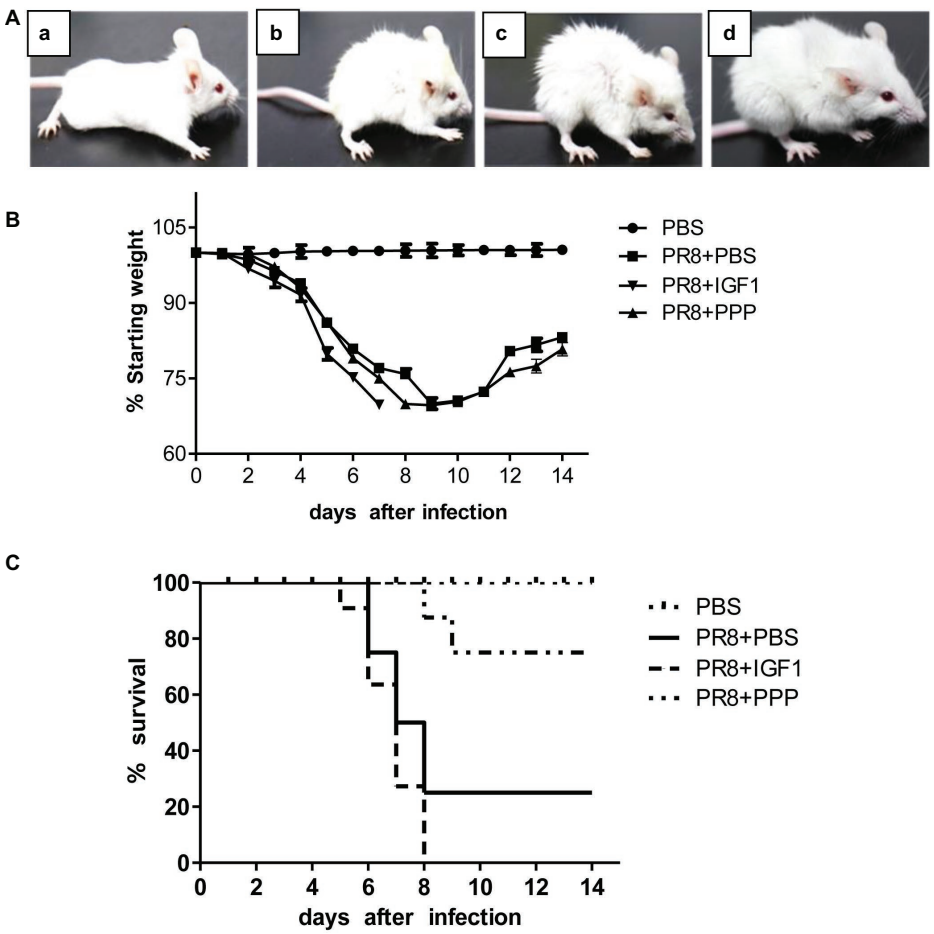

FIGURE 4 | Changes in the clinical manifestations, body weight, and survival rate of BALB/c mice following PR8 infection. **(A)** Clinical symptoms of BALB/c mice after PR8 infection ($50LD_{50}$) [**(a)** PBS; **(b)** PR8 + PBS; **(c)** PR8 + IGF1; **(d)** PR8 + PPP]; **(B)** changes in body weight in BALB/c mice after PR8 infection ($50LD_{50}$); and **(C)** survival rate of BALB/c mice after PR8 infection ($50LD_{50}$; n = 15).

Figure 4B showed that the body weight of the mice decreased significantly on day 3 post-infection of PR8, and the body weight of the mice on day 9 decreased to the lowest. Although the changes in body weight were similar between the PR8 + PPP group and PR8 + PBS group, the survival rate of the PR8 + PPP group was dramatically increased up to 75% compared with the survival rate of the PR8 + PBS group was only 25%, with the first death not occurring until the day 8 post-infection (**Figure 4C**). The first death in the PR8 + IGF1 group was accelerated to day 5 post-infection, and all mice have succumbed to the infection by day 8. These findings indicated that the intraperitoneal injection of IGF1 promoted the death of PR8-infected mice, whereas the inhibition of IGF1 increased the survival rate of PR8-infected mice.

Figure 5A showed that in IAV PR8-infected mice, the lungs exhibited differential degrees of damage, and the color of the damaged parts changed from pink to dark red, with the presence of edema. The extent of lung injury in the PR8 + IGF1 group was significantly more severe than that of the PR8 + PBS group, as the lung color was darker, and the lesion area was larger. The degree of lung injury in the PR8 + PPP group was significantly less severe than that of the PR8 + PBS group. **Figures 5B,C** showed that the lung index of uninfected mice was approximately 1%. Compared with the PR8+ PBS group, the lung index of the PR8 + IGF1 group increased significantly from 1.953 ± 0.074 to 2.515 ± 0.121%, and the area of lung injury also increased from 0.38 ± 0.042 to 0.78 ± 0.069, approximately twice that of the control group. In the PR8 + PPP group, the lung index decreased to 1.393 ± 0.032%, and the lung injury area also decreased to 0.25 ± 0.062, which were both lower than that of the PR8 + PBS group. As shown in **Figure 5D**, the lung structure of the mice in the PBS group was clear, with intact pulmonary alveoli, clear alveolar septum, and without hemorrhaging and inflammatory cell infiltration. The pulmonary alveoli of the PR8 + PBS, PR8 + IGF1, and PR8 + PPP groups exhibited varying degrees of damage. The level of inflammatory cell infiltration in the lung tissue of the PR8 + IGF1 group was greater than that of the PR8 + PBS group, and there was lower inflammatory infiltration in the PR8 + PPP group than the PR8 + PBS group.

Whether IGF1 regulates the viral replication of IAV, qPCR was used to detect changes of the viral matrix protein 1 (M1) expression in the lungs of PR8-infected mice, which could indirectly reflect the viral load. The viral load in the lungs of the PR8 + IGF1 group was significantly increased to nearly two-fold of the PR8 + PBS group (**Figure 5E**). However, the viral load of the PR8 + PPP group and the PR8 + PBS group was similar, indicating that IGF1 responded to influenza infection *via* the host immune response rather than targeting viral replication.

The cytokine content in the serum of PR8-infected mice was detected. **Figures 6A–D** showed that there was a significant increase in the serum inflammatory following PR8 infection.

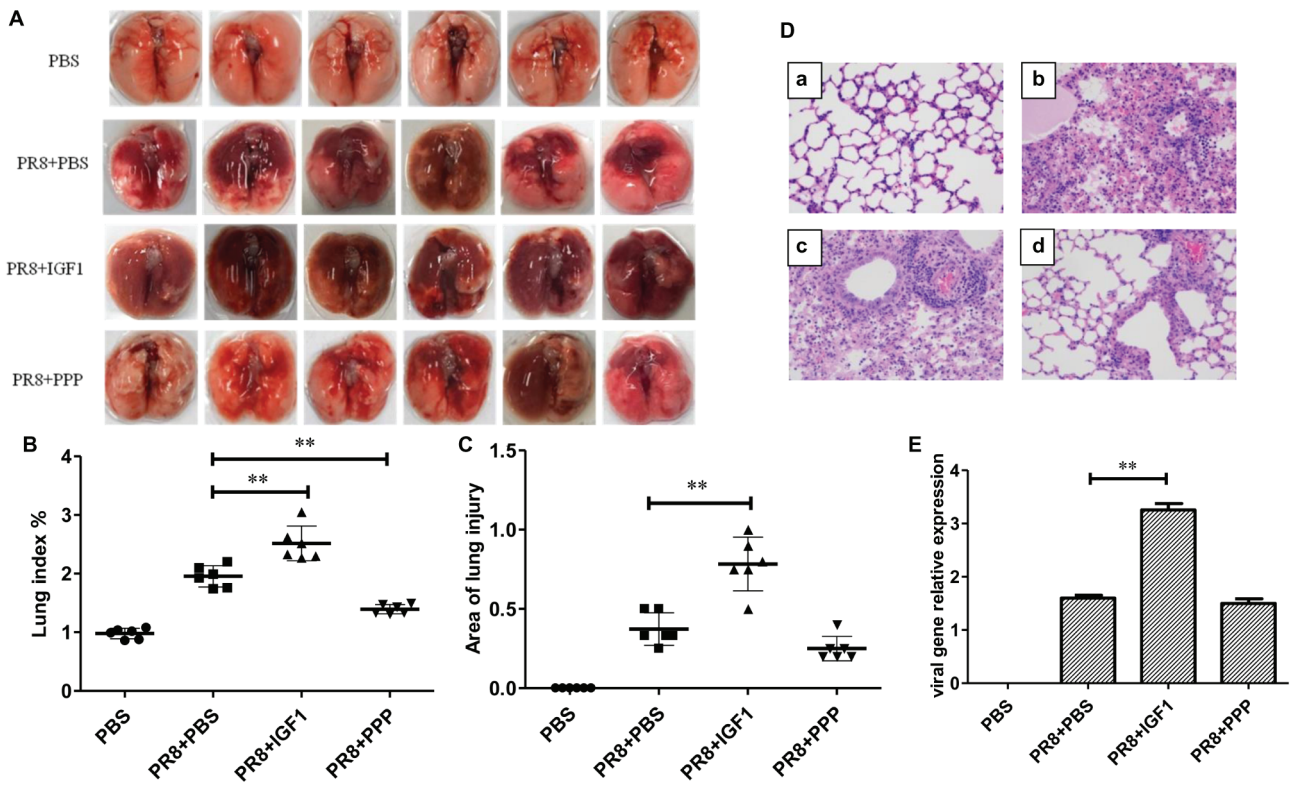

FIGURE 5 | Lung injury following PR8 infection in BALB/c mice. Groups of BALB/c mice (n = 6, females, 6–8 weeks) were intranasally infected with PR8 ($50LD_{50}$), treated with IGF1 or PPP, and at day 5 post-infection, the mice lungs were examined for changes in **(A)** morphology, **(B)** lung injury, **(C)** injury areas, **(D)** histopathology, and **(E)** viral load. Data were the means ± SD from three independent experiments. $^{**}p < 0.01$ vs. PR8 + PBS group by t test.

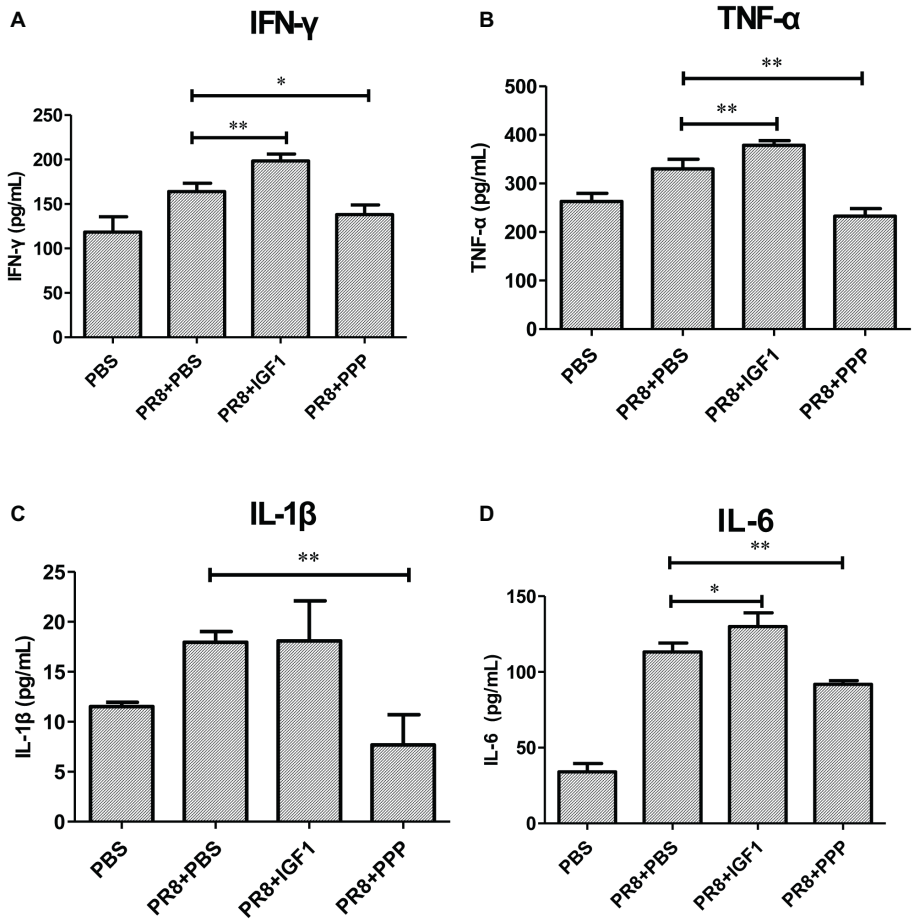

FIGURE 6 | Cytokine expression in BALB/c mice after PR8 infection. Groups of BALB/c mice (n = 6, females, 6–8 weeks) were intranasally infected with PR8 ($50LD_{50}$), treated with IGF1 or PPP, and at day 5 post-infection, the mice serum were examined for changes in **(A)** IFN-γ mRNA, **(B)** TNF-α mRNA, **(C)** IL-1β mRNA, and **(D)** IL-6 mRNA. Data were the means ± SD from three independent experiments. $^{*}p < 0.05$; $^{**}p < 0.01$ vs. PR8 + PBS group by t test.

Moreover, the inflammatory cytokine levels in the intraperitoneal injected IGF1 protein group were further increased, in which IL-1β was highly variable, and there was no statistical difference with the PR8 + PBS group. The levels of inflammatory factors IFN-γ, TNF-α, IL-6, and IL-1β in the serum of the PR8 + PPP group were significantly decreased, and IL-1β was lower than that of the uninfected mice. The results further confirm that IGF1 induced an inflammatory response following influenza virus infection, which can be alleviated by inhibiting IGF1.

IGF1 Regulates Acute Inflammatory Lung Injury in PR8-Infected Mice *via* the PI3K/AKT and MAPK Pathways

To explore the mechanism by which IGF1 regulates acute inflammatory lung injury induced by IAV infection, a Western blot was used to detect the expression of molecules in key signaling pathways in the lung tissue of PR8-infected mice ($50LD_{50}$ PR8). Each sample was from six mice in a group and was tested for three times. Figures were representative of three independent experiments. **Figure 7A** showed that the phosphorylation level of IGF1R increased gradually following PR8 infection, peaked at day 7 post-infection, and then decreased slightly on day 9, which was consistent with the changes in the trend of IGF1 protein expression (**Figure 3B**). **Figures 7B–D** showed that the PI3K/AKT and MAPK signaling pathways were activated following PR8 infection; p-AKT expression was upregulated in the PI3K/AKT signaling pathway; and p-p38 and p-JNK expression were upregulated in the MAPK signaling pathway. The levels of p-AKT and p-p38 expression were further increased in the PR8 + IGF1 group. The expression level in the PR8 + PPP group was between that of the PBS and PR8 + PBS groups. There was no significant difference in the level of p-JNK expression between the groups infected with influenza virus. The results indicated that the administration of IGF1 protein following influenza virus infection promoted the activation of the PI3K/AKT and MAPK signaling pathway. Intervention with the IGF1R inhibitor PPP inhibited influenza virus mediated PI3K/AKT and MAPK signaling pathways. These results suggest that IGF1 affected the expression of key proteins associated with MAPK and the PI3K/AKT signaling pathway in response to IAV-mediated inflammation.

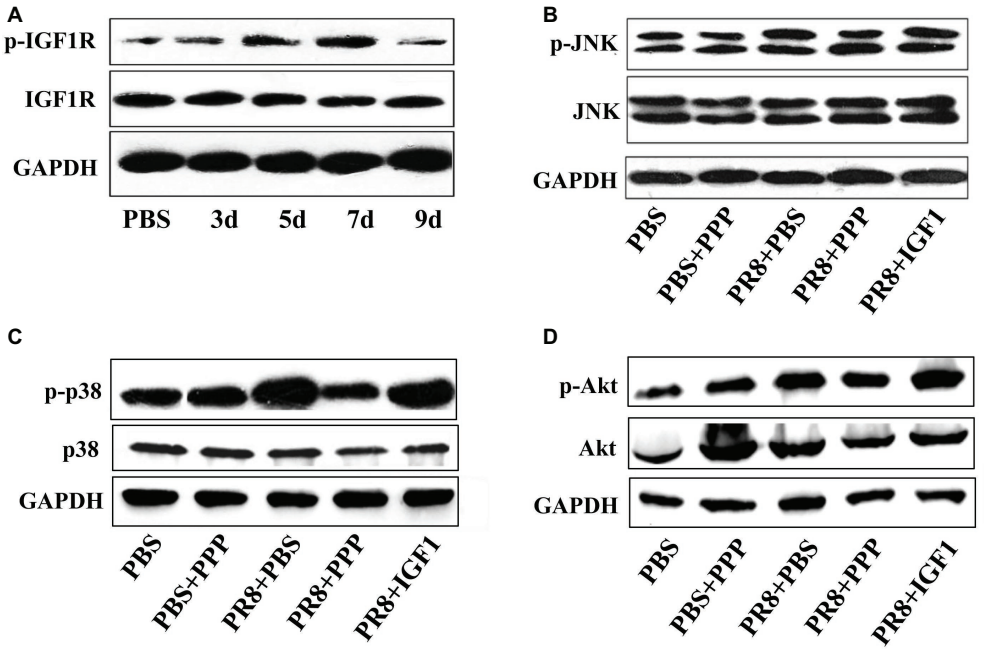

FIGURE 7 | Changes in the level of protein expression in the IGF1 signaling pathway. **(A)** Changes in the level of IGF1R and p-IGF1R protein over time in the lung tissue of BALB/c mice infected with PR8 ($50LD_{50}$); groups of BALB/c mice (n = 6, females, 6–8 weeks) were intranasally infected with PR8 ($50LD_{50}$) treated with IGF1 or PPP, and at day 5 post-infection, the mice lungs were examined for changes in **(B)** JNK and p-JNK protein, **(C)** p38 and p-p38 protein, and **(D)** Akt and p-Akt protein. The lung sample was mixed from six mice in the group. Figures were representative of three independent experiments.

DISCUSSION

In this study, we investigated that IGF1 played a significant role in mediating inflammation and pathology during IAV infection. IGF1 expression was upregulated in A549 cells and BALB/c mice infected with PR8, which modulated inflammatory cytokine expression. IGF1 overexpression aggravated influenza-mediated inflammatory responses, whereas the inhibition of IGF1 expression reduced such inflammatory responses. The phosphorylation of IGF1R triggered the PI3K/AKT and MAPK signaling pathways to induce inflammation. Thus, inhibiting IGF1 or IGF1R expression to block downstream signaling may be a novel treatment strategy for influenza infection.

Following an influenza virus infection, a series of immunological responses are initiated. First, the host's innate immune system, consisting of interferon, cytokines, macrophages, neutrophils, NK cells, and Dendritic cells (DCs), all rapidly respond to the viral infection and activate adaptive immunity (Gu et al., 2019). Although the innate immune response is important, the host typically eliminates the viral infection with the aid of the adaptive response (Bonilla and Oettgen, 2010). In humoral immunity, neutralizing antibodies can prevent the adsorption of the virus, *via* opsonization, and primarily interact with extracellular free viruses (Murasko et al., 2002). Activated Th1 cells release various cytokines (i.e., IFN-γ and TNF), activate macrophages and NK cells to induce further inflammatory reactions, and promote the proliferation and differentiation of cytotoxic T lymphocytes (CTLs), which play an important role in antiviral infection (Julkunen et al., 2001; Farsakoglu et al., 2019). However, studies have shown that while an inflammatory response helps to clear pathogens, excessive inflammatory reactions do not only protect the host organism but also cause the additional damage. Many studies have shown that the cause of death from an influenza virus infection is the pulmonary respiratory syndrome induced by inflammation caused by an excessive reaction of the body's immune system (Blach-Olszewska and Leszek, 2007).

In the present study, changes in the level of IGF1 mRNA and protein expression in A549 cells were detected. The results showed that IGF1 mRNA and protein expression were significantly altered following IAV infection. To further confirm the important role of IGF1 in IAV-mediated inflammation and the associated signaling mechanism, IGF1 protein was administered as an intervention to PR8-infected mice. Compared with the untreated infected mice, the infected mice administered IGF1 displayed more severe clinical symptoms; in particular, the serum levels of IFN-γ, TNF-α, and IL-1β were significantly increased, and lung damage was more serious. IGF1 is known to function by binding to the receptor, IGF1R. In this study, the IGF1R inhibitor PPP was used to inhibit IGF1R function, thereby disrupting its downstream signaling capacity. By monitoring the clinical symptoms and inflammation indicators in mice, it was found that during the same period of viral infection, when PPP was used to inhibit IGF1, the clinical symptoms of mice were alleviated; the lung injury area of the mice was reduced; the degree of lung injury was reduced; the lung index was significantly decreased; the serum levels of inflammatory cytokines IFN-γ, TNF-α, IL-1β, and IL-6 were

significantly decreased; and the survival rate increased from 25 to 75% compared with the untreated group. The viral proliferation in the lungs of mice treated with IGF1 was significantly increased; however, the viral proliferation of the mice treated with PPP was similar to that of the PR8 + PBS group. Thus, the inhibition of IGF1 only affects the immune response but has no significant effect on IAV replication. Thus, the inhibition of IGF1, rather than antiviral pathways that affect viral replication, may provide a new therapeutic avenue for influenza that limits detrimental inflammatory responses to infection. This is consistent with the previously reported effective treatments for influenza-mediated inflammation, which prolong the survival of older influenza-infected individuals, compared to those treated with antivirals (Pillai et al., 2016).

The inflammation-associated PI3K/AKT and MAPK signaling pathways are known to be activated in response to influenza virus infection (Dong et al., 2014; Hirata et al., 2014). Although IGF1 primarily regulates cell growth and apoptosis through the PI3K/AKT and MAPK signaling pathways, whether IGF1 plays a role in these pathways in the context of influenza virus-mediated inflammation remains unknown. In this study, a Western blot was used to detect the expression of key proteins in the PI3K/AKT and MAPK signaling pathways. The results showed that p-IGF1R was upregulated following PR8 infection; p-AKT expression was upregulated in the PI3K/AKT signaling pathway; and p-p38 and p-JNK expression were upregulated in the MAPK signaling pathway compared with the PBS group. The expression of p-AKT and p-p38 in the PR8 + IGF1 group was higher than that of the PR8 + PBS group, and the expression in the PR8 + PPP group was between that of the PBS and PR8 + PBS group. There was no significant difference in the level of p-JNK expression between the groups infected with influenza virus. This suggested that IGF1 affected the expression of key proteins associated with P38 in the MAPK and the PI3K/AKT signaling pathways in the context of influenza virus-mediated inflammation, which confirmed our hypothesis. Therefore, we conclude that IGF1 expression is upregulated following influenza virus infection, and IGF1 receptor phosphorylation is elevated, triggering two signaling pathways downstream of PI3K/AKT and MAPK to induce inflammation. Thus, the inhibition of IGF1 or IGF1R expression to block such downstream signaling pathways may represent a novel approach for the treatment of influenza virus infection.

DATA AVAILABILITY STATEMENT

The data used to support the findings of this study are available from the corresponding author upon request.

ETHICS STATEMENT

The animal study was reviewed and approved by Academy of Military Medical Sciences (AMMS; ID: SYXK2012-05).

AUTHOR CONTRIBUTIONS

ChZ and GL contributed to conceptualization. ChZ, GL, and LZ contributed to methodology. LZ, CaZ, and YS contributed to investigation. RW and ChZ contributed to writing the original draft. RW and ChZ contributed to writing, reviewing, and editing. ChZ contributed to funding acquisition. LZ, DD, and MB contributed to resources. RW, GL, and ChZ helped in supervision.

FUNDING

This work was supported by the National High-tech Research and Development Program (863; 2014AA020516) and the China Mega-Project on Infectious Disease Prevention (2018ZX10713-003).

ACKNOWLEDGMENTS

The authors thank Prof. Shihui Sun (Beijing Institute of Microbiology and Epidemiology) for kindly providing the IAV A/Puerto Rico/8/1934 (H1N1).

REFERENCES

Aikawa, N. E., Campos, L. M., Silva, C. A., Carvalho, J. F., Saad, C. G., Trudes, G., et al. (2012). Glucocorticoid: major factor for reduced immunogenicity of 2009 influenza A (H1N1) vaccine in patients with juvenile autoimmune rheumatic disease. *J. Rheumatol.* 39, 167–173. doi: 10.3899/jrheum.110721

Allen, I. C., Scull, M. A., Moore, C. B., Holl, E. K., Mcelvania-Tekippe, E., Taxman, D. J., et al. (2009). The NLRP3 inflammasome mediates in vivo innate immunity to influenza A virus through recognition of viral RNA. *Immunity* 30, 556–565. doi: 10.1016/j.immuni.2009.02.005

Arroba, A. I., Rodriguez-De La Rosa, L., Murillo-Cuesta, S., Vaquero-Villanueva, L., Hurle, J. M., Varela-Nieto, I., et al. (2016). Autophagy resolves early retinal inflammation in Igf1-deficient mice. *Dis. Model. Mech.* 9, 965–974. doi: 10.1242/dmm.026344

Basler, C. F., and Aguilar, P. V. (2008). Progress in identifying virulence determinants of the 1918 H1N1 and the southeast Asian H5N1 influenza A viruses. *Antivir. Res.* 79, 166–178. doi: 10.1016/j.antiviral.2008.04.006

Blach-Olszewska, Z., and Leszek, J. (2007). Mechanisms of over-activated innate immune system regulation in autoimmune and neurodegenerative disorders. *Neuropsychiatr. Dis. Treat.* 3, 365–372.

Bonilla, F. A., and Oettgen, H. C. (2010). Adaptive immunity. *J. Allergy Clin. Immunol.* 125, S33–S40. doi: 10.1016/j.jaci.2009.09.017

Cohen, D. H., and Leroith, D. (2012). Obesity, type 2 diabetes, and cancer: the insulin and IGF connection. *Endocr. Relat. Cancer* 19, F27–F45. doi: 10.1530/ERC-11-0374

Dong, W., Wei, X., Zhang, F., Hao, J., Huang, F., Zhang, C., et al. (2014). A dual character of flavonoids in influenza A virus replication and spread through modulating cell-autonomous immunity by MAPK signaling pathways. *Sci. Rep.* 4:7237. doi: 10.1038/srep07237

Egan, S. E., Giddings, B. W., Brooks, M. W., Buday, L., Sizeland, A. M., and Weinberg, R. A. (1993). Association of Sos Ras exchange protein with Grb2 is implicated in tyrosine kinase signal transduction and transformation. *Nature* 363, 45–51.

Farsakoglu, Y., Palomino-Segura, M., Latino, I., Zanaga, S., Chatziandreou, N., Pizzagalli, D. U., et al. (2019). Influenza vaccination induces NK-cell-mediated

type-II IFN response that regulates humoral immunity in an IL-6-dependent manner. *Cell Rep.* 26, 2307–2315.e2305. doi: 10.1016/j.celrep.2019.01.104

Ge, D., Dauchy, R. T., Liu, S., Zhang, Q., Mao, L., Dauchy, E. M., et al. (2013). Insulin and IGF1 enhance IL-17-induced chemokine expression through a GSK3B-dependent mechanism: a new target for melatonin's anti-inflammatory action. *J. Pineal Res.* 55, 377–387. doi: 10.1111/jpi.12084

Granata, R., Trovato, L., Garbarino, G., Taliano, M., Ponti, R., Sala, G., et al. (2004). Dual effects of IGFBP-3 on endothelial cell apoptosis and survival: involvement of the sphingolipid signaling pathways. *FASEB J.* 18, 1456–1458. doi: 10.1096/fj.04-1618fje

Gu, Y., Hsu, A. C., Pang, Z., Pan, H., Zuo, X., Wang, G., et al. (2019). Role of the innate cytokine storm induced by the influenza A virus. *Viral Immunol.* 32, 244–251. doi: 10.1089/vim.2019.0032

Hirata, N., Suizu, F., Matsuda-Lennikov, M., Edamura, T., Bala, J., and Noguchi, M. (2014). Inhibition of Akt kinase activity suppresses entry and replication of influenza virus. *Biochem. Biophys. Res. Commun.* 450, 891–898. doi: 10.1016/j.bbrc.2014.06.077

Hoshino, M., Nakamura, Y., Sim, J. J., Yamashiro, Y., Uchida, K., Hosaka, K., et al. (1998). Inhaled corticosteroid reduced lamina reticularis of the basement membrane by modulation of insulin-like growth factor (IGF)-I expression in bronchial asthma. *Clin. Exp. Allergy* 28, 568–577.

Hubbard, S. R. (1997). Crystal structure of the activated insulin receptor tyrosine kinase in complex with peptide substrate and ATP analog. *EMBO J.* 16, 5572–5581.

Imai, Y., Kuba, K., Rao, S., Huan, Y., Guo, F., Guan, B., et al. (2005). Angiotensin-converting enzyme 2 protects from severe acute lung failure. *Nature* 436, 112–116. doi: 10.1038/nature03712

Jewell, N. A., Cline, T., Mertz, S. E., Smirnov, S. V., Flano, E., Schindler, C., et al. (2010). Lambda interferon is the predominant interferon induced by influenza A virus infection in vivo. *J. Virol.* 84, 11515–11522. doi: 10.1128/JVI.01703-09

Jogie-Brahim, S., Feldman, D., and Oh, Y. (2009). Unraveling insulin-like growth factor binding protein-3 actions in human disease. *Endocr. Rev.* 30, 417–437. doi: 10.1210/er.2008-0028

Johannesson, B., Sattler, S., Semenova, E., Pastore, S., Kennedy-Lydon, T. M., Sampson, R. D., et al. (2014). Insulin-like growth factor-1 induces regulatory T cell-mediated suppression of allergic contact dermatitis in mice. *Dis. Model. Mech.* 7, 977–985. doi: 10.1242/dmm.015362

Julkunen, I., Sareneva, T., Pirhonen, J., Ronni, T., Melen, K., and Matikainen, S. (2001). Molecular pathogenesis of influenza A virus infection and virus-induced regulation of cytokine gene expression. *Cytokine Growth Factor Rev.* 12, 171–180. doi: 10.1016/s1359-6101(00)00026-5

Kobasa, D., Jones, S. M., Shinya, K., Kash, J. C., Copps, J., Ebihara, H., et al. (2007). Aberrant innate immune response in lethal infection of macaques with the 1918 influenza virus. *Nature* 445, 319–323. doi: 10.1038/nature05495

Lee, H., Kim, S. R., Oh, Y., Cho, S. H., Schleimer, R. P., and Lee, Y. C. (2014). Targeting insulin-like growth factor-I and insulin-like growth factor-binding protein-3 signaling pathways. A novel therapeutic approach for asthma. *Am. J. Respir. Cell Mol. Biol.* 50, 667–677. doi: 10.1165/rcmb.2013-0397TR

Li, H., and Cao, B. (2017). Pandemic and avian influenza A viruses in humans: epidemiology, virology, clinical characteristics, and treatment strategy. *Clin. Chest Med.* 38, 59–70. doi: 10.1016/j.ccm.2016.11.005

Murasko, D. M., Bernstein, E. D., Gardner, E. M., Gross, P., Munk, G., Dran, S., et al. (2002). Role of humoral and cell-mediated immunity in protection from influenza disease after immunization of healthy elderly. *Exp. Gerontol.* 37, 427–439. doi: 10.1016/s0531-5565(01)00210-8

Myers, M. G. Jr., Backer, J. M., Sun, X. J., Shoelson, S., Hu, P., Schlessinger, J., et al. (1992). IRS-1 activates phosphatidylinositol 3′-kinase by associating with src homology 2 domains of p85. *Proc. Natl. Acad. Sci. USA* 89, 10350–10354.

Nicholls, J., and Peiris, M. (2005). Good ACE, bad ACE do battle in lung injury, SARS. *Nat. Med.* 11, 821–822. doi: 10.1038/nm0805-821

Ocana-Macchi, M., Bel, M., Guzylack-Piriou, L., Ruggli, N., Liniger, M., McCullough, K. C., et al. (2009). Hemagglutinin-dependent tropism of H5N1 avian influenza virus for human endothelial cells. *J. Virol.* 83, 12947–12955. doi: 10.1128/JVI.00468-09

Oda, T., Akaike, T., Hamamoto, T., Suzuki, F., Hirano, T., and Maeda, H. (1989). Oxygen radicals in influenza-induced pathogenesis and treatment with pyran polymer-conjugated SOD. *Science* 244, 974–976.

Onnureddy, K., Ravinder Onteru, S. K., and Singh, D. (2015). IGF-1 attenuates LPS induced pro-inflammatory cytokines expression in buffalo (*Bubalus bubalis*) granulosa cells. *Mol. Immunol.* 64, 136–143. doi: 10.1016/j.molimm.2014.11.008

Pillai, P. S., Molony, R. D., Martinod, K., Dong, H., Pang, I. K., Tal, M. C., et al. (2016). Mx1 reveals innate pathways to antiviral resistance and lethal influenza disease. *Science* 352, 463–466. doi: 10.1126/science.aaf3926

Reed, L. J., and Muench, H. (1938). A simple method of estimating fifty percent endpoints. *Am. J. Epidemiol.* 27, 493–497.

Siddle, K., Urso, B., Niesler, C. A., Cope, D. L., Molina, L., Surinya, K. H., et al. (2001). Specificity in ligand binding and intracellular signalling by insulin and insulin-like growth factor receptors. *Biochem. Soc. Trans.* 29, 513–525. doi: 10.1042/bst0290513

Stewart, C. E., and Rotwein, P. (1996). Growth, differentiation, and survival: multiple physiological functions for insulin-like growth factors. *Physiol. Rev.* 76, 1005–1026.

Taubenberger, J. K., and Morens, D. M. (2006). 1918 influenza: the mother of all pandemics. *Emerg. Infect. Dis.* 12, 15–22. doi: 10.3201/eid1201.050979

Wilden, P. A., Kahn, C. R., Siddle, K., and White, M. F. (1992). Insulin receptor kinase domain autophosphorylation regulates receptor enzymatic function. *J. Biol. Chem.* 267, 16660–16668.

Xagorari, A., and Chlichlia, K. (2008). Toll-like receptors and viruses: induction of innate antiviral immune responses. *Open Microbiol. J.* 2, 49–59. doi: 10.2174/1874285800802010049

Conflict of Interest: The authors declare that the research was conducted in the absence of any commercial or financial relationships that could be construed as a potential conflict of interest.

Copyright © 2019 Li, Zhou, Zhang, Shi, Dong, Bai, Wang and Zhang. This is an open-access article distributed under the terms of the Creative Commons Attribution License (CC BY). The use, distribution or reproduction in other forums is permitted, provided the original author(s) and the copyright owner(s) are credited and that the original publication in this journal is cited, in accordance with accepted academic practice. No use, distribution or reproduction is permitted which does not comply with these terms.

frontiers in Microbiology

ORIGINAL RESEARCH
published: 03 December 2019
doi: 10.3389/fmicb.2019.02765

Estimating Transmission Potential of H5N1 Viruses Among Humans in Egypt Using Phylogeny, Genetic Distance and Sampling Time Interval

*Wessam Mohamed, Kimihito Ito and Ryosuke Omori**

Division of Bioinformatics, Research Center for Zoonosis Control, Hokkaido University, Sapporo, Japan

In 2014 and 2015, the number of human cases of H5N1 avian influenza virus infections had increased dramatically in Egypt. This increase might be related to increase in the transmission potential of the virus among humans. To clarify the cause of the increase in H5N1 human cases, we investigate the transmissibility of H5N1 viruses among humans via estimating the basic reproduction number R_0 using nucleotide sequences and sampling dates of viruses. To this end, full-length hemagglutinin gene sequences of human and avian H5N1 influenza viruses isolated from 2006 to 2016 in Egypt were obtained from the NCBI influenza virus resource. Taking into account the phylogeny, genetic distance, sampling time difference among viruses, R_0 was estimated to be 0.05 (95% CI: 0.01, 0.13) assuming that human-to-human transmissions occurred within a city, 0.23(95% CI: 0.14, 0.35) assuming human-to-human transmissions among cities. Our results indicate that human-to-human transmission of H5N1 viruses in Egypt is limited, and the large increase in human cases is likely attributed to other factor than increase in human-to-human transmission potential.

Keywords: avian influenza, Egypt, H5N1, human-to-human transmission, R_0, statistical model

OPEN ACCESS

Edited by:
Ahmed Sayed Abdel-Moneim, Taif University, Saudi Arabia

Reviewed by:
Daniela Rajao, University of Georgia, United States
Gloria Consuelo Ramirez-Nieto, Universidad Nacional de Colombia, Colombia

***Correspondence:**
Ryosuke Omori
omori@czc.hokudai.ac.jp

Specialty section:
This article was submitted to Virology, a section of the journal Frontiers in Microbiology

Received: *06 August 2019*
Accepted: *13 November 2019*
Published: *03 December 2019*

Citation:
Mohamed W, Ito K and Omori R (2019) Estimating Transmission Potential of H5N1 Viruses Among Humans in Egypt Using Phylogeny, Genetic Distance and Sampling Time Interval. Front. Microbiol. 10:2765. doi: 10.3389/fmicb.2019.02765

INTRODUCTION

The H5N1 avian influenza virus is of great concern to the public health in the world. According to the World Health Organization (WHO), more than 860 human cases have been clinically diagnosed as H5N1 infections in 17 countries by the 24th of June 2019 (World Health Organization [WHO], 2019). In 2009, the World Organisation for Animal Health (OIE) reported that H5N1 viruses became enzootic in poultry populations in Bangladesh, Cambodia, China, Egypt, India, Indonesia, Laos, Nepal and Vietnam (Tarantola et al., 2010). H5N1 viruses have occasionally transmitted to humans and caused severe respiratory disorders leading to death (Yuen et al., 1998). Previous studies have shown that H5N1 can acquire the ability to transmit in ferrets (Herfst et al., 2012; Imai et al., 2012). Although the human-to-human transmission of the virus is limited, family case clusters of H5N1 infections were reported from Sumatra (Yang et al., 2007), Cambodia (Chea et al., 2014), Thailand (Ungchusak et al., 2005), China (Wang et al., 2008), and Pakistan (World Health Organization [WHO], 2008).

H5N1 influenza viruses were first identified in Egypt among poultry in 2006 (Aly et al., 2008) and declared to be enzootic in 2008 (Kayali et al., 2016). The number of human cases in Egypt has been increasing dramatically since 2014 (Refaey et al., 2015). Two-thirds of the human cases reported in the world by 2019 were from Egypt (World Health Organization [WHO], 2019). The increase in 2014 might be either related to increase in the transmission potential of the H5N1 virus among

human populations or other factors. Furthermore, Arafa A. S. et al. (2016) found that some H5N1 viruses isolated in Egypt during 2014–2015 had the ability to be transmitted via respiratory droplets between ferrets, although the transmission efficiency of these H5N1 viruses in ferrets may be very low. However, in the slight possibility that H5N1 viruses may acquire airborne transmission in a natural environment, the identification of the transmission potential of H5N1 viruses in humans is crucial to improve the control measures that can be used to contain virus spread in Egypt.

One way to estimate the transmissibility of infectious diseases is by measuring the basic reproduction number (R_0), which is defined as the average number of secondary cases originating from a primary infected case in a whole susceptible population (Vynnycky, 2010). To estimate R_0 of avian virus infections in a human population, the number of human cases and/or cases with history of bird contact are frequently used (Nishiura et al., 2013). However, the data on contact with poultry may not be accurate, because data are biased by the recall bias or missing data. Lack of epidemiological data is an obstacle for the estimation of R_0 of avian virus infections in a human population.

Recently, various types of epidemiological information have been used to estimate R_0. Chong et al. used travel data, i.e., arrival times of infected cases in different countries (Chong et al., 2017). Farrington et al. used age-stratified serological survey data to estimate R_0 of hepatitis A, mumps, rubella, parvovirus, *Haemophilus influenzae*, and measles infection (Farrington and Kanaan, 2001). On the other hand, Pybus et al. (2001) developed a method to estimate R_0 of an infectious disease using nucleotide sequences of pathogens, showing nucleotide sequences have the ability to infer the magnitude of infectious diseases transmission.

In this study, we assess the transmission potential of H5N1 viruses among humans in Egypt. We measure transmission potential by R_0 estimated from nucleotide sequences, sampling time, and sampling location of H5N1 viruses isolated in Egypt during 2006–2016.

MATERIALS AND METHODS

Sequence Data

Nucleotide sequences of the hemagglutinin (HA) gene of H5N1 influenza viruses isolated from humans and birds in Egypt were downloaded from the NCBI Influenza Virus Database (Bao et al., 2008). We selected full-length and nearly full-length HA sequences in the database, and nucleotide sequences of HA of 73 human isolates and 531 avian isolates from 2006 to 2016 were obtained. For each nucleotide sequence we recorded the city and the date where and when its virus was sampled. Thirteen human sequences that lacked sampling date information were excluded from subsequent analyses. The GenBank accession numbers, strain names, sampling dates, and sampling locations of nucleotide sequences used in this study can be found in the **Supplementary Table S1**. For the clustering analysis described below, *p*-distance (Nei and Kumar, 2000) among all pairs of sequences were calculated. For each city where viruses were sampled, the latitude and longitude of the city were obtained from Egypt Cities Database in Simplemaps.Com (2019). Then, geographical distances between cities were calculated using the "geosphere" library in R software.

Phylogenetic Analysis

To visualize evolutionary relationships among Egyptian H5N1 viruses isolated from birds and humans, a phylogenetic tree was constructed using HA sequences of avian and human isolates. We used the maximum composite likelihood with general time reversible substitution model in MEGA software version 6.06 (Tamura et al., 2013) to construct the phylogenetic tree. The genetic distance between two viruses are depicted to be proportional to the summation of horizontal distances of branches connecting them. Clade information of H5N1 viruses are shown using different colors. Human viruses are emphasized by marks.

Detection of Human Case Clusters in Phylogenetic Tree

To find possible human-to-human transmissions, we first identified clusters of human isolates in the phylogenetic tree. Clusters of human isolates were identified as follows. Each human isolate is considered to belong to a cluster. There may be a cluster with a single virus, and we call such a cluster a singleton cluster. Two human isolates are considered to belong to the same cluster if they are connecting with one or two internal nodes in the phylogenetic tree. Applying this criterion for all pairs of human isolates, we get clusters of human isolates.

Estimation of Human-to-Human Transmission Potential

To estimate the number of human-to-human transmission events in an infection chain, we employ a mathematical model describing human-to-human transmission. We hypothesized all human index cases of H5N1 viruses are avian-to-human transmission. Let n be the number of avian-to-human transmissions and S be the total number of human cases. For an infectious chain i, which starts from an individual infected from a bird and ends with a person who has not transmitted virus to another person, let x_i denote the number of individuals in the infectious chain i. We assume the probability of observing the "i"-th chains with length x_i follows a geometric distribution with the "success" probability p, which is considered as the probability of a human-to-human transmission. The likelihood function L of human-to-human transmission probability p can be written as follow:

$$L\left(p; x_1, \ldots, x_n\right) = \prod_{i=1}^{n} p^{x_i - 1}\left(1 - p\right).$$

Since, the summation of x_i over i is equal to the total number of human cases S, the maximum likelihood estimate of p is given by,

$$\hat{p} = \frac{\sum_{i=1}^{n} x_i - n}{\sum_{i=1}^{n} x_i} = 1 - \frac{n}{S}.$$

R_0 is the expected number of secondary cases from single case in the entire susceptible population. Assuming that R_0 is smaller

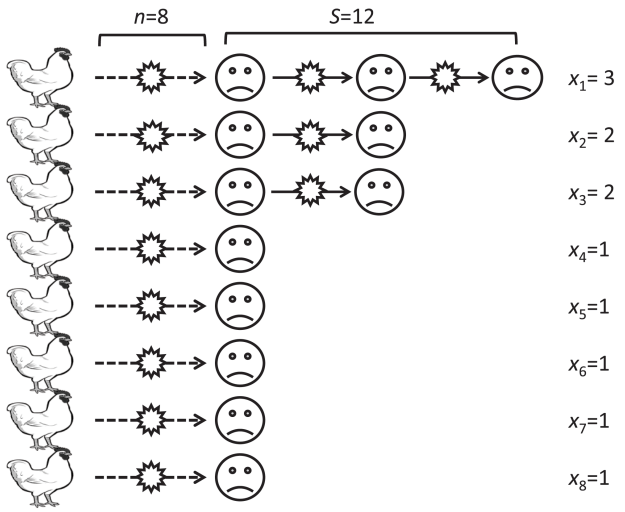

FIGURE 1 | An illustrative example of infection chains in our model. A virus transmits from a bird to a human (broken lines) then transmits from a human to another human and so on (solid lines). The x_i represent the length of the ith transmission chain.

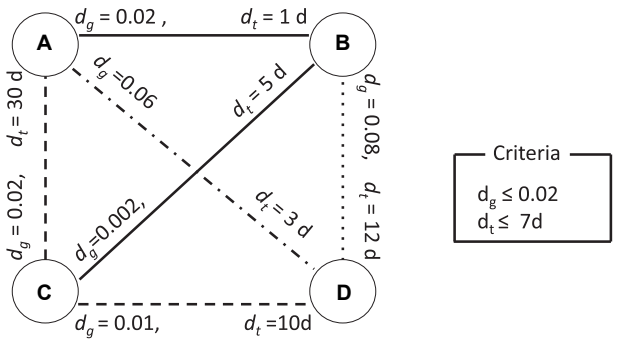

FIGURE 2 | An illustrative example of clustering analysis using two criteria. The nodes A, B, C, and D represent viruses isolated from humans. The d_g on each edge connecting two nodes represents the genetic distance between corresponding viruses. The d_t on each edge represents the sampling time interval between the corresponding viruses. This example uses 0.02 as clustering threshold for genetic distance and 7 days for sampling time interval. A solid line represents a pair of viruses satisfying both criteria. A dashed line represents a pair of viruses satisfying only the criteria for genetic distance. A dash-dot line represents a pair of viruses satisfying only the criteria for sampling time interval. A dotted line represents a pair of viruses which does not satisfy with any of the criteria.

than or equal to 1, the representative value for the estimate of R_0 can be given by,

$$R_0 = \hat{p} = 1 - \frac{n}{S}.$$

Figure 1 illustrates an example of infection chains. In this example, the number of avian to human transmissions, n, is eight. The length of infection chains started from these avian-to-human transmissions are three, two, two, one, one, one, one, and one, and the total number of human cases, S, is 12. The R_0 for this example is calculated to be 1–8/12 = 0.33.

We calculate the confidence interval (CI) for the R_0 estimate using a likelihood ratio test. The critical value of R_0 in our analysis is 1.0, because no major epidemic will occur when R_0 is smaller than 1.0. Our method can applicable only for infections in sporadic outbreaks and cannot be used for infections in an endemic situation, since the length of transmission chain is assumed follow the geometric distribution. All the analysis was done using the statistical software R, and its R codes are available in **Supplementary Data Sheet S1**. The detailed process of statistical analysis is described in **Supplementary Data Sheet S2**.

Clustering Analysis Using Genetic Distance, Sampling Time Interval, and Geographical Distance

Possible human-to-human transmissions were identified using criteria of genetic distance, sampling time interval, and geographical distance. **Figure 2** illustrates how our clustering algorithm works with genetic distance and sampling time interval. In this example, we have four viruses isolated from humans. The d_g on edges connecting two viruses represents the genetic distance between corresponding viruses. The d_t on edges represents the sampling time interval between the corresponding viruses. If we set genetic distance threshold to 0.02 and use only genetic distance as a criterion, then edges A–B, A–C, B–C, and C–D satisfy the criterion and A, B, C, and D are considered as a single cluster. The clustered sequences were sorted by their sampling time and transmission chains were reconstructed. We consider adjacent pairs in the transmission chain as candidate transmission pairs. In this case, we have 4 human cases and one transmission chain and R_0 is calculated to be 1–1/4 = 0.75. If we set the sampling time interval threshold to 7 days and use sampling time as another criterion in addition to the genetic distance criterion, then A–B and B–C satisfy these two criteria, grouping A, B, and C to the same cluster and making D to be a singleton cluster. Then R_0 is calculated to be 1–2/4 = 0.5. We can extend this to work with geographical distance in the same manner.

Sensitivity Analysis

To assess the robustness of the R_0 estimate, we conducted sensitivity analyses with respect to combinations of threshold values for the genetic distance, sampling time interval, and geographical distance. First, we varied genetic distance from 0 to 0.01 and calculated R_0 and its 95% CIs. The 95% CI was calculated using the likelihood ratio test method. To obtain the distribution of sampling time interval and geographical distance between candidate transmission pairs, we used a fixed threshold for genetic distance between human viruses at a p-distance of 0.004488. This p-distance value is the between-households genetic variation, which is calculated by adding the mean value of between-households genetic distance and 1.96 times its standard deviation according to a previous study (Thai et al., 2014). Sequences in the clusters identified by phylogenetic analysis were also analyzed in the same manner.

To investigate the effect of sampling time interval threshold on the R_0 estimate, we fixed the genetic distance threshold

at the between-households genetic variation and varied the sampling time threshold from 0 to 60 days, which is a sufficient time for the infectious period of human influenza. For the sensitivity analysis using geographical distance, we fixed the genetic distance threshold at the between-households genetic variation and varied the geographical distance threshold from 0 to 700 km, which is the maximum distance within human clusters identified from genetic distance. We also conducted sensitivity analyses of sequences in the clusters identified by phylogenetic analysis in the same manner.

Estimation of R_0 From Phylogeny, Genetic Distance, Sampling Time Interval, and Geographical Distance

To obtain representative estimates of R_0, we set threshold values of genetic distance, sampling time interval, and geographical distance. The threshold of genetic distance was set to 0.004488, which is the genetic distance observed in the between-household transmissions of H1N1 viruses (Thai et al., 2014). Threshold of sampling time interval was set to 30 days, which is the maximum value of the first cluster in the histogram of sampling time intervals. Since maximum duration of viral shedding is around 20 days (Loeb et al., 2012; Ng et al., 2016), the thresh hold of 30 days is an enough period to capture human-to-human transmissions. If it is assumed that human-to-human transmissions occurred only within household, we set the geographical distance threshold was 0 km (within a city), which is the geographical distance between the same city.

RESULTS

Phylogenetic Analysis

A phylogenetic tree was constructed from HA sequences of avian and human viruses isolated in Egypt from 2006 to 2016 (**Figure 3**). The phylogenetic tree has four major clades of clade 2.2, 2.2.1, 2.2.1.1, and 2.2.1.2 (Arafa A. et al., 2016). The 60 human sequences (cross and diamond marks) were distributed on subtrees of clade 2.2 (blue), 2.2.1 (red), and 2.2.1.2 (light blue) while clade 2.2.1.1 (green) did not contain human isolates, indicating that most avian-to-human transmissions were attributed to the avian viruses of clade 2.2, 2.2.1, and 2.2.1.2. From 60 sequences of human isolates, a total of 26 human clusters were found from connecting patterns of human sequences in the phylogenetic tree. Of these clusters, 12 were singleton clusters (diamonds) and 14 have more than one human sequence. These 14 clusters (cross marks) are candidates of possible human-to-human transmissions. The clade 2.2.1 has 9 candidate clusters of human-to-human transmissions, clade 2.2.1.2 has 4, and clade 2.2 has 1. Clade 2.2.1.1 has no candidate clusters for human-to-human transmissions. In total, 34 human-to-human transmission events were suggested from the phylogenetic tree. R_0 was estimated to be 1–26/60 = 0.57 with its 95% CI from 0.44 to 0.69.

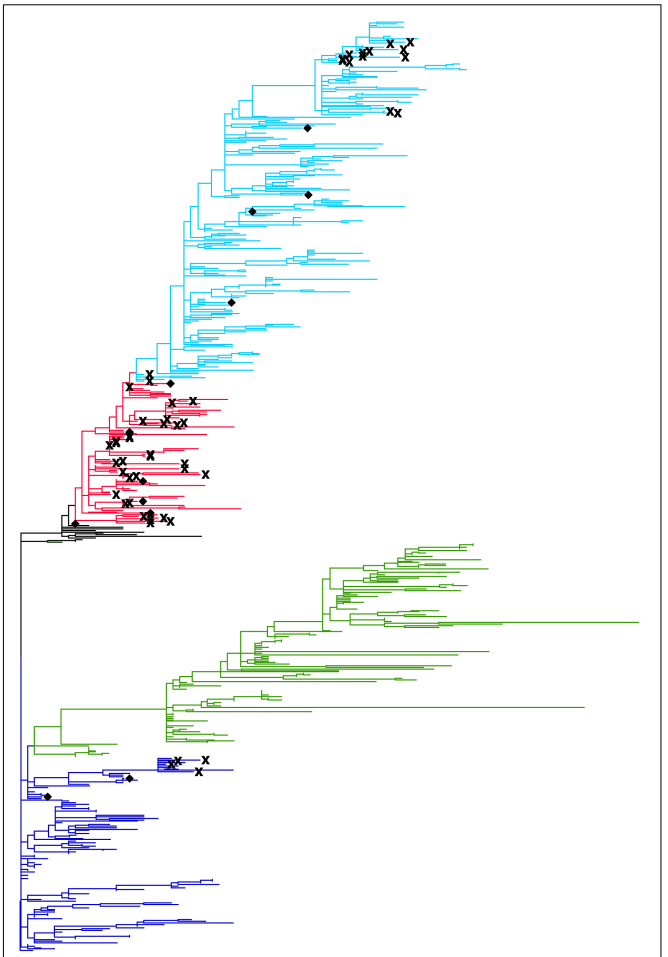

FIGURE 3 | Phylogenetic tree of the HA gene of H5N1 avian influenza A viruses isolated in Egypt. The tree was constructed with the maximum composite likelihood with general time reversible substitution model in MEGA software version 6.06. Tips of the tree represent reported viral sequences. The genetic distance between two viruses are depicted to be proportional to the summation of horizontal distances of branches connecting them. Human viruses are emphasized by marks; human viruses identified in a human cluster containing more than one human isolate were represented by cross marks. Human viruses in a singleton cluster were represented by diamonds. Clade information of H5N1 viruses are shown using different colors; clade 2.2 are shown in blue, clade 2.2.1.1 in green, clade 2.2.1 in red, and clade 2.2.1.2 in light blue.

Estimation of R_0 From Genetic Distance

Human isolates were clustered by genetic distances, and R_0 and its CI were calculated from the clustering results. **Figure 4** shows the sensitivity of R_0 estimate with respect to genetic distance. In **Figure 4A**, clusters were identified using only genetic distances among human viruses without using the phylogenetic tree. R_0 was estimated to be 0.00 with its 95% CI from 0.00 to 0.032 when the genetic distance threshold was 0.00. R_0 increased as the genetic distance threshold increased, and R_0 was estimated to be 0.883 with its 95% CI from 0.79 to 0.95 when the genetic distance threshold was 0.01. R_0 was estimated to be 0.55 with its 95% CI from 0.42 to 0.67

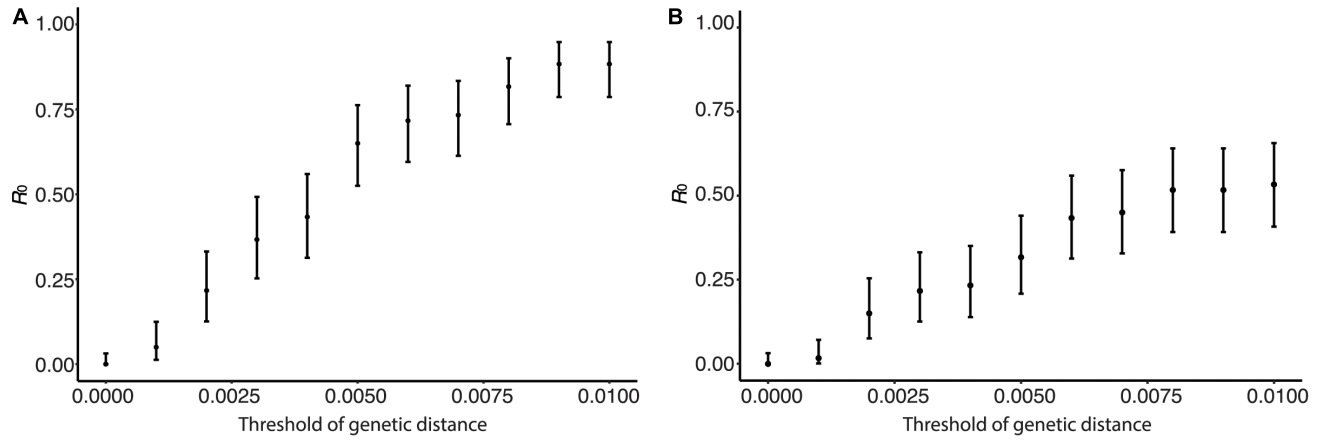

FIGURE 4 | Effect of genetic distance threshold on the estimate of R_0 using genetic distance. **(A)** Human viruses were clustered by genetic distances. **(B)** Human viruses were clustered by phylogeny and genetic distances.

when the genetic distance threshold was 0.004488, which is the between-household genetic variation. In **Figure 4B**, clusters were identified using phylogenetic tree of human and avian viruses and genetic distances among viruses clustered together. R_0 was estimated to be 0.30 with its 95% CI from 0.19 to 0.42 when the genetic distance threshold was the between-household genetic variation. R_0 was estimated to be 0.53 with its 95% CI from 0.41 to 0.66 when the genetic distance threshold was 0.01.

Distribution of Sampling Time Interval and Geographical Distance Among Human Viruses

To determine the range of parameter values in the sensitivity analysis of R_0 estimate, we analyzed the distribution of the parameters. The distribution of sampling time intervals and geographical distances among candidate transmission pairs were obtained by fixing the threshold for genetic distance between human viruses at the between-households genetic variation (**Figure 5**). **Figure 5A** shows histogram of time intervals among candidate transmission pairs in the cluster obtained using the between-households genetic distance among human sequences. **Figure 5B** uses phylogeny and the between-households genetic distance to obtain clusters of human sequences. The time intervals of candidate transmission pairs range from 0 to 149 days in clusters identified using genetic distance and from 1 to 170 days in clusters identified using phylogeny and genetic distance. **Figure 5C** shows histogram of geographical distances among candidate transmission pairs in the cluster obtained using the between-households genetic distance. **Figure 5D** uses phylogeny and the between-households genetic distance to obtain clusters of human sequences. The geographical distances of candidate transmission pairs ranges from 0 to 682.2 km in clusters identified using genetic distance and ranges from 0 to 383.3 km in clusters identified using phylogeny and genetic distance.

Estimation of R_0 From Genetic Distance and Sampling Time Interval

Human viruses were clustered by genetic distances and sampling time interval, and R_0 and its CI were calculated from the clustering results. **Figure 6** shows sensitivity of R_0 estimate with respect to sampling time interval threshold when genetic distance threshold was fixed at the between-household distance. **Figure 6A** uses genetic distances and sampling time intervals, and **Figure 6B** uses phylogeny and genetic distances and sampling time interval among human sequence clusters. R_0 was estimated to be 0.55 (95% CI: 0.42, 0.67) without phylogeny and 0.30 (95% CI: 0.19, 0.42) with phylogeny when the sampling time interval threshold was 220 days, and these values decreased as sampling time interval threshold decreased. R_0 was estimated to be 0.42 (95% CI: 0.30, 0.54) without phylogeny and 0.23 (95% CI: 0.14, 0.35) with phylogeny when the sampling time interval threshold was 30 days, which is the upper bound of sampling time interval between-household transmissions (Loeb et al., 2012; Ng et al., 2016).

Estimation of R_0 From Genetic Distance and Geographical Distance

Human viruses were clustered by genetic distances and geographical distances, and R_0 and its CI were calculated from the clustering results. **Figure 7** shows sensitivity of R_0 estimate with respect to geographical distance threshold when genetic distance threshold was fixed at the between-household distance. **Figure 7A** uses genetic and geographical distances, and **Figure 7B** uses phylogeny and genetic distances and geographical distances among human sequence clusters. R_0 was estimated to be 0.55 (95% CI: 0.42, 0.67) without phylogeny and 0.30 (95% CI: 0.19, 0.42) with phylogeny when the geographical distance threshold was 700 km, and these values decreased as geographical distance threshold decreased. R_0 was estimated to be 0.15 (95% CI: 0.0751, 0.254) without phylogeny and 0.1

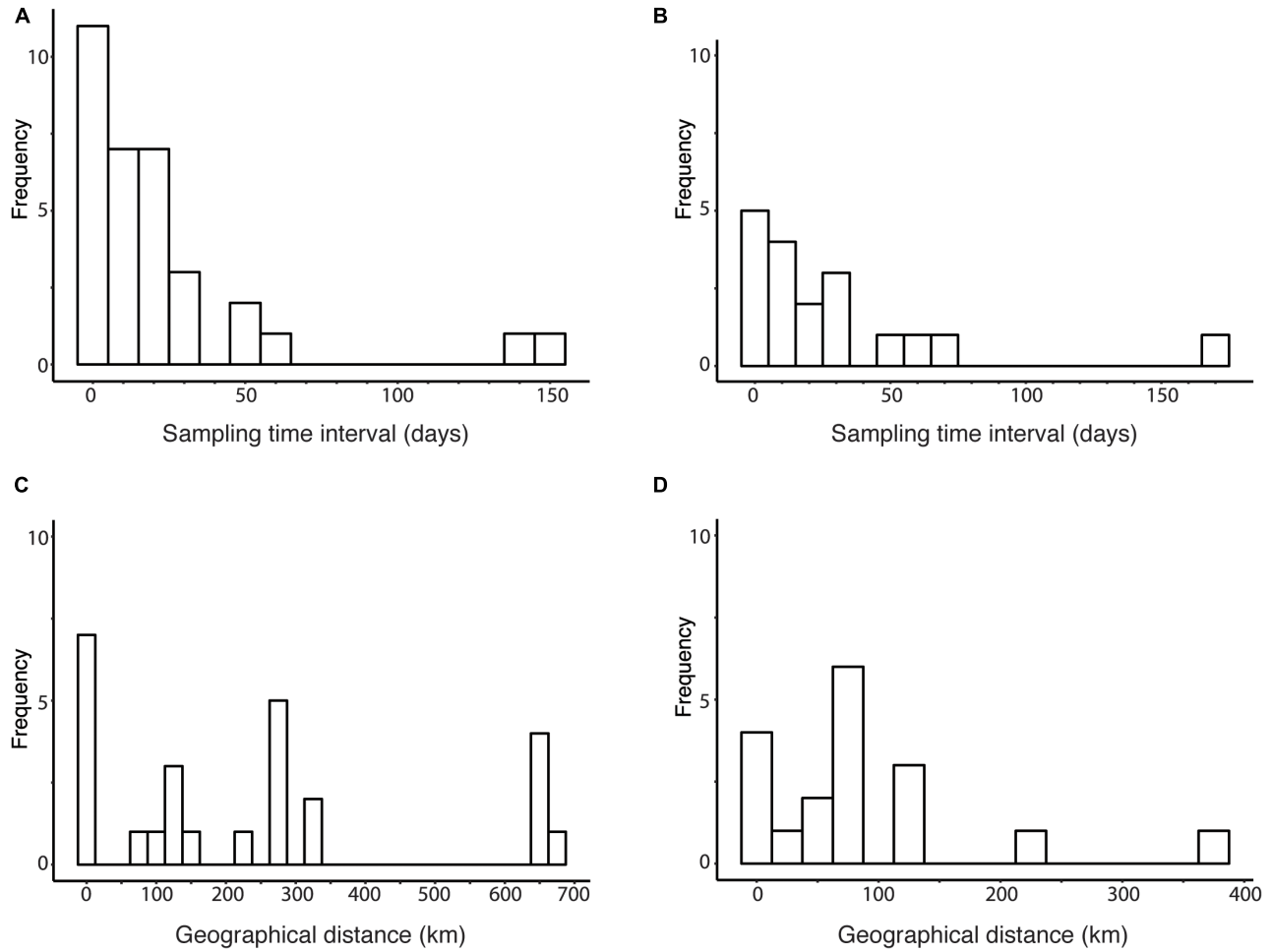

FIGURE 5 | Distribution of sampling time interval and geographical distance among human viruses. **(A)** Histogram of sampling time intervals between human viruses clustered by genetic distances threshold at the between-household genetic variation. **(B)** Histogram of sampling time intervals between human viruses clustered by phylogeny and genetic distances threshold at the between-household genetic variation. **(C)** Histogram of geographical distances between human viruses clustered by genetic distances threshold at the between-household genetic variation. **(D)** Histogram of geographical distances between human viruses clustered by phylogeny and genetic distances threshold at the between-household genetic variation.

(95% CI: 0.041, 0.1923) with phylogeny when the geographical distance threshold was 0 km, which is the geographical distance between the same city.

Estimation of R_0 From Genetic Distance, Sampling Time Interval, and Geographical Distance

Using genetic distance threshold of 0.004488 and sampling time interval threshold of 30 days, human viruses were clustered by phylogeny, genetic distances, sampling time interval. Since, we do not have any restriction on the sampling location, this setting assumes that human-to-human transmissions can occur among different cities. In this setting, fourteen human-to-human transmissions were detected, and R_0 was estimated to be 0.23(95% CI: 0.14, 0.35). If it is assumed that human-to-human transmissions occurred only within household and we set the geographical distance threshold was 0 km (within a city), which is the geographical distance between the same city, three human-to-human transmissions were detected. Based on this result, R_0 was estimated to be 0.05 (95% CI: 0.01, 0.13).

Supplementary Table S2 shows the estimates of R_0 for different combinations of genetic distance threshold, sampling time interval threshold, and geographical distance threshold. The upper bounds of 95% CI of our estimates of R_0 using various thresholds were below 1.0.

DISCUSSION

In this paper, to elucidate the cause of the rapid increase in human cases of H5N1 influenza infections from 2014 to 2015 in Egypt, we have estimated the R_0 of H5N1 infections in human population in Egypt using candidate transmission pairs identified from the nucleotide sequences, infection time, and geographic location of viruses. Sensitivity analysis shows that R_0

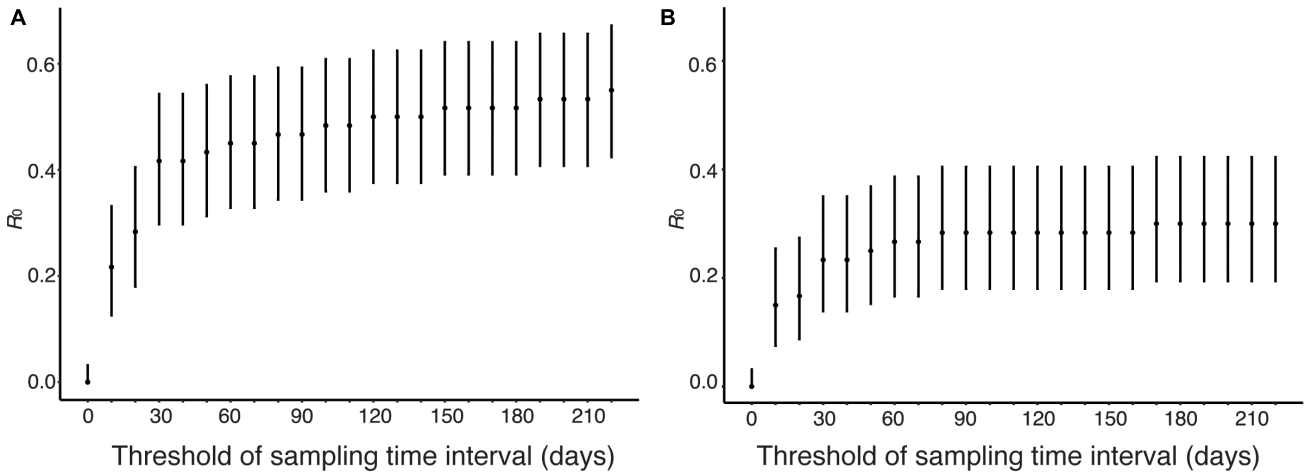

FIGURE 6 | Estimation of R_0 from genetic distance and sampling time interval. The effect of time interval threshold on the estimate of R_0 is shown when genetic distance threshold fixed at the between-household variation. **(A)** Genetic distances and sampling time intervals were used to obtain candidate transmission pairs. **(B)** Phylogeny, genetic distances, and sampling time interval were used to obtain candidate transmission pairs.

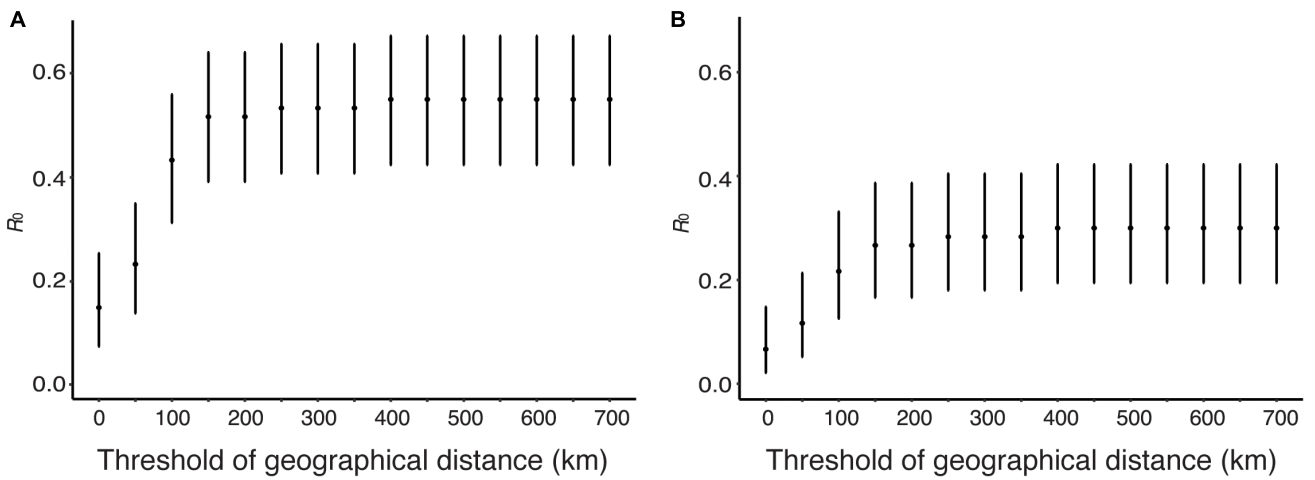

FIGURE 7 | Estimation of R_0 from genetic distance and geographical distance. The effect of geographical distance threshold on the estimate of R_0 is shown when genetic distance threshold fixed at the between-household variation. **(A)** Genetic distances and geographical distance were used to obtain candidate transmission pairs. **(B)** Phylogeny, genetic distances, and geographical distance were used to obtain candidate transmission pairs.

is below unity, suggesting that major outbreak will not occur, with broad range of threshold values of genetic distance, sampling time interval, and geographical distance (**Figures 4**, **6**, **7**). Using phylogeny, genetic distance, sampling time interval, and geographical distance, we estimated R_0 of 0.05 (95% CI: 0.01, 0.13) assuming that human-to-human transmissions occurred within a city, 0.23(95% CI: 0.14, 0.35) assuming human-to-human transmissions among cities, confirming previous studies that suggest human-to-human transmission of H5N1 viruses is rare in Egypt.

We have estimated the R_0 of H5N1 infections in human population in Egypt using candidate transmission pairs identified from the nucleotide sequences, infection time, and geographic location of viruses. The nucleotide sequences of H5N1 influenza viruses were used to obtain candidate transmission pairs in two different ways. The first approach makes clusters of human viruses using genetic distances with respect to a given threshold value. This approach does not use nucleotide sequences of avian viruses. The second approach use a phylogenetic tree of influenza viruses constructed from nucleotide sequences of humans and birds and use genetic distance to divide clusters into transmission chains. The second approach reduces a possibility that two avian-to-human transmissions are clustered together. In fact, the estimated values of R_0 were smaller when we analyzed sequences with phylogeny than without phylogeny (**Figures 4A,B**, **6A,B**, **7A,B**). There is a possibility that the R_0 would further decrease if we had more avian sequences similar to human viruses. In sensitivity analysis, the effect of threshold values on R_0 were

smaller when with a phylogenetic tree (**Figure 4B**) than without a phylogenetic tree (**Figure 4A**).

Sensitivity analysis of sampling time interval showed a large effect on R_0 between 0 days and 30 days (**Figures 6A,B**). R_0 was estimated as 0.22, 0.28, and 0.42 when the sampling time interval threshold was 10, 20, and 30 days, respectively. It is known that the sampling time interval of transmission period is less than 30 days. Sensitivity analysis of geographical distance showed a large effect on R_0 between 0and 150 km (**Figures 7A,B**). R_0 was estimated as 0.067, 0.12, 0.22, 0.27 when the geographical distance threshold was 0, 50, 100, and 150 km, respectively. These results indicate that the threshold of sampling time interval and geographical distance are important variables to estimate R_0 using our data. We estimated R_0 with combinations of different threshold values for genetic distance, sampling time difference and spatial difference as sensitivity analyses. In all analyses, the upper bound of the 95% CI of R_0 was below unity.

Although sensitivity of R_0 against geographical distance is also high, the setting of geographical distance to detect clusters of human cases is not straightforward. Since several studies reported that most human-to-human transmissions of H5N1 occurred within their household (Ungchusak et al., 2005; Wang et al., 2008; Centers for Disease Control and Prevention, 2015), the threshold of geographical distance might be suitable to set 0 km, i.e., human-to-human transmissions occurred only within the same city. If this is the case, the R_0 estimate is 0.05 (95% CI: 0.01, 0.13). However, the human cases of H5N1 in Egypt have not been well-understood whether they occur within or between household so far, and this assumption may underestimate R_0. If we do not set any threshold of geographical distance, the R_0 estimate is 0.23 (95% CI: 0.14, 0.35). However, this setting may overestimate R_0. This setting assumes that genetic distance and sampling time difference are enough to determine the cluster of human cases formed by only human-to-human transmission. If multiple introductions of H5N1 viruses from avian to human occur, this setting may lead to misinterpret them as human-to-human transmission events. It is difficult to determine which of the two representative estimates of R_0 is more reasonable because we cannot set the upper limit distance for human-to-human transmissions. To estimate an accurate R_0, a detailed surveillance, e.g., contact tracing, is required. Regardless of the settings for threshold of geographical distance, the upper bound of the 95% CI of R_0 was below unity.

Several studies have estimated R_0 of H5N1 influenza viruses in human populations, most studies estimated R_0 smaller than unity, ranges from 0.06 to 1.14 (Ferguson et al., 2004; Yang et al., 2007; Bettencourt and Ribeiro, 2008; Aditama et al., 2012; Saucedo et al., 2019). Our estimate of R_0 assuming transmissions among cities, 0.23(95% CI: 0.14, 0.35), is comparable with most of estimates from these studies.

Human cases of the highly pathogenic avian influenza H5N1 had increased in 2014–2015, and three hypotheses for this increase can be raised; the increase in (i) human-to-human transmission potential, (ii) the susceptibility of humans to infection with these H5N1 viruses, (iii) avian-to-human transmissions. The upper bounds of 95% CI of our estimates of R_0 using various methods were below unity, suggesting that major outbreaks due to human-to-human transmission are unlikely to occur in the current situation. Naguib et al. (2016) showed that human infections of H5N1 in Egypt in 2014–2015 are statistically linked to the increased outbreaks in poultry. This suggested that human cases were likely to be attributed to avian-to-human transmissions, although the increase in the susceptibility cannot be rejected. Furthermore, the distribution of geographical distance between human cases show unclear trend (**Figures 5C,D**), meanwhile, the distribution should be right-skewed if most human cases are attributed to human-to-human transmission. Sensitivity of R_0 against geographical distance suggests that the outbreak of H5N1 among birds in Egypt occurs widely (diameter of the area is 200 km hypothesized from the saturation of R_0 estimate in **Figures 7A,B** with assuming that human-to-human transmission is rare). The dramatic increase in human cases in Egypt would be attributed to the increase in the prevalence of H5N1 viruses among avian species, and avian-to-human transmissions in wide regions of Egypt may explain the unclear trend in the distribution of geographical distance between human cases.

This study proposed a method to estimate human-to-human transmissibility of zoonotic pathogens using nucleotide sequences as well as temporal and geographic information of infections. The integration of multiple types of data to the analyses can lead a more accurate estimation than analysis using a single type of data. However, there are some limitations in this study. First, we did not include exposure history to birds in our analysis. WHO reported 65 human cases from January 26 to March 3, 2015, of which 63 cases had exposure to poultry or poultry markets, and the exposure history of one case was still under investigation at the time of the report (World Health Organization [WHO], 2015a). From March 3 to 31, 2015, there were 37 human cases, of which all but one case had exposure to poultry or poultry markets, and the exposure history of the one case was still under investigation (World Health Organization [WHO], 2015b). The inclusion of bird contact information may change the estimates of R_0. There is no link between the sequence data used in this study and exposure history data so far, the improvement of surveillance system that can link them is required to estimate an accurate R_0. Second, the number of available sequences in the database is limited. There would be difference in the sampling probability between human and avian sequences. Assuming that the sampling probability in human sequences is higher than that of avian sequences, we may have overestimated the R_0. Third, we did not model movement of hosts, both of human and avian due to the lack of data. Modeling movement of hosts explicitly can improve accuracy of estimates. Fourth, our method can applicable only for infections in sporadic outbreaks and cannot be used for infections in an endemic situation, since the length of transmission chain is assumed follow the geometric distribution.

The small value of R_0 estimate, i.e., below unity, suggests that human-to-human transmission of H5N1 viruses in Egypt is limited. The large increase in human cases in Egypt since 2014 is likely attributed to other factors than the increase in human-to-human transmission potential. Therefore the increase in human cases should be attributed to the increase in avian-to-human transmissions. A possible cause of the increase in avian-to-human transmissions is the spread of the viruses in avian populations,

which increase the chance of avian-to-human transmissions. Another possibility is the increase in the susceptibility of humans to infection with these H5N1 viruses due to virus evolution. Thus, monitoring the spread and evolution of viruses in avian population as well as those in human populations is required to prevent major outbreaks of H5N1 infections among the human population.

DATA AVAILABILITY STATEMENT

All datasets generated for this study are included in the article/**Supplementary Material**.

AUTHOR CONTRIBUTIONS

WM and RO designed the study. WM and KI analyzed the data. WM, KI, and RO wrote the manuscript.

FUNDING

This work was supported by the Program for Leading Graduate Schools from the Ministry of Education, Culture, Sports, Science and Technology, Japan (http://www.mext.go.jp/) and CREST (grant number JPMJCR1413) and PRESTO programs (grant number JPMJPR15E1) from Japan Science and Technology Agency (http://www.jst.go.jp/). The funders had no role in the study design, data collection and analysis, decision to publish, or preparation of the manuscript.

SUPPLEMENTARY MATERIAL

The Supplementary Material for this article can be found online at: https://www.frontiersin.org/articles/10.3389/fmicb.2019.02765/full#supplementary-material

TABLE S1 | The GenBank accession numbers, strain names, sampling dates, and sampling locations of nucleotide sequences used in this study.

TABLE S2 | Sensitivity analysis of R_0 against genetic distance, time difference, geographical distance. Lb and ub are the upper and lower bound of 95% confidence interval for the R_0 estimate.

DATA SHEET S1 | R codes for estimation of R_0 and its confidence interval from phylogeny, genetic distance, time difference, and geographical distance.

DATA SHEET S2 | Detailed process of statistical analysis for estimation of R_0 and its confidence interval from phylogeny, genetic distance, time difference, and geographical distance.

REFERENCES

Aditama, T. Y., Samaan, G., Kusriastuti, R., Sampurno, O. D., Purba, W., Santoso, H., et al. (2012). Avian influenza H5N1 transmission in households, Indonesia. *PLoS One* 7:e29971. doi: 10.1371/journal.pone.0029971

Aly, M. M., Arafa, A., and Hassan, M. K. (2008). Epidemiological findings of outbreaks of disease caused by highly pathogenic H5N1 avian influenza virus in poultry in Egypt during 2006. *Avian Dis.* 52, 269–277. doi: 10.1637/8166-103007-reg.1

Arafa, A., El-Masry, I., Kholosy, S., Hassan, M. K., Dauphin, G., Lubroth, J., et al. (2016). Phylodynamics of avian influenza clade 2.2.1 H5N1 viruses in Egypt. *Virol. J.* 13:49. doi: 10.1186/s12985-016-0477-7

Arafa, A. S., Yamada, S., Imai, M., Watanabe, T., Yamayoshi, S., Iwatsuki-Horimoto, K., et al. (2016). Risk assessment of recent Egyptian H5N1 influenza viruses. *Sci. Rep.* 6:38388. doi: 10.1038/srep38388

Bao, Y. M., Bolotov, P., Dernovoy, D., Kiryutin, B., Zaslavsky, L., Tatusova, T., et al. (2008). The influenza virus resource at the national center for biotechnology information. *J. Virol.* 82, 596–601. doi: 10.1128/jvi.02005-07

Bettencourt, L. M. A., and Ribeiro, R. M. (2008). Real time Bayesian estimation of the epidemic potential of emerging infectious diseases. *PLoS One* 3:e2185. doi: 10.1371/journal.pone.0002185

Centers for Disease Control and Prevention (2015). *Highly Pathogenic Asian Avian Influenza A(H5N1) in People*. Available at: https://www.cdc.gov/flu/avianflu/h5n1-people.htm (accessed August 1, 2019).

Chea, N., Yi, S. D., Rith, S., Seng, H., Ieng, V., Penh, C., et al. (2014). Two clustered cases of confirmed influenza A(H5N1) virus infection, Cambodia, 2011. *Eurosurveillance* 19, 6–13.

Chong, K. C., Zee, B. C. Y., and Wang, M. H. (2017). A statistical method utilizing information of imported cases to estimate the transmissibility for an influenza pandemic. *BMC Med. Res. Methodol.* 17:31. doi: 10.1186/s12874-017-0300-1

Farrington, C. P., and Kanaan, M. N. (2001). Estimation of the basic reproduction number for infectious diseases from age-stratified serological survey data. *J. R. Statist. Soc. Ser. C Appl. Statist.* 50, 251–283.

Ferguson, N. M., Fraser, C., Donnelly, C. A., Ghani, A. C., and Anderson, R. M. (2004). Public health risk from the avian H5N1 influenza epidemic. *Science* 304, 968–969. doi: 10.1126/science.1096898

Herfst, S., Schrauwen, E. J. A., Linster, M., Chutinimitkul, S., De Wit, E., Munster, V. J., et al. (2012). Airborne transmission of influenza A/H5N1 virus between ferrets. *Science* 336, 1534–1541. doi: 10.1126/science.1213362

Imai, M., Watanabe, T., Hatta, M., Das, S. C., Ozawa, M., Shinya, K., et al. (2012). Experimental adaptation of an influenza H5 HA confers respiratory droplet transmission to a reassortant H5 HA/H1N1 virus in ferrets. *Nature* 486, 420–428. doi: 10.1038/nature10831

Kayali, G., Kandeil, A., Ei-Shesheny, R., Kayed, A. S., Maatouq, A. M., Cai, Z. P., et al. (2016). Avian influenza A(H5N1) virus in Egypt. *Emerg. Infect. Dis.* 22, 379–388. doi: 10.3201/eid2203.150593

Loeb, M., Singh, P. K., Fox, J., Russell, M. L., Pabbaraju, K., Zarra, D., et al. (2012). Longitudinal study of influenza molecular viral shedding in hutterite communities. *J. Infect. Dis.* 2006, 1078–1084. doi: 10.1093/infdis/jis450

Naguib, M. M., Abdelwhab, E. M., and Harder, T. C. (2016). Evolutionary features of influenza A/H5N1 virus populations in Egypt: poultry and human health implications. *Arch. Virol.* 161, 1963–1967. doi: 10.1007/s00705-016-2849-0

Nei, M., and Kumar, S. (2000). *Molecular Evolution and Phylogenetics*. New York, NY: Oxford University Press.

Ng, S., Lopez, R., Kuan, G., Gresh, L., Balmaseda, A., Harris, E., et al. (2016). The timeline of influenza virus shedding in children and adults in a household transmission study of influenza in Managua, Nicaragua. *Pediatr. Infect. Dis. J.* 35, 583–586. doi: 10.1097/INF.0000000000001083

Nishiura, H., Mizumoto, K., and Ejima, K. (2013). How to interpret the transmissibility of novel influenza A(H7N9): an analysis of initial epidemiological data of human cases from China. *Theor. Biol. Med. Model.* 10:30. doi: 10.1186/1742-4682-10-30

Pybus, O. G., Charleston, M. A., Gupta, S., Rambaut, A., Holmes, E. C., and Harvey, P. H. (2001). The epidemic behavior of the hepatitis C virus. *Science* 292, 2323–2325. doi: 10.1126/science.1058321

Refaey, S., Azziz-Baumgartner, E., Amin, M. M., Fahim, M., Roguski, K., Abd Elaziz, H. A., et al. (2015). Increased number of human cases of influenza virus A(H5N1) infection, Egypt, 2014-15. *Emerg. Infect. Dis/* 21, 2171–2173. doi: 10.3201/eid2112.150885

Saucedo, O., Martcheva, M., and Annor, A. (2019). Computing human to human avian influenza R0 via transmission chains and parameter estimation. *Math. Biosci. Eng.* 16, 3465–3487. doi: 10.3934/mbe.2019174

Simplemaps.Com (2019). *Egypt Cities Database*. Available at: https://simplemaps.com/data/eg-cities (accessed August 1, 2019).

Tamura, K. S., Peterson, D., Filipski, A., and Kumar, S. (2013). MEGA6: molecular evolutionary genetics analysis version 6.0. *Mol. Biol. Evol.* 30, 2725–2729. doi: 10.1093/molbev/mst197

Tarantola, A., Barboza, P., Gauthier, V., Ioos, S., El Omeiri, N., Gastellu-Etchegorry, M., et al. (2010). The influenza A(H5N1) epidemic at six and a half years: 500 notified human cases and more to come. *Eurosurveillance* 15, 8–12.

Thai, P. Q., Mai, L. Q., Welkers, M. R. A., Hang, N. L. K., Hanh, L. T., Dung, V. T. V., et al. (2014). Pandemic H1N1 virus transmission and shedding dynamics in index case households of a prospective vietnamese cohort. *J. Infect.* 68, 581–590. doi: 10.1016/j.jinf.2014.01.008

Ungchusak, K., Auewarakul, P., Dowell, S. F., Kitphati, R., Auwanit, W., Puthavathana, P., et al. (2005). Probable person-to-person transmission of avian influenza A (H5N1). *N. Engl. J. Med.* 352, 333–340. doi: 10.1056/nejmoa044021

Vynnycky, E. (2010). *An Introduction to Infectious Disease Modelling*. Oxford: Oxford University Press.

Wang, H., Feng, Z., Shu, Y., Yu, H., Zhou, L., Zu, R. Q., et al. (2008). Probable limited person-to-person transmission of highly pathogenic avian influenza A (H5N1) virus in China. *Lancet* 371, 1427–1434. doi: 10.1016/s0140-6736(08)60493-6

World Health Organization [WHO] (2008). Human cases of avian influenza A (H5N1) in North-West frontier province, Pakistan, october-november 2007. *Wkly Epidemiol. Rec.* 83, 359–364.

World Health Organization [WHO], (2015a). *Influenza at the Human-Animal Interface Summary and Assessment as of 3 March 2015*. Available at: https://www.who.int/influenza/human_animal_interface/HAI_Risk_Assessment/en/ (accessed August 1, 2019).

World Health Organization [WHO], (2015b). *Influenza at the Human-Animal Interface Summary and Assessment as of 31 March 2015*. Available at: https://www.who.int/influenza/human_animal_interface/HAI_Risk_Assessment/en/ (accessed August 1, 2019).

World Health Organization [WHO] (2019). *Cumulative Number of Confirmed Human Cases of Avian Influenza A(H5N1) Reported to WHO*. Available at: https://www.who.int/influenza/human_animal_interface/H5N1_cumulative_table_archives/en/ (accessed August 1, 2019).

Yang, Y., Halloran, M. E., Sugimoto, J. D., and Longini, I. M. (2007). Detecting human-to-human transmission of avian influenza A (H5N1). *Emerg. Infect. Dis.* 13, 1348–1353. doi: 10.3201/eid1309.07-0111

Yuen, K. Y., Chan, P. K. S., Peiris, M., Tsang, D. N. C., Que, T. L., Shortridge, K. F., et al. (1998). Clinical features and rapid viral diagnosis of human disease associated with avian influenza A H5N1 virus. *Lancet* 351, 467–471. doi: 10.1016/s0140-6736(98)01182-9

Conflict of Interest: The authors declare that the research was conducted in the absence of any commercial or financial relationships that could be construed as a potential conflict of interest.

Copyright © 2019 Mohamed, Ito and Omori. This is an open-access article distributed under the terms of the Creative Commons Attribution License (CC BY). The use, distribution or reproduction in other forums is permitted, provided the original author(s) and the copyright owner(s) are credited and that the original publication in this journal is cited, in accordance with accepted academic practice. No use, distribution or reproduction is permitted which does not comply with these terms.

frontiers in Microbiology

ORIGINAL RESEARCH
published: 06 December 2019
doi: 10.3389/fmicb.2019.02818

Neglected Australian Arboviruses Associated With Undifferentiated Febrile Illnesses

Narayan Gyawali[1,2,3], Andrew W. Taylor-Robinson[4], Richard S. Bradbury[2], Wayne Pederick[2], Helen M. Faddy[5] and John G. Aaskov[1]*

[1] Institute of Health and Biomedical Innovation, Queensland University of Technology, Brisbane, QLD, Australia, [2] School of Health, Medical and Applied Sciences, Central Queensland University, Rockhampton, QLD, Australia, [3] Mosquito Control Laboratory, QIMR Berghofer Medical Research Institute, Brisbane, QLD, Australia, [4] School of Health, Medical and Applied Sciences, Central Queensland University, Brisbane, QLD, Australia, [5] Research and Development, Australian Red Cross Blood Service, Brisbane, QLD, Australia

OPEN ACCESS

Edited by:
Ahmed Sayed Abdel-Moneim, Taif University, Saudi Arabia

Reviewed by:
Adam Taylor, Griffith University, Australia
Kevin Joseph Sokoloski, University of Louisville, United States

***Correspondence:**
Narayan Gyawali
narayan.gyawali@qimrberghofer.edu.au;
gyawali123@gmail.com

Specialty section:
This article was submitted to Virology, a section of the journal Frontiers in Microbiology

Received: *20 September 2019*
Accepted: *20 November 2019*
Published: *06 December 2019*

Citation:
Gyawali N, Taylor-Robinson AW, Bradbury RS, Pederick W, Faddy HM and Aaskov JG (2019) Neglected Australian Arboviruses Associated With Undifferentiated Febrile Illnesses. Front. Microbiol. 10:2818. doi: 10.3389/fmicb.2019.02818

Infections with commonly occurring Australian *ar*thropod-*bo*rne arboviruses such as Ross River virus (RRV) and Barmah Forest virus (BFV) are diagnosed routinely by pathology laboratories in Australia. Others, such as Murray Valley encephalitis (MVEV) and Kunjin (KUNV) virus infections may be diagnosed by specialist reference laboratories. Although Alfuy (ALFV), Edge Hill (EHV), Kokobera (KOKV), Sindbis (SINV), and Stratford (STRV) viruses are known to infect humans in Australia, all are considered 'neglected.' The aetiologies of approximately half of all cases of undifferentiated febrile illnesses (UFI) in Australia are unknown and it is possible that some of these are caused by the neglected arboviruses. The aims of this study were to determine the seroprevalence of antibodies against several neglected Australian arboviruses among residents of Queensland, north-east Australia, and to ascertain whether any are associated with UFI. One hundred age- and sex-stratified human plasma samples from blood donors in Queensland were tested to determine the prevalence of neutralising antibodies against ALFV, BFV, EHV, KOKV, KUNV, MVEV, RRV, SINV, and STRV. The seroconversion rates for RRV and BFV infections were 1.3 and 0.3% per annum, respectively. The prevalence of antibodies against ALFV was too low to enable estimates of annual infection rates to be determined, but the values obtained for other neglected viruses, EHV (0.1%), KOKV (0.05%), and STRV (0.05%), indicated that the numbers of clinical infections occurring with these agents are likely to be extremely small. This was borne out by the observation that only 5.7% of a panel of 492 acute phase sera from UFI patients contained IgM against any of these arboviruses, as detected by an indirect immunofluorescence assay. While none of these neglected arboviruses appear to be a cause of a significant number of UFIs in Australia at this time, each has the potential to emerge as a significant human pathogen if there are changes to their ecological niches.

Keywords: alphavirus, arbovirus, Australia, flavivirus, prevalence, Queensland, Ross River virus, undifferentiated febrile illness

INTRODUCTION

Arboviruses, defined as viruses that replicate in both vertebrate hosts and invertebrate vectors and which are transmitted between vertebrate hosts by biting arthropods (such as mosquitoes, ticks, sandflies, and midges), present a significant public health risk in Australia and internationally (Wilder-Smith et al., 2017). The recent epidemics and intercontinental spread of hitherto obscure diseases such as chikungunya and Zika have highlighted the significant threat to global health security presented by emerging arthropod-borne viruses (Gyawali et al., 2016). More than 75 arboviruses have been identified in Australia (Centers for Disease Control and Prevention, 2019), and while only a few of these are known to cause disease in humans there are limited or no data regarding the potential pathogenicity for humans of most others (Gyawali et al., 2017b).

Although most infections caused by arboviruses are mild or asymptomatic, those known to cause disease in humans in Australia include Ross River (RRV) and Barmah Forest (BFV), alphaviruses that elicit a debilitating and sometimes chronic polyarthritis (Fraser, 1986; Phillips et al., 1990). The flaviviruses Murray Valley encephalitis (MVEV) and West Nile virus (Kunjin strain, KUNV) cause encephalitis, while dengue viruses (DENV) cause a febrile illness and, less commonly, haemorrhagic fever (French, 1952; Halstead et al., 1970; Muller et al., 1986).

For almost a decade after the identification of RRV (Doherty et al., 1963), only small numbers of patients were diagnosed with a clinical infection with this agent because diagnostic testing was available only in a research setting and using an in-house methodology. Following the development and commercial release of an enzyme-linked immunosorbent assay (ELISA) to detect anti-RRV immunoglobulin IgM (Oseni et al., 1983), the number of patients diagnosed annually rose from 50 to 200 during the 1980s and 4,000 to 9,000 in the present decade. A similar but smaller increase in the number of cases of BFV disease was observed when a commercial diagnostic assay for that infection became available (Australian Government Department of Health, 2019). Moreover, epidemic polyarthritis, the disease caused by RRV infection, was made a nationally notifiable disease in 1991 (Hargreaves et al., 1995). Clinical infections with the viruses Edge Hill (EHV), Kokobera (KOKV), KUNV, and MVEV can be confirmed in some reference laboratories but only tests for suspected KUNV and MVEV are performed in these specialised facilities on a routine basis (Australian Government Department of Health, 2019).

Other Australian arboviruses, such as Alfuy (ALFV), Sindbis (SINV), and Stratford (STRV), have been associated with human disease (Doherty et al., 1969; Doherty, 1973; Hawkes et al., 1985, 1993; Boughton et al., 1986; Aaskov et al., 1993). However, each is thought to cause mild symptoms and no outbreaks of disease due to any of these have been reported in Australia (Australian Government Department of Health, 2019). In the absence of routine testing by all diagnostic laboratories for infection with these remaining neglected alpha- and flaviviruses, it remains possible that some patients with undifferentiated febrile illnesses (UFIs) – fever without diagnosed cause – are experiencing an infection with one of these 'neglected' viruses (Gyawali et al., 2017a). A retrospective study in Western Australia, undertaken from July 2000 to July 2003, identified 3,218 UFI cases (Ingarfield et al., 2007). Another investigation, from July 2008 to June 2011, conducted in a hospital in Far North Queensland found that 58.8% of patients with febrile illnesses received no definitive diagnosis (Susilawati and McBride, 2014).

Many UFIs go undiagnosed because the aetiological agent is novel or not known to cause human disease or because the tests to diagnose the infection are not available or are not sufficiently sensitive to be of clinical utility. The funding model for diagnostic pathology in Australia restricts the likelihood that a patient's treating physician would request tests for infection with a little-known arbovirus even if they have considered one in their differential diagnosis (Gyawali et al., 2016). This study aimed to determine rates of infection among adult residents of Queensland with neglected alphaviruses and flaviviruses – and to determine whether any of these are associated with UFIs.

MATERIALS AND METHODS

Study Design, Samples, and Research Setting

Two sets of samples were collected for this study. For the first, 100 de-identified plasma samples (3–5 mL) from 50 female and from 50 male, age-stratified, adult (20–69 years) Australian blood donors were provided by the Australian Red Cross Blood Service (approved by the Australian Red Cross Blood Service Human Research Ethics Committee, approval no. 12-03QLD-10). The samples were collected in 2015 throughout the state of Queensland. The prevalence of anti-RRV IgG in subjects from northern Australia observed by Aaskov et al. (1981) was 28/62 (45.1%). If it is assumed that the infection rate with neglected arboviruses is the same as that of RRV infections, the minimum sample size (for blood donor samples) required to detect the prevalence of such arboviral infections with 95% confidence at 0.1 margin of error would be 96. Hence, a sample collection of 100 was considered to provide statistically valid data.

The second sample set consisted of 492 de-identified sera from UFI patients, collected during January 2015 and December 2016 (during the Queensland wet season) by QML Pathology (Central Queensland University Human Research Ethics Committee approval no. H15/03-041). Inclusion criteria were that samples were submitted to QML Pathology from febrile patients for a variety of laboratory tests, including arbovirus serology, and with clinical notes such as 'fever,' 'fever of unknown origin,' 'pyrexia of unknown origin,' 'viral studies,' or 'undifferentiated fever/febrile illness.' Samples from patients with a laboratory diagnosis of an autoimmune or neoplastic condition, or of an infection with a bacterial, parasitic or viral agent – including RRV, BFV, and DENV – were excluded.

Determination of Background Infection Rates With Australian Alphaviruses and Flaviviruses Among Adults in Queensland

Neutralisation tests with plasma from blood donors employed the following prototype strains of viruses: ALFV MRM3929 (Whitehead et al., 1968), BFV BH2193 (Marshall et al., 1982), EHV C281, KOKV CH112820, KUNV MRM16, RRV T48, SINV MRM 39, STRV C338 (Doherty et al., 1963), and MVEV MVE/1/1951 (French, 1952). Australian alphaviruses and flaviviruses were reported to produce plaques on monolayers of porcine stable equine kidney cells (PS-EK; Gorman et al., 1975) but BFV did not do so in our experience. As all alphaviruses of interest, including BFV, formed plaques on baby hamster kidney (BHK-21) cells, the study employed PS-EK cells for neutralisation tests involving flaviviruses and BHK cells for tests involving alphaviruses.

Two hundred μL of plasma was inactivated by heating at 56°C for 30 min, then diluted 1 in 10 in serum-free Roswell Park Memorial Institute 1640 (RPMI-1640) medium (Sigma-Aldrich, St. Louis, MO, United States). This solution was mixed with an equal volume of virus stock diluted to contain between 50 and 60 plaque forming units (pfu) and added to cell monolayers at 37°C for 2 h to enable non-neutralised virus to adsorb to cells. Two mL of 0.75% w/v carboxymethyl cellulose (CMC, Sigma-Aldrich)/RPMI 1640 was then added and the plates were incubated at 37°C in an atmosphere of 5% v/v CO_2/air for an additional 2–4 days, depending on the virus being employed, i.e., 2 days for alphaviruses and 4 days for flaviviruses. The CMC medium was then removed and the cell monolayers were fixed and stained with 0.05% w/v crystal violet (Sigma-Aldrich) in formaldehyde (1% v/v) and methanol (1% v/v). Plasma samples that reduced virus plaque numbers by $\geq$ 50% were recorded as reactive.

The prevalence of antibodies against each virus was plotted against the age of the donors and the line of best fit was determined by linear regression (**Figure 1**). The annual infection rate was calculated from the slope of the line of best fit. Given previous reports of cross-reactivity between flaviviruses by polyclonal antisera (De Madrid and Porterfield, 1974; Calisher et al., 1989; Hall et al., 1990), and of mouse monoclonal antibodies that recognise epitopes on the E1 or E2 proteins of multiple alphaviruses, e.g., 2A2C3 (Roehrig, 1986), it is possible that plasma samples that recognised more than one alphavirus or more than one flavivirus might represent serological cross-reactivity, rather than be due to infections with multiple viruses. Therefore, the results shown in **Tables 1**, **2** were analysed based on three different assumptions: (1) The presence of neutralising antibody against any virus represented an infection with that virus; i.e., ignoring the possibility of serological cross-reactions (**Figure 1**, line A); (2) Analyses were performed with samples that neutralised only one virus; i.e., excluding all samples that may have contained cross-reactive antibodies (**Figure 1**, line B); and (3) Each subject was infected with only a single virus and it was the one against which the highest neutralising activity was observed; i.e., all other neutralising activity was due to cross-reacting antibodies (**Figure 1**, line C).

Detection of IgM Antibodies Against Australian Alphaviruses and Flaviviruses in Acute Phase Sera From UFI Patients in Queensland

A modification of the indirect immunofluorescence assay (IFA) of Aaskov and Davies (1979) was employed to detect IgM antibodies against a range of alphaviruses (BFV, RRV, and SINV) and flaviviruses (ALFV, EHV, KOKV, KUNV, MVEV, and STRV) in sera from UFI patients. Briefly, 40 μL of a suspension of virus-infected C6/36 cells (approximately 1.25×10^4 cells) was aliquoted onto each well of a 12-well Teflon-coated IFA slide (Cell Line Diagnostic, Thermo Scientific, Dreieich, Germany). After allowing cells to settle, the liquid in each well was aspirated and cells were air-dried (at room temperature for 15 min) before being fixed in ice-cold acetone (2 min). Fifty μL of serum from each UFI patient was diluted 1 in 20 in phosphate-buffered saline (PBS), pH 7.2, and added to each spot on the IFA slide containing infected cells before the slide was incubated at room temperature for 45 min. Slides were then washed in PBS, three times for 10 min each. Secondary antibody [FITC-labelled polyclonal rabbit anti-human IgM (Dako, Glostrup, Denmark)], was added to the cells and incubated at room temperature for 30–45 min before undergoing three further washes in PBS. A glass cover slip was placed over the slide and cells were viewed under a UV microscope (Eclipse, Nikon, Minato, Japan) using phloem illumination. Cells were considered to be infected if a clear green fluorescent signal was observed in the cytoplasm.

In order to exclude the possibility that the apparent anti-viral IgM reactions in IFAs were due to IgM rheumatoid factor (RF) attaching to anti-viral IgG, all IgM-reactive samples were tested for the presence of RF using a latex agglutination assay, performed according to the manufacturer's instructions (Dutch Diagnostics, Zutphen, Netherlands). Briefly, 50 μL of the UFI sample and one drop of RF-latex reagent were mixed with a stirrer and then shaken at 100 rpm for 2 min. Semi-quantitative assays were performed by making twofold dilutions of serum in normal saline before being added to the RF-latex reagent. The approximate concentration of RF was calculated by multiplying the RF titre by 8 IU/mL, as suggested by the manufacturer.

All IgM-reactive sera were then tested for the presence of neutralising antibodies against the viruses recognised by IgM antibody in the IFA assay, by the method described above.

RESULTS

Prevalence of Neutralising Antibodies to Australian Alphavirues and Flaviviruses in Blood Donors

Plasma samples from 63 of the panel of 100 donors neutralised one or more of the arboviruses against which they were tested. Thirty-eight samples neutralised one or more flavivirus (**Table 1**),

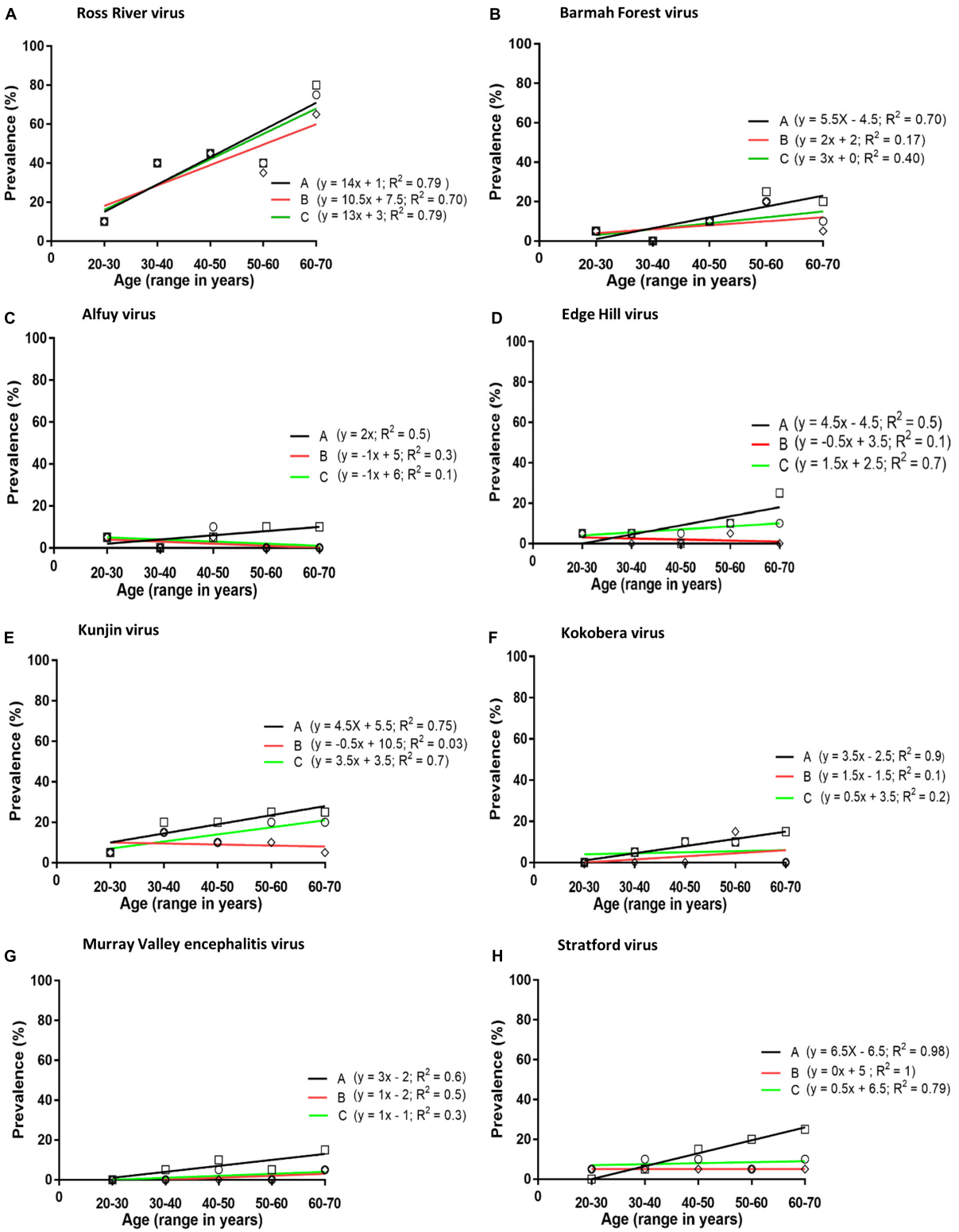

FIGURE 1 | Prevalence of neutralising antibodies against arboviruses **(A–H)** in plasma obtained from blood donors. Analysis performed by plotting prevalence of neutralising antibodies against age groups: Line A (squares), neutralising antibodies against any virus considered to represent an infection with that virus; i.e., ignoring the possibility of serological cross-reactions; Line B (diamonds), including samples that neutralised only one virus; i.e., excluding all samples which may have contained cross-reactive antibodies; Line C (circles), each subject was infected with only a single virus and it was the one against which the highest neutralising activity was observed; i.e., all other neutralising activity was assumed to be due to cross-reactive antibodies.

TABLE 1 | Plasma samples that neutralised one or more Australian flaviviruses by fifty *per cent* or more (n = 100).

Sample identifier	Reduction in mean plaque count (*per cent*)						Viruses neutralised to similar levels*
	KUNV (A)	KOKV (B)	STRV (C)	EHV (D)	ALFV (E)	MVEV (F)	
482	79	2	26	40	57	0	
347	70	48	39	15	21	6	
992	63	56	60	33	21	18	A&B; A&C; B&C
475	63	5	56	3	38	11	A&C
104	62	3	24	13	2	46	
689	61	34	67	6	38	36	A&C
839	61	12	14	24	23	12	
429	56	37	41	50	29	43	A&D; D&F
569	56	51	47	42	7	30	A&B; B&C; A&C
879	56	1	46	0	21	7	A&C
385	54	9	43	9	17	15	
226	54	5	39	44	35	5	A&D
983	52	15	19	45	28	20	A&D
637	51	22	53	9	29	48	A&C; A&F; C&F
793	51	2	33	4	20	29	
262	51	30	31	12	46	0	A&E
26	50	43	66	41	18	62	C&F
864	50	44	35	55	27	9	A&B; A&D
518	50	63	0	4	18	32	A&B
601	45	61	24	52	46	54	B&D; A&D; D&E; E&F; D&F
541	40	59	47	31	7	39	
754	17	57	29	21	16	12	
633	24	51	50	36	60	61	B&C; B&E; C&E
199	17	51	48	10	24	27	B&C
151	44	10	52	44	24	36	A&C; C&D
141	7	47	60	19	34	7	
522	5	3	63	10	27	10	
902	1	27	50	20	16	0	
321	1	16	90	8	33	25	
933	37	44	52	57	34	1	B&C, C&D
361	−42	33	87	100	36	79	
405	37	48	47	83	27	9	
86	34	3	12	52	49	19	D&E
241	−39	39	42	91	51	57	E&F; C&E
452	33	48	35	50	63	51	B&D; B&F; D&F
611	0	8	2	4	69	14	
488	15	7	9	14	61	31	
184	34	26	17	31	24	50	
#Total reactive	14	5	8	6	3	2	

*Values for reactive samples are shaded, with the darker shade notifying the most reactive. *There was no significant difference ($p > 0.05$, Student's t-test) between the neutralisation of the virus pairs indicated. #Numbers are based on an assumption that the subject had been infected with a single virus and it was the one against which the highest neutralising activity (darker shade) was observed.*

and for 21 of these reactive samples no single virus was neutralised to a greater extent than all others ($p > 0.05$; Student's t-test). Samples 361 and 241 consistently enhanced the number of plaques formed by KUNV.

Similarly, 51 of the 100 samples neutralised one or more alphaviruses (**Table 2**). Of these, samples from 39 donors neutralised RRV and eight neutralised BFV to a greater extent than another; i.e., there was a significant difference between the reductions in plaque count ($p < 0.05$). Only four samples neutralised both RRV and BFV.

The prevalence of antibody to a virus increased with the age of the donor, except for ALFV, but only with RRV, EHV, and KUNV was there a significant linear association between antibody prevalence and age ($p < 0.05$). If it is assumed that each subject was infected with only a single virus and it was the one against which the highest neutralising activity was observed (assumption number 3, section 'Materials and Methods'), the annual infection rate calculated for viruses among blood donors in Queensland were: RRV 1.3%, BFV 0.3%, EHV 0.15%, KUNV 0.15%, MVEV 0.1%, and STRV 0.05%.

TABLE 2 | Plasma samples that neutralised one or more Australian alphaviruses by fifty *per cent* or more (n = 100).

	Reduction in mean plaque count (*per cent*)				
Sample identifier	**RRV**	**BFV**	**Sample identifier**	**RRV**	**BFV**
412	100.00	42.03	768	58.16	39.86
347	100.00	33.33	980	58.16	11.59
482	100.00	31.88	452	57.14	44.93
653	98.98	31.16	151	57.14	39.86
284	98.98	30.43	405	57.14	34.78
262	95.92	33.33	933	57.14	27.54
992	94.90	23.19	633	56.12	36.23
328	93.88	36.23	598	56.12	25.36
77	93.88	31.88	601	53.06	47.10
351	93.88	31.88	864	53.06	21.74
717	89.80	36.23	754	51.02	31.88
361	89.80	26.09	212	50.00	26.09
242	85.71	23.19	518	50.00	21.74
531	78.57	21.74	199	*89.80	55.07
26	77.55	46.38	241	*77.55	65.22
12	76.53	30.43	982	*77.55	55.07
385	70.41	17.39	541	54.08	*95.65
497	69.39	36.23	368	48.98	89.86
429	67.35	22.46	457	48.98	55.07
569	67.35	18.84	415	47.96	51.45
709	65.31	24.64	290	46.94	50.00
488	63.27	27.54	562	36.73	70.29
293	61.22	30.43	306	30.61	55.80
680	60.20	28.26	141	26.53	50.72
902	59.18	31.16	475	22.45	62.32
600	59.18	21.74			
#Total reactive			RRV 41; BFV 9		

#*The numbers are based on an assumption that the subject had been infected with a single virus and it was the one against which the highest neutralising activity (darker shade) was observed.* **The value is significantly greater ($p < 0.05$, Student's t-test) than the corresponding value in the same row.*

Prevalence of IgM Antibodies to Australian Alphavirues and Flaviviruses in Acute Phase Sera From UFI Patients

Four-hundred and ninety-two acute phase sera were obtained from patients between 12 and 75 years of age (median of 45 years); 238 (48.4%) were male and 254 (51.6%) were female. Thirty-two samples contained IgM antibody that reacted with C6/36 cells infected by either an alphavirus or a flavivirus, or by several viruses. As the extent of cross-reactivity observed in these assays to detect anti-arboviral IgM was unexpected (Calisher et al., 1989), neutralisation tests were performed with each sample against all of the viruses to which IgM appeared to be reacting. The four samples (35, 91, 440, and 456 in **Table 3**) that failed to neutralise any of the arboviruses, by $\geq$ 50%, with which they reacted in IFA were regarded as non-reactive and excluded from subsequent analyses. Sample 456 consistently enhanced the number of plaques formed by incubation with KUNV.

Twenty-eight of the 32 IgM-reactive samples (5.7% of 492) neutralised one or more alphavirus or flavivirus (**Table 3**). Of these, 16 samples (3.2% of 492) neutralised a single virus (2 RRV, 3 BFV, 4 KUNV, 3 KOKV, 2 EHV, and 2 STRV). Twelve IgM-reactive samples neutralised more than one virus with one (331 in **Table 3**) neutralising both alphaviruses and flaviviruses. Only two of the 28 (7.1%) arbovirus-neutralising sera contained RF (274,64 IU/mL; 331,1104 IU/mL).

Estimates of numbers of clinical infections with these viruses were made using a range of total infection to clinical (symptomatic) infection ratios and the seroprevalence data employing assumptions 3, section 'Materials and Methods,' above (**Table 4**).

DISCUSSION

This study suggests that only a small proportion of UFIs in Australia are caused by flaviviruses for which virological and serological diagnostic testing is not performed on a routine basis. The low clinical infection rate is supported by the low rate of sub-clinical or inapparent infection with these viruses among blood donors.

The annual RRV infection rate determined by our investigation (1.3%) is in close agreement with that observed by Doherty et al. (1966) (1.4 to 3.2% for residents of Cape York Peninsula, North Queensland), by Doherty et al. (1968) (1.5% for residents of Innisfail, Far North Queensland) and by Aaskov et al. (1981) (1.4% for residents of Central and North Queensland). Taken together, these results suggest that there have been constant and continuous RRV infections in Queensland for decades. Furthermore, these findings also indicate that there was no major bias in the sampling of sera used in the current study.

The annual rate of infections with BFV (0.3%) and its seroprevalence (9.0%) were similar to those reported previously for Queensland residents [0.23% prevalence rate and 6.5% seroprevalence (Phillips et al., 1990)]. However, the seroprevalence was significantly higher (Chi–square test, $p < 0.05$) than that reported previously in Australia by Faddy et al. (2015) among blood donors in Queensland (2.9%), by Vale et al. (1986) among blood donors on the south coast of New South Wales (2.9%), by Hawkes et al. (1987) in inland (0.3%) and coastal regions (6%) of New South Wales. Some of these differences may reflect the sensitivities and specificities of the various assays employed; e.g., the neutralisation test employed in the current study and a commercial ELISA used by Faddy et al. (2015), or the type of sample collection and hypothesis of the particular study. While use of separate assay methodologies may have influenced the differences in seroprevalence values observed between Queensland and other states, it is also possible that both the abundance and species of mosquito vectors at geographically distant localities played a role (Webb et al., 2016).

The prevalence of antibodies against several neglected flaviviruses suggested they are associated with human infection. This conclusion is broadly in line with prior reports from Queensland (Doherty, 1973), New South Wales (Hawkes et al., 1985, 1993), and Victoria (Williams et al., 2013). In the present investigation annual seroconversion rates for flaviviruses (EHV 0.15%, KOKV 0.05%, MVEV 0.10%, and STRV 0.05%)

TABLE 3 | Recognition of Australian alphaviruses and flaviviruses by IgM antibody in sera from UFI patients in indirect immunofluorescence assays.

Identifier	Age/Sex	Recognition of virus by IgM antibody (R, reactive; N, non-reactive)								
		RRV	BFV	SINV	ALFV	EHV	KOKV	KUNV	MVEV	STRV
323	31/F	R (99)	N	N	N	N	N	N	N	N
274	47/M	R (98)	N	N	N	N	N	N	N	N
220	35/F	N	R (66)	N	N	N	N	N	N	N
152	43/F	N	R (51)	N	N	N	N	N	N	N
424	41/F	N	R (57)	N	N	N	N	N	N	N
425	27/M	N	N	N	N (10)	R (57)	N	N	N	N
103	39/F	N	N	N	N	R (50)	N	N (13)	N	N
88	40/F	N	N	N	N	N (44)	R (74)	N (36)	N	N
432	29/M	N	N	N	N (29)	N (13)	R (54)	N	N	N
43	32/F	N	N	N	N	N	R (59)	N	N	N
86	36/F	N	N	N	N	N	N (12)	R (51)	N	N
259	49/M	N	N	N	N	N	N	R (53)	N	N
474	34/M	N	N	N	N	N	N	R (50)	N	N
215	43/F	N	N	N	N	N	N	R (57)	N	N
347	75/F	N	N	N	N	N	N	N	N	R (88)
1	35/M	N	N	N	N	N	N	N	N	R (87)
14	46/F	N	N	N	N	N	R (71)	R (63)	N	N
468	22/F	N	N	N	N	N	R (73)	N	R (55)	N
47	66/M	N	N	N	R (89)	N	N	N	R (95)	N
33	18/M	N	N	N	R (55)	N	N	N	N	R (*98)
148	70/M	N	N	N	R (78)	R (55)	R (59)	N	N	N
253	61/F	N	N	N	R (74)	R (66)	N	N	R (*87)	N
257	51/F	N	N	N	R (64)	N	R (65)	N	R (*79)	N
299	32/M	N	N	N	R (58)	N	N	N	R (72)	R (87)
305	48/F	N	N	N	N	N	R (*74)	N	R (65)	R (58)
79	64/F	N	N	N	R (77)	R (74)	R (83)	N	R (77)	N
185	20/M	N	N	N	R (71)	N	R (78)	N	R (83)	R (*95)
331	56/M	R (84)	R (*98)	N	R (58)	N	R (65)	N (20)	N	N
91	53/M	N (24)	N (7)	N	N	N	N	N	N	N
35	25/F	N	N (27)	N	N	N	N	N	N	N
456	45/F	N	N	N	N (29)	N (27)	N	N (−36)	N	N
440	12/F	N	N	N	N	N	N	N	N	N (8)

*Values for reactive samples are shaded, with the darker shade notifying the most reactive. The neutralisation (per cent) of viruses recognised by IgM antibodies, identified by the patient serum, is shown in parenthesis. *Neutralisation value is significantly greater ($p < 0.05$, Student's t-test) than any other values within the same row (i.e., for the same serum sample).*

(**Figures 1A–E**) were significantly lower than those that have been determined for the alphaviruses RRV and BFV. However, an annual seroconversion rate for KUNV of 0.3% is similar to that for BFV. This overall disparity between rates of infection with alphaviruses and flaviviruses might reflect differences in their transmission cycles, particularly the vectors and reservoirs that are involved.

Kunjin shares a number of epidemiological characteristics with MVEV, including reservoir hosts (wading birds, particularly the rufous night heron; *Nycticorax caledonicus*) and mosquito vector species (particularly the common banded mosquito; *Culex annulirostris*) (Evans et al., 2009; Prow, 2013). However, in this study, antibodies against KUNV were more prevalent than those against MVEV among, predominantly, urban dwelling blood donors. This is in contrast to the observations of Doherty et al. (1959) in Far North Queensland, where approximately 50% of the residents of one aboriginal community had antibodies to MVEV but only 8% possessed anti-KUNV antibodies. Lower rates of infection with MVEV compared to those reported by Doherty et al. (1959) may reflect the transitory presence of the putative hosts of MVEV in nature, migratory water birds (Kingsford and Thomas, 1995). It may also reflect greater transmission of MVEV at the more northern latitude of Doherty's study than that which occurs elsewhere in the state of Queensland, from where the samples for this study were acquired. The most northerly part of Queensland from which samples were collected for this study was Cairns, which is 500 km south of Doherty's study site. In Western Australia also, MVEV transmission is more common in the northernmost Kimberley region than in the more southern central Pilbara region, where KUNV is most prevalent (Prow, 2013). Moreover, both annual and longer-term alterations in rainfall and climate patterns in the 60 years since the

TABLE 4 | Estimates of subclinical and clinical infection rates with Australian arboviruses in the Queensland population using the annual infection rates determined from this study.

Virus	*Annual infection rate per cent per annum	Estimated annual number of infections	Assumed clinical infection rate (clinical/total infection rate)	Clinical infections estimated annually	Average annual number of cases reported
RRV	1.3	63,960	20%	12,792	2,779
			10%	6,396	
			5%	3,195	
			1%	639	
BFV	0.3	14,760	20%	2,952	857
			10%	1,476	
			5%	723	
			1%	148	
ALFV	0.2	9,840	20%	1,968	NA
			10%	984	
			5%	492	
			1%	98	
EHV	0.15	7,380	20%	1,478	NA
			10%	784	
			5%	362	
			1%	73	
KOKV	0.05	2,460	20%	492	NA
			10%	246	
			5%	123	
			1%	24	
KUNV	0.3	14,760	20%	2,952	4
			10%	1,476	
			5%	738	
			1%	148	
MVEV	0.10	4,920	20%	984	1
			10%	492	
			5%	246	
			1%	49	
STRV	0.05	2,460	20%	492	NA
			10%	246	
			5%	123	
			1%	24	

*2017 census of Queensland estimated 4.92 million population. *The values presented are the annual infection rate per annum for each virus determined in this study. NA, data not available.*

publication of Doherty's data may have altered the transmission rates of KUNV and MVEV in Queensland (Prow, 2013). Further investigation is required to substantiate our finding of a potential emergence of KUNV in north-east Australia. The number of sera containing anti-ALFV antibodies were too small to detect an increase in the prevalence of anti-ALFV antibodies with increasing age of the blood donors, even if it was occurring, suggesting that ALFV infections may occur sporadically rather than on a regular basis.

Confounders of the observed seroprevalence of anti-flavivirus antibodies were the failure to test for anti-DENV antibodies and the possibility that blood donors had been vaccinated against either yellow fever or Japanese encephalitis. However, neither yellow fever nor Japanese encephalitis is endemic to Australia so immunisation would be recommended only in the event of international travel. Use of these vaccines among the Australian population, especially in regional communities, is assumed to be very low and this is unlikely to have influenced the results obtained. There are both locally acquired DENV infections and large numbers of Australian tourists returning with DENV infection acquired overseas. However, few, if any, of the levels of anti-flavivirus neutralising activity detected among plasma from blood donors could have been attributed to cross-reactive anti-DENV antibody from healthy blood donors.

For many of the viruses studied, the ratio of total infections to clinical infections in humans is unknown. From estimates made with the data obtained in this study (**Table 4**), it appears that approximately 5% of infections with RRV and BFV in Queensland are clinical infections severe enough to require medical attention and so be reported. If it is assumed that only a small proportion, e.g., 1%, of infections caused by flaviviruses studied in the current study results in disease, there would be at least 416 clinical infections caused by these viruses in Queensland annually.

Approximately 5.7% of UFI subjects had been infected recently (i.e., this proportion of sera contained anti-viral IgM) by one of the neglected Australian flaviviruses for which a diagnostic test was not requested or is not available in commercial laboratories. However, as these samples were collected during the wet summer months when the rate of transmission of the common arboviruses RRV, BFV, and DENV is highest, the annual value might be less than 5.7%. The detection of anti-RRV and anti-BFV IgM antibody in sera from a small number of these patients was unexpected because serology tests to determine the infection caused by these viruses might have been requested and performed on these samples using commercial ELISA. However, the ethical constraints on this study prevented retrospective access to any related serology that may have been conducted on these samples by a pathology laboratory. The PanBio ELISA kits, the only commercial tests for diagnosis of RRV and BFV currently available in Australia, have a sensitivity of 98.5% for IgM detection (Harley et al., 2001).

The extent of IgM cross-reactivity between the flaviviruses also was unexpected, but is reflected in the number of 'flavivirus-unspecified' reports made to the Australian Government National Notifiable Disease Surveillance System (Australian Government Department of Health, 2019). However, by combining the IgM data with those for neutralisation tests (**Table 3**), it was possible to implicate a given virus as the likely causative agent of a recent UFI. In most instances in which cross-reactive IgM antibody was detected, neutralising antibodies could be identified against the same viruses. The absence of detectable RF in almost all samples suggested it was not responsible for false positive IgM reactions.

Enhancement of infection with KUNV was noted with some samples examined in this study. There is an extensive literature describing enhancement of flavivirus infection *in vitro* by cross-reactive and non-neutralising antibodies, starting with the report of Hawkes (1964), who also described enhancement of infection by West Nile virus (Hawkes, 1964). However, antibody-mediated enhancement of infection with KUNV, an Australian strain of West Nile virus, by human antisera has not been reported previously. It is not known if the PS-EK cells that were used in this study express the Fc receptors required for antibody-dependent enhancement of viral infection to occur (Kliks and Halstead, 1983) or if another mechanism was responsible for our observations.

While this study identified neglected arboviruses that may cause UFI, the prevalence of these infections may have been elevated by the samples tested coming from a collection for which arbovirus serology or 'viral studies' had been requested and while the presence of anti-viral IgM indicates a recent infection, it does not indicate that the infection has caused the clinical signs and symptoms observed. It should be noted that the aetiology of disease in at least 94% of the patients remained undetermined.

CONCLUSION

The occurrence of UFI due to 'neglected' Australian flaviviruses like ALFV, EHV, KOKV, and STRV appears to be extremely low and the reported annual infection rates of these viruses suggest that this has always been the case. However, they do infect humans and so population growth, societal changes (such as increased urbanisation and travel) and variations in the ecosystem (climate-related or other) could have a profound effect on their transmission cycles, with consequent changes to the rates of human infection. Under these circumstances the current routine diagnostic testing regimes would not detect a rise in the rate of infection with ALFV, EHV, KOKV, and STRV. In order to monitor any future changes in the transmission of these viruses, there is a strong case to be made for the systematic testing of a sub-sample of UFI cases by state or national public health laboratories.

DATA AVAILABILITY STATEMENT

All datasets generated for this study are included in the article/supplementary material.

ETHICS STATEMENT

The studies involving human participants were reviewed and approved by the Central Queensland University Human Research Ethics Committee approval no. H15/03-041. Written informed consent for participation was not required for this study in accordance with the national legislation and the institutional requirements.

AUTHOR CONTRIBUTIONS

NG, AT-R, RB, and JA conceived the project. HF and WP collected the specimens. NG carried out the laboratory experiments and drafted the manuscript. JA supervised the project. NG, AT-R, RB, HF, WP, and JA critically reviewed and revised various versions of the manuscript. RB was co-authored this manuscript in his personal capacity and his capacity as an adjunct academic at Central Queensland University. All authors read and approved the final manuscript.

FUNDING

NG was in receipt of an International Postgraduate Research Scholarship and an Australian Postgraduate Award administered by Central Queensland University. This study was supported in part through a Health Collaborative Research Network Merit Grant awarded jointly to AT-R and JA, and funds provided from the Cook Estate to JA. The Australian governments fund the Australian Red Cross Blood Service to provide blood, blood products, and services to the Australian community.

ACKNOWLEDGMENTS

We thank Dr. Francesca D. Frentiu and Debbie Phillips from the Queensland University of Technology for technical advice and Mr. James Sinclair from the University of Queensland for assisting with the collection and transportation of sera.

REFERENCES

Aaskov, J., Phillips, D., and Wiemers, M. (1993). Possible clinical infection with Edge Hill virus. *Trans. R. Soc. Trop. Med. Hyg.* 87, 452–453. doi: 10.1016/0035-9203(93)90032-l

Aaskov, J. G., and Davies, C. E. (1979). An immunofluorescence assay for human antibodies to Ross River virus. *J. Immunol. Methods* 25, 37–41. doi: 10.1016/0022-1759(79)90162-5

Aaskov, J. G., Ross, P., Davies, C. E., Innis, M. D., Guard, R. W., Stallman, N. D., et al. (1981). Epidemic polyarthritis in northeastern Australia, 1978–1979. *Med. J. Aust.* 2, 17–19. doi: 10.5694/j.1326-5377.1981.tb132047.x

Australian Government Department of Health, (2019). *National Notifiable Diseases: Australia's Notifiable Diseases Status: Annual Report of the National Notifiable Diseases Surveillance System. The Department of Health, Australian Government*. Available at: http://www.health.gov.au/internet/main/publishing.nsf/content/cda-pubs-annlrpt-nndssar.htm (accessed August 30, 2019).

Boughton, C., Hawkes, R., and Naim, H. (1986). Illness caused by a Kokobera-like virus in south-eastern Australia. *Med. J. Aust.* 145, 90–92. doi: 10.5694/j.1326-5377.1986.tb101087.x

Calisher, C. H., Karabatsos, N., Dalrymple, J. M., Shope, R. E., Porterfield, J. S., Westaway, E. G., et al. (1989). Antigenic relationships between *Flaviviruses* as determined by cross-neutralization tests with polyclonal antisera. *J. Gen. Virol.* 70, 37–43. doi: 10.1099/0022-1317-70-1-37

Centers for Disease Control and Prevention, (2019). *Arbovirus Catalog*. Available at: https://wwwn.cdc.gov/Arbocat/Default.aspx (accessed August 30, 2019).

De Madrid, A. T., and Porterfield, J. S. (1974). The *Flaviviruses* (group B arboviruses): a cross-neutralization study. *J. Gen. Virol.* 23, 91–96. doi: 10.1099/0022-1317-23-1-91

Doherty, R., Whitehead, R., Gorman, B., and O'Gower, A. (1963). The isolation of a third group a arbovirus in Australia, with preliminary observations on its relationship to epidemic polyarthritis. *Aust. J. Sci.* 26, 183–184.

Doherty, R. L. (1973). Surveys of haemagglutination-inhibiting antibody to arboviruses in aborigines and other population groups in northern and eastern Australia, 1966–1971. *Trans. R. Soc. Trop. Med. Hyg.* 67, 197–205. doi: 10.1016/0035-9203(73)90144-2

Doherty, R. L., Bodey, A. S., and Carew, J. S. (1969). Sindbis virus infection in Australia. *Med. J. Aust.* 2, 1016–1017. doi: 10.5694/j.1326-5377.1969.tb107563.x

Doherty, R. L., Carley, J. G., and Lee, P. E. (1959). Studies of arthropod-borne virus infections in Queensland I. a serological survey of aboriginal missions bordering the Gulf of carpentaria. *Aust. J. Exp. Biol. Med. Sci.* 37, 365–372. doi: 10.1038/icb.1959.38

Doherty, R. L., Gorman, B. M., Whitehead, R. H., and Carley, J. G. (1966). Studies of arthropod-borne virus infections in Queensland. V. survey of antibodies to group A arboviruses in man and other animals. *Aust. J. Exp. Biol. Med. Sci.* 44, 365–377. doi: 10.1038/icb.1966.35

Doherty, R. L., Whitehead, R. H., Wetters, E. J., and Gorman, B. M. (1968). Studies of the epidemiology of arthropod-borne virus infections at Mitchell River Mission, Cape York Peninsula, North Queensland: II. arbovirus infections of mosquitoes, man and domestic fowls, 1963–1966. *Trans. R. Soc. Trop. Med. Hyg.* 62, 430–438. doi: 10.1016/0035-9203(68)90095-3

Evans, I. A., Hueston, L., and Doggett, S. L. (2009). Murray Valley encephalitis virus. *NSW Public Health Bull.* 20, 195–196.

Faddy, H., Dunford, M., Seed, C., Olds, A., Harley, D., Dean, M., et al. (2015). Seroprevalence of antibodies to Ross River and barmah forest viruses: possible implications for blood transfusion safety after extreme weather events. *EcoHealth* 12, 347–353. doi: 10.1007/s10393-014-1005-0

Fraser, J. (1986). Epidemic polyarthritis and Ross River virus disease. *Clin. Rheum. Dis.* 12, 369–388.

French, E. L. (1952). Murray Valley encephalitis: isolation and characterization of the aetiological agent. *Med. J. Aust.* 1, 100–103. doi: 10.5694/j.1326-5377.1952.tb74985.x

Gorman, B. M., Leer, J. R., Filippich, C., Goss, P. D., and Doherty, R. L. (1975). Plaquing and neutralization of arboviruses in the PS-EK line of cells. *Aust. J. Med. Technol.* 6, 65–71.

Gyawali, N., Bradbury, R. S., Aaskov, J. G., and Taylor-Robinson, A. W. (2017a). Neglected Australian arboviruses and undifferentiated febrile illness: addressing public health challenges arising from the 'Developing Northern Australia'. Government policy. *Front. Microbiol.* 8:2150. doi: 10.3389/fmicb.2017.0215

Gyawali, N., Bradbury, R. S., Aaskov, J. G., and Taylor-Robinson, A. W. (2017b). Neglected Australian arboviruses: quam gravis? *Microbes Infect.* 19, 388–401. doi: 10.1016/j.micinf.2017.05.002

Gyawali, N., Bradbury, R. S., and Taylor-Robinson, A. W. (2016). The global spread of zika virus: is public and media concern justified in regions currently unaffected? *Infect. Dis. Poverty* 5:37. doi: 10.1186/s40249-016-0132-y

Hall, R. A., Kay, B. H., Burgess, G. W., Clancy, P., and Fanning, I. D. (1990). Epitope analysis of the envelope and non-structural glycoproteins of Murray Valley encephalitis virus. *J. Gen. Virol.* 71, 2923–2930. doi: 10.1099/0022-1317-71-12-2923

Halstead, S. Á, Nimmannitya, S., and Cohen, S. N. (1970). Observations related to pathogenesis of dengue hemorrhagic fever. IV. relation of disease severity to antibody response and virus recovered. *Yale J. Biol. Med.* 42, 311–328.

Hargreaves, J., Longbottom, H., Myint, H., Herceg, A., Oliver, G., Curran, M., et al. (1995). Annual report of the national notifiable diseases surveillance system, 1994. *Commun. Dis. Intell.* 19, 542–574.

Harley, D., Sleigh, A., and Ritchie, S. (2001). Ross River virus transmission, infection, and disease: a cross-disciplinary review. *Clin. Microbiol. Rev.* 14, 909–932. doi: 10.1128/CMR.14.4.909-932.2001

Hawkes, R., Boughton, C., Naim, H., Wild, J., and Chapman, B. (1985). Arbovirus infections of humans in new south wales. seroepidemiology of the *Flavivirus* group of togaviruses. *Med. J. Aust.* 143, 555–561. doi: 10.5694/j.1326-5377.1985.tb119949.x

Hawkes, R. A. (1964). Enhancement of the infectivity of arboviruses by specific antisera produced in domestic fowls. *Aust. J. Exp. Biol. Med. Sci.* 42, 465–482. doi: 10.1038/icb.1964.44

Hawkes, R. A., Boughton, C. R., Naim, H. M., Myrick, B. A., and Ramsay, L. G. (1987). Barmah forest virus infections in humans in new south wales. *Med. J. Aust.* 146, 569–573. doi: 10.5694/j.1326-5377.1987.tb120416.x

Hawkes, R. A., Pamplin, J., Boughton, C. R., and Naim, H. M. (1993). Arbovirus infections of humans in high-risk areas of south-eastern Australia: a continuing study. *Med. J. Aust.* 159, 159–162. doi: 10.5694/j.1326-5377.1993.tb137778.x

Ingarfield, S. L., Celenza, A., Jacobs, I. G., and Riley, T. V. (2007). Outcomes in patients with an emergency department diagnosis of fever of unknown origin. *Emerg. Med. Australas.* 19, 105–112. doi: 10.1111/j.1742-6723.2007.00915.x

Kingsford, R. T., and Thomas, R. F. (1995). The Macquarie Marshes in arid Australia and their waterbirds: a 50-year history of decline. *J. Environ. Manage.* 19, 867–878. doi: 10.1007/bf02471938

Kliks, S. C., and Halstead, S. B. (1983). Role of antibodies and host cells in plaque enhancement of Murray Valley encephalitis virus. *J. Virol.* 46, 394–404.

Marshall, I. D., Woodroofe, G. M., and Hirsch, S. (1982). Viruses recovered from mosquitoes and wildlife serum collected in the Murray Valley of south-eastern Australia. February 1974, during an epidemic of encephalitis. *Aust. J. Exp. Biol. Med. Sci.* 60, 457–470. doi: 10.1038/icb.1982.51

Muller, D., McDonald, M., King, J., and Stallman, N. (1986). Kunjin viras encephalomyelitis. *Med. J. Aust.* 144, 41–42. doi: 10.5694/j.1326-5377.1986.tb113633.x

Oseni, R. A., Donaldson, M. D., Dalglish, D. A., and Aaskov, J. G. (1983). Detection by ELISA of IgM antibodies to Ross River virus in serum from patients with suspected epidemic polyarthritis. *Bull. World Health Organ.* 61, 703–708.

Phillips, D., Murray, J., Aaskov, J., and Wiemers, M. (1990). Clinical and subclinical Barmah Forest virus infection in Queensland. *Med. J. Aust.* 152, 463–466. doi: 10.5694/j.1326-5377.1990.tb125304.x

Prow, N. A. (2013). The changing epidemiology of Kunjin virus in Australia. *Int. J. Environ. Res. Public Health* 10, 6255–6272. doi: 10.3390/ijerph10126255

Roehrig, J. (1986). "The use of monoclonal antibodies in studies of the structural proteins of alphaviruses and *Flaviviruses*," in *The Viruses – The Togaviridae and Flaviviridae*, eds S. Schlesinger, and M. J. Schlesinger, (New York, NY: Plenum), 251–278. doi: 10.1007/978-1-4757-0785-4_9

Susilawati, T. N., and McBride, W. J. H. (2014). Undiagnosed undifferentiated fever in Far North Queensland, Australia: a retrospective study. *Int. J. Infect. Dis.* 27, 59–64. doi: 10.1016/j.ijid.2014.05.022

Vale, T., Carter, I., McPhie, K., James, G. S., and Cloonan, M. (1986). Human arbovirus infections along the south coast of New South Wales. *Aust. J. Exp. Biol. Med. Sci.* 64, 307–309. doi: 10.1038/icb.1986.32

Webb, C., Doggett, S., and Russell, R. (2016). *A Guide to Mosquitoes of Australia. Clayton South*. Victoria: CSIRO Publishing.

Whitehead, R. H., Doherty, R. L., Domrow, R., Standfast, H. A., and Wetters, E. J. (1968). Studies of the epidemiology of arthropod-borne virus infections

at Mitchell River Mission, Cape York Peninsula, North Queensland: III. virus studies of wild birds, 1964–1967. *Trans. R. Soc. Trop. Med. Hyg.* 62, 439–445. doi: 10.1016/0035-9203(68)90096-5

Wilder-Smith, A., Gubler, D. J., Weaver, S. C., Monath, T. P., Heymann, D. L., and Scott, T. W. (2017). Epidemic arboviral diseases: priorities for research and public health. *Lancet Infect. Dis.* 17, e101–e106. doi: 10.1016/S1473-3099(16)30518-7

Williams, S. A., Richards, J. S., Faddy, H. M., Leydon, J., Moran, R., Nicholson, S., et al. (2013). Low seroprevalence of Murray Valley encephalitis and Kunjin viruses in an opportunistic serosurvey, victoria 2011. *Aust. N. Z. J. Public Health* 37, 427–433. doi: 10.1111/1753-6405.12113

Conflict of Interest: The authors declare that the research was conducted in the absence of any commercial or financial relationships that could be construed as a potential conflict of interest.

Copyright © 2019 Gyawali, Taylor-Robinson, Bradbury, Pederick, Faddy and Aaskov. This is an open-access article distributed under the terms of the Creative Commons Attribution License (CC BY). The use, distribution or reproduction in other forums is permitted, provided the original author(s) and the copyright owner(s) are credited and that the original publication in this journal is cited, in accordance with accepted academic practice. No use, distribution or reproduction is permitted which does not comply with these terms.

frontiers in Microbiology

MINI REVIEW
published: 11 December 2019
doi: 10.3389/fmicb.2019.02885

The Host Heat Shock Protein MRJ/DNAJB6 Modulates Virus Infection

Shih-Han Ko[1,2], Li-Min Huang[1,2] and Woan-Yuh Tarn[3]**

[1] Institute of Clinical Medicine, National Taiwan University College of Medicine, Taipei, Taiwan, [2] Department of Pediatrics, National Taiwan University Children's Hospital, National Taiwan University College of Medicine, Taipei, Taiwan, [3] Institute of Biomedical Sciences, Academia Sinica, Taipei, Taiwan

A variety of pathogens take advantage of cellular heat shock proteins (HSPs) to complete their life cycle and exert pathogenic effects. MRJ (DNAJB6), a member of the heat shock protein 40 family, acts as a molecular chaperone for a wide range of cellular processes. MRJ mutations are linked to human diseases, such as muscular dystrophy and neurodegenerative diseases. There are two MRJ isoforms generated by alternative use of terminal exons, which differ in their C-terminus. This mini-review summarizes how these two MRJ isoforms participate differentially in viral production and virulence, and the possibility for MRJ as a therapeutic target.

Keywords: heat shock protein, Hsp40, MRJ, virus, morpholino oligonucleotide

OPEN ACCESS

Edited by:
Ian M. Jones,
University of Reading,
United Kingdom

Reviewed by:
Arun Upadhyay,
Northwestern University,
United States
Yize Li,
University of Pennsylvania,
United States

****Correspondence:***
Li-Min Huang
lmhuang@ntu.edu.tw
Woan-Yuh Tarn
wtarn@ibms.sinica.edu.tw

Specialty section:
This article was submitted to Virology, a section of the journal Frontiers in Microbiology

Received: *08 July 2019*
Accepted: *29 November 2019*
Published: *11 December 2019*

Citation:
Ko S-H, Huang L-M and Tarn W-Y (2019) The Host Heat Shock Protein MRJ/DNAJB6 Modulates Virus Infection. Front. Microbiol. 10:2885. doi: 10.3389/fmicb.2019.02885

INTRODUCTION

Heat shock proteins (HSPs) function as molecular chaperones, thereby assisting protein folding, and non-covalent assembly or disassembly of macromolecules (Whitley et al., 1999). HSPs are structurally related proteins and classified based on their molecular weights, ranging from 10 to >100 kDa (Jee, 2016). HSP subfamily members exert similar functions across species. For example, small HSPs (HspB1 to HspB10) prevent the aggregation of misfolded proteins in an ATP-independent manner (Bakthisaran et al., 2015). ATP-dependent chaperones include Hsp60, Hsp70, and Hsp90. Hsp60 assists protein refolding throughout transport from the cytoplasm to the mitochondrial matrix (Cheng et al., 1989), while Hsp70 exerts the anti-aggregation activity with co-chaperones Hsp40 or Hsp110 (Kampinga and Craig, 2010). Hsp40 presents unfolded proteins to Hsp70 and stimulates its ATP hydrolysis (Bascos et al., 2017). Hsp90 regulates assembling, refolding and stabilizing of substrate proteins (Wandinger et al., 2008). HSPs function in a wide range of cellular processes to maintain protein homeostasis under physiological conditions and in response to environmental stresses (Hipp et al., 2019).

Invasion of pathogens, such as bacteria or viruses, may trigger cell stress responses and hence induces the production of cellular HSPs. Various viruses take advantage of cellular HSPs to overcome host environmental challenges and complete their infectious cycles (Neckers and Tatu, 2008). HSPs may participate in distinct steps during infection processes, such as viral entry, replication, and viral particle assembly and movement (**Table 1**). It is noteworthy that dengue virus particularly utilizes a set of Hsp70 family members for its entry, RNA replication and virion production (Taguwa et al., 2015). Moreover, some of the HSPs, particularly Hsp70, even become an integral component of virions (Santoro et al., 2009). All these findings emphasize the importance of HSPs in viral infection.

Heat shock proteins may also negatively impact viral infection. For example, two Hsp40 members inhibit the replication of human hepatitis B virus (HBV) (Sohn et al., 2006). Hsp70 interferes with nuclear import of the human immunodeficiency viruses (HIV) preinitiation complex, and viral gene expression and replication (Kumar et al., 2011). In addition, HSPs have immunomodulatory roles, although opposing. HSPs may act as a pro-inflammatory molecule by facilitating pathogenic antigen presentation on the antigen-presenting cells (Binder, 2014). On the other hand, HSPs may prevent immune activation by reducing inflammatory damages and promoting anti-inflammatory cytokines production (Hauet-Broere et al., 2006; Broere et al., 2011). Together, HSPs are engaged in both host immune response and viral pathogenesis during infection.

THE MRJ PROTEIN AND ITS FUNCTIONAL DOMAINS

Mammalian relative of DnaJ (MRJ/DNAJB6) is an Hsp40 family member. The Hsp40 family can be categorized into three major types (I, II, and III), all of which share the ∼70-amino acid J-domain (Li et al., 2009; **Figure 1A**). In type-I Hsp40 proteins, the J-domain is at the N-terminus, followed by the glycine/phenylalanine (G/F)-rich region, the zinc finger domain, and the peptide-binding domain in the C-terminus. Type-II is similar to type-I but lacks a zinc finger domain. Type-III members contain only the J-domain, whose location differs between members (Qiu et al., 2006). Many, but not all, Hsp40 members act as cochaperones of Hsp70 by forming a heterodimer through the J-domain (Langer et al., 1992; Meacham et al., 1999; Lee et al., 2002). The J-domain of Hsp40 containing the invariant histidine-proline-aspartic acid (HPD) tripeptide stimulates the ATPase activity of Hsp70 and increases the affinity of Hsp70 for the polypeptide substrate released from Hsp40 (Summers et al., 2009). The G/F-rich region of MRJ contains several hydrophobic residues responsible for substrate recognition; phenylalanine mutations disrupt its anti-aggregation activity (Sarparanta et al., 2012; Palmio et al., 2015). The C-terminal part of MRJ contains a serine/threonine (S/T)-rich region, which is important for substrate binding (Kakkar et al., 2016). Nevertheless, Hsp40s bind and transfer non-native polypeptides to Hsp70 through distinct mechanisms, which are subject to further processing (Summers et al., 2009). In addition, the C-terminal region of MRJ is also involved in polydisperse oligomeric complexes and oligomerization (Hageman et al., 2010; **Figure 1B**, protein). All these functional domains are present in both splice isoforms of MRJ (see below).

REGULATION OF MRJ ISOFORM EXPRESSION

MRJ is ubiquitously expressed in human tissues, with a higher level in the brain (Chuang et al., 2002). MRJ is upregulated during mitosis in HeLa cells perhaps to support mitotic activities (Dey et al., 2009). Human *MRJ* has two splice isoforms, *MRJ-L* and *MRJ-S*, generated through alternative splicing (Hanai and Mashima, 2003). The *MRJ* gene has ten exons. The first eight exons are included in both isoforms, while the last two exons are missing in *MRJ-S* (Ko et al., 2018; **Figure 1B**, mRNA). MRJ-L and MRJ-S proteins are comprised of 326 and 241 amino acid residues, respectively; both possess the aforementioned three functional domains. MRJ-L has a nuclear localization signal (NLS) in its very C-terminal region. Suppression of splicing in conjunction with activation of aberrant polyadenylation signals in intron 8 leads to *MRJ-S* expression. *MRJ* has been identified as a potential target transcript of cleavage stimulation factor subunit 2 (CstF64/CSTF2), a cleavage stimulation factor for mRNA 3'-end processing (Yao et al., 2012). Knockdown or overexpression of CstF64, respectively, increases and decreases the L/S isoform ratio (Ko et al., 2018). A decline in the CstF64 level during macrophage differentiation favors *MRJ-L* expression (**Figure 1B**, mRNA). In addition, serine/arginine-rich splicing factor 3 (SRSF3) may promote *MRJ-S* expression (Ko et al., 2018). Cyclin-dependent kinase 12 (CDK12) amplification in breast cancer results in downregulation of *MRJ-L* via modulating its terminal exon selection (Tien et al., 2017). Thus, the *MRJ* isoform ratio may be modulated in response to different cellular signals. Moreover, *MRJ-L* expression can be enhanced by increasing the strength of the 5' splice site of intron 8. Single nucleotide variations in the proximal polyadenylation signal and the polypyrimidine tract of intron 8 also affect *MRJ* isoform ratios. Thus, both alternative splicing and alternative polyadenylation activities determine *MRJ* isoform expression (Ko et al., 2018).

CELLULAR FUNCTIONS OF MRJ

MRJ knockout mice show embryonic lethality due in part to placental abnormalities and neural tube defects (Hunter et al., 1999; Watson et al., 2009). MRJ is involved in a variety of physiological processes, from transcription, cellular signaling to cell adhesion. MRJ suppresses the transcriptional activity of nuclear factors of activated T-cells (NFAT) by recruiting class II histone deacetylases, and hence, reduces calcineurin-induced cardiac myocyte growth. This observation suggests a role of MRJ in preventing cardiac hypertrophy (Dai et al., 2005). More notably, MRJ suppresses Wnt/β-catenin signaling through multiple pathways. Essentially, MRJ upregulates the secretary glycoprotein and Wnt inhibitor dickkopf 1 (DKK1) and maintains the dephosphorylation status of glycogen synthase kinase 3β (GSK3β) through the protein phosphatase PP2A and hence promotes degradation of β-catenin (Meng et al., 2016). This suppressive effect of MRJ on Wnt-β-catenin signaling negatively regulates tumor growth and metastases. Accordingly, a reduction of the MRJ level is present in various invasive and metastatic cancers as earlier mentioned. On the other hand, MRJ influences cytoskeletal organization, which is responsible for cell growth, division, and migration. For example, MRJ modulates intermediate filament organization via its direct interaction with keratins (Izawa et al., 2000). *MRJ* knockout causes actin cytoskeletal collapse in chorionic trophoblast cells (Watson et al., 2011). MRJ also contributes to cell adhesion and migration

TABLE 1 | Function of the HSP-virus interaction.

HSP family	Member	Virus	Interacting viral proteins	Engrave roles in HSP-virus interaction	References
Hsp40	DNAJA1, DNAJB1	IAV	NP, PB2, PA	Enhance nuclear import of vRNP complex and viral RNA synthesis	Cao et al., 2014; Batra et al., 2016
	DNAJA2	HCV	NS5A	NS5A-mediated IRES translation	Gonzalez et al., 2009
Hsp60	HSPD	HBV	HBx	Enhance HBx-induced apoptosis and HBx protein folding	Tanaka et al., 2004; Zhang et al., 2005
			Virus polymerase	Enhance viral polymerase activity	Park et al., 2002
Hsp70	HSPA1A	HIV	Virion	Virion assembly	Gurer et al., 2005
	HSPA1A	MuV	P protein	Facilitate IBs formation and modulate degradation of P protein	Katoh et al., 2015
	HSPA1A	HCV	NS5A	NS5A-mediated IRES translation	Gonzalez et al., 2009
	HSPA1, HSPA2, HSPA8	KSHV	RTCs	Facilitate RTCs formation and nuclear import	Baquero-Perez and Whitehouse, 2015
	HSPA5	RSV	Viral IBs	Enhance viral polymerase activity	Brown et al., 2005
	HSPA9	HBV	HBx	Viral protein folding	Zhang et al., 2005
Hsp90	HSP90AA1, HSP90AB1	IAV	PB1, PB2	Facilitate vRNP stabilization and nuclear import, viral RNA synthesis	Momose et al., 2002; Naito et al., 2007
	HSP90AA1	Rotavirus	NSP3	Viral protein folding and stabilization	Dutta et al., 2011
	HSP90A	RSV	Viral filaments and IBs	Viral particle assembly	Radhakrishnan et al., 2010
	HSP90	MuV	L protein	Viral protein stabilization	Katoh et al., 2017
	HSP90	HCV	NS3	Viral protein stabilization	Ujino et al., 2009

IAV, influenza A virus; NP, nucleoprotein; vRNP, viral ribonucleoprotein complex; PB2, polymerase basic protein 2; PB1, polymerase basic protein 1; PA, polymerase acidic protein; HCV, hepatitis C virus; NS5A, non-structural 5A protein; HBV, hepatitis B virus; HBx, hepatitis B virus X protein; HIV, human immunodeficiency virus; MuV, mumps virus; P protein, phophoprotein; KSHV, kaposi's sarcoma-associated herpes virus; RTCs, replication and transcription compartments; RSV, respiratory syncytial virus; IBs, inclusion bodies; NSP3, non-structural protein 3; L protein, large protein; NS3, non-structural protein 3.

via its interaction with urokinase-type plasminogen activator receptor (uPAR) (De Bock et al., 2010; Lin et al., 2014). A recent report reveals that MRJ promotes spindle pole focusing via its interaction with dynactin, which is essential for chromosome segregation during cell division (Rosas-Salvans et al., 2019).

PATHOLOGICAL EFFECTS OF DEFECTIVE MRJ

Genetic mutations or dysfunction of MRJ have been observed in human diseases such as limb-girdle muscular dystrophy (LGMD), myopathy and neurodegenerative diseases. Phenylalanine mutations in the (G/F)-rich region of MRJ are found in LGMD and distal myopathy, indicating that the chaperone activity of MRJ is critical for preventing proteinopathy (Harms et al., 2012; Sarparanta et al., 2012; Li et al., 2016; Jonson et al., 2018). MRJ mutations result in myofibrillar aggregates containing ubiquitin, ubiquitin-binding protein p62 and TAR DNA-binding protein 43 (TDP-43) (Sato et al., 2013; Sandell et al., 2016). Notably, TDP-43 aggregation is a characteristics of amyotrophic lateral sclerosis (Tamaki et al., 2018), emphasizing the pathological effect of defective MRJ in neurodegenerative disorders. The C-terminal S/T-rich region in MRJ exhibits the suppressive effect on the formation of different aggregation-prone peptides such as amyloid-β and polyglutamine peptides that are involved in the pathogenesis of Alzheimer's disease and Huntington's disease, respectively (Kakkar et al., 2016; Mansson et al., 2018; Bason et al., 2019). MRJ has also been implicated in Parkinson's disease. Upregulation of MRJ in parkinsonian astrocytes prevents the neuronal release of α-synuclein/SNCA, which has the potential to form toxic aggregates, suggesting a protective role of MRJ (Durrenberger et al., 2009; Aprile et al., 2017). A more recent study indicates that the chaperone activity of MRJ also suppresses mutant parkin aggregation (Kakkar et al., 2016). Thus, it is likely that the chaperone function of MRJ contributes to preventing protein misfolding in neurodegenerative diseases.

ROLE OF MRJ IN VIRUS INFECTION

In addition to the cellular functions above mentioned, both MRJ isoforms have been implicated in infection and pathogenesis of multiple human viruses. A recent report unveils the involvement of a translocon complex factor, Sec61, in the biogenesis of several different viral proteins, suggesting that targeting Sec61 can provide an antiviral strategy against multiple viruses (Heaton et al., 2016). In light of this finding, we review the roles of MRJ in infection and propagation of several viruses and discuss the potential of targeting MRJ as an antiviral strategy.

Human Immunodeficiency Viruses (HIV)

Human immunodeficiency viruses is a retrovirus that causes acquired immunodeficiency syndrome (AIDS), which destroys the immune system of infections (Sharp and Hahn, 2011). HIV infects macrophages and $CD4^+$ T helper cells through the CD4 receptor and its coreceptor, i.e., chemokine receptor CCR5 or

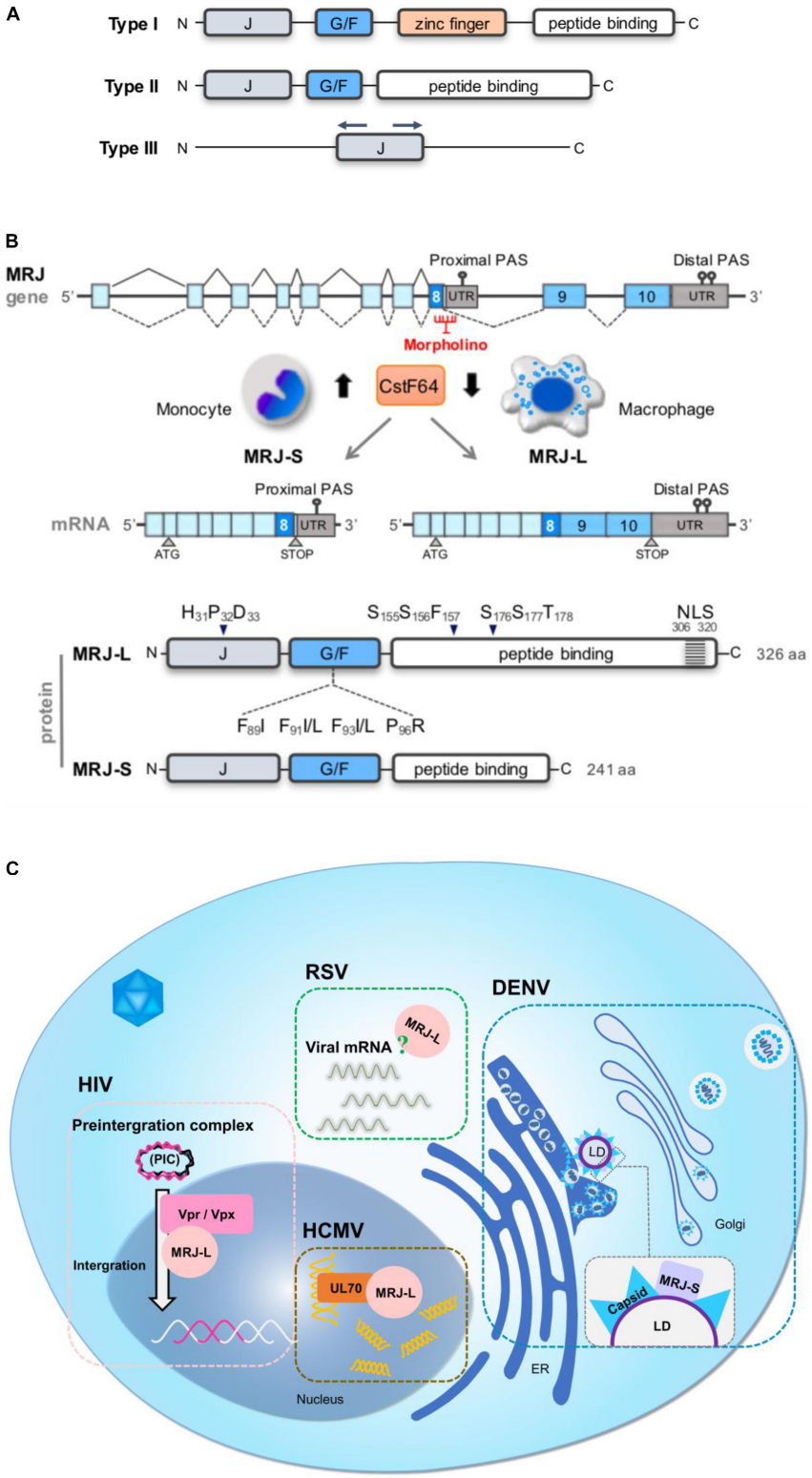

FIGURE 1 | Human MRJ gene and functions in the viral life cycle. **(A)** Schematic diagram of three major types of Hsp40. All contain the J-domain. The J-domain is located at the N-terminus of type I and II Hsp40 but is found at various locations within the type III members. Additional domains are as depicted. **(B)** Schematic diagram (upper) shows genomic organization of the human MRJ gene and its transcript isoforms that are generated by alternative splicing and polyadenylation. A reduction in the CstF64 level in macrophages favors MRJ-L production. A morpholino oligonucleotide targeting the 5' splice site of intron 8 suppresses

(Continued)

FIGURE 1 | Continued
MRJ-L expression. The bottom schematic diagram shows three major domains of the MRJ protein, including the J-domain followed by the G/F-rich domain in the N-terminal part, and the C-terminal peptide-binding domain, which interacts with denatured polypeptides and also directs the function of Hsp70. The conserved HPD motif of the J-domain, the SSF and SST motifs (namely the S/T-rich region) in the C-terminal peptide-binding domain and LGMD-associated mutations in the G/F domain are indicated. MRJ-S has a truncated C-terminal domain that lacks the NLS. **(C)** The two MRJ isoforms participate in the infection of the following viruses. HIV, MRJ-L facilitates nuclear import of the PIC via its interaction with Vpr (HIV-1) or Vpx (HIV-2), and hence facilitates the integration of the HIV genome into host chromosomes. HCMV, MRJ-L interacts with the DNA polymerase UL70 of HCMV and facilitates its nuclear import so that MRJ-L enhances viral genome synthesis. RSV, MRJ-L is essential for the expression of viral mRNAs and proteins, and viral production, but how it functions remains yet unclear. DENV: DENV replicates its genomes released from the pore of DENV-induced vesicle-like structures. The newly synthesized genome is packaged in the nucleocapsid with the capsid protein, which subsequently buds form proximal ER membranes. MRJ-S is colocalized with the viral capsid protein on the LD surface and facilitates viral assembly. Assembled viruses are transported to the Golgi apparatus for the maturation processes.

CXCR4 (Maartens et al., 2014). After infection, HIV is integrated into the human genome, which is essential for the viral life cycle (Moir et al., 2011). For integration, HIV establishes the pre-integration complex (PIC), consisting of the cDNA that is converted from its genomic RNA and several cellular and viral proteins including the viral protein R (Vpr). Vpr participates in proviral integration into the host genome (Chiang et al., 2014; Pirrone et al., 2014). MRJ-L facilitates nuclear localization of the HIV-1 pre-integration complex via its direct interaction with Vpr (Chiang et al., 2014). As compared to MRJ-L, MRJ-S displays a relatively weak activity in nuclear localization of Vpr/Vpx likely due to its lack of the C-terminal NLS of MRJ-L (Cheng et al., 2008; Chiang et al., 2014). Notably, mutations in the HPD motif of MRJ-L disrupt the activity of MRJ-L in facilitating Vpx (or HIV) nuclear import, indicating the involvement of Hsp70 (Cheng et al., 2008). Analogously, MRJ-L assists nuclear import of the HIV-2 viral protein X (Vpx), the paralog of HIV-1 Vpr. Depletion of MRJ-L restricts HIV-2 replication due to reduced nuclear import of the PIC (Cheng et al., 2008). On the other hand, overexpression of MRJ-S suppresses HIV proviral transcription and hence compromises HIV-1 production (Urano et al., 2013). These observations together suggest that a higher L/S ratio of MRJ may promote HIV infection (**Figure 1C**, HIV). A cohort study reveals that HIV-infected individuals indeed exhibit a slightly higher level of MRJ-L in macrophages than healthy subjects (Chiang et al., 2014), supporting the positive role of MRJ-L in HIV-1 infection. It is speculated that *cis*-element polymorphisms of *MRJ* that favor L isoform expression may increase the probability of HIV infection (Ko et al., 2018). Therefore, the MRJ-L level difference between individuals may predict HIV susceptibility. On the other hand, the negative regulatory factor (Nef) of HIV facilitates nuclear translocation of Hsp40, which subsequently facilitates viral gene expression. Nevertheless, Hsp70 can counteract the nuclear import of Vpr-mediated PIC complex and hence inhibits viral replication (Iordanskiy et al., 2004).

Human Cytomegalovirus (HCMV)

Human cytomegalovirus is a common opportunistic pathogen that may establish long-life latency without any symptoms in healthy individuals but may threaten immunocompromised individuals and neonates (Kenneson and Cannon, 2007). HCMV has the largest genome among the human herpesviruses and replicates in the nucleus of cells. The HCMV DNA-dependent RNA polymerase, i.e., the primase UL70, forms the helicase-primase complex with UL102/105 to synthesize short RNA primers for viral DNA replication (McMahon and Anders, 2002). MRJ-L interacts with UL70 through a fragment containing the G/F-rich region and facilitates nuclear entry of UL70, thereby promoting viral DNA synthesis (**Figure 1C**, HCMV). On the other hand, MRJ-S is co-localized with the primase in the cytoplasm that reduces viral genome expression and synthesis (Pei et al., 2012). Thus, MRJ isoforms differentially modulate HCMV replication. Reduction of the MRJ-L expression level conceivably inhibits viral lytic infection and can be used as an anti-HCMV strategy (Biron, 2006).

Respiratory Syncytial Virus (RSV)

Human RSV causes lower respiratory tract infection in infants and children worldwide. RSV infection shows a higher risk of mortality compared to seasonal influenza infection in elder individuals (Kwon et al., 2017). RSV belongs to the Paramyxoviridae family, consisting of a negative-sense single-stranded RNA genome that replicates in the host cytoplasm. The viral RNA-dependent RNA polymerase is responsible for both viral transcription and replication (Noton et al., 2019). Intriguingly, knockdown of MRJ-L reduces viral mRNA and protein expression and virion production, while depletion of MRJ-S has no such effects (Ko et al., 2018), indicating the critical role of MRJ-L in RSV propagation. Nevertheless, whether MRJ-L interferes with the RNA polymerase activity of RSV remains to be determined. Additionally, whether the nuclear localization property of MRJ-L is required for RSV viral production also remains puzzling (**Figure 1C**, RSV). If this were the case, it would be interesting to elucidate why an RNA virus, which completes its life cycle in the cytoplasm, requires the nuclear function(s) of MRJ-L for propagation.

Dengue Virus (DENV)

Dengue virus is a mosquito-transmitted pathogen and its infection may cause haemorrhagic fever (Brady et al., 2012; Bhatt et al., 2013). DENV is a member of the Flaviviridae family with a positive-sense single-stranded RNA genome. Viral genome replication and package solely occur in the host cytoplasm. DENV infection induces autophagy that targets cellular lipid droplets (LDs), which are endoplasmic reticulum-derived storage organelles of neutral lipids, and hence stimulates lipid metabolism (Randall, 2018). On the other hand, LDs are essential for DENV production. During virion assembly, the DENV capsid protein binds to an LD surface protein and forms the nucleocapsids with viral genomes in the endoplasmic reticulum (Samsa et al., 2009; Heaton and Randall, 2010).

HSPs participate in multiple steps in the DENV life cycle (Taguwa et al., 2015). Among them, MRJ-S is colocalized with the capsid protein on LDs and aids viral particle assembly (Taguwa et al., 2015; **Figure 1C**, DENV). Depletion of MRJ-S impairs viral RNA replication and virion production (Taguwa et al., 2015). MRJ-S with mutations in the HPD motif fails to rescue viral production in MRJ-S-depleted cells, indicating the cooperative role of MRJ-S and Hsp70 in viral particle biogenesis. Nevertheless, MRJ-L is not engaged in the process of DENV propagation (Taguwa et al., 2015).

TARGETING MRJ AS AN ANTIVIRAL STRATEGY

Antisense morpholino oligonucleotides targeting viral RNAs or host mRNAs that encode proteins essential for viral propagation have been designed for treatment of viral infection (Warren et al., 2012). For example, a splice switching morpholino oligonucleotide can restrict influenza viral replication by suppressing exon inclusion of the host *transmembrane serine protease 2 (TMPRSS2)* (Bottcher-Friebertshauser et al., 2011). In light of the findings that MRJ is involved in viral propagation, it is possible to interfere with viral infection by targeting MRJ or modulating its splice isoform expression. Depletion of *MRJ-L* by siRNAs inhibits viral life cycles of HCMV and HIV (Cheng et al., 2008; Pei et al., 2012). Our recent report shows that a morpholino oligonucleotide complementary to the 5' splice site of *MRJ* intron 8 efficiently inhibits *MRJ-L* expression *in vitro* (Ko et al., 2018). This morpholino disrupts the propagation of both pesudotyped and native HIV-1 in macrophage-like cells, and also effectively restricts subgenomic synthesis of RSV (Ko et al., 2018). It is likewise possible that masking the polyadenylation signal in intron 8 can suppress *MRJ-S* production. Since flaviviruses share a similar viral processing mechanism in LDs, it would be interesting to know whether MRJ-S-targeting agents may have a broad-spectrum antiviral effect. Since small molecule splicing modulators developed recently demonstrate their therapeutic potentials (Bates et al., 2017), it is worthy to evaluate whether any of them could influence MRJ isoform ratios, and hence impact viral infection. As described above, MRJ acts as an efficient suppressor of polyglutamine aggregation (Chuang et al., 2002). Therefore, harnessing the expression or chaperone activity of MRJ would be used for treatment of neurodegenerative disorders. Together, MRJ holds a great potential as drug targets.

CONCLUSION

It has been demonstrated that single nucleotide polymorphisms near splice sites or polyadenylation sites of MRJ affect its isoform expression ratio (Ko et al., 2018). Thus, individuals may vary their susceptibility to viral infection, cancer or other disorders. Although the chaperone activity of MRJ is likely important for protein proteostasis, particularly disease-causing proteins, it is yet unclear whether this activity is critical for its various functions in viral infection. Nevertheless, the importance of the MRJ HPD motif in supporting HIV and dengue viral production suggests that the ATPase activity of Hsp70 contributes to viral propagation. Identification of small molecule compounds that selectively target HSPs has the values in prevention and treatment of viral infection. It has been demonstrated that Hsp70 inhibitors exert substantial antiviral activities against DENV as well as other flaviviruses (Taguwa et al., 2015, 2019). Small molecules targeting different domains of Hsp90 or interfering with its cochaperone or substrate protein binding have also shown the potential in therapeutic treatment of cancer or neurodegenerative disorders (Shrestha et al., 2016). However, pharmacologically manipulating the activity of Hsp40 is not yet available. Therefore, to have a better understanding of the isoform expression and domain structure-function relations of MRJ would be important for drug design toward viral infection.

AUTHOR CONTRIBUTIONS

S-HK and W-YT designed the figures and wrote the manuscript. L-MH and W-YT edited the manuscript.

FUNDING

The authors acknowledge the funding supported by an intramural grant from the National Taiwan University to L-MH and M-RC, an NTU-Academia Sinica grant (NTU-AS-106R104514 to L-MH and W-YT), and the Ministry of Science and Technology, Taiwan (Grant 103-2314-B-002-056-MY3 to L-MH).

REFERENCES

Aprile, F. A., Kallstig, E., Limorenko, G., Vendruscolo, M., Ron, D., and Hansen, C. (2017). The molecular chaperones DNAJB6 and Hsp70 cooperate to suppress alpha-synuclein aggregation. *Sci. Rep.* 7:9039. doi: 10.1038/s41598-017-08324-z

Bakthisaran, R., Tangirala, R., Rao, and Ch, M. (2015). Small heat shock proteins: role in cellular functions and pathology. *Biochim. Biophys. Acta* 1854, 291–319. doi: 10.1016/j.bbapap.2014.12.019

Baquero-Perez, B., and Whitehouse, A. (2015). Hsp70 isoforms are essential for the formation of Kaposi's Sarcoma-associated herpesvirus replication and transcription compartments. *PLoS Pathog.* 11:e1005274. doi: 10.1371/journal.ppat.1005274

Bascos, N. A. D., Mayer, M. P., Bukau, B., and Landry, S. J. (2017). The Hsp40 J-domain modulates Hsp70 conformation and ATPase activity with a semi-elliptical spring. *Protein Sci.* 26, 1838–1851. doi: 10.1002/pro.3223

Bason, M., Meister-Broekema, M., Alberts, N., Dijkers, P., Bergink, S., Sibon, O. C. M., et al. (2019). Astrocytic expression of the chaperone DNAJB6 results in non-cell autonomous protection in Huntington's disease. *Neurobiol. Dis.* 124, 108–117. doi: 10.1016/j.nbd.2018.10.017

Bates, D. O., Morris, J. C., Oltean, S., and Donaldson, L. F. (2017). Pharmacology of modulators of alternative splicing. *Pharmacol. Rev.* 69, 63–79. doi: 10.1124/pr.115.011239

Batra, J., Tripathi, S., Kumar, A., Katz, J. M., Cox, N. J., Lal, R. B., et al. (2016). Human Heat shock protein 40 (Hsp40/DnaJB1) promotes influenza A virus replication by assisting nuclear import of viral ribonucleoproteins. *Sci. Rep.* 6:19063. doi: 10.1038/srep19063

Bhatt, S., Gething, P. W., Brady, O. J., Messina, J. P., Farlow, A. W., Moyes, C. L., et al. (2013). The global distribution and burden of dengue. *Nature* 496, 504–507. doi: 10.1038/nature12060

Binder, R. J. (2014). Functions of heat shock proteins in pathways of the innate and adaptive immune system. *J. Immunol.* 193, 5765–5771. doi: 10.4049/jimmunol.1401417

Biron, K. K. (2006). Antiviral drugs for cytomegalovirus diseases. *Antiviral Res.* 71, 154–163. doi: 10.1016/j.antiviral.2006.05.002

Bottcher-Friebertshauser, E., Stein, D. A., Klenk, H. D., and Garten, W. (2011). Inhibition of influenza virus infection in human airway cell cultures by an antisense peptide-conjugated morpholino oligomer targeting the hemagglutinin-activating protease TMPRSS2. *J. Virol.* 85, 1554–1562. doi: 10.1128/JVI.01294-10

Brady, O. J., Gething, P. W., Bhatt, S., Messina, J. P., Brownstein, J. S., Hoen, A. G., et al. (2012). Refining the global spatial limits of dengue virus transmission by evidence-based consensus. *PLoS Negl. Trop. Dis.* 6:e1760. doi: 10.1371/journal.pntd.0001760

Broere, F., Van Der Zee, R., and Van Eden, W. (2011). Heat shock proteins are no DAMPs, rather 'DAMPERs'. *Nat. Rev. Immunol.* 11:565. doi: 10.1038/nri2873-c1

Brown, G., Rixon, H. W., Steel, J., Mcdonald, T. P., Pitt, A. R., Graham, S., et al. (2005). Evidence for an association between heat shock protein 70 and the respiratory syncytial virus polymerase complex within lipid-raft membranes during virus infection. *Virology* 338, 69–80. doi: 10.1016/j.virol.2005.05.004

Cao, M., Wei, C., Zhao, L., Wang, J., Jia, Q., Wang, X., et al. (2014). DnaJA1/Hsp40 is co-opted by influenza A virus to enhance its viral RNA polymerase activity. *J. Virol.* 88, 14078–14089. doi: 10.1128/JVI.02475-14

Cheng, M. Y., Hartl, F. U., Martin, J., Pollock, R. A., Kalousek, F., Neupert, W., et al. (1989). Mitochondrial heat-shock protein hsp60 is essential for assembly of proteins imported into yeast mitochondria. *Nature* 337, 620–625. doi: 10.1038/337620a0

Cheng, X., Belshan, M., and Ratner, L. (2008). Hsp40 facilitates nuclear import of the human immunodeficiency virus type 2 Vpx-mediated preintegration complex. *J. Virol.* 82, 1229–1237. doi: 10.1128/jvi.00540-07

Chiang, Y. P., Sheng, W. H., Shao, P. L., Chi, Y. H., Chen, Y. M., Huang, S. W., et al. (2014). Large isoform of mammalian relative of DnaJ is a major determinant of human susceptibility to HIV-1 infection. *EBioMedicine* 1, 126–132. doi: 10.1016/j.ebiom.2014.10.002

Chuang, J. Z., Zhou, H., Zhu, M., Li, S. H., Li, X. J., and Sung, C. H. (2002). Characterization of a brain-enriched chaperone, MRJ, that inhibits Huntingtin aggregation and toxicity independently. *J. Biol. Chem.* 277, 19831–19838. doi: 10.1074/jbc.m109613200

Dai, Y. S., Xu, J., and Molkentin, J. D. (2005). The DnaJ-related factor Mrj interacts with nuclear factor of activated T cells c3 and mediates transcriptional repression through class II histone deacetylase recruitment. *Mol. Cell Biol.* 25, 9936–9948. doi: 10.1128/mcb.25.22.9936-9948.2005

De Bock, C. E., Lin, Z., Mekkawy, A. H., Byrne, J. A., and Wang, Y. (2010). Interaction between urokinase receptor and heat shock protein MRJ enhances cell adhesion. *Int. J. Oncol.* 36, 1155–1163.

Dey, S., Banerjee, P., and Saha, P. (2009). Cell cycle specific expression and nucleolar localization of human J-domain containing co-chaperone Mrj. *Mol. Cell Biochem.* 322, 137–142. doi: 10.1007/s11010-008-9950-y

Durrenberger, P. F., Filiou, M. D., Moran, L. B., Michael, G. J., Novoselov, S., Cheetham, M. E., et al. (2009). DnaJB6 is present in the core of Lewy bodies and is highly up-regulated in parkinsonian astrocytes. *J. Neurosci. Res.* 87, 238–245. doi: 10.1002/jnr.21819

Dutta, D., Chattopadhyay, S., Bagchi, P., Halder, U. C., Nandi, S., Mukherjee, A., et al. (2011). Active participation of cellular chaperone Hsp90 in regulating the function of rotavirus nonstructural protein 3 (NSP3). *J. Biol. Chem.* 286, 20065–20077. doi: 10.1074/jbc.m111.231878

Gonzalez, O., Fontanes, V., Raychaudhuri, S., Loo, R., Loo, J., Arumugaswami, V., et al. (2009). The heat shock protein inhibitor Quercetin attenuates hepatitis C virus production. *Hepatology* 50, 1756–1764. doi: 10.1002/hep.23232

Gurer, C., Hoglund, A., Hoglund, S., and Luban, J. (2005). ATPgammaS disrupts human immunodeficiency virus type 1 virion core integrity. *J. Virol.* 79, 5557–5567. doi: 10.1128/jvi.79.9.5557-5567.2005

Hageman, J., Rujano, M. A., Van Waarde, M. A., Kakkar, V., Dirks, R. P., Govorukhina, N., et al. (2010). A DNAJB chaperone subfamily with HDAC-dependent activities suppresses toxic protein aggregation. *Mol. Cell* 37, 355–369. doi: 10.1016/j.molcel.2010.01.001

Hanai, R., and Mashima, K. (2003). Characterization of two isoforms of a human DnaJ homologue. HSJ2. *Mol. Biol. Rep.* 30, 149–153.

Harms, M. B., Sommerville, R. B., Allred, P., Bell, S., Ma, D., Cooper, P., et al. (2012). Exome sequencing reveals DNAJB6 mutations in dominantly-inherited myopathy. *Ann. Neurol.* 71, 407–416. doi: 10.1002/ana.22683

Hauet-Broere, F., Wieten, L., Guichelaar, T., Berlo, S., Van Der Zee, R., and Van Eden, W. (2006). Heat shock proteins induce T cell regulation of chronic inflammation. *Ann. Rheum. Dis.* 65(Suppl. 3), iii65–iii68. doi: 10.1136/ard.2006.058495

Heaton, N. S., Moshkina, N., Fenouil, R., Gardner, T. J., Aguirre, S., Shah, P. S., et al. (2016). Targeting viral proteostasis limits influenza virus, hiv, and dengue virus infection. *Immunity* 44, 46–58. doi: 10.1016/j.immuni.2015.12.017

Heaton, N. S., and Randall, G. (2010). Dengue virus-induced autophagy regulates lipid metabolism. *Cell Host Microbe* 8, 422–432. doi: 10.1016/j.chom.2010.10.006

Hipp, M. S., Kasturi, P., and Hartl, F. U. (2019). The proteostasis network and its decline in ageing. *Nat. Rev. Mol. Cell Biol.* 20, 421–435. doi: 10.1038/s41580-019-0101-y

Hunter, P. J., Swanson, B. J., Haendel, M. A., Lyons, G. E., and Cross, J. C. (1999). Mrj encodes a DnaJ-related co-chaperone that is essential for murine placental development. *Development* 126, 1247–1258.

Iordanskiy, S., Zhao, Y., Dimarzio, P., Agostini, I., Dubrovsky, L., and Bukrinsky, M. (2004). Heat-shock protein 70 exerts opposing effects on Vpr-dependent and Vpr-independent HIV-1 replication in macrophages. *Blood* 104, 1867–1872. doi: 10.1182/blood-2004-01-0081

Izawa, I., Nishizawa, M., Ohtakara, K., Ohtsuka, K., Inada, H., and Inagaki, M. (2000). Identification of Mrj, a DnaJ/Hsp40 family protein, as a keratin 8/18 filament regulatory protein. *J. Biol. Chem.* 275, 34521–34527. doi: 10.1074/jbc.m003492200

Jee, H. (2016). Size dependent classification of heat shock proteins: a mini-review. *J. Exerc. Rehabil.* 12, 255–259. doi: 10.12965/jer.1632642.321

Jonson, P. H., Palmio, J., Johari, M., Penttila, S., Evila, A., Nelson, I., et al. (2018). Novel mutations in DNAJB6 cause LGMD1D and distal myopathy in French families. *Eur. J. Neurol.* 25, 790–794. doi: 10.1111/ene.13598

Kakkar, V., Mansson, C., De Mattos, E. P., Bergink, S., Van Der Zwaag, M., Van Waarde, M., et al. (2016). The S/T-Rich motif in the DNAJB6 chaperone delays polyglutamine aggregation and the onset of disease in a mouse model. *Mol. Cell* 62, 272–283. doi: 10.1016/j.molcel.2016.03.017

Kampinga, H. H., and Craig, E. A. (2010). The HSP70 chaperone machinery: J proteins as drivers of functional specificity. *Nat. Rev. Mol. Cell Biol.* 11, 579–592. doi: 10.1038/nrm2941

Katoh, H., Kubota, T., Kita, S., Nakatsu, Y., Aoki, N., Mori, Y., et al. (2015). Heat shock protein 70 regulates degradation of the mumps virus phosphoprotein via the ubiquitin-proteasome pathway. *J. Virol.* 89, 3188–3199. doi: 10.1128/JVI.03343-14

Katoh, H., Kubota, T., Nakatsu, Y., Tahara, M., Kidokoro, M., and Takeda, M. (2017). Heat shock protein 90 ensures efficient mumps virus replication by assisting with viral polymerase complex formation. *J. Virol.* 91:e02220. doi: 10.1128/JVI.02220-16

Kenneson, A., and Cannon, M. J. (2007). Review and meta-analysis of the epidemiology of congenital cytomegalovirus (CMV) infection. *Rev. Med. Virol.* 17, 253–276. doi: 10.1002/rmv.535

Ko, S. H., Liau, Y. J., Chi, Y. H., Lai, M. J., Chiang, Y. P., Lu, C. Y., et al. (2018). Interference of DNAJB6/MRJ isoform switch by morpholino inhibits replication of HIV-1 and RSV. *Mol. Ther. Nucleic Acids* 14, 251–261. doi: 10.1016/j.omtn.2018.12.001

Kumar, M., Rawat, P., Khan, S. Z., Dhamija, N., Chaudhary, P., Ravi, D. S., et al. (2011). Reciprocal regulation of human immunodeficiency virus-1 gene expression and replication by heat shock proteins 40 and 70. *J. Mol. Biol.* 410, 944–958. doi: 10.1016/j.jmb.2011.04.005

Kwon, Y. S., Park, S. H., Kim, M. A., Kim, H. J., Park, J. S., Lee, M. Y., et al. (2017). Risk of mortality associated with respiratory syncytial virus and influenza infection in adults. *BMC Infect. Dis.* 17:785. doi: 10.1186/s12879-017-2897-4

Langer, T., Lu, C., Echols, H., Flanagan, J., Hayer, M. K., and Hartl, F. U. (1992). Successive action of DnaK, DnaJ and GroEL along the pathway of chaperone-mediated protein folding. *Nature* 356, 683–689. doi: 10.1038/356683a0

Lee, S., Fan, C. Y., Younger, J. M., Ren, H., and Cyr, D. M. (2002). Identification of essential residues in the type II Hsp40 Sis1 that function in polypeptide binding. *J. Biol. Chem.* 277, 21675–21682. doi: 10.1074/jbc.m111075200

Li, J., Qian, X., and Sha, B. (2009). Heat shock protein 40: structural studies and their functional implications. *Protein Pept. Lett.* 16, 606–612. doi: 10.2174/092986609788490159

Li, S., Zhang, P., Freibaum, B. D., Kim, N. C., Kolaitis, R. M., Molliex, A., et al. (2016). Genetic interaction of hnRNPA2B1 and DNAJB6 in a Drosophila model of multisystem proteinopathy. *Hum. Mol. Genet.* 25, 936–950. doi: 10.1093/hmg/ddv627

Lin, Y., Peng, N., Zhuang, H., Zhang, D., Wang, Y., and Hua, Z. C. (2014). Heat shock proteins HSP70 and MRJ cooperatively regulate cell adhesion and migration through urokinase receptor. *BMC Cancer* 14:639. doi: 10.1186/1471-2407-14-639

Maartens, G., Celum, C., and Lewin, S. R. (2014). HIV infection: epidemiology, pathogenesis, treatment, and prevention. *Lancet* 384, 258–271. doi: 10.1016/s0140-6736(14)60164-1

Mansson, C., Van Cruchten, R. T. P., Weininger, U., Yang, X., Cukalevski, R., Arosio, P., et al. (2018). Conserved S/T residues of the human chaperone DNAJB6 are required for effective inhibition of abeta42 amyloid fibril formation. *Biochemistry* 57, 4891–4902. doi: 10.1021/acs.biochem.8b00353

McMahon, T. P., and Anders, D. G. (2002). Interactions between human cytomegalovirus helicase-primase proteins. *Virus Res.* 86, 39–52. doi: 10.1016/s0168-1702(02)00054-0

Meacham, G. C., Lu, Z., King, S., Sorscher, E., Tousson, A., and Cyr, D. M. (1999). The Hdj-2/Hsc70 chaperone pair facilitates early steps in CFTR biogenesis. *EMBO J.* 18, 1492–1505. doi: 10.1093/emboj/18.6.1492

Meng, E., Shevde, L. A., and Samant, R. S. (2016). Emerging roles and underlying molecular mechanisms of DNAJB6 in cancer. *Oncotarget* 7, 53984–53996. doi: 10.18632/oncotarget.9803

Moir, S., Chun, T. W., and Fauci, A. S. (2011). Pathogenic mechanisms of HIV disease. *Annu. Rev. Pathol.* 6, 223–248. doi: 10.1146/annurev-pathol-011110-130254

Momose, F., Naito, T., Yano, K., Sugimoto, S., Morikawa, Y., and Nagata, K. (2002). Identification of Hsp90 as a stimulatory host factor involved in influenza virus RNA synthesis. *J. Biol. Chem.* 277, 45306–45314. doi: 10.1074/jbc.m206822200

Naito, T., Momose, F., Kawaguchi, A., and Nagata, K. (2007). Involvement of Hsp90 in assembly and nuclear import of influenza virus RNA polymerase subunits. *J. Virol.* 81, 1339–1349. doi: 10.1128/jvi.01917-06

Neckers, L., and Tatu, U. (2008). Molecular chaperones in pathogen virulence: emerging new targets for therapy. *Cell Host Microbe* 4, 519–527. doi: 10.1016/j.chom.2008.10.011

Noton, S. L., Tremaglio, C. Z., and Fearns, R. (2019). Killing two birds with one stone: how the respiratory syncytial virus polymerase initiates transcription and replication. *PLoS Pathog.* 15:e1007548. doi: 10.1371/journal.ppat.1007548

Palmio, J., Jonson, P. H., Evila, A., Auranen, M., Straub, V., Bushby, K., et al. (2015). Novel mutations in DNAJB6 gene cause a very severe early-onset limb-girdle muscular dystrophy 1D disease. *Neuromuscul. Disord.* 25, 835–842. doi: 10.1016/j.nmd.2015.07.014

Park, S. G., Lim, S. O., and Jung, G. (2002). Binding site analysis of human HBV pol for molecular chaperonin, hsp60. *Virology* 298, 116–123. doi: 10.1006/viro.2002.1496

Pei, Y., Fu, W., Yang, E., Shen, A., Chen, Y. C., Gong, H., et al. (2012). A Hsp40 chaperone protein interacts with and modulates the cellular distribution of the primase protein of human cytomegalovirus. *PLoS Pathog.* 8:e1002968. doi: 10.1371/journal.ppat.1002968

Pirrone, V., Mell, J., Janto, B., and Wigdahl, B. (2014). Biomarkers of HIV susceptibility and disease progression. *EBioMedicine* 1, 99–100. doi: 10.1016/j.ebiom.2014.11.003

Qiu, X. B., Shao, Y. M., Miao, S., and Wang, L. (2006). The diversity of the DnaJ/Hsp40 family, the crucial partners for Hsp70 chaperones. *Cell Mol. Life Sci.* 63, 2560–2570. doi: 10.1007/s00018-006-6192-6

Radhakrishnan, A., Yeo, D., Brown, G., Myaing, M. Z., Iyer, L. R., Fleck, R., et al. (2010). Protein analysis of purified respiratory syncytial virus particles reveals an important role for heat shock protein 90 in virus particle assembly. *Mol. Cell Proteomics* 9, 1829–1848. doi: 10.1074/mcp.M110.001651

Randall, G. (2018). Lipid droplet metabolism during dengue virus infection. *Trends Microbiol.* 26, 640–642. doi: 10.1016/j.tim.2018.05.010

Rosas-Salvans, M., Scrofani, J., Modol, A., and Vernos, I. (2019). DnaJB6 is a RanGTP-regulated protein required for microtubule organization during mitosis. *J. Cell Sci.* 132:jcs227033. doi: 10.1242/jcs.227033

Samsa, M. M., Mondotte, J. A., Iglesias, N. G., Assuncao-Miranda, I., Barbosa-Lima, G., Da Poian, A. T., et al. (2009). Dengue virus capsid protein usurps lipid droplets for viral particle formation. *PLoS Pathog.* 5:e1000632. doi: 10.1371/journal.ppat.1000632

Sandell, S., Huovinen, S., Palmio, J., Raheem, O., Lindfors, M., Zhao, F., et al. (2016). Diagnostically important muscle pathology in DNAJB6 mutated LGMD1D. *Acta Neuropathol. Commun.* 4:9. doi: 10.1186/s40478-016-0276-9

Santoro, M. G., Amici, C., and Rossi, A. (2009). "Role of hear shock proteins in viral infection," in *Prokaryotic and Eukaryotic Heat Shock Proteins in Infectious Disease Heat Shock Proteins*, Vol. 4, eds A. G. Pockley, S. K. Calderwood, and M. G. Santoro, (Springer), 51–84. doi: 10.1007/978-90-481-2976-8_3

Sarparanta, J., Jonson, P. H., Golzio, C., Sandell, S., Luque, H., Screen, M., et al. (2012). Mutations affecting the cytoplasmic functions of the co-chaperone DNAJB6 cause limb-girdle muscular dystrophy. *Nat. Genet.* 44, S451–S452. doi: 10.1038/ng.1103

Sato, T., Hayashi, Y. K., Oya, Y., Kondo, T., Sugie, K., Kaneda, D., et al. (2013). DNAJB6 myopathy in an Asian cohort and cytoplasmic/nuclear inclusions. *Neuromuscul. Disord.* 23, 269–276. doi: 10.1016/j.nmd.2012.12.010

Sharp, P. M., and Hahn, B. H. (2011). Origins of HIV and the AIDS pandemic. *Cold Spring Harb. Perspect. Med.* 1:a006841. doi: 10.1101/cshperspect.a006841

Shrestha, L., Bolaender, A., Patel, H. J., and Taldone, T. (2016). Heat shock protein (HSP) drug discovery and development: targeting heat shock proteins in disease. *Curr. Top. Med. Chem.* 16, 2753–2764. doi: 10.2174/1568026616666160413141911

Sohn, S. Y., Kim, S. B., Kim, J., and Ahn, B. Y. (2006). Negative regulation of hepatitis B virus replication by cellular Hsp40/DnaJ proteins through destabilization of viral core and X proteins. *J. Gen. Virol.* 87, 1883–1891. doi: 10.1099/vir.0.81684-0

Summers, D. W., Douglas, P. M., Ramos, C. H., and Cyr, D. M. (2009). Polypeptide transfer from Hsp40 to Hsp70 molecular chaperones. *Trends Biochem Sci* 34, 230–233. doi: 10.1016/j.tibs.2008.12.009

Taguwa, S., Maringer, K., Li, X., Bernal-Rubio, D., Rauch, J. N., Gestwicki, J. E., et al. (2015). Defining Hsp70 subnetworks in dengue virus replication reveals key vulnerability in flavivirus infection. *Cell* 163, 1108–1123. doi: 10.1016/j.cell.2015.10.046

Taguwa, S., Yeh, M. T., Rainbolt, T. K., Nayak, A., Shao, H., Gestwicki, J. E., et al. (2019). Zika virus dependence on host Hsp70 provides a protective strategy against infection and disease. *Cell Rep.* 26:e903. doi: 10.1016/j.celrep.2018.12.095

Tamaki, Y., Shodai, A., Morimura, T., Hikiami, R., Minamiyama, S., Ayaki, T., et al. (2018). Elimination of TDP-43 inclusions linked to amyotrophic lateral sclerosis by a misfolding-specific intrabody with dual proteolytic signals. *Sci. Rep.* 8:6030. doi: 10.1038/s41598-018-24463-3

Tanaka, Y., Kanai, F., Kawakami, T., Tateishi, K., Ijichi, H., Kawabe, T., et al. (2004). Interaction of the hepatitis B virus X protein (HBx) with heat shock protein 60 enhances HBx-mediated apoptosis. *Biochem. Biophys. Res. Commun.* 318, 461–469. doi: 10.1016/j.bbrc.2004.04.046

Tien, J. F., Mazloomian, A., Cheng, S. G., Hughes, C. S., Chow, C. C. T., Canapi, L. T., et al. (2017). CDK12 regulates alternative last exon mRNA splicing and promotes breast cancer cell invasion. *Nucleic Acids Res.* 45, 6698–6716. doi: 10.1093/nar/gkx187

Ujino, S., Yamaguchi, S., Shimotohno, K., and Takaku, H. (2009). Heat-shock protein 90 is essential for stabilization of the hepatitis C virus nonstructural protein NS3. *J. Biol. Chem.* 284, 6841–6846. doi: 10.1074/jbc.M806452200

Urano, E., Morikawa, Y., and Komano, J. (2013). Novel role of HSP40/DNAJ in the regulation of HIV-1 replication. *J. Acquir. Immune Defic. Syndr.* 64, 154–162. doi: 10.1097/QAI.0b013e31829a2ef8

Wandinger, S. K., Richter, K., and Buchner, J. (2008). The Hsp90 chaperone machinery. *J. Biol. Chem.* 283, 18473–18477. doi: 10.1074/jbc.r800007200

Warren, T. K., Shurtleff, A. C., and Bavari, S. (2012). Advanced morpholino oligomers: a novel approach to antiviral therapy. *Antiviral Res.* 94, 80–88. doi: 10.1016/j.antiviral.2012.02.004

Watson, E. D., Hughes, M., Simmons, D. G., Natale, D. R., Sutherland, A. E., and Cross, J. C. (2011). Cell-cell adhesion defects in Mrj mutant trophoblast cells are associated with failure to pattern the chorion during early placental development. *Dev. Dyn.* 240, 2505–2519. doi: 10.1002/dvdy.22755

Watson, E. D., Mattar, P., Schuurmans, C., and Cross, J. C. (2009). Neural stem cell self-renewal requires the Mrj co-chaperone. *Dev. Dyn.* 238, 2564–2574. doi: 10.1002/dvdy.22088

Whitley, D., Goldberg, S. P., and Jordan, W. D. (1999). Heat shock proteins: a review of the molecular chaperones. *J. Vasc. Surg.* 29, 748–751.

Yao, C., Biesinger, J., Wan, J., Weng, L., Xing, Y., Xie, X., et al. (2012). Transcriptome-wide analyses of CstF64-RNA interactions in global regulation of mRNA alternative polyadenylation. *Proc. Natl. Acad. Sci. U.S.A.* 109, 18773–18778. doi: 10.1073/pnas.1211101109

Zhang, S. M., Sun, D. C., Lou, S., Bo, X. C., Lu, Z., Qian, X. H., et al. (2005). HBx protein of hepatitis B virus (HBV) can form complex with mitochondrial HSP60 and HSP70. *Arch. Virol.* 150, 1579–1590. doi: 10.1007/s00705-005-0521-1

Conflict of Interest: The authors declare that the research was conducted in the absence of any commercial or financial relationships that could be construed as a potential conflict of interest.

Copyright © 2019 Ko, Huang and Tarn. This is an open-access article distributed under the terms of the Creative Commons Attribution License (CC BY). The use, distribution or reproduction in other forums is permitted, provided the original author(s) and the copyright owner(s) are credited and that the original publication in this journal is cited, in accordance with accepted academic practice. No use, distribution or reproduction is permitted which does not comply with these terms.

frontiers in Microbiology

ORIGINAL RESEARCH
published: 13 December 2019
doi: 10.3389/fmicb.2019.02879

Epstein-Barr Virus Nuclear Antigen 1 Recruits Cyclophilin A to Facilitate the Replication of Viral DNA Genome

Shuyu Xin[1,2†], Shujuan Du[1,2†], Lingzhi Liu[1,2], Yan Xie[1,2], Lielian Zuo[1], Jing Yang[1], Jingjin Hu[2], Wenxing Yue[1,2], Jing Zhang[1,2], Pengfei Cao[1,2], Fanxiu Zhu[1,3] and Jianhong Lu[1,2]*

[1] NHC Key Laboratory of Carcinogenesis, The Key Laboratory of Carcinogenesis and Cancer Invasion of the Chinese Ministry of Education, Department of Hematology, Xiangya Hospital, Central South University, Changsha, China,
[2] Department of Medical Microbiology, School of Basic Medical Science, Central South University, Changsha, China,
[3] Department of Biological Sciences, Florida State University, Tallahassee, FL, United States

Epstein-Barr virus (EBV) nuclear antigen 1 (EBNA1)-mediated DNA episomal genome replication and persistence are essential for the viral pathogenesis. Cyclophilin A (CYPA) is upregulated in EBV-associated nasopharyngeal carcinoma (NPC) with unknown roles. In the present approach, cytosolic CYPA was found to be bound with EBNA1 into the nucleus. The amino acid 376-459 of the EBNA1 domain was important for the binding. CYPA depletion attenuated and ectopic CYPA expression improved EBNA1 expression in EBV-positive cells. The loss of viral copy number was also accelerated by CYPA consumption in daughter cells during culture passages. Mechanistically, CYPA mediated the connection of EBNA1 with oriP (origin of EBV DNA replication) and subsequent oriP transcription, which is a key step for the initiation of EBV genome replication. Moreover, CYPA overexpression markedly antagonized the connection of EBNA1 to Ubiquitin-specific protease 7 (USP7), which is a strong host barrier with a role of inhibiting EBV genome replication. The PPIase activity of CYPA was required for the promotion of oriP transcription and antagonism with USP7. The results revealed a strategy that EBV recruited a host factor to counteract the host defense, thus facilitating its own latent genome replication. This study provides a new insight into EBV pathogenesis and potential virus-targeted therapeutics in EBV-associated NPC, in which CYPA is upregulated at all stages.

Keywords: Epstein-Barr virus nuclear antigen 1, latent genome, cyclophilin A, replication, persistence, pathogenesis

OPEN ACCESS

Edited by:
Zhengli Shi,
Wuhan Institute of Virology (CAS), China

Reviewed by:
Takayuki Murata,
Fujita Health University, Japan
Mu-Sheng Zeng,
Sun Yat-sen University, China

***Correspondence:**
Jianhong Lu
jianhlu@csu.edu.cn

† These authors have contributed equally to this work

Specialty section:
This article was submitted to Virology, a section of the journal Frontiers in Microbiology

Received: *06 August 2019*
Accepted: *28 November 2019*
Published: *13 December 2019*

Citation:
Xin S, Du S, Liu L, Xie Y, Zuo L, Yang J, Hu J, Yue W, Zhang J, Cao P, Zhu F and Lu J (2019) Epstein-Barr Virus Nuclear Antigen 1 Recruits Cyclophilin A to Facilitate the Replication of Viral DNA Genome. Front. Microbiol. 10:2879. doi: 10.3389/fmicb.2019.02879

INTRODUCTION

Epstein-Barr virus (EBV) is a member of the gamma herpesviruses and was the first confirmed human tumor virus (Ding et al., 2013; Lu et al., 2017). EBV ubiquitously infects more than 90% of the global population and is closely associated with the development of several malignancies, including Burkitt's lymphoma and nasopharyngeal carcinoma (NPC) (Shair et al., 2008; Yu et al., 2012; Young, 2014; Young and Dawson, 2014; Liu et al., 2017). NPC, which is primarily of epithelial origin, is a type of metastatic head-and-neck neoplasm that is highly prevalent in southern China and some other areas in East Asia and Africa (Tang et al., 2016; Tu et al., 2017; Jiang et al., 2018).

EBV is able to establish life-long persistence in the human host (Young and Murray, 2003; Zuo L. et al., 2017). It contains a large genome approximately 172 kb in size and has two phases in its life cycle (the latent and lytic stages) (Yu et al., 2011; Hammerschmidt and Sugden, 2013). EBV mainly spreads through the saliva of human host, infects B cells through the oral mucosal epithelium, and then transforms B lymphocytes into resting memory B cells through a series of viral latent transcription programs, thus establishing a lifelong latent infection pattern (Thorley-Lawson et al., 2013). The majority of EBV infections *in vivo* are latent (Thorley-Lawson, 2015). During EBV latency, the EBV genome exists in the form of episome DNA, few viral genes are expressed, and no virion is produced. EBV nuclear antigen 1 (EBNA1) is the only viral protein that is expressed in all types of EBV-associated tumors (Lu et al., 2010; Tao et al., 2015). Determining how EBV is able to maintain its stable latent status in host cells is a topic of interest, because it may provide understanding about the pathogenesis of EBV and new targets to inhibit the persistence of EBV genome in the therapy of EBV-associated cancers. EBV replication is under the control of some host and viral factors that are not fully understood. EBNA1 plays a key role in the replication and mitotic segregation of EBV DNA episomes to daughter cells (Yates and Guan, 1991; Frappier, 2012b). EBNA1-mediated S-phase episome replication depends on binding of EBNA1 to the EBV origin of genome replication (oriP) (Reisman et al., 1985). Viruses are obligate intracellular parasites, and their replication cycles depend on some host cell factors. For example, some studies suggested that cellular origin recognition complex (ORC) and minichromosome maintenance (MCM) complex are related to the DS element of oriP, implicating them in the initiation of EBV DNA replication (Frappier, 2012a; Capone et al., 2015). These host factors may also be potential targets for antiviral therapy.

Cyclophilin A (CYPA) is a protein with multiple functions as a typical member of the cellular peptidyl-prolyl *cis-trans* isomerase (PPIase) family (Braaten et al., 1996; Bahmed et al., 2012). CYPA was discovered initially as an intracellular receptor of the immunosuppressive drug cyclosporin A (CsA) (Braaten et al., 1996; Bahmed et al., 2012). Studies have shown that CYPA can use IL-6 to induce cell signal conversion, activate tyrosine phosphorylation and nuclear transport of transcription factor 3, and can bind and activate NF-κB (Tang et al., 2015). CYPA is involved in the life cycles of multiple viruses and plays a critical role in their successful infectivity and replication, including human immunodeficiency virus type 1 (HIV-1), hepatitis C virus (HCV), hepatitis B virus (HBV), vesicular stomatitis virus (VSV), vaccinia virus (VV), coronaviruses (CoVs), and feline coronavirus (Bose et al., 2003; Naoumov, 2014; Jyothi et al., 2015; Phillips et al., 2015). The interaction between CYPA and HIV protein promotes the replication and infection of HIV particles; CD147 is the main signal receptor of CYPA, and the two interact to regulate the early steps of HIV replication (Ciesek et al., 2009; Tang et al., 2015). Conversely, CYPA suppresses the replication of some viruses, such as rotavirus, infectious bursal disease virus and influenza virus (Xu et al., 2010; Liu et al., 2012). However, the role and mechanism of CYPA in the function of EBV remain unknown. Our laboratory previously performed a proteomics study using NPC tissues and found that CYPA was upregulated from the early stages of NPC (atypical hyperplasia and stage I) to the malignancy stages (Yang et al., 2014). Since EBV infection also occurs during the early stage of NPC (Morrison et al., 2004), we speculated that a potential relationship might exist between CYPA and EBV, which initiated the present approach. Recently, we have reported that the exosomal CYPA level in NPC is positively related that of exosomal latent membrane protein 1, which is another latent protein of EBV. The result suggests a relationship between CYPA and EBV (Liu et al., 2019).

Ubiquitin-specific protease 7 (USP7) is a type of deubiquitinase that is also known as herpesvirus-associated ubiquitin specific protease (HAUSP) and has been documented as a host factor that inhibits EBV replication (Holowaty et al., 2003a). The USP7-EBNA1 interaction was selectively disrupted by deletion of EBNA1 residues 395–450 just upstream of the DNA binding domain, and the resulting EBNA1 mutant exhibited significantly increased DNA replication activity (Holowaty et al., 2003b). USP7 also plays a role in the replication inhibition of Kaposi's sarcoma-associated herpesvirus (KSHV) by interacting with the latency-associated nuclear antigen 1 (LANA), which is the homology of EBNA1 (Jager et al., 2012). As it is known, KSHV also persists in infected cells mainly in a latent state, and LANA, is expressed in all latently KSHV-infected cells (Rainbow et al., 1997). However, the mechanism by which EBV overcomes host suppression to maintain its own pathogenesis remains to be investigated.

Here, we demonstrate that EBNA1 binds to and recruits CYPA to the nucleus to support the function of EBNA1 in the replication of the viral latent genome. CYPA overexpression could antagonize the host barrier, USP7. The results revealed a strategy that EBV recruited one host factor to counteract another, thus favoring the viral DNA replication and persistence in latent infection. The study provides novel insights into understanding EBV pathogenesis in epithelial cells.

MATERIALS AND METHODS

Cell Lines and Plasmids

The p2089 plasmid (Maxi-EBV), which contains the complete EBV genome of the B95–8 strain, was kindly provided by Dr. W Hammerschmidt (Delecluse et al., 1998). The human embryonic kidney HEK293 cell line (HEK293) was originally obtained from ATCC and was used to establish latent infection of the whole EBV genome (p2089) by using hygromycin for the screening, resulting in the C2089 cell line that was previously described by our group (Zuo et al., 2015). Subsequently, the cells were divided into groups of shRNA (using pRNAT-U6.1-shRNA-CYPA treated cells), the NC shRNA group (pRNAT-U6.1-shRNA treated cells CYPA NC), Liposomal transfected cells are based on Lipofectamine 3000 transfection reagent (Invitrogen-Thermo Fisher; United States). The day after transfection, cells were treated with G418 was added (Sigma-Merck; Germany) for cell selection. Cells were subcultured every 2 days. The cells were grown in Dulbecco's modified Eagle's medium (DMEM; Sigma) supplemented with 10%

FCS. The C666-1 cell line is an EBV-positive NPC cell line (Zuo L.L. et al., 2017).

All recombinant plasmids used for bimolecular fluorescence complementation (BiMC) were constructed using standard cloning techniques according to the schematic diagram (**Supplementary Figure S1**) by using the pCAGGS vector, which is a gift from Dr. Harty (Lu et al., 2013). CYPA and CYPB were amplified from 93 cells by RT-PCR. CYPA or CYPB gene was fused with the N-terminal fragment of the yellow fluorescent protein (YFP), constructing the plasmids of pCAGGS-Flag-CYPA-NY (CYPA-NY) and pCAGGS-Flag-CYPB-NY (CYPB-NY), respectively. The EBNA1 protein was expressed as a fusion protein with the C-terminal fragment of (YFP), constructing the plasmid pCAGGS-Myc-EBNA1-CY (EBNA1-CY). The expression plasmids pCAGGS-Flag-CYPA and pCAGGS-Flag-CYPB were also constructed respectively. The Myc tag sequence was added to the N-terminal of EBNA1. Myc-tagged EBNA1 was generated by cloning into the *Sph*I and *Nhe*I sites of the pCAGGS vector to produce the pCAGGS-Myc-EBNA1 plasmid. The truncations EBNA1 (NT, 1-90) and EBNA1 (607-641) were generated by PCR based on the plasmid pCAGGS-Myc-EBNA1 using the primers listed in **Supplementary Table S1**. The EBNA1 deletion mutants EBNA1 (NT, 90-376), EBNA1 (376-459) and EBNA1 (459-607) were generated by inverse PCR. For example, primer complementary to 243–67 bp (anti-sense) and 1129–1156 bp (sense) of EBNA1 were used for amplification, and the resulting PCR.

product was gel-purified and self-ligated, resulting in EBNA1 (Δaa 90-376). Then a *Sph*I-*Nhe*I fragment from EBNA1 (Δaa 90-376) was inserted into the *Sph*I and *Nhe*I sites of the pCAGGS-Myc-EBNA1 to produce the pCAGGS-Myc-EBNA1 (Δaa 90-376).

The oriP-SV40-Luc expression vector was obtained by introducing the flanking sequence of oriP amplified from the pc3-oriP plasmid, which was a gift from Prof. Frappier (Sivachandran et al., 2011). The oriP sequence was cloned into the *Sac*I and *Xho*I sites of the luciferase reporter vector, PGL3-enhancer.

RT and Real-Time Quantitative PCR (RT-qPCR)

The RT-qPCR was performed as previously described (Yu et al., 2012). Briefly, total RNA was isolated from cells using the TRIzol reagent (Invitrogen). First, TRIzol was added to lyse the cells, then 1/5 volume of chloroform was added to the lysate to separate the DNA, protein and RNA, followed by the isopropanol and 75% absolute ethanol to precipitate the RNA. For RT, 1 μg of RNA was reversely transcribed into cDNA using the One-Step gDNA Removal and cDNA Synthesis SuperMix kit (TransGen Biotech, Beijing, China). Real-time quantitative PCR (RT-qPCR) was then performed by using the kit of *TransStart*® Top Green qPCR SuperMix (TransGen Biotech, Beijing, China) according to the manufacturer's instructions. The following program was used for the RT reaction: 65°C for 5 min, ice for 2 min, followed by 42°C for 15 min and then 85°C for 5 s. The CFX Multicolor Detection System (Bio-Rad) was employed for the detection. Primers for RNA detection by qRT-PCR were designed based on RNA sequences, and bate-actin was used as an endogenous control. The following procedure was used for the RT-qPCR: 95°C for 3 min, followed by 40 cycles of 95°C for 12 s and 62°C for 35 s. Data obtained by the conventional method of calculating comparative method $2^{(-\Delta\Delta ct)}$. Repeated three times for each sample in parallel in each experiment, and the results were expressed as the mean of three independent experiments. The sequences of the qRT-PCR primers are provided in **Supplementary Table S1**.

Western Blotting Analysis

Western blotting (WB) was performed using a standard protocol as described previously (Zuo L.L. et al., 2017). cells was lysed in RIPA (50 mM Tris, pH 7.4, 150 mM NaCl, 1% NP-40, 0.5% sodium deoxycholate, 0.1% SDS, sodium orthovanadate, sodium fluoride, EDTA, leupeptin) followed by incubation on ice for 30 min, protein quantification according to the specification of BCA kit (Beyotime, Shanghai, China). The cells lysates were centrifuged at 12000 × *g* for 20 min at 4°C. Supernatant fractions were used for detection. Samples with equivalent amounts of denatured protein were separated using 10% SDS polyacrylamide gels (Epizyme, Shanghai, China). After electrophoretic separation, the proteins were transferred to a polyvinylidene difluoride (PVDF) membrane (Millipore, Danvers, MA, United States). The membrane was blocked with 5% skimmed milk for 1 h at room temperature, followed by an overnight incubation with the primary antibody at 4°C. After washing three times, the membrane was incubated with a secondary antibody for 1 h at 37°C. Finally, the proteins of interest were detected using the Luminata Crescendo HRP Substrate (Millipore) and viewed with the ChemiDoc XRS + Molecular Imager (Bio-Rad). The results were analyzed using the Image Lab software (Bio-Rad).

The following antibodies were used for the immune detection: anti-EBNA1 (Santa Cruz Biotech, DE, United States, sc-81579), anti-CYPA (Proteintech, Chicago, IL, United States, 10720-1-AP), anti-C-Myc (Sigma, St. Louis, MO, United States, C3956), and anti-Flag (Sigma, H9658). GAPDH (Proteintech, Chicago, IL, United States, 10494-I-AP) and bate-actin (Proteintech, Chicago, IL, United States, 66009-I-Ig) were used as the loading controls. The secondary antibodies used for WB and IF were as follows: HRP-conjugated anti-rabbit (CST, Chicago, IL, United States, #7074P2), HRP-conjugated anti-mouse (GE Healthcare, United Kingdom, NA931V) and Alexa Fluor 488 donkey anti–rabbit IgG (Life technologies, United States, 1480770).

Cell Counting Kit-8 Assay

C2089 cells were plated in a 96-well plate at a density of 1×10^3 cells per well. The next day, different CsA concentrations as indicated were applied for treatment. At 24, 48 and 72 h post-treatment, the Cell Counting Kit-8 (CCK8) was used to test cell viability according to the manufacturer's instructions. The absorbance was detected at the 450 nm wavelength using a microplate reader.

Cyclosporin A (CsA) Treatment

Cyclosporin A (Dalian Meilun, China) is a type of immunosuppressive preparation that targets CYPA (Chatterji et al., 2009). The drug was dissolved in dimethyl sulfoxide (DMSO). EBV-positive cells were cultured in medium containing 40 μM of CsA. After 48 h of treatment, the cellular proteins and total RNA were extracted and subjected to detection.

Bimolecular Fluorescence Complementation (BiMC) Assay

Bimolecular fluorescence complementation assay was performed as described previously (Liu et al., 2011; Lu et al., 2013, 2014). The schematic diagram of BiMC assay is shown in **Supplementary Figure S1**. In brief, human HEK293T cells were grown on coverslips in six-well plates. The pCAGGS-Myc-EBNA1-CY plasmid or the mutant constructs and the pCAGGS-Flag-CYPB-NY plasmid were cotransfected into the cells using the Lipofectamine 3000 transfection reagent (Invitrogen) according to the manufacturer's instructions. Approximately 0.25 μg of each plasmid was used for the transfection. Transfection of a single plasmid for each used in BiMC assay was performed as a negative control. After 24 h, the cells were gently washed for three times with PBS and fixed with cold 4% paraformaldehyde for 30 min at room temperature. Then, the cells were washed and subsequently stained with Hoechst 33342 (Sigma) for 3 min at room temperature. Finally, the cells were washed again, and the slides were observed for the specific YFP signal under a fluorescence microscope.

Co-immunoprecipitation (co-IP)

A typical co-IP procedure was performed as described (Liu et al., 2011; Lu et al., 2013, 2014). Cell lysates were harvested directly or at 48 h post-transfection as indicated. The lysed sample was centrifuged at 13,000 rpm for 20 min at 4°C. The supernatant lysates of about 1 mg were incubated with a primary antibody, such as an anti-Flag monoclonal antibody (mAb) (H9658, Sigma, 1:100) or anti-mouse IgG antibody (control) (sc-0025, Santa Cruz, 1:200), for 10 h at 4°C. After centrifugation, the supernatant was transferred to a new tube containing 40 μl of protein G beads (TransGen Biotech, Beijing, China) and incubated for 6 h at 4°C. After extensive washes with cold lysis buffer, the immunoprecipitated proteins were eluted in SDS sample loading buffer (Aurigene Biotech, Changsha, China), separated by SDS-PAGE, transferred onto polyvinylidene difluoride membranes (Millipore), and detected by WB (Zheng et al., 2012).

RNA Interference

Three small interfering RNAs (siRNAs) targeting CYPA (GenBank accession number: NM 001166326) were designed and synthesized by Guangzhou RIBOBIO Company. To evaluate the knock-down efficiency of the siRNAs, 100 pmol of each siRNA was transfected into HEK293 cells. The cells were lysed with RIPA as described by WB, and lysates were used for western blotting with anti-CYPA and anti-bate-actin antibodies. The siRNA with the best knock-down efficiency was chosen for the subsequent experiments. A scramble siRNA-NC was used as the control.

Immunofluorescence (IF) Assay

HEK293T and Vero cells grown on coverslips in six-well plates for 24 h were washed gently three times with PBS, fixed with 4% formaldehyde in PBS for 15 min, and then permeabilized with 0.5% Triton X-100 in PBS for 5 min. Subsequently, the cells were blocked with fresh 10% goat serum. The cells were incubated with an anti-CYPA rabbit polyclonal antibody and anti-Flag mouse mAb overnight at 4°C, respectively. After washing five times with PBS, the secondary antibody was added for 1 h of incubation at 37°C. Then, Hoechst 33342 was applied for nuclear staining for 3 min at room temperature. The coverslips were finally mounted onto slides and observed under a florescent microscope (BX53, Olympus, Japan).

Chromatin Immunoprecipitation (ChIP) Assay

The ChIP assay was performed to detect the binding of EBNA1-oriP according to previous reports (Shen et al., 2016). The Immunoprecipitation Kit (Millipore) was used for the assay. HEK293 cells were transfected with Lipofectamine 3000 (Invitrogen) according to the manufacturer's protocol. Cells were collected after 48 h and lysed with lysis buffer (Beyotime, Shanghai, China) [20 mM Tris (pH7.5), 150 mM NaCl, 1% Triton X-100, sodium pyrophosphate, β-glycerophosphate, EDTA, Na_3VO_4, leupeptin]. The immunoprecipitated nucleoprotein complexes were eluted by incubation twice for 15 min at 25°C with 200 μl of elution buffer (1% SDS and 100 mM $NaHCO_3$), and the crosslinks were reversed by incubation at 65°C for 4 h. The DNA was extracted with phenol/chloroform and precipitated with ethanol. Then oriP DNA was amplified by qRT-PCR using the primers listed in **Supplementary Table S1**.

Luciferase Reporter Assay

The experimental procedure for the detection of oriP transcription activation mediated by EBNA1 was carried out according to previous description from other group (Chen et al., 2014). Cells were seeded into 24-well plates 24 h prior to transfection. The following day, 1000 ng of the orip-SV40-Luc reporter plasmid was transfected into the cells using Lipofectamine 3000. The SV40-Luc reporter plasmid was transfected as a control. Cell lysates were collected at 24 h post-transfection and assayed for luciferase activity using a luciferase assay kit (Promega, Madison, WI, United States) on the Panomics Luminometer. The Renilla luciferase activity was also measured using an enzyme assay kit (Promega). The results were normalized to the Renilla activity. Three parallel repeats were performed for each sample in each experiment, and the results were expressed as the mean of three independent experiments.

Detection of the EBV Copy Number

The detection of EBV copy number was performed as described previously (Zuo et al., 2015). DNA was extracted from the C2089-shNC and C2089-shCYPA cells using the General AllGen

Kit (CWBio, Hunan, China) and quantified. The relative EBV copy number was determined by RT-qPCR using the EBV DNA Quantitative Fluorescence Diagnostic Kit (Sansure Biotech, Hunan, China) according to the manufacturer's instruction. In this product, *Bam*HI-W fragment in EBV genome is designed as the specific primers and probes. The EBV copy number concentration (copies/cell) of the samples was calculated according to the level of internal reference. The experiment was repeated for three times.

Statistical Analysis

The statistical analyses were performed using GraphPad Prism 5 (GraphPad Software, CA, United States). Differences between groups were determined using Student's *t*-test or one-way analysis of variance (ANOVA). The data are expressed as the means ± standard deviations (SDs). Single, double and triple asterisks indicate statistical significance ($^{*}P < 0.05$, $^{**}P < 0.01$ and $^{***}P < 0.001$).

RESULTS

CYPA, but Not CYPB, Binds to EBNA1

By immunofluorescence (IF) assay, CYPA was detected to be mainly localized in the cytoplasm in Vero and HEK293T cells (**Supplementary Figure S2**). To study the potential interaction between EBNA1 and CYPA, BiMC assay was performed. The BiMC assay is a useful tool for detection of protein-protein interactions in living cells, and the results can be visualized under a fluorescence microscope (Hudry et al., 2012; Yang et al., 2014). A diagram of the basic principle of the BiMC assay is shown in **Supplementary Figure S1**. The EBNA1 protein was expressed as a fusion protein with the C-terminal fragment of the YFP (pCAGGS-Myc-EBNA1-CY), and CYPA was fused with the N-terminal fragment of YFP (pCAGGS-Flag-CYPA-NY). These two plasmids were co-transfected into HEK293T cells, with the single pCAGGS-Flag-CYPA-NY plasmid transfection as a negative control. The results showed that EBNA1 and CYPA interacted with each other in the nucleus (**Figure 1A**, Top). When the nuclear localization signal (NLS) sequence of EBNA1 was deleted, the proteins interacted in the cytoplasm (**Figure 1A**). This translocation showed the specificity of the interaction mediated by EBNA1 with an NLS. Cyclophilin B (CYPB) is another member of the cyclophilin family, but we did not detect any binding signal for CYPB-EBNA1 in the BiMC assay (**Figure 1A**). There was no fluorescence signal in the cells transfected with only single plasmid which was a negative control (**Figure 1A**, Lower). EBNA1 and CYPA/B expression in the BiMC assay was detected by WB (**Figure 1B**). We further evaluated EBNA1 and CYPA intracellular localization in EBV-positive cells by IF assays (**Figure 1C**). The result showed that CYPA expressed in both cytoplasm and nucleus in EBV-positive C2089 cells, while mainly in the cytoplasm of the EBV-negative HEK293 cells (**Figure 1C**). The co-immunoprecipitation (co-IP) assay was used to verify the interaction of EBNA1 with CYPA. These results showed that both endogenous and exogenous CYPA interacted with EBNA1 (**Figures 1D–F**). The plasmids pCAGGS-Myc-EBNA1 and pCAGGS-Flag-CYPA or pCAGGS-Flag-CYPB were transfected in HEK293 cells, Myc-EBNA1 was immune-precipitated with anti-Flag antibody. As shown in **Figure 1G**, the result of co-IP assay further validated that EBNA1 interacted with CYPA but not CYPB.

EBNA1 Domain With Amino Acids 376-459 Is Essential for the CYPA-EBNA1 Interaction

To identify the contribution of the functional domains of EBNA1 to the CYPA-EBNA1 interaction, we constructed five deletion mutants of Myc-tagged EBNA1 named EBNA1Δ1-90, EBNA1Δ90-376, EBNA1Δ376-459, EBNA1Δ459-607, and EBNA1Δ607-641. The plasmid structures are illustrated in **Figure 2A**. The BiMC assay revealed that YFP was reconstructed in HEK293T cells using wild-type EBNA1 and four of the mutants (EBNA1Δ1-90-CY, EBNA1Δ90-376-CY, EBNA1Δ459-607-CY and EBNA1Δ607-641-CY) but not the EBNA1Δ376-459-CY mutant (**Supplementary Figure S3A**). Each negative control with single plasmid transfection is shown in **Supplementary Figure S3C**. Subsequently, we co-transfected pCAGGS-Myc-EBNA1 or a pCAGGS-Myc-EBNA1 mutant plasmid with pCAGGS -Flag-CYPA into HEK293 cells. A co-IP assay using a Flag-tag antibody for the pulldown showed the same result (i.e., CYPA did not interact with EBNA1Δ376-459) (**Figure 2B**). This domain, which is also the region containing the USP7-binding domain in EBNA1 (**Figure 2A**), was thus critical for the binding of EBNA1 to CYPA. Co-expression of EBNA1 376-459-CY (only this one domain of EBNA1) and CYPA-NY recovered their binding function based on the BiMC assay results (**Supplementary Figure S3B**). The NLS (amino acids 379-386) is also included in the domain containing amino acids 376-459, and thus YFP was detected in the nucleus (**Supplementary Figure S3B**). These results indicated that amino acids 376-459 of EBNA1, which contain the USP7-binding domain, were essential for the interaction between EBNA1 and CYPA.

CYPA Influences EBNA1 Expression and Maintenance of EBV Genome During Cell Culture Passages

We designed three siRNAs to observe their efficiency on CYPA protein expression in HEK293 cells (**Figure 3A**). The results showed that the knock-down of siCYPA-1 was best, and this siRNA was used in the subsequent experiments, whereas a scrambled control siRNA (siNC) had no effect on CYPA expression. As shown in **Figures 3B,C**, EBNA1 protein and mRNA expression decreased in response to siCYPA in EBV-positive NPC C666-1 and C2089 cells. Conversely, ectopic CYPA overexpression in the EBV-positive cell lines resulted in an increase in the EBNA1 expression levels detected by WB and qRT-PCR (**Figures 3D,E**).

As EBV episomal genome is easy to be lost with culture passages *in vitro* (Frappier, 2012b), we investigated whether CYPA depletion might expedite this process in consecutive passages. Then we collected gDNA from different generations

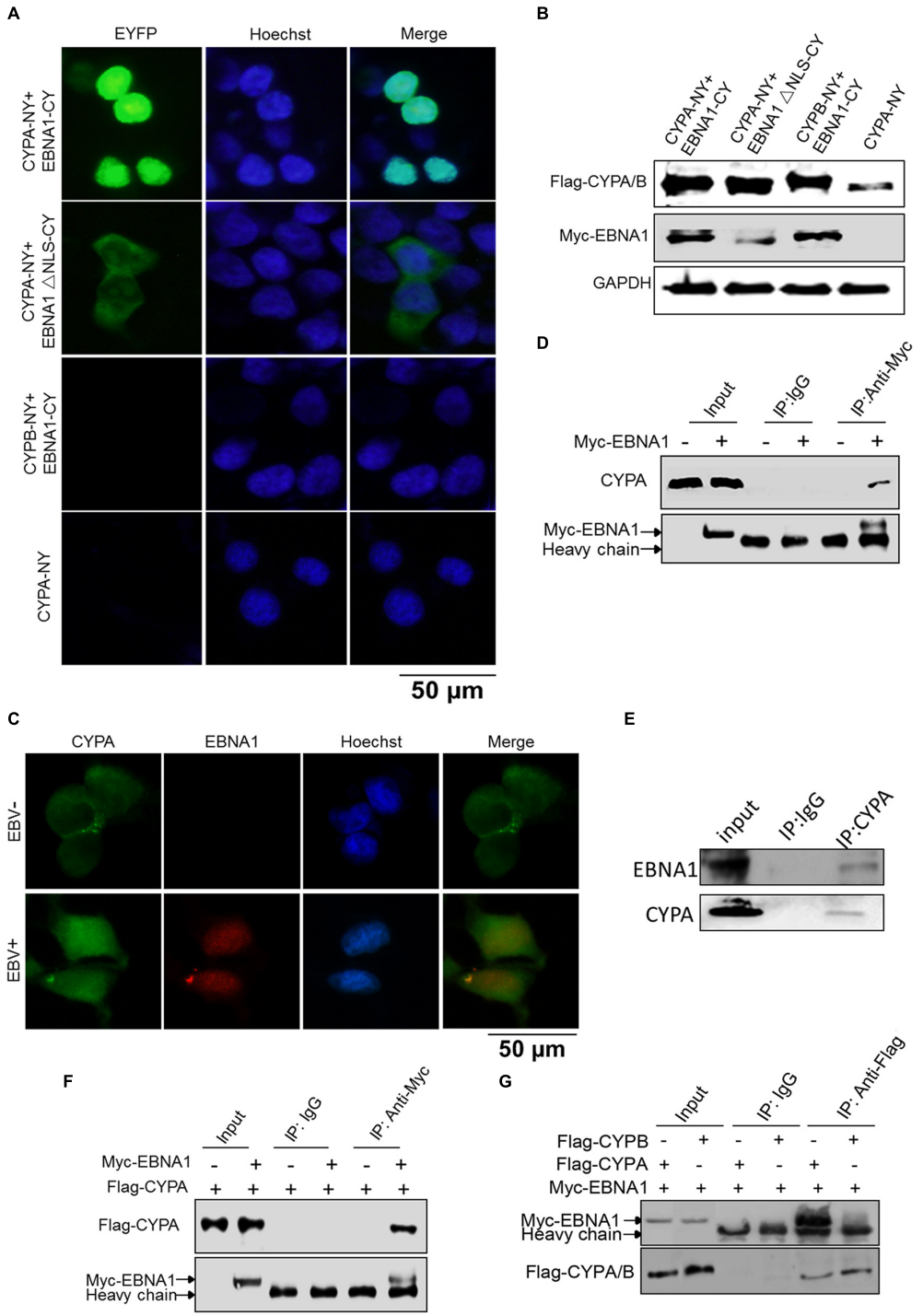

FIGURE 1 | Detection of CYPA-EBNA1 binding by the BiMC and co-IP assays. **(A)** Detection of the EBNA1-CYPA interaction by the BiMC assay. HEK293T cells were transfected with the indicated plasmids, including CYPA-NY, EBNA1-CY, EBNA1ΔNLS-CY, and CYPB-NY following by BiMC analysis, and fluorescence was observed. Transfection of a single CYPA-NY plasmid did not lead to the production of fluorescence. Scale bar, 50 μm. **(B)** The proteins expressed from the plasmids used in the BiMC assay were detected by WB. **(C)** The detection of CYPA and EBNA1 in EBV-negative and EBV-positive HEK293 cells by IF assay. Scale bar, 50 μm. **(D)** Endogenous CYPA interacts with EBNA1 in HEK293 cells. The plasmid pCAGGS-Myc-EBNA1 was transfected into cells. An anti-Myc antibody was used for the pull-down the CYPA, and the WB assay was carried out for detection. **(E)** Endogenous CYPA interacts with EBNA1 in C2089 cells. EBNA1 was immune-precipitated with anti-CYPA. EBNA1 was detected by WB **(F)** Exogenous CYPA interacts with EBNA1. HEK293 cells were transiently transfected with Flag-CYPA alone or with Myc-EBNA1. Flag-CYPA was immune-precipitated with anti-Myc antibody. IgG was used as a negative control for the pull-down in the co-IP assay. Flag-CYPA was detected by WB. **(G)** Co-IP assay for comparison of the interactions of CYPA and CYPB with EBNA1. PCAGGS-Myc-EBNA1 and pCAGGS-Flag-CYPA or pCAGGS-Flag-CYPB were transfected in HEK293 cells. Myc-EBNA1 was immune-precipitated with anti-Flag antibody.

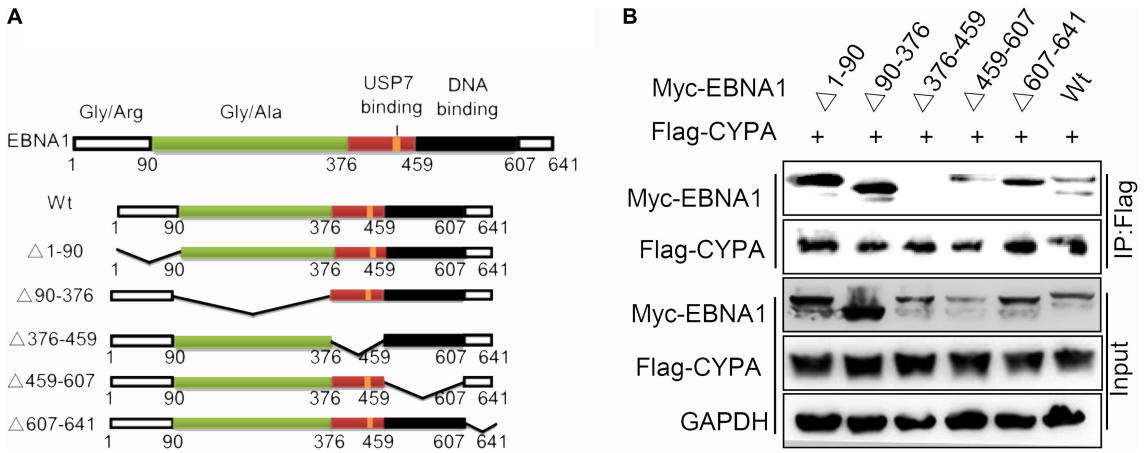

FIGURE 2 | Identification of the EBNA1 domain required for binding to CYPA. **(A)** Diagram of the EBNA1 deletion mutants. The start and end amino acid residues for each fragment are indicated according to a previous report (Young and Murray, 2003). **(B)** Validation of the interaction between each mutant EBNA1 and CYPA by the co-IP assay. PCAGGS-Myc-EBNA1, pCAGGS-Myc-EBNA1 mutants, and pCAGGS-Flag-CYPA were transfected into HEK293 cells. Myc-EBNA1 was immune-precipitated with anti-FLAG antibody. Flag-CYPA and Myc-EBNA1 were detected by WB.

of cells and detected the copy number of each cell. As it shown in **Figure 3F**, CYPA depletion significantly facilitated loss of EBV copy numbers.

CYPA Regulates Transcription Initiation of the EBV Genome via Promoting the EBNA1-Mediated OriP Transcription

EBNA1-oriP binding has been validated to be necessary for the replication initiation of EBV genome (Shen et al., 2016). Here, we investigated the effect of CYPA knockdown on the oriP luciferase activity in cells transfected with an oriP luciferase reporter in C2089 cells. EBV-positive C2089 and EBV-negative HEK293 cells were stably transfected with a lentivirus expressing a short hairpin (sh) of CYPA and a scramble control (shNC) (**Figure 4A**), and the results showed that CYPA was successfully knocked down. EBNA1 protein expression was restored in the C2089-shCYPA cells transfected with the wild-type CYPA expression plasmid (**Figure 4B**). In these cells, an oriP luciferase reporter, oriP-SV40-Luc was transiently transfected. After 24 h transfection, luciferase activities were detected. The EBNA1 activated oriP Luciferase was decreased by 3.5-fold in the luciferase assay compared to that in the control cells (C2089-shNC) due to CYPA depletion. In contrast, there was no effect on the transfection of an SV40-Luc reporter plasmid with CYPA depletion ($P < 0.001$, **Figure 4C**), EBNA1 mRNA was detected by qRT-PCR. When EBNA1 was lacked, CYPA knockdown did not affect luciferase activity of oriP-SV40-Luc (**Figure 4C**). The results indicated that CYPA enhanced the EBNA1 activation of oriP transcription. The ChIP assay was used to further validate that CYPA played a role in EBNA1-oriP binding. pCAGGS-Myc-EBNA1 and oriP-SV40-Luc were co-transfected into HEK293-shNC and HEK293-shCYPA cells. As shown in **Figure 4D**, CYPA interference (shCYPA) reduced the EBNA1 binding to oriP DNA by approximately 50% compared to that of the control (shNC) in HEK293 cells ($P < 0.05$).

The PPIase Activity of CYPA Is Required for Its Role in Viral Replication

CYPA is an intracellular receptor of CsA, which in turn inhibits the PPIase activity of CYPA through binding to the hydrophobic pocket of CYPA (Chatterji et al., 2009). Based on above data about CYPA regulation in EBV genome transcription initiation, we further investigated the possibility of CsA against EBV replication. The working concentration of CsA was considered as 40 μm according to its inhibition effectiveness and low cytotoxicity by the Cell Counting Kit-8 assay (**Figure 5A**). Rescue experiments showed that EBNA1 protein levels were restored compared to the CsA treatment group (**Figure 5B**). EBNA1 protein expression was evaluated by WB after treated or untreated with CsA (**Figure 5C**, left). RT-qPCR analysis showed that there was a significant reduction for the EBNA1 following the decrease of CYPA caused by CsA (**Figure 5C**, right). Subsequently, C2089 cells were transiently transfected with the CYPA expression plasmid together with oriP-SV40-Luc. Luciferase activities were increased at 24 h post-transfection compared with that of no CYPA overexpression, but there was no change for SV40-Luc (without oriP), and EBNA1-oriP-Luc activity increased in CYPA overexpression (**Figure 5D**). The protein level of CYPA and the mRNA level of EBNA1 are detected (**Figure 5D**).

We further investigate the role of CsA in EBNA1-mediated oriP transcription. After transfection of oriP-SV40-Luc, the cells were treated with CsA. The result showed that CsA decreased EBNA-oriP-Luc activity compared to the untreated group, with a decrease in CYPA and EBNA1 (**Figure 5E**). However, overexpression of CYPA and treatment of CsA in HEK293 cells did not affect the activity of oriP-SV40-Luc (**Figure 5F**). These data indicated that CsA inhibited the EBNA1-mediated oriP activation. ChIP assay followed by quantitative PCR (ChIP-qPCR) was used to evaluate the

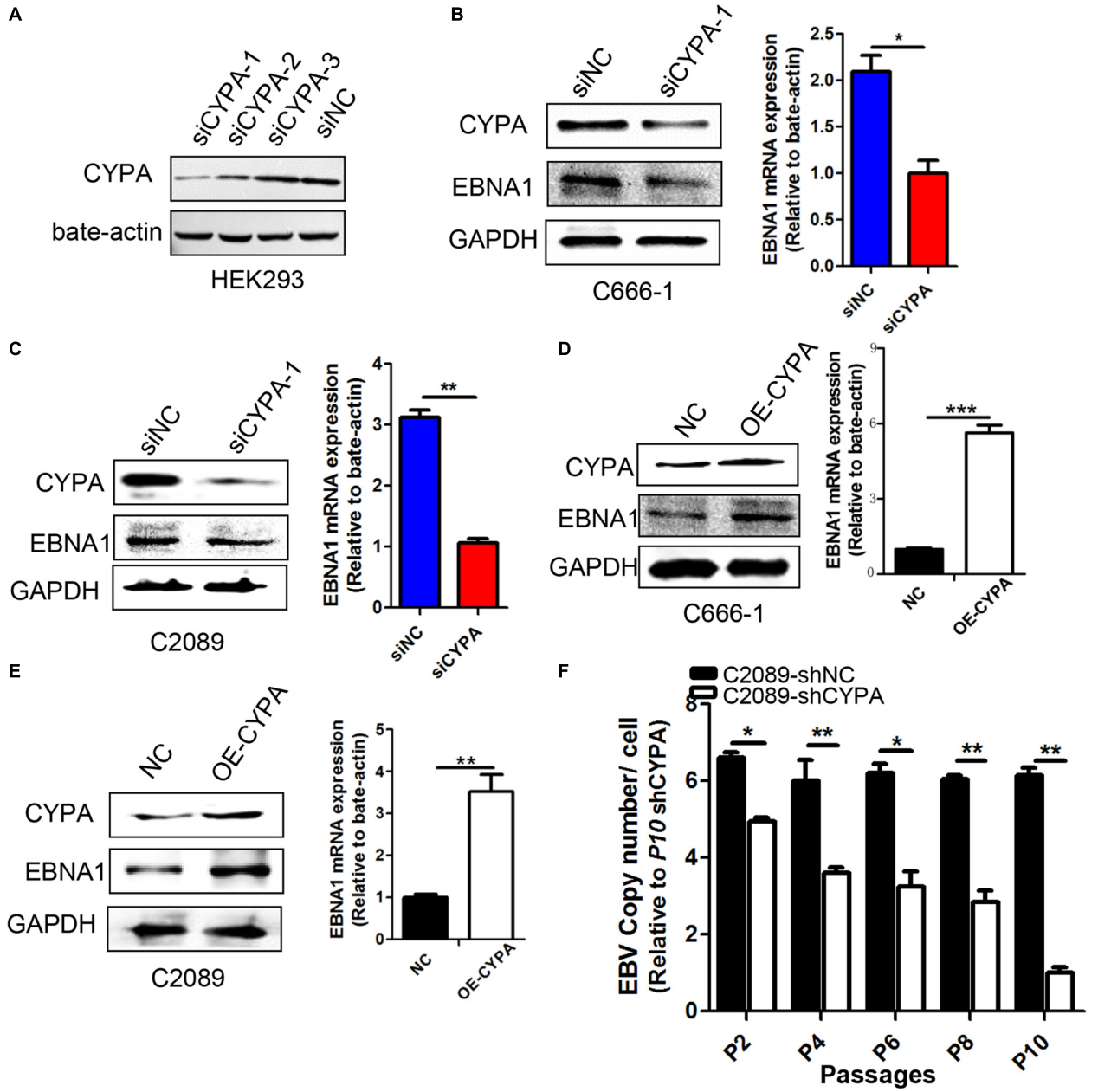

FIGURE 3 | Effect of CYPA on EBNA1 expression and loss of viral copy numbers. **(A)** Designations of the CYPA siRNAs. Three siRNAs for CYPA and a control siRNA were designed and used for detection of the interference efficiency. HEK293 cells were transfected with one of the siRNAs, and a WB assay was performed at 48 h post-transfection for analysis of the CYPA protein level. **(B,C)** Effect of siCYPA on EBNA1 expression in EBV-positive cells. Two EBV-positive cell lines [C666-1 **(B)** and C2089 **(C)**] were used for siRNA transfection. At 48 h post-transfection, the cell lysates and RNA were subjected to the WB and RT-qPCR assays respectively, with siCYPA standarized to 1. **(D,E)** Effect of CYPA overexpression on EBNA1 expression at protein and mRNA levels in EBV-positive cells [C666-1 **(D)** and C2089 **(E)**]. **(F)** The effect of CYPA depletion on loss of EBV copy numbers during passages. EBV-positive C2089 was used for shRNA stable transfection and selection. Cell lines stably transfected with shRNA-CYPA or shRNA-NC were established for the experiment. Cell dispersal for each passage was performed at a ratio 1:2. The copy number of the C2089-shCYPA cells was decreased compared with the C2089-shNC, with passage 10th of C2089-shCYPA set to 1. $^{*}P < 0.05$, $^{**}P < 0.01$, $^{***}P < 0.001$.

effect of CYPA overexpression and CsA treatment on EBNA1 binding to oriP in HEK293 cells. Myc antibody (for Myc-EBNA1) efficiently pulled down oriP-DNA from the above samples, and the results showed that CsA treatment eliminates EBNA1-oriP binding, while CYPA overexpression increases its binding (**Figure 5G**). The results suggested that the PPIase activity of CYPA was required for the role of CYPA in EBV latent replication.

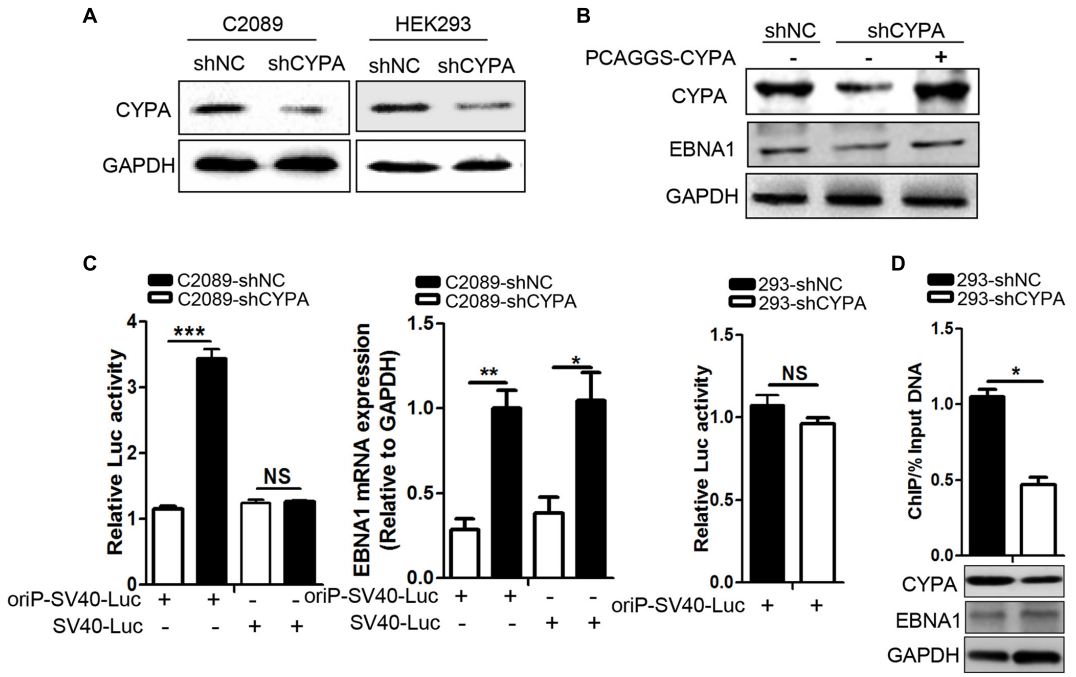

FIGURE 4 | The effect of CYPA knockdown on EBNA1–mediated oriP transcription activity. **(A)** The detection of CYPA expression in stably transfected cell lines with shRNA-CYPA and shRNA-NC. **(B)** Restoration of EBNA1 protein expression in C2089-shCYPA cells transfected with wild-type CYPA expression plasmids. CYPA and EBNA1 proteins were detected by WB. **(C)** Effect of CYPA knockdown on EBNA1-oriP-mediated transcription activity in the luciferase reporter assay. The EBNA1 mRNA was detected by RT-qPCR. **(D)** Effect of CYPA knockdown on binding of EBNA1 to oriP in the ChIP assay. CYPA was depleted from HEK293 with shRNA. Antibodies against Myc and IgG control were respectively used for the pulldown in ChIP assaysHEK293. The precipitation of oriP DNA was quantitated by RT-qPCR. CYPA and EBNA1 proteins were detected by WB. $^{*}P < 0.05$, $^{**}P < 0.01$, $^{***}P < 0.001$.

CYPA Overexpression Antagonizes EBNA1-USP7 Binding

Ubiquitin-specific protease 7 has been implicated in strong inhibition of EBV replication through its tight connection with EBNA1 (Holowaty et al., 2003b). In this study, as the above results demonstrated, the CYPA binding domain was located within the domain containing amino acids 376-459, which spanned the USP7-binding domain in EBNA1. Because CYPA played an opposite role in regulating EBNA1 function compared with USP7, HEK293-shNC and HEK293-shCYPA cells were transiently transfected with pCAGGS-Flag-CYPA alone or with pCAGGS-Myc-EBNA1, a co-IP assay was carried out. The results showed that USP7-EBNA1 binding was strong in the HEK293-shCYPA and HEK293-shNC cells. However, when CYPA was overexpressed, the amount of USP7 bound with EBNA1 was decreased remarkably (**Figure 6A**). In order to study the PPIase activity of CYPA in this mechanism in EBV replication, a co-IP assay was performed to using the treatment of CsA. The result verified that CsA eliminated the antagonism of CYPA on EBNA1-USP7 interaction (**Figure 6B**).

To investigate the ability of CYPA to influence the EBNA1-oriP connection through antagonizing USP7, in HEK293 cells, oriP-SV40-Luc was transfected with pCAGGS -Myc-EBNA1, pCAGGS-Flag-CYPA or pCAGGS-Myc-EBNA1 mutant, a ChIP assay was designed based on ectopic CYPA expression. As shown in **Figure 6C**, the interaction of oriP and the EBNA1 mutant with deletion of amino acids 376-459 (EBNA1Δ376-459) was significantly enhanced. In contrast, CYPA overexpression increased EBNA1-oriP binding to a high level. The result demonstrated that the deletion of the binding site for both USP7 and CYPA exhibited the enhancement of EBNA1-oriP binding (**Figure 6C**). This was a priority effect of the release of USP7 inhibition but not CYPA facilitation. Only when CYPA was overexpressed, could the effect of USP7 inhibition be reversed. The results further showed that CYPA overexpression was essential to overcome the USP7 suppression in regulating EBNA1 replication function.

DISCUSSION

EBV latent infection is an important causative factor in the development of related cancers such as NPC (Dittmer et al., 2008; Zheng et al., 2014, 2018), although the mechanism is largely unclear. Viral replication and genome maintenance in host cells are important for the pathogenesis. CYPA was found to be highly expressed in NPC in the previous work from our laboratory (Yang et al., 2014; Liu et al., 2019) and played an unknown role related to EBV. Herein, we reveal that CYPA, especially when increasingly expressed, contributes to the replication function of EBNA1. CYPA first was recruited by EBNA1 into the nucleus and then mediated EBNA1-oriP binding and replication activity.

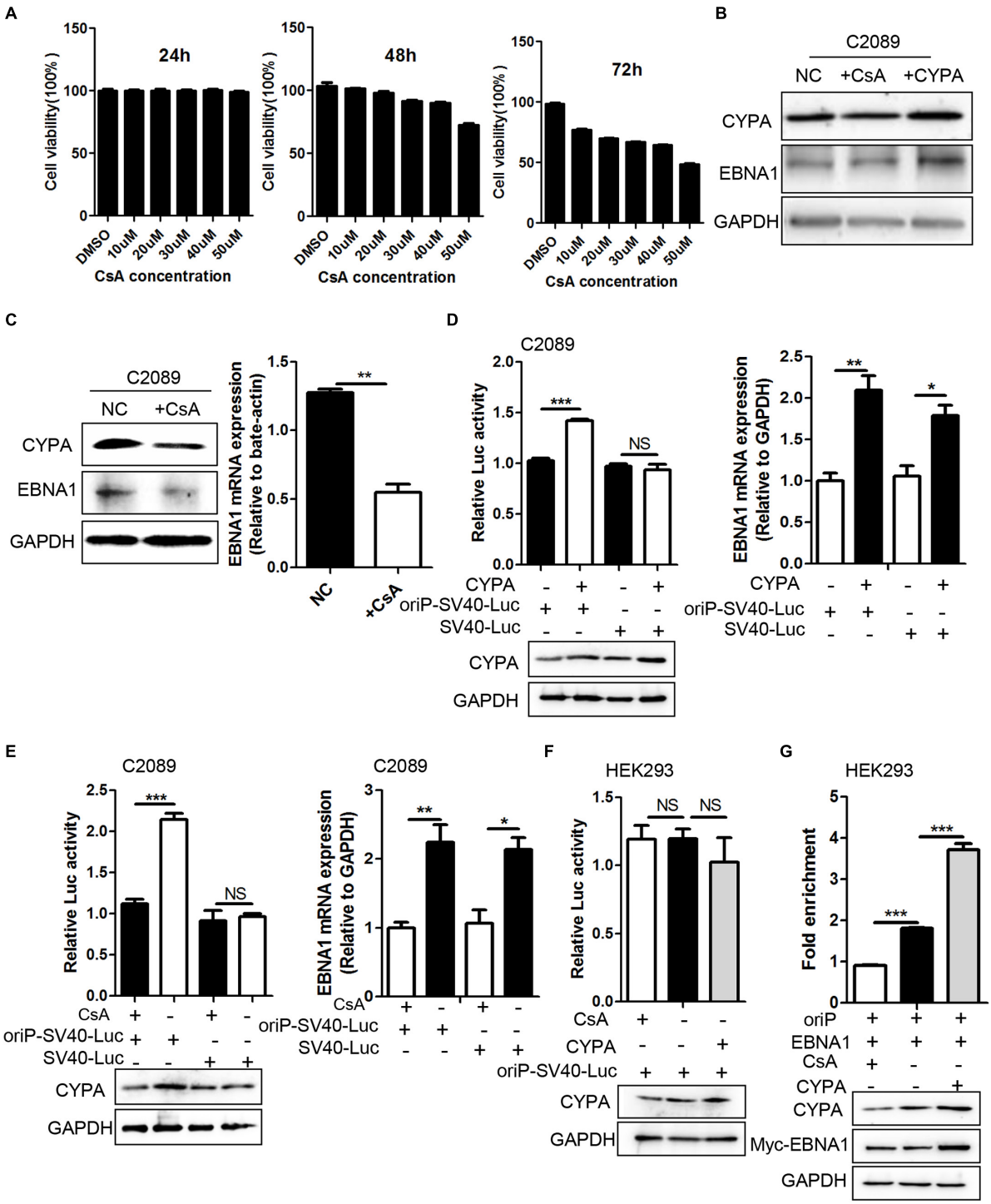

FIGURE 5 | The effect of CYPA-specific inhibitor CsA on EBNA1–mediated oriP transcription and EBNA1-oriP binding. **(A)** The concentration determination of CsA by Cell Counting Kit-8 (CCK-8) assay. The concentration of 40 μM at 48 h was determined as the working concentration for treatment. **(B)** Rescue experiment of EBNA1 protein level after CsA treatment in C2089 cells. **(C)** The protein expression of CYPA and EBNA1 detected by WB assay at 48 h post-treatment with CsA. The mRNA expression of EBNA1 measured by RT-qPCR. EBV-positive C2089 cell lines were used for the test. **(D)** C2089 cells were transfected with oriP-SV40-Luc reporter plasmid and CYPA expression plasmids. Overexpressed CYPA significantly increased EBNA1- oriP-dependent luciferase activity, but had no effect on SV40 promoter dependent luciferase activity (left). EBNA1 mRNA was measured by RT-qPCR (right). **(E)** OriP-SV40-Luc reporter plasmid was transfected into C2089 cells, following the CsA treatment. CsA treatment greatly reduced EBNA1- oriP luciferase activity compared with untreatment. **(F)** CsA and elevated CYPA on EBNA1-oriP-mediated transcription activity in the luciferase reporter assay in HEK293 cells. **(G)** ChIP- qPCR was used to determine EBNA1-oriP binding. CsA treatment reduced EBNA1-oriP binding while elevated CYPA increased binding. CYPA and EBNA1 proteins were analyzed by WB. $^{*}P < 0.05$, $^{**}P < 0.01$, $^{***}P < 0.001$.

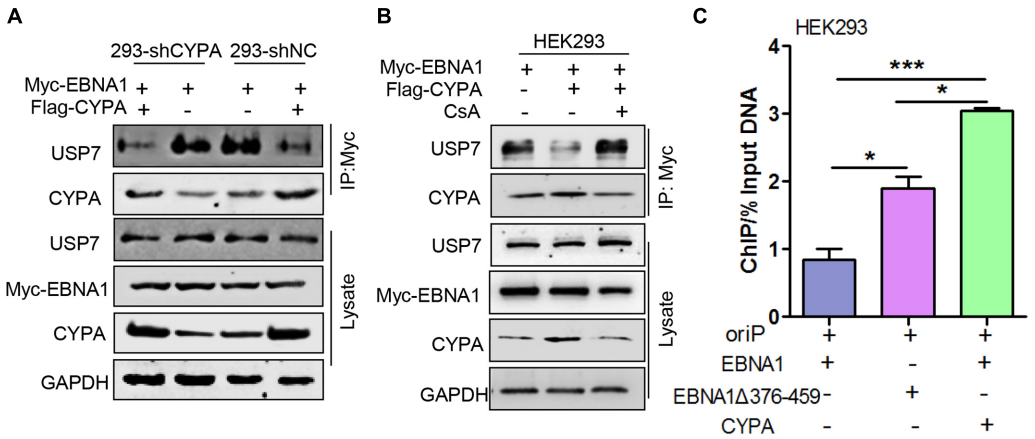

FIGURE 6 | The effect of ectopic CYPA expression on USP7-EBNA1 and EBNA1-oriP binding. **(A)** Effect of CYPA overexpression on EBNA1-USP7 binding in HEK293-shCYPA and HEK293-shNC cells. These cells were transiently transfected with pCAGGS-Flag-CYPA alone or with pCAGGS-Myc-EBNA1, a co-IP assay was performed with the anti-Myc antibody for the pulldown. **(B)** The inhibition of CsA on CYPA-USP7 antagonism in the binding with EBNA1. pCAGGS-Myc-EBNA1 was transfected with pCAGGS-Flag-CYPA or alone, and treated with CsA. The anti-Myc antibody was used for the pulldown, and proteins were detected by WB. **(C)** Effect of CYPA overexpression and EBNA1 Δ376-459 mutation on the EBNA1-oriP binding detected by ChIP assay. $*P < 0.05$, $***P < 0.001$.

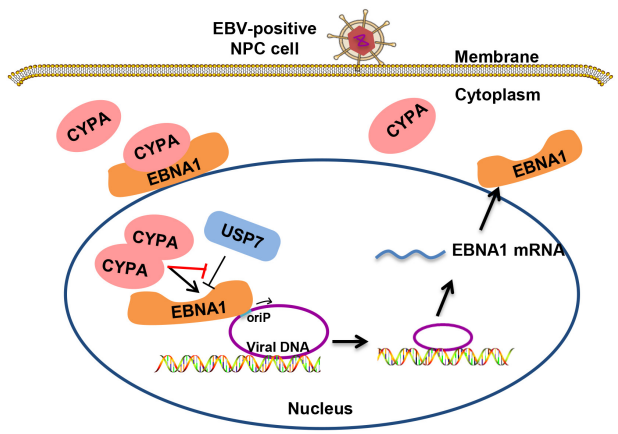

FIGURE 7 | Schematic for the mechanism of CYPA in supporting the replication function of EBNA1. EBV genomic DNA exists within the host genome in the form of extrachromosomal episomes. Cytoplasmic CYPA can be hijacked by EBNA1 into the nucleus. Overexpressed CYPA can overcome the suppression of USP7 in binding to EBNA1. Nuclear CYPA mediates EBNA1-oriP transcription, and thus contributing to the viral genome replication and maintenance.

On the other hand, when CYPA was upregulated, the USP7 suppression in EBNA1-mediated replication could be reversed. This interaction is a type of quantity-driven winning for CYPA, because its rival USP7 is too powerful. It was reported that the affinity of USP7-EBNA1 was 10-fold higher than USP7-p53, implying the strong binding of USP7-EBNA1 (Saridakis et al., 2005). The CsA treatment demonstrated that the PPIase activity of CYPA was required for this function. The schematic working model is shown as in **Figure 7**.

Cyclophilin A has been implicated in the life cycles of several viruses and plays a critical role in the successful infectivity and replication of these viruses, including some tumor viruses, such as HBV and HCV (Bose et al., 2003; Naoumov, 2014; Jyothi et al., 2015; Phillips et al., 2015). It has not been reported for the relationship between CYPA and KSHV, another tumor virus in the same family of gamma herpesvirus as EBV. Though CYPA is involved in the regulation of several viruses, its function mode is different from that in other viruses depending on the different mode of viral infection and replication. For example, the interaction between CYPA and HIV Gag was proposed to facilitate disassembly of the viral RNA containing core following virus entry and thus supports the efficient reverse transcription of the HIV-1 genome (Luban et al., 1993; Ott, 2002) CYPA also enhances virus attachment to the host cell membrane through interactions with heparans (Saphire et al., 2000) and after membrane fusion through interaction with CD147, thereby promoting viral infection. In the present study, for the first time, we showed that CYPA was also utilized by EBV in the modulation of viral replication function in epithelial cells. Thus, CYPA is involved in the maintenance of the virus during its latency in host cells. EBNA1 mediates DNA episome replication from oriP (Frappier, 2012a). Our results revealed that CYPA was recruited to influence EBNA1-oriP-mediated transcription. CYPA depletion significantly facilitated loss of EBV copy numbers (**Figure 3F**), suggesting that impairment of EBNA-oriP binding further weakened successful replication and maintenance of the EBV genome.

Epstein-Barr virus can naturally infected B cells and latently maintained in resting B cells (Thorley-Lawson et al., 2013). As CYPA is a multi-functional protein, which can be expressed in all kinds of cells, and EBNA1 is the only expressed protein of EBV in all latency types. Therefore, we think that both CYPA and EBNA1 may be expressed in resting B cells. How CYPA plays a role in the function of EBV in B cells remains to be further investigated.

The deubiquitinase USP7 is also known as a HAUSP and has been found to be associated with several herpesviruses, including HSV-1, EBV, and KSHV (Holowaty et al., 2003b; Jager et al., 2012; Hammerschmidt and Sugden, 2013). A previous study demonstrated that USP7 suppressed EBV replication (Holowaty et al., 2003b). Here, we showed that EBV hijacked the host factor of elevated CYPA to counteract USP7, thereby adding to the definition of HAUSP. Additionally, our data showed that deletion of the binding domain in EBNA1 for both USP7 and CYPA resulted in significantly increased EBNA1-oriP binding activity (**Figure 6C**), mainly due to release of USP7 inhibition. The result was consistent with that of previous report (Holowaty et al., 2003a), demonstrating that the suppressive role of USP7 was strong enough to greatly overshadow the improved role of CYPA.

In summary, the study reveals that CYPA is a novel critical host factor utilized by EBNA1 in the viral DNA replication in epithelial cells. Elevated CYPA levels remarkably antagonize USP7 in the interaction with EBNA1. The results revealed a strategy that EBV recruited a host factor to counteract the host defense, thus facilitating its own latent genome replication and efficient persistence. Our findings implied that EBV has evolved sophisticatedly. This study provides a new insight into EBV pathogenesis and potential virus-targeted therapeutics in EBV-associated NPC, in which CYPA is upregulated.

DATA AVAILABILITY STATEMENT

The data used to support the findings of this study are available from the corresponding author upon request.

AUTHOR CONTRIBUTIONS

SX, SD, and JL designed and conceived the experiments. JL supervised the research. SX, SD, LL, YX, LZ, JY, JH, WY, JZ, and PC performed the experiments and analyzed the data. SX, FZ, and JL wrote and revised the manuscript.

FUNDING

This work was supported by the National Key Research and Development Program and National Natural Science Foundations of China (2017YFC1200204, 31670171, 81728011, and 81974427).

ACKNOWLEDGMENTS

We thank Dr. Wolfgang Hammerschmidt (GSF-National Research Center for Environment and Health, Germany) for kindly providing us the Maxi-EBV system, which was used in the establishment of C2089 cell line. We thank Dr. Lori Frappier (University of Toronto, Canada) for the kind gift, plasmid pc3-oriP. We also thank Dr. Ronald N. Harty (University of Pennsylvania, United States) for providing us the pCAGGS vector.

SUPPLEMENTARY MATERIAL

The Supplementary Material for this article can be found online at: https://www.frontiersin.org/articles/10.3389/fmicb.2019.02879/full#supplementary-material

FIGURE S1 | The schematic diagram of the BiMC assay.

FIGURE S2 | CYPA expression was detected by IF assay in Vero and HEK293T cells. Scale bar, 100 μm. After transfected the pCAGGS-Flag-CYPA plasmid for 24 h in Vero cells, the Flag antibody was incubated overnight in 4°C, followed by green fluorescent secondary antibody in 37°C for 1 h, hoechst33342 stained nucleus. HEK293T cells, CYPA antibody incubated overnight, followed by red fluorescent secondary antibody, stained nucleus.

FIGURE S3 | Detection of EBNA1 mutants and CYPA using BiMC assays. **(A)** Detection of the interaction between each mutant and CYPA by BiMC assay. Scale bar, 50 μm. **(B)** Verification of the interaction between the single EBNA1 domain containing aa 376-459 and CYPA by the BiMC assay. Scale bars, 50 μm. **(C)** Negative controls for each single plasmid in BiMC assay.

TABLE S1 | Primer sequences used in the study.

REFERENCES

Bahmed, K., Henry, C., Holliday, M, Redzic, J., Ciobanu, M., Zhang, F., et al. (2012). Extracellular cyclophilin-A stimulates ERK1/2 phosphorylation in a cell-dependent manner but broadly stimulates nuclear factor kappa B. *Cancer Cell Int.* 12, 19. doi: 10.1186/1475-2867-12-19

Bose, S., Mathur, M., Bates, P., Joshi, N., and Banerjee, A. K. (2003). Requirement for cyclophilin A for the replication of vesicular stomatitis virus New Jersey serotype. *J. Gen. Virol.* 84, 1687–1699. doi: 10.1099/vir.0.19074-0

Braaten, D., Franke, E. K., and Luban, J. (1996). Cyclophilin A is required for an early step in the life cycle of human immunodeficiency virus type 1 before the initiation of reverse transcription. *J. Virol.* 70, 3551–3560.

Capone, G., Fasano, C., Lucchese, G., Calabro, M., and Kanduc, D. (2015). EBV-associated cancer and autoimmunity: searching for therapies. *Vaccines* 3, 74–89. doi: 10.3390/vaccines3010074

Chatterji, U., Bobardt, M., Selvarajah, S., Yang, F., Tang, H., Sakamoto, N., et al. (2009). The isomerase active site of cyclophilin A is critical for hepatitis C virus replication. *J. Biol. Chem.* 284, 16998–17005. doi: 10.1074/jbc.M109.007625

Chen, Y. L., Liu, C. D., Cheng, C. P., Zhao, B., Hsu, H. J., Shen, C. L., et al. (2014). Nucleolin is important for Epstein-Barr virus nuclear antigen 1-mediated episome binding, maintenance, and transcription. *Proc. Natl. Acad. Sci. U.S.A.* 111, 243–248. doi: 10.1073/pnas.1321800111

Ciesek, S., Steinmann, E., Wedemeyer, H., Manns, M. P., Neyts, J., Tautz, N., et al. (2009). Cyclosporine A inhibits hepatitis C virus nonstructural protein 2 through cyclophilin A. *Hepatology* 50, 1638–1645. doi: 10.1002/hep.23281

Delecluse, H. J., Hilsendegen, T., Pich, D., Zeidler, R., and Hammerschmidt, W. (1998). Propagation and recovery of intact, infectious Epstein-Barr virus from prokaryotic to human cells. *Proc. Natl. Acad. Sci. U.S.A.* 95, 8245–8250. doi: 10.1073/pnas.95.14.8245

Ding, Y., Li, X. R., Yang, K. Y., Huang, L. H., Hu, G., and Gao, K. (2013). Proteomics analysis of gastric epithelial AGS cells infected with Epstein-Barr virus. *Asian Pac. J. Cancer Prev.* 14, 367–372. doi: 10.7314/apjcp.2013.14.1.367

Dittmer, D. P., Hilscher, C. J., Gulley, M. L., Yang, E. V., Chen, M., and Glaser, R. (2008). Multiple pathways for Epstein-Barr virus episome loss from nasopharyngeal carcinoma. *Int. J. Cancer* 123, 2105–2112. doi: 10.1002/ijc.23685

Frappier, L. (2012a). EBNA1 and host factors in Epstein-Barr virus latent DNA replication. *Curr. Opin. Virol.* 2, 733–739. doi: 10.1016/j.coviro.2012.09.005

Frappier, L. (2012b). The Epstein-Barr Virus EBNA1 Protein. *Scientifica* 2012:438204. doi: 10.6064/2012/438204

Hammerschmidt, W., and Sugden, B. (2013). Replication of Epstein-Barr viral DNA. *Cold Spring Harb. Perspect. Biol.* 5:a013029. doi: 10.1101/cshperspect.a013029

Holowaty, M. N., Sheng, Y., Nguyen, T., Arrowsmith, C., and Frappier, L. (2003a). Protein interaction domains of the ubiquitin-specific protease. USP7/HAUSP. *J. Biol. Chem.* 278, 47753–47761. doi: 10.1074/jbc.M307200200

Holowaty, M. N., Zeghouf, M., Wu, H., Tellam, J., Athanasopoulos, V., Greenblatt, J., et al. (2003b). Protein profiling with Epstein-Barr nuclear antigen-1 reveals an interaction with the herpesvirus-associated ubiquitin-specific protease HAUSP/USP7. *J. Biol. Chem.* 278, 29987–29994. doi: 10.1074/jbc.M303977200

Hudry, B., Remacle, S., Delfini, M. C., Rezsohazy, R., Graba, Y., and Merabet, S. (2012). Hox proteins display a common and ancestral ability to diversify their interaction mode with the PBC class cofactors. *PLoS Biol.* 10:e1001351. doi: 10.1371/journal.pbio.1001351

Jager, W., Santag, S., Weidner-Glunde, M., Gellermann, E., Kati, S., Pietrek, M., et al. (2012). The ubiquitin-specific protease USP7 modulates the replication of Kaposi's sarcoma-associated herpesvirus latent episomal DNA. *J. Virol.* 86, 6745–6757. doi: 10.1128/JVI.06840-11

Jiang, C., Chen, J., Xie, S., Zhang, L., Xiang, Y., Lung, M., et al. (2018). Evaluation of circulating EBV microRNA BART2-5p in facilitating early detection and screening of nasopharyngeal carcinoma. *Int. J. Cancer* 143, 3209–3217. doi: 10.1002/ijc.31642

Jyothi, K. R., Beloor, J., Jo, A., Nguyen, M. N., Choi, T. G., Kim, J. H., et al. (2015). Liver-targeted cyclosporine A-encapsulated poly (lactic-co-glycolic) acid nanoparticles inhibit hepatitis C virus replication. *Int. J. Nanomed.* 10, 903–921. doi: 10.2147/IJN.S74723

Liu, L., Zhou, Q., Xie, Y., Zuo, L., Zhu, F., and Lu, J. (2017). Extracellular vesicles: novel vehicles in herpesvirus infection. *Virol. Sin.* 32, 349–356. doi: 10.1007/s12250-017-4073-9

Liu, L., Zuo, L., Yang, J., Xin, S., Zhang, J., Zhou, J., et al. (2019). Exosomal cyclophilin A as a novel noninvasive biomarker for Epstein-Barr virus associated nasopharyngeal carcinoma. *Cancer Med.* 8, 3142–3151. doi: 10.1002/cam4.2185

Liu, X., Zhao, Z., Xu, C., Sun, L., Chen, J., Zhang, L., et al. (2012). Cyclophilin A restricts influenza A virus replication through degradation of the M1 protein. *PLoS One* 7:e31063. doi: 10.1371/journal.pone.0031063

Liu, Y., Stone, S., and Harty, R. N. (2011). Characterization of filovirus protein-protein interactions in mammalian cells using bimolecular complementation. *J. Infect. Dis.* 204(Suppl. 3), S817–S824. doi: 10.1093/infdis/jir293

Lu, J., Han, Z., Liu, Y., Liu, W., Lee, M. S., Olson, M. A., et al. (2014). A host-oriented inhibitor of Junin Argentine hemorrhagic fever virus egress. *J. Virol.* 88, 4736–4743. doi: 10.1128/JVI.03757-13

Lu, J., Qu, Y., Liu, Y., Jambusaria, R., Han, Z., Ruthel, G., et al. (2013). Host IQGAP1 and Ebola virus VP40 interactions facilitate virus-like particle egress. *J. Virol.* 87, 7777–7780. doi: 10.1128/JVI.00470-13

Lu, J. H., Tang, Y. L., Yu, H. B., Zhou, J. H., Fu, C. Y., Zeng, X., et al. (2010). Epstein-Barr virus facilitates the malignant potential of immortalized epithelial cells: from latent genome to viral production and maintenance. *Lab. Invest.* 90, 196–209. doi: 10.1038/labinvest.2009.130

Lu, Y., Qin, Z., Wang, J., Zheng, X., Lu, J., Zhang, X., et al. (2017). Epstein-Barr Virus miR-BART6-3p Inhibits the RIG-I Pathway. *J Innate Immun.* 9, 574–586. doi: 10.1159/000479749

Luban, J., Bossolt, K. L., Franke, E. K., Kalpana, G. V., and Goff, S. P. (1993). Human immunodeficiency virus type 1 Gag protein binds to cyclophilins A and B. *Cell* 73, 1067–1078. doi: 10.1016/0092-8674(93)90637-6

Morrison, J. A., Gulley, M. L., Pathmanathan, R., and Raab-Traub, N. (2004). Differential signaling pathways are activated in the Epstein-Barr virus-associated malignancies nasopharyngeal carcinoma and Hodgkin lymphoma. *Cancer Res.* 64, 5251–5260. doi: 10.1158/0008-5472.CAN-04-0538

Naoumov, N. V. (2014). Cyclophilin inhibition as potential therapy for liver diseases. *J. Hepatol.* 61, 1166–1174. doi: 10.1016/j.jhep.2014.07.008

Ott, D. E. (2002). Potential roles of cellular proteins in HIV-1. *Rev. Med. Virol.* 12, 359–374. doi: 10.1002/rmv.367

Phillips, S., Chokshi, S., Chatterji, U., Riva, A., Bobardt, M., Williams, R., et al. (2015). Alisporivir inhibition of hepatocyte cyclophilins reduces HBV replication and hepatitis B surface antigen production. *Gastroenterology* 148:e407. doi: 10.1053/j.gastro.2014.10.004

Rainbow, L., Platt, G. M., Simpson, G. R., Sarid, R., Gao, S. J., Stoiber, H., et al. (1997). The 222- to 234-kilodalton latent nuclear protein (LNA) of Kaposi's sarcoma-associated herpesvirus (human herpesvirus 8) is encoded by orf73 and is a component of the latency-associated nuclear antigen. *J. Virol.* 71, 5915–5921.

Reisman, D., Yates, J., and Sugden, B. (1985). A putative origin of replication of plasmids derived from Epstein-Barr virus is composed of two cis-acting components. *Mol. Cell. Biol.* 5, 1822–1832. doi: 10.1128/mcb.5.8.1822

Saphire, A. C., Bobardt, M. D., and Gallay, P. A. (2000). Human immunodeficiency virus type 1 hijacks host cyclophilin A for its attachment to target cells. *Immunol. Res.* 21, 211–217. doi: 10.1385/IR:21:2-3:211

Saridakis, V., Sheng, Y., Sarkari, F., Holowaty, M. N., Shire, K., Nguyen, T., et al. (2005). Structure of the p53 binding domain of HAUSP/USP7 bound to Epstein-Barr nuclear antigen 1 implications for EBV-mediated immortalization. *Mol. Cell.* 18, 25–36. doi: 10.1016/j.molcel.2005.02.029

Shair, K. H., Schnegg, C. I., and Raab-Traub, N. (2008). EBV latent membrane protein 1 effects on plakoglobin, cell growth, and migration. *Cancer Res.* 68, 6997–7005. doi: 10.1158/0008-5472.CAN-08-1178

Shen, C. L., Liu, C. D., You, R. I., Ching, Y. H., Liang, J., Ke, L. R., et al. (2016). Ribosome Protein L4 is essential for Epstein-Barr Virus Nuclear Antigen 1 function. *Proc. Natl. Acad. Sci. U.S.A.* 113, 2229–2234. doi: 10.1073/pnas.1525444113

Sivachandran, N., Thawe, N. N., and Frappier, L. (2011). Epstein-Barr virus nuclear antigen 1 replication and segregation functions in nasopharyngeal carcinoma cell lines. *J. Virol.* 85, 10425–10430. doi: 10.1128/JVI.05293-11

Tang, F. C., Wang, H. Y., Ma, M. M., Guan, T. W., Pan, L., Yao, D. C., et al. (2015). CyPA-CD147-ERK1/2-cyclin D2 signaling pathway is upregulated during rat left ventricular hypertrophy. *Sheng Li Xue Bao* 67, 393–400.

Tang, L. L., Chen, W. Q., Xue, W. Q., He, Y. Q., Zheng, R. S., Zeng, Y. X., et al. (2016). Global trends in incidence and mortality of nasopharyngeal carcinoma. *Cancer Lett.* 374, 22–30. doi: 10.1016/j.canlet.2016.01.040

Tao, Y., Shi, Y., Jia, J., Jiang, Y., Yang, L., and Cao, Y. (2015). Novel roles and therapeutic targets of Epstein-Barr virus-encoded latent membrane protein 1-induced oncogenesis in nasopharyngeal carcinoma. *Expert Rev. Mol. Med.* 17:e15. doi: 10.1017/erm.2015.13

Thorley-Lawson, D. A. (2015). EBV persistence-introducing the virus. *Curr. Top. Microbiol.* 390, 151–209. doi: 10.1007/978-3-319-22822-8-8

Thorley-Lawson, D. A., Hawkins, J. B., Tracy, S. I., and Shapiro, M. (2013). The pathogenesis of Epstein-Barr virus persistent infection. *Curr. Opin. Virol.* 3, 227–232. doi: 10.1016/j.coviro.2013.04.005

Tu, C., Zeng, Z., Qi, P., Li, X., Yu, Z., Guo, C., et al. (2017). Genome-Wide Analysis of 18 Epstein-Barr Viruses Isolated from Primary Nasopharyngeal Carcinoma Biopsy Specimens. *J. Virol.* 91:JVI.00301-17 doi: 10.1128/JVI.00301-17

Xu, C., Meng, S., Liu, X., Sun, L., and Liu, W. (2010). Chicken cyclophilin A is an inhibitory factor to influenza virus replication. *Virol. J.* 7:372. doi: 10.1186/1743-422X-7-372

Yang, J., Zhou, M., Zhao, R., Peng, S., Luo, Z., Li, X., et al. (2014). Identification of candidate biomarkers for the early detection of nasopharyngeal carcinoma by quantitative proteomic analysis. *J. Proteomics* 109, 162–175. doi: 10.1016/j.jprot.2014.06.025

Yates, J. L., and Guan, N. (1991). Epstein-Barr virus-derived plasmids replicate only once per cell cycle and are not amplified after entry into cells. *J. Virol.* 65, 483–488.

Young, L. S. (2014). Epstein-Barr virus at 50-future perspectives. *Chin. J. Cancer* 33, 527–528. doi: 10.5732/cjc.014.10208

Young, L. S., and Dawson, C. W. (2014). Epstein-Barr virus and nasopharyngeal carcinoma. *Chin. J. Cancer* 33, 581–590. doi: 10.5732/cjc.014.10197

Young, L. S., and Murray, P. G. (2003). Epstein-Barr virus and oncogenesis: from latent genes to tumours. *Oncogene* 22, 5108–5121. doi: 10.1038/sj.onc.1206556

Yu, H. B., Lu, J. H., Zuo, L. L., Yan, Q. J., Yu, Z. Y., Li, X. Y., et al. (2012). Epstein-Barr virus downregulates microRNA 203 through the oncoprotein latent membrane protein 1: a contribution to increased tumor incidence in epithelial cells. *J. Virol.* 86, 3088–3099. doi: 10.1128/Jvi.05901-5911

Yu, Z., Lu, J., Yu, H., Yan, Q., Zuo, L., and Li, G. (2011). A precise excision of the complete Epstein-Barr virus genome in a plasmid based on a bacterial artificial chromosome. *J. Virol. Methods* 176, 103–107. doi: 10.1016/j.jviromet.2011.06.015

Zheng, X., Wang, J., Wei, L., Peng, Q., Gao, Y., Fu, Y., et al. (2018). Epstein-Barr Virus MicroRNA miR-BART5-3p Inhibits p53 Expression. *J. Virol.* 92:JVI.01022-1018 doi: 10.1128/JVI.01022-1018

Zheng, Y., Qin, Z. L., Ye, Q. R., Chen, P., Wang, Z., Yan, Q., et al. (2014). Lactoferrin suppresses the Epstein-Barr virus-induced inflammatory response by interfering with pattern recognition of TLR2 and TLR9. *Lab. Invest.* 94, 1188–1199. doi: 10.1038/labinvest.2014.105

Zheng, Y., Zhang, W., Ye, Q., Zhou, Y., Xiong, W., He, W., et al. (2012). Inhibition of Epstein-Barr virus infection by lactoferrin. *J Innate Immun.* 4, 387–398. doi: 10.1159/000336178

Zuo, L., Yu, H., Liu, L., Tang, Y., Wu, H., Yang, J., et al. (2015). The copy number of Epstein-Barr virus latent genome correlates with the oncogenicity by the activation level of LMP1 and NF-kappaB. *Oncotarget.* 6, 41033–41044. doi: 10.18632/oncotarget.5708

Zuo, L., Yue, W., Du, S., Xin, S., Zhang, J., Liu, L., et al. (2017). An update: Epstein-Barr virus and immune evasion via microRNA regulation. *Virol. Sin.* 32, 175–187. doi: 10.1007/s12250-017-3996-3995

Zuo, L. L., Zhang, J., Liu, L. Z., Zhou, Q., Du, S. J., Xin, S. Y., et al. (2017). Cadherin 6 is activated by Epstein-Barr virus LMP1 to mediate EMT and metastasis as an interplay node of multiple pathways in nasopharyngeal carcinoma. *Oncogenesis* 6:402. doi: 10.1038/s41389-017-0005-7

Conflict of Interest: The authors declare that the research was conducted in the absence of any commercial or financial relationships that could be construed as a potential conflict of interest.

Copyright © 2019 Xin, Du, Liu, Xie, Zuo, Yang, Hu, Yue, Zhang, Cao, Zhu and Lu. This is an open-access article distributed under the terms of the Creative Commons Attribution License (CC BY). The use, distribution or reproduction in other forums is permitted, provided the original author(s) and the copyright owner(s) are credited and that the original publication in this journal is cited, in accordance with accepted academic practice. No use, distribution or reproduction is permitted which does not comply with these terms.

frontiers in Microbiology

ORIGINAL RESEARCH
published: 13 December 2019
doi: 10.3389/fmicb.2019.02869

Host Gene SEL1L Involved in Endoplasmic Reticulum-Associated Degradation Pathway Could Inhibit Hepatitis B Virus at RNA, DNA, and Protein Levels

Jinyu Wang[1†], Jing Li[1†], Jingwen Wu[1†], Minhui Dong[1], Zhongliang Shen[1], Yong Lin[2], Fahong Li[1], Yongmei Zhang[1], Richeng Mao[1], Mengji Lu[2] and Jiming Zhang[1,3]**

[1]Department of Infectious Diseases, Huashan Hospital, Fudan University, Shanghai, China, [2]Institute of Virology, University Hospital Essen, University Duisburg-Essen, Essen, Germany, [3]Key Laboratory of Medical Molecular Virology of the Ministry of Education (MOE) and Ministry of Health (MOH), Fudan University, Shanghai, China

OPEN ACCESS

Edited by:
Zhengli Shi,
Wuhan Institute of Virology (CAS), China

Reviewed by:
Ying Zhu,
Wuhan University, China
Lin Deng,
Kobe University, Japan

***Correspondence:**
Mengji Lu
mengji.lu@uni-due.de
Jiming Zhang
jmzhang@fudan.edu.cn

[†]These authors share first authorship

Specialty section:
This article was submitted to Virology, a section of the journal Frontiers in Microbiology

Received: 13 June 2019
Accepted: 27 November 2019
Published: 13 December 2019

Citation:
Wang J, Li J, Wu J, Dong M, Shen Z, Lin Y, Li F, Zhang Y, Mao R, Lu M and Zhang J (2019) Host Gene SEL1L Involved in Endoplasmic Reticulum-Associated Degradation Pathway Could Inhibit Hepatitis B Virus at RNA, DNA, and Protein Levels. Front. Microbiol. 10:2869. doi: 10.3389/fmicb.2019.02869

Hepatitis B virus (HBV) belongs to the Hepadnaviridae family of enveloped DNA viruses. Recent studies have found that host factors can suppress HBV replication. HBV envelope proteins are reported to be degraded by the endoplasmic reticulum-associated degradation (ERAD) pathway. As a component of the ERAD pathway, suppressor of lin-12-like 1 (SEL1L) was earlier found to be upregulated in the inactive carrier phase of chronic HBV infection relative to that in the immune tolerant phase. However, the role of SEL1L in regulating HBV replication remains largely unknown. In this study, we found the levels of HBV RNA, DNA, and core and envelope proteins to be significantly downregulated by SEL1L overexpression and upregulated by SEL1L silencing in Huh7 cells transiently transfected with an overlength HBV genome. Similar upregulation was observed in HepG2.2.15 cells as well. SEL1L co-localized with HBV surface antigen (HBsAg), which changed its staining pattern. Treatment with an inhibitor of ERAD pathway remarkably increased intracellular S protein. Surprisingly, silencing SEL1L to block the ERAD pathway activated an alternative ER quality control (ERQC)-autophagy pathway, which might account for the increased HBV RNAs and core protein. Together, our results demonstrate that SEL1L is a host restriction factor that exerts anti-HBV effect through ERAD and alternative ERQC-autophagy pathway.

Keywords: hepatitis B virus, SEL1L, endoplasmic reticulum-associated degradation, endoplasmic reticulum quality control-autophagy, immune tolerant, inactive carrier

INTRODUCTION

Hepatitis B virus (HBV) infection is a common public health concern worldwide (Schweitzer et al., 2015). Patients with chronic hepatitis B (CHB) are at high risk of developing liver cirrhosis and hepatocellular carcinoma (Tiollais et al., 1985). The natural history of chronic HBV infection refers to four phases, which is immune tolerant (IT), immune active (IA),

inactive carrier status (IC), and HBeAg-negative active chronic hepatitis (ENH; European Association for the Study of the Liver. Electronic address: easloffice@easloffice.eu and European Association for the Study of the Liver, 2017).

Although the immune tolerant (IT) and inactive carrier (IC) phases of CHB are considered to maintain a similar inactivated host immune status, they have entirely different virological characteristics. Thus, viral loads are typically very high (>10^7 IU/ml) in IT subjects although usually <2,000 IU/ml in patients at IC phase, suggesting the existence of host immunity-independent restrictive factors against the virus. Recently, we found the intrahepatic mRNA level of host gene suppressor of lin-12-like 1 (SEL1L) to be significantly upregulated in patients at IC phase compared to that in patients at IT phase (Liu et al., 2018). SEL1L protein is a core component of an endoplasmic reticulum (ER) quality control pathway, namely the endoplasmic reticulum-associated degradation (ERAD) pathway, which in turn plays a vital role in preserving a secretory function by recognizing terminally misfolded polypeptides and processing them for proteasomal degradation (Vembar and Brodsky, 2008).

HBV is a non-cytopathic, hepatotropic virus belonging to the Hepadnaviridae family. The virion is an enveloped icosahedral nucleocapsid containing a partially double-stranded relaxed circular (RC) DNA genome of 3.2 kb. The synthesized envelope proteins of HBV-infected hepatocytes are translocated into the endoplasmic reticulum (ER), where *N*-glycosylation, folding, followed by oligomerization occurring (Gerlich et al., 1992). Several viruses were found to trigger the ERAD pathway (Isler et al., 2005; Yu et al., 2006; Barry et al., 2010). A previous report had found HBV to activate the ERAD pathway by increased expression of ER degradation-enhancing mannosidase-like proteins (EDEMs), thus leading to reduced amount of intracellular envelope proteins (Lazar et al., 2012). However, whether SEL1L, a vital component of ERAD pathway, can regulate HBV life cycle, still remains unknown.

In the present study, we demonstrated that SEL1L functioned as a host restriction factor against HBV replication. Interestingly, silencing SEL1L could activate ER quality control (ERQC)-autophagy pathway, which was considered as an alternative route for protein degradation.

MATERIALS AND METHODS

Cell Culture and Transfection

Human hepatoma cell line Huh7 was maintained in DMEM medium (Gibco, USA), supplemented with 10% fetal bovine serum, 10 mM HEPES, 100 U/ml penicillin, and 100 μg/ml streptomycin. Cells were seeded in 12-well plates at a density of 1.0×10^6 cells per well. Each well was transfected with a total of 3 μg of plasmid using Lipofectamine 3000 (Invitrogen, USA) following the manufacturer's instruction. The human hepatoma cell line HepG2.2.15 harboring the integrated dimer of HBV genome (GenBank accession number: U95551) was cultured using the same medium, except for supplementation with 400 μg/ml of G418 (Gibco, USA).

Plasmids and Reagents

HBV replication competent plasmid pHBV1.3 (genotype D, subtype ayw, GenBank accession number V01460.1), in which the transcription of viral pregenomic RNA (pgRNA) is governed by an authentic HBV core promoter, was constructed as described previously (Mao et al., 2011). Plasmids SEL1L-FLAG and SEL1L-GFP were synthesized by GeneChem Co. (China). Plasmid HBsAg-mCherry was given as a gift from Prof. Xinwen Chen, Wuhan, China. Plasmid HBs-2-s, expressing low level of HBsAg, was kindly provided by Dr. Reinhold Schirmbeck and Dr. William Carman.

The siRNA designed to silence SEL1L expression (siSEL1L, cat.no. SI02664494) and negative control siRNA (siNC, cat.no. 1022076) was purchased from Qiagen (Germany). Kifunensine (KIF, K1140), 3-methyladenine (3-MA, M928), and chloroquine (CQ, C6628) were purchased from Sigma-Aldrich (USA).

Analysis of Hepatitis B Virus DNA and RNA

Intracellular HBV core DNA and total RNA were extracted as described previously (Mao et al., 2011). For DNA analysis, HBV core DNA was separated by electrophoresis on a 1.5% agarose gel and transferred onto Hybond-XL membrane (GE Healthcare). For RNA analysis, 10 μg of total cellular RNA was resolved in a 1.5% agarose gel containing 2.2 M formaldehyde and transferred onto a Hybond-N+ membrane (GE Healthcare). Membranes were probed with either α-^{32}P-UTP-labeled minus or plus strand-specific full-length HBV riboprobe and then exposed to a phosphor imager screen. Hybridization signals were measured with a computerized imaging system (ImageJ software).

Western Blot Assay

Cells were seeded in 12-well plates and washed twice with PBS followed by lysing in 200 μl of Red Loading Buffer (Cell Signaling Technology). Ten microliters of the cell lysate were then resolved by electrophoresis in 12% SDS-PAGE, and proteins were transferred onto nitrocellulose filter membrane (GE Healthcare, USA). The membranes were blocked with 5% skim milk and incubated with antibodies against SEL1L (ab78298, Abcam, UK), EDEM1 (ab209660, Abcam, UK), HBsAg (ab9193, Abcam, UK), HBcAg (ab8639, Abcam, UK), LC3 (Cell Signaling Technology, USA), p62 (Cell Signaling Technology, USA), or β-actin (Cell Signaling Technology, USA). The membranes were washed with 1× TBST (as appropriate) and incubated with secondary antibodies (315-035-048, 111-035-045, Jackson ImmunoResearch, USA). Immunoreactive bands were captured by enhanced chemiluminescence system (RPN2106, GE Healthcare, USA).

Luciferase Reporter Assay

The Dual-Glo luciferase reporter assay system (E2940, Promega, USA) was used to detect both firefly and *Renilla* (as internal control) luciferase activity. The firefly luciferase reporter plasmids pSP1, pSP2, pCP, and pXP (containing HBV promoters) were generated and used as previously described (Zhang et al., 2011).

Immunofluorescence

Huh7 cells were seeded on cover slips and transfected with plasmids or siRNAs. Forty-eight hours after transfection, cells were fixed in 4% paraformaldehyde for 10 min and permeabilized with 0.1% Triton X-100 for 10 min. Nuclei were stained with DAPI. HBsAg and LC3 were stained with Anti-Hepatitis B Virus Surface Antigen (Ad/Ay) antibody (ab9193, Abcam, UK) and LC3B (D11) XP® Rabbit mAb (3,868, Cell Signaling Technology, USA). Co-localization of SEL1L or LC3 (green) with HBsAg (red) was determined using a confocal microscope (LSM 710; Carl Zeiss) with objectives Plan-Apochromat 63×/1.40 oil Iris M27. Images were visualized by ZEN acquisition software (2012; Carl Zeiss) and analyzed by ImageJ.

Histological Analysis and Immunohistochemistry Staining

Pieces of liver tissues from patients at IT and IC phases were fixed in 10% (vol/vol) neutralized formalin. Pathological examination of tissue section was performed by a collaborating pathologist in our hospital. For immunohistochemistry staining (IHC), paraffin-embedded liver tissues were rehydrated, boiled in 1 mM EDTA for antigen retrieval, and stained with DAB substrate from Invitrogen. After incubation with SEL1L antibody (Abcam, 1:200), IHC sections were scanned using the Aperio Scanscope, and pictures were acquired at various magnifications.

Statistical Analysis

We undertook two-way ANOVA, including multiple comparisons, using GraphPad Prism 5 (GraphPad Software, Inc., San Diego, CA), and specifying $p < 0.05$ as the standard for statistical significance. Compared and other means are shown ± standard error of the mean. All experiments were replicated three or more times.

RESULTS

Intrahepatic SEL1L Expression Was Significantly Higher in Inactive Carrier Subjects Than in Immune Tolerant Ones

Liver biopsies of 83 treatment-naïve patients, from four natural-history phases, were followed by subsequent RNA extraction and microarray analysis. **Supplementary Table 1** contains an overview of the CHB patients' clinical and virological characteristics. Patients in IT and IC phases had different HBV DNA loads, with normal alanine aminotransferase (ALT) levels. Our previous study had revealed a set of host genes, including SEL1L, which may be involved in the control of HBV replication in IC phase (Liu et al., 2018). As shown in **Figure 1A**, SEL1L expression was significantly higher in IC phase than in IT phase. Next, we investigated SEL1L distribution *in vivo*. Liver tissues from treatment-naïve patients with chronic hepatitis B were fixed and stained with SEL1L antibody. For patients in IT phase, representative images showed SEL1L to be mostly distributed homogeneously. However, for patients in IC phase, SEL1L accumulated as visible coarse granules, which suggested the possibility of SEL1L protein to aggregate and form a functional complex (**Figure 1B**).

Hepatitis B Virus RNA, DNA, and Core and Envelope Proteins Were Increased by SEL1L Silencing and Decreased by Its Overexpression in Human Hepatoma Cells

Huh7 cells were transiently transfected with a 1.3-mer construct of the HBV genome, together with SEL1L siRNA, thereby increasing HBV DNA levels relative to that in co-transfection with control siRNA. Reduced expression of SEL1L was confirmed by western blot (**Figure 2B**, bottom panels) with no cytotoxic effect observed. Knockdown of SEL1L increased the secreted HBsAg (**Figure 2A**, $p = 0.0142$) and HBeAg ($p = 0.1331$) in the supernatant compared to control group and generated higher levels of HBV DNA (**Figure 2B**, top panels) as well as intracellular core and S proteins (**Figure 2B**, bottom panels). Similar results were obtained in HepG2.2.15 cells (**Supplementary Figure 1A**) as well. Conversely, co-transfection with a 1.3-mer construct of the HBV genome, together with empty vector or increasing concentrations of an expression construct for human SEL1L, reduced the secreted HBV proteins (**Figure 3A**, HBsAg, SEL1L 1.5 μg and vector, $p = 0.0463$; HBeAg, SEL1L 1.5 μg and vector, $p = 0.0477$) and intracellular levels of replicative HBV DNA in a dose-dependent manner (**Figure 3B**, top panels). Similar tendencies were observed for intracellular levels of S and core proteins as well (**Figure 3B**, bottom panels). Secreted HBsAg from HBs-2-s could be reduced by more than 50% by SEL1L overexpression (**Supplementary Figure 1B**), which indicated a limited ability of SEL1L to reduce HBsAg. HBV genotypes B and C responded similarly, with overexpressed SEL1L resulting in reduced replication (**Supplementary Figures 2B,D**), while reduced SEL1L increased HBV DNA and secreted HBsAg (**Supplementary Figures 2A,C**). Collectively, these results suggested that host SEL1L protein negatively regulates HBV RNA, DNA, and proteins.

SEL1L Could Regulate Hepatitis B Virus Replication *via* a Post-transcriptional Mechanism

In order to clarify whether SEL1L-mediated downregulation of HBV RNA may be attributed to a transcriptional or post-transcriptional mechanism, HBV RNA analysis and promoter reporter assays were performed. Knockdown of SEL1L did not significantly alter HBV RNAs, including the 3.5-kb pregenomic (pg) RNA, the precursor for HBV DNA replication, and subgenomic RNAs of 2.4/2.1 kb for HBV envelope protein translation (**Figure 4A**). SEL1L overexpression decreased HBV RNA levels slightly (**Figure 4B**). Moreover, SEL1L did not significantly inhibit the activities of HBV core promoter or X promoter. It, in fact, increased the activities of SP1 and SP2 promoters, although the difference did not reach statistical significance (**Figure 4C**).

The decay kinetics of HBV RNA were measured with and without SEL1L overexpression. HepDES19 cells were transfected with control vector or plasmid SEL1L without tetracycline and

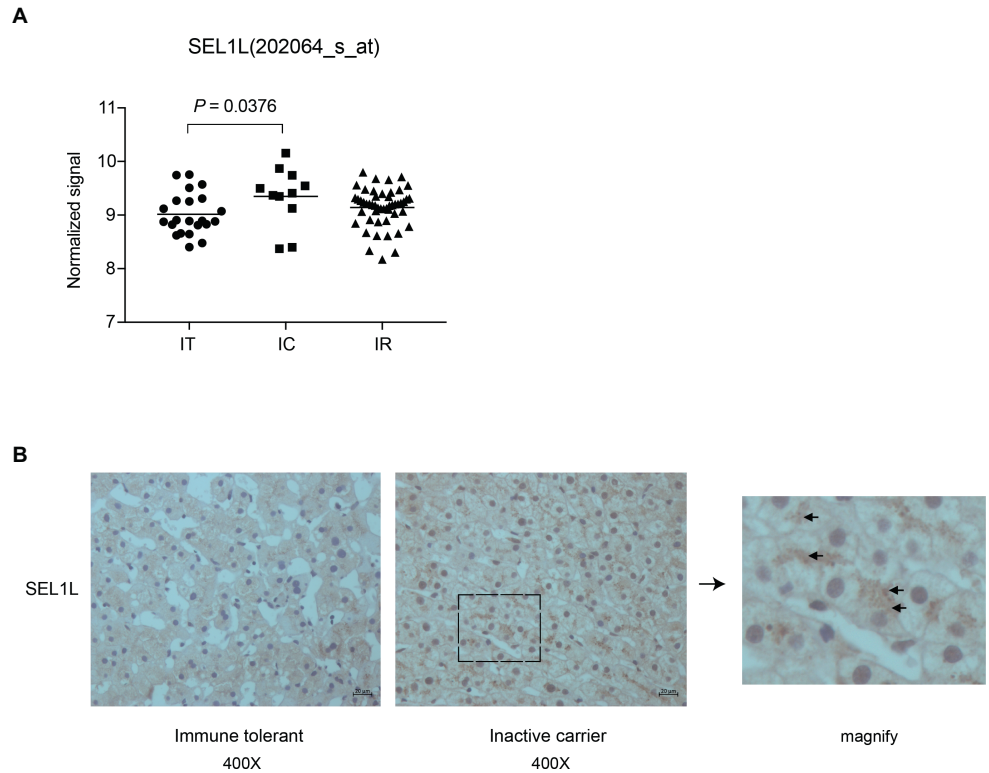

FIGURE 1 | Intrahepatic expression of SEL1L was significantly higher in inactive carrier patients than in immune tolerant patients. **(A)** Liver biopsies were performed in the patients and then subjected to RNA extraction and microarray analysis using Affymetrix Human Genome U133 Plus 2.0 Array in our previous studies (Liu et al., 2018). The intrahepatic SEL1L expression was displayed in scatter plots. The mean expression levels of SEL1L in the immune tolerant (IT), inactive carrier state (IC), and immune reactive (IR) patients were calculated and compared. $p < 0.05$ was considered significant. **(B)** Two sheets of liver tissues from immune tolerant and inactive carrier patients, respectively, were fixed and stained with SEL1L antibody (yellow).

incubated for 36 h to induce HBV RNA transcription. Tetracycline was then added so that *de novo* transcription of HBV pgRNA from the transgene ceased (**Supplementary Figure 3A**). Time-course measurements of the decay kinetics of HBV RNA were made following cessation of expression (**Supplementary Figure 3B**). HBV RNA degraded no faster in HepDES19 cells with overexpressed SEL1L than that in the controls. Thus, we concluded that SEL1L did not promote such degradation and therefore had no significant effect on the stability of HBV RNA. SEL1L-mediated HBV RNA reduction was not due to transcriptional inhibition but most likely attributed to a post-transcriptional mechanism.

Blocking the Endoplasmic Reticulum-Associated Degradation Pathway Increased Intracellular and Secreted Levels of Hepatitis B Virus Envelope Proteins

SEL1L is an adaptor protein for the ubiquitin ligase HRD1 in ERAD pathway. A previous study had demonstrated the activation of ERAD pathway by HBV, which in turn reduced the levels of three envelope proteins (Lazar et al., 2012). In the present study, we treated HBV-transfected cells with kifunensine (KIF), a potent inhibitor of ER mannosidase to block the ERAD pathway. It increased the secreted HBsAg levels in the supernatant of cultured cells in a dose-dependent manner (**Figure 5A**). Similar trend was observed for intracellular HBV envelope proteins (**Figure 5B**). Moreover, two important components of ERAD pathway, SEL1L and EDEM1, were also increased (**Figure 5B**), which probably resulted from the less consumption after ERAD inhibition. However, KIF did not increase HBV core protein level (**Figure 5B**), indicating that the decrease of core protein by SEL1L overexpression was not *via* ERAD pathway.

SEL1L Co-localized With HBsAg in the Cytoplasm to Generate a Granular Distribution

To check the interaction of SEL1L with HBV envelope proteins, we first examined its intracellular distribution in the absence of HBV. Immunofluorescence staining showed cytoplasmic localization of SEL1L protein (**Supplementary Figure 4A**), with homogeneous distribution. Strikingly, when HBsAg was also expressed in Huh7 cells, SEL1L accumulated into visible coarse granules (green spots) co-localizing with HBsAg-cherry (red spots) as obvious granules (yellow spots; **Figure 5C**). Nevertheless,

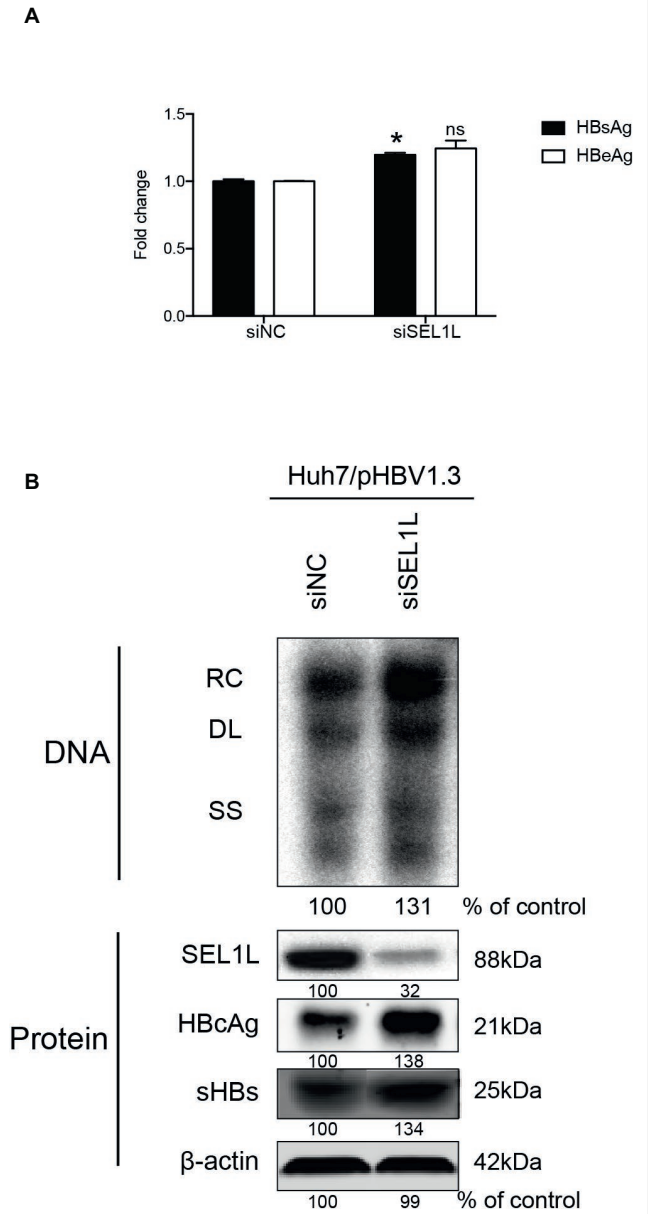

FIGURE 2 | Knocking down of SEL1L increased HBV replication in Huh7 cells. **(A)** Huh7 cells in 12-well plates were co-transfected with 1.5 μg pHBV 1.3 containing 1.3 mer genome-length HBV sequences and 20 nM control siRNA or siSEL1L and harvested after 72 h. Secreted HBsAg and HBeAg from the supernatant of cell culture were measured and reported as fold change. **(B)** Core DNA and proteins were analyzed by southern blot (upper panels) and western blot (lower panels) assays, respectively. The positions of relaxed circular (RC), single-stranded (SS) DNA were indicated. The expression of intracellular viral proteins including surface and core proteins was also measured. The levels of β-actin served as a loading control. The relative gray-scale value for each lane of DNA and proteins was measured by Image J software as the percentage of DNA in control cells. *$p < 0.05$; ns, not significant.

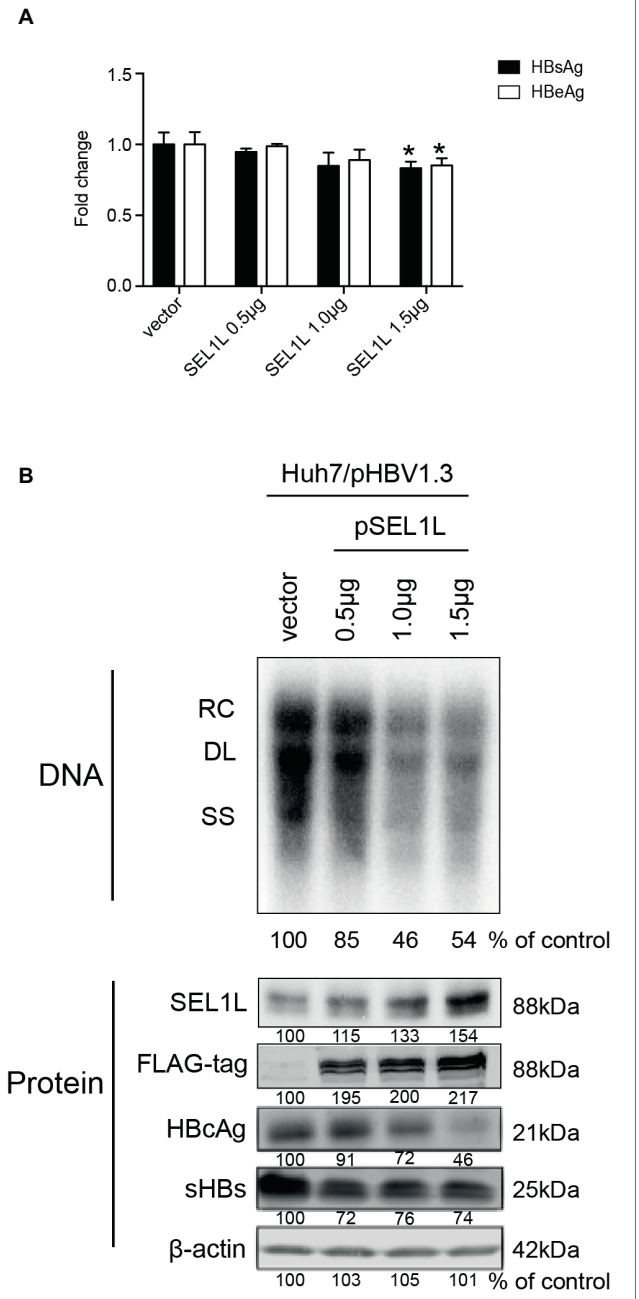

FIGURE 3 | Overexpression of SEL1L decreased HBV replication in Huh7 cells. Huh7 cells in 12-well plates were co-transfected with 1.5 μg pHBV1.3 and control empty vector or constructed plasmid expressing flag-tagged pSEL1L in a dose-dependent manner. Secreted viral proteins **(A)**, HBV DNA, and proteins **(B)** were detected as described above. The expression of SEL1L was revealed by western blot analysis with FLAG antibodies. *$p < 0.05$.

the pattern of homogeneous distribution could still be observed in some sections, despite HBsAg co-expression (**Figure 5C**, bottom panels). The separate localizations of SEL1L-GFP and HBsAg-cherry were shown in **Supplementary Figures 4B,C**. We further noted that SEL1L maintained a homogeneous, non-granular distribution where HBcAg expression was occurring in Huh7 cells (**Supplementary Figure 4D**). Incomplete co-localization was observed for SEL1L and HBcAg. The results suggested the association of SEL1L with HBsAg, which might be an intermediate in HBsAg degradation. Another mode is

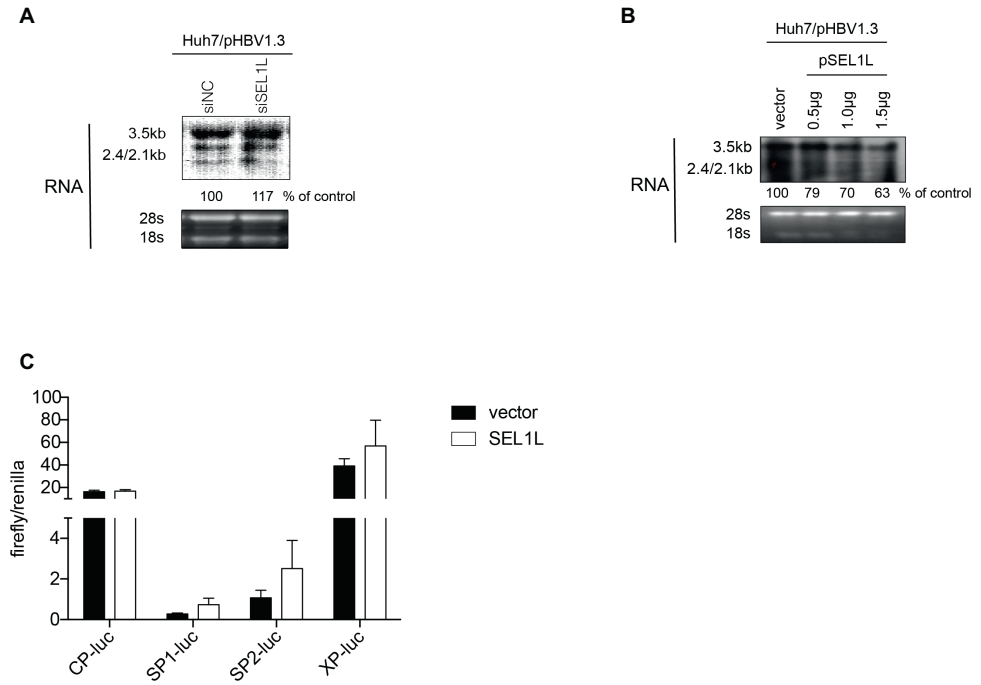

FIGURE 4 | SEL1L had no significant impact on HBV RNA and promoter activities. **(A,B)** Huh7 cells in 12-well plates were co-transfected with 1.5 μg pHBV1.3 and control empty vector or constructed plasmid expressing flag-tagged pSEL1L in a dose-dependent manner, or with 20 nM control siRNA or siSEL1L and harvested after 72 h. HBV RNAs were analyzed by northern blot assay. Ribosomal RNAs (28S and 18S) were presented as loading controls. The positions of HBV 3.5, 2.4, and 2.1 kb RNAs were indicated. The relative gray-scale value for each lane of RNA was measured by Image J software as the percentage of RNA in control cells. **(C)** Huh7 cells in 24-well plates were co co-transfected with 100 ng of four HBV promoters Cp-Luc, SP1-Luc, SP2-Luc, or XP-Luc, and 100 ng of *Renilla*, plus 300 ng of control vector or plasmid SEL1L. Forty-eight hours after transfection, cells were harvested, and luciferase activity was measured.

suspected as the explanation for the decrease of HBcAg when SEL1L was expressed.

SEL1L Silencing May Promote Hepatitis B Virus Replication Through the Activation of Endoplasmic Reticulum Quality Control-Autophagy Pathway

ERAD is not the only pathway for degradation of misfolded proteins. Buchberger had demonstrated another ER quality control-autophagy (ERQC-autophagy) pathway that allows the entry of ERAD-resistant conformers, followed by degradation through the autophagosome-lysosome format (Buchberger, 2014; Houck et al., 2014). However, whether ERQC-autophagy is a compensatory pathway or parallel option for proteins that cannot be recognized, ubiquitinated, or transported by ERAD pathway remains to be clarified.

To examine the effect of SEL1L knockdown on autophagy, plasmid pHBV1.3 and siRNAs were co-transfected into Huh7 cells. As shown in **Figure 6A**, knockdown of SEL1L increased LC3 and HBsAg expression, which was observed to be co-localized. CQ, which is an autophagy activator, was used as a positive control. It, therefore, suggests that knockdown of SEL1L induced autophagy activation.

As described above, SEL1L overexpression decreased HBV RNA and core protein, which cannot be otherwise explained by the ERAD pathway. Hence, we added 3-methyladenine (3-MA), an autophagy inhibitor, to the culture medium, either alone or together with the knockdown of SEL1L, in Huh7 cells transfected with pHBV 1.3 plasmid. Results showed that HBV core DNA secreted and intracellular HBsAg and HBeAg levels were reduced by 3-MA treatment, as was the level of LC3-II (**Figures 6B,C**), thus suggesting a reduction in autophagy (consistent with previous studies; Lin et al., 2018). Interestingly, knockdown of SEL1L had the opposite effect and led to a significant increase in LC3-II. If 3-MA treatment was performed along with knockdown of SEL1L, LC3-II levels were still higher than 3-MA treatment alone but slightly lower than in SEL1L knockdown alone (**Figure 6C**). HBV DNA and core protein have been earlier reported to be increased by autophagy (Liu et al., 2014; Lin et al., 2017). Thus, we suspect that knockdown of SEL1L blocked the ERAD pathway due to deficiency of a key component. The alternative ERQC-autophagy is then activated as a compensatory mechanism for degradation of conformers (**Figure 6D**). As for HBV, ERQC-autophagy activation may increase both HBV RNA and core protein levels.

DISCUSSION

Our present study raised the possibility of SEL1L playing an indispensable role in either ERAD or ERQC-autophagy pathway

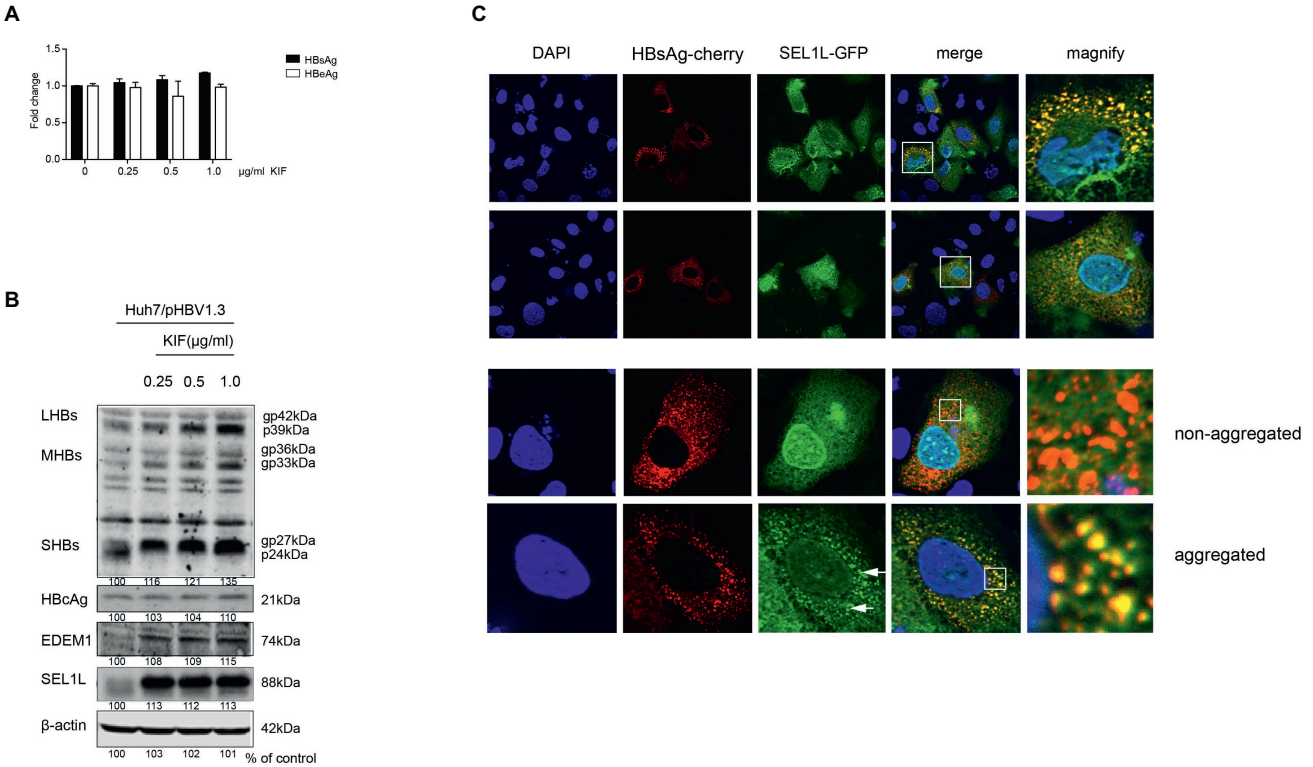

FIGURE 5 | SEL1L decreased HBV envelope proteins through the ERAD pathway and may be aggregated to form granules. **(A,B)** Huh7 cells in 12-well plates were transfected with 1.5 μg pHBV1.3, followed by treating cells with ER mannosidase inhibitor KIF in a dose-dependent manner for 48 h post transfection. The expression levels of intracellular and secreted viral proteins as well as SEL1L and EDEM1 were measured as previously described. **(C)** Huh7 cells were co-transfected with 1.5 μg pSEL1L-GFP (green) and 1.5 μg HBsAg-cherry (red). The cells were fixed and stained with DAPI (blue). The colocalization of SEL1L and HBsAg was measured by confocal microscopy.

to degrade viral proteins and inhibit HBV replication. Overexpression of SEL1L resulted in the reduction of HBV DNA, RNA, and viral proteins, whereas knockdown of SEL1L showed opposite results. We noticed that SEL1L did not inhibit HBV promoters, which suggested post-transcriptional mechanisms to be involved in the reduction of HBV RNA and core proteins. Furthermore, our data suggested that while SEL1L probably decreased HBV envelope proteins through the ERAD pathway, SEL1L silencing increased HBV RNAs and core protein possibly *via* the ERQC-autophagy pathway.

SEL1L is a highly conserved ER-resident trans-membrane protein involved in the degradation of a subset of misfolded ER proteins through ERAD pathway [13,14,17]. SEL1L was found to be indispensable for mammalian ERAD and ER homeostasis (Sun et al., 2014). However, the relationship between SEL1L and HBV infection had not been investigated earlier. Infection of several viruses has been shown to induce unfolded protein response (UPR; Ambrose and Mackenzie, 2011; Trujillo-Alonso et al., 2011). Recently, importance of the ERAD pathway in modulating HCV and HBV infection was demonstrated with more attention on EDEMs. EDEMs interact with HCV glycoproteins, inducing increased ubiquitylation (Saeed et al., 2011). As for HBV, ERAD pathway was found to reduce the intracellular level of envelope proteins (Lazar et al., 2012). The downstream SEL1L is usually thought to form a complex with HRD1 and OS9, and control HRD1 stability (Cattaneo et al., 2008). Our data demonstrated the decrease of HBV envelope proteins by SEL1L overexpression, thus resulting in ERAD pathway activation; however, no effect was observed on HBV core protein when ERAD was blocked by kifunensine. Besides, silencing OS9 and HRD1 did not alter HBsAg or core protein levels (data not shown). We, therefore, suspected that SEL1L may occupy an important site in another pathway for the reduction of core protein.

SEL1L may function as HRD1-independent pattern in cells [15]. A recent study showed that a SEL1L-LC3-I complex was formed to deliver ERAD-associated proteins, which controlled the efficacy of ERAD (Noack et al., 2014). Sharma et al. found replication of Japanese encephalitis virus to be suppressed by autophagy occurring on LC3-I-containing membranes, which are activated by silencing of SEL1L and EDEM1 (Sharma et al., 2014); this suggested that SEL1L deficiency activates autophagy. On the contrary, Sun et al. proposed that SEL1L deficiency did not induce increase of autophagy in the pancreas, as evidenced by LC3B cleavage in mice (Sun et al., 2014).

Autophagy is known to impact on HBV replication significantly (Sir et al., 2010; Li et al., 2011; Liu et al., 2014). Independent

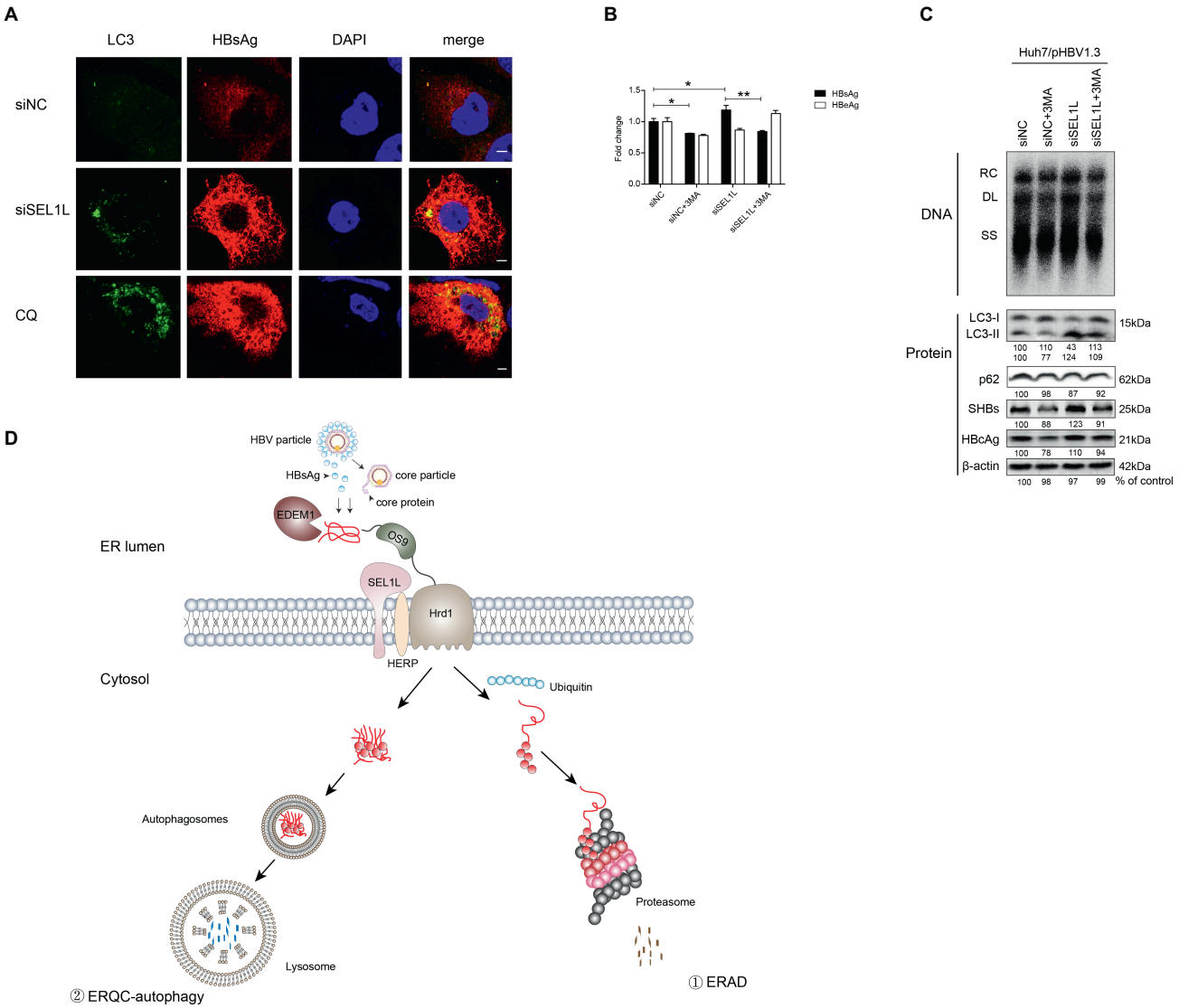

FIGURE 6 | Silencing of SEL1L induced ERQC-autophagy activation. **(A)** Huh7 cells were co-transfected with 1.5 μg pHBV 1.3 and 20 nM control siRNA or siSEL1L. After 48 h, wells were fixed and incubated with primary anti-LC3, followed by staining with Alexa Fluor 488-conjugated anti-rabbit secondary antibody IgG. As for HBsAg staining, primary anti-HBsAg and Alexa Fluor 594-conjugated anti-rabbit secondary antibody IgG were used. The cells were treated with 10 μmol/L CQ for 24 h as a positive control. The images were captured by confocal microscopy. **(B,C)** Huh7 cells in 12-well plates were co-transfected with 1.5 μg pHBV 1.3 and 20 nM control siRNA or siSEL1L. A 3-MA (10 mM) was treated for 24 h before harvest. Secreted HBsAg and HBeAg from the supernatant of cell culture were measured. Analysis of LC3, p62, intracellular HBsAg, and HBcAg expression was performed by western blotting. **(D)** Degradation pathways for proteins at the endoplasmic reticulum. EDEM1 and OS-9 facilitate delivery of misfolded polypeptides to the adaptor proteins SEL1L and the HRD1 dislocation machinery. As for HBV, envelope and core proteins proceed to the ER membrane. Misfolded proteins dislocated across the ER membrane, which are polyubiquitylated, and degraded by cytosolic proteasomes (route 1). Under conditions that limit proteasomal capacity, the dislocated substrates aggregate in the cytoplasm and accumulate in aggresomes, which are then transferred to the lysosome for selective degradation by autophagy (route 2). After fusion of the autophagosome with lysosome, ERAD-resistant protein aggregates are engulfed by autophagosomes and degraded by lysosomal hydrolases (route 2). *$p < 0.05$; **$p < 0.01$.

studies have consistently demonstrated that autophagy inhibition strongly decreases HBV replication in hepatic cells (Sir et al., 2010; Li et al., 2011). Additionally, autophagy deficiency was found to strongly reduce HBV replication in a transgenic mouse model (Tian et al., 2011). In fact, at the late stage of autophagy, HBV replication is enhanced (Lin et al., 2018). In yeast, autophagy function is a distinct degradation pathway to remove proteins from the ER (Kruse et al., 2006). Relation between ERAD and autophagy was established when Houck et al. reported that novel ERQC-autophagy could degrade ER-resistant proteins (Houck et al., 2014). The key structure of polypeptide substrate, which can be recognized by ERQC-autophagy, is yet to be defined, and the relationship between ERAD and ERQC-autophagy remains largely unknown. It is, however, tempting to suggest that in case of insufficient degradation by ERAD, usually due to abnormally structured polypeptides or deficiency of ERAD

components, proteins aggregate on the ER membrane to increase ER stress and stimulate autophagy. Our data suggested that SEL1L deficiency is actually related to the increase of autophagy in liver, suggesting the possibility of organ-specific properties of ERQC-autophagy. Due to the differential structures of HBV core protein and surface proteins, they might enter different degradation pathways induced by SEL1L overexpression. However, we did not clarify the details of this event, which deserves further investigation. The demonstration of host-virus interaction will be definitely helpful in exploring new methods for therapy of chronic hepatitis B.

In summary, our study suggested SEL1L as indispensable in ERAD as well as alternative ERQC-autophagy pathway for degradation of HBV proteins and control of HBV replication. Although the exact mechanisms for degradation of HBV proteins remain unclear at the moment, the novel function of SEL1L is worth further investigation.

DATA AVAILABILITY STATEMENT

All datasets generated for this study are included in the article/**Supplementary Material**.

ETHICS STATEMENT

The studies involving human participants were reviewed and approved by the ethics committee of Fudan University affiliated Hushan Hospital. The patients/participants provided their written informed consent to participate in this study.

AUTHOR CONTRIBUTIONS

JWa conceived the project. JWa and JL wrote the manuscript. JWa, JL, JWu MD, ZS, and YL conducted the experiments. FL, YZ, RM, ML, and JZ offered the helpful guidance of this study.

FUNDING

This work was supported by the National Natural Science Foundation of China (81700526, 81471933, 81871640, 81701986, 81800529, 81800526), National Science and Technology Major Project of China (2017ZX10202203-007-002, 2017ZX10202202-001-001).

ACKNOWLEDGMENTS

We thank Dr. Jinke Pang and Mrs. Thekla Kemper (Essen University, Germany) for helpful suggestion in this study.

SUPPLEMENTARY MATERIAL

The Supplementary Material for this article can be found online at: https://www.frontiersin.org/articles/10.3389/fmicb.2019.02869/full#supplementary-material

REFERENCES

Ambrose, R. L., and Mackenzie, J. M. (2011). West Nile virus differentially modulates the unfolded protein response to facilitate replication and immune evasion. *J. Virol.* 85, 2723–2732. doi: 10.1128/JVI.02050-10

Barry, G., Fragkoudis, R., Ferguson, M. C., Lulla, A., Merits, A., Kohl, A., et al. (2010). Semliki forest virus-induced endoplasmic reticulum stress accelerates apoptotic death of mammalian cells. *J. Virol.* 84, 7369–7377. doi: 10.1128/JVI.02310-09

Buchberger, A. (2014). ERQC autophagy: yet another way to die. *Mol. Cell* 54, 3–4. doi: 10.1016/j.molcel.2014.03.037

Cattaneo, M., Otsu, M., Fagioli, C., Martino, S., Lotti, L. V., Sitia, R., et al. (2008). SEL1L and HRD1 are involved in the degradation of unassembled secretory Ig-mu chains. *J. Cell. Physiol.* 215, 794–802. doi: 10.1002/jcp.21364

European Association for the Study of the Liver. Electronic address: easloffice@easloffice.eu and European Association for the Study of the Liver (2017). EASL 2017 Clinical Practice Guidelines on the management of hepatitis B virus infection. *J. Hepatol.* 67, 370–398. doi: 10.1016/j.jhep.2017.03.021

Gerlich, W. H., Heermann, K. H., and Lu, X. (1992). Functions of hepatitis B surface proteins. *Arch. Virol. Suppl.* 4, 129–132.

Houck, S. A., Ren, H. Y., Madden, V. J., Bonner, J. N., Conlin, M. P., Janovick, J. A., et al. (2014). Quality control autophagy degrades soluble ERAD-resistant conformers of the misfolded membrane protein GnRHR. *Mol. Cell* 54, 166–179. doi: 10.1016/j.molcel.2014.02.025

Isler, J. A., Skalet, A. H., and Alwine, J. C. (2005). Human cytomegalovirus infection activates and regulates the unfolded protein response. *J. Virol.* 79, 6890–6899. doi: 10.1128/JVI.79.11.6890-6899.2005

Kruse, K. B., Brodsky, J. L., and McCracken, A. A. (2006). Characterization of an ERAD gene as VPS30/ATG6 reveals two alternative and functionally distinct protein quality control pathways: one for soluble Z variant of human alpha-1 proteinase inhibitor (A1PiZ) and another for aggregates of A1PiZ. *Mol. Biol. Cell* 17, 203–212. doi: 10.1091/mbc.e04-09-0779

Lazar, C., Macovei, A., Petrescu, S., and Branza-Nichita, N. (2012). Activation of ERAD pathway by human hepatitis B virus modulates viral and subviral particle production. *PLoS One* 7:e34169. doi: 10.1371/journal.pone.0034169

Li, J., Liu, Y., Wang, Z., Liu, K., Wang, Y., Liu, J., et al. (2011). Subversion of cellular autophagy machinery by hepatitis B virus for viral envelopment. *J. Virol.* 85, 6319–6333. doi: 10.1128/JVI.02627-10

Lin, Y., Deng, W., Pang, J., Kemper, T., Hu, J., Yin, J., et al. (2017). The microRNA-99 family modulates hepatitis B virus replication by promoting IGF-1R/PI3K/Akt/mTOR/ULK1 signaling-induced autophagy. *Cell. Microbiol.* 19, 1–15. doi: 10.1111/cmi.12709

Lin, Y., Wu, C., Wang, X., Kemper, T., Squire, A., Gunzer, M., et al. (2018). Hepatitis B virus is degraded by autophagosome-lysosome fusion mediated by Rab7 and related components. *Protein Cell* 10, 60–66. doi: 10.1007/s13238-018-0555-2

Liu, B., Fang, M., Hu, Y., Huang, B., Li, N., Chang, C., et al. (2014). Hepatitis B virus X protein inhibits autophagic degradation by impairing lysosomal maturation. *Autophagy* 10, 416–430. doi: 10.4161/auto.27286

Liu, H., Li, F., Zhang, X., Yu, J., Wang, J., Jia, J., et al. (2018). Differentially expressed intrahepatic genes contribute to control of hepatitis B virus replication in the inactive carrier phase. *J. Infect. Dis.* 217, 1044–1054. doi: 10.1093/infdis/jix683

Mao, R., Zhang, J., Jiang, D., Cai, D., Levy, J. M., Cuconati, A., et al. (2011). Indoleamine 2,3-dioxygenase mediates the antiviral effect of gamma interferon against hepatitis B virus in human hepatocyte-derived cells. *J. Virol.* 85, 1048–1057. doi: 10.1128/JVI.01998-10

Noack, J., Bernasconi, R., and Molinari, M. (2014). How viruses hijack the ERAD tuning machinery. *J. Virol.* 88, 10272–10275. doi: 10.1128/JVI.00801-14

Saeed, M., Suzuki, R., Watanabe, N., Masaki, T., Tomonaga, M., Muhammad, A., et al. (2011). Role of the endoplasmic reticulum-associated degradation (ERAD) pathway in degradation of hepatitis C virus envelope proteins and production of virus particles. *J. Biol. Chem.* 286, 37264–37273. doi: 10.1074/jbc.M111.259085

Schweitzer, A., Horn, J., Mikolajczyk, R. T., Krause, G., and Ott, J. J. (2015). Estimations of worldwide prevalence of chronic hepatitis B virus infection: a systematic review of data published between 1965 and 2013. *Lancet* 386, 1546–1555. doi: 10.1016/S0140-6736(15)61412-X

Sharma, M., Bhattacharyya, S., Nain, M., Kaur, M., Sood, V., Gupta, V., et al. (2014). Japanese encephalitis virus replication is negatively regulated by autophagy and occurs on LC3-I- and EDEM1-containing membranes. *Autophagy* 10, 1637–1651. doi: 10.4161/auto.29455

Sir, D., Tian, Y., Chen, W. L., Ann, D. K., Yen, T. S., and Ou, J. H. (2010). The early autophagic pathway is activated by hepatitis B virus and required for viral DNA replication. *Proc. Natl. Acad. Sci. U. S. A.* 107, 4383–4388. doi: 10.1073/pnas.0911373107

Sun, S., Shi, G., Han, X., Francisco, A. B., Ji, Y., Mendonca, N., et al. (2014). Sel1L is indispensable for mammalian endoplasmic reticulum-associated degradation, endoplasmic reticulum homeostasis, and survival. *Proc. Natl. Acad. Sci. U. S. A.* 111, E582–E591. doi: 10.1073/pnas.1318114111

Tian, Y., Sir, D., Kuo, C. F., Ann, D. K., and Ou, J. H. (2011). Autophagy required for hepatitis B virus replication in transgenic mice. *J. Virol.* 85, 13453–13456. doi: 10.1128/JVI.06064-11

Tiollais, P., Pourcel, C., and Dejean, A. (1985). The hepatitis B virus. *Nature* 317, 489–495. doi: 10.1038/317489a0

Trujillo-Alonso, V., Maruri-Avidal, L., Arias, C. F., and Lopez, S. (2011). Rotavirus infection induces the unfolded protein response of the cell and controls it through the nonstructural protein NSP3. *J. Virol.* 85, 12594–12604. doi: 10.1128/JVI.05620-11

Vembar, S. S., and Brodsky, J. L. (2008). One step at a time: endoplasmic reticulum-associated degradation. *Nat. Rev. Mol. Cell Biol.* 9, 944–957. doi: 10.1038/nrm2546

Yu, C. Y., Hsu, Y. W., Liao, C. L., and Lin, Y. L. (2006). Flavivirus infection activates the XBP1 pathway of the unfolded protein response to cope with endoplasmic reticulum stress. *J. Virol.* 80, 11868–11880. doi: 10.1128/JVI.00879-06

Zhang, X., Zhang, E., Ma, Z., Pei, R., Jiang, M., Schlaak, J. F., et al. (2011). Modulation of hepatitis B virus replication and hepatocyte differentiation by microRNA-1. *Hepatology* 53, 1476–1485. doi: 10.1002/hep.24195

Conflict of Interest: The authors declare that the research was conducted in the absence of any commercial or financial relationships that could be construed as a potential conflict of interest.

Copyright © 2019 Wang, Li, Wu, Dong, Shen, Lin, Li, Zhang, Mao, Lu and Zhang. This is an open-access article distributed under the terms of the Creative Commons Attribution License (CC BY). The use, distribution or reproduction in other forums is permitted, provided the original author(s) and the copyright owner(s) are credited and that the original publication in this journal is cited, in accordance with accepted academic practice. No use, distribution or reproduction is permitted which does not comply with these terms.

frontiers in Microbiology

ORIGINAL RESEARCH
published: 20 December 2019
doi: 10.3389/fmicb.2019.02955

Comparative Pathogenicity and Transmissibility of Pandemic H1N1, Avian H5N1, and Human H7N9 Influenza Viruses in Tree Shrews

*Shuai Xu, Xuyong Li, Jiayun Yang, Zhengxiang Wang, Yane Jia, Lu Han, Liang Wang and Qiyun Zhu**

State Key Laboratory of Veterinary Etiological Biology, Lanzhou Veterinary Research Institute, Chinese Academy of Agricultural Sciences, Lanzhou, China

Influenza A viruses (IAVs) continuously challenge the poultry industry and human health. Studies of IAVs are still hampered by the availability of suitable animal models. Chinese tree shrews (*Tupaia belangeri chinensis*) are closely related to primates physiologically and genetically, which make them a potential animal model for human diseases. In this study, we comprehensively evaluated infectivity and transmissibility in Chinese tree shrews by using pandemic H1N1 (A/Sichuan/1/2009, pdmH1N1), avian-origin H5N1 (A/Chicken/Gansu/2/2012, H5N1) and early human-origin H7N9 (A/Suzhou/SZ19/2014, H7N9) IAVs. We found that these viruses replicated efficiently in primary tree shrew cells and tree shrews without prior adaption. Pathological lesions in the lungs of the infected tree shrews were severe on day 3 post-inoculation, although clinic symptoms were self-limiting. The pdmH1N1 and H7N9 viruses, but not the H5N1 virus, transmitted among tree shrews by direct contact. Interestingly, we also observed that unadapted H7N9 virus could transmit from tree shrews to naïve guinea pigs. Virus-inoculated tree shrews generated a strong humoral immune response and were protected from challenge with homologous virus. Taken together, our findings suggest the Chinese tree shrew would be a useful mammalian model to study the pathogenesis and transmission of IAVs.

Keywords: H1N1, H5N1, H7N9, tree shrew, infectivity, transmissibility

OPEN ACCESS

Edited by:
Zhengli Shi,
Wuhan Institute of Virology (CAS), China

Reviewed by:
Gloria Consuelo Ramirez-Nieto,
Universidad Nacional de Colombia, Colombia
Jae-Keun Park,
National Institutes of Health (NIH), United States

***Correspondence:**
Qiyun Zhu
zhuqiyun@caas.cn

Specialty section:
This article was submitted to Virology, a section of the journal Frontiers in Microbiology

Received: *17 September 2019*
Accepted: *09 December 2019*
Published: *20 December 2019*

Citation:
Xu S, Li X, Yang J, Wang Z, Jia Y, Han L, Wang L and Zhu Q (2019) Comparative Pathogenicity and Transmissibility of Pandemic H1N1, Avian H5N1, and Human H7N9 Influenza Viruses in Tree Shrews. Front. Microbiol. 10:2955. doi: 10.3389/fmicb.2019.02955

INTRODUCTION

Influenza A viruses (IAVs) are segmented, single-stranded, negative-sense RNA viruses, whose genome comprises eight gene segments, including basic polymerase 2 (PB2), basic polymerase 1 (PB1), acidic polymerase (PA), hemagglutinin (HA), nucleoprotein (NP), neuraminidase (NA), matrix (M), and nonstructural protein (NS). IAVs are divided into 18 HA and 11 NA subtypes on the basis of the antigenicity of their HA and NA surface glycoproteins.

IAVs continuously challenge the poultry industry and human health due to antigenic shift and drift. In the twentieth century, H1N1, H2N2, and H3N2 viruses caused four influenza pandemics in humans, resulting in widespread disease and severe loss of life (Medina and Garcia-Sastre, 2011; Lipsitch, 2013). In 2009, a novel swine-origin influenza A (H1N1) pandemic

caused huge economic losses and casualties (Novel Swine-Origin Influenza A (H1N1) Virus Investigation Team et al., 2009). In addition, since 1997, increasing numbers of humans have been infected with highly pathogenic avian influenza H5N1 viruses, with a mortality rate of about 60% among confirmed cases (WHO, 2017). Most recently, avian influenza A (H7N9) viruses have emerged and infected human. To date, the H7N9 avian influenza virus has caused multiple outbreaks of severe disease in humans (Shi et al., 2018; WHO, 2018).

Animal models are essential for studies on the infection, immunity, and transmission of IAVs. Animal models such as mouse, cotton rat, pig, guinea pig, ferret, and nonhuman primate have been extensively developed, but many gaps remain in our understanding (Margine and Krammer, 2014). Each laboratory animal has its advantages and drawbacks. Generally, mouse and guinea pig models are used for pathogenicity and transmission studies. However, these animals do not exhibit some of the clinical symptoms experienced by humans, such as nasal exudates, fever, sneezing, and coughing, and their genetic backgrounds are far from those of humans. Ferrets and nonhuman primates (e.g., macaques) are excellent mammalian animal models for influenza virus pathogenicity and host immunity. Also, ferrets have been used as an important model for influenza virus transmission (Sun et al., 2016, 2019). Moreover, the clinical symptoms of influenza virus-infected ferrets are similar to those of humans (Maines et al., 2006; Shinya et al., 2012). However, availability, cost, livestock requirements, and ethical constraints limit the widespread use of these animals. Therefore, efforts remain focused on the development of new animal models in the influenza field.

The Chinese tree shrew (*Tupaia belangeri chinensis*) is a squirrel-like mammal widely distributing in south and southwest China. It has a small body size (100–150 g), a low maintenance cost, a short reproductive cycle (~6 weeks) and life span (6–8 years), and a much closer affinity to primates than that of ferrets and rodents (Xu et al., 2013). A comparative analysis of the tree shrew and human genome identified 28 genes in the tree shrew genome that were previously considered to be primate-specific (Fan et al., 2013). The high level of similarity in gene sequences between the tree shrew and humans has laid the foundation for the genetic basis to evaluate the tree shrew as a feasible animal model to study related diseases. In contrast, the unique genetic characteristics of tree shrews provide an opportunity for us to understand specific pathways mediated by the unique genes. For instance, loss of the important antiviral gene DDX58/RIG-I (retinoic acid inducible gene I) in the Chinese tree shrew has made the tree shrew a suitable animal model for studying viral infections (Fan et al., 2013; Xu et al., 2016; Yao, 2017).

Since 1970s, tree shrews have been used as animal models for various viruses. Herpes simplex virus (HSV) was the first virus known to infect tree shrews, and tree shrews proved to be a viable model to study HSV latency (Darai et al., 1978; Li et al., 2015, 2016). Moreover, the tree shrew was the only non-primate animal found to be susceptible to hepatitis B virus (HBV) infection, and therefore was used to study HBV infection for many years (Guo et al., 2018). In 2012, the cellular functional receptor of HBV, sodium taurocholate cotransporting polypeptide (NTCP), was identified in tree shrew model (Yan et al., 2012). Tree shrews have been demonstrated to possess all of the essential factors required for hepatitis C virus (HCV) infection and can be used as a potential platform for studying HCV infection (Tong et al., 2011; Feng et al., 2017). Most recently, the tree shrew was used as an animal model to study Zika virus (ZIKV) infection, exhibiting robust viral secretions in sera and saliva as well as cutaneous inflammation and dermatological manifestations, which were similar to those in ZIKV-infected patients (Zhang et al., 2019).

In 2013, Yang et al. analyzed the distribution of α2,3 and α2,6 sialic acid receptors in the respiratory tract of tree shrew (Yang et al., 2013), and investigated the pathological change, seroconversion, and cytokine response of tree shrews infected with H1N1, H9N2 IAVs, and influenza B virus (Yang et al., 2013; Li et al., 2018; Yuan et al., 2019). Most recently, Sanada et al. assessed the pathogenicity of H5N1 and H7N9 IAVs in tree shrews and found that H5N1 influenza virus infection caused severe diffuse pneumonia with fever and weight loss; in contrast, H7N9 influenza virus infection caused focal pneumonia in this tree shrew model (Sanada et al., 2019). These studies suggested that tree shrews could be a useful alternative mammalian model to study the pathogenesis of influenza virus. However, transmissibility and immune responses in the tree shrew model for different IAVs have not been comprehensively investigated.

To better prepare for IAV pandemics and develop more effective prevention and control strategies, a comprehensive understanding of the biological characteristics of the various influenza virus infections is necessary through the use of a suitable animal model. In the present study, we investigated the susceptibility and transmissibility of H1N1, H5N1, and H7N9 IAVs in tree shrews, and assessed the humoral immune response in this model.

MATERIALS AND METHODS

Biosafety and Ethical Statements

All experiments with live influenza viruses were conducted within enhanced animal biosafety level 3+ (ABSL3+) facilities. This study was carried out in strict accordance with the recommendations in the Guide for the Care and Use of Laboratory Animals of the Ministry of Science and Technology of the People's Republic of China. The details of the facility and the biosafety and biosecurity measures used have been previously reported (Zhang et al., 2013b). The protocols for animal studies were approved by Animal Ethics Committee of Lanzhou Veterinary Research Institute, Chinese Academy of Agricultural Sciences.

Animals

One to four-month-old female Chinese tree shrews weighing 90–110 g was obtained from the experimental animal core facility of the Kunming Institute of Zoology, Chinese Academy of Sciences (Kunming, China). Six-week-old female Balb/c mice and five- to six-week-old female Hartley strain guinea pigs (250–300 g) were purchased from Vital River Co. Ltd., Beijing, China. All animals were housed in ventilated cages, and provided food and water *ad libitum*.

Cells and Viruses

Madin-Darby canine kidney (MDCK, American Type Culture Collection, USA) cells were grown in DMEM (Gibco-BRL; 11965-092) supplemented with 10% (vol/vol) FBS (Gibco-BRL; 10099-141) and 1× penicillin/streptomycin (Gibco-BRL; 10378016) at 37°C in 5% CO_2. Primary renal cells (TSPRCs) and lung cells (TSPLCs) were established from Chinese tree shrews (aged 1–4 months) as follows: kidneys or lungs were taken from the sacrificed tree shrew and minced into small pieces (about 1 mm^3) in pre-cold PBS, and the pieces were transferred into a 50 ml sterile plastic tube containing 5 mg/ml collagenase type IV (Invitrogen, USA) solution for 30 min in a 37°C water bath. After digestion, the solution was filtered through a 200-mesh sieve to remove tissue pieces. The TSPRCs or TSPLCs were suspended and washed three times with pre-cold PBS. Finally, the cells were resuspended and cultured at a density of 2×10^6 cells/ml in high-glucose DMEM supplemented with 10% FBS and 1× penicillin/streptomycin at 37°C in 5% CO_2 until confluent. The cells were passaged three times and then used for the indicated experiments.

H1N1 virus A/Sichuan/1/2009 (pdmH1N1) was isolated from the first human case of the 2009 influenza pandemic in China. H5N1 highly pathogenic avian influenza virus A/Chicken/Gansu/2/2012 (H5N1) was isolated in Gansu Province in China in 2012 (Yang et al., 2019). H7N9 virus A/Suzhou/SZ19/2014 (H7N9) was isolated from Jiangsu Province in China in 2014. Virus stocks were propagated in specific-pathogen-free (SPF) chicken eggs and stored at −70°C until use.

Experimental Infection of Animals

Each animal was inoculated with viruses at 10^6 EID_{50} in a volume of 200 μl for tree shrews, 50 μl for mice or 300 μl for guinea pigs after they were lightly anesthetized with 0.5% pentobarbital sodium or carbon dioxide. The control animals were inoculated with an equal volume of PBS. Clinical signs of infection and body weight were recorded daily. The animals were sacrificed on the indicated days post-inoculations for virologic and pathological assays.

Viral Growth Kinetics

TSPRCs and TSPLCs were infected with viruses at a multiplicity of infection (MOI) of 0.01. One hour after infection, the mediums were replaced with fresh OPTI-MEM (containing 0.05 μg/ml TPCK-trypsin) and the cells were maintained at 37°C. Virus-containing culture supernatants were collected at the indicated timepoints, and titrated in eggs. Growth data are presented as the average of three independent experiments.

Receptor Binding Specificity Assay

We tested the receptor binding specificity of the HA protein for α2,3- or α2,6-linked sialic acid using a solid-phase binding assay with two different glycopolymers: α-2,6 glycans (6′SLN, Neu5Aca2-6Galb1-4GlcNAcb-PAA-biotin) and α-2,3 glycans (3′SLN, Neu5Aca2-3Galb1-4GlcNAcb-PAA-biotin), as previously described (Imai et al., 2012). Briefly, a streptavidin-coated high-binding capacity 96-well plate (Pierce) was incubated with PBS containing different concentrations (starting from 2.4 μM) of biotinylated glycans at 4°C overnight. After the glycan solution was removed, the plates were washed four times with ice-cold PBS and then incubated at 4°C overnight with PBS containing 128 HA units of purified influenza virus. After washing, the plates were incubated for 4 h at 4°C with mouse antibody against influenza NP. The plates were then washed four times and incubated with horseradish peroxidase (HRP)-conjugated goat-anti-mouse antibody (Sigma-Aldrich) for 2 h at 4°C. After four washes, the plates were finally incubated with tetramethylbenzidine substrate (Thermo Scientific), and the reaction was stopped with 50 μl of 2 M H2SO4. Absorbance was determined at 450 nm.

RNA Isolation and Quantitative PCR

Total RNA from tree shrew primary cells was extracted with TRIzol (Invitrogen), following the manufacturer's instructions, and was subsequently transcripted into cDNA using M-MLV Reverse Transcriptase, according to the manufacturer's protocol (Promega). Real-time PCR was carried out using the ABI 7500 detection System (Applied Biosystems, CA). The mRNA level of each cytokine or chemokine was shown as fold of induction ($2^{-\Delta\Delta CT}$) in the graph. The sequences of the gene-specific primers used for qPCR were shown in **Table 1**.

Virus Titration

Virus titers of virus stocks and homogenized tissue samples were determined by end-point titration in eggs and/or MDCK cells. For end-point viral titration in eggs, 10-fold serial dilutions of each sample were inoculated into eggs. Sixty hours after inoculation, fluid from the allantoic cavity was collected and tested for the ability to agglutinate chicken erythrocytes as an indicator of viral replication. Infectious virus titers are reported as log10 EID_{50}/ml, and were calculated from three replicates by the method of Reed-Muench.

Pathological Analysis

Lung tissue was collected and fixed in 10% neutral buffered formalin for histopathological examination, which was performed as described previously (Masic et al., 2009). Tissue sections of lungs were stained with hematoxylin and eosin (H&E) and examined microscopically for alveolar edema, interstitial edema, hemorrhage, and inflammatory infiltration. The lesion severity of each of four pathological lesions was scored according to the distribution or extent of lesions within the sections examined

TABLE 1 | Primers for qRT-PCR used in this study.

Primer name	Sequence (5′-3′)
GAPDH-F	TCATTGACCTGAACTACAT
GAPDH-R	GAAGATGGTGATGGACTT
IFNβ-F	CTGAGGAAATTCAACGACCAC
IFNβ-R	ATAATAGCTCTTCAGGTGCAT
IFIT2-F	GGCCAATGGAAATCTCTACCAG
IFIT2-R	AGATAGCCTTTTCTTCGCACT
OASL-F	CTCGAGCTACTAACCATCTACGC
OASL-R	TCTGCCTCCTTCTGCTACGTT

according to the following scale: 0, no visible changes; 1, mild focal or multifocal change; 2, moderate multifocal change; 3, moderate diffuse change; or 4, severe diffuse change. Two independent pathologists scored all slides from blinded experimental groups.

Protein Content and Differential Blood Count of Bronchoalveolar Lavage Fluid

The bronchoalveolar lavage fluid (BALF) was obtained from tree shrews on day 3 post-inoculation. BALF was obtained from individual animals *via* tracheal cannulation and lavage with 2 ml of PBS. Protein content as a surrogate metric of lung barrier function was quantified by use of a BCA assay. For BALF cell analysis, BALF was centrifuged at 500 $\times g$ for 10 min to spin down the cells and the collected cells were resuspended in 2 ml of PBS. The cell suspension was washed three times in PBS buffer. Differential cell counts were obtained from smears stained with May-Grünwald-Giemsa. At least 200 cells were counted for each animal.

Antibody Response Assessment

Tree shrews were prime-inoculated intranasally (i.n.) with 10^6 EID_{50} of test viruses. Sera were collected from all animals 1 day before and on day 14 post-inoculation (p.i.). Twenty-one days post prime-inoculation, the tree shrews were challenged i.n. with 10^6 EID_{50} of the same virus. Nasal washes were collected from all of the animals at 2-day intervals, beginning on day 2 post-challenge and titrated in eggs. Sera were collected from all tree shrews on day 14 post-challenge for hemagglutinin inhibition (HI) and virus neutralization (VN) tests.

Intra- or Inter-Species Transmission Study

For the intra-species transmission study, groups of three guinea pigs or tree shrews were inoculated i.n. with 10^6 EID_{50} of test virus and housed in a ventilated cage. After 24 h, three guinea pigs or tree shrews were cohoused in the same cage as the inoculated animals. For the interspecies transmission study, three animals (tree shrews or guinea pigs) were inoculated i.n. with 10^6 EID_{50} of test virus and three animals of the other species (guinea pigs or tree shrews) were cohoused in the same cage at 24 h post-inoculation. Body weights of the inoculated and exposed animals were recorded at 2-day intervals, starting on day 0 p.i. Nasal washes were collected from all of the animals at 2-day intervals, starting on day 2 p.i. [1 day post-exposure (p.e.)], which was performed as descripted previously (Lowen et al., 2006). The nasal wash samples were first kept in −80°C and titrated in eggs. Sera were collected from each animal on day 2 before inoculation and day 21 p.i. for HI and VN tests.

Serological Assays

After serum samples were pretreated with receptor-destroying enzyme to eliminate inhibitors of hemagglutination, serum antibody titers were determined by using the HI test with 0.5% chicken red blood cells (prepared in our laboratory from SPF chickens) and VN in MDCK cells, which were performed as described previously (Maines et al., 2006; Laursen et al., 2018). The cutoff value used for the HI and VN antibody assays was 10.

Statistical Analysis

The statistical significance of comparisons between two groups was determined with the Student's *t*-test. p less than 0.05 were considered statistically significant. Comparisons of more than two groups were made with ANOVA with Bonferroni corrections. Survival analysis was performed with GraphPad Prism 6.

RESULTS

Pandemic H1N1, Avian H5N1, and Human H7N9 Influenza Viruses Efficiently Replicate in Primary Tree Shrew Cells

Yang and his colleagues demonstrated that H1N1 and H9N2 influenza viruses replicate in the upper respiratory tract of tree shrews, and exhibited moderate respiratory symptoms and pathological signs (Yang et al., 2013; Li et al., 2018). In the present study, to characterize the susceptibility of tree shrews to different IAVs, pandemic 2009 H1N1 virus A/Sichuan/1/2009 (pdmH1N1), avian-origin H5N1 virus A/Chicken/Gansu/2/2012 (H5N1), and human-origin H7N9 virus A/Suzhou/SZ19/2014 (H7N9) were selected as representative viruses. We found that the growth and infectivity of all three viruses were comparable in 9-day-old specific-pathogen-free (SPF) chicken eggs, but diverse in MDCK cells (**Table 2**). Our recent study showed that A/Chicken/Gansu/2/2012 (H5N1) was lethal to chickens and intravenous pathogenicity index was 2.97, indicating that the H5N1 virus was highly pathogenic for chickens (Yang et al., 2019). Molecular characterization indicated that the H5N1 virus possesses a polybasic cleavage site motif (PQRERRRKR/GLF), whereas pdmH1N1 and H7N9 viruses lack this feature (PSIQSR/GLF or PEIPKGR/GLF), suggesting pdmH1N1 and H7N9 viruses may be low pathogenic for chickens (**Table 2**). Additionally, we tested the receptor-binding properties of three viruses and found that pdmH1N1 virus only bound to α2, 6-siaylglycopolymer (human-type receptor), H5N1 virus only bound to α2, 3-siaylglycopolymer (avian-type receptor), and H7N9 virus bound to both receptors, which had greater affinity with α2, 6-siaylglycopolymer than that with the α2, 3-siaylglycopolymer (**Supplementary Figure S1**).

Next, we evaluated the infectivity of tree shrew primary renal and primary lung cells (TSPRCs or TSPLCs) by infected them with three viruses at a MOI of 0.01 in the presence of trypsin. Supernatants were collected at the indicated time-points for virus titration. As shown in **Figure 1A**, each virus replicated efficiently in the two cell types. The H5N1 virus titer reached a higher level in both cell types compared with the titers of the pdmH1N1 and H7N9 viruses at 24, 48, and 72 h post-infection (hpi). Virus replication in the TSPLCs reached a peak at 48 hpi, whereas in the TSPRCs, the titers of all three viruses continued to increase during

TABLE 2 | Growth and pathogenicity characteristics of three viruses.

Viruses	Virus growth[a]		HA cleavage site motif	Receptor-binding preference	
	$log_{10}EID_{50}$/ml	$log_{10}TCID_{50}$/ml		SA α-2, 3	SA α-2, 6
pdmH1N1	8.35 ± 0.13	5.58 ± 0.14	PSIQSR/GLF	No	Yes
H5N1	8.69 ± 0.17	6.64 ± 0.13	PQRERRRKR/GLF	Yes	No
H7N9	8.24 ± 0.08	4.69 ± 0.17	PEIPKGR/GLF	Yes	Yes

[a]*All data are the mean ± SD from three independent experiments.*

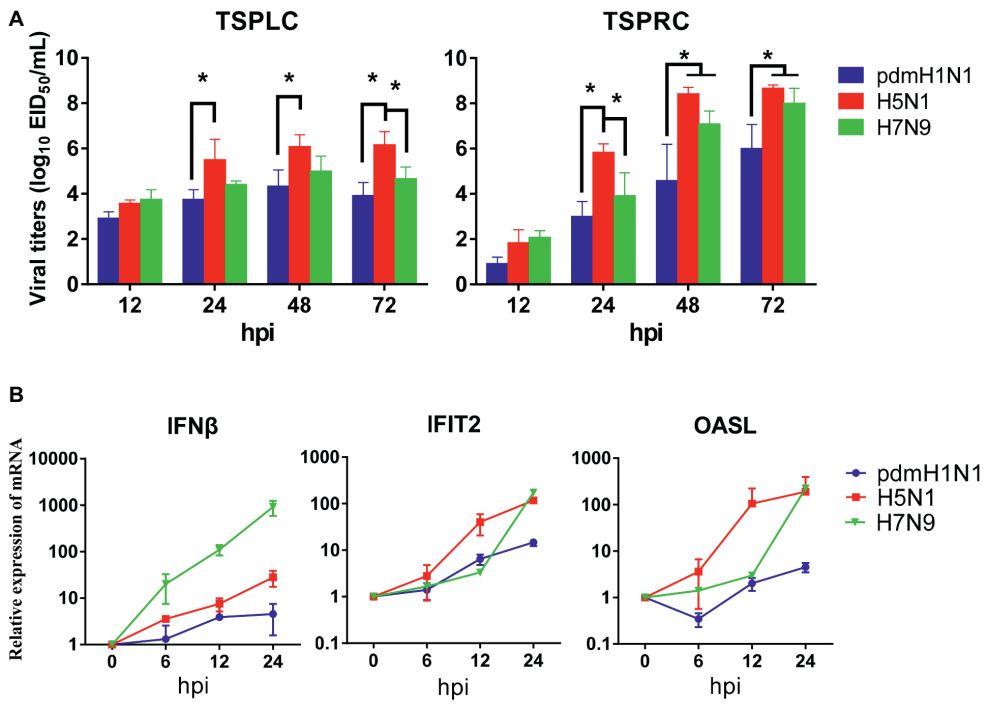

FIGURE 1 | Growth kinetics of influenza viruses and cytokine response in primary tree shrew cells. **(A)** Virus titers in tree shrew primary cells infected with pdmH1N1, H5N1, and H7N9 influenza viruses. Virus growth characteristics were determined by use of multi-cycle growth curves in tree shrew primary lung (left) or renal (right) cells infected with viruses at a MOI of 0.01. Viral titers were quantitated in SPF embryonated chicken eggs. **(B)** Cytokine expression at the transcription level in primary tree shrew renal cells infected with pdmH1N1, H5N1, or H7N9 influenza viruses. Primary tree shrew cells were either mock-infected or infected with one of the three viruses at a MOI of 1. Total RNAs were prepared at the indicated time points and analyzed by qRT-PCR to quantitate the cytokine mRNA levels. The data shown represent three independent experiments; bars represent the mean ± SD of the three independent experiments ($n = 3$). *$p < 0.05$.

the observation period (72 hpi) and were relatively high compared with those in the TSPLCs. We also assessed the mRNA levels of three major cytokines in the TSPRCs infected with the viruses (**Figure 1B**). Within the observation period, H7N9 virus induced a sharp increase of IFNβ expression at the mRNA level to about 1,000 folds at 24 hpi, while only 28 folds or even less induced by the H5N1 or pdmH1N1 virus. As for the IFNβ associated genes (IFIT2 and OASL), the H5N1 virus induced an upregulated expression within three viruses at the earliest stage. While at 24 hpi the H5N1 and H7N9 viruses induced higher expression of IFIT2 and OASL, compared with the pdmH1N1 virus. These results indicate that the pdmH1N1, H5N1, and H7N9 influenza viruses can efficiently replicate and activate innate immune responses in primary tree shrew cells.

PdmH1N1, H5N1, and H7N9 Viruses Efficiently Replicate in Tree Shrews and Cause Subclinical Symptoms

To evaluate virologic characteristics in tree shrews, we intranasally inoculated tree shrews and balb/c mice (as controls) with pdmH1N1, H5N1, and H7N9 viruses. As shown in **Figure 2A**, all three influenza viruses replicated well in the respiratory tract. In the tree shrew respiratory tract, the viral titers reached a peak on day 1 or 2 post-inoculation (dpi), with infectious viral loads of over 10^5 and up to 10^7 EID_{50}/g. The H5N1 virus also replicated in the brains and spleens of the infected tree shrews on 1, 2, and 3 dpi, although the virus titers only ranged from $10^{0.58}$ to $10^{1.5}$ EID_{50}/g. The viruses were not detected in the spleens or brains of tree shrews inoculated with the pdmH1N1 or H7N9 viruses within the experimental time period. The virus titers

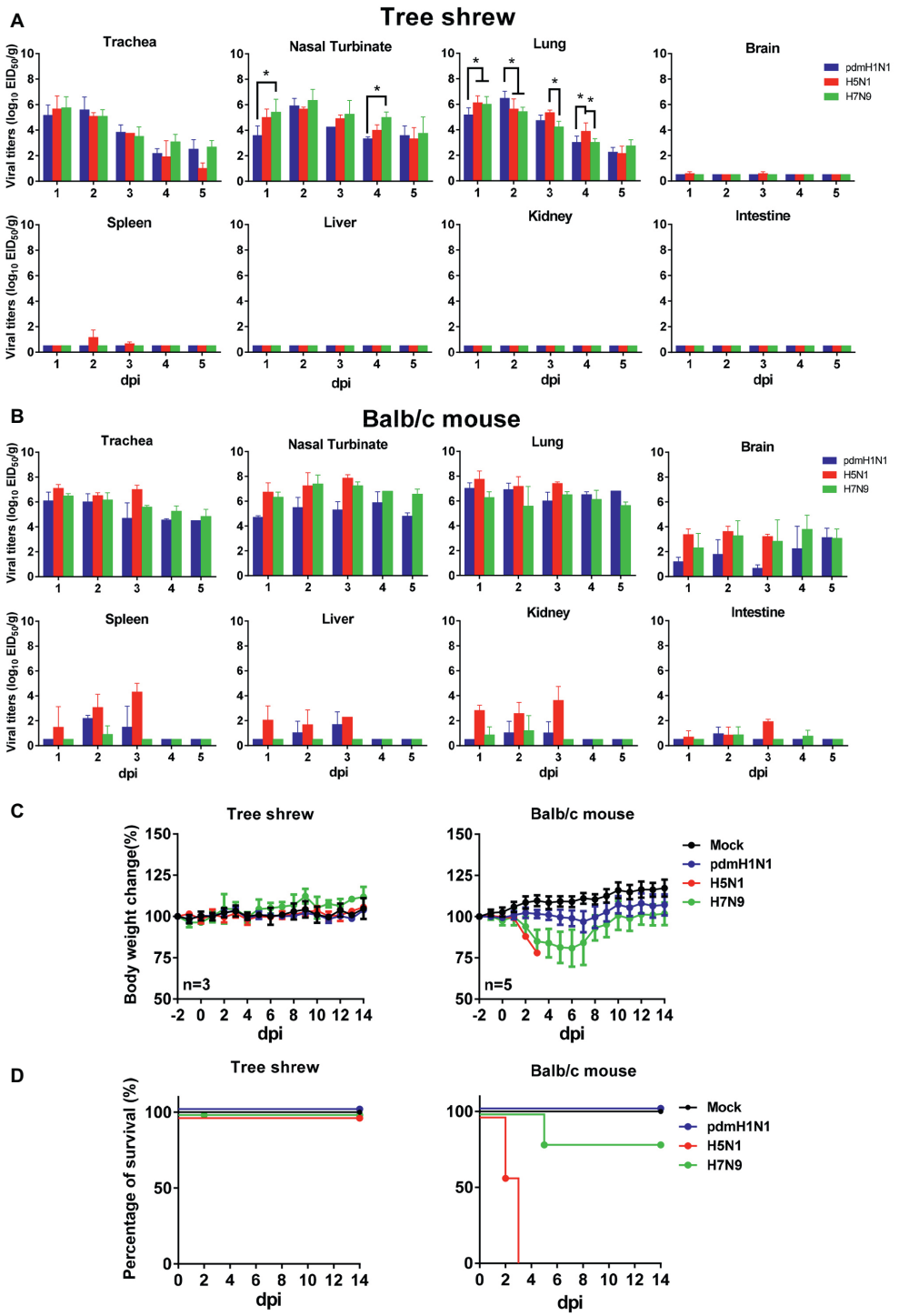

FIGURE 2 | Pathogenicity and virus titers in tissues of animals inoculated with pdmH1N1, H5N1, or H7N9 viruses. Three tree shrews or mice in each group were inoculated with pdmH1N1, H5N1, or H7N9 viruses or were mock-inoculated on day 0. Three tree shrews **(A)** or BALB/c mice **(B)** in each group were euthanized on days 1–5 post-inoculation, and the trachea, nasal turbinate, lung, brain, kidney, spleen, liver, and intestine were collected for viral titration in chicken eggs. Data shown are viral titers (log_{10} EID_{50}/g) from three animals; error bars indicate standard deviations. Averages and standard deviations of body weight changes **(C)** and survival **(D)** of three tree shrews in each group were calculated daily. Body weights are presented as percentages of the body weights before virus inoculation. Body weight changes of individual animals on each day after virus inoculation were compared with the average body weight days 2 before virus inoculation. Thereafter, averages and standard deviations of the body weight changes of the animals are indicated in the graphs. The values for body weights are means ± SD from live animals. *$p < 0.05$.

declined dramatically from 3 dpi in the trachea and in almost all lung lobes of animals inoculated with the pdmH1N1 and H7N9 viruses, and reached a very low level ($<10^3$ EID_{50}/g) by 4 dpi. However, the virus titers in these same tissues of animals inoculated with H5N1 virus remained high ($>10^5$ EID_{50}/g) until 3 dpi, and decreased to a very low level ($<10^3$ EID_{50}/g) by 5 dpi. As a control, we noted that the three viruses effectively replicated in the respiratory tract of the mice, and even saw systemic replication in the brain, liver, spleen, kidneys, and intestine (**Figure 2B**). These results indicate that tree shrews are susceptible to H1N1, H5N1, and H7N9 influenza viruses, as are mice, and that the tissue tropism of IAVs in the tree shrew model is mainly restricted in the respiratory tract.

Clinical observation during the course of infection revealed occasional snivel and sneezing. None of the infected tree shrews showed any weight loss during the observation period (**Figure 2C**). However, the infected mice showed varying degrees of decreased body weight, especially the H5N1-infected mice, which died within 5 days of infection (**Figures 2C,D**). These data suggest that, compared with the mouse model, tree shrews show a subclinical pathotype on infection with pdmH1N1, H5N1, and H7N9 viruses.

PdmH1N1, H5N1, and H7N9 Influenza Viruses Induce Pathological Lesions and Inflammatory Responses in the Lung of Tree Shrews

We assessed whether histological changes occurred in the lung tissues of tree shrews and mice inoculated with pdmH1N1, H5N1, or H7N9 viruses. The lungs of virus-infected tree shrews at 3 dpi showed obvious alveolar edema, interstitial edema, hemorrhage, and inflammatory infiltration. The inflammation was slightly milder at 5 dpi (**Figure 3A**). The histopathology score of the infected lungs from tree shrews was as high as 9.0 at 3 dpi and 6.0 at 5 dpi (**Figure 3B**). Of note, pdmH1N1 induced more severe lesions in infected lungs than H5N1 and H7N9. Lung inflammation in inoculated mice was relatively worse at 5 dpi compared with at 3 dpi, which may have been due to persistent high-level virus loads.

The physiopathology and disease progression induced by influenza virus involve destruction of the pulmonary capillary endothelium and alveolar epithelium as a result of neutrophil, macrophage, and erythrocyte accumulation, as well as protein-rich fluid in the alveolar spaces (Herold et al., 2006). Proteins in the bronchoalveolar lavage fluid (BALF) are usually measured as surrogates for disruption of the alveolar-capillary barrier (Ware and Matthay, 2000). As shown in **Figure 3C**, the alveolar-capillary barrier integrity following H5N1 virus infection was seriously disturbed, as indicated by the increased BALF protein content. For pdmH1N1 and H7N9 viruses, the BALF protein content was increased to different degrees compared with the mock infection. The total white cell count in the BALF was significantly increased following virus infection, especially for H5N1 virus (**Figure 3D**). Differential cell counts of BALF from infected tree shrew showed a significant increase in neutrophil and lymphocyte numbers compared with mock-infected tree shrews. These results suggest that influenza viruses induce pathological lesions and inflammatory responses in the lungs of tree shrews.

PdmH1N1, H5N1, and H7N9 Influenza Viruses Induce Protective Responses Against Homologous Challenge in Tree Shrews

Next, we examined sera from the inoculated tree shrews for antibodies against the influenza viruses by using hemagglutination inhibition (HI) and virus neutralization (VN) tests (**Table 3**). All tree shrews inoculated with pdmH1N1, H5N1, or H7N9 viruses generated specific antibodies at 3 weeks post-inoculation. The HI antibody against pdmH1N1 virus showed the highest titers in the sera of the inoculated tree shrews, whereas H5N1 virus induced the lowest antibody level in the sera. The VN test showed antibodies from the inoculated tree shrews had high neutralizing activity against the corresponding viruses. Not surprisingly, pre-inoculation sera were negative for influenza virus-specific antibodies by the HI and VN tests.

To test the protection efficacy against homologous challenge, we first inoculated tree shrews with 10^6 EID_{50}/ml of pdmH1N1, H5N1, or H7N9 virus and then challenged them with 10^6 EID_{50}/ml of homologous viruses at 3 weeks after inoculation. During the observation period, no clinic symptoms appeared in the tree shrews. Sera were collected at 14 days post-inoculation and 14 days post-challenge for HI and VN tests, which revealed a significant increase in the antibody level in each challenge group (**Figures 4A,B**). In addition, considerable virus shedding was detected in the nasal wash collected from the inoculated tree shrews from day 1 to day 7 post-inoculation, whereas almost no virus was detected in any of the nasal wash collected from the challenged tree shrews within the observation period (**Figure 4C**). These data suggest that single dose inoculation of tree shrews induced protective immunity against homologous influenza virus challenge.

PdmH1N1 and H7N9, but not H5N1, Influenza Viruses Are Transmissible in Tree Shrews

To test whether the three different influenza viruses can transmit in the tree shrew model, we evaluated their transmissibility among tree shrews by using a direct-contact approach, and employed a well-defined transmission model (guinea pig) for influenza virus as a control. The pre-inoculation sera from each animal at day 2 before inoculation were negative for influenza virus-specific antibodies by the HI and VN tests (data not shown). In the transmission experiment for pdmH1N1 virus, virus efficiently replicated in the upper respiratory tract of guinea pigs with titers of $\geq 10^{4.25}$, $\geq 10^{3.5}$, and $\geq 10^{2.25}$ EID_{50}/ml on days 2, 4, and 6 post-inoculation, respectively. Low titers of virus were detected in the nasal washings of exposed guinea pigs from day 1 p.e. (**Figure 5A**). Only one of three exposed guinea pigs seroconverted, with an HI titer of 80 and a VN titer of 531, whereas all pdmH1N1

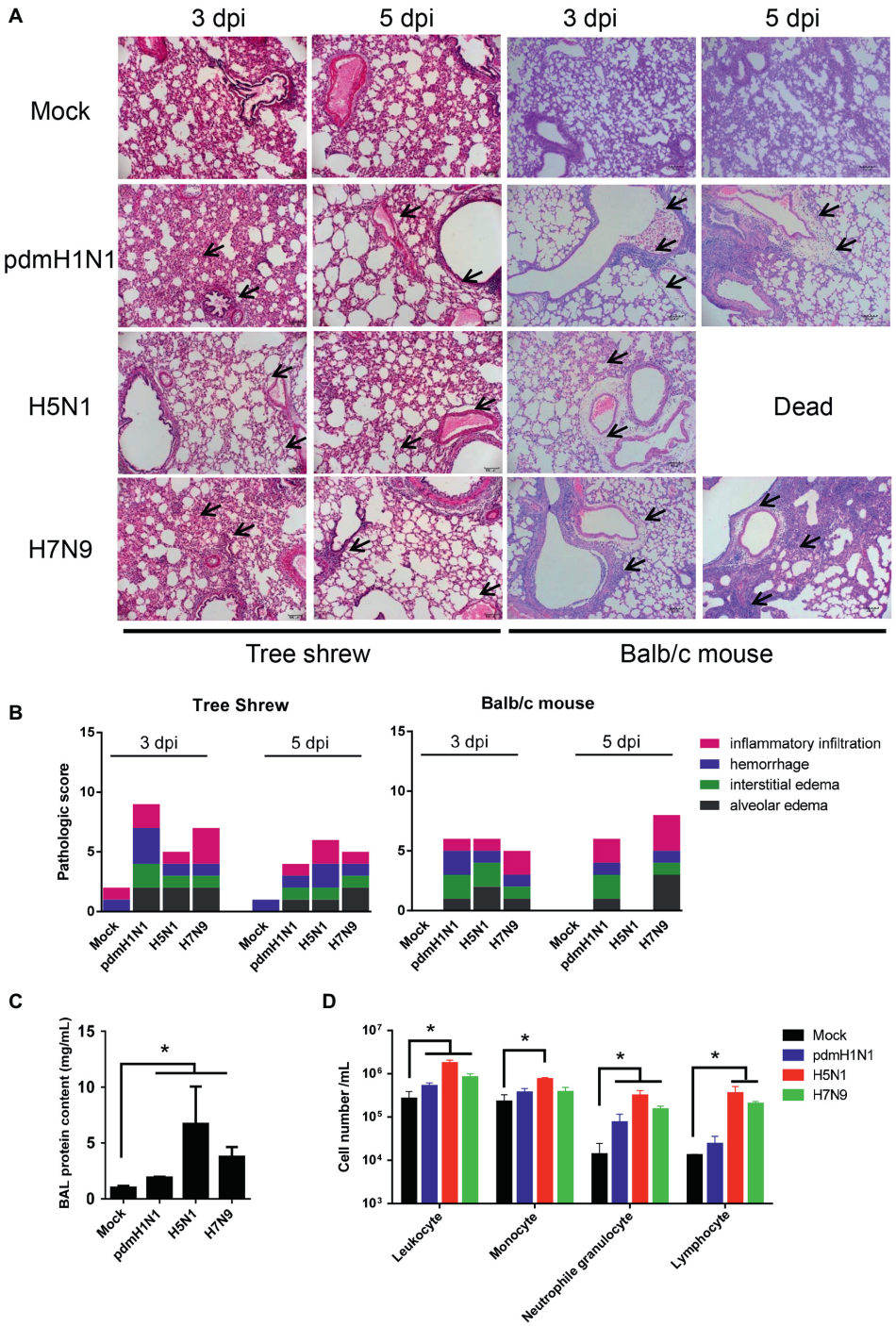

FIGURE 3 | Histopathology and inflammatory response in the lungs of tree shrews inoculated with influenza viruses. **(A)** Representative pathological images of inoculated lungs on days 3 and 5 post-inoculation. Scale bars, 100 μm. **(B)** Histopathological lung lesion scores from tree shrews inoculated with one of the three test viruses. Black arrows indicate edema, hemorrhage, or inflammatory infiltration. **(C)** Protein content was quantified by using a BCA assay with the BALF obtained from tree shrews at day 3 p.i. **(D)** Differential cell counts of BALF obtained from tree shrews at day 3 p.i. The data are presented as means ± SDs for samples of three animals ($n = 3$). $^*p < 0.05$.

virus-inoculated guinea pigs possessed HI titers ≥80 and VN titers ≥376 (**Table 4**). A similar trend was observed in the tree shrew groups; however, viruses were detectable in three nasal wash samples from day 5 p.e. in the exposed tree shrews (**Figure 5B**). Serum antibodies from two of three exposed tree shrews were seroconverted with HI titers of 40

and 320 and VN titers of 266 and 1,259 against pdmH1N1, respectively, whereas all inoculated tree shrews possessed HI titers ≥80 and VN titers ≥447 (**Table 4**). In the H7N9 transmission experiment, not surprisingly, H7N9 virus was readily transmitted from the three inoculated guinea pigs to the three contact ones with viral loads of up to $10^{4.5}$ EID_{50}/mL on day 5 p.e. (**Figure 5A**). Sera from all guinea pigs exposed to H7N9 virus were seroconverted with HI titers of 40–160 and VN titers of 79–447, whereas the inoculated guinea pigs possessed higher antibody titers with HI titers of 80–160 and VN titers 224–531 (**Table 4**). H7N9 virus also transmitted from the inoculated tree shrews to the contact animals (**Figure 5B**). Detectable virus persisted in nasal wash samples until day 9 p.e., while the viral load reached its peak on day 5 at $10^{4.17}$ EID_{50}/ml (**Figure 5B**). Sera from the exposed tree shrews were all seroconverted with HI titers of 20–80 and VN titers of 94–112, whereas the inoculated tree shrews induced higher antibody levels with HI titers of 80–160 and VN titers of 56–447 (**Table 4**). However, avian-origin H5N1 did not transmit in guinea pigs or tree shrews by direct contact in the present study (**Figures 5A,B**). No virus was detected in any of the nasal wash samples collected from the exposed guinea pigs or tree shrews within the observation period, and sera collected from the contact animals were negative against H5N1 virus at 21 days post-exposure (**Figures 5A,B** and **Table 4**). Together, these results indicate that pdmH1N1 and H7N9 viruses can transmit among guinea pigs and tree shrews in a direct contact model and that H7N9 has stronger transmissibility among guinea pigs than tree shrews compared with pdmH1N1 and H5N1 viruses.

TABLE 3 | Seroconversion of tree shrews pre- and post-inoculated with different influenza viruses.

Tree shrews inoculated with	Seroconversion (positive/total)[a]			
	Pre-inoculation sera		Post-inoculation sera	
	HI titer	VN titer	HI titer	VN titer
pdmH1N1	–[b]	–	3/3 (80–160)	3/3 (447–1,778)
H5N1	–	–	3/3 (20–80)	3/3 (158–447)
H7N9	–	–	3/3 (80–160)	3/3 (56–447)

[a]*Sera were collected from the animals at 2 days pre- or 3 weeks after the virus inoculation. The range of antibody titers obtained is indicated in parentheses.*
[b]*No antibody titer was detected.*

Interspecies Transmission of H7N9 Influenza Virus From Tree Shrews to Guinea Pigs

The interspecies transmission of IAVs poses a potential threat to humans and animals (Shi et al., 2018; WHO, 2018;

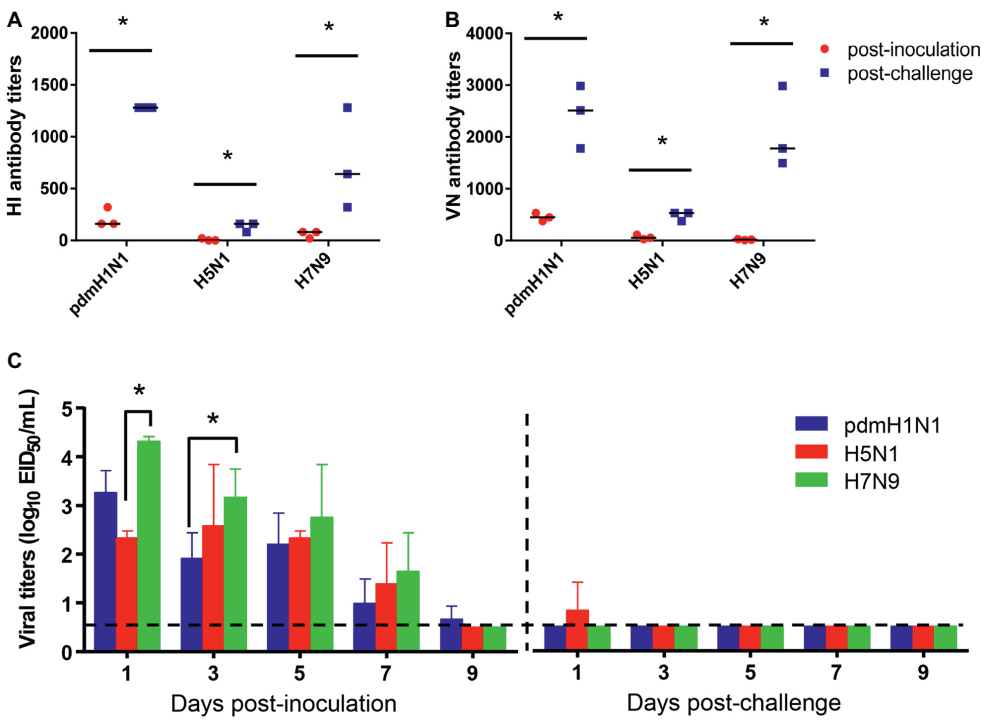

FIGURE 4 | Antibody response and virus shedding in tree shrews inoculated or challenged with influenza viruses. **(A,B)** Serum antibody titers were measured by using the HI method and virus neutralization test with serum collected at 14 days post-inoculation (red dots) and 14 days post-challenge (blue dots). **(C)** Nasal washes for virus shedding detection were collected every other day from tree shrews from day 2 post-inoculation or -challenge. Viral titers in nasal wash samples from each of three individual tree shrews are expressed as log_{10} EID_{50}/ml. The data are presented as means ± SDs for nasal wash samples of three animals ($n = 3$). *$p < 0.05$. Horizontal dashed lines indicate the lower limit of virus detection.

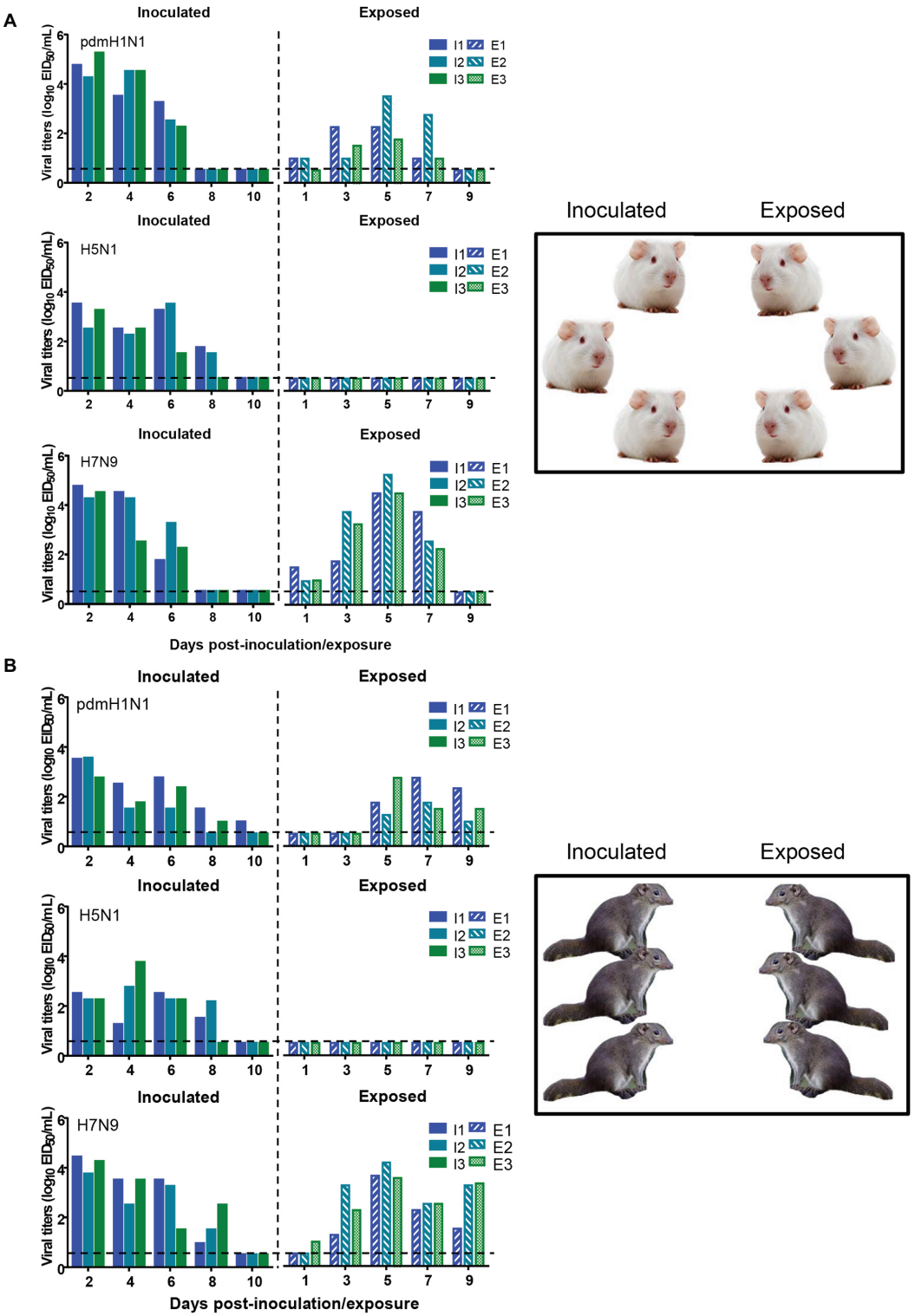

FIGURE 5 | Transmission of pdmH1N1, H5N1, and H7N9 viruses in guinea pigs **(A)** and tree shrews **(B)**. Groups of three guinea pigs or tree shrews were inoculated with 10^6 EID_{50} of the indicated viruses. The next day, the inoculated animals were cohoused with three guinea pigs or tree shrews. Nasal washes for virus shedding detection were collected every other day from all animals from day 2 of the initial infection. Viral titers in nasal wash samples from each of three individual inoculated animals (solid bars, left) and contact animals (dotted/diagonal bars, right) are expressed as $\log_{10}$ EID_{50}/ml. Each color bar represents a value from an individual animal. Horizontal dashed lines indicate the lower limit of virus detection. I or E means Inoculated or Exposed, respectively.

TABLE 4 | Seroconversion of guinea pigs and tree shrews inoculated with or exposed to different influenza viruses.

Virus	Animals	Seroconversion (positive/total)[a]			
		Inoculated		Exposed	
		HI titer	VN titer	HI titer	VN titer
H1N1	Guinea pig	3/3 (80–320)	3/3 (376–631)	1/3 (80)	1/3 (531)
H5N1	Guinea pig	3/3 (20–40)	3/3 (112–447)	0/3	0/3
H7N9	Guinea pig	3/3 (80–160)	3/3 (224–531)	3/3 (40–160)	3/3 (79–447)
H1N1	Tree shrew	3/3 (80–160)	3/3 (447–1,778)	2/3 (40–320)	2/3 (266–1,259)
H5N1	Tree shrew	3/3 (20–80)	3/3 (158–447)	0/3	0/3
H7N9	Tree shrew	3/3 (80–160)	3/3 (56–447)	3/3 (20–80)	3/3 (94–112)

[a]*Sera were collected from the animals at 3 weeks after the virus inoculation or exposure; these animals are the same ones that were used for the transmission studies shown in* **Figure 5**. *The range of antibody titers obtained was indicated in parentheses.*

Zeng et al., 2018). Based on the transmissibility of pdmH1N1 and H7N9 viruses in guinea pigs and tree shrews described above, we next sought to test whether these two viruses could transmit from guinea pig to tree shrew, or vice versa. For pandemic H1N1 virus, as shown in **Figures 6A,B**, the virus was not detected in the respiratory tract of the exposed guinea pigs or tree shrews, although pdmH1N1 was detectable in the nasal wash from the inoculated guinea pigs and tree shrews, suggesting that pdmH1N1 is not transmissible from tree shrews to guinea pigs, or vice versa. For H7N9 virus, viral shedding was detected on days 3–7 p.e. from the three exposed guinea pigs housed with the tree shrews inoculated with H7N9 virus (**Figure 6C**), but the corresponding interspecies transmission model was not established (**Figure 6D**). Consistent with the above, in the four groups of exposed animals, only the serum antibodies from two of the exposed guinea pigs co-housed with the H7N9-inoculated tree shrews were seroconverted with HI titers of 80 and VN titers of 316 (**Table 5**). These results suggest that the H7N9 virus, but not pdmH1N1, is transmissible from tree shrews to guinea pigs.

DISCUSSION

Previous studies have demonstrated that H1N1 and H9N2 influenza viruses replicate in the upper respiratory tract of tree shrews, which showed moderate respiratory symptoms and pathological signs (Yang et al., 2013; Li et al., 2018). Furthermore, while our manuscript was in preparation, Sanada and colleagues documented the pathogenicity of H5N1 and H7N9 IAVs in tree shrews (Sanada et al., 2019). In the present study, we performed a more comprehensive and in-depth investigations and comparison of the suitability of the tree shrew as an animal model for the study of three different IAV subtypes from various species. Three influenza viruses, pdmH1N1, H5N1, and H7N9, were isolated from humans and birds, respectively, and represent a severe threat to human health. Our integrated evaluation of the tree shrew model enriched the study about the infectivity and transmissibility of animal influenza viruses in the field.

Numerous human and non-human cell lines have been used to study the pathogenicity, replication, and innate immune response of influenza viruses (Steel et al., 2009; Elbahesh et al., 2014; Wang et al., 2018). Compared with cell lines, primary cells could reflect viral infectivity and pathogenicity *in vivo* from another facet since primary cells from animal models possess their inherent biological properties. For instance, primary tree shrew cells have been used as an *in vitro* platform for HBV, HCV, and ZIKV (Glebe et al., 2003; Feng et al., 2017; Zhang et al., 2019). In the present study, we demonstrated that primary renal and lung epithelial cells from the tree shrew were suitable to study the infectivity and innate immune response induced by pdmH1N1, H5N1, and H7N9 viruses (**Figure 1**).

The clinical manifestations of influenza virus are various in humans. Most infected people develop a fever, cough, runny nose, loss of appetite, etc. In the worst cases, influenza virus may cause pneumonia, respiratory distress syndrome, and even death (Carrat et al., 2008). Previous studies have demonstrated that tree shrews infected with H1N1, H7N9, or H9N2 virus showed moderate respiratory symptoms and pathological signs (Yang et al., 2013; Li et al., 2018; Sanada et al., 2019). Sanada et al. reported that H5N1 infection induced severe clinical symptoms including pneumonia, fever, weight loss, and death in tree shrews (Sanada et al., 2019). However, in our study, tree shrews infected with H1N1, H5N1, or H7N9 virus did not show significant weight loss or obvious clinical signs (**Figure 2**). The reasonable explanation for this discrepancy is the origin of the virus strains. The H5N1 virus used in our study was isolated from chickens, whereas the H5N1 virus (A/Vietnam/UT3040/2004) used in Sanada's study was from a human patient and possessed adaptive mutations (PB2 E627K, G309D) that can lead to enhanced virulence in mammals. In addition, pdmH1N1, H5N1, and H7N9 viruses possessed different abilities to replicate in the non-respiratory organs of mice and tree shrews because of a distinct tissue tropism. (**Figure 2**), suggesting that these three IAVs could be used for the study on the respiratory tract-related diseases in the tree shrew model. Finally, in the tree shrew, we observed obvious pulmonary lesions and inflammatory responses and a large number of neutrophils, monocytes, and proteins in the BALF, which similarly appeared in many human clinical cases infected with influenza viruses (Yokoyama et al., 2010; Shen et al., 2015). Therefore, tree shrews have potential as a mammalian model for the study of influenza virus pathogenesis.

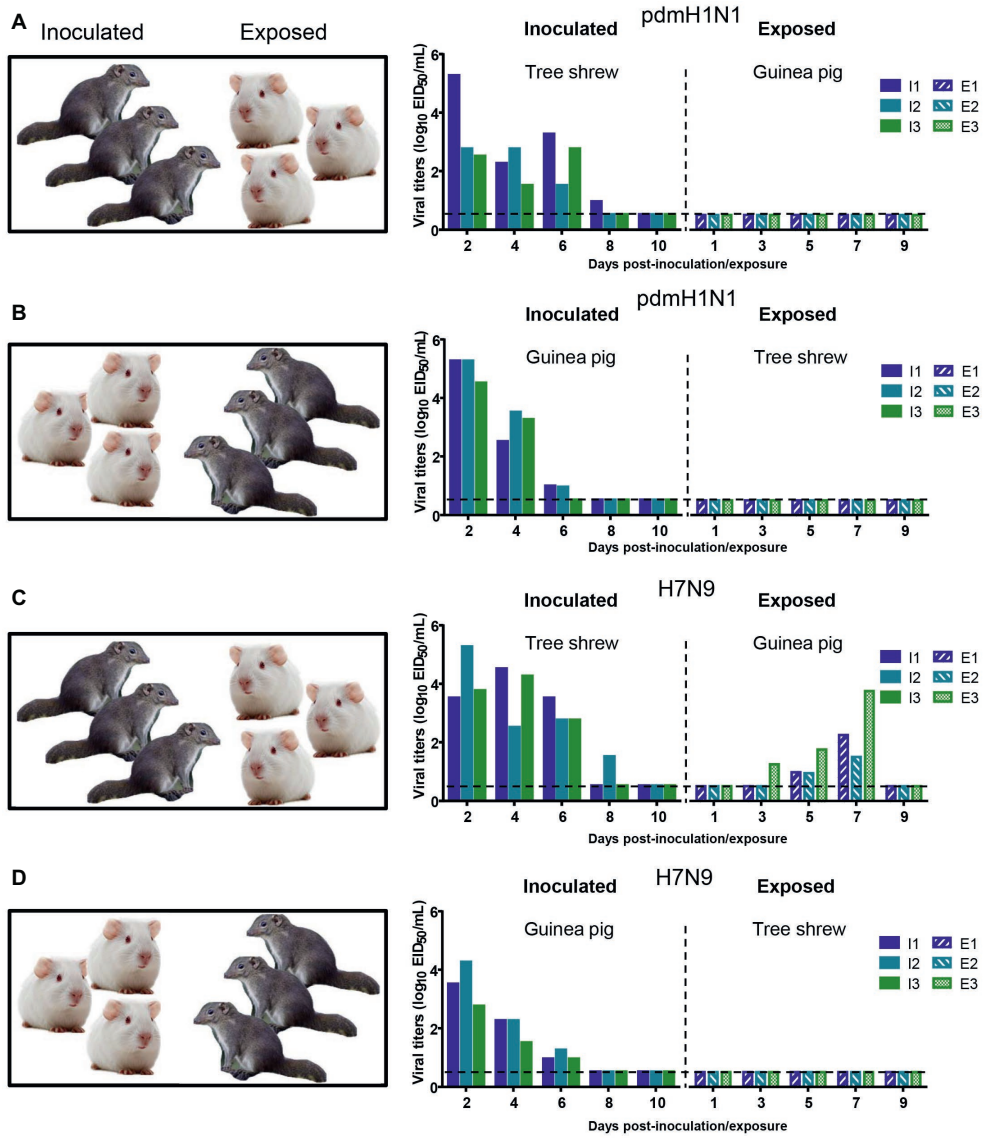

FIGURE 6 | Interspecies transmission of pdmH1N1 and H7N9 viruses between guinea pigs and tree shrews. Three animals were inoculated with 10^6 EID_{50} of pdmH1N1 virus **(A,B)** or H7N9 virus **(C,D)**, respectively. The next day, for **A** and **C**, the inoculated tree shrews were cohoused with three naive guinea pigs; for **B** and **D**, the inoculated guinea pigs were cohoused with three naive tree shrews. Nasal washes for virus shedding detection were collected every other day from all animals from day 2 of the initial infection. Viral titers in nasal wash samples from each of three individual inoculated animals (solid bars, left) and contact animals (dotted/diagonal bars, right) are expressed as log_{10} EID_{50}/ml. Each color bar represents a value from an individual animal. Horizontal dashed lines indicate the lower limit of virus detection. I or E means Inoculated or Exposed, respectively.

Vaccination is the most effective and cost-effective healthcare intervention to prevent influenza infection. However, the frequent antigenic shift and drift of influenza virus results in mismatches between the vaccine and circulating influenza virus strains, making it important to assess vaccine potency promptly in a suitable animal model (Singanayagam et al., 2018). Animal models not only play an important role in our understanding of viral pathogenicity, but also serve as a platform for the evaluation of vaccine candidates and new therapeutics (Margine and Krammer, 2014). In the present study, tree shrews induced an ideal humoral immune response upon infection with different influenza viruses. Infected tree shrews were protected against a second challenge with the homologous virus. Although the magnitude of the antibody responses in the tree shrews was variable, this variation appears to be due to the different viruses, which would assist us in selecting appropriate vaccine candidate strains. Therefore, we believe that the tree shrew model would be helpful for evaluating the efficacy of vaccines for the prevention of influenza infection.

Studies of influenza virus transmission in mammals are essential to assess potential public health risks and for pandemic preparedness. Previous work has shown that both strong binding to human

TABLE 5 | Seroconversion of animals in the interspecies transmission study.

Virus	Seroconversion (positive/total)[a]					
	Inoculated			Exposed		
	Animals	HI titer	VN titer	Animals	HI titer	VN titer
pdmH1N1	Tree shrew	3/3 (80–640)	3/3 (188–376)	Guinea pig	0/3	0/3
pdmH1N1	Guinea pig	3/3 (40–320)	3/3 (40–266)	Tree shrew	0/3	0/3
H7N9	Tree shrew	3/3 (20–40)	3/3 (79–188)	Guinea pig	2/3 (80)	2/3 (316)
H7N9	Guinea pig	3/3 (80–160)	3/3 (224)	Tree shrew	0/3	0/3

[a]*Sera were collected from the animals at 3 weeks after virus inoculation or exposure; these animals are the same ones that were used for the transmission studies shown in* **Figure 6**. *The range of antibody titers obtained was indicated in parentheses.*

like α2,6 sialic acid receptors and potent replication in the respiratory tract are necessary for efficient transmission in mammals (Schrauwen and Fouchier, 2014). Previous findings indicate that human-like α2,6 sialic acid receptors are mainly distributed in the nasal mucosa, trachea, and bronchus of tree shrews, and avian-like α2,3 sialic acid receptors are primarily distributed in the trachea, bronchiole, and alveolus of tree shrews (Yang et al., 2013). In our study, the H5N1 avian influenza virus prior to adaptation in mammals had no affinity for α2,6 sialic acid receptors (**Table 2; Supplementary Figure S1**), it is not surprising that the H5N1 virus failed to transmit in either the guinea pig or tree shrew model, consistent with previous studies in other animal models (mouse, guinea pig, and ferret) (Lowen et al., 2006; Maines et al., 2006). In contrast, the low pathogenic pdmH1N1 and H7N9 viruses tested in this study transmitted efficiently between tree shrews with high-titer virus shedding in nasal wash and seroconversion of directly inoculated and exposed groups. To our knowledge this represents the first reporting of an unadapted H7N9 influenza virus being transmitted among tree shrews by direct contact. Further studies should examine whether aerosol spread of H7N9 influenza virus occurs in tree shrews.

The risk of a new influenza pandemic increases with repeated interspecies transmission events (Wang et al., 2013; Zhang et al., 2017). In early 2013, a novel reassortant a*vian*-origin influenza A (H7N9) virus crossed the species barrier and caused the first human infection (Gao et al., 2013; Zhang et al., 2013a). So far, five waves of human H7N9 infection have caused 1,567 cases, with a fatality rate of approximately 39% (WHO, 2018; Zeng et al., 2018). Moreover, in 2017, H7N9 highly pathogenic influenza viruses were detected in poultry and humans (Shi et al., 2017, 2018). H7N9 viruses easily acquire the PB2 E627K or D701N mutation upon replication in mammals (Chen et al., 2013; Shi et al., 2017). Additionally, the viral PA protein and host ANP32A protein are crucial for the emergence of PB2 E627K during adaptation of H7N9 avian influenza viruses to humans (Liang et al., 2019). Nevertheless, there is currently no evidence that the H7N9 influenza virus can spread from person to person. Among the mammalian hosts, pigs, possessing both avian-like and human-like receptors in the respiratory tract, are susceptible to infection with various influenza viruses and have been deemed to be "mixing vessels" (Hass et al., 2011). Two studies reported that H7N9 isolate was able to infect and easily adapted to pigs, and the six internal gene combination of H7N9 virus, which are probably derived from H9N2 viruses, functions in viral replication and transmission in mammals (Zhu et al., 2013; Li et al., 2014; Xu et al., 2014). Therefore, human or avian H7N9 influenza virus could be potentially introduced into swine population and initiate a multiple gene reassortment in nature. In the present study, the tree shrew-guinea pig interspecies transmission model can mimic the transmission between porcine and human to some extent. Our data suggest that H7N9 virus can cross the species-barrier from tree shrews to guinea pigs (**Figure 6**), which implies the importance of implementing biosecurity measures in pig farms and the necessity of changing the co-habitation pattern of different livestock and poultry to prevent interspecies transmission. Future studies will examine why this interspecies transmission is unidirectional and why H7N9 virus rather than pdmH1N1 virus was able to transmit interspecies. The tree shrew is thus a promising tool for studies on the interspecies transmission of H7N9 influenza virus.

In summary, our comprehensive study suggests that tree shrew is susceptible to different subtypes of IAVs that replicate efficiently in the both the upper and lower respiratory tracts prior to adaptation. Virus inoculation may protect tree shrews against challenge from homologous virus. Importantly, this study revealed that unadapted H7N9 virus is transmissible among tree shrews and interspecies transmission can occur from tree shrews to guinea pigs *via* the direct-contact mode. Therefore, taken together with all of the merits of tree shrews in our or previous studies, we believe that tree shrews could be a promising alternative animal model for the study of influenza virus pathogenesis and transmission, and for assessments of antiviral agents and vaccines.

DATA AVAILABILITY STATEMENT

All datasets generated for this study are included in the article/**Supplementary Material**.

ETHICS STATEMENT

The animal study was reviewed and approved by Animal Ethics Committee of Lanzhou Veterinary Research Institute, Chinese Academy of Agricultural Sciences.

AUTHOR CONTRIBUTIONS

SX and QZ conceived this study. SX, XL, JY, ZW, YJ, LH, and LW conducted the experiments. SX and QZ analyzed the data and wrote the paper. SX and XL contributed equally to this work.

FUNDING

This work was supported by the National Natural Science Foundation of China under Grant (81571998, 31961133013, and 31772716 to QZ and 31802178 to SX); and National Key R&D program under Grant (2016YFD0500207 to QZ).

ACKNOWLEDGMENTS

We thank Drs. Hualan Chen (Harbin Veterinary Research Institute, CAAS) and Yong-Gang Yao (Kunming Institute of Zoology, CAS) for critical suggestions and core facility assistance.

SUPPLEMENTARY MATERIAL

The Supplementary Material for this article can be found online at: https://www.frontiersin.org/articles/10.3389/fmicb.2019.02955/full#supplementary-material

REFERENCES

Carrat, F., Vergu, E., Ferguson, N. M., Lemaitre, M., Cauchemez, S., Leach, S., et al. (2008). Time lines of infection and disease in human influenza: a review of volunteer challenge studies. *Am. J. Epidemiol.* 167, 775–785. doi: 10.1093/aje/kwm375

Chen, Y., Liang, W., Yang, S., Wu, N., Gao, H., Sheng, J., et al. (2013). Human infections with the emerging avian influenza A H7N9 virus from wet market poultry: clinical analysis and characterisation of viral genome. *Lancet* 381, 1916–1925. doi: 10.1016/S0140-6736(13)60903-4

Darai, G., Schwaier, A., Komitowski, D., and Munk, K. (1978). Experimental infection of *Tupaia belangeri* (tree shrews) with herpes simplex virus types 1 and 2. *J. Infect. Dis.* 137, 221–226. doi: 10.1093/infdis/137.3.221

Elbahesh, H., Cline, T., Baranovich, T., Govorkova, E. A., Schultz-Cherry, S., and Russell, C. J. (2014). Novel roles of focal adhesion kinase in cytoplasmic entry and replication of influenza A viruses. *J. Virol.* 88, 6714–6728. doi: 10.1128/JVI.00530-14

Fan, Y., Huang, Z. Y., Cao, C. C., Chen, C. S., Chen, Y. X., Fan, D. D., et al. (2013). Genome of the Chinese tree shrew. *Nat. Commun.* 4:1426. doi: 10.1038/ncomms2416

Feng, Y., Feng, Y. M., Lu, C., Han, Y., Liu, L., Sun, X., et al. (2017). Tree shrew, a potential animal model for hepatitis C, supports the infection and replication of HCV in vitro and in vivo. *J. Gen. Virol.* 98, 2069–2078. doi: 10.1099/jgv.0.000869

Gao, R., Cao, B., Hu, Y., Feng, Z., Wang, D., Hu, W., et al. (2013). Human infection with a novel avian-origin influenza A (H7N9) virus. *N. Engl. J. Med.* 368, 1888–1897. doi: 10.1056/NEJMoa1304459

Glebe, D., Aliakbari, M., Krass, P., Knoop, E. V., Valerius, K. P., and Gerlich, W. H. (2003). Pre-s1 antigen-dependent infection of Tupaia hepatocyte cultures with human hepatitis B virus. *J. Virol.* 77, 9511–9521. doi: 10.1128/jvi.77.17.9511-9521.2003

Guo, W. N., Zhu, B., Ai, L., Yang, D. L., and Wang, B. J. (2018). Animal models for the study of hepatitis B virus infection. *Zool. Res.* 39, 25–31. doi: 10.24272/j.issn.2095-8137.2018.013

Hass, J., Matuszewski, S., Cieslik, D., and Haase, M. (2011). The role of swine as "mixing vessel" for interspecies transmission of the influenza A subtype H1N1: a simultaneous Bayesian inference of phylogeny and ancestral hosts. *Infect. Genet. Evol.* 11, 437–441. doi: 10.1016/j.meegid.2010.12.001

Herold, S., von Wulffen, W., Steinmueller, M., Pleschka, S., Kuziel, W. A., Mack, M., et al. (2006). Alveolar epithelial cells direct monocyte transepithelial migration upon influenza virus infection: impact of chemokines and adhesion molecules. *J. Immunol.* 177, 1817–1824. doi: 10.4049/jimmunol.177.3.1817

Imai, M., Watanabe, T., Hatta, M., Das, S. C., Ozawa, M., Shinya, K., et al. (2012). Experimental adaptation of an influenza H5 HA confers respiratory droplet transmission to a reassortant H5 HA/H1N1 virus in ferrets. *Nature* 486, 420–428. doi: 10.1038/nature10831

Laursen, N. S., Friesen, R. H. E., Zhu, X., Jongeneelen, M., Blokland, S., Vermond, J., et al. (2018). Universal protection against influenza infection by a multidomain antibody to influenza hemagglutinin. *Science* 362, 598–602. doi: 10.1126/science.aaq0620

Li, L., Li, Z., Li, X., Wang, E., Lang, F., Xia, Y., et al. (2016). Reactivation of HSV-1 following explant of tree shrew brain. *J. Neurovirol.* 22, 293–306. doi: 10.1007/s13365-015-0393-4

Li, L., Li, Z., Wang, E., Yang, R., Xiao, Y., Han, H., et al. (2015). Herpes simplex virus 1 infection of tree shrews differs from that of mice in the severity of acute infection and viral transcription in the peripheral nervous system. *J. Virol.* 90, 790–804. doi: 10.1128/JVI.02258-15

Li, X., Shi, J., Guo, J., Deng, G., Zhang, Q., Wang, J., et al. (2014). Genetics, receptor binding property, and transmissibility in mammals of naturally isolated H9N2 Avian Influenza viruses. *PLoS Pathog.* 10:e1004508. doi: 10.1371/journal.ppat.1004508

Li, R., Yuan, B., Xia, X., Zhang, S., Du, Q., Yang, C., et al. (2018). Tree shrew as a new animal model to study the pathogenesis of avian influenza (H9N2) virus infection. *Emerg. Microbes Infect.* 7:166. doi: 10.1038/s41426-018-0167-1

Liang, L., Jiang, L., Li, J., Zhao, Q., Wang, J., He, X., et al. (2019). Low polymerase activity attributed to PA drives the acquisition of the PB2 E627K mutation of H7N9 avian influenza virus in mammals. *mBio* 10:e01162-19. doi: 10.1128/mBio.01162-19

Lipsitch, M. (2013). Avian influenza: Ferret H7N9 flu model questioned. *Nature* 501:33. doi: 10.1038/501033e

Lowen, A. C., Mubareka, S., Tumpey, T. M., Garcia-Sastre, A., and Palese, P. (2006). The Guinea pig as a transmission model for human influenza viruses. *Proc. Natl. Acad. Sci. USA* 103, 9988–9992. doi: 10.1073/pnas.0604157103

Maines, T. R., Chen, L. M., Matsuoka, Y., Chen, H., Rowe, T., Ortin, J., et al. (2006). Lack of transmission of H5N1 avian-human reassortant influenza viruses in a ferret model. *Proc. Natl. Acad. Sci. USA* 103, 12121–12126. doi: 10.1073/pnas.0605134103

Margine, I., and Krammer, F. (2014). Animal models for influenza viruses: implications for universal vaccine development. *Pathogens* 3, 845–874. doi: 10.3390/pathogens3040845

Masic, A., Booth, J. S., Mutwiri, G. K., Babiuk, L. A., and Zhou, Y. (2009). Elastase-dependent live attenuated swine influenza A viruses are immunogenic and confer protection against swine influenza A virus infection in pigs. *J. Virol.* 83, 10198–10210. doi: 10.1128/JVI.00926-09

Medina, R. A., and Garcia-Sastre, A. (2011). Influenza A viruses: new research developments. *Nat. Rev. Microbiol.* 9, 590–603. doi: 10.1038/nrmicro2613

Novel Swine-Origin Influenza A (H1N1) Virus Investigation TeamDawood, F. S., Jain, S., Finelli, L., Shaw, M. W., Lindstrom, S., et al. (2009). Emergence of a novel swine-origin influenza A (H1N1) virus in humans. *N. Engl. J. Med.* 360, 2605–2615. doi: 10.1056/NEJMoa0903810

Sanada, T., Yasui, F., Honda, T., Kayesh, M. E. H., Takano, J. I., Shiogama, Y., et al. (2019). Avian H5N1 influenza virus infection causes severe pneumonia in the northern tree shrew (*Tupaia belangeri*). *Virology* 529, 101–110. doi: 10.1016/j.virol.2019.01.015

Schrauwen, E. J., and Fouchier, R. A. (2014). Host adaptation and transmission of influenza A viruses in mammals. *Emerg. Microbes Infect.* 3:e9. doi: 10.1038/emi.2014.9

Shen, Y., Lu, H., Qi, T., Gu, Y., Xiang, M., Lu, S., et al. (2015). Fatal cases of human infection with avian influenza A (H7N9) virus in Shanghai, China in 2013. *Biosci. Trends* 9, 73–78. doi: 10.5582/bst.2014.01113

Shi, J., Deng, G., Kong, H., Gu, C., Ma, S., Yin, X., et al. (2017). H7N9 virulent mutants detected in chickens in China pose an increased threat to humans. *Cell Res.* 27, 1409–1421. doi: 10.1038/cr.2017.129

Shi, J., Deng, G., Ma, S., Zeng, X., Yin, X., Li, M., et al. (2018). Rapid evolution of H7N9 highly pathogenic viruses that emerged in China in 2017. *Cell Host Microbe* 24, 558–568 e557. doi: 10.1016/j.chom.2018.08.006

Shinya, K., Gao, Y., Cilloniz, C., Suzuki, Y., Fujie, M., Deng, G., et al. (2012). Integrated clinical, pathologic, virologic, and transcriptomic analysis of H5N1 influenza virus-induced viral pneumonia in the rhesus macaque. *J. Virol.* 86, 6055–6066. doi: 10.1128/JVI.00365-12

Singanayagam, A., Zambon, M., Lalvani, A., and Barclay, W. (2018). Urgent challenges in implementing live attenuated influenza vaccine. *Lancet Infect. Dis.* 18, e25–e32. doi: 10.1016/S1473-3099(17)30360-2

Steel, J., Lowen, A. C., Pena, L., Angel, M., Solorzano, A., Albrecht, R., et al. (2009). Live attenuated influenza viruses containing NS1 truncations as vaccine candidates against H5N1 highly pathogenic avian influenza. *J. Virol.* 83, 1742–1753. doi: 10.1128/JVI.01920-08

Sun, X., Belser, J. A., Pappas, C., Pulit-Penaloza, J. A., Brock, N., Zeng, H., et al. (2019). Risk assessment of fifth-wave H7N9 influenza A viruses in mammalian models. *J. Virol.* 93:e01740-18. doi: 10.1128/JVI.01740-18

Sun, H., Pu, J., Wei, Y., Sun, Y., Hu, J., Liu, L., et al. (2016). Highly pathogenic avian influenza H5N6 viruses exhibit enhanced affinity for human type sialic acid receptor and in-contact transmission in model ferrets. *J. Virol.* 90, 6235–6243. doi: 10.1128/JVI.00127-16

Tong, Y., Zhu, Y., Xia, X., Liu, Y., Feng, Y., Hua, X., et al. (2011). Tupaia CD81, SR-BI, claudin-1, and occludin support hepatitis C virus infection. *J. Virol.* 85, 2793–2802. doi: 10.1128/JVI.01818-10

Wang, D. Y., Qi, S. X., Li, X. Y., Guo, J. F., Tan, M. J., Han, G. Y., et al. (2013). Human infection with Eurasian avian-like influenza A (H1N1) virus, China. *Emerg. Infect Dis.* 19, 1709–1711. doi: 10.3201/eid1910.130420

Wang, J., Zeng, Y., Xu, S., Yang, J., Wang, W., Zhong, B., et al. (2018). A naturally occurring deletion in the effector domain of H5N1 swine influenza virus nonstructural protein 1 regulates viral fitness and host innate immunity. *J. Virol.* 92:e00149-18. doi: 10.1128/JVI.00149-18

Ware, L. B., and Matthay, M. A. (2000). The acute respiratory distress syndrome. *N. Engl. J. Med.* 342, 1334–1349. doi: 10.1056/NEJM200005043421806

WHO (2017). Monthly risk assessment summary [Online]. Available at: http://www.who.int/influenza/human_animal_interface/HAI_Risk_Assessment/en/ (Accessed October 30, 2017).

WHO (2018). Monthly Risk Assessment Summary (World Health Organization) [Online]. Available at: http://www.who.int/influenza/human_animal_interface/Influenza_Summary_IRA_HA_interface_02_03_2018.pdf?ua=1 (Accessed March 02, 2018).

Xu, L., Bao, L., Deng, W., Zhu, H., Li, F., Chen, T., et al. (2014). Rapid adaptation of avian H7N9 virus in pigs. *Virology* 452-453, 231–236. doi: 10.1016/j.virol.2014.01.016

Xu, L., Fan, Y., Jiang, X. L., and Yao, Y. G. (2013). Molecular evidence on the phylogenetic position of tree shrews. *Dongwuxue Yanjiu* 34, 70–76. doi: 10.3724/SP.J.1141.2013.02070

Xu, L., Yu, D., Fan, Y., Peng, L., Wu, Y., and Yao, Y. G. (2016). Loss of RIG-I leads to a functional replacement with MDA5 in the Chinese tree shrew. *Proc. Natl. Acad. Sci. USA* 113, 10950–10955. doi: 10.1073/pnas.1604939113

Yan, H., Zhong, G., Xu, G., He, W., Jing, Z., Gao, Z., et al. (2012). Sodium taurocholate cotransporting polypeptide is a functional receptor for human hepatitis B and D virus. *elife* 1:e00049. doi: 10.7554/eLife.00049

Yang, J., Wang, Z., Du, Y., Jia, Y., Wang, L., Xu, S., et al. (2019). Clade 2.3.2.1 H5N1 avian influenza viruses circulate at the interface of migratory and domestic birds around Qinghai Lake in China. *Vet. Microbiol.* 235, 234–242. doi: 10.1016/j.vetmic.2019.07.009

Yang, Z. F., Zhao, J., Zhu, Y. T., Wang, Y. T., Liu, R., Zhao, S. S., et al. (2013). The tree shrew provides a useful alternative model for the study of influenza H1N1 virus. *Virol. J.* 10:111. doi: 10.1186/1743-422X-10-111

Yao, Y. G. (2017). Creating animal models, why not use the Chinese tree shrew (*Tupaia belangeri chinensis*)? *Zool. Res.* 38, 118–126. doi: 10.24272/j.issn.2095-8137.2017.032

Yokoyama, T., Tsushima, K., Ushiki, A., Kobayashi, N., Urushihata, K., Koizumi, T., et al. (2010). Acute lung injury with alveolar hemorrhage due to a novel swine-origin influenza A (H1N1) virus. *Intern. Med.* 49, 427–430. doi: 10.2169/internalmedicine.49.3022

Yuan, B., Yang, C., Xia, X., Zanin, M., Wong, S. S., Yang, F., et al. (2019). The tree shrew is a promising model for the study of influenza B virus infection. *Virol. J.* 16:77. doi: 10.1186/s12985-019-1171-3

Zeng, X., Tian, G., Shi, J., Deng, G., Li, C., and Chen, H. (2018). Vaccination of poultry successfully eliminated human infection with H7N9 virus in China. *Sci. China Life Sci.* 61, 1465–1473. doi: 10.1007/s11427-018-9420-1

Zhang, Y., Chen, M., Huang, Y., Zhu, W., Yang, L., Gao, L., et al. (2017). Human infections with novel reassortant H5N6 avian influenza viruses in China. *Emerg. Microbes Infect.* 6:e50. doi: 10.1038/emi.2017.38

Zhang, L., Shen, Z. L., Feng, Y., Li, D. Q., Zhang, N. N., Deng, Y. Q., et al. (2019). Infectivity of Zika virus on primary cells support tree shrew as animal model. *Emerg. Microbes Infect.* 8, 232–241. doi: 10.1080/22221751.2018.1559707

Zhang, Q., Shi, J., Deng, G., Guo, J., Zeng, X., He, X., et al. (2013a). H7N9 influenza viruses are transmissible in ferrets by respiratory droplet. *Science* 341, 410–414. doi: 10.1126/science.1240532

Zhang, Y., Zhang, Q., Kong, H., Jiang, Y., Gao, Y., Deng, G., et al. (2013b). H5N1 hybrid viruses bearing 2009/H1N1 virus genes transmit in Guinea pigs by respiratory droplet. *Science* 340, 1459–1463. doi: 10.1126/science.1229455

Zhu, H., Wang, D., Kelvin, D. J., Li, L., Zheng, Z., Yoon, S. W., et al. (2013). Infectivity, transmission, and pathology of human-isolated H7N9 influenza virus in ferrets and pigs. *Science* 341, 183–186. doi: 10.1126/science.1239844

Conflict of Interest: The authors declare that the research was conducted in the absence of any commercial or financial relationships that could be construed as a potential conflict of interest.

Copyright © 2019 Xu, Li, Yang, Wang, Jia, Han, Wang and Zhu. This is an open-access article distributed under the terms of the Creative Commons Attribution License (CC BY). The use, distribution or reproduction in other forums is permitted, provided the original author(s) and the copyright owner(s) are credited and that the original publication in this journal is cited, in accordance with accepted academic practice. No use, distribution or reproduction is permitted which does not comply with these terms.

frontiers in Microbiology

ORIGINAL RESEARCH
published: 08 January 2020
doi: 10.3389/fmicb.2019.02962

Dual NDP52 Function in Persistent CSFV Infection

Shuangqi Fan†, Keke Wu†, Chaowei Luo, Xin Li, Mengpo Zhao, Dan Song, Shengming Ma, Erpeng Zhu, Yuming Chen, Hongxing Ding, Lin Yi, Jun Li, Mingqiu Zhao and Jinding Chen**

College of Veterinary Medicine, South China Agricultural University, Guangzhou, China

Viruses have evolved many mechanisms to escape host antiviral responses. Previously, we found that classical swine fever virus (CSFV) infection induces autophagy using the autophagosome as a self-replication site, thereby evading the host immune response and promoting long-term infection. However, the underlying mechanisms used by CSFV to enter autophagosomes and the mechanism by which autophagy promotes viral replication remain unclear. We found that CSFV infection inhibited autophagy receptor nuclear dot protein 52 kDa (NDP52) expression, ubiquitination, and SUMO2-4 modification. Further analyses revealed that CSFV mediated ubiquitination and SUMOylation of NDP52 via Pten-induced kinase 1 (PINK1)-Parkin. Moreover, NDP52 inhibition also inhibited CSFV replication and the induction of mitophagy marker proteins expression. Inhibition of NDP52 reduced CD63 expression and binding to CSFV E2 protein, which has an essential role in persistent CSFV infection. As NDP52 has a close relationship with the NF-κB innate immunity pathway and plays an important role in the antiviral response, we investigated whether NDP52 inhibited CSFV replication through the release of immune factors and antivirus signals. Our results showed that inhibiting NDP52 boosted interferon and TNF release and promoted NF-κB pathway activation. In summary, we found that NDP52 inhibition not only reduces CSFV binding and entry into autophagic vesicles, but also inhibits CSFV replication by active NF-κB antiviral immune pathways. Our data reveal a novel mechanism by which NDP52, an autophagy receptor, mediates CSFV infection, and provide new avenues for the development of antiviral strategies.

Keywords: classical swine fever virus, NDP52, ubiquitination, CD63, NF-κB

OPEN ACCESS

Edited by:
Zhengli Shi,
Wuhan Institute of Virology (CAS), China

Reviewed by:
Pinghui Feng,
University of Southern California, United States
Dang Wang,
Huazhong Agricultural University, China

****Correspondence:***
Mingqiu Zhao
zmingqiu@scau.edu.cn
Jinding Chen
jdchen@scau.edu.cn

† These authors have contributed equally to this work

Specialty section:
This article was submitted to Virology, a section of the journal Frontiers in Microbiology

Received: *31 August 2019*
Accepted: *09 December 2019*
Published: *08 January 2020*

Citation:
Fan S, Wu K, Luo C, Li X, Zhao M, Song D, Ma S, Zhu E, Chen Y, Ding H, Yi L, Li J, Zhao M and Chen J (2020) Dual NDP52 Function in Persistent CSFV Infection. Front. Microbiol. 10:2962. doi: 10.3389/fmicb.2019.02962

INTRODUCTION

Swine fever, caused by classical swine fever virus (CSFV) infection, is characterized by acute fever and death, and is classified as a Class A infectious disease by the World Organization for Animal Health (OIE) (Paton and Greiser-Wilke, 2003). CSFV belongs to the genus *Pestivirus* within the family Flaviviridae. The virus has a small, enveloped, single-stranded, positive-sense 12.3 kb RNA genome with a long, open reading frame that encodes a 3898 amino acid polypeptide (Becher et al., 2003). Co-and post-translational processing of the polypeptide by cellular and viral proteases yields 12 cleavage products, including four structural proteins (C, Erns, E1, and E2) and eight non-structural proteins (N^{pro}, p7, NS2, NS3, NS4A, NS4B, NS5A, and NS5B) (Heinz-Jurgen et al., 1991).

CSFV can infect several cells types, including immune cells, leading to cellular immunosuppression (Fan et al., 2018). However, CSFV infection does not cause typical pathological changes, and the underlying infection mechanisms remain unclear (Bensaude, 2004; Johns et al., 2009).

Macroautophagy, hereafter referred to as autophagy, is an internal balancing mechanism for maintaining homeostasis in eukaryotic cells. After receiving an autophagy induction signal, such as pathogen infection (Deretic et al., 2013), starvation (Tattoli et al., 2012), growth factor withdrawal (Lum et al., 2005), endoplasmic reticulum (ER) stress (Ciechomska et al., 2013), or oxidative stress (Scherz-Shouval et al., 2007), the cell forms a small liposome-like membrane structure in the cytosol, which expands to form a bowl-like structure consisting of two layers of lipid bilayers that can be observed under electron microscopy. The bowl structure is called a phagophore. Many components in the cytoplasm, including protein aggregates, damaged organelles, and foreign invading pathogens, are wrapped in vesicles and then closed into a closed spherical autophagosome (Høyer-Hansen and Jäättelä, 2008). Microtubule-associated protein 1 light chain 3 (MAP1LC3 or simply LC3), consisting of the interconvertible forms LC3-I and LC3-II, is involved in the formation of autophagosome membranes. Early pro-LC3 cleavage by ATG4 exposes the C-terminal glycine to form the cytosolic soluble form LC3-I, which is modified by ubiquitination and coupled with the substrate PE on the surface of the autophagosome membrane under the action of the E1-like enzyme ATG7, the E2-like enzyme ATG3, and the E3-like enzyme ATG5-ATG12-ATG16L complex to form the membrane-bound form LC3-II. After autophagosome formation, this fuses with lysosomes to form autolysosomes. Under the action of various hydrolases, the substrate in the autophagosomes is degraded (Bizargity and Schröppel, 2014). Autophagy is a way for cells respond to unfavorable environmental factors. Many RNA viruses, such as enteroviruses, hepatitis C virus (HCV), and CSFV, circumvent and utilize host autophagic machinery to promote viral propagation (Pei et al., 2013; Mohamud and Luo, 2018; Wang and Ou, 2018). During CSFV infection, the viral proteins NS5A and E2 colocalize with the autophagy marker CD63 on autophagosome-like vesicle membranes. Moreover, CSFV infection can use mitophagy to inhibit cell apoptosis to create a persistent environment for viral infection (Pei et al., 2016; Gou et al., 2017). However, the mechanisms underlying CSFV-autophagosome entry are unclear.

Autophagy was initially considered to be non-selective, but recent studies have found that autophagy can also be selective. The most important feature of the selective autophagy pathway is the involvement of autophagy receptors that recognize and transport autophagic substrates, thereby regulating autophagy substrate degradation under very precise dynamic control (Lazarou et al., 2015). These autophagy receptors contain a conserved LC3-interacting region (LIR) domain, which binds to Atg8 molecules on autophagosomes and mediate autophagy degradation (Zaffagnini and Martens, 2016). Ubiquitin acts as a signaling molecule, inducing polyubiquitination of autophagy substrates (Kocaturk and Gozuacik, 2018). Autophagy receptor proteins recognize and bind autophagic substrates in a UBA domain-dependent or -independent manner. The LIR is anchored to the autophagosome membrane, followed by autophagosome fusion, lysosome fusion, and substrate degradation in lysosomes (cargo recognition and trafficking in selective autophagy) (Shaid et al., 2012; Nakamura and Yoshimori, 2017). In addition to the autophagy receptor functions, the protein itself is also ubiquitinated. Hou et al. found that the ubiquitin ligase HACE1 with tumor suppressor activity binds to the OPTN protein and catalyzes the polyubiquitination of OPTN. OPTN is modified by HACE1 with a K48-linked polyubiquitin chain, followed by autophagy–lysosomal pathway degradation. HACE1 mediates the modification of the 193th lysine of OPTN by a ubiquitin chain, which specifically interacts with the UBA domain of p62 to activate autophagy. Clearly, ubiquitinated OPTN interacts with p62 to increase the efficiency of autophagy receptor-mediated transport of substrates to autophagic vacuoles, significantly increasing autophagic flux and thereby more effectively recruiting and transporting autophagy substrates (Liu et al., 2014).

It is well known that NF-κB plays a key role in regulating the immune response to infection. It participates in the inflammatory response and immune response and regulates apoptosis and the stress response (Liu et al., 2017). There are three main signal transduction pathways that activate NF-κB: the classical pathway, bypass pathway, and atypical pathway (Oeckinghaus and Ghosh, 2009). Several proteins encoded by NF-κB target genes are involved in the activation of immune and inflammatory responses. NF-κB activation during viral infection is interpreted as a host protective response to viral pathogens (Schmitz et al., 2014). Type I interferons (IFNs) also play an important role in the immune response to viruses. The production of type I IFN in immune cells is mediated by pattern recognition receptors in the host cell (Ivashkiv and Donlin, 2013). There are four main ways to induce the production of type I IFN: (1) DNA virus activates the second messenger cGAMP (cyclic GMP-AMP) induction pathway; (2) RNA virus activates the RIG-I-like receptor (RLR) induction pathway; (3) the Toll-like receptors TLR3 and TLR4 activate the adaptor protein TRIF induction pathway; and (4) TLR7/TLR8 and TLR9 activate the transcription factor IRF7 induction pathway (Majzoub et al., 2019). Interestingly, CSFV replication in cells suppresses type I IFN-inducible antiviral activity and apoptosis by interfering with IFN production, resulting in the persistent survival of CSFV in host cells *in vitro*.

Nuclear dot protein 52 kDa (NDP52), also called CALCOCO2, has been well studied in xenophagy and primary adaptation to Parkin-mediated mitophagy (Sharma et al., 2018; Ravenhill et al., 2019). Pten-induced kinase 1 (PINK1) can promote NDP52 recruitment and ubiquitination. Further, the xenophagy kinase TBK1 forms a complex with NDP52, thus promoting xenophagy (Fu et al., 2018). In *Salmonella typhimurium* infection, NDP5 promotes pathogen-containing autophagosome maturation and independently regulates targeting of bacteria to mature autophagosomes (Verlhac et al., 2015a). Further studies have found that Rab35 GTPase and myosin VI play important

roles in NDP52-microorganism binding and autophagosome maturation (Minowa-Nozawa et al., 2017). During viral infection, NDP52 not only interacts with viral proteins, but also activates RIG-I and NF-κB signaling pathways to exert antiviral effects (Jin et al., 2017). Many studies have shown that NDP52 has a negative regulatory effect on the NF-κB pathway. Moreover, in CVB virus infection, CALCOCO2, but not SQSTM1, suppresses antiviral type I IFN signaling by promoting autophagy-mediated degradation of the mitochondrial antiviral signaling (MAVS) protein (Mohamud et al., 2018). Therefore, we sought to explore the regulatory effect of NDP52 on NF-κB and IFN in swine fever virus infection and hypothesized that it plays an important role in CSFV infection.

Here, we found that CSFV infection activates the PINK1-Parkin pathway, resulting in NDP52 SUMOylation, which inhibits NDP52 and permits CSFV replication. Further, NDP52 colocalizes with viral protein E2, thereby inhibiting CD63 expression, promoting CSFV binding by NDP52 and increasing cytokine release and NF-κB signaling activation.

MATERIALS AND METHODS

Cells, Viruses, and Virus Titration Assays

The swine kidney cell line PK-15 (ATCC, CCL-33) was grown in Dulbecco's modified Eagle's medium (DMEM) supplemented with 10% fetal bovine serum (FBS) at 37°C in a 5% CO_2 incubator. The CSFV strain (Shimen) used in the study was propagated in PK-15 cells. Viral titers in CSFV-infected cell culture media were determined as previously described (Hongchao et al., 2017). Briefly, cells cultivated in 96-well plates were inoculated with 10-fold serial dilutions of virus and incubated at 37°C for 3 days. Cells were fixed with 80% acetone at –20°C for 30 min, and viruses were detected by immunofluorescence assay using mouse anti-CSFV E2 antibody and FITC-conjugated goat anti-mouse secondary antibody. Viral titers are expressed as 50% tissue culture infective doses (TCID50)/0.1 ml.

Reagents and Antibodies

The chemical reagents MG-132 (M8699) and BAY (11-7082, S2913) were purchased from Sigma-Aldrich and Selleck. The following primary antibodies were used in this study: rabbit polyclonal anti-PARK2 (Abnova, PAB0714), rabbit polyclonal anti-LC3B (Cell Signaling, 2775), rabbit polyclonal anti-MFN2 (Santa Cruz, sc-50331), goat polyclonal anti-VDAC1 (Santa Cruz, sc-32063), goat polyclonal anti-TOM20 (Santa Cruz, sc-11021), mouse monoclonal anti-Beclin-1 (Cell Signaling, 2A4), rabbit polyclonal anti-CD63 (Beyotime, AF1471), mouse monoclonal anti-Ub(A-5) (Santa Cruz, sc-166553), mouse monoclonal anti-CSFV E2 (JBT, 9011), mouse monoclonal anti-IkBa (Cell Signaling, 112B2), mouse monoclonal anti-kB-Ras2 (Santa Cruz, sc-374311), rabbit monoclonal anti-P65 (Santa Cruz, sc-AF1870), mouse monoclonal anti-GAPDH (Beyotime, AG019), mouse monoclonal anti-tubulin (Beyotime, AT819), normal rabbit IgG (Beyotime, A7016), and normal goat IgG (Beyotime, A7007). The polyclonal anti-CSFV Npro was kindly provided by Dr. Xinglong Yu (Veterinary Department, Hunan Agricultural University, China). The secondary antibodies used for immunofluorescence were Alexa Fluor 350 goat anti-mouse IgG (Beyotime, A0412), Alexa Fluor 488 goat anti-mouse IgG (Beyotime, A0428), and Alexa Fluor 647 goat anti-rabbit IgG (Beyotime, A0468). The secondary antibodies used for immunoblotting analysis were HRP-conjugated goat anti-mouse IgG (Bioworld Technology, BS12478), HRP-conjugated goat anti-rabbit IgG (Bioworld Technology, BS13278), and HRP-conjugated rabbit anti-goat IgG (Bioworld Technology, BS30503).

Plasmids and RNA Interference

The EGFP-LC3 plasmid was prepared in our laboratory. Plasmid pAT016 (p-mito-mRFP-EGFP) was a kind gift from Dr. Andreas Till (University of California, United States). Parkin-targeting shRNAs and scrambled shRNA were obtained from Cyagen. Small interfering RNAs (siRNAs) for NDP52 were synthesized by Sangon Biotech. The shRNA and siRNA sequences are listed in **Table 1**. PK-15 cells grown to 60% confluence in six-well cell culture plates were transfected with siRNA and shRNA using Lipofectamine 3000 reagent (Thermo Fisher, L3000015). Targeted protein knockdown was evaluated by western blotting.

Virus Infection

Twenty-four hours after siNC or siRNA transfection, cells were infected with CSFV at a multiplicity of infection (MOI) of 0.1. Two hours later, the viral inoculum was removed and the infected cells were washed twice with phosphate-buffered saline (PBS) (pH 7.4). DMEM containing 2% FBS was then added to each culture. At various time points post-infection, cell-free culture supernatants and cell lysates were harvested and stored at −80°C until use.

Immunoprecipitation

For immunoprecipitation analysis, PK-15cells were infected with CSFV at an MOI of 0.1 for 24 h. SUMOylated NDP52 and ubiquitinated Parkin or NDP52 from whole cell lysates (WCL) were incubated on ice with IP lysis buffer (Beyotime, P0013) containing 1 mM PMSF (Beyotime, ST506) for 10 min. The precipitates were removed by centrifugation at 14,000 × *g* for 10 min at 4°C. The supernatant was immunoprecipitated with the appropriate antibodies (anti-Parkin or anti-NDP52) and protein A + G Sepharose (7sea

TABLE 1 | shRNA and siRNA sequences of targeted genes.

Gene	Sequence (5′∼3′)
shParkin	GCATCACCTGTACGGACATTCTCTTGAAATGTCCGTACAG GTGATGC
scrambled	GCGCGCTTTGTAGGATTCGTTCAAGAGACGAATCCTACAAA GCGCGC
siNDP52	Sense: GCAGGAAGUCCAGUUCAAATT
	Antisense: UUUGAACUGGACUUCCUGCTT
siNC	Sense: UUCUCCGAACGUGUCACGUTT
	Antisense: ACGUGACACGUUCGGAGAATT

biotech, P001-2). The immunoprecipitated proteins were then analyzed by western blotting with SUMO or ubiquitin antibodies.

Quantitative Real-Time RT-PCR (qPCR)

For targeted gene expression analysis, total RNA was prepared using a total RNA Kit I (Omega, R6834-01). Complementary DNA (cDNA) was synthesized using PrimeScript RT Master Mix (Takara, RR036A). Real-time qPCR was performed using SYBR Premix Ex Taq II (Takara, RR820A) using an iQ5 iCycler detection system (Bio-Rad, United States). Relative mRNA expression was assessed using the $2^{-\Delta\Delta Ct}$ method and normalized to the housekeeping gene GAPDH. The primers used are described in **Table 2**. For virus copy detection, viral RNA was extracted using a MiniBEST Viral RNA/DNA Extraction Kit Ver.5.0 (Takara, 9766) and reverse-transcribed using PrimeScript RT Master Mix (Perfect Real Time; Takara, RR036A). The resulting cDNA was then amplified using SYBR Premix Ex Taq (Tli RNaseH Plus; Takara, RR420B) and an iQ5 iCycler detection system (Bio-Rad, United States). Primer sequences targeting the CSFV NS5B gene were: CSFV1: CCTGAGGACCAAACACATGTTG; CSFV2: TGGTGGAAGTTGGTTGTGTCTG. Viral copy number was calculated using a standard curve from a recombinant plasmid containing the CSFV NS5B gene.

Western Blot Analysis

After treatment, cells were washed with cold PBS and incubated on ice with RIPA lysis buffer (Beyotime, P0013B) supplemented with 1 mM PMSF (Beyotime, ST506) for 10 min. Cell lysates were centrifuged at 14,500 × *g* for 20 min at 4°C. Protein concentration was determined using a BCA protein assay kit (Beyotime, P0012). Samples with equal protein amounts were diluted in 5× SDS-PAGE loading buffer and boiled for 5 min. Proteins (20 mg) were separated by SDS-PAGE and transferred onto polyvinylidene fluoride membranes (Beyotime, FFP30). After blocking with PBS containing 2% non-fat milk powder and 0.05% Tween 20 (Sigma-Aldrich, P2287) for 2 h at 25°C, the membrane was incubated with primary antibodies overnight at 4°C. Then, membranes were incubated with corresponding HRP-conjugated secondary antibodies at 37°C for 2 h at appropriate dilutions. The protein bands were visualized using an ECL Plus kit (Beyotime, P0018). Blots were imaged with a CanoScan LiDE 100 scanner (Canon, Japan) and quantified with Image Pro Plus 6.0 software.

TABLE 2 | Primers used in this study.

Gene	Sequence (5′∼3′)	GenBank
NDP52	F: CGGAATTCCATGAGGGGCGGGCCCCG R: GGGGTACCTCACAGGTCCTTCAGATCCTT	XM003131552.4
IFNA	F: CTCAGCCAGGACAGAAGCA R: TCACAGCCCAGAGAGCAGA	NM_214393.1
IFNB1	F: TCGCTCTCCTGATGTGTTTCTC R: AAATTGCTGCTCCTTTGTTGGT	NM_001003923.1
TNF	F: TGGCCCAAGGACTCAGATCAT R: TCGGCTTTGACATTGGCTACA	EU682384
GAPDH	F: TGGAGTCCACTGGTGTCTTCAC R: TTCACGCCCATCACAAACA	NM_001206359.1

Confocal Microscopy

Cells were grown in 35 mm glass-bottom petri dishes (NEST, GBD-35-20). The indicated interfering RNA was transfected at various time points. Cells were washed with PBS, fixed with 4% paraformaldehyde for 30 min, and washed with 0.2% Triton X-100 (Sigma-Aldrich, T8787) in PBS for 10 min. The cells were blocked in PBS containing 5% bovine serum albumin (BSA; Beyotime, ST023) for 30 min. Next, the cells were stained with primary antibodies and appropriate secondary antibodies for 1 h at 37°C. Wherever indicated, nuclei were stained with DAPI (Beyotime). Fluorescence was visualized with a TCS SP2 confocal fluorescence microscope (Leica).

Cell Viability Assay

Cell viability was detected by the CCK8 assay according to the manufacturer's instructions (Dojindo, CK04). In brief, PK-15 cells were cultivated in 96-well plates at a density of 1×10^4 cells per well and cultured for 24 h at 37°C. The cells were transfected with siNDP52, siNC, shParkin or non-targeting shRNA using Lipofectamine 3000 reagent. After 48 h, the medium was replaced with 100 μl of fresh medium containing 10 μl of CCK8. The cells were further cultured for 1 h at 37°C, and the optical density was measured at 570 nm using a model 680 microplate reader (Bio-Rad).

Statistical Analysis

Statistical analysis was performed with unpaired Student's *t*-tests, as implemented in GraphPad Prism 5 software (mean ± SD; $n = 3$; $^*P < 0.05$; $^{**}P < 0.01$; $^{***}P < 0.001$; $^{\#}P > 0.05$).

RESULTS

CSFV Infection Inhibits NDP52 (CALCOCO2) Ubiquitination and SUMOylation

To explore whether CSFV infection affects NDP52, we first evaluated changes in NDP52 mRNA and protein expression after CSFV infection. PK-15 cells were tested at several time points post-CSFV infection. NDP52 mRNA and protein expression was decreased by CSFV infection at 24, 36, and 48 h post-infection (hpi) (**Figures 1A,B**). These results suggest that CSFV infection has a negative effect on the expression of NDP52. Several reports indicate that autophagy receptors undergo self-modification (Liu et al., 2014). Therefore, we examined NDP52 ubiquitination and SUMOylation after CSFV infection. CSFV-infected cell lysate was immunoprecipitated with an NDP52-specific antibody and immunoblotted with SUMO2-4 or Ub(A-5) antibody. These results showed that NDP52 ubiquitination and SUMOylation were decreased in CSFV-infected cells compared to that in un-infected PK-15 cells (**Figures 1C,D**). The above results indicate

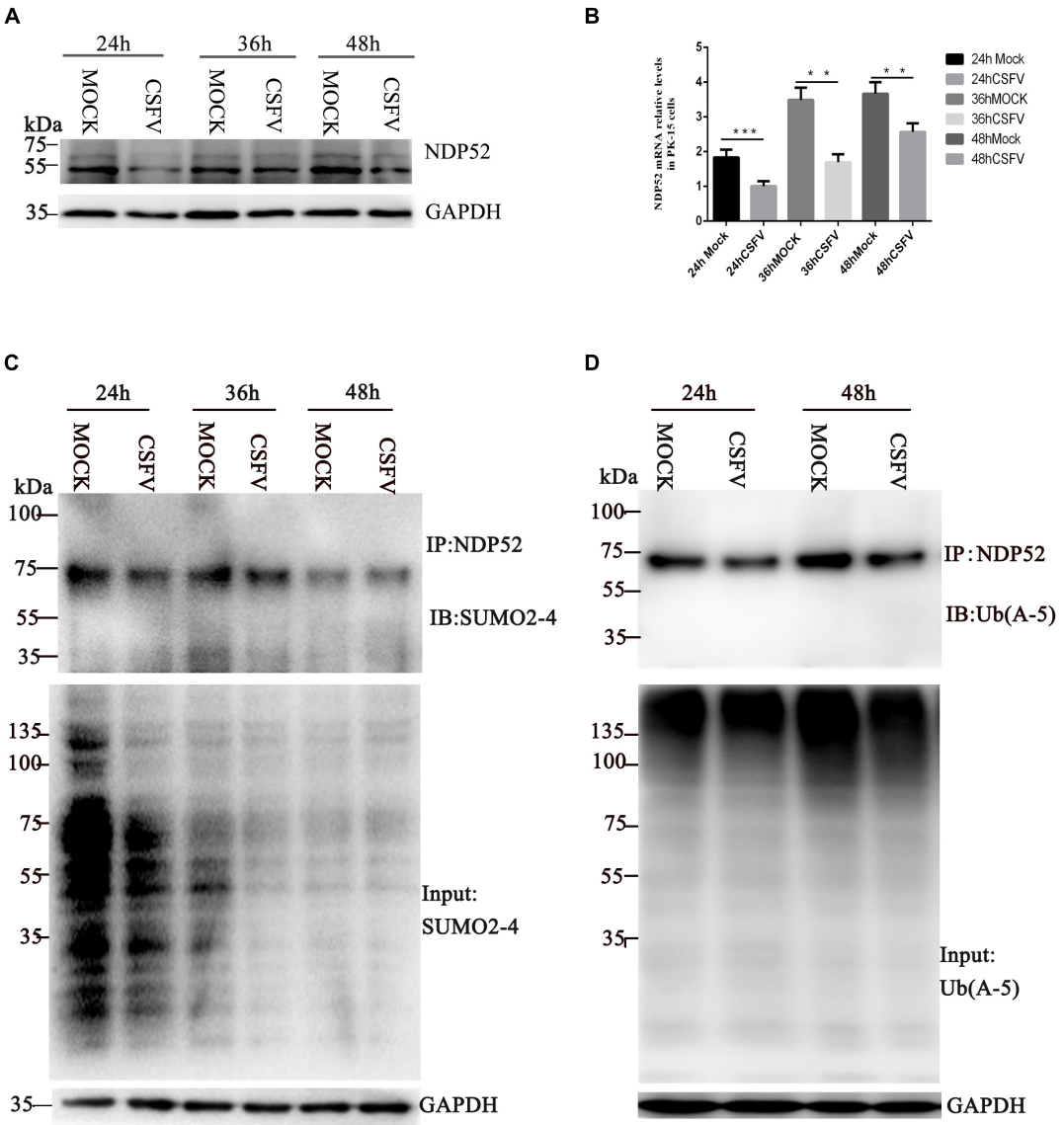

FIGURE 1 | Classical swine fever virus (CSFV) inhibits NDP52 (CALCOCO2) ubiquitination and SUMOylation. **(A)** PK-15 cells were infected with CSFV (MOI = 0.1) or un-infected (MOCK) at the indicated time points. CALCOCO2, N^{pro}, and GAPDH levels were analyzed by Western blot. **(B)** After CSFV infection, CALCOCO2 mRNA was detected by qRT-PCR. The data represent the mean ± SD of three independent experiments. Data were tested by one-way ANOVA with Fisher's least significant difference (LSD) *post hoc* correction. $^{*}P < 0.05$; $^{**}P < 0.01$; $^{***}P < 0.001$; $\#P > 0.05$. **(C)** PK-15 cells were infected with CSFV. NDP52 SUMOylation was analyzed by immunoblot using anti-SUMO2-4 antibody. SUMO2-4 expression in CSFV-infected cells was used as the input control. **(D)** Ubiquitinated NDP52 was immunoblotted with anti-Ub(A-5) antibody. Ub(A-5) expression in CSFV-infected cells was used as the input control. GAPDH was used as the internal loading control.

that CSFV infection not only inhibits the expression of NDP52, but also mediates the protein modification of NDP52.

CSFV Infection Promotes Ubiquitination of Parkin and Mediates NDP52 Modification via PINK1-Parkin

Several reports suggest that NDP52 is closely related to the PINK1-Parkin pathway (Heo et al., 2015). To verify whether CSFV infection affects NDP52 modification via the PINK1-Parkin pathway, we first examined Parkin expression and ubiquitination at 24 h post-CSFV infection. We observed that CSFV infection promotes Parkin2 protein expression and ubiquitination (**Figures 2A,B**). The shParkin interference plasmid (**Table 1**) was applied to PK-15 cells for 24 h. Then, cells were infected with CSFV at an MOI of 0.1. Cell lysate was immunoprecipitated with anti-NDP52 antibody and immunoblotted with SUMO2-4 antibody or Ub(A-5) antibody. The results showed that ubiquitinated and SUMOylation NDP52 were significantly increased with shParkin, suggesting that Parkin plays a key role in NDP52 protein modification (**Figure 2C**). Thus, CSFV can activate the PINK1-Parkin pathway and promote the expression

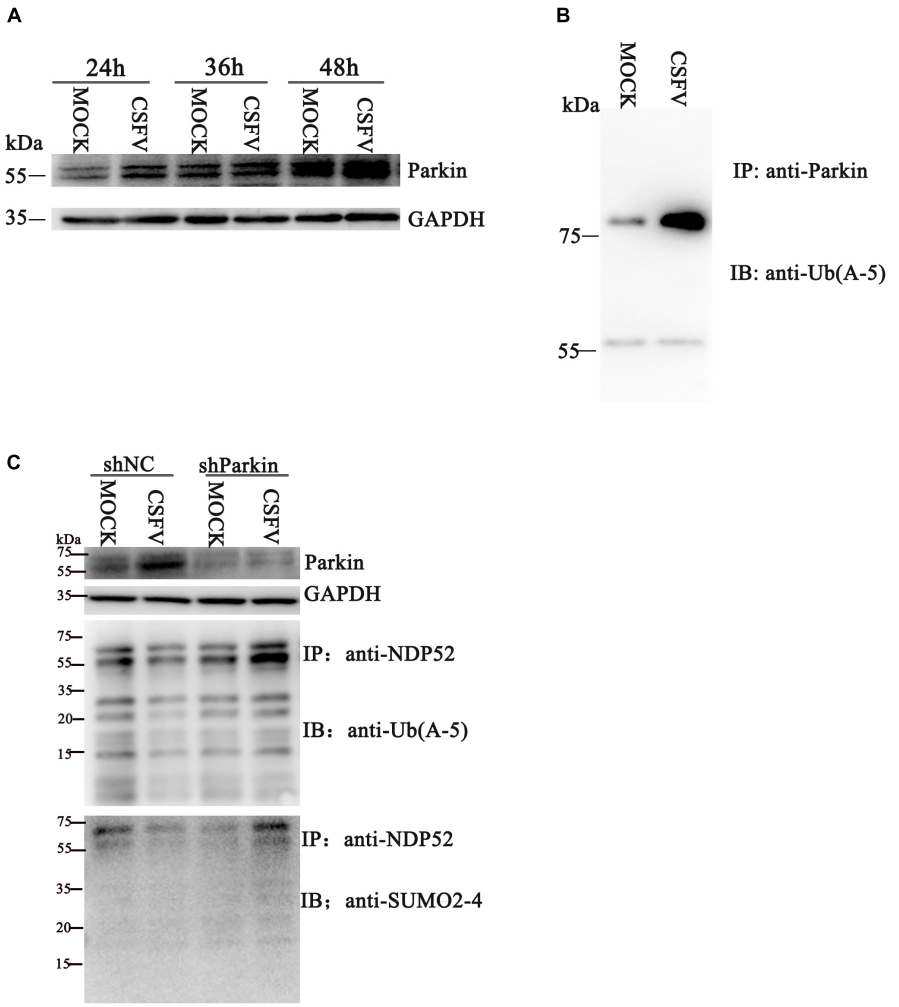

FIGURE 2 | CSFV infection promotes ubiquitination of Parkin2 and mediates NDP52 modification via the PINK1-Parkin pathway. **(A)** PK-15 cells were treated as in **Figure1 A**. Western blotting was used to examine Parkin2, N^{pro} and GAPDH protein expression 24, 36, and 48 h after CSFV infection. **(B)** PK-15 cells were infected with CSFV (MOI = 0.1) for 24 h. Cell lysates were immunoprecipitated with an anti-Parkin antibody and assayed for Parkin2 with anti-Ub(A-5) antibody. **(C)** PK-15 cells were infected with CSFV (MOI = 0.1) for 24 h, followed by shParkin2 or shNC plasmid (MOI = 10) for 24 h. After immunoprecipitation with an anti-NDP52 antibody, NDP52 ubiquitination and SUMOylation were blotted with anti-Ub-5a and anti-SUMO2-4 antibodies.

of Parkin. After inhibition of Parkin, the protein modification of NDP52 induced by CSFV is attenuated. These results show that CSFV infection promotes the ubiquitination of Parkin and mediates NDP52 modification via the PINK1-Parkin pathway.

NDP52 Inhibition Decreases CSFV Replication

To assess the functional effects of NDP52 on CSFV infection, we performed RNA knockdown experiments to silence endogenous NDP52 expression in CSFV-infected PK-15 cells. As shown in **Figure 3A**, the silencing effect on NDP52 expression was verified by western blotting. Decreased expression of CSFV N^{pro} protein in NDP52-silenced cells suggested that CSFV replication is promoted by NDP52. To verify this finding, we analyzed CSFV replication after treatment with NDP52 siRNA, by measuring viral titers and RNA copy numbers. These results indicated that NDP52 silencing decreased viral replication in PK-15 cells (**Figures 3B,C**), demonstrating a positive role for NDP52 in CSFV replication. Moreover, we found that CSFV E2 protein and NDP52 colocalize to the cytoplasm by confocal microscopy (**Figure 3D**). The above results indicated that NDP52 promotes replication of CSFV and can colocalize with CSFV structural proteins.

NDP52 Inhibition Reduces Autophagy Related Proteins Expression, but Decreases Ubiquitin and LC3 Binding

Several studies show that NDP52 is essential for autophagosome maturation (Tumbarello et al., 2012; Verlhac et al., 2015b). To investigate the role of NDP52 in CSFV-mediated autophagy, we examined the effect of NDP52 on autophagy and mitophagy. We assessed expression of the autophagy marker LC3 by

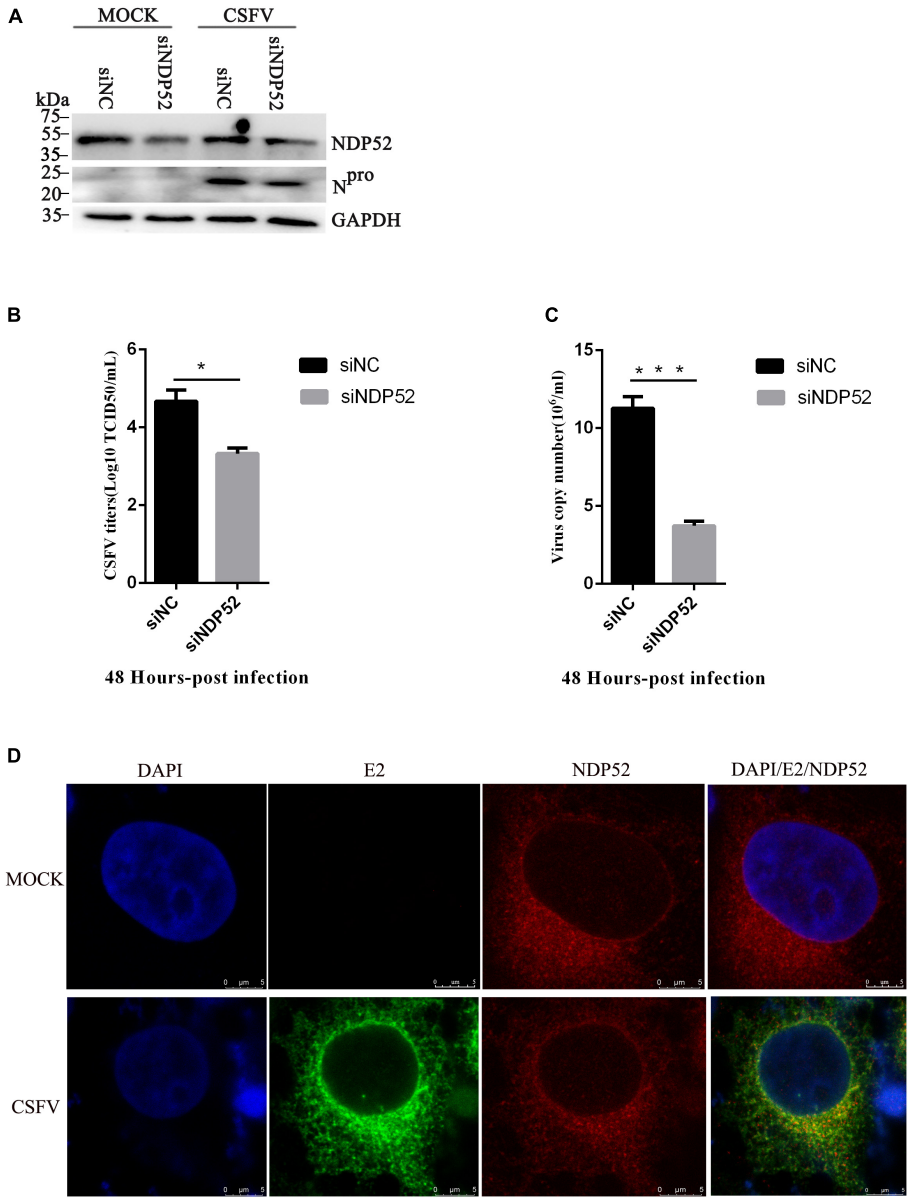

FIGURE 3 | NDP52 inhibition reduces CSFV replication. **(A)** PK-15 cells were mock-infected or infected with CSFV (MOI = 0.1) after transfection with siNDP52 for 24 h. NDP52 expression was analyzed by Western blotting at 24 hpi. CSFV infection was verified by immunoblotting with anti-CSFV N^{pro} antibody. GAPDH was used as an internal loading control. **(B)** Statistical analysis of the effect of NDP52 siRNA transfection on the viral copy numbers in CSFV-infected cells. PK-15 cells were transfected with scrambled or NDP52 siRNA for 24 h, followed by mock infection and CSFV infection (MOI = 0.1). At 48 hpi, CSFV RNA levels were analyzed by real-time qRT-PCR (mean ± SD; $n = 3$; $^{*}P < 0.05$; $^{**}P < 0.01$; $^{***}P < 0.001$; $^{\#}P > 0.05$). *P*-values were calculated using an unpaired Student's *t*-test. **(C)** Statistical analysis of the effect of NDP52 siRNA transfection on virus titers in CSFV-infected cells. PK-15 cells were transfected with scrambled or NDP52 siRNA for 24 h, followed by mock infection and CSFV infection (MOI = 0.1). At 48 hpi, CSFV titers were analyzed (mean ± SD; $n = 3$; $^{*}P < 0.05$; $^{**}P < 0.01$; $^{***}P < 0.001$; $^{\#}P > 0.05$). *P*-values were calculated using an unpaired Student's *t*-test. **(D)** PK-15 cells were mock-infected or infected with CSFV (MOI = 0.1), after 24 h infection, cells were immunostained with antibodies against CSFV E2 (green) and NDP52 (red). In the merged images, protein colocalization is displayed as yellow.

transfecting the plasmid of GFP-LC3 and observed by fluorescence microscopy (**Figure 4A**). We also used the plasmid of GFP-RFP-LC3 to detect its distribution in cells. The results showed that LC3B in the cytoplasm was reduced and the yellow spots more than red spots in NDP52-inhibited cells. Thus, inhibition of NDP52 reduced LC3 expression and the normal fusion of autophagosomes with lysosomes. We also assessed the mitochondrial autophagy marker Tom20 using laser confocal microscopy and found that inhibition of NDP52 enhanced Tom20 expression (**Figure 4B**), suggesting positive regulation of autophagy by NDP52. At the same time, we detected expression of cellular and mitochondrial autophagy markers LC3B and Beclin-1 expression decreased, while VDAC1 and Tom20 expression increased (**Figure 4C**), indicating that

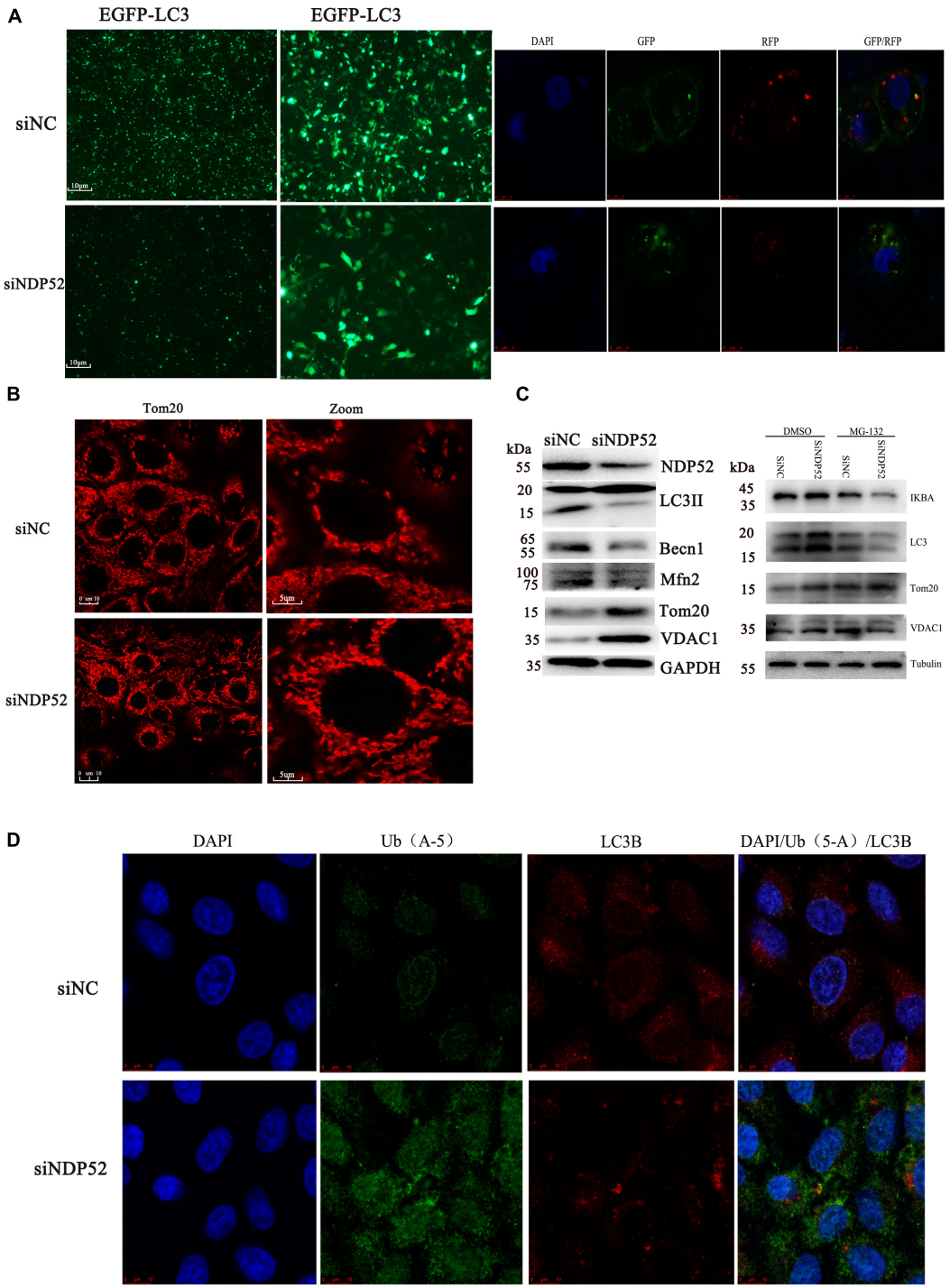

FIGURE 4 | Inhibition of NDP52 reduces autophagy and mitophagy, and decreases ubiquitin and LC3 binding. **(A)** PK-15 cells were transfected with scrambled or NDP52 siRNA for 24 h. Then, cells were transfected with EGFP-LC3 or GFP-RFP-LC3 plasmid or immunostained with antibodies against LC3 (red). After NDP52 inhibition, eGFP levels were significantly reduced, the yellow dots were more than red dots and the LC3B expression in the cytoplasm. **(B)** PK-15 cells were treated as above, after 24 h transfection, cells were immunostained with antibodies against Tom20 (red). After NDP52 inhibition, Tom20 expression was enhanced. **(C)** The expression of the autophagy markers, LC3 and Beclin-I, and mitophagy markers, Mfn2, VDAC, and Tom20, in PK-15 cells were analyzed by Western blotting after transfection with scrambled or NDP52 siRNA for 24 h. GAPDH was used as the internal loading control. The expression of IκB-a, LC3, VDAC, and Tom20 in PK-15 cells were analyzed by Western blotting after co-transfection with scrambled or NDP52 siRNA with DMSO or MG-132 for 24 h. Tubulin was used as the internal loading control. **(D)** Ub(A-5) (green) and LC3 (red) expression in PK-15 cells. In the merged images, protein colocalization is displayed as yellow.

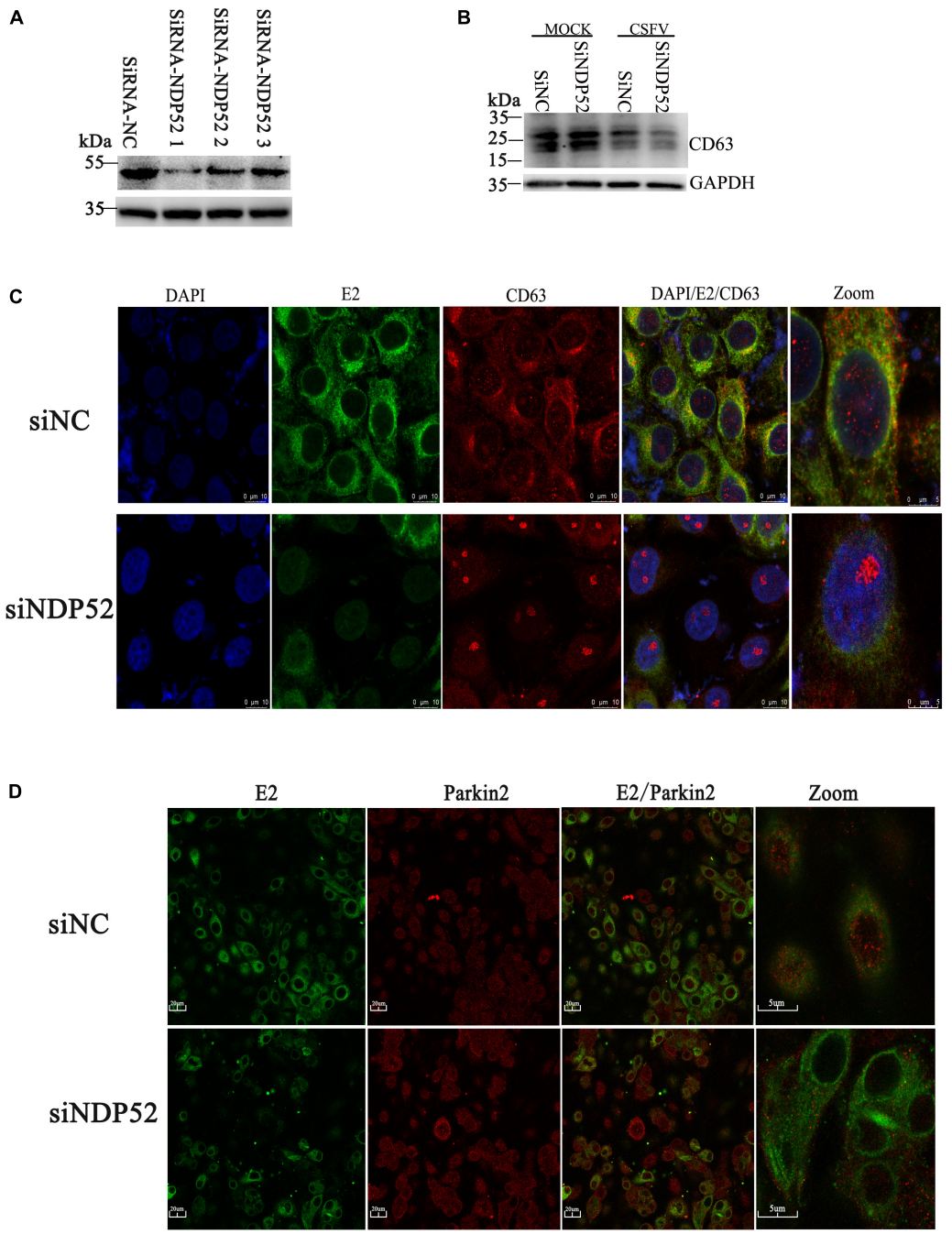

FIGURE 5 | Inhibition of NDP52 reduces CD63 and Ub(A-5) binding to E2. **(A)** Three different NDP52 interference plasmids were verified by Western blot. GAPDH was used as the internal loading control. siRNA-NDP52-1 was used to inhibit NDP52 expression for subsequent experiments. **(B)** PK-15 cells were transfected with scrambled or NDP52 siRNA for 24 h, followed by mock or CSFV infection (MOI = 0.1). CD63 protein expression was detected by Western blot. GAPDH was used as the internal loading control. **(C)** Treated PK-15 cells were immunostained with antibodies against CSFV E2 (green) and CD63 (red). **(D)** PK-15 cells were immunostained with antibodies against CSFV E2 (green) and Ub(A-5) (red).

inhibition of NDP52 has an inhibitory effect on the expression of autophagy proteins. To explore the role of ubiquitin in this process, we co-transfected NDP52 interfering RNA with MG-132 (5 μM), a ubiquitin-proteasome system inhibitor. We found that in the cells treated with MG-132, the effect of SiNDP52 on the autophagy-related protein disappeared, indicated that ubiquitin-proteasome system affects the effect of NDP52 on autophagy. In selective autophagy, the function of NDP52 is closely related to LC3 and ubiquitin, so we examined the expression and colocalization of LC3 and Ub(A-5) in cells.

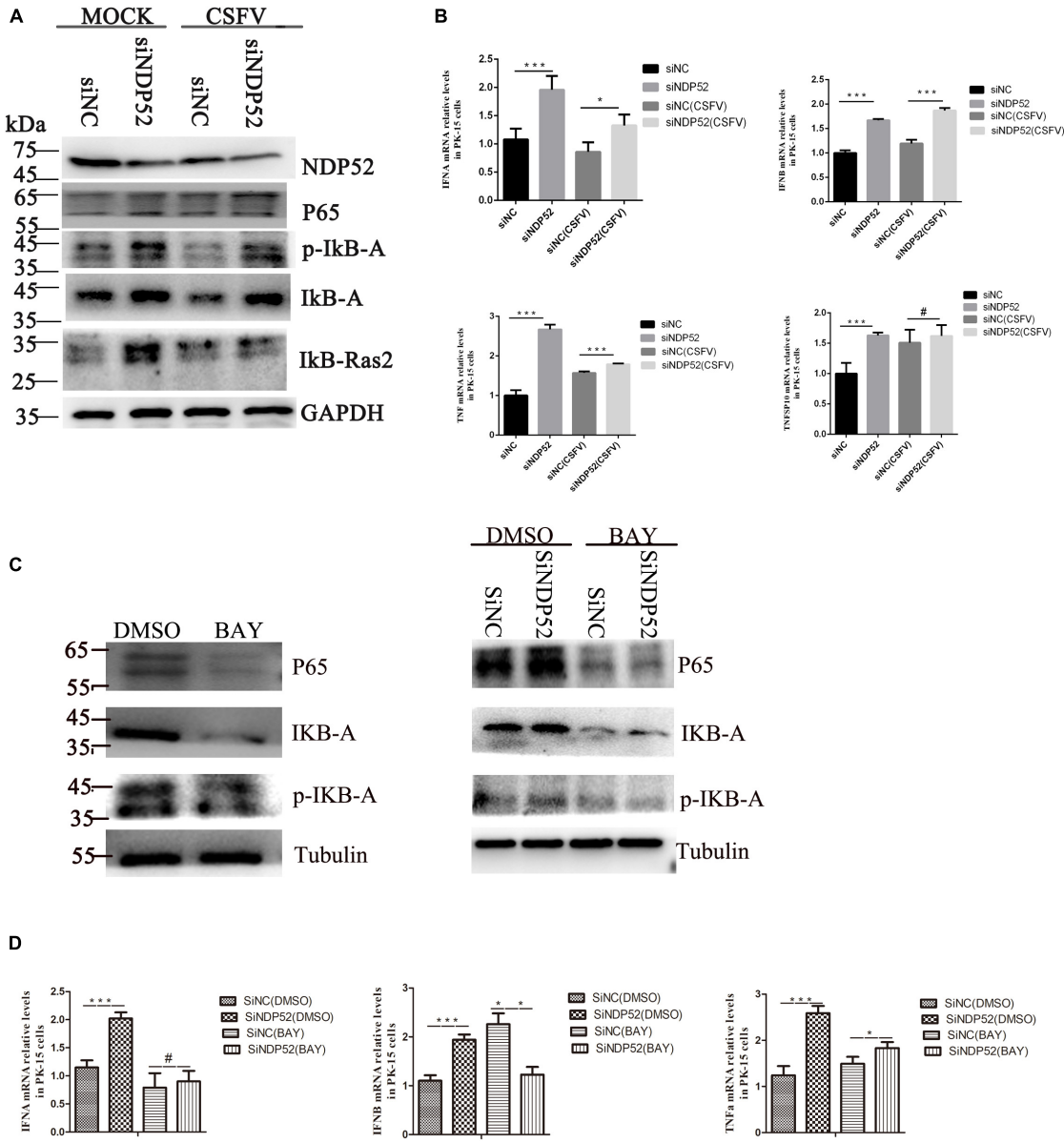

FIGURE 6 | Inhibition of NDP52 promotes innate immunity through the NF-κB signaling pathway. **(A)** Inhibition of NDP52 has a positive effect on NF-κB signaling pathway. PK-15 cells were mock-infected or infected with CSFV (MOI = 0.1) after transfection with siNDP52 for 24 h. NF-κB signaling pathway proteins IκB-A, P65, IκB-Ras expression were analyzed by western blotting at 24 hpi. **(B)** PK-15 cells were treated as above. mRNA levels of the cytokines IFN-α, IFN-β, and TNF were detected by qRT-PCR. **(C)** PK-15 cells were co-transfection with scrambled or NDP52 siRNA with DMSO or BAY (5 μM) for 24 h. NF-κB signaling pathway proteins IκB-A, P65, p-IκB-A expression were analyzed by western blotting at 24 hpi. **(D)** PK-15 cells were treated as **(C)**, mRNA levels of the cytokines IFN-α, IFN-β, and TNF were detected by qRT-PCR. The data represent mean ± SD in three independent experiments. Data were tested by one-way ANOVA with *post hoc* LSD (L). $^{*}P < 0.05$; $^{**}P < 0.01$; $^{***}P < 0.001$; $\#P > 0.05$.

Indeed, NDP52 inhibition also decreased LC3 expression and subsequent binding to Ub(A-5) (**Figure 4D**).

Inhibition of NDP52 Reduces Colocalization of Autophagy Vesicle CD63 With CSFV E2 Protein

Our previous studies showed that CSFV induces autophagy, with autophagosomes as self-replication sites. However, the specific mechanism of CSFV-autophagosome entry is unclear (Pei et al., 2013). Because NDP52 regulates autophagy, we investigated the role of NDP52 in autophagic vesicles mediated by CSFV infection. We screened NDP52-interfering RNAs using western blotting and found that SiNDP52-1 had the best interference effect (**Figure 5A**). After NDP52 RNA interference for 24 h, PK-15 cells were infected with CSFV or mock-infected. Western blots showed that NDP52 inhibition decreased expression of CD63, a marker of autophagic vesicles (**Figure 5B**). Moreover, in the

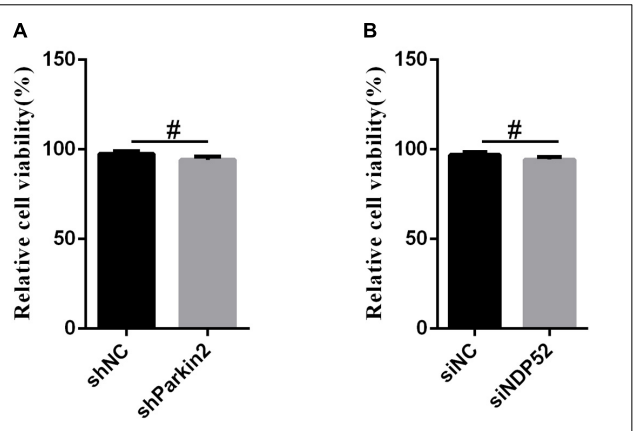

FIGURE 7 | The effect of RNA interference on cell viability. The cell viability of PK-15 cells transfected with scrambled or Parkin shRNA **(A)** and siNC or NDP52 siRNA **(B)** was analyzed using the CCK8 assay as described in section "Materials and Methods" (mean ± SD; $n = 3$; $^{*}P < 0.05$; $^{**}P < 0.01$; $^{***}P < 0.001$; $^{\#}P > 0.05$).

case of CSFV infection, this inhibition was more pronounced, indicating that NDP52 has a positive effect on the expression of CD63. To further verify the effect of NDP52 on CD63 and E2 colocalization, we used laser confocal microscopy to observe the localization of CD63. The results showed that CD63 binding to the CSFV E2 protein was decreased in the cytoplasm after NDP52 suppression (**Figure 5C**). We also found that Ub-5a binding to the CSFV E2 protein was reduced after NDP52 suppression (**Figure 5D**), suggesting that NDP52 plays an import role in CSFV entry into autophagosomes. These results indicate that NDP52 promotes colocalization of E2 with CD63 and Ub(A-5).

Inhibition of NDP52 Activates the NF-κB Pathway to Release IFN/TNF Cytokines

NF-κB activation during viral infection is part of the protective response to pathogens (Santoro et al., 2003). Interestingly, CSFV replication in cells suppresses type I IFN-inducible antiviral activity and apoptosis by interfering with IFN production, thereby resulting in the persistent survival of CSFV in host cells *in vitro* (Bensaude, 2004). To examine the effect of NDP52 on the innate antiviral immune pathway, we first examined NF-κB signaling activation following NDP52 inhibition. We observed increased expression of NF-κB signaling pathway proteins after NDP52 inhibition, indicating that inhibition of NDP52 promotes the activation of the NF-κB signaling pathway (**Figure 6A**). We also found that inhibition of NDP52 promotes release of cytokines, including IFN-α, IFN-β, and TNF (**Figure 6B**), indicating that NDP52 also plays an important role in the innate immune response. Therefore, NDP52 may inhibit CSFV infection via the NF-κB signaling pathway. In order to verify whether the release of SiNDP52 on the above cytokines is regulated by the NF-κB pathway, we treated cells with NF-κB inhibitor BAY 11-7082 (5 μM) and found that BAY 11-7082 had no effect on cytokine release, but BAY 11-7082 affects the effect of SiNDP52 on IFN-α release (**Figures 6C,D**).

Cell Viability Was Not Affected by RNA Interference

To exclude the possibility that NDP52 siRNA inhibited CSFV replication or that Parkin shRNA inhibited NDP52 protein modification by downregulating cell viability, we assessed the effects of RNA interference on the viability of PK-15 cells. The results showed no significant changes in the viability of cells following silencing of NDP52 or Parkin ($P > 0.05$) (**Figure 7**).

DISCUSSION

The body has several cellular immune mechanisms to maintain the internal environment and prevent invasion by pathogenic microorganisms. However, many viruses have evolved replication strategies to cope with the adverse host environment. Indeed, virus-induced autophagy as a protective mechanism has been widely reported (Sugden et al., 2005). In our previous study, we found that CSFV infection induces complete and high-yield autophagic flux and that CSFV replicates in the autophagosome. Together, these processes provide a suitable environment for long-term viral infection in host cells. Further research found that the viral E2 protein colocalizes with the autophagosome marker CD63 (Metzelaars et al., 1991), but the function of this interaction was unclear. As an autophagy receptor, NDP52 plays an important role both in bacterial and viral infection. NDP52 mediates targeting of cytosolic substrates to autophagy machinery, and promotes the maturation of autophagic vesicles (Von muhlinen et al., 2012; Cemma et al., 2014; Leymarie et al., 2017). Therefore, we wanted to define the role of the autophagy receptor NDP52 in CSFV infection. The current study provides further insights into the role of NDP52 in CSFV-autophagic vesicle entry and the mechanism of induction of virus-mediated autophagy.

In the case of viral infection, Mohamud et al. (2018) reported that NDP52 binds to the coxsackievirus B3 viral protein VP1 and mediates VP1 ubiquitination via the K48 ubiquitin pathway. Other studies have shown that CALCOCO2 binds the non-structural protein 2 of the Chikungunya virus to promote viral replication in humans (Judith et al., 2013), and plays a pro-viral role in measles viral infection (Petkova et al., 2017). In this study, our results showed that CSFV infection inhibits NDP52 expression. Moreover, NDP52-interfering RNA inhibits CSFV replication, indicating that NDP52 plays an important role in the infection of swine fever virus.

During viral infection, autophagy receptors can induce viral phagocytosis in a ubiquitin-dependent manner and can bind directly to viral capsid proteins or indirectly to host ubiquitin factors via E3 ubiquitin ligase (Mohamud et al., 2018). In the present study, we found that CSFV infection can reduce NDP52 ubiquitination and SUMO2-4 protein modification. Since the PINK1-Parkin pathway and autophagy receptors are closely related to functional ubiquitin modification, we examined the CSFV-mediated regulation of NDP52 protein modification after Parkin inhibition. CSFV can mediate NDP52 ubiquitination by PINK1-Parkin. Interestingly, when we inhibited NDP52 expression by RNA interference,

we found that Ub(A-5) expression increased while LC3 expression decreased. Ubiquitin acts as a signaling molecule, which causes polyubiquitination of autophagic substrates (Lu et al., 2017a,b). Autophagy receptor proteins recognize and bind autophagic substrates through a ubiquitin domain-dependent or independent manner (Walinda et al., 2014). The substrate is anchored to the autophagosome membrane by its LIR, followed by autophagosome-lysosome fusion and substrate degradation. We speculate polyubiquitination is required to recruit NDP52 or other autophagy receptors and reduce LC3 expression, and thus virus-induced ubiquitin molecules persist within the cell.

Because NDP52 mediates bacterial entry into autophagosomes (Sudhakar et al., 2019), we investigated whether NDP52 plays a role in CSFV entry into autophagosomes. We first assessed the effect of NDP52 on autophagy and observed that autophagy markers LC3 and Beclin-I decreased. Further analyses revealed that after NDP52 inhibition, CD63 protein expression was reduced, leading to decreased binding of CD63 to the viral E2 protein. These results suggest that NDP52 plays an important role in the mechanism of CSFV entry into autophagic vesicles. However, it is unclear whether NDP52 is modified by self-protein or by modifying CSFV protein to promote CSFV entry into autophagic vesicles.

NDP52 is involved in the negative regulation of the classical NF-κB pathway (Inomata et al., 2011). Our previous studies confirmed that CSFV can bind to MDA5 and RIG-1, inducing NF-κB nuclear translocation via RIG-1 signaling (Xiao-Ying et al., 2013). Moreover, NF-κB signaling also regulates CSFV replication (Ling et al., 2018). However, the effect of NDP52 on the NF-κB signaling pathway during CSFV infection was unclear. Therefore, we used RNA interference to inhibit NDP52 after CSFV infection. We found that NDP52 inhibition activates the NF-κB pathway, including P65, Iκb-Ras, IκBa, and p-IκBa. Furthermore, NDP52 inhibition promotes TNF and type I IFN release. CSFV infection attenuates this activation, suggesting that CSFV may have an inhibitory effect on the NF-κB signaling pathway.

In summary, our study provides the first evidence that CSFV infection regulates and modifies the autophagy receptor NDP52. Further, we uncovered the dual CD63 and NF-κB-induced mechanisms used by NDP52 to promote viral propagation.

DATA AVAILABILITY STATEMENT

All datasets generated for this study are included in the article/supplementary material.

AUTHOR CONTRIBUTIONS

SF, MiZ, KW, and JC conceived and designed the study. SF, KW, CL, MiZ, JC, EZ, and SM performed the experiments. SF, YC, MeZ, DS, and XL analyzed the data. SF, MiZ, KW, HD, JL, LY, and JC wrote the manuscript. All authors read and agreed upon the final manuscript.

FUNDING

This work was supported by grants from the National Natural Science Foundation of China (31672590), National Key Research and Development Program (2017YFD0501104 and 2016YFD0500600), and Science and Technology Program of Guangzhou, China (Nos. 2019B020211003 and 201803020005).

REFERENCES

Becher, P., Avalos Ramirez, R., Orlich, M., Cedillo Rosales, S., König, M., Schweizer, M., et al. (2003). Genetic and antigenic characterization of novel pestivirus genotypes: implications for classification. *Virology* 311, 96–104. doi: 10.1016/s0042-6822(03)00192-2

Bensaude, E. (2004). Classical swine fever virus induces proinflammatory cytokines and tissue factor expression and inhibits apoptosis and interferon synthesis during the establishment of long-term infection of porcine vascular endothelial cells. *J. Gen. Virol.* 85, 1029–1037. doi: 10.1099/vir.0.19637-0

Bizargity, P., and Schröppel, B. (2014). Autophagy: basic principles and relevance to transplant immunity. *Am. J. Transplant.* 14, 1731–1739. doi: 10.1111/ajt.12743

Cemma, M., Kim, P. K., and Brumell, J. H. (2014). The ubiquitin-binding adaptor proteins p62/SQSTM1 and NDP52 are recruited independently to bacteria-associated microdomains to target *Salmonella* to the autophagy pathway. *Autophagy* 7, 341–345. doi: 10.4161/auto.7.3.14046

Ciechomska, I. A., Gabrusiewicz, K., Szczepankiewicz, A. A., and Kaminska, B. (2013). Endoplasmic reticulum stress triggers autophagy. *Oncogene* 32, 1518–1529. doi: 10.1038/onc.2012.174

Deretic, V., Saitoh, T., and Akira, S. (2013). Autophagy in infection, inflammation and immunity. *Nat. Rev. Immunol.* 13, 722–737. doi: 10.1038/nri3532

Fan, S., Yuan, J., Deng, S., Chen, Y., Xie, B., Wu, K., et al. (2018). Activation of Interleukin-1β Release by the Classical Swine Fever Virus Is Dependent on the NLRP3 Inflammasome, Which Affects Virus Growth in Monocytes. *Front. Cell. Infect. Microbiol.* 8:225. doi: 10.3389/fcimb.2018.00225

Fu, T., Liu, J., Wang, Y., Xie, X., Hu, S., and Pan, L. (2018). Mechanistic insights into the interactions of NAP1 with the SKICH domains of NDP52 and TAX1BP1. *Proc. Natl. Acad. Sci. U.S.A.* 115, E11651–E11660. doi: 10.1073/pnas.1811421115

Gou, H., Zhao, M., Fan, S., Yuan, J., Liao, J., He, W., et al. (2017). Autophagy induces apoptosis and death of T lymphocytes in the spleen of pigs infected with CSFV. *Sci. Rep.* 7:13577. doi: 10.1038/s41598-017-14082-9

Heinz-Jurgen, T. R. S., Emilie, W., Tillmann, R., and Gregor, M. (1991). Hog cholera virus_ molecular composition of virgins from a pestiferous. *J. Virol.* 65, 4705–4712.

Heo, J.-M., Ordureau, A., Paulo, J. A., Rinehart, J., and Harper, J. W. (2015). The PINK11-PARKIN mitochondrial ubiquitylation pathway drives a program of OPTN/NDP52 recruitment and TBK1 activation to promote mitophagy. *Mol. Cell* 60, 7–20. doi: 10.1016/j.molcel.2015.08.016

Hongchao, G., Mingqiu, Z., Hailuan, X., Jin, Y., Wencheng, H., Mengjiao, Z., et al. (2017). CSFV induced mitochondrial fission and mitophagy to inhibit apoptosis. *Oncotarget* 24, 39382–39400. doi: 10.18632/oncotarget.17030

Høyer-Hansen, M., and Jäättelä, M. (2008). Autophagy An emerging target for cancer therapy. *Autophagy* 4, 574–580. doi: 10.4161/auto.5921

Inomata, M., Niida, S., Shibata, K.-I., and Into, T. (2011). Regulation of Toll-like receptor signaling by NDP52-mediated selective autophagy is normally inactivated by A20. *Cell. Mol. Life Sci.* 69, 963–979. doi: 10.1007/s00018-011-0819-y

Ivashkiv, L. B., and Donlin, L. T. (2013). Regulation of type I interferon responses. *Nat. Rev. Immunol.* 14, 36–49. doi: 10.1038/nri3581

Jin, S., Tian, S., Luo, M., Xie, W., Liu, T., Duan, T., et al. (2017). Tetherin suppresses type I interferon signaling by targeting MAVS for NDP52-mediated selective autophagic degradation in human cells. *Mol. Cell* 68, 308.e6–322.e6. doi: 10.1016/j.molcel.2017.09.005

Johns, H. L., Bensaude, E., La Rocca, S. A., Seago, J., Charleston, B., Steinbach, F., et al. (2009). Classical swine fever virus infection protects aortic endothelial cells from pIpC-mediated apoptosis. *J. Gen. Virol.* 91, 1038–1046. doi: 10.1099/vir.0.016576-0

Judith, D., Mostowy, S., Bourai, M., Gangneux, N., Lelek, M., Lucas-Hourani, M., et al. (2013). Species-specific impact of the autophagy machinery on Chikungunya virus infection. *EMBO Rep.* 14, 534–544. doi: 10.1038/embor.2013.51

Kocaturk, N. M., and Gozuacik, D. (2018). Crosstalk between mammalian autophagy and the ubiquitin-proteasome system. *Front. Cell Dev. Biol.* 6:128. doi: 10.3389/fcell.2018.00128

Lazarou, M., Sliter, D. A., Kane, L. A., Sarraf, S. A., Wang, C., Burman, J. L., et al. (2015). The ubiquitin kinase PINK11 recruits autophagy receptors to induce mitophagy. *Nature* 524, 309–314. doi: 10.1038/nature14893

Leymarie, O., Meyer, L., Tafforeau, L., Lotteau, V., Costa, B. D., Delmas, B., et al. (2017). Influenza virus protein PB1-F2 interacts with CALCOCO2 (NDP52) to modulate innate immune response. *J. Gen. Virol.* 98, 1196–1208. doi: 10.1099/jgv.0.000782

Ling, S., Luo, M., Jiang, S., Liu, J., Ding, C., Zhang, Q., et al. (2018). Cellular Hsp27 interacts with classical swine fever virus NS5A protein and negatively regulates viral replication by the NF-κB signaling pathway. *Virology* 518, 202–209. doi: 10.1016/j.virol.2018.02.020

Liu, T., Zhang, L., Joo, D., and Sun, S.-C. (2017). NF-κB signaling in inflammation. *Signal Transduct. Target. Ther.* 2:17023.

Liu, Z., Chen, P., Gao, H., Gu, Y., Yang, J., Peng, H., et al. (2014). Ubiquitylation of autophagy receptor optineurin by HACE1 activates selective autophagy for tumor suppression. *Cancer Cell* 26, 106–120. doi: 10.1016/j.ccr.2014.05.015

Lu, K., Den Brave, F., and Jentsch, S. (2017a). Pathway choice between proteasomal and autophagic degradation. *Autophagy* 13, 1799–1800. doi: 10.1080/15548627.2017.1358851

Lu, K., Den Brave, F., and Jentsch, S. (2017b). Receptor oligomerization guides pathway choice between proteasomal and autophagic degradation. *Nat. Cell Biol.* 19, 732–739. doi: 10.1038/ncb3531

Lum, J. J., Bauer, D. E., Kong, M., Harris, M. H., Li, C., Lindsten, T., et al. (2005). Growth factor regulation of autophagy and cell survival in the absence of apoptosis. *Cell* 120, 237–248. doi: 10.1016/j.cell.2004.11.046

Majzoub, K., Wrensch, F., and Baumert, T. F. (2019). The innate antiviral response in animals: an evolutionary perspective from flagellates to humans. *Viruses* 11:758. doi: 10.3390/v11080758

Metzelaars, M. J., Wijngaard, P. L., Peter, P. J., Sixma, J. J., Nieuwenhuiss, H. K., and Cleversb, H. C. (1991). CD63 antigen. A novel lysosomal membrane glycoprotein, cloned by a screening procedure for intracellular antigens in eukaryotic cells. *J. Biol. Chem.* 266, 3239–3245.

Minowa-Nozawa, A., Nozawa, T., Okamoto-Furuta, K., Kohda, H., and Nakagawa, I. (2017). Rab35 GTPase recruits NDP52 to autophagy targets. *EMBO J.* 36, 2790–2807. doi: 10.15252/embj.201796463

Mohamud, Y., and Luo, H. (2018). The intertwined life cycles of enterovirus and autophagy. *Virulence* 10, 470–480. doi: 10.1080/21505594.2018.1551010

Mohamud, Y., Qu, J., Xue, Y. C., Liu, H., Deng, H., and Luo, H. (2018). CALCOCO2/NDP52 and SQSTM1/p62 differentially regulate coxsackievirus B3 propagation. *Cell Death Differ.* 26, 1062–1076. doi: 10.1038/s41418-018-0185-5

Nakamura, S., and Yoshimori, T. (2017). New insights into autophagosome–lysosome fusion. *J. Cell Sci.* 130, 1209–1216. doi: 10.1242/jcs.196352

Oeckinghaus, A., and Ghosh, S. (2009). The NF- B family of transcription factors and its regulation. *Cold Spring Harb. Perspect. Biol.* 1:a000034. doi: 10.1101/cshperspect.a000034

Paton, D. J., and Greiser-Wilke, I. (2003). Classical swine fever–an update. *Res. Vet. Sci.* 75, 169–178. doi: 10.1016/s0034-5288(03)00076-6

Pei, J., Deng, J., Ye, Z., Wang, J., Gou, H., Liu, W., et al. (2016). Absence of autophagy promotes apoptosis by modulating the ROS-dependent RLR signaling pathway in classical swine fever virus-infected cells. *Autophagy* 12, 1738–1758. doi: 10.1080/15548627.2016.1196318

Pei, J., Zhao, M., Ye, Z., Gou, H., Wang, J., Yi, L., et al. (2013). Autophagy enhances the replication of classical swine fever virus in vitro. *Autophagy* 10, 93–110. doi: 10.4161/auto.26843

Petkova, D., Verlhac, P., Rozières, A., Baguet, J., Claviere, M., Kretz-Remy, C., et al. (2017). Distinct contributions of autophagy receptors in measles virus replication. *Viruses* 9:123. doi: 10.3390/v9050123

Ravenhill, B. J., Boyle, K. B., Von Muhlinen, N., Ellison, C. J., Masson, G. R., Otten, E. G., et al. (2019). The cargo receptor NDP52 initiates selective autophagy by recruiting the ULK complex to cytosol-invading bacteria. *Mol. Cell* 74, 320.e6–329.e6. doi: 10.1016/j.molcel.2019.01.041

Santoro, M. G., Rossi, A., and Amici, C. (2003). NF-κB and virus infection_ who controls whom. *EMBO J.* 22, 2552–2560. doi: 10.1093/emboj/cdg267

Scherz-Shouval, R., Shvets, E., Fass, E., Shorer, H., Gil, L., and Elazar, Z. (2007). Reactive oxygen species are essential for autophagy and specifically regulate the activity of Atg. *EMBO J.* 26, 1749–1760. doi: 10.1038/sj.emboj.7601623

Schmitz, M. L., Kracht, M., and Saul, V. V. (2014). The intricate interplay between RNA viruses and NF-κB. *Biochim. Biophys. Acta Mol. Cell Res.* 1843, 2754–2764. doi: 10.1016/j.bbamcr.2014.08.004

Shaid, S., Brandts, C. H., Serve, H., and Dikic, I. (2012). Ubiquitination and selective autophagy. *Cell Death Differ.* 20, 21–30. doi: 10.1038/cdd.2012.72

Sharma, V., Verma, S., Seranova, E., Sarkar, S., and Kumar, D. (2018). Selective autophagy and xenophagy in infection and disease. *Front. Cell Dev. Biol.* 6:147. doi: 10.3389/fcell.2018.00147

Sudhakar, P., Jacomin, A.-C., Hautefort, I., Samavedam, S., Fatemian, K., Ari, E., et al. (2019). Targeted interplay between bacterial pathogens and host autophagy. *Autophagy* 15, 1620–1633. doi: 10.1080/15548627.2019.1590519

Sugden, B., Jackson, W. T., Giddings, T. H., Taylor, M. P., Mulinyawe, S., Rabinovitch, M., et al. (2005). Subversion of cellular autophagosomal machinery by RNA viruses. *PLoS Biol.* 3:e156. doi: 10.1371/journal.pbio.0030156

Tattoli, I., Sorbara, M. T., Vuckovic, D., Ling, A., Soares, F., Carneiro, L. A., et al. (2012). Amino acid starvation induced by invasive bacterial pathogens triggers an innate host defense program. *Cell Host Microbe* 11, 563–575. doi: 10.1016/j.chom.2012.04.012

Tumbarello, D. A., Waxse, B. J., Arden, S. D., Bright, N. A., Kendrick-Jones, J., and Buss, F. (2012). Autophagy receptors link myosin VI to autophagosomes to mediate Tom1-dependent autophagosome maturation and fusion with the lysosome. *Nat. Cell Biol.* 14, 1024–1035. doi: 10.1038/ncb2589

Verlhac, P., Grégoire, I. P., Azocar, O., Petkova, D. S., Baguet, J., Viret, C., et al. (2015a). Autophagy receptor NDP52 regulates pathogen-containing autophagosome maturation. *Cell Host Microbe* 17, 515–525. doi: 10.1016/j.chom.2015.02.008

Verlhac, P., Viret, C., and Faure, M. (2015b). Dual function of CALCOCO2/NDP52 during xenophagy. *Autophagy* 11, 965–966. doi: 10.1080/15548627.2015.1046672

Von muhlinen, N., Akutsu, M., Ravenhill, B. J., Foeglein, A., Bloor, S., Rutherford, T. J., et al. (2012). LC3C, bound selectively by a noncanonical LIR motif in NDP52, is required for antibacterial autophagy. *Mol. Cell* 48, 329–342. doi: 10.1016/j.molcel.2012.08.024

Walinda, E., Morimoto, D., Sugase, K., Konuma, T., Tochio, H., and Shirakawa, M. (2014). Solution structure of the ubiquitin-associated (UBA) domain of human autophagy receptor NBR1 and its interaction with ubiquitin and polyubiquitin. *J. Biol. Chem.* 289, 13890–13902. doi: 10.1074/jbc.M114.555441

Wang, L., and Ou, J. J. (2018). Regulation of autophagy by Hepatitis C virus for its replication. *DNA Cell Biol.* 37, 287–290. doi: 10.1089/dna.2017.4115

Xiao-Ying, D., Wen-Jun, L., Ming-Qiu, Z., Jia-Ying, W., Jing-Jing, P., Yong-Wen, L., et al. (2013). Classical swine fever virus triggers RIG-I and MDA5-dependent signaling pathway to IRF-3 and NF-κB activation to promote secretion of interferon and inflammatory cytokines in porcine alveolar macrophages.*pdf* >. *Virol. J.* 10, 1–11.

Zaffagnini, G., and Martens, S. (2016). Mechanisms of selective autophagy. *J. Mol. Biol.* 428, 1714–1724. doi: 10.1016/j.jmb.2016.02.004

Conflict of Interest: The authors declare that the research was conducted in the absence of any commercial or financial relationships that could be construed as a potential conflict of interest.

Copyright © 2020 Fan, Wu, Luo, Li, Zhao, Song, Ma, Zhu, Chen, Ding, Yi, Li, Zhao and Chen. This is an open-access article distributed under the terms of the Creative Commons Attribution License (CC BY). The use, distribution or reproduction in other forums is permitted, provided the original author(s) and the copyright owner(s) are credited and that the original publication in this journal is cited, in accordance with accepted academic practice. No use, distribution or reproduction is permitted which does not comply with these terms.

frontiers in Microbiology

ORIGINAL RESEARCH
published: 21 January 2020
doi: 10.3389/fmicb.2019.03085

Transmissible Gastroenteritis Virus Infection Up-Regulates FcRn Expression via Nucleocapsid Protein and Secretion of TGF-β in Porcine Intestinal Epithelial Cells

*Shaoju Qian[1], Zitong Gao[1], Rui Cao[1], Kang Yang[1], Yijie Cui[1], Shaowen Li[1,2,3], Xianrong Meng[1,2,3], Qigai He[1,2,3] and Zili Li[1,2,3]**

[1] State Key Laboratory of Agricultural Microbiology, College of Veterinary Medicine, Huazhong Agricultural University, Wuhan, China, [2] Key Laboratory of Preventive Veterinary Medicine in Hubei Province, The Cooperative Innovation Center for Sustainable Pig Production, Wuhan, China, [3] Key Laboratory of Development of Veterinary Diagnostic Products, Ministry of Agriculture of the People's Republic of China, Wuhan, China

OPEN ACCESS

Edited by:
Ian M. Jones, University of Reading, United Kingdom

Reviewed by:
Pinghuang Liu, Harbin Veterinary Research Institute (CAAS), China
Guochun Jiang, The University of North Carolina at Chapel Hill, United States

***Correspondence:**
Zili Li
lizili@mail.hzau.edu.cn

Specialty section:
This article was submitted to Virology, a section of the journal Frontiers in Microbiology

Received: *14 October 2019*
Accepted: *20 December 2019*
Published: *21 January 2020*

Citation:
Qian S, Gao Z, Cao R, Yang K, Cui Y, Li S, Meng X, He Q and Li Z (2020) Transmissible Gastroenteritis Virus Infection Up-Regulates FcRn Expression via Nucleocapsid Protein and Secretion of TGF-β in Porcine Intestinal Epithelial Cells. Front. Microbiol. 10:3085. doi: 10.3389/fmicb.2019.03085

Transmissible gastroenteritis virus (TGEV) is a porcine intestinal coronavirus that causes fatal severe watery diarrhea in piglets. The neonatal Fc receptor (FcRn) is the only IgG transport receptor, its expression on mucosal surfaces is triggered upon viral stimulation, which significantly enhances mucosal immunity. We utilized TGEV as a model pathogen to explore the role of FcRn in resisting viral invasion in overall intestinal mucosal immunity. TGEV induced FcRn expression by activating NF-κB signaling in porcine small intestinal epithelial (IPEC-J2) cells, however, the underlying mechanisms are unclear. First, using small interfering RNAs, we found that TGEV up-regulated FcRn expression via TLR3, TLR9 and RIG-I. Moreover, TGEV induced IL-1β, IL-6, IL-8, TGF-β, and TNF-α production. TGF-β-stimulated IPEC-J2 cells highly up-regulated FcRn expression, while treatment with a JNK-specific inhibitor down-regulated the expression. TGEV nucleocapsid (N) protein also enhanced FcRn promoter activity via the NF-κB signaling pathway and its central region (aa 128–252) was essential for FcRn activation. Additionally, N protein-mediated FcRn up-regulation promotes IgG transcytosis. Thus, TGEV N protein and TGF-β up-regulated FcRn expression, further clarifying the molecular mechanism of up-regulation of FcRn expression by TGEV.

Keywords: transmissible gastroenteritis virus, nucleocapsid protein, TGF-β, neonatal Fc receptor, toll-like receptor, NF-κB

INTRODUCTION

Transmissible gastroenteritis virus (TGEV) infection mainly causes severe watery diarrhea, vomiting, dehydration, and mortality in suckling piglets less than 2 weeks old, as well as colossal economic losses in the worldwide pig industry (Zhao et al., 2014). TGEV has a 28.5-kb single-stranded, positive-sense RNA genome, including at least nine open reading frames (ORFs): ORF1a, ORF1b, Structural proteins, nucleocapsid (N) protein, membrane (M) glycoprotein, spike (S) glycoprotein, a small envelope (E) glycoprotein, and accessory proteins 3a, 3b, and 7

(Escors et al., 2003). ORF1a and ORF1b, located in the 5′ two-thirds of the viral genome, are cleaved into 16 non-structural proteins (nsp1 to nsp16) by the nsp3 and nsp5 proteases. These nsps are responsible for viral replication, viral transcription, and the antagonization of host innate immune responses.

Transmissible gastroenteritis virus replication occurs in the small intestinal epithelial cells, while viral entry and release are restricted to the apical surface of polarized epithelial cells. Neonatal Fc receptor (FcRn) is a specific receptor for the immunoglobulin IgG, which is expressed in many cells, including epithelial cells, macrophages, and dendritic cells (Ye et al., 2008). FcRn transports of IgG in the female reproductive tract plays an important role in combating infection (Li et al., 2011). In addition to IgG, FcRn binds albumin, which regulates liver damage (Pyzik et al., 2017). It has been found that FcRn can enhance HIV-I endocytosis in transmucosal epithelial cells (Gupta et al., 2013). It has also been documented that the use of fusion proteins of the Fc fragment as immunogenic antigens can improve the impact of vaccines. Intranasally inoculated fusion protein, HSV-2 gD, HIV Gag fused with the Fc region of IgG, and targeted FcRn can all induce systemic and mucosal immunity to genital infections (Lu et al., 2011; Ye et al., 2011). Most studies on FcRn have focused on the function of FcRn in humans and mice; so far, only a few relevant studies about pathogenic infection and FcRn expression regulation have been reported. In our previous study, TGEV induced FcRn expression via the NF-κB pathway in IPEC-J2 cells (Guo et al., 2016b), but the regulatory mechanisms underlying this remain unclear; thus, we need to further explore the involvement of pattern recognition receptors (PRRs), inflammatory factors, and virus-coding proteins in the regulation of FcRn.

In the innate immune system, PRRs recognize pathogen-associated molecular patterns (PAMPs) as the first step in the host's resistance to infection. After recognition of PAMPs, these receptors interact with their corresponding binding molecules to trigger downstream signaling events that activate NF-κB and IFN regulatory factors that induce several types of antiviral cytokines (Thompson and Locarnini, 2007). TGEV infection activates transcriptional activator 1 (JAK-STAT1) signaling pathways according to a quantitative proteomics study in PK-15 cells (An et al., 2014). TGEV infection has been reported to activate the mitogen-activated protein kinase (MAPK) pathway and destroy epithelial barrier integrity in IPEC-J2 cells (Zhao et al., 2014). TGEV N, nsp2 and nsp14 proteins all induce NF-κB activation (Zhou et al., 2017; Wang et al., 2018; Zhang et al., 2018), but the regulatory mechanism of FcRn is still unknown. Most studies on TGEV have focused on the induction and activation of NF-κB and IFN, but host cell biology may affect cell function. However, the detailed mucosal immunity mechanism during TGEV pathogenesis remains unknown.

Viral invasion always triggers an inflammatory response, which is the key mediator of host response to microbial pathogens (McDonnell et al., 2016). TGEV infection has been shown to induce the production of IFNs and pro-inflammatory cytokines *in vitro* and *in vivo* (Cruz et al., 2013). A direct correlation between dsRNA antiviral response induction and TGEV virulence has been demonstrated (Cruz et al., 2011). Moreover, the inflammatory factors produced will also contribute to the production of a strong immune response. TNF-α and IL-1β can activate NF-κB to up-regulate the expression of human FcRn, which enhances FcRn-mediated IgG transport (Liu et al., 2007). TGEV infection was also found to induce EMT via TGF-β in IPEC-J2 cells (Xia et al., 2017). The aim of this study was to identify the TGEV-encoded proteins involved in inducing FcRn production.

MATERIALS AND METHODS

Cells, Virus, and Antibodies

IPEC-J2 cells donated by Xiaoping Li from Huazhong Agricultural University (Hubei Province, Wuhan, China) were cultured in Dulbecco's modified Eagle's medium (DMEM; Hyclone, United States) containing 10% fetal bovine serum (FBS; Gibco, United States) and 1% penicillin/streptomycin at 37°C in a 5% CO_2 atmosphere. The isolated TGEV strain WH-1 (GenBank HQ462571) was propagated in IPEC-J2 cells. In our laboratory, AffiniPure rabbit anti-cytoplasmic tails of porcine FcRn (anti-FcRn-CT) polyclonal antibodies were prepared (Guo et al., 2016a). Horseradish peroxidase (HRP)-conjugated goat anti-rabbit and goat anti-mouse IgG were purchased from Abclona (China). Monoclonal antibody (mAb) against GAPDH in mice was purchased from Abclona (China). Mouse mAbs against HA, IκBα, NF-κB, p65 and rabbit mAbs against phospho-NF-κB and p65 were obtained from Cell Signaling Technology (United States).

Plasmid Construction and siRNA

Luciferase reporter plasmids FcRn-Luc, NF-κB-Luc, pR-TK, p65-EGFP, and p65-Tag2B were prepared in our laboratory and have been described previously. Genes encoding TGEV proteins were amplified from the genomic RNA of the TGEV strain WH-1 and then cloned into the expression vector pCAGGS-HA (Guo et al., 2016b) (**Table 1**). pCAGGS-N was used as a template to amplify several deletion mutants of the virus N gene. These mutants were then cloned into the pCAGGS-HA (**Table 2**). Small interfering RNA (siRNA) molecules targeting TLR2, TLR3, TLR4, TLR8, TLR9, RIG-I, MyD88, TRIF, and negative controls were obtained from Shanghai GenePharma (**Table 3**). MAPK inhibitors SB203580, SP600125, U0126 and DMSO were purchased from Sigma-Aldrich (United States).

RNA Extraction and Real-Time RT-qPCR

Total RNA was prepared using TRIzol® reagent (Invitrogen). RT-qPCR was performed using SYBR Green PCR Master Mix (Takara, Osaka, Japan) in the Bio-Rad Sequence Detection System (Bio-Rad). Each transcript from each sample was determined three times. The delta threshold cycle ($2^{-\Delta\Delta CT}$) method was used to calculate the fold-change compared to the normal gene expression. The specific pig gene primers (**Table 4**) were designed using Primer Express software (version 3.0; Applied Biological Systems, Carlsbad, CA, United States) as previously described with some modifications (Temeeyasen et al., 2018).

TABLE 1 | Sequences of primers for cloning the TGEV genomic fragments.

Primer	Sequence (5′–3′)	Restriction enzyme site
nsp1-F	GCGGTACCATGAGTTCCAAACAATTCAAG	*Kpn*I
nsp1-R	ATTAGATCTACCTCTGCCAGTGCGAGCAAT	*Bgl*II
nsp2-F	GGCGGTACCGCCATATATGTTGATCAATA	*Eco*RI
nsp2-R	GCCCTCGAGACCACCCATTTTATTATAC	*Xho*I
nsp3-F	GGCGGTACCGGTGACAAAACTGTCTCAT	*Kpn*I
nsp3-R	GCCCTCGAGACCACTTTTTGGAGACACA	*Xho*I
nsp4-F	CTCGGTACCTCAGGCTTTTTCGATGTAAT	*Kpn*I
nsp4-R	CGACTCGAGCTGAAGTGTAGAATTAACAC	*Xho*I
nsp5-F	GCGAATTCTCAGGTTTGCGGAAAATGGC	*Xho*I
nsp5-R	CGGGGTACCCTGAAGATTTACACCATAC	*Bgl*II
nsp6-F	GGCGGTACCGCTGGTAAAGTAAAATCTTT	*Kpn*I
nsp6-R	GGCCTCGAGCTGTACAGTTGAAATTTTG	*Xho*I
nsp7-F	GCCGGTACCTCAAAACTTACAGAGATGAA	*Kpn*I
nsp7-R	TAGAGATCTCTGGAGTATGGTGGTGTTCT	*Bgl*II
nsp8-F	TCGAATTCAGTGTGGCTTCAGCTTATGC	*Eco*RI
nsp8-R	TAACTCGAGCTGAAGCTTTGTGGTTCTCT	*Xho*I
nsp9-F	CCGGTACCAACAATGAAATTATGCCAGG	*Kpn*I
nsp9-R	TACTCGAGTTGCAGACGAACTGTTGCA	*Xho*I
nsp10-F	CGGAATTCGCTGGTAAACCCACTGAA	*Eco*RI
nsp10-R	TGCTCGAGATAGAAGTACGATCGCACATG	*Xho*I
nsp11-F	CGGGGTACCATGAGTTTTACTGTTGATCAA	*Kpn*I
nsp11-R	AAGCTCGAGTGTTGCAGCAATTGACTT	*Xho*I
nsp12-F	ATTGGTACCTAGAACCCTGCAATGGTACT	*Kpn*I
nsp12-R	CAACTCGAGTTGCAAGACAGTGGACTTTT	*Xho*I
nsp13-F	TAAGAATTCGCTGCAGGCATGTGTGTAGT	*Eco*RI
nsp13-R	CGGCTCGAGTTGTAAACCAATCTTTGAA	*Xho*I
nsp14-F	GCGAATTCGCAAAACCTGAAACTTGTGG	*Eco*RI
nsp14-R	TGGCTCGAGCTGAAGTGCTTTGCTATTAA	*Xho*I
nsp15-F	GCCGGTACCAGTCTAGAAAATGTGGCTTT	*Kpn*I
nsp15-R	AGCTCGAGTTGGAGTTGTGGATAGAAGG	*Xho*I
nsp16-F	TAAGAATTCTCTGCTGAATGGAATCCCGG	*Eco*RI
nsp16-R	ATACTCGAGTGGTGTGTTAACGAAGTGGT	*Xho*I
S1-F	CCG*GAATTCGCCATG*AAAAAACTATTTGTGG	*Eco*RI
S1-R	CCAACTAT*GGTACC*ATCAATAACAGCTGC	*Kpn*I
S2-F	GCAGCTGTTATTGAT*GGTACC*ATAGTTGG	*Kpn*I
S2-R	GCG*GTCGAC*AATTTAATGGACGTGCACT	*Sal*I
M-F	GCGGGTACCATGAAGATTTTGTTAATA	*Kpn*I
M-R	GCGCTCGAGTAGTTATACCATATGTAA	*Xho*I
N-F	CATGAATTCATGGCCAACCAGGGACAAC	*Eco*RI
N-R	CACCTCGAGTTAGTTCGTTACCTCATC	*Xho*I
E-F	CTCGAATTCATGACGTTTCCTAGGGCATTG	*Eco*RI
E-R	ACTAGATCTTCAAGCAAGGAGTGCTCCATC	*Bgl*II
3b -F	GCCCTCGAGATGATTGGTGGACTTTTTCTT	*Eco*RI
3b -R	CGGGAATTCCTAGGAAACGTCATAGGTATG	*Xho*I

TABLE 2 | Sequences of primers used for cloning the TGEV N-protein deletion mutants.

Primer	Sequence (5′–3′)	Restriction enzyme site
ΔN1-F	CATGAATTCATGGCCAACCAGGGACAAC	*Eco*RI
ΔN1-R	CACCTCGAGAAGCGTGGTTGGTTTGTTCAT	*Xho*I
ΔN2-F	CATGAATTCATGGGTAGTCGTGGTGCTAAT	*Eco*RI
ΔN2-R	CACCTCGAGAGCTCCATAAAATCTTGTCAC	*Xho*I
ΔN3-F	CATGAATTCATGAGAAGCAGTTCAGCCA	*Eco*RI
ΔN3-R	CACCTCGAGTTAGTTCGTTACCTCATC	*Xho*I
ΔN4-F	CGCGAATTCATGAAAGCTTTGAAATTCGAT	*Eco*RI
ΔN4-R	CGCCTCGAGACGTTCTTTAGATTTAGAACG	*Xho*I

TABLE 3 | Sequences of siRNA used in the study.

Gene name	siRNA sequence (sense)	siRNA sequence (anti-sense)
siTLR2	GCC CUU CCU ACA CAC UUU ATT	UAA AGU GUG UAG GAA GGG CTT
siTLR3	GCUUAAGUGUGAUUGGU AATT-	UUACCAAUCACACUUAA GCTT
siTLR4	GCAUGGAGCUGAAUUUC UATT	UAGAAAUUCAGCUCCAU GCTT
siTLR8	GCUGGAAGACAACCAGU UATT	UAACUGGUUGUCUUCCA GCTT
siTLR9	GCCUCUCCUUACUCUCC AATT	UUGGAGAGUAAGGAGAG GCTT
siRIG-I	GGUACAAAGUUGCAGG CAUTT	AUGCCUGCAACUUUGUA CCTT
siMyD88	CAG CUG AGA AGC CUU UAC ATT	UGU AAA GGC UUC UCA GCU GTT
siTRIF	GGA GUU AUC GGA ACA GAA ATT	UUU CUG UUC CGA UAA CUC CTT
Negative control	UUC UCC GAA CGU GUC ACG UTT	ACG UGA CAC GUU CGG AGA ATT

Western Blot and Porcine Cytokine Array

The samples were harvested with lysis buffer (4% sodium dodecyl sulfate, 3% dithiothreitol, 65 mM Tris–HCl [pH 6.8], and 30% glycerol). Proteins were separated via SDS-PAGE and then electrotransferred onto a polyvinylidene difluoride membrane (Bio-Rad, United States). Western blot analysis was performed using the indicated antibodies following the procedure as described previously (Guo et al., 2016b).

IPEC-J2 cells grown in a six-well plate were infected with TGEV, the supernatant of IPEC-J2 cells was harvested, and IL-1β, IL-6, IL-8, TGF-β, and TNF-α protein levels were measured with a Quantibody Porcine Cytokine Array 1 (Ray Biotech, Norcross, GA, United States) according to the manufacturer's instructions.

Transfection and Dual-Luciferase Assay

IPEC-J2 cells at 80% confluence were co-transfected with 0.2 μg FcRn-Luc and 0.1 μg pRL-TK using Lipofectamine 2000 (Invitrogen) reagent before treatment with TGEV, specific siRNA molecules, or recombinant plasmids. Cell lysates were collected at the indicated time points over 36 h and measured using a dual-luciferase assay kit (Promega).

Eukaryotic Expression of TGEV N Protein and IgG Transcytosis

The recombinant TGEV N protein were prepared using a baculovirus/insect cell expression system as previously described (Chen et al., 2017). IPEC-J2 cells were added (0, 10, 20, 50, 100

TABLE 4 | Sequences of the primers used for RT-qPCR.

Gene name	sequence (sense)	sequence (anti-sense)
TLR2	TCATCTCCCAAATCTGCGAAT	GGCTGATGTTCTGAATTG ACCTC
TLR3	GCGGTCCTGTTCAGTTTCT	AAGGCATCTGCTGGGATTT
TLR4	CCTGCCTGTGCTGAGTTTCA	AAGGTGAGAACTGACGCAC TAATG
TLR8	CTTTGATGATGACGCTGC TTTC	GGTGTGTCACTCCTGCT ATTC
TLR9	CCTCACACATCTCTCACT CAAG	GGTGACAATGTGGTTGT AGGA
RIG-I	GAGCCCTTGTGGATGCTTTA	GGGTCATCCCTATGTTCTG ATTC
MyD88	GGCAGCTGGAACAGACCAA	GGTGCCAGGCAGGACATC
TRIF	ACTCGGCCTTCACCATCCT	GGCTGCTCATCAGAGACT GGTT
FcRn	GGCGACGAGCACCACT ACTG	AGCCGACCATGATTCCA ACC
TGF-β	ACGTGGAGCTATACCAGAAAT ACAG	ACAACTCCGGTGACATCA AAGG
IL-1β	GGCCGCCAAGATATAACTGA	GGACCTCTGGGTATGGC TTTC
IL-6	AACCTGAACCTTCCAAAA ATGG	ACCGGTGGTGATTCTCA TCA
IL-8	AGTTTTCCTGCTTTCTGCA GCT	TGGCATCGAAGTTCTGC ACT
TNF-α	TCCACCAACGTTTTCCTCACT	AGGGCTCTTGATGGCA GAGA
GAPDH	CCCCAACGTGTCGGTTGT	CCTGCTTCACCACCTTC TTGA

or 200 ng/mL) recombinant TGEV N protein in medium and its FcRn expression detected by RT-qPCR and Western blot.

IgG transport was performed as previously described methods (Guo et al., 2016a). Transepithelial electrical resistance (TEER) was measured with planar electrodes (World Precision Instruments). IPEC-J2 cells were grown on 0.4-μm pore size transwell filter inserts (Corning Costar, United States) to form a monolayer exhibiting TEER > 1000 Ω/cm^2 about 6–7 days. Monolayers were stimulated with recombinant TGEV N protein (100 ng/mL) for 12 h. Thereafter, Biotin-IgG (200 μg/mL) were applied to the basolateral or apical DMEM medium and incubated for 3 h at 37°C. Meanwhile, the opposite chamber was incubated in DMEM medium. Three hours later, samples were collected in which apically and basolaterally directed IgG transports were conducted. Subsequently, the bidirectional transport (apical-to-basolateral or basolateral-to-apical) of IgG were measured by Western blot and avidin blot analysis.

Statistical Analysis

All experiments were repeated a minimum of three times. Differences among groups were determined by one-way ANOVA using GraphPad Prism (version 5.0; GraphPad Software). The significance levels for all analyses were set as $p < 0.05$ (*) and $p < 0.01$ (**).

RESULTS

TGEV-Induced FcRn Activation Is Closely Related to Viral Replication

To examine if TGEV infection induces FcRn promoter activation, IPEC-J2 cells were co-transfected with FcRn-luc or pRL-TK. Twenty-four hours later, the cells were incubated with live or UV-inactivated TGEV for 12, 24, 36, and 48 h post-infection (hpi). Enhanced FcRn luciferase activities tended to increase during the progression of TGEV infection from 24 to 48 hpi, and this increase was significantly different compared with mock-infected IPEC-J2 cells (**Figure 1A**). Therefore, the up-regulation of FcRn is closely related to the replication of TGEV.

In order to determine whether TGEV induces FcRn expression in IPEC-J2 cells, live or UV-inactivated TGEV at a multiplicity of infection (MOI) of 1 was used to inoculate IPEC-J2 cells, which were then harvested for FcRn analysis at 12, 24, 36, and 48 hpi by RT-qPCR and Western blot (**Figures 1B,C**). TGEV induced FcRn mRNA expression about two fold higher at 24, 36, and 48 hpi, and the elevation in protein levels correlated with the increased mRNA. However, UV-inactivated viral treatment resulted in only a 1.3-fold up-regulation of FcRn expression compared with that in simulated infected cells, indicating that the replicating virus is more effective than the UV-inactivated virus.

Role of TLR and NF-κB in TGEV-Mediated Activation of FcRn

The small intestine of pigs expressed different TLRs, such as TLR1, TLR2, TLR3, TLR4, TLR6, TLR8, TLR9, and TLR10 (Arce et al., 2010). It has been reported that viral nucleic acids are recognized by TLR3, TLR8, and TLR9, whereas viral proteins are recognized by TLR2 and TLR4 (Thompson and Locarnini, 2007). To determine whether TLRs are involved in mediating TGEV-induced FcRn activation, specific siRNAs were synthesized to target binding molecules in the TLR2, TLR3, TLR4, TLR8, TLR9, TRIF, MyD88, and RIG-I pathways. Transient transfection and RT-qPCR assays proved the low knockout efficiency of each siRNA, and the silencing efficiencies of the siRNAs to these receptors were over 50% (**Figure 2A**). The cells were transfected with each siRNA and then infected with TGEV; then, the changes in FcRn expression were detected by RT-qPCR and Western blot. The results showed that, compared with the cells transfected with NC siRNA, siRNA knockdown of TLR3, TLR9, RIG-I, TRIF, and MyD88 effectively reduced the TGEV-induced up-regulation of FcRn, while FcRn mRNA expression was not inhibited in cells transfected with siRNA targeting TLR2, TLR4, or TLR8 (**Figure 2B**). Next, IPEC-J2 cells were transfected with TLR-specific siRNA or NC siRNA. After 12 h, the cells were infected with 1 MOI TGEV for an additional 36 h. Compared with NC siRNA, TLR3, TLR9, RIG-I, TRIF, and MyD88-specific siRNAs inhibited TGEV-induced FcRn expression, while no significant change was detected in s TLR2, TLR4 and TLR8-specific siRNAs (**Figures 2C,D**). These data suggest that TGEV infection activates FcRn via TLR3, TLR9, TRIF, MyD88, and RIG-I.

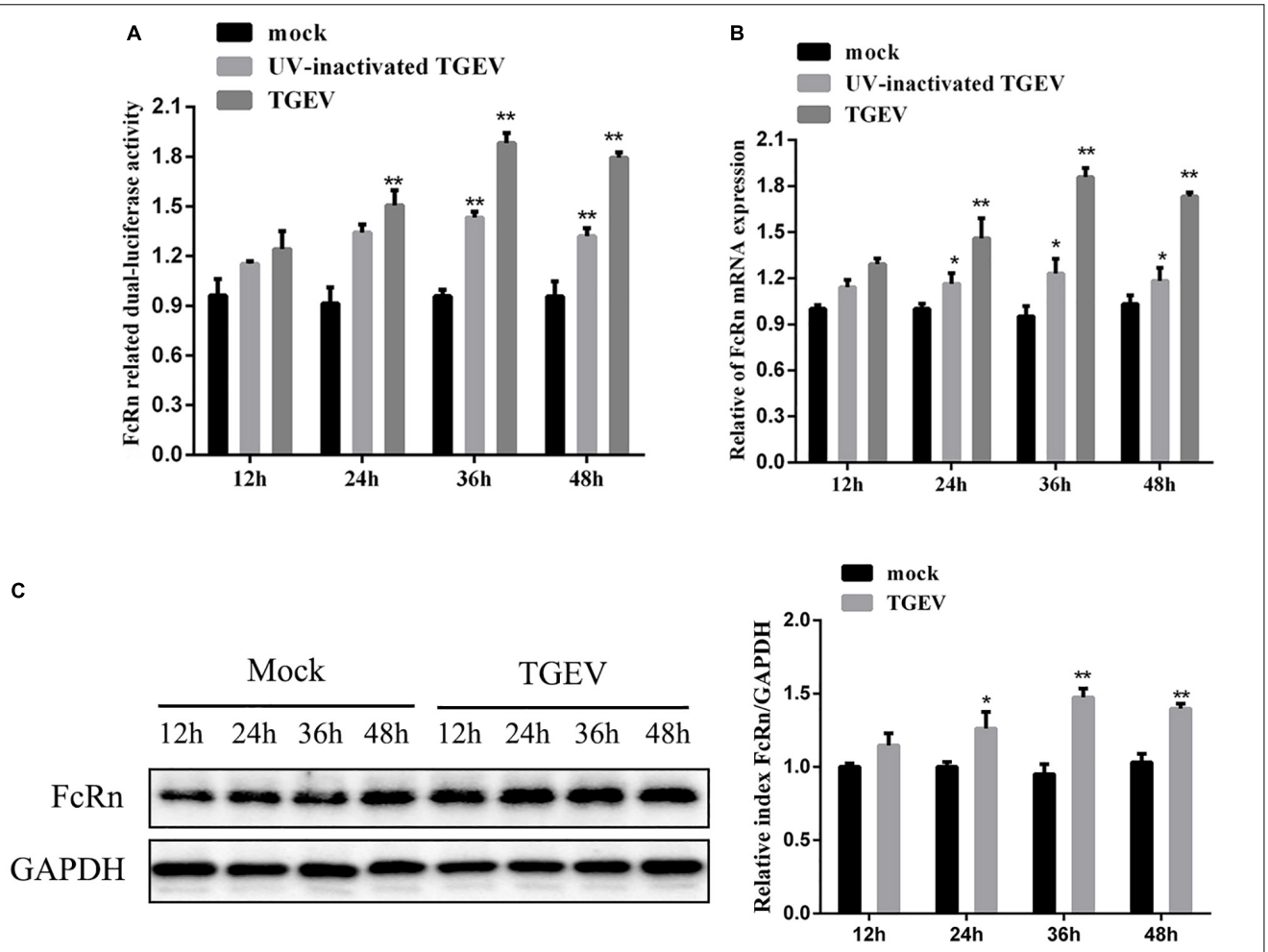

FIGURE 1 | TGEV-induced activation of FcRn depends on viral replication. **(A)** IPEC-J2 were co-transfected with pRL-TK and FcRn-Luc, followed by alive TGEV or UV-inactivated TGEV (MOI 1). Cells were harvested at 12, 24, 36 or 48 hpi, and the lysates were analyzed by dual-luciferase assay. **(B)** IPEC-J2 cells were infected with alive TGEV or UV-inactivated TGEV at a MOI of 1. Cells were harvested at 12, 24, 36 or 48 hpi, and the lysates were analyzed by RT-qPCR. **(C)** IPEC-J2 were infected with alive TGEV at a MOI of 1. Cells were harvested at 12, 24, 36 or 48 hpi, and the lysates were analyzed by Western blot. *$p < 0.05$, **$p < 0.01$.

TGF-β Stimulated by TGEV Promotes the Expression of FcRn

To detect the effect of TGEV infection on inflammatory cytokines, RT-qPCR and a porcine cytokine array were used to detect the expression levels of IL-1β, IL-6, IL-8, TGF-β, and TNF-α in IPEC-J2 cells infected with TGEV at 36 h. TGEV significantly increased the expression levels of five cytokines, especially TGF-β (**Figures 3A,B**).

We treated IPEC-J2 cells with TNF-α and IL-1β in different concentrations. TNF-α and IL-1β induced FcRn expression in a dose-dependent manner, increasing mRNA levels 1.5–1.7-fold after 2 h (**Figures 3C,D**). Interestingly, we found that TGF-β can also up-regulate FcRn, increasing the mRNA level 1.9-fold after 2 h (**Figure 3E**). Meanwhile, IPEC-J2 cells were treated with SB202190 (p38 inhibitor), SP600125 (JNK1/2 inhibitor) and U0126 (ERK1/2 inhibitor), followed by TGF-β incubation. Treatment with SP600125 sharply reduced FcRn expression, indicating that TGF-β up-regulated FcRn expressions via the c-Jun amino-terminal kinase (JNK)-MAPK pathway in IPEC-J2 cells (**Figure 3F**).

TGEV N Protein Enhances FcRn Expression via NF-κB Signaling Pathways

Because NF-κB is a necessary transcription factor for FcRn production, we examined the effects of all TGEV-encoded proteins on NF-κB promoter activity. TGEV encodes 16 non-structural proteins (nsp1–16), four structural proteins (S, E, M, and N), and three helper proteins (ORF7, ORF3a, and ORF3b), which were constructed recombinant plasmids by using the pCAGGS-HA vector. However, efficient expression occurred only for the plasmids encoding N, E, 3a, nsp1, nsp2, nsp5, nsp7, nsp8, nsp9, nsp10, nsp13, and nsp14 (**Figure 4C**). IPEC-J2 cells were co-transfected with NF-κB-Luc or FcRn, pRL-TK and different TGEV protein expression vectors. We found that TGEV N, nsp2 and nsp14 can all activate NF-κB (**Figure 4A**), and TGEV N, 3a,

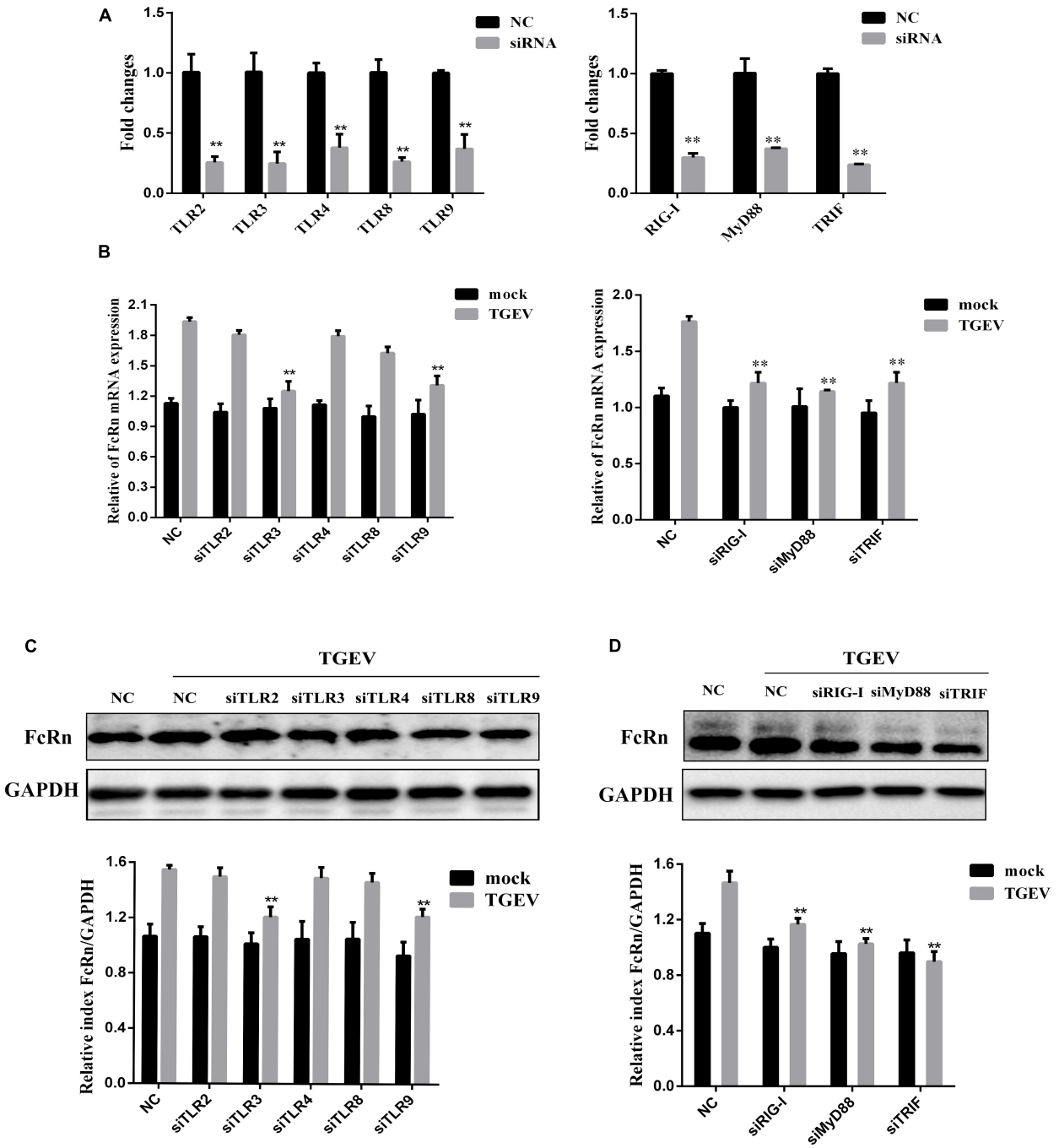

FIGURE 2 | Involvement of TLR signaling cascades in FcRn activation by TGEV. **(A)** IPEC-J2 cells were transfected with 50 nM specific siRNAs targeting TLR2/3/4/8/9, TRIF, MyD88, RIG-I or NC siRNA, respectively for 24 h, then cells were collected for analysis of mRNA levels using RT-qPCR assays. **(B)** IPEC-J2 cells were transfected with the siRNAs TLR2/3/4/8/9, TRIF, MyD88, RIG-I or NC siRNA, respectively for 24 h, then with/without TGEV infection (MOI = 1). At 24 hpi, total RNA was extracted and FcRn or GAPDH mRNA expression was analyzed by RT-qPCR. **(C,D)** IPEC-J2 cells were transfected with the siRNAs TLR2/3/4/8/9, TRIF, MyD88, RIG-I or NC siRNA, respectively for 24 h, then with/without TGEV infection (MOI 1). IPEC-J2 cells were harvested at 36 hpi and measured by Western blot. The right panel represents the quantification of the bands by densitometry, corrected by the amount of GAPDH. $^{**}p < 0.01$.

nsp1 and nsp5 can up-regulate FcRn by about 1.5–2-fold and N was the most significant inducer produced by FcRn (**Figure 4B**).

To confirm the involvement of N protein in NF-κB or FcRn promoter activation, IPEC-J2 cells were co-transfected with pRL-TK, NF-κB-Luc or FcRn-Luc and N expression vectors were added at different concentrations. Interestingly, N enhanced the activation of NF-κB and FcRn in a dose-dependent manner (**Figures 4D,E**), following Western blot analysis with antibodies

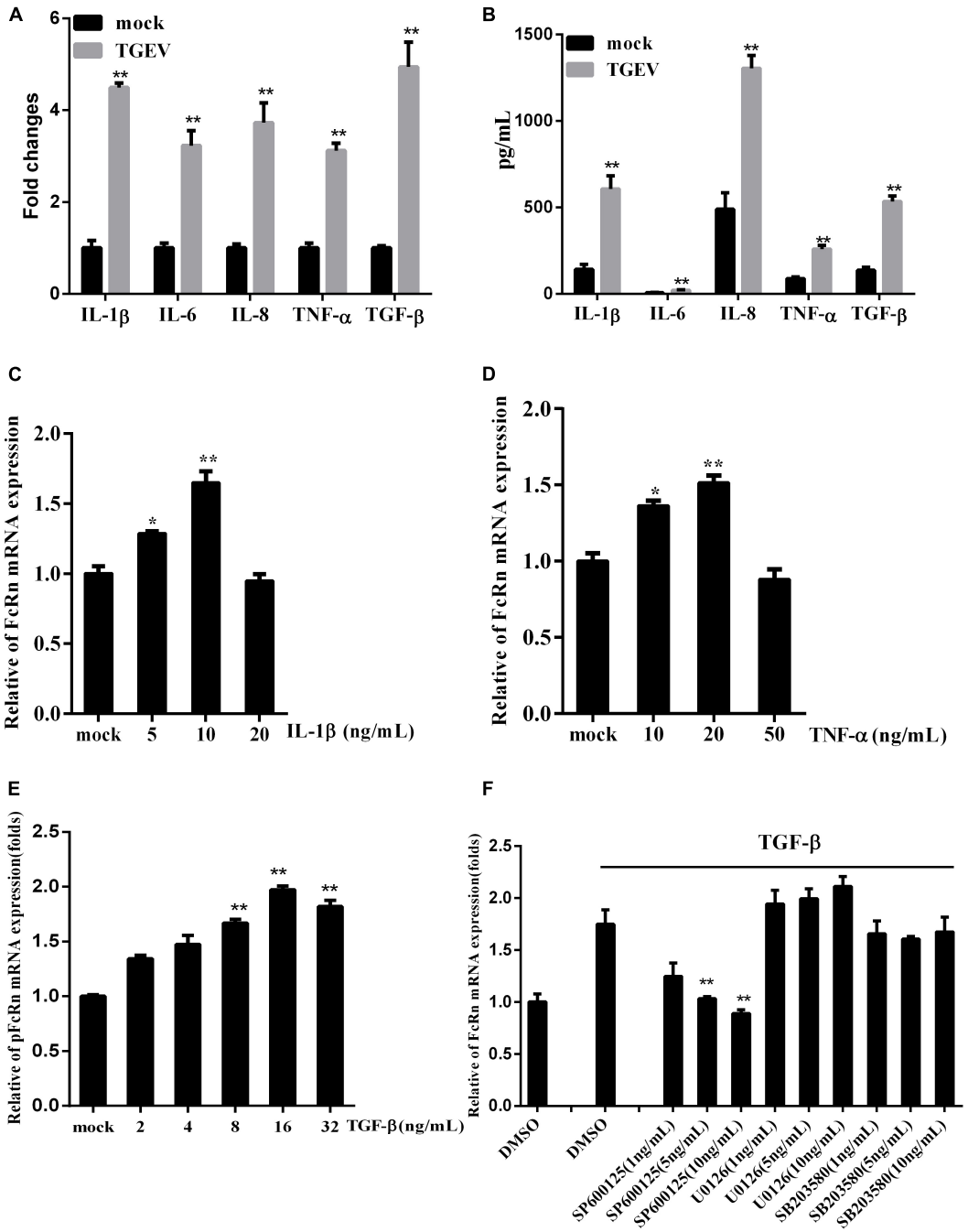

FIGURE 3 | Regulation of FcRn mRNA on IPEC-J2 cells stimulated by TGF-β. **(A,B)** The relative mRNA and protein levels of IL-1β, IL-6, IL-8, TNF-α, and TGF-β in IPEC-J2 infected with TGEV for 36 hpi by RT-PCR and porcine cytokine array. **(C–E)** IPEC-J2 cells were stimulated with TNF-α, IL-1β, TGF-β for 2 h, and the levels of FcRn mRNA were detected using RT-qPCR. **(F)** IPEC-J2 cells were pretreated with SB202190 (1, 5, and 10 ng/mL), SP600125 (1, 5, and 10 ng/mL), or U0126 (1, 5, and 10 ng/mL) or DMSO (control) for 2 h, followed by with/without TGF-β for 2 h and the levels of FcRn mRNA were detected using RT-qPCR. $^{*}p < 0.05$, $^{**}p < 0.01$.

against FcRn, IκBα, phospho-p65, total-p65. The results showed that the expression of N had no significant effects on the total amount of p65; however, the level of phosphorylated p65 (p-p65) and nuclear p65 increased markedly, and the level of IκBα decreased significantly (**Figure 4F**). As shown in **Figure 4G**, pre-treatment of cells with siRIG-I impaired FcRn expression by TGEV N protein in comparison with IPEC-J2 cells transfected with NC siRNA. This result showed that RIG-I may be responsible for TGEV N-protein-induced FcRn expression. In this study, we used confocal microscopy to identify that the

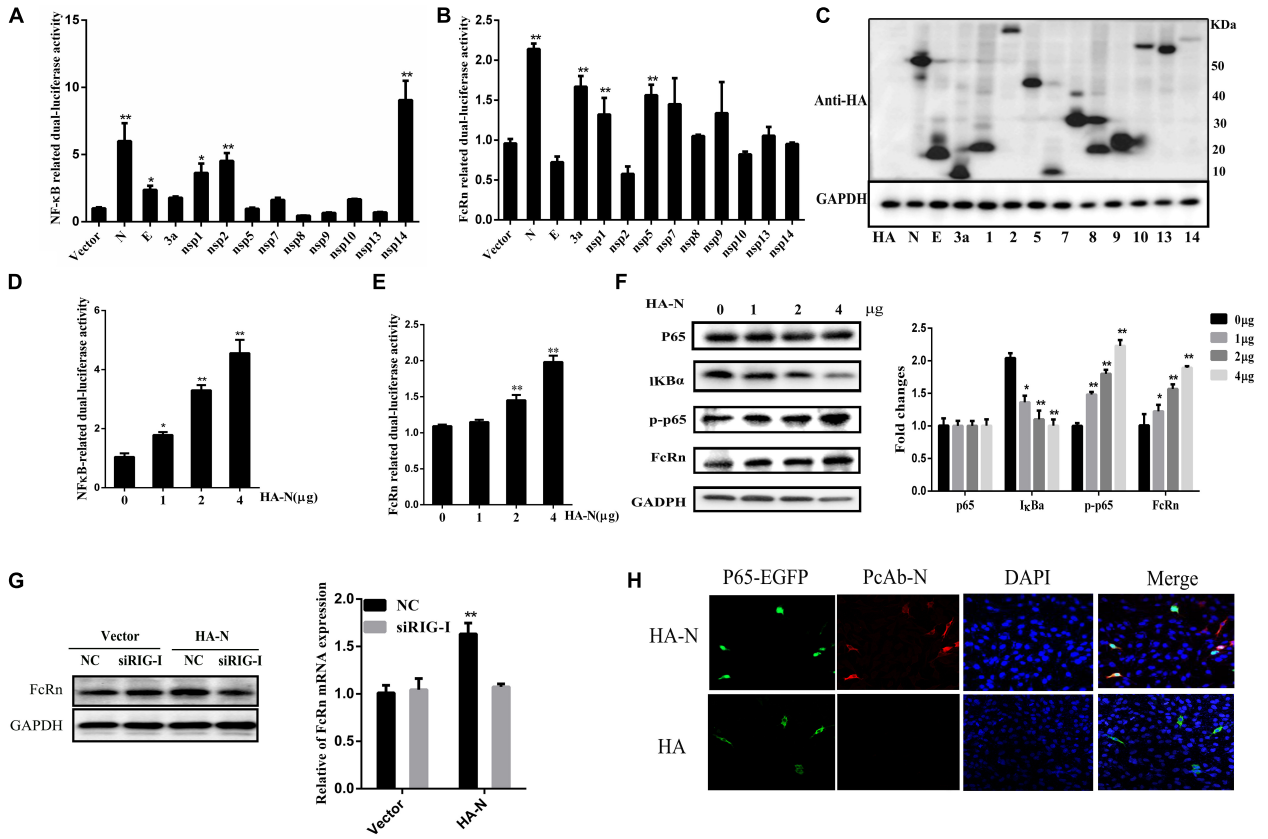

FIGURE 4 | Transmissible gastroenteritis virus N induces FcRn and NF-κB activation. **(A,B)** IPEC-J2 cells were co-transfected with pRL-TK and FcRn-Luc or NF-κB-Luc together with each expression plasmid of TGEV proteins. **(C)** Lysates of transfected cells were subjected to Western blot with anti-HA antibody to detect viral protein expression. **(D,E)** IPEC-J2 were co-transfected with pRL-TK, FcRn-Luc or NF-κB-Luc, and TGEV N expression plasmids (1, 2 or 4 μg) for 36 h. The cell lysates were analyzed by dual-luciferase assay. **(F)** FcRn, IκBα, p65 and phosphorylated p65 (p-p65), and GAPDH was assayed by Western blot analysis. **(G)** IPEC-J2 cells were transfected with siRIG or NC siRNA for 24 h and subsequently retransfected with TGEV N-expression plasmids (4 μg) for an additional 24 h. FcRn expression were detected by Western blot analysis. The right panel represents the quantification of the bands by densitometry, corrected by the amount of GAPDH. **(H)** IPEC-J2 cells were co-transfected with the p65-EGFP fusion protein vector and an empty vector (HA) or the TGEV N expression vector (HA-N) for 24 h. NF-κB p65 (green), TGEV N (red), and the nuclei (blue) were visualized by confocal microscopy. $^{*}p < 0.05$, $^{**}p < 0.01$.

TGEV N protein has an effect on the nuclear translocation of the NF-κB subunit p65. We observed the control vector-transfected IPEC-J2 cells and p65-EGFP was mainly present in the cytoplasm. Interestingly, the overexpression of TGEV N could lead to p65-EGFP expression in the nucleus in transfected IPEC-J2 cells (**Figure 4G**). Taken together, these results demonstrated that TGEV N protein can both significantly activate NF-κB and up-regulate the expression of FcRn.

Mutations in N Protein Can Reduce FcRn Expression

In order to further explore N functional domains, N protein truncations were expressed in this study. According to the Lasergene DNASTAR Protean 9.0 software prediction, the N-protein contains two nuclear export signal (NES) sequences at aa 221–236 (NES-1), aa 330–353 (NES-2), an RNA-binding region at aa 33–159, a specific SR-rich region at aa 156–198 and a ZnF region at aa 137–219 (**Figure 5A**). TGEV N protein is mainly located at aa 128–252 and this region has high hydrophilicity and flexibility. In order to study the TGEV N protein, the structure of which is essential for FcRn activation, four truncation mutants were cloned into the eukaryotic expression plasmid, pCAGGS-HA, named as N1(1–128), N2(128–382), N3(252–382), and N4(128–252). The relationship between these mutants and FcRn activation was analyzed through luciferase reporter assays and Western blot. As shown in **Figure 5**, N4, which contains NES1 and the immune dominant area, compared with the total length of the TGEV N protein, increased the FcRn activation and expression (**Figures 5B,C**). The result showed that the central region (128–252) of N protein is critical for FcRn activation.

Recombinant TGEV N Protein Mediated Induced FcRn-Mediated IgG in Polarized IPEC-J2 Cells

Transmissible gastroenteritis virus N protein was expressed by Bac-to-Bac baculovirus expression systems, the secreted 49 KDa was verified as we expected by Western blot (**Figure 6A**). IPEC-J2 cells were stimulated with different doses of recombinant TGEV

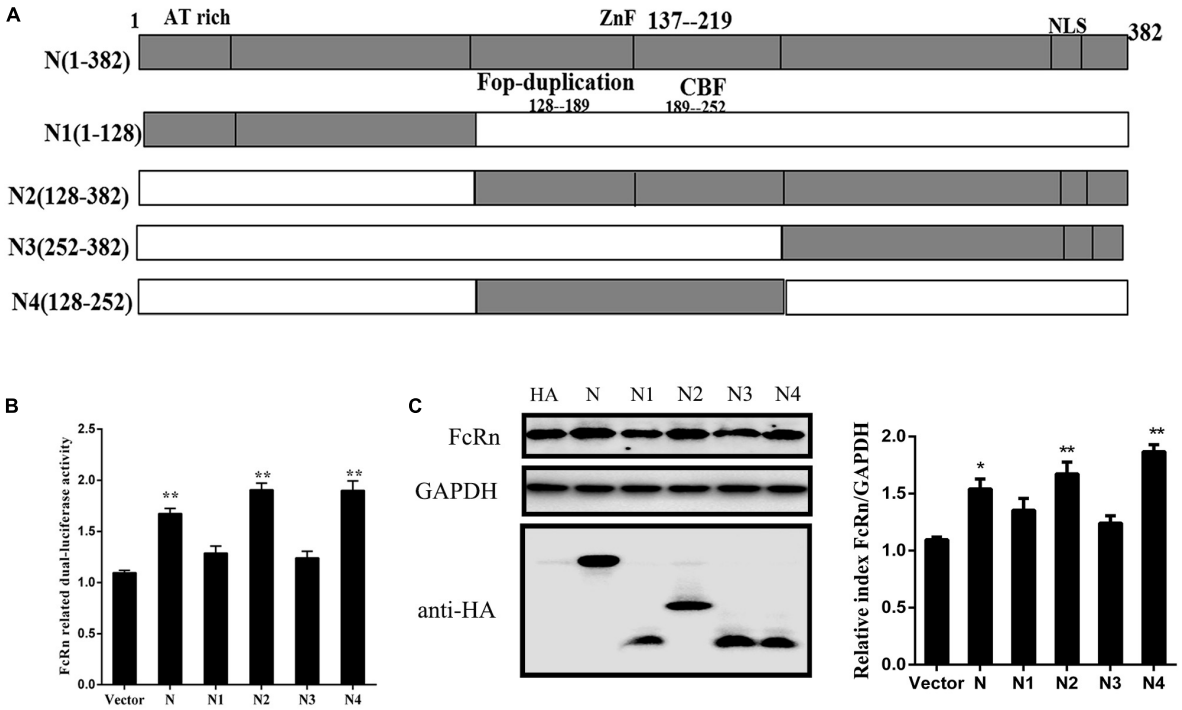

FIGURE 5 | Schematic representation of the TGEV N-protein serial-deletion mutant constructs. **(A)** Schematic representation of the TGEV N-protein serial-deletion mutant constructs. **(B)** IPEC-J2 cells were co-transfected with pRL-TK, FcRn-Luc, and TGEV N deletion-mutant expression plasmids. The cell lysates were harvested for dual luciferase assays at 24 hpi. **(C)** IPEC-J2 cells were co-transfected with TGEV N deletion-mutant expression plasmids for 36 h and protein expression in cell lysates was measured by Western blot using anti-HA antibody and anti-FcRn antibody. The right panel represents the quantification of the bands by densitometry, corrected by the amount of GAPDH. $^{*}p < 0.05$, $^{**}p < 0.01$.

N protein. We further verified the FcRn up-regulation up to two times by recombinant TGEV N stimulation, as assessed by RT-qPCR and Western blot (**Figures 6B,C**).

The FcRn protein has been well known to transport IgG bidirectionally in polarized epithelial cells. Therefore, we hypothesized TGEV N protein could alter the role of IgG transcytosis epithelial cells and constructed the transwell system to mimic the porcine intestinal microenvironment using IPEC-J2 cells (**Figure 6D**). The polarized monolayers (TEER > 1000 Ω/cm^2) were stimulated with recombinant TGEV N protein (100 ng/mL) for 12 h. Then, porcine biotin-IgG was added to the apical or basolateral surface of a IPEC-J2 cell monolayer, after 3 h at 37°C we assessed the IgG transported to the opposite basolateral or apical chamber, respectively. The IgG H chain was detected in medium by Western blot (**Figure 6D**, lane 1). Importantly, IgG transport was enhanced 1.3-fold in the apical to basolateral (**Figure 6D**, lane 3) direction or 1.8-fold in the basolateral to apical (**Figure 6D**, lane 5) direction by TGEV N in comparison to the mock-treated monolayer (**Figure 6D**, lanes 2 and 4).

DISCUSSION

The secretory IgA and IgG play major roles in mucosal anti-infection immunity and are obtained primarily through the polymeric immunoglobulin receptor (plgR) and FcRn-mediated transport. Reovirus, dsRNA (a ligand for TLR3), LPS (a ligand for TLR4), IFN-γ, IL-4, IL-1β, TNF-α, and TGF-β all regulate pIgR expression (Johansen and Brandtzaeg, 2004; Pal et al., 2005; Schneeman et al., 2005). Therefore, LPS, IL-1β, and TNF-α could up-regulate the expression of FcRn via the NF-κB pathway. NF-κB appears to be a positive regulator of FcRn expression. In our previous study, we identified that TGEV infection up-regulated FcRn via the activation of the NF-κB pathway (Guo et al., 2016b). Consistent with this, the replication of the virus is directly related to FcRn expression.

Transmissible gastroenteritis virus infection up-regulates the expression levels of IL-1β, IL-6, IL-8, TNF-α, and TGF-β, which are important factors in chronic inflammation. The expression of FcRn was up-regulated by the inflammatory cytokine TNF-α and IL-1β in a dose-dependent manner, as determined by RT-qPCR (**Figures 3A,B**), and this was consistent with that observed in a previous study (Liu et al., 2007). MAPK is a highly conserved serine protein kinase in the cytoplasm that mediates a signaling pathway that plays an important role in the body's inflammatory response. The MAPK family is mainly divided into three classes: extracellular signal-regulated kinases (ERKs), JNKs, and p38 MAPK kinases. Multiple stimulating factors activate the MAPK pathway, including inflammatory factors, growth factors, and cellular responses (Huang et al., 2004). TGF-β dose-dependently induces pIgR production via the p38/MAPK pathway in human

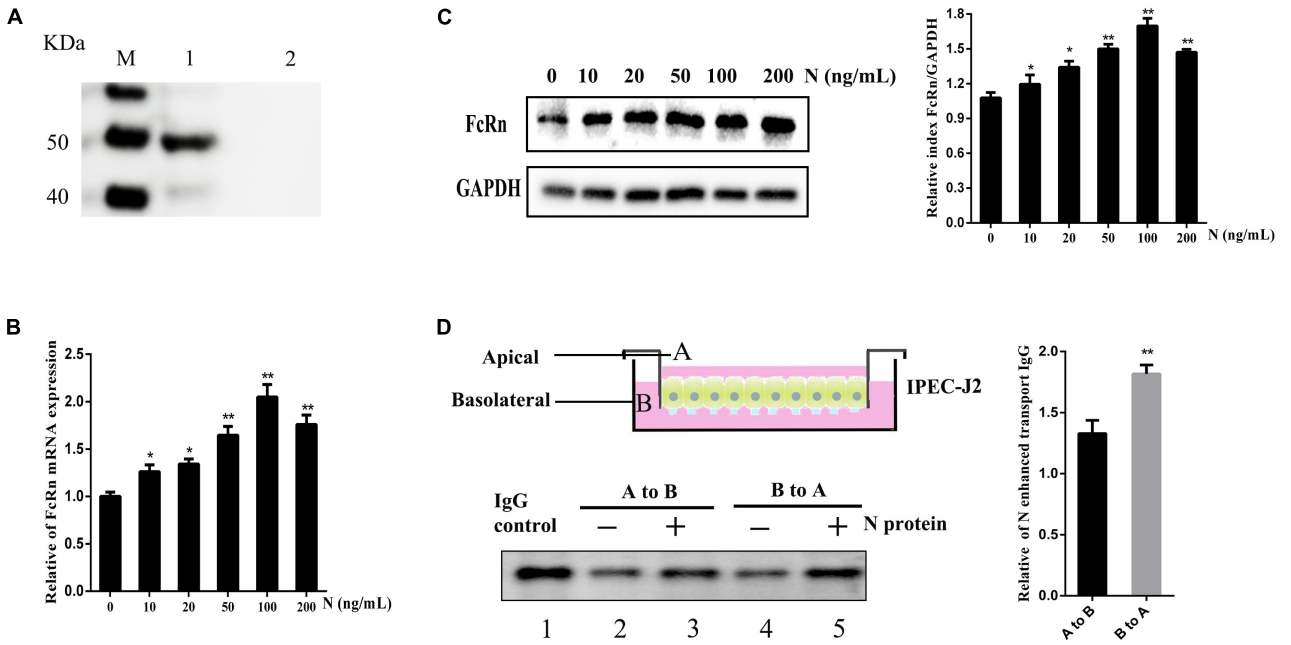

FIGURE 6 | Effects of recombinant TGEV N stimulation on the IgG transcytosis in IPEC-J2 cells. **(A)** Analysis of recombinant TGEV N protein by Western blot. M: Protein marker. 1: TGEV recombinant N. 2: Negative Control. IPEC-J2 cells were treated with recombinant TGEV N protein (0, 10, 20, 50, 100 or 200 ng/mL) for 12 h. **(B,C)** FcRn expression levers were detected by RT-qPCR and Western blot. The right panel represents the quantification of the bands by densitometry, corrected by the amount of GAPDH. **(D)** Transwell system used throughout this study. A, apical; B, basolateral. IPEC-J2 cells were grown in a 12-well transwell plate about 6–7 day until TEER > 1000 Ω/cm^2. IPEC-J2 cells were stimulated with or without recombinant TGEV N (100 ng/ml) for 12 h. Cells were loaded with porcine biotin-IgG at 37°C in either the apical (lanes 2 and 3) or basolateral (lanes 4 and 5) chamber. Lane 1 represents an IgG. *$p < 0.05$, **$p < 0.01$.

bronchial epithelial cells (Ratajczak et al., 2010). Moreover, TGF-β was said to inhibit pIgR production in bronchial epithelium (Gohy et al., 2014). In this study, we observed that TGF-β up-regulates FcRn via the JNK MAPK pathway, perhaps because TGEV activates the JNK MAPK pathway in porcine cells.

The ability of TGEV proteins to stimulate the FcRn promoter was identified by constructing a series of recombinant expression plasmids. However, efficient expression was obtained only from plasmids encoding the N, E, 3a, nsp1, nsp2, nsp5, nsp7, nsp8, nsp9, nsp10, nsp13, and nsp14. The expression of viral protein was not high or related to cell type and state. Among these proteins, N was the most potent NF-κB activator, and it induced FcRn expression. The proteins 3a, nsp1, and nsp5 also enhance but have little influence on NF-κB promoter activity. While nsp2 and nsp14 are also potential NF-κB activators, consistent with that reported in previous studies (Zhou et al., 2017; Wang et al., 2018). Since the essential and multifunctional N protein is fundamental for immune regulation and pathogenesis, we examined it more closely. Porcine epidemic diarrhea virus (PEDV) N protein mediates NF-κB activation through TLR pathways and has functions in cell growth, cell cycle and ER stress (Xu et al., 2013). In fact, the interaction of TGEV N protein with several host cell proteins has been shown (Zhang et al., 2014, 2015). In addition, overexpression of TGEV N protein induces cell cycle arrest (Ding et al., 2014a). Using domain-specific mutations, we determined that the domain at aa 128–252 of the N protein (immunodominant central region) is critical for FcRn activation; it contains a ZnF structure and a SR-rich region. Both the SR-rich truncated proteins of the N protein of SARS coronavirus and PEDV can effectively promote the activation of the NF-κB signaling pathway (Zhang et al., 2007; Cao et al., 2015a).

Epithelial TLR expression plays an important role in the innate and adaptive immune responses. NF-κB is a branch of the downstream signaling pathways of TLR and RLR, which also play important roles in various immune responses. Diverse coronaviruses can escape host immune responses via NF-κB activation through different pathways. PEDV activates NF-κB signaling through TLRs, while mouse hepatitis virus (MHV) does so through RLRs (Li et al., 2010; Cao et al., 2015a). IPEC-J2 cells express mRNA encoding TLR1, TLR2, TLR3, TLR4, TLR6, TLR8, TLR9, TLR10, IL-1α, IL-6, IL-7, IL-8, IL-18, TNF-α, and GM-CSF (Bowie and Haga, 2005; Burkey et al., 2009; Mariani et al., 2009). Rotavirus infection triggers the production of IL-8, IL-6, and TNF-α in IECs by activating the TLR3 and RIG-I pathways (Broquet et al., 2011). Compared with the NC siRNA, TLR3-, TLR9-, RIG-, MyD88-, and TRIF-specific siRNAs inhibited TGEV-induced FcRn activation, while TLR2-, TLR4-, and TLR8-specific siRNAs did not. We speculate that TGEV activates NF-κB via the TLR3, TLR9, and RIG-I pathways. Our results suggest that TLR3, TLR9, and RIG-I may be used to activate the FcRn signaling pathway when TGEV infects IPEC-J2 cells. Recently, our research has shown that PEDV down-regulate the NF-κB signaling pathway to inhibit FcRn by TLR3 and

RIG-I pathway in the early stage of infected piglets (Qian et al., 2019). PEDV and PDCoV N protein inhibited IFN-β by RIG-I pathway (Ding et al., 2014b; Likai et al., 2019), and we found that TGEV N protein up-regulated FcRn by RIG-I pathway. Moreover, TGEV infection induced IFN-β production and PEDV inhibited IFN-β production (An et al., 2014; Cao et al., 2015b). These results may be important causes of PEDV being more pathogenic than TGEV.

Transgenic mice that overexpress hFcRn can improve the antigen presentation ability of dendritic cells and enhance the humoral immune response of the body (Végh et al., 2012). FcRn not only transports IgG, but also transports antigen-antibody complexes, which are taken up by antigen-presenting cells (APCs) (Rath et al., 2013). When the pathogen stimulates the mucosal epithelium, the expression of FcRn may be regulated. Simian/human immunodeficiency virus (SHIV) infection decreases FcRn and pIgR expression, which may also be the mechanism responsible for its pathogenesis in rhesus monkeys (Wang and Yang, 2016). On the other hand, TGEV up-regulates FcRn expression, which is potentially what provides the mucosal protection. To observe and measure IgG transcytosis *in vitro*, we applied the transwell system to mimic the porcine intestinal microenvironment, using IPEC-J2 cells to construct the transwell model, our previous research showed that FcRn not only transports specific antibodies across the mucosal epithelium *in vitro*, but also reduces the yield of TGEV (Guo et al., 2016a). We speculated that the up-regulation of FcRn by N protein may mediates more TGEV-specific antibody transcytosis across the mucosal epithelium, thereby enhancing the host's anti-infective ability. On the other hand, N protein-enhanced FcRn mediates more IgG immune complex transcytosis, followed by antigen uptake by specialized APCs to activate adaptive immune responses. Overall, we elucidated the immune mechanism of TGEV induced FcRn expression and provided a scientific and theoretical basis for the prevention and control of TGEV infection.

DATA AVAILABILITY STATEMENT

All datasets generated for this study are included in the article/supplementary material.

AUTHOR CONTRIBUTIONS

SQ wrote the manuscript. SQ and ZL conceived and initiated the study. SQ, ZG, RC, and KY extracted the dataset. SQ, YC, SL, XM, QH, and ZL performed the analysis. All authors reviewed the manuscript.

FUNDING

This work was supported by the National Natural Science Foundation of China (31572500 to ZL).

REFERENCES

An, K., Fang, L., Luo, R., Wang, D., Xie, L., Yang, J., et al. (2014). Quantitative proteomic analysis reveals that transmissible gastroenteritis virus activates the JAK-STAT1 signaling pathway. *J. Proteome Res.* 13, 5376–5390. doi: 10.1021/pr500173p

Arce, C., Ramirez-Boo, M., Lucena, C., and Garrido, J. J. (2010). Innate immune activation of swine intestinal epithelial cell lines (IPEC-J2 and IPI-2I) in response to LPS from *Salmonella typhimurium*. *Comp. Immunol. Microbiol. Infect. Dis.* 33, 161–174. doi: 10.1016/j.cimid.2008.08.003

Bowie, A. G., and Haga, I. R. (2005). The role of Toll-like receptors in the host response to viruses. *Mol. Immunol.* 42, 859–867. doi: 10.1016/j.molimm.2004.11.007

Broquet, A. H., Hirata, Y., McAllister, C. S., and Kagnoff, M. F. (2011). RIG-I/MDA5/MAVS are required to signal a protective IFN response in rotavirus-infected intestinal epithelium. *J. Immunol.* 186, 1618–1626. doi: 10.4049/jimmunol.1002862

Burkey, T. E., Skjolaas, K. A., Dritz, S. S., and Minton, J. E. (2009). Expression of porcine Toll-like receptor 2, 4 and 9 gene transcripts in the presence of lipopolysaccharide and *Salmonella enterica* serovars *Typhimurium* and *Choleraesuis*. *Vet. Immunol. Immunopathol.* 130, 96–101. doi: 10.1016/j.vetimm.2008.12.027

Cao, L., Ge, X., Gao, Y., Ren, Y., Ren, X., and Li, G. (2015a). Porcine epidemic diarrhea virus infection induces NF-kappaB activation through the TLR2, TLR3 and TLR9 pathways in porcine intestinal epithelial cells. *J. Gen. Virol.* 96, 1757–1767. doi: 10.1099/vir.0.000133

Cao, L., Ge, X., Gao, Y., Herrler, G., Ren, Y., Ren, X., et al. (2015b). Porcine epidemic diarrhea virus inhibits dsRNA-induced interferon-beta production in porcine intestinal epithelial cells by blockade of the RIG-I-mediated pathway. *Virol. J.* 12:127. doi: 10.1186/s12985-015-0345-x

Chen, X., Zhang, Q., Bai, J., Zhao, Y., Wang, X., Wang, H., et al. (2017). The nucleocapsid protein and nonstructural protein 10 of highly pathogenic porcine reproductive and respiratory syndrome virus enhance CD83 production via NF-kappaB and Sp1 signaling pathways. *J. Virol.* 91:JVI.00986-17. doi: 10.1128/JVI.00986-17

Cruz, J. L., Becares, M., Sola, I., Oliveros, J. C., Enjuanes, L., and Zuniga, S. (2013). Alphacoronavirus protein 7 modulates host innate immune response. *J. Virol.* 87, 9754–9767. doi: 10.1128/JVI.01032-13

Cruz, J. L., Sola, I., Becares, M., Alberca, B., Plana, J., Enjuanes, L., et al. (2011). Coronavirus gene 7 counteracts host defenses and modulates virus virulence. *PLoS Pathog.* 7:e1002090. doi: 10.1371/journal.ppat.1002090

Ding, L., Huang, Y., Du, Q., Dong, F., Zhao, X., Zhang, W., et al. (2014a). TGEV nucleocapsid protein induces cell cycle arrest and apoptosis through activation of p53 signaling. *Biochem. Biophys. Res. Commun.* 445, 497–503. doi: 10.1016/j.bbrc.2014.02.039

Ding, Z., Fang, L., Jing, H., Zeng, S., Wang, D., Liu, L., et al. (2014b). Porcine epidemic diarrhea virus nucleocapsid protein antagonizes beta interferon production by sequestering the interaction between IRF3 and TBK1. *J. Virol.* 88, 8936–8945. doi: 10.1128/JVI.00700-14

Escors, D., Izeta, A., Capiscol, C., and Enjuanes, L. (2003). Transmissible gastroenteritis coronavirus packaging signal is located at the 5′ end of the virus genome. *J. Virol.* 77, 7890–7902. doi: 10.1128/jvi.77.14.7890-7902.2003

Gohy, S. T., Detry, B. R., Lecocq, M., Bouzin, C., Weynand, B. A., Amatngalim, G. D., et al. (2014). Polymeric immunoglobulin receptor down-regulation in chronic obstructive pulmonary disease. Persistence in the cultured epithelium and role of transforming growth factor-beta. *Am. J. Respir. Crit. Care Med.* 190, 509–521. doi: 10.1164/rccm.201311-1971OC

Guo, J., Li, F., He, Q., Jin, H., Liu, M., Li, S., et al. (2016a). Neonatal Fc receptor-mediated IgG transport across porcine intestinal epithelial cells: potentially provide the mucosal protection. *DNA Cell Biol.* 35, 301–309. doi: 10.1089/dna.2015.3165

Guo, J., Li, F., Qian, S., Bi, D., He, Q., Jin, H., et al. (2016b). TGEV infection up-regulates FcRn expression via activation of NF-kappaB signaling. *Sci. Rep.* 6:32154. doi: 10.1038/srep32154

Gupta, S., Gach, J. S., Becerra, J. C., Phan, T. B., Pudney, J., Moldoveanu, Z., et al. (2013). The Neonatal Fc receptor (FcRn) enhances human immunodeficiency virus type 1 (HIV-1) transcytosis across epithelial cells. *PLoS Pathog.* 9:e1003776. doi: 10.1371/journal.ppat.1003776

Huang, C., Jacobson, K., and Schaller, M. D. (2004). MAP kinases and cell migration. *J. Cell Sci.* 117, 4619–4628. doi: 10.1242/jcs.01481

Johansen, F. E., and Brandtzaeg, P. (2004). Transcriptional regulation of the mucosal IgA system. *Trends Immunol.* 25, 150–157. doi: 10.1016/j.it.2004.01.001

Li, J., Liu, Y., and Zhang, X. (2010). Murine coronavirus induces type I interferon in oligodendrocytes through recognition by RIG-I and MDA5. *J. Virol.* 84, 6472–6482. doi: 10.1128/JVI.00016-10

Li, Z., Palaniyandi, S., Zeng, R., Tuo, W., Roopenian, D. C., and Zhu, X. (2011). Transfer of IgG in the female genital tract by MHC class I-related neonatal Fc receptor (FcRn) confers protective immunity to vaginal infection. *Proc. Natl. Acad. Sci. U.S.A.* 108, 4388–4393. doi: 10.1073/pnas.1012861108

Likai, J., Shasha, L., Wenxian, Z., Jingjiao, M., Jianhe, S., Hengan, W., et al. (2019). Porcine deltacoronavirus nucleocapsid protein suppressed IFN-beta production by interfering porcine RIG-I dsRNA-binding and K63-linked polyubiquitination. *Front. Immunol.* 10:1024. doi: 10.3389/fimmu.2019.01024

Liu, X., Ye, L., Christianson, G. J., Yang, J. Q., Roopenian, D. C., and Zhu, X. (2007). NF-kappaB signaling regulates functional expression of the MHC class I-related neonatal Fc receptor for IgG via intronic binding sequences. *J. Immunol.* 179, 2999–3011. doi: 10.4049/jimmunol.179.5.2999

Lu, L., Palaniyandi, S., Zeng, R., Bai, Y., Liu, X., Wang, Y., et al. (2011). A neonatal Fc receptor-targeted mucosal vaccine strategy effectively induces HIV-1 antigen-specific immunity to genital infection. *J. Virol.* 85, 10542–10553. doi: 10.1128/JVI.05441-11

Mariani, V., Palermo, S., Fiorentini, S., Lanubile, A., and Giuffra, E. (2009). Gene expression study of two widely used pig intestinal epithelial cell lines: IPEC-J2 and IPI-2I. *Vet. Immunol. Immunopathol.* 131, 278–284. doi: 10.1016/j.vetimm.2009.04.006

McDonnell, K., Nienaber, V., Andersen, J. T., Mizoguchi, A., Blumberg, L., Purohit, S., et al. (2016). Viral evasion strategies in type I IFN signaling - a summary of recent developments. *Proc. Natl. Acad. Sci. U.S.A.* 7:498.

Pal, K., Kaetzel, C. S., Brundage, K., Cunningham, C. A., and Cuff, C. F. (2005). Regulation of polymeric immunoglobulin receptor expression by reovirus. *J. Gen. Virol.* 86, 2347–2357. doi: 10.1099/vir.0.80690-0

Pyzik, M., Rath, T., Kuo, T. T., Win, S., Baker, K., Hubbard, J. J., et al. (2017). Hepatic FcRn regulates albumin homeostasis and susceptibility to liver injury. *Proc. Natl. Acad. Sci. U.S.A.* 114, E2862–E2871. doi: 10.1073/pnas.1618291114

Qian, S., Zhang, W., Jia, X., Sun, Z., Zhang, Y., Xiao, Y., et al. (2019). Isolation and identification of porcine epidemic diarrhea virus and its effect on host natural immune response. *Front. Microbiol.* 10:2272. doi: 10.3389/fmicb.2019.02272

Ratajczak, C., Guisset, A., Detry, B., Sibille, Y., and Pilette, C. (2010). Dual effect of neutrophils on pIgR/secretory component in human bronchial epithelial cells: role of TGF-beta. *J. Biomed. Biotechnol.* 2010:428618. doi: 10.1155/2010/428618

Rath, T., Kuo, T. T., Baker, K., Qiao, S. W., Kobayashi, K., Yoshida, M., et al. (2013). The immunologic functions of the neonatal Fc receptor for IgG. *J. Clin. Immunol.* 33(Suppl. 1), S9–S17. doi: 10.1007/s10875-012-9768-y

Schneeman, T. A., Bruno, M. E., Schjerven, H., Johansen, F. E., Chady, L., and Kaetzel, C. S. (2005). Regulation of the polymeric Ig receptor by signaling through TLRs 3 and 4: linking innate and adaptive immune responses. *J. Immunol.* 175, 376–384. doi: 10.4049/jimmunol.175.1.376

Temeeyasen, G., Sinha, A., Gimenez-Lirola, L. G., Zhang, J. Q., and Piñeyro, P. E. (2018). Differential gene modulation of pattern-recognition receptor TLR and RIG-I-like and downstream mediators on intestinal mucosa of pigs infected with PEDV non S-INDEL and PEDV S-INDEL strains. *Virology* 517, 188–198. doi: 10.1016/j.virol.2017.11.024

Thompson, A. J., and Locarnini, S. A. (2007). Toll-like receptors, RIG-I-like RNA helicases and the antiviral innate immune response. *Immunol. Cell Biol.* 85, 435–445. doi: 10.1038/sj.icb.7100100

Végh, A., Farkas, A., Kövesdi, D., Papp, K., Cervenak, J., Schneider, Z., et al. (2012). FcRn overexpression in transgenic mice results in augmented APC activity and robust immune response with increased diversity of induced antibodies. *PLoS One* 7:e36286. doi: 10.1371/journal.pone.0036286

Wang, L., Qiao, X., Zhang, S., Qin, Y., Guo, T., Hao, Z., et al. (2018). Porcine transmissible gastroenteritis virus nonstructural protein 2 contributes to inflammation via NF-kappaB activation. *Virulence* 9, 1685–1698. doi: 10.1080/21505594.2018.1536632

Wang, Y., and Yang, G. B. (2016). Alteration of polymeric immunoglobulin receptor and neonatal Fc receptor expression in the Gut Mucosa of immunodeficiency virus-infected rhesus macaques. *Scand. J. Immunol.* 83, 235–243. doi: 10.1111/sji.12416

Xia, L., Dai, L., Yu, Q., and Yang, Q. (2017). Persistent transmissible gastroenteritis virus infection enhances enterotoxigenic *Escherichia coli* K88 adhesion by promoting epithelial-mesenchymal transition in intestinal epithelial cells. *J. Virol.* 91:JVI.01256-17. doi: 10.1128/JVI.01256-17

Xu, X., Zhang, H., Zhang, Q., Huang, Y., Dong, J., Liang, Y., et al. (2013). Porcine epidemic diarrhea virus N protein prolongs S-phase cell cycle, induces endoplasmic reticulum stress, and up-regulates interleukin-8 expression. *Vet. Microbiol.* 164, 212–221. doi: 10.1016/j.vetmic.2013.01.034

Ye, L., Tuo, W., Liu, X., Simister, N. E., and Zhu, X. (2008). Identification and characterization of an alternatively spliced variant of the MHC class I-related porcine neonatal Fc receptor for IgG. *Dev. Comp. Immunol.* 32, 966–979. doi: 10.1016/j.dci.2008.01.008

Ye, L., Zeng, R., Bai, Y., Roopenian, D. C., and Zhu, X. (2011). Efficient mucosal vaccination mediated by the neonatal Fc receptor. *Nat. Biotechnol.* 29, 158–163. doi: 10.1038/nbt.1742

Zhang, Q., Xu, Y., Chang, R., Tong, D., and Xu, X. (2018). Transmissible gastroenteritis virus N protein causes endoplasmic reticulum stress, up-regulates interleukin-8 expression and its subcellular localization in the porcine intestinal epithelial cell. *Res. Vet. Sci.* 119, 109–115. doi: 10.1016/j.rvsc.2018.06.008

Zhang, X., Shi, H., Chen, J., Shi, D., Dong, H., and Feng, L. (2015). Identification of the interaction between vimentin and nucleocapsid protein of transmissible gastroenteritis virus. *Virus Res.* 200, 56–63. doi: 10.1016/j.virusres.2014.12.013

Zhang, X., Shi, H., Chen, J., Shi, D., Li, C., and Feng, L. (2014). EF1A interacting with nucleocapsid protein of transmissible gastroenteritis coronavirus and plays a role in virus replication. *Vet. Microbiol.* 172, 443–448. doi: 10.1016/j.vetmic.2014.05.034

Zhang, X., Wu, K., Wang, D., Yue, X., Song, D., Zhu, Y., et al. (2007). Nucleocapsid protein of SARS-CoV activates interleukin-6 expression through cellular transcription factor NF-kappaB. *Virology* 365, 324–335. doi: 10.1016/j.virol.2007.04.009

Zhao, S., Gao, J., Zhu, L., and Yang, Q. (2014). Transmissible gastroenteritis virus and porcine epidemic diarrhoea virus infection induces dramatic changes in the tight junctions and microfilaments of polarized IPEC-J2 cells. *Virus Res.* 192, 34–45. doi: 10.1016/j.virusres.2014.08.014

Zhou, Y., Wu, W., Xie, L., Wang, D., Ke, Q., Hou, Z., et al. (2017). Cellular RNA helicase DDX1 is involved in transmissible gastroenteritis virus nsp14-induced interferon-beta production. *Front. Immunol.* 8:940. doi: 10.3389/fimmu.2017.00940

Conflict of Interest: The authors declare that the research was conducted in the absence of any commercial or financial relationships that could be construed as a potential conflict of interest.

Copyright © 2020 Qian, Gao, Cao, Yang, Cui, Li, Meng, He and Li. This is an open-access article distributed under the terms of the Creative Commons Attribution License (CC BY). The use, distribution or reproduction in other forums is permitted, provided the original author(s) and the copyright owner(s) are credited and that the original publication in this journal is cited, in accordance with accepted academic practice. No use, distribution or reproduction is permitted which does not comply with these terms.

frontiers in Microbiology

ORIGINAL RESEARCH
published: 04 February 2020
doi: 10.3389/fmicb.2020.00042

Coxsackievirus A6 Induces Necroptosis for Viral Production

Shuxia Zhang[1†], Xiaoyan Yu[1†], Xiangling Meng[1], Wenbo Huo[1], Ying Su[1], Jinming Liu[1], Yumeng Liu[1], Jun Zhang[2], Shaohua Wang[2] and Jinghua Yu[2]*

[1] Department of Experimental Pharmacology and Toxicology, School of Pharmaceutical Science, Jilin University, Changchun, China, [2] Institute of Virology and AIDS Research, The First Hospital of Jilin University, Jilin University, Changchun, China

Hand, foot, and mouth disease (HFMD) is a febrile exanthematous disease with typical or atypical symptoms. Typical HFMD is usually caused by enterovirus 71 (EV71) or coxsackievirus A16, while atypical HFMD is usually caused by coxsackievirus A6 (CA6). In recent years, worldwide outbreaks of CA6-associated HFMD have dramatically increased, although the pathogenic mechanism of CA6 is still unclear. EV71 has been established to induce caspase-dependent apoptosis, but in this study, we demonstrate that CA6 infection promotes a distinct pathway of cell death that involves loss of cell membrane integrity. Necrostatin-1, an inhibitor of necroptosis, blocks the cell death induced by CA6 infection, but Z-DEVD-FMK, an inhibitor of caspase-3, has no effect on CA6-induced cell death. Furthermore, CA6 infection up-regulates the expression of the necroptosis signaling molecule RIPK3. Importantly, necrostatin-1 inhibits CA6 viral production, as assessed by its ability to inhibit levels of VP1 protein and genomic RNA and infectious particles. CA6-induced necroptosis is not dependent on the generation of reactive oxygen species; however, viral 3D protein can directly bind RIPK3, which is suggestive of a direct mechanism of necroptosis induction. Therefore, these results indicate that CA6 induces a mechanism of RIPK3-dependent necroptosis for viral production that is distinct from the mechanism of apoptosis induced by typical HFMD viruses.

Keywords: CA6, necroptosis, viral production, RIPK3, host–pathogen interaction

OPEN ACCESS

Edited by:
Zhengli Shi,
Wuhan Institute of Virology (CAS), China

Reviewed by:
Varpu Seija Marjomäki,
University of Jyväskylä, Finland
Zhenhua Zheng,
Wuhan Institute of Virology (CAS), China

***Correspondence:**
Jinghua Yu
yjh-0-2002@163.com

† These authors have contributed equally to this work

Specialty section:
This article was submitted to Virology, a section of the journal Frontiers in Microbiology

Received: *25 September 2019*
Accepted: *09 January 2020*
Published: *04 February 2020*

Citation:
Zhang S, Yu X, Meng X, Huo W, Su Y, Liu J, Liu Y, Zhang J, Wang S and Yu J (2020) Coxsackievirus A6 Induces Necroptosis for Viral Production. Front. Microbiol. 11:42. doi: 10.3389/fmicb.2020.00042

INTRODUCTION

Hand, food, and mouth disease (HFMD) is a highly contagious disease caused by enterovirus infection. It especially poses a health problem in young children under 5 years of age worldwide. The most common causative agents of typical HFMD are enterovirus 71 (EV71) and coxsackievirus A 16 (CA16), though coxsackievirus 6 (CA6) has emerged as a causative agent of an atypical form of the disease. In recent years, outbreaks of CA6-associated HFMD have markedly increased worldwide, and especially in China (Gao et al., 2016; Laga et al., 2016; Li J.S. et al., 2016; Li W. et al., 2016; Mirand et al., 2016; Anh et al., 2018; Wang S.H. et al., 2018; Du et al., 2019). Although vaccines and drug have been developed for HFMD, they principally target EV71 and CA16; strategies for preventing and treating CA6-related-HFMD are scarce, and the current understanding of the pathogenic mechanism of CA6 remains limited.

The typical symptoms of HFMD caused by EV71 or CA16 include flat discolored spots or bumps and sometime, heart inflammation, brain inflammation, or acute flaccid paralysis (Chan et al., 2003; Wang et al., 2012); however, CA6 causes atypical HFMD, characterized by severe rash, onychomadesis in young children, and a higher rate of infection in adults. Furthermore, the pathogenic mechanism of EV71 has been heavily investigated. For example, EV71 has been shown to induce apoptosis that is characterized by cell shrinkage, nuclear condensation, and plasma membrane blebbing in different cell lines (Chang et al., 2004; Lu et al., 2013; Song et al., 2018). EV71-associated apoptosis has also been shown to involve the activation of caspases during viral replication (Chang et al., 2004). Indeed, many viruses induce apoptosis, including but not limited to CA16 (Li et al., 2014), human immunodeficiency virus HIV-1 (Westendorp et al., 1995), hepatitis C virus (Zhu et al., 1998), Epstein–Barr virus (Le Clorennec et al., 2006), and human papillomavirus (Wang et al., 2011). Therefore, apoptosis represents the dominant mechanism by which virus-infected cells undergo programmed cell death. Nevertheless, it remains unknown whether CA6 induces apoptosis.

Coxsackievirus 6 belongs to the *Enterovirus* genus of the Picornaviridae family, which has a single-stranded, positive-sense RNA genome of about 7400 bp that could encode a poly-protein (about 2200 amino acids). In host cells, this poly-protein is further cleaved into four structural (VP1 to VP4) and seven non-structural (2A to 3D) proteins by viral non-structural 2A and 3C proteases (Solomon et al., 2010). Besides 2A and 3C proteins, non-structural 3D protein as an RNA-dependent RNA polymerase is responsible for viral genome replication via incorporating nucleotides into RNA strand (Baltimore, 1964). Recently our studies have demonstrated that 3C and 3D exert other roles that affect the life cycle of the virus (Song et al., 2018; Wang Z. et al., 2018).

As an alternative to apoptosis, necroptosis is an inflammatory type of cell death characterized with cell swelling, loss of plasma membrane integrity, and release of cytosolic contents into the extracellular space (Orzalli and Kagan, 2017). Unlike apoptosis, necroptosis is independent of caspase activity. Generally, when membrane receptors or cytosolic receptors are activated, RIPK1 (receptor-interacting protein kinase 1) associates with RIPK3 via the RIP homotypic interaction motif domain, and this interaction promotes RIPK3-mediated phosphorylation of RIPK1, which then phosphorylates RIPK3. Activated RIPK3 recruits and phosphorylates MLKL, resulting in cell lysis (Cho et al., 2009; He et al., 2009), or activates Ca^{2+}-calmodulin-dependent protein kinase (CaMKII) to induce necroptosis (Zhang et al., 2016). RIPK3-dependent necroptosis has been demonstrated to be activated in response to bovine parvovirus (BPV) (Abdel-Latif et al., 2006), murine cytomegalovirus (Upton et al., 2012), Influenza A virus (Thapa et al., 2016), and reovirus (Berger et al., 2017). Furthermore, high amounts of reactive oxygen species (ROS) have been shown to induce necroptosis (Takemoto et al., 2014; Schenk and Fulda, 2015; Muraro, 2018).

In this study, we demonstrate that the CA6-induced cell death mechanism is distinct from the apoptotic mechanism of EV71 and is instead characterized by RIPK3-dependent necroptosis. CA6-induced necroptosis is not dependent on the generation of ROS, although viral 3D protein can directly bind to RIPK3. Importantly, necrostatin-1 inhibits necroptosis and viral production. These results further advance our understanding of the pathogenic mechanisms of CA6 and provide a potential target for the treatment and prevention of HFMD.

MATERIALS AND METHODS

Cells and Viruses

Human rhabdomyosarcoma RD cells (No CCL-136), human embryonic kidney cells (HEK 293T cells) (No CRL-11268), and human cervix epithelial HeLa (No CCL-2) were purchased from the ATCC (Manassas, VA, United States). Cells were grown in Dulbecco's Modified Eagle's Medium (DMEM, Hyclone, Logan, UT, United States) supplemented with 10% fetal bovine serum (FBS, GIBCO BRL, Grand Island, NY, United States). The 98 strain of CA6[1] was provided by the Jilin Provincial Center for Diseases Control and Prevention (Changchun, China). Viruses were propagated in RD cells, and the supernatants were collected and stored at −80°C as our previous studies (Yu et al., 2015; Wang et al., 2017).

Viral Titer Determination

As previous study (Zhong et al., 2017), the viral titer in a microtitration assay was determined by measuring the $TCID_{50}$ in RD cells. Virus was serially prepared after 10-fold dilution, and 100 μL virus/well was inoculated in octuplicate in 96-well plates. The cytopathic effect was measured once per day until the experimental endpoint was reached. The $TCID_{50}$ was determined according to the Reed–Muench method (Reed and Muench, 1983) based on that viruses of 1×10^5 $TCID_{50}$/mL will produce 0.7×10^5 plaque forming units/mL as our previous studies (Yu et al., 2015; Wang et al., 2017).

Propidium Iodide Staining

After gently removing the culture medium, RD cells were stained *in situ* with 4.5 μM of propidium iodide (PI) (40747-B, Yeasen, Shanghai, China) in buffer (40747-C, Yeasen, Shanghai, China) for 15 min at room temperature in the dark place. The morphological changes were observed and photographed by optical microscopy (Olympus, Tokyo, Japan). PI staining was observed at excitation wavelength 488 nm with emission filter 630 nm by fluorescence microscopy (Leica, Nussloch, Germany).

Infection

Cells were mock-infected or infected with CA6 at an MOI of 5, or EV71 at an MOI of 1. After 2 h of virus absorption, cells were washed once with PBS, and cells were cultured with fresh culture medium or drug treated medium.

Drugs Treatment

After 2 h of virus absorption, cells were washed once with PBS, and cells were cultured with different dose (100, 150,

[1]https://www.ncbi.nlm.nih.gov/nuccore/1071451807

and 200 μM) of necrostatin-1 (A4213, ApexBio, United States), different dose (100, 180, and 260 μM) of necrostatin-2 (A3652, ApexBio, United States) or different dose (1, 2, and 4 mM) of *N*-acetyl-L-cysteine (NAC, A9165, Sigma, St. Louis, MO, United States) for determination of applied concentration. And 20 μM of Z-DEVD-FMK (A1920, ApexBio, United States) as apoptosis inhibitor, 150 μM of necrostatin-1 as necroptosis inhibitor, 180 μM of necrostatin-2 as necroptosis inhibitor, or 2 mM of NAC as ROS scavengers was treated at 2 h post infection of CA6 or EV71.

Cell Counting Using a Hemocytometer

Trypan Blue (Sigma, St. Louis, MO, United States) was used as a vital stain. Live cells appeared colorless and bright (refractile) under phase contrast, while dead cells stained blue and were non-refractile. After staining with a final concentration 0.2% trypan blue, live cells were visualized and counted using a hemocytometer.

Western Blot Analysis

As our previous studies (Yu et al., 2015; Wang et al., 2017), virus-infected and mock-infected cells and/or together with drug treatment were collected at indicated times. Cells were lysed directly in sodium dodecyl sulfate (SDS) sample buffer [60 mM Tris–HCl (pH 6.8), 2% SDS, 10% glycerol, 5% 2-mercaptoethanol, 0.01% bromophenol blue], followed by boiling for 10 min. Whole-cell lysates were further subjected to SDS–PAGE. Proteins were transferred to nitrocellulose membranes (Bio-Rad) and detected with corresponding primary and alkaline phosphatase-conjugated secondary antibody. The membranes were then reacted with 5-bromo-4-chloro-39-indolylphosphate (BCIP) and nitro-blue tetrazolium (NBT) substrate (Sigma, St. Louis, MO, United States). The following antibodies were used: anti-RIPK3 (17563-1-AP, Proteintech), anti-p-MLKL (#91689, Cell Signal), anti-MLKL (#14993, Cell Signal), anti-VP1 (GTX132346, Genetex), anti-histone and anti-HA (GenScript), and anti-tubulin (11224-1-AP, Proteintech). Anti-mouse or rabbit secondary antibodies from goat were obtained from Jackson ImmunoResearch.

Immunofluorescence Staining

RD cells (1×10^6) were cultured in 6 cm culture dishes for 24 h and then were mock-infected or infected with CA6 (MOI = 5) for 36 h. At 36 h after post-infection, cells were fixed with 4% paraformaldehyde for 15 min. The cells were then rinsed three times with 1× PBS (5 min per wash) and blocked for 60 min in blocking buffer (1× PBS/5% normal serum/0.3% Triton X-100) at room temperature. The cells were then incubated with mouse anti-RIPK3 (17563-1-AP, Proteintech) antibody or together with HA antibody (715500, Invitrogen, United States) overnight at 4°C. After three washes in PBS, samples were incubated with FITC-goat anti-Mouse IgG (H + L) (Sungene Biotech, China), or CoraLite 594-conjugated Goat Anti-Mouse IgG (H + L) (Proteintech, China), or FITC-goat anti-Rabbit IgG (H + L) (Sungene Biotech, China) for another 2 h at room temperature. Cells were counterstained with Hoechst 33258 (Sigma, St. Louis, MO, United States) to visualize nuclear DNA on fluorescence microscopy at excitation wavelength 350 nm with emission filter 460 nm (Leica, Nussloch, Germany).

Quantitative Real-Time RT-PCR

According to our previous studies (Yu et al., 2015; Wang et al., 2017), intracellular viral genome RNA was detected through targeting VP1 primers, and GAPDH was chose as internalization control. VP1 forward primer: AATGAGGCGAGTGTGGAAC; VP1 reverse primer: AGGTTGGACACAAAAGTGAACT; GAPDH forward primer: GCAAATTCCATGGCACCGT; GAPDH reverse primer: TCGCCCCACTTGATTTTGG. The fold changes were calculated relative to GAPDH using the $2^{-\Delta\Delta Ct}$ method for VP1, and $\Delta\Delta Ct$ = [(VP1-GAPDH) of drug treatment − (VP1-GAPDH) of control treatment].

Flow Cytometric Analysis by the 2′,7′-Dichlorofluorescin Diacetate Staining

Mock infected or CA6 infected RD cells were trypsinized and collected. Then the cells were stained with 10 μM of 2′,7′-dichlorofluorescin diacetate (DCF-DA) in DMEM with 10% FBS at 37°C for 60 min in the dark. After incubation, the cells were washed once with PBS. Mock infected RD cells are designed as negative control. The samples were analyzed by flow cytometry at excitation wavelength 480 nm with emission filter 525 nm (Yang et al., 2002).

Plasmid Transfection

According to our previous studies (Yu et al., 2015; Wang et al., 2017), 2 μg of VR1012-HA plasmid, VR1012-3C-HA plasmid, or VR1012-3D-HA plasmid with 6 μL of Lipofectamine 2000 (Invitrogen, United States) were transfected into cells in 3.5-cm cell culture dishes. We replenished the empty plasmid VR1012 to maintain a final concentration of 2 μg plasmid/well for dose-dependent test of 3D. Amounts of plasmid and Lipofectamine 2000 were increased for other experiments.

Immunoprecipitation

293T cells (5 × 105 cells/well) were cultured in 10 cm dishes for 24 h and then were mock-transfected or transfected with 10 μg of VR1012-HA, VR1012-3D-HA, or VR1012-3C-HA for 36 h. Then the cells were harvested in IP-lysis buffer [50 mM Tris (pH 7.4), 150 mM NaCl, 1% NP-40, 0.25% sodium deoxycholate, 1 mM EDTA], and the lysates were added to mouse anti-RIPK3 (sc-374639, Santa Cruz, United States) antibody for immunoprecipitation of RIPK3 in HA-, 3C-HA-, and 3D-HA-expressed cells. The bound proteins were analyzed by Western blotting by RIPK3 (17563-1-AP, Proteintech) and HA (715500, Invitrogen, United States) antibody.

Statistical Analyses

Statistical differences were analyzed using the Student's *t*-test. Multiple group differences were assessed using one-way ANOVA in SPSS 10.0. Data are presented as means and standard deviations (SD). **P*-values of <0.05 were considered statistically significant.

RESULTS

CA6 Infection Induces Cytopathic Effects, Though the Morphology After CA6 and EV71 Infection Is Different

Given that EV71, a causative agent for typical HFMD, is known to induce an obvious cytopathic effect in RD cells (Chang et al., 2004; Lu et al., 2013; Song et al., 2018), we sought to determine whether CA6, a causative agent for atypical HFMD, also induces a cytopathic effect. At 24 h post infection, CA6 did not cause a statistical decrease in the cell number (data not shown); however, at 36 h post infection, CA6 decreased the cell number from $5.1 \pm 0.26 \times 10^5$ to $3.33 \pm 0.23 \times 10^5$ (**Figure 1A**). By comparison, at 24 h post infection, EV71 decreased the cell number from $4.83 \pm 0.45 \times 10^5$ to $1.93 \pm 0.15 \times 10^5$ (**Figure 1B**). These results suggest that CA6 can induce a cytopathic effect, although the time course for CA6-mediated cytopathy is extended relative to the time course for EV71-mediated cytopathy.

To determine whether the cytopathic effect caused by CA6 at 36 h post infection is similar to the cytopathic effect caused by EV71 at 24 h post infection, we performed morphology analysis. At 36 h after CA6 infection, many cells were floating, and others appeared ruptured (**Figure 1C**). In contrast, at 24 h after EV71 infection, the cells were condensed, rounded up, and detached from the bottom of the dish (**Figure 1D**). Therefore, although both viruses induced cytopathy, the mechanism of cell death induction by CA6 and EV71 appeared to differ.

To further distinguish the cell death induced by CA6 infection and EV71 infection, we utilized PI to assess plasma membrane rupture. After CA6 infection, the dying cells showed signs of cellular membrane permeability (**Figure 1E**), which is a mark of necroptosis (Abdel-Latif et al., 2006; Cho et al., 2009; He et al., 2009). In contrast, cellular PI staining was not observed after EV71 infection (**Figure 1F**), which is more suggestive of apoptosis and is consistent with the findings of previous studies (Chang et al., 2004; Song et al., 2018). Therefore, these results raise the possibility that CA6 might induce cytopathic effects through necroptosis, rather than apoptosis.

CA6 Infection Induces a Necroptotic Form of Cell Death

To further evaluate the possibility that CA6 induces necroptosis, the necroptosis inhibitor, necrostatin-1 (150 μM, A4213, ApexBio, United States), and the apoptosis inhibitor, Z-DEVD-FMK (20 μM, A1920, ApexBio, United States), were added (**Figures 2A,B**). The results demonstrated that necrostatin-1 inhibited the morphological changes and PI permeability induced by CA6, although Z-DEVD-FMK had no effect (**Figure 2C**). On the other hand, Z-DEVD-FMK, but not necrostatin-1, inhibited the morphological changes induced by EV71 infection (**Figure 2D**). These results suggest that CA6 induces cell death by a mechanism that differs from the mechanism of apoptosis induced by EV71.

To verify that necrostain-1 modulates the cytopathic effect caused by CA6 virus, we examined the effect of necrostatin-1 on the cell number. Our results demonstrated that necrostatin-1 reversed the decrease in the cell number caused by CA6 infection ($4.53 \pm 0.06 \times 10^5$ versus $3.33 \pm 0.31 \times 10^5$; $P < 0.01$), but Z-DEVD-FMK could not reverse the decrease induced by CA6 infection (**Figure 2E**). However, Z-DEVD-FMK reversed the decrease in the cell number caused by EV71 infection ($3.90 \pm 0.10 \times 10^5$ versus $1.93 \pm 0.15 \times 10^5$; $P < 0.001$), but necrostatin-1 could not reverse this decrease induced by EV71 infection (**Figure 2F**). Therefore, these results are consistent with the ability of CA6 to induce necroptosis.

RIPK3, a Protein in the Pathway of Necroptosis, Is Up-Regulated After CA6 Infection

Next, we investigated the mechanism of necroptosis induced by CA6 infection by assessing the effects of CA6 infection on necroptosis proteins. The expression of RIPK3 was up-regulated by CA6 infection, with a similar time course of upregulation as that of the viral protein VP1, while the expression of P-MLKL and MLKL was not consistently altered (**Figure 3A**), and especially at 48 h post infection, the expression of RIPK3 was significantly up-regulated by CA6 infection comparing to mock infection ($P < 0.01$, **Figure 3B**); however, EV71 infection did not affect RIPK3 expression as well as the expression of P-MLKL and MLKL with time (**Figure 3C**), which proved that CA6 could regulate necroptotic pathway protein, but not EV71. Furthermore, the expression of the apoptotic proteins pro-caspase-3 and cleaved caspase-3 was not changed after CA6 infection (**Supplementary Figure S1A**), but was changed after EV71 infection (**Supplementary Figure S1B**), which further confirmed that CA6 infection did not induce apoptosis and was different from EV71. For further confirmation that RIPK3 is up-regulated by CA6 infection, we performed immunofluorescence analysis. The results confirm CA6 infection induced necroptosis (**Figure 3D2**) compared to mock infection (**Figure 3D1**), and the increased expression of RIPK3 was visualized in necroptotic cells induced by CA6-infection (**Figure 3D4**) compared to mock-infection (**Figure 3D3**). Furthermore, the up-regulated RIPK3 was also localized to the cytoplasm, where viral genome replication, protein translation, and viral package occur (**Figure 3D8**). We additionally assessed the effects of necrostatin-1 on RIPK3 expression. At 36 h post infection, the expression of RIPK3 underwent consistent decreased in response to necrostatin-1 treatment ($P < 0.05$, **Figures 3E,F**). Therefore, the necroptosis induced by CA6 infection is associated with the up-regulation of RIPK3.

Necroptosis Promotes Viral Production

Necrostatin-1 is (R)-5-([7-chloro-1H-indol-3-yl]methyl)-3-methylimidazolidine-2,4-dione (**Figure 4A**). Below the concentration of 200 μM, the inhibitory ratio of necrostatin-1 is <5%, the inhibitory ratio of 360 μM of necrostatin-1 is about 37% at 36 h post-treatment (**Supplementary Figure S1C**). To evaluate whether the necroptosis induced by CA6 infection affects viral production, we examined the effect of different doses of necrostatin-1 treatment (100, 150, and 200 μM) on viral

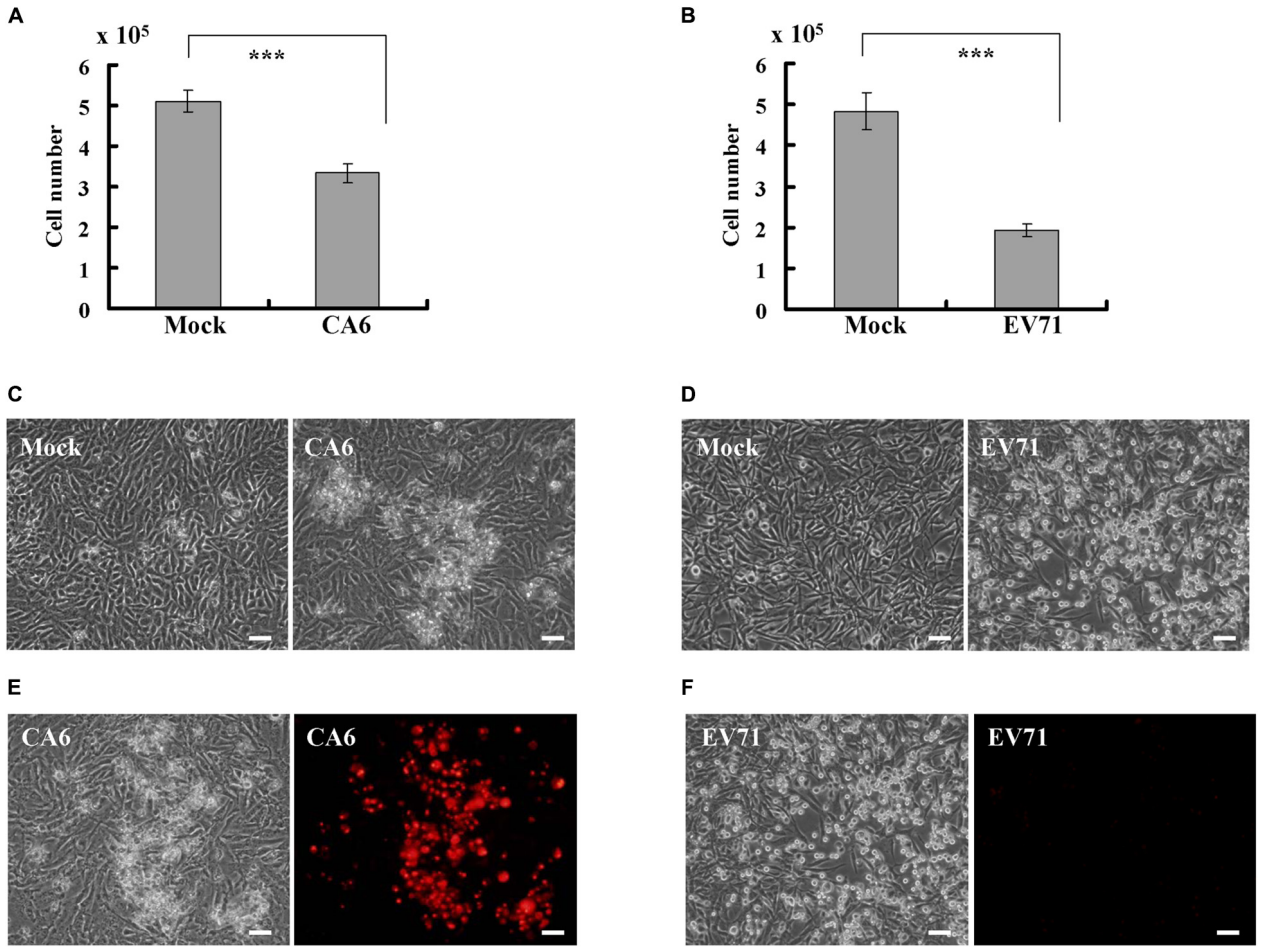

FIGURE 1 | CA6 induces cytopathic effects in RD cells. **(A)** Cell number analysis after CA6 infection (MOI = 5) at 36 h. The cell numbers were counted by trypan blue staining. The results represent the mean ± SD of three independent experiments. ***$P < 0.001$. **(B)** Cell number analysis after EV71 infection (MOI = 1) at 24 h. The cell numbers were counted by trypan blue staining. The results represent the mean ± SD of three independent experiments. ***$P < 0.001$. **(C)** Cell morphologic analysis after mock or CA6 (MOI = 5) infection was performed at 36 h post infection. Results are representative of three independent experiments. Bar = 20 μm. **(D)** Cell morphologic analysis after mock or EV71 (MOI = 1) infection was performed at 24 h post infection. Results are representative of three independent experiments. Bar = 20 μm. **(E)** Cell morphologic analysis with propidium iodide staining after CA6 (MOI = 5) infection was performed at 36 h post infection by light microscopy (left) or fluorescence microscopy (right). Results are representative of three independent experiments. Bar = 20 μm. **(F)** Cell morphologic analysis with propidium iodide staining after EV71 (MOI = 1) infection was performed at 24 h post infection and assessed by light microscopy (left) or fluorescence microscopy (right). Results are representative of three independent experiments. Bar = 20 μm.

protein expression at 36 h post infection. The expression of VP1 was decreased by necrostatin-1 in a dose-dependent manner (**Figure 4B**). To verify these findings, the effects of necrostatin-1 on CA6 genomic levels were evaluated. Necrostatin-1 obviously inhibited the intracellular viral genomic level as assessed by real-time PCR of the VP1 coding sequence ($P < 0.001$) (**Figure 4C**). Finally, we analyzed CA6 virus production at 36 h post-infection. The TCID50/mL of CA6-infected cells ($45.27 \pm 16.16 \times 10^5$) was dramatically reduced by the addition of necrostatin-1 ($4.66 \pm 0.81 \times 10^5$) ($P < 0.05$) (**Figure 4D**). At the same time, another necroptosis inhibitor, necrostatin-2, was utilized to confirm necroptosis affecting CA6 viral production. Necrostatin-2 is an analog of necrostatin-1 (Teng et al., 2007; **Figure 4E**) and has more powerful ability of inhibiting necroptosis and less cytotoxicity than necrostatin-1. Below the concentration of 280 μM, the inhibitory ratio of necrostatin-2 is <5%, the inhibitory ratio of 360 μM of necrostatin-2 is about 16% at 36 h post-treatment (**Supplementary Figure S1D**). And it was confirmed that necrostatin-2 had a similar inhibitory ability on viral production (**Figures 4F–H**). To further confirm the mechanism of necroptosis affecting viral production, we analyzed the effect of necrostatin-1 on viral release. Considering the alteration of cell number after virus infection and necrostain-1 treatment, before calculating intracellular and extracellular viral genome level and TCID50, the cell number was detected, and it was found that different dose of necrostatin-1 (**Supplementary Figure S2A**) and necrostatin-2 (**Supplementary Figure S2B**) could prevent the damage induced by CA6 infection, but not caspase-3 inhibitor (**Supplementary Figure S2C**). Especially, the survival ratio of CA6 infected cells is 66%, while together

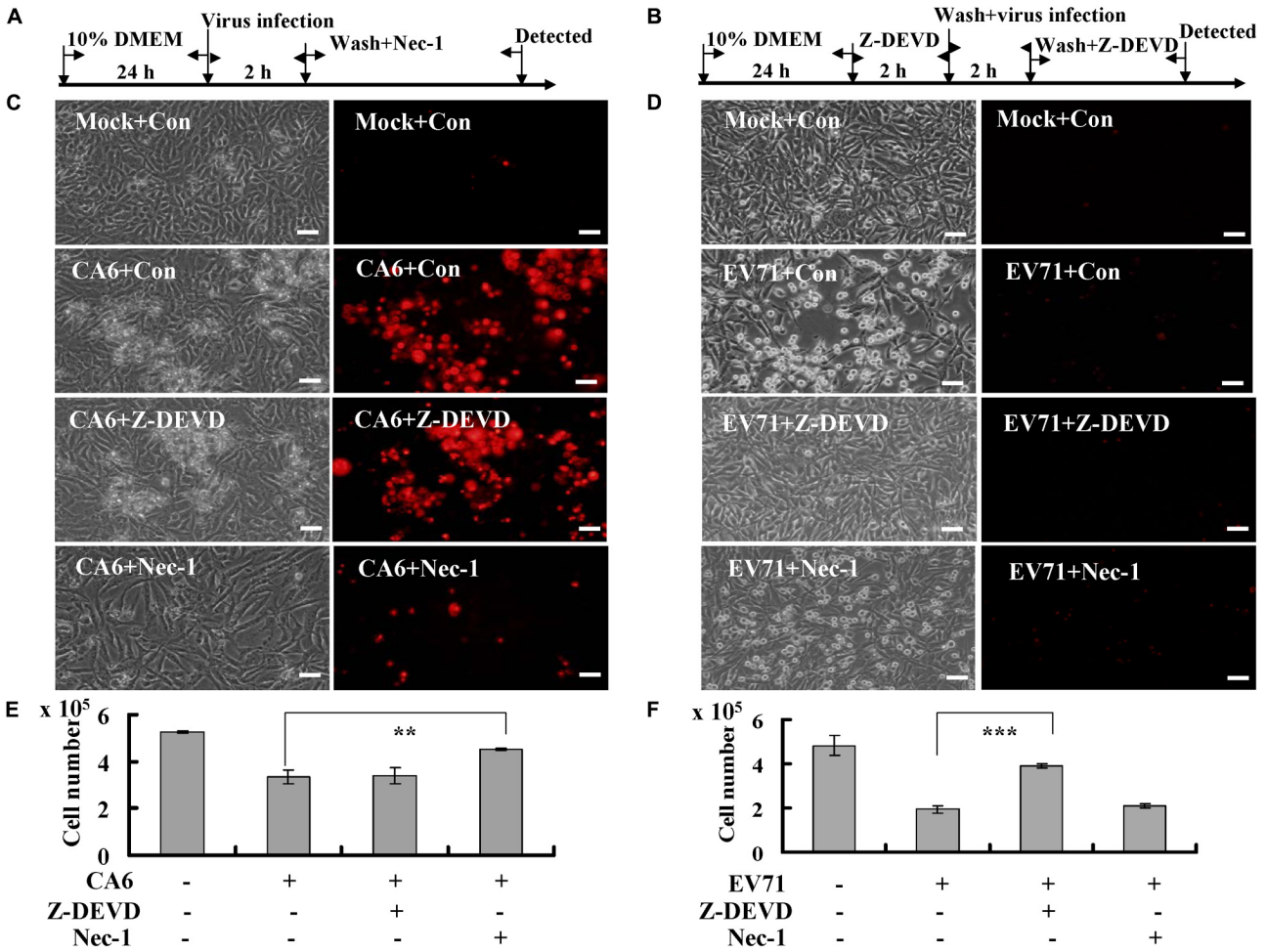

FIGURE 2 | Necrostatin-1 inhibits cell death induced by CA6 infection. **(A)** Flow diagram of RD cells treated with necroptosis inhibitor (necrostatin-1). RD cells were mock-infected or infected with CA6 (MOI = 5) or EV71 (MOI = 1). After 2 h, the cells were washed again with PBS and treated with 150 μM of necrostatin-1 (Nec-1) or 0.05% DMSO in 10% DMEM (Con) for the indicated times. **(B)** Flow diagram of RD cells treated with caspase-3 inhibitor (Z-DEVD-FMK). RD cells were pre-treated with 20 μM of Z-DEVD-FMK inhibitor (Z-DEVD) or 0.05% DMSO in 10% DMEM (Con) for 2 h. The cells were then washed with PBS and mock-infected or infected with CA6 (MOI = 5) or EV71 (MOI = 1). After 2 h, the cells were washed again with PBS and re-treated with 20 μM of Z-DEVD-FMK or 0.05% DMSO in 10% DMEM for the indicated times. **(C)** Cell morphologic analysis with propidium iodide staining after CA6 (MOI = 5) infection was performed at 36 h post infection with necrostatin-1 or Z-DEVD-FMK treatment by light microscopy (left) or fluorescence microscopy (right). Results are representative of three independent experiments. Bar = 20 μm. **(D)** Cell morphologic analysis with propidium iodide staining after EV71 (MOI = 1) infection was performed at 24 h post infection with necrostatin-1 or Z-DEVD-FMK treatment by light microscopy (left) or fluorescence microscopy (right). Results are representative of three independent experiments. Bar = 20 μm. **(E)** Cell number analysis after CA6 infection (MOI = 5) at 36 h treatment with control, necrostatin-1, or Z-DEVD-FMK. The cell numbers were counted by trypan blue staining. The results represent the mean ± SD of three independent experiments. $^{**}P < 0.01$. **(F)** Cell number analysis after EV71 infection (MOI = 1) at 24 h treatment with control, necrostatin-1, or Z-DEVD-FMK. The cell numbers were counted by trypan blue staining. The results represent the mean ± SD of three independent experiments. $^{***}P < 0.001$. Nec-1, necrostatin-1; Z-DEVD, Z-DEVD-FMK; Mock, Mock infection; Con, control.

with 150 μM of necrostatin-1 the survival ratio of CA6 infected cells is 85% at 36 h post infection (**Supplementary Figure S2A**). Followed that, we detected the mRNA level of CA6 in extracellular, intracellular, and total samples by real-time PCR, then the relative extracellular and intracellular mRNA level was calculated assuming the same cell number in each group of control and necrostatin-1 treatment (150 μM), and it was found that excluding the effect of cell number, for extracellular mRNA level, control treatment was 123 times as large as the necrostatin-1 treatment, and for intracellular mRNA level, control treatment was 2.73-fold of the necrostation-1 treatment, while for total mRNA level, control treatment was 2.54 times than the necrostation-1 treatment (**Figure 4I**). Meanwhile, for extracellular virions production, control treatment was 229 times as large as the necrostatin-1 treatment, and for intracellular virions production, there was no obvious difference between control treatment and necrostation-1 treatment, while for total virions production, control treatment was 10 times than the necrostation-1 treatment (**Figure 4J** and **Supplementary Figure S2D**). Therefore, these results suggest that CA6-induced necroptosis promotes viral production, especially through inhibiting viral release.

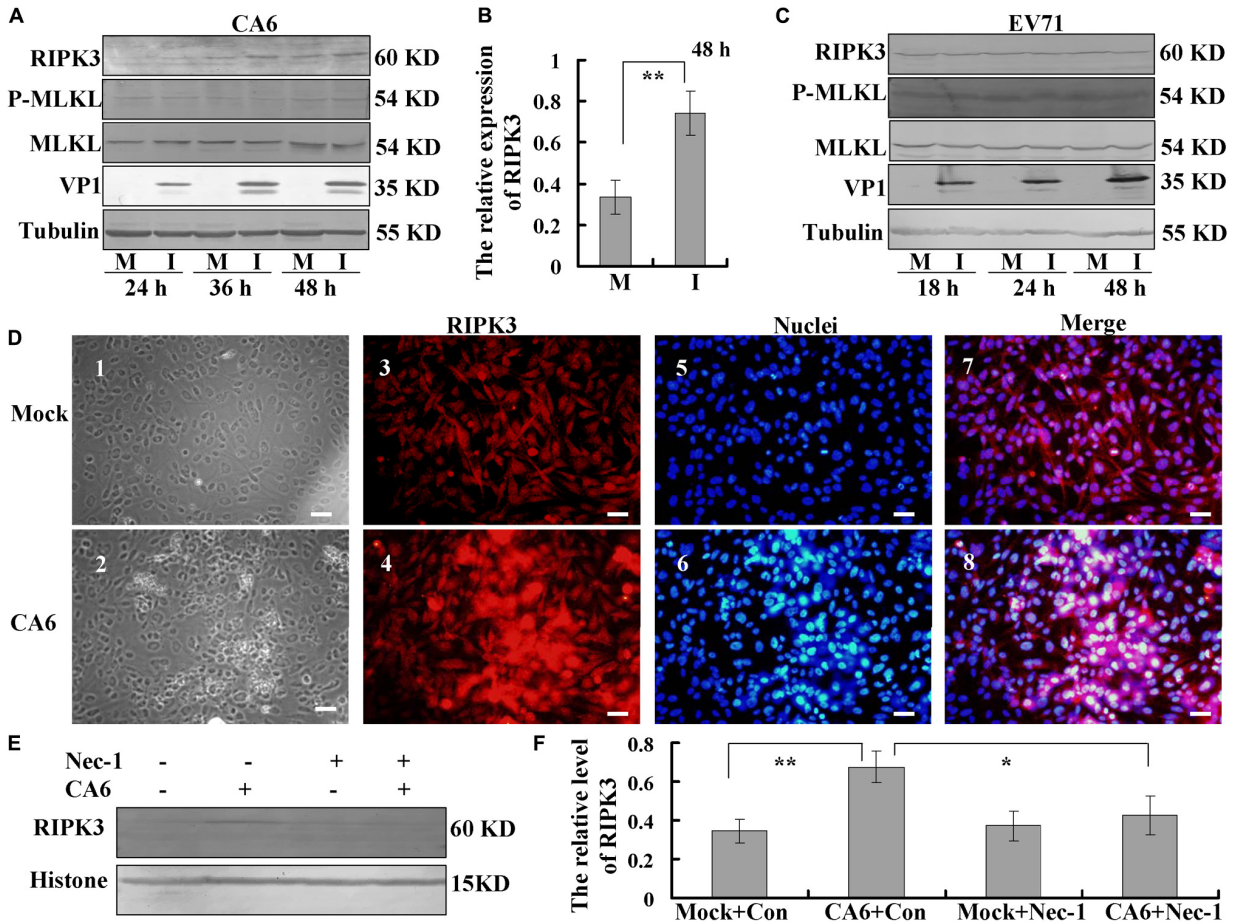

FIGURE 3 | Analysis of host necroptosis regulatory proteins. **(A)** RD cells were mock-infected (M) or infected with CA6 at a MOI of 5 (I) and then collected at the indicated times. RIPK3, p-MLKL, MLKL, and VP1 were detected by Western blot analysis. Tubulin is shown as a loading control. Results are representative of three independent experiments. **(B)** RD cells were mock-infected (M) or infected with CA6 at a MOI of 5 (I) and then collected at the 48 h post infection. The band of RIPK 3 and corresponding tubulin was processed by ImageJ, and the ratio of intensity of RIPK3 to corresponding tubulin was shown. The results represent the mean ± SD of three independent experiments. $^{**}P < 0.01$. **(C)** RD cells were mock-infected (M) or infected with EV71 at a MOI of 1 (I) and then collected at the indicated times. RIPK3, p-MLKL, MLKL, and VP1 were detected by Western blot analysis. Tubulin is shown as a loading control. Results are representative of three independent experiments. **(D)** RIPK3 distribution as assessed by fluorescence microscopy at 36 h post-infection with CA6 at a MOI of 5. Cells were stained with RIPK3 antibody, and then co-stained with CoraLite594-conjugated-second antibody (Red). DNA was counterstained with Hoechst 33258 (Blue). Cell morphology was visualized by light microscope. Merged images of RIPK3 with DNA are shown. Results are representative of three independent experiments. Scale bar = 20 μm. **(E)** Necrostatin-1 inhibited the expression of RIPK3-induced by CA6. Histone is shown as a loading control. Results are representative of three independent experiments. **(F)** The band of panel **(E)** was processed by ImageJ, and the ratio of intensity of RIPK3 to corresponding histone was shown. The results represent the mean ± SD of three independent experiments. $^{**}P < 0.01$. $^{*}P < 0.05$.

ROS Scavenger Do Not Inhibit CA6 Proliferation

Often, necroptosis is associated with increases in the level of ROS (Takemoto et al., 2014; Schenk and Fulda, 2015; Muraro, 2018). To investigate the relationship between CA6 infection and ROS, the level of ROS was detected, CA6 infection did not change the level of ROS compared to the mock-infection (**Figure 5A**). To further confirm the relationship between CA6 infection and ROS, scavengers of ROS (NAC, *N*-Acetyl-L-cysteine, Sigma, St. Louis, MO, United States, A9165) were applied to CA6-infected cells. Increasing doses of NAC had no effect on the expression of VP1 (**Figure 5B**), the necroptotic death induced by CA6 (**Figures 5C,D**), or virion production (**Figure 5E**). To prove the effectiveness of ROS detection and NAC, pseudolaric acid (3 μM) was used as positive control (Qi et al., 2013), and it was found that pseudolaric acid increased the level of ROS ($P < 0.001$) and NAC inhibited the increase of ROS ($P < 0.05$) (**Supplementary Figures S3A,B**). Therefore, these results suggest that necroptosis induced by CA6 is not dependent on ROS.

Viral Non-structural Protein 3D Directly Hijacks RIPK3

As an alternative to ROS induction, we speculated that CA6 virus might directly hijack the pathway of necroptosis by targeting RIPK3 protein. Viral non-structural protein 3C as a protease and 3D as an RNA-dependent RNA polymerase play important role in

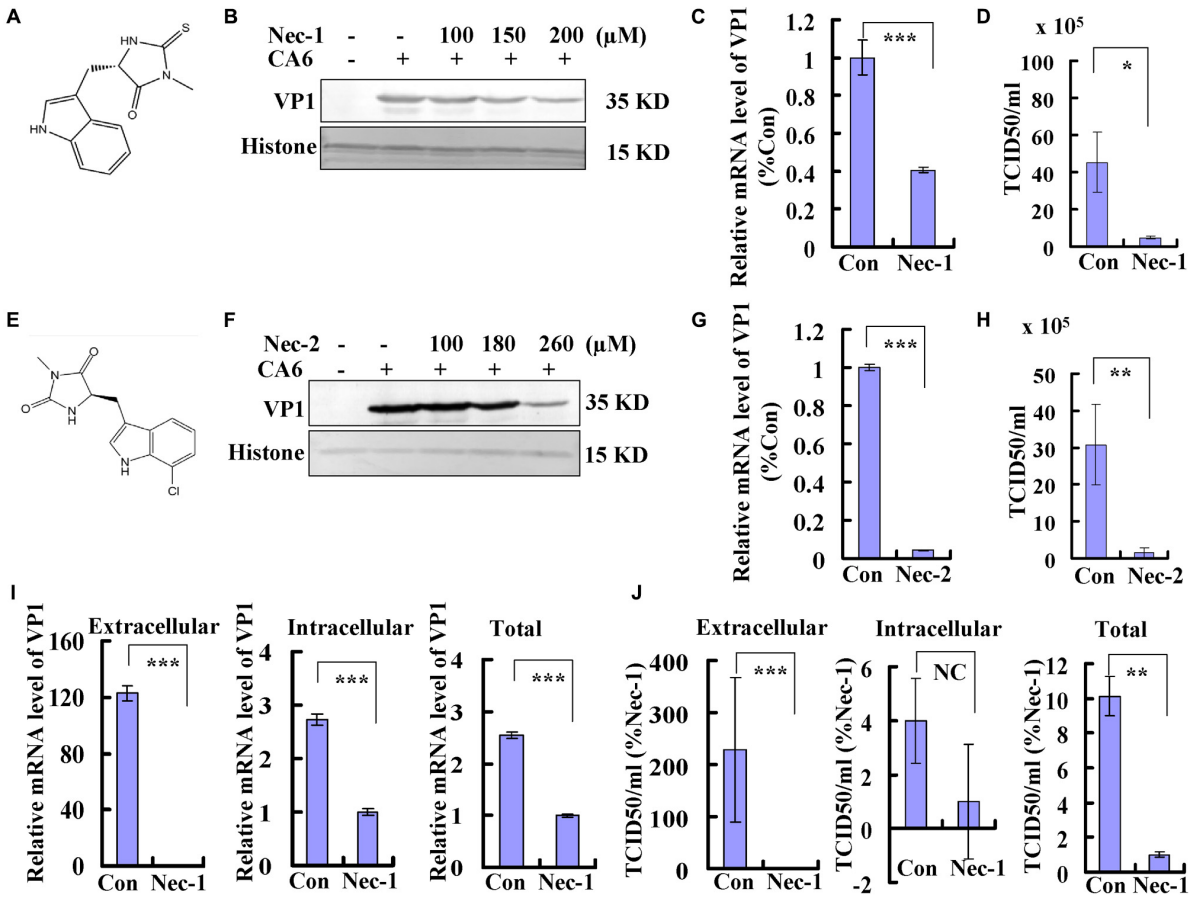

FIGURE 4 | Necrostatin-1 or necrostatin-2 inhibits viral production. **(A)** The chemical structure of necrostatin-1. **(B)** VP1 expression in cellular lysates was determined after growth in control medium or different doses of necrostatin-1 medium at 36 h post-infection. The results are representative of three independent experiments. Histone is shown as loading control. **(C)** At 36 h post-infection, intracellular CA6 RNA levels were detected in control, necrostatin-1 (150 μM)-treated RD cells by real-time quantitative PCR. The results were standardized to GAPDH mRNA as a control and normalized to 1.0 in Con-treated cells. ***$P < 0.001$. **(D)** Total progeny viruses collected at 36 h post-infection of CA6 (MOI = 5) were titrated using RD cells. The results indicate the means ± SD of three independent experiments. *$P < 0.05$. **(E)** The chemical structure of necrostatin-2. **(F)** VP1 expression in cellular lysates was determined after growth in control medium or different doses of necrostatin-2 medium at 36 h post-infection. The results are representative of three independent experiments. Histone is shown as loading control. **(G)** At 36 h post-infection, intracellular CA6 RNA levels were detected in control, necrostatin-2 (180 μM)-treated RD cells by real-time quantitative PCR. The results were standardized to GAPDH mRNA as a control and normalized to 1.0 in Con-treated cells. ***$P < 0.001$. **(H)** Total progeny viruses collected at 36 h post-infection of CA6 (MOI = 5) were titrated using RD cells. The results indicate the means ± SD of three independent experiments. **$P < 0.01$. **(I)** At 36 h post-infection, extracellular, intracellular, and total CA6 RNA levels were detected in control, necrostatin-1 (150 μM)-treated RD cells by real-time quantitative PCR. The results of extracellular and intracellular were standardized to corresponding cell number and normalized to 1.0 in Nec-1-treated cells. ***$P < 0.001$. **(J)** At 36 h post-infection, extracellular, intracellular, and total virions were detected in control, necrostatin-1 (150 μM)-treated RD cells by TCID50. The results of extracellular and intracellular were standardized to corresponding cell number and normalized to 1.0 in Nec-1-treated cells. ***$P < 0.001$, **$P < 0.01$. NC, no significant difference; Con, control treatment; Nec-1, necrostatin-1; Nec-2, necrostatin-2.

viral life cycle (Song et al., 2018; Wang Z. et al., 2018), and 3C and 3D of CA6 induce G0/G1 cell cycle arrest (Wang Z. et al., 2018). Therefore, we firstly evaluated the interaction between these proteins by immunoprecipitation assay, RIPK3 protein antibody was able to pull down 3D-HA but not 10 KD of HA which was constructed by our previous study (Song et al., 2018; **Figure 6A**). However, RIPK3 protein antibody was not able to pull down 3C-HA (**Figure 6B**). Therefore, RIPK3 possibly was hijacked by viral 3D protein but not 3C protein. In the following study, it was found that with the increase of 3D protein, the expression of RIPK3 was correspondingly up-regulated (**Figure 6C**), and with the 3D increase, necroptosis occurred more and more (**Figure 6D**). We further evaluated that RIPK3 can co-localize with the viral non-structural 3D. The results demonstrate that RIPK3 was up-regulated by 3D-HA and co-localized with 3D-HA but not HA (**Figure 6E**). On the basis of these results, 3D protein may regulate necroptosis by binding RIPK3.

DISCUSSION

Apoptosis is a prevalent form of programmed cell death that is activated by many viruses, such as CA16 (Li et al., 2014), human immunodeficiency virus (HIV-1) (Westendorp et al., 1995),

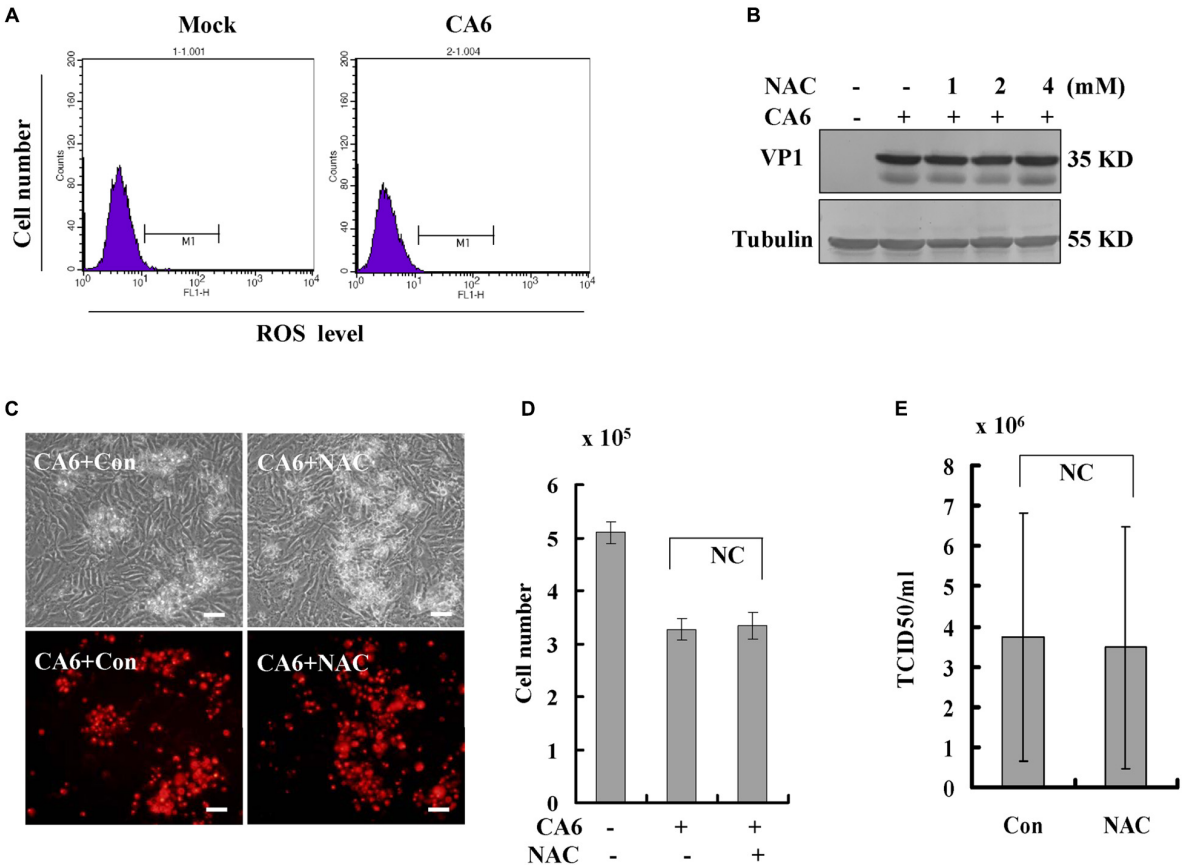

FIGURE 5 | Scavengers of ROS (NAC) do not inhibit necroptosis or viral production. **(A)** The level of ROS was determined after CA6 infection (MOI = 5) at 36 h post-infection by flow cytometery. The results are representative of three independent experiments. **(B)** VP1 expression in cellular lysates was determined after growth in control medium or different doses of NAC medium at 36 h post-infection. The results are representative of three independent experiments. Tubulin is shown as loading control. The results are representative of three independent experiments. **(C)** Cell morphologic analysis with propidium iodide staining after CA6 (MOI = 5) infection was performed at 36 h post infection with control or NAC treatment (2 mM) by light microscopy (upper) or fluorescence microscopy (lower). Results are representative of three independent experiments. Bar = 20 μm. **(D)** Cell number analysis after CA6 infection at 36 h. The cell numbers were counted by trypan blue staining. The results represent the mean ± SD of three independent experiments. NC, no significant difference. **(E)** Total progeny viruses collected at 36 h post-infection of CA6 were titrated using RD cells. The results indicate the mean ± SD of three independent experiments. NC, no significant difference.

hepatitis C virus (Zhu et al., 1998), Epstein–Barr virus (Le Clorennec et al., 2006), and human papillomavirus (Wang et al., 2011). Previous studies show that EV71, which is a major pathogen of typical HFMD, induces apoptosis (Chang et al., 2004) and activates caspase-3 for own production (Song et al., 2018). However, when we investigated the death mechanism of the CA6 virus, the major causative agent of atypical HFMD, we found that CA6 does not induce the same program of apoptosis as EV71.

Apoptotic cells display characteristic morphological features, including membrane blebbing, condensed cells, and the formation of apoptotic bodies, which can be observed after EV71 infection. However, our results reveal that after CA6 infection, membrane rupture and organelle swelling occur, which are the hallmarks of necroptosis. Furthermore, the cell death induced by CA6 infection was attenuated by necrostatin-1, but not caspase-3 inhibitor. Therefore, our results suggest that CA6 induces necroptosis rather than apoptosis.

The induction of necroptosis by CA6 virus could potentially explain the atypical manifestation of HFMD. HFMD is a febrile exanthematous disease with typical or atypical symptoms in children younger than 5 years of age. EV71 infection induces typical symptoms of HFMD, including flat discolored spots or bumps, even heart inflammation, brain inflammation, or acute flaccid paralysis (Chan et al., 2003; Wang et al., 2012), while CA6 leads to atypical HFMD characterized by severe rash, onychomadesis in young children, and a higher rate of infection in adults. In recent years, the large outbreaks of HFMD are usually caused by EV71 infection, while CA6-associated HFMD has lower rates that have markedly increased worldwide. Therefore, apoptosis or necroptosis might be related to varying clinical characteristics, such as the epidemic region, epidemic frequency, clinical symptoms, and epidemic size.

Although CA6 diverges from the typical HFMD viruses in its ability to promote necroptosis, there are many other viruses that activate necroptosis. BPV (Abdel-Latif et al., 2006),

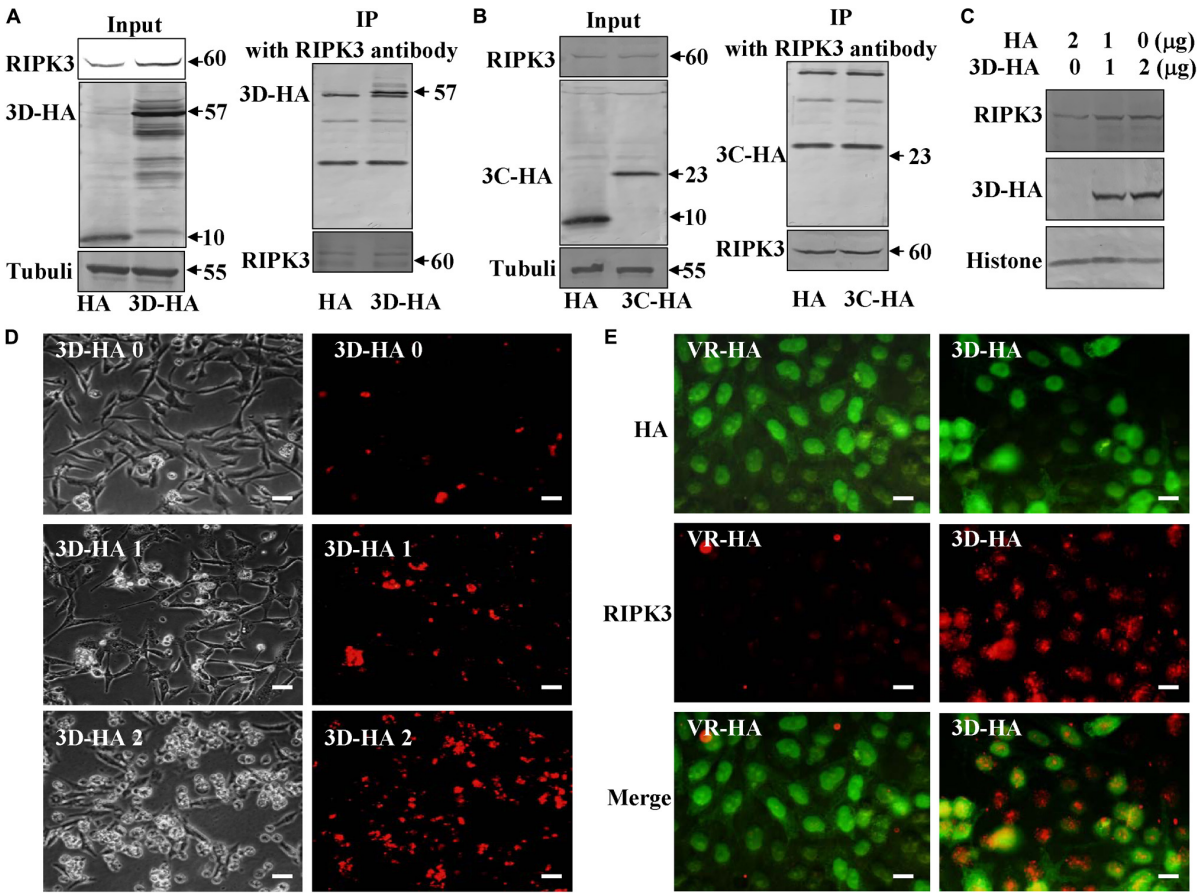

FIGURE 6 | Non-structural protein 3D binds RIPK3. **(A)** Non-structural protein 3D in 3D-transfected cells was evaluated by Western blotting before or after immunoprecipitation (IP) with RIPK3 antibody (Santa) at 36 h post transfection. Results are representative of three independent experiments. **(B)** Non-structural protein 3C in 3C-transfected cells was evaluated by Western blotting before or after immunoprecipitation (IP) with RIPK3 antibody (Santa) at 36 h post transfection. Results are representative of three independent experiments. **(C)** The expression of RIPK3 in 293T cells was analyzed at 36 h after transfection with 0, 1, or 2 μg of 3D-HA-VR1012 plasmid as indicated. Results are representative of three independent experiments. Histone is loading control. **(D)** Transfection of 0, 1, or 2 μg of 3D-HA-VR1012 plasmid into RD cells (HA-VR1012 plasmid was used to replenish 2 μg/well) for 36 h, cell morphologic analysis with propidium iodide staining by light microscopy (left) or fluorescence microscopy (right). Results are representative of three independent experiments. Bar = 20 μm. **(E)** The localization of RIPK3 and HA was analyzed by fluorescence microscopy at 48 h post-transfection of VR1012-HA and VR1012-3D-HA. Cells were fixed in 4% paraformaldehyde, stained with RIPK3 and HA antibodies, and then co-stained FITC labeled-secondary antibody (Green, HA) and CoraLite594-conjugated-second antibody (Red, RIPK3). Merged images of HA and RIPK3 are shown. Data are representative of three individual experiments. Scale bar = 10 μm.

murine cytomegalovirus (Upton et al., 2012), influenza A virus (Thapa et al., 2016), and reovirus (Berger et al., 2017) are among numerous other viruses that have this ability (Upton et al., 2012; Nogusa et al., 2016; Berger et al., 2017; Maelfait, 2017; Schock et al., 2017; Guo et al., 2018; Muraro, 2018; Gaba et al., 2019; Lee et al., 2019). Furthermore, some viruses, such as Epstein–Barr virus (Liu et al., 2018) and human cytomegalovirus (Omoto et al., 2015), can inhibit necroptosis. Therefore, the regulation of necroptosis is a common theme among a subset of viruses, and our results provide a new model to investigate mechanisms associated with necroptosis regulation.

The core of the necroptotic pathway involves the activities of the RIP kinases, RIPK1 and RIPK3, and their ability to phosphorylate and activate the pseudokinase mixed lineage kinase domain-like (MLKL) protein. We demonstrated that RIPK3 is up-regulated after CA6 infection and that the up-regulation of RIPK3 is reversed by the necroptosis inhibitor necrostatin-1, suggesting that RIPK3 may mediate CA6-induced necroptosis. However, the expression of MLKL and p-MLKL was not affected by CA6 infection. Therefore, our results are consistent with the possibility that RIPK3 plays a role in CA6-induced necroptosis that is independent of its ability to phosphorylate MLKL. Future studies to identify downstream effectors of RIPK3 activation in CA6-infected cells may address this possibility.

Necroptosis induced by viral infection has been shown to inhibit viral proliferation (Nogusa et al., 2016; Guo et al., 2018; Lee et al., 2019) or to promote viral magnification (Bozym et al., 2011), depending on the virus and the context. In this study, we demonstrated that necrostatin-1 inhibits viral production. These results were verified by measurement of VP1 genomic levels and

protein expression and by assessing the TCID50. In the further study, it was found that necrostatin-1 decreased the extracellular (123-fold), intracellular (2.73-fold), and total (2.54-fold) viral mRNA level, decreased extracellular (229-fold) and total (10-fold) virions, which indicated that necrostatin-1 inhibited virus production, especially viral release. Therefore, our results suggest that necroptosis is beneficial to the CA6 virus, especially viral release, although further analysis will be needed to elucidate the exact mechanism.

It has been reported that necroptosis is associated with the generation of ROS (Muraro, 2018). However, in our study, we found that CA6 infection did not increase the ROS level, and scavengers of ROS did not affect the necroptosis induced by CA6 or the production of CA6. As an alternate mechanism, viral 3D protein was shown to bind RIPK3 protein, but not viral 3C protein. Further study confirmed that 3D protein up-regulated the expression of RIPK3 and induced necroptosis. Therefore, it is speculated that the virus might directly hijack a factor related to necroptosis to induce necroptosis, which provides a mechanism to explain CA6 induction of necroptosis.

CONCLUSION

In conclusion, necroptosis is exploited functionally by CA6 to facilitate its production, which suggests a novel therapeutic approach for the treatment and prevention of HFMD.

DATA AVAILABILITY STATEMENT

All datasets generated for this study are included in the article/**Supplementary Material**.

AUTHOR CONTRIBUTIONS

JY designed the experiments and wrote the manuscript. JY, SZ, and XY analyzed the results. SZ, XM, WH, YS, JL, YL, and JZ conducted the experiments. JY, SZ, XY, XM, WH, YS, JL, YL, JZ, and SW prepared the viruses, the cell lines, and the reagents, and discussed the data.

FUNDING

This work was supported by the National Natural Science Foundation of China (81871634 and 81301416) to JY, Postdoctoral Science Foundation of China (2014M561302 and 2015T80299) to JY, Norman Bethune Program of Jilin University (2015202) to JY, the Jilin Provincial Science and Technology Department (20140204004YY, 20160414025GH, and 20190304064YY) to JY, and the Department of Human Resources and Social Security of Jilin Province (2016014) to JY.

ACKNOWLEDGMENTS

We would like to thank LetPub (www.letpub.com) for providing linguistic assistance during the preparation of this manuscript.

SUPPLEMENTARY MATERIAL

The Supplementary Material for this article can be found online at: https://www.frontiersin.org/articles/10.3389/fmicb.2020.00042/full#supplementary-material

REFERENCES

Abdel-Latif, L., Murray, B. K., Renberg, R. L., O'Neill, K. L., Porter, H., Jensen, J. B., et al. (2006). Cell death in bovine parvovirus-infected embryonic bovine tracheal cells is mediated by necrosis rather than apoptosis. *J. Gen. Virol.* 87(Pt 9), 2539–2548. doi: 10.1099/vir.0.81915-0

Anh, N. T., Nhu, L. N. T., Van, H. M. T., Hong, N. T. T., Thanh, T. T., Hang, V. T. T., et al. (2018). Emerging coxsackievirus A6 causing hand, foot and mouth disease, vietnam. *Emerg. Infect. Dis.* 24, 654–662. doi: 10.3201/eid2404.171298

Baltimore, D. (1964). *In Vitro* synthesis of viral RNA by the poliovirus RNA polymerase. *Proc. Natl. Acad. Sci. U.S.A.* 51, 450–456. doi: 10.1073/pnas.51.3.450

Berger, A. K., Hiller, B. E., Thete, D., Snyder, A. J., Perez, E. Jr., Upton, J. W., et al. (2017). Viral RNA at two stages of reovirus infection is required for the induction of necroptosis. *J. Virol.* 91:e02404-16. doi: 10.1128/jvi.02404-16

Bozym, R. A., Patel, K., White, C., Cheung, K. H., Bergelson, J. M., Morosky, S. A., et al. (2011). Calcium signals and calpain-dependent necrosis are essential for release of coxsackievirus B from polarized intestinal epithelial cells. *Mol. Biol. Cell* 22, 3010–3021. doi: 10.1091/mbc.E11-02-0094

Chan, K. P., Goh, K. T., Chong, C. Y., Teo, E. S., Lau, G., and Ling, A. E. (2003). Epidemic hand, foot and mouth disease caused by human enterovirus 71, Singapore. *Emerg. Infect. Dis.* 9, 78–85. doi: 10.3201/eid0901.020112

Chang, S. C., Lin, J. Y., Lo, L. Y., Li, M. L., and Shih, S. R. (2004). Diverse apoptotic pathways in enterovirus 71-infected cells. *J. Neurovirol.* 10, 338–349. doi: 10.1080/13550280490521032

Cho, Y. S., Challa, S., Moquin, D., Genga, R., Ray, T. D., Guildford, M., et al. (2009). Phosphorylation-driven assembly of the RIP1-RIP3 complex regulates programmed necrosis and virus-induced inflammation. *Cell* 137, 1112–1123. doi: 10.1016/j.cell.2009.05.037

Du, Z., Zhao, Y., Luo, Y., Du, L., Gan, Q., Zhang, H., et al. (2019). Ongoing change of severe hand, foot, and mouth disease pathogens in Yunnan, China, 2012 to 2016. *J. Med. Virol.* 91, 881–885. doi: 10.1002/jmv.25393

Gaba, A., Xu, F., Lu, Y., Park, H. S., and Liu, G. (2019). The NS1 protein of influenza a virus participates in necroptosis by interacting with MLKL and increasing its oligomerization and membrane translocation. *J. Virol.* 93:e001835-18. doi: 10.1128/jvi.01835-18

Gao, F., Mao, Q. Y., Chen, P., Bian, L. L., Yao, X., Li, J. X., et al. (2016). Seroepidemiology of coxsackievirus A6, coxsackievirus A16, and enterovirus 71 infections in infants and children: a prospective cohort study in Jiangsu, China. *J. Infect.* 73, 509–512. doi: 10.1016/j.jinf.2016.08.008

Guo, H., Gilley, R. P., Fisher, A., Lane, R., Landsteiner, V. J., Ragan, K. B., et al. (2018). Species-independent contribution of ZBP1/DAI/DLM-1-triggered necroptosis in host defense against HSV1. *Cell Death Dis.* 9:816. doi: 10.1038/s41419-018-0868-3

He, S., Wang, L., Miao, L., Wang, T., Du, F., Zhao, L., et al. (2009). Receptor interacting protein kinase-3 determines cellular necrotic response to TNF-alpha. *Cell* 137, 1100–1111. doi: 10.1016/j.cell.2009.05.021

Laga, A. C., Shroba, S. M., and Hanna, J. (2016). Atypical hand, foot and mouth disease in adults associated with coxsackievirus A6: a clinico-pathologic study. *J. Cutan. Pathol.* 43, 940–945. doi: 10.1111/cup.12775

Le Clorennec, C., Youlyouz-Marfak, I., Adriaenssens, E., Coll, J., Bornkamm, G. W., and Feuillard, J. (2006). EBV latency III immortalization program

sensitizes B cells to induction of CD95-mediated apoptosis via LMP1: role of NF-kappaB, STAT1, and p53. *Blood* 107, 2070–2078. doi: 10.1182/blood-2005-05-2053

Lee, A. C. Y., Zhang, A. J. X., Chu, H., Li, C., Zhu, H., Mak, W. W. N., et al. (2019). H7N9 influenza A virus activation of necroptosis in human monocytes links innate and adaptive immune responses. *Science* 10:442. doi: 10.1038/s41419-019-1684-0

Li, J. S., Dong, X. G., Qin, M., Feng, H. R., Yang, J. Y., Li, R. X., et al. (2016). Outbreak of hand, foot, and mouth disease caused by coxsackievirus A6 in a Juku in Fengtai District Beijing, China, 2015. *Springerplus* 5:1650. doi: 10.1186/s40064-016-3307-x

Li, W., Gao, H. H., Zhang, Q., Liu, Y. J., Tao, R., Cheng, Y. P., et al. (2016). Large outbreak of herpangina in children caused by enterovirus in summer of 2015 in Hangzhou, China. *Sci. Rep.* 6:35388. doi: 10.1038/srep35388

Li, Z., Yu, J., Liu, L., Wei, Z., Ehrlich, E. S., Liu, G., et al. (2014). Coxsackievirus A16 infection induces neural cell and non-neural cell apoptosis in vitro. *PLoS One* 9:e111174. doi: 10.1371/journal.pone.0111174

Liu, X., Li, Y., Peng, S., Yu, X., Li, W., Shi, F., et al. (2018). Epstein-Barr virus encoded latent membrane protein 1 suppresses necroptosis through targeting RIPK1/3 ubiquitination. *Cell Death Dis.* 9:53. doi: 10.1038/s41419-017-0081-9

Lu, J. R., Lu, W. W., Lai, J. Z., Tsai, F. L., Wu, S. H., Lin, C. W., et al. (2013). Calcium flux and calpain-mediated activation of the apoptosis-inducing factor contribute to enterovirus 71-induced apoptosis. *J. Gen. Virol.* 94(Pt 7), 1477–1485. doi: 10.1099/vir.0.047753-0

Maelfait, J. (2017). Sensing of viral and endogenous RNA by ZBP1/DAI induces necroptosis. *Cell Death Dis.* 36, 2529–2543. doi: 10.15252/embj.201796476

Mirand, A., le Sage, F. V., Pereira, B., Cohen, R., Levy, C., Archimbaud, C., et al. (2016). Ambulatory pediatric surveillance of hand, foot and mouth disease as signal of an outbreak of coxsackievirus A6 infections, France, 2014-2015. *Emerg. Infect. Dis.* 22, 1884–1893. doi: 10.3201/eid2211.160590

Muraro, S. P. (2018). Respiratory syncytial virus induces the classical ROS-DEPENDENT NETosis through PAD-4 and necroptosis pathways activation. *Sci. Rep.* 8:14166. doi: 10.1038/s41598-018-32576-y

Nogusa, S., Thapa, R. J., Dillon, C. P., Liedmann, S., Oguin, T. H. III, Ingram, J. P., et al. (2016). RIPK3 Activates Parallel Pathways of MLKL-Driven necroptosis and FADD-mediated apoptosis to protect against influenza a virus. *Cell Host Microb.* 20, 13–24. doi: 10.1016/j.chom.2016.05.011

Omoto, S., Guo, H., Talekar, G. R., Roback, L., Kaiser, W. J., and Mocarski, E. S. (2015). Suppression of RIP3-dependent necroptosis by human cytomegalovirus. *J. Biol. Chem.* 290, 11635–11648. doi: 10.1074/jbc.M115.646042

Orzalli, M. H., and Kagan, J. C. (2017). Apoptosis and necroptosis as host defense strategies to prevent viral infection. *Trends Cell Biol.* 27, 800–809. doi: 10.1016/j.tcb.2017.05.007

Qi, M., Fan, S., Yao, G., Li, Z., Zhou, H., Tashiro, S., et al. (2013). Pseudolaric acid B-induced autophagy contributes to senescence via enhancement of ROS generation and mitochondrial dysfunction in murine fibrosarcoma L929 cells. *J. Pharmacol. Sci.* 121, 200–211. doi: 10.1254/jphs.12269fp

Reed, L. J., and Muench, H. (1983). A simple method of estimating fifty percent endpoints. *J. Hyg.* 27, 493–497. doi: 10.1093/oxfordjournals.aje.a118408

Schenk, B., and Fulda, S. (2015). Reactive oxygen species regulate Smac mimetic/TNFalpha-induced necroptotic signaling and cell death. *Sci. Rep.* 34, 5796–5806. doi: 10.1038/onc.2015.35

Schock, S. N., Chandra, N. V., Sun, Y., Irie, T., and Kitagawa, Y. (2017). Induction of necroptotic cell death by viral activation of the RIG-I or STING pathway. *Cell Death Differ.* 24, 615–625. doi: 10.1038/cdd.2016.153

Solomon, T., Lewthwaite, P., Perera, D., Cardosa, M. J., McMinn, P., and Ooi, M. H. (2010). Virology, epidemiology, pathogenesis, and control of enterovirus 71. *Lancet Infect. Dis.* 10, 778–790. doi: 10.1016/S1473-3099(10)70194-8

Song, F., Yu, X., Zhong, T., Wang, Z., Meng, X., Li, Z., et al. (2018). Caspase-3 inhibition attenuates the cytopathic effects of EV71 infection. *Front. Microbiol.* 9:817. doi: 10.3389/fmicb.2018.00817

Takemoto, K., Hatano, E., Iwaisako, K., Takeiri, M., Noma, N., Ohmae, S., et al. (2014). Necrostatin-1 protects against reactive oxygen species (ROS)-induced hepatotoxicity in acetaminophen-induced acute liver failure. *FEBS Open Bio.* 4, 777–787. doi: 10.1016/j.fob.2014.08.007

Teng, X., Keys, H., Jeevanandam, A., Porco, J. A. Jr., Degterev, A., Yuan, J., et al. (2007). Structure-activity relationship study of [1,2,3] thiadiazole necroptosis inhibitors. *Bioorg. Med. Chem. Lett.* 17, 6836–6840. doi: 10.1016/j.bmcl.2007.10.024

Thapa, R. J., Ingram, J. P., Ragan, K. B., Nogusa, S., Boyd, D. F., Benitez, A. A., et al. (2016). DAI senses influenza a virus genomic RNA and activates RIPK3-dependent cell death. *Cell Host Microb.* 20, 674–681. doi: 10.1016/j.chom.2016.09.014

Upton, J. W., Kaiser, W. J., and Mocarski, E. S. (2012). DAI/ZBP1/DLM-1 complexes with RIP3 to mediate virus-induced programmed necrosis that is targeted by murine cytomegalovirus vIRA. *Cell Host Microb.* 11, 290–297. doi: 10.1016/j.chom.2012.01.016

Wang, S. H., Wang, A., Liu, P. P., Zhang, W. Y., Du, J., Xu, S., et al. (2018). Divergent pathogenic properties of circulating coxsackievirus A6 associated with emerging hand, foot, and mouth disease. *J. Virol.* 92:e00303-18. doi: 10.1128/jvi.00303-18

Wang, Z., Wang, Y., Wang, S., Meng, X., Song, F., Huo, W., et al. (2018). Coxsackievirus A6 induces cell cycle arrest in G0/G1 phase for viral production. *Front. Cell Infect. Microbiol.* 8:279. doi: 10.3389/fcimb.2018.00279

Wang, W., Fang, Y., Sima, N., Li, Y., Li, W., Li, L., et al. (2011). Triggering of death receptor apoptotic signaling by human papillomavirus 16 E2 protein in cervical cancer cell lines is mediated by interaction with c-FLIP. *Apoptosis* 16, 55–66. doi: 10.1007/s10495-010-0543-3

Wang, X., Zhu, C., Bao, W., Zhao, K., Niu, J., Yu, X. F., et al. (2012). Characterization of full-length enterovirus 71 strains from severe and mild disease patients in northeastern China. *PLoS One* 7:e32405. doi: 10.1371/journal.pone.0032405

Wang, Z. Y., Zhong, T., Wang, Y., Song, F. M., Yu, X. F., Xing, L. P., et al. (2017). Human Enterovirus 68 interferes with the host cell cycle to facilitate viral production. *Front. Cell Infect. Microbiol.* 7:29. doi: 10.3389/fcimb.2017.00029

Westendorp, M. O., Frank, R., Ochsenbauer, C., Stricker, K., Dhein, J., Walczak, H., et al. (1995). Sensitization of T cells to CD95-mediated apoptosis by HIV-1 Tat and gp120. *Nature* 375, 497–500. doi: 10.1038/375497a0

Yang, M. L., Huang, T. S., Lee, Y., and Lu, F. J. (2002). Free radical scavenging properties of sulfinpyrazone. *Free Radic. Res.* 36, 685–693. doi: 10.1080/10715760290009137

Yu, J. H., Zhang, L. Y., Ren, P. Y., Zhong, T., Li, Z. L., Wang, Z. Y., et al. (2015). Enterovirus 71 mediates cell cycle arrest in S phase through non-structural protein 3D. *Cell Cycle* 14, 425–436. doi: 10.4161/15384101.2014.980631

Zhang, T., Zhang, Y., Cui, M., Jin, L., Wang, Y., Lv, F., et al. (2016). CaMKII is a RIP3 substrate mediating ischemia- and oxidative stress-induced myocardial necroptosis. *Nat. Med.* 22, 175–182. doi: 10.1038/nm.4017

Zhong, T., Zhang, L. Y., Wang, Z. Y., Wang, Y., Song, F. M., Zhang, Y. H., et al. (2017). Rheum emodin inhibits enterovirus 71 viral replication and affects the host cell cycle environment. *Acta Pharmacol. Sin.* 38, 392–401. doi: 10.1038/aps.2016.110

Zhu, N., Khoshnan, A., Schneider, R., Matsumoto, M., Dennert, G., Ware, C., et al. (1998). Hepatitis C virus core protein binds to the cytoplasmic domain of tumor necrosis factor (TNF) receptor 1 and enhances TNF-induced apoptosis. *J. Virol.* 72, 3691–3697. doi: 10.1128/jvi.72.5.3691-3697.1998

Conflict of Interest: The authors declare that the research was conducted in the absence of any commercial or financial relationships that could be construed as a potential conflict of interest.

Copyright © 2020 Zhang, Yu, Meng, Huo, Su, Liu, Liu, Zhang, Wang and Yu. This is an open-access article distributed under the terms of the Creative Commons Attribution License (CC BY). The use, distribution or reproduction in other forums is permitted, provided the original author(s) and the copyright owner(s) are credited and that the original publication in this journal is cited, in accordance with accepted academic practice. No use, distribution or reproduction is permitted which does not comply with these terms.

frontiers in Microbiology

ORIGINAL RESEARCH
published: 11 February 2020
doi: 10.3389/fmicb.2020.00146

Transcriptome Analysis Reveals New Insight of Fowl Adenovirus Serotype 4 Infection

Yuan Chen[1,2], *Ruiling Huang*[1,2], *Guishu Qu*[1,2], *Yaoshun Peng*[1], *Lihui Xu*[1], *Changkang Wang*[1], *Cuiqin Huang*[3] *and Quanxi Wang*[1,2]*

[1] College of Animal Science (College of Fee Science), Fujian Agriculture and Forestry University, Fuzhou, China, [2] Fujian Key Laboratory of Traditional Chinese Veterinary Medicine and Animal Health, Fujian Agriculture and Forestry University, Fuzhou, China, [3] Fujian Provincial Key Laboratory for the Prevention and Control of Animal Infectious Diseases and Biotechnology, Longyan, China

Since 2015, Fowl adenovirus serotype 4 (FAdV-4) infection has caused serious economic losses to the poultry industry worldwide. We isolated and identified the FAdV-4 strain NP, from infected chickens on a layer farm, using chicken embryo allantoic cavity inoculation, electron microscopy, viral genome sequencing, and regression analysis. To explore the pathogenesis of FAdV-4 infection, we conducted transcriptome sequencing analysis of the liver in chickens infected with FAdV-4, using the Illumina® HiSeq 2000 system. Two days after infection with the FAdV-4 NP strain, 13,576 differentially expressed genes (DEGs) were screened in the liver, among which, 7,480 were up-regulated and 6,096 were down-regulated. Gene ontology (GO) analysis indicated that these genes were involved in 52 biological functions. Furthermore, Kyoto Encyclopedia of Genes and Genomes (KEGG) analysis showed that those DEGs were involved in 33 pathways. We then focused on the KEGG pathway of phagosome and found that mRNA levels of the 25 DEGs in that pathway were up-regulated, and seven DEGs were down-regulated. Real-time quantitative polymerase chain reaction (qPCR) confirmed the accuracy and reliability of these findings. Moreover, 24 h after LMH cells were infected with FAdV-4, the mRNA levels of *F-actin*, *Rab7*, *TUBA*, and *DVnein* were significantly increased. These four genes were all subsequently silenced by RNA interference, and viral replication of FAdV-4 was then significantly down-regulated. These findings demonstrate the isolation and identification of the FAdV-4 NP strain, and the DEGs in KEGG pathway of phagosome were utilized by FAdV-4 to benefit its infection.

Keywords: transcriptome, fowl adenovirus serotype 4, virus genome, viral invasion, intracellular trafficking

OPEN ACCESS

Edited by:
Ian M. Jones,
University of Reading, United Kingdom

Reviewed by:
Dahlene N. Fusco,
Tulane University, United States
Ramón A. Gonzalez,
Universidad Autónoma del Estado de Morelos, Mexico

***Correspondence:**
Quanxi Wang
wqx608@126.com

Specialty section:
This article was submitted to Virology, a section of the journal Frontiers in Microbiology

Received: *10 October 2019*
Accepted: *21 January 2020*
Published: *11 February 2020*

Citation:
Chen Y, Huang R, Qu G, Peng Y, Xu L, Wang C, Huang C and Wang Q (2020) Transcriptome Analysis Reveals New Insight of Fowl Adenovirus Serotype 4 Infection. Front. Microbiol. 11:146. doi: 10.3389/fmicb.2020.00146

INTRODUCTION

Based on the genomic profiles, Fowl adenovirus (FAdV) is divided into three groups (I–III) and 12 serotypes (Hess, 2000). It is a non-encapsulated, double-stranded DNA virus (Griffin and Nagy, 2011). Its main structural proteins include the penton, hexon, and fiber proteins (Shah et al., 2017). Infection with different serotypes of group I FAdV leads to different clinical symptoms. Infection with FAdV serotype 4 (FAdV-4) causes hydropericardium hepatitis syndrome (HHS) (Asthana et al., 2013). Broilers at 21–35 days old are easily infected with FAdV-4. The morbidity and mortality rates are high (Chandra et al., 2000). In 1987, FAdV-4 was first reported in Pakistan, and then in India (Mittal et al., 2014) and South Korea (Kim et al., 2008), among other countries. Before 2014,

only sporadic cases had been reported in China. Since 2015, FAdV-4 infection has caused a major outbreak in China. However, little is known about the pathogenic mechanisms of FAdV-4 infection.

Viruses evade the defense responses of host in order to efficiently infect host cells. Furthermore, viruses often utilize the host cell machinery to replicate, spread, and survive (Toscano and de Haan, 2018). Receptors are located on the cytomembranes or endosomal membranes. The receptors are internalized within endosomes, from which they are transferred to lysosomes for degradation, while others are recycled and transported back to the plasma membrane. After binding with the receptor, viral structural proteins serve as pathogen-associated molecular patterns that bind to toll-like receptors (TLRs). Some viral particles could inhibit the activation of TLRs to evade the proteasome, and the antigen presentation to cells of the host's immune system during the initial stages of infection (Horvath et al., 1992).

In this study, we identified FAdV-4 strain NP from sick layers that were pre-laying Hy-Line Variety Brown hens and investigated the transcriptomic profile of livers infected with FAdV-4 strain NP. We then focused on the KEGG pathway of phagosome and used qPCR and ribonucleic acid (RNA) interference to determine whether the KEGG pathway of phagosome was used to facilitate FAdV-4 invasion.

MATERIALS AND METHODS

Compliance With Ethical Standards

The animal protocol used in this study was approved by the Research Ethics Committee of the College of Animal Science, Fujian Agriculture and Forestry University. All experimental procedures were performed in accordance with the Regulations for the Administration of Affairs Concerning Experimental Animals, approved by the State Council of China.

Main Reagents

The PEASY-T1 cloning vector kit, total RNA extraction kit, and reverse transcription kit, qPCR kit, Trans1-T1 competent cells (Full-type Golden Biotechnology Co., Ltd., Beijing, China), and agar rapid recovery kit were purchased from Tiangen Biochemical Technology Co., Ltd. (Beijing, China). The deoxyribonucleic acid (DNA) extraction kit was purchased from Promega Biotechnology Co., Ltd. (Beijing, China). The hematoxylin and eosin (H&E) stains were purchased from Nanjing Jiancheng Technology Co., Ltd. (Nanjing, China), whereas the Dulbecco's modified Eagle medium (DMEM), fetal bovine serum, and the real-time fluorescent quantitative polymerase chain reaction kit were purchased from TaiJing Biotechnology Co., Ltd. (Xiamen, China).

Embryonated Eggs

Specific-pathogen-free (SPF) embryonated eggs were provided by Jinan Sais Poultry Co. Ltd. The eggs were hatched to 10 day-old in an incubator at 37°C.

Virus Isolation

The virus was isolated from diseased layers in Nanping city of Fujian province. The liver from each of the infected layers was collected, ground with sterile phosphate-buffered saline (PBS, pH 7.2), and centrifuged at 10,000 g for 10 min. After the supernatants were filtered through a 0.22-μm syringe-driven filter, they were inoculated into the allantoic cavities of 10-day-old SPF embryonated eggs, and cultured in an incubator at 37°C. After inoculation, the embryonated eggs were checked daily and the allantoic fluid was collected from days 1–3. The virus was propagated through more than three passages. The harvested allantoic fluid was frozen at −80°C for viral DNA extraction and subsequent observation using electron microscopy. The median embryo lethal dose (ELD_{50}) was calculated using the Reed-Muench method (Wang et al., 2014). The virus was named FAdV4 strain NP.

Observation by Electron Microscope

The allantoic fluid from the infected embryonated eggs was again centrifuged at 10,000 g for 45 min. The virus was suspended in ultrapure water, and then doubly treated with 2.5% glutaraldehyde for 2 h at 4°C, and 1% osmic acid fixation for 1 h. It was then embedded in epoxy resin and sliced into 50–60 nm sections, and then stained with 3% uranium acetate-citric acid. The morphology of the virus was observed using an HT7700 electron microscope (Wang et al., 2019).

Identification by PCR and Sequencing of PCR Products

Specific primers based on the A fragment of the hexon gene (AJ554049.1) were designed as follows: F:5′-TGGACATGG GGGCGACCTA-3′ and R:5′-AAGGGATTGACGTTGTCCA-3′. They were then sent to Shanghai Sangon Biological Co., Ltd. for synthesis.

The DNA of FAdV4 was extracted using a viral DNA extraction kit (Promega Biotechnology Co. Ltd., Beijing, China). The PCR was then conducted with specific primers for the A fragment of the hexon gene. The PCR reaction system (25 μL) comprised 1 μL of template, 12.5 μL of PCR Nucleotide Mix (10 mmol/L), 9.5 μL of nuclease-free water, and 1 μL of each of the upstream and downstream primers. The reaction conditions were as follows: denaturation at 95°C for 30 s, annealing at 55°C for 30 s, and extension at 72°C for 30 s, over 35 cycles. After amplification, the PCR products were analyzed via 1% agarose gel electrophoresis. Then the PCR products were sent to sequence by Sangon Biotech (Shanghai) Co., Ltd. At last, the genetic tree was analyzed by DNAMAN9.0 software (Lynnon Biosoft, San Ramon, USA).

Sequencing Analysis of the FAdV4 Genome

The FAdV-4 strain NP [median tissue culture infective dose ($TCID_{50}$) = $10^{-6.23}$/0.01 mL] was multiplied in a chick embryonic fibroblast cell line (DF-1) with 5% fetal bovine serum in Dulbecco's modified Eagle medium (DMEM; Hyclone, Logan, USA). At 24 h post-infection, the cells were collected, and viral DNA was extracted with a viral DNA extraction kit (Promega Biotechnology Co., Ltd., Beijing, China). The DNA sample was

sent to Wuhan Thermofly Co. Ltd. for sequencing (PE150, HiSeq X^{TM} Ten, Illumina, USA). The genomic library of FAdV4 was constructed with 200–300 bp fragments, which were amplified by PCR with specific primers (shown in **Table 1**) based on the reference genome of FAdV-4 strain CH/AHMC (GenBank: KU558760.1). The overlap between the amplified bands was about 50 bp. All PCR products were further evaluated for end repair, A-tailing and adapter ligation. The genomic library of FAdV4 was sequenced (PE150; Hiseq X ten, Illumina, USA).

TABLE 1 | Special primers of the FAdV 4 genome.

Genes	Sequences (5′-3′)
V1	F:5′-CATCATCTTATATAACCGCGTCTTT-3′ R:5′-CGGTCCGAAGCCATCTGTAAT-3′
V2	F:5′-GAACTGGCTGCGATGCTAGA-3′ R:5′-AAGAGCGACTACACGCGAAA-3′
V3	F:5′-TGTTTCGTCCTTGCACGCAT-3′ R:5′-ACAACGCCAGAGTAGCATCC-3′
V4	F:5′-AGCATTTTGGCGTTGGAGTG-3′ R:5′ACTGTGTTCGGGTTCTAGCG-3′
V5	F:5′-GAGAGTGGGGACGTTACCGA-3′ R:5′-TGTCACGCTTCTCAACGACA-3′
V6	F:5′-GTCATCGCTCTCTTCTGGGG-3′ R:5′-ACAGGTAGCGAAATGTGGCA-3′
V7	F:5′-GGTCTCCGCTGAGCATGAAA-3′ R:5′-CTTTCAACGCCGACGATCAC-3′
V8	F:5′-CAGCGAACACTTCCGATCCA-3′ R:5′-AACTCATCCTCCTCTCCGCT-3′
V9	F:5′-AGAAGCGGATGAGCGAGATT-3′ R:5′-CAACTGGATGGACTCGGTGG-3′
V10	F:5′-CCATAGCAATTTCCGCACCA-3′ R:5′-CAGGGACGGTACAAAGTCGT-3′
V11	F:5′-CTACCGTCGCCTCCATCTAC-3′ R:5′-GGTGTTGGCGTTTTGTACCC-3′
V12	F:5′-CGAGCACCTCCAAAGACACG-3′ R:5′-TCCACAGGTAGTTGTCGCAG-3′
V13	F:5′-AACTCTGGGTTTATCGCCCC-3′ R:5′-CGGTATGCGCGAAAGACAAG-3′
V14	F:5′-TCCAACTCAGGTCGTGCTTC-3′ R:5′-GTCCCCCATCTGCCGAATAG-3′
V15	F:5′-TTGTCTAGGTAGGCGTTGGC-3′ R:5′-TTGTCTAGGTAGGCGTTGGC-3′
V16	F:5′-GAACTGCTCGCCATCAACAC-3′ R:5′-GCTGGGACCTTGAACACGTA-3′
V17	F:5′-GCAATTATCGGGCGGACTGA-3′ R:5′-GGGGGAGTAGACGTAACCCT-3′
V18	F:5′-TAGCCTTCACTGTCTCGCTG-3′ R:5′-CTCCCCTGTCACTACTTGCG-3′
V19	F:5′-CTTTGTTCCCGCGTCCAATC-3′ R:5′-ATTAGGTCGCGCATTCCGAT-3′
V20	F:5′-CCGAAACCGAACTCACCGAT-3′ R:5′-TGTATAACGGAGGAGGCGGA-3′
V21	F:5′-CATGGACCTTGTCCTGTTTGTT-3′ R:5′-TAACGAGGGATACGCGCAAG-3′
V22	F:5′-CGCTCCGAACACAAGGTACA-3′ R:5′-CGAAGGGTGAGAGCTGGTTT-3′
V23	F:5′-TATGCTGAGAACCCTCCCCAA-3′ R:5′-GATCGGTTCCGTGCTGTTTT-3′
V24	F:5′-ACCTCAGAACCAACTACTGCTG-3′ R:5′-CATCATCTTATATATAACCGCGT-3′

Animal Infection

Eighteen 40-day-old chicks (FAdV4 antigen and antibody negative) were randomly divided into the control group or infection group. Chicks in the infection group were administered an intramuscular injection of 0.5 mL FAdV4 ($TCID_{50} = 10^{-6.23}$/0.1 mL), and those in the control group were injected with the same volume of sterile saline.

Observation of Pathological Changes

When clinical signs were apparent in the infected group, the birds were sacrificed, and sections of the heart, liver, and kidney of each were collected, stained with H&E and subjected to pathological evaluation.

Transcriptome Sequencing and Screening of Differentially Expressed Genes (DEGs) in the Liver

At 2 days post-infection with FAdV4, the livers in the two groups were collected and total RNA was extracted using an RNA extraction kit (Saffer, China). The mRNA was separated with magnetic beads to generate a sequence library using the Illumina® HiSeq TM 2000 (Illumina, Shenzhen,

TABLE 2 | Sequences of qPCR primers in this study.

Genes	Sequences (5′-3′)	Expected size (bp)
β-actin	F:5′-CCAAAGCCAACAGAGAGAAGAT-3′ R:5′-CATCACCAGAGTCCATCACAAT-3′	138
CR3	F:5′-GCTTTGGCTTTGGTGCATGG-3′ R:5′-CTCCTTCTGTCTTGCGCTGG-3′	108
αMβ2	F:5′-GAGACCACCAGTAGCCAGGT-3′ R:5′-AGCACCAGGAGCTAGGACAG-3′	181
αVβ3	F:5′-CTCACCAGCAACCTTCGCAT-3′ R:5′-TTGAAGCGCATCACCTCGTC-3′	179
MR	F:5′-AGTGTCCCTTGGCTGGACTT-3′ R:5′-CTACAGCGCACGTACTGCAA-3′	161
F-actin	F:5′-GCTTCCATCCAGTGCGGAGTATTC-3′ R:5′-GCTTAGAACGGCGGCGACAG-3′	88
Rab7	F:5′-CCTGCTGCTTGGATCTGCTCTC-3′ R:5′-CTGTAAGGTGGCTGGCACTGC-3′	108
TUBA	F:5′-GCGGCACGGCAAGTACATGG-3′ R:5′-CTTGGTCTTGATGGTGGCGATGG-3′	94
DVnein	F:5′-AGATGTTCAAGCAGGAGCCAACC-3′ R:5′-TCCATACAGGTGACAACACGATGC-3′	87
VAMP-3	F:5′-CGGCAGGATGTCAGCCAATGTC-3′ R:5′-TTCCAGCACCTTGTCCACATTCAC-3′	133
VATPase	F:5′-GAGGAACTGCTGCGCTCTGTG-3′ R:5′-GCCAGAACTCCGACATGATCCG-3′	85
MHCII	F:5′-CATGCTAGCTTGGAGGAGCC-3′ R:5′-GGTAGTTGTGACCGGGAAGC-3′	187
MHCI	F:5′-TGGGTGTGGGATGGGCTC-3′ R:5′-GAAACACAGCCGGGCAGG-3′	200
SRB1	F:5′-AGATCACCACCAGTCTCCAGAAGG-3′ R:5′-CAGAACGACAGATGAGCCAGCAG-3′	197

China). The concentration of total RNA was quantified with a NanoDrop® 1000 spectrophotometer (OD260/280 = 1.8–2.0) (Thermo Scientific, Shanghai, China) and its purity assessed with electrophoresis in 1% (w/v) agarose gel, which was to detect whether the RNA was degradation or was contaminated with proteins and eoxyribonucleic acid (DNA) (Wang et al., 2015).

We then evaluated the quality of sequenced reads and analyzed their saturation following as our previous study (Wang et al., 2015). Sequencing results of Illumina ®HiSeq TM 2000 is raw reads, in which the impurities as reads with adapter, need to be removed. After removing the impurities, the reads is clean reads. The clean reads should be further filtrated to high quality clean reads, in which the reads with adapter, reads containing N more than 10% were further removed. The map of classification of clean read was present.

Then first, the high quality clean reads were compared with sequences of ribosome using the short-read comparison software Bowtie. Second the ribosome reads were removed. The clean reads-removed ribosome reads were compared with avian genomes and gene sequences using the software TopHat2. Third, the sequencing saturation was used to assess whether the sequencing amount of the sample was saturated. Because when the sequencing amount reaches a certain value, the rate of transcription tends to be gentle, indicating that it is saturated. The data was present with saturation curve.

The number of genes expressed was calculated as the reads per kilobase per million mapped reads (RPKM) and genes were compared to determine their relevant features. The differential test was then conducted and the multiple hypothesis tests were calculated by the detection method based on sequencing of DEGs (Audic and Claverie, 1997). The field value of P was controlled by the false discovery rate (FDR). The DEGs were defined as those for which the FDR was ≤0.05 and its difference ratio was <2-fold (Wang et al., 2015; Wang Q. X. et al., 2018).

Gene Ontology (GO) analysis and Kyoto Encyclopedia of Genes and Genomes (KEGG) pathway analysis of DEGs. The DEGs were first mapped to the respective terms of the GO database (http://www.geneontology.org/), and the number of genes per term was calculated. A list of genes was thereby obtained with specific

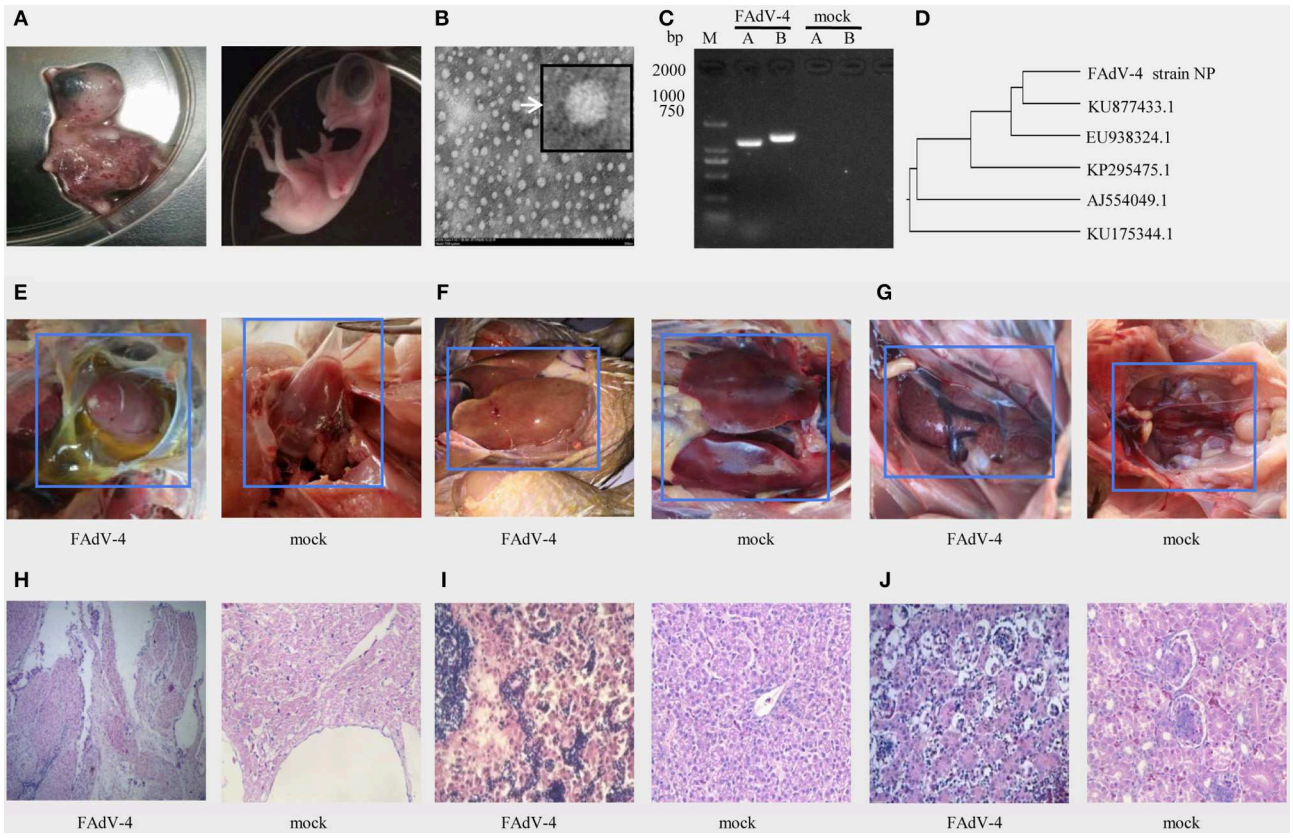

FIGURE 1 | Isolation and identification of FAdV-4 strain NP. Chickens on a layer farm in Fujian province of China were affected by an outbreak of the infectious disease. Ten-day-old specific-pathogen-free (SPF) embryonated eggs were inoculated with 200 μL of filter liquid. (**A**, left) At 24–48 h post-inoculation, the embryos died and showed severe hemorrhage. (**A**, right) The embryonated eggs in control group were inoculated with 200 μL of Sterilized saline. The allantoic fluid of chicken embryos was collected and concentrated. **(B)** The allantoic fluid was examined using electron microscopy (10,000×). **(C)** Viral serotypes were identified by PCR. **(D)** The hexon gene sequence was analyzed using a genetic evolution tree. **(E–G)** Chickens in FAdV-4 infection group (at left) and in control group (at right) were dissected and observed. Tissue sections of the heart (**H**, FAdV-4 infection at left, control group at right), liver (**I**, FAdV-4 infection at left, control group at right), and kidneys (**J**, FAdV-4 infection at left, control group at right) were prepared and stained with hematoxylin and eosin **(H,E)**. Sections were then observed microscopically (400×).

numbers and GO functions. The hypergeometric test was then applied to find GO entries that were significantly enriched in the DEGs compared with the entire genomic background.

The corrected $p \leq 0.05$ was used as the threshold, and the GO term satisfying this condition was defined as the significantly enriched GO term in the differentially expressed transcript (Wang et al., 2015; Wang Q. X. et al., 2018).

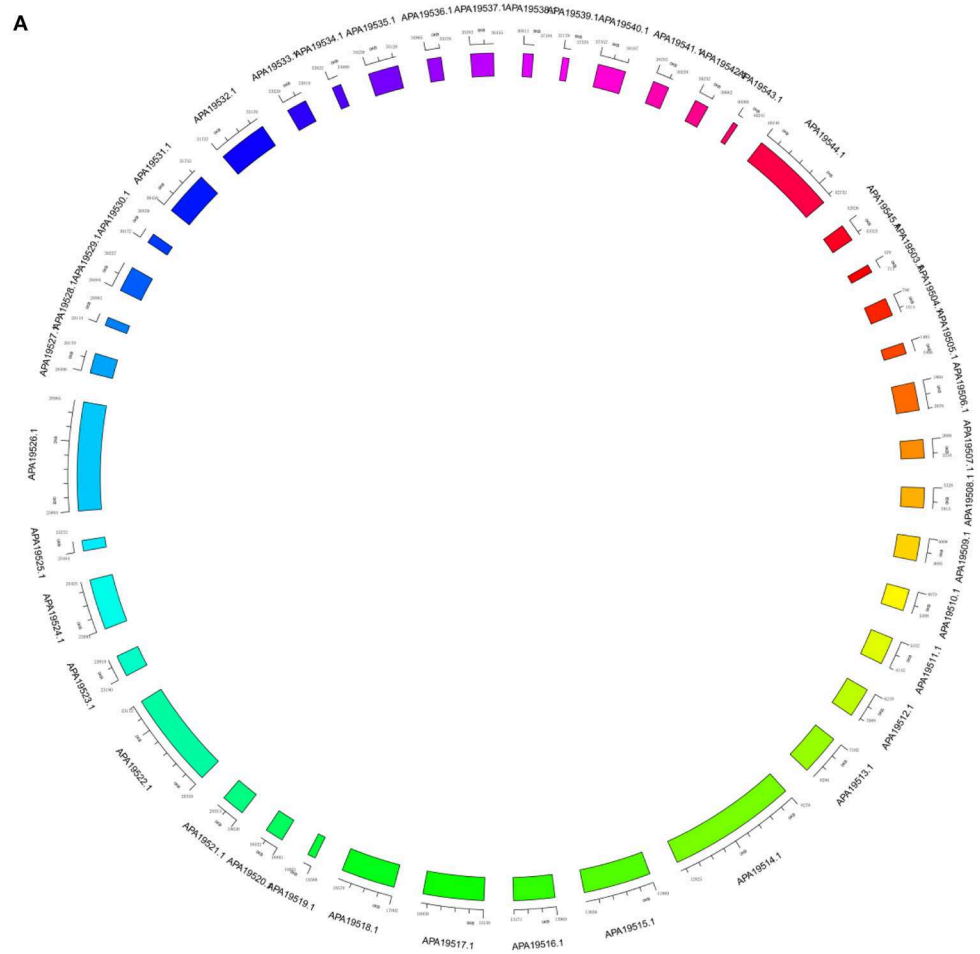

FIGURE 2 | Genome map of FAdV-4 strain NP. The sequences were compiled and edited using the SeqMan program (laser gene) to produce the whole-genome sequence of strain NP. **(A)** The genome was mapped. **(B)** The homology of FAdV-4 strain NP was analyzed through genetic evolution tree.

KEGG Enrichment Analysis

The KEGG enrichment analysis was applied to find the pathways that were significantly enriched in the differentially expressed transcripts compared with the whole genome. Pathways with a $Q \leq 0.05$ were defined as significantly enriched pathways in the differentially expressed transcripts. Significant pathway enrichment was able to identify the most important biochemical metabolic pathways and signal transduction pathways involved in the differentially expressed transcripts.

Fluorescence Quantitative PCR

In this study, we focused on the pathways associated with the process of viral infection. The mRNA expression of genes in these pathways were determined by qPCR, using specific primers (shown in **Table 2**), which were designed based on the sequences in Genebank (β-actin: X00182.1, CR: XM_015289135.2, αMβ2: XM_015289136.2, αVβ3: XM_015299304.2, MR: XM_015853441.1, F-actin: NM_001308613.2, Rab7: XM_003212919.3, TUBA: NM_001305272.1, DVnein:XM_015281907.2, VAMP-3: NM_001039489.1, VATPase: XM_004935760.3, MHCII:XM_015294966.2, MHCI:HQ141386.1, SRB1:XM_415106.4). At 24 h post-infection with FAdV4, the mRNA expression of those genes was further examined by qPCR. Furthermore, β-actin was used as a reference gene and mRNA levels were calculated using the ΔΔCT method. The mRNA expression of the *hexon* gene of FAdV4 was calculated based on a standard curve.

F-actin, *Rab7*, *TUBA*, and *DVnein* Gene Silencing

The LMH cells were prepared in 6-well plates with DMEM containing 10% fetal bovine serum at 37°C, under 5% carbon dioxide (CO_2). The F-actin-, Rab7-, TUBA-, and DVnein-specific siRNA oligonucleotides were designed (based on: F-actin: NM_001308613.2, Rab7: XM_003212919.3, TUBA: NM_001305272.1, DVnein:XM_015281907.2) and synthesized by Biomics Biotechnology Co. Ltd. (Nantong, China). The siRNA sequences were as follows: si-F-actin F:CGAUGAAGAUCAAGAUCAUdTdT, R:AUGAUCUUGAUCUUCAUCGdTdT; si-Rab7 F:CCAUGGUGUCGACCUUCUAdTdT, R:UAGAAGGUCGACACCAUGGdTdT; si-DVnein F:GAAAGAUGGAGAUGUUCAAdTdT, R:UUGAACAUCUCCAUCUUUCdTdT; and si-TUBA F:AGCUGGAGUUCUCCAUCUdTdT, R:UAGAUG

TABLE 3 | Genomic alignment results.

Samples	Control group	FAdV-4-infected
Total paired reads, number (%)	78,924,070 (100.00)	78,033,860 (100.00)
Unmapped paired reads, number (%)	11,226,317 (14.22)	19,282,033 (24.71)
Unique mapped paired reads, number (%)	67,322,232 (85.30)	58,369,327 (74.80)
Multiple mapped paired reads, number (%)	375,521 (0.48)	382,500 (0.49)
Mapping ratio (%)	85.78	75.29

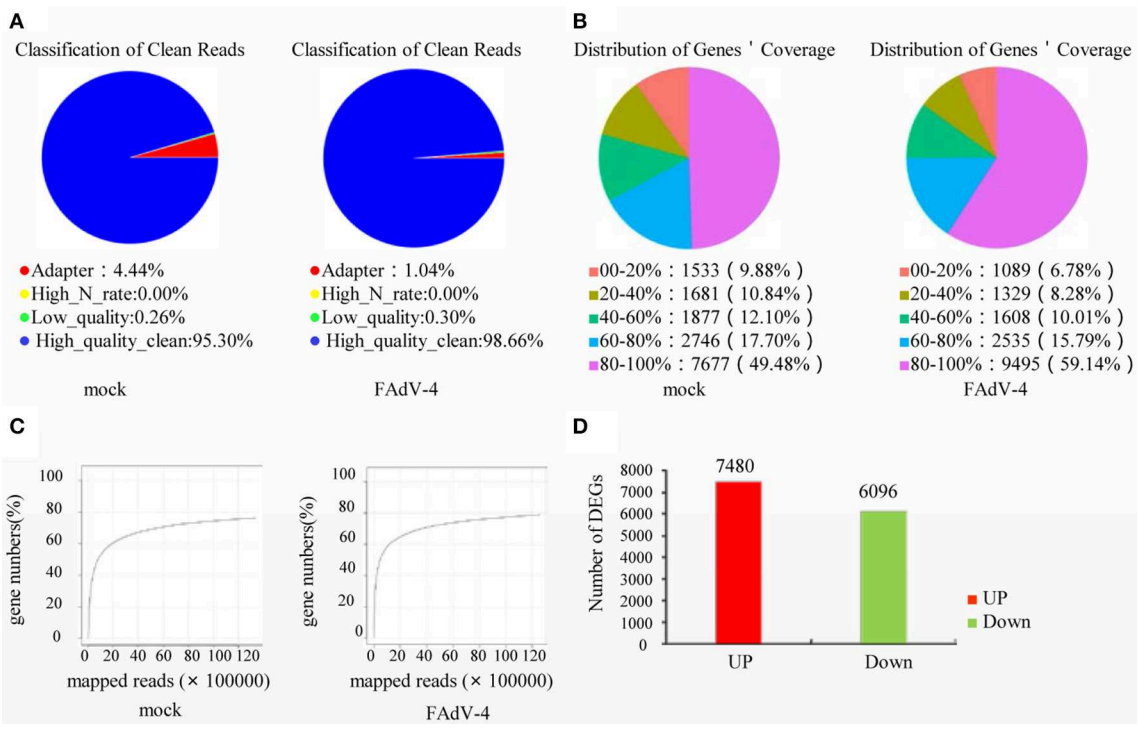

FIGURE 3 | Screening of differentially expressed genes (DEGs) in livers infected with FAdV-4. Two days after infection with FAdV-4, the genes expressed in the livers were subjected to transcription and sequencing analysis. **(A)** Classification of clean reads. **(B)** Distribution of gene coverage. **(C)** Mapped reads were evaluated in FAdV-4 infected livers and control livers. **(D)** Histogram showing screened DEGs.

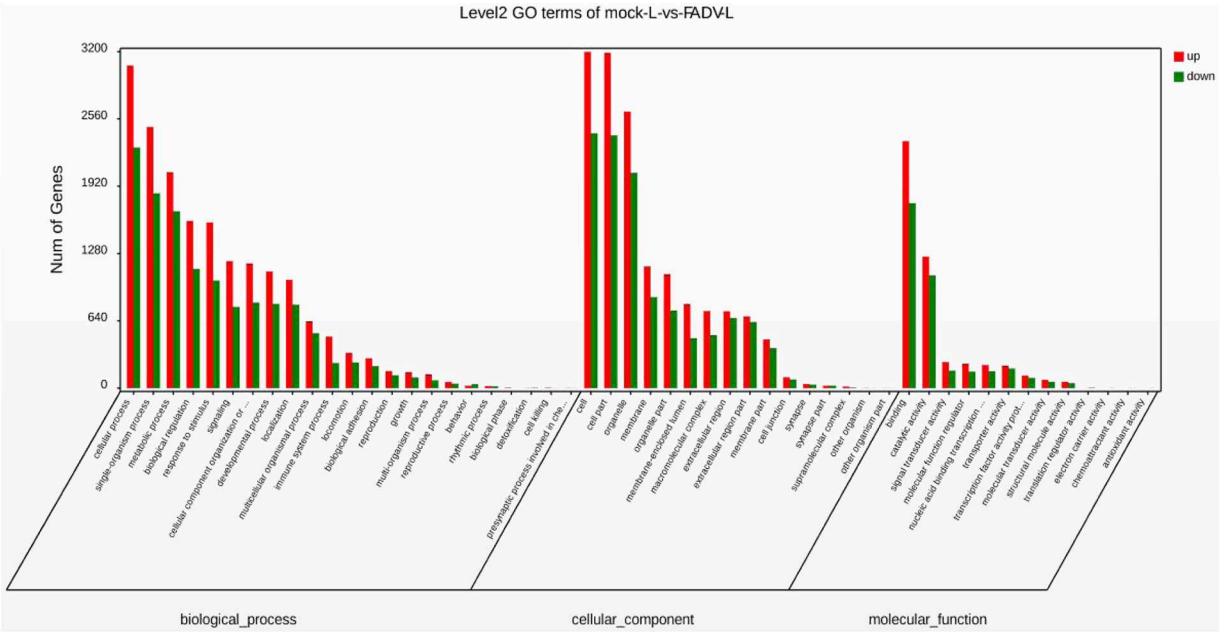

FIGURE 4 | Gene Ontology (GO) functional annotation and classification of differentially expressed genes (DEGs). Functional classification of DEGs was performed using GO analysis (http://www.geneontology.org/) and the categories "biological process," "molecular function," and "cellular component" were analyzed.

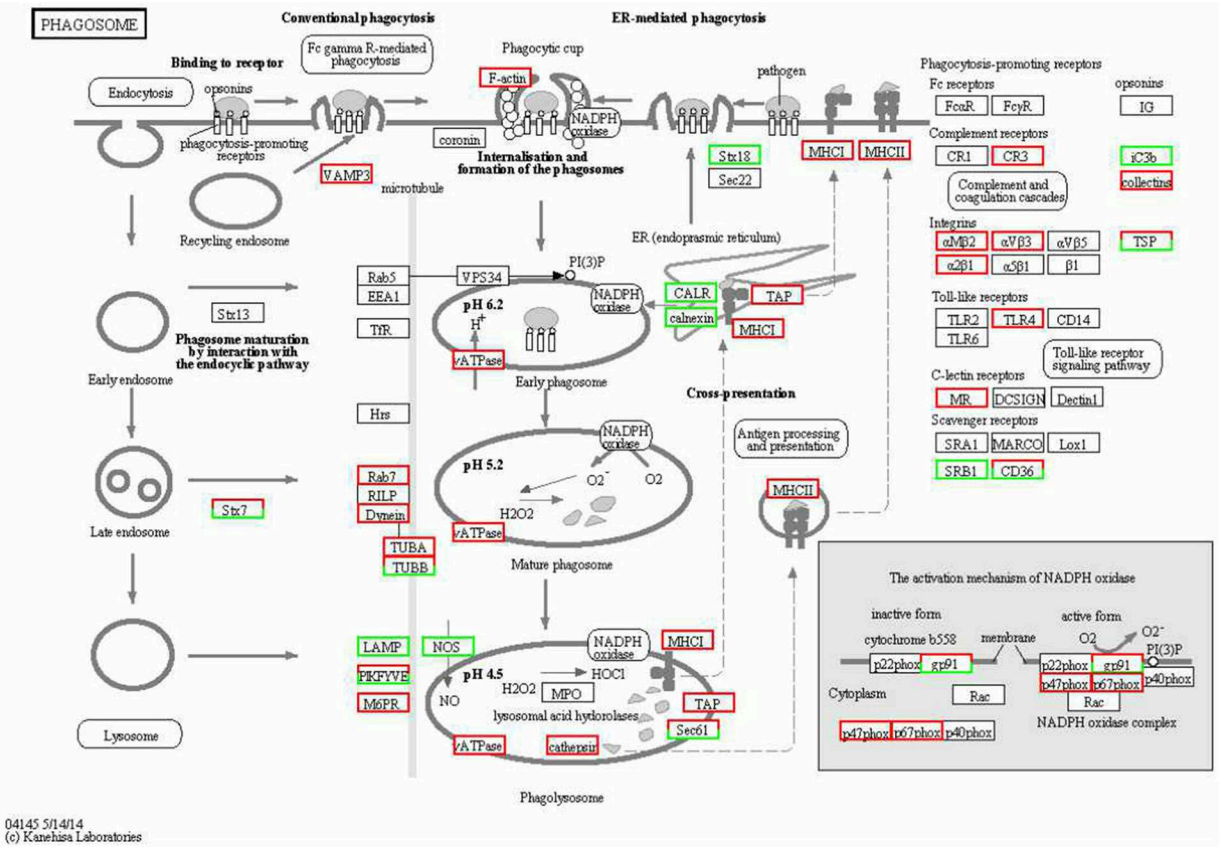

FIGURE 5 | KEGG functional annotation of differentially expressed genes (DEGs) involved in the cell phagosome pathway. A red rectangle denotes that the DEGs are significantly up-regulated [log fold change > 1, false discovery rate (FDR) < 0.001]; A green rectangle denotes that the DEGs are significantly down-regulated (log fold change > 1, FDR < 0.001) in the FAdV-4-infected liver, compared with the control liver.

GAGAACUCCAGCUdTdT. When the siRNA sequences were transfected into LMH cells for 6 h, the cells were subsequently infected with FAdV4. The mRNA levels of *F-actin, Rab7, TUBA, DVnein*, and the hexon gene of FAdV4 were detected by qPCR at 24 h post-infection.

Statistical Analysis

Statistical analyses were performed via *t*-tests or one-way analysis of variance (ANOVA) and the least significant difference (LSD) test using the SPSS 20.0 software.

RESULTS

Isolation and Identification of FAdV4 Strain NP

The results of inoculation of 10-day-old SPF chicken embryos showed that they all died 24–48 h after infection, were severely swollen, with oedema and hemorrhage (**Figure 1A** left), compared with the control embryo (**Figure 1A** right). Observation of the viral structure by electron microscopy revealed that the virus was 70–90 nm in size, spherical, non-encapsulated, and with a typical icosahedral structure (**Figure 1B**).

The PCR amplification with specific primers of the A and B fragments of the hexon gene showed specific bands around 1,219 and 1,350 bp (**Figure 1C**). The sequence of the A fragment of the hexon gene indicated that the virus was FAdV4 (**Figure 1D**).

TABLE 4 | Results of qPCR verification.

Genes	Results of expression spectrum Up (+)/Down (–)	Results of qPCR Up (+)/Down (–)	Folds
CR3	+	+	1.33 ± 0.001
αMβ2	+	+	1.95 ± 0.001
αVβ3	+	+	2.04 ± 0.001
MR	+	+	5.67 ± 0.001
F-actin	+	+	2.27 ± 0.001
Rab7	+	+	2.65 ± 0.001
TUBA	+	+	1.40 ± 0.001
DVnein	+	+	2.92 ± 0.001
VAMP-3	+	+	1.28 ± 0.001
VATPase	+	+	2.55 ± 0.001
MHCI	+	+	2.37 ± 0.001
MHCII	+	+	1.24 ± 0.001
SRB1	–	–	0.52 ± 0.001

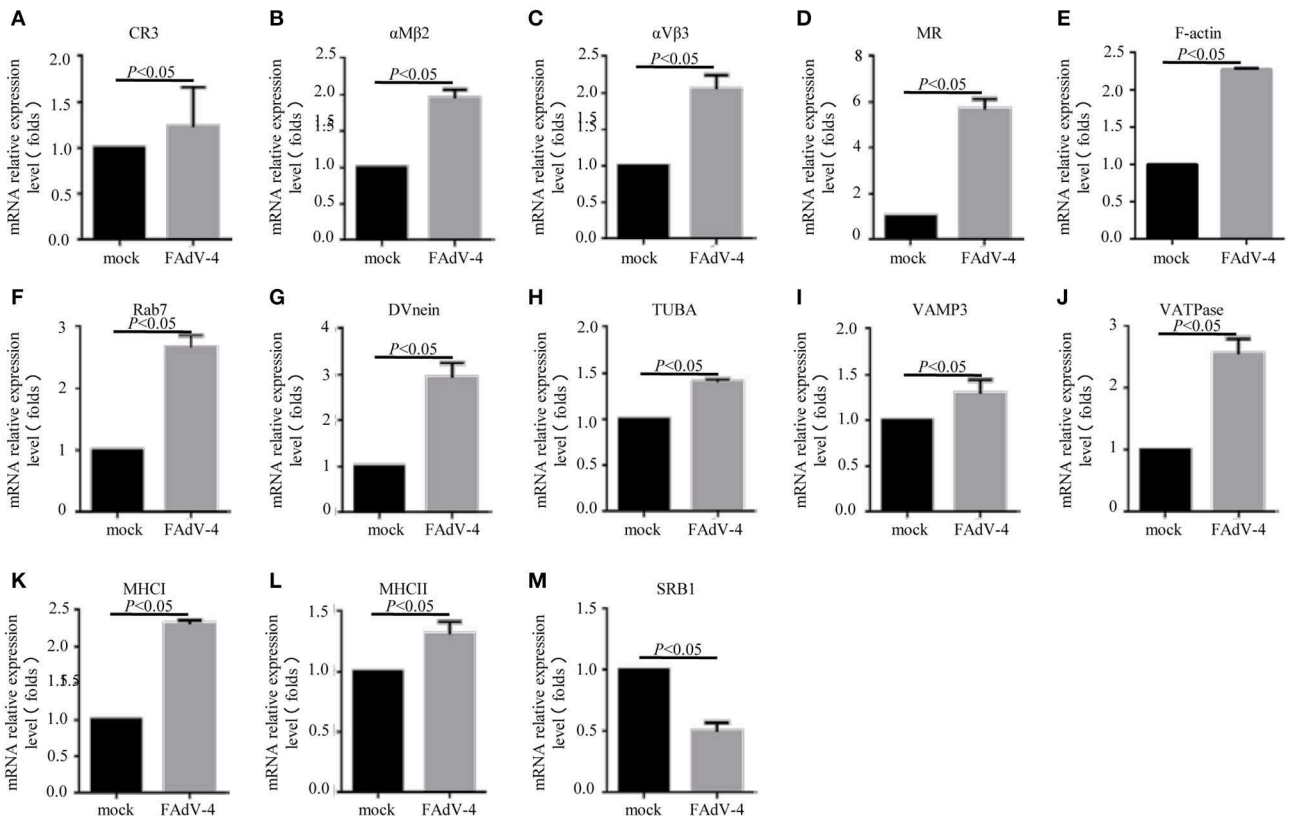

FIGURE 6 | The mRNA levels of genes involved in the phagosome pathway in the liver, as revealed by qPCR. Two days after infection with FAdV-4, the livers were collected and the mRNA levels of *CR3* **(A)**, *αMβ2* **(B)**, *αVβ3* **(C)**, *MR* **(D)**, *F-actin* **(E)**, *Rab7* **(F)**, *DVnein* **(G)**, *TUBA* **(H)**, *VATPase* **(I)**, *VATPasw* **(J)**, *MHCI* **(K)**, *MHCII* **(L)**, and *SRB1* **(M)** were detected by qPCR. All data are presented as the mean ± SE of three independent experiments. Significant differences between the treatments were determined by the Student's *t*-test, using the SPSS software (version 20.0). Label of $p < 0.05$ denotes significance between the treatments.

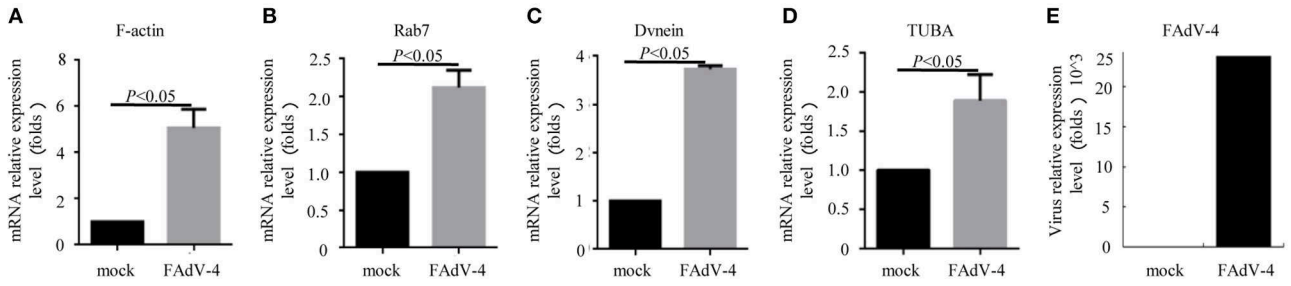

FIGURE 7 | The mRNA levels of genes involved in the cell phagosome pathway in the LMH cell line, as revealed by qPCR. LMH cells were prepared in cell culture plates; one was the control, and the other was infected with 200 μL FAdV-4. The mRNA levels of **(A)** *F-actin*, **(B)** *Rab7*, **(C)** *DVnein*, and **(D)** *TUBA* were analyzed by qPCR, 24 h after transfection with FAdV-4 **(E)**. All data are presented as the mean ± SE of three independent experiments. Significance between the treatments was determined by the Student's *t*-test using the SPSS software (version 20.0). Label of $p < 0.05$ denotes significance between the treatments.

In another animal experiment, 8 out of 9 40-day-old SPF chickens died within 3 days of being inoculated intramuscularly with the NP virus ($TCID_{50} = 10^{-6.23}$/0.01 mL), and all chickens of control treatment were alive. Pathological evaluation of the pericardial sac showed that it was filled with transparent or straw-colored fluid (**Figure 1E** left), the pericardium of the control group had no inflammatory exudate (**Figure 1E** right). And the liver-infected with FAdV-4 is swollen, embrittlement, and xanthochromia (**Figure 1F** left), compared with the control group (**Figure 1F** right). The kidney-infected with FAdV-4 showed swollen with white necrotic foci (**Figure 1G** left), compared with the control group (**Figure 1G** right). The pathological sections of hart-infected with FAdV-4 showed that there were many lymphocyte infiltration between the myocardiums (**Figure 1H** left), compared with hart in the control group (**Figure 1H** right). In the pathological section of liver-infected with FAdV-4, hepatocytes were present to degeneration and necrosis (**Figure 1I** left), compared with the livers in control group (**Figure 1I** right). And the cells in renal tubular-infected with FAdV-4 also showed degeneration and necrosis (**Figure 1J** left), compared with the kidney in control group (**Figure 1I** right).

Genomic Profile of FAdV4 Strain NP

The complete genome of FAdV4 strain NP was 43,738 bp in length (the sequence has been submitted to Genbank, the submission ID is 2266218) (**Supplemental Data 1**), with 54.9% G+C content and 42 open reading frames (ORFs) (**Figure 2A**) (the sequence has been submitted to Genbank, accession numbers MN604703 to MN604744). The FAdV4 strain NP showed a typical genome organization of FAdV-4, with two fiber genes (protein fiber-1 and fiber-2). Compared with the genomic sequences of other published FAdV-4 strains, 98.3–100% homology was observed at the nucleotide level. The NP strain was most closely matched to the CH/HNJZ2015 strain, isolated in China in 2015 (**Figure 2B**).

DEG Screening in the Livers Infected With FAdV-4

Based on the results of the sequencing quality evaluation, the high-quality clean reads in the two groups were all higher than 95.00% (**Figure 3A**). The distribution of gene coverage in the control group was up to 49.48%, and up to 59.14% in the FAdV4-infected group (**Figure 3B**). The mapped reads were >60% (**Figure 3C**). These results indicated that the sequencing quality in the livers of the two groups were favorable for further study. In the current study, the genome of Gallus gallus-5.0 (chicken) (GRCg6a, GCF_000002315. 6, https://www.ncbi.nlm.nih.gov/genome/?term=Gallus%20 domesticus) was as our reference genome. A total of 78,924,070 paired reads were detected in the control livers and 78,033,860 paired reads in the livers infected with FAdV-4. The mapping ratio in the control was 85.78%, and in livers infected with FAdV-4, 75.29% (**Table 3**). And a total of 26,512 transcripts were annotated in the control livers and 28,708 in the livers infected with FAdV 4 strain NP. In the current study, 10,024 novel annotation transcript were found in the control livers and 10,567 in the livers infected with FAdV 4 strain NP (the sequence of novel annotation transcript has been submitted to Genbank, the submission ID is 6338149).

A total of 13,576 DEGs were then screened from the livers infected with FAdV-4 and compared with the control livers. These DEGs included 7,480 up-regulated unigenes and 6,096 down-regulated unigenes (**Figure 3D**).

GO Functional Classification

The GO functional classification of the 13,576 unigenes revealed three categories: "biological processes," "cellular compounds," and "molecular function." As shown in **Figure 4**, the numbers of up-regulated unigenes and down-regulated unigenes in "cell processes" were highest in "biological processes." Furthermore, the numbers of up-regulated unigenes and down-regulated unigenes in "cell" were highest in the category of "cellular compounds." In the category of "molecular function," the DEGs associated with binding were the highest in number (**Figure 4**).

KEGG Enrichment Analysis and Real-Time qPCR Confirmation

The KEGG enrichment analysis helped us to further understand the biological functions of DEGs. We found that the *Q*-value of the phagosome was significantly up-regulated (**Figure 5**). The mRNA levels of *CR3, αMβ2, αVβ3, α2β1, TLR4, MR, F-actin, Rab7, TUBA, DVnein, VATPase, VAMP-3, MHCI*, and

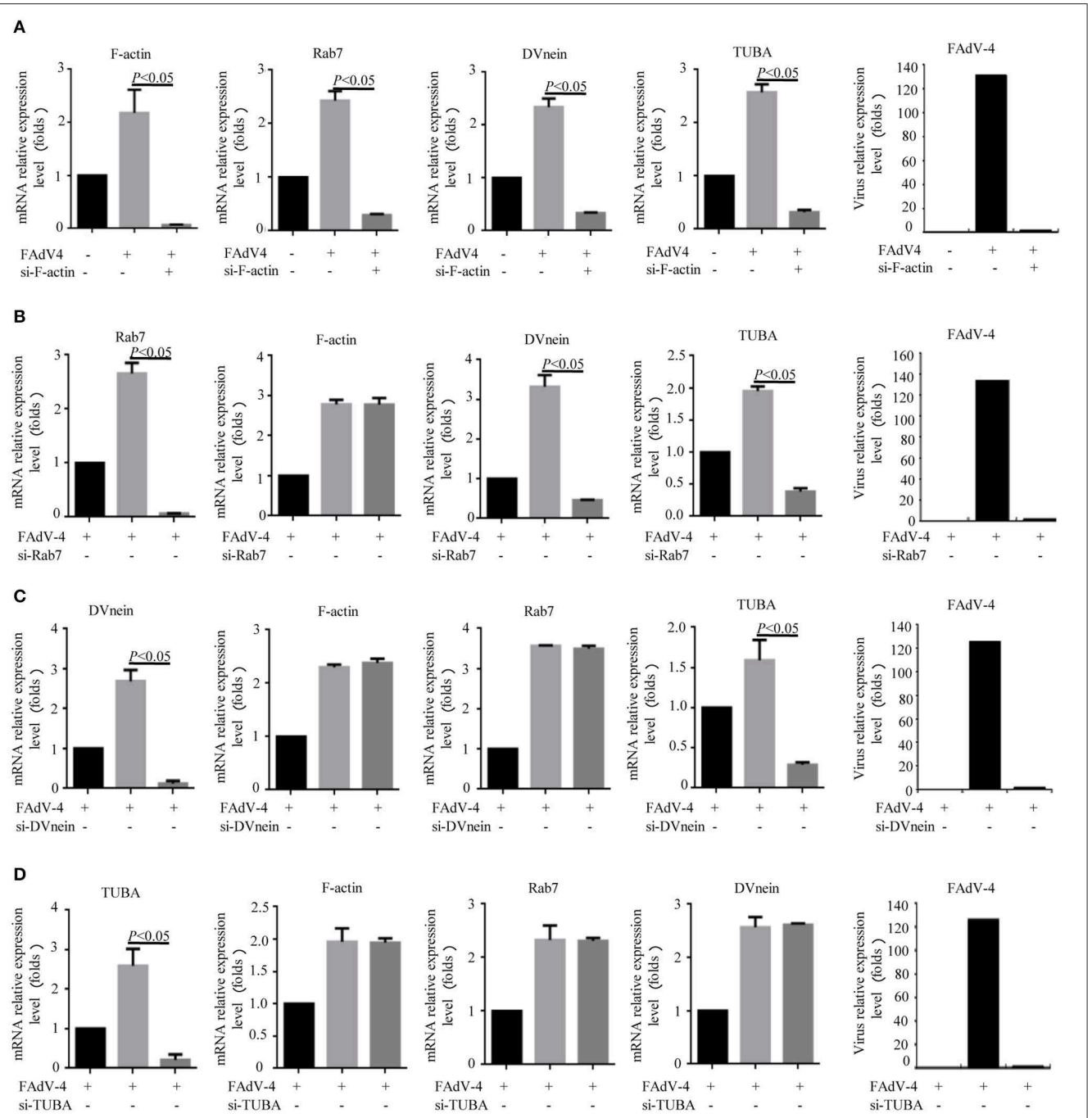

FIGURE 8 | Knockdown of *F-actin, Rab7, DVnein*, and *TUBA* reduced replication of FAdV-4. LMH cells were cultured in 6-well-plates for 24 h. Three treatments were conducted. One was the control group, in which cells were siRNA and FAdV-4 free. The second, was the FAdV-4 infection group, in which cells were infected with FAdV-4 but siRNA free. The third group was transfected with **(A)** si-F-actin, **(B)** si-Rab7, **(C)** si-DVnein, and **(D)** si-TUBA, respectively, and 6 h after transfection, cells were infected with FAdV-4. At 24 h post-infection, all cells were collected. The mRNA levels of *F-actin, Rab7, DVnein,* and *TUBA* were determined by real-time fluorescent quantitative (fq)-PCR. All data are presented as the mean ± SE of three independent experiments. Significance between the treatments was determined by the Single factor analysis of variance and least-significant different multiple comparison using the SPSS software (version 20.0). Label of $p < 0.05$ denotes significance between the treatments.

MHCII were significantly up-regulated in FAdV-4 infected livers, compared with the control livers.

In order to confirm the DEGs levels, we evaluated the mRNA levels of *CR3, αMβ2, αVβ3, MR, F-actin, Rab7, TUBA, DVnein, VAMP-3, VATPase, MHCI, MHCII*, and *SRB1* in livers infected with FAdV-4 strain NP. After infection, the mRNA levels of *CR3, αMβ2, αVβ3, MR, F-actin, Rab7, TUBA, DVnein, VAMP-3, VATPase, MHCI*, and *MHCII* were up-regulated and the mRNA

level of *SRB1* was down-regulated (**Figures 6A–M**). These results were consistent with those of the KEGG analysis (**Table 4**).

F-actin, *Rab7*, *TUBA*, and *DVnein* Gene Silencing Reduced the Replication of FAdV-4

Firstly, 24 h after LMH cells were infected with FAdV-4, the mRNA levels of *F-actin, Rab7, TUBA*, and *DVnein* were significantly up-regulated (**Figures 7A–E**). The four genes were then silenced by RNA interference. The results indicated that when *F-actin* was silenced, the mRNA levels of *Rab7*, *TUBA*, and *DVnein* were reduced, as the viral load declined (**Figure 8A**). When *Rab7* was silenced, the mRNA level of *F-actin* showed no decline, but the mRNA levels of *TUBA* and *DVnein* were both reduced, as the viral load declined (**Figure 8B**). In addition, we found that when *TUBA* was silenced, the mRNA levels of *DVnein* were reduced, as the viral load declined (**Figure 8C**). The viral load of FAdV-4 declined after silencing of the *DVnein* gene (**Figure 8D**). These results further indicated that genes of *F-actin*, *Rab7*, *TUBA*, and *DVnein* in KEGG pathway of phagosome was used to facilitate FAdV-4 invasion.

DISCUSSION

Hydropericardium syndrome (HPS) is an infectious viral disease in chickens, 3–5 weeks of age. The first outbreak was reported in Angara Goth, Pakistan in 1987 (Asthana et al., 2013). It is characterized by hydropericardium and hepatic necrosis. Reports indicated that broiler birds are more susceptible to infection (Dahiya et al., 2002). In the current study, we isolated a virulent strain of FAdV-4 from sick pre-laying hens, which also had typical hydropericardium and hepatic necrosis.

Virus would attach to target cells after they pass through the extracellular medium. F-actin reinforces the plasma membrane and imposes a barrier toward the outside of the cell (Wang I. H. et al., 2018). The F-actin participates the formation of endocytic pits and vesicles, which often is used by virus to bind to cell extensions (Mercer and Helenius, 2009). Then virus transmits forward signals into cells and prepares to endocytic uptake and infection (Greber, 2002). F-actin is required when the endocytic vesicles containing the virus separate from the plasma membrane (Liu et al., 2016). Furthermore, Rab7 mediates the process by which endocytic vesicles are transported to the lysosome (mature phagosome) (Suwandittakul et al., 2017). If the virus is released from, or is able to escape the lysosome, it would enter the nucleus. However, it requires the assistance of a motor protein and tubulin, such as TUBA and the DVnein protein (Leopold et al., 2000). Nevertheless, the detailed mechanisms by which FAdV-4 invasion and intracellular trafficking in host cells occur, require further investigation.

Transcriptome analysis provides a novel research tool that may reveal the interactions between host and virus (Wang et al., 2015). Researchers have revealed new insights into the host immune response to Muscovy duck reovirus (MDRV) infection using transcriptome analysis (Wang et al., 2015). They then elucidated the molecular mechanism of hepatic steatosis induced by MDRV (Wang Q. X. et al., 2018).

In the present study, our team found 13,576 DEGs that were screened in livers infected with FAdV-4. These DEGs were involved in "biological processes," "cellular compounds," and "molecular function." The KEGG analysis revealed that the phagosome pathway was significantly up-regulated. The DEGs in that pathway were evaluated against by qPCR, and results supported the KEGG analysis. Then four genes as *F-actin, Rab7, TUBA*, and *DVnein* in phagosome pathway, were determined in LMH cells-infected with FAdV-4 by qPCR and RNAi, results also supported the KEGG analysis. The DEGs in phagosome pathway are involved in the formation of a phagocytic cup, intracellular trafficking along microtubules, and the internalization and formation of phagosomes. But how FAdV-4 regulates these genes to contribute its proliferation need to further investigation.

CONCLUSION

In this study, the FAdV-4 strain NP was isolated from sick young hens. And transcriptome analysis revealed that the KEGG pathway of phagosome was used to facilitate FAdV-4 invasion.

DATA AVAILABILITY STATEMENT

The raw data generated during this study has been submitted to genbank, accession numbers MN604703 to MN604744, SRR10350642.

ETHICS STATEMENT

The animal study was reviewed and approved by Research Ethics Committee of the College of Animal Science, Fujian Agriculture and Forestry University.

AUTHOR CONTRIBUTIONS

All authors listed have made a substantial, direct and intellectual contribution to the work, and approved it for publication.

FUNDING

This work was supported by the China Fujian Natural Science Foundation under Grant number 2019J0658, the China Fujian Avian Industry System Program (2019–2022), and the opening program of Fujian Provincial Key Laboratory for the Prevention and Control of Animal Infectious Diseases and Biotechnology (2019KF03).

SUPPLEMENTARY MATERIAL

The Supplementary Material for this article can be found online at: https://www.frontiersin.org/articles/10.3389/fmicb.2020.00146/full#supplementary-material

REFERENCES

Asthana, M., Chandra, R., and Kumar, R. (2013). Hydropericardium syndrome: current state and future developments. *Arch. Virol.* 158, 921–931. doi: 10.1007/s00705-012-1570-x

Audic, S., and Claverie, J. M. (1997). The significance of digital gene expression profiles. *Genome. Res.* 7, 986–995. doi: 10.1101/gr.7.10.986

Chandra, R., Shukla, S. K., and Kumar, M. (2000). The hydropericardium syndrome and inclusion body hepatitis in domestic fowl. *Trop. Anim. Health Prod.* 32, 99–111. doi: 10.1023/A:1005230703093

Dahiya, S., Srivastava, R. N., Hess, M., and Gulati, B. R. (2002). Fowl adenovirus serotype 4 associated with outbreaks of infectious hydropericardium in Haryana, India. *Avian Dis.* 46, 230–233. doi: 10.1637/0005-2086(2002)046[0230:FASAWO]2.0.CO;2

Greber, U. F. (2002). Signalling in viral entry. *Cell. Mol. Life Sci.* 59, 608–626. doi: 10.1007/s00018-002-8453-3

Griffin, B. D., and Nagy, E. (2011). Coding potential and transcript analysis of fowl adenovirus 4: insight into upstream ORFs as common sequence features in adenoviral transcripts. *J. General Virol.* 92, 1260–1272. doi: 10.1099/vir.0.030064-0

Hess, M. (2000). Detection and differentiation of avian adenoviruses: a review. *Avian Pathol.* 29, 195–206. doi: 10.1080/03079450050045440

Horvath, C. J., Simon, M. A., Bergsagel, D. J., Pauley, D. R., King, N. W., Garcea, R. L., et al. (1992). Simian virus 40-induced disease in rhesus monkeys with simian acquired immunodeficiency syndrome. *Am. J. Pathol.* 140, 1431–1440.

Kim, J. N., Byun, S. H., Kim, M. J., Kim, J. J., Sung, H. W., and Mo, I. P. (2008). Outbreaks of hydropericardium syndrome and molecular characterization of Korean fowl adenoviral Isolates. *Avian Dis.* 52, 526–530. doi: 10.1637/8178-112207-Case

Leopold, P. L., Kreitzer, G., Miyazawa, N., Rempel, S., Pfister, K. K., Rodriguez-Boulan, E., et al. (2000). Dynein- and microtubule-mediated translocation of adenovirus serotype 5 occurs after endosomal lysis. *Hum. Gene Ther.* 11, 151–165. doi: 10.1089/104303400500 16238

Liu, Z., Ning, G., Xu, R., Cao, Y., Meng, A., and Wang, Q. (2016). Fscn1 is required for the trafficking of TGF-β family type I receptors during endoderm formation. *Nat. Commun.* 7:12603. doi: 10.1038/ncomms12603

Mercer, J., and Helenius, A. (2009). Virus entry by macropinocytosis. *Nat. Cell Biol.* 11, 510–520. doi: 10.1038/ncb0509-510

Mittal, D., Jindal, N., Tiwari, A. K., and Khokhar, R. S. (2014). Characterization of fowl adenoviruses associated with hydropericardium syndrome and inclusion body hepatitis in broiler chickens. *Virus Dis.* 25, 114–119. doi: 10.1007/s13337-013-0183-7

Shah, M. A., Ullah, R., De March, M., Shah, M. S., Ismat, F., Habib, M., et al. (2017). Overexpression and characterization of the 100K protein of Fowl adenovirus-4 as an antiviral target. *Virus Res.* 238, 218–225. doi: 10.1016/j.virusres.2017.06.024

Suwandittakul, N., Reamtong, O., Molee, P., Maneewatchararangsri, S., Sutherat, M., Chaisri, U., et al. (2017). Disruption of endocytic trafficking protein Rab7 impairs invasiveness of cholangiocarcinoma cells. *Cancer Biomark.* 20, 255–266. doi: 10.3233/CBM-170030

Toscano, M. G., and de Haan, P. (2018). How Simian Virus 40 Hijacks the intracellular protein trafficking pathway to its own benefit … and ours. *Front. Immunol.* 9:1160. doi: 10.3389/fimmu.2018.01160

Wang, I. H., Burckhardt, C. J., Yakimovich, A., and Greber, U. F. (2018). Imaging, tracking and computational analyses of virus entry and egress with the cytoskeleton. *Viruses* 10:E166. doi: 10.3390/v10040166

Wang, Q. X., Liu, M. X., Chen, Y., Xu, L. H., Wu, B. C., Wu, Y. J., et al. (2019). Muscovy duck reovirus p10.8 protein induces ER stress and apoptosis through the Bip/IRE1/XBP1 pathway. *Vet. Microbiol.* 228, 234–245. doi: 10.1016/j.vetmic.2018.12.011

Wang, Q. X., Liu, M. X., Xu, L. H., Wu, Y. J., and Huang, Y. F. (2018). Transcriptome analysis reveals the molecular mechanism of hepatic fat metabolism disorder caused by Muscovy Duck Reovirus infection. *Avian Pathol.* 47, 127–139. doi: 10.1080/03079457.2017.13 80294

Wang, Q. X., Wen, Y. P., Huang, Y. F., Wu, Y. J., Cai, Y. L., Xu, L. H., et al. (2014). Isolation and identification of Duck Tembusu Virus Strain LH and development of latex-agglutination diagnostic method for rapid detection of antibodies. *Avian Dis.* 58, 616–622. doi: 10.1637/10795-021114-Reg

Wang, Q. X., Wu, Y. J., Cai, Y. L., Zhuang, Y. B., Xu, L. H., Wu, B. C., et al. (2015). Spleen transcriptome profile of Muscovy ducklings in response to infection with Muscovy duck reovirus. *Avian Dis.* 59, 282–290. doi: 10.1637/10992-112514-Reg

Conflict of Interest: The authors declare that the research was conducted in the absence of any commercial or financial relationships that could be construed as a potential conflict of interest.

Copyright © 2020 Chen, Huang, Qu, Peng, Xu, Wang, Huang and Wang. This is an open-access article distributed under the terms of the Creative Commons Attribution License (CC BY). The use, distribution or reproduction in other forums is permitted, provided the original author(s) and the copyright owner(s) are credited and that the original publication in this journal is cited, in accordance with accepted academic practice. No use, distribution or reproduction is permitted which does not comply with these terms.

frontiers in Microbiology

ORIGINAL RESEARCH
published: 20 February 2020
doi: 10.3389/fmicb.2020.00260

A Long Non-coding RNA IVRPIE Promotes Host Antiviral Immune Responses Through Regulating Interferon β1 and ISG Expression

Lingna Zhao[1], Min Xia[1], Keyu Wang[1], Chengcai Lai[1], Hongxia Fan[1], Hongjing Gu[1], Penghui Yang[2] and Xiliang Wang[1]**

[1] State Key Laboratory of Pathogen and Biosecurity, Beijing Institute of Microbiology and Epidemiology, Beijing, China, [2] The Fifth Medical Center of Chinese PLA General Hospital, Beijing, China

Accumulating studies have shown that long non-coding RNAs (lncRNAs) modulate multiple biological processes, including immune response. However, the underlying mechanisms of lncRNAs regulating host antiviral immune response are not well elucidated. In this study, we report that analysis of the existing dataset transcriptome of blood immune cells of patients with influenza A virus (IAV) infection and after recovery (GSE108807) identified a novel lncRNA, termed as IVRPIE (Inhibiting IAV Replication by Promoting IFN and ISGs Expression), was involved in antiviral innate immunity. *In vitro* studies showed that IVRPIE was significantly upregulated in A549 cells after IAV infection. Gain-and-loss of function experiments displayed that enforced IVRPIE expression significantly inhibited IAV replication in A549 cells. Conversely, silencing IVRPIE promoted IAV replication. Furthermore, IVRPIE positively regulates the transcription of interferon β1 and several critical interferon-stimulated genes (ISGs), including IRF1, IFIT1, IFIT3, Mx1, ISG15, and IFI44L, by affecting histone modification of these genes. In addition, hnRNP U was identified as an interaction partner for IVRPIE. Taken together, our findings suggested that a novel lncRNA IVRPIE is a critical regulator of host antiviral response.

Keywords: lncRNA – long non-coding RNA, IFNβ1, IAV, ISGs, IVRPIE

OPEN ACCESS

Edited by:
Ian M. Jones,
University of Reading,
United Kingdom

Reviewed by:
Dahlene N. Fusco,
Tulane University, United States
David Olagnier,
Aarhus University, Denmark

****Correspondence:***
Penghui Yang
ypenghuiamms@hotmail.com
Xiliang Wang
xiliangw@126.com

Specialty section:
This article was submitted to Virology, a section of the journal Frontiers in Microbiology

Received: *15 October 2019*
Accepted: *04 February 2020*
Published: *20 February 2020*

Citation:
Zhao L, Xia M, Wang K, Lai C, Fan H, Gu H, Yang P and Wang X (2020) A Long Non-coding RNA IVRPIE Promotes Host Antiviral Immune Responses Through Regulating Interferon β1 and ISG Expression. Front. Microbiol. 11:260. doi: 10.3389/fmicb.2020.00260

INTRODUCTION

Influenza A virus (IAV) infection poses great challenges to the public health (Neumann et al., 2009). Numerous researches attempted to explore the mechanisms of host antiviral immune responses. The innate immune system builds the first line defense against IAV infection. The initial sensing of IAV infection is mediated by innate pattern recognition receptors (PRRs), such as retinoic acid-inducible gene I (RIG-I), melanoma differentiation factor 5 (MDA5), and toll-like receptor 3 (TLR3) (Alexopoulou et al., 2001; Kato et al., 2005; Gitlin et al., 2006; Takeuchi and Akira, 2010). After sensing IAV infection, they signal through different adaptor proteins, MAVS or TRIF, to activate two cytosolic protein kinase complexes, one consisting of IKKα, IKKβ and NEMO, and the other comprising TBK1 (TANK-binding kinase 1) or IKK-i/ε. The IKKα, IKKβ and NEMO complex subsequently free NF-κB to translocate into the nucleus and activate expression of proinflammatory cytokine genes. And the TBK1 complex leads to phosphorylation and dimerization of the transcription factors IRF3 and IRF7, which translocate to the nucleus, triggering a rapid production of type I IFN genes (Kawai et al., 2005; Seth et al., 2005;

Takeuchi and Akira, 2010). Then type I IFN stimulates cells to initiates a signaling cascade that leads to phosphorylation and heterodimerization of STAT1 and STAT2, which interact with IRF9 to form ISGF3, regulating the synthesis of many IFN-stimulated genes (ISGs), including IRF1, IFIT1, IFIT3, Mx1, ISG15, and IFI44L, serving as an essential primary barrier for virus infection (Darnell et al., 1994; Kotenko et al., 2003; Stark and Darnell, 2012; Au-Yeung et al., 2013).

Although cell signaling pathways of host antiviral immune responses have been well understood, the majority of studies have focused on the function of proteins, and less is known about the roles of RNA in this process. In the past two decades, studies have demonstrated that thousands of non-coding RNAs are universally transcribed from the Genome, one of which is classified as long non-coding RNAs (lncRNAs) (Kapranov et al., 2002, 2007; Birney et al., 2007; Djebali et al., 2012). LncRNAs are generally defined as transcripts longer than 200 nucleotides that lack protein-coding potential (Derrien et al., 2012; Djebali et al., 2012). Accumulating data indicate that lncRNAs play essential roles in nearly every biological process, including transcription, splicing, translation, imprinting, cell "stemness," differentiation, adaptation and death (Mercer et al., 2009; Johnsson et al., 2014). Recent studies have found that lncRNAs also have important roles in host immune response (Atianand and Fitzgerald, 2014; Chen et al., 2017). In viral infections, several lncRNAs were reported to regulate viral replication. For example, 7SL and NEAT1 are involved in modulating HIV-1 posttranscriptional expression (Wang et al., 2007; Zhang et al., 2013). NRAV and lnc-ISG20 were found to affect IAV replication and virulence (Ouyang et al., 2014; Chai et al., 2018). CCR5AS can diminish infection of $CD4^+$ T cells with HIV (Kulkarni et al., 2019). However, the vast majority of lncRNAs during IAV replication remain uncharacterized.

In this study, we defined a novel human lncRNA, termed as IVRPIE, as a critical regulator in anti-IAV infection. A549 cells with IAV infection upregulated IVRPIE, compared with control cells. *In vitro* data revealed that IVRPIE served the function of antiviral activity by promoting IFNβ1 and several ISG production. Furthermore, we found that IVRPIE promoted the expression of these genes through affecting chromatin remodeling at their transcription starting site by interaction with heterogeneous nuclear ribonuclear protein U (hnRNP U). These results demonstrate that IVRPIE is a positive regulator of IFNβ1 and ISG expression, establishing a critical role in host innate defense during the IAV infection.

MATERIALS AND METHODS

Cell Lines and Virus Strains

Human lung adenocarcinoma epithelial cells (A549) and human bronchial epithelium BEAS-2B cells were grown in F12 supplemented with 10% (vol/vol) FBS (Royacel) and antibiotics (penicillin and streptomycin) (Invitrogen) at 37°C under 5% CO_2 concentration. Madin-Darby canine kidney (MDCK) cells and BabyHamster Syrian Kidney (BHK21) cells were grown in DMEM supplemented with 10% (vol/vol) FBS (Royacel) and antibiotics (penicillin and streptomycin) (Invitrogen).

A/Beijing/501/2009 (H1N1; BJ501), A/Puerto Rico/8/34 (H1N1; PR8), A/Singapore/INFIMH-16-0019/2016 (H3N2; SI16) and Sendai virus (SeV) were propagated in embryonated chicken eggs. VSV New Jersey (VSNJV) and VSV Indiana (VSIV) were propagated in BHK21 cells. Respiratory Syncytial Virus (RSV) was propagated in Hep2 cells. Adenovirus was propagated in Vero cells.

All of the experimental protocols used in this study were approved by the Institutional Animal Care and Use Committees of the Beijing Institute of Microbiology and Epidemiology (permit number: SYXK2015-008). And all of the experiments were performed in strict accordance with the approved guidelines.

Antibodies and Reagents

The antibodies used were IRF-1 (8478S, Cell Signaling), IFIT1 (14769S, Cell Signaling), IFIT3 (sc-393512, Santa Cruz Biotechnology), Mx1 (37849S, Cell Signaling), ISG15 (2758T, Cell Signaling), IFI44L (HK7931, Hushi Pharmaceutical Technology), Tri-Methyl-Histone H3 (Lys27) (C36B11) Rabbit mAb (9733, Cell Signaling), Tri-Methyl-Histone H3 (Lys4) (C42D8) Rabbit mAb (9751, Cell Signaling), anti-rabbit IgG, HRP-linked antibody (7074P2, Cell Signaling), anti-mouse IgG, HRP-linked antibody (7076P2, Cell Signaling). Anti-A/California/7/2009-like HA serum (sheep 606 and 610) (14/310) was purchased from National Institute for Biological Standards and Control (NIBSC). Anti-sheep IgG, HRP-linked antibody (F030231) was purchased from Beijing BioRab Technology. Mouse anti-hnRNP U monoclonal antibody (ab10297) was purchased from Abcam.

Polyinosinic-polycytidylic acid sodium salt (P9582) was purchased from Sigma-Aldrich. Human IFN-β (10704-H02H) was purchased from Sino Biological. MRT67307 HCl (T5162) and Pyrrolidinedithiocarbamate ammonium (T3147) were purchased from TargetMol.

Plasmids, siRNAs, and ASOs

The IVRPIE gene was cloned into the pcDNA 3.1(+) plasmid. Primers used in RT-PCR were listed in **Supplementary Table S1**.

IVRPIE-specific Antisense oligonucleotides (ASOs), and negative control ASO were synthesized by Guangzhou RiboBio Co., Ltd. (RiboBio). The targeting sequences of the ASOs were as follows: ASO1: GCACTACACTCTTGGCATAT; ASO2: ACCTATCCCGTGCTGTAAAT. hnRNP U-specific siRNAs and negative control siRNAs were synthesized by GenePharma Ltd. The targeting sequence of the hnRNP U-specific siRNA was as follows: hnRNP U-2443: CGUGGUAGUUACUCAAACATT, negative control: UUCUCCGAACGUGUCACGUTT. ASOs and siRNAs were transfected into A549 cells using Lipofectamine 3000 (Invitrogen) according to the manufacturer's instructions.

Bioinformatics Analysis of Non-coding Potential

Non-coding potential of IVRPIE was analyzed by coding potential calculator 2[1] (Kang et al., 2017).

[1] http://cpc2.cbi.pku.edu.cn

Quantitative PCR

RNA was extracted from A549 cells using TRIzol Reagent (Invitrogen) according to the manufacturer's instructions. cDNA was synthesized from total RNA using TransScript First-Strand cDNA Synthesis SuperMix (TransGen Biotech) and subjected to quantitative PCR using UltraSYBR Mixture (Low ROX) (CW2601M, ComWin Biotech) performed on QuantStudio 6 Flex system (ABI). Primers used in quantitative PCR were listed in **Supplementary Table S1**. The relative amounts of the tested RNAs were calculated using the $2^{-\Delta\Delta Ct}$ method against GAPDH.

Rapid Amplification of cDNA Ends (RACE)

RACE of IVRPIE was performed using a SMARTer™ RACE cDNA Amplification Kit (Clontech) according to the manufacturer's instructions. The primers for IVRPIE 5′ RACE were as follows: IVRPIE outer R, 5′-TCTGTGGTGCACATGC TGTCTTCCGT-3′ and IVRPIE inner R, 5′-GATTACGCC AAGCTTAAGCATTTCCCGAGTTTGCTGGAACACA-3′. The primers for IVRPIE 3′ RACE were as follows: IVRPIE outer F, 5′-GATGAGAAGTCTGAGGCTTTACCTAAACTTCA-3′ and IVRPIE inner F, 5′- AAACTTATGATTAAAGGCTTCTA CGTACTCA-3′.

Plaque Forming Assay (PFU), HA Assay and 50% Tissue Culture Infectious Dose ($TCID_{50}$) Assay

For plaque forming assay, MDCK cells were seeded in 6-well plates and infected with serial dilutions of virus in serum-free DMEM for 1 h. Then, the cells were supplemented with DMEM containing 1% agarose (Promega) and 2 μg/mL of TPCK-trypsin. After the agar solidified at 4°C, plates were incubated upside-down at 37°C for 5 days. Then the virus plaques were stained with 1% crystal violet and counted, and PFUs of the virus were determined. For HA assay, the supernatants of cell culture were diluted with physiological saline and mixed with an equal volume of 1% chicken erythrocytes. The viral titers were counted from the highest dilution factors that produced a positive reading (Wang et al., 2012). For $TCID_{50}$ assay, BHK21 cells were seeded in 96-well cell culture plates and infected with serial 10-fold dilutions of VSNJV made in DMEM medium containing 2% (vol/vol) FBS for 48 h. Then cytopathic effect (CPE) of each of the wells of the plate was examined and $TCID_{50}$ was calculated by Reed-Muench method.

Western Blotting

Cells were washed once by ice-cold PBS, and then were lysed using RIPA buffer (R0010, Solarbio) containing Phenylmethanesulfonyl fluoride (PMSF) (P0100, Solarbio). Proteins were separated by SDS-PAGE, and then transferred onto PVDF membrane (Roche Diagnostics). PVDF membranes were incubated with the following diluted primary antibodies: Anti-A/California/7/2009-like HA serum (sheep 606 and 610) (14/310, NIBSC), IRF-1 (8478S, Cell Signaling), IFIT1 (14769S, Cell Signaling), IFIT3 (sc-393512, Santa Cruz Biotechnology), Mx1 (37849S, Cell Signaling), ISG15 (2758T, Cell Signaling), IFI44L (HK7931, Hushi Pharmaceutical Technology). Membranes were washed three times in Tris-buffered saline containing 1% Triton X-100 and then were incubated with horseradish peroxidase (HRP)-conjugated secondary antibodies (7074P2, Cell Signaling, F030231, Beijing BioRab Technology). Immunoreactive bands were visualized by enhanced chemiluminescence using Super ECL Plus Detection Reagent (P1050, Applygen) using Tanon-5200 (Tanon).

Subcellular Fractionation

Cytoplasmic and nuclear fractions were separated using PARIS Kit Protein and RNA Isolation System (Invitrogen) according to the manufacturer's instructions. Briefly, A549 cells were lysed with Cell Fractionation Buffer on ice for 5–10 min. The lysates were centrifuged 1–5 min at 4°C and 500 × *g*. The supernatant cytoplasmic fraction was aspirated away from the nuclear pellet and transferred to a new tube. The nuclear pellets were washed with Cell Fractionation Buffer once and lysed with Cell Disruption Buffer by vigorous vortex or pipet. RNA was extracted using TRIzol Reagent and quantitative PCR was performed to detect IVRPIE expression in cytoplasmic and nuclear fraction.

RNA Pull-Down Assay and Mass Spectrometry

RNA pull-down assay was carried out using Magnetic RNA-Protein Pull-Down Kit (Thermo Scientific Pierce). Label the target RNA using the included Thermo Scientific Pierce RNA 3′ Desthiobiotinylation Kit. 25–100 pmol of labeled RNA was bound to Streptavidin Magnetic Beads. Add 400 μL of Master Mix containing A549 nuclear lysate to the RNA-bound beads. Add 50 μL of Elution Buffer to the beads and mix well by vortexing. The eluted proteins were subjected to silver-staining (Invitrogen Silver Staining Kit, Thermo) and whole bands were excised and sent for LC-MS/MS analysis which was performed by Shanghai Luming Biological Technology Co., Ltd.

RNA Immunoprecipitation (RIP)

hnRNP U RIP experiments were performed in nuclear extracts isolated from unstimulated A549 cells under native conditions. Assays were performed as previously described (Tsai et al., 2010). Nuclear extracts were immunoprecipitated with 2.5 μg hnRNP U (Abcam, clone 4D11, ab6106) and isotype-matched control IgG antibodies overnight. RNA-protein-antibody complexes were captured using Dynabead Protein A/G (Thermo Fisher Scientific). RNA was eluted by adding TRIzol directly to magnetic beads and isolated as per manufacturer's instructions. cDNA was synthesized using TransScript First-Strand cDNA Synthesis SuperMix (TransGen Biotech) and analyzed by qPCR. Results were normalized to input RNA and shown as fold-enrichment over control IgG RIP.

Chromatin Immunoprecipitation (ChIP)

A549 cells overexpressing or knocking down IVRPIE were infected with BJ501 (MOI = 1, 24 hpi) and subjected to ChIP

assays using the SimpleChIP® Enzymatic Chromatin IP Kit (Magnetic Beads) (Cell Signaling Technology) following the manufacturer's instruction. Briefly, 4×10^6 cells were fixed and lysed in 1× Buffer A per immunoprecipitation. Nucleus fraction was pelleted and resuspended in 100 μL 1× Buffer B, followed by enzymic digestion of DNA by 0.5 μL of Micrococcal Nuclease for 20 min at 37°C to the length of approximately 150–900 bp and sonication to break nuclear membrane. Sheared chromatin was immunoprecipitated with 5 μL anti-H3K4me3 (CST; 9751), anti-H3K27me3 (CST; 9733) or Normal Rabbit IgG (CST) antibody at 4°C for 4 h to overnight followed by incubation with 30 μL ChIP-Grade Protein G Magnetic Beads for 2 h at 4°C with rotation. To reverse the cross-links, protein digestion with proteinase K and 5 M NaCl was performed. Immunoprecipitated DNA was purified and quantified by qPCR analysis using UltraSYBR Mixture (Low ROX) (CW2601M, ComWin Biotech). Primers used in qPCR were listed in **Supplementary Table S1**. Modificated histone enrichment in the ChIP samples were normalized to the input DNA. Experiments were performed at least three times with independent chromatin samples.

Statistical Analysis

Statistical analyses were performed using GraphPad Prism version 5.0 (GraphPad Software Inc.). Student's *t*-test was used to analyze the significance of data. $P < 0.05$ was considered statistically significant. Error bars represent standard error (± SEM).

RESULTS

LncRNA IVRPIE Is Preferentially Up-Regulated in Patients With IAV Infection

To define lncRNAs involved in IAV infection, we analyzed the existing dataset (GSE108807) which utilized RNA sequencing to define the transcriptome of peripheral blood leucocyte samples from patients infected with IAV in the acute stage which were confirmed by molecular diagnostics and their matched recovery-stage (9 months after recovery), to depict the lncRNA profiles involved in IAV infection (Lai et al., 2019). As shown in **Figure 1A** and **Supplementary Table S2**, several lncRNAs that were differentially expressed in patients with IAV infection were chosen for function studies after confirmation by RT-qPCR (**Supplementary Figure S1A**).

To identify lncRNAs affecting IAV infection, virus titers were detected by HA assay after transient transfection of lncRNAs in A549 cells (**Supplementary Figure S1B**). IVRPIE was found to inhibit IAV replication most significantly, and thus it was selected for further study. The human lncRNA gene *virpie* (XLOC_026516) is located on chromosome 2q24.2, transcribed from the antisense strand of promotor region of *tank* locus (**Figure 1B**). Protein-coding potential analysis was performed by coding potential calculator 2[2], and the low coding potential score (−1.0565) suggested that it's a non-coding transcript (Kang et al., 2017) (**Supplementary Figure S1C**). 5′ and 3′ RACE studies were performed to define the exact length and sequence of IVRPIE. IVRPIE is exactly 1316 nt (**Supplementary Table S3**), and the 5′ and 3′ sequences are shown in **Figure 1C**. And IVRPIE is most located in nucleus (**Figure 1D**).

Furthermore, we observed that IVRPIE was upregulated in a virus dose- and infection time-dependent manner in A549 cells (**Figures 1E,F**). Besides, IVRPIE was significantly upregulated by some other RNA virus infections, including Sendai virus (SeV), Vesicular Stomatitis Virus (VSV) (**Figure 1G**), and Poly (I:C) (**Supplementary Figure S1D**), but not upregulated by some RNA viruses, like RSV, DNA viruses, like Adenovirus (AdV) (**Figure 1G**) and IFNβ (**Supplementary Figure S1E**). Similar results were obtained from another normal human bronchial epithelium cells, BEAS-2B cells (**Supplementary Figures S1F,G**). Surprisingly, except for A549 cells and BEAS-2B cells, IVRPIE was not significantly upregulated in other human cell lines (**Supplementary Figure S1H**), which revealed that it mainly exerted its function in blood immune cells and lung cells. To explore the regulatory mechanisms involved in IVRPIE expression, we evaluated the role of TBK1 and NF-κB in controlling the expression of IVRPIE. A549 cells were pretreated with DMSO, MRT67307 HCl, a kinase inhibitor of TBK1 and IKKε, or Pyrrolidinedithiocarbamate ammonium, a selective NF-κB inhibitor, followed by BJ501 infection for 24 h. Interestingly, upregulation of IVRPIE was not affected in MRT67307 HCl or Pyrrolidinedithiocarbamate ammonium-treated A549 cells relative to the control cells (**Supplementary Figure S1I**). These results indicate that IVRPIE expression is not regulated by TBK1 and NF-κB, which needs to be further studied. Together, these experiments demonstrate that upregulation of IVRPIE is mainly associated with some RNA viral infections, especially IAV virus.

Upregulation of IVRPIE Inhibits IAV Replication *in vitro*

To study the effect of IVRPIE on viral load, an *in vitro* infection assay was performed in which A549 cells were transfected with IVRPIE or specific Anti-sense oligos (ASO) targeting IVRPIE. For IVRPIE overexpression, A549 cells were transfected with IVRPIE and then infected with IAV (BJ501) (**Supplementary Figures S2A,B**). The virus growth kinetics results showed that viral titers were lower in IVRPIE-overexpressing cells than control cells (**Figures 2A,B**). We further confirmed inhibition of IAV replication in IVRPIE-overexpressing cells by western blotting using an antibody against the IAV hemagglutinin (HA) (**Figure 2C**). Next, A549 cells were transfected with IVRPIE specific ASOs to downregulate IVRPIE (**Supplementary Figure S2C**), and the effect of IVRPIE downregulation on IAV viral load was analyzed as above. Virus titers were significantly higher in IVRPIE-reduced cells compared to control cells (**Figures 2D–F**). Similar results were obtained from IVRPIE-overexpressing and knockdown BEAS-2B cells (**Supplementary Figures S2D,E**). Besides, IVRPIE overexpression can inhibit the replication of

[2]http://cpc2.cbi.pku.edu.cn

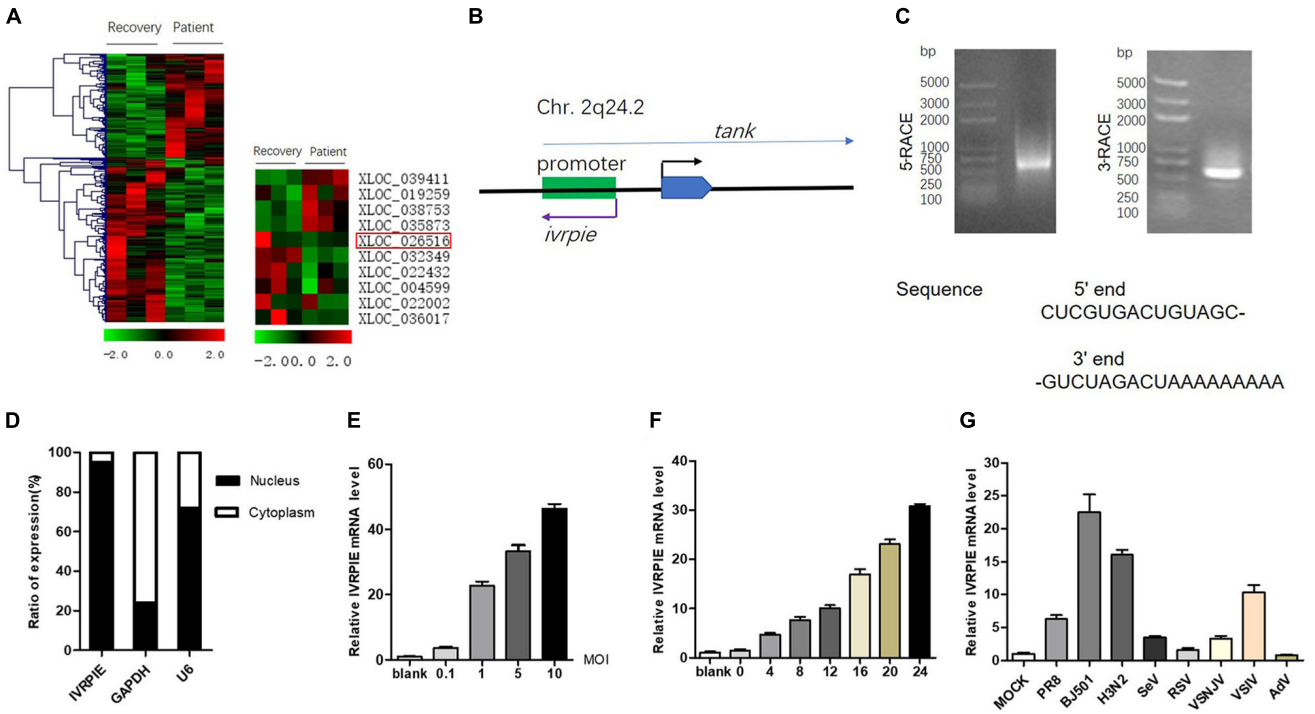

FIGURE 1 | Identification and characterization of IVRPIE. **(A)** Analysis of existing dataset (GSE108807) of RNA sequencing of patients with IAV infection and after recovery revealed 118 upregulated and 187 downregulated lncRNAs (left). Ten lncRNAs are selected and shown in heatmaps (right). **(B)** Schematic diagram of IVRPIE and *tank*. **(C)** The 5′ and 3′ end sequences of IVRPIE determined by RACE. **(D)** Cytoplasmic and nuclear fractions from A549 cells were separated, and the RNA levels of IVRPIE in different subcellular fractions were determined by RT-qPCR. GAPDH mRNA and U6 RNA were respectively used as cytoplasmic and nuclear control. Data are shown as % input (means ± SD; $n = 3$). **(E,F)** A549 cells were infected with BJ501 at the indicated MOI for 24 h **(E)** or at 1 MOI for indicated hours **(F)**, and RT-qPCR was performed to determine the IVRPIE expression. **(G)** A549 cells were infected with different viruses, and RT-qPCR was performed to determine the IVRPIE expression. Data were normalized to GAPDH. Data are shown as the mean ± SD; $n = 3$.

other RNA viruses, such an VSV (**Supplementary Figure S2F**), while IVRPIE knockdown can promote the replication of VSV (**Supplementary Figure S2G**), determined by $TCID_{50}$ assay. These results suggest that upregulation of IVRPIE in infected cells might be a host self defense mechanism to virus infection.

IVRPIE Positively Regulates the Expression of IFNβ1 and Several Critical ISGs

To define the mechanism by which IVRPIE inhibited IAV replication, we tested the IFN and ISGs mRNA and protein level by RT-qPCR, ELISA, or western blotting after overexpressing or knocking down IVRPIE in A549 cells. Notably, mRNA and protein levels of IFNβ1 and some critical ISGs were significantly upregulated in IVRPIE-overexpressing cells, including IRF1, IFIT1, IFIT3, Mx1, ISG15, and IFI44L (**Figures 3A–C**). Conversely, the mRNA and protein levels of IFNβ1 and these ISGs were reduced in IVRPIE knockdown cells compared to control cells (**Figures 3D–F**). Collectively, these results indicate that IVRPIE exerts antiviral functions by upregulating IFNβ1 and some critical ISGs.

IVRPIE Was Involved in Regulation of Histone Modifications of IFNβ1 and ISGs

Next, we explored the mechanism involved in IVRPIE regulation of IFNβ1 and ISG expression. As IVRPIE is located in the nucleus, we investigated the relationship between IVRPIE and its adjacent gene, TRAF family member associated NFκB activator (TANK). It has been reported that TANK is involved in antiviral activities (Chariot et al., 2002; Lee et al., 2013), so we examined TANK expression levels after altering IVRPIE expression. Importantly, there was not significant change after overexpression or knocking down IVRPIE (**Supplementary Figures S3A,B**). These results demonstrated that other mechanisms might be involved in IVRPIE regulation of IFNβ1 and ISG expression. It was reported that lncRNAs can modulate the chromatin state at the transcription start site (TSS) of protein coding genes, so we investigated whether IVRPIE regulated IFNβ1 and ISG expression through this mechanism. We tested the histone modification at transcription start sites of IFNβ1 and ISGs by performing ChIP-qPCR in which histone 3 lysine 4 trimethylation (H3K4me3) and histone 3 lysine 27 trimethylation (H3K27me3) were, respectively, selected as an active mark and repressive mark of transcription. Notably, the H3K4me3 enrichments at the *ifnb1*, *irf1*, *ifit1*, *ifit3*, *mx1*, *isg15*, and *ifi44l*

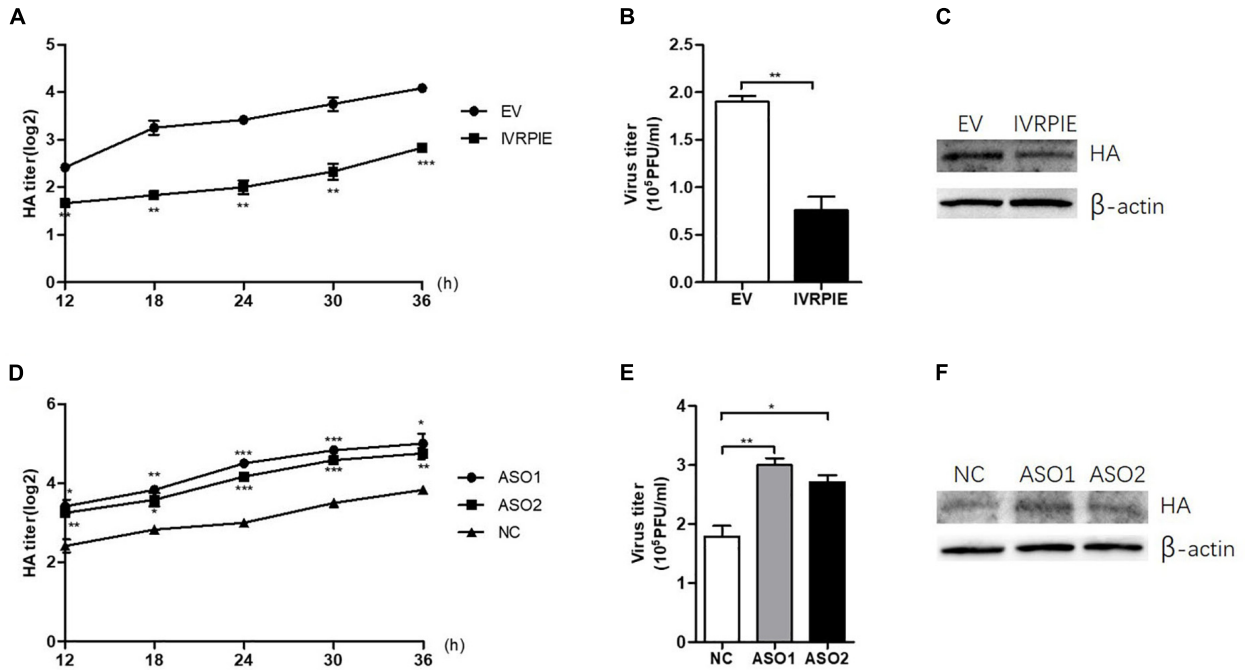

FIGURE 2 | IVRPIE regulates IAV replication in A549 cells. **(A–C)** IVRPIE were transiently overexpressed in A549 cells, and IAV titers were respectively determined by HA assay **(A)**, PFU assay **(B)**, and western blotting **(C)**. **(D–F)** IVRPIE was knocked down by specific ASOs in A549 cells, and IAV titers were respectively determined by HA assay **(D)**, PFU assay **(E)**, and western blotting **(F)**. Data are shown as the mean ± SD; $n = 3$. $^{*}P < 0.05$; $^{**}P < 0.01$; $^{***}P < 0.001$ (Student's *t*-test).

TSSs were significantly increased in IVRPIE-overexpressing cells than those in control cells following IAV infection (**Figure 4A**). In contrast, the H3K27me3 levels at *ifnb1*, *irf1*, *ifit1*, *ifit3*, *mx1*, *isg15*, and *ifi44l* TSSs were impaired in infected IVRPIE-overexpressing cells than that in control cells (**Figure 4B**). Consistently, we observed a significant decrease in H3K4me3 levels and a significant increase in H3K27me3 levels at *ifnb1*, *irf1*, *ifit1*, *ifit3*, *mx1*, *isg15*, and *ifi44l* TSSs in knock down cells compared to control cells (**Figures 4C,D**). Taken together, these data suggest that IVRPIE may promote the IFN β1 and ISG transcription by affecting the histone modifications at the TSSs of these genes.

hnRNP U Is Identified as an Interaction Partner for IVRPIE

To further understand the mechanism how IVRPIE affected the histone modifications of IFN β1 and ISGs, we performed RNA pull down assays to identify the protein partners of IVRPIE. To this end, we used *in vitro*-transcribed biotinylated IVRPIE or its antisense control RNA to pull down proteins from nuclear extracts of A549 cells. RNA-protein complexes were captured using streptavidin magnetic beads and subjected to SDS-PAGE and viewed by silver staining, and whole protein bands were sent for mass spectrometry. This approach identified several proteins that specifically bound with IVRPIE, one of which was identified to be hnRNP U (**Figure 5A** and **Supplementary Table S4**). We next confirmed the ability of hnRNP U to bind IVRPIE by western blotting (**Figure 5B**). RNA immunoprecipitation (RIP) was further performed to purify endogenous hnRNP U in A549 cells and qRT-PCR was used to analyze IVRPIE level. As predicted, the enrichment of IVRPIE in hnRNP U immunoprecipitates was significantly higher than that of control IgG antibodies (**Figure 5C**). Importantly, IVRPIE level in immunoprecipitates was also higher than other nuclear RNAs including U6 (**Figure 5D**). These results suggest that hnRNP U is a protein partner for IVRPIE's antiviral function. We next explored the role of hnRNP U in IFNβ1, IRF1, IFIT1, IFIT3, Mx1, ISG15, and IFI44L expression. Specific siRNAs targeting hnRNP U were used to silence hnRNP U (**Supplementary Figure S4A**), and the IFN β1 and ISG mRNA levels were detected by RT-qPCR. Consistently, the siRNA-mediated silencing of hnRNP U led to significant decrease of IFN β1, IRF1, IFIT1, IFIT3, Mx1, and IFI44L expression in both IVRPIE overexpressing and natural cells (**Figures 5E–G**). These data indicate that hnRNP U is involved in IVRPIE regulation of IFN β1 and several ISG transcription (**Figure 5H**). However, we didn't detect significant decrease of ISG15 expression, suggesting that there might be other mechanisms involved in regulation of IVRPIE in ISG expression.

DISCUSSION

Although antiviral signaling pathways in IAV infection have been well understood, the functions of non-coding RNA, especially lncRNA in these processes remain largely unclear. lncRNA NEAT, 7SL, NRAV, lnc-ISG20, and CCR5AS have been reported to

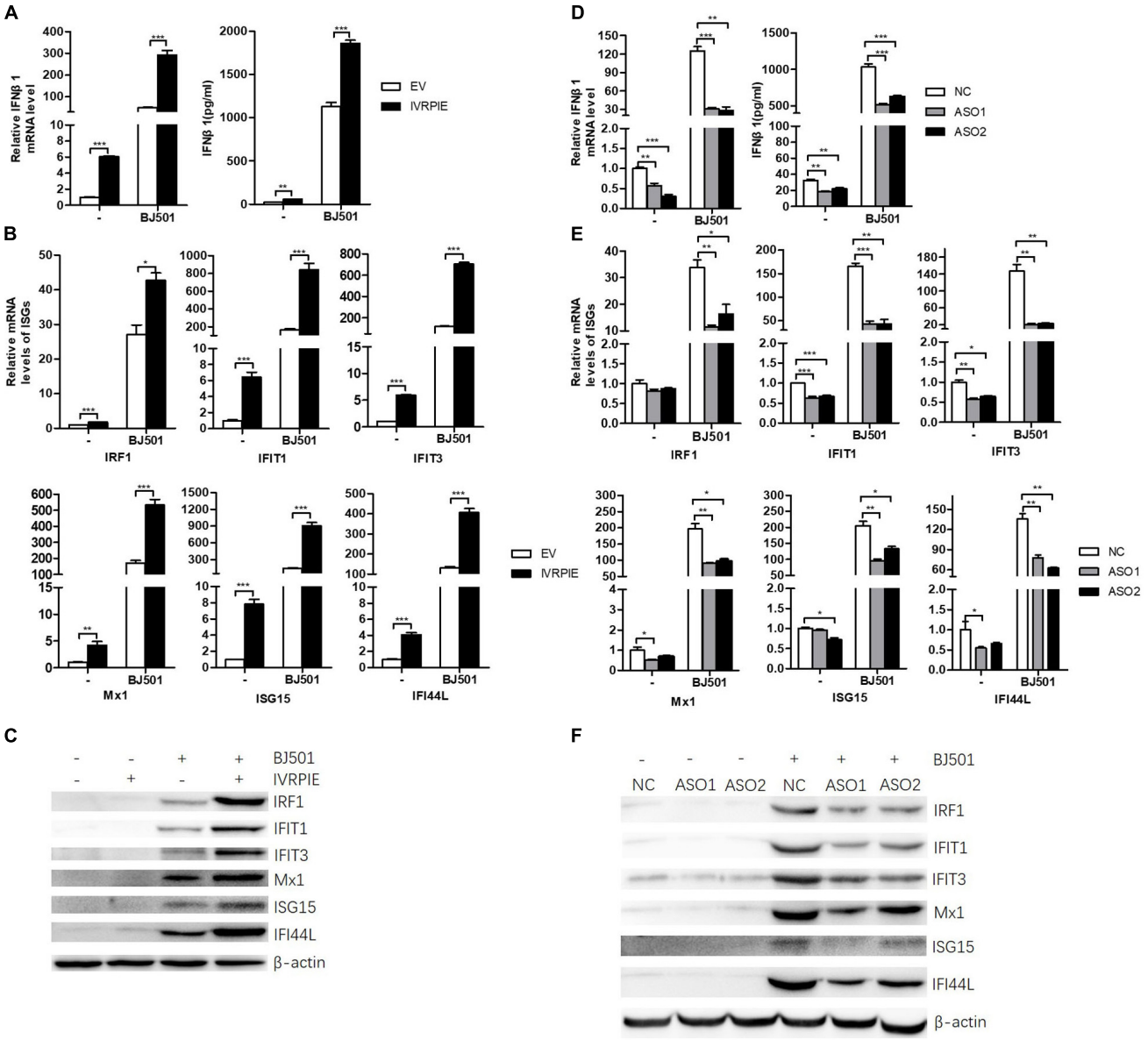

FIGURE 3 | Altering IVRPIE expression in A549 cells changes the expression of IFNβ1 and several critical ISGs. **(A)** IVRPIE was transiently overexpressed in A549 cells, and mRNA level and protein level of IFNβ1 were detected by RT-qPCR and ELISA respectively. **(B,C)** mRNA levelsand protein levels of several critical ISGs were detected by RT-qPCR **(B)** and western blotting **(C)**. **(D)** IVRPIE was knocked down by specific ASOs in A549 cells, and mRNA level and protein level of IFNβ1 were detected by RT-qPCR and ELISA respectively. **(E,F)** mRNA levels and protein levels of several critical ISGs were detected by RT-qPCR **(E)** and western blotting **(F)**. For RT-qPCR, data were normalized to GAPDH. Data are shown as the mean ± SD; $n = 3$. $^{*}P < 0.05$; $^{**}P < 0.01$; $^{***}P < 0.001$ (Student's *t*-test).

regulate the innate immune responses to virus infection (Wang et al., 2007; Zhang et al., 2013; Ouyang et al., 2014; Chai et al., 2018; Kulkarni et al., 2019). In this study, we report a novel human lncRNA termed as IVRPIE, inhibits the IAV infection through promotion of the expression of IFNβ1 and several ISGs, such as IRF1, IFIT1, IFIT3, Mx1, ISG15, and IFI44L. hnRNP U was identified to be the protein partner for IVRPIE in this biological process. Our results further support the idea that lncRNAs play important roles in antiviral immune response.

As IFNβ stimulation did not promote the IVRPIE expression, we propose that IVRPIE is not one of the ISGs. Interestingly, some RNA viruses such as IAV, SeV, and VSV, or Poly (I:C) which is a TLR3 and MDA5 ligand, can induce IVRPIE while other RNA viruses such as RSV and DNA virus such as AdV cannot. We presume this may be related with different cellular receptors that different viruses bind to. Many candidate cellular receptors have been described for RSV entry, including annexin II, CX3 chemokine receptor 1 (CX3CR1), epidermal growth factor (EGF) receptor, calcium-dependent lectins, Toll-like receptor 4

(TLR4), intercellular adhesion molecule 1 (ICAM-1) receptors and heparan sulfate proteoglycans (HSPGs) (Griffiths et al., 2017). Recent studies have shown that IAV, SeV, and VSV are all recognized by RIG-I, and Poly (I:C) is recognized by TLR3 or MDA5, while AdV, as a DNA virus, is recognized by cGAS (Takeuchi and Akira, 2010). Thus, we presume that IVRPIE expression may be regulated by RIG-I, TLR3, MDA5, or the common downstream components shared by these pathways. However, our results showed that IVRPIE expression is not regulated by TBK1 or NF-κB. Further studies need to be done to investigate the mechanism involved in regulation of IVRPIE production. In this study, we found that the histone modifications (active mark H3K4me3 and repressive mark H3K27me3) at the TSSs of several ISGs were altered by IVRPIE, lending support to that lncRNAs regulate gene expression through chromatin remodeling. Since multiple mechanisms are involved in regulation of gene transcription, it may be worth investigating whether other mechanisms involved in regulation of IFNβ and ISG transcription.

We observed that IVRPIE altered the histone modifications of IFNβ1 and several ISGs through interaction with hnRNP U. It was reported that hnRNP U can inhibit HIV-1 gene expression by an N-terminal fragment specifically targeting the 3′ long terminal repeat (3′LTR) in the viral mRNA (Valente and Goff, 2006). In this study, hnRNP U exerted its antiviral function through a totally different way. In recent years, hnRNPs are identified as important functional partners for lncRNAs (Huarte et al., 2010; Carpenter et al., 2013; Atianand et al., 2016). A role for hnRNP U in the epigenetic regulation of gene expression by lncRNAs is also beginning to emerge (Hasegawa et al., 2010; Hacisuleyman et al., 2014). For example, hnRNP U is required for chromosomal localization of Xist RNA in the formation of the inactive X chromosome. hnRNP U is also required for cross-chromosomal co-localization of *Firre* in proper adipogenesis. In this study, hnRNP U was identified as a partner for IVRPIE, which adds further support to the role of hnRNPs in epigenetic regulation by lncRNAs. Secondary structure is important for molecular interaction between lncRNAs and proteins. Of course, further investigations need to be explored, such as the association between the sequence of lncRNA IVRPIE and secondary structures.

IVRPIE is located in the promoter region of TRAF family member associated NFκB activator (TANK). It has been reported that TANK is involved in antiviral activities by modulating NF-kappa B activation through interaction with TANK-binding kinase 1 (TBK1) or IKK epsilon (Chariot et al., 2002; Lee et al., 2013). Herein, our data indicated that TANK expression was not affected by IVRPIE and IVRPIE likely exerted antiviral function through non-TANK pathway. In addition, IVRPIE was mainly upregulated in peripheral blood immune cells and lung cells, not upregulated by other tissues, indicating that IVRPIE is mainly an antiviral regulator for blood and lung immune response.

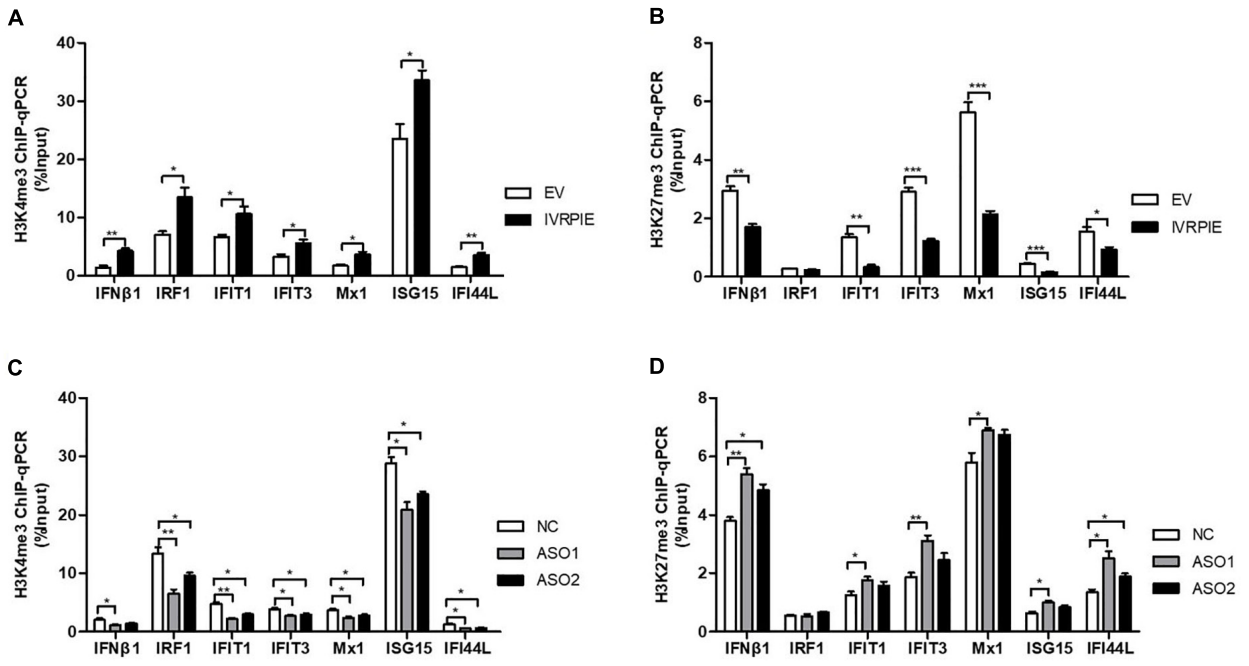

FIGURE 4 | IVRPIE regulates the expression of IFNβ1 and ISGs through histone modifications of these genes. **(A,B)** ChIP-qPCR analysis of H3K4me3 **(A)** and H3K27me3 **(B)** at IFNβ1 and ISGs in IVRPIE overexpressing A549 cells that were infected with BJ501 for 24 h. **(C,D)** ChIP-qPCR analysis of H3K4me3 **(C)** and H3K27me3 **(D)** at IFNβ1 and ISGs in IVRPIE knock-down A549 cells that were infected with BJ501 for 24 h. DNA immuno precipitated by the anti-H3K4me3 antibody or anti-H3K27me3 antibody was calculated using the Percent Input Method. Data are shown as the mean ± SD; $n = 3$. $^{*}P < 0.05$; $^{**}P < 0.01$; $^{***}P < 0.001$ (Student's *t*-test).

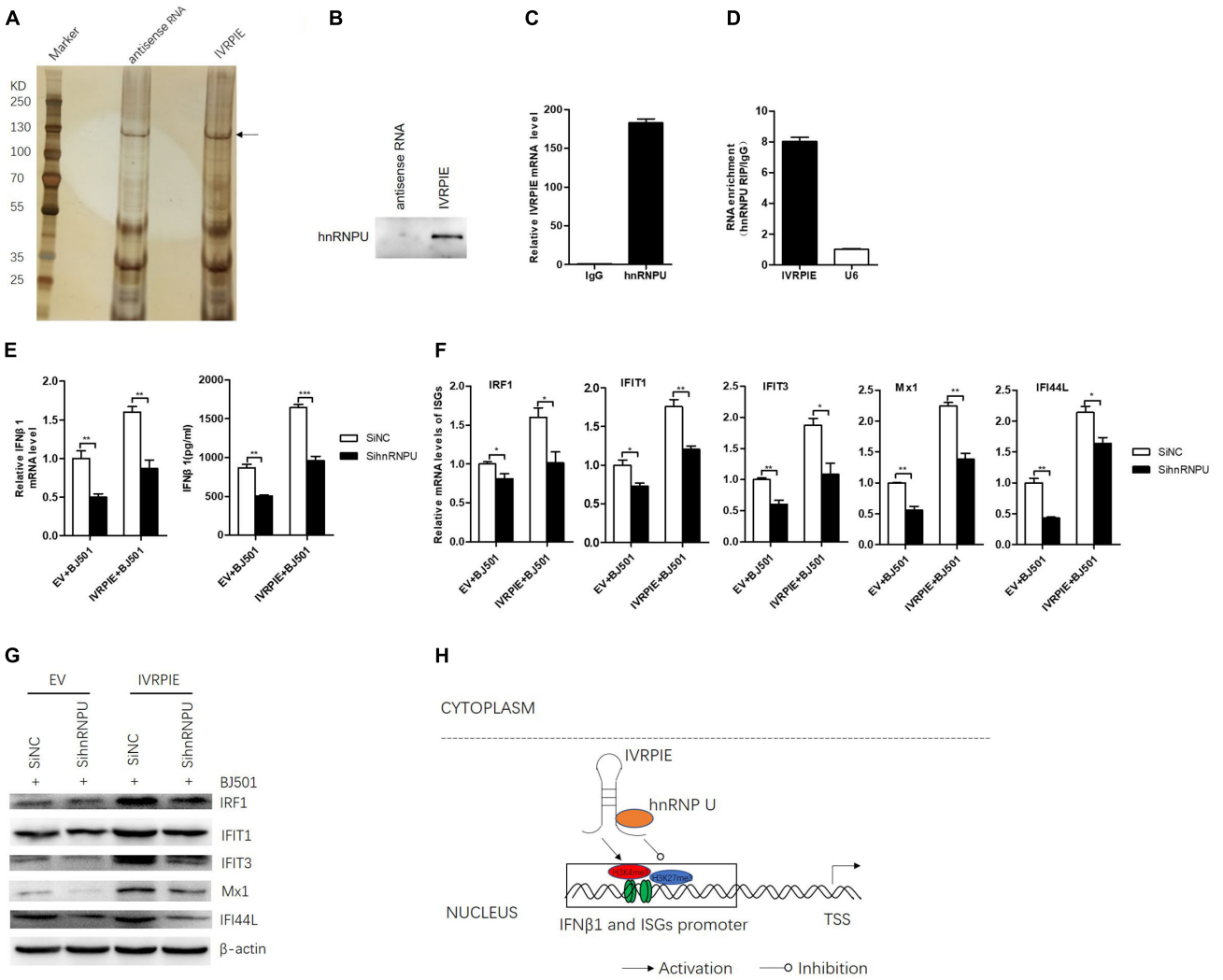

FIGURE 5 | hnRNP U is identified as a protein partner of IVRPIE. **(A)** Silver staining of proteins pulled down by IVRPIE from A549 nuclear lysate. The whole bands were sent for mass spectrometry. **(B)** Western blotting confirms interaction between IVRPIE and hnRNP U *in vitro*. **(C,D)** hnRNP U RIP followed by RT-qPCR analysis of co-purified RNAs in A549 cells. IVRPIE level is significantly higher than that of control IgG antibody **(C)** and other nuclear RNAs normalized to IgG antibody **(D)**. **(E)** mRNA level and protein level of IFNβ1 were detected by RT-qPCR and ELISA respectively in hnRNP U knock-down IVRPIE overexpressing A549 cells and mRNA level of IFNβ1 was normalized to that of control cells. **(F,G)** mRNA levels and protein levels of ISGs were detected by RT-qPCR **(F)** and western blotting **(G)** in hnRNP U knock-down IVRPIE overexpressing A549 cells. **(H)** Schematic diagram of the mechanism for IVRPIE regulating IFNβ1 and ISG transcription.

DATA AVAILABILITY STATEMENT

Publicly available datasets were analyzed in this study. This data can be found here: GSE108807.

AUTHOR CONTRIBUTIONS

LZ contributed to the conception and design of the study, performed the experiments, analyzed the data, and the first draft of the manuscript. CL organized the database. MX, KW, and HF participated in the experiments. HG contributed to the conception and design of the study and provided important advice for experiment improvement. PY supervised the study, wrote sections of the manuscript, and revised it critically. XW supervised the study. PY and XW take primary responsibility for communication with the journal and editorial office during the submission process, throughout peer review and during publication.

FUNDING

This work was supported by the National Natural Science Foundation of China (81771700). The funders had no role in the study design, data analysis, or decision to publish.

SUPPLEMENTARY MATERIAL

The Supplementary Material for this article can be found online at: https://www.frontiersin.org/articles/10.3389/fmicb.2020.00260/full#supplementary-material

FIGURE S1 | Identification and characterization of IVRPIE. **(A)** RT-qPCR was used to validate the gene expression in RNA sequencing. **(B)** A549 cells were infected with several lncRNAs, and virus titers were detected using HA assay. **(C)** Protein-coding potential analysis was performed by coding potential calculator 2. **(D)** A549 cells were transfected with poly I:C (0.25 μg/mL) for indicated hours, and RT-qPCR was performed to determine the IVRPIE expression. **(E)** A549 cells were stimulated with IFNβ for indicated hours, and RT-qPCR was performed to determine the IVRPIE expression. **(F)** BEAS-2B cells were infected with different viruses, and RT-qPCR was performed to determine the IVRPIE expression. **(G)** BEAS-2B cells were transfected with poly I:C (2μg/mL) for 16 h or stimulated with IFNβ for 24 h, and RT-qPCR was performed to determine the IVRPIE expression. RT-qPCR was performed to determine the IVRPIE expression. **(H)** Different cell lines were infected with BJ501, and RT-qPCR was performed to determine the IVRPIE expression. **(I)** A549 cells were pretreated with DMSO, MRT67307 HCl, or Pyrrolidinedithiocarbamate ammonium, followed by BJ501 infection for 24 h. RT-qPCR was performed to determine the IVRPIE expression. Data were normalized to GAPDH. Data are shown as the mean ± SD; $n = 3$.

FIGURE S2 | Altering IVRPIE expression regulates IAV or VSV replication. **(A)** RT-PCR was used to amplify IVRPIE. **(B)** IVRPIE was overexpressed in A549 cells and mRNA level was detected by RT-qPCR. **(C)** IVRPIE was silenced by specific ASOs in A549 cells and mRNA level was detected by RT-qPCR. **(D,E)** IVRPIE was transiently overexpressed **(D)** or specifically knocked down **(E)** in BEAS-2B cells, and viral hemagglutinin (HA) was detected by western blotting. **(F,G)** A549 cells were transfected with pcDNA 3.1-IVRPIE **(F)** or specific ASOs targeting IVRPIE **(G)**, followed by VSNJV infection (100μL, 5×10^7 $TCID_{50}$/mL) for 24 h, and virus titers were determined using $TCID_{50}$ assay. Data were normalized to GAPDH. Data are shown as the mean ± SD; $n = 3$. $^*P < 0.05$; $^{**}P < 0.01$; $^{***}P < 0.001$ (Student's *t*-test).

FIGURE S3 | Regulation of TANK expression by IVRPIE. **(A,B)** IVRPIE was overexpressed **(A)** or knocked down **(B)** in A549 cells, and RT-qPCR was used to detect TANK expression. Data were normalized to GAPDH. Data are shown as the mean ± SD; $n = 3$.

FIGURE S4 | Knock-down of hnRNP Uin A549 cells. **(A)** hnRNP U was knock down in A549 cells, and RT-qPCR was used to detect hnRNP U expression. Data were normalized to GAPDH. Data are shown as the mean ± SD; $n = 3$. $^*P < 0.05$; $^{**}P < 0.01$; $^{***}P < 0.001$ (Student's *t*-test).

TABLE S1 | Primers used for RT-PCR, RT-qPCR and ChIP-qPCR.

TABLE S2 | lncRNAs Differentially Expressed in Patients with IAV Infection.

TABLE S3 | Exact sequence of IVRPIE.

TABLE S4 | Top 10 Proteins Pulled Down by IVRPIE.

REFERENCES

Alexopoulou, L., Holt, A. C., Medzhitov, R., and Flavell, R. A. (2001). Recognition of double-stranded RNA and activation of NF-kappaB by Toll-like receptor 3. *Nature* 413, 732–738. doi: 10.1038/35099560

Atianand, M., Hu, W., Satpathy, A., Shen, Y., Ricci, E., Alvarez-Dominguez, J., et al. (2016). A long noncoding RNA lincRNA-EPS acts as a transcriptional brake to restrain inflammation. *Cell* 165, 1672–1685. doi: 10.1016/j.cell.2016.05.075

Atianand, M. K., and Fitzgerald, K. A. (2014). Long non-coding RNAs and control of gene expression in the immune system. *Trends Mol. Med.* 20, 623–631. doi: 10.1016/j.molmed.2014.09.002

Au-Yeung, N., Mandhana, R., and Horvath, C. M. (2013). Transcriptional regulation by STAT1 and STAT2 in the interferon JAK-STAT pathway. *JAK-STAT* 2:e23931. doi: 10.4161/jkst.23931

Birney, E., Stamatoyannopoulos, J. A., Dutta, A., Guigó, R., Gingeras, T. R., Margulies, E. H., et al. (2007). Identification and analysis of functional elements in 1% of the human genome by the ENCODE pilot project. *Nature* 447, 799–816. doi: 10.1038/nature05874

Carpenter, S., Aiello, D., Atianand, M. K., Ricci, E. P., Gandhi, P., Hall, L. L., et al. (2013). A long noncoding RNA mediates both activation and repression of immune response genes. *Science* 341, 789–792. doi: 10.1126/science.1240925

Chai, W., Li, J., Shangguan, Q., Liu, Q., Li, X., Qi, D., et al. (2018). Lnc-ISG20 inhibits influenza A virus replication by enhancing ISG20 expression. *J. Virol.* 92:e00539-18. doi: 10.1128/JVI.00539-18

Chariot, A., Leonardi, A., Muller, J., Bonif, M., Brown, K., and Siebenlist, U. (2002). Association of the adaptor TANK with the Ikappa B Kinase (IKK) regulator NEMO connects IKK complexes with IKKepsilon and TBK1 Kinases. *J. Biol. Chem.* 277, 37029–37036. doi: 10.1074/jbc.M205069200

Chen, Y. G., Satpathy, A. T., and Chang, H. Y. (2017). Gene regulation in the immune system by long noncoding RNAs. *Nat. Immunol.* 18, 962–972. doi: 10.1038/ni.3771

Darnell, J., Kerr, I., and Stark, G. (1994). Jak-STAT pathways and transcriptional activation in response to IFNs and other extracellular signaling proteins. *Science* 264, 1415–1421. doi: 10.1126/science.8197455

Derrien, T., Johnson, R., Bussotti, G., Tanzer, A., Djebali, S., Tilgner, H., et al. (2012). The GENCODE v7 catalog of human long noncoding RNAs: analysis of their gene structure, evolution, and expression. *Genome Res.* 22, 1775–1789. doi: 10.1101/gr.132159.111

Djebali, S., Davis, C. A., Merkel, A., Dobin, A., Lassmann, T., Mortazavi, A., et al. (2012). Landscape of transcription in human cells. *Nature* 489, 101–108. doi: 10.1038/nature11233

Gitlin, L., Barchet, W., Gilfillan, S., Cella, M., Beutler, B., Flavell, R. A., et al. (2006). Essential role of mda-5 in type I IFN responses to polyriboinosinic:polyribocytidylic acid and encephalomyocarditis picornavirus. *Proc. Natl. Acad. Sci. U.S.A.* 103, 8459–8464. doi: 10.1073/pnas.0603082103

Griffiths, C., Drews, S. J., and Marchant, D. J. (2017). Respiratory syncytial virus: infection, detection, and new options for prevention and treatment. *Clin. Microbiol. Rev.* 30, 277–319. doi: 10.1128/CMR.00010-16

Hacisuleyman, E., Goff, L. A., Trapnell, C., Williams, A., Henao-Mejia, J., Sun, L., et al. (2014). Topological organization of multichromosomal regions by the long intergenic noncoding RNA Firre. *Nat. Struct. Mol. Biol.* 21, 198–206. doi: 10.1038/nsmb.2764

Hasegawa, Y., Brockdorff, N., Kawano, S., Tsutui, K., Tsutui, K., and Nakagawa, S. (2010). The matrix protein hnRNP U is required for chromosomal localization of Xist RNA. *Dev. Cell* 19, 469–476. doi: 10.1016/j.devcel.2010.08.006

Huarte, M., Guttman, M., Feldser, D., Garber, M., Koziol, M. J., Kenzelmann-Broz, D., et al. (2010). A large intergenic noncoding RNA induced by p53 mediates global gene repression in the p53 response. *Cell* 142, 409–419. doi: 10.1016/j.cell.2010.06.040

Johnsson, P., Lipovich, L., Grandér, Dan, and Morris, K. V. (2014). Evolutionary conservation of long non-coding RNAs; sequence, structure, function. *Biochim. Biophys. Acta.* 1840, 1063–1071. doi: 10.1016/j.bbagen.2013.10.035

Kang, Y. J., Yang, D. C., Kong, L., Hou, M., and Meng, Y. Q. (2017). CPC2: a fast and accurate coding potential calculator based on sequence intrinsic features. *Nucleic Acids Res.* 45, W12–W16. doi: 10.1093/nar/gkx428

Kapranov, P., Cawley, S. E., Drenkow, J., Bekiranov, S., Strausberg, R. L., Fodor, S. P., et al. (2002). Large-scale transcriptional activity in chromosomes 21 and 22. *Science* 296, 916–919. doi: 10.1126/science.1068597

Kapranov, P., Cheng, J., Dike, S., Nix, D. A., Duttagupta, R., Willingham, A. T., et al. (2007). RNA maps reveal new RNA classes and a possible function for pervasive transcription. *Science* 316, 1484–1488. doi: 10.1126/science.1138341

Kato, H., Sato, S., Yoneyama, M., Yamamoto, M., Uematsu, S., Matsui, K., et al. (2005). Cell type-specific involvement of RIG-I in antiviral response. *Immunity* 23, 19–28. doi: 10.1016/j.immuni.2005.04.010

Kawai, T., Takahashi, K., Sato, S., Coban, C., Kumar, H., Kato, H., et al. (2005). IPS-1, an adaptor triggering RIG-I- and Mda-5-mediated type I interferon induction. *Nat. Immunol.* 6, 981–988. doi: 10.1038/ni1243

Kotenko, S. V., Gallagher, G., Baurin, V. V., Lewis-Antes, A., Shen, M., Shah, N. K., et al. (2003). IFN-lambdas mediate antiviral protection through a distinct class II cytokine receptor complex. *Nat. Immunol.* 4, 69–77. doi: 10.1038/ni875

Kulkarni, S., Lied, A., Kulkarni, V., Rucevic, M., Martin, M. P., Walker-Sperling, V., et al. (2019). CCR5AS lncRNA variation differentially regulates CCR5, influencing HIV disease outcome. *Nat. Immunol.* 20, 824–834. doi: 10.1038/s41590-019-0406-1

Lai, C., Liu, L., Liu, Q., Cheng, S., and Wang, K. (2019). Long noncoding RNA AVAN promotes antiviral innate immunity by interacting with TRIM25 and enhancing the transcription of FOXO3a. *bioRxiv* [preprint]. doi: 10.1101/623132

Lee, Y., Song, B., Park, C., and Kwon, K. S. (2013). TRIM11 Negatively Regulates IFNβ Production and Antiviral Activity by Targeting TBK1. *PLoS One* 8:e63255. doi: 10.1371/journal.pone.0063255

Mercer, T. R., Dinger, M. E., and Mattick, J. S. (2009). Long non-coding RNAs: insights into functions. *Nat. Rev. Genet.* 10, 155–159. doi: 10.1038/nrg2521

Neumann, G., Noda, T., and Kawaoka, Y. (2009). Emergence and pandemic potential of swine-origin H1N1 influenza virus. *Nature* 459, 931–939. doi: 10.1038/nature08157

Ouyang, J., Zhu, X., Chen, Y., Wei, H., Chen, Q., Chi, X., et al. (2014). NRAV, a long noncoding RNA, modulates antiviral responses through suppression of interferon-stimulated gene transcription. *Cell Host Microbe* 16, 616–626. doi: 10.1016/j.chom.2014.10.001

Seth, R. B., Sun, L., Ea, C. K., and Chen, Z. J. (2005). Identification and characterization of MAVS, a mitochondrial antiviral signaling protein that activates NF kappaB and IRF 3. *Cell* 122, 669–682. doi: 10.1016/j.cell.2005.08.012

Stark, G. R., and Darnell, J. E. Jr. (2012). The JAK-STAT pathway at twenty. *Immunity* 36, 503–514. doi: 10.1016/j.immuni.2012.03.013

Takeuchi, O., and Akira, S. (2010). Pattern recognition receptors and inflammation. *Cell* 140, 805–820. doi: 10.1016/j.cell.2010.01.022

Tsai, M. C., Manor, O., Wan, Y., Mosammaparast, N., Wang, J. K., Lan, F., et al. (2010). Long noncoding RNA as modular scaffold of histone modification complexes. *Science* 329, 689–693. doi: 10.1126/science.1192002

Valente, S. T., and Goff, S. P. (2006). Inhibition of HIV-1 Gene Expression by a Fragment of hnRNP U. *Mol. Cell* 23, 597–605. doi: 10.1016/j.molcel.2006.07.021

Wang, S., Li, H., Chen, Y., Wei, H., Gao, G. F., Liu, H., et al. (2012). Transport ofinfluenza virus neuraminidase (NA) to host cell surface is regulated by ARHGAP21 and Cdc42 proteins. *J. Biol. Chem.* 287, 9804–9816. doi: 10.1074/jbc.M111.312959

Wang, T., Tian, C., Zhang, W., Luo, K., Sarkis, P. T., Yu, L., et al. (2007). 7SL RNA mediates virion packaging of the antiviral cytidine deaminase APOBEC3G. *J. Virol* 81, 13112–13124. doi: 10.1128/JVI.00892-07

Zhang, Q. H., Chen, C. Y., Yedavalli, V. S., and Jeang, K. T. (2013). NEAT1 long noncoding RNA and paraspeckle bodies modulate HIV-1 posttranscriptional expression. *mBiol* 4, 596–512. doi: 10.1128/mBio.00596-12

Conflict of Interest: The authors declare that the research was conducted in the absence of any commercial or financial relationships that could be construed as a potential conflict of interest.

Copyright © 2020 Zhao, Xia, Wang, Lai, Fan, Gu, Yang and Wang. This is an open-access article distributed under the terms of the Creative Commons Attribution License (CC BY). The use, distribution or reproduction in other forums is permitted, provided the original author(s) and the copyright owner(s) are credited and that the original publication in this journal is cited, in accordance with accepted academic practice. No use, distribution or reproduction is permitted which does not comply with these terms.

frontiers in Microbiology

ORIGINAL RESEARCH
published: 20 February 2020
doi: 10.3389/fmicb.2020.00105

MiR-10a-5p-Mediated Syndecan 1 Suppression Restricts Porcine Hemagglutinating Encephalomyelitis Virus Replication

Shiyu Hu[1†], Zi Li[1†], Yungang Lan[1], Jiyu Guan[1], Kui Zhao[1], Dianfeng Chu[2], Gencheng Fan[2], Yuguang Guo[2], Feng Gao[1] and Wenqi He[1]*

[1] Key Laboratory of Zoonosis Research, Ministry of Education, College of Veterinary Medicine, Jilin University, Changchun, China, [2] State Key Laboratory of Genetically Engineered Veterinary Vaccines, Yebio Bioengineering Co., Ltd. of Qingdao, Qingdao, China

Porcine hemagglutinating encephalomyelitis virus (PHEV) is a single-stranded RNA coronavirus that causes nervous dysfunction in the infected hosts and leads to widespread alterations in the host transcriptome by modulating specific microRNA (miRNA) levels. MiRNAs contribute to RNA virus pathogenesis by promoting antiviral immune response, enhancing viral replication, or altering miRNA-mediated host gene regulation. Thus, exploration of the virus–miRNA interactions occurring in PHEV-infected host may lead to the identification of novel mechanisms combating the virus life cycle or pathogenesis. Here, we discovered that the expression of miR-10a-5p was constitutively up-regulated by PHEV in both the N2a cells *in vitro* and mice brain *in vivo*. Treatment with miR-10a-5p mimics allowed miR-10a-5p enrichment and resulted in a significant restriction in PHEV replication, suggesting widespread negative regulation of the RNA virus infection by miR-10a-5p. The outcomes were also evidenced by miR-10a-5p inhibitor over-expression. Luciferase reporter, quantitative real-time PCR (qRT-PCR), and western blotting analysis further showed that Syndecan 1 (SDC1), a cell surface proteoglycan associated with host defense mechanisms, acts as a target gene of miR-10a-5p during PHEV infection. Naturally, siRNA-mediated knockdown of SDC1 leads to a reduction in viral replication, implying that SDC1 expression is likely a favorable condition for viral replication. Together, the findings demonstrated that the abundant miR-10a-5p leads to downstream suppression of SDC1, and it functions as an antiviral mechanism in the PHEV-induced disease, providing a potential strategy for the prevention and treatment of PHEV infection in the future work.

Keywords: porcine hemagglutinating encephalomyelitis virus, miR-10a-5p, Syndecan 1, virus replication, antiviral mechanism

OPEN ACCESS

Edited by:
Zhengli Shi,
Wuhan Institute of Virology (CAS), China

Reviewed by:
Guruprasad R. Medigeshi,
Translational Health Science and Technology Institute (THSTI), India
Rod Russell,
Memorial University of Newfoundland, Canada

****Correspondence:***
Wenqi He
hewq@jlu.edu.cn

† These authors have contributed equally to this work

Specialty section:
This article was submitted to Virology, a section of the journal Frontiers in Microbiology

Received: *10 October 2019*
Accepted: *17 January 2020*
Published: *20 February 2020*

Citation:
Hu S, Li Z, Lan Y, Guan J, Zhao K, Chu D, Fan G, Guo Y, Gao F and He W (2020) MiR-10a-5p-Mediated Syndecan 1 Suppression Restricts Porcine Hemagglutinating Encephalomyelitis Virus Replication. Front. Microbiol. 11:105. doi: 10.3389/fmicb.2020.00105

INTRODUCTION

Porcine hemagglutinating encephalomyelitis virus (PHEV) is a neurotropic coronavirus and causes central nervous system (CNS) disorders and digestive illnesses in piglets (Li et al., 2016). PHEV is an enveloped positive strand RNA virus and coding five structural proteins, including small envelope (E), membrane (M), nucleocapsid (N), spike (S), and hemagglutinin-esterase

protein (HE) (Dong et al., 2014). The main host of PHEV infection is the piglets under 3 weeks of age, manifested by vomiting and wasting disease (VWD) or encephalomyelitis, with a mortality rate of nearly 100% (Vijgen et al., 2006). Previous studies have shown that the disease is widespread worldwide (Gao et al., 2011), although it is often in a subclinical state in conventional swine farms owing to the colostrum antibodies and age-related resistance (Rho et al., 2011). By now, there are no effective preventive vaccines or drugs for prevention; thus, research on PHEV infection is vital to prevent outbreaks.

MicroRNAs (miRNAs) are a group of endogenous non-coding RNA and act as post-transcriptional regulators of target genes mRNAs (Panoutsopoulou et al., 2018). The mature miRNAs are single-stranded RNA of ∼20 nucleotides, which participate in almost biological processes, including host–pathogen interactions (Huang et al., 2017). Increasing studies demonstrate that miRNAs are involved in host–virus interactions and actively regulate the replication of pathogenic viruses (Haasnoot and Berkhout, 2011). For example, miR-30e* inhibits the dengue virus (DENV) replication by restoring IFN-β production (Zhu et al., 2014). Host cells utilized miR-26a to defend against porcine reproductive and respiratory syndrome virus (PRRSV) infection by activating innate antiviral immunity (Jia et al., 2015). MiR-185-5p inhibits hepatitis B virus (HBV) transcription and replication by targeting ETS transcription factor 1 (ELK1) (Fan et al., 2018), whereas miR-520a inhibited HBV replication by inactivating the AKT signaling pathway (Sun et al., 2018). Furthermore, several viruses hijack host miRNAs to promote their replication, such as miR-146a, which promotes HBV replication by targeting zinc finger e-box binding homeobox 2 (ZEB2) (Wang and Li, 2018). Our previous research found that some miRNAs, such as miR-21a and miR-142-5p, are involved in PHEV infection (Li et al., 2017; Lv et al., 2017), and these findings lead to a better understanding of miRNA-mediated regulation of PHEV infection.

In this paper, we found that the cellular miR-10a-5p was up-regulated by PHEV infection and the enriched miR-10a-5p conversely repressed PHEV replication. Further studies suggested that the miR-10a-5p may potentially bind to the 3′-UTR of SDC1 mRNA and may play an antiviral effect on PHEV-infected cells. The data marked that the altered miR-10a-5p directly affects viral pathogenesis and acts as a potential inhibitor of PHEV replication, thereby implying a new therapeutic strategy for PHEV-infected disease. Therefore, understanding the role of cellular miRNAs during viral infection may lead to the identification of novel mechanisms to block RNA virus replication or cell-specific regulation of viral vector targeting.

MATERIALS AND METHODS

Cells and Viruses

The human embryonic kidney cells (HEK293T) and mouse neuroblastoma N2a (N2a) cells were maintained in Dulbecco modified Eagle medium (DMEM; Sigma) supplemented with 10% fetal bovine serum (Gibco, United States) and 1% penicillin/streptomycin. These cells were incubated at 37°C in a humidified atmosphere with 5% CO_2. The PHEV strain HEV 67N (GenBank accession: AY048917) was propagated and titrated on N2a cells.

Animals

BALB/c mice were provided from the Laboratory Animal Center of Jilin University. All animal studies were conducted according to experimental practices and standards approved by the Animal Welfare and Research Ethics Committee of the College of Veterinary Medicine, Jilin University, China (no. KT201904002).

Antibodies

Mouse monoclonal antibody against PHEV was generated in our laboratory. Mouse monoclonal anti-beta actin was purchased from Proteintech, and rabbit polyclonal anti-SDC1 was obtained from Abcam. Horseradish peroxidase secondary anti-mouse and rabbit IgG antibodies were obtained from Proteintech. Goat anti-mouse IgG–Alexa 568 and goat anti-rabbit IgG–Alexa 488 were purchased from Cell Signaling Technology.

MicroRNA Target Prediction

The potential targets of miR-10a-5p were predicted by some bioinformatics website, including DIANA-microT-CDS[1], miRanda[2], PicTar[3], and TargetScan[4] databases. The target sites of miR-10a-5p in the 3′-UTR region of the potential genes were predicted by TargetScan.

In vivo and *in vitro* Infection

Three-week-old BALB/c mice were nasally inoculated with 2×10^6 50% tissue culture infection dose ($TCID_{50}$)/ml of PHEV. The brain tissues were collected on 0, 3, and 5 days post infection. N2a cells were seeded in six-well plates, cultured to 70–80% confluence, and then infected with or without the PHEV at 2×10^6 $TCID_{50}$/ml within the indicated time. Total RNA and protein were extracted and detected by quantitative real-time PCR (qRT-PCR) and western blotting ($n = 3$).

MicroRNA Array

Treated mice were anesthetized with 3.5% chloral hydrate (1.0 ml/100 g; Sigma), and then cerebral cortex tissue was exfoliated under aseptic conditions. Total RNA was harvested using TRIzol (Invitrogen) according to manufacturer's instructions. After having passed RNA quantity measurement, the samples were labeled and hybridized on the miRCURY LNA Array (v.18.0). The heat map diagram shows the result of the two-way hierarchical clustering of miRNAs and samples. T indicates PHEV treated group, whereas C represents control group. The result of hierarchical clustering shows distinguishable miRNA expression profiling among samples.

[1]http://www.microrna.gr/microT-CDS

[2]http://www.microrna.org/microrna/microrna/getDownloads.do

[3]https://pictar.mdc-berlin.de/

[4]http://www.targetscan.org/mmu_61/

Plasmid Construction

To construct the wild-type reporter plasmid, the 3′-UTR sequence of mouse SDC1 gene, which contains the putative miR-10a-5p binding site, was amplified and cloned into pmirGLO luciferase reporter vector (SDC1-WT). On the other hand, the sequence of SDC1 mRNA 3′-UTR that contains the mutant binding site was amplified by overlap extension of PCR and then constructed as a mutant-type reporter (SDC1-MUT). All plasmids were verified by DNA sequencing. The primers were designed as follows: SDC1-WT sense primer, 5′-GAG CTC ACC TCG CTT CCC TAA TCT AC-3′; SDC1-WT anti-sense primer, 5′-CTC GAG ACA GGC TCT TCC AAT GTC AC-3′; SDC1-MUT primer 1, 5′-GAG CTC ACC TCG CTT CCC TAA TCT AC-3′, SDC1-MUT primer 2, 5′-CTC ATG CGT ACA ATG CGG TAT GGA CTA TC-3′; SDC1-MUT primer 3, 5′-GAT AGT CCA TAC CGC ATT GTA CGC ATG AG-3′; and SDC1-MUT primer 4, 5′-CTC GAG ACA GGC TCT TCC AAT GTC AC-3′.

Transfection and Viral Infection

For siRNA transfection, cells are seeded on a six-well plate to reach 30–40% confluence after 12 h. Then SDC1 siRNA or the negative control siRNA (NC) was transfected with X-tremeGENE HD DNA Transfection Reagent (Roche, Sweden) in OPTI-MEM medium (Gibco), according to the instruction of the manufacturer. For miRNA transfection, cells were plated as the previous method and transfected with miR-10a-5p mimic, miR-10a-5p inhibitor, and negative control (RiboBio). In the viral infection experiment, cells were infected with PHEV at 2×10^6 $TCID_{50}$/ml at 48 h after transfection and were then collected at 24, 48, and 72 h post infection. All the transfection experiments were repeated at least three times.

Quantitative Real-Time PCR

To analyze SDC1 mRNA expression, total RNA was extracted using TRIzol (Invitrogen) and reverse transcribed into cDNA by using the reverse transcription kit (Takara, Japan). For miRNA isolation and analysis, miRNA was extracted by a miRNApure Mini Kit (cwbio, China), and then, the Bulge-Loop miRNA qRT-PCR Primer Set (RiboBio, China) was utilized to analyze mature miRNA expression. qRT-PCR was performed using SYBR Green Master Mix kit with the StepOne Real-Time PCR System. The relative expression of mRNAs and miRNAs was normalized using GAPDH and U6, respectively, followed by being analyzed by the $2^{-\Delta\ \Delta\ Ct}$ method. U6 and mmu-miR-10a-5p primers were purchased from RiboBio. The primers for SDC1 and GAPDH were designed as follows: SDC1 sense primer, 5′-CCT CAT CTT TGC TGT GTG CC-3′; SDC1 anti-sense primer, 5′-GCT TGG TGG GTT TCT GGT AG-3′; GAPDH sense primer, 5′-CTC AAC TAC ATG GTC TAC ATG TTC-3′; GAPDH anti-sense primer, and 5′-ATT TGA TGT TAG TGG GGT CTC GCT C-3′.

Luciferase Reporter Assay

For the SDC1 mRNA 3′-UTR luciferase reporter assay, HEK293T cells were plated in 12-well plates and co-transfected with 1 μg of SDC1-WT or 1 μg of SDC1-MUT plasmid as described above, along with miR-10a-5p mimics, miR-10a-5p inhibitors, or negative controls (RiboBio). After 48 h post-transfection, the luciferase reporter assay system (Promega) was used to detect firefly and Renilla luciferase activities. These data are represented as the firefly luciferase activity relative to the Renilla luciferase activity. The experiment was repeated at least three times.

Western Blotting Analysis

The cells and brain tissues were lysed by using Radio Immunoprecipitation Assay Lysis Buffer containing phenylmethylsulfonyl fluoride protease inhibitor (Beyotime). After being lyse on ice for 30 min, the BCA Protein Assay Kit (Pierce) was used to determine protein concentration. The samples were separated on 12% sodium dodecyl sulfate polyacrylamide gel electrophoresis gels and were then transferred to 0.45 μm polyvinylidene fluoride membranes. Non-specific binding was blocked using 5% non-fat dry milk in 0.01 M of phosphate-buffered saline (PBS) for 1 h at room temperature. Following that, membranes were washed five times with PBS and incubated in rabbit polyclonal anti-SDC1 or mouse monoclonal anti-beta actin antibody dilution buffer with gentle agitation overnight at 4°C. Then the membranes were washed and incubated with horseradish peroxidase-linked secondary anti-mouse or anti-rabbit IgG antibodies for 1 h at room temperature. Finally, the binds were detected using ECL reagents (Proteintech).

Indirect Immunofluorescence Assay

For immunofluorescence staining, N2a cells plated in 24-well plates were infected with PHEV at 2×10^6 $TCID_{50}$/ml. At 48 h post infection, N2a cells were washed twice with PBS and fixed with 4% paraformaldehyde for 15 min and then incubated with 5% non-fat dry milk in PBS for 1 h at 37°C, followed by incubation with a monoclonal antibody against the PHEV (1:1,000) and a polyclonal antibody against SDC1 for 1 h at 37°C. Cells were washed five times with PBS and incubated with goat anti-mouse IgG–Alexa 568 conjugates and goat anti-rabbit IgG–Alexa 488 (1:300) for 1 h at 37°C. After being washed five times with PBS, the nuclei were visualized with 4′,6-diamidino-2-phenylindole (DAPI, 1:500). The stained cells were observed using a confocal microscope.

Cell Proliferation Assays

Cell growth and viability were measured using Cell Counting Kit-8 (CCK-8) assay kit (Meilunbio, China). The treated cells were grown in 96-well plate with $\sim 5 \times 10^3$ per well and incubated for 24, 48, and 72 h. At the indicated time, 10 μl of CCK-8 solution was added to the cell culture medium for 1-h incubation. The absorbance of the converted dye at 450 nm was measured by a microplate reader.

Statistical Analysis

All experiments presented were repeated three times. The data are presented the mean ± SD. Statistical analysis was performed with either Student's *t*-test or one-way ANOVA in GraphPad Prism version 5 software. All data were considered statistically significant at a p-value < 0.05.

RESULTS

Porcine Hemagglutinating Encephalomyelitis Virus Infection Up-Regulates MiR-10a-5p Expression

Investigating the miRNA profiling during PHEV infection may provide insight into the CNS injury diseases. A miRNA array was previously performed to identify the miRNAs involved in neurological dysfunction as a result of PHEV infection (**Figure 1A** and **Supplementary Data Sheet S1**). Of these up-regulated miRNAs, we found that miR-10a-5p was of research value and practical significance. To investigate the role of miR-10a-5p during PHEV infection, N2a cells and BALB/c mice were infected with PHEV. Cell lyses were collected at the indicated time, and the expression of miR-10a-5p RNA and PHEV genome

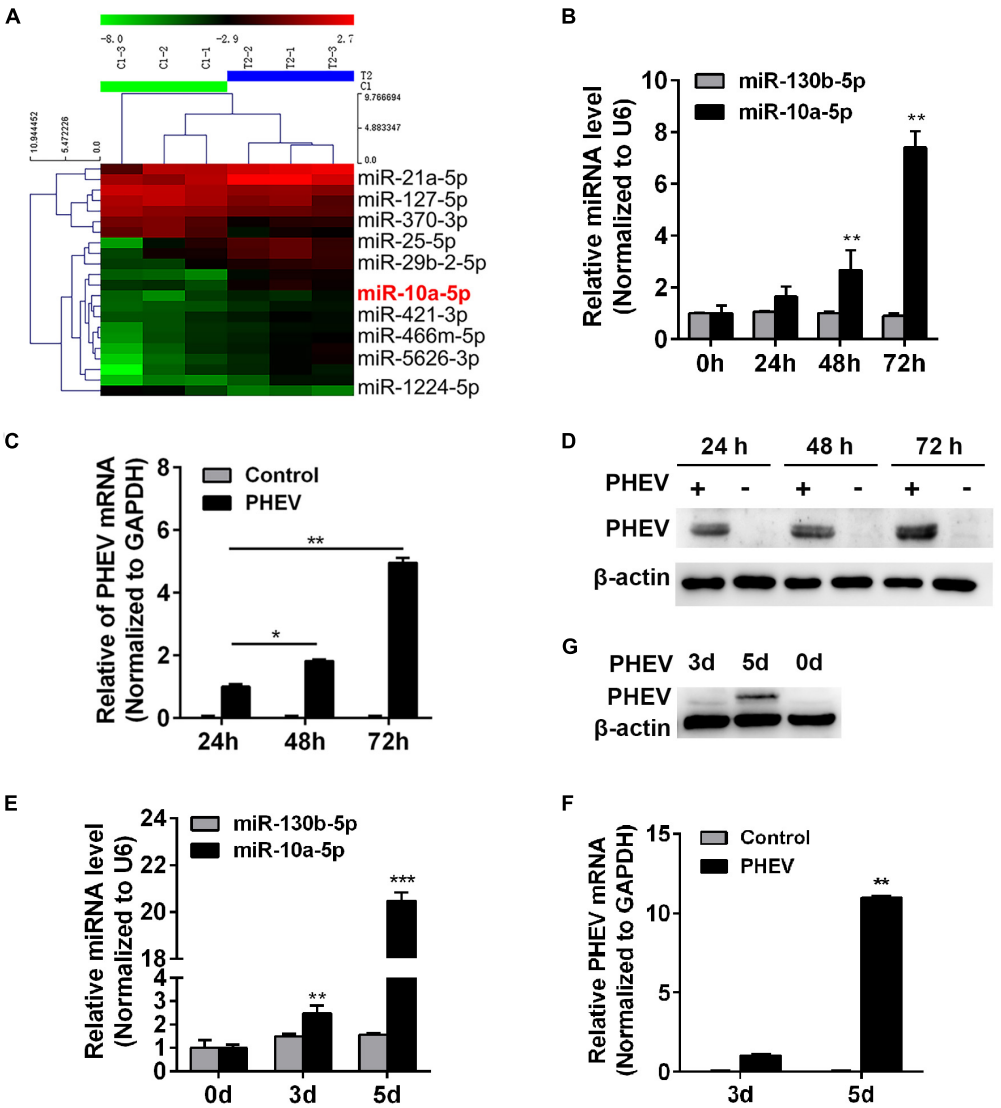

FIGURE 1 | Porcine hemagglutinating encephalomyelitis virus (PHEV) infection up-regulates miR-10a-5p expression. **(A)** MiRNA array of PHEV-infected and uninfected mice. Hierarchical clustering shows distinguishable miRNA expression profiling among samples. **(B)** N2a cells were infected with PHEV at 2×10^6 $TCID_{50}$/ml and harvested at 0, 24, 48, and 72 h post infection. The expression of miR-10a-5p was determined by qRT-PCR. U6 was chosen as a housekeeping gene to normalize miR-142a-3p expression. Another irrelative miR-130b-5p is used as a negative control. **(C)** Cells were treated as described in panel **(B)**, then the total RNA was extracted, and the relative expression of PHEV mRNA was determined by qRT-PCR. Data were normalized to GAPDH. **(D)** N2a cells treated as described in panel **(B)**, and the cell lysates were collected and subjected to examine the expression of PHEV protein by western blotting. Beta actin expression was verified as loading control. **(E)** BALB/c mice were infected with PHEV for 3 or 5 days, and then the cerebral cortexes were harvested, and miR-10a-5p level was determined by qRT-PCR. $N = 4$ mice per group, three independent experiments. **(F)** The lysis from cerebral cortexes of mice as described in panel **(E)** was collected, and then the relative expression of PHEV mRNA was determined by qRT-PCR. **(G)** The cerebral cortical lysis was detected by western blotting, and the PHEV protein was normalized to beta actin. All of data are representative of at least three independent experiments, with the error bars representing the standard deviations (SDs). $^*p < 0.05$, $^{**}p < 0.01$ vs. normal controls.

was detected by qRT-PCR (**Figures 1B,C**), whereas the viral protein levels were determined by western blotting (**Figure 1D**). The results showed that the miR-10a-5p level was significantly higher than that in the control group at 48 and 72 h post infection, during which PHEV RNA replication and protein expression were remarkably strengthening (**Figures 1B–D**). Likewise, 3-week-old BALB/c mice were intranasal inoculated with PHEV, and the cerebral cortex was obtained at 0, 3, and 5 days post infection. And we confirmed a heightened expression of miR-10a-5p by qRT-PCR analyses, which is tightly correlative to enhanced PHEV propagation (**Figures 1E–G**). These data indicate that miR-10a-5p level was up-regulated by the increasing amount of PHEV during infection.

MiR-10a-5p Suppresses the Replication of Porcine Hemagglutinating Encephalomyelitis Virus

To examine whether miR-10a-5p has a biological function on PHEV replication, the N2a cells were transfected with miR-10a-5p mimic or inhibitor for 24 h, and then the expression of miR-10a-5p was detected by qRT-PCR. Our results showed a significant increase in the miR-10a-5p level with the mimic transfection at a dose of 50 or 100 nM (**Figure 2A**). In contrast, the level of miR-10a-5p decreased after treatment with miR-10a-5p inhibitors (**Figure 2B**). These miR-10a-5p mimic- or inhibitor-treated cells were then seeded in 96-well plates, and virus titers were determined by $TCID_{50}$/ml. As shown in **Figure 2C**, the RNA virus titers in the miR-10a-5p mimic-overexpressing cells ($10^{4.59}$ $TCID_{50}$/ml) were

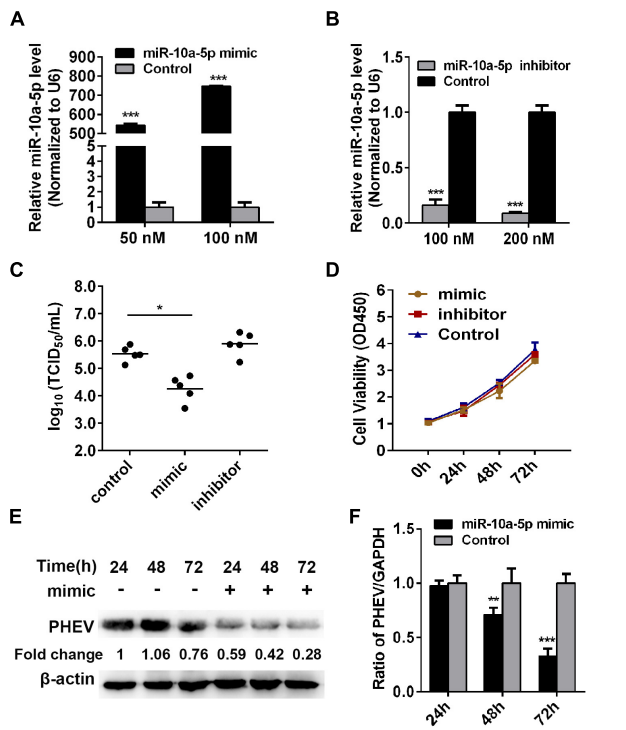

FIGURE 2 | Abundant miR-10a-5p suppresses the replication of porcine hemagglutinating encephalomyelitis virus (PHEV). **(A)** N2a cells were transfected with different concentrations of miR-10a-5p mimic for 24 h, and then the expression of miR-10a-5p was analyzed by qRT-PCR and normalized to U6. **(B)** N2a cells were transfected with 100 or 200 nM miR-10a-5p inhibitor, and miR-10a-5p level was detected by qRT-PCR. **(C)** N2a cells pre-transfected with miR-10a-5p mimic, miR-10a-5p inhibitor, or miRNA NC were seeded in 96-well plates followed by PHEV infection. The cytopathic effect was monitored for 24 to 96 h. The virus titers were determined by $TCID_{50}$/ml and calculated according to the Reed–Muench method. **(D)** Cell Counting Kit- (CCK-8) assay was performed to determine the cell proliferation at the indicated times. **(E)** N2a cells were pre-transfected with 100 nM of miR-10a-5p mimic and then infected with PHEV at 2×10^6 $TCID_{50}$/ml. The cells lystate were harvested at 24, 48, and 72 h post infection, and PHEV protein levels were determined by western blotting and normalized to beta actin. **(F)** Cells were treated as described in panel **(E)** and determined by qRT-PCR by analyzing PHEV mRNA level. GAPDH was chosen as a housekeeping gene for normalization. Data are shown as means ± SD of at least three independent experiments. $^*p < 0.05$; $^{***}p < 0.01$.

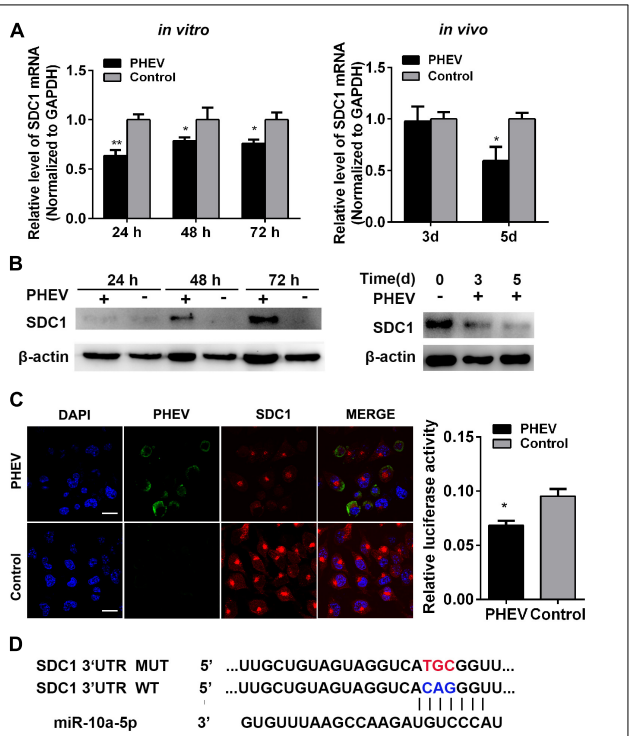

FIGURE 3 | Syndecan 1 (SDC1) expression was inhibited during porcine hemagglutinating encephalomyelitis virus (PHEV) infection. **(A)** N2a cells were incubated with PHEV for 24∼72 h *in vitro*, whereas the BALB/c mice were infected with PHEV for 3 or 5 days *in vivo*. *N* = 4 mice per group, three independent experiments. The endogenous SDC1 mRNA expression was determined by qRT-PCR. **(B)** The lysates from cells or mice that treated as described as (A) were harvested and detected by western blotting using primary antibodies against SDC1 or beta actin. **(C)** N2a cells were incubated with PHEV for 24 h and then fixed and labeled with antibodies against PHEV (green) and SDC1 (red). The cell nucleus was stained with DAPI (blue). Representative micrograph is shown, and quantitative analyses of the Rab3a staining are listed on the right. Bars indicate 20 μm. All of the data are representative of at least three independent experiments ($^*p < 0.05$, $^{**}p < 0.01$). **(D)** Sequence alignment of miR-10a-5p in TargetScan website and its target site in 3′ UTR of SDC1 mRNA are shown. Model of wild- and mutant-type constructs of SDC1 mRNA 3′ UTR. The red letters indicate the point mutation.

significantly lower than those in the NC-overexpressing cells ($10^{5.57}$ $TCID_{50}$/ml) after 72 h post infection, whereas the viral titers were not significantly changed in the miR-10a-5p inhibitor-overexpressing cells compared with the NC-overexpressing cells (**Figure 2C**). Hereafter, we infected the miR-10a-5p mimic-treated cells with PHEV, followed by western blotting and qRT-PCR assays, to detect the intracellular viral proliferation. Cytotoxicity experiment showed that cell viability was not significantly influenced after transfection (**Figure 2D**). As shown in **Figures 2E,F**, we observed that the enhanced miR-10a-5p significantly restricts PHEV replication at 72 h post infection. The data suggested the host miR-10a-5p's widespread negative regulation of PHEV replication and that any antiviral effects at the cellular level should be considered in the context of the overall effect of PHEV-induced miR-10a-5p alteration in the infected hosts.

Syndecan 1 Is a Target Gene of MiR-10a-5p

To identify miR-10a-5p target genes, some publically available miRNA target-prediction websites were used, including Pictar, TargetScan, and miRanda. Among all predicted target genes, the potential target Syndecan 1 (SDC1) acts as an important factor that participates in cancer, inflammatory diseases, and pathogen infection (Teng et al., 2012). Its expression was dramatically inhibited during PHEV infection *in vivo* and *in vitro*, which was determined by qRT-PCR and western blotting (**Figures 3A,B**).

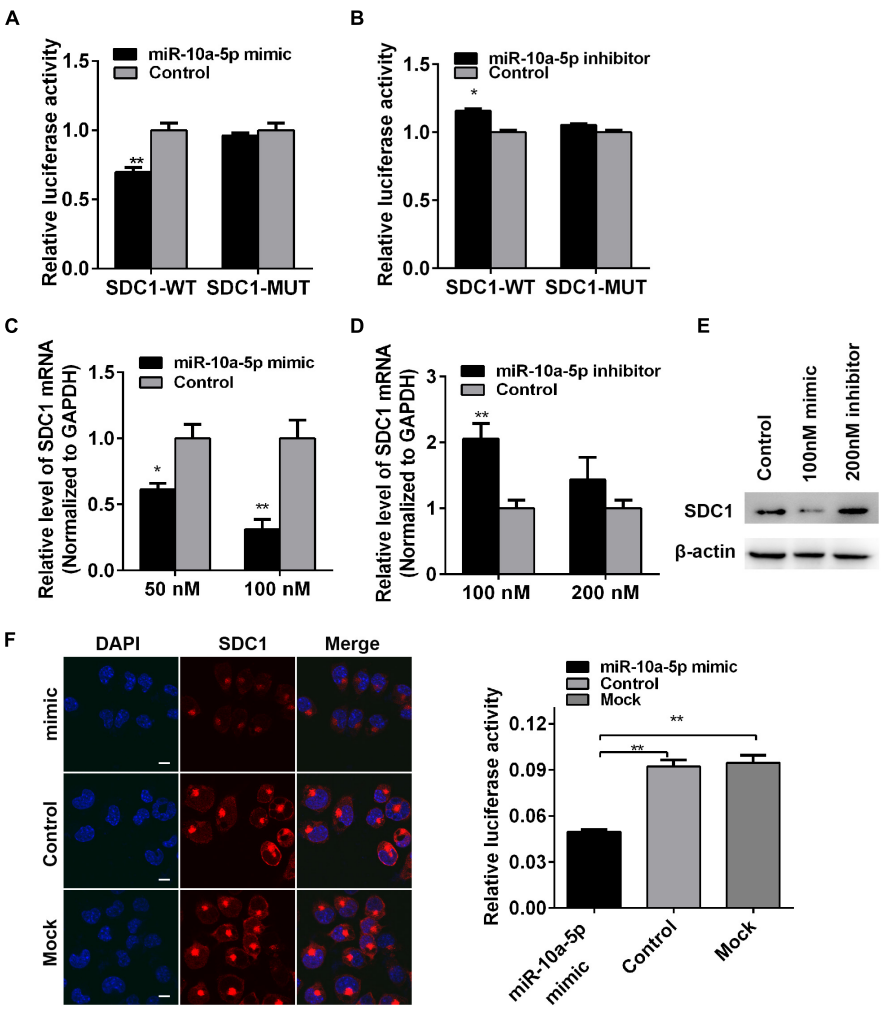

FIGURE 4 | Syndecan 1 (SDC1) mRNA is a target of miR-10a-5p. **(A)** Wild-type (WT) or mutant-type (MUT) reporter constructs of SDC1 3'-UTR were co-transfected with 100 nM of miR-10a-5p mimic into HEK293T cells. After 24 h, the Renilla and firefly luciferase activities were assayed. **(B)** SDC1-WT or SDC1-MUT reporter was co-transfected with 200 nM of miR-10a-5p inhibitor into HEK293T cells for 24 h and were then harvested and subjected to luciferase activities detection. **(C)** N2a cells were transfected with different concentrations of miR-10a-5p mimic for 48 h, and the SDC1 mRNA expression was determined by qRT-PCR. **(D)** N2a cells pre-transfected with miR-10a-5p inhibitor for 48 h were subjected to SDC1 level determination by qRT-PCR. **(E)** Cells were pre-treated as indicated in panels **(C,D)**, lysed, and detected by western blotting assay to examine the level of PHEV protein. Data were normalized to beta actin. All of the data are representative of at least three independent experiments (*$p < 0.05$, **$p < 0.01$). **(F)** Representative micrograph of IFA showed the expressed level of SDC1 (red) in the miR-10a-5p mimic- or mock-transfected N2a cells. Nucleus was stained with DAPI (blue). Quantitative analyses of the SDC1 staining are listed on the right. Bars, 20 μm.

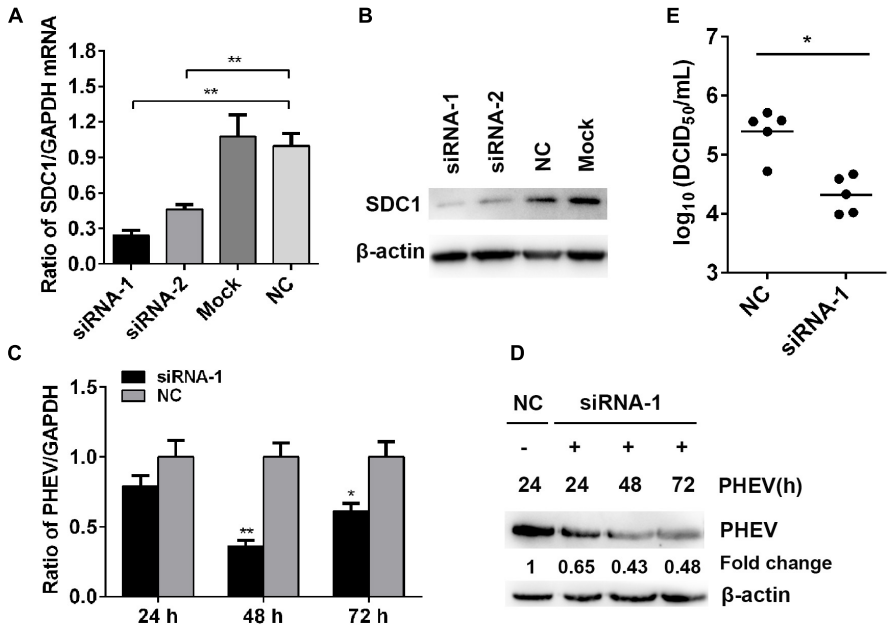

FIGURE 5 | Effects of Syndecan 1 (SDC1) defect in porcine hemagglutinating encephalomyelitis virus (PHEV) replication *in vitro*. **(A)** N2a cells were transfected with 50 nM of SDC1-siRNA-1, SDC1-siRNA-2, or negative control (NC) siRNA, and the expression of SDC1 mRNA was determined by qRT-PCR at 24 h post transfection. **(B)** The protein levels of SDC1 in the cell treated as described in panel **(A)** were determined by western blotting. **(C)** N2a cells were infected with PHEV for 24∼72 h, following SDC1-siRNA-1 transfection, and the levels of the viral genome RNA were detected by qRT-PCR. **(D)** Cells treated as indicated in panel **(C)** were harvested and determined by western blotting. **(E)** Viral titers in the supernatants were measured by $TCID_{50}$/ml assay. Data are shown as means ± SD of at least three independent experiments. $^{*}p < 0.05$; $^{**}p < 0.001$.

An immunofluorescence assay (IFA) analysis further confirmed that SDC1 expression decreased in the PHEV-infected N2a cells compared with the uninfected ones (**Figure 3C**). Moreover, the sequences of miR-10a-5p and its target site in the 3′-UTR of SDC1 mRNA were then obtained from TargetScan software. It suggests that miR-10a-5p specifically binds to SDC1 mRNA 3′-UTR, through bioinformatics prediction (**Figure 3D**). Therefore, we hypothesized that SDC1 mRNA was a putative miR-10a-5p target gene and may be involved in PHEV infection.

To determine whether miR-10a-5p binding to SDC1 depends on this site in the 3′-UTR, we constructed dual-luciferase reporter plasmid carrying the complementary sequence (SDC1-WT) or three base pair mutations (SDC1-MUT) of the seed region in the SDC1 mRNA 3′-UTR (**Figure 3D**). We found that the luciferase activity of SDC1-WT was significantly decreased when it was co-transfected with the miR-10a-5p mimic for 24 h in the HEK293T cells (**Figure 4A**). In contrast, miR-10a-5p inhibitors increased the luciferase activity of SDC1-WT reporter (**Figure 4B**). No significant changes of luciferase activity were observed when co-transfecting with SDC1-MUT reporter and either miR-10a-5p mimics or inhibitors (**Figures 4A,B**). To further validate the effect of the interaction between miR-10a-5p and SDC1, expression of endogenous SDC1 was analyzed in the N2a cells that pre-transfected with miR-10a-5p mimics or inhibitors. The application of miR-10a-5p mimics significantly decreased the mRNA and protein level of SDC1 at both doses of 50 and 100 nM (**Figures 4C,E,F**). The promotion effects on SDC1 expression were observed in the miR-10a-5p inhibitor-transfected group (**Figures 4D,F**). Together, PHEV-induced miR-10a-5p up-regulation was shown to lead to decreased SDC1 protein level, and SDC1 mRNA is a direct target of miR-10a-5p.

Effects of Syndecan 1 Knockdown on Porcine Hemagglutinating Encephalomyelitis Virus Replication in N2a Cells

To confirm whether SDC1 is involved in PHEV infection, we silenced SDC1 with specific siRNA and verified the effects on PHEV replication. The knockdown of gene level was determined by qRT-PCR and western blotting, and we found that the SDC1 mRNA was cut down by more than 70% at 50 nM of siRNA-1-transfected cells (**Figures 5A,B**). We next determined the effect of SDC1 defect on PHEV infection. N2a cells were transfected with 50 nM of SDC1 siRNA-1, followed by infection of PHEV at 37°C for indicated times. At 24, 48, and 72 h post infection, the levels of PHEV replication were analyzed by qRT-PCR and western blotting, and the viral titers were measured by $TCID_{50}$/ml on 96-well plates as well. We found that the viral load was markedly reduced in these cells (**Figures 5C–E**). These results demonstrated that SDC1 is positively related with PHEV replication. Therefore, we draw a conclusion by summarizing several tentative findings of the study above and pointing out that the host cells make use of miR-10a-5p to reduce SDC1 levels, in response to PHEV infection.

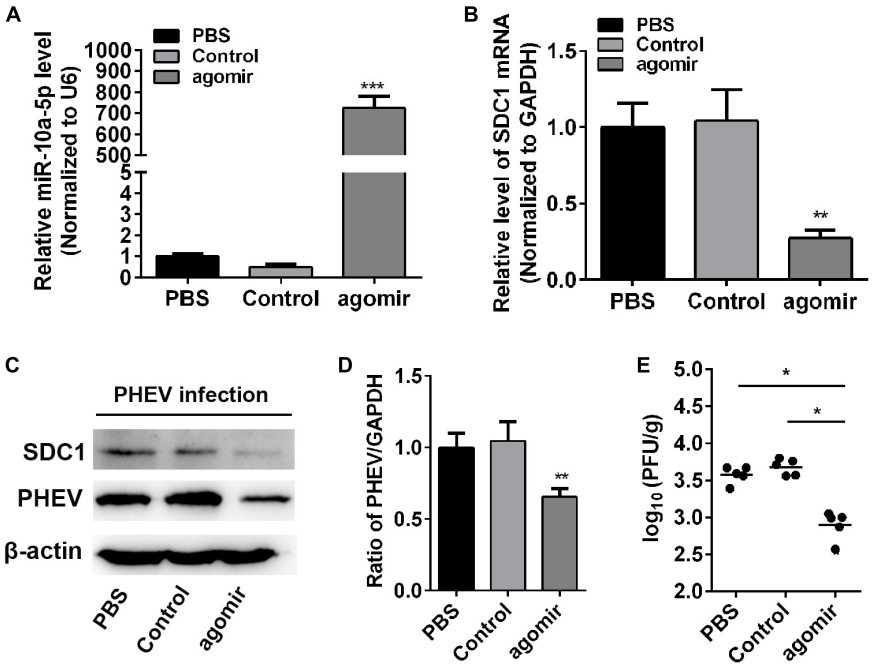

FIGURE 6 | MiR-10a-5p agomir reduced porcine hemagglutinating encephalomyelitis virus (PHEV) replication *in vivo*. BALB/c mice were injected with miR-10a-5p agomir at 1 and 3 days post infection following PHEV infection. *N* = 6 mice per group, three independent experiments. The brain tissues were collected, and qRT-PCR and western blotting assay were performed to assess miR-10a-5p miRNA level **(A)**, Syndecan 1 (SDC1) mRNA transcription **(B)**, SDC1 protein expression **(C)**, and viral replication and load **(C,D)**. Phosphate-buffered saline (PBS)-injected mice were identified as mock injection, whereas mice in the control group were only infected with PHEV without agomir or PBS injection. **(E)** The titer of infectious virus in brain were measured by using a standard plaque assay in N2a cells. Data are shown as means ± SD of at least three independent experiments. $^{*}p < 0.05$; $^{**}p < 0.01$; $^{***}p < 0.001$.

MiR-10a-5p Agomir Reduced Porcine Hemagglutinating Encephalomyelitis Virus Replication in Mice

To determine whether miR-10a-5p was effective against PHEV *in vivo*, the healthy BALB/c mice received an intracerebral injection of miR-10a-5p agomir, a specially chemically modified miRNA agonist that functions by mimicking the entry of endogenous miRNAs into the miRISC complex to regulate the expression of target gene mRNA. PBS-injected mice were used as a mock control. Then, the brain tissues were collected and assigned to assess the expression of miR-10a-5p and SDC1. In the miR-10a-5p agomir-injected mice, an apparent accumulation of miR-10a-5p RNA was observed at 24 h after injection (**Figure 6A**), thereby leading to SDC1 mRNA and protein level restriction, in compared with the control groups (**Figures 6B,C**). Next, we infected the mice with PHEV, followed by miR-10a-5p agomir injection at 24 and 72 h post infection. At 5 days post infection, the expression of PHEV was analyzed by qRT-PCR and western blotting. We found that the viral replication appears to be considerably reduced in the brain of PHEV-infected mice after being injected with miR-10a-5p agomir (**Figures 6C,D**). And also, the brain tissue was weighed and lysed in serum-free MEM, and the viral titration was performed by using a standard plaque assay. As shown in **Figure 6E**, the infectious viral titer was generally lower in the agomir-treated mice than that in the PBS or control group (**Figure 6E**). Taken together with the research and analysis above, we concluded that SDC1 is a potential antiviral target, which is controlled by host miR-10a-5p miRNA at the post-transcriptional level in PHEV-induced disease.

DISCUSSION

Over the past decades, miRNAs have been reported to play critical roles in a variety of cellular processes, including inflammation, cancer, and virus infections (Lee and Dutta, 2009). Of particular note is that many of novel miRNAs and related target genes have been identified to be involved in different stages of virus infections, but in-depth molecular mechanism studies are lacking. Cellular miRNAs can affect virus replication in a direct or indirect way. The former acts as an effected pathway by combining with the virus or viral components. For instance, cellular miR-17 promotes the stability and translation of viral RNA by targeting the 3′-UTR of RNA viruses (Scheel et al., 2016). The latter affects virus replication by targeting host cellular mRNAs (Balasubramaniam et al., 2018). For example, miR-200b and miR-429 suppress the expression of zinc finger E-box binding homeobox 1 (ZEB1) and zinc finger E-box binding homeobox 2 (ZEB2), the two cellular proteins that have key roles to establish and maintain latent infections of Epstein–Barr virus, thus leading to lytic reactivation of

latently infected cells (Ellis-Connell et al., 2010). The miRNA-mediated activity plays a critical role in cellular responses to viral infections.

Previous efforts have suggested that the miRNAs mediated variable functions in the infection of PHEV. For example, miR-21a-5p accelerates PHEV proliferation by down-regulating Caskin1 (Lv et al., 2017), and miR-142-5p disrupted the neuronal morphogenesis during PHEV infection by targeting Ulk1 (Li et al., 2017). Yet more miRNA–PHEV interactome research is lacking. Our paper focuses on the host miR-10a-5p and how it evolved to use target gene to join PHEV replication and pathogenesis. The findings presented here firstly identified SDC1 as a promising and novel target of the miR-10a-5p and also provided the evidence that miR-10a-5p could weaken the function of SDC1, which is a cell surface proteoglycan that bears both heparan sulfate and chondroitin sulfate and necessary for host defense mechanisms, angiogenesis, cancer proliferation and invasion, and microbial attachment and entry (Teng et al., 2012).

The therapeutic miRNAs have emerged as novel or functionally relevant targets against the viral infection. Agomir mixture of hsa-mir-127-3p, hsa-mir-486-5p, hsa-mir-593-5p, mmu-mir-487b-5p, and hsa-miR-1-3p protected mice from influenza (H1N1) virus infection (Peng et al., 2018), whereas miR-m01-3-5p and miR-M23-1-5p agomirs have protective effects on reactivation of murine cytomegalovirus (MCMV) in animals (Deng et al., 2017). Therefore, understanding the host regulatory machinery hijacked by miRNAs during PHEV infection has a potential sense in antiviral therapies. Advancement of knowledge on the interaction between RNA viruses and cellular miRNAs focuses on how the RNA viruses have evolved to use host miRNAs to evade antiviral immune responses, leading to enhanced viral replication and pathogenesis. In our study, miR-10a-5p agomir treatment decreased the virus load in the brain tissue of PHEV-infected mice, by miRNA-mediated changes in antiviral-associated effector activity, further supporting the validation of specific miRNAs as potential antiviral agents in the PHEV-induced disease. However, the role of SDC1 activity during PHEV infection remains unclear. Although the data of SDC1 knockdown assay preliminarily suggests that SDC1 might identify as a novel protein involved in the life cycle of PHEV, or specific functional contribution to viral pathogenesis, further experiments would be required to elucidate this point. It is likely that future work will obtain insights into the downstream signaling processes of the SDC1-dependent PHEV replication restriction. And identifying more miRNAs that are involved in down-regulating the innate immune response during PHEV infection is also of great significance.

DATA AVAILABILITY STATEMENT

The raw data supporting the conclusions of this article will be made available by the authors, without undue reservation to any qualified researcher.

ETHICS STATEMENT

The animal study was reviewed and approved by the Animal Welfare and Research Ethics Committee of the College of Veterinary Medicine, Jilin University, China.

AUTHOR CONTRIBUTIONS

SH and WH designed and supervised the experiments. SH, ZL, and YL performed most of the experiments and interpreted the data. JG cultured cells and conducted the statistical analysis. KZ and DC carried out the bioinformatics prediction analysis and prepared the figures. FG and YG drafted the manuscript and GF and WH revised it critically for important intellectual content.

FUNDING

This study was supported by the National Key Research and Development Program of China (Grant No. 2016YFD0500102), the National Natural Science Foundation of China (Grant Nos. 31902262, 31872446, 31772704, and 31672519), the State Key Laboratory of Genetically Engineered Veterinary Vaccines No. AGVSKL-ZD-201808, the Scientific and Technological Project of Jilin Province (Grant No. 20180101270JC), and the China Postdoctoral Science Foundation (Grant 2018M640285). The funders had no role in the study design, data collection and interpretation, or the decision to submit the work for publication.

SUPPLEMENTARY MATERIAL

The Supplementary Material for this article can be found online at: https://www.frontiersin.org/articles/10.3389/fmicb.2020.00105/full#supplementary-material

DATA SHEET S1 | A miRNA array was previously performed to identify the miRNAs involved in neurological dysfunction as a result of PHEV infection. Supplemental table includes a sheet showing the differentially miRNAs expression profiling with statistical significance among the cerebral cortex samples of mice, which treated with PHEV for 0 days (C1), 3 days (T1), 5 days (T2), respectively.

REFERENCES

Balasubramaniam, M., Pandhare, J., and Dash, C. (2018). Are microRNAs important players in HIV-1 infection? an update. *Viruses* 10:E110. doi: 10.3390/v10030110

Deng, J., Xiao, J., Ma, P., Gao, B., Gong, F., Lv, L., et al. (2017). Manipulation of viral microRNAs as a potential antiviral strategy for the treatment of cytomegalovirus infection. *Viruses* 9:E118. doi: 10.3390/v9050118

Dong, B., Lu, H., Zhao, K., Liu, W., Gao, W., Lan, Y., et al. (2014). Identification and genetic characterization of porcine hemagglutinating encephalomyelitis virus from domestic piglets in China. *Arch. Virol.* 159, 2329–2337. doi: 10.1007/s00705-014-2070-y

Ellis-Connell, A. L., Iempridee, T., Xu, I., and Mertz, J. E. (2010). Cellular microRNAs 200b and 429 regulate the epstein-barr virus switch between latency and lytic replication. *J. Virol.* 84, 10329–10343. doi: 10.1128/JVI.00923-10

Fan, H. X., Feng, Y. J., Zhao, X. P., He, Y. Z., and Tang, H. (2018). MiR-185-5p suppresses HBV gene expression by targeting ELK1 in hepatoma carcinoma cells. *Life Sci.* 213, 9–17. doi: 10.1016/j.lfs.2018.10.016

Gao, W., Zhao, K., Zhao, C., Du, C., Ren, W., Song, D., et al. (2011). Vomiting and wasting disease associated with hemagglutinating encephalomyelitis viruses infection in piglets in Jilin, China. *Virol. J.* 8:130. doi: 10.1186/1743-422X-8-130

Haasnoot, J., and Berkhout, B. (2011). "RNAi and cellular miRNAs in Infections by Mammalian Viruses," in *Antiviral RNAi. Methods in Molecular Biology (Methods and Protocols)*, Vol. 721, ed. R. van Rij, (Totowa, NJ: Humana Press).

Huang, J. Y., Kang, S. T., Chen, I. T., Chang, L. K., Lin, S. S., Kou, G. H., et al. (2017). Shrimp miR-10a is co-opted by white spot syndrome virus to increase viral gene expression and viral replication. *Front. Immunol.* 8:1084. doi: 10.3389/fimmu.2017.01084

Jia, X., Bi, Y., Li, J., Xie, Q., Yang, H., and Liu, W. (2015). Cellular microRNA miR-26a suppresses replication of porcine reproductive and respiratory syndrome virus by activating innate antiviral immunity. *Sci. Rep.* 5:10651. doi: 10.1038/srep10651

Lee, Y. S., and Dutta, A. (2009). MicroRNAs in cancer. *Annu. Rev. Pathol.* 4, 199–227. doi: 10.1146/annurev.pathol.4.110807.092222

Li, Z., He, W., Lan, Y., Zhao, K., Lv, X., Lu, H., et al. (2016). The evidence of porcine hemagglutinating encephalomyelitis virus induced nonsuppurative encephalitis as the cause of death in piglets. *PeerJ* 4:e2443. doi: 10.7717/peerj.2443

Li, Z., Lan, Y., Zhao, K., Lv, X., Ding, N., Lu, H., et al. (2017). miR-142-5p disrupts neuronal morphogenesis underlying porcine hemagglutinating encephalomyelitis virus infection by targeting Ulk1. *Front. Cell. Infect. Microbiol.* 7:155. doi: 10.3389/fcimb.2017.00155

Lv, X., Zhao, K., Lan, Y., Li, Z., Ding, N., Su, J., et al. (2017). miR-21a-5p contributes to porcine hemagglutinating encephalomyelitis virus proliferation via targeting CASK-interactive protein1 in vivo and vitro. *Front. Microbiol.* 8:304. doi: 10.3389/fmicb.2017.00304

Panoutsopoulou, K., Avgeris, M., and Scorilas, A. (2018). miRNA and long non-coding RNA: molecular function and clinical value in breast and ovarian cancers. *Expert. Rev. Mol. Diagn.* 18, 963–979. doi: 10.1080/14737159.2018.1538794

Peng, S., Wang, J., Wei, S., Li, C., Zhou, K., Hu, J., et al. (2018). Endogenous cellular MicroRNAs mediate antiviral defense against influenza A virus. *Mol. Ther. Nucleic Acids* 10, 361–375. doi: 10.1016/j.omtn.2017.12.016

Rho, S., Moon, H. J., Park, S. J., Kim, H. K., Keum, H. O., Han, J. Y., et al. (2011). Detection and genetic analysis of porcine hemagglutinating encephalomyelitis virus in South Korea. *Virus Genes* 42, 90–96. doi: 10.1007/s11262-010-0551-y

Scheel, T. K., Luna, J. M., Liniger, M., Nishiuchi, E., Rozen-Gagnon, K., Shlomai, A., et al. (2016). A broad RNA virus survey reveals both miRNA dependence and functional sequestration. *Cell. Host Microb.* 19, 409–423. doi: 10.1016/j.chom.2016.02.007

Sun, W., Zhang, J., and Chen, J. (2018). MicroRNA-520a suppresses HBV replication in HepG2.2.15 cells by inactivating AKT. *J. Int. Med. Res.* 46, 4693–4704. doi: 10.1177/0300060518792780

Teng, Y. H., Aquino, R. S., and Park, P. W. (2012). Molecular functions of syndecan-1 in disease. *Matrix Biol.* 31, 3–16. doi: 10.1016/j.matbio.2011.10.001

Vijgen, L., Keyaerts, E., Lemey, P., Maes, P., Van Reeth, K., Nauwynck, H., et al. (2006). Evolutionary history of the closely related group 2 coronaviruses: porcine hemagglutinating encephalomyelitis virus, bovine coronavirus, and human coronavirus OC43. *J. Virol.* 80, 7270–7274. doi: 10.1128/JVI.02675-05

Wang, Y., and Li, Y. (2018). miR-146 promotes HBV replication and expression by targeting ZEB2. *Biomed. Pharmacother.* 99, 576–582. doi: 10.1016/j.biopha.2018.01.097

Zhu, X., He, Z., Hu, Y., Wen, W., Lin, C., Yu, J., et al. (2014). MicroRNA-30e* suppresses dengue virus replication by promoting NF-kappaB-dependent IFN production. *PLoS Negl. Trop. Dis.* 8:e3088. doi: 10.1371/journal.pntd.0003088

Conflict of Interest: DC, FG, and YG were employed by the company Yebio Bioengineering Co., Ltd. of Qingdao.

The remaining authors declare that the research was conducted in the absence of any commercial or financial relationships that could be construed as a potential conflict of interest.

Copyright © 2020 Hu, Li, Lan, Guan, Zhao, Chu, Fan, Guo, Gao and He. This is an open-access article distributed under the terms of the Creative Commons Attribution License (CC BY). The use, distribution or reproduction in other forums is permitted, provided the original author(s) and the copyright owner(s) are credited and that the original publication in this journal is cited, in accordance with accepted academic practice. No use, distribution or reproduction is permitted which does not comply with these terms.

frontiers in Microbiology

ORIGINAL RESEARCH
published: 24 March 2020
doi: 10.3389/fmicb.2020.00392

Phylogeographic Dynamics of Influenza A(H9N2) Virus Crossing Egypt

Ruiyun Li[1], Amany Adel[2], Jon Bohlin[3], Åke Lundkvist[4], Björn Olsen[5], John H.-O. Pettersson[4,6]† and Mahmoud M. Naguib[2,4]*†*

[1] MRC Centre for Global Infectious Disease Analysis, Department of Infectious Disease Epidemiology, School of Public Health, Faculty of Medicine, Imperial College London, London, United Kingdom, [2] National Laboratory for Veterinary Quality Control on Poultry Production, Animal Health Research Institute, Agriculture Research Center, Giza, Egypt, [3] Department of Infectious Disease Epidemiology and Modelling, Domain for Infection Control and Environmental Health, Norwegian Institute of Public Health, Oslo, Norway, [4] Department of Medical Biochemistry and Microbiology, Zoonosis Science Center, Uppsala University, Uppsala, Sweden, [5] Department of Medical Sciences, Zoonosis Science Center, Uppsala University, Uppsala, Sweden, [6] Marie Bashir Institute for Infectious Diseases and Biosecurity, Charles Perkins Centre, School of Life & Environmental Sciences and Sydney Medical School, The University of Sydney, Sydney, NSW, Australia

OPEN ACCESS

Edited by:
Ian M. Jones, University of Reading, United Kingdom

Reviewed by:
Ahmed Mohamed Kandeil, National Research Centre, Egypt
Muhammad Zubair Shabbir, University of Veterinary and Animal Sciences, Pakistan

***Correspondence:**
John H.-O. Pettersson
john.pettersson@imbim.uu.se
Mahmoud M. Naguib
Mahmoud.naguib@imbim.uu.se; mahmoud.mnaguib@yahoo.com

† These authors have contributed equally to this work and share last authorship

Specialty section:
This article was submitted to Virology, a section of the journal Frontiers in Microbiology

Received: *15 December 2019*
Accepted: *25 February 2020*
Published: *24 March 2020*

Citation:
Li R, Adel A, Bohlin J, Lundkvist Å, Olsen B, Pettersson JH-O and Naguib MM (2020) Phylogeographic Dynamics of Influenza A(H9N2) Virus Crossing Egypt. Front. Microbiol. 11:392. doi: 10.3389/fmicb.2020.00392

Low pathogenic avian influenza (LPAI) virus of subtype H9N2 is the most frequently detected subtype among domestic poultry and is a public health concern because of its zoonotic potential. Due to the multiple and complex routes of LPAIV H9N2 between geographic regions, little is known about the spatial diffusion of H9N2 virus to, within, and from Egypt, where it is endemic among poultry since 2011. Using close to 800 publicly available hemagglutinin (HA) segment nucleotide sequences, associated location and temporal data, we conducted a Bayesian discrete phylogeographic analysis. Here, we reconstructed and traced the origin, spread and principal transmission routes of H9N2 across large geographical regions, in addition to the transmission between Egypt and the rest of the world and between different Egyptian governorates. Our analysis suggests that during the last few decades, H9N2 has been introduced back and forth continuously between the countries where it is endemic. Amongst these regions, Saudi Arabia, United Arab Emirates and Iraq act as main distribution hubs and drive the viral migration worldwide, with bi-directional and long-distance diffusions. It is noteworthy that H9N2 was introduced once to Egypt via Israel in mid 2009, and that the descendants of the Egyptian LAIVs H9N2 were back-transmitted to Israel in 2015. Additionally, governorates in middle Egypt (Giza, Fayoum and Bani Souwaif) are major hubs in the LPAIV H9N2 transmission network in Egypt. This knowledge highlights that H9N2 is both a global and a national concern and can aid in updating the surveillance program and vaccine strain selection.

Keywords: avian influenza, H9N2, phylogeography, virus evolution, Egypt

INTRODUCTION

Low pathogenic avian influenza virus (LPAIV) of subtype H9N2 is a subtype of influenza A viruses that circulate among different bird species and possess a public health concern because of its zoonotic potential (Peacock et al., 2019). Based on their genetic features, H9N2 viruses are classified into two major lineages, i.e., the "North American" and "Eurasian" lineages, circulating in poultry and wild birds. The Eurasian lineage is subdivided into three major lineages: 1-Korean lineage: A/duck/Hong Kong/Y439/97 (Y439-like) and A/chicken/Korea/38349-p96323/96 (Korean-like); 2-Y280 lineage: A/duck/Hong Kong/Y280/97-like (Y280-like), A/Chicken/Hong Kong/G9/97 (G9-like) and A/Chicken/Beijing/1/94 (BJ94-like); and 3-G1 lineage: A/quail/Hong Kong/G1/97-like (G1-like) (Guo et al., 2000). Since its emergence in 1996 and according to the clustering scheme described by Fusaro et al. (2011), the G1-like lineage displays the largest geographic spread extending from Eastern Asia to the Middle East. Further, the G1-like H9N2 viruses circulating in Central-Asian and Middle Eastern countries, have been diversified into four distinct groups (A, B, C, and D) (Fusaro et al., 2011; Naguib et al., 2017). Although H9N2 is endemic in many Asian and African countries, little is known about the ongoing viral diversifications and spatial expansions.

In particular, Egypt has experienced incursion of LPAI H9N2 viruses of the G1-like clade in late 2010 (Monne et al., 2012). Since then, LPAIV H9N2 has established endemic status among the Egyptian poultry population, causing serious economic problems to the poultry industry. In addition, the co-circulation with other endemic highly pathogenic AIVs (HPAIVs) of subtypes H5N1 and H5N8, has also been reported in wide parts of the Egyptian poultry population (Arafa et al., 2012; Kim, 2018; Samy and Naguib, 2018). In 2014, a reassortant LPAIV H9N2 was reported in pigeon containing five internal gene segments (PB2, PB1, PA, NP, and NS) form Eurasian AIV subtypes (Kandeil et al., 2017). The same genotype was found in backyard chickens in three Egyptian governorates in 2015 (Samir et al., 2019). Recently a new genotype was described similar to the reassortant H9N2 but inherited its NP gene segment from the Egyptian 2010 H9N2 viruses (Kandeil et al., 2019). It is also noteworthy that the continuous spread and circulation of LPAIV H9N2 in the Egyptian poultry population has been linked LPAIV H9N2 cases in humans and pigs (World Health Organization [WHO], 2016; Gomaa et al., 2018). In January 2015, three human cases of LPAI H9N2 following exposure to infected poultry was recorded indicating the zoonotic potential of these viruses (World Health Organization [WHO], 2016). Importantly, this ranks Egypt as the third country, after China and Bangladesh, reporting H9N2 infections in humans. The vast majority of the Egyptian H9N2 viruses encoded amino acid residues H183 and L226 (H3 numbering), the same feature as a vast majority of viruses in the G1-like lineage, which are described to correlate with a shift in affinity of the HA from the "avian" alpha 2–3 toward the "human-like" alpha 2–6 sialic acid linkage (Matrosovich et al., 2001; Naguib et al., 2017). LPAIVs H9N2 in Egypt form the majority of group B, G1 lineage along with viruses from Saudi Arabia, United Arab Emirates, Jordon, Israel, and Bangladesh (Kayali et al., 2014; Naguib et al., 2015). Phylogenetically, the Egyptian LPAIVs H9N2 have been described to be diversified further into three groups clustered within G1-B lineage based on their HA gene segment (Kandeil et al., 2014; Naguib et al., 2017). It is generally acknowledged that waterfowl migration and poultry trade play an important role in the spread of AIVs (Peacock et al., 2019). However, the geographic diffusion of H9N2 globally and into and within Egypt is not fully understood. In particular, the probability of backward transmission of Egyptian H9N2 viruses to the rest of the world is still unclear.

Understanding virus spread and migration patterns could aid in better preparation for epidemics and provide useful guidelines for virus control. In this study, we conducted a phylogeographic analysis of LPAIVs H9N2 obtained from our institutional repositories and public databases, including >700 viruses from 1997–2018, to illustrate the dissemination of LPAIVs H9N2 from far Asia to the Middle East and North Africa, in addition to uncovering the transmission pathways of LPAIVs H9N2 in Egypt. The findings of this study should contribute to the strategic surveillance and targeted planning of control and prevention activities of not only LPAIVs H9N2 but also other subtypes co-circulating in Egypt.

MATERIALS AND METHODS

Sequence Data Collection and Phylogenetic Analysis

Initially, the genetic sequence data of more than 3,500 HA segments of global H9N2 viruses in 1997–2018 were retrieved from GenBank and Global Initiative on Sharing All Influenza Data (GISAID) platforms. To reduce the dataset size, several steps were taken. Initially, identical sequences were removed by keeping the sequence with the earliest date. Secondly, a maximum-likelihood tree was computed using PhyML v.3.0 (Guindon et al., 2009), employing the GTR + g model of nucleotide substitution, whereafter sequences from high-density monophyletic clades from China were subsampled to reflect the current diversity. With this reduced dataset, new maximum-likelihood tree, using the same approach as above, was computed. Temporal structure was subsequently assessed with TempEst v.1.5.1 (Rambaut et al., 2016) after which additional sequences were excluded. The final dataset contained 740 representative sequences (alignment length of 1,738 nucleotides) with the corresponding virus name, host, collection time and geographical location. The majority of samples were distributed in Bangladesh, Israel and Egypt, with over 120 sequences in each country. By contrast, less than 10 samples were obtained in Iraq, Lebanon, Libya, Morocco, and Tunisia. More details on sample distribution in **Supplementary Table S1**. Details on sequences in the final dataset re-provided in **Supplementary Table S6** where those previously generated in our institutional repositories are marked bold.

Global H9N2 Phylogeographic Pathways

To investigate the main global-level spatial diffusion routes between 1997 and 2018, locations were assigned to different regions: Middle East 1 (Saudi Arabia, United Arab Emirates and Iraq), Middle East 2 (Jordan, Lebanon and Israel), North Africa (Egypt, Morocco, Libya, Tunisia, and Algeria), China, Iran and South Asia (Bangladesh, India and Pakistan) (**Supplementary Table S1**). In a parallel analysis, Egypt was designated as a separate region from other North African countries (Morocco, Libya, Tunisia, and Algeria) to prioritize viral migrations between Egypt and the rest regions. The reconstruction of viral migration network was conducted through a Bayesian statistical inference framework using a Bayesian Markov chain Monte Carlo (MCMC) method available in the BEAST package (version 1.7.5) (Drummond et al., 2012). More specifically, a discrete phylogeography was inferred using the general time reversible (GTR) substitution model and a constant size coalescent prior. Three MCMC chains were run independently for 100,000,000 iterations and sampled every 10,000 steps. The convergence of MCMC was assessed by the effective sample size (ESS) of at least 200 using Tracer. Following a burn-in of 10% of each run, the three chains were combined and resampled to 1,000 trees to create the maximum clade credibility (MCC) tree. The reconstructed MCC tree was visualized and edited using FigTree (version 1.4.0). 'Markov jump' counts was used to quantify the expected number of transitions among different locations (Minin and Suchard, 2008). Additionally, the Bayesian stochastic search variable selection (BSSVS) was applied to undertake the Bayes factor (BF) test and estimate the transition rates. We assumed Poisson prior for the BSSVS, assigning 50% prior probability to the minimal rate configuration (Lemey et al., 2009). The strength of transition rates was assessed using SPREAD (version 1.0.6) (Bielejec et al., 2011) with a Bayes factor threshold of ≥ 3. The region with the highest bayes factor support was denoted as the most probable transmission hub for global viral migrations. To investigate the time when the inter-regional transmission between Israel and Egypt occurred, the time to the most recent common ancestors and 95% HPD intervals of the collected Israeli and Egyptian H9N2 viruses were also estimated. Given the spatial-temporal heterogeneity in viral isolation, temporal variation of transmission rate was not evaluated.

Egyptian H9N2 Phylogeographic Pathways

In total 97 out of 171 available Egyptian sequences had known governorate information and were used to reconstruct the diffusing pattern within Egypt (**Supplementary Table S2**). By using the same molecular clock model, nucleotide substitution model and coalescent prior as above, two MCMC chains were run independently for 100,000,000 iterations and sampled every 5,000 steps. Governorates with the highest bayes factor support is denoted as the most probable transmission hub of viral migration within Egypt. To facilitate the interpretation of the results, governorates were categorized into three areas, i.e., Lower Egypt (the Nile Delta), Middle Egypt (including Giza, Fayoum and Bani Souwaif) and Upper Egypt.

RESULTS

Global Hierarchical Viral Diffusion Network

Our reconstruction of the H9N2 transmission pathways shows that the propagation network of H9N2 is highly structured, with significant inter-regional expansions with distinct source-sink dynamics (**Figures 1**, **2** and **Supplementary Table S3**). Amongst these regions investigated, Middle East 1 was shown to be a major inter-regional transmission hub of H9N2 viruses, as indicated by the much higher posterior probability (>70%), linking viruses isolated from all other regions (except for Egypt). Similarly, Iran was also shown to be important in the global spread and maintenance of H9N2, although not in the same magnitude as Middle East 1. By contrast, the lack of posterior probability support for Middle East 2, Egypt and North Africa suggests that they are less likely to act as sources of H9N2 in other regions. Furthermore, bi-directional transmissions were inferred between some regions, i.e., North Africa and Middle East 2, and Middle East 1 and Iran, which may due primarily to their spatial adjacency. In particular, Egyptian viruses were closely related to those isolated from Jordan, Lebanon and Israel, with bi-directional viral migrations between these two regions (**Figure 2** and **Supplementary Table S4**). However, when viewed in detail [**Supplementary Figure S1** and given the sample size (**Supplementary Table S1**)], the Egyptian H9N2 was most likely introduced via Israel around mid 2009 (95% HPD: March 2009–October 2009). Subsequently, H9N2 was back-transmitted from Egypt to Israel ca. 2015 (95% HPD: December 12, 2014–December 30, 2015).

Transmission Pathways of H9N2 in Egypt

There is a distinct spatial viral diffusion structure within Egypt, including both intra- and inter-area transmission pathways (**Figures 3**, **4** and **Supplementary Table S5**). Intra-area viral diffusions were primarily concentrated in Lower Egypt, with bi-directional transmission between El-Beheira and Dakahliya. Additionally, inter-area transmissions are generally migrated from Middle or Upper Egypt to Lower Egypt. It is noteworthy that governorates located in the Middle Egypt, i.e., Giza, Fayoum and Bani Souwaif, are most likely transmission hubs, linking viral migrations between Lower and Upper Egypt. In the interim, direct long-distance diffusions between Upper and Lower Egypt are also observed, particularly the Suez – Sohag and Ismailia – New Valley viral migrations. Of note, transmission from New Valley to Fayoum is of the highest significance compared with the others. Given the localized circulation and viral incursion from Upper and Middle Egypt, we suggest that Lower Egypt may be the reservoir of H9N2 viruses.

DISCUSSION

In Egypt, LPAIV H9N2 continues to cause a significant impact on poultry production industry since its introduction in 2010 (Kandeil et al., 2014; Naguib et al., 2015); in addition, it poses threat to the public health due to its zoonotic potential where

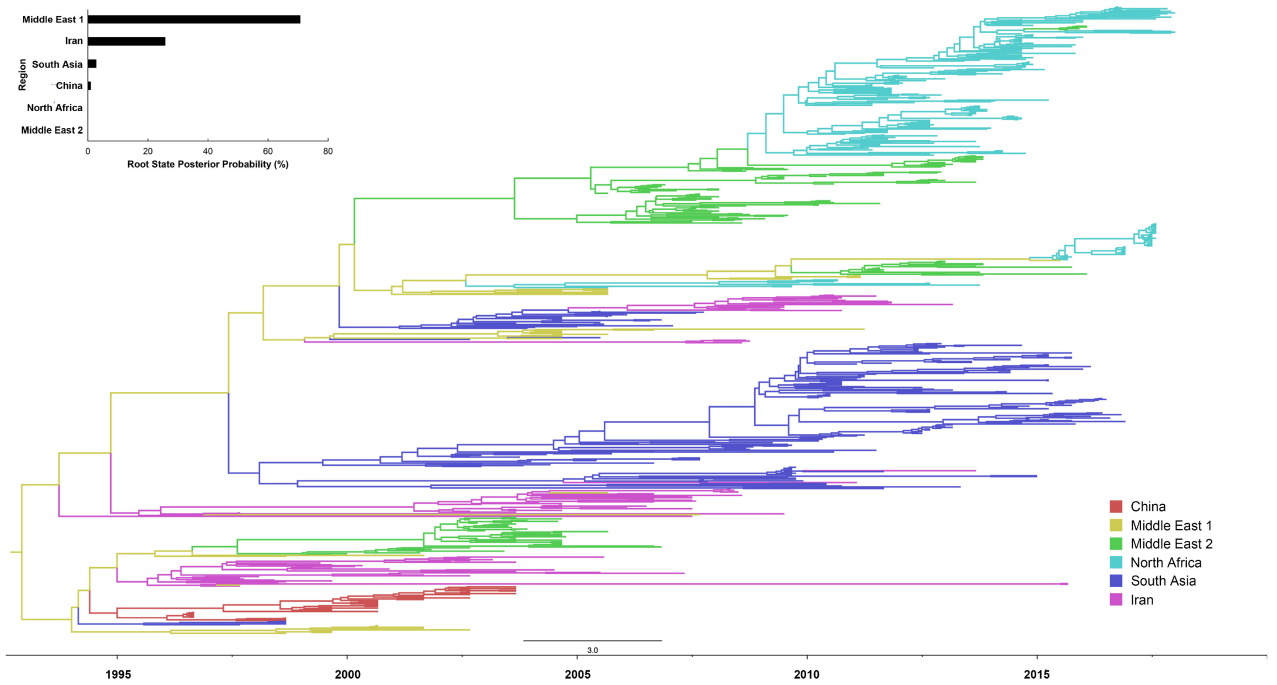

FIGURE 1 | Bayesian evolutionary tree of global LPAI H9N2 viruses based on the nucleotide sequence of the HA gene between 1997 and 2018. Locations were assigned to six regions: Middle East 1 (Saudi Arabia, United Arab Emirates and Iraq), Middle East 2 (Jordan, Lebanon and Israel), Africa (Egypt, Morocco, Libya, Tunisia and Algeria), East Asia (China), West Asia (Iran), and South Asia (Bangladesh, India and Pakistan). The posterior probability of each location acting as transmission hub, i.e., root state posterior probability, was also presented.

subsequent human infections have been reported (Naguib et al., 2017; Nagy et al., 2017). Despite many reports on the molecular features, the transmission dynamics of LPAIVs H9N2 in Egypt is yet to be defined. In this study, we aimed, by using discrete state Bayesian phylogeography, to reveal the evolutionary history and spatial diffusion process of LPAIV H9N2 to, in, and from Egypt, which will in turn aid in establishing more effective avian influenza control strategies.

We find a hierarchical viral propagation network of LPAIV H9N2 being active since the past twenty years. Overall, there is a strong evidence of geographically structured viral diffusions both at the global and the regional scale. Saudi Arabia, United Arab Emirates and Iraq are likely to have played a dominant role in driving the global diffusions of LPAIV H9N2, which was supported by its highest probability as being the transmission sources and multiple transmission events to the rest of the world. This predominant role may potentially be due to its specific location, i.e., in the intersection of the Central Asian and Black Sea-Mediterranean flyways (Birdlife, 2019). It might be also possible that the increased probability of transmission reflects the commercial trade of poultry between regions.

The LPAIVs H9N2 isolated in North Africa has been demonstrated to share a close genetic relationship with those sampled from the Middle East (Peacock et al., 2019). Notably, we proposed a diverse genetic relationship between Africa and the Middle East, with distinct sources of LPAIVs H9N2 between Egypt and the rest of the North African countries. More specific, the close genetic relationship between viruses circulating in Egypt and the neighboring Middle Eastern countries indicated that Jordan, Lebanon and, in particular, Israel are the primary sources of Egyptian H9N2 viruses. By contrast, Saudi Arabia, Emirates and Iraq are most likely to be the source of H9N2 viruses in North Africa (Libya, Algeria, Tunisia, and Morocco). Given the different vaccination strategies implemented in African and Middle Eastern countries (Nagy et al., 2017), we suggest that these strategies may have facilitated the continuous evolution and diversification of LPAIVs H9N2, forming complicated genetic relationship among countries. Additionally, the lack of the direct wild bird movements (Birdlife, 2019) between Egypt and North Africa may have favored viral divergence between two regions as well.

Considering our analysis span more than 20 years of global H9N2 evolution, i.e., 1997–2018, the inferred transmission pathways and sources for the explored regions and time periods should more so be seen as a general pattern for the time-period as a whole. However, although we have subsampled all of the available H9N2 HA genetic diversity, it is important to note that reporting LPAIVs H9N2 varies between different countries our analysis is just reflecting the currently available data. Previous studies have shown extensive expansions to the Middle East after its first emergence in Asia, forming a close genetic linkage between two regions (Fusaro et al., 2011; Nagy et al., 2017; Wei and Li, 2018). Furthermore, phylogenetic divergence of Asian and the Middle Eastern H9N2 viruses

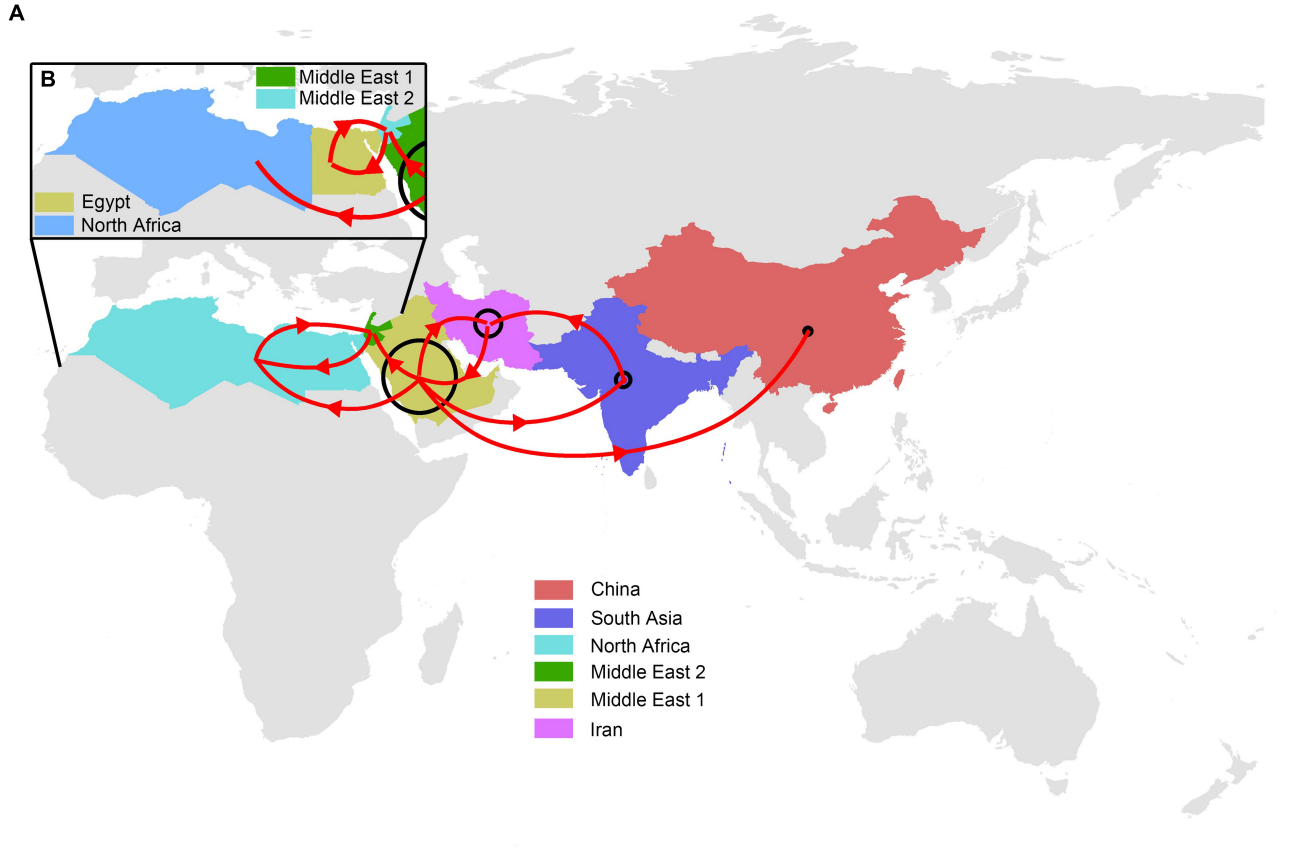

FIGURE 2 | Migration pathways of global LPAI H9N2 viruses. **(A)** Locations were assigned to six regions: Middle East 1 (Saudi Arabia, Emirates and Iraq), Middle East 2 (Jordan, Lebanon and Israel), North Africa (Egypt, Morocco, Libya, Tunisia and Algeria), China, Iran and South Asia (Bangladesh, India and Pakistan). **(B)** Egypt was designated as a separate region from North African countries (Morocco, Libya, Tunisia and Algeria). Lines with arrows illustrate main migration routes. The size of the circle indicates relative chance of a region acting as a migration source. The color of each region is consistent with those shown in **Figure 1**.

has also been reported through the ongoing viral evolution (Fusaro et al., 2011; Hu et al., 2017; Naguib et al., 2017; Wei and Li, 2018). Together, these finding indicated that Asia served as the original transmission source of global H9N2 viruses, but our analyses give heighten the distinct role of Middle East as transmission hub in shaping the following spatial expansions.

From this study, it is observed that Egyptian LPAIVs H9N2 have evolved into three major groups (**Supplementary Figure S2**) and was shown to have been introduced from Israel in mid 2009 (**Supplementary Figure S1**), which is in accordance with a previous study (Naguib et al., 2015). Following this incursion, no further introduction of LPAIV H9N2 has been observed from other countries. Determinants of viral diffusion in Egypt differed markedly between locations, where rural population density (Delta regions) was found to be a strong disseminator for LPAIV H9N2 viral migration in Egypt. This shows that movement dynamics within the Nile Delta region of Egypt are complex and important for the understanding of H9N2 circulation in Egypt. The data in this study suggests that governorates in middle Egypt (Giza, Fayoum and Bani Souwaif) are the major hubs in the LPAIV H9N2 transmission network in Egypt and has a strong connection between upper and lower Egyptian governorates (**Figure 4**). The spread of LPAIV H9N2 across Egypt primarily occurs through movements of domestic poultry. Moreover, the phylogeographic networks of LPAIV H9N2 in Egypt, shown in this study, are likely to be indicative of poultry movements across Egypt. Therefore, our findings propose that transportation networks of live poultry between lower (Nile Delta) and upper regions should be considered key routes for LPAIV H9N2 dissemination in Egypt.

Taken together, our study showed the transmission of H9N2 influenza viruses to, in and from Egypt, is part of the complex migration network from far Asia to the Middle East to Africa. Data generated on LPAIVs H9N2 on the transmission patterns in our study can be informative for AIV control strategies for the local administrative authorities. Note that This inferred transmission pattern of HA gene should not be projected to other gene segments, given the different evolutionary and transmission dynamics. Continuous monitoring and characterization of AIV in Egypt is recommended to fully understand the transmission patterns of this virus.

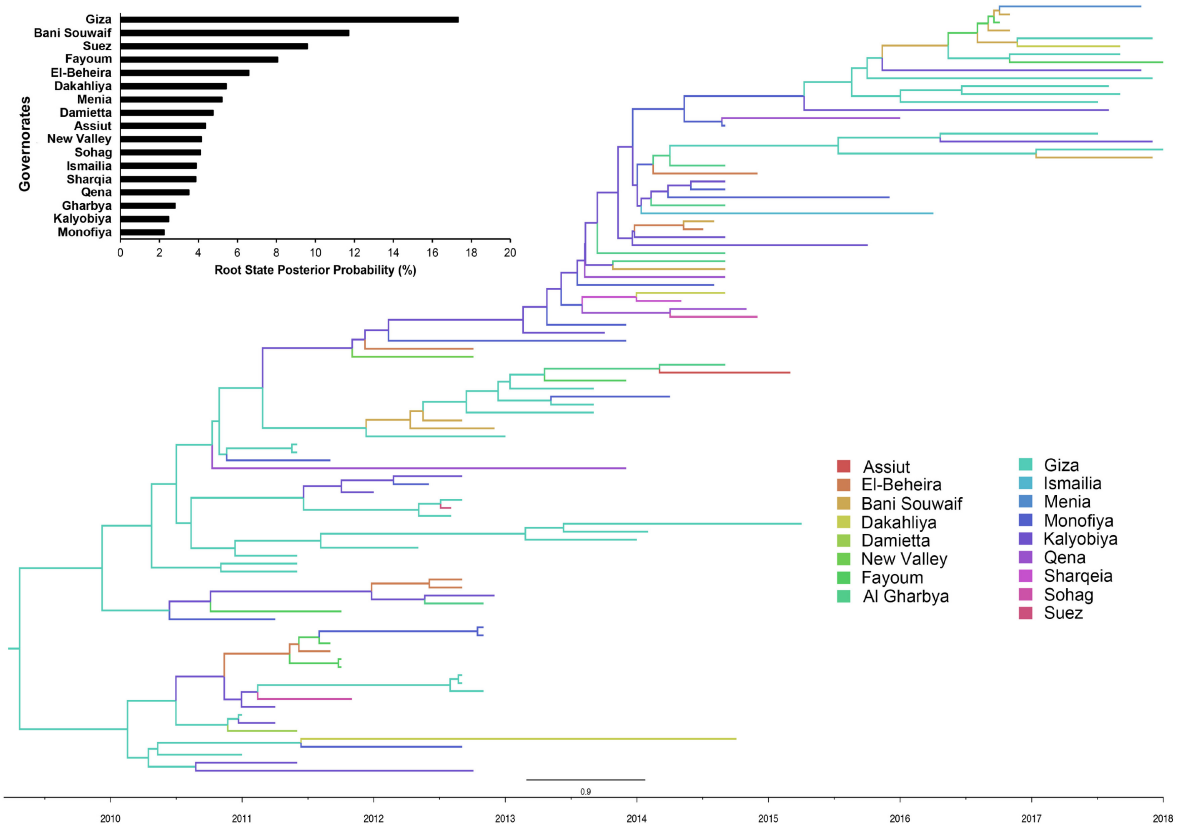

FIGURE 3 | Bayesian evolutionary tree of Egyptian LPAI H9N2 viruses based on the nucleotide sequence of the HA gene between 2010 to 2018. The posterior probability of each governorate as transmission hub, i.e., root state posterior probability, were also presented.

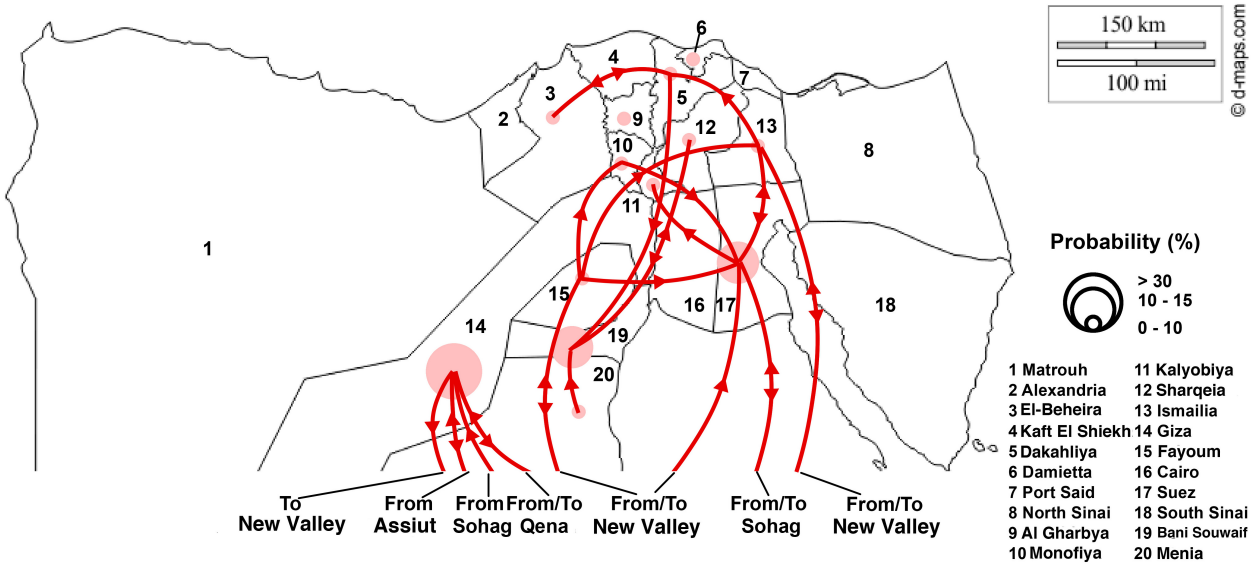

FIGURE 4 | Migration pathways of LPAI H9N2 viruses in Egypt. Lines with arrows illustrate main migration routes between the different governorates (1–20). The size of the circle indicates relative chance of a governorate acting as a migration source.

DATA AVAILABILITY STATEMENT

The datasets generated for this study can be found in the GenBank (National Center for Biotechnology Information), Global Initiative on Sharing All Influenza Data (GISAID) platforms.

AUTHOR CONTRIBUTIONS

RL, JP, and MN conceived the study, produced, analyzed, and interpreted the phylogeographic data. AA, JB, and JP provided the epidemiological data and performed the viruses sub-sampling. RL and MN drafted the manuscript. All authors critically analyzed and revised the manuscript, and provided final approval.

FUNDING

This work was supported by the Swedish Research Council VR (grant numbers: 2016-02596 and 2018–02569 to MN, BO, and ÅL), a research program by the Swedish Foundation for International Cooperation in Research and Higher Education STINT (grant number IB2017-7363 to MN). JP is funded by the Swedish research council FORMAS (grant no: 2015-710).

ACKNOWLEDGMENTS

We sincerely acknowledge the authors and submitting laboratories of the sequences deposited in the GenBank and GISAID database, on which the sequence analyses of this research were based. We do not have any financial or other relationships that may pose conflicts of interest.

SUPPLEMENTARY MATERIAL

The Supplementary Material for this article can be found online at: https://www.frontiersin.org/articles/10.3389/fmicb.2020.00392/full#supplementary-material

REFERENCES

Arafa, A., Hagag, N. M., Yehia, N., Zanaty, A. M., Naguib, M. M., and Nasef, S. A. (2012). Effect of cocirculation of highly pathogenic avian influenza H5N1 subtype with low pathogenic H9N2 subtype on the spread of infections. *Avian Dis.* 56, 849–857. doi: 10.1637/10152-040812-reg.1

Bielejec, F., Rambaut, A., Suchard, M. A., and Lemey, P. (2011). SPREAD: spatial phylogenetic reconstruction of evolutionary dynamics. *Bioinformatics* 27, 2910–2912. doi: 10.1093/bioinformatics/btr481

Birdlife (2019). *Migratory Birds & Flyways*. Available online at: https://www.birdlife.org/worldwide/programmes/migratory-birds (accessed December 10, 2019).

Drummond, A. J., Suchard, M. A., Xie, D., and Rambaut, A. (2012). Bayesian phylogenetics with BEAUti and the BEAST 1.7. *Mol. Biol. Evol.* 29, 1969–1973. doi: 10.1093/molbev/mss075

Fusaro, A., Monne, I., Salviato, A., Valastro, V., Schivo, A., Amarin, N. M., et al. (2011). Phylogeography and evolutionary history of reassortant H9N2 viruses with potential human health implications. *J. Virol.* 85, 8413–8421. doi: 10.1128/JVI.00219-11

Gomaa, M. R., Kandeil, A., El-Shesheny, R., Shehata, M. M., Mckenzie, P. P., Webby, R. J., et al. (2018). Evidence of infection with avian, human, and swine influenza viruses in pigs in Cairo, Egypt. *Arch. Virol.* 163, 359–364. doi: 10.1007/s00705-017-3619-3

Guindon, S., Delsuc, F., Dufayard, J. F., and Gascuel, O. (2009). Estimating maximum likelihood phylogenies with PhyML. *Methods Mol. Biol.* 537, 113–137. doi: 10.1007/978-1-59745-251-9_6

Guo, Y. J., Krauss, S., Senne, D. A., Mo, I. P., Lo, K. S., Xiong, X. P., et al. (2000). Characterization of the pathogenicity of members of the newly established H9N2 influenza virus lineages in Asia. *Virology* 267, 279–288. doi: 10.1006/viro.1999.0115

Hu, M., Jin, Y., Zhou, J., Huang, Z., Li, B., Zhou, W., et al. (2017). Genetic characteristic and global transmission of influenza A H9N2 virus. *Front. Microbiol.* 8:2611. doi: 10.3389/fmicb.2017.02611

Kandeil, A., El-Shesheny, R., Maatouq, A., Moatasim, Y., Cai, Z., Mckenzie, P., et al. (2017). Novel reassortant H9N2 viruses in pigeons and evidence for antigenic diversity of H9N2 viruses isolated from quails in Egypt. *J. Gen. Virol.* 98, 548–562. doi: 10.1099/jgv.0.000657

Kandeil, A., El-Shesheny, R., Maatouq, A. M., Moatasim, Y., Shehata, M. M., Bagato, O., et al. (2014). Genetic and antigenic evolution of H9N2 avian influenza viruses circulating in Egypt between 2011 and 2013. *Arch. Virol.* 159, 2861–2876. doi: 10.1007/s00705-014-2118-z

Kandeil, A., Hicks, J. T., Young, S. G., El Taweel, A. N., Kayed, A. S., Moatasim, Y., et al. (2019). Active surveillance and genetic evolution of avian influenza viruses in Egypt, 2016-2018. *Emerg. Microb. Infect.* 8, 1370–1382. doi: 10.1080/22221751.2019.1663712

Kayali, G., Kandeil, A., El-Shesheny, R., Kayed, A. S., Gomaa, M. M., Maatouq, A. M., et al. (2014). Active surveillance for avian influenza virus, Egypt, 2010-2012. *Emerg. Infect. Dis.* 20, 542–551. doi: 10.3201/eid2004.131295

Kim, S. H. (2018). Challenge for one health: co-circulation of zoonotic H5N1 and H9N2 avian influenza viruses in egypt. *Viruses* 10:E121. doi: 10.3390/v10030121

Lemey, P., Rambaut, A., Drummond, A. J., and Suchard, M. A. (2009). Bayesian phylogeography finds its roots. *PLoS Comput. Biol.* 5:e1000520. doi: 10.1371/journal.pcbi.1000520

Matrosovich, M. N., Krauss, S., and Webster, R. G. (2001). H9N2 influenza A viruses from poultry in asia have human virus-like receptor specificity. *Virology* 281, 156–162. doi: 10.1006/viro.2000.0799

Minin, V. N., and Suchard, M. A. (2008). Counting labeled transitions in continuous-time Markov models of evolution. *J. Math. Biol.* 56, 391–412. doi: 10.1007/s00285-007-0120-8

Monne, I., Hussein, H. A., Fusaro, A., Valastro, V., Hamoud, M. M., Khalefa, R. A., et al. (2012). H9N2 influenza A virus circulates in H5N1 endemically infected poultry population in Egypt. *Influen. Respir. Virus.* 7, 240–243. doi: 10.1111/j.1750-2659.2012.00399.x

Naguib, M. M., Arafa, A. S., El-Kady, M. F., Selim, A. A., Gunalan, V., Maurer-Stroh, S., et al. (2015). Evolutionary trajectories and diagnostic challenges of potentially zoonotic avian influenza viruses H5N1 and H9N2 co-circulating in Egypt. *Infect Genet. Evol.* 34, 278–291. doi: 10.1016/j.meegid.2015.06.004

Naguib, M. M., Arafa, A. S., Parvin, R., Beer, M., Vahlenkamp, T., and Harder, T. C. (2017). Insights into genetic diversity and biological propensities of potentially zoonotic avian influenza H9N2 viruses circulating in Egypt. *Virology* 511, 165–174. doi: 10.1016/j.virol.2017.08.028

Nagy, A., Mettenleiter, T. C., and Abdelwhab, E. M. (2017). A brief summary of the epidemiology and genetic relatedness of avian influenza H9N2 virus in birds and mammals in the Middle East and North Africa. *Epidemiol. Infect.* 145, 3320–3333. doi: 10.1017/S0950268817002576

Peacock, T. H. P., James, J., Sealy, J. E., and Iqbal, M. (2019). A global perspective on H9N2 avian influenza virus. *Viruses* 11:E620. doi: 10.3390/v11070620

Rambaut, A., Lam, T. T., Max Carvalho, L., and Pybus, O. G. (2016). Exploring the temporal structure of heterochronous sequences using TempEst (formerly Path-O-Gen). *Virus Evol.* 2:vew007. doi: 10.1093/ve/vew007

Samir, A., Adel, A., Arafa, A., Sultan, H., and Hussein Ahmed, H. A. (2019). Molecular pathogenic and host range determinants of reassortant Egyptian low pathogenic avian influenza H9N2 viruses from backyard chicken. *Int. J. Vet. Sci. Med.* 7, 10–19. doi: 10.1080/23144599.2019.1637046

Samy, A., and Naguib, M. M. (2018). Avian respiratory coinfection and impact on avian influenza pathogenicity in domestic poultry: field and experimental findings. *Vet. Sci.* 5:E23. doi: 10.3390/vetsci5010023

Wei, K., and Li, Y. (2018). Global genetic variation and transmission dynamics of H9N2 avian influenza virus. *Transbound. Emerg. Dis.* 65, 504–517. doi: 10.1111/tbed.12733

World Health Organization [WHO] (2016). *Influenza at the Human-Animal Interface*. Geneva: WHO.

Conflict of Interest: The authors declare that the research was conducted in the absence of any commercial or financial relationships that could be construed as a potential conflict of interest.

Copyright © 2020 Li, Adel, Bohlin, Lundkvist, Olsen, Pettersson and Naguib. This is an open-access article distributed under the terms of the Creative Commons Attribution License (CC BY). The use, distribution or reproduction in other forums is permitted, provided the original author(s) and the copyright owner(s) are credited and that the original publication in this journal is cited, in accordance with accepted academic practice. No use, distribution or reproduction is permitted which does not comply with these terms.

frontiers in Microbiology

ORIGINAL RESEARCH
published: 09 April 2020
doi: 10.3389/fmicb.2020.00620

Accumulation and Competition Amongst Deformed Wing Virus Genotypes in Naïve Australian Honeybees Provides Insight Into the Increasing Global Prevalence of Genotype B

Amanda M. Norton, Emily J. Remnant, Gabriele Buchmann and Madeleine Beekman*

Behaviour, Ecology and Evolution (BEE) Laboratory, School of Life and Environmental Sciences, The University of Sydney, Sydney, NSW, Australia

OPEN ACCESS

Edited by:
Declan C. Schroeder, University of Minnesota, United States

Reviewed by:
Lena Wilfert, Ulm University, Germany
Miguel Angel Martinez, IrsiCaixa, Spain

***Correspondence:**
Amanda M. Norton
amanda.norton@sydney.edu.au

Specialty section:
This article was submitted to Virology, a section of the journal Frontiers in Microbiology

Received: *24 January 2020*
Accepted: *19 March 2020*
Published: *09 April 2020*

Citation:
Norton AM, Remnant EJ, Buchmann G and Beekman M (2020) Accumulation and Competition Amongst Deformed Wing Virus Genotypes in Naïve Australian Honeybees Provides Insight Into the Increasing Global Prevalence of Genotype B. Front. Microbiol. 11:620. doi: 10.3389/fmicb.2020.00620

Honeybee colony deaths are often attributed to the ectoparasitic mite *Varroa destructor* and deformed wing virus (DWV), vectored by the mite. In the presence of *V. destructor* both main genotypes (DWV-A and DWV-B) have been correlated with colony loss. Studies show that DWV-B is the most prevalent genotype in the United Kingdom and Europe. More recently DWV-B has increased in prevalence in the United States. The increasing prevalence of DWV-B at the expense of DWV-A suggests that competition exists between the genotypes. Competition may be due to disparities in virulence between genotypes, differences in fitness, such as rate of replication, or a combination of factors. In this study we investigated if DWV genotypes differ in their rate of accumulation in Australian honeybees naïve to both *V. destructor* and DWV, and if viral load was associated with mortality in honeybee pupae. We singly and co-infected pupae with DWV-A, DWV-B, and a recombinant strain isolated from a *V. destructor* tolerant bee population. We monitored viral accumulation throughout pupation, up to 192 h post-injection. We found significant differences in accumulation, where DWV-A accumulated to significantly lower loads than DWV-B and the DWV-recombinant. We also found evidence of competition, where DWV-B loads were significantly reduced in the presence of DWV-A, but still accumulated to the highest loads overall. In contrast to previous studies, we found significant differences in virulence between pupae injected with DWV-A and DWV-B. The average mortality associated with DWV-B (0.4% ± 0.33 SE) and DWV-recombinant (2.2% ± 0.83 SE) injection were significantly less than observed for DWV-A (11% ± 1.2 SE). Our results suggest that a higher proportion of DWV-B infected pupae will emerge into adults, compared to DWV-A. Overall, our data suggest that low mortality in pupae and the ability of DWV-B to accumulate to higher loads relative to DWV-A even during co-infection may favor vector transmission by *V. destructor*, and may thus be contributing factors to the increasing prevalence of DWV-B globally.

Keywords: RNA viruses, accumulation, competition, virulence, honeybee, parasites, pathogens, *Varroa*

INTRODUCTION

Varroa destructor is arguably one of the biggest threats to Western honeybee (*Apis mellifera*) populations worldwide. Over the past 60 years, *V. destructor* has spread globally from its origin in Asia where the mite originally parasitized the Asian honeybee *Apis cerana* (Solignac et al., 2005). *V. destructor* parasitism is particularly destructive to *A. mellifera* (hereafter simply honeybees), and is associated with significant colony losses. Australia is currently the only major beekeeping country to remain free from *V. destructor* (Oldroyd, 1999; Roberts et al., 2017).

Honeybee colony losses associated with *V. destructor* have often been attributed to viruses vectored by mites during feeding. One virus in particular, deformed wing virus (DWV), is frequently associated with *V. destructor* (Highfield et al., 2009; Martin et al., 2012; Mondet et al., 2014; Martin and Brettell, 2019). DWV is a single-stranded positive sense RNA virus belonging to the *Iflaviridae* family. Prior to the spread of *V. destructor*, DWV was rarely detected whereas now the virus is found in virtually all honeybee populations worldwide, excluding Australia (Roberts et al., 2017). In some *Varroa*-free honeybee populations, DWV has been shown to have low prevalence and accumulate to very low levels (Martin et al., 2012; Ryabov et al., 2014; Shutler et al., 2014; McMahon et al., 2016). In contrast, numerous studies have found a positive correlation between *V. destructor* infestation levels and increased DWV loads (Martin et al., 2012; Nazzi et al., 2012; Mondet et al., 2014; Wu et al., 2017). Within a *V. destructor* infested colony, vector transmission of DWV is associated with approximately 20% pupal mortality (Martin, 2001; Martin et al., 2013). Such relatively low mortality allows the majority of DWV infected brood to emerge as adults. And because *V. destructor* reproduces within honeybee brood cells (Martin, 1995), low brood mortality results in a continuing increase in the number of mites and transmission of DWV.

Three DWV genotypes have been described: DWV-A, DWV-B, and DWV-C (Mordecai et al., 2016b); only DWV-A (formally DWV) and DWV-B [formally *V. destructor virus* 1 or VDV-1 (Ongus et al., 2004)] are currently recognized by the International Committee on Taxonomy of Viruses. For clarity, we have employed the types A and B nomenclature widely adopted in recent publications (Martin et al., 2012; McMahon et al., 2016; Mordecai et al., 2016a,b; Brettell and Martin, 2017; Kevill et al., 2017; Gisder et al., 2018; Brettell et al., 2019; Dubois et al., 2019; Kevill et al., 2019; Remnant et al., 2019; Tehel et al., 2019).

An immediate effect of *V. destructor* appears to be a reduction in the genetic diversity of DWV in honeybees both in the field (Martin et al., 2012) and in experiments using injection of DWV to mimic vector transmission (Ryabov et al., 2014). Over time, the distribution of DWV genotypes changes so that one DWV genotype prevails within honeybee populations. DWV-B has become the most common variant in the United Kingdom (UK) and Europe (McMahon et al., 2016; Kevill et al., 2019; Manley et al., 2019). In North-America DWV-A remains the most common genotype (Ryabov et al., 2017; Kevill et al., 2019). However, Ryabov et al. (2017) found that DWV-B prevalence in the United States increased from 3% in 2010 to 65% in 2016. Similarly, Kevill et al. (2019) found that DWV-B was prevalent in 56% of tested colonies in 2016, and the dominant genotype in 23% of those colonies. Kevill et al. (2019) predicted that DWV-B prevalence will continue to increase and supersede DWV-A with time, as observed in England and Wales. Such change in relative prevalence suggests that the different DWV genotypes compete within their host. The increased prevalence of DWV-B may potentially be explained by differences in replication rate within the host, difference in virulence and associated host mortality, or a combination of both.

Understanding the exact relationship between DWV genotype and host virulence is far from straightforward. Not all studies distinguish between DWV genotypes. In those studies that do both DWV-A (Highfield et al., 2009; Martin et al., 2012; Mondet et al., 2014; Kevill et al., 2017, 2019; Barroso-Arévalo et al., 2019b) and DWV-B (Natsopoulou et al., 2017) have been associated with colony deaths in the presence of *V. destructor*. At the same time, high viral loads of DWV-B have been associated with low levels of colony mortality in the United Kingdom and Spain (Mordecai et al., 2016a; Barroso-Arévalo et al., 2019b; Kevill et al., 2019). High DWV-B loads in surviving colonies that were untreated for *V. destructor* led Mordecai et al. (2016a) to hypothesize that DWV-B may outcompete DWV-A via 'superinfection exclusion.' If DWV-B is a superior competitor, it could prevent DWV-A from replicating to high levels. If, then, DWV-B causes less damage to the host, the exclusion of the more harmful DWV-A genotype could result in the association between DWV-B and low honeybee mortality.

Despite evidence of colonies surviving with high DWV-B loads, experimental evidence thus far indicates that DWV-B is more harmful to adult honeybees than DWV-A. After DWV-B was injected into adult bees, the virus was detected in brain tissue which was associated with impairment of cognitive function (Gisder et al., 2018). The inocula were then serially passaged in pupae before a second round of adult injections. After one round of serial passage viral particles were not detected in the bees' brain and the bees did not suffer from cognitive impairment. Gisder et al. (2018) associated the decreased tissue tropism and virulence of the passaged inoculum with a concurrent sequence shift from DWV-B to DWV-A. In a different study, injection of DWV-B into newly emerged adults resulted in significantly altered foraging behavior and higher mortality compared to controls (Benaets et al., 2017). However, the same experiment was not conducted on DWV-A (Benaets et al., 2017). When DWV-A and DWV-B were compared in a separate study, injection of DWV-B into newly emerged adults resulted in a significant reduction in survival compared to DWV-A (McMahon et al., 2016).

The most likely life stage to be infected with DWV is the pupal stage. Models have suggested that vector transmission of DWV to pupae results in reduced longevity in emerging adult honeybees and can lead to colony death in temperate climates, due to significantly reduced overwinter workforce (Martin, 2001; Sumpter and Martin, 2004). Thus, some studies have assessed whether DWV genotypes affect pupae differently. Gisder et al. (2018) found that injection of DWV-B into pupae resulted in significantly higher mortality compared to pupae injected with

the passaged inoculum. Lamp et al. (2016) did not test DWV-B, but showed that both DWV-A directly isolated from infected bees and a constructed molecular clone both caused pupal death. However, Tehel et al. (2019) found no difference in survival between pupae injected with DWV-A or DWV-B when pupae were injected with the same source inocula as McMahon et al. (2016). Dubois et al. (2019) also found no difference in mortality between pupae infected with DWV-A and DWV-B obtained from heads of naturally infected bees. Similarly, a study using *V. destructor* and DWV naïve Australian honeybee pupae found no significant pupal mortality when white-eyed pupae were injected with DWV-A isolated from adult bees with overt disease symptoms, including deformed wings (Remnant et al., 2019).

Clearly while the global association between *V. destructor* and DWV seems irrefutable, determining whether virulence differences exist between DWV genotypes remains a challenge. The aforementioned experimental studies differ in many attributes, such as source inocula [with the exception of (McMahon et al., 2016; Tehel et al., 2019)], bee populations, life stage infected, experiment duration, and potential presence of other pathogens. In addition, covert infections with DWV may affect results as injection with buffered salt solutions can activate DWV replication (Dubois et al., 2019; Posada-Florez et al., 2019; Tehel et al., 2019). Similarly, previous infestations with *V. destructor* may have changed the viral landscape within honeybee populations by selecting for particular DWV genotypes that are better adapted to vector-based transmission. Australian honeybees are naïve to both *V. destructor* and DWV and are therefore an ideal model to determine the dynamics between different DWV genotypes. We infected white-eyed pupae to reflect the life stage at which *V. destructor* first vectors DWV to honeybees (Bailey and Ball, 1991). We infected pupae by injecting either a single DWV genotype or two genotypes (co-infection). Co-infection allowed us to determine the extent to which different DWV genotypes compete within the same host. We further determined if there is a relationship between viral load and host damage (mortality).

MATERIALS AND METHODS

DWV Source Material and Strain Confirmation

Inocula were prepared from individual asymptomatic adult bees collected from Blenheim, New Zealand (DWV-A) and Amsterdam Water Dunes, the Netherlands (DWV-B and DWV-recombinant). The New Zealand bees were collected from *V. destructor* treated colonies and the Netherlands bees were collected from colonies that were part of a selection program for *V. destructor* tolerance (Panziera et al., 2017). The bees were imported on dry ice and stored at −80°C (Import permit and Quarantine details below). As we intended to use the source material as inocula, we firstly extracted viral material from individual bees from each population [protocol adapted from Remnant et al. (2019)]. We homogenized the thorax and abdomen [as eye pigments have been shown to inhibit PCR reactions (Boncristiani et al., 2011)] of individual adults in 2 mL 0.5 M potassium phosphate buffer (PPB) pH 8. Within a fume hood, we added 5% v/v diethyl ether and 10% v/v chloroform and shook vigorously for 30 s, before centrifuging at max speed ($>20{,}000 \times g$) for 2 min. We then collected the supernatant and passed it through a 0.22 μm nitrocellulose filter to remove bacterial or particulate contaminants. We portioned the filtrate into aliquots, which were later used for RNA extraction or inoculation of pupae after strain identification.

For inocula identification, we obtained RNA from 100 μL of the partitioned filtrate using the RNeasy mini kit (Qiagen). For our sequencing negative control, we extracted RNA from a single juvenile velvet worm (*Euperipatoides rowelli*) using the Direct-zol RNA MiniPrep Plus (Zymo Research). To avoid any potential cross contamination we prepared the velvet worm sample in the Evolutionary and Integrative Zoology Laboratory, University of Sydney. All RNA samples were treated with DNase (Ambion® TURBO DNA-free kit) according to manufacturer's instructions. We shipped treated RNA (80–150 ng/μL) on dry ice to the Australian Genome Research Facility (AGRF) laboratory (Melbourne, Australia) for preparation of whole transcriptome, 150 bp paired-end libraries with ribosome depletion and MiSeq (Illumina) sequencing.

Sequencing reads were checked for quality using FastQC[1] and trimmed to remove residual adaptor sequences and low-quality sequences using Trimmomatic (Bolger et al., 2014). Trimmed reads were assembled *de novo* into contigs using the metagenomic assembler Megahit (Li et al., 2015). Resulting contigs were compared to a custom reference library containing previously identified honeybee virus genome sequences using BLASTn, including but not limited to acute bee paralysis virus (ABPV), *Apis* rhabdovirus (ARV) (Remnant et al., 2017), black queen cell virus (BQCV), chronic bee paralysis virus (CBPV), Israeli acute paralysis virus (IAPV), Kashmir bee virus (KBV), Lake Sinai virus (LSV), and sacbrood virus (SBV). The DWV-A and DWV-rec inocula were negative for all other honeybee viruses, including BQCV. The DWV-B inoculum contained low amounts of LSV and ARV-1 and ARV-2, however, this did not impact our study as we found that these viruses were not transmissible to pupae via injection of our DWV-B inoculum (see section "Results"). In addition, we examined a general viral reference database containing a comprehensive library of viral protein sequences downloaded from GenBank by using BLASTx to identify any potential novel viral sequences. Identified DWV contigs from each source inoculum were aligned to the DWV-A and DWV-B reference genomes in Geneious [Version 10.2.4, (Kearse et al., 2012); accession numbers AJ489744 and AY251269], to produce alternate DWV strain sequence assemblies for each source inoculum. The DWV-A and DWV-B inocula sequences only contained the DWV genotype of interest. The DWV-rec inoculum contained one predominant genotype (**Figure 1**), where the average coverage per base was approximately 2,800-fold, as estimated by Megahit. Additionally within the DWV-rec inoculum, we detected low frequencies of DWV-B, and an additional recombinant with an extended DWV-A fragment to position 2,140, with low coverage per base values of 26

[1]http://www.bioinformatics.babraham.ac.uk/projects/fastqc/

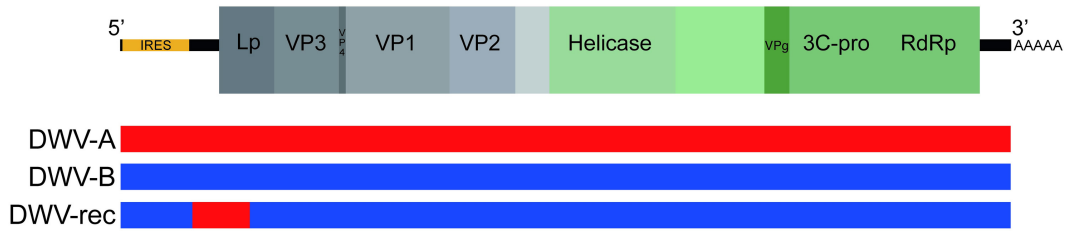

FIGURE 1 | Schematic of the DWV genome structure. Location of coat proteins as per de Miranda and Genersch (2010). DWV-A and DWV-B sequence shown in red and blue, respectively. The Netherlands recombinant (DWV-rec) predominantly corresponds to DWV-B, with a DWV-A region between nucleotide positions 829 and 1487. The first recombination breakpoint occurs after the predicted internal ribosome entry site (IRES), which is predicted to fall within the first 810 nucleotides (Ongus et al., 2006).

and 408, respectively (partial contig sequences available as **Supplementary Texts S1, S2**). The DWV-A, DWV-B and DWV-rec inocula sequences used in this study were deposited to GenBank [accession numbers MN538208–MN538210]. We also compared our inocula sequences to strains previously injected by Gisder et al. (2018), Remnant et al. (2019) and Tehel et al. (2019). We performed pairwise comparisons and nucleotide alignments in Geneious using Muscle, and generated a maximum likelihood phylogenetic tree using PhyML (**Supplementary Figure S1** and **Supplementary Table S1**). We found that our DWV-A and DWV-B inoculum were the most similar to the reference genomes, and more closely related to the inocula used by Remnant et al. (2019) and Tehel et al. (2019), compared to the isolates injected by Gisder et al. (2018).

Inocula Standardization

Quantification of Inocula Viral Load

First strand cDNA was synthesized from DNase treated RNA (0.2–0.4 μg) (Ambion® TURBO DNA-free kit) using SuperScript III Reverse Transcriptase (Invitrogen) with random hexamer primers, in 10 μL reaction volumes. The resulting cDNA was diluted in 30 μL UltraPure nuclease-free dH_2O (Invitrogen). To determine the viral load of each inoculum we used quantitative PCR (qPCR) to compare quantitation cycle (Cq) values against the DWV-A and DWV-B standard curves (described below), and multiplied by dilution factor of 1/6,400. We diluted inocula in 0.5 M PPB pH 8.0 to standardize DWV concentration to 1×10^7 genome equivalents (GE). Next, we added 10% green food coloring (Queen, Australia) to visually aid injection.

Preparation of DWV-A and DWV-B qPCR Standards

We used absolute quantification with DWV-A and DWV-B plasmid standards to accurately determine viral loads in inocula and injected pupae (**Supplementary Figure S2**). DWV-A and DWV-B RdRp plasmid standards were prepared from the source material cDNA after strain confirmation (above), using the method adapted from Kevill et al. (2017). We analyzed the cDNA by PCR with the Kapa2G Robust PCR Kit (Kapa Biosystems), as per manufacturer's instructions, using DWV strain specific RdRp primers (**Supplementary Table S2**). PCR cycling conditions for all reactions were 94°C (3 min), followed by 35 cycles of 94, 58, and 72°C (30 s), and 72°C (5 min). We analyzed PCR products by gel electrophoresis on 1% agarose gel with SB buffer and SYBR Safe DNA stain (Life Technologies). We cleaned the PCR fragments with GF-1 PCR Clean-up Kit (Vivantis). Plasmid vectors containing DWV-A or DWV-B fragments were prepared with TOPO Cloning reaction and transfected into Transform One Shot TOP10 competent *Escherichia coli* cells (Invitrogen). LB plates with 50 μg/mL kanamycin were prepared as per manufacturer's instruction, plated with 100 μL cells and incubated at 37°C overnight. We performed colony PCR with DWV strain specific primers to ensure that transformation had occurred, and visualized PCR products on 1% agarose gel (as above). Colonies positive for DWV-A or DWV-B clones were added to 2 mL LB broth with 2 μL kanamycin and incubated at 37°C overnight. We then isolated plasmid DNA with Wizard SV Plus Minipreps DNA Purification System (Promega). As circular plasmids are known to supercoil and produce unreliable absolute qPCR results (Hou et al., 2010), we linearized our plasmids with *PmeI* restriction digest (New England Biolabs). We confirmed linearization on 1% agarose gel, cleaned plasmids (as above), and quantified DNA concentration with Qubit Broad Range Assay. We calculated plasmid copy numbers as per Staroscik (2004), and diluted DWV-A and DWV-B linear plasmids to 5 ng/μL, which was equivalent to 1×10^9 genome copies of DWV.

qPCR of DWV Plasmid Standards

We prepared 10-fold serial dilutions from the 1×10^9 plasmid stock to generate DWV-A and DWV-B standard curves from 10^8 to 10^2, prior to qPCR analysis with a Bio-Rad CFX384 Touch real-time PCR detection system. We performed all 5 μL qPCR reactions in triplicate with SsoAdvanced Universal SYBR Green supermix (Bio-Rad), forward and reverse primers (final concentration 500 nM each), and 1 μL cDNA, in both DWV-A and DWV-B master mixes. We used the following cycling conditions: 95°C (10 min), followed by 35 cycles of 95°C (30 s), 58°C (30 s) and 72°C (30 s). Melt curve analysis immediately followed between 55 and 95°C, at 0.5°C increments. We plotted average Cq values against the $\log_{10}$ of the plasmid copy number to give a standard curve for DWV-A and DWV-B. PCR primer efficiency ($E = 10^{[-1/\text{slope}]}$) was 1.91 for DWV-A (slope = −3.5557, Y-intercept = 35.165, $R^2 = 0.9998$) and 1.92 for DWV-B (slope = −3.5343, Y-intercept = 35.125, $R^2 = 0.9998$).

Pupal Injection Assay and Sample Preparation

Experimental Injection of Pupae

We collected approximately 650 white-eyed pupae per colony, from capped brood cells of three unrelated *A. mellifera* colonies kept at the University of Sydney's apiary. These colonies are naïve to both *V. destructor* and DWV, neither of which are established in Australia (Roberts et al., 2017). Pupae that showed signs of melanization or damage from uncapping were excluded from the assay prior to injection. Mated *V. destructor* females enter a honeybee brood cell just prior to the cell being capped and the bee undergoing pupation (Donzé and Guerin, 1994). The mother mite and her offspring feed on the fat bodies of the developing bee (Ramsey et al., 2019), during which the mother mite can transmit viruses acquired from her previous meal (Bowen-Walker et al., 1999). To mimic the natural vector-mediated infection route as closely as possible, we injected 475 white-eyed pupae per colony; each colony consisted of five treatment groups of 95 pupae. We adapted the injection protocol used by McMahon et al. (2016), to reflect the same viral load and similar DWV treatments. In our study, we injected pupae with either 2 μL of: (1) 0.5 M PPB pH 8 ('buffer control'), (2–4), 1×10^7 GE of DWV-A, DWV-B, or the recombinant strain (DWV-rec), or (5) an equal mixture ('co-injection') containing 5×10^6 GE of DWV-A and DWV-B. In contrast to McMahon et al. (2016), we co-injected pupae with the mixture to assess strain competition during co-infection.

We injected white-eyed pupae with a 32G needle attached to a 10 μL Hamilton syringe inserted between the 3rd and 4th tergites at the side of the abdomen [the typical *V. destructor* feeding site (Donzé and Guerin, 1994)], underneath but parallel to the cuticle to avoid puncturing the gut. After injection, we immediately placed pupae into Petri dishes lined with sterile filter paper (10 pupae/Petri dish). We placed the Petri dishes onto shallow racks within clip-locked plastic tubs (Sistema) and incubated at 34.5°C for 8 days (192 h) in the dark. To keep the humidity high, we added 30 mL sterile H_2O to the plastic tubs housing the Petri dishes.

After injection, we randomly selected four pupae per treatment and colony at regular time-points (1, 4, 8, 12, and 24 h) and every subsequent 24 h for 192 h (just prior to eclosion). Sampled pupae were immediately frozen at −80°C. We continued to incubate the pupae not collected for RNA extraction until 192 h [when remaining pupae were terminated due to Quarantine permit conditions (see below)]. We visually monitored the survival of pupae throughout the experiment, using an adapted version of the method described by Remnant et al. (2019). We used the continual pigment changes in pupal eye and body color (Jay, 1962) as indicators of healthy development. A pupa was classed as dead when eye or body pigments has ceased changing color for 48 h.

RNA Extraction and cDNA Synthesis

We extracted RNA from each frozen pupa separately in 1 mL of TRI Reagent (Sigma) with a TissueLyser, according to the manufacturer's protocol. We suspended RNA pellets in 200 μL ultra-pure water (Invitrogen) and quantified the concentration with Qubit Broad Range Assay (Life Technologies). Samples were standardized to 200 μg/mL RNA to account for body mass differences between individual pupae. First strand cDNA was synthesized from 0.8 μg DNase treated RNA in 10 μL reaction volumes, as described above. The resulting cDNA was diluted in 30 μL UltraPure nuclease-free dH_2O (Invitrogen).

qPCR Analysis

Viral Analysis of Pupae

For DWV analysis, cDNA from all individual pupae were analyzed in both DWV-A and DWV-B master mixes alongside DWV-A and DWV-B plasmid standards, and positive and negative controls. cDNA from the source inocula was used as positive DWV controls and water served as a negative (no template) control. In addition, we screened all samples for BQCV, SBV and amplified the endogenous control gene, *Actin* (**Supplementary Table S2**). Whole transcriptome sequencing results indicated that the DWV-B source material was positive for LSV, and ARV-1 and ARV-2. We screened DWV-B injected pupae for ARV-1 and ARV-2 by qPCR, and LSV by endpoint PCR with primers that amplify multiple LSV strains (**Supplementary Table S2**). The qPCR and 1% agarose gel results showed that these viruses were not transmitted to pupae via injection of DWV-B inoculum.

Data Analyses

Relative Viral Loads

Average *C*q values from triplicate qPCR analyses were confirmed to have a standard deviation of ≤0.3 and we considered *C*q values ≥ 35 to be DWV free. A small number of samples (3.2% of 720 pupae) randomly distributed across each treatment and colony had abnormal amplification of DWV or *Actin*. These cases included two pupae which had very high average *C*q values of 31.2 and 28.3 for *Actin*, three pupae with abnormally low DWV loads for their time-point, and 17 pupae where DWV-A or DWV-B was detected in the opposing qPCR master mix to what was injected. We excluded these pupae from further analyses and attributed these anomalies to possible pupal death, error during injection, and contamination during downstream processing, respectively. Though we suspected it unlikely, we wanted to ensure that the three pupae with low DWV loads for their time point (one pupa injected with DWV-rec from Colony 2 at 192 h post-injection, and two co-injected pupae from Colony 3 at 144 h post-injection) were not true reflections of natural variation between individual pupae. Thus, we repeated the statistical analyses with these three individuals included (see section "Results" for further details).

We measured the accumulation of viral loads in pupae from 8 to 192 h post-injection, relative to housekeeping gene *Actin* to account for any precision error during preparation and handling of samples. Primer efficiencies were calculated using the slope of the standard curve constructed with a 10-fold dilution series of cDNA, from 10^0 to 10^{-6} (**Supplementary Table S2**). We determined the relative loads of DWV strains or BQCV with the Pfaffl expression ratio (Pfaffl, 2001), which mathematically corrects for differences in primer efficiencies. The calculation compares the primer efficiency (E) and *C*q difference (Δ) of the

target virus (DWV strain or BQCV) to those of reference gene *Actin*, in individual pupae versus buffer controls. We assigned buffer injected pupae a Cq of 40 for their viral value, as they were negative for DWV and BQCV.

Absolute DWV Viral Loads

Absolute viral loads in DWV injected pupae were interpolated from mean Cq values against the associated standard curve and multiplied by dilution factor (9/4000). This gave the absolute viral load as DWV genome equivalents in cDNA synthesized from 0.8 μg RNA. Mean absolute viral loads per treatment and colony (8–192 h post-injection) have been provided in the **Supplementary Material** (**Supplementary Figure S2**) so that our results can be compared to other studies.

Statistical Analyses

Accumulation and Competition

To determine if there were significant differences in mean viral loads (relative to *Actin*) between genotypes over time we used a two-way ANOVA followed by Tukey (HSD) *post hoc* analysis. As viral loads rapidly increased over many orders of magnitude within the first 48 h (exponential phase of replication) and were visibly different between genotypes, we chose to analyze the most linear and consistent phase of the data, from 48 to 192 h post injection. A visual assessment of the homogeneity of variance (Residual vs. Fitted plot) and normality (Normal QQ plot) assumptions showed that a fourth root transformation of the response variable (mean DWV load) substantially improved the model. We used backward elimination based on Akaike's Information Criterion (AIC) values to fit the most parsimonious model. All statistical analyses were performed with RStudio software (R version 3.5.0).

Survival

We analyzed the survival of pupae throughout the incubation period when exposed to the five different injection treatments. At each specific time-point pupae were assigned a survival value of 0 if alive or censored (removed for viral analysis), or 1 if dead. As the data did not meet the Cox proportional hazards assumption, we analyzed the mean proportion of pupal survival with a generalized linear mixed effects model (glmer) with binomial distribution and logit link function ("lme4" package) (Bates et al., 2018). Again, the most parsimonious model was determined with backward elimination based on AIC values. We then analyzed the final model as a type II ANOVA ("car" package) (Fox et al., 2018), followed by Tukey pairwise comparison analysis using lsmeans function ("lsmeans" package) (Lenth, 2018).

Quarantine Permit

Frozen adult honeybees (workers) containing Deformed wing virus were imported from New Zealand and the Netherlands under our Department of Agriculture and Water Resources import permit 0000917783. The permit allows us to infect local honeybee pupae with DWV within our strictly controlled Quarantine approved laboratory at the University of Sydney; however, all pupae must be terminated prior to eclosion. Thus, the remaining pupae that were not collected at earlier time points for viral analysis were terminated at 192 h post-injection, prior to eclosion.

RESULTS

Viral Accumulation Post-injection

We measured the accumulation of viral loads relative to housekeeping gene *Actin* and as absolute genome copy equivalents by standard curve (**Supplementary Figure S2**) in individual pupae using qPCR with cDNA synthesized from 0.8 μg RNA. Our method does not measure any level of viral degradation by the honeybee immune response and therefore reflects the net virus levels, assuming that a combination of viral replication and degradation occurs. DWV was not detected in any of our buffer injected pupae (n = 144). The average Cq values for DWV in pupae at 1 and 4 h post-injection were >30, inconsistent between samples, and in some individuals DWV was not detected at all. Thus, these time points were excluded from further analyses. DWV was detected in all DWV-injected pupae from 8 h post-injection onwards. Viral loads of all genotypes (DWV-A, DWV-B, and DWV-rec) rapidly increased within the first 48 h post-injection, either when injected alone (**Figure 2** and **Supplementary Figure S3**) or co-injected (DWV-A and DWV-B) (**Figure 3** and **Supplementary Figure S4**), and plateaued between 72 and 96 h post-injection. We found that accumulation patterns were more dynamic within the first 48 h, with high variation between genotypes and colonies. Despite this variation, DWV-B loads were generally lower than DWV-A and DWV-rec, particularly in colonies 1 and 2. However, DWV-B loads in all colonies exceeded DWV-A from 72 h post-injection. This remained true when DWV-A and DWV-B were co-injected excluding DWV-B loads in colony 1 compared to DWV-A loads in colonies 2 and 3 (**Figure 3**).

To determine if there was a significant difference in the net accumulation of viral loads from 48 to 192 h post-injection, we compared the mean viral loads of all genotypes relative to *Actin* (injected singly or co-injected) with an ANOVA followed by Tukey (HSD) *post hoc* analysis. We found significant differences in mean viral loads amongst all genotypes (F = 248.642; df = 4, 381; $p < 0.0001$), and found that the strains differed in the rate at which they accumulated, as indicated by a significant strain × time interaction (F = 15.325; df = 4, 381; $p < 0.0001$) (**Supplementary Table S3**). DWV-B accumulated to significantly higher loads compared to DWV-A in all colonies [Tukey (HSD) *post hoc* $p < 0.0001$; **Figure 2** and **Supplementary Table S4**], and viral loads were 5- to 10-fold higher than DWV-A. The accumulation of DWV-B and DWV-rec were not significantly different within the same colonies ($p < 0.05$). However, mean viral loads were significantly affected by colony (F = 147.876; df = 2, 381; $p < 0.0001$), although the overall pattern of increase over time remained the same. We found that colony 1 pupae injected with DWV-A or DWV-rec had significantly lower loads compared to colonies 2 and 3 ($p < 0.0001$), and that DWV-rec loads in colony 1 were not significantly different to DWV-A loads in colony 3 (p = 0.1358). Similarly, DWV-B loads were significantly different between all colonies ($p < 0.05$). We

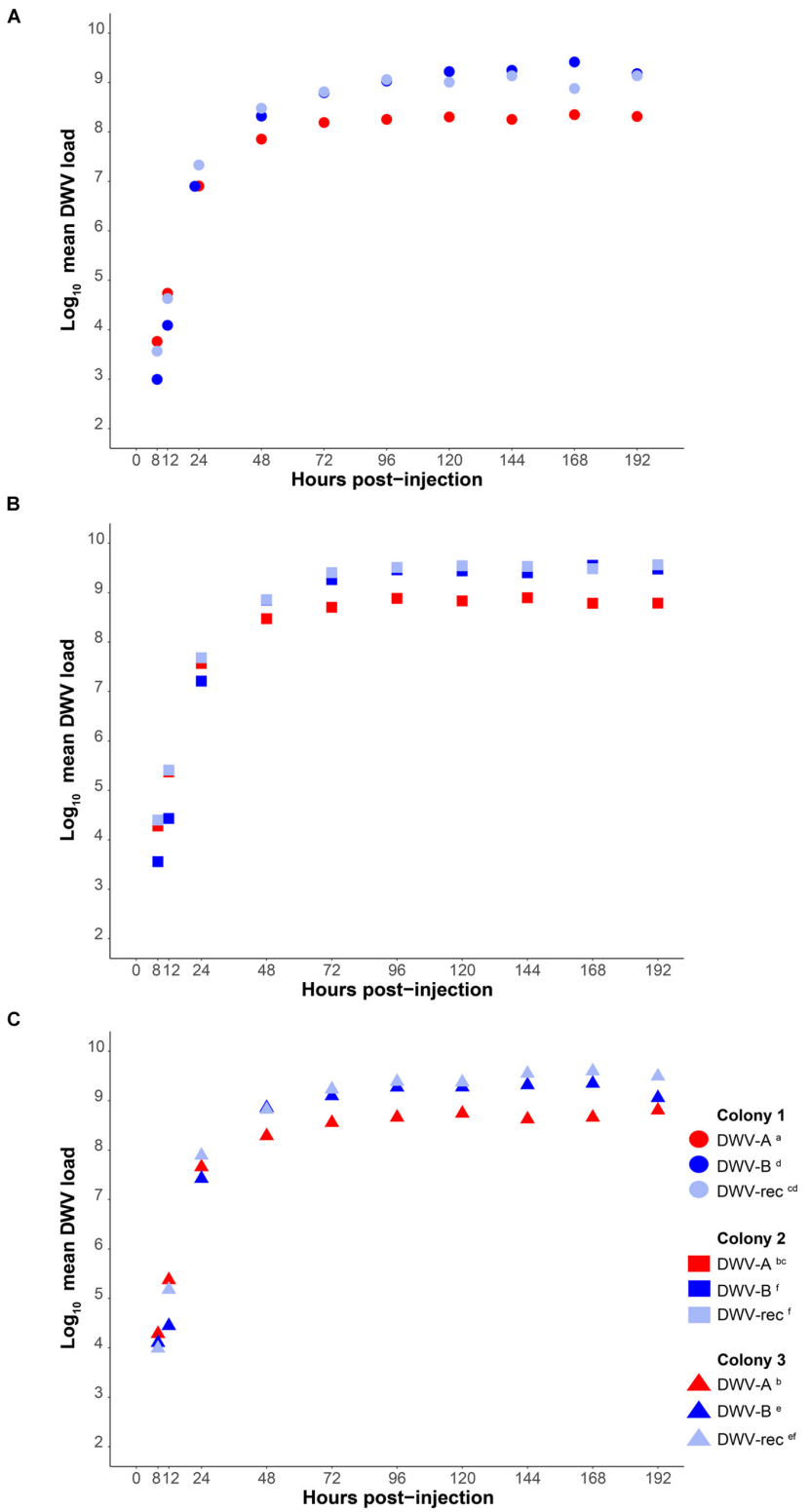

FIGURE 2 | Mean DWV viral loads of individually infected pupae from 8 to 192 h post-injection (n = 120 per treatment), relative to housekeeping gene *Actin* in cDNA synthesized from 0.8 μg RNA. White-eyed pupae from three naïve colonies **(A–C)** were singly injected with 1×10^7 genome equivalents of DWV-A, DWV-B or recombinant strain ('DWV-rec'). Viral loads rapidly increased over several orders of magnitude within the first 48 h of infection (exponential replication phase). Statistical analyses were performed in the linear phase of the data, from 48 to 192 h post-injection. Significant ($p < 0.05$) differences between genotypes and colonies indicated with lettering. See the electronic **Supplementary Material**, **Supplementary Tables S3, S4** for details of the statistical analyses.

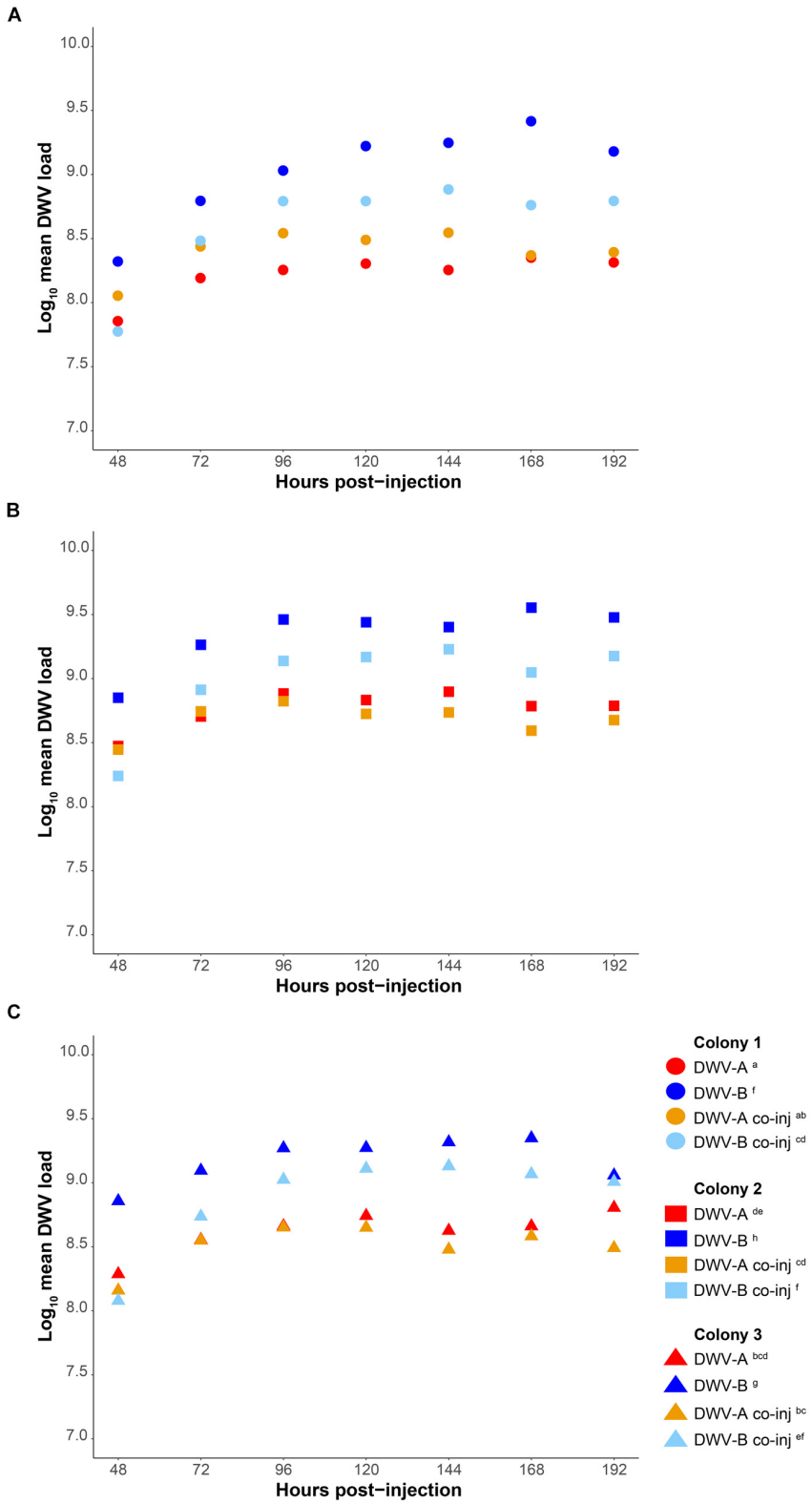

FIGURE 3 | Comparison of mean DWV viral loads of individual pupae singly infected with DWV-A or DWV-B versus pupae co-injected with 5×10^6 genome equivalents of DWV-A and DWV-B, from 48 to 192 h post-injection. Viral loads are relative to housekeeping gene *Actin* in cDNA synthesized from 0.8 μg RNA. Accumulation loads are displayed by colony **(A–C)**. Significant ($p < 0.05$) differences between genotypes and colonies indicated with lettering. Viral loads of singly injected pupae also shown in **Figure 2**.

also found a significant interaction between strain and colony ($F = 4.837$; $df = 8, 381$; $p < 0.0001$). Upon reanalysis, the inclusion of the three pupae with low loads for their time point did not alter the significance of any of the predictor variables (**Supplementary Table S5**). However, we did find slight differences in the pairwise comparisons of colonies; DWV-B loads between colonies 1 and 3, and 2 and 3 were no longer significantly different ($p > 0.05$) (**Supplementary Table S6**).

We classified competition between DWV genotypes as a significant reduction in mean viral loads of DWV-A or DWV-B when co-injected compared to singly from 48 to 192 h post-injection, relative to *Actin*. Co-injected DWV-B loads were significantly lower than when DWV-B was injected alone in all colonies ($p < 0.0001$; **Figure 3** and **Supplementary Table S4**). In contrast, DWV-A loads did not differ when injected singly or when co-injected ($p > 0.05$). As when injected singly, we found that DWV-A loads in co-injected pupae were significantly lower in colony 1 compared to colony 2, and DWV-B loads were significantly lower in colony 1 compared to colonies 2 and 3 ($p < 0.05$). We found slight differences in these results with the inclusion of the three additional pupae, whereby DWV-A loads in co-injected pupae were significantly higher ($p < 0.05$) in colony 2 compared to both colony 1 and 3 (**Supplementary Table S6**).

Survival

We monitored the survival of pupae throughout the incubation period when exposed to the five different injection treatments. At each specific time-point pupae were assigned a survival value of 0 if alive or censored (removed for viral analysis), or 1 if dead. While the vast majority of pupae survived the injections, survival was significantly affected by treatment ($\chi^2 = 44.472$; $df = 4$; $p \leq 0.0001$) (**Supplementary Table S7**). The survival of pupae singly or co-injected with DWV-A did not significantly differ ($p = 0.1095$; **Figure 4A** and **Supplementary Table S8**). However, only pupae singly injected with DWV-A had mortality that significantly differed from the buffer control ($p \leq 0.0001$), and only after 120 h post-injection (**Figure 4B**). The survival of pupae injected with DWV-B or DWV-rec did not significantly differ from that of the buffer controls ($p > 0.05$). 'Colony' had no effect on survival (using Akaike's information criterion during backward elimination; **Supplementary Table S9**).

Presence of Other Viruses in Injected Pupae

Because our DWV-B inoculum contained LSV, and ARV-1 and ARV-2 we screened the DWV-B injected pupae for LSV by endpoint PCR with primers designed to amplify multiple variant strains, and ARV-1 and ARV-2 by qPCR (**Supplementary Table S2**). LSV, ARV-1 and ARV-2 were not detected in any of the DWV-B injected pupae, suggesting that these viruses were not transmissible via injection of the DWV-B inoculum. The DWV-A and DWV-rec inocula were negative for all other known honeybee viruses. However, we additionally chose to screen all injected pupae for BQCV and SBV via qPCR as Remnant et al. (2019) previously found covert infections of both viruses in our honeybee population. We did not detect SBV in any pupae across all colonies. In contrast, we detected BQCV in some of the DWV-A and co-injected pupae, yet BQCV was not detected in any of the DWV-B, DWV-rec or buffer injected pupae across the three colonies. The relative BQCV loads varied highly between individuals and colonies (**Figure 5**). BQCV had higher prevalence in pupae singly injected with DWV-A, where the virus accumulated to loads $\geq 1 \times 10^7$ in 4.9% of pupae, predominantly between 48 and 96 h post-injection (**Figure 5**). Less than 1% of co-injected pupae had BQCV loads of 10^7 or more. Unlike the DWV strains, BQCV loads did not continuously increase over time. Peak BQCV loads coincided with the commencement of mortality observed with DWV-A injections, at 120 h post-injection (**Figure 4B**).

DISCUSSION

Our aim was to assess the ability of three genotypes of DWV (DWV-A, DWV-B, and DWV-rec) to accumulate in honeybee pupae naïve to DWV and *V. destructor*, both in isolation and during co-infection. Our experimental protocol resulted in a rapid infection with all DWV genotypes accumulating to viral loads exceeding 1×10^7 (relative to housekeeping gene *Actin* or 1×10^9 genome copy equivalents by standard curve) within 48 h. Viral loads typically plateaued at 96 h post-infection, in agreement with previous analysis by ELISA (Martin et al., 2013). We found significant differences in the relative mean viral loads of the two master variants, which differed by an order of magnitude in colony 1, and approximately fivefold in colonies 2 and 3. While DWV-A loads initially accumulated faster, DWV-B ultimately reached significantly higher levels from 72 h post-injection. Our results are consistent with the experimental findings of McMahon et al. (2016); Dubois et al. (2019), and Tehel et al. (2019) who also found that DWV-B accumulates to higher loads than DWV-A when injected into pupae or adults, despite all four studies using different honeybee populations. While McMahon et al. (2016) and Tehel et al. (2019) used the same source of inocula, the inocula used by Dubois et al. (2019) and our study were different. Given the consistency in results despite the differences amongst the four studies, we can safely conclude that DWV-B reaches higher viral loads than DWV-A after injection. Similarly to our study, in English and Welsh colonies (Kevill et al., 2019) and in the United States (Ryabov et al., 2017; Kevill et al., 2019), mean DWV-B loads were approximately sevenfold higher than DWV-A when colonies contain both genotypes. Yet there are exceptions. In some co-infected colonies in the United States that died over winter, Kevill et al. (2019) found significantly higher DWV-A loads relative to DWV-B.

Only DWV-B appears to be affected by competition when co-injected. We found that DWV-B loads were significantly reduced in pupae co-injected with DWV-A across all colonies. Interestingly by 96 h post-infection, DWV-B still accumulated to higher loads than DWV-A during co-infection, excluding colony 1. DWV-A loads, when co-injected, were not significantly different to single DWV-A injections, despite containing half the starting dose. Thus, competition appears to be independent of the initial dose. Our results are in accordance with Tehel et al. (2019)

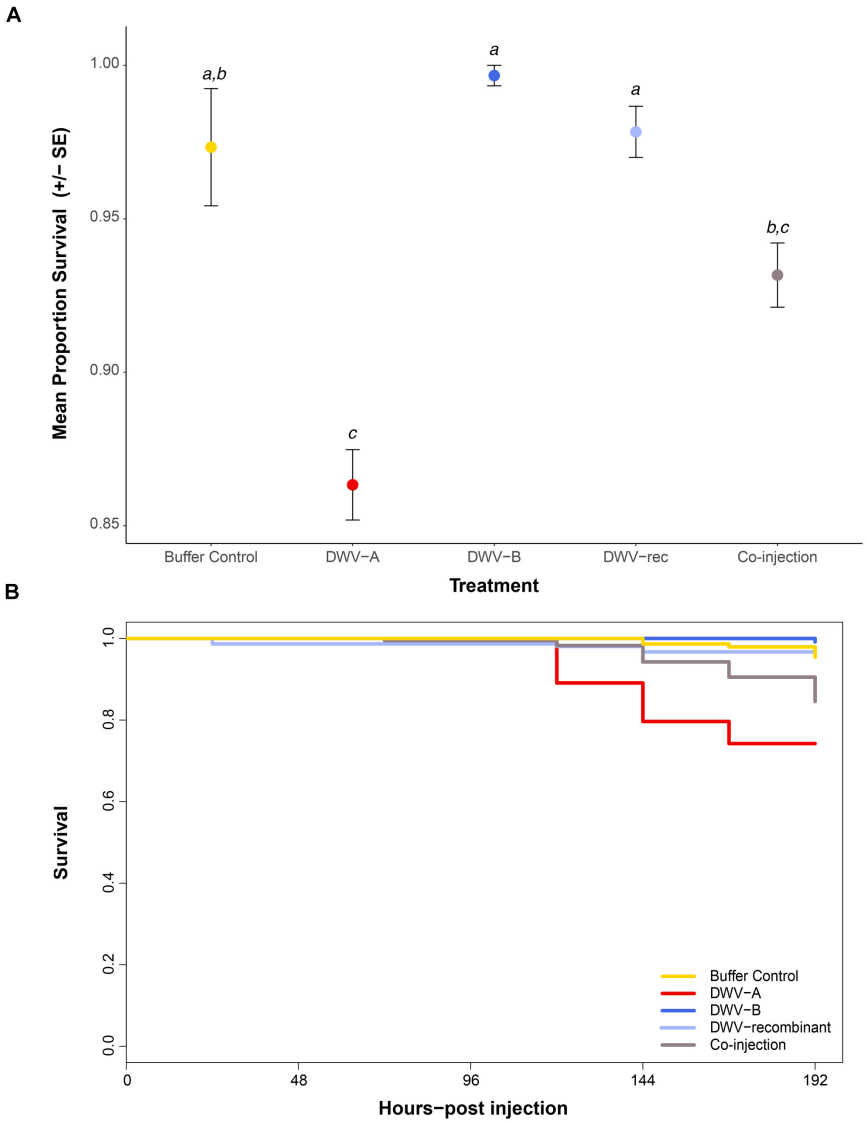

FIGURE 4 | Survival of individual naïve pupae singly injected with DWV-A, DWV-B, DWV recombinant ('DWV-rec'), buffer control, or co-injected with DWV-A and DWV-B (n = 285 per treatment). Pupal survival was monitored throughout the incubation period, up to 192 h post-injection. Pupae collected at regular time points for viral analysis were recorded as censored, thus the final number of remaining pupae at 192 h post-injection was $n \leq 141$ per treatment (depending on mortality). **(A)** Mean proportion and standard error of pupal survival at 192 h post-injection. Letters show significant differences between treatments ($p < 0.05$) based on pairwise comparisons of the final model. See the electronic Supplementary Material, **Supplementary Tables S7–S9** for details of statistical analyses. **(B)** Survival curve of pupae by treatment up to 192 h post-injection. Data did not meet the Cox proportional hazards assumption, thus **(B)** only used to illustrate the pattern of mortality over time.

even though Tehel et al. (2019) injected a much lower dose (10^2–10^4 genome equivalents) and quantified virus levels in far fewer samples (n = 4–11). It thus seems there is a maximum level that DWV-A can accumulate to. This is in agreement with Ryabov et al. (2019), who found that five divergent DWV-A clones all accumulated to the same level. While we observed evidence of competition between DWV-A and DWV-B, we did not see strong competitive exclusion between the genotypes, suggesting that the reduction in DWV-B loads was not due to a lack of some critical resource required for viral replication. In contrast, Israeli acute paralysis virus (IAPV) and closely related Kashmir bee virus (KBV) appear to compete directly for cellular resources. In the presence of KBV, accumulation of IAPV was reduced by four orders of magnitude (Carrillo-Tripp et al., 2016). Lastly, we found significant differences in both single and co-injected DWV loads between colonies, indicating that colony-level factors, such as immune response (Niu et al., 2014; Brutscher et al., 2015), might additionally affect DWV accumulation.

Our recombinant strain (DWV-rec) accumulated to equally high loads as DWV-B within the same colonies. Previous studies have shown that some recombinant strains can replicate to higher loads than the master variants (Moore et al., 2011;

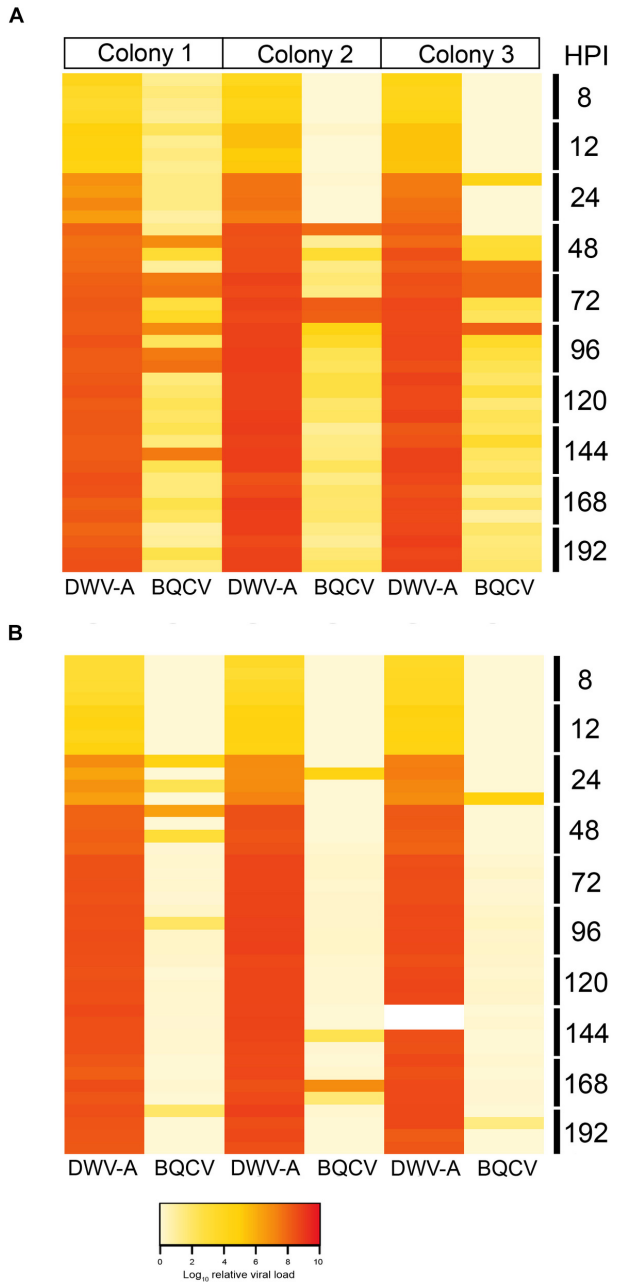

FIGURE 5 | Heat map showing the $\log_{10}$ relative viral loads of DWV-A in comparison to BQCV per pupa and colony, in single DWV-A **(A)** and co-injected pupae **(B)**, from 8 to 192 h post-injection. The two white cells in colony 3 (co-injected DWV-A at 144 h post-injection) had abnormally low DWV loads for their time-point, thus were excluded from analyses.

Zioni et al., 2011; Ryabov et al., 2014). The genome structure of DWV-rec predominantly corresponds to DWV-B, with two recombination breakpoints at positions 829 and 1487 (when aligned to DWV-B AY251269), resulting in a DWV-A region from the 5′ untranslated region (UTR) up to approximately the first half of the Leader protein (Lp). This structure differs from previously characterized recombinants, which have a breakpoint within the helicase region and subsequent non-structural proteins corresponding to DWV-A (Moore et al., 2011; Zioni et al., 2011; Ryabov et al., 2014; Dalmon et al., 2017). Interestingly, the 5′ end of our DWV-rec strain is similar to the RecVT-Fr1 strain isolated from a *V. destructor* tolerant colony in France (Dalmon et al., 2017), although our breakpoints occur earlier.

The difference in accumulation amongst the genotypes may potentially be due to the way viruses interact with cellular translational machinery. Many RNA viruses, including *Dicistroviridae*, *Flaviviridae*, and *Picornaviridae*, use internal ribosome entry site (IRES) secondary structures to initiate translation of their open read frame(s) (Martínez-Salas, 2008). The predicted IRES of DWV-A and DWV-B fall approximately within the first 810 nucleotides (Ongus et al., 2006), prior to our first breakpoint at position 829 for DWV-rec. Thus, the IRES of DWV-rec corresponds to DWV-B. DWV-A and DWV-B share approximately 84% nucleotide and 95% amino acid homology (Ongus et al., 2004). While their 5′ UTR sequences differ, the overall IRES structures were predicted to be the same (Ongus et al., 2006). Nevertheless, small sequence differences may result in different translational efficiencies. For example, a single nucleotide mutation (C472U) in the IRES reduces poliovirus type 3 replication and virulence in mouse neural tissue (La Monica et al., 1987), but does not affect organ tropism (Kauder and Racaniello, 2004). At this stage, it is unclear exactly what part of the genome is most important for DWV replication. However, it is possible that the increased accumulation of DWV-B and DWV-rec compared to DWV-A might be associated with sequence differences within the IRES.

We found differences in mortality between pupae injected with different genotypes. In agreement with Dubois et al. (2019) and Tehel et al. (2019), we found no relationship between viral accumulation and mortality in pupae. In our study, only pupae singly injected with DWV-A showed mortality statistically different from the buffer control, but mortality was low (11% ± 1.2 SE). Interestingly, the 0.4% mortality we observed in DWV-B injected pupae up to 192 h (8 days) post-injection was less than the 55%, 0-75%, and 18% mortality observed by Gisder et al. (2018), Dubois et al. (2019), and Tehel et al. (2019), respectively, after 7 or 10 days post-injection.

Gisder et al. (2018) postulate that their high pupal mortality is further evidence that DWV-B is more virulent than DWV-A, yet the independent DWV-B isolates injected in our study and by Tehel et al. (2019) were found to be more similar (99.3 and 98.9% pairwise identity, respectively) to the DWV-B reference genome [AY251269; isolated from *V. destructor* by Ongus et al. (2004)] than the three isolates injected by Gisder et al. (2018) (91.4–96.9%). Furthermore, the DWV-$_{P0}$ I isolate injected by Gisder et al. (2018) shows recombination with DWV-A, however, Gisder et al. (2018) did not indicate whether mortality differed between their three DWV-$_{P0}$ isolates. Dubois et al. (2019) associated their high mortality with SBV, initially present at very low levels in their inocula. While Dubois et al. (2019) and Tehel et al. (2019) found no difference in mortality between DWV-A and DWV-B injected pupae, this may be affected by background DWV infection in their pupae. Both studies detected accumulation of both DWV

genotypes upon injection of a single genotype, accumulation of both genotypes in buffer injected pupae and had higher control mortality (11–25%) than observed in our study (2.7% ± 1.9 SE).

While we did find significant mortality when pupae were injected with DWV-A, we caution that we cannot exclude that the mortality was attributed to BQCV and not DWV-A, particularly as BQCV is known to kill brood (Chen and Siede, 2007). Unfortunately, we were unable to screen our 48-h dead pupae for viruses due to extreme RNA degradation, thus cannot determine if dead pupae were infected with BQCV. Nevertheless, we only detected significant mortality in pupae injected with DWV-A, and only detected BQCV in pupae injected with the DWV-A genotype. As BQCV was not detected in any of our inocula by whole transcriptome sequencing, it seems unlikely that we injected BQCV together with DWV. While we cannot completely exclude the possibility that BQCV was present in our DWV-A inoculum at levels too low to be detected, we think this unlikely because we did detect low amounts of LSV and ARV in the DWV-B inoculum. It could be that DWV-A has an immunosuppressive effect that then allows other viruses, such as BQCV, to replicate to high viral loads as suggested by Barroso-Arévalo et al. (2019a). In a 21 months study of honeybee colonies in Spain, Barroso-Arévalo et al. (2019a) found that BQCV, in addition to DWV and *V. destructor*, was highly prevalent and negatively correlated with colony vigor. As our study was conducted in the absence of *V. destructor*, our results may point to a synergistic interaction between DWV-A and BQCV, such that injection with DWV-A activates an endogenous BQCV infection, potentially by disrupting immune response of pupae more than other DWV genotypes. D'Alvise et al. (2019) also suggested a potential synergistic interaction between DWV and BQCV. Their regression analysis showed that DWV was the most significant predictor of BQCV accumulation in German honeybees, despite contrasting seasonal dynamics and BQCV being significantly correlated to virtually all of the tested viral pathogens and intestinal parasites (D'Alvise et al., 2019). In agreement with Barroso-Arévalo et al. (2019a), D'Alvise et al. (2019) postulated this interaction may be associated with a reduction in host immune defense by DWV. As DWV-A and DWV-B were combined for analysis (D'Alvise et al., 2019), it is unclear if their results would differ between DWV genotypes. We found no evidence of a relationship between DWV-B and BQCV, or between our DWV-rec strain and BQCV. Previous modeling has shown that 20% pupal mortality associated with *Varroa* transmission of DWV to pupae can lead to colony mortality, due to a reduction in workforce longevity (Martin, 2001). While the mortality observed for DWV-A in our study was less than this, any increased effect of DWV-A on the mortality of pupae, with or without an interaction with BQCV, can explain the shift from DWV-A to DWV-B observed globally. Because the reproductive success of *V. destructor* depends on the pupa surviving to adulthood, DWV-A associated pupal mortality will negatively affect the transmission of DWV-A in favor of the transmission of DWV-B.

Our data provide some explanation for the continued global increase in prevalence of DWV-B over DWV-A. Low mortality in pupae and the ability of DWV-B to accumulate to higher loads relative to DWV-A, even during co-infection, are likely to be contributing factors to the increasing prevalence of DWV-B. Further, our observed interaction between DWV-A and BQCV highlights the complex relationships between viruses. Previous studies have suggested, implicitly and explicitly, that studying a single virus in isolation does not provide the whole picture (Mondet et al., 2014; Carrillo-Tripp et al., 2016; Dubois et al., 2019; Remnant et al., 2019), particularly as honeybees are frequently infected with multiple pathogens (Bailey et al., 1981; Chen et al., 2004; Berényi et al., 2006; Berthoud et al., 2010; Nguyen et al., 2011; Cornman et al., 2012; Locke et al., 2014; Mondet et al., 2014; Amiri et al., 2015; Natsopoulou et al., 2017; D'Alvise et al., 2019). While a direct relationship between DWV-A and BQCV requires experimental validation, our results suggest that future studies should continue to incorporate a broader ecological approach by experimentally investigating how multiple pathogens interact with their honeybee hosts.

DATA AVAILABILITY STATEMENT

The inocula sequences used in this study were deposited to GenBank [accession numbers MN538208-MN538210].

AUTHOR CONTRIBUTIONS

AN, ER, and MB conceived the study. AN conducted the experimental work. AN and GB carried out molecular laboratory work. AN analyzed the data. AN, ER, and MB contributed to data interpretation and writing the manuscript. All authors gave final approval for publication.

FUNDING

This work was supported by the Australian Research Council (grant DP170100844 to MB). The funders had no role in study design, data collection and analysis, preparation of the manuscript or the decision to publish.

ACKNOWLEDGMENTS

We thank Boris Yagound at the University of Sydney for statistical advice; Tjeerd Blacquière at Wageningen University & Research, Netherlands, and Gertje Petersen at University of Otago, New Zealand, for providing the samples used as source inocula; and Camilla Whittington at the Evolutionary and Integrative Zoology Laboratory, The University of Sydney, for use of her laboratory and reagents in preparing the velvet worm sample.

SUPPLEMENTARY MATERIAL

The Supplementary Material for this article can be found online at: https://www.frontiersin.org/articles/10.3389/fmicb.2020.00620/full#supplementary-material

REFERENCES

Amiri, E., Meixner, M., Nielsen, S.L., and Kryger, P. (2015). Four categories of viral infection describe the health status of honey bee colonies. *PLoS One* 10:e0140272. doi: 10.1371/journal.pone.0140272

Bailey, L., and Ball, B.V. (1991). *Honey Bee Pathology*.San Diego, CA: Academic Press.

Bailey, L., Ball, B.V., and Perry, J. (1981). The prevalence of viruses of honey bees in Britain. *Ann. Appl. Biol.* 97, 109–118. doi: 10.1371/journal.pone.0133228

Barroso-Arévalo, S., Fernández-Carrión, E., Goyache, J., Molero, F., Puerta, F., and Sánchez-Vizcaíno, J.M. (2019a). High load of deformed wing virus and *Varroa destructor* infestation are related to weakness of honey bee colonies in Southern Spain. *Front. Microbiol.*10:1331. doi: 10.3389/fmicb.2019.01331

Barroso-Arévalo, S., Vicente-Rubiano, M., Molero, F., Puerta, F., and Sánchez-Vizcaíno, J.M. (2019b). Nucleotide sequence variations may be associated with virulence of deformed wing virus. *Apidologie* 50, 482–496. doi: 10.1007/s13592-019-00660-5

Bates, D., Maechler, M., Bolker, B., and Walker, S. (2018). *Package 'lme4': Linear Mixed-Effects Models Using Eigen and S4*.

Benaets, K., Van Geystelen, A., Cardoen, D., De Smet, L., de Graaf, D.C., Schoofs, L., et al. (2017). Covert deformed wing virus infections have long-term deleterious effects on honey bee foraging and survival. *Proc. R. Soc. B Biol. Sci.* 284:20162149. doi: 10.1098/rspb.2016.2149

Berényi, O., Bakonyi, T., Derakhshifar, I., Köglberger, H., and Nowotny, N. (2006). Occurrence of six honeybee viruses in diseased Austrian apiaries. *Appl. Environ. Microbiol.* 72, 2414–2420. doi: 10.1128/aem.72.4.2414-2420.2006

Berthoud, H., Imdorf, A., Haueter, M., Radloff, S., and Neumann, P. (2010). Virus infections and winter losses of honey bee colonies (*Apis mellifera*). *J. Apicult. Res.* 49, 60–65. doi: 10.3896/IBRA.1.49.1.08

Bolger, A.M., Lohse, M., and Usadel, B. (2014). Trimmomatic: a flexible trimmer for Illumina sequence data. *Bioinformatics* 30, 2114–2120. doi: 10.1093/bioinformatics/btu170

Boncristiani, H., Li, J., Evans, J.D., Pettis, J., and Chen, Y. (2011). Scientific note on PCR inhibitors in the compound eyes of honey bees, *Apis mellifera*. *Apidologie* 42, 457–460. doi: 10.1007/s13592-011-0009-9

Bowen-Walker, P., Martin, S., and Gunn, A. (1999). The transmission of deformed wing virus between honeybees (*Apis mellifera* L.) by the Ectoparasitic Mite *Varroa jacobsoni* Oud. *J. Invertebr. Pathol.* 73, 101–106. doi: 10.1006/jipa.1998.4807

Brettell, L., and Martin, S. (2017). Oldest *Varroa* tolerant honey bee population provides insight into the origins of the global decline of honey bees. *Sci. Rep.* 7:45953. doi: 10.1038/srep45953

Brettell, L.E., Schroeder, D.C., and Martin, S.J. (2019). RNAseq analysis reveals virus diversity within hawaiian apiary insect communities. *Viruses* 11:397. doi: 10.3390/v11050397

Brutscher, L.M., Daughenbaugh, K.F., and Flenniken, M.L. (2015). Antiviral defense mechanisms in honey bees. *Curr. Opin. Insect Sci.* 10, 71–82. doi: 10.1016/j.cois.2015.04.016

Carrillo-Tripp, J., Dolezal, A.G., Goblirsch, M.J., Miller, W.A., Toth, A.L., and Bonning, B.C. (2016). *In vivo* and *in vitro* infection dynamics of honey bee viruses. *Sci. Rep.* 6:22265. doi: 10.1038/srep22265

Chen, Y., Zhao, Y., Hammond, J., Hsu, H.-T., Evans, J., and Feldlaufer, M. (2004). Multiple virus infections in the honey bee and genome divergence of honey bee viruses. *J. Invertebr. Pathol.* 87, 84–93. doi: 10.1016/j.jip.2004.07.005

Chen, Y.P., and Siede, R. (2007). "Honey bee viruses," in *Advances in Virus Research*, eds K. Maramorosch, S.A. Shabalina and F.A. Murphy (San Diego, CA: Elsevier Academic Press Inc), 33–80.

Cornman, R.S., Tarpy, D.R., Chen, Y., Jeffreys, L., Lopez, D., Pettis, J.S., et al. (2012). Pathogen webs in collapsing honey bee colonies. *PLoS One* 7:e43562. doi: 10.1371/ journal.pone.0043562 doi: 10.1371/journal.pone.0043562

D'Alvise, P., Seeburger, V., Gihring, K., Kieboom, M., and Hasselmann, M. (2019). Seasonal dynamics and co-occurrence patterns of honey bee pathogens revealed by high-throughput RT-qPCR analysis. *Ecol. Evol.* 9, 10241–10252. doi: 10.1002/ece3.5544

Dalmon, A., Desbiez, C., Coulon, M., Thomasson, M., Le Conte, Y., Alaux, C., et al. (2017). Evidence for positive selection and recombination hotspots in deformed wing virus (DWV). *Sci. Rep.* 7:41045. doi: 10.1038/srep41045

de Miranda, J.R., and Genersch, E. (2010). Deformed wing virus. *J. Invertebr. Pathol.* 103, S48–S61. doi: 10.1016/j.jip.2009.06.012

Donzé, G., and Guerin, P.M. (1994). Behavioral attributes and parental care of *Varroa* mites parasitizing honey bee brood. *Behav. Ecol. Sociobiol.* 34, 305–319. doi: 10.1007/BF00197001

Dubois, E., Dardouri, M., Schurr, F., Cougoule, N., Sircoulomb, F., and Thiéry, R. (2019). Outcomes of honeybee pupae inoculated with deformed wing virus genotypes A and B. *Apidologie* 51, 18–34. doi: 10.1007/s13592-019-00701-z

Fox, J., Weisberg, S., and Price, B. (2018). Package 'car': Companion to Applied Regression.

Gisder, S., Möckel, N., Eisenhardt, D., and Genersch, E. (2018). In vivo evolution of viral virulence: switching of deformed wing virus between hosts results in virulence changes and sequence shifts. *Environ. Microbiol.* 20, 4612–4628. doi: 10.1111/1462-2920.14481

Highfield, A.C., El Nagar, A., Mackinder, L.C., Laure, M.-L.N., Hall, M.J., Martin, S.J., et al. (2009). Deformed wing virus implicated in overwintering honeybee colony losses. *Appl. Environ. Microbiol.* 75, 7212–7220. doi: 10.1128/AEM.02227-09

Hou, Y., Zhang, H., Miranda, L., and Lin, S. (2010). Serious overestimation in quantitative PCR by circular (supercoiled) plasmid standard: microalgal pcna as the model gene. *PLoS One* 5:e9545. doi: 10.1371/journal.pone.0009545

Jay, S.C. (1962). Colour changes in honeybee pupae. *Bee World* 43:119–122. doi: 10.1080/0005772x.1962.11096960

Kauder, S.E., and Racaniello, V.R. (2004). Poliovirus tropism and attenuation are determined after internal ribosome entry. *J. Clin. Invest.* 113, 1743–1753. doi: 10.1172/JCI200421323

Kearse, M., Moir, R., Wilson, A., Stones-Havas, S., Cheung, M., Sturrock, S., et al. (2012). Geneious basic: an integrated and extendable desktop software platform for the organization and analysis of sequence data. *Bioinformatics* 28, 1647–1649. doi: 10.1093/bioinformatics/bts199

Kevill, J.L., de Souza, F.S., Sharples, C., Oliver, R., Schroeder, D.C., and Martin, S.J. (2019). DWV-a lethal to honey bees (*Apis mellifera*): a colony level survey of DWV variants (A, B, and C) in England, Wales, and 32 states across the US. *Viruses* 11:426. doi: 10.3390/v11050426

Kevill, L.J., Highfield, A., Mordecai, J.G., Martin, J.S., and Schroeder, C.D. (2017). ABC assay: method development and application to quantify the role of three DWV master variants in overwinter colony losses of European honey bees. *Viruses* 9:314. doi: 10.3390/v9110314

La Monica, N., Almond, J., and Racaniello, V. (1987). A mouse model for poliovirus neurovirulence identifies mutations that attenuate the virus for humans. *J. Virol.* 61, 2917–2920. doi: 10.1128/jvi.61.9.2917-2920.1987

Lamp, B., Url, A., Seitz, K., Eichhorn, J., Riedel, C., Sinn, L.J., et al. (2016). Construction and rescue of a molecular clone of deformed wing virus (DWV). *PLoS One* 11:e0164639. doi: 10.1371/journal.pone.0164639

Lenth, R.V. (2018). Package 'lsmeans': Least-Squares Means.

Li, D., Liu, C.-M., Luo, R., Sadakane, K., and Lam, T.-W. (2015). MEGAHIT: an ultra-fast single-node solution for large and complex metagenomics assembly via succinct de Bruijn graph. *Bioinformatics* 31, 1674–1676. doi: 10.1093/bioinformatics/btv033

Locke, B., Forsgren, E., and De Miranda, J.R. (2014). Increased tolerance and resistance to virus infections: a possible factor in the survival of *Varroa destructor*-resistant honey bees (*Apis mellifera*). *PLoS One* 9:e99998. doi: 10.1371/journal.pone.0099998

Manley, R., Temperton, B., Doyle, T., Gates, D., Hedges, S., Boots, M., et al. (2019). Knock-on community impacts of a novel vector: spillover of emerging DWV-B from *Varroa*-infested honeybees to wild bumblebees. *Ecol. Lett.* 22, 1306–1315. doi: 10.1111/ele.13323

Martin, S. (1995). Reproduction of *Varroa jacobsoni* in cells of *Apis mellifera* containing one or more mother mites and the distribution of these cells. *J. Apicult. Res.* 34, 187–196. doi: 10.1080/00218839.1995.11100904

Martin, S.J. (2001). The role of *Varroa* and viral pathogens in the collapse of honey bee colonies: a modelling approach. *J. Appl. Ecol.* 38, 1082–1093. doi: 10.1046/j.1365-2664.2001.00662.x

Martin, S.J., Ball, B.V., and Carreck, N.L. (2013). The role of deformed wing virus in the initial collapse of varroa infested honey bee colonies in the UK. *J. Apicult. Res.* 52, 251–258. doi: 10.3896/ibra.1.52.5.12

Martin, S.J., and Brettell, L.E. (2019). Deformed wing virus in honeybees and other insects. *Annu. Rev. Virol.* 6, 227–253. doi: 10.1146/annurev-virology-092818-015700

Martin, S.J., Highfield, A.C., Brettell, L., Villalobos, E.M., Budge, G.E., Powell, M., et al. (2012). Global honey bee viral landscape altered by a parasitic mite. *Science* 336, 1304–1306. doi: 10.1126/science.1220941

Martínez-Salas, E. (2008). The impact of RNA structure on picornavirus IRES activity. *Trends Microbiol.* 16, 230–237. doi: 10.1016/j.tim.2008.01.013

McMahon, D.P., Natsopoulou, M.E., Doublet, V., Fürst, M., Weging, S., Brown, M.J., et al. (2016). Elevated virulence of an emerging viral genotype as a driver of honey bee loss. *Proc. R. Soc. B Biol. Sci.* 283:20160811. doi: 10.1098/rspb.2016.0811

Mondet, F., de Miranda, J.R., Kretzschmar, A., Le Conte, Y., and Mercer, A.R. (2014). On the front line: quantitative virus dynamics in honey bee (*Apis mellifera* L.) colonies along a new expansion front of the parasite *Varroa destructor*. *PLoS Pathog.* 10:e1004323. doi: 10.1371/journal.ppat.1004323

Moore, J., Jironkin, A., Chandler, D., Burroughs, N., Evans, D.J., and Ryabov, E.V. (2011). Recombinants between deformed wing virus and *Varroa destructor* virus-1 may prevail in *Varroa destructor*-infested honey bee colonies. *J. Gen. Virol.* 92, 156–161. doi: 10.1099/vir.0.025965-0

Mordecai, G.J., Brettell, L.E., Martin, S.J., Dixon, D., Jones, I.M., and Schroeder, D.C. (2016a). Superinfection exclusion and the long-term survival of honey bees in *Varroa*-infested colonies. *ISME J.* 10, 1182–1191. doi: 10.1038/ismej.2015.186

Mordecai, G.J., Wilfert, L., Martin, S.J., Jones, I.M., and Schroeder, D.C. (2016b). Diversity in a honey bee pathogen: first report of a third master variant of the deformed wing virus quasispecies. *ISME J.* 10, 1264–1273. doi: 10.1038/ismej.2015.178

Natsopoulou, M.E., McMahon, D.P., Doublet, V., Frey, E., Rosenkranz, P., and Paxton, R.J. (2017). The virulent, emerging genotype B of deformed wing virus is closely linked to overwinter honeybee worker loss. *Sci. Rep.* 7:5242. doi: 10.1038/s41598-017-05596-3

Nazzi, F., Brown, S.P., Annoscia, D., Del Piccolo, F., Di Prisco, G., Varricchio, P., et al. (2012). Synergistic parasite-pathogen interactions mediated by host immunity can drive the collapse of honey bee colonies. *PLoS Pathog.* 8:e1002735. doi: 10.1371/journal.ppat.1002735

Nguyen, B.K., Ribière, M., vanEngelsdorp, D., Snoeck, C., Saegerman, C., Kalkstein, A.L., et al. (2011). Effects of honey bee virus prevalence, *Varroa destructor* load and queen condition on honey bee colony survival over the winter in Belgium. *J. Apicult. Res.* 50, 195–202. doi: 10.3896/IBRA.1.50.3.03

Niu, J., Meeus, I., Cappelle, K., Piot, N., and Smagghe, G. (2014). The immune response of the small interfering RNA pathway in the defense against bee viruses. *Curr. Opin. Insect Sci.* 6, 22–27. doi: 10.1016/j.cois.2014.09.014

Oldroyd, B.P. (1999). Coevolution while you wait: *Varroa jacobsoni*, a new parasite of western honey bees. *Trends Ecol. Evol.* 14, 312–315. doi: 10.1016/S0169-5347(99)01613-4

Ongus, J.R., Peters, D., Bonmatin, J.M., Bengsch, E., Vlak, J.M., and van Oers, M.M. (2004). Complete sequence of a picorna-like virus of the genus *Iflavirus* replicating in the mite *Varroa destructor*. *J. Gen. Virol.* 85, 3747–3755. doi: 10.1099/vir.0.80470-0

Ongus, J.R., Roode, E.C., Pleij, C.W.A., Vlak, J.M., and van Oers, M.M. (2006). The 5' non-translated region of *Varroa destructor* virus 1 (genus *Iflavirus*): structure prediction and IRES activity in *Lymantria dispar* cells. *J. Gen. Virol.* 87, 3397–3407. doi: 10.1099/vir.0.82122-0

Panziera, D., van Langevelde, F., and Blacquière, T. (2017). *Varroa* sensitive hygiene contributes to naturally selected *varroa* resistance in honey bees. *J. Apicult. Res.* 56, 635–642. doi: 10.1080/00218839.2017.1351860

Pfaffl, M.W. (2001). A new mathematical model for relative quantification in real-time RT–PCR. *Nucleic Acids Res.* 29**:**e45. doi: 10.1093/nar/29.9.e45

Posada-Florez, F., Childers, A.K., Heerman, M.C., Egekwu, N.I., Cook, S.C., Chen, Y., et al. (2019). Deformed wing virus type A, a major honey bee pathogen, is vectored by the mite *Varroa destructor* in a non-propagative manner. *Sci. Rep.* 9**:**12445. doi: 10.1038/s41598-019-47447-3

Ramsey, S.D., Ochoa, R., Bauchan, G., Gulbronson, C., Mowery, J.D., Cohen, A., et al. (2019). *Varroa destructor* feeds primarily on honey bee fat body tissue and not hemolymph. *Proc. Natl. Acad. Sci.* 116, 1792–1801. doi: 10.1073/pnas.1818371116

Remnant, E.J., Mather, N., Gillard, T., Yagound, B., and Beekman, M. (2019). Direct transmission by injection affects competition amongst RNA viruses in honeybees. *Proc. R. Soc. B Biol. Sci.* 286:20182452. doi: 10.1098/rspb.2018.2452

Remnant, E.J., Shi, M., Buchmann, G., Blacquière, T., Holmes, E.C., Beekman, M., et al. (2017). A diverse range of novel RNA viruses in geographically distinct honey bee populations. *J. Virol.* 91:e00158-17. doi: 10.1128/JVI.00158-17

Roberts, J.M., Anderson, D.L., and Durr, P.A. (2017). Absence of deformed wing virus and *Varroa destructor* in Australia provides unique perspectives on honeybee viral landscapes and colony losses. *Sci. Rep.* 7**:**6925. doi: 10.1038/s41598-017-07290-w

Ryabov, E.V., Childers, A.K., Chen, Y., Madella, S., Nessa, A., vanEngelsdorp, D., et al. (2017). Recent spread of *Varroa destructor* virus-1, a honey bee pathogen, in the United States. *Sci. Rep.* 7**:**17447. doi: 10.1038/s41598-017-17802-3

Ryabov, E.V., Childers, A.K., Lopez, D., Grubbs, K., Posada-Florez, F., Weaver, D., et al. (2019). Dynamic evolution in the key honey bee pathogen deformed wing virus: novel insights into virulence and competition using reverse genetics. *PLoS Biol.* 17:e3000502. doi: 10.1371/journal.pbio.3000502

Ryabov, E.V., Wood, G.R., Fannon, J.M., Moore, J.D., Bull, J.C., Chandler, D., et al. (2014). A virulent strain of deformed wing virus (DWV) of honey bees (*Apis mellifera*) prevails after *Varroa destructor*-mediated, or *in vitro*, transmission. *PLoS Pathog.* 10:e1004230. doi: 10.1371/journal.ppat.1004230

Shutler, D., Head, K., Burgher-MacLellan, K.L., Colwell, M.J., Levitt, A.L., Ostiguy, N., et al. (2014). Honey bee *Apis mellifera* parasites in the absence of *Nosema ceranae* fungi and *Varroa destructor* mites. *PLoS One* 9:e98599. doi: 10.1371/journal.pone.0098599

Solignac, M., Cornuet, J.M., Vautrin, D., Le Conte, Y., Anderson, D., Evans, J., et al. (2005). The invasive Korea and Japan types of *Varroa destructor*, ectoparasitic mites of the western honey bee (*Apis mellifera*), are two partly isolated clones. *Proc. R. Soc. Lond. B Biol. Sci.* 272, 411–419. doi: 10.1098/rspb.2004.2853

Staroscik, A. (2004). *Calculator for Determining the Number of Copies of a Template* [Online]. Available onile at: https://cels.uri.edu/gsc/cndna.html (accessed October 16, 2017).

Sumpter, D.J., and Martin, S.J. (2004). The dynamics of virus epidemics in *Varroa*−infested honey bee colonies. *J. Anim. Ecol.* 73, 51–63. doi: 10.1111/j.1365-2656.2004.00776.x

Tehel, A., Vu, Q., Bigot, D., Gogol-Döring, A., Koch, P., Jenkins, C., et al. (2019). The two prevalent genotypes of an emerging infectious disease, deformed wing virus, cause equally low pupal mortality and equally high wing deformities in host honey bees. *Viruses* 11:114. doi: 10.3390/v11020114

Wu, Y., Dong, X., and Kadowaki, T. (2017). Characterization of the copy number and variants of deformed wing virus (DWV) in the pairs of honey bee pupa and infesting *Varroa destructor* or *Tropilaelaps mercedesae*. *Front. Microbiol.* 8**:**1558. doi: 10.3389/fmicb.2017.01558

Zioni, N., Soroker, V., and Chejanovsky, N. (2011). Replication of *Varroa destructor* virus 1 (VDV-1) and a *Varroa destructor* virus 1–deformed wing virus recombinant (VDV-1–DWV) in the head of the honey bee. *Virology* 417, 106–112. doi: 10.1016/j.virol.2011.05.009

Conflict of Interest: The authors declare that the research was conducted in the absence of any commercial or financial relationships that could be construed as a potential conflict of interest.

Copyright © 2020 Norton, Remnant, Buchmann and Beekman. This is an open-access article distributed under the terms of the Creative Commons Attribution License (CC BY). The use, distribution or reproduction in other forums is permitted, provided the original author(s) and the copyright owner(s) are credited and that the original publication in this journal is cited, in accordance with accepted academic practice. No use, distribution or reproduction is permitted which does not comply with these terms.

frontiers in Microbiology

REVIEW
published: 21 April 2020
doi: 10.3389/fmicb.2020.00736

Friend or Enemy: A Dual Role of Autophagy in Plant Virus Infection

Xiuqin Huang[1,2], *Siping Chen*[1,2], *Xiaorong Yang*[1,2], *Xin Yang*[1,2], *Tong Zhang*[1,2]* and *Guohui Zhou*[1,2]*

[1] Guangdong Province Key Laboratory of Microbial Signals and Disease Control, College of Agriculture, South China Agricultural University, Guangzhou, China, [2] Guangdong Laboratory of Lingnan Modern Agriculture, South China Agricultural University, Guangzhou, China

Autophagy is a primary protective process that involves removing damaged organelles or dysfunctional proteins in eukaryotes. The autophagy pathway not only maintains cellular homeostasis, but also modulates the host's cellular response to pathogen infection. Several studies proved that autophagy plays a dominant role in plant fitness and immunity. As intracellular parasites, the replication and spread of viruses entirely rely upon the molecular machinery of the host cell, including the autophagy process. Plant viruses severely affect crop yields and quality. During infection, complex interactions occur between viral proteins and host factors in relation to plant defense and virus counter-defense. An increasing number of studies demonstrated that plants use autophagy to eliminate and inhibit viruses; some viruses were shown to manipulate the process of autophagy to promote their own replication and survival in plant cells. In this review, we summarize recent advances in plant autophagy, with an emphasis on the role of autophagy in plant virus infection.

Keywords: plant virus, autophagy, ATGs, antiviral mechanism, counter-defense

OPEN ACCESS

Edited by:
Akio Adachi,
Kansai Medical University, Japan

Reviewed by:
Hernan Garcia-Ruiz,
University of Nebraska-Lincoln, United States
Fabien P. Blanchet,
Institut National de la Santé et de la Recherche Médicale (INSERM), France

***Correspondence:**
Tong Zhang
zhangtong@scau.edu.cn
Guohui Zhou
ghzhou@scau.edu.cn

Specialty section:
This article was submitted to Virology, a section of the journal Frontiers in Microbiology

Received: *05 January 2020*
Accepted: *30 March 2020*
Published: *21 April 2020*

Citation:
Huang X, Chen S, Yang X, Yang X, Zhang T and Zhou G (2020) Friend or Enemy: A Dual Role of Autophagy in Plant Virus Infection. Front. Microbiol. 11:736. doi: 10.3389/fmicb.2020.00736

INTRODUCTION

Autophagy is a conserved intracellular degradation pathway through which damaged organelles, non-functional proteins, and harmful microbial invaders are delivered to vacuoles in yeast and plants or lysosomes in animals to be degraded (Liu and Bassham, 2012; Marshall and Vierstra, 2018; Shimamura et al., 2019). This process achieves intracellular recycling and plays a paramount role in energy balance. The autophagy phenomenon was first observed in 1963, but its mechanism was not revealed until 1993 (Deter and de Duve, 1967; Tsukada and Ohsumi, 1993). The mechanism of autophagy in yeast was characterized first, with researchers making considerable progress in plant models for more than a decade. The genes involved in autophagy were named autophagy-related genes (*ATG*s) (Klionsky et al., 2003; Mizushima et al., 2011). In recent years, many *ATGs* have been identified in *Arabidopsis*, tobacco, rice, and many other plants (Yoshimoto et al., 2010; Xia et al., 2011; Yoshimoto, 2012; Zhou et al., 2015).

Plant viruses include some of the most devastating crop pathogens, leading to significant agricultural losses worldwide and seriously threatening global food security (Oerke and Dehne, 2004; Fargette et al., 2006). Due to the systematic infection characteristics of plant viruses, no chemical pesticides target viral diseases directly. Autophagy is a major homoeostatic process through which cytoplasmic components are delivered to vacuoles as a regulatory pathway to coordinate the host's response to various intracellular pathogens, including viruses (Shoji-Kawata and Levine, 2009). Therefore, this pathway is a potential target for modulation by chemical agents or molecular breeding to establish resistance to viruses in crops.

In the past decade, a lot of progress has been made in the relationship between plant autophagy and virus infection. Autophagy can promote virus infection or inhibit it (**Figure 1**). In this work, we summarize the current state of autophagy in plant systems and discuss the dual roles of autophagy in the arms race between the defense and counter-defense of plants and viruses, respectively.

AUTOPHAGY AND ITS MOLECULAR MECHANISM IN PLANTS

Autophagy is an evolutionarily conserved process observed in yeast, plants, and animals, and whose regulatory mechanisms and induction factors are quite similar (Hurley and Young, 2017). The three major types of autophagy include macroautophagy, microautophagy, and molecular chaperone-mediated autophagy (CMA) (Mizushima et al., 2008; Kaushik and Cuervo, 2018). Macroautophagy (hereafter called autophagy) occurs when cytoplasmic components are engulfed by double-membrane structures, termed autophagosomes, and subsequently delivered to vacuoles for breakdown and turnover in plants (Ohsumi, 2001; Klionsky and Codogno, 2013; Marshall and Vierstra, 2018). Tremendous progress has been made regarding the molecular mechanism of macroautophagy. From its inception at the preautophagosomal structure (PAS), the phagophore expands into a cup-shaped structure and ultimately forms a double-membrane vesicle called an autophagosome (Marshall and Vierstra, 2018). By contrast, microautophagy refers to the direct depression of a plant's vacuolar membrane, with the trapped tonoplast swallowing cytoplasmic material into the vacuole for degradation. However, information regarding microautophagy is limited and no reliable markers are available for monitoring purposes (Li et al., 2012). CMA targets proteins bearing the KEFRQ residue, which is recognized by the chaperone heat shock-cognate protein that is 70 KDa in mass (Hsc70). The chaperone delivers the substrate to the lysosome where they bind to lysosome-associated membrane protein type 2A (LAMP-2A), allowing the soluble proteins to be selectively degrade. To date, the CMA pathway has been described only in mammals and birds (Cuervo and Wong, 2014; Catarino et al., 2017; Kaushik and Cuervo, 2018). The autophagy process of plants includes the initiation of autophagy, nucleation, elongation, completion, fusion with vacuoles, and breakdown. These are also the key steps in the life-cycle of an autophagosome (Lamb et al., 2013; Ismayil et al., 2019).

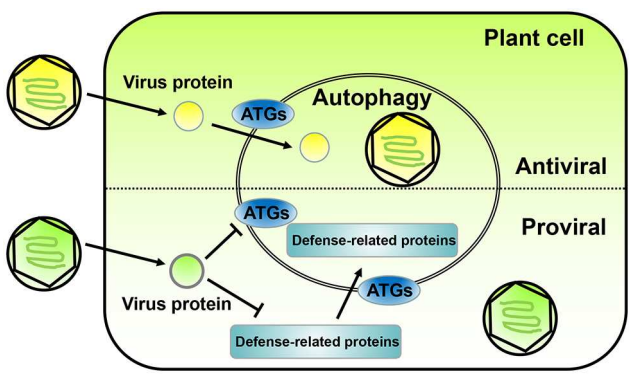

FIGURE 1 | The opposite roles of autophagy in plant-virus interaction. The diagram on the top shows an antiviral role for autophagy during plant infection by viruses. Plant viruses express proteins (yellow ball) to promote infection; however, sometimes the autophagy of the plant infected cell is activated and directly or indirectly targets the virus protein or vision toward degradation. The diagram on the bottom shows a proviral role for autophagy during plant infection by viruses. In some cases, plant virus proteins (green ball) can interact with ATGs to inhibit autophagy and prevent degradation. Also, some plant virus encoded proteins can promote the degradation of plant defense-related proteins through the autophagy pathway. Both case scenarios lead to an enhancement of viral replication and infection in the host plant.

The complicated molecular machinery of autophagy has been unveiled over the past 15 years (Klionsky and Codogno, 2013; Medina-Puche and Lozano-Duran, 2019; Signorelli et al., 2019). Autophagy, which always occurs at a basal level in all plant cells, is responsible for the elimination of harmful cellular debris (Marshall and Vierstra, 2018). The execution of autophagy requires many ATG proteins (Wang et al., 2018; Levine and Kroemer, 2019). When cells are stimulated by nutrient-starved conditions, abiotic stresses, or pathogen infection, the activity of TOR kinase in plant cells is inhibited and ATG13 is rapidly dephosphorylated. The dephosphorylated ATG13 then binds to ATG1 to form an activated ATG1 kinase complex called an autophagy precursor, thereby initiating autophagy as a key activator. Autophagy precursors interact with PI3K kinase complexes (including ATG6/Vps30, ATG14, etc.) to form autophagic vesicles, in which the ATG9 circulation system (including ATG2, ATG9, ATG18, etc.) is involved in forming the membrane of the autophagic vesicles. Under the action of two ubiquitin-like systems, i.e., the ATG8 lipidation system (including ATG3, ATG4, ATG7, and ATG8) and the ATG12 conjugation system (including ATG5, AT7, ATG10, ATG12, and ATG16), the autophagosomes gradually mature (Xie and Klionsky, 2007; Yoshimoto et al., 2010). Finally, the soluble N-ethylmaleimide-sensitive factor attachment protein receptor (SNARE) mediates the fusion of the autophagosome and vacuole, thereby forming an autolysosome and causing the autophagosomal content to bedegrade in the vacuole (Wang et al., 2016) (**Figure 2**).

METHODS FOR ASSESSING AUTOPHAGY DURING PLANT VIRUS INFECTION

The establishment of suitable approaches to assess autophagy is a key challenge in revealing the role of the pathway in plant and virus interaction. Here, we describe some common methods of autophagy investigation.

Transmission Electron Microscope Observation

Direct observation of autophagosomes by transmission electron microscope (TEM) is an effective method of analyzing autophagy (Klionsky et al., 2016). TEM allows for the visualization of the

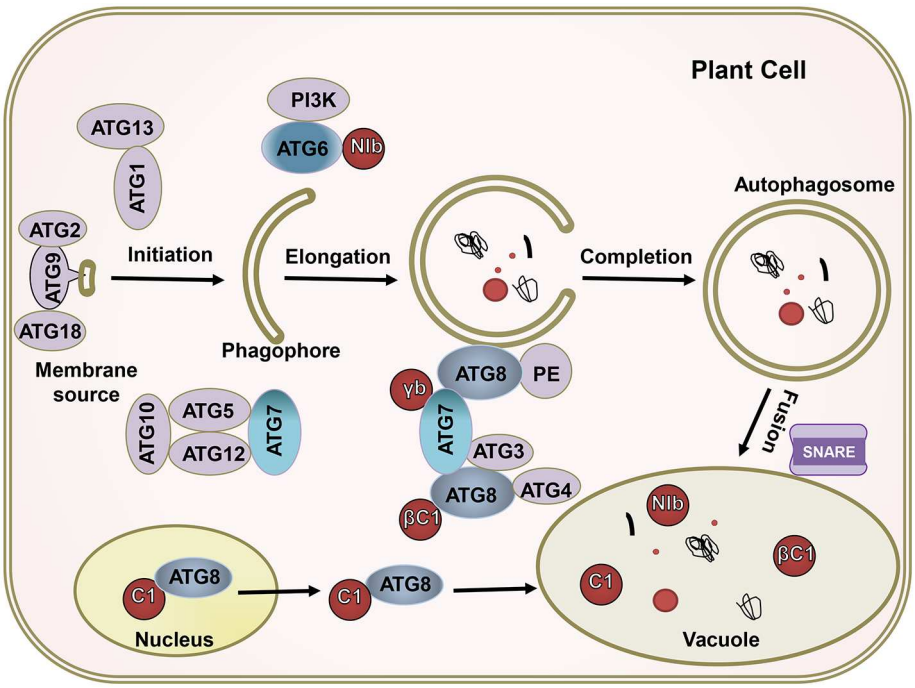

FIGURE 2 | The ATGs target viral proteins for degradation by the autophagy pathway. The autophagy pathway includes four key steps including initiation, elongation, completion, and fusion. Most ATGs drive this process; βC1 of geminivirus, NIb of PVY, γb of BSMV, and C1 of TLCYnV; these virus effectors (red) interact with crucial autophagy genes, like ATG6, ATG7, and ATG8. The ATGs target viral proteins for their degradation.

autophagosome's double-membrane circular structure, which has a diameter from 100 to 1000 nm in plant cells; the electron density of the contents in an autophagosome is similar to that of cytoplasm. Exhibiting the morphology of autophagosomes by TEM in nanometer range can help researchers confirm the occurrence and dynamics of autophagy during virus infection (Barth et al., 2010; Klionsky et al., 2016; Yoshii and Mizushima, 2017).

Fluorescent Protein-Based Autophagy Monitoring

The ATG8 lipidation system is essential for autophagosome formation. Therefore, fluorescent proteins (FPs) that are fused with ATG8 under laser scanning confocal microscope (LSCM) can be used to track autophagy in plant cells. ATG8 is located on both the inner and outer membranes of autophagosomes. After an autophagosome fuses with a vacuole, the autophagic bodies in the vacuole also exhibit the ATG8 protein (Bassham, 2015). Compared with other detection methods, FP-ATG8 fusion protein accurately quantifies autophagosomes in living cells (Bassham, 2015; Izumi et al., 2015). Many plant species encode several ATG8 homologs, all of which are located on autophagosomes and allowing most of them to be used as markers of autophagic vesicles (Bassham, 2015). FP-ATG8 fusion protein can be expressed consistently in transgenic plants or transiently by agrobacterium inoculation, allowing autophagy in living plant cells to be monitored in real time (Contento et al., 2005; Bassham, 2015; Izumi et al., 2015).

Methods for Assessing Autophagic Flux

Autophagic flux refers to the entire process of autophagy. The most common method to indicate autophagic flux in plants is by detecting the protein level of ATG8-PE or NBR1 by Western blot, which provides reliable evidence about autophagic flux (Minina et al., 2013; Klionsky et al., 2016). ATG8 is covalently attached to the lipid phosphatidylethanolamine (PE) to produce ATG8–PE, which is imbedded in the membrane of the autophgosome. Thus, ATG8 and ATG8–PE turnover indicates the strength of autophagic flux. NBR1, as an autophagy substrate, can be degraded by autophagy pathway; the protein level of NBR1 indicates autophagy activity. In addition, assays using pharmacological drugs affecting vacuolar hydrolases are quite similar to those performed in mammalian cells with drugs affecting lysosomal hydrolases, which will benefit the observation of autophagic flux. Concanamycin A (ConA), an inhibitor of vacuolar H^+-ATPase, can block vacuolar degradation, while E64d, an inhibitor of lysosomal/vacuolar cysteine proteases, can also block vacuolar degradation. Autophagic bodies within the vacuole are in proportion to autophagic activity. The autophagic bodies can be observed by fluorescence microscopy when labeled with fluorescent protein fused ATG8, like GFP-ATG8, or can be monitored by TEM (Bassham, 2015; Li et al., 2018).

Chemical Inducers and Inhibitors of Autophagy

Besides the above cell biological means used to directly observe autophagy, various chemical inhibitors affect different stages of

autophagy which can be used to test the role of autophagy in virus infection. Rapamycin acts as an allosteric inhibitor of mTOR upon association with the FK506-binding protein 12 (FKBP12) (Yang et al., 2013); however, many plants are insensitive to it (Xiong and Sheen, 2015). Another TOR inhibitor, AZD8055, an efficient autophagy inducer that works by suppressing TOR signaling, is widely used in plants (Dong et al., 2015; Pu et al., 2017; Song et al., 2019). Several inhibitors of autophagy in plant cells have been reported to impact on different stages of the process. ConA blocks vacuolar hydrolysis and suppresses autophagic vesicle degradation in vacuoles (Hafrén et al., 2017), whereas 3-methyladenine (3-MA) inhibits PI3K activity, and E64d, a cysteine protease inhibitor, blocks the flux of autophagy (Takatsuka et al., 2004; Kim et al., 2008; Pasquier, 2016; Xu et al., 2017). These chemical inducers and inhibitors can be directly sprayed onto or inoculated into the plant leaf to trigger autophagy, thereby allowing the role of autophagy in relation to biotic or abiotic stresses to be investigated.

Silencing or Mutation of *ATGs* in Plants

In addition to chemical treatments, numerous key *ATG* genes of plants are appropriate targets for autophagy inhibition. Virus-induced gene silencing (VIGS) is widely used to silence *ATG* genes to address whether autophagy plays a role in pathogen infection (Liu et al., 2005). In *Arabidopsis*, many *atg* T-DNA insertion mutants are available (Zheng et al., 2006; Yoshimoto et al., 2009; Zhou et al., 2013). For instance, *atg5* and *atg7* mutants were inoculated with cauliflower mosaic virus (CaMV) and exhibited more severe symptoms than the wild type, indicating that the process of autophagy may involve an antiviral mechanism (Hafrén et al., 2017). In recent years, the clustered regularly interspaced short palindromic repeats (CRISPR)/CRISPR-associated9 (Cas9) (CRISPR/Cas9) system was developed for genome editing (Doudna and Charpentier, 2014; Ma et al., 2016), allowing the scientific community to obtain *atg* mutants in different species and therefore promoting the study of the function and mechanism of autophagy (O'Prey et al., 2017; Norizuki et al., 2019).

PLANT DEFENSE AGAINST VIRUS INFECTION BY AUTOPHAGY

Although autophagy provides different contributions to plant immunity, research on the relationship between plant autophagy and virus infection is relatively lagging. Liu et al. (2005) reported the first case of plant virus-induced autophagy using the fluorescent dye LysoTracker Red to probe autolysosomes in tobacco cells that were infected by tobacco mosaic virus (TMV). The mRNA and protein levels of Beclin1 increased in the early stages of the TMV-induced hypersensitive response (HR) of programmed cell death (PCD) in N gene-containing *Nicotiana benthamiana* plants. Knocking down the expression levels of *ATG3*, *Beclin1*, and *ATG7* using VIGS exhibited unrestricted HR PCD and demonstrated enhanced TMV accumulation (Liu et al., 2005). These results indicated that autophagy plays an essential role in the N-mediated defense against TMV and requires Beclin1 for induction. Recently, both PCD and reactive oxygen species (ROS) level were reported to be regulated by autophagy during the compatible interplay between plant and virus (Ismayil et al., 2019). Some other components, such as sugar levels, are also modulated by virus infection (Llave, 2016; de Haro et al., 2019). Whether sugar has a relationship with autophagy induction during plant virus infection remains to be investigated.

For most plant viruses, autophagy is an antiviral mechanism, which directly targets viral components for degradation (**Figure 1**, upper part and **Table 1**). Cotton leaf curl Multan virus (CLCuMV) induces autophagy in host plants, and the virulence factor βC1 of CLCuMV directly interacts with ATG8f, which is a key autophagy protein. This interaction occurs in autophagy vesicles and targets βC1 for breakdown. When *ATG5* or *ATG7* were silenced to inhibit the autophagy pathway, more severe symptoms were caused by the virus in plants, indicating that autophagy plays an important antiviral role in CLCuMV infections (Haxim et al., 2017). These same autophagy effects were observed in other geminiviruses, like tomato yellow leaf curl virus (TYLCV) and tomato yellow leaf curl China virus (TYLCCNV). Silencing of *ATG5* or *ATG7* caused more severe symptoms and increased viral DNA accumulation (Haxim et al., 2017), indicating that autophagy may be a general antiviral mechanism against diverse geminiviruses. Recently, a study clarified the mechanism of CLCuMV-encoded βC1 inducing autophagy (Ismayil et al., 2020). Cytosolic glyceraldehyde-3-phosphate dehydrogenase (GAPC), is a negative autophagy regulator that interacts with ATG3 to inhibit autophagy in *N. benthamiana* (Han et al., 2015). Wherever, βC1 interacts with GAPC by disrupting GAPCs-ATG3 interactions to activate autophagy pathway (Ismayil et al., 2020). Turnip mosaic virus (TuMV) of the potyvirus group also induces autophagy in plants. Beclin1 (ATG6) is a key protein that interacts with ATG8a to mediate the autophagy process; expression levels of Beclin1 were shown to be significantly upregulated by TuMV infection. Interestingly, Beclin1 directly interacts with NIb, the RNA-dependent RNA polymerase (RdRp) of TuMV, and targets NIb degradation via the autophagy pathway. Silencing *Beclin1* or *ATG8a* increased NIb accumulation and promoted TuMV infection (Li et al., 2018). Two other RNA viruses, namely cucumber green mottle mosaic virus (CGMMV) of the *Tobamovirus* genus and pepino mosaic virus (PepMV) of the *Potexvirus* genus, face similar antiviral mechanisms. Their encoded RdRps also interact with Beclin1, and silencing *Beclin1* caused more severe symptoms than those observed in control plants. As a critical autophagy regulator, Beclin1 restricts RNA virus infection via the autophagy pathway to suppress and degrade viral RdRps (Li et al., 2018). CaMV of the *Caulimovirus* genus also induces the formation of autophagosomes in *N. benthamiana* cells. In *Arabidopsis atg*-mutants, the symptoms caused by CaMV were more severe than in wild type plants. Intriguingly, CaMV-encoded P4 interacts with NEIGHBOR of BRCA1 (NBR1), which is an autophagy receptor selectively targeting polyubiquitinated aggregates to nascent autophagosomes (Kirkin et al., 2009; Svenning et al., 2011; Hafrén et al., 2017). The P4–NBR1–ATG8 complex promotes selective autophagy to target P4

TABLE 1 | Summary of reported interactions between plant virus and host factors involved in autophagy.

Role	Virus	Host plants	Virus effector	Host factors	References
Antiviral function	Cucumber mosaic virus	Tobacco	2b	rgs-CaM	Nakahara et al., 2012
	Tomato aspermy virus		2b	rgs-CaM	
	Turnip mosaic virus	Tobacco	HC-Pro	rgs-CaM	Nakahara et al., 2012
	Tobacco etch virus		HC-Pro	rgs-CaM	
	Clover yellow vein virus		HC-Pro	rgs-CaM	
	Turnip mosaic virus	Arabidopsis Tobacco	HC-Pro	NBR1	Hafrén et al., 2018
	Watermelon mosaic virus	Arabidopsis	HC-Pro	NBR1	
	Cauliflower mosaic virus	Arabidopsis Tobacco	P4	NBR1	Hafrén et al., 2017
	Cotton leaf curl Multan virus	Tobacco	βC1	ATG8	Haxim et al., 2017
	Tomato yellow leaf curl virus		βC1	ATG8	
	Tomato yellow leaf curl China virus		βC1	ATG8	
	Turnip mosaic virus	Arabidopsis Tobacco	NIb	Beclin1(ATG6)	Li et al., 2018
	Cucumber green mottle virus	Tobacco	RdRp	Beclin1(ATG6)	
	Pepino mosaic virus		RdRp	Beclin1(ATG6)	
	Tomato leaf curl Yunnan virus	Tobacco	C1	ATG8h	Li et al., 2019
Pro-viral function	Potato leafroll virus	Potato Arabidopsis	P0	AGO1	Derrien et al., 2012
	Turnip mosaic virus	Tobacco Arabidopsis	VPg	SGS3	Cheng and Wang, 2017
	Tobacco etch virus		VPg	SGS3	
	Soybean mosaic virus		VPg	SGS3	
	Rice stripe virus	Tobacco Rice	NSvc4	NbREM1/OsREM1.4	Fu et al., 2018
	Barley stripe mosaic virus	Tobacco Barley	γb	ATG7	Yang et al., 2018
	Cauliflower mosaic virus	Arabidopsis Tobacco	P6	NBR1	Hafrén et al., 2017

and viral particles for degradation to fight against CaMV infection (Hafrén et al., 2017). Similarly, the autophagy cargo receptor NBR1 mediates selective autophagy by targeting helper-component proteinase (HC-Pro) and RNA-silencing suppressors (RSS) of TuMV for degradation to suppress viral accumulation (Hafrén et al., 2018). A study reported that the replication-initiator protein C1 of tomato leaf curl Yunnan virus (TLCYnV) induced plant autophagy. The direct interaction between C1 of TLCYnV and ATG8h led to the translocation of C1 from the nucleus to the cytoplasm, resulting in degradation by autophagy. This process depends on the interaction between ATG8h and XPO1a, which is a crucial component of the nuclear export pathway. Treatment with autophagy inhibitors or silencing of *ATG5*, *ATG7*, and *ATG8h* promoted TLCYnV infection in solanaceous plants (Li et al., 2019). These studies confirmed that the autophagy pathway of plants plays a direct antiviral role by interacting with virus-encoded proteins. In addition, the expression of TLCYnV-encoded C1 alone is sufficient to induce autophagy, although how TLCYnV or C1 protein activate autophagy is unclear (Li et al., 2019).

Besides the direct antiviral mechanism, autophagy is indirectly involved in plant defense against virus infection by targeting host factors (**Table 1**). Two well-studied RSSs, 2b and HC-Pro, of *Cucumovirus* and *Potyvirus* genera, were reported to interact with the regulator of gene silencing calmodulin-like protein (rgs-CaM), a cellular suppressor of post-transcriptional gene silencing (PTGS) in plants. The protein levels of endogenous rgs-CaM and viral RSSs significantly increased after autophagy inhibitor 3-MA treatment, indicating that rgs-CaM and RSSs were degraded by autophagy (Nakahara et al., 2012).

PLANT VIRUS COUNTER-DEFENSE ACTING ON AUTOPHAGY

Plants defend against virus infection by autophagy, but, as a result of long-term co-evolution, viruses produced counter-defense strategies. As mentioned above, CaMV-encoded P4 interacts with NBR1 and promotes selective autophagy to target P4 and viral particles to fight against CaMV infection. On the other hand, virus-encoded P6 can interfere with the interaction between P4 and NBR1, thus allowing CaMV-induced viral inclusions and transmission bodies to antagonize NBR1 and therefore impeding the degradation of viral proteins and particles. This report revealed a potential strategy of viruses to evade autophagy degradation for successful infection (Hafrén et al., 2017). Autophagy also plays an antiviral role in barley stripe mosaic virus (BSMV) infection. However, BSMV suppresses autophagy via its encoded-γb protein, which directly interacts with ATG7 and competes for the ATG7–ATG8 interaction, which is essential for autophagy induction. As such, BSMV-encoded γb subverts autophagy-mediated antiviral defense responses by disrupting the ATG7–ATG8 interaction to facilitate infection (Yang et al., 2018) (**Figure 1**, lower part). More cases regarding

the resolution of autophagy-mediated antiviral defense by plant viruses are reported hereafter. Further research is needed to unravel how viruses finely adjust to the induction and inhibition of the host autophagy pathway to achieve a perfect balance for their successful infection and colonization.

PLANT VIRUS PROMOTES INFECTION THROUGH HOST AUTOPHAGY

Apart from their direct interference with host plant autophagy, many viruses use autophagy to degrade some host plant factors, which have adverse effect on viruses, to promote their infection (Derrien et al., 2012; Cheng and Wang, 2017; Li et al., 2017) (**Figure 1**, lower part and **Table 1**).

In the course of plant–virus interactions, many viruses evolved mechanisms to manipulate host autophagy to meet their own needs. By degrading defense-related proteins through the autophagy pathway, plant viruses adversely affect plants to facilitate infection. Polerovirus encodes RSS P0 to trigger the degradation of the key RNA-silencing component ARGONAUTE1 (AGO1) via the autophagy pathway. Because AGO1 is co-localized with ATG8a in autophagic structures, the degradation of AGO1 was blocked following E64d or 3-MA inhibition treatment. Polerovirus-induced degradation of AGO1 via the autophagy pathway suppressed virus resistance and promoted viral infection in plants (Derrien et al., 2012). Similarly, TuMV infection caused the degradation of SGS3 and its preferential partner, RNA-dependent RNA polymerase 6 (RDR6). Treatment with the proteasome inhibitor MG132 or autophagy inhibitor 3-MA significantly attenuated virus-induced degradation of SGS3 and RDR6, suggesting that the ubiquitin proteasome and autophagy pathway are both involved in the degradation of important RNA-silencing components. TuMV-encoded VPg directly interacts with SGS3 and triggers SGS3 and RDR6 degradation, thereby attenuating host RNA-silencing and facilitating virus infection. Two other potyvirus-encoded VPgs, belonging to tobacco etch virus (TEV) and soybean mosaic virus (SMV), also interact with SGS3, indicating that the interaction between SGS3 and VPg and the degradation of the RNA-silencing component are general mechanisms of potyviruses (Cheng and Wang, 2017). The betasatellite of tomato yellow leaf China virus (TYLCCNV)-encoded βC1 up-regulates the expression of calmodulin-like protein (CaM), which interacts with the SGS3 protein in *N. benthamiana*. Transient co-expression of CaM and SGS3 induces autophagosomal activity to degrade SGS3 in host cells, while 3-MA treatment or silencing of *Beclin1*, *PI3K*, or *VPS15* in *N. benthasmiana* leading to inhibition of SGS3 degradation. TYLCCNV-induced CaM mediates RNA-silencing component SGS3 degradation, leading to successful infection of the virus in plants (Li et al., 2017).

Remorins are membrane-associated proteins found in *N. benthamiana* and rice plants that play crucial roles in cell-to-cell signaling and defense against biotic stress via the S-acylation (also known as palmitoylation) of C-terminal cysteine, a reversible post-translational modification contributing to cell plasma membrane (PM) localization and protein stability. Rice stripe virus (RSV) infection interferes with S-acylation of the C-terminal of remorin (NbREM1/OsREM1.4) through the viral movement protein NSvc4, which interacts with the NbREM1 C-terminal. NSvc4 competitively binds to the C-terminal of NbREM1/OsREM1.4 decreasing the S-acylated NbREM1/OsREM1.4 anchor to PM. S-acylation-deficient NbREM1/OsREM1.4 are sequestrated in the endoplasmic reticulum (ER) and induced autophagy for its degradation. Less S-acylated NbREM1/OsREM1.4 accumulation at the PM enhances the permeability of plasmodesma (Pd), thereby promoting virus infection (Fu et al., 2018). A study found that bamboo mosaic virus (BaMV) infection upregulated the expression of several *ATGs* and induced autophagy in *N. benthamiana* leaves. Autophagy inhibitor 3-MA treatment blocked autophagosome formation and reduced the accumulation of the viral coat protein, whereas rapamycin, an inducer treatment, enhanced the expression of the viral coat protein. BaMV-induced autophagy may offer an environment more conductive to viral replication or a shelter to evade from the RNA silencing (Huang et al., 2019). However, the autophagy mechanism contributing to BaMV RNA increase, and which viral protein of BaMV plays the crucial role in autophagy induction require further study.

CONCLUSIONS AND FUTURE DIRECTIONS

Autophagy plays a crucial role in the interaction between pathogens and mammalian cells (Shelly et al., 2009; Münz, 2017; Wang et al., 2018). In the past decade, an increasing number of studies expanded our understanding of autophagy in virus-attacked plants (Liu et al., 2005; Derrien et al., 2012; Hafrén et al., 2017; Haxim et al., 2017; Yang et al., 2018; Li et al., 2019). Most viruses trigger the autophagy pathway of host plants as a defense mechanism to counter virus infection. Notably, many viruses evolved to escape the autophagic machinery using distinct strategies, such as inhibiting autophagy induction, suppressing autophagosome nucleation, and blocking autophagosome fusion with vacuoles. Some viruses even hijack autophagic machinery for their replication and to increase movement within autophagosome-like vesicles. Therefore, accurate manipulation of plant autophagy has the potential to combat viral infections of plants in the agriculture field.

Both animal and plant viruses activate the autophagy pathway, which then induces viral protein and particle degradation as a defense mechanism (Shelly et al., 2009; Chan and Qu, 2017; Haxim et al., 2017; Sparrer and Gack, 2018; Li et al., 2019). The mechanism by which virus infection induces plant autophagy is still obscure, which viral proteins are key to inducing autophagy remains unknown, and the upstream signal of autophagy initiation upon virus infection is not yet clear. Understanding the induction of the autophagy mechanism in plants during virus infection will allow easier control of the autophagy pathway in the future.

Several ATGs act as cargo receptors or autophagy regulators to selectively interact with viral effectors, such as ATG8,

which interacts with CLCuMuV βC1; ATG6, which interacts with TuMV NIb; and ATG7, which interacts with BSMV γb (**Figure 1**). These findings suggest that more autophagy-related proteins may interact with viral effectors and are involved in host immunity. Notably, βC1 binds to ATG8f, whereas Beclin1 binds to ATG8a but not ATG8f, and C1 binds to ATG8h but not to other ATG8s. This suggests that ATG8 has multiple homologs in plants to perform diverse functions. In addition, ATG8a binds to Beclin1 at the N-terminal AIM motif. NIb binds to Beclin1 at the C-terminal, and Beclin1-mediated degradation of NIb depends on ATG8a, indicating that Beclin1 acts as a bridge to guide viral proteins to autophagosomes for breakdown.

Furthermore, some ATGs are involved in other cellular signaling pathways, including cell death, cell–cycle regulation, and innate immune signaling (Wang, 2008; Xu et al., 2017; Levine and Kroemer, 2019). For instance, Beclin1, PI3K/VPS30, and ATG3 are all required to limit HR PCD to the pathogen infection site (Liu et al., 2005), ATG5 and ATG7 regulate glucose-induced ROS in *Arabidopsis* (Huang et al., 2018), and ATG9 is a negative regulator of innate immune signaling (Cadwell and Debnath, 2018; Levine and Kroemer, 2019). Investigating autophagy crosstalk with other cellular processes may provide researchers with new methods to modulate the autophagy pathway.

In the future, the molecular mechanisms and roles of autophagy during plant and virus interactions require further and deeper study. Genetic engineering approaches or chemical treatments can be harnessed to modulate autophagy to fight against plant viruses.

AUTHOR CONTRIBUTIONS

GZ and TZ designed the project. XH wrote the manuscript and reviewed the manuscript. SC, XiaY, XinY, and TZ edited the manuscript. All authors reviewed and approved the final version of the manuscript.

FUNDING

This work was supported by the National Natural Science Foundation of China (31671993, 31871928), the Pearl River S&T Nova Program of Guangzhou (201906010093), Research and Development Project in Major Fields of Guangdong (2019B020238001), Guangdong Provincial Innovation Team for General Key Technologies in Modern Agricultural Industry (2019KJ133), and Guangdong Special Branch Plan for Young Talent with Scientific and Technological Innovation (2019TQ05N158).

ACKNOWLEDGMENTS

All authors listed have made a substantial and intellectual contribution to the work, and the authors apologize to all investigators whose researches are not cited in the review owing to space limitations.

REFERENCES

Barth, S., Glick, D., and Macleod, K. F. (2010). Autophagy: assays and artifacts. *J. Pathol.* 221, 117–124. doi: 10.1002/path.2694

Bassham, D. C. (2015). Methods for analysis of autophagy in plants. *Methods* 75, 181–188. doi: 10.1016/j.ymeth.2014.09.003

Cadwell, K., and Debnath, J. (2018). Beyond self-eating: the control of nonautophagic functions and signaling pathways by autophagy-related proteins. *J. Cell Biol.* 217, 813–822. doi: 10.1083/jcb.201706157

Catarino, S., Pereira, P., and Girão, H. (2017). Molecular control of chaperone-mediated autophagy. *Essays Biochem.* 61, 663–674. doi: 10.1042/EBC20170057

Chan, S. T., and Qu, J. J. (2017). Hepatitis C virus-induced autophagy and host innate immune response. *Viruses* 9:224. doi: 10.3390/v9080224

Cheng, X., and Wang, A. (2017). The potyvirus silencing suppressor protein VPg mediates degradation of SGS3 via ubiquitination and autophagy pathways. *J. Virol.* 91:e01478-16. doi: 10.1128/JVI.01478-16

Contento, A. L., Xiong, Y., and Bassham, D. C. (2005). Visualization of autophagy in *Arabidopsis* using the fluorescent dye monodansylcadaverine and a GFP-AtATG8e fusion protein. *Plant J.* 42, 598–608. doi: 10.1111/j.1365-313X.2005.02396.x

Cuervo, A. M., and Wong, E. (2014). Chaperone-mediated autophagy: roles in disease and aging. *Cell Res.* 24, 92–104. doi: 10.1038/cr.2013.153

de Haro, L. A., Arellano, S. M., Novák, O., Feil, R., Dumón, A. D., Mattio, M. F., et al. (2019). Mal de río cuarto virus infection causes hormone imbalance and sugar accumulation in wheat leaves. *BMC Plant Biol.* 19:112. doi: 10.1186/s12870-019-1709-y

Derrien, B., Baumberger, N., Schepetilnikov, M., Viotti, C., Cillia, J. D., Ziegler-Graff, V., et al. (2012). Degradation of the antiviral component ARGONAUTE1 by the autophagy pathway. *Proc. Natl. Acad. Sci. U.S.A.* 109, 15942–15946. doi: 10.1073/pnas.1209487109

Deter, R. L., and de Duve, C. (1967). Influence of glucagon, an inducer of cellular autophagy, on some physical properties of rat liver lysosomes. *J. Cell Biol.* 33, 437–449. doi: 10.1083/jcb.33.2.437

Dong, P., Xiong, F., Que, Y., Wang, K., Yu, L., Li, Z., et al. (2015). Expression profiling and functional analysis reveals that TOR is a key player in regulating photosynthesis and phytohormone signaling pathways in *Arabidopsis*. *Front. Plant Sci.* 6:677. doi: 10.3389/fpls.2015.00677

Doudna, J. A., and Charpentier, E. (2014). The new frontier of genome engineering with crispr-cas9. *Science* 346:1258096. doi: 10.1126/science.1258096

Fargette, D., Konaté, G., Fauquet, C., Muller, E., Peterschmitt, M., and Thresh, J. M. (2006). Molecular ecology and emergence of tropical plant viruses. *Annu. Rev. Phytopathol.* 44, 235–260. doi: 10.1146/annurev.phyto.44.120705.104644

Fu, S., Xu, Y., Li, C., Li, Y., Wu, J., and Zhou, X. (2018). Rice stripe virus interferes with S-acylation of remorin and induces its autophagic degradation to facilitate virus infection. *Mol. Plant* 11, 269–287. doi: 10.1016/j.molp.2017.11.011

Hafrén, A., Macia, J., Love, A. J., Milner, J. J., Drucker, M., and Hofius, D. (2017). Selective autophagy limits cauliflower mosaic virus infection by NBR1-mediated targeting of viral capsid protein and particles. *Proc. Natl. Acad. Sci. U.S.A.* 114, E2026–E2035. doi: 10.1073/pnas.1610687114

Hafrén, A., Üstün, S., Hochmuth, A., Svenning, S., Johansen, T., and Hofius, D. (2018). Turnip mosaic virus counteracts selective autophagy of the viral silencing suppressor HCpro. *Plant Physiol.* 176, 649–662. doi: 10.1104/pp.17.01198

Han, S., Wang, Y., Zheng, X., Jia, Q., Zhao, J., Bai, F., et al. (2015). Cytoplastic glyceraldehyde-3-phosphate dehydrogenases interact with atg3 to negatively regulate autophagy and immunity in *Nicotiana benthamiana*. *Plant Cell* 27, 1316–1331. doi: 10.1105/tpc.114.134692

Haxim, Y., Ismayil, A., Jia, Q., Wang, Y., Zheng, X., Chen, T., et al. (2017). Autophagy functions as an antiviral mechanism against geminiviruses in plants. *eLife* 6:e14859. doi: 10.7554/eLife.23897

Huang, L., Yu, L., Zhang, X., Fan, B., Wang, F., Dai, Y., et al. (2018). Autophagy regulates glucose-mediated root meristem activity by modulating ROS production in *Arabidopsis*. *Autophagy* 15, 407–422. doi: 10.1080/15548627.2018.1520547

Huang, Y., Huang, Y., Hsiao, Y. J., Li, S., Hsu, Y. H., and Tsai, C. H. (2019). Autophagy is involved in assisting the replication of *Bamboo mosaic virus* in *Nicotiana benthamiana*. *J. Exp. Bot.* 70, 4657–4669. doi: 10.1093/jxb/erz244

Hurley, J. H., and Young, L. N. (2017). Mechanisms of autophagy initiation. *Annu. Rev. Biochem.* 86, 225–244. doi: 10.1146/annurev-biochem-061516-044820

Ismayil, A., Yang, M., Haxim, Y., Wang, Y., Li, J., Han, L., et al. (2020). Cotton leaf curl Multan virus βC1 protein induces autophagy by disrupting the interaction of Autophagy-Related protein 3 with glyceraldehyde-3-phosphate dehydrogenases. *Plant Cell* 32, 1124–1135. doi: 10.1105/tpc.19.00759

Ismayil, A., Yang, M., and Liu, Y. (2019). Role of autophagy during plant-virus interactions. *Semin. Cell Dev. Biol.* 101, 36–40. doi: 10.1016/j.semcdb.2019.07.001

Izumi, M., Hidema, J., Wada, S., Kondo, E., Kurusu, T., Kuchitsu, K., et al. (2015). Establishment of monitoring methods for autophagy in rice reveals autophagic recycling of chloroplasts and root plastids during energy limitation. *Plant Physiol.* 167, 1307–1320. doi: 10.1104/pp.114.254078

Kaushik, S., and Cuervo, A. M. (2018). The coming of age of chaperone-mediated autophagy. *Nat. Rev. Mol. Cell Bio.* 19, 365–381. doi: 10.1038/s41580-018-0001-6

Kim, K. W., Hwang, M., Moretti, L., Jaboin, J. J., Cha, Y. I., and Lu, B. (2008). Autophagy upregulation by inhibitors of caspase-3 and mTOR enhances radiotherapy in a mouse model of lung cancer. *Autophagy* 4, 659–668. doi: 10.4161/auto.6058

Kirkin, V., Lamark, T., Sou, Y., Bjørkøy, G., Nunn, J. L., Bruun, J. A., et al. (2009). A role for NBR1 in autophagosomal degradation of ubiquitinated substrates. *Mol. Cell* 33, 505–516. doi: 10.1016/j.molcel.2009.01.020

Klionsky, D. J., Abdelmohsen, K., Abe, A., Abedin, M. J., Abeliovich, H., Arozena, A. A., et al. (2016). Guidelines for the use and interpretation of assays for monitoring autophagy (3rd edition). *Autophagy* 12, 1–222. doi: 10.1080/15548627.2015.1100356

Klionsky, D. J., and Codogno, P. (2013). The mechanism and physiological function of macroautophagy. *J. Innate Immun.* 5, 427–433. doi: 10.1159/000351979

Klionsky, D. J., Cregg, J. M., Dunn, W. A Jr., Emr, S. D., Sakai, Y., Sandoval, I. V., et al. (2003). A unified nomenclature for yeast autophagy-related genes. *Dev. Cell* 5, 539–545. doi: 10.1016/s1534-5807(03)00296-x

Lamb, C. A., Yoshimori, T., and Tooze, S. A. (2013). The autophagosome: origins unknown, biogenesis complex. *Nat. Rev. Mol. Cell Bio.* 14, 759–774. doi: 10.1038/nrm3696

Levine, B., and Kroemer, G. (2019). Biological functions of autophagy genes: a disease perspective. *Cell* 176, 11–42. doi: 10.1016/j.cell.2018.09.048

Li, F., Zhang, C., Li, Y., Wu, G., Hou, X., Zhou, X., et al. (2018). Beclin1 restricts RNA virus infection in plants through suppression and degradation of the viral polymerase. *Nat. Commun.* 9:1268. doi: 10.1038/s41467-018-03658-2

Li, F., Zhang, M., Zhang, C., and Zhou, X. (2019). Nuclear autophagy degrades a geminivirus nuclear protein to restrict viral infection in solanaceous plants. *New Phytol.* 225, 1746–1761. doi: 10.1111/nph.16268

Li, F., Zhao, N., Li, Z., Xu, X., Wang, Y., Yang, X., et al. (2017). A calmodulin-like protein suppresses RNA silencing and promotes geminivirus infection by degrading SGS33 via the autophagy pathway in Nicotiana benthamiana. *PLOS Pathog.* 13:e1006213. doi: 10.1371/journal.ppat.1006213

Li, W., Li, J., and Bao, J. (2012). Microautophagy: lesser-known self-eating. *Cell. Mol. Life Sci.* 69, 1125–1136. doi: 10.1007/s00018-011-0865-5

Liu, Y., and Bassham, D. C. (2012). Autophagy: pathways for self-eating in plant cells. *Annu. Rev. Plant Biol.* 63, 215–237. doi: 10.1146/annurev-arplant-042811-105441

Liu, Y., Schiff, M., Czymmek, K., Tallóczy, Z., Levine, B., and Dinesh-kumar, S. P. (2005). Autophagy regulates programmed cell death during the plant innate immune response. *Cell* 121, 567–577. doi: 10.1016/j.cell.2005.03.007

Llave, C. (2016). Dynamic cross-talk between host primary metabolism and viruses during infections in plants. *Curr. Opin. Virol.* 19, 50–55. doi: 10.1016/j.coviro.2016.06.013

Ma, X., Zhu, Q., Chen, Y., and Liu, Y. (2016). CRISPR/Cas9 platforms for genome editing in plants: developments and applications. *Mol. Plant* 9, 961–974. doi: 10.1016/j.molp.2016.04.009

Marshall, R. S., and Vierstra, R. D. (2018). Autophagy: the master of bulk and selective recycling. *Annu. Rev. Plant Biol.* 69, 173–208. doi: 10.1146/annurev-arplant-042817-040606

Medina-Puche, L., and Lozano-Duran, R. (2019). Tailoring the cell: a glimpse of how plant viruses manipulate their hosts. *Curr. Opin. Plant Biol.* 52, 164–173. doi: 10.1016/j.pbi.2019.09.007

Minina, E. A., Sanchez-Vera, V., Moschou, P. N., Suarez, M. F., Sundberg, E., Weih, M., et al. (2013). Autophagy mediates caloric restriction-induced lifespan extension inarabidopsis. *Aging Cell* 12, 327–329. doi: 10.1111/acel.12048

Mizushima, N., Levine, B., Cuervo, A. M., and Klionsky, D. J. (2008). Autophagy fights disease through cellular self-digestion. *Nature* 451, 1069–1075. doi: 10.1038/nature06639

Mizushima, N., Yoshimori, T., and Ohsumi, Y. (2011). The role of Atg proteins in autophagosome formation. *Annu. Rev. Cell Dev. Biol.* 27, 107–132. doi: 10.1146/annurev-cellbio-092910-154005

Münz, C. (2017). The autophagic machinery in viral exocytosis. *Front. Microbiol.* 8:269. doi: 10.3389/fmicb.2017.00269

Nakahara, K. S., Masuta, C., Yamada, S., Shimura, H., Kashihara, Y., Wada, T. S., et al. (2012). Tobacco calmodulin-like protein provides secondary defense by binding to and directing degradation of virus RNA silencing suppressors. *Proc. Natl. Acad. Sci. U.S.A.* 109, 10113–10118. doi: 10.1073/pnas.1201628109

Norizuki, T., Kanazawa, T., Minamino, N., Tsukaya, H., and Ueda, T. (2019). Marchantia polymorpha, a new model plant for autophagy studies. *Front. Plant Sci.* 10:935. doi: 10.3389/fpls.2019.00935

Oerke, E. C., and Dehne, H. W. (2004). Safeguarding production-losses in major crops and the role of crop protection. *Crop Prot.* 23, 275–285. doi: 10.1016/j.cropro.2003.10.001

Ohsumi, Y. (2001). Molecular dissection of autophagy: two ubiquitin-like systems. *Nat. Rev. Mol. Cell Bio.* 2, 211–216. doi: 10.1038/35056522

O'Prey, J., Sakamaki, J., Baudot, A. D., New, M., van Acker, T., Tooze, S. A., et al. (2017). Application of CRISPR/Cas9 to autophagy research. *Methods Enzymol.* 588, 79–108. doi: 10.1016/bs.mie.2016.09.076

Pasquier, B. (2016). Autophagy inhibitors. *Cell. Mol. Life Sci.* 73, 985–1001. doi: 10.1007/s00018-015-2104-y

Pu, Y., Luo, X., and Bassham, D. C. (2017). TOR-dependent and -independent pathways regulate autophagy in *Arabidopsis* thaliana. *Front. Plant Sci.* 8:1204. doi: 10.3389/fpls.2017.01204

Shelly, S., Lukinova, N., Bambina, S., Berman, A., and Cherry, S. (2009). Autophagy is an essential component of *drosophila* immunity against vesicular stomatitis virus. *Immunity* 30, 588–598. doi: 10.1016/j.immuni.2009.02.009

Shimamura, S., Miyazaki, T., Tashiro, M., Takazono, T., Saijo, T., Yamamoto, K., et al. (2019). Autophagy-inducing factor Atg1 is required for virulence in the pathogenic fungus *Candida* glabrata. *Front. Microbiol.* 10:27. doi: 10.3389/fmicb.2019.00027

Shoji-Kawata, S., and Levine, B. (2009). Autophagy, antiviral immunity, and viral countermeasures. *Biochim. Biophys. Acta.* 1793, 1478–1484. doi: 10.1016/j.bbamcr.2009.02.008

Signorelli, S., Tarkowski, A. P., van den Ende, W., and Bassham, D. C. (2019). Linking autophagy to abiotic and biotic stress responses. *Trends Plant Sci.* 24, 413–430. doi: 10.1016/j.tplants.2019.02.001

Song, Y., Li, L., Yang, Z., Zhao, G., Zhang, X., Wang, L., et al. (2019). Target of rapamycin (TOR) regulates the expression of lncRNAs in response to abiotic stresses in cotton. *Front. Genet.* 9:690. doi: 10.3389/fgene.2018.00690

Sparrer, K. M. J., and Gack, M. U. (2018). TRIM proteins: new players in virus-induced autophagy. *PLOS Pathog.* 14:e1006787. doi: 10.1371/journal.ppat.1006787

Svenning, S., Lamark, T., Krause, K., and Johansen, T. (2011). Plant NBR1 is a selective autophagy substrate and a functional hybrid of the mammalian autophagic adapters NBR1 and p62/SQSTM1. *Autophagy* 7, 993–1010. doi: 10.4161/auto.7.9.16389

Takatsuka, C., Inoue, Y., Matsuoka, K., and Moriyasu, Y. (2004). 3-methyladenine inhibits autophagy in tobacco culture cells under sucrose starvation conditions. *Plant Cell Physiol.* 45, 265–274. doi: 10.1093/pcp/pch031

Tsukada, M., and Ohsumi, Y. (1993). Isolation and characterization of autophagy-defective mutants of *saccharomyces cerevesiae*. *FEBS Lett.* 333, 169–174. doi: 10.1016/0014-5793(93)80398-E

Wang, J. (2008). Beclin 1 bridges autophagy, apoptosis and differentiation. *Autophagy* 4, 947–948. doi: 10.4161/auto.6787

Wang, Y., Jiang, K., Zhang, Q., Meng, S., and Ding, C. (2018). Autophagy in negative RNA virus. *Front. Microbiol.* 9:206. doi: 10.3389/fmicb.2018.00206

Wang, Y., Li, L., Hou, C., Lai, Y., Long, J., Liu, J., et al. (2016). SNARE-mediated membrane fusion in autophagy. *Semin. Cell Dev. Biol.* 60, 97–104. doi: 10.1016/j.semcdb.2016.07.009

Xia, K., Liu, T., Ouyang, J., Wang, R., Fan, T., and Zhang, M. (2011). Genome-wide identification, classification, and expression analysis of autophagy-associated gene homologues in rice (*Oryza sativa* L.). *DNA Res.* 18, 363–377. doi: 10.1093/dnares/dsr024

Xie, Z., and Klionsky, D. J. (2007). Autophagosome formation: core machinery and adaptations. *Nat. Cell Biol.* 9, 1102–1109. doi: 10.1038/ncb1007-1102

Xiong, Y., and Sheen, J. (2015). Novel links in the plant tor kinase signaling network. *Curr. Opin. Plant Biol.* 28, 83–91. doi: 10.1016/j.pbi.2015.09.006

Xu, G., Wang, S., Han, S., Xie, K., Wang, Y., Li, J., et al. (2017). Plant Bax inhibitor-1 interacts with ATG6 to regulate autophagy and programmed cell death. *Autophagy* 13, 1161–1175. doi: 10.1080/15548627.2017.1320633

Yang, H., Rudge, D. G., Koos, J. D., Vaidialingam, B., Yang, H. J., and Pavletich, N. P. (2013). mTOR kinase structure, mechanism and regulation. *Nature* 497, 217–223. doi: 10.1038/nature12122

Yang, M., Zhang, Y., Xie, X., Yue, N., Li, J., Wang, X. B., et al. (2018). Barley stripe mosaic virus γb protein subverts autophagy to promote viral infection by disrupting the ATG7-ATG8 interaction. *Plant Cell* 30, 1582–1595. doi: 10.1105/tpc.18.00122

Yoshii, S. R., and Mizushima, N. (2017). Monitoring and measuring autophagy. *Int. J. Mol. Sci.* 18:1865. doi: 10.3390/ijms18091865

Yoshimoto, K. (2012). Beginning to understand autophagy, an intracellular self-degradation system in plants. *Plant Cell Physiol.* 53, 1355–1365. doi: 10.1093/pcp/pcs099

Yoshimoto, K., Jikumaru, Y., Kamiya, Y., Kusano, M., Consonni, C., Panstruga, P., et al. (2009). Autophagy negatively regulates cell death by controlling NPR1-dependent Salicylic acid signaling during senescence and the innate immune response in *Arabidopsis*. *Plant Cell* 21, 2914–2927. doi: 10.1105/tpc.109.068635

Yoshimoto, K., Takano, Y., and Sakai, Y. (2010). Autophagy in plants and phytopathogens. *FEBS Lett.* 584, 1350–1358. doi: 10.1016/j.febslet.2010.01.007

Zheng, Z., Qamar, S. A., Chen, Z., and Mengiste, T. (2006). *Arabidopsis* WRKY33 transcription factor is required for resistance to necrotrophic fungal pathogens. *Plant J.* 48, 592–605. doi: 10.1111/j.1365-313X.2006.02901.x

Zhou, J., Wang, J., Cheng, Y., Chi, Y. J., Fan, B., Yu, J. Q., et al. (2013). NBR1-mediated selective autophagy targets insoluble ubiquitinated protein aggregates in plant stress responses. *PLOS Genet.* 9:e1003196. doi: 10.1371/journal.pgen.1003196

Zhou, X., Zhao, P., Wang, W., Zou, J., Cheng, T., Peng, X., et al. (2015). A comprehensive, genome-wide analysis of autophagy-related genes identified in tobacco suggests a central role of autophagy in plant response to various environmental cues. *DNA Res.* 22, 245–257. doi: 10.1093/dnares/dsv012

Conflict of Interest: The authors declare that the research was conducted in the absence of any commercial or financial relationships that could be construed as a potential conflict of interest.

Copyright © 2020 Huang, Chen, Yang, Yang, Zhang and Zhou. This is an open-access article distributed under the terms of the Creative Commons Attribution License (CC BY). The use, distribution or reproduction in other forums is permitted, provided the original author(s) and the copyright owner(s) are credited and that the original publication in this journal is cited, in accordance with accepted academic practice. No use, distribution or reproduction is permitted which does not comply with these terms.

frontiers in Microbiology

ORIGINAL RESEARCH
published: 30 April 2020
doi: 10.3389/fmicb.2020.00766

Interactions Between Thiamethoxam and *Deformed Wing Virus* Can Drastically Impair Flight Behavior of Honey Bees

Marianne Coulon[1,2†], Anne Dalmon[1†], Gennaro Di Prisco[3,4], Alberto Prado[1,5], Florine Arban[1], Eric Dubois[2], Magali Ribière-Chabert[2], Cedric Alaux[1], Richard Thiéry[2] and Yves Le Conte[1]*

[1] INRAE, UR 406 Abeilles et Environnement, Site Agroparc, Avignon, France, [2] ANSES Sophia Antipolis, Unit of Honey bee Pathology, Sophia Antipolis, France, [3] CREA-AA, Research Centre for Agriculture and Environment, Council for Agricultural Research and Economics, Bologna, Italy, [4] Department of Agriculture, University of Naples "Federico II", Portici, Italy, [5] Escuela Nacional de Estudios Superiores Juriquilla, UNAM, Juriquilla, Mexico

OPEN ACCESS

Edited by:
Declan C. Schroeder, University of Minnesota, United States

Reviewed by:
Stephen Martin, University of Salford, United Kingdom
Ian Michael Traniello, University of Illinois at Urbana–Champaign, United States

***Correspondence:**
Anne Dalmon
anne.dalmon@inrae.fr

† These authors have contributed equally to this work

Specialty section:
This article was submitted to Virology, a section of the journal Frontiers in Microbiology

Received: *29 January 2020*
Accepted: *31 March 2020*
Published: *30 April 2020*

Citation:
Coulon M, Dalmon A, Di Prisco G, Prado A, Arban F, Dubois E, Ribière-Chabert M, Alaux C, Thiéry R and Le Conte Y (2020) Interactions Between Thiamethoxam and Deformed Wing Virus Can Drastically Impair Flight Behavior of Honey Bees. Front. Microbiol. 11:766. doi: 10.3389/fmicb.2020.00766

Exposure to multiple stress factors is believed to contribute to honey bee colony decline. However, little is known about how co-exposure to stress factors can alter the survival and behavior of free-living honey bees in colony conditions. We therefore studied the potential interaction between a neonicotinoid pesticide, thiamethoxam, and a highly prevalent honey bee pathogen, *Deformed wing virus* (DWV). For this purpose, tagged bees were exposed to DWV by feeding or injection, and/or to field-relevant doses of thiamethoxam, then left in colonies equipped with optical bee counters to monitor flight activity. DWV loads and the expression of immune genes were quantified. A reduction in vitellogenin expression level was observed in DWV-injected bees and was associated with precocious onset of foraging. Combined exposure to DWV and thiamethoxam did not result in higher DWV loads compared to bees only exposed to DWV, but induced precocious foraging, increased the risk of not returning to the hive after the first flight, and decreased survival when compared to single stress exposures. We therefore provided the first evidence for deleterious interactions between DWV and thiamethoxam in natural conditions.

Keywords: neonicotinoid, pesticide, synergy, pathogen, colony collapse, sub-lethal effects, foraging

INTRODUCTION

Heavy losses of honey bee colonies in the Northern hemisphere have been documented since the beginning of the 21st century (Lee et al., 2015). It is crucial to study such losses as it is known that 84% of the 264 most important crops in Europe depend on, at least to some extent, animal pollination (Williams, 1994). There is now a scientific consensus on the fact that honey bee colony losses are the result of multifactorial causes, including a decrease in floral resource availability, the spread of pathogens and pesticide use (Goulson et al., 2015).

Honey bee colonies are frequently co-exposed to several pesticides and their corresponding metabolites, even when foraging in grasslands or non-agricultural areas (Hladik et al., 2016; Long and Krupke, 2016; Alburaki et al., 2018). Indeed, pesticides are carried to the hive via contaminated

pollen and nectar by forager bees. For instance, neonicotinoids have increasingly been used as insecticides for a wide range of crops for the past 20 years (Simon-Delso et al., 2015), which has resulted in frequent detection in honey bee hives (Lawrence et al., 2016) and hive products like honey (Jones and Turnbull, 2016; Mitchell et al., 2017). Despite EU policy measures for banning neonicotinoids they still persist in the environment (Wintermantel et al., 2020).

In addition, the high density of individuals inside the honey bee colony facilitates pathogen transmission. Honey bee colonies are favorable to pathogens due to the high concentration of individuals and stored food in the colony (Schmid-Hempel, 1998). Therefore, honey bees can often be co-exposed to stress factors, like pathogens and pesticides (Mullin et al., 2010; vanEngelsdorp and Meixner, 2010; Cornman et al., 2012; Simon-Delso et al., 2014). Interactions between pesticides and pathogens have been reviewed by Poquet et al. (2016). Specifically, pesticides can interact with bee viruses. DeGrandi-Hoffman et al. (2013) showed that the number of nurse bees contaminated with *Black queen cell virus* (BQCV) increased significantly when they were fed with pollen containing a mix of the insecticide chlorpyrifos (organophosphates) and a commercial fungicide solution. In the field, Alburaki et al. (2015) found higher BQCV loads in colonies located in treated corn fields grown from neonicotinoid-coated seeds but a subsequent study did not confirm this result (Osterman et al., 2019). Combined exposure to sublethal doses of the neonicotinoid thiacloprid and BQCV was also found to significantly increase mortality and BQCV viral loads in honey bee larvae (Doublet et al., 2015). This latter effect could be explained by the immune suppression induced by the pesticide. Indeed, Di Prisco et al. (2013) reported an inhibition of an immune cascade effector by the neonicotinoid clothianidin, which hinders the bee's control of *Deformed wing virus* (DWV) replication. We also observed that tolerance to chronic bee paralysis virus (CBPV) infection was changed by co-exposure to thiamethoxam but this effect may depend on the honey bee's physiology (Coulon et al., 2018, 2019). Most studies were performed in laboratories in controlled conditions. As a result, little is known about their consequences on bee behavior, such as orientation flights and foraging activity. We therefore tested the potential effects of a co-exposure to a pathogen (DWV) and a common pesticide (thiamethoxam) in natural conditions.

Deformed wing virus is one of the most prevalent honey bee viruses in the world (Martin and Brettell, 2019); for example, it was detected in 97% of tested French apiaries in 2002 (Tentcheva et al., 2004). It is a single strand positive RNA virus, of the *Picornavirales* order, which contains many of the viruses infecting honey bees (Remnant et al., 2017). However, as for many honey bee viruses, DWV mostly causes covert infections in hives (de Miranda and Genersch, 2010). Overt infections often occur when the virus is transmitted to the pupae by the *Varroa destructor* mite through injection while the mite feeds (de Miranda and Genersch, 2010; Möckel et al., 2011), causing deformed wings. In addition, DWV infection is known to impair associative learning and memory formation (Iqbal and Mueller, 2007), weaken flight ability (Wells et al., 2016), induce precocious foraging trips (Benaets et al., 2017) and drastically reduce bee lifespan (Rueppell et al., 2017). Thiamethoxam is a neonicotinoid insecticide commonly used around the world (Sanchez-Bayo, 2014), especially on rapeseed oil, a crop that is widespread and attractive to honey bees (Simon-Delso et al., 2015). It can be quickly metabolized both in insects and plants into clothianidin (Nauen et al., 2003; Coulon et al., 2018), which is also commercialized as an insecticide. Sublethal doses of thiamethoxam have been shown to cause negative effects on homing flights in foragers (Henry et al., 2012). Such impaired foraging behavior after chronic exposure to sublethal doses of another neonicotinoid (thiachloprid) was correlated with a disruption in learning and memory functions (Tison et al., 2016, 2017). Furthermore thiamethoxam or its metabolite clothianidin have been found to cause a significant reduction in foraging activity and longer foraging trips in exposed foragers (Schneider et al., 2012), impair memory consolidation and retrieval (Tison et al., 2019) and inhibit the honey bee immune system (Brandt et al., 2016) and detoxification genes (Coulon et al., 2019). Altogether, loss of bees and poor performance of foragers may affect the colony homeostasis and development, and ultimately lead to colony failure (Perry et al., 2015; Prado et al., 2019).

To better understand the influence of DWV and thiamethoxam co-exposure on honey bees, we recorded survival and the onset of foraging of bees with optical bee counters (Dussaubat et al., 2013; Alaux et al., 2014; Bordier et al., 2017b; Prado et al., 2019). In parallel we measured variation in viral loads as well as the expression levels of immune, detoxification genes, and vitellogenin, which promotes the longevity of bees by acting as an antioxidant (Seehuus et al., 2006) and has an important role in immune function (Amdam et al., 2004).

MATERIALS AND METHODS

Experimental Set Up

Two 5-frame colonies were selected based on low DWV infection levels ($<2.5 \times 10^6$ copies DWV/bee) and then equipped with optical counters at the hive entrance in early May 2016 and April 2017. Colonies were treated against varroa at the end of the summer using Apivar (Veto-pharma, Palaiseau, France) and overwintered successfully. They were screened for common viruses (DWV, SBV, BQCV, ABPV, IAPV, CBPV) before starting the experiment by analyzing a pool of 40 honey bees per colony (see below for virus quantification). Emerging bees were collected from brood frames originating from the same "DWV-low" colonies, and incubated overnight at 34°C. Newly emerged bees were randomly distributed in cages and marked with either a 3-mm wide barcode printed on laminated paper and glued (Sader) onto the thorax (66 and 60 bees per treatment, colony and replicate in 2016 and 2017, respectively; see **Supplementary Table S1**), or a paint mark on the abdomen (one color per treatment, 80–100 bees per treatment and replicate, **Supplementary Table S1**). In total 3024 bees were barcoded and 3125 painted. After tagging or painting, bees were kept overnight in an incubator at 34°C with saturated humidity and 50% sucrose syrup. On the next day, they were assigned to the following treatments: (1) control bees; (2) bees individually fed

with 0.25 ng of thiamethoxam in 5 µl of syrup; (3) bees injected with PBS (Phosphate Buffer Saline solution); (4) bees injected with PBS and individually fed with 0.25 ng of thiamethoxam; (5) bees injected with DWV ($\sim 10^4$ copies/bee), and 6. bees injected with DWV ($\sim 10^4$ copies/bee) and individually fed with 0.25 ng of thiamethoxam. The experiment was replicated five times, in May and July 2016, and three times between April and May 2017. The PBS injection treatments were performed as a control for the effects of the injection, as it has been shown that piercing honey bee cuticle can challenge their immunity (Evans et al., 2006; Siede et al., 2012; Alaux et al., 2014).

In the three replicates from 2017 (**Supplementary Table S1**), additional experimental groups were included: (7) bees individually fed with an inoculum of $\sim 10^8$ copies of DWV, (8) bees individually fed with 1.00 ng of thiamethoxam, (9) bees injected with DWV ($\sim 10^4$ copies/bee) and individually fed with 1.00 ng of thiamethoxam, and (10) bees individually fed with $\sim 10^8$ copies of DWV and with 0.25 ng of thiamethoxam.

Thiamethoxam and DWV Exposures

To obtain the DWV inoculum, the stored DWV sample already described (KX373899, Dalmon et al., 2017) was injected in pupae for multiplication. After 24 h at 34°C and saturated humidity, five pupae were crushed into 500 µl of PBS and then centrifuged twice for 10 min at 8,000 × *g* and 4°C to eliminate most tissue and cell debris. Bees were injected with supernatant from the second centrifugation, and an aliquot of supernatant was later quantified using real-time RT-PCR to retrospectively assess the exact number of viral copies injected. Dilution was calculated to result in 10^8 copies of DWV in the 5 µl sucrose syrup for DWV-*per os* or to 2.75×10^4 copies of DWV in the 46 nl of the inoculum that was injected into each bee. No quantifiable levels of BQCV, SBV, CBPV, ABPV, IAPV, and KBV were found. Injections were performed using a Nanoject (Drummond Scientific, Broomall, PA, United States) and heat-elongated glass microcapillary tubes, between the third and fourth tergites of bees previously anesthetized with CO_2 and maintained on ice. These doses corresponded to DWV levels observed from low to high varroa infestations in the colonies (Traynor et al., 2016).

Exposure to thiamethoxam was performed as follows. After 2 h of starvation (control bees included), bees were individually fed with 5 µl of syrup. The 0.25 and 1.00 ng doses of thiamethoxam in 5 µl of syrup solution were obtained from successive dilutions from a 1 mg/ml solution of thiamethoxam, first in water, then in 30% syrup. Syrup was prepared by mixing 30% w/v powdered sugar in water. The same technique was used to feed the 10^8 copies/bee of DWV for the *per os* treatments.

After treatments, 396–725 bees per hive were introduced into the hives. For viral and gene expression analysis, three samples of three bees for each replicate and treatment (identified from their paint mark on the abdomen) were collected from colony frames and immediately put on dry ice 24 and 48 h after their re-introduction into the colony, and then stored at −80°C (**Supplementary Table S1**).

Onset of Foraging and Survival

In total, 3024 bees tagged with barcodes were followed using optical counters, as previously described in Alaux et al. (2014) and Bordier et al. (2017b). Briefly, the bee counter is composed of a modified entrance with eight tunnels, a camera monitoring the entrance, a computer for image acquisition and software that analyses the images and records the in-and-out activity of bees. For each detection event, we recorded the bee's ID, direction (in or out of the hive) and the time (day, hour, minute, and second). From these raw data, we retrieved the duration of each flight and identified the first day of foraging for each individual, defined as the age at which each bee performs a trip lasting longer than 10 min (Marco Antonio et al., 2008; Woyciechowski and Moroń, 2009; Benaets et al., 2017). All tagged bees were followed until no bee could be detected (up to 51 days); for each bee the last day of detection was considered as time of death. 2306 out of the 3024 barcoded bees were recorded at least once, corresponding to 76% detection.

Virus and Gene Transcription Quantification

The number of DWV copies was determined by quantitative PCR using a StepOne-Plus Real-Time PCR System (Applied Biosystems, Life Technologies) and the SYBR Green detection method. Pools of 3 bees were crushed directly in 900 µl of Qiazol with a 0.8 cm-diameter bead using a TissueLyser (Qiagen) (four times 30 s at 30 Hz). The homogenate was centrifuged for 2 min at 12,000 × *g* and 4°C, and the supernatant was transferred into a new tube to be processed for RNA extraction. Then, total RNA was extracted using Qiagen's RNeasy Universal Plus Mini Kit, following the manufacturer's instructions (QIAGEN, Hilden, Germany). RNA was quantified using a spectrophotometer (Nanodrop 2000, Thermo Fisher Scientific) and then diluted to obtain a concentration of 500 ng/µl. RNA solutions were stored at −80°C. Reverse transcription was performed from 1 µg RNA with the High capacity RNA to cDNA kit (Applied Biosystems, Saint Aubin, France) according to the manufacturer's protocol.

For virus quantification, 3 µl of 10-fold diluted cDNA were mixed with 7 µl of SYBR Green master mix (Applied Biosystems) containing 10 pmol of primers. DWV, but also ABPV, CBPV, BQCV and *Sacbrood bee virus* (SBV) loads were quantified using a qPCR absolute quantification. Amplification was performed with the following program: 10 min 95°C, 40 cycles of 15 s at 95°C, and 1 min at 60°C. A melting curve was generated from 60 to 95°C. Quantification was performed twice. Sequence primers and viral sequences used as reference are shown in **Supplementary Table S2**. A standard curve, obtained for each virus from serial dilutions of viral synthetic fragments of known concentration (MWG, Germany), was used to calculate viral loads from Ct values in the samples (Dalmon et al., 2019).

Expression level of immune response [vitellogenin, dorsal-1-a, apidaecin, pro-phenoloxydase (*ppo*)] and detoxification (glutathione-*S*-transferase 3, catalase and *cyp6as11*) genes were assessed using the primer pairs reported in **Supplementary Table S2**. We focused on DWV injected bees co-exposed, or not, to thiamethoxam at 0.25 ng, because for coexposure to DWV and

1.00 ng of thiamethoxam, honey bee mortality was too high to allow for sufficient sampling (**Supplementary Table S1**). Relative gene expression data were analyzed using β-actin and RpL32 and the geometric mean of both as a reference (Reim et al., 2013). The qRT-PCR mix for one sample was prepared according to the recommendations of the Power SYBR Green RNA-to-Ct 1-Step Kit (Thermo Fisher Scientific): 10 μl of RT-PCR SYBR Green mix, 0.2 μl of 10 μM forward and reverse primer each, 0.16 μl of Retro-transcriptase enzyme from the kit, 8.44 μl of H_2O, and finally 1 μl of RNA sample. All primer pairs were designed using PrimerExpress 3.0 software (Life Technologies) following the standard procedure. Negative (H_2O) and positive controls (previously identified positive samples) were included in each qRT-PCR run. To ensure that the amplification efficiencies of the target and reference genes were approximately equal, the amplification of five 10-fold dilutions of the total RNA sample (from 1.0 to 0.1 ng per reaction) were analyzed in triplicate. The efficiency plot for Log input total RNA vs. ΔCt had a slope lower than ± 0.1. Amplifications for relative gene expression quantification were performed using the StepOne Real-Time PCR System (Applied Biosystems, Life Technologies) with the following thermal cycling profiles: one cycle at 48°C for 15 min for reverse transcription, one cycle at 95°C for 10 min, 40 cycles at 95°C for 15 s and 60°C for 1 min, and one cycle at 68°C for 7 min.

Statistics

For statistical analysis, bees exposed to DWV via oral ingestion (*per os*) or injection were analyzed separately. *Per os* treatments included Control, thiamethoxam at 0.25 ng, thiamethoxam at 1.00 ng, DWV *per os* and co-exposure to DWV *per os* and thiamethoxam at 1.00 ng. Injection treatments included PBS injection (control), co-exposure to PBS and thiamethoxam at 0.25 ng (control for injected bees exposed to thiamethoxam), DWV injection, co-exposure to DWV and 0.25 ng of thiamethoxam, and co-exposure to DWV and 1.00 ng of thiamethoxam.

Bee mortality was analyzed with a Kaplan–Meier estimation (Efron, 1988; Pepe and Fleming, 1989) and survival rates were calculated using the Cox proportional hazards model (Cox, 1972). The age at the first foraging flight (first flight longer than 10 min) was determined for each bee. The proportion of bees lost after their first exit from the hive was calculated using the χ^2 of compliance, and by comparing observed and expected proportions. A χ^2 table was used first to compare all treatments with 9 degrees of freedom, then separately for each pairwise combination of treatments with 1 degree of freedom. Variations in the age at which honey bees performed their first foraging trip were analyzed via a general linear mixed model fit by maximum likelihood (Laplace Approximation) using the Poisson probability distribution function. Treatment and month (April as basal level) were considered as fixed factors and the source colony as a random factor. The total time spent outside the hive was analyzed via pairwise Wilcoxon rank-sum tests; *p*-values were adjusted using the Holm–Bonferroni method. Flights less than 10 min were included to take into account all flights and not only foraging trips. Variations in the time spent outside were analyzed via a generalized least square model for 1–30 and 6–23 days old bees from the oral inoculation and injection treatments, respectively, to avoid a low sampling bias when mortality increased.

For genes, analyses were carried out on ΔCt values ($\log_2$ scale). Viral loads were analyzed from the $\log_{10}$ of the number of copies per bee. Analyses were carried out using either ANOVA followed by Tukey HSD when data followed a normal distribution (non-significant Shapiro–Wilk test) or a pairwise Wilcoxon test with Bonferroni correction when data did not follow a normal distribution (significant Shapiro–Wilk test). All statistical analyses were run with the software R (Version 1.0.143 – 2009–2016 RStudio).

RESULTS

Thiamethoxam Influence on DWV Load in Honey Bees

We assessed whether exposure to DWV, thiamethoxam alone or a combination of both modified the virus levels in experimentally infected bees using pairwise Wilcoxon tests (df = 10, n = 228 pools of three bees). While *per os* infection with DWV did not induce a higher level of DWV as compared to control bees (p = 1, **Supplementary Figure S1**), exposure by injection triggered a slight increase of DWV level in bees (p = 0.049, n = 82). Thiamethoxam exposure did not affect DWV levels; neither did its combination with DWV infection *per os*. A significant increase of DWV loads was observed after DWV injection in bees exposed to 0.25 ng of thiamethoxam (p = 0.003, n = 30) but was not higher than in DWV injected bees. No increase in DWV level was found in bees co-exposed to DWV injection and 1.00 ng of thiamethoxam, but sampling size was low (only seven samples could be retrieved, **Supplementary Table S1**).

For all other tested viruses (ABPV, BQCV, CBPV, SBV) no significant variation due to treatments was detected using Wilcoxon pairwise tests with Bonferroni correction, df = 10, n = 228 pools of three bees (**Supplementary Figure S2**).

Honey Bee Survival and Onset of Foraging Activity

Survival

Regardless of the dose, thiamethoxam did not affect bee survival when compared to control bees (control: n = 338, 0.25 ng: n = 305, p = 0.384 and 1.00 ng: n = 150, p = 0.836, **Figure 1A**), which was expected for these sublethal doses.

Surprisingly, *per os* infection with DWV significantly increased survival probability as compared to control bees (n = 156, df = 4, p = 0.018). As expected, bee survival strongly decreased after DWV injection (**Figure 1B**) in comparison to non-injected bees (**Figure 1A**). Moreover, the injection of DWV significantly increased mortality when compared to bees injected with PBS (PBS control: n = 310, injected DWV: n = 369, $p < 0.001$, **Figure 1B**).

Co-exposure to 1.00 ng thiamethoxam and DWV-*per os* (n = 150) did not influence bee survival as compared to

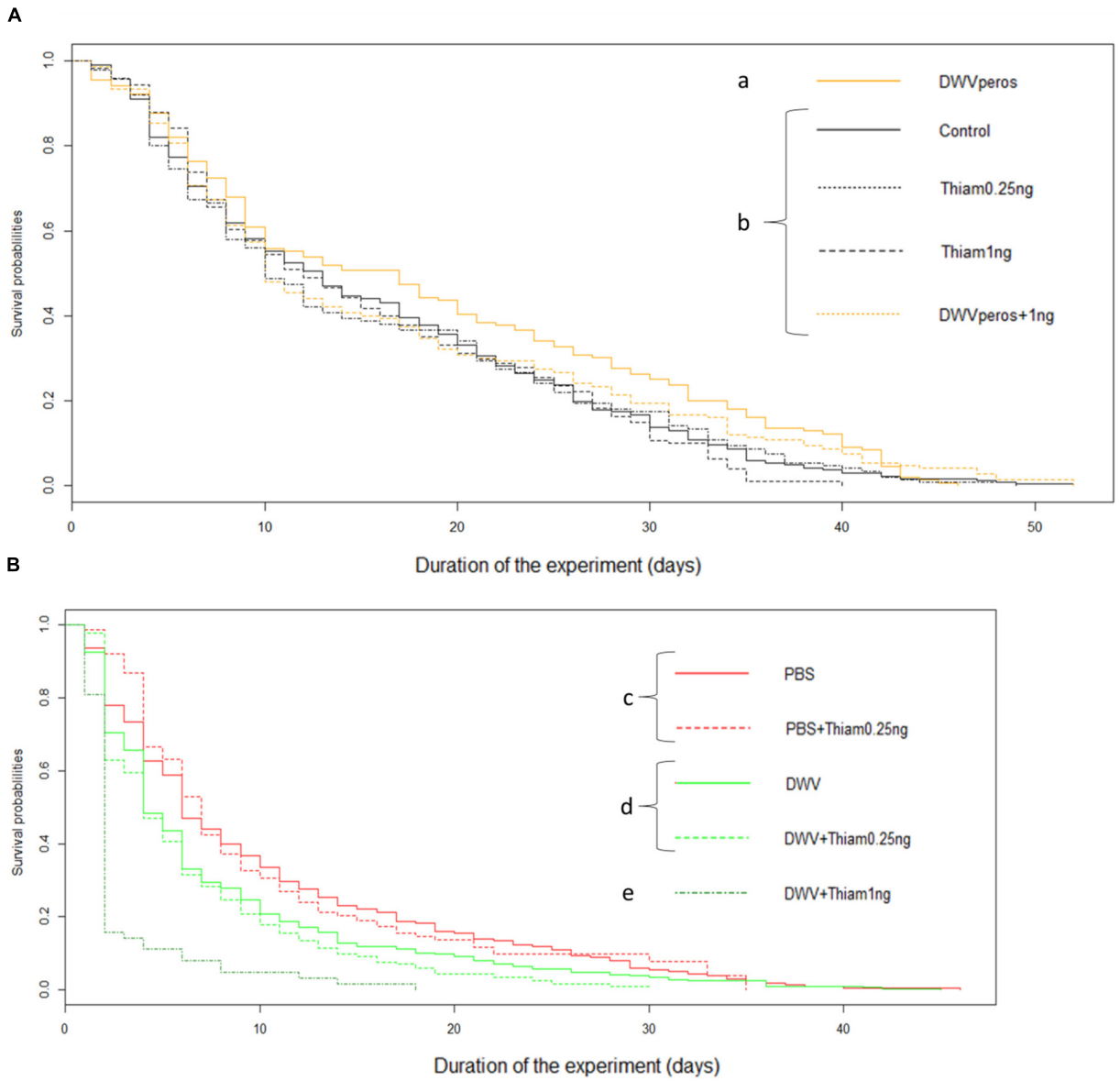

FIGURE 1 | Survival curves of bees exposed to thiamethoxam and/or DWV. While oral exposure to thiamethoxam and/or DWV did not decrease survival compared to the control group, injection of DWV did. A drastic decrease of survival was observed in bees co-exposed to DWV and thiamethoxam 1.00 ng. **(A)** Exposure to pesticide and virus *per os*: untreated bees (Control, n = 339 bees), Thiamethoxam at 0.25 ng/bee (Thiam 0.25 ng, n = 302), Thiamethoxam at 1.00 ng/bee (Thiam 1 ng, n = 150), DWV *per os* (n = 153), DWV *per os* co-exposed with Thiamethoxam at 1.00 ng (DWV *per os* + Thiam 1 ng, n = 150); **(B)** Exposure to pesticide *per os* and to DWV by injection: bees injected with PBS (PBS, used here as control, n = 311 bees), PBS co-exposed with Thiamethoxam at 0.25 ng (PBS + Thiam 0.25 ng, n = 209), DWV (n = 368), DWV co-exposed with thiamethoxam at 0.25 ng/bee (DWV + Thiam 0.25 ng, n = 253), DWV co-exposed with thiamethoxam at 1.00 ng/bee (DWV + Thiam 1 ng, n = 63). Different letters show statistical differences ($p < 0.05$) between groups (log-rank test).

control bees (n = 338) or 1.00 ng thiamethoxam-exposed bees (n = 150) (p = 0.212 and p = 0.276, respectively). The lowest dose of thiamethoxam (0.25 ng) did not affect the survival of DWV- or PBS-injected bees (n = 253, n = 212, respectively) when compared to bees only exposed to DWV (injected DWV: n = 369) or PBS (PBS control: n = 310), (df = 4, p = 0.122 and p = 0.876, respectively). However, exposure to the highest dose of thiamethoxam (1.00 ng) drastically decreased the survival of DWV-injected bees (n = 63, df = 4, $p < 0.001$ for all treatment comparisons). In fact, 4 days after the co-exposure, only 10% of bees from this group were alive compared to 66% for DWV-injected bees and 80% for bees exposed to 1.00 ng of thiamethoxam.

Lost Bees

The optical counter allowed us to record the number of bees that never returned to the colony after their first flight. The lowest proportion of lost bees was found among bees exposed

to 0.25 ng of thiamethoxam ($p < 0.001$ when compared to all others groups, $\chi^2 = 20.83$, df = 1). Exposure to thiamethoxam at 1.00 ng, DWV *per os*, DWV *per os*/1.00 ng of thiamethoxam, PBS injection, and PBS injection/0.25 ng of thiamethoxam induced significantly higher proportions of lost bees ($\chi^2 = 62.33$, df = 9, $p < 0.001$) as compared to control bees. Nevertheless, the highest proportions of lost bees were observed in the following groups: DWV injection, DWV injection/0.25 ng of thiamethoxam, and DWV injection/1.00 ng of thiamethoxam (**Figure 2**). Finally, co-exposure to DWV injection and 1.00 ng of thiamethoxam caused a significantly higher proportion of lost bees than DWV alone ($\chi^2 = 21.79$, df = 1, $p < 0.001$).

Onset of Foraging

The age at onset of foraging differed between replicates (**Supplementary Table S3**). Indeed, for all treatments, bees started foraging overall significantly earlier in May and July than in April (**Supplementary Table S3**).

Regarding the treatment effects, among the non-injected bees (*per os*) only bees exposed to 0.25 ng of thiamethoxam exhibited a later onset of foraging ($p = 0.015$), but this difference was only observed in July (**Supplementary Table S3**). Among the injected bees, DWV, with or without co-exposure to thiamethoxam (0.25 and 1 ng), caused an earlier onset of foraging (at least 1 day earlier) as compared to PBS-injected bees (respectively $p = 0.002$, $p = 0.004$, $p = 0.007$, **Figure 3** and **Supplementary Table S3**). The strongest impact was observed in bees co-exposed to DWV and 1.00 ng of thiamethoxam (**Figure 3** and **Supplementary Table S3**, $n = 21$ surviving bees after their first exit out of 120 treated and 63 detected at least once), with an earlier onset of foraging than bees exposed to DWV alone ($n = 195$) or in combination with 0.25 ng of thiamethoxam ($n = 119$), suggesting a synergistic effect.

Daily Flight Duration and Total Time Spent Outside

As bees became older their foraging activity increased (around 3.2 and 4.7 min. each day in control bees and PBS injected bees, respectively, **Supplementary Table S4**). Among oral exposure treatments (df = 12696), from day one to day 30 both doses of thiamethoxam and DWV reduced the daily flight duration as compared to control bees (**Figure 4A**). Injections (df = 3633), on the contrary, tended to increase the daily flight duration from day 6 to 23 (**Figure 4B**); this was observed for bees exposed to DWV, 0.25 ng of thiamethoxam, or a combination of both. Due to the early mortality of bees co-exposed to DWV by injection and thiamethoxam at 1.00 ng/bee, this treatment could not be included in this analysis (**Figure 1**).

Total time spent outside was calculated using all exit data, including those shorter than 10 min, from day one until last recorded day. Co-exposure to DWV (injection) and 1 ng of thiamethoxam reduced the time accumulated outside (**Figure 5**), which was significantly shorter than all other treatments (about 24 min compared to 397–738 min, $p < 0.001$, **Figure 5**). Interestingly no effect was observed between others treatments, even though DWV and/or thiamethoxam fed groups spent less daily time outside, because they survived for a longer period of time.

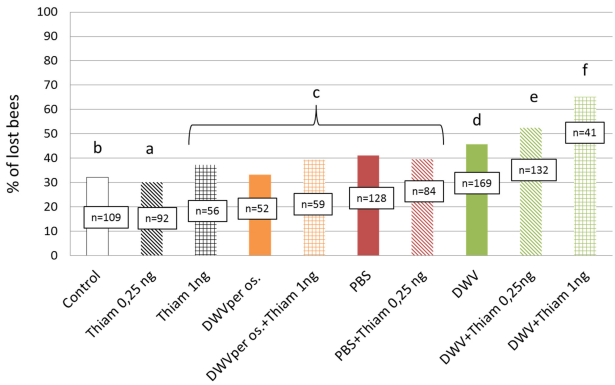

FIGURE 2 | Proportion of bees that were lost after their first exit when exposed to thiamethoxam and/or DWV. Number of lost bees are given for each treatment. DWV injection significantly increased the loss of bees at the first exit; bee losses being higher when co-exposed to thiamethoxam. Treatments are: untreated control bees, bees fed with 0.25 ng of thiamethoxam, bees fed with 1.00 ng of thiamethoxam, bees fed with DWV (*per os*), bees co-exposed to thiamethoxam at 1.00 ng and DWV *per os*, bees injected with PBS (PBS, used here as control), PBS co-exposed with 0.25 ng of thiamethoxam (PBS + Thiam 0.25 ng), DWV, DWV co-exposed with thiamethoxam at 0.25 ng/bee (DWV + Thiam 0.25 ng), DWV co-exposed with thiamethoxam at 1.00 ng/bee (DWV + Thiam 1 ng). Letters show significant differences between groups ($p < 0.05$) from lowest to highest proportion of lost bees (a << f).

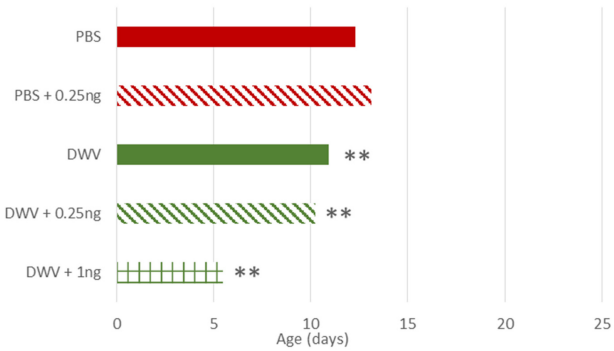

FIGURE 3 | Estimation of age of injected-honey bees at first foraging flight. DWV- injected bees performed their first foraging flight earlier than control bees, as well as bees co-exposed to thiamethoxam 0.25 ng or much thiamethoxam 1.00 ng. Treatments are: bees injected with PBS (PBS, used as control), injected with PBS co-exposed with thiamethoxam at 0.25 ng/bee (PBS + 0.25 ng), injected with DWV (DWV), injected with DWV co-exposed with thiamethoxam at 0.25 ng/bee (DWV + 0.25 ng), injected with DWV co-exposed with thiamethoxam at 1.00 ng/bee (DWV + 1 ng). For oral exposures, see **Supplementary Table S3**. ** indicates a significant difference ($p < 0.01$) based on the ANOVA performed from the general linear mixed model.

Expression Level of Immune and Detoxification Genes

Dorsal-1-a, apidaecin, pro-phenoloxydase, glutathione-S-transferase 3, catalase and *cyp6as11* genes did not show any significant variation in their expression level between experimental treatments ($p > 0.05$) (data not shown).

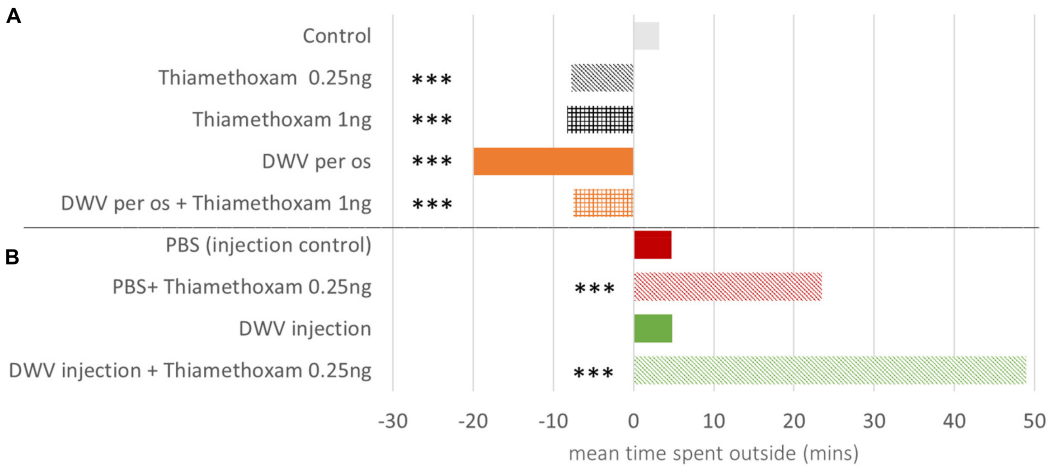

FIGURE 4 | Daily increase in honey bee flight duration as compared to control bees. Honey bees orally exposed to DWV and/or thiamethoxam exhibit a slower daily increase of flight duration compared to control bees (negative values) **(A)**. Bees injected and co-exposed to thiamethoxam 0.25 ng/bee exhibit a faster daily increase of flight duration compared to the injected control bees (PBS) (positive values) **(B)**. *** indicates significant difference ($p < 0.001$) based on ANOVA performed from the general linear mixed model. Variations in the daily time spent outside the hive are considered for 1–30 and 6–23 days old bees from the oral inoculation and injection treatments, respectively, to avoid a low sampling bias when mortality increased. DWV injection + Thiamethoxam 1.00 ng is missing because of the high mortality (>80% on the 6–23 days old bees period, **Figure 1**). Detailed data are in **Supplementary Table S4**.

No difference in vitellogenin expression levels was found between treatments 24 h post exposure ($p > 0.05$). At 48 h post exposure, vitellogenin expression in control bees was not significantly different between bees injected with PBS ($p = 0.940$), bees exposed to thiamethoxam at 0.25 ng ($p = 0.999$), or bees co-exposed to 0.25 ng of thiamethoxam and PBS injection ($p = 0.081$; **Figure 6**). However bees injected with DWV or co-exposed to DWV and 0.25 ng of thiamethoxam exhibited significantly lower vitellogenin expression levels than control bees ($p < 0.001$ for both), bees injected with PBS ($p = 0.011$ and $p < 0.001$, respectively), or bees exposed to 0.25 ng of thiamethoxam ($p = 0.015$ and $p < 0.001$, respectively). Vitellogenin expression was not significantly different between bees injected with DWV and bees co-exposed to DWV injection and 0.25 ng of thiamethoxam ($p = 0.603$).

DISCUSSION

By co-exposing honey bees to DWV and thiamethoxam at environmentally relevant doses in their natural environment (colony), we showed that the combination of both stressors caused premature foraging, a higher rate of failure to return to the colony and a steep decrease in survival.

We demonstrated that honey bees co-exposed to DWV and 1.00 ng of thiamethoxam exhibited the lowest survival rate. Interestingly, exposure to thiamethoxam (0.25 ng or 1.00 ng) as a single stressor did not affect bee survival at all, but mortality was increased in bees injected with DWV alone or co-exposed to DWV and 0.25 ng of thiamethoxam. These results correspond with previous studies showing that DWV has a deleterious effect on honey bee lifespan (Woyciechowski and Moroń, 2009; Dainat et al., 2012; Martin et al., 2013; Benaets et al., 2017; Rueppell et al., 2017). Notably, by using a Radio-Frequency Identification device, Benaets et al. (2017) found that experimentally DWV infected bees had a greater early-life mortality (up to 81%) as compared to control bees (up to 67%), and Martin et al. (2013) observed a high decrease in longevity of adults that were parasitized by varroa during the larvae/pupae stages. In our study, no high increase of DWV loads was observed in virus-injected bees, which is congruent with the absence of variation of several immune genes (dorsal-1-a, apidaecin, pro-phenoloxydase) and with the native background of DWV infection. The injection of DWV did increase DWV loads in the bees and viral loads tend to be higher when they were co-exposed with 1.00 ng of thiamethoxam. However, the mortality due to co-exposure to DWV and the neonicotinoid was so high that sampling size decreased dramatically compared to the other treatments, resulting in a low number of replicates. Most of the infected bees may have been excluded by nest mates as part of social immunity (Baracchi et al., 2012; McDonnell et al., 2013), or may have altruistically removed themselves (Rueppell et al., 2010) or simply died and could not be sampled. Indeed, during the experiments, some co-exposed bees were removed by workers from the colony while still alive. In a previous *in vitro* study, bees co-exposed to CBPV and thiamethoxam (5.00 ng/bee) showed higher CBPV loads in dead bees, as opposed to live bees (Coulon et al., 2018), which suggests that higher DWV loads may be present in dead bees, but could not be measured, as bees did not return or were excluded from the hive.

We did not find any significant effect of *per os* DWV inoculation on viral loads, even when we performed exposure with higher numbers of DWV copies (inoculum with 10^8 copies of DWV per bee). Ryabov et al. (2014) showed that larvae reared in DWV symptomatic hives (thus exposed through

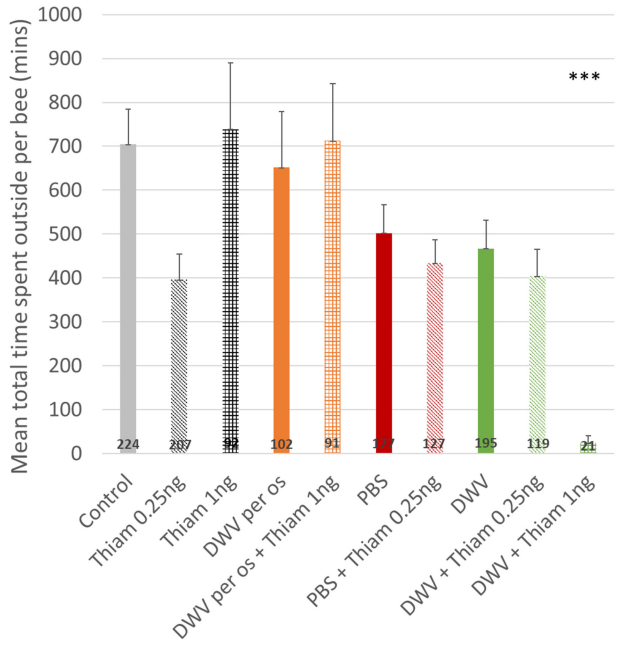

FIGURE 5 | Total time spent outside for honey bees. The total time spent outside for honey bees co-exposed to DWV (injection) and thiamethoxam 1.00 ng was drastically lower (***: $p < 0.001$, Wilcoxon rank sum test). The number of bees per treatment is at the bottom of the bars. Treatments are oral exposure to thiamethoxam at 0.25 ng/bee (Thiam 0.25 ng), thiamethoxam at 1.00 ng/bee (Thiam 1 ng); bees injected with PBS (PBS, used as control), injected with PBS co-exposed with 0.25 ng of thiamethoxam (PBS + Thiam 0.25 ng), injected with DWV (DWV), injected with DWV co-exposed with thiamethoxam at 0.25 ng/bee (DWV + Thiam 0.25 ng), injected with DWV co-exposed with thiamethoxam at 1.00 ng/bee (DWV + Thiam 1 ng).

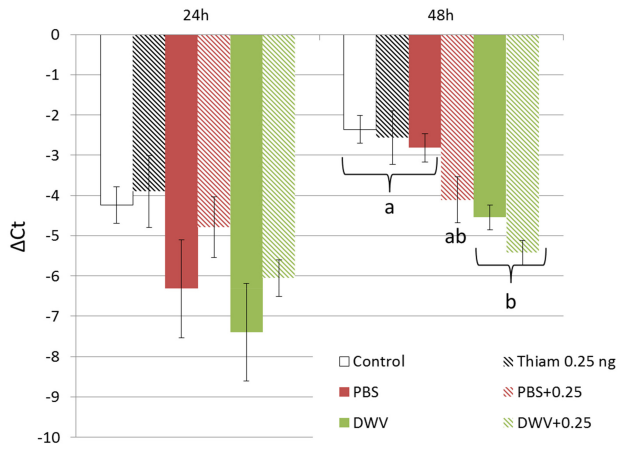

FIGURE 6 | Vitellogenin expression level in bees exposed to DWV and/or thiamethoxam. Mean vitellogenin expression significantly decreased 48 h after exposure to DWV alone (green bars) or in combination with 0.25 ng of thiamethoxam (hatched green bars) compared to control bees, bees exposed to 0.25 ng of thiamethoxam, and PBS-injected bees (injection control). Analyses were performed on bees sampled 24 or 48 h post exposure. Letters indicate significant differences ($p < 0.05$).

alimentation), but not infested by *Varroa,* showed low DWV loads close to control (larvae raised in colonies with low DWV levels and no *Varroa*), while *Varroa* parasitized pupae developed very high loads of DWV (direct *Varroa* transmission). Feeding does not seem to be an efficient way of experimental transmission of DWV in honey bees (Bailey and Ball, 1991). However, we measured viral loads 48 h after virus feeding and we cannot exclude that DWV loads may have increased later. The infection may have been delayed due to the degradation of viral particles in the gut and may be first restricted to the midgut epithelium before breaching this barrier (Möckel et al., 2011). The absence of a significant effect on the number of lost bees, onset of foraging and flight behavior is, however, congruent with an inefficient transmission of DWV *per os*. Surprisingly, survival was slightly higher when feeding the bees with DWV extracts. These extracts originated from pupae ground in buffer and sequentially centrifuged, and may contain associated beneficial microbiota, which could enhance bee survival (Raymann et al., 2017). Moreover, the ingested DWV could have triggered non-specific defense mechanisms preventing its multiplication (Evans and Spivak, 2010). The lower daily flight duration we observed in DWV orally exposed bees may also explain why they outlived control bees. Behavioral maturation may have been delayed, thus increasing bee survival (Perry et al., 2015).

The survival decline in bees co-exposed to DWV and 1.00 ng of thiamethoxam was related to a very high proportion of bees that never returned to the colony after their first exit (65%). One simple explanation is that co-exposed bees got lost on their return trips, which has been observed for foragers after a similar dose of thiamethoxam (Henry et al., 2012). However, contrary to Henry et al. (2012), we did not find a significant loss in bees only exposed to thiamethoxam. The main difference is that honey bees in Henry et al. (2012) were released 1 km away from their colonies, while in our study, bees were not exposed to this return flight challenge. Moreover, our trial required us to anesthetize and/or starve bees, which were also kept for some hours in the lab before re-introducing them into the colonies. This experimental procedure may have stressed bees and increased overall mortality.

The lowest survival rate and higher rate of lost bees in the DWV injected and 1.00 ng thiamethoxam co-exposed group could be explained by their early onset of foraging. Indeed, such young honey bees may not be optimally adapted to foraging tasks and are usually less resilient than normal-aged foragers (Woyciechowski and Moroń, 2009). Young workers are heavier and exhibit lower flight performance (Vance et al., 2009), likely due to different flight metabolic rates and muscle biochemistry (Schippers et al., 2006). Precocious foraging has been previously observed from DWV injections by Benaets et al. (2017) in the same range (2.3 days earlier vs. 2.4 days earlier in our study), but also with other stressors, such as *Varroa destructor* (Downey et al., 2000) and *Nosema apis* (Wang and Moffler, 1970). Considering that there is no effect of thiamethoxam alone, and the fact that honey bees that were co-exposed to DWV and thiamethoxam started foraging

earlier (2–5 days earlier depending on thiamethoxam dose) our results suggest that the effect of co-exposure between DWV injection and thiamethoxam on this specific trait could be synergistic.

Virus and pesticide treatments could affect physiological traits of bees. To further explore the influence of both DWV and thiamethoxam on bees, we analyzed potential physiological changes, by focusing on immune and detoxification genes. Except for vitellogenin, none of the tested genes were affected by the treatments, suggesting a lack of effect on the immune and detoxification system in our experiments (at least 24 and 48 h post treatments). This contradicts previous *in vitro* studies, which, for example, showed that immune genes under control of *dorsal-1a (Apidaecin)* were down-regulated by sublethal doses of clothianidin (Di Prisco et al., 2013); or that dorsal-1a was down-regulated in bees with high levels of DWV in the presence of Varroa (Nazzi et al., 2012) or exposed to CBPV and/or thiamethoxam (Coulon et al., 2019). Up-regulation of some immune genes in bees with high levels of DWV in natural conditions has already been observed (Steinmann et al., 2015) and illustrates that gene expression, and especially immune response, varies greatly (Doublet et al., 2017) and depends on the experimental conditions and time of sampling from exposure, and may be tissue-specific (here, whole bee bodies were analyzed). Moreover, we cannot exclude that these genes may have been down- or up-regulated earlier or later after co-exposure.

However we noticed a significant decrease of vitellogenin expression level. Vitellogenin is involved in the regulation of division of labor, notably a key player in the regulation of behavioral maturation, with a higher expression in nurses than in foragers (Nelson et al., 2007; Marco Antonio et al., 2008). The maintenance of stable conditions within colonies relies on a division of labor, with bees spending the first 2–3 weeks of their adult life working in the hive (feeding and taking care of the brood, building comb), and then the rest of their life outside of the hive (foraging for nectar and pollen to supply the colony growth) (Seeley, 1995). However, a significant loss of foragers for the colony will accelerate the behavioral maturation of young bees to replace them (Robinson, 1992). Similarly, parasitism also leads to precocious foragers (Dussaubat et al., 2013; Goblirsch et al., 2013; Natsopoulou et al., 2015), which may not be optimally adapted to foraging tasks (Schippers et al., 2006; Vance et al., 2009). The down-regulation of vitellogenin we observed here upon DWV injection is consistent with previous studies performed on other stress factors such as simulated heat waves (Bordier et al., 2017a). Nelson et al. (2007) and Marco Antonio et al. (2008) showed that an RNAi-mediated inhibition of the transcription of vitellogenin made bees start foraging significantly earlier. We therefore propose that injection of DWV, reinforced by co-exposure to thiamethoxam, induced a precocious shift toward foraging activity through down-regulation of the transcription of vitellogenin. Here co-exposed bees may become precocious, but immature, foragers that could induce a high cost on the hive for collecting nectar and pollen resources. Depending on the number of affected bees, this could result in a breakdown of division of labor, as indicated by Perry et al. (2015).

CONCLUSION

Our results underscore the importance of translating laboratory experiments to the field. By performing behavioral experiments, we could identify highly negative effects of pesticide/virus co-exposure on honey bee survival and identify some underlying mechanisms (early onset of foraging, lost bees and flight duration). The relationship between survival and flight behavior could not be assessed from previous cage experiments (Di Prisco et al., 2013; Coulon et al., 2018, 2019). Our results provide new insights on the negative synergism of viruses (DWV) and pesticides (neonicotinoids) on bees, even at sublethal environmental pesticide doses. Such a great impact on honey bee survival and flight behavior was quite unexpected from a single acute oral exposure to a sublethal dose of thiamethoxam. In the field, honey bees may be exposed to higher thiamethoxam doses (from 13.3 ng/g in nectar to 20.2 ng/g in honey, 53.3 ng/g in stored pollen or 86 ng/g in pollen from field margin plants; Mullin et al., 2010; Bargañska et al., 2013; Botías et al., 2015) and may not be exposed only once but probably several times while foraging and/or feeding on honey and stored pollen. As co-exposure to both viruses and pesticides likely occurs in natural conditions, field relevant experiments are essential to better understand the influence of these stress factors in bees and the underlying mechanisms potentially leading to colony failure.

DATA AVAILABILITY STATEMENT

All datasets generated for this study are included in the article/**Supplementary Material**.

AUTHOR CONTRIBUTIONS

AD, MC, YL, and GD conceptualized and designed the experiments. ED, AP, MR-C, RT, CA, and AP provided conceptualization advice. MC and AD performed the experiments with assistance from FA. AD, GD, and YL provided lab facilities and resources for experiments. AD and YL supervised the research. MC, AP, and AD did the statistical analysis. MC and AD drafted the manuscript. All authors participated in the revisions of the manuscript, read and approved the final manuscript.

FUNDING

This study was supported by INRAE (Institut national de recherche pour l'agriculture, l'alimentation et l'environnement) for the 2016 experiments, by the "Fondation Lune de Miel" for the 2017 experiments, and by a Ph.D. grant from ANSES and INRA. GD is currently supported by European Horizon 2020 Research and Innovation Programme under grant agreement no. 773921.

ACKNOWLEDGMENTS

The authors thank Didier Crauser, Jacques Sénéchal, Marion Larribe, Julien Proust, and François Steffen (INRAE) for their technical support in beekeeping activities or lab work, and all colleagues who contributed to bee tagging. Thanks to Prof. Pennacchio Francesco for the permission to use the molecular biology laboratory at University of Naples Federico II. The authors also thank Jean-Luc Brunet (INRAE) and Cyril Vidau (ITSAP) for their expertise and advice in setting up the experiment, and Cynthia Mc Donnell for English editing.

SUPPLEMENTARY MATERIAL

The Supplementary Material for this article can be found online at: https://www.frontiersin.org/articles/10.3389/fmicb.2020.00766/full#supplementary-material

REFERENCES

Alaux, C., Crauser, D., Pioz, M., Saulnier, C., and Le Conte, Y. (2014). Parasitic and immune modulation of flight activity in honey bees tracked with optical counters. *J. Exp. Biol.* 217, 3416–3424. doi: 10.1242/jeb.105783

Alburaki, M., Boutin, S., Mercier, P. L., Loublier, Y., Chagnon, M., and Derome, N. (2015). Neonicotinoid-coated zea mays seeds indirectly affect honeybee performance and pathogen susceptibility in field trials. *PLoS One* 10:e125790. doi: 10.1371/journal.pone.0125790

Alburaki, M., Chen, D., Skinner, J. A., Meikle, W. G., Tarpy, D. R., Adamczyk, J., et al. (2018). Honey bee survival and pathogen prevalence: from the perspective of landscape and exposure to pesticides. *Insects* 9:65. doi: 10.3390/insects9020065

Amdam, G. V., Simões, Z. L., Hagen, A., Norberg, K., Schrøder, K., Mikkelsen, Ø., et al. (2004). Hormonal control of the yolk precursor vitellogenin regulates immune function and longevity in honeybees. *Exp. Gerontol.* 39, 767–773. doi: 10.1016/j.exger.2004.02.010

Bailey, L., and Ball, B. V. (1991). "3 - VIRUSES," in *Honey Bee Pathology (Second Edition)*, eds L. Bailey and B. V. Ball (London: Academic Press), 10–34.

Baracchi, D., Fadda, A., and Turillazzi, S. (2012). Evidence for antiseptic behavior towards sick adult bees in honey bee colonies. *J. Insect Physiol.* 58, 1589–1596. doi: 10.1016/j.jinsphys.2012.09.014

Bargańska, Z., Slebioda, M., and Namieśnik, J. (2013). Pesticide residues levels in honey from apiaries located of Northern Poland. *Food Control* 31, 196–201. doi: 10.1016/j.foodcont.2012.09.049

Benaets, K., Geystelen, A. V., Cardoen, D., Smet, L. D., Graaf, D. C. D., Schoofs, L., et al. (2017). Covert deformed wing virus infections have long-term deleterious effects on honeybee foraging and survival. *Proc. R. Soc. B* 284:20162149. doi: 10.1098/rspb.2016.2149

Bordier, C., Dechatre, H., Suchail, S., Peruzzi, M., Soubeyrand, S., Pioz, M., et al. (2017a). Colony adaptive response to simulated heat waves and consequences at the individual level in honeybees (*Apis mellifera*). *Sci. Rep.* 7:3760. doi: 10.1038/s41598-017-03944-x

Bordier, C., Suchail, S., Pioz, M., Devaud, J. M., Collet, C., Charreton, M., et al. (2017b). Stress response in honeybees is associated with changes in task-related physiology and energetic metabolism. *J. Insect Physiol.* 98, 47–54. doi: 10.1016/j.jinsphys.2016.11.013

Botías, C., David, A., Horwood, J., Abdul-Sada, A., Nicholls, E., Hill, E., et al. (2015). Neonicotinoid residues in wildflowers, a potential route of chronic exposure for bees. *Environ. Sci. Technol.* 49, 12731–12740. doi: 10.1021/acs.est.5b03459

Brandt, A., Gorenflo, A., Siede, R., Meixner, M., and Büchler, R. (2016). The neonicotinoids thiacloprid, imidacloprid, and clothianidin affect the immunocompetence of honey bees (*Apis mellifera* L.). *J. Insect Physiol.* 86, 40–47. doi: 10.1016/j.jinsphys.2016.01.001

Cornman, R. S., Tarpy, D. R., Chen, Y. P., Jeffreys, L., Lopez, D., Pettis, J. S., et al. (2012). Pathogen webs in collapsing honey bee colonies. *PLoS One* 7:e43562. doi: 10.1371/journal.pone.0043562

Coulon, M., Schurr, F., Martel, A. C., Cougoule, N., Begaud, A., Mangoni, P., et al. (2018). Metabolisation of thiamethoxam (a neonicotinoid pesticide) and interaction with the Chronic bee paralysis virus in honeybees. *Pest. Biochem. Physiol.* 144, 10–18. doi: 10.1016/j.pestbp.2017.10.009

Coulon, M., Schurr, F., Martel, A.-C., Cougoule, N., Bégaud, A., Mangoni, P., et al. (2019). Influence of chronic exposure to thiamethoxam and chronic bee paralysis virus on winter honey bees. *PLoS One* 14:e0220703. doi: 10.1371/journal.pone.0220703

Cox, D. R. (1972). Regression models and life-tables. *J. Royal Stat. Soc.* 34, 187–202. doi: 10.1007/978-1-4612-4380-9_37

Dainat, B., Evans, J. D., Chen, Y. P., Gauthier, L., and Neumann, P. (2012). Dead or alive: deformed wing virus and Varroa destructor reduce the life span of winter honeybees. *Appl. Environ. Microbiol.* 78, 981–987. doi: 10.1128/aem.06537-11

Dalmon, A., Desbiez, C., Coulon, M., Thomasson, M., Conte, Y. L., Alaux, C., et al. (2017). Evidence for positive selection and recombination hotspots in Deformed wing virus (DWV). *Sci. Rep.* 7:41045. doi: 10.1038/srep41045

Dalmon, A., Peruzzi, M., Le Conte, Y., Alaux, C., and Pioz, M. (2019). Temperature-driven changes in viral loads in the honey bee *Apis mellifera*. *J. Invert. Pathol.* 160, 87–94. doi: 10.1016/j.jip.2018.12.005

de Miranda, J. R., and Genersch, E. (2010). Deformed wing virus. *J. Invert. Pathol.* 103, S48–S61. doi: 10.1016/j.jip.2009.06.012

DeGrandi-Hoffman, G., Chen, Y. P., and Simonds, R. (2013). The effects of pesticides on queen rearing and virus titers in honey bees (*Apis mellifera* L.). *Insects* 4, 71–89. doi: 10.3390/insects4010071

Di Prisco, G., Cavaliere, V., Annoscia, D., Varricchio, P., Caprio, E., Nazzi, F., et al. (2013). Neonicotinoid clothianidin adversely affects insect immunity and promotes replication of a viral pathogen in honey bees. *Proc. Natl. Acad. Sci.* 110, 18466–18471. doi: 10.1073/pnas.1314923110

Doublet, V., Natsopoulou, M. E., Zschiesche, L., and Paxton, R. J. (2015). Within-host competition among the honey bees pathogens Nosema ceranae and Deformed wing virus is asymmetric and to the disadvantage of the virus. *J. Invert. Pathol.* 124, 31–34. doi: 10.1016/j.jip.2014.10.007

Doublet, V., Poeschl, Y., Gogol-Doring, A., Alaux, C., Annoscia, D., Aurori, C., et al. (2017). Unity in defence: honeybee workers exhibit conserved molecular responses to diverse pathogens. *BMC Genomics* 18:207. doi: 10.1186/s12864-017-3597-6

Downey, D. L., Higo, T. T., and Winston, M. L. (2000). Single and dual parasitic mite infestations on the honey bee, *Apis mellifera* L. *Insect. Soc.* 47, 171–176. doi: 10.1007/PL00001697

Dussaubat, C., Maisonnasse, A., Crauser, D., Beslay, D., Costagliola, G., Soubeyrand, S., et al. (2013). Flight behavior and pheromone changes associated to *Nosema ceranae* infection of honey bee workers (*Apis mellifera*) in field conditions. *J. Invert. Pathol.* 113, 42–51. doi: 10.1016/j.jip.2013.01.002

Efron, B. (1988). Logistic regression, survival analysis, and the kaplan-meier curve. *J. Am. Stat. Assoc.* 83, 414–425. doi: 10.2307/2288857

Evans, J. D., and Spivak, M. (2010). Socialized medicine: individual and communal disease barriers in honey bees. *J. Invert. Pathol.* 103, S62–S72.

Evans, J. D., Aronstein, K., Chen, Y. P., Hetru, C., Imler, J.-L., Jiang, H., et al. (2006). Immune pathways and defence mechanisms in honey bees *Apis mellifera*. *Insect Mol. Biol.* 15, 645–656. doi: 10.1111/j.1365-2583.2006.00682.x

Goblirsch, M., Huang, Z. Y., and Spivak, M. (2013). Physiological and behavioral changes in honey bees (*Apis mellifera*) induced by *Nosema ceranae* infection. *PLoS One* 8:e58165. doi: 10.1371/journal.pone.0058165

Goulson, D., Nicholls, E., Botias, C., and Rotheray, E. L. (2015). Bee declines driven by combined stress from parasites, pesticides, and lack of flowers. *Science* 347:1255957. doi: 10.1126/science.1255957

Henry, M., Beguin, M., Requier, F., Rollin, O., Odoux, J. F., Aupinel, P., et al. (2012). A common pesticide decreases foraging success and survival in honey bees. *Science* 336, 348–350. doi: 10.1126/science.1215039

Hladik, M. L., Vandever, M., and Smalling, K. L. (2016). Exposure of native bees foraging in an agricultural landscape to current-use pesticides. *Scie. Total Environ.* 542, 469–477. doi: 10.1016/j.scitotenv.2015.10.077

Iqbal, J., and Mueller, U. (2007). Virus infection causes specific learning deficits in honeybee foragers. *Proc. Biol. Sci.* 274, 1517–1521. doi: 10.1098/rspb.2007.0022

Jones, A., and Turnbull, G. (2016). Neonicotinoid concentrations in UK honey from 2013. *Pest Manag. Sci.* 72, 1897–1900. doi: 10.1002/ps.4227

Lawrence, T. J., Culbert, E. M., Felsot, A. S., Hebert, V. R., and Sheppard, W. S. (2016). Survey and risk assessment of *Apis mellifera* (Hymenoptera: Apidae) exposure to neonicotinoid pesticides in Urban, Rural, and agricultural settings. *J. Econ. Entomol.* 109:529.

Lee, K. V., Steinhauer, N., Rennich, K., Wilson, M. E., Tarpy, D. R., Caron, D. M., et al. (2015). A national survey of managed honey bee 2013-2014 annual colony losses in the USA. *Apidologie* 46, 292–305. doi: 10.1007/s13592-015-0356-z

Long, E. Y., and Krupke, C. H. (2016). Non-cultivated plants present a season-long route of pesticide exposure for honey bees. *Nat. Commun.* 7:11629. doi: 10.1038/ncomms11629

Marco Antonio, D. S., Guidugli-Lazzarini, K. R., do Nascimento, A. M., Simões, Z. L. P., and Hartfelder, K. (2008). RNAi-mediated silencing of vitellogenin gene function turns honeybee (*Apis mellifera*) workers into extremely precocious foragers. *Naturwissenschaften* 95, 953–961. doi: 10.1007/s00114-008-0413-9

Martin, S. J., Ball, B. V., and Carreck, N. L. (2013). The role of deformed wing virus in the initial collapse of varroa infested honey bee colonies in the UK. *J. Apicult. Res.* 52, 251–258. doi: 10.3896/IBRA.1.52.5.12

Martin, S. J., and Brettell, L. E. (2019). Deformed wing virus in honeybees and other insects. *Ann. Rev. Virol.* 6, 49–69. doi: 10.1146/annurev-virology-092818-015700

McDonnell, C., Alaux, C., Parrinello, H., Desvignes, J.-P., Crauser, D., Durbesson, E., et al. (2013). Ecto- and endoparasite induce similar chemical and brain neurogenomic responses in the honey bee (*Apis mellifera*). *BMC Ecol.* 13:25. doi: 10.1186/1472-6785-13-25

Mitchell, E. A. D., Mulhauser, B., Mulot, M., Mutabazi, A., Glauser, G., and Aebi, A. (2017). A worldwide survey of neonicotinoids in honey. *Science* 358, 109–111. doi: 10.1126/science.aan3684

Möckel, N., Gisder, S., and Genersch, E. (2011). Horizontal transmission of deformed wing virus: pathological consequences in adult bees (*Apis mellifera*) depend on the transmission route. *J. Gen. Virol.* 92, 370–377. doi: 10.1099/vir.0.025940-0

Mullin, C. A., Frazier, M., Frazier, J. L., Ashcraft, S., Simonds, R., vanEngelsdorp, D., et al. (2010). High levels of miticides and agrochemicals in North American apiaries: implications for honey bee health. *PLoS One* 5:e9754. doi: 10.1371/journal.pone.0009754

Natsopoulou, M. E., McMahon, D. P., and Paxton, R. J. (2015). Parasites modulate within-colony activity and accelerate the temporal polyethism schedule of a social insect, the honey bee. *Behav. Ecol. Sociobiol.* 70, 1019–1031. doi: 10.1007/s00265-015-2019-5

Nauen, R., Ebbinghaus-Kintscher, U., Salgado, V. L., and Kaussmann, M. (2003). Thiamethoxam is a neonicotinoid precursor converted to clothianidin in insects and plants. *Pest. Biochem. Physiol.* 76, 55–69. doi: 10.1016/S0048-3575(03)00065-8

Nazzi, F., Brown, S. P., Annoscia, D., Del Piccolo, F., Di Prisco, G., Varricchio, P., et al. (2012). Synergistic parasite-pathogen interactions mediated by host immunity can drive the collapse of honeybee colonies. *PLoS Pathog.* 8:e1002735. doi: 10.1371/journal.ppat.1002735

Nelson, C. M., Ihle, K. E., Fondrk, M. K., Page, R. E., and Amdam, G. V. (2007). The gene vitellogenin has multiple coordinating effects on social organization. *PLoS Biol.* 5:e62. doi: 10.1371/journal.pbio.0050062

Osterman, J., Wintermantel, D., Locke, B., Jonsson, O., Semberg, E., Onorati, P., et al. (2019). Clothianidin seed-treatment has no detectable negative impact on honeybee colonies and their pathogens. *Nat. Commun.* 10:692. doi: 10.1038/s41467-019-08523-4

Pepe, M. S., and Fleming, T. R. (1989). Weighted kaplan-meier statistics: a class of distance tests for censored survival data. *Biometrics* 45, 497–507. doi: 10.2307/2531492

Perry, C. J., Sovik, E., Myerscough, M. R., and Barron, A. B. (2015). Rapid behavioral maturation accelerates failure of stressed honey bee colonies. *Proc. Natl. Acad. Sci. U.S.A.* 112, 3427–3432.

Poquet, Y., Vidau, C., and Alaux, C. (2016). Modulation of pesticide response in honeybees. *Apidologie* 47, 412–426. doi: 10.1007/s13592-016-0429-7

Prado, A., Pioz, M., Vidau, C., Requier, F., Jury, M., Crauser, D., et al. (2019). Exposure to pollen-bound pesticide mixtures induces longer-lived but less efficient honey bees. *Sci. Total Environ.*650, 1250–1260. doi: 10.1016/j.scitotenv.2018.09.102

Raymann, K., Shaffer, Z., and Moran, N. A. (2017). Antibiotic exposure perturbs the gut microbiota and elevates mortality in honeybees. *PLoS Biol.* 15:e2001861. doi: 10.1371/journal.pbio.2001861

Reim, T., Thamm, M., Rolke, D., Blenau, W., and Scheiner, R. (2013). Suitability of three common reference genes for quantitative real-time PCR in honey bees. *Apidologie* 44, 342–350. doi: 10.1007/s13592-012-0184-3

Remnant, E. J., Shi, M., Buchmann, G., Blacquiere, T., Holmes, E. C., Beekman, M., et al. (2017). A diverse range of novel RNA viruses in geographically distinct honey bee populations. *J. Virol.* 91:JVI.00158-17. doi: 10.1128/JVI.00158-17

Robinson, G. E. (1992). Regulation of division of labor in insect societies. *Ann. Rev. Entomol.* 37, 637–665.

Rueppell, O., Hayworth, M. K., and Ross, N. P. (2010). Altruistic self-removal of health-compromised honey bee workers from their hive. *J. Evol. Biol.* 23, 1538–1546. doi: 10.1111/j.1420-9101.2010.02022.x

Rueppell, O., Yousefi, B., Collazo, J., and Smith, D. (2017). Early life stress affects mortality rate more than social behavior, gene expression or oxidative damage in honey bee workers. *Exp. Gerontol.* 90, 19–25. doi: 10.1016/j.exger.2017.01.015

Ryabov, E. V., Wood, G. R., Fannon, J. M., Moore, J. D., Bull, J. C., Chandler, D., et al. (2014). A Virulent Strain of Deformed Wing Virus (DWV) of Honeybees (*Apis mellifera*) Prevails after Varroa destructor-Mediated, or In Vitro. Transmission. *PLoS Pathog.* 10:e1004230. doi: 10.1371/journal.ppat.1004230

Sanchez-Bayo, F. (2014). The trouble with neonicotinoids. *Science* 346, 806–807. doi: 10.1126/science.1259159

Schippers, M. P., Dukas, R., Smith, R. W., Wang, J., Smolen, K., and McClelland, G. B. (2006). Lifetime performance in foraging honeybees: behaviour and physiology. *J. Exp. Biol.* 209, 3828–3836. doi: 10.1242/jeb.02450

Schmid-Hempel, P. (1998). *Parasites in Social Insects*. Princeton, NJ: Princeton University Press.

Schneider, C. W., Tautz, J., Grünewald, B., and Fuchs, S. (2012). RFID tracking of sublethal effects of two neonicotinoid insecticides on the foraging behavior of *Apis mellifera*. *PLoS One* 7:e30023. doi: 10.1371/journal.pone.0030023

Seehuus, S. C., Norberg, K., Gimsa, U., Krekling, T., and Amdam, G. V. (2006). Reproductive protein protects functionally sterile honey bee workers from oxidative stress. *Proc. Natl. Acad. Sci. U.S.A.* 103, 962–967.

Seeley, T. D. (1995). *The Wisdom of the Hive. The Social Physiology of Honey Bee Colonies*. Cambridge, MA: Harvard University Press.

Siede, R., Meixner, M. D., and Büchler, R. (2012). Comparison of transcriptional changes of immune genes to experimental challenge in the honey bee (*Apis mellifera*). *J. Apicult. Res.* 51, 320–328. doi: 10.3896/IBRA.1.51.4.05

Simon-Delso, N., Amaral-Rogers, V., Belzunces, L. P., Bonmatin, J. M., Chagnon, M., Downs, C., et al. (2015). Systemic insecticides (neonicotinoids and fipronil): trends, uses, mode of action and metabolites. *Environ. Sci. Pollut. Res.* 22, 5–34. doi: 10.1007/s11356-014-3470-y

Simon-Delso, N., San Martin, G., Bruneau, E., Minsart, L.-A., Mouret, C., and Hautier, L. (2014). Honeybee colony disorder in crop areas: the role of pesticides and viruses. *PLoS One* 9:e103073. doi: 10.1371/journal.pone.0103073

Steinmann, N., Corona, M., Neumann, P., and Dainat, B. (2015). Overwintering is associated with reduced expression of immune genes and higher susceptibility to virus infection in honey bees. *PLoS One* 10:e0129956. doi: 10.1371/journal.pone.0129956

Tentcheva, D., Gauthier, L., Zappulla, N., Dainat, B., Cousserans, F., Colin, M. E., et al. (2004). Prevalence and seasonal variations of six bee viruses in *Apis mellifera* L. and Varroa destructor mite populations in France. *Appl. Environ. Microbiol.* 70, 7185–7191. doi: 10.1128/Aem.70.12.7185-7191.2004

Tison, L., Hahn, M. L., Holtz, S., Rossner, A., Greggers, U., Bischoff, G., et al. (2016). Honey bees' behavior is impaired by chronic exposure to the neonicotinoid thiacloprid in the field. *Environ. Sci. Technol.* 50, 7218–7227. doi: 10.1021/acs.est.6b02658

Tison, L., Holtz, S., Adeoye, A., Kalkan, O., Irmisch, N. S., Lehmann, N., et al. (2017). Effects of sublethal doses of thiacloprid and its formulation Calypso (R) on the learning and memory performance of honey bees. *J. Exp. Biol.* 220, 3695–3705. doi: 10.1242/jeb.154518

Tison, L., Roessner, A., Gerschewski, S., and Menzel, R. (2019). The neonicotinoid clothianidin impairs memory processing in honey bees. *Ecotoxicol. Environ. Safety* 180, 139–145. doi: 10.1016/j.ecoenv.2019.05.007

Traynor, K. S., Rennich, K., Forsgren, E., Rose, R., Pettis, J., Kunkel, G., et al. (2016). Multiyear survey targeting disease incidence in US honey bees. *Apidologie* 47, 325–347. doi: 10.1007/s13592-016-0431-0

Vance, J. T., Williams, J. B., Elekonich, M. M., and Roberts, S. P. (2009). The effects of age and behavioral development on honey bee (*Apis mellifera*) flight performance. *J. Exp. Biol.* 212(Pt 16), 2604–2611. doi: 10.1242/jeb.028100

vanEngelsdorp, D., and Meixner, M. D. (2010). A historical review of managed honey bee populations in Europe and the United States and the factors that may affect them. *J. Invert. Pathol.* 103, S80–S95. doi: 10.1016/j.jip.2009.06.011

Wang, D.-I., and Mofller, F. (1970). The division of labor and queen attendance behavior of Nosema-infected worker honey bees. *J. Econ. Entomol.* 63, 1539–1541.

Wells, T., Wolf, S., Nicholls, E., Groll, H., Lim, K. S., Clark, S. J., et al. (2016). Flight performance of actively foraging honey bees is reduced by a common pathogen. *Environ. Microbiol. Rep.* 8, 728–737. doi: 10.1111/1758-2229.12434

Williams, I. H. (1994). The dependence of crop production within the European Union on pollination by honey bees. *Agricult. Zool. Rev.* 6, 229–257.

Wintermantel, D., Odoux, J.-F., Decourtye, A., Henry, M., Allier, F., and Bretagnolle, V. (2020). Neonicotinoid-induced mortality risk for bees foraging on oilseed rape nectar persists despite EU moratorium. *Sci. Total Environ.* 704:135400. doi: 10.1016/j.scitotenv.2019.135400

Woyciechowski, M., and Moroń, D. (2009). Life expectancy and onset of foraging in the honeybee (*Apis mellifera*). *Insectes Soc.* 56, 193–201. doi: 10.1007/s00040-009-0012-6

Conflict of Interest: The authors declare that the research was conducted in the absence of any commercial or financial relationships that could be construed as a potential conflict of interest.

Copyright © 2020 Coulon, Dalmon, Di Prisco, Prado, Arban, Dubois, Ribière-Chabert, Alaux, Thiéry and Le Conte. This is an open-access article distributed under the terms of the Creative Commons Attribution License (CC BY). The use, distribution or reproduction in other forums is permitted, provided the original author(s) and the copyright owner(s) are credited and that the original publication in this journal is cited, in accordance with accepted academic practice. No use, distribution or reproduction is permitted which does not comply with these terms.

frontiers in Microbiology

ORIGINAL RESEARCH
published: 08 May 2020
doi: 10.3389/fmicb.2020.00767

Cleavage of Desmosomal Cadherins Promotes γ-Catenin Degradation and Benefits Wnt Signaling in Coxsackievirus B3-Induced Destruction of Cardiomyocytes

Guangze Zhao[1,2], Huifang M. Zhang[1,2], Ye Qiu[1,3], Xin Ye[1,2†] and Decheng Yang[1,2]*

[1] Department of Pathology and Laboratory Medicine, University of British Columbia, Vancouver, BC, Canada, [2] Centre for Heart Lung Innovation, St. Paul's Hospital, Vancouver, BC, Canada, [3] College of Biology, Hunan University, Changsha, China

OPEN ACCESS

Edited by:
Ian M. Jones, University of Reading, United Kingdom

Reviewed by:
Jianwei Wang, Chinese Academy of Medical Sciences and Peking Union Medical College, China
Daniel Adesse, Oswaldo Cruz Foundation (Fiocruz), Brazil

***Correspondence:**
Decheng Yang
decheng.yang@hli.ubc.ca

†Present address:
Xin Ye, Genevant Science Corp., Burnaby, BC, Canada

Specialty section:
This article was submitted to Virology, a section of the journal Frontiers in Microbiology

Received: *16 January 2020*
Accepted: *31 March 2020*
Published: *08 May 2020*

Citation:
Zhao G, Zhang HM, Qiu Y, Ye X and Yang D (2020) Cleavage of Desmosomal Cadherins Promotes γ-Catenin Degradation and Benefits Wnt Signaling in Coxsackievirus B3-Induced Destruction of Cardiomyocytes. Front. Microbiol. 11:767. doi: 10.3389/fmicb.2020.00767

Coxsackievirus B3 (CVB3) is the primary etiologic agent of viral myocarditis, a major heart disease that occurs predominantly in children and young adolescents. In the heart, intercalated disks (ICD) are important structural formations that connect adjacent cardiomyocytes to maintain cardiac architecture and mediate signal communication. Deficiency in ICD components, such as desmosome proteins, leads to heart dysfunction. γ-catenin, a component protein of desmosomes, normally binds directly to desmocollin-2 and desmoglein-2. In this study, we found that CVB3 infection downregulated γ-catenin at the protein level but not the mRNA level in mouse HL-1 cardiomyocytes. We further found that this reduction of γ-catenin protein is a result of ubiquitin proteasome-mediated degradation, since the addition of proteasome inhibitor MG132 inhibited γ-catenin downregulation. In addition, we found that desmocollin-2 and desmoglein-2 were cleaved by both viral protease 3C and virus-activated cellular caspase, respectively. These cleavages led to the release of bound γ-catenin from the desmosome into the cytosol, resulting in rapid degradation of γ-catenin. Since γ-catenin shares high sequence homology with β-catenin in binding the TCF/LEF transcription factor, we further studied the effect of γ-catenin degradation on Wnt/β-catenin signaling. Luciferase assay showed that γ-catenin expression inhibited Wnt/β-catenin signaling. This finding was substantiated by qPCR to show that overexpression of γ-catenin downregulated transcription of Wnt signal target genes, c-myc and MMP9, while silencing γ-catenin upregulated these target genes. Finally, we demonstrated that γ-catenin expression inhibited CVB3 replication. In search for the underlying mechanism, we found that silencing γ-catenin caused down-regulation of interferon-β and its stimulated antiviral genes MDA5, MAVS, and ISG15. Taken together, our results indicate, for the first time, that CVB3 infection causes cardiomyocyte death through, at least in

part, direct damage to the desmosome structure and reduction of γ-catenin protein, which in return promotes Wnt/β-catenin signaling and downregulates interferon-β stimulated immune responses.

Keywords: Coxsackievirus B3, desmocollin-2, desmoglein-2, γ-catenin, Wnt/β-catenin signal, intercalated disks, interferon-β

INTRODUCTION

Coxsackievirus B3 (CVB3) is a primary etiologic pathogen of viral myocarditis (Fairweather et al., 2012). Acute viral myocarditis can enter its chronic phase, dilated cardiomyopathy, which is a severe heart disease that may lead to heart failure or sudden death (Davies and McKenna, 1994; Mason, 2003). Numerous studies have shown that CVB3 replicates quickly in the heart after infection and causes direct cardiomyocyte injury or death, ultimately leading to loss of cardiac function (McManus et al., 1993). However, the pathway through which CVB3 infection causes direct cardiomyocyte destruction is still not fully understood.

Coxsackievirus B3 is a member of the *Picornaviridae* family. Its positive, single-stranded RNA genome can be directly translated into a polyprotein, which is cleaved into 11 mature viral proteins by viral proteases 2A and 3C. In addition to processing viral polyproteins to complete viral life cycle, proteases 2A and 3C also cleave a number of host proteins involved in host gene transcription and translation as well as signal transduction (Yang et al., 2003; Laitinen et al., 2016); these viral proteases thus play a critical role in viral pathogenesis.

Intercalated disks (ICD) are substantial structures that connect adjacent cardiomyocytes in the myocardium. The entire ICD structure is composed of three major complexes: desmosomes, gap junctions, and fascia adherens (Zhao et al., 2019). Desmosomes are essential for mechanically maintaining the architecture of cardiomyocytes (Sheikh et al., 2009), as well as for withstanding the strong forces imposed by heart contraction (Vermij et al., 2017). Disorganization of desmosome proteins in the myocardium results in multiple cardiac diseases, such as arrhythmogenic ventricle cardiomyopathy, which is caused by mutations in desmosome proteins (Campuzano et al., 2013; Rasmussen et al., 2014). In addition, several desmosome-related diseases, such as wooly hair and palmoplantar keratoderma have been reported (Rao et al., 1996; Carvajal-Huerta, 1998). These studies, however, largely focused on pharmacological reagent-induced disorganization of desmosomes in skin cells, and not on desmosome destruction in the heart due to viral infection, which has previously not been well investigated. A recent study from our laboratory found that reduction of ICD proteins in CVB3-infected cardiomyocytes is related to upregulation of certain microRNAs (Ye et al., 2014). For example, vinculin and α-catenin levels in the heart are decreased due to CVB3-induced upregulation of miR-21. We have also shown that γ-catenin (also called plakoglobin, encoded by the JUP gene), another important component of the desmosome, is robustly reduced during CVB3 infection; however, this decrease is not due to upregulation of miR-21, implying that other mechanisms are responsible for the downregulation of γ -catenin.

In addition to localizing in the desmosome as a structural protein, γ-catenin also participates in cell signaling in the cytosol. This protein is critical for desmosome assembly, especially the vertical linkage of desmosomal cadherins (desmoglein and desmocollin) to desmoplakin (Kowalczyk et al., 1999). Interestingly, in the presence of either desmoglein or desmocollin, γ-catenin's half-life increases from 10–15 min to approximately 3–4 h (Kowalczyk et al., 1994), indicating that the binding of γ-catenin to neighboring desmosomal cadherins enhances its stability. γ-catenin is a close homolog of β-catenin, and they share many common interacting proteins, suggesting that γ-catenin may also be involved in the Wnt/β-catenin signaling pathway. However, the functional role of γ-catenin in Wnt/β-catenin signaling remains controversial and needs to be further investigated (Miravet et al., 2002; Maeda et al., 2004; Lombardi et al., 2011).

In this study, we first found that the reduction of γ-catenin was primarily due to the ubiquitin proteasome-mediated degradation caused by CVB3 infection. We further found that desmosome cadherins, desmocollin-2 (DSC-2) and desmoglein-2 (DSG-2), were cleaved by both CVB3 protease and virus-activated caspases. These cleavages promoted cellular relocalization and subsequent degradation of γ-catenin. To our knowledge, this is the first report on the cleavage of ICD proteins by cardiotropic viral proteases. In addition, we also found by luciferase assay that γ-catenin played an inhibitory role in Wnt/β-catenin signaling by competing with β-catenin to interact with the LEF/TCF transcription factor. As a result, overexpression of γ-catenin suppressed Wnt/β-catenin target gene transcription and also inhibited CVB3 replication. These data imply that CVB3-induced reduction of γ-catenin benefits CVB3 replication and generates a positive feedback effect on the destruction of ICD proteins and eventually cardiomyocyte death. Taken together, our studies revealed a previously unrecognized mechanism of CVB3-mediated cardiomyocyte destruction, based on reduction of cardiomyocyte structural integrity and inhibition of an integral signaling pathway.

MATERIALS AND METHODS

Cell Culture, Animals, and Viral Infection

HeLa cells (ATCC) were cultured in Dulbecco's modified eagle's medium (DMEM) supplemented with 10% fetal bovine serum (FBS) (Sigma), 100 μg/ml penicillin-streptomycin and

2 mM glutamine (Thermo Fisher) at 37°C in 5% CO_2. HL-1 cardiomyocytes, a mouse cardiac muscle cell line established from a cardiomyocyte tumor linage, were a gift from Dr. William C. Claycomb (Louisiana State University Health Science Center). These cells were cultured in Claycomb medium (Sigma) with 10% FBS, 100 μg/ml penicillin-streptomycin, 4 mM L-glutamine (Thermo Fisher) and 100 μM norepinephrine. For *in vivo* studies, 4-week-old male A/J mice were purchased from Jackson Laboratories (United States). Animal work was conducted by strictly following the Guide to the Care and Use of Experimental Animals – Canadian Council on Animal Care. All protocols were approved by the Animal Care Committee of Faculty of Medicine, University of British Columbia (protocol number A16-0093). The CVB3 (CG) strain was obtained from Dr. Charles Gauntt (University of Texas Health Science Center) and propagated in HeLa cells. Viral infection of cultured cells was conducted by incubation with CVB3 at a multiplicity of infection (MOI) of 10 for 1 h (for HeLa) or at a MOI of 50 for 2 h (for HL-1) in a serum free medium, washed with phosphate-buffered saline (PBS) (Thermo Fisher) twice, and then replenished with fresh medium containing 10% FBS. Mice were infected with CVB3 at a plaque forming unit (pfu) of 10^5 or sham-infected with PBS by intraperitoneal injection. Infected mice were then euthanized at day 6 post-infection and the ventricular walls of the hearts were collected for analysis of target protein expression. The indicated MOI or pfu amounts and infection procedures were used throughout the entire work, unless otherwise specified.

Cell Treatment With Inhibitor Against Proteasome, GSK3, or Caspase

HeLa cells were pre-treated with proteasome inhibitor MG132 (Selleckchem) to block protein degradation at 5 μM or an equal volume of DMSO for 1 h and then infected with CVB3. Cellular proteins were then collected at 5 and 7 h post infection (pi) to detect target protein degradation by Western blot analysis. To inhibit caspases, HeLa cells were pre-treated with z-VAD-fmk (Selleckchem) at 50 μM or equal volume of DMSO for 1 h and then infected with CVB3. Cellular proteins were collected at 5 and 7 h pi to detect the blockage of caspase-3-mediated cleavage of target protein by Western blot analysis. To inhibit glucose synthase kinase-3 (GSK3), HL-1 cells were pre-treated with inhibitor SB216763 (Selleckchem) at 40 μM or equal volume of DMSO for 1 h and then infected with CVB3. Cellular proteins were then collected at 12 and 24 h pi to determine the effect of inhibition on γ-catenin level by Western blot analysis. All these inhibitors were used at a lower concentration that could not significantly affect CVB3 replication based on our previous experience (Yuan et al., 2005b; Qiu et al., 2017; Zhang et al., 2020).

Transfection of Plasmids and siRNAs

All the plasmids used in this study were purchased from Addgene (United States), including 1105-desmoglein2-FLAG-eGFP, 476-desmocollin2-myc and 330-plakoglobin-myc. The γ-catenin siRNA (human) and DSC-2 siRNA (human) were purchased from Santa Cruz (United States). To perform the transient transfection, HeLa cells (2×10^5) were seeded in 6-well plates and grown to 60∼80% confluence (for plasmid) or 30∼40% confluence (for siRNA) before transfection. Plasmid DNA was then transfected into the cells using Lipofectamine 2000 (Life Technologies) and Opti-MEM™ (Thermo Fisher) complex for 6 h, and then incubated for 48 h after replacing the medium with DMEM containing 10% FBS. The siRNA was transfected using the same procedures as those described for plasmid except that Oligofectamine was used as transfection reagent. Scrambled siRNA and empty vector were used as controls in these transfections, respectively. Further, CVB3 infection was conducted at 36 h (for plasmid) or 48 h (for siRNA) post transfection before final analysis.

RNA Extraction and Quantitative Real-Time PCR (qPCR)

Total cellular RNAs were isolated using the PureLink™ RNA mini kit (Invitrogen) according to the manufacturer's instructions. cDNAs were then synthesized by reverse transcription using 5 μg of RNA and the SuperScript IV First-Strand Synthesis System (Invitrogen). The target genes were detected by qPCR using 2 × SYBR Green qPCR Master Mix (Bimake), 100 ng of first-strand cDNA and 1 μM of each primer. Glyceraldehyde 3-phosphate dehydrogenase (GAPDH) expression level was used as the endogenous control to normalize the data. All PCR experiments were performed in triplicates and repeated twice. The PCR primer sequences are listed in **Supplementary Table S1**.

Western Blot Analysis

Cultured cells were washed with ice cold PBS twice and then lysed with an appropriate volume of RIPA Lysis and Extraction Buffer (Thermo Fisher) on ice for 20 min. Cell lysates were centrifuged at 13,000 × *g* for 20 min at 4°C and the protein-containing supernatant was collected. The protein concentration was determined by BCA Protein Assay (Thermo Fisher). For preparing mouse heart tissue lysates, the heart tissue sections were first rinsed with PBS to remove the blood and then lysed in RIPA lysis buffer using the TissueLyser LT (Qiagen). Samples were briefly sonicated at 50 Hz for 5 min to release the proteins. The protein-containing supernatants were collected by centrifugation and protein concentrations were determined as described above. Western blot was conducted by following the standard method (Qiu et al., 2017). Briefly, proteins were separated by sodium dodecyl sulfate-polyacrylamide gel electrophoresis (SDS-PAGE) with a corresponding polyacrylamide concentration according to the protein molecular weights and transferred onto BioTrace™ NT nitrocellulose membranes. The membranes were blocked with 5% skim milk in Tris-buffered saline with 0.1% Tween 20 (TBST) for 1 h and then incubated overnight with one of the following primary antibodies: monoclonal rat anti-VP1 (Doka), polyclonal rabbit anti-γ-catenin (Cell Signaling), monoclonal mouse anti-desmocollin-2 and monoclonal rabbit anti-desmoglein-2 (Abcam), monoclonal mouse anti-cleaved-caspase-3 (Cell Signaling), monoclonal rabbit anti-c-myc (Abcam) and K48-linkage specific polyubiquitin rabbit antibody

(Cell Signaling) and monoclonal mouse anti-β-actin-HRP (Santa Cruz). After three washes with TBST, each blot was further incubated with a corresponding secondary antibody (goat anti-mouse or donkey anti-rabbit IgG) conjugated to horseradish peroxidase (Amersham). Detection was carried out by enhanced chemiluminescence (Amersham) as per the manufacturer's instructions. β-actin was used as the loading control. Signal intensities were quantified by densitometric analysis using the NIH ImageJ program and then normalized to the loading control.

In vitro Cleavage Assay

The *in vitro* cleavage assay was conducted as described previously (Skern and Liebig, 1994). In brief, cultured HeLa cells were collected in RIPA lysis buffer and centrifuged at 13,000 × *g* at 4°C for 20 min. 10 μl of supernatant containing 25 μg of total protein were mixed with 20 μl of reaction buffer (20 mM PH 7.4 Hepes, 150 mM potassium acetate, and 1 mM DDT) and 10 μl of recombinant wild-type or mutant (inactive catalytic site) CVB3 protease 2A or 3C (kind gifts from Drs. Eric Jan and Honglin Luo, respectively) containing 10 μg of protease (Jagdeo et al., 2018). This reaction was then incubated at 37°C for defined periods of time (0 min, 15 min, 30 min, 1 h, and 2 h) and stopped by the addition of SDS-PAGE sample buffer. Cleavage products were detected by Western blot analysis as described above.

Viral Plaque Assay

Viral titer was determined following the procedure published previously (Yuan et al., 2005a). Briefly, samples of cells and medium from plates receiving the various treatments were freeze-thawed and then centrifuged at 4,000 × *g* to collect the supernatant containing the viruses. HeLa cells were seeded onto 6-well plates (8×10^5 cells/well) and incubated at 37°C for 20 h to reach confluence of approximately 90% and then washed with PBS and overlaid with 800 μl of virus-containing samples serially diluted (10^{-1} to 10^{-7}) in cell culture medium. After a viral adsorption period of 60 min at 37°C, the supernatant was removed and the cells were overlaid with 2 ml of sterilized soft (0.75%) Bacto-agar-minimal essential medium, cultured at 37°C for 72 h, fixed with Carnoy's fixative for 30 min, stained with 1% crystal violet for 2 min and then washed with PBS twice. The number of plaques was counted, and the virus titer was calculated as the pfu/ml. All the assays were conducted three times.

Immunofluorescence Staining and Confocal Microscopy

Cells cultured in μ-Slide 8 Well ibiTreat:#1.5 polymer coverslip (Ibidi, Cat. No. 80826) were washed with PBS and fixed with 4% paraformaldehyde in PBS for 20 min at room temperature. After removing the fixative, cells were further washed with fresh 0.1 M glycine in PBS for three times (5 min each). Fixed cells were permeabilized with 0.1% Triton X-100 in PBS for 2 min, washed with PBS three times and then blocked with 3% bovine serum albumin (BSA) in PBS for 1 h at room temperature, which was followed by removing the blocking buffer and incubating the cells with a corresponding primary antibody (same antibodies as for the Western blot) at 4°C overnight. The cells were then washed with PBS and incubated with corresponding secondary antibodies: goat anti-rabbit IgG labeled with Alexa Fluor 488 (green), goat anti-mouse IgG labeled with Alexa Flour 594 (red), or goat anti-rat IgG labeled with Alexa Flour 633 (purple) (Invitrogen). The nuclei were stained with 4′,6′-diamidine-2′-phenylindole dihydrochloride (DAPI) (Sigma). Images were captured using a Zeiss LSM 880 confocal microscope and merged using the Zen Black and Zen Blue programs. To quantify the intensity of fluorescence signals, the same imaging setting parameters were applied to all the samples. Relative protein levels were then quantified by converting the captured photos to 8 bit-pictures and measuring the mean gray value of the entire image using the NIH ImageJ program.

Immunoprecipitation and Ubiquitination Assay

Cell lysates of CVB3-infected and sham-infected cells were prepared using lysis buffer containing 50 mM Tris HCl, pH 7.4, 150 mM NaCl, 1 mM EDTA, 1% Triton X-100, and protease inhibitor cocktail (Roche), and centrifuged at 14,000 × *g* for 5 min at 4°C. After preclearing for 2 h, the supernatants were immunoprecipitated overnight using the anti-myc antibody and the Pierce Crosslink IP Kit (Thermo Fisher) according to the manufacturer's instructions. The enriched proteins were separated by a 6% SDS-PAGE and then immunoblotted using the K48-linkage anti-polyubiquitin antibody (Cell Signaling).

Dual Luciferase Assay

The β-catenin firefly reporter (M50 Super 8 × TOPFlash), the Renilla reporter (pcDNA-RLuc8) and 330-plakoglobin-myc plasmids were purchased from Addgene. The β-catenin firefly reporter plasmid contains a TCF/LEF binding motif upstream of a firefly luciferase reporter, while the Renilla reporter is a constitutively expressed reporter, serving as a control. Thus, the expression of firefly luciferase is regulated by the activity of TCF/LEF binding proteins (such as β-catenin). To determine the effect of γ-catenin on the TCF/LEF-regulated luciferase activity, HeLa cells were co-transfected with two luciferase reporters (M50 Super 8 × TOPFlash and pcDNA-RLuc8) and the 330-plakoglobin-myc plasmid. For the negative control group, an empty vector was used to replace the 330-plakoglobin-myc plasmid for co-transfection. At 36 h post transfection, cells were infected with CVB3 for 6 h and then the cell lysates were harvested for luciferase assay on a Tecan GENios luminescence reader to determine the relative luciferase activity (firefly/Renilla) using the Dual-Luciferase Reporter Assay System (Promega) following the manufacturer's instructions. Each treatment was verified by three biological repeats.

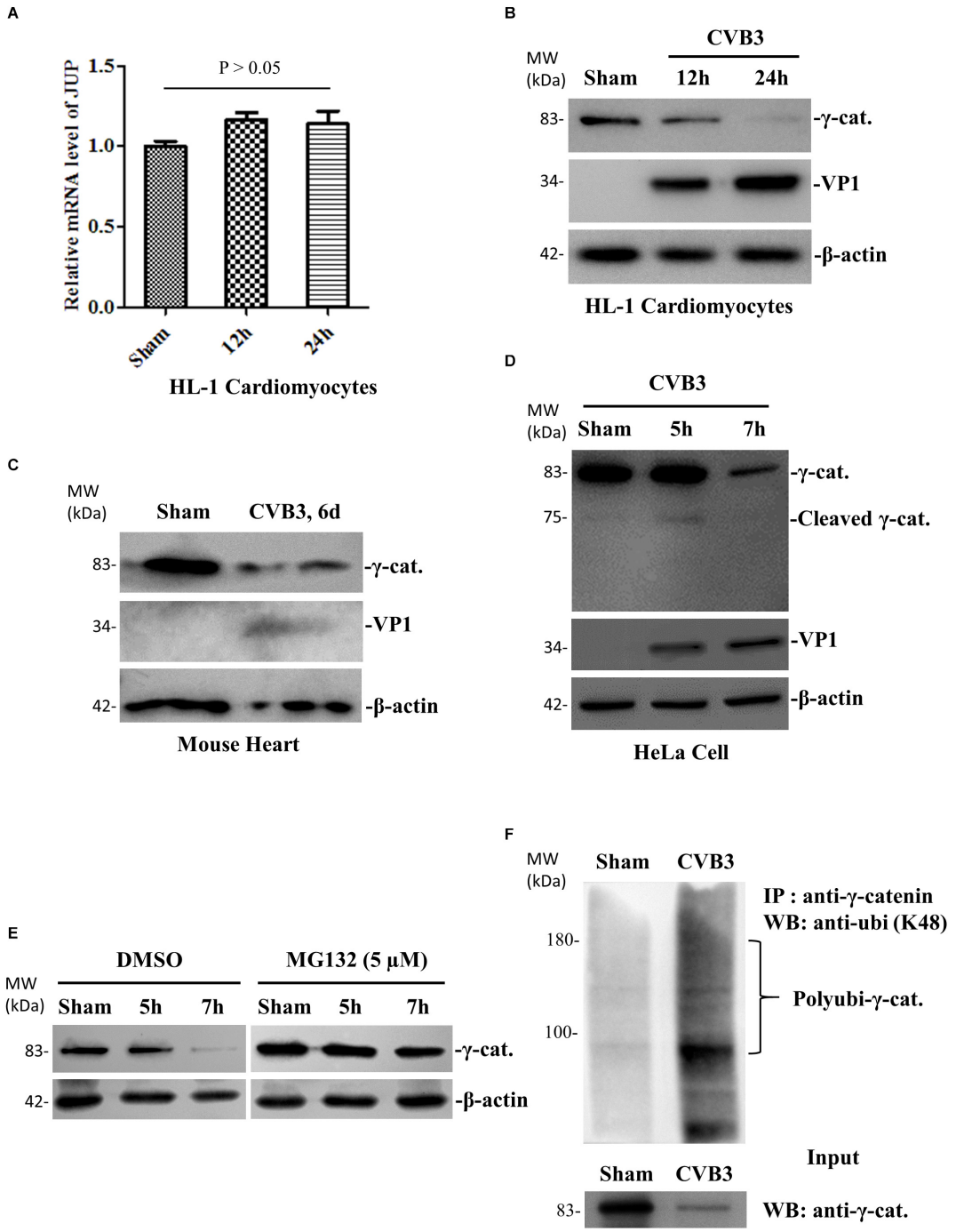

FIGURE 1 | CVB3 infection decreases γ-catenin level through the ubiquitin-proteasome pathway of protein degradation. **(A)** HL-1 mouse cardiomyocytes were infected with CVB3 at a MOI of 50 or sham-infected with PBS and the cell lysates were harvested at the indicated time points pi. Total cellular RNAs were isolated for qPCR to measure the mRNA of γ-catenin (encoded by JUP gene). The relative level of the mRNA at each time point was normalized to the level of GAPDH in the sample. Three biological repeats were performed for each assay, and the Student's *t*-test was used to analyze the data. $p > 0.05$ (not significant). **(B)** HL-1 mouse cardiomyocytes were infected with CVB3 or sham-infected as described in **(A)** and the cell lysates were harvested at the indicated time points pi for Western blot analysis of γ-catenin and CVB3 VP1 protein. β-actin was used as a loading control. **(C)** 4-week-old A/J mice were infected with CVB3 at 10^5 pfu or sham-infected with PBS. At 6 days pi, the mice were sacrificed and the heart tissues were homogenized for Western blot analysis of γ-catenin protein. **(D)** HeLa cells were infected with CVB3 at a MOI of 10 or sham-infected with PBS and cell lysates were prepared for Western blot analysis of γ-catenin cleavage. **(E)** HeLa cells were pretreated with 5 μM MG132 and then infected with CVB3 at a MOI of 10. At the indicated time points pi, the cellular proteins were subjected to Western blot analysis of γ-catenin protein. **(F)** HeLa cells were infected or sham-infected as described above for 7 h. Cell lysates were prepared and first immunoprecipitated (IP) with the anti-γ-catenin antibody and then subjected to Western blot (WB) analysis of K48-linked polyubiquitin chains. The input (non-immunoprecipitated) samples were detected with the anti-γ-catenin antibody.

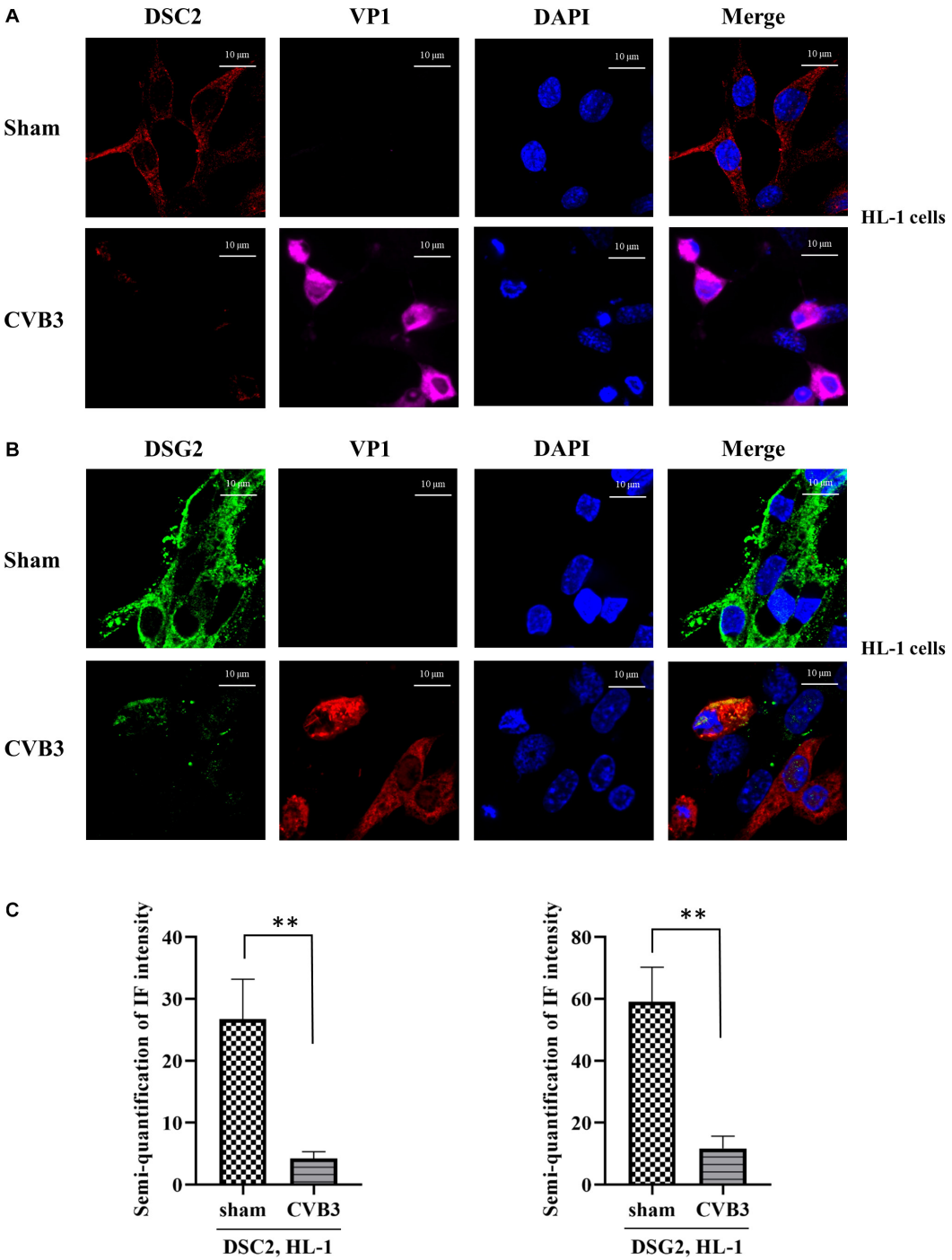

FIGURE 2 | CVB3 induces destabilization of desmosomal cadherins in HL-1 mouse cardiomyocytes. **(A,B)** HL-1 cells were infected with CVB3 at a MOI of 50 for 24 h. Cells were subjected to immunofluorescence staining of DSC-2 (red) **(A)** and DSG-2 (green) **(B)**. Nuclei were stained using DAPI (blue). Images were captured by Zeiss confocal microscope and Zeiss Black program, scale bars = 10 μM. Fluorescence signal intensities were quantified by using ImageJ **(C)**. Data were statistically analyzed, $n = 3$, $^{**}p < 0.01$.

Statistical Analysis

Two-way ANOVA analysis of variances was performed for determining differences between groups on multiple variables, and Student's *t*-test was conducted to analyze the paired groups. Results are shown as means ± standard deviation (SD) of three independent experiments. A *p*-value less than 0.05 (indicated by *) was considered statistically significant. Additionally, $^{**}p < 0.01$; $^{***}p < 0.001$; $^{****}p < 0.0001$.

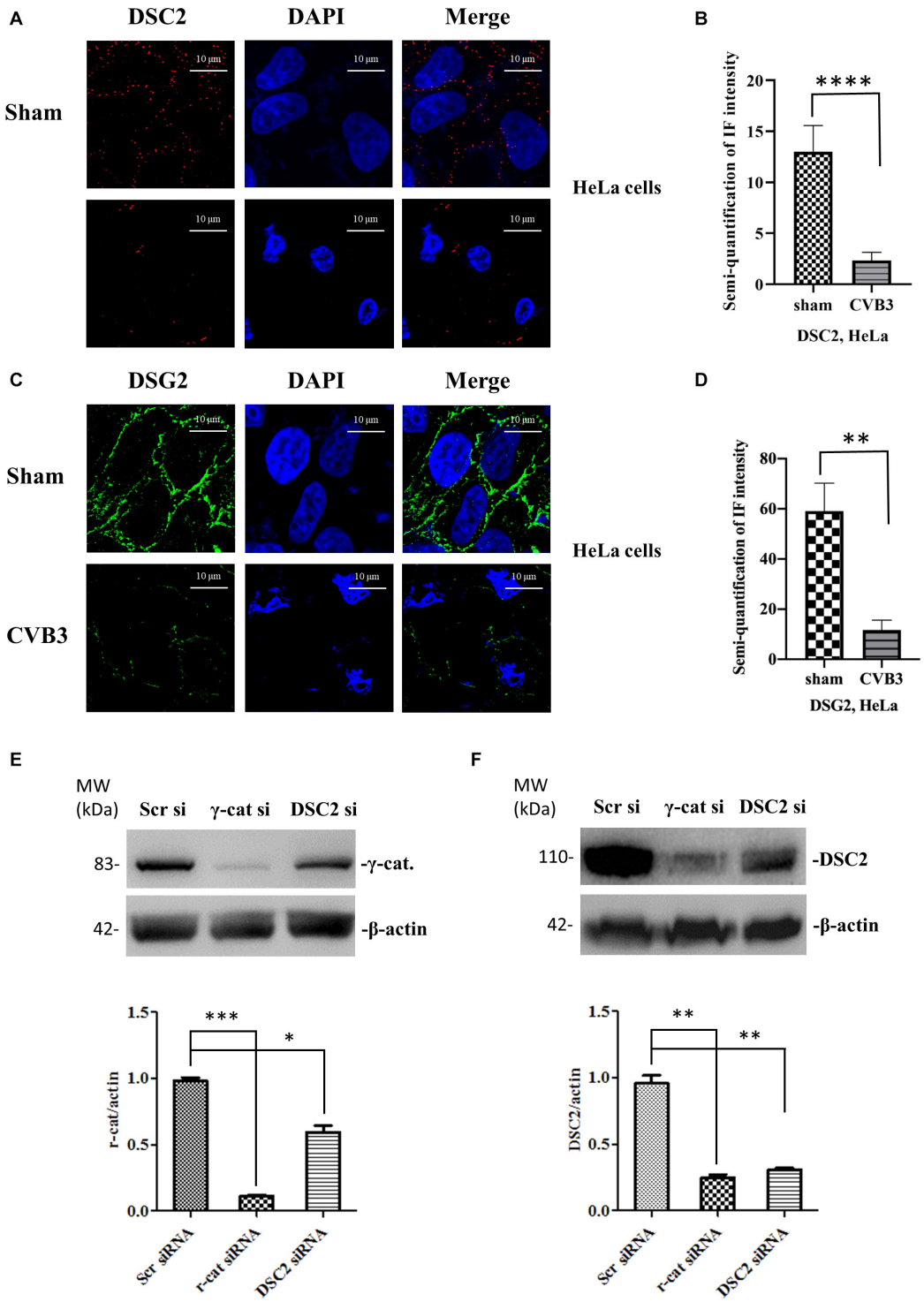

FIGURE 3 | CVB3-induced decrease of desmosomal cadherins leads to reduction of γ-catenin. HeLa cells were infected with CVB3 at a MOI of 10 for 6 h. Cells were then subjected to immunofluorescence staining of DSC-2 (red) **(A,B)** and DSG-2 (green) **(C,D)**, scale bars = 10 μM. Fluorescence signal intensities were quantified as described in **Figure 2**. HeLa cells were transfected with the indicated specific siRNAs for 48 h and the cell lysates were collected for Western blot analysis of γ-catenin **(E)** and DSC-2 **(F)**. β-actin was used as a loading control. The intensities of the bands were measured using the NIH ImageJ program and normalized to the loading control. Data were statistically analyzed, $n = 3$, $^{*}p < 0.05$, $^{**}p < 0.01$, $^{***}p < 0.001$.

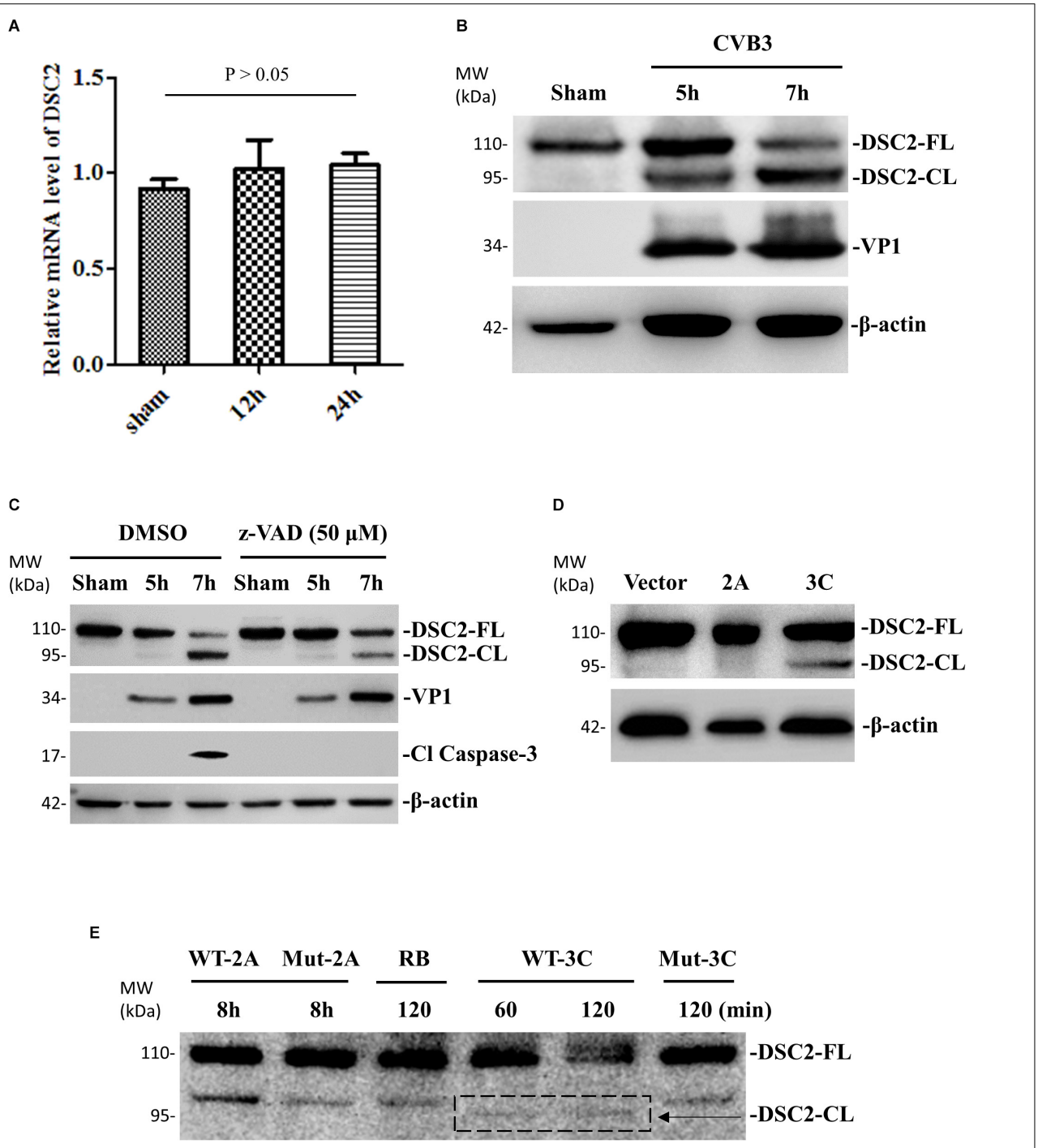

FIGURE 4 | DSC-2 is cleaved during CVB3 infection. **(A)** HeLa cells were infected with CVB3 at a MOI of 10 or sham-infected with PBS and collected at the indicated time points pi. Cellular RNAs were extracted for measuring the mRNA level of DSC-2 by qPCR. Three biological repeats were performed for each assay. Data were normalized to the level of GAPDH in the sample. $p > 0.05$ (not significant). **(B)** HeLa cells were infected or sham-infected as described in **(A)**. Cell lysates were prepared for Western blot analysis of DSC-2 using an anti-N-terminal antibody. VP1 detection was a marker for CVB3 replication. β-actin was used as the loading control. **(C)** HeLa cells were treated with 50 μM z-VAD-fmk or DMSO (negative control), and then infected with CVB3 at a MOI of 10. At the indicated time points pi, the cell lysates were harvested for Western blot analysis using the indicated antibodies. The level of cleaved caspase-3 was used as an indicator of caspase activation. **(D)** HeLa cells were transfected with a viral protease 2A or 3C plasmid, or an empty vector as the negative control. Cell lysates were harvested at 36 h post transfection for Western blot analysis of DSC-2 cleavage products. **(E)** *In vitro* cleavage assay. Non-infected HeLa cell lysates were incubated with recombinant CVB3 wild-type (WT) and mutant (Mut) 2A or 3C protease. At the indicated time points post incubation, the reaction samples were subjected to Western blot analysis of DSC-2 cleavage products. Reaction buffer (RB) only was used as another negative control.

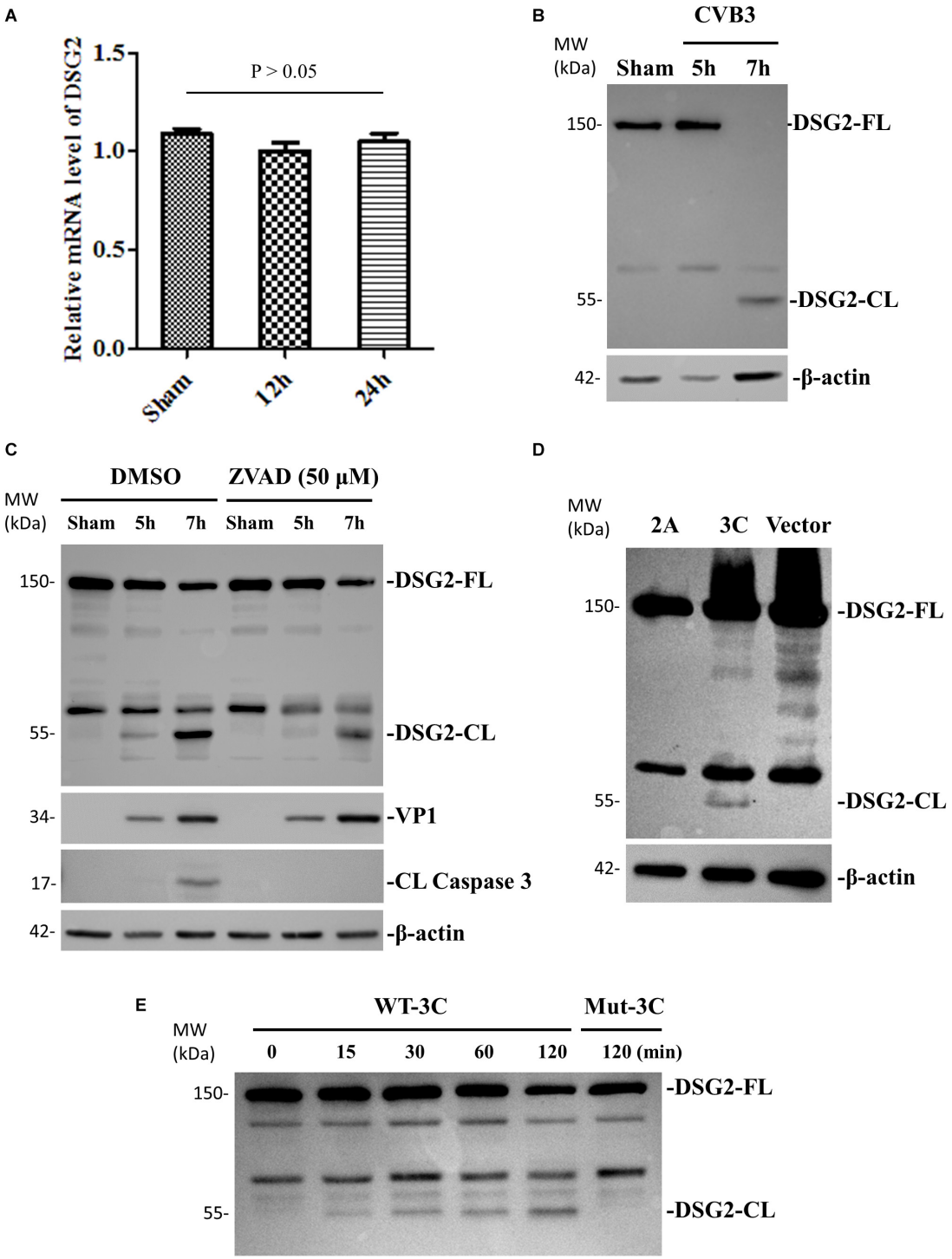

FIGURE 5 | DSG-2 is cleaved during CVB3 infection. **(A)** HeLa cells were infected with CVB3 at a MOI of 10 or sham-infected with PBS and collected at the indicated time points pi. Cellular RNAs were extracted for measuring the mRNA levels of DSG2 by qPCR. Three biological repeats were performed for each assay. Data were normalized to the level of GAPDH in the sample, $p > 0.05$ (not significant). **(B)** HeLa cells were infected or sham-infected as described in **(A)**. Cell lysates were prepared for Western blot analysis of DSG-2 using an anti-DSG-2 antibody targeting the C-terminal of the protein. β-actin level was used as the loading control. **(C)** HeLa cells were treated with 50 μM z-VAD-fmk or DMSO to block caspase activation, and then infected with CVB3 at a MOI of 10. At the indicated time points pi, cellular lysates were subjected to Western blot analysis of DSG-2 cleavage products. **(D)** HeLa cells were transfected with a viral protease 2A or 3C plasmid or an empty vector as the negative control. Cell lysates were harvested at 36 h post transfection for Western blot analysis of DSG-2 cleavage products. **(E)** *In vitro* cleavage assay. Non-infected HeLa cell lysates were incubated for the indicated time points with purified recombinant CVB3 wild-type and mutant 3C protease. Lysates were subjected to Western blot analysis of DSG-2 cleavage products.

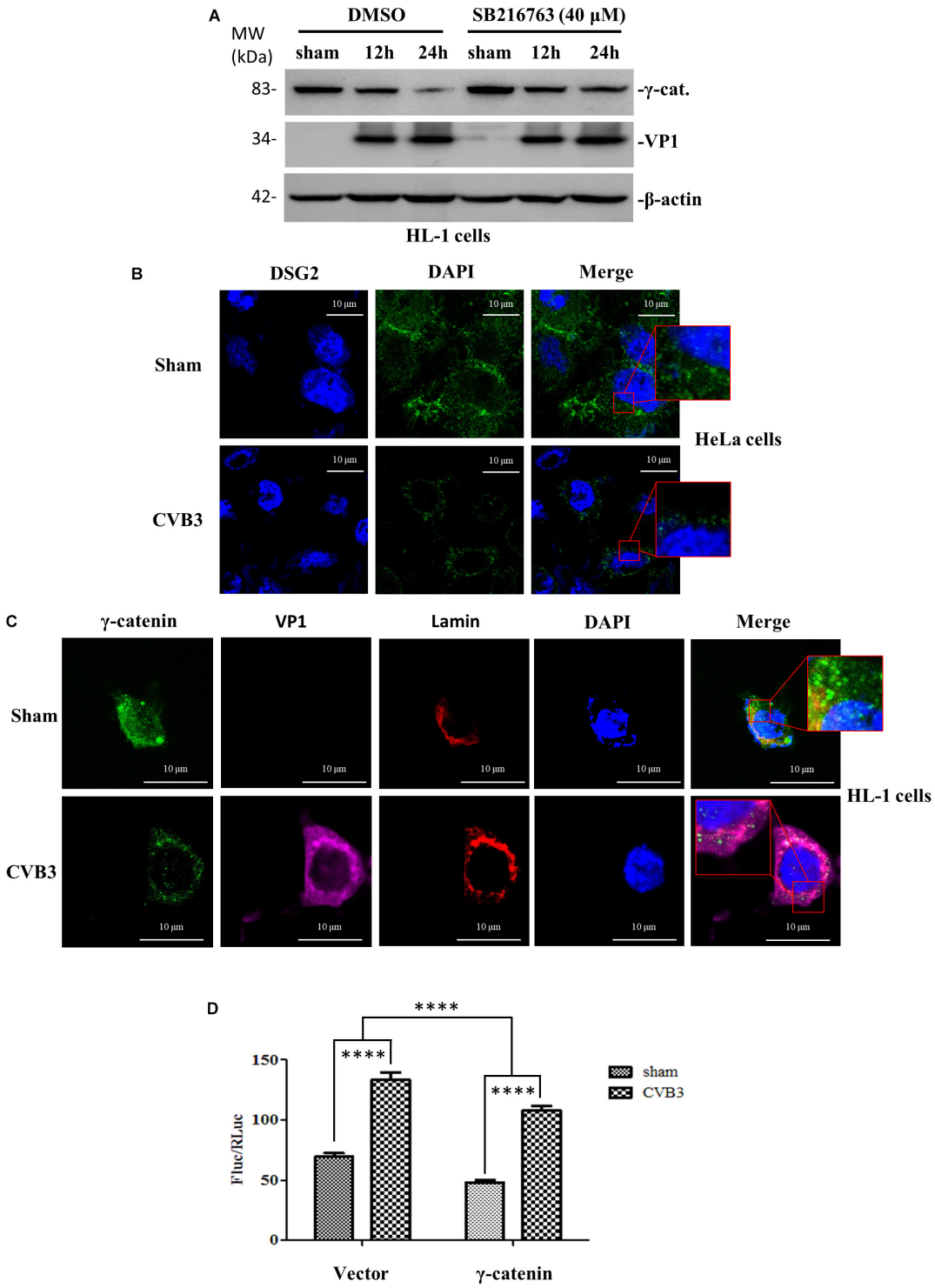

FIGURE 6 | γ-Catenin suppresses the activity of Wnt/β-catenin signaling. **(A)** Murine HL-1 cardiomyocytes were treated with SB216763 or DMSO, and then infected with CVB3 at a MOI of 50 or sham-infected. Cell lysates were collected at the indicated time points pi and subjected to Western blot analysis of γ-catenin. β-actin was used as the loading control. **(B,C)** HeLa cells and HL-1 cardiomyocytes were infected with CVB3 at a MOI of 10 and 50 for 6 h and 24 h, respectively. Cells were subjected to immunofluorescence staining to detect the γ-catenin (green), lamin (red) and CVB3 VP1 protein (purple). Nuclei were stained using DAPI (blue). Images were captured by confocal microscopy, scale bars = 10 μM. The insets show the magnified regions of colocalization. **(D)** HeLa cells were co-transfected with the γ-catenin plasmid or the empty vector and two luciferase reporters (firefly and Renilla luciferase plasmids) for 36 h, and then infected with CVB3 for 6 h. The cell lysates were harvested for dual luciferase assay to detect the relative luciferase activities (Firefly/Renilla). Data were statistically analyzed, $n = 9$, $^{****}p < 0.0001$.

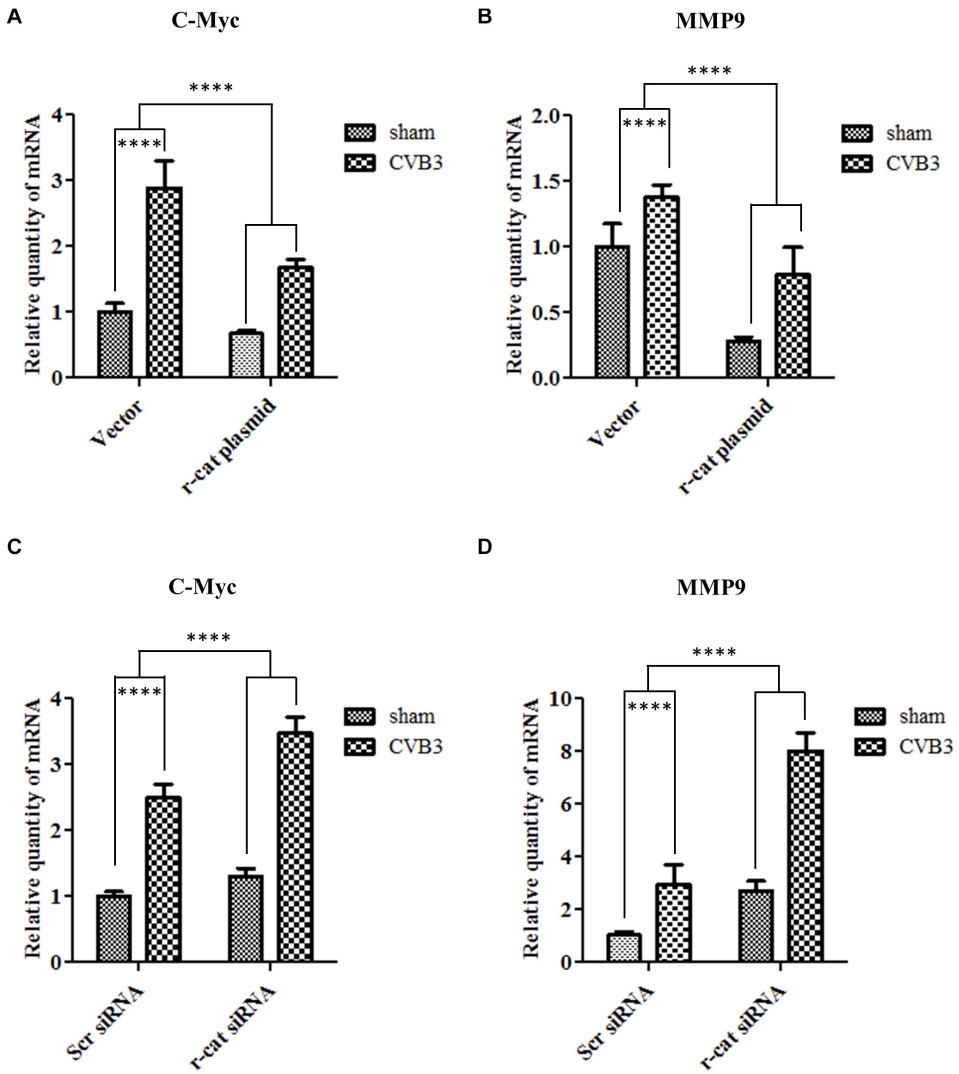

FIGURE 7 | γ-Catenin inhibits target gene transcription of Wnt/β-catenin signaling during CVB3 infection. **(A,B)** HeLa cells were transfected with the γ-catenin plasmid for 36 h to overexpress γ-catenin and then infected with CVB3 at a MOI of 10 or sham-infected. Cellular RNAs were extracted at 6 h pi and then subjected to qPCR analysis of c-myc (A) and MMP9 (B) mRNAs using specific primers. **(C,D)** HeLa cells were transfected with γ-catenin siRNA for 48 h to silence γ-catenin expression and then infected with CVB3 at a MOI of 10 or sham-infected. Cellular RNAs were extracted at 6 h pi and the mRNA levels of c-myc and MMP9 were measured as described in **(A)**. The transcriptional levels of target genes were normalized to that of GAPDH and statistically analyzed, $n = 3$, $^{****}p < 0.0001$.

RESULTS

CVB3 Infection Decreases γ-Catenin Through Ubiquitin Proteasome-Mediated Degradation

Our previous studies demonstrated downregulation of γ-catenin during CVB3 infection (Ye et al., 2014). To further investigate how γ-catenin levels are decreased, we first asked whether γ-catenin expression is downregulated at the transcriptional level. qPCR using total mouse HL-1 cardiomyocyte RNAs and specific primers targeting the γ-catenin gene (**Supplementary Table S1**) showed that CVB3 infection did not alter the mRNA levels of γ-catenin (encoded by the JUP gene) (**Figure 1A**). We then measured the changes in protein translation as well as potential post-translational cleavage and degradation. We first confirmed, by Western blot, that γ-catenin protein levels are downregulated in CVB3-infected HL-1 cardiomyocytes (**Figure 1B**) and in mouse hearts (**Figure 1C**). To determine if γ-catenin is cleaved by viral and/or cellular proteases, we performed a Western blot using a short running SDS-PAGE gel to capture the cleavage products. Although a very faint band (∼75 kDa) appeared at 5 h pi, a similar band also appeared in the sham-infected control, suggesting that this cleavage is not by CVB3 protease but rather by activated cellular protease (**Figure 1D**). Considering the faintness of this band at 5 h pi and its disappearance at 7 h pi, the reduction of γ-catenin might be mainly due to degradation. To verify this, we treated HeLa cells with

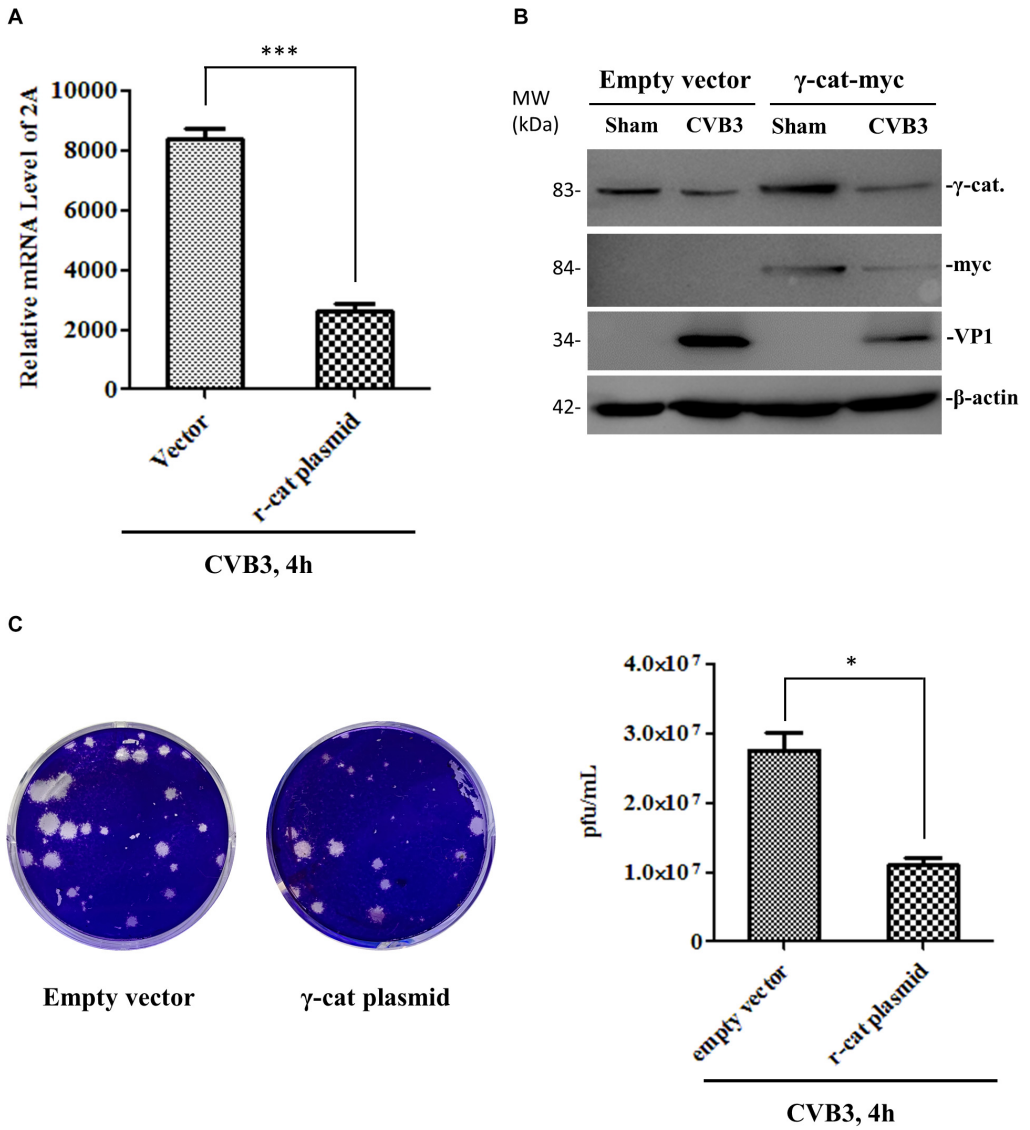

FIGURE 8 | γ-Catenin expression inhibits CVB3 replication. HeLa cells were transfected with the γ-catenin-myc plasmid or empty vector for 36 h and then infected with CVB3 for 4 h. Part of the cell culture was used for cellular RNA extraction to measure the RNA level of CVB3 2A by qPCR **(A)**, and the other part of the culture was used for cell lysate preparation to detect CVB3 VP1 and other proteins by Western blot using the indicated antibodies **(B)**. The cell culture supernatants were used for plaque assay to measure the CVB3 particle release **(C)**. Data were statistically analyzed and graphically presented, $n = 3$, $^{*}p < 0.05$, $^{***}p < 0.001$.

proteasome inhibitor MG-132 for 1 h before CVB3 infection. In this experiment, Western blot showed that compared to DMSO control, the downregulation of γ-catenin levels at 7 h pi was significantly rescued (**Figure 1E**), indicating that γ-catenin reduction is a consequence of proteasome-mediated degradation. To further determine if this degradation occurred through poly-ubiquitination before being processed in the 26S proteasome, we conducted immunoprecipitation using a primary antibody against γ-catenin and then detected poly-ubiquitinated γ-catenin using another antibody against K48-linked poly-ubiquitin. We found that CVB3 infection induced γ-catenin poly-ubiquitination compared to the sham-infected control, while the input γ-catenin level significantly decreased (**Figure 1F**).

CVB3-Induced Decrease of Desmosomal Cadherins Leads to Destabilization of γ-Catenin

Since the half-life of γ-catenin is known to be prolonged in the desmosome compared to that in the cytoplasm (Kowalczyk et al., 1994), we speculated that CVB3 infection might cause release of γ-catenin from the desmosome into the cytoplasm by destroying its co-localized binding partners in the desmosome, leading to the promotion of γ-catenin degradation. To verify this, we first determined the protein levels and localization of DSC-2 and DSG-2 in CVB3-infected murine HL-1 cardiomyocytes by immunostaining and confocal microscopy. We found that

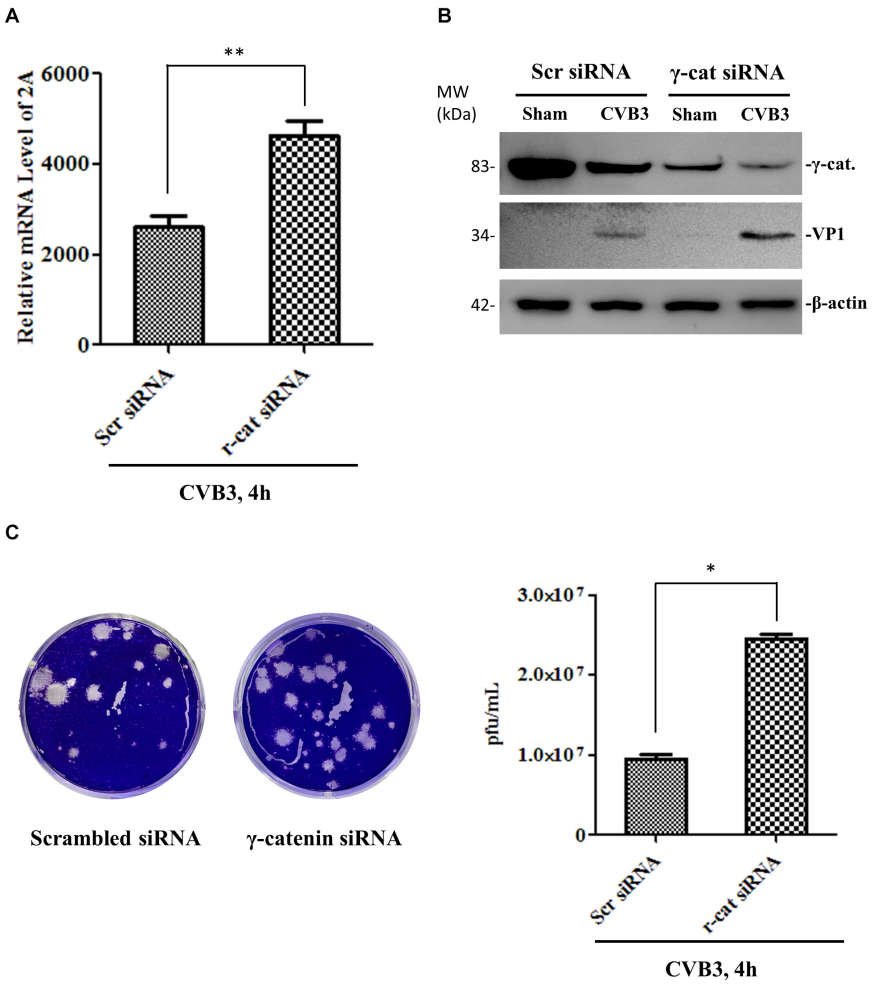

FIGURE 9 | Knockdown of γ-catenin expression enhances CVB3 replication. HeLa cells were transfected with γ-catenin siRNA or scrambled siRNA for 48 h and then infected with CVB3 at a MOI of 10 or sham-infected for 4 h. Part of the cell culture was used for qPCR to measure CVB3 2A RNA **(A),** and the other part was used either for Western blot analysis of CVB3 VP1 protein **(B)** or for plaque assay to determine the released viral particles **(C)**. Data were statistically analyzed and graphically presented, $n = 3$, $^{*}p < 0.05$, $^{**}p < 0.01$.

in sham-infected control groups, both DSC-2 and DSG-2 were mainly localized along the cell border where the cells contact each other. After CVB3 infection, however, these protein levels were dramatically decreased and their regular localization pattern was disrupted (**Figures 2A,B**). Furthermore, the fluorescence signal intensities were also quantified (**Figure 2C**).

These findings were further verified by immunostaining using CVB3-infected HeLa cells (**Figures 3A–D**). In addition, to determine whether the silencing of desmosomal cadherins could lead to γ-catenin reduction in the absence of CVB3 infection, HeLa cells were transfected with DSC-2 siRNA or scrambled siRNA, and cell lysates were then collected for Western blot; in parallel, γ-catenin siRNA was used to transfect HeLa cells as a positive control. As shown in **Figure 3E**, transfection of DSC-2 siRNA led to a ∼45% decrease in γ-catenin protein compared to cells transfected with scrambled siRNAs. Additionally, we found that silencing of γ-catenin could also reduce DSC-2 levels by ∼75% (**Figure 3F**); this reduction was even higher than that in DSC-2 siRNA-treated cells (∼46%), indicating that γ-catenin and DSC-2 stabilize each other in the desmosome complex.

DSC-2 Protein Is Cleaved During CVB3 Infection

To investigate the effect of CVB3 infection on the expression and integrity of desmosomal cadherins, we first selected DSC-2 as a target and performed qPCR and Western blot to determine DSC-2 mRNA and protein levels after CVB3 infection. We found that CVB3 infection did not alter the mRNA level of DSC-2 (**Figure 4A**) while Western blot using an anti-N terminal antibody showed the production of a ∼95 kDa band (**Figure 4B**). Since CVB3 can induce apoptosis by activating caspase-3, we used the pan-caspase inhibitor to test whether the ∼95 kDa fragment was produced by caspase-3 cleavage. We showed that z-VAD-fmk completely blocked caspase-3 cleavage; production of the ∼95 kDa product, however, was

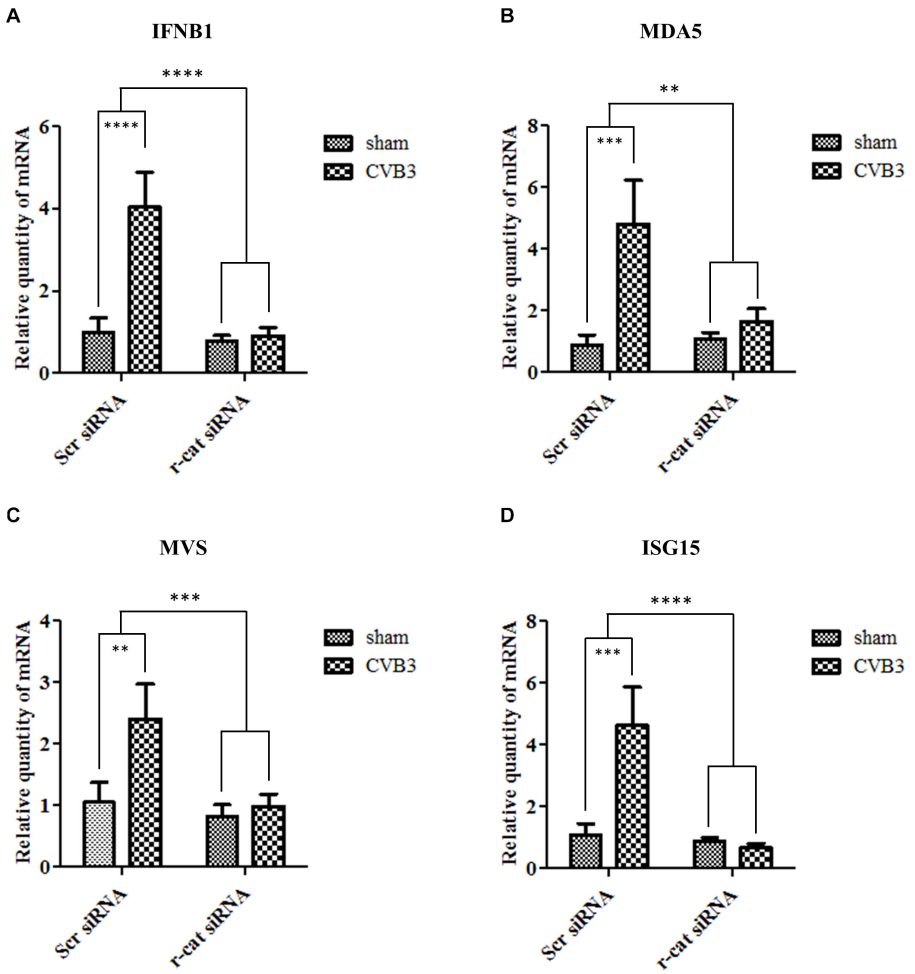

FIGURE 10 | γ-Catenin supports the induction of interferon β1 and its stimulated genes. HeLa cells were transfected with siRNA to knockdown the expression of γ-catenin and then infected with CVB3 at 10 MOI. Scrambled siRNA was used as a negative control. Cellular RNAs were extracted at 6 h pi and then subjected to qPCR analysis of the mRNA levels of IFNB1 gene **(A)**, MDA5 **(B)**, MAVS **(C)**, and ISG15 **(D)**. The transcriptional level of each gene was normalized to GAPDH level and statistically analyzed, $n = 3$, $^{**}p < 0.01$, $^{***}p < 0.001$, $^{****}p < 0.0001$.

only partially inhibited (**Figure 4C**), suggesting that DSC-2 is cleaved by both CVB3 protease and activated caspase. To identify the viral protease responsible for this cleavage, we transfected HeLa cells with protease expressing plasmids pIRES-2A or pIRES-3C and analyzed the cleavage at 36 h post transfection; results showed that compared to the empty pIRES vector, only the pIRES-3C plasmid induced the production of a ∼95 kDa product (**Figure 4D**). Meanwhile, we also conducted an *in vitro* cleavage assay using purified CVB3 wild-type and mutant (control) proteases 3C to treat the cell lysates containing DSC-2 protein (**Figure 4E**). Our data showed that protease 3C, but not 2A, could cleave DSC-2. These data were further supported by a motif search for 3C cleavage site according to a previous publication (Blom et al., 1996). This search found amino acids Q766-G767 as the potential cleavage site (**Supplementary Figure S1**), which would result in a ∼95 kDa N-terminal fragment, matching the fragment size produced during CVB3 infection.

DSG-2 Protein Is Cleaved During CVB3 Infection

Next, we used the same experimental design and methods to verify that DSG-2 gene was not downregulated at the transcriptional level but its protein was cleaved during CVB3 infection, producing a ∼55-kDa C-terminal fragment (**Figures 5A,B**). We confirmed that both CVB3 protease 3C and cellular caspase could execute this cleavage. However, CVB3 2A protease could not (**Figures 5C–E**).

γ-Catenin Suppresses the Activity of Wnt/β-Catenin Signaling

To determine the role of γ-catenin in Wnt/β-catenin signaling during CVB3 infection, we first focused on glycogen synthase kinase 3 (GSK-3), an important kinase in Wnt signaling regulation that works via phosphorylation and destabilization of β-catenin (Wu and Pan, 2010). We treated HL-1 cardiomyocytes

with 40 μM SB216763, an inhibitor of GSK-3, and then infected cells with CVB3. Western blot showed that the reduction of γ-catenin was rescued in SB216763-treated cells compared to DMSO-treated cells (**Figure 6A**), indicating that γ-catenin is also a target of GSK-3 and may play an important role in Wnt/β-catenin signaling. To determine the localization of γ-catenin during Wnt signal activation, we performed immunostaining using HeLa cells and HL-1 cardiomyocytes and both showed that γ-catenin was translocated to perinucleus upon CVB3 infection (**Figures 6B,C**). This translocation may enable γ-catenin to participate in the interaction with the LEF/TCF transcription factor and affect the Wnt signaling. To identify the nature of this effect, a luciferase assay was conducted by co-transfection of HeLa cells with two reporters (firefly luciferase and Renilla luciferase) and γ-catenin plasmid (or empty vector) for 36 h. After CVB3 infection, a dual luciferase assay was performed to determine the ratio (FLuc/RLuc) of these two luciferases (**Figure 6D**). The results showed that γ-catenin overexpression inhibited the activation of Wnt/β-catenin signaling.

γ-Catenin Inhibits Target Gene Transcription of Wnt/β-Catenin Signaling During CVB3 Infection

Having identified the role of γ-catenin in inhibiting Wnt/β-catenin signaling using a luciferase assay, our next step was to further confirm this notion by detecting the expression of Wnt signaling target genes. To this end, qPCR was conducted to detect transcription of c-myc and MMP9 using total RNAs isolated from HeLa cells transfected with γ-catenin plasmid and infected with CVB3 for 6 h. Results demonstrated that CVB3 infection upregulated the transcription of these two genes, indicating that CVB3 infection induces activation of Wnt signaling. Overexpressing γ-catenin, however, decreased transcription of both c-myc and MMP9 compared to their respective vector-transfected cells (**Figures 7A,B**). These results suggest that γ-catenin plays an inhibitory role in the Wnt/β-catenin signaling pathway. These data were further solidified by silencing γ-catenin with its specific siRNAs, showing that decreased γ-catenin expression upregulated the transcription of c-myc and MMP9, compared to the transcription in control cells treated with scrambled siRNAs (**Figures 7C,D**).

γ-Catenin Expression Inhibits CVB3 Replication While Knockdown of γ-Catenin Expression Enhances CVB3 Replication

To determine the effect of γ-catenin on viral replication, we transfected HeLa cells with a plasmid expressing myc-tagged γ-catenin for 36 h and then infected with CVB3. At 4 h pi, the cell culture was divided into two parts. One part was used to extract total RNAs for qPCR measurement of CVB3 RNA using primers targeting the CVB3 2A gene. The other part was used for (i) Western blotting analysis of CVB3 VP1 using total proteins, and (ii) plaque assay of viral particle formation using culture supernatants. Results showed that γ-catenin overexpression dramatically reduced the levels of 2A RNA (**Figure 8A**), VP1 protein (**Figure 8B**) and CVB3 particle release (**Figure 8C**) compared to the vector-transfected cells, indicating that γ-catenin has a potent inhibitory role in CVB3 replication. These data were further substantiated by siRNA-mediated silencing of γ-catenin and detection of CVB3 RNA, VP1 protein and particle formation using the methods described above. As expected, silencing γ-catenin promoted CVB3 replication, which was demonstrated by the increased levels of CVB3 RNA, VP1 protein, and particle formation (**Figures 9A–C**).

γ-Catenin Supports the Induction of Interferon-β and Interferon-Stimulated Genes

To further determine the mechanism by which γ-catenin inhibits CVB3 replication, we selected several mediators in type I interferon (IFN) immune responses for further investigation. We treated cells with γ-catenin siRNA or scrambled siRNA before CVB3 infection and then isolated the cellular RNAs to measure the transcription levels of IFNB1, MDA5 (melanoma differentiation-associated gene 5), MAVS (mitochondrial antiviral-signaling protein) and ISG15 (interferon-stimulated gene of 15 kDa) using qPCR. Data demonstrated that silencing γ-catenin significantly decreased the CVB3-activated transcription of IFNB1 (**Figure 10A**) and its ISGs (**Figures 10B–D**) compared to the scrambled siRNA-treated and CVB3-infected cells. These data suggest that γ-catenin expression is essential for CVB3-induced type I IFN immune response.

DISCUSSION

We found that both DSC-2 and DSG-2 were cleaved during CVB3 infection. These cleavages likely cause a domino effect, resulting in the destruction of other partner proteins, such as γ-catenin, in the desmosome complex. We speculated that cleavage of DSC-2 or DSG-2 led to the release of γ-catenin into the cytosol, where it is quickly degraded through the ubiquitin proteasome pathway. This speculation was verified by using proteasome inhibitor MG132. We further found that γ-catenin reduction benefited Wnt/β-catenin signaling and enhanced viral replication by suppressing the interferon-β antiviral immune response. These findings may provide a two-fold explanation of the pathogenesis of CVB3 infection (**Figure 11**): first, the cleavage of ICD structural proteins may directly damage myocardium architecture, leading to cardiomyocyte death and subsequent heart dysfunction since our previous studies and others have shown that CVB3 infection can cause cardiomyocyte apoptosis (Henke et al., 2000; Jensen et al., 2013); second, reduction of γ-catenin levels in the cell may increase viral load and promote viral pathogenicity.

Previously, it was unknown which protease(s) is/are responsible for the cleavage of DSG-2. Several proteases, such as caspase-8 (Yulis et al., 2018) and ADAM-17 (matrix metalloprotease 17) (Wang et al., 2015), have been shown to be involved in generating a DSG-2 fragment in experiments using human epithelial cells. Caspase-8 cleavage produces a 50-kDa

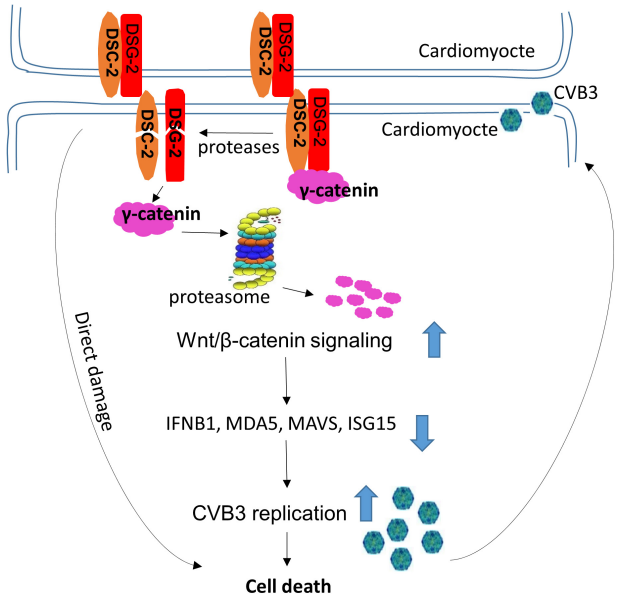

FIGURE 11 | Proposed model of action and mechanism by which CVB3 infection causes cardiomyocyte death. CVB3 infection causes cleavage of desmosomal cadherins by both CVB3 protease and virus-activated caspase, which leads to the direct damage of cardiomyocytes and the release of γ-catenin from the desmosomal complex to the cytosol, where it degrades through the ubiquitin proteasome pathway. The degradation of γ-catenin benefits Wnt/β-catenin signaling and downregulates the IFN-β antiviral immune response, which promotes CVB3 replication and eventually causes cell death. Large arrows indicate up- or down-regulation.

intracellular fragment during cell apoptosis induced by IFN-γ or TNF-α, while cellular ADAM-17 can produce an 80-kDa extracellular fragment of DSG-2 during adenovirus infection. In our study using cardiotropic CVB3 infection, we found that besides virus-activated caspase-3, CVB3 protease 3C, but not 2A, could also cleave DSG-2 and generate a ∼55-kDa intracellular fragment during infection. According to the size of the cleavage products, the caspase and CVB3 3C likely cut the protein at sites that are very close to each other. This would explain why only one single cleavage band (50–55 kDa) was observed on the Western blot membrane. For DSC-2, it was reported that this protein cannot be cleaved by caspases during apoptosis induced by camptothecin or IFN-γ (Nava et al., 2007). However, our experiments showed that both CVB3 protease 3C and the virus-activated caspase-3 could cleave DSC-2, since the pan-caspase inhibitor z-VAD-fmk only partially decreased the amount of DSC-2 cleavage products. It is worth noting that z-VAD-fmk has been reported to have antiviral activities via inhibition of viral proteases (Martin et al., 2007). Thus, the decrease of DSC-2 cleavage fragments during z-VAD-fmk treatment was probably due to either the inhibition of viral protease activity or the blockage of caspase activation, or both, which may explain the inconsistency of our observation with the previous report.

Intercalated disk component proteins not only maintain the architecture of the myocardium, but also participate in signaling transduction pathways (Zhao et al., 2019). Thus, our next goal was to elucidate the effect of CVB3-induced cleavage of desmosome proteins on signal transduction. DSG-2 and DSC-2 are transmembrane anchoring components that stabilize the desmosome structure and serve as bridging cables that connect the intracellular components (Li and Radice, 2010; Sohier et al., 2018). γ-Catenin is a cytoplasmic protein that binds to the intracellular parts of desmosomal cadherins. It has been reported that γ-catenin is rapidly degraded when expressed in a fibroblast model system in the absence of interactions with either desmoglein or desmocollin (Kowalczyk et al., 1994). As a member of the armadillo family of proteins and a paralog of β-catenin, γ-catenin also participates in cell signaling in addition to its role as a structural protein (Manring et al., 2018). The protein level of γ-catenin was dramatically decreased during CVB3 infection and no significant amount of cleaved products was observed in our Western blot analysis. This implies that CVB3-induced downregulation of γ-catenin mainly occurs through post-translational degradation. This speculation was further verified via co-immunoprecipitation assay of the poly-ubiquitinated γ-catenin.

γ-Catenin and β-catenin share many common interacting protein partners, such as cadherins, LEF/TCF transcription factors, and the APC/Axin degradation machinery, and these proteins can fulfill certain common functions (Zhurinsky et al., 2000b; Zhao et al., 2019). Furthermore, the competition between these two catenin proteins mediates the cross-talk of cadherin-based adhesion, catenin-dependent transcription and Wnt signaling (Zhurinsky et al., 2000a). However, how γ-catenin affects Wnt signaling is still debatable. For instance, using a human malignant mesothelioma cell line, researchers found that γ-catenin has TCF/LEF family-dependent transcriptional activity in a β-catenin deficient cell line (Maeda et al., 2004). This implies that γ-catenin may compete with β-catenin for binding to TCF/LEF family members and thus inhibit Wnt signaling. Another group reported that Wnt-3a activation of LEF/TCF-dependent transcription depends on β-catenin, but not on γ-catenin (Shimizu et al., 2008). However, the role of γ-catenin in the Wnt signaling – particularly in the setting of picornavirus infection – has not been studied. Our results showed that degradation of γ-catenin was suppressed when treating the cells with GSK3 inhibitor SB216763, indicating that β-catenin and γ-catenin potentially compete to serve as a phosphorylation target of GSK3 kinase. C-myc and MMP9 are two target genes of Wnt signaling associated with heart development (Foulquier et al., 2018). We found that overexpression of γ-catenin downregulated the transcription of these two genes, implying the suppression of Wnt/β-catenin signaling by γ-catenin. MMP9 is reported to be induced by Wnt signaling during the course of vascular calcifications (Freise et al., 2016), and is also induced during CVB3 infection (Cheung et al., 2008). Our qPCR analysis showed that γ-catenin-induced suppression of Wnt signaling reduced the transcriptional level of MMP9, but that CVB3 infection rescued this reduction. These data are consistent with the above-mentioned reports. In addition, c-myc was also decreased by the overexpression of γ-catenin and recovered by CVB3 infection. In summary, our data support the previous reports that γ-catenin plays an inhibitory role in Wnt/β-catenin signaling.

In searching for the central role of γ-catenin in viral pathogenesis, we found that γ-catenin overexpression reduced CVB3 particle formation, suggesting an antiviral effect for γ-catenin. To reveal the underlying mechanism by which γ-catenin activates an antiviral effect during CVB3 infection, we focused on the type I interferon response. This is because type I IFNs are produced early during viral infection; mice deficient in type I IFN receptor display delayed CVB3 clearance and accelerated myocardial disease, and die more rapidly than wild-type mice (Wessely et al., 2001; Althof et al., 2014). More importantly, β-catenin and γ-catenin have recently been reported to be important regulators in innate immune response, suppressing influenza A virus through induction of expression of IFNB1 and its related genes, such as RIG-1, MDA5, MAVS, etc. (Hillesheim et al., 2014). Similarly, our data demonstrated that γ-catenin significantly enhanced the expression of interferon-β by activating the MDA5/MAVS pathway. MDA5, like RIG-1, is an important mediator of intracellular viral nucleic acid sensing and uses the signaling adaptor (MAVS) to coordinate the activation of interferon regulatory factor-3 to induce the production of the type I IFNs (Kawai et al., 2005; Seth et al., 2005). MDA5 and RIG-I both consist of a C-terminal DEXD/H-box RNA-helicase domain and an N-terminal caspase recruitment domain and can induce IFN gene transcription in response to dsRNA (Yoneyama et al., 2005). CVB3, as a single-stranded RNA virus, replicates its genome via production of a dsRNA intermediate. Thus, MDA5 likely plays a role in the immune response to CVB3 infection, inducing IFN gene transcription upon recognition of the CVB3 dsRNA intermediate. Finally, we also determined the expression of another IFN-stimulated gene, ISG15, a small ubiquitin family protein playing an important antiviral role via ubiquitin-like modification of viral or host proteins (Loeb and Haas, 1992; Albert et al., 2018). ISG15 has been shown to defend against heart failure in virus-induced cardiomyopathy (Rahnefeld et al., 2014). We therefore also measured the expression of ISG15 as the target gene of type I interferon response. As expected, ISG15 was dramatically increased during CVB3 infection; however, when γ-catenin was silenced with siRNAs, the ISG15 expression levels were reduced to their basal level in both CVB3-infected and sham-infected cells. These data, combined with the detection of other ISG gene expression, indicate that γ-catenin expression suppresses CVB3 replication via induction of the type I IFN signaling and activation of antiviral ISGs.

CONCLUSION

We have provided the first evidence on how CVB3 destroys the integrity of desmosome by cleaving DSC-2 and DSG-2. The destruction of desmosomal cadherins causes γ-catenin to be released into the cytosol for further degradation via the ubiquitin-proteasome pathway. Since γ-catenin executes its anti-CVB3 function through activation of the IFN-β immune response, virus-induced degradation of γ-catenin benefits CVB3 replication, enhancing viral pathogenicity. Based on this new understanding of the underlying mechanism by which CVB3 infection causes direct damage or death of cardiomyocytes, searching for novel inhibitors to block cleavage and prevent γ-catenin degradation could be an effective strategy for therapeutic intervention to protect the integrity of the myocardium and treat viral myocarditis.

DATA AVAILABILITY STATEMENT

All datasets generated for this study are included in the article/**Supplementary Material**.

ETHICS STATEMENT

The animal study was reviewed and approved by the Animal Care Committee, Faculty of Medicine, University of British Columbia. Animal work was conducted by strictly following the Guide to the Care and Use of Experimental Animals – Canadian Council on Animal Care.

AUTHOR CONTRIBUTIONS

DY, XY, and GZ conceived the study. GZ, HZ, and YQ conducted the experiments and data analyses. GZ and DY wrote the manuscript. All authors read and approved the final manuscript.

FUNDING

This work was supported by grants from the Heart and Stroke Foundation of Canada and the National Science and Engineering Research Council of Canada. Funding support for the confocal microscope was provided by the Canadian Foundation for Innovation (Grant #31080) to the Imaging and Biophysics Core, Centre for Heart Lung Innovation.

ACKNOWLEDGMENTS

We thank Drs. Eric Jan and Honglin Luo, University of British Columbia, for providing recombinant 2A and 3C proteases, respectively.

SUPPLEMENTARY MATERIAL

The Supplementary Material for this article can be found online at: https://www.frontiersin.org/articles/10.3389/fmicb.2020.00767/full#supplementary-material

REFERENCES

Albert, M., Becares, M., Falqui, M., Fernandez-Lozano, C., and Guerra, S. (2018). ISG15, a Small Molecule with Huge Implications: regulation of Mitochondrial Homeostasis. *Viruses* 10:E629.

Althof, N., Harkins, S., Kemball, C. C., Flynn, C. T., Alirezaei, M., and Whitton, J. L. (2014). In vivo ablation of type I interferon receptor from cardiomyocytes delays coxsackieviral clearance and accelerates myocardial disease. *J. Virol.* 88, 5087–5099.

Blom, N., Hansen, J., Blaas, D., and Brunak, S. (1996). Cleavage site analysis in picornaviral polyproteins: discovering cellular targets by neural networks. *Protein Sci.* 5, 2203–2216.

Campuzano, O., Alcalde, M., Allegue, C., Iglesias, A., Garcia-Pavia, P., Partemi, S., et al. (2013). Genetics of arrhythmogenic right ventricular cardiomyopathy. *J. Med. Genet.* 50, 280–289.

Carvajal-Huerta, L. (1998). Epidermolytic palmoplantar keratoderma with woolly hair and dilated cardiomyopathy. *J. Am. Acad. Dermatol.* 39, 418–421.

Cheung, C., Marchant, D., Walker, E. K., Luo, Z., Zhang, J., Yanagawa, B., et al. (2008). Ablation of matrix metalloproteinase-9 increases severity of viral myocarditis in mice. *Circulation* 117, 1574–1582.

Davies, M. J., and McKenna, W. J. (1994). Dilated cardiomyopathy: an introduction to pathology and pathogenesis. *Br. Heart J.* 72, S24.

Fairweather, D., Stafford, K. A., and Sung, Y. K. (2012). Update on coxsackievirus B3 myocarditis. *Curr. Opin. Rheumatol.* 24, 401–407.

Foulquier, S., Daskalopoulos, E. P., Lluri, G., Hermans, K. C. M., Deb, A., and Blankesteijn, W. M. (2018). WNT signaling in cardiac and vascular disease. *Pharmacol. Rev.* 70, 68–141.

Freise, C., Kretzschmar, N., and Querfeld, U. (2016). Wnt signaling contributes to vascular calcification by induction of matrix metalloproteinases. *BMC Cardiovasc. Disord.* 16:185. doi: 10.1186/s12872-016-0362-8

Henke, A., Launhardt, H., Klement, K., Stelzner, A., Zell, R., and Munder, T. (2000). Apoptosis in coxsackievirus B3-caused diseases: interaction between the capsid protein VP2 and the proapoptotic protein siva. *J. Virol.* 74, 4284–4290.

Hillesheim, A., Nordhoff, C., Boergeling, Y., Ludwig, S., and Wixler, V. (2014). beta-catenin promotes the type I IFN synthesis and the IFN-dependent signaling response but is suppressed by influenza A virus-induced RIG-I/NF-kappaB signaling. *Cell Commun. Signal.* 12, 29.

Jagdeo, J. M., Dufour, A., Klein, T., Solis, N., Kleifeld, O., Kizhakkedathu, J., et al. (2018).N-terminomics TAILS identifies host cell substrates of poliovirus and coxsackievirus B3 3C proteinases that modulate virus infection. *J. Virol.* 92:e02211-17.

Jensen, K. J., Garmaroudi, F. S., Zhang, J., Lin, J., Boroomand, S., Zhang, M., et al. (2013). An ERK-p38 subnetwork coordinates host cell apoptosis and necrosis during coxsackievirus B3 infection. *Cell Host Microbe.* 13, 67–76.

Kawai, T., Takahashi, K., Sato, S., Coban, C., Kumar, H., Kato, H., et al. (2005). IPS-1, an adaptor triggering RIG-I- and Mda5-mediated type I interferon induction. *Nat. Immunol.* 6, 981–988.

Kowalczyk, A. P., Hatzfeld, M., Bornslaeger, E. A., Kopp, D. S., Borgwardt, J. E., Corcoran, C. M., et al. (1999). The head domain of plakophilin-1 binds to desmoplakin and enhances its recruitment to desmosomes. Implications for cutaneous disease. *J. Biol. Chem.* 274, 18145–18148.

Kowalczyk, A. P., Palka, H. L., Luu, H. H., Nilles, L. A., Anderson, J. E., Wheelock, M. J., et al. (1994). Posttranslational regulation of plakoglobin expression. Influence of the desmosomal cadherins on plakoglobin metabolic stability. *J. Biol. Chem.* 269, 31214–31223.

Laitinen, O. H., Svedin, E., Kapell, S., Nurminen, A., Hytonen, V. P., and Flodstrom-Tullberg, M. (2016). Enteroviral proteases: structure, host interactions and pathogenicity. *Rev. Med. Virol.* 26, 251–267.

Li, J., and Radice, G. L. (2010). A new perspective on intercalated disc organization: implications for heart disease. *Dermatol. Res. Pract.* 2010:207835.

Loeb, K. R., and Haas, A. L. (1992). The interferon-inducible 15-kDa ubiquitin homolog conjugates to intracellular proteins. *J. Biol. Chem.* 267, 7806–7813.

Lombardi, R., da Graca Cabreira-Hansen, M., Bell, A., Fromm, R. R., Willerson, J. T., and Marian, A. J. (2011). Nuclear plakoglobin is essential for differentiation of cardiac progenitor cells to adipocytes in arrhythmogenic right ventricular cardiomyopathy. *Circ. Res.* 109, 1342–1353.

Maeda, O., Usami, N., Kondo, M., Takahashi, M., Goto, H., Shimokata, K., et al. (2004). Plakoglobin (gamma-catenin) has TCF/LEF family-dependent transcriptional activity in beta-catenin-deficient cell line. *Oncogene* 23, 964–972.

Manring, H. R., Dorn, L. E., Ex-Willey, A., Accornero, F., and Ackermann, M. A. (2018). At the heart of inter- and intracellular signaling: the intercalated disc. *Biophys. Rev.* 10, 961–971.

Martin, U., Jarasch, N., Nestler, M., Rassmann, A., Munder, T., Seitz, S., et al. (2007). Antiviral effects of pan-caspase inhibitors on the replication of coxsackievirus B3. *Apoptosis* 12, 525–533.

Mason, J. W. (2003). Myocarditis and dilated cardiomyopathy: an inflammatory link. *Cardiovasc. Res.* 60, 5–10.

McManus, B. M., Chow, L. H., Wilson, J. E., Anderson, D. R., Gulizia, J. M., Gauntt, C. J., et al. (1993). Direct myocardial injury by enterovirus: a central role in the evolution of murine myocarditis. *Clin. Immunol. Immunopathol.* 68, 159–169.

Miravet, S., Piedra, J., Miro, F., Itarte, E., Garcia, de Herreros, A., et al. (2002). The transcriptional factor Tcf-4 contains different binding sites for beta-catenin and plakoglobin. *J. Biol. Chem.* 277, 1884–1891.

Nava, P., Laukoetter, M. G., Hopkins, A. M., Laur, O., Gerner-Smidt, K., Green, K. J., et al. (2007). Desmoglein-2: a novel regulator of apoptosis in the intestinal epithelium. *Mol. Biol. Cell* 18, 4565–4578.

Qiu, Y., Ye, X., Zhang, H. M., Hanson, P., Zhao, G., Tong, L., et al. (2017). Cleavage of osmosensitive transcriptional factor NFAT5 by coxsackieviral protease 2A promotes viral replication. *PLoS Pathog.* 13:e1006744. doi: 10.1371/journal.ppat.1006744

Rahnefeld, A., Klingel, K., Schuermann, A., Diny, N. L., Althof, N., Lindner, A., et al. (2014). Ubiquitin-like protein ISG15 (interferon-stimulated gene of 15 kDa) in host defense against heart failure in a mouse model of virus-induced cardiomyopathy. *Circulation* 130, 1589–1600.

Rao, B. H., Reddy, I. S., and Chandra, K. S. (1996). Familial occurrence of a rare combination of dilated cardiomyopathy with palmoplantar keratoderma and curly hair. *Indian Heart J.* 48, 161–162.

Rasmussen, T. B., Nissen, P. H., Palmfeldt, J., Gehmlich, K., Dalager, S., Jensen, U. B., et al. (2014). Truncating plakophilin-2 mutations in arrhythmogenic cardiomyopathy are associated with protein haploinsufficiency in both myocardium and epidermis. *Circ. Cardiovasc. Genet.* 7, 230–240.

Seth, R. B., Sun, L., Ea, C. K., and Chen, Z. J. (2005). Identification and characterization of MAVS, a mitochondrial antiviral signaling protein that activates NF-kappaB and IRF 3. *Cell* 122, 669–682.

Sheikh, F., Ross, R. S., and Chen, J. (2009). Cell-cell connection to cardiac disease. *Trends Cardiovasc. Med.* 19, 182–190.

Shimizu, M., Fukunaga, Y., Ikenouchi, J., and Nagafuchi, A. (2008). Defining the roles of beta-catenin and plakoglobin in LEF/T-cell factor-dependent transcription using beta-catenin/plakoglobin-null F9 cells. *Mol. Cell. Biol.* 28, 825–835.

Skern, T., and Liebig, H. D. (1994). Picornains 2A and 3C. *Methods Enzymol.* 244, 583–595.

Sohier, P., Legrand, L., Aktary, Z., Grill, C., Delmas, V., Bernex, F., et al. (2018). A histopathological classification system of Tyr::NRAS(Q61K) murine melanocytic lesions: a reproducible simplified classification. *Pigment Cell Melanoma Res.* 31, 423–431.

Vermij, S. H., Abriel, H., and van Veen, T. A. (2017). Refining the molecular organization of the cardiac intercalated disc. *Cardiovasc. Res.* 113, 259–275.

Wang, H., Ducournau, C., Saydaminova, K., Richter, M., Yumul, R., Ho, M., et al. (2015). Intracellular signaling and desmoglein 2 shedding triggered by human adenoviruses Ad3, Ad14, and Ad14P1. *J. Virol.* 89, 10841–10859.

Wessely, R., Klingel, K., Knowlton, K. U., and Kandolf, R. (2001). Cardioselective infection with coxsackievirus B3 requires intact type I interferon signaling: implications for mortality and early viral replication. *Circulation* 103, 756–761.

Wu, D., and Pan, W. (2010). GSK3: a multifaceted kinase in Wnt signaling. *Trends Biochem. Sci.* 35, 161–168.

Yang, D., Cheung, P., Sun, Y., Yuan, J., Zhang, H., Carthy, C. M., et al. (2003). A shine-dalgarno-like sequence mediates in vitro ribosomal internal entry and subsequent scanning for translation initiation of coxsackievirus B3 RNA. *Virology* 305, 31–43.

Ye, X., Zhang, H. M., Qiu, Y., Hanson, P. J., Hemida, M. G., Wei, W., et al. (2014). Coxsackievirus-induced miR-21 disrupts cardiomyocyte interactions via the downregulation of intercalated disk components. *PLoS Pathog.* 10:e1004070. doi: 10.1371/journal.ppat.1004070

Yoneyama, M., Kikuchi, M., Matsumoto, K., Imaizumi, T., Miyagishi, M., Taira, K., et al. (2005). Shared and unique functions of the DExD/H-box helicases RIG-I, MDA5, and LGP2 in antiviral innate immunity. *J. Immunol.* 175, 2851–2858.

Yuan, J., Cheung, P. K., Zhang, H. M., Chau, D., and Yang, D. (2005a). Inhibition of coxsackievirus B3 replication by small interfering RNAs requires perfect sequence match in the central region of the viral positive strand. *J. Virol.* 79, 2151–2159.

Yuan, J., Zhang, J., Wong, B. W., Si, X., Wong, J., Yang, D., et al. (2005b). Inhibition of glycogen synthase kinase 3beta suppresses coxsackievirus-induced cytopathic effect and apoptosis via stabilization of beta-catenin. *Cell Death Differ.* 12, 1097–1106.

Yulis, M., Quiros, M., Hilgarth, R., Parkos, C. A., and Nusrat, A. (2018). Intracellular Desmoglein-2 cleavage sensitizes epithelial cells to apoptosis in response to pro-inflammatory cytokines. *Cell Death Dis.* 9:389.

Zhang, H. M., Qiu, Y., Zhao, G., Wang, H., Chen, Y. T., Aghakeshmiri, S., et al. (2020). Cleavage and degradation of EDEM1 promotes coxsackievirus B3 replication via ATF6a-mediated unfolded protein response signalling. *Cell Microbiol.* e13198.

Zhao, G., Qiu, Y., Zhang, H. M., and Yang, D. (2019). Intercalated discs: cellular adhesion and signaling in heart health and diseases. *Heart Fail Rev.* 24, 115–132.

Zhurinsky, J., Shtutman, M., and Ben-Ze'ev, A. (2000a). Differential mechanisms of LEF/TCF family-dependent transcriptional activation by beta-catenin and plakoglobin. *Mol. Cell. Biol.* 20, 4238–4252.

Zhurinsky, J., Shtutman, M., and Ben-Ze'ev, A. (2000b). Plakoglobin and beta-catenin: protein interactions, regulation and biological roles. *J. Cell Sci.* 113(Pt 18), 3127–3139.

Conflict of Interest: The authors declare that the research was conducted in the absence of any commercial or financial relationships that could be construed as a potential conflict of interest.

Copyright © 2020 Zhao, Zhang, Qiu, Ye and Yang. This is an open-access article distributed under the terms of the Creative Commons Attribution License (CC BY). The use, distribution or reproduction in other forums is permitted, provided the original author(s) and the copyright owner(s) are credited and that the original publication in this journal is cited, in accordance with accepted academic practice. No use, distribution or reproduction is permitted which does not comply with these terms.

frontiers in Microbiology

ORIGINAL RESEARCH
published: 19 May 2020
doi: 10.3389/fmicb.2020.00986

Distinct Cell Transcriptomic Landscapes Upon Henipavirus Infections

Mingyue Chen[1,2,3], Mary Tachedjian[2], Glenn A. Marsh[4], Jie Cui[2,3] and Lin-Fa Wang[4,5]**

[1] Key Laboratory of Fermentation Engineering, National 111 Center for Cellular Regulation and Molecular Pharmaceutics, Hubei University of Technology, Wuhan, China, [2] CAS Key Laboratory of Molecular Virology and Immunology, Institut Pasteur of Shanghai, Chinese Academy of Sciences, Shanghai, China, [3] Center for Biosafety Mega-Science, Wuhan Institute of Virology, Chinese Academy of Sciences, Wuhan, China, [4] Australian Animal Health Laboratory, CSIRO Health and Biosecurity, Geelong, VIC, Australia, [5] Programme in Emerging Infectious Diseases, Duke-NUS Medical School, Singapore, Singapore

Hendra virus (HeV) and Cedar virus (CedV) are henipaviruses, which fall into the *Paramyxoviridae* family of single-stranded, negative-sense RNA viruses. HeV is classified as a Biosafety Level-4 (BSL-4) agent, as it is highly pathogenic and is often fatal to humans. To date, no HeV prevention or treatment methods for human are available. In contrast, previous experimental infection studies have suggested that CedV is non-pathogenic. Flying foxes (pteropid bats) in Australia are the natural reservoirs of both viruses, but the cellular responses of bats to these viral infections remain unclear. Here, we infected bat and human cells with these viruses. We then examined the total transcriptomic landscapes of the cells at 6 or 24 h post infection. Unexpectedly, despite the close phylogenetic relationship between HeV and CedV, there was a dramatic difference in cellular gene expression patterns in response to the two different infections. It is likely that minor differences in the phosphoprotein (P) gene coding strategy between the two viruses cause the observed incongruence in host transcriptomic divergence and viral lethality. This study greatly expands our understanding of the pathogenic mechanisms of henipaviruses.

Keywords: bats (Chiroptera), Hendra virus (HeV), Cedar virus, transcriptomatics, cell infection

OPEN ACCESS

Edited by:
Ahmed Sayed Abdel-Moneim, Taif University, Saudi Arabia

Reviewed by:
Alexander Freiberg, The University of Texas Medical Branch at Galveston, United States
Rekha Khandia, Barkatullah University, India

****Correspondence:***
Jie Cui
jcui@ips.ac.cn
Lin-Fa Wang
linfa.wang@duke-nus.edu.sg

Specialty section:
This article was submitted to Virology, a section of the journal Frontiers in Microbiology

Received: *20 January 2020*
Accepted: *23 April 2020*
Published: *19 May 2020*

Citation:
Chen M, Tachedjian M, Marsh GA, Cui J and Wang L-F (2020) Distinct Cell Transcriptomic Landscapes Upon Henipavirus Infections. Front. Microbiol. 11:986. doi: 10.3389/fmicb.2020.00986

INTRODUCTION

Two viruses in the genus *Henipavirus* (Eaton et al., 2006; Marsh et al., 2012), Hendra (HeV) and Nipah (NiV), are the only known Biosafety Level 4 (BSL-4) pathogens in the family *Paramyxoviridae* (Marsh et al., 2012). Both of these viruses cause 40–100% mortality in humans and other animals (Eaton et al., 2006). The natural reservoir of HeV is the Australian flying foxes (pteropid bats) (Field et al., 2001). Another henipaviral species, Cedar virus (CedV), was isolated from fruit bats in Australia (Marsh et al., 2012). HeV has a broad host range as it uses a highly conserved cellular protein, ephrin-B2, as an entry receptor (Marsh et al., 2012; Field, 2016). CedV also uses ephrin-B2 (Marsh et al., 2012). However, CedV and HeV use different coding strategy of the viral phosphoprotein (P) gene, which play fundamental role in antagonizing the innate immune system of the host (Marsh et al., 2012; Glennon et al., 2015). Unlike HeV, P gene of CedV lacks the coding capacity for the highly conserved V and W proteins (**Figure 1A**). V protein could be the

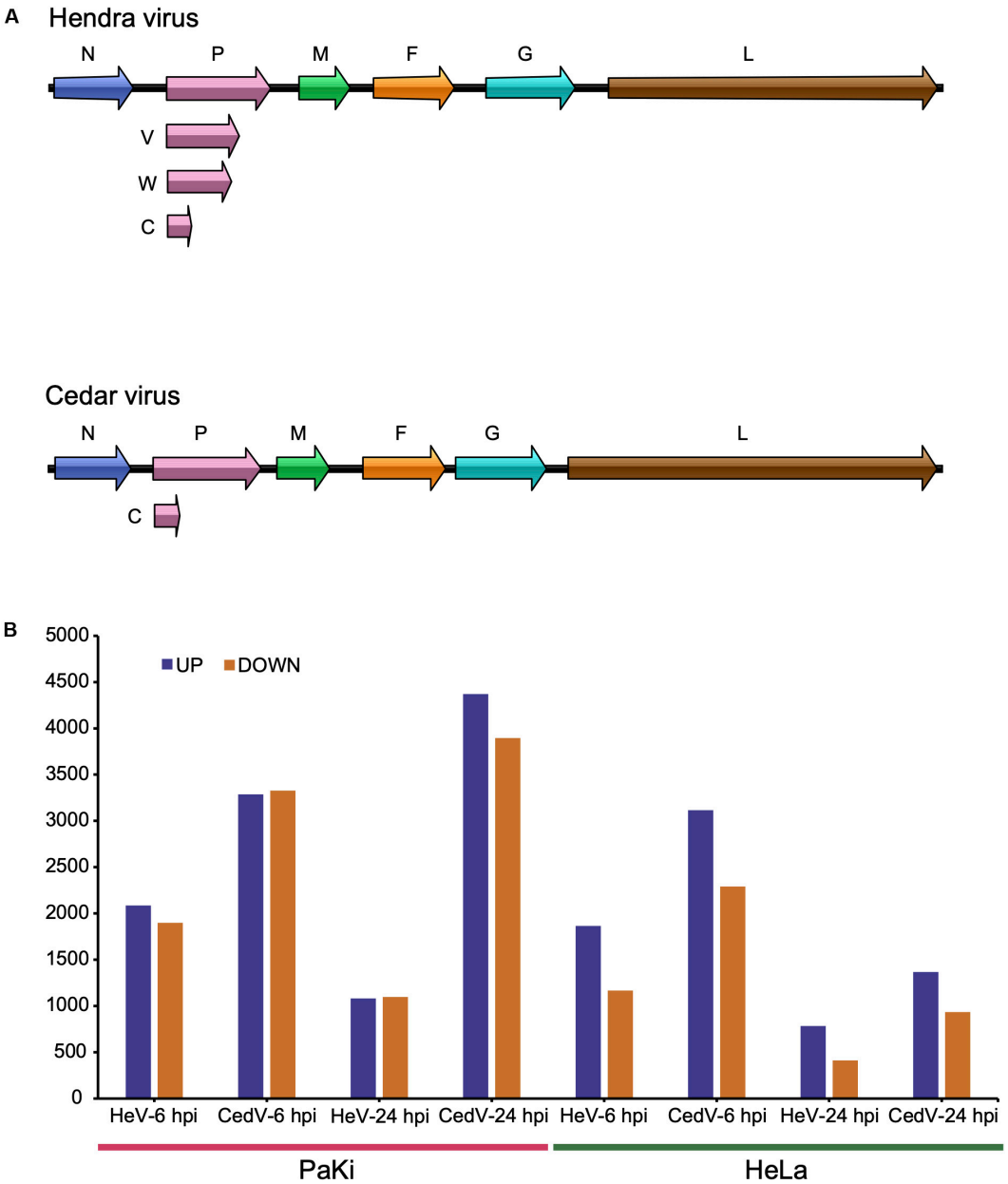

FIGURE 1 | HeV and CedV genome organization and RNA-seq profiles**. (A)** Genome organization of HeV and CedV. **(B)** DEGs in HeV- or CedV-infected HeLa and PaKi cells at 6 and 24 hpi. HeV-6 hpi and CedV-6 hpi represent HeV- or CedV-infected corresponding PaKi or HeLa at 6 hpi. HeV-24 hpi and CedV-24 hpi represent HeV- or CedV-infected corresponding PaKi or HeLa at 24 hpi.

major determinant of pathogenesis while W protein determines the disease course (Satterfield et al., 2015). When ferrets and guinea pigs were experimentally challenged with CedV, viral replication and the generation of neutralizing antibodies were observed, but no clinical disease was identified (Marsh et al., 2012).

Many bat-borne zoonotic viruses are highly pathogenic to spillover hosts, but bats are predominantly clinically asymptomatic and rarely display any signs of disease (Wynne et al., 2014). The mechanisms used by bats to balance the support and control of viral infections remain largely unknown. Transcriptomic profiling of viral infections is ideal for studying these mechanisms. We thus used RNA sequencing (RNA-seq) to identify differences in human and bat cell lines after two periods of infection with either HeV or CedV. Surprisingly, both cell lines exhibited a stronger immune response to CedV than to HeV. Our study provides novel insight into the host response to infection with phylogenetically similar, but pathogenically dissimilar viruses.

RESULTS

Host Gene Transcription Following Infection With HeV or CedV

To explore the effects of HeV and CedV on host gene expression, we used RNA-seq to analyze HeV-, CedV-, or mock-infected immortalized cells lines from bats (PaKi) and humans (HeLa) 6 and 24 h post infection (hpi). Across all infection groups, the most differentially expressed genes (DEGs) were identified in CedV-infected PaKi cells at 24 hpi (4371 genes upregulated and 3896 downregulated, as compared to uninfected PaKi cells; **Figure 1B**). The fewest DEGs were identified in HeV-infected HeLa cells at 24 hpi (784 genes upregulated and 411 downregulated, as compared to uninfected HeLa cells). And more DEGs were identified in the CedV-infected cells than in HeV-infected cells, irrespective of cell type. Therefore, the host response to HeV and CedV differed, with CedV inducing more differential expression of host genes than HeV. In addition, more DEGs were identified in the bat cells than in the human cells, irrespective of infection type.

Pattern Recognition Receptors (PRRs)

PRRs, which include toll-like receptors (TLRs) and retinoic acid inducible gene I (RIG-I) like receptors (RLRs), are vital to the host immune system as they form the first line of defense against infection (Baker et al., 2013). The RLR family comprises RIG-I, melanoma differentiation-associated protein 5 (MDA5), laboratory of genetics and physiology 2 (LGP2) (Satoh et al., 2010). RIG-I, MDA5, LGP2, and TLR3 were significantly upregulated in CedV-infected PaKi and HeLa cells at 24 hpi (**Table 1**). These genes were more strongly upregulated in PaKi cells than in HeLa cells.

NOD-like receptor family CARD domain containing 5 (NLRC5) is an important regulator of MHC class I gene expression (Ranjan et al., 2015). NLRC5 interacts with RIG-I to induce a robust response to the influenza virus; overexpression of NLRC5 resulted in impaired influenza viral replication (Ranjan et al., 2015). Here, NLRC5 was upregulated in CedV-infected PaKi and HeLa cells at 24 hpi, with more differential expression observed in PaKi cells. This indicated that NLRC5 may also interact with RIG-I to impair CedV replication. The presence of highly expressed PRRs in both CedV-infected cell lines suggested that both bats and humans have a strong antiviral response to CedV infection.

Interferon (IFN) Response to Infection

To determine the role of IFNs in the host response to viral infections, RNA-seq reads from PaKi cells (HeV-, CedV-, or mock-infected) were separately mapped to type I IFN locus (three IFN-α, one IFN-β, one IFN-ε, and five IFN-ω), using the type I IFN locus from *Pteropus alecto* as a reference (Zhou et al., 2016). IFN-α1, IFN-α2, IFN-α3, IFN-β, IFN-ω3, IFN-ω4, and IFN-ω5 were highly expressed in CedV-infected PaKi cells at 24 hpi, based on the read depth counts of the IFN transcripts, especially IFN-α2, IFN-α3, IFN-β, and IFN-ω4 (**Figure 2**). In contrast, type I IFN expression in PaKi cells showed little change following HeV infection. RNA-seq reads from PaKi cells were also mapped to the IFN-λ1 and IFN-λ2 genes of *P. Alecto* (Zhou et al., 2011). At 24 hpi with CedV, IFN-λ2 expression in PaKi cells was high, while IFN-λ1 expression was relatively low. Consistent with our results for type I IFN genes, IFN-λ1 and IFN-λ2 expression did not increase in HeV-infected PaKi cells. HeV-, CedV-, or Mock-infected HeLa cells were also mapped against human genome. In CedV-infected HeLa cells, IFN-λ (λ1, λ2, and λ3) and IFN-β were both upregulated at 24 hpi, but no IFN genes were differentially expressed in HeV-infected HeLa cells (**Table 1**).

IFNs stimulate antiviral activity by inducing interferon-stimulated genes (ISGs), including the IFN-induced protein with the tetratricopeptide repeats (IFIT) (Fensterl and Sen, 2015). We examined the expression of IFITs during HeV and CedV infection. IFIT1, IFIT2, IFIT3, and IFIT5 were significantly upregulated in CedV-infected HeLa and PaKi cells (**Table 2**). Indeed, the expression of IFIT1, IFIT2, and IFIT3 increased over 2000-fold in the CedV-infected PaKi cells, as compared to uninfected PaKi cells. Unexpectedly, IFIT1, IFIT2, and IFIT3 were also upregulated in HeV-infected HeLa cells at 24 hpi.

The 2′,5′-oligoadenylate synthetase (OAS) proteins can be induced by type I IFNs (Sadler and Williams, 2008). Consistent with this, OAS2, OAS3, and OASL were significantly upregulated in CedV-infected HeLa and PaKi cells at 24 hpi, with OAS1 upregulated in CedV-infected PaKi cells at 24 hpi. The HeV V and W proteins block IFN production, with V inhibiting MDA5

TABLE 1 | Log2 fold change (log2FC) of DEGs involved in pattern recognition in HeV- or CedV-infected PaKi and HeLa cells.

	PaKi				HeLa			
	HeV-6 hpi[a]	CedV-6 hpi[b]	HeV-24 hpi[c]	CedV-24 hpi[d]	HeV-6 hpi	CedV-6 hpi	HeV-24 hpi	CedV-24 hpi
RIG-I	–	–	–	7.79	–	0.62	–	5.23
MDA5	−0.49	−0.84	0.52	7.51	–	–	1.79	6.36
LGP2	–	–	–	9.68	–	–	–	3.99
TLR3	−0.95	−0.42	0.59	2.14	–	–	0.57	3.02
TLR4	–	–	–	–	0.42	0.83	–	0.36
TLR6	−0.47	-0.38	–	–	−0.30	-0.19	–	–
NLRC5	–	–	–	9.72	–	−0.59	–	0.75

[a]HeV-infected corresponding PaKi or HeLa cell at 6 hpi. [b]CedV-infected corresponding PaKi or HeLa cell at 6 hpi. [c]HeV-infected corresponding PaKi or HeLa cell at 24 hpi. [d]CedV-infected corresponding PaKi or HeLa cell at 24 hpi. [e]The corresponding gene was not differentially expressed.

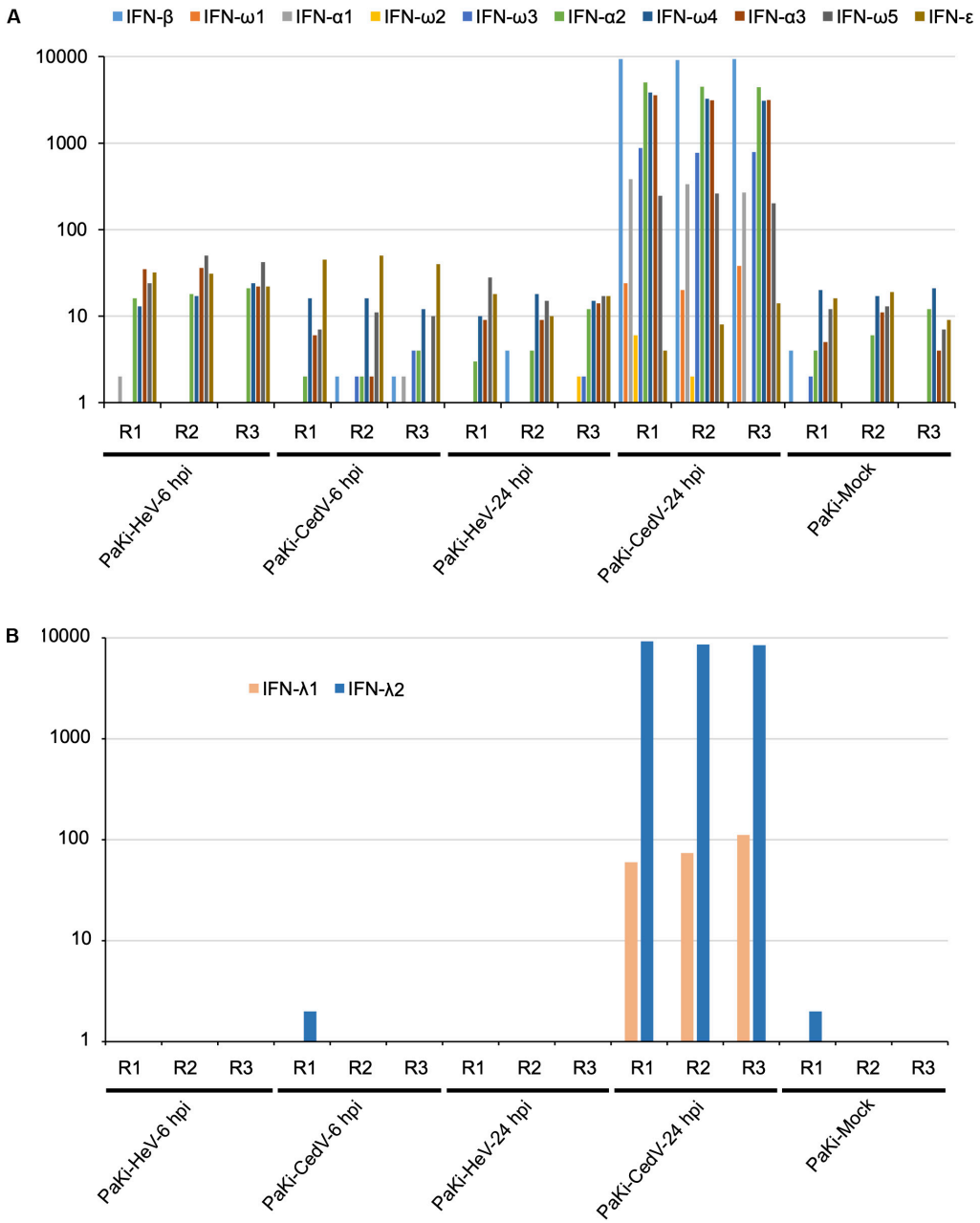

FIGURE 2 | The transcriptional profiles of type I **(A)** and type III **(B)** interferon (IFN) in PaKi cells (HeV-, CedV-, or mock-infected at 6 or 24 hpi). The y-axes indicate the read counts per gene for type I and III IFN locus from *P. alecto*. R1, R2, and R3 represent the three biological replicates.

signaling and W blocking IFN synthesis from TLRs after IFN regulatory factor 3 (IRF3) activation (Glennon et al., 2015). At 24 hpi, MDA5 and TLRs were upregulated in CedV-infected PaKi and HeLa cells, while IRF3 was upregulated in CedV-infected PaKi cells only (**Table 2**).

Apoptosis

Several host mechanisms that prevent viral replication, viral dissemination, or persistent viral infection involve programmed cell death, or apoptosis (Barber, 2001). The extrinsic apoptosis pathway is triggered by the binding of death receptors (TNF receptor 1 (TNFR1), TNF-related apoptosis-inducing ligand (TRAIL) receptor 1/2 (TNFRSF10A/B), and FasL-related receptor Fas to their respective ligands (TNF-α, TRAIL, and FasL) (Cuda et al., 2016). At 24 hpi, the ligands TNF-α and TRAIL, death receptors TNFR1, TNFRSF10B, Fas, as well as apoptosis signaling protein DAXX were upregulated in CedV-infected PaKi cells, suggesting that TNF-α-, TRAIL-, and FasL-mediated apoptosis may be induced (**Figure 3**). And the expression of TNF-α, TRAIL, TNFRSF10B, and DAXX in

TABLE 2 | Log2FC of the DEGs involved in the IFN response to HeV and CedV infection in PaKi and HeLa cells.

	PaKi				HeLa			
	HeV-6 hpi[a]	CedV-6 hpi[b]	HeV-24 hpi[c]	CedV-24 hpi[d]	HeV-6 hpi	CedV-6 hpi	HeV-24 hpi	CedV-24 hpi
IFN-β	N[e]	N	N	N	–[f]	–	–	13.92
IFN-λ1	N	N	N	N	–	–	–	13.36
IFN-λ2	N	N	N	N	–	–	–	10.68
IFN-λ3	N	N	N	N	–	–	–	10.88
IFIT1	–	–	–	11.90	−0.85	−1.50	1.06	5.91
IFIT2	–	–	–	11.96	–	–	1.46	6.53
IFIT3	–	–	–	11.00	0.36	0.60	1.23	5.86
IFIT5	–	−0.81	–	1.86	–	0.51	–	2.85
OAS1	–	–	–	–	–	–	–	3.71
OAS2	–	–	–	8.46	–	–	–	9.31
OAS3	–	−0.62	0.52	5.85	0.54	0.24	0.53	3.66
OASL	–	–	–	11.42	–	–	1.18	5.22
IRF3	–	–	–	0.93	–	–	–	–

[a]HeV-infected corresponding PaKi or HeLa cell at 6 hpi. [b]CedV-infected corresponding PaKi or HeLa cell at 6 hpi. [c]HeV-infected corresponding PaKi or HeLa cell at 24 hpi. [d]CedV-infected corresponding PaKi or HeLa cell at 24 hpi. [e]The expression of corresponding gene was measured based on the read depth counts, and Log2FC of was not calculated. [f]The corresponding gene was not differentially expressed.

CedV-infected PaKi increased more than 3-fold over uninfected PaKi cells (**Table 3**). According to **Table 3**, bat induced a relatively stronger apoptosis response at 24 hpi than at 6 hpi. However, at 24 hpi, in CedV-infected HeLa cells, TNFR1, TNFRSF10A, TNFRSF10B and Fas were only slightly upregulated as compared to uninfected HeLa cells. In addition, few genes were upregulated in HeV-infected PaKi and HeLa cells at 6 and 24 hpi.

Caspase-8 was only upregulated in CedV-infected PaKi and HeLa cells, as well as in HeV-infected PaKi cells at 24 hpi. There was an over 2-fold increase in the expression of caspase-8 in CedV-infected PaKi cells, as compared to uninfected cells. It is therefore probable that CedV sensitizes human and bat cells to TNF-α-, TRAIL-, and FasL-mediated apoptosis more effectively than does HeV (**Figure 3**). The overexpression of caspase-7 indicated that this protein may be also involved in apoptosis-mediated cell death. Caspase-3 was only upregulated in HeV-infected HeLa cells (**Table 3**). At 24 hpi, another pro-apoptotic group of genes (DAXX, RIP1, TRAF2, ASK1, JUN, AP1, and Bim) were induced by over 2-fold in CedV-infected PaKi cells, implying that PaKi cells were also subjected to strong pro-apoptotic signals.

Cytokines

In response to viral infection, target cells produce cytokines and chemokines to control viral replication (Klotman and Chang, 2006). Here, the cytokines IL6, IL8, CCL2, CXCL2, and CXCL16 were upregulated in HeV- or CedV-infected PaKi and HeLa cells at 6 and 24 hpi, suggesting that cytokines may function during HeV or CedV infection in PaKi and HeLa cells. It is notable that more cytokines were significantly upregulated in CedV-infected PaKi cells than in HeV-infected PaKi cells or in HeLa cells infected with either virus at 24 hpi (**Figure 4**). In particular, the expression levels of TNF-α, IL12A, CCL5, and CCL8 increased over 1000-fold in CedV-infected PaKi cells, as compared to uninfected cells. The large number of highly expressed cytokines in CedV-infected PaKi cells suggested that the bat immune system responds strongly to CedV infection.

NF-κB Signaling

The nuclear factor-κB (NF-κB) family of transcription factors regulate innate and acquired host immune responses, and is thus critical for the host response to microbial pathogen infection (Rahman and McFadden, 2011). The mammalian NF-κB proteins are members of the Rel domain-containing protein family: RELA, RELB, c-REL, the NF-κB p105 subunit (NF-κB1), and the NF-κB p100 subunit (NF-κB2). The expression levels of RELA, RELB, c-REL, NF-κB1, NF-κB2, and NF-κB inhibitor-α (IκBα) were affected by HeV and CedV infection in both PaKi and HeLa cells at 6 and 24 hpi, but the majority of these genes were most highly expressed in CedV-infected PaKi cells at 24 hpi (**Supplementary Table S1**). Both TRAF2 and RIP1, which interact with TNFR1 in the classical NF-κB pathway, were highly expressed in CedV-infected PaKi cells at 24 hpi (**Table 3**), suggesting that TNF-α is involved in the activation of NF-κB, leading to the transcription of genes that encode pro-inflammatory and proliferative factors. Thus, both HeV and CedV might induce an immune response in PaKi and HeLa cells via NF-κB signaling. The immune response was strongest in CedV-infected PaKi cells.

JAK–STAT Signaling

The cytokine-activated Janus kinase (JAK)–signal transducer and activator of transcription (STAT) pathway play an important role in the control of immune responses (Shuai and Liu, 2003). Here, JAK2, JAK3, STAT1, STAT2, and STAT3 were over 2-fold upregulated in CedV-infected PaKi cells at 24 hpi. In contrast, at 24 hpi, JAKs and STATs were expressed at relatively low levels in CedV-infected HeLa cells. The expression levels of JAKs and STATs in HeLa and PaKi cells showed little change following HeV infection (**Supplementary Table S2**) at 6 and 24 hpi,

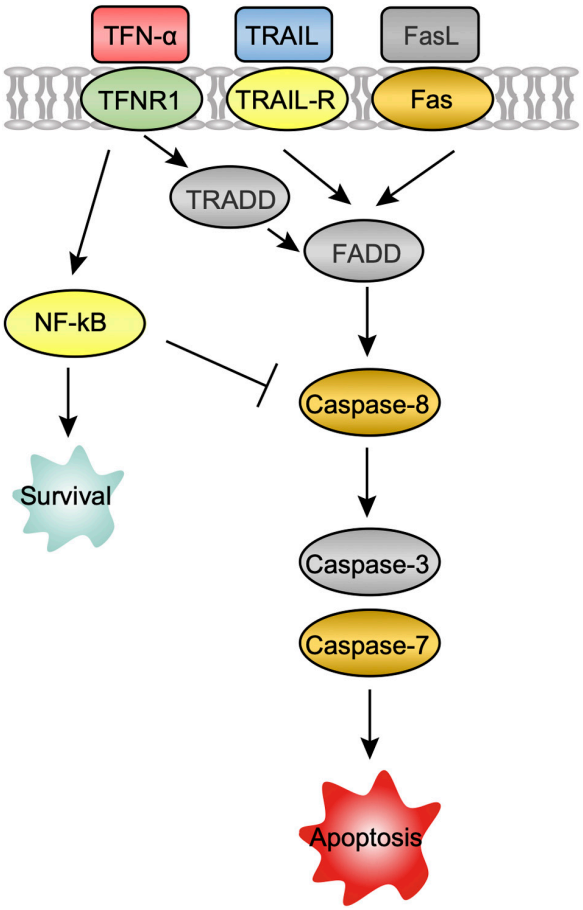

FIGURE 3 | A potential apoptosis pathway in PaKi cells following CedV infection. The challenge groups in which genes were upregulated at 24 hpi are indicated with color. Red: CedV-infected PaKi cells only; Green: CedV-infected HeLa and PaKi cells; Blue: HeV- or CedV-infected PaKi cells; Orange: HeV- or CedV-infected PaKi cells and CedV-infected HeLa cells; Yellow: HeV- or CedV-infected HeLa and PaKi cells. Genes that were not upregulated in any challenge group at 24 hpi are colored gray.

indicating that CedV infection stimulated JAK-STAT signaling but HeV infection might not. Interestingly, the suppressor of cytokine signaling (SOCS) proteins that regulate the JAK-STAT were also upregulated in CedV-infected PaKi cells at 24 hpi (**Supplementary Table S2**). As SOCS inhibits JAK-STAT signaling (Shuai and Liu, 2003), its upregulation indicates a classic negative-feedback loop.

Genes Highly Differentially Expressed Following HeV and CedV Infection

To better understand the functions of genes strongly up- and downregulated post infection, we selected DEGs with > 2-fold changes in expression level in both cell lines after HeV or CedV infection, as compared to uninfected cells. At 24 hpi, CedV-infected PaKi cells had the most DEGs with a > 2-fold change in expression (1441 DEGs upregulated and 1039 downregulated) (**Figure 5**). At 24 hpi, the fewest DEGs with a > 2-fold change in expression were observed in HeV-infected HeLa cells (46 upregulated and 4 downregulated).

We then used Kyoto encyclopedia of genes and genomes (KEGG) pathway enrichment analysis to predict potential interactions among these selected DEGs. Our KEGG pathway analysis indicated that for DEGs with a > 2-fold upregulation the most frequently predicted pathways were the TNF signaling pathway, the NF-κB signaling pathway, and the NOD-like receptor signaling pathway (**Supplementary Table S3**). Notably, all genes significantly upregulated at 6 or 24 hpi in all challenge groups were enriched in the TNF signaling pathway. In addition, selected DEGs upregulated in the HeV-infected PaKi cells, HeV-infected HeLa cells, and CedV-infected HeLa cells were enriched in the NF-κB signaling pathway at 24 hpi. However, CedV-infected PaKi cells were not highly enriched in the NF-κB pathway at 24 hpi. We did not perform a KEGG pathway analysis on the selected DEGs downregulated in the HeV-infected HeLa cells at 24 hpi, as only four genes were highly downregulated. In contrast to the upregulated genes, distinct pathways were enriched in the downregulated DEGs, and there were no shared pathways across the challenge groups (**Supplementary Table S4**).

DISCUSSION

Here, we used the expression profiles of PaKi and HeLa cells infected with HeV or CedV to identify differences in host response to these henipaviruses. We found that host responses to HeV and CedV infection differed dramatically. The large number of DEGs in CedV-infected PaKi cells at 24 hpi indicated that the bat response to CedV infection was strong. In contrast, relatively few DEGs were identified in HeV-infected HeLa cells at 24 hpi. Various immune related proteins (e.g., PRRs, IFNs, and cytokines) and pathways (e.g., apoptosis, NF-κB signaling, and JAK–STAT signaling) were upregulated in PaKi and HeLa cells following CedV infection. The immune response was relatively stronger in PaKi cells than in HeLa cells. One possible explanation for this discrepancy is that the CedV P gene does not encode V and W proteins; these proteins may antagonize host innate immunity, including blocking IFN production (Glennon et al., 2015). Because our results indicated that CedV infection induces interferon expression and other immune signaling pathways in both HeLa and PaKi cells, it is probable that V and W proteins affect several pathways related to immunity.

Previous study showed that no clinical disease was observed when Cedar virus was tested in experimental challenge models in ferrets and guinea pigs (Marsh et al., 2012). One explanation for this is that ferrets and guinea pigs may control viral replication as part of an innate antiviral response, such as PRRs, IFNs, cytokines, and apoptosis-related factors. The immune responses of HeLa and PaKi cells to HeV infection were weak, possibly because V and W proteins were present. This is consistent with a recent study showing that V and W proteins were crucial for pathogenesis and disease progression, respectively (Satterfield et al., 2015).

The greater production of cytokines by CedV-infected PaKi cells compared to HeV-infected PaKi cells observed here was

TABLE 3 | Log2FC of DEGs involved in apoptosis in HeV- or CedV-infected PaKi and HeLa cells.

	PaKi				HeLa			
	HeV-6 hpi[a]	CedV-6 hpi[b]	HeV-24 hpi[c]	CedV-24 hpi[d]	HeV-6 hpi	CedV-6 hpi	HeV-24 hpi	CedV-24 hpi
TNF-α	–[e]	–	–	12.41	–	–	–	–
TRAIL	−1.25	−3.28	0.86	3.47	–	–	–	–
TNFR1	–	0.84	–	0.54	–	–	–	0.38
TNFRSF10A	–	–	–	–	0.74	1.01	–	0.37
TNFRSF10B	1.66	2.52	0.93	3.31	0.45	0.78	0.29	0.32
FAS	–	0.24	0.44	0.95	–	0.54	–	0.76
FADD	–	–	–	−0.30	–	–	–	–
DAXX	0.45	0.45	–	2.29	–	–	–	–
TRADD	–	–	–	–	–	−0.56	–	–
CASP8	–	–	0.45	1.70	–	–	–	0.62
CASP3	–	−0.23	–	−1.04	0.31	0.43	–	–
CASP7	0.93	−0.82	0.31	0.64	0.45	0.63	–	0.93
RIP1	–	–	–	1.11	–	0.28	–	0.33
TRAF2	0.49	0.65	–	1.36	0.61	0.71	–	–
AIP	−0.37	−0.53	–	−0.99	–	0.37	–	–
ASK1	–	−0.62	–	1.47	0.29	–	–	–
JNK1	–	0.95	–	0.27	–	0.39	–	–
JNK2	–	−0.44	–	−0.82	–	–	–	–
JUN	–	−0.34	–	2.11	0.62	0.88	–	0.53
AP1	–	1.23	–	4.01	−0.76	0.38	0.67	0.68
p53	0.37	–	0.42	0.59	−0.95	−0.95	0.32	0.40
Bim	–	1.47	–	1.34	–	0.77	–	0.27

[a]HeV-infected corresponding PaKi or HeLa cell at 6 hpi. [b]CedV-infected corresponding PaKi or HeLa cell at 6 hpi. [c]HeV-infected corresponding PaKi or HeLa cell at 24 hpi. [d]CedV-infected corresponding PaKi or HeLa cell at 24 hpi. [e]The corresponding gene was not differentially expressed.

likely due to the absence of the W protein in CedV, as it has been shown that cells infected with W-deficient NiV produce more cytokines than in cells infected with wild-type NiV (Satterfield et al., 2015). The W protein may control the cytokine response of target endothelial cells, thus affecting disease progression without altering disease lethality (Satterfield et al., 2015). Therefore, although cytokine production may not be directly responsible for the distinct clinical outcomes of HeV and CedV infections, cytokine production may affect disease progression.

Several genes upregulated in HeV-infected HeLa and PaKi cells encoded cytokines or elements of the NF-κB signaling pathway. Moreover, our KEGG pathway analysis of highly upregulated DEGs indicated that the TNF and NF-κB signaling pathways were enriched in HeV-infected HeLa and PaKi cells, suggesting that HeV-infection induced certain innate antiviral responses in both cell lines. Several proteins crucial to apoptosis, such as TRAIL, TNFRSF10B, FAS, CASP7, and CASP8, were upregulated in HeV-infected PaKi cells at 24 hpi, suggesting that HeV infection may trigger apoptosis in PaKi cells. This is consistent with a previous study, which indicated that HeV induces apoptosis in bat cells, but not human cells (Wynne et al., 2014). Both HeV and CedV could induce apoptosis in bat, which implied that apoptosis pathway may contribute to control the viral infection in bat. However, apoptosis could not be induced by HeV in HeLa cells and the immune response is extremely weak compared to HeLa cells infected with CedV, thus may result in divergent clinical outcomes of human infected with HeV or CedV. A comparative analysis based on the relative codon deoptimization index (RCDI) for host adaptation of HeV, CedV, Nipah virus, and Hendra like Mojiang virus revealed that except for dog and hamster, all other evaluated hosts (human, bat, horse, pig, cat, ferret, squirrel monkey, and African green monkey) were most susceptible to HeV while all hosts were least susceptible to CedV (Khandia et al., 2019), which may also provide insight to the distinct clinical outcomes of HeV and CedV. At 24 hpi, the expression levels of IFIT1, IFIT2, and IFIT3 were over 2-fold up-regulated in HeV-infected HeLa cells (**Table 2**), probably because genes such as IRF7 can induce the expression of ISGs in the absence of type I or III IFN (Schmid et al., 2010). In PaKi cells, there were several DEGs (e.g., MDA5, TLR3, IFIT5, TRAIL, and JUN) downregulated at 6 hpi but significantly upregulated at 24 hpi, especially infected with CedV. In general, the host response to viral infection is stronger at 24 hpi than that at 6 hpi. Probably 24 h post infection could be more appropriate to analyze the host response.

We observed several points of similarity between the two viruses. For example, some DNA damage checkpoint and innate immune genes shown to be under positive selection in bats (e.g., p53, c-REL, and RAD50) (Zhang et al., 2013) were upregulated in PaKi cells infected with either virus, suggesting that the certain innate antiviral mechanisms activated by henipaviruses are conserved across bat lineages. In summary, we used RNA-seq to compare bat and human cell lines infected with HeV or CedV. We found that CedV caused a stronger innate immune response

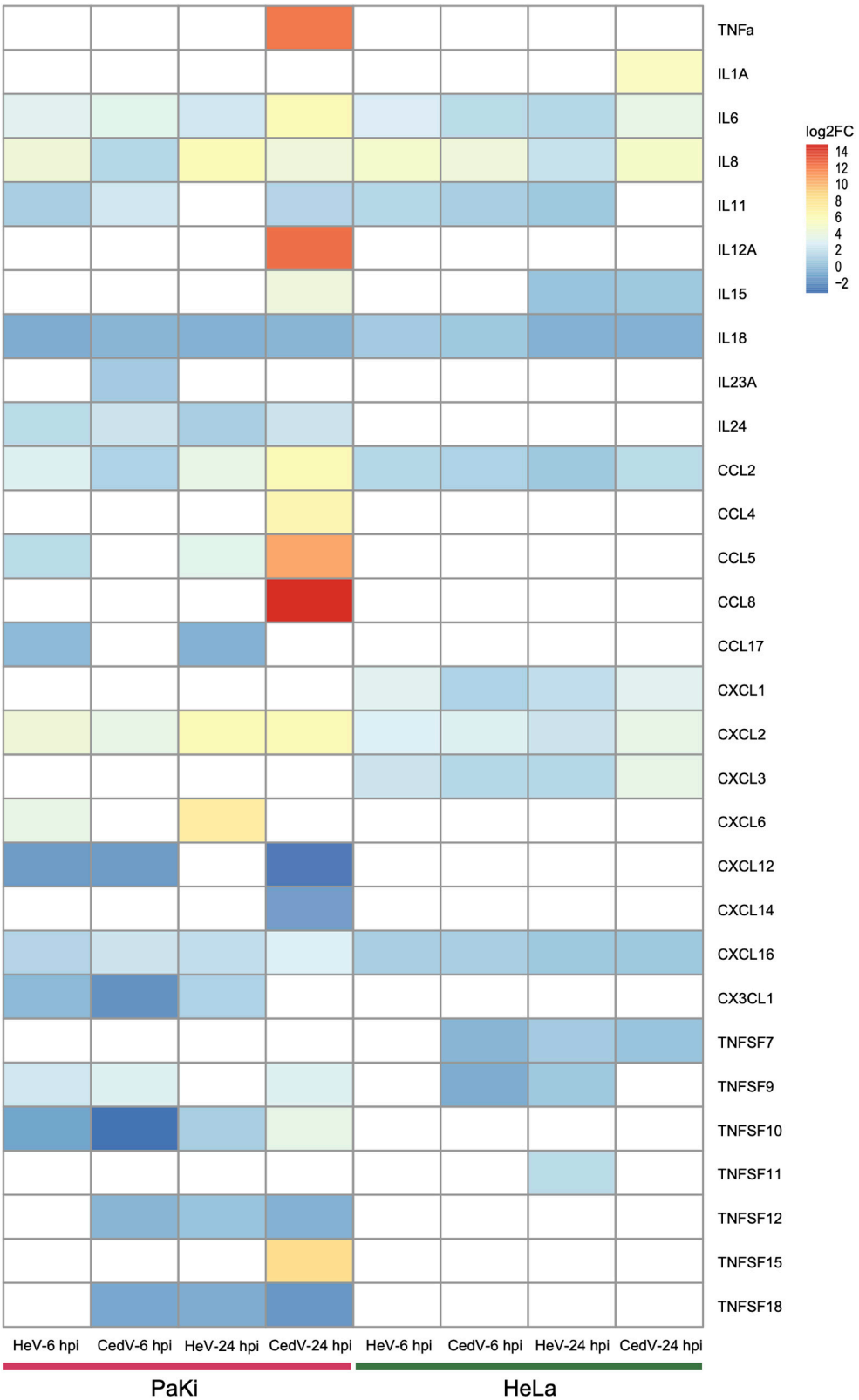

FIGURE 4 | Cytokine expression in HeV- or CedV-infected HeLa and PaKi cells at 6 or 24 hpi. The color scale for log2FC is shown at the top right of the figure. Genes that were not differentially expressed are colored white. HeV-6 hpi and CedV-6 hpi represent HeV- or CedV-infected corresponding PaKi or HeLa at 6 hpi. HeV-24 hpi and CedV-24 hpi represent HeV- or CedV-infected corresponding PaKi or HeLa at 24 hpi.

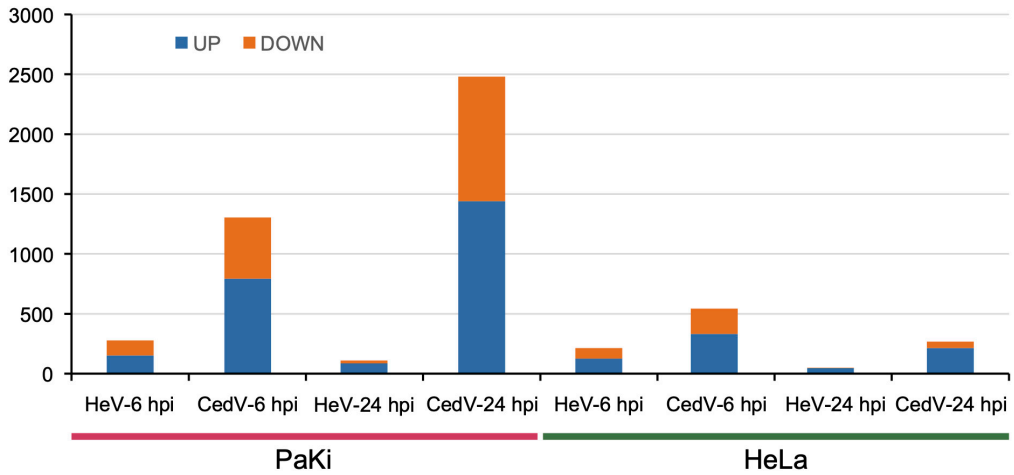

FIGURE 5 | Genes highly up- and downregulated (>2-fold change in expression as compared to uninfected cells) in HeV- or CedV-infected HeLa and PaKi cells at 6 or 24 hpi. HeV-6 hpi and CedV-6 hpi represent HeV- or CedV-infected corresponding PaKi or HeLa at 6 hpi. HeV-24 hpi and CedV-24 hpi represent HeV- or CedV-infected corresponding PaKi or HeLa at 24 hpi.

than did HeV. It is possible that differences in the phosphoprotein gene coding strategy between the two viruses lead to host transcriptomic divergence and alterations in viral lethality. Further work is required to understand how henipaviruses evade the host immune response.

MATERIALS AND METHODS

Cell Culture

The *P. alecto* immortalized kidney-derived PaKi cell line (Crameri et al., 2009) and the human HeLa cell line were used in this study. Cell lines were grown in either Dulbecco's modified Eagle's medium (DMEM)/F12 (PaKiT03) or DMEM GlutaMAX (HeLa), both supplemented with 10% (v/v) fetal calf serum (FCS) and 100 U/mL penicillin/streptomycin. All cells were incubated at 37°C in a humidified atmosphere containing 5% CO_2.

HeV and CedV Infection of Bat and Human Cell Lines

All virology work was conducted at the BSL-4 facility of the CSIRO Australian Animal Health Laboratory (Geelong, Australia). Approximately 2×10^7 PaKi and HeLa cells per challenge were mock infected or infected with HeV (Hendra virus/Australia/horse/1994/Hendra) or CedV (Cedar virus/Australia/bat/2009/Cedar) for 6 or 24 h at a MOI of 10. We performed three biological replicates for each challenge in T75cm^2 flasks. All cells were harvested with trypsinization and resuspended in RLT buffer (Qiagen, Hilden, Germany). Mock-infected cells were used as controls.

RNA Isolation, Sequencing, and RNA-Seq Analysis

Total RNA was isolated using the Qiagen RNeasy Mini kit (Qiagen, Hilden, Germany) and treated with DNase I (Qiagen, Hilden, Germany). The quality and quantity of total RNA was assessed using a Bioanalyzer (Agilent, Santa Carla, CA, United States). mRNA was sequenced on an Illumina HiSeq 2000 sequencer (Illumina, San Diego, CA, United States). Adapter sequences were trimmed from the resulting reads. The quality of reads was assessed using FastQC[1]. High-quality reads were mapped to either the *P. alecto* or human genomes using TopHat (version 2.1.1) (Trapnell et al., 2009). Based on the resulting alignments, we assembled our transcripts separately by challenge group. Grouped transcripts were assembled and merged using Cufflinks and Cuffmerge (version 2.2.1) (Trapnell et al., 2012). Differential expression analysis was performed with Cuffdiff (version 2.2.1) (Trapnell et al., 2012). Transcripts with a fragments per kilobase of transcript per million mapped reads (FPKM) value < 1 before or after HeV or CedV infection were discarded. We considered a transcript statistically significant if the FDR-adjusted p-value of the test statistic (q-value) was < 0.05.

Analysis of IFN Expression

As IFN genes are only partially characterized in the *P. alecto* genome, PaKi RNA-seq reads were mapped separately to the *P. alecto* type I IFN locus (Zhou et al., 2016), IFN-λ1 (GenBank accession no. HQ201956.1) and IFN-λ2 (GenBank accession no. HQ201955.1) using bowtie2 (Langmead and Salzberg, 2012). We used these mappings to measure the expression of type I and III IFNs. We used SAMtools to compile and count the number of reads mapped (Li et al., 2009).

Functional Enrichment Analysis

To predict the molecular interactions of the DEGs, we performed KEGG enrichment analysis with KOBAS (Xie et al., 2011), using a hypergeometric test. We considered KEGG pathways with $p < 0.05$ significantly enriched. The -log10 (p-value) indicates

[1]http://www.bioinformatics.babraham.ac.uk/projects/fastqc/

the enrichment score, which represents the significance of the corresponding pathway enrichment.

DATA AVAILABILITY STATEMENT

The original contributions presented in the study are publicly available. This data can be found here: https://bigd.big.ac.cn/gsa, accession number CRA002578.

AUTHOR CONTRIBUTIONS

L-FW and JC designed the research and supervised the experiments. JC, MT, and GM performed the experiments. JC and MC analyzed the data. JC, MC, and L-FW wrote the manuscript.

FUNDING

This study was supported by National Science and Technology Major Project (Grant No. 2018ZX10301101), CAS Pioneer Hundred Talents Program to JC; Singapore National Research Foundation (Grant No. NRF2012NRF-CRP001–056), and CSIRO OCE Science Leader award to L-FW.

SUPPLEMENTARY MATERIAL

The Supplementary Material for this article can be found online at: https://www.frontiersin.org/articles/10.3389/fmicb.2020.00986/full#supplementary-material

REFERENCES

Baker, M. L., Schountz, T., and Wang, L. F. (2013). Antiviral immune responses of bats: a review. *Zoonoses Public Health* 60, 104–116. doi: 10.1111/j.1863-2378.2012.01528.x

Barber, G. N. (2001). Host defense, viruses and apoptosis. *Cell Death Differ.* 8, 113–126. doi: 10.1038/sj.cdd.4400823

Crameri, G., Todd, S., Grimley, S., McEachern, J. A., Marsh, G. A., Smith, C., et al. (2009). Establishment, immortalisation and characterisation of pteropid bat cell lines. *PLoS One* 4:e8266. doi: 10.1371/journal.pone.0008266

Cuda, C. M., Pope, R. M., and Perlman, H. (2016). The inflammatory role of phagocyte apoptotic pathways in rheumatic diseases. *Nat. Rev. Rheumatol.* 12, 543–558. doi: 10.1038/nrrheum.2016.132

Eaton, B. T., Broder, C. C., Middleton, D., and Wang, L. F. (2006). Hendra and Nipah viruses: different and dangerous. *Nat. Rev. Microbiol.* 4, 23–35. doi: 10.1038/nrmicro1323

Fensterl, V., and Sen, G. C. (2015). Interferon-induced Ifit proteins: their role in viral pathogenesis. *J. Virol.* 89, 2462–2468. doi: 10.1128/jvi.02744-14

Field, H., Young, P., Yob, J. M., Mills, J., Hall, L., and Mackenzie, J. (2001). The natural history of Hendra and Nipah viruses. *Microbes Infect.* 3, 307–314. doi: 10.1016/s1286-4579(01)01384-3

Field, H. E. (2016). Hendra virus ecology and transmission. *Curr. Opin. Virol.* 16, 120–125. doi: 10.1016/j.coviro.2016.02.004

Glennon, N. B., Jabado, O., Lo, M. K., and Shaw, M. L. (2015). Transcriptome profiling of the virus-induced innate immune response in *Pteropus vampyrus* and its attenuation by Nipah virus interferon antagonist functions. *J. Virol.* 89, 7550–7566. doi: 10.1128/JVI.00302-15

Khandia, R., Singhal, S., Kumar, U., Ansari, A., Tiwari, R., Dhama, K., et al. (2019). Analysis of Nipah virus codon usage and adaptation to hosts. *Front. Microbiol.* 10:886. doi: 10.3389/fmicb.2019.00886

Klotman, M. E., and Chang, T. L. (2006). Defensins in innate antiviral immunity. *Nat. Rev. Immunol.* 6, 447–456. doi: 10.1038/nri1860

Langmead, B., and Salzberg, S. L. (2012). Fast gapped-read alignment with Bowtie 2. *Nat. Methods* 9, 357–359. doi: 10.1038/nmeth.1923

Li, H., Handsaker, B., Wysoker, A., Fennell, T., Ruan, J., Homer, N., et al. (2009). The sequence alignment/map format and SAMtools. *Bioinformatics* 25, 2078–2079. doi: 10.1093/bioinformatics/btp352

Marsh, G. A., de Jong, C., Barr, J. A., Tachedjian, M., Smith, C., Middleton, D., et al. (2012). Cedar virus: a novel Henipavirus isolated from Australian bats. *PLoS Pathog.* 8:e1002836. doi: 10.1371/journal.ppat.1002836

Rahman, M. M., and McFadden, G. (2011). Modulation of NF-kappaB signalling by microbial pathogens. *Nat. Rev. Microbiol.* 9, 291–306. doi: 10.1038/nrmicro2539

Ranjan, P., Singh, N., Kumar, A., Neerincx, A., Kremmer, E., Cao, W., et al. (2015). NLRC5 interacts with RIG-I to induce a robust antiviral response against influenza virus infection. *Eur. J. Immunol.* 45, 758–772. doi: 10.1002/eji.201344412

Sadler, A. J., and Williams, B. R. (2008). Interferon-inducible antiviral effectors. *Nat. Rev. Immunol.* 8, 559–568. doi: 10.1038/nri2314

Satoh, T., Kato, H., Kumagai, Y., Yoneyama, M., Sato, S., Matsushita, K., et al. (2010). LGP2 is a positive regulator of RIG-I- and MDA5-mediated antiviral responses. *Proc. Natl. Acad. Sci. U.S.A.* 107, 1512–1517. doi: 10.1073/pnas.0912986107

Satterfield, B. A., Cross, R. W., Fenton, K. A., Agans, K. N., Basler, C. F., Geisbert, T. W., et al. (2015). The immunomodulating V and W proteins of Nipah virus determine disease course. *Nat. Commun.* 6:7483. doi: 10.1038/ncomms8483

Schmid, S., Mordstein, M., Kochs, G., García-Sastre, A., and Tenoever, B. R. (2010). Transcription factor redundancy ensures induction of the antiviral state. *J. Biol. Chem.* 285, 42013–42022. doi: 10.1074/jbc.M110.165936

Shuai, K., and Liu, B. (2003). Regulation of JAK-STAT signalling in the immune system. *Nat. Rev. Immunol.* 3, 900–911. doi: 10.1038/nri1226

Trapnell, C., Pachter, L., and Salzberg, S. L. (2009). TopHat: discovering splice junctions with RNA-Seq. *Bioinformatics* 25, 1105–1111. doi: 10.1093/bioinformatics/btp120

Trapnell, C., Roberts, A., Goff, L., Pertea, G., Kim, D., Kelley, D. R., et al. (2012). Differential gene and transcript expression analysis of RNA-seq experiments with TopHat and Cufflinks. *Nat. Protoc.* 7, 562–578. doi: 10.1038/nprot.2012.016

Wynne, J. W., Shiell, B. J., Marsh, G. A., Boyd, V., Harper, J. A., Heesom, K., et al. (2014). Proteomics informed by transcriptomics reveals Hendra virus sensitizes bat cells to TRAIL-mediated apoptosis. *Genome Biol.* 15:532. doi: 10.1186/PREACCEPT-1718798964145132

Xie, C., Mao, X., Huang, J., Ding, Y., Wu, J., Dong, S., et al. (2011). KOBAS 2.0: a web server for annotation and identification of enriched pathways and diseases. *Nucleic Acids Res.* 39, W316–W322. doi: 10.1093/nar/gkr483

Zhang, G., Cowled, C., Shi, Z., Huang, Z., Bishop-Lilly, K. A., Fang, X., et al. (2013). Comparative analysis of bat genomes provides insight into the evolution of flight and immunity. *Science* 339, 456–460. doi: 10.1126/science.1230835

Zhou, P., Cowled, C., Todd, S., Crameri, G., Virtue, E. R., Marsh, G. A., et al. (2011). Type III IFNs in pteropid bats: differential expression patterns provide evidence for distinct roles in antiviral immunity. *J. Immunol.* 186, 3138–3147. doi: 10.4049/jimmunol.1003115

Zhou, P., Tachedjian, M., Wynne, J. W., Boyd, V., Cui, J., Smith, I., et al. (2016). Contraction of the type I IFN locus and unusual constitutive expression of IFN-alpha in bats. *Proc. Natl. Acad. Sci. U.S.A.* 113, 2696–2701. doi: 10.1073/pnas.1518240113

Conflict of Interest: The authors declare that the research was conducted in the absence of any commercial or financial relationships that could be construed as a potential conflict of interest.

Copyright © 2020 Chen, Tachedjian, Marsh, Cui and Wang. This is an open-access article distributed under the terms of the Creative Commons Attribution License (CC BY). The use, distribution or reproduction in other forums is permitted, provided the original author(s) and the copyright owner(s) are credited and that the original publication in this journal is cited, in accordance with accepted academic practice. No use, distribution or reproduction is permitted which does not comply with these terms.

frontiers in Microbiology

OPINION
published: 21 May 2020
doi: 10.3389/fmicb.2020.00810

Canine Distemper Virus (CDV) Transit Through the Americas: Need to Assess the Impact of CDV Infection on Species Conservation

Santiago Rendon-Marin[1], *Marlen Martinez-Gutierrez*[1,2], *José Antonio Suarez*[3] and *Julian Ruiz-Saenz*[1,4*†]

[1] Grupo de Investigación en Ciencias Animales—GRICA, Universidad Cooperativa de Colombia, Bucaramanga, Colombia, [2] Infettare, Facultad de Medicina, Universidad Cooperativa de Colombia, Medellín, Colombia, [3] Investigador SNI Senacyt Panamá, Clinical Research Deparment, Instituto Conmemorativo Gorgas de Estudios de la Salud, Panama City, Panama, [4] Asociación Colombiana de Virología, Bogotá, Colombia

OPEN ACCESS

Edited by:
Ahmed Sayed Abdel-Moneim, Taif University, Saudi Arabia

Reviewed by:
Sara Louise Cosby, Agri-Food and Biosciences Institute (AFBI), United Kingdom
Fumio Seki, National Institute of Infectious Diseases, Japan

***Correspondence:**
Julian Ruiz-Saenz
julianruizsaenz@gmail.com; julian.ruizs@campusucc.edu.co

†ORCID:
Julian Ruiz-Saenz
orcid.org/0000-0002-1447-1458

Specialty section:
This article was submitted to Virology, a section of the journal Frontiers in Microbiology

Received: *12 February 2020*
Accepted: *06 April 2020*
Published: *21 May 2020*

Citation:
Rendon-Marin S, Martinez-Gutierrez M, Suarez JA and Ruiz-Saenz J (2020) Canine Distemper Virus (CDV) Transit Through the Americas: Need to Assess the Impact of CDV Infection on Species Conservation. Front. Microbiol. 11:810. doi: 10.3389/fmicb.2020.00810

Keywords: canine distemper, conservation, interspecies transmission, morbillivirus, wildlife corridors

Canine Morbillivirus (also known as Canine Distemper Virus—CDV) is the causative agent of one of the most important diseases in domestic dogs and wild fauna. It belongs to the *Paramyxoviridae* family, order *Mononegavirales*, which has a non-segmented, single-stranded linear negative polarity RNA genome (Lamb and Parks, 2013). The clinical disease is characterized by moderate to severe respiratory signs, gastrointestinal issues, immune suppression, and/or neurological disease (De Vries et al., 2015; Pfeffermann et al., 2018).

Beyond domestic dogs (*Canis lupus familiaris*), CDV infects multiple species within the Order Carnivora, including several wild species as *Canidae*, *Felidae*, *Procyonidae*, *Mustelidae*, *Hyaenidae*, *Ursidae*, and *Viverridae* families. CDV infection has also been reported in other Orders such as Rodentia (rodents), Primates, Artiodactyla, and Proboscidea (Martinez-Gutierrez and Ruiz-Saenz, 2016). More recently, CDV has been confirmed as the etiological agent of clinical illness in two different families of the Order Pilosa in South America and in one in North America. The first case was reported on a captive southern tamandua (*Tamandua tetradactyla*) with neurological signs (Lunardi et al., 2018). The other case was described in a young giant anteater, showing prostration, nasal, and eye discharge (*Myrmecophaga tridactyla*). Both of these belong to the *Myrmecophagidae* Family (Debesa Belizario Granjeiro et al., 2020). Also, in the USA, a Linnaeus's 2-toed sloth (*Choloepus didactylus*), family *Choloepodidae*, order Pilosa, was reported with clinical signs that included hyporexia, lethargy, mucopurulent nasal discharge, and oral and facial ulcers confirmed as CDV South America/North America-4 lineage (Watson et al., 2020). However, the complete distribution of different CDV strains and Lineages among wildlife species throughout the Americas have not been thoroughly investigated.

Phylogenetic analysis has demonstrated the circulation of a new CDV lineage in the Americas. Classified as "South America/North America-4" due to its intercontinental distribution and the monophyletic grouping, strains have been isolated in dogs from Ecuador and Colombia (South America) and wild and domestic dogs in the United States (North America) (Duque-Valencia et al., 2019a). As plylogeography confirmed, the "South America/North America-4" lineage circulated first in Colombia and Ecuador, then in the United States, and again in Colombia [see Figures 3, 4 in Duque-Valencia et al. (2019a)]. It has been stated that the uncontrolled commercialization of puppies from South America to the United States could be the route of transmission of the "South America/North America-4" lineage among these two continent regions; the role of wildlife in virus dissemination throughout the entire continent can also not be ruled out.

In this context, it is important to understand the impact of the intercontinental transmission of CDV, since the implementation of control policies should cross borders and generate unified international policies that prevent the presentation of cases in domestic and wild fauna. This type of regional disease control program has proven to face multiple challenges in political interaction between countries and requires the leadership of multilateral entities to help unify criteria and policies (Hukic et al., 2010; Sleeman et al., 2017).

On the other hand, wildlife corridors are connections across the landscape that link up areas of habitats, which supports natural processes, including the movement of species to find resources such as food and water (Chetkiewicz et al., 2006). Corridors are species and process specific (e.g., migration and dispersal). They do not necessarily consist of breeding habitats, but rather are intended to provide connectivity between habitat patches (Beier et al., 2008). Different corridors have been designed to protect wild fauna among the Americas. The Mesoamerican Biological Corridor (Holland, 2012) or the Jaguar Corridor Initiative (Zeller et al., 2013) are a wide range of initiatives to protect species and habitats through maintaining or enhancing connectivity between populations, which contributes to the survival of the species by allowing the dispersion of individuals from their native ranges to new territories, enabling the exchange of genetic material among different isolated populations (Zeller et al., 2013).

However, it has been postulated that wildlife corridors may be at risk of contracting diseases through interaction with domestic and livestock fauna (Grootenhuis, 2000). Moreover, it is well known that viral diseases could have a negative role in animal conservation. For example, highly contagious diseases with high mortality rates, such as CDV and rinderpest, have decimated wildlife populations in the past (Loots et al., 2017). It is possible that diverse pathogens may have negative effects on population health due to reconnecting fragmented habitats, which could cause pathogen invasions and would

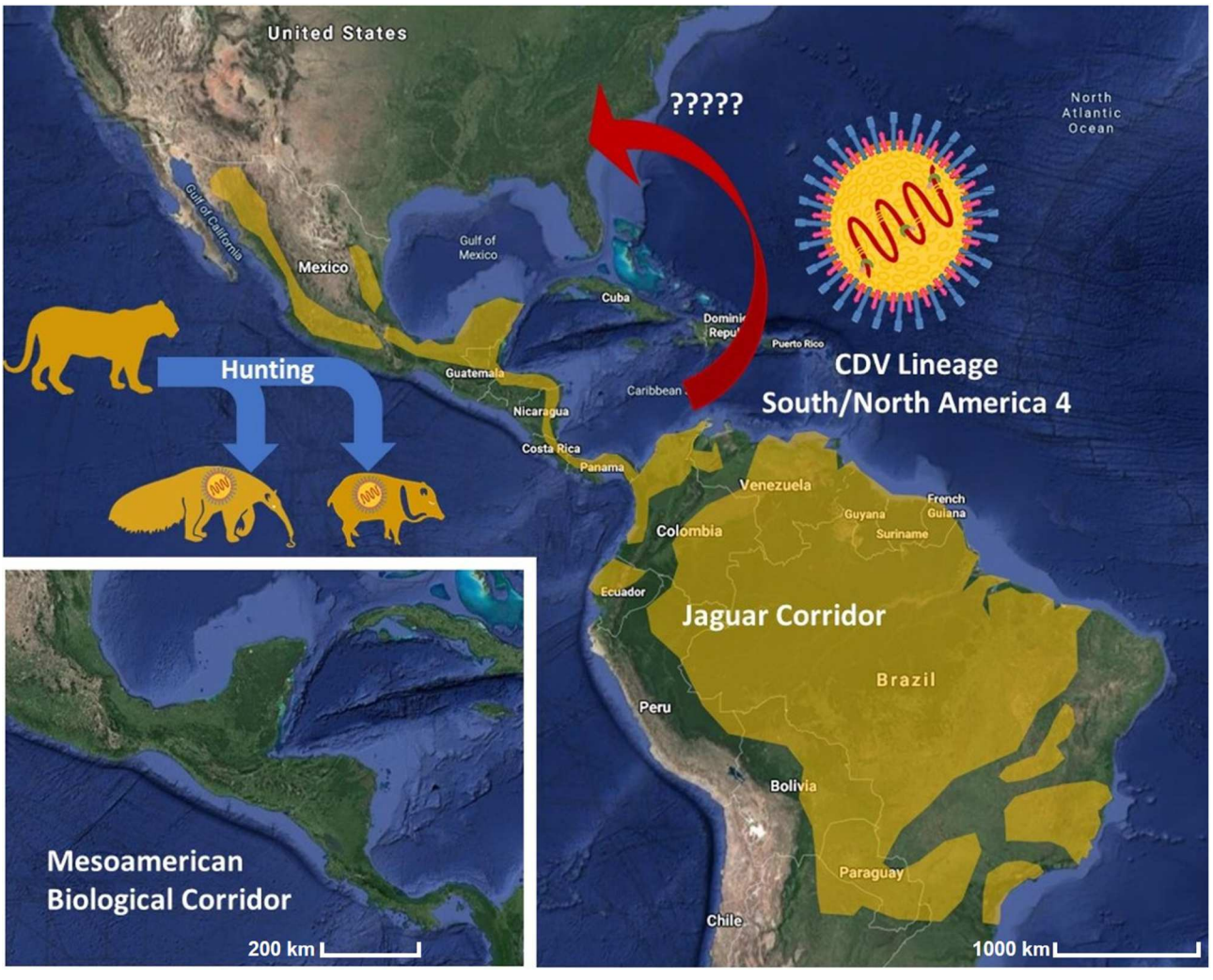

FIGURE 1 | Schematic representation of the possible transmission route of CDV trough the biological corridors. Box below highlights the Mesoamerican Biological Corridor. Yellow shadow highlights the Jaguar Corridor. See text for references.

result in a negative effect on species conservation (Hess, 1994).

Previously, the main role of Panamá for the movement and gene flow of numerous neotropical forest species has been described (Leigh et al., 2014), mainly due to the geographical location in the Mesoamerican Biological Corridor. Moreover, recent assessments have reported that the Atlantic side of the isthmus is critical for the occupancy and connectivity of important mammal species. These include ungulates such as the Baird's tapir (*Tapirus bairdii*), white-lipped peccary (*Tayassu pecari*), collared peccary (*Pecari tajacu*), white-tailed deer (*Odocoileus virginianus*) and the Central American red brocket deer (*Mazama temama*), carnivores such as the jaguar (*Panthera onca*), puma (*Puma concolor*), and ocelot (*Leopardus pardalis*), and insectivores like the giant anteater (*Myrmecophaga tridactyla*); all of them are mostly forest specialists (Meyer et al., 2020a,b).

The mentioned list includes a vast array of large and medium-sized mammals (both carnivorous and non-carnivorous) ranging from ungulates to carnivores and even insectivorous species, and CDV has been reported to infect most of those species (Martinez-Gutierrez and Ruiz-Saenz, 2016). In fact, the reported case of a giant anteater showing clinical illness confirmed to be canine distemper (Debesa Belizario Granjeiro et al., 2020) could just represent the tip of the iceberg, relative to the total number of infections in the wild. When we analyse the connectivity of the Mesoamerican Biological Corridor or the Jaguar Corridor in the Americas, we could observe the successful bridge between central and South America (**Figure 1**). However, this same bridge could possibly be used as a transmission bridge for "Multi-Host viruses" such as the CDV (Duque-Valencia et al., 2019b). A similar phenomena has been described for other important viruses such as the West Nile Virus and the Avian Influenza Virus that efficiently use migratory routes, leading to dissemination and intercontinental transmission of viruses in animal populations (Lee et al., 2015; Afanador-Villamizar et al., 2017; Kramer et al., 2019).

The continuous reports of CDV infection in wild felids and endangered species such as the Anteater from central and South America has raised a concern over the critical role of CDV in big cat conservation in the Americas. The same occurred with wild Siberian tigers (*Panthera tigris altaica*) (Gilbert et al., 2014, 2015; Zhang et al., 2017) and Giant pandas (*Ailuropoda melanoleuca*) (Feng et al., 2016; Jin et al., 2017; Zhao et al., 2017) in which the risk of extinction of the species associated with CDV infection has been characterized.

In the Mesoamerican and South American areas, CDV has been described as infecting the cougar (*Puma concolor*), margay (*Leopardus wiedii*), jaguarundi (*Herpailurus yagouaroundi*), Jaguars (*Panther onca*), ocelots (*Leopardus pardalis*), jaguarundis (*Puma yaguaroundi*), pampas cat (*Leopardus colocolo*), and other wild canids such as the maned wolf (*Chrysocyon brachyurus*), crab-eating fox (*Cerdocyon thous*), hoary fox (*Pseudalopex vetulus*), striped hog-nosed skunk (*Conepatus semistriatus*), and coati (*Nasua nasua*), among others (Avendano et al., 2016; Furtado et al., 2016; Viana et al., 2020). The animals mentioned above such as cougars, jaguars, and other medium and big carnivorous often prey on livestock and native prey including mesocarnivorous and medium-sized mammals such as anteaters and tamanduas (Cavalcanti and Gese, 2010) which could be shown to be a new reservoir for CDV. In fact, it has been described that Giant anteaters (*Myrmecophaga tridactyla*) contribute more than 75 % of biomass to the observed diet of the jaguar (*Panthera onca*) in the Cerrado, central Brazil (Sollmann et al., 2013). Also, it has been shown that 21% of the jaguar diet includes peccaries (mostly *Tayassu pecari*), another species that has been commonly been reported as being at risk of infection with CDV (Noon et al., 2003), suggesting the imminent risk in those species to get infected with a multi-host viral pathogen such as CDV when they hunt their prey.

CONCLUDING REMARKS

Our understanding of the circulation of CDV in the Americas allows us to speculate on the number of critical factors. These factors include the presence of specific viral lineages in large geographical areas, and the susceptibility of circulating species in interconnected regions which favors viral exchange across the continent and represents a risk for wild endangered populations. For this reason, it is imperative to establish not only the dynamics but also diverse aspects of the circulation of CDV among wildlife in the Americas, such as prevalent linages and their associations that would enable us to elucidate the main circulating stains.

There is a great possibility that there is an underreporting of CDV infection and that the published cases only represent the tip of the iceberg in the epidemiology of CDV in wild populations in the Americas.

We recommend enhancing the monitoring of CDV among wildlife corridors and to evaluate the CDV dynamics among different target populations regardless of whether clinical signs are observed. Moreover, we encourage the implementation of an interdisciplinary approach that would enable us to understand the critical role of high impact/mortality diseases such as CDV on the wildlife conservation. Also we encourage the assessment of the impact of CDV circulation and vaccine coverage of domestic dogs on wildlife epidemics, as this topic has not been evaluated in the America corridor areas.

AUTHOR CONTRIBUTIONS

JR-S conceived the study. SR-M, MM-G, JS, and JR-S were involved in all other aspects of the study, including data collection, data analysis, drafting and editing the paper. All authors read and approved the final manuscript.

FUNDING

This work was financially supported by the Departamento Administrativo de Ciencia, Tecnología e Innovación—COLCIENCIAS Grant No. 123171249669 to JR-S.

REFERENCES

Afanador-Villamizar, A., Gomez-Romero, C., Diaz, A., and Ruiz-Saenz, J. (2017). Avian influenza in Latin America: a systematic review of serological and molecular studies from 2000-2015. *PLoS ONE* 12:e0179573. doi: 10.1371/journal.pone.0179573

Avendano, R., Barrueta, F., Soto-Fournier, S., Chavarria, M., Monge, O., Gutierrez-Espeleta, G. A., et al. (2016). Canine distemper virus in wild felids of costa rica. *J. Wildl. Dis.* 52, 373–377. doi: 10.7589/2015-02-041

Beier, P., Majka, D. R., and Spencer, W. D. (2008). Forks in the road: choices in procedures for designing wildland linkages. *Conserv. Biol.* 22, 836–851. doi: 10.1111/j.1523-1739.2008.00942.x

Cavalcanti, S. M., and Gese, E. M. (2010). Kill rates and predation patterns of jaguars (Panthera onca) in the southern Pantanal, Brazil. *J. Mammal.* 91, 722–736. doi: 10.1644/09-MAMM-A-171.1

Chetkiewicz, C.-L. B., St. Clair, C. C., and Boyce, M. S. (2006). Corridors for conservation: integrating pattern and process. *Annu. Rev. Ecol. Evol. Syst.* 37, 317–342. doi: 10.1146/annurev.ecolsys.37.091305.110050

De Vries, R. D., Duprex, W. P., and De Swart, R. L. (2015). Morbillivirus infections: an introduction. *Viruses* 7, 699–706. doi: 10.3390/v7020699

Debesa Belizario Granjeiro, M., Lima Kavasaki, M., Morgado, T. O., Avelino Dandolini Pavelegini, L., Alves De Barros, M., Fontana, C., et al. (2020). First report of a canine morbillivirus infection in a giant anteater (Myrmecophaga tridactyla) in Brazil. *Vet Med Sci*. doi: 10.1002/vms3.246. [Epub a head of print].

Duque-Valencia, J., Forero-Munoz, N. R., Diaz, F. J., Martins, E., Barato, P., and Ruiz-Saenz, J. (2019a). Phylogenetic evidence of the intercontinental circulation of a Canine distemper virus lineage in the Americas. *Sci. Rep.* 9:15747. doi: 10.1038/s41598-019-52345-9

Duque-Valencia, J., Sarute, N., Olarte-Castillo, X. A., and Ruiz-Saenz, J. (2019b). Evolution and interspecies transmission of canine distemper virus-an outlook of the diverse evolutionary landscapes of a multi-host virus. *Viruses* 11:582. doi: 10.3390/v11070582

Feng, N., Yu, Y., Wang, T., Wilker, P., Wang, J., Li, Y., et al. (2016). Fatal canine distemper virus infection of giant pandas in China. *Sci. Rep.* 6, 1–7. doi: 10.1038/srep27518

Furtado, M. M., Hayashi, E. M., Allendorf, S. D., Coelho, C. J., De Almeida Jacomo, A. T., Megid, J., et al. (2016). Exposure of free-ranging wild carnivores and domestic dogs to canine distemper virus and parvovirus in the cerrado of central Brazil. *Ecohealth* 13, 549–557. doi: 10.1007/s10393-016-1146-4

Gilbert, M., Miquelle, D. G., Goodrich, J. M., Reeve, R., Cleaveland, S., Matthews, L., et al. (2014). Estimating the potential impact of canine distemper virus on the Amur tiger population (Panthera tigris altaica) in Russia. *PLoS ONE* 9:e110811. doi: 10.1371/journal.pone.0110811

Gilbert, M., Soutyrina, S. V., Seryodkin, I. V., Sulikhan, N., Uphyrkina, O. V., Goncharuk, M., et al. (2015). Canine distemper virus as a threat to wild tigers in Russia and across their range. *Integr. Zool.* 10, 329–343. doi: 10.1111/1749-4877.12137

Grootenhuis, J. G. (2000). "Wildlife, livestock and animal disease reservoirs," in *Wildlife Conservation by Sustainable Use*, eds H. H. T. Prins, J. G. Grootenhuis, and T. T. Dolan (London, UK: Springer), 81–113. doi: 10.1007/978-94-011-4012-6_6

Hess, G. R. (1994). Conservation corridors and contagious disease: a cautionary note. *Conserv. Biol.* 8, 256–262. doi: 10.1046/j.1523-1739.1994.08010256.x

Holland, M. B. (2012). "Mesoamerican biological corridor," in *Climate and Conservation*, eds J. A. Hilty, C. C. Chester, and M. S. Cross (Washington, DC: Island Press), 56–66. doi: 10.5822/978-1-61091-203-7_5

Hukic, M., Numanovic, F., Sisirak, M., Moro, A., Dervovic, E., Jakovec, S., et al. (2010). Surveillance of wildlife zoonotic diseases in the Balkans Region. *Med. Glas (Zenica).* 7, 96–105.

Jin, Y., Zhang, X., Ma, Y., Qiao, Y., Liu, X., Zhao, K., et al. (2017). Canine distemper viral infection threatens the giant panda population in China. *Oncotarget* 8:113910. doi: 10.18632/oncotarget.23042

Kramer, L. D., Ciota, A. T., and Kilpatrick, A. M. (2019). Introduction, spread, and establishment of west nile virus in the Americas. *J. Med. Entomol.* 56, 1448–1455. doi: 10.1093/jme/tjz151

Lamb, R. A., and Parks, G. D. (2013). "Paramyxoviridae: the viruses and their replication," in *Fields Virology: Sixth Edition. Vol. 1*, eds B. N. Fields, D. M. Knipe, and P. M. Howley (Philadelphia, PA: Lippincott; Williams; Wilkins), 957–995.

Lee, D. H., Torchetti, M. K., Winker, K., Ip, H. S., Song, C. S., and Swayne, D. E. (2015). Intercontinental spread of asian-origin H5N8 to north america through beringia by migratory birds. *J. Virol.* 89, 6521–6524. doi: 10.1128/JVI.00728-15

Leigh, E. G., O'dea, A., and Vermeij, G. J. (2014). Historical biogeography of the I sthmus of P anama. *Biol. Rev.* 89, 148–172. doi: 10.1111/brv.12048

Loots, A. K., Mitchell, E., Dalton, D. L., Kotze, A., and Venter, E. H. (2017). Advances in canine distemper virus pathogenesis research: a wildlife perspective. *J. Gen. Virol.* 98, 311–321. doi: 10.1099/jgv.0.000666

Lunardi, M., Darold, G. M., Amude, A. M., Headley, S. A., Sonne, L., Yamauchi, K. C. I., et al. (2018). Canine distemper virus active infection in order Pilosa, family Myrmecophagidae, species Tamandua tetradactyla. *Vet. Microbiol.* 220, 7–11. doi: 10.1016/j.vetmic.2018.04.030

Martinez-Gutierrez, M., and Ruiz-Saenz, J. (2016). Diversity of susceptible hosts in canine distemper virus infection: a systematic review and data synthesis. *BMC Vet. Res.* 12:78. doi: 10.1186/s12917-016-0702-z

Meyer, N. F., Moreno, R., Reyna-Hurtado, R., Signer, J., and Balkenhol, N. (2020a). Towards the restoration of the Mesoamerican Biological Corridor for large mammals in Panama: comparing multi-species occupancy to movement models. *Mov. Ecol.* 8, 1–14. doi: 10.1186/s40462-019-0186-0

Meyer, N. F. V., Moreno, R., Sutherland, C., de la Torre, J. A., Esser, H. J., Jordan, C. A., et al. (2020b). Effectiveness of Panama as an intercontinental land bridge for large mammals. *Conserv. Biol.* 34, 207–219. doi: 10.1111/cobi.13384

Noon, T. H., Heffelfinger, J. R., Olding, R. J., Wesche, S. L., and Reggiardo, C. (2003). Serologic survey for antibodies to canine distemper virus in collared peccary (*Tayassu tajacu*) populations in Arizona. *J. Wildl. Dis.* 39, 221–223. doi: 10.7589/0090-3558-39.1.221

Pfeffermann, K., Dorr, M., Zirkel, F., and Von Messling, V. (2018). Morbillivirus pathogenesis and virus-host interactions. *Adv. Virus Res.* 100, 75–98. doi: 10.1016/bs.aivir.2017.12.003

Sleeman, J. M., Deliberto, T., and Nguyen, N. (2017). Optimization of human, animal, and environmental health by using the One Health approach. *J. Vet. Sci.* 18, 263–268. doi: 10.4142/jvs.2017.18.S1.263

Sollmann, R., Betsch, J., Furtado, M. M., Hofer, H., Jácomo, A. T., Palomares, F., et al. (2013). Note on the diet of the jaguar in central Brazil. *Eur. J. Wildl. Res.* 59, 445–448. doi: 10.1007/s10344-013-0708-9

Viana, N. E., De Mello Zanim Michelazzo, M., Oliveira, T. E. S., Cubas, Z. S., De Moraes, W., and Headley, S. A. (2020). Immunohistochemical identification of antigens of canine distemper virus in neotropical felids from Southern Brazil. *Transbound. Emerg. Dis*. doi: 10.1111/tbed.13422. [Epub ahead of print].

Watson, A. M., Cushing, A. C., Sheldon, J. D., Anis, E., Wilkes, R. P., Dubovi, E. J., et al. (2020). Natural canine distemper virus infection in linnaeus's 2-toed sloths (*Choloepus didactylus*). *Vet. Pathol.* 57, 311–315. doi: 10.1177/0300985819900017

Zeller, K. A., Rabinowitz, A., Salom-Perez, R., and Quigley, H. (2013). *The Jaguar Corridor Initiative: A Range-Wide Conservation Strategy. Molecular Population Genetics, Evolutionary Biology and Biological Conservation of Neotropical Carnivores*. New York (NY): Nova Science Publishers, 629–657.

Zhang, H., Shan, F., Zhou, X., Li, B., Zhai, J.-Q., Zou, S.-Z., et al. (2017). Outbreak and genotyping of canine distemper virus in captive Siberian tigers and red pandas. *Sci. Rep* 7, 1–7. doi: 10.1038/s41598-017-08462-4

Zhao, N., Li, M., Luo, J., Wang, S., Liu, S., Wang, S., et al. (2017). Impacts of canine distemper virus infection on the giant panda population from the perspective of gut microbiota. *Sci. Rep.* 7, 1–10. doi: 10.1038/srep39954

Conflict of Interest: The authors declare that the research was conducted in the absence of any commercial or financial relationships that could be construed as a potential conflict of interest.

Copyright © 2020 Rendon-Marin, Martinez-Gutierrez, Suarez and Ruiz-Saenz. This is an open-access article distributed under the terms of the Creative Commons Attribution License (CC BY). The use, distribution or reproduction in other forums is permitted, provided the original author(s) and the copyright owner(s) are credited and that the original publication in this journal is cited, in accordance with accepted academic practice. No use, distribution or reproduction is permitted which does not comply with these terms.

frontiers in Microbiology

ORIGINAL RESEARCH
published: 22 May 2020
doi: 10.3389/fmicb.2020.01180

The Coronavirus PEDV Evades Type III Interferon Response Through the miR-30c-5p/SOCS1 Axis

Changlin Wang[1†], Lingling Shan[2†], Shuxin Qu[1], Mei Xue[2], Keliang Wang[1], Fang Fu[2], Lu Wang[1], Ziqi Wang[1], Li Feng[2], Wanhai Xu[1] and Pinghuang Liu[2*]*

[1] Department of Urology, the Fourth Affiliated Hospital of Harbin Medical University, Harbin, China, [2] State Key Laboratory of Veterinary Biotechnology, Harbin Veterinary Research Institute, Chinese Academy of Agricultural Sciences, Harbin, China

Porcine epidemic diarrhea virus (PEDV) is an economically important pathogen that has evolved several mechanisms to evade type I IFN responses. Type III interferon (IFN-λ), an innate cytokine that primarily targets the mucosal epithelia, is critical in fighting mucosal infection in the host and has been reported to potently inhibit PEDV infection *in vitro*. However, how PEDV escapes IFN-λ antiviral response remains unclear. In this study, we found that PEDV infection induced significant IFN-λ expression in type I IFN-defective Vero E6 cells, but virus-induced endogenous IFN-λ did not reduce PEDV titers. Moreover, we demonstrated that PEDV escaped IFN-λ responses by substantially upregulating the suppressor of cytokine signaling protein 1 (SOCS1) expression, which impaired the induction of IFN-stimulated genes (ISGs) and dampened the IFN-λ antiviral response and facilitated PEDV replication in Vero E6 cells. We further showed that PEDV infection increased SOCS1 expression by decreasing host miR-30c-5p expression. MiR-30c-5p suppressed SOCS1 expression through targeting the 3′ untranslated region (UTR) of SOCS1. The inhibition of IFN-λ elicited ISGs expression by SOCS1 was specifically rescued by overexpression of miR-30c-5p. Collectively, our findings identify a new strategy by PEDV to escape IFN-λ-mediated antiviral immune responses by engaging the SOCS1/miR-30c axis, thus improving our understanding of its pathogenesis.

Keywords: coronavirus, PEDV, IFN-λ, SOCS1, microRNA, miR-30c-5p

OPEN ACCESS

Edited by:
Ahmed Sayed Abdel-Moneim, Taif University, Saudi Arabia

Reviewed by:
Ana Angulo, University of Barcelona, Spain
Yashpal S. Malik, Indian Veterinary Research Institute (IVRI), India

***Correspondence:**
Wanhai Xu
xuwanhai@hrbmu.edu.cn
Pinghuang Liu
liupinghuang@caas.cn

†These authors have contributed equally to this work

Specialty section:
This article was submitted to Virology, a section of the journal Frontiers in Microbiology

Received: *13 December 2019*
Accepted: *08 May 2020*
Published: *22 May 2020*

Citation:
Wang C, Shan L, Qu S, Xue M, Wang K, Fu F, Wang L, Wang Z, Feng L, Xu W and Liu P (2020) The Coronavirus PEDV Evades Type III Interferon Response Through the miR-30c-5p/SOCS1 Axis. Front. Microbiol. 11:1180. doi: 10.3389/fmicb.2020.01180

INTRODUCTION

Porcine epidemic diarrhea virus (PEDV), a member of the *Alphacoronavirus* family, is an enteropathogenic coronavirus with economic importance (Madson et al., 2014; Wang et al., 2014; Zhang and Yoo, 2016). PEDV infection in newborn piglets is characterized by vomiting, anorexia, watery diarrhea, and dehydration (Song and Park, 2012). The virus primarily infects small intestinal epithelial cells *in vivo* and causes high morbidity and mortality in piglets (Li et al., 2012). Interferons (IFNs) are the key components of innate immunity in response to viral infection (Zhang et al., 2018). Among three types of IFNs (types I, II, and III), type III IFN-lambda (IFN-λ) primarily acts on mucosal surfaces, including epithelial surfaces of the liver, respiratory, and gastrointestinal systems, and plays vital roles in controlling viral infection within mucosal surfaces (Mordstein et al., 2010; Pott et al., 2011; Lazear et al., 2015). We and other groups previously demonstrated that porcine IFN-λdisplays powerful antiviral activity against PEDV infection in both Vero E6 cells and porcine intestinal epithelia (Li et al., 2017, 2019). PEDV has evolved multiple strategies to escape

IFN responses, including the degradation of STAT1 and the suppression of type I IFN production (Guo et al., 2016). Although type I and type III IFNs have a large overlap in the spectrum of induced antiviral ISG responses, recent studies demonstrated that type III IFN is a critical non-redundant antiviral mediator of type I IFNs in the GI tract and elicits a unique transcriptional profile that does not completely overlap with that induced by IFN-α (Wells and Coyne, 2018). It is necessary to clarify how PEDV evades type III IFN following infection.

Unlike ample studies reporting that PEDV escapes type I IFNs, limited studies demonstrate that PEDV escapes IFN-λ response. PEDV suppresses IRF1-mediated type III IFN responses by reducing the number of peroxisomes and counteracting type III IFN response by PEDV nsp15 endoribonuclease (Zhang et al., 2018; Deng et al., 2019). Deng et al. showed that type I and type III IFNs exhibit different modulation in response to PEDV infection and that the discrepancy of type I and type III IFN responses is independent of PEDV endoribonuclease activity (Deng et al., 2019), suggesting that there are distinct strategies to modify host type I and type III IFN responses during PEDV infection. Because cells generally produce both type I and type III IFNs in response to viral infection, it is challenging to elucidate how viruses escape IFN-λ response separately to type I response. In this study, we used Vero cells, a cell line with a defective function, to produce endogenous type I IFNs. Vero cells are widely used as an *in vitro* model to study the interactions between viruses and hosts including PEDV. We and others reported that Vero cells respond well to both porcine type I and type III IFNs (Guo et al., 2016; Shen et al., 2016; Li et al., 2017). IFN-λ is rapidly produced after infection and following engagement with its receptor induces IFN-stimulated gene (ISG) expression to mediate antiviral activity (Kotenko et al., 2003; Dellgren et al., 2009; Lazear et al., 2015). Binding of IFN-λ to its receptor, which consists of two subunits, IFN-λR1 and IL-10R2, leads to activation of JAK1 and Tyk2, which mediates the phosphorylation of STAT1 and STAT2 proteins (Sheppard et al., 2003; Palma-Ocampo et al., 2015). The suppressor of cytokine signaling protein 1 (SOCS1), a negative regulator of Janus family kinase (JAK) signal transducer, simultaneously binds the receptors and JAKs and prevents STATs from accessing the receptor kinase complex (de Weerd and Nguyen, 2012; Palma-Ocampo et al., 2015). Previous reports demonstrated that SOCS1 is an inducible negative regulator of IFN-λ-induced gene expression *in vivo* (Blumer et al., 2017). SOCS1 was also associated with DENV-2 escape from IFN-λ response during infection (Palma-Ocampo et al., 2015). However, the role of SOCS1 during PEDV infection remains unclear.

MicroRNAs (miRNAs), as important post-transcriptional modulators of gene expression, participate in modulating the host innate and adaptive immune responses in response to pathogen invasion (Baltimore et al., 2008; Gottwein and Cullen, 2008; O'Neill et al., 2011). Increasing evidence has shown that miRNAs of viral and cellular origin can help viruses evade host immune responses by targeting critical components in the host immune system (Cullen, 2006; Sullivan et al., 2006; Kincaid and Sullivan, 2012). For example, miR-30c is a potent negative regulator of type I IFN signaling by targeting JAK1, resulting in the enhancement of PRRSV infection (Zhang et al., 2016). The miR-30 family is a well-studied host miRNA that plays an important role in viral infection by modulating IFN signaling (Zhu et al., 2014; Zhang et al., 2016; Liu et al., 2018; Ma et al., 2018). Our previous study revealed that TGEV escapes type I IFN response by engaging the IRE1-miR-30a-5p/SOCS1/3 axis (Ma et al., 2018). The potential role of miRNAs in coronavirus escape from IFN-λ response remains elusive.

In this study, we showed that PEDV escaped IFN-λ responses by upregulating SOCS1 expression in type I IFN-defective Vero E6 cells. In addition, we demonstrated that PEDV infection increased SOCS1 expression by decreasing the expression of host miR-30c-5p, which modulates SOCS1 expression by specifically targeting the 3′ UTR of SOCS1. Our findings identify a new strategy by PEDV to escape IFN-λ-mediated host innate immune defenses.

TABLE 1 | Sequences of miRNA mimics, inhibitors, and shRNAs.

Small RNA	Sequence(5′-3′)
miR-30c-5p	UGUAAACAUCCUACACUCUCAGC
miR-30c-5p inhibitor	GCUGAGAGUGUAGGAUGUUUACA
shSOCS1 #1	GTATGACAAGAGCCTCAAG
shSOCS1 #2	GTTCTCCGAACGTGTCACGT
shSOCS1 #3	GCGAGAGCTTCGACTGCCTCT

MATERIALS AND METHODS

Cells and Viruses

African green monkey kidney cells (Vero E6 cells) were stocked by our laboratory and grown in DMEM (Gibco, Gaithersburg, MD, USA) supplemented with 10% FBS (Gibco) and antibiotics (100 U/mL of penicillin and 100 μg/mL of streptomycin) at 37°C in a humidified atmosphere of 5% CO2. PEDV-CV777 (GenBank accession no. KT323979) stocked in our laboratory was propagated in Vero E6 cells as previously described (Hofmann and Wyler, 1988; Sun et al., 2015). To evaluate the anti-PEDV activity of porcine IFN-λ (Prosit Sole Biotechnology, Co., Ltd., Beijing, China), Vero E6 cells were pretreated with designated concentrations of IFN-λ for 12 h and then infected with PEDV (MOI of 0.1).

Synthetic miRNAs, shRNAs, and Transfection

All of the miRNA mimics, miRNA inhibitors, and short hairpin RNAs (shRNAs) were synthesized by Gene Pharma (Shanghai, China). The miRNAs and shRNAs sequences are listed in **Table 1**. Lipofectamine 2000 (Invitrogen, Carlsbad, CA, USA) or Lipofectamine RNAiMAX (Invitrogen) was used to transfect cells with plasmid DNA or synthetic oligonucleotides according to the manufacturer's instructions. The cells were infected with PEDV as previously described after transfection for 24 h. The cells were harvested for quantitative real-time PCR (RT-qPCR) or treated with NP-40 lysis buffer for Western blotting after infection for 36 h.

TABLE 2 | Sequences of primers used in the present study.

Primer	Sequences(5′-3′)
miR-30c-5p-qPCR-F	TGTAAACATCCTACACTCTCAGC
Uni-miR-qPCR-R	GCGAGCACAGAATTAATACGACTCAC
ISG15-qPCR-F	ACGCAGACTGTGGCCCACCT
ISG15-qPCR-R	CATTTATTTCCAGCCCTTGA
SOCS1-qPCR-F	CGCCCTCAGTGTGAAGATGG
SOCS1-qPCR-R	GCTCGAAGAGGCAGTCGAAG
GAPDH-qPCR-F	ATGGGGAAGGTGAAGGTCGG
GAPDH-qPCR-R	TCCTGGAAGATGGTGATGGG
IFN-λ-qPCR-F	ACCGCAGGAGTTGGCAAG
IFN-λ-qPCR-R	CCGGGGAAGACAGGAGAG
MxA-qPCR-F	CTGCTGCATCCCAACCTCTAT
MxA-qPCR-R	GGCGCACCTTCTCCTCGTACT
IFIT1-qPCR-F IFIT1-qPCR-R	GGTCTTGGAGGAGATTGA ATACAGCCAGGCATAGTT
SOCS1-EcoR I–F	CGGAATTCATGGTAGCACACAACCAGGTG
SOCS1-Kpn I–R	GGGGTACCTCATATCTGGAAGGGGAAGGAG
SOCS1-3′ UTR-Nhe I-F	CTAGCTAGCATTATTTCCTTGGAACCATGTG
SOCS1-3′ UTR-Xba I-R	GCTCTAGACACAGCAGAAAAATAAAGCCAG
SOCS1-3′ UTR-MT–F	CTTCATAGGGTCATATACCCAGTATCTTTG CACAAAC
SOCS1-3′ UTR-MT–R	TATATGACCCTATGAAGAGGTAGGAGGTAC TGAGTTC

Total RNA Isolation, Reverse Transcription, and qPCR

Total cellular RNA was isolated using an RNeasy Mini kit (Qiagen Sciences, Hilden, Germany) according to the manufacturer's instructions. Total RNA was extracted and reverse transcribed as previously described (Ma et al., 2018). For miRNA reverse transcription, cDNA was prepared with a miRNA First Strand cDNA Synthesis kit (Sangon Biotech, Shanghai, China). qPCR was conducted in triplicate with Power SYBR Green PCR Master Mix reagents (Takara) on a LightCycler480 II system (Thermo Fisher Scientific, Waltham, MA, USA) as previously described (Ma et al., 2018). The miRNA expression levels were normalized to the internal control of U6. The sequences of RT-qPCR primers for PEDV, IFN-λ, SOCS1, IFIT1, ISG15, MxA, GAPDH, miR-30c, and Uni-miR transcription are listed in **Table 2**. The results are presented as the means ± SEM from three separate trials.

miRNA Target Projections and Plasmid Construction

TargetScan Release 7.1 (http://www.targetscan.org) was used to predict the targets of miR-30c-5p. SOCS1 3′ UTRs as a prospective target was cloned and constructed as previously described (Ma et al., 2018). To construct the monkey SOCS1 expression vector, the full-length CDS region of monkey SOCS1 was amplified from Vero E6 cellular mRNA PCR and cloned into pCAGGS-HA vector (Clontech, Mountain View, CA, USA) using EcoR I and Kpn I restriction sites. The 3′UTR of SOCS1 (GenBank:100307052) was amplified and inserted into the pmirGLO luciferase reporter vector. The SOCS1 3′UTR mutant vector was produced by mutating five seed nucleotides using a site-directed mutagenic kit (Stratagene, La Jolla, CA, USA) according to the manufacturer's instructions. The constructed plasmids were verified by sequencing.

Dual-Luciferase Assays

The luciferase activities were tested using a Dual-Luciferase Reporter Assay System (Promega, Madison, WI, USA) based on the manufacturer's instructions. Wild- or mutant-type SOCS1 3′UTR luciferase reporter vectors were co-transfected with miR-30c-5p mimics (miR-30c), mimic NC (NC), miR-30c-5p inhibitor (miR-30c-i), or inhibitor NC (NC-i) into Vero E6 cells for 24 h. Then pRL-TK was co-transfected with either miR-30c, NC, miR-30c-i, or NC-i for 24 h. The cells were collected and the luciferase activity was evaluated with a dual-luciferase reporter assay system (Promega). The pRL-TK vector expressing the Renilla luciferase gene was used as a normalization control.

Immunofluorescence Assay (IFA)

Vero E6 cells were fixed with 4% paraformaldehyde for 30 min at 4°C and permeabilized with 0.2% Triton X-100 for 15 min, then blocked with blocking buffer (PBS with 5% FBS) for 2 h at 37°C. The cells were incubated with an anti-HA monoclonal antibody (Sigma-Aldrich, Munich, Germany, 1:5000) at 37°C for 2 h, followed by labeling with an Alexa Fluor 546 goat anti-mouse IgG antibody (Thermo Fisher Scientific, 1:500) at 37°C for 1 h. 4′,6-diamidino-2-phenylindole (DAPI, 1:100) was used to stain the cellular nuclei. The stained cells were visualized using an AMG EVOS F1 fluorescence microscope.

Western Blotting

Vero E6 cells were lysed with NP-40 lysis buffer (Beyotime, China) supplemented with 0.1 mM of phenylmethylsulfonyl fluoride (PMSF) (Roche, Indianapolis, IN, USA). Target proteins were separated on SDS-PAGE gels then transferred onto nitrocellulose membranes (GE Healthcare, Chicago, IL, USA). After blocking with TBS-T containing 5% non-fat milk at room temperature (RT), the membranes were incubated with primary antibody at 4°C for 18 h. Antibodies included: β-actin (Sigma-Aldrich, 1:5000) and SOCS1 (Sigma-Aldrich, 1:500). The membranes were incubated with secondary antibody goat anti-mouse-HRP or goat anti-rabbit-HRP, diluted at 1:2000 for 1 h at room temperature, and visualized using an ECL system (Thermo Fisher). The results were analyzed using ImageJ software.

Statistical Analysis

All of the data are described as the means ± the standard error of the mean (SEM). GraphPad Prism (GraphPad Software, Inc.) was used to analyze the data using Student's *t*-test. Each experiment was repeated three times. *P*-values < 0.05 were considered significant: $^{*}P < 0.05$; $^{**}P < 0.01$; $^{***}P < 0.001$; $^{****}P < 0.0001$, and NS, not significant.

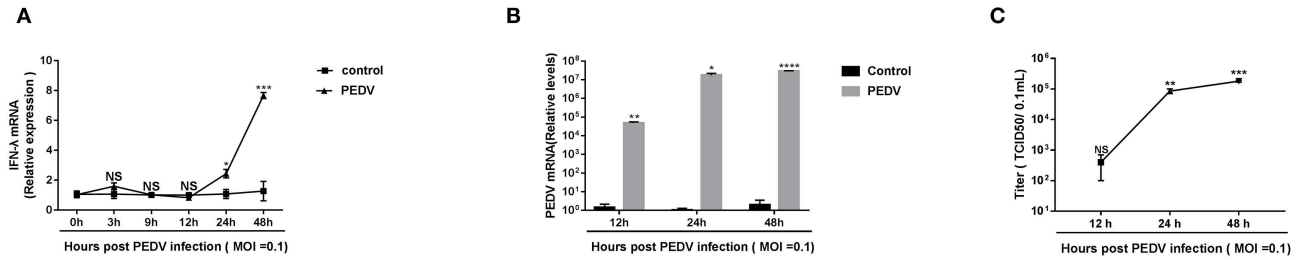

FIGURE 1 | PEDV replicated successfully despite the induction of endogenous IFN-λ responses during late infection. **(A)** PEDV infection induced IFN-λ expression. IFN-λ expression was monitored in Vero E6 cells after infection with PEDV at MOIs of 0.1 and the results were normalized by the mock uninfected controls. **(B,C)** Kinetic curve of PEDV replication in Vero E6 cells. Vero E6 cells were inoculated with PEDV at an MOI of 0.1, and the level of PEDV infection compared to mock controls at 12, 24, and 48 h was quantified by RT-qPCR and $TCID_{50}$. The results were obtained from three independent experiments. Mean ± SEM, $^{*}P < 0.05$; $^{**}P < 0.01$; $^{***}P < 0.001$; $^{****}P < 0.0001$, and NS, not significant.

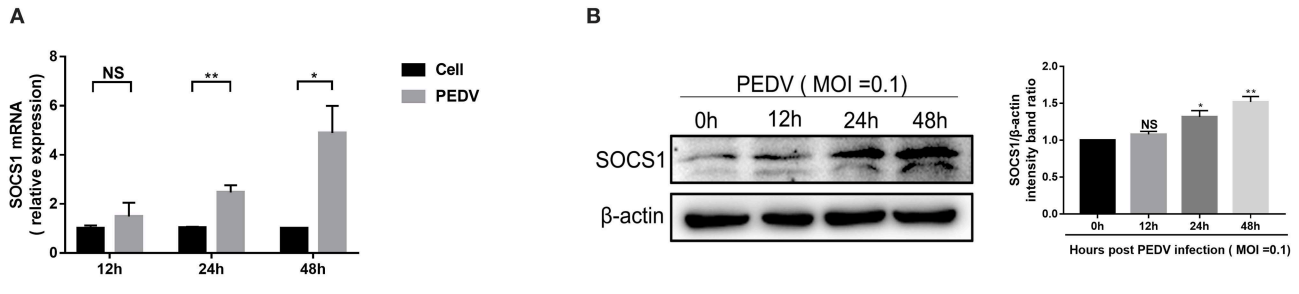

FIGURE 2 | PEDV infection increased the expression of SOCS1 in Vero E6 cells. **(A,B)** PEDV infection increased the mRNA levels and protein levels of SOCS1. Vero E6 cells were infected with PEDV at MOI 0.1. The level of SOCS1 RNA was measured by RT-qPCR **(A)**. Cell lysates of Vero E6 cells were analyzed by Western blotting using an antibody against SOCS1 (left panel); β-actin was used as a loading control. The SOCS1 bands were normalized to β-actin using ImageJ software (right panel) **(B)**. The results were represented as Mean ± SEM of three independent experiments. $^{*}P < 0.05$, $^{**}P < 0.01$, and NS, not significant.

RESULTS

PEDV Replicated Well Despite the Induction of Endogenous IFN-λ Responses During Late Infection

Previous research showed that the pretreatment of porcine IFN-λ inhibits PEDV infection in Vero E6 cells and IPEC-J2 (Li et al., 2017). It is well-established that PEDV replicates efficiently in Vero E6 cells. To determine whether PEDV elicits an endogenous IFN-λ response in Vero E6 cells following infection, we initially infected Vero E6 cells with PEDV at MOI = 0.1 and monitored the IFN-λ expression. Compared with a mock uninfected control, PEDV did not increase the expression of IFN-λ transcripts as observed until 12 hpi, and then gradually induced IFN-λ expression, indicating that PEDV infection elicits type III IFN expression at the late stage of infection instead of the early stage of infection in the Vero E6 cells (**Figure 1A**), which was consistent with the results in porcine enteroids (Li et al., 2019). And PEDV propagated efficiently in Vero E6 cells by quantifying viral genomes and titers (**Figures 1B,C**). The virus titer increased up to 10^5/0.1 mL at 48 hpi (**Figure 1C**). Interestingly, despite the increased expression of endogenous IFN-λ at the late stage of infection, the PEDV virus titer did not decrease. This indicates that there are mechanisms explored by PEDV to antagonize the endogenous IFN-λ ISG response at the late-stage infection.

PEDV Infection Increased the Expression of SOCS1 in Vero E6 Cells

SOCS1, a typical member of the SOCS family of proteins, is a well-known negative feedback inhibitor of JAK/STAT signaling pathway induced by cytokines (Ma et al., 2018). To explore the underlying mechanisms exploited by PEDV to escape IFN-λ-induced antiviral responses, we initially assessed whether PEDV infection induces SOCS1 expression in Vero E6 cells. The mRNA levels of SOCS1 significantly increased following PEDV infection and displayed a time-dependent response (**Figure 2A**). The induction of SOCS1 by PEDV infection was further verified by SOCS1 Western blotting (**Figure 2B**).

SOCS1 Counteracted the Anti-PEDV Activity of IFN-λ

SOCS1 is a potent inhibitor of the type I and type II IFN signaling pathway (Skjesol et al., 2014). We next investigated whether SOCS1 suppresses IFN-λ-mediated antiviral activity. First, we silenced endogenous SOCS1 expression by specific shRNAs. SOCS1 shRNAs or a non-targeting shRNA (NC) were transfected into Vero E6 cells. The efficiency of SOCS1 knockdown was confirmed by Western blotting (**Figure 3A**). shSOCS1 #2 and #3 led to a 55 and 65% decrease in SOCS1 expression, respectively, compared with NC (**Figure 3A**). Silencing of

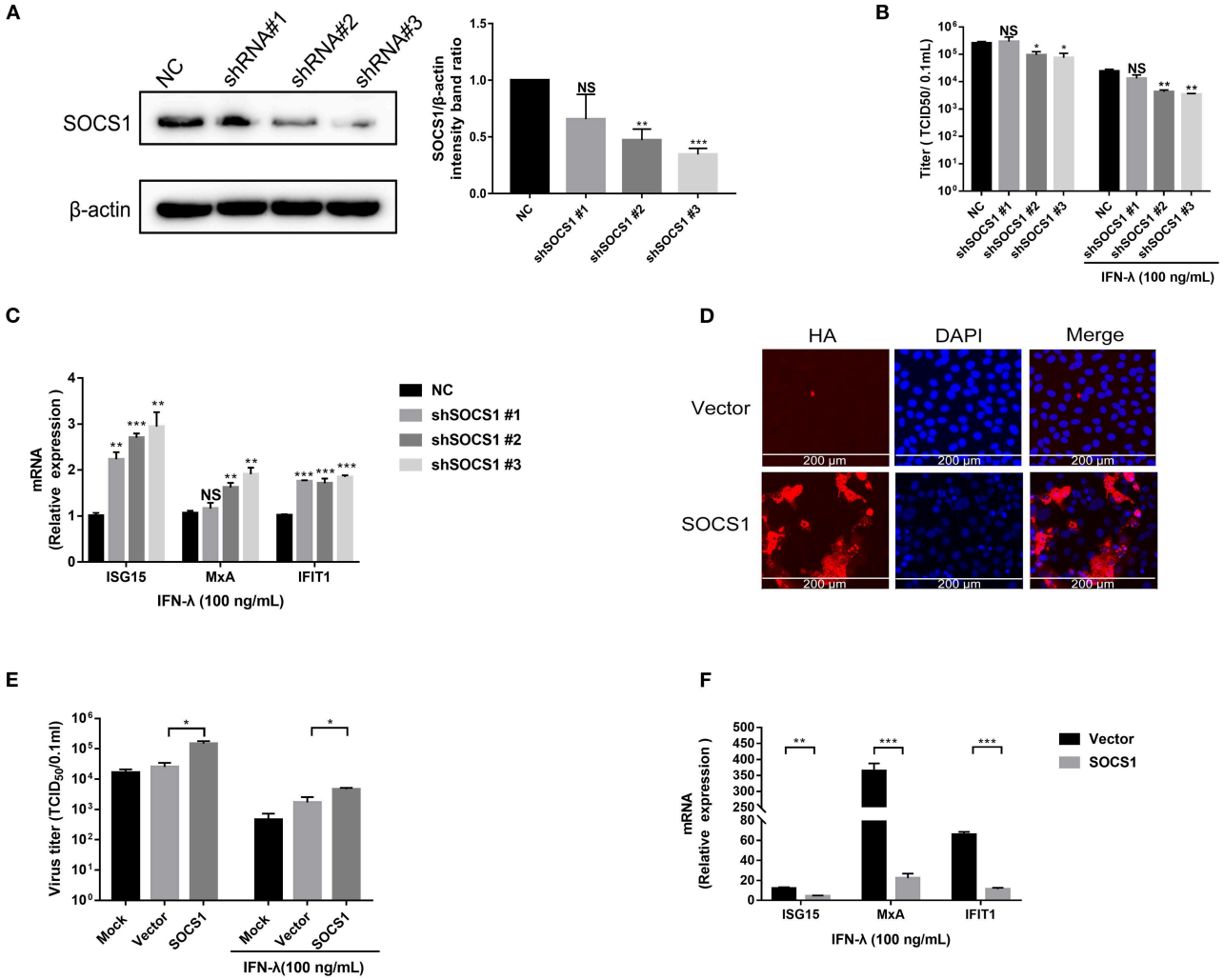

FIGURE 3 | SOCS1 counteracted the anti-PEDV activity of IFN-λ. **(A)** The knockdown efficiency of shSOCS1 was determined by Western blotting (left panel); β-actin was used as a loading control. The SOCS1 bands were quantified using ImageJ software as normalized to β-actin (right panel). **(B)** Knockdown of SOCS1 decreased PEDV replication. Vero E6 cells were treated with 100 ng/mL of IFN-λ and transfected with NC or shSOCS1s, followed by infection with PEDV (MOI = 0.1). After 36 h, cell culture supernatants were harvested for virus titration. **(C)** Silencing of SOCS1 increased IFN-λ signaling induced by IFN-λ stimulation. Vero E6 cells were stimulated with IFN-λ 12 h after transfection with shSOCS1 #1, shSOCS1 #2, shSOCS1 #3, or scrambled control shRNA, and then the cells were collected for RT-qPCR analysis of ISG15, IFIT1, or MxA expression relative to that of GAPDH after 24 h of stimulation. **(D)** Transient expression of SOCS1 in Vero E6 cells. SOCS1 was cloned and expressed in the eukaryotic expression vector pCAGGS-HA. The overexpression efficiency of SOCS1 in Vero E6 cells was confirmed by IFA. **(E)** Transient expression of SOCS1 enhanced PEDV infection in Vero E6 cells. Vero E6 cells were stimulated with IFN-λ 12 h after the transient expression of SOCS1 promoted PEDV infection. Vero E6 cells were transfected with SOCS1-HA for 24 h and then infected with PEDV (MOI = 0.1). PEDV infection was determined by measuring PEDV titers. **(F)** Transient expression of SOCS1 disrupted the IFN-λ antiviral response. Vero E6 cells were stimulated with IFN-λ after being transfected with SOCS1 for 24 h. The cells were collected for RT-qPCR analysis of ISG15, MxA, and IFIT1 expression relative to that of GAPDH after 24 h of stimulation. Error bars, mean ±SEM. ($n = 3$ independent experiments). $^*P < 0.05$, $^{**}P < 0.01$, $^{***}P < 0.001$, and NS, not significant.

endogenous SOCS1 by shSOCS1 #2 or #3 significantly reduced PEDV replication in Vero E6 cells without the addition of exogenous IFN-λ (**Figure 3B**). The decreased levels of PEDV infection were in line with the knockdown efficiency of SOCS1 shRNAs, indicating the specific effect of SOCS1 shRNAs. As previously reported, exogenous IFN-λ significantly inhibited PEDV infection, whereas silencing of endogenous SOCS1 by shSOCS1 #2 or #3 further enhanced the PEDV inhibition by IFN-λ in Vero E6 cells compared with untreated IFN-λ mock control (**Figure 3B**). The knockdown of endogenous SOCS1 by shSOCS1 #3 resulted in a more than 3.4-fold decrease in PEDV titer (**Figure 3B**) and degraded to 7.2-fold of PEDV titers with IFN-λ treatment in Vero E6 cells (**Figure 3B**), indicating that SOCS1 knockdown increases the antiviral effects of IFN-λ. Inconsistent with the viral results, SOCS1 knockdown increased the mRNA levels of ISG15, MxA, and IFIT1 (**Figure 3C**). We subsequently investigated the role of SOCS1 overexpression on the anti-PEDV effects of IFN-λ. The transient overexpression of SOCS1 in Vero E6 cells was verified by HA IFA (**Figure 3D**). As expected, SOCS1 overexpression substantially elevated PEDV

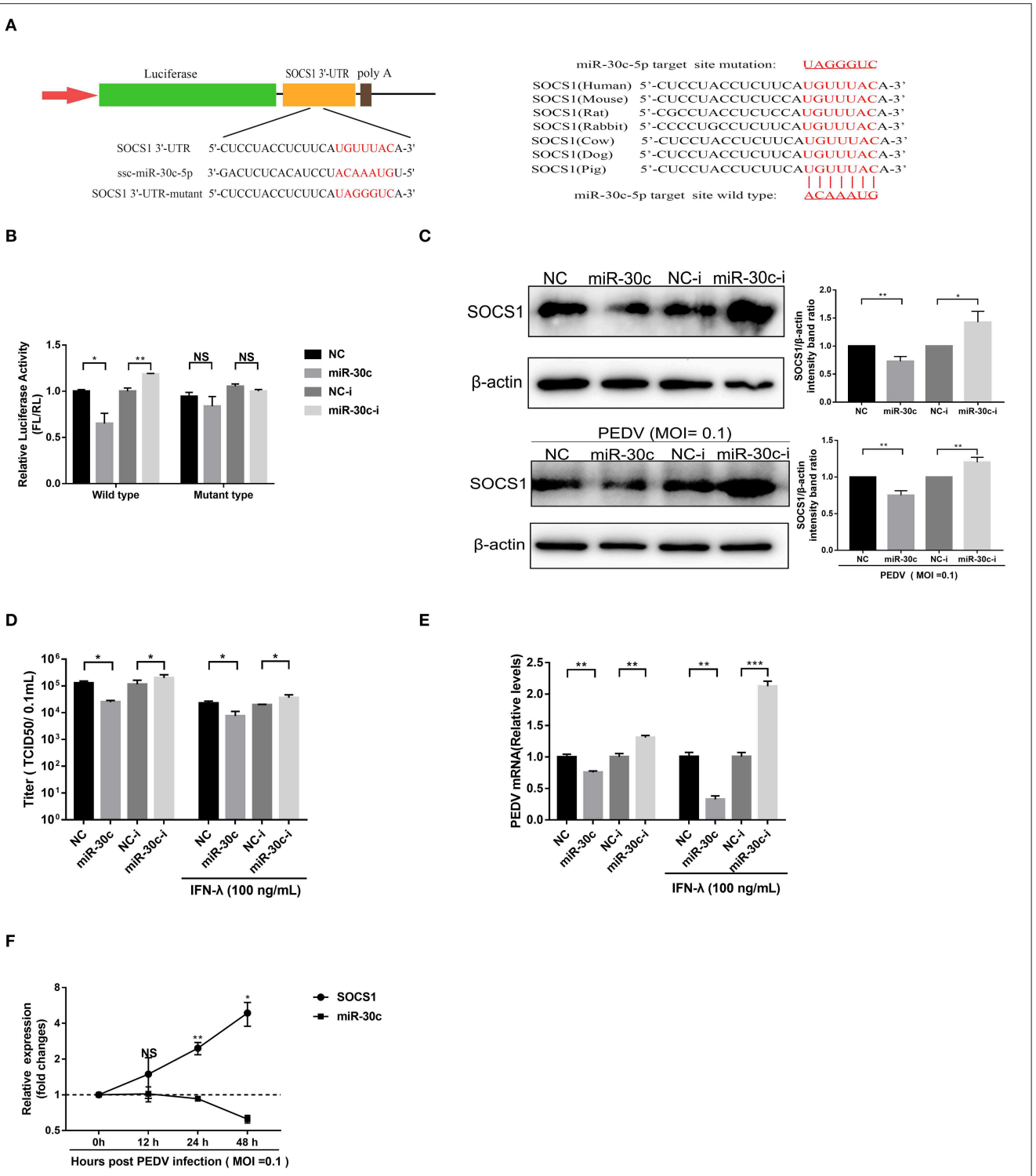

FIGURE 4 | MiR-30c-5p targeted the 3′ UTRs of SOCS1. **(A)** Schematic diagram of the left panel is the predicted target sites of miR-30c-5p in the SOCS1 3′ UTRs of seven representative mammals. The predicted target sites and mutated target sites of miR-30c-5p are underlined and mutated as indicated (right panel). **(B)** Results of the luciferase assay. Vero E6 cells were co-transfected with SOCS1 wild-type or mutant luciferase vectors (500 ng) and 160 nM of miR-30c-5p mimics or NC mimics, miR-30c-5p inhibitor, or NC inhibitor, and the luciferase activity was analyzed at 24 h after transfection. FL, firefly luciferase; RL, Renilla luciferase. **(C)** The suppression of SOCS1 protein levels by miR-30c-5p under PEDV-uninfected and -infected conditions. Vero E6 cells were transfected as described in the legend for panel B for 24 h, followed by infection with PEDV (MOI=0.1) or mock infection with DMEM, and the samples were collected at 36 h for Western blotting of SOCS1 or β-actin. Quantifications were normalized to those of uninfected NC. **(D,E)** MiR-30c-5p increased the anti-PEDV activity of IFN-λ. After transfection with miR-30c-5p

(Continued)

FIGURE 4 | mimics or inhibitor for 24 h, cells were pretreated with IFN-λ or DMEM for 12 h and then infected with PEDV (MOI = 0.1) and harvested at 36 hpi for viral RNA quantification and $TCID_{50}$. **(F)** The SOCS1 expression levels in Vero E6 cells were measured by RT-qPCR at 36 hpi at different MOIs. P values represent the difference from the mock-infected control for time kinetics, the SOCS1, and miR-30c-5p levels. Error bars, mean ± SEM. ($n = 3$ independent experiments). $^{*}P < 0.05$, $^{**}P < 0.01$, $^{***}P < 0.001$, and NS, not significant.

infection (**Figure 3E**) and blunted the expression of ISG15, MxA, and IFIT1 (**Figure 3F**). Thus, these data indicate that SOCS1 counteracts the anti-PEDV activity of IFN-λ.

PEDV Upregulated SOCS1 Expression by Modulating miR-30c-5p

The porcine miR-30 family (five members: miR30a-e) has been demonstrated to modulate host type I IFN response during virus infection (Zhu et al., 2014; Zhang et al., 2016; Liu et al., 2018; Ma et al., 2018). The TargetScan (http://www.targetscan.org) prediction program indicated that SOCS1 was targeted by miR-30c-5p through a site in the 3′UTR conserved in the SOCS1 of seven representative mammals (**Figure 4A**). To investigate whether miR-30c-5p is involved in modulating IFN-λ signaling by directly targeting SOCS1 and downregulating endogenous SOCS1 expression, we conducted a computational analysis using TargetScan Release 7.1 (http://www.targetscan.org). The result showed that miR-30c could directly target the site on the 3′UTRs of SOCS1 (**Figure 4A**). We cloned the predicted target sites in porcine SOCS1 3′UTR, and constructed the firefly luciferase reporter vector of porcine SOCS1 3′UTR (**Figure 4A**). Overexpression of miR-30c-5p, the luciferase reporter containing the SOCS1 wild-type target sequence, decreased to ∼65% relative to NC mimics, whereas the blockage of miR-30c by miR-30c inhibitor increased SOCS1 3′UTR luciferase activity. However, the mutation of the SOCS1 target 3′UTR site of miR-30c-5p disrupted the effects of miR-30c-5p on modifying the luciferase activity in Vero E6 cells relative to the NCs (**Figure 4B**). These results confirmed that miR-30c-5p directly targets the 3′ UTR of SOCS1. Consistent with the luciferase results, miR-30c-5p overexpression reduced SOCS1 expression measured by Western blotting (**Figure 4C**). Conversely, blockage of endogenous miR-30c-5p increased the expression of SOCS1 in Vero E6 cells compared with the NC inhibitor. To further validate the modulation of SOCS1 expression by miR-30c-5p during PEDV infection, we examined the expression of SOCS1 in PEDV-infected Vero E6 cells with overexpression or inhibition of miR-30c-5p, and found that the expression pattern of SOCS1 in PEDV infected Vero E6 cells was similar to that in PEDV-uninfected E6 cells (**Figure 4C**). Taken together, these data demonstrated that miR-30c-5p downregulates the expression of SOCS1 by directly targeting SOCS1 3′UTR.

To verify whether PEDV escape the IFN-λ antiviral signaling through miR-30c-5p mediated modification of SOCS1 expression, we then explored the effect of miR-30c-5p on PEDV infection and IFN-λ antiviral signaling. Transient miR-30c expression reduced PEDV titers and promoted IFN-λ anti-PEDV activity compared with the mock control NCs, whereas miR-30c-5p inhibitor significantly increased PEDV infection and undermined the anti-PEDV activity of IFN-λ (**Figures 4D,E**). Furthermore, the SOCS1 expression increased starting at 12 hpi and substantially increased at 24 hpi, which was inversely correlated with the kinetic expression profiles of miR-30c-5p (**Figure 4F**). In agreement with the kinetics pattern of miR-30c-5p and SOCS1 in Vero E6 cells, PEDV infection reduced the levels of miR-30c-5p and increased SOCS1 expression in IPEC-J2 starting at 12 h post-infection (data not shown). Collectively, PEDV infection upregulates SOCS1 expression by modulating host miR-30c-5p abundance at the late stage of infection.

miR-30c-5p Facilitated PEDV Infection via Antagonizing IFN-λ Signaling by Targeting SOCS1

To further verify whether PEDV escape IFN-λ response through the miR-30c-5p/SOCs1 axis, we co-transfected miR-30c-5p with SOCS1 and measured the replication of PEDV with or without IFN-λ treatment. SOCS1 overexpression promoted PEDV replication with or without IFN-λ treatment. MiR-30c-5p largely abolished the role of SOCS1 in promoting PEDV replication, and the effect was more pronounced in the presence of IFN-λ stimulation (**Figure 5A**). Consistent with this, SOCS1 inhibited IFN downstream ISGs expression such as IFIT1 and ISG15 expression (**Figures 5B,C**), whereas overexpression of miR-30c-5p abrogated the ISG inhibition of SOCS1, which was more pronounced in the presence of IFN-λ priming (**Figures 5B,C**). In summary, these data indicate that PEDV escapes the response of IFN-λ through the miR-30a-5p/SOCS1 axis.

DISCUSSION

IFN-λ is an antiviral innate cytokine induced by virus infection that plays vital roles in controlling mucosal infection (Blumer et al., 2017). We and other groups previously showed that IFN-λ substantially inhibits PEDV (Li et al., 2017; Zhang et al., 2018). However, whether PEDV has evolved a mechanism to counteract endogenous IFN-λ just as PEDV does the type I IFN response remains unclear. In this study, we found that PEDV propagated well despite the significant production of endogenous IFN-λ induced at the late stage of infection in Vero E6 cells, indicating that PEDV escaped the IFN-λ response at the late stage of infection not through suppressing IFN-λ production. We further defined the mechanism that PEDV counteracted IFN-λ-elicited antiviral ISG responses by exploiting the miR-30c-5p/SOCS1 axis.

PEDV has evolved multiple strategies to escape type I IFN response. Whether PEDV exploits similar mechanisms to counteract type III IFN remains elusive. One previous study demonstrated that PEDV escaped type III IFN by suppressing IRF1-mediated IFN-λ production through PEDV viral nsp1 protein (Zhang et al., 2018). In that study, PEDV actually upregulates IFN-λ expression at 3 h post-infection and then decreased to minimal levels of IFN-λ expression until 12 hpi

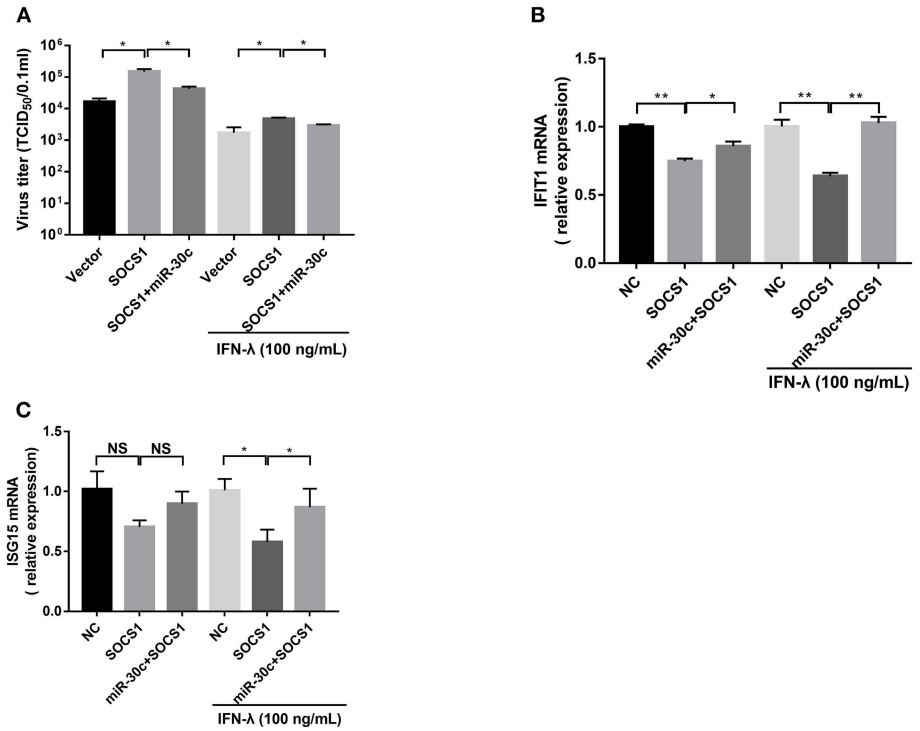

FIGURE 5 | Mir-30c-5p inhibited the infection of PEDV by regulating the expression of SOCS1. **(A)** SOCS1 overexpression increased PEDV infection and undermined the anti-PEDV activity of IFN-λ. Vero E6 cells were transfected as described with pCAGGS-HA, pCAGGS-SOCS1, and miR-30c-5p for 24 h, followed by incubation with porcine IFN-λ (100 ng/ml) or DMEM for 12 h. The cells then were infected with PEDV at an MOI of 0.1; PEDV infection was determined at 36 hpi. **(B,C)** miR-30c-5p abolished the impairment of the overexpression of SOCS1 to IFN-λ signaling under IFN-λ-stimulated or PEDV-infected conditions. E6 cells were treated as described in the legend for panel A. The cells were collected for RT-qPCR analysis of IFIT1 and ISG15 expression relative to that of GAPDH. Error bars, mean ± SEM ($n = 3$ independent experiments). $^{*}P < 0.05$, $^{**}P < 0.01$, and NS, not significant.

(Zhang et al., 2018). In agreement with this, we did not observe increased IFN-λ expression at 12 hpi (**Figure 1A**). They did not show the IFN-λ expression at the late stage of PEDV infection. In the current study, we observed that PEDV elicited substantially increased IFN-λ expression in Vero E6 cells only after 24 hpi (**Figure 1A**), which is consistent with the results observed in porcine enteroids following PEDV infection (Li et al., 2019), indicating that PEDV has evolved mechanisms to escape IFN-λ antiviral response instead of IFN-λ production at the late stage of infection. It is possible that PEDV exploits varying strategies at different infection stages. This is also observed in other RNA viruses such as influenza virus (Chung et al., 2018). To prevent over-activation of the IFN signaling pathways, the host evolves a few negative regulators of IFN signaling, and SOCS1 is one of the canonical inhibitors of IFN signaling (Shao et al., 2013). SOCS1 has been reported to be exploited by multiple viruses to abrogate IFN antiviral signaling (Shao et al., 2013; Wei et al., 2014; Ma et al., 2018). We showed that PEDV significantly induced the expression of SOCS1 at the late stage of infection (**Figure 2**). As expected, increased SOCS1 impaired the antiviral ISGs expression and impaired the anti-PEDV activity of IFN-λ (**Figure 3**). This is in agreement with the results of TGEV, another swine alphacoronavirus (Ma et al., 2018). Therefore, unlike previously published studies with the modification of IFN production mediated by viral proteins such as nsp1, our study found that PEDV largely evades innate immunity of IFN-λ by modulating the antiviral signal of IFN-λ rather than manipulating the production of IFN-λ at the late stage of infection.

MiRNA plays a vital role in regulating gene expression through post-transcription modification. Increasing evidence demonstrates that viruses escape IFN antiviral activity for optimal infection by modifying the cellular abundance of miRNA targeting vital components of the IFN response (Zhu et al., 2014; Zhang et al., 2016; Liu et al., 2018; Ma et al., 2018). JEV infection downregulates the expression of miRNA miR-432, which directly targets the suppressor of cytokine signaling protein 5 (SOCS5) and manipulates the JAK-STAT1 signaling cascade (Sharma et al., 2016). The miR-30 family has been reported to target SOCS family members and manipulate the JAK/STAT signaling pathway (Zou et al., 2017; Ma et al., 2018; Yuan et al., 2019). In this study, we showed that PEDV infection suppressed miR-30c-5p expression, which was conversely related to SOCS1 expression during PEDV infection (**Figure 4**). Just as other members of miR-30, miR-30c-5p specifically targeted the 3′ UTR of SOCS1 and inhibited SOCS1 expression (Kobayashi et al., 2012; Ma et al., 2018; Yuan et al., 2019) (**Figure 4**). However, the mechanism of PEDV decreasing miR-30a-5p remains unclear and deserves further study.

In summary, we determined that PEDV escaped IFN-λ response at the late stage of infection by downregulating miR-30c-5p, thus increasing SOCS1 expression. Therefore, unlike previously published studies with defined mechanisms such as nsp1, we demonstrated that PEDV escapes IFN-λ response through another pathway of the miR-30c-5p/SOCS1 axis. Our results highlight the important role of miR-30c-5p in the regulation of interferon pathways during PEDV infection, improve the current knowledge of PEDV infection, and expand the role of micro-RNA in viral infection.

DATA AVAILABILITY STATEMENT

The datasets generated for this study are available on request to the corresponding author.

AUTHOR CONTRIBUTIONS

PL, CW, LS, and WX designed the research studies and analyzed and interpreted the data. CW, LS, SQ, MX, KW, FF, LW, ZW, and LF conducted the experiments and collected the data. PL, CW, and LS drafted the manuscript. All of the authors contributed revisions.

FUNDING

This study was supported by the China Postdoctoral Science Foundation (2018M641841), the Special Fund for Scientific and Technological Innovative Talents in Harbin (2017RAXYJ050), the Heilongjiang Postdoctoral Fund (grant no. LBH-Z18207), and the Spark Research Fund from the Fourth Affiliated Hospital of Harbin Medical University (grant no. HYDSYXH201914).

REFERENCES

Baltimore, D., Boldin, M. P., O'Connell, R. M., Rao, D. S., and Taganov, K. D. (2008). MicroRNAs: new regulators of immune cell development and function. *Nat. Immunol.* 9, 839–845. doi: 10.1038/ni.f.209

Blumer, T., Coto-Llerena, M., Duong, F. H. T., and Heim, M. H. (2017). SOCS1 is an inducible negative regulator of interferon lambda (IFN-lambda)-induced gene expression *in vivo*. *J. Biol. Chem*. 292, 17928–17938. doi: 10.1074/jbc.M117.788877

Chung, M., Cho, S. Y., and Lee, Y. S. (2018). Construction of a Transcriptome-driven network at the early stage of infection with Influenza A H1N1 in human lung alveolar epithelial cells. *Biomol. Therap.* 26, 290–297. doi: 10.4062/biomolther.2017.240

Cullen, B. R. (2006). Viruses and microRNAs. *Nat. Genet.* 38 (Suppl):S25–30. doi: 10.1038/ng1793

de Weerd, N. A., and Nguyen, T. (2012). The interferons and their receptors–distribution and regulation. *Immunol. Cell Biol.* 90, 483–491. doi: 10.1038/icb.2012.9

Dellgren, C., Gad, H. H., Hamming, O. J., Melchjorsen, J., and Hartmann, R. (2009). Human interferon-lambda3 is a potent member of the type III interferon family. *Genes Immun.* 10, 125–131. doi: 10.1038/gene.2008.87

Deng, X., van Geelen, A., Buckley, A. C., O'Brien, A., Pillatzki, A., Lager, K. M., et al. (2019). Coronavirus endoribonuclease activity in porcine epidemic diarrhea virus suppresses type I and Type III interferon responses. *J. Virol.* 93:e02000-18. doi: 10.1128/JVI.02000-18

Gottwein, E., and Cullen, B. R. (2008). Viral and cellular microRNAs as determinants of viral pathogenesis and immunity. *Cell Host Microbe* 3, 375–387. doi: 10.1016/j.chom.2008.05.002

Guo, L., Luo, X., Li, R., Xu, Y., Zhang, J., Ge, J., et al. (2016). Porcine epidemic diarrhea virus infection inhibits interferon signaling by targeted degradation of STAT1. *J. Virol.* 90, 8281–8292. doi: 10.1128/JVI.01091-16

Hofmann, M., and Wyler, R. (1988). Propagation of the virus of porcine epidemic diarrhea in cell culture. *J. Clin. Microbiol.* 26, 2235–2239. doi: 10.1128/JCM.26.11.2235-2239.1988

Kincaid, R. P., and Sullivan, C. S. (2012). Virus-encoded microRNAs: an overview and a look to the future. *PLoS Pathog* 8:e1003018. doi: 10.1371/journal.ppat.1003018

Kobayashi, N., Uemura, H., Nagahama, K., Okudela, K., Furuya, M., Ino, Y., et al. (2012). Identification of miR-30d as a novel prognostic maker of prostate cancer. *Oncotarget* 3, 1455–1471. doi: 10.18632/oncotarget.696

Kotenko, S. V., Gallagher, G., Baurin, V. V., Lewis-Antes, A., Shen, M., Shah, N. K., et al. (2003). IFN-lambdas mediate antiviral protection through a distinct class II cytokine receptor complex. *Nat. Immunol.* 4, 69–77. doi: 10.1038/ni875

Lazear, H. M., Nice, T. J., and Diamond, M. S. (2015). Interferon-lambda: immune functions at barrier surfaces and beyond. *Immunity* 43, 15–28. doi: 10.1016/j.immuni.2015.07.001

Li, L., Fu, F., Guo, S., Wang, H., He, X., Xue, M., et al. (2019). Porcine intestinal enteroids: a new model for studying enteric coronavirus porcine epidemic diarrhea virus infection and the host innate response. *J. Virol.* 93:e01682-18. doi: 10.1128/JVI.01682-18s

Li, L., Fu, F., Xue, M., Chen, W., Liu, J., Shi, H., et al. (2017). IFN-lambda preferably inhibits PEDV infection of porcine intestinal epithelial cells compared with IFN-alpha. *Antiviral Res.* 140, 76–82. doi: 10.1016/j.antiviral.2017.01.012

Li, W., Li, H., Liu, Y., Pan, Y., Deng, F., Song, Y., et al. (2012). New variants of porcine epidemic diarrhea virus China 2011. *Emerg. Infect. Dis.* 18, 1350–1353. doi: 10.3201/eid1803.120002

Liu, F., Wang, H., Du, L., Wei, Z., Zhang, Q., and Feng, W. H. (2018). MicroRNA-30c targets the interferon-alpha/beta receptor beta chain to promote type 2 PRRSV infection. *J. Gen. Virol.* 99, 1671–1680. doi: 10.1099/jgv.0.001166

Ma, Y., Wang, C., Xue, M., Fu, F., Zhang, X., Li, L., et al. (2018). The coronavirus transmissible gastroenteritis virus evades the type i interferon response through IRE1alpha-mediated manipulation of the MicroRNA miR-30a-5p/SOCS1/3 Axis. *J. Virol.* 92, e00728-18. doi: 10.1128/JVI.00728-18

Madson, D. M., Magstadt, D. R., Arruda, P. H., Hoang, H., Sun, D., Bower, L. P., et al. (2014). Pathogenesis of porcine epidemic diarrhea virus isolate (US/Iowa/18984/2013) in 3-week-old weaned pigs. *Vet. Microbiol.* 174, 60–68. doi: 10.1016/j.vetmic.2014.09.002

Mordstein, M., Neugebauer, E., Ditt, V., Jessen, B., Rieger, T., Falcone, V., et al. (2010). Lambda interferon renders epithelial cells of the respiratory and gastrointestinal tracts resistant to viral infections. *J. Virol.* 84, 5670–5677. doi: 10.1128/JVI.00272-10

O'Neill, L. A., Sheedy, F. J., and McCoy, C. E. (2011). MicroRNAs: the fine-tuners of Toll-like receptor signalling. *Nat. Rev. Immunol.* 11, 163–175. doi: 10.1038/nri2957

Palma-Ocampo, H. K., Flores-Alonso, J. C., Vallejo-Ruiz, V., Reyes-Leyva, J., Flores-Mendoza, L., Herrera-Camacho, I., et al. (2015). Interferon lambda inhibits dengue virus replication in epithelial cells. *Virol. J.* 12:150. doi: 10.1186/s12985-015-0383-4

Pott, J., Mahlakoiv, T., Mordstein, M., Duerr, C. U., Michiels, T., Stockinger, S., et al. (2011). IFN-lambda determines the intestinal epithelial antiviral host defense. *Proc. Natl. Acad. Sci. U.S.A.* 108, 7944–7949. doi: 10.1073/pnas.1100552108

Shao, R. X., Zhang, L., Hong, Z., Goto, K., Cheng, D., Chen, W. C., et al. (2013). SOCS1 abrogates IFN's antiviral effect on hepatitis C virus replication. *Antiviral Res.* 97, 101–107. doi: 10.1016/j.antiviral.2012.12.001

Sharma, N., Kumawat, K. L., Rastogi, M., Basu, A., and Singh, S. K. (2016). Japanese encephalitis virus exploits the microRNA-432 to regulate the expression of Suppressor of Cytokine Signaling (SOCS) 5. *Sci. Rep.* 6:27685. doi: 10.1038/srep27685

Shen, H., Zhang, C., Guo, P., Liu, Z., Sun, M., Sun, J., et al. (2016). Short communication: antiviral activity of porcine IFN-lambda3 against

porcine epidemic diarrhea virus *in vitro*. *Virus Genes* 52, 877–882. doi: 10.1007/s11262-016-1374-2

Sheppard, P., Kindsvogel, W., Xu, W., Henderson, K., Schlutsmeyer, S., Whitmore, T. E., et al. (2003). IL-28, IL-29 and their class II cytokine receptor IL-28R. *Nat. Immunol.* 4, 63–68. doi: 10.1038/ni873

Skjesol, A., Liebe, T., Iliev, D. B., Thomassen, E. I., Tollersrud, L. G., Sobhkhez, M., et al. (2014). Functional conservation of suppressors of cytokine signaling proteins between teleosts and mammals: Atlantic salmon SOCS1 binds to JAK/STAT family members and suppresses type I and II IFN signaling. *Dev. Comp. Immunol.* 45, 177–189. doi: 10.1016/j.dci.2014.02.009

Song, D., and Park, B. (2012). Porcine epidemic diarrhoea virus: a comprehensive review of molecular epidemiology, diagnosis, and vaccines. *Virus Genes* 44, 167–175. doi: 10.1007/s11262-012-0713-1

Sullivan, C. S., Grundhoff, A., Tevethia, S., Treisman, R., Pipas, J. M., and Ganem, D. (2006). Expression and function of microRNAs in viruses great and small. *Cold Spring Harb. Symp. Quant. Biol.* 71, 351–356. doi: 10.1101/sqb.2006.71.065

Sun, D., Shi, H., Guo, D., Chen, J., Shi, D., Zhu, Q., et al. (2015). Analysis of protein expression changes of the Vero E6 cells infected with classic PEDV strain CV777 by using quantitative proteomic technique. *J. Virol. Methods* 218, 27–39. doi: 10.1016/j.jviromet.2015.03.002

Wang, L., Byrum, B., and Zhang, Y. (2014). New variant of porcine epidemic diarrhea virus United States 2014. *Emerg. Infect. Dis.* 20, 917–919. doi: 10.3201/eid2005.140195

Wei, H., Wang, S., Chen, Q., Chen, Y., Chi, X., Zhang, L., et al. (2014). Suppression of interferon lambda signaling by SOCS-1 results in their excessive production during influenza virus infection. *PLoS Pathog.* 10:e1003845. doi: 10.1371/journal.ppat.1003845

Wells, A. I., and Coyne, C. B. (2018). Type III interferons in antiviral defenses at barrier surfaces. *Trends Immunol.* 39, 848–858. doi: 10.1016/j.it.2018.08.008

Yuan, F. H., Chen, Y. L., Zhao, Y., Liu, Z. M., Nan, C. C., Zheng, B. L., et al. (2019). microRNA-30a inhibits the liver cell proliferation and promotes cell apoptosis through the JAK/STAT signaling pathway by targeting SOCS-1 in rats with sepsis. *J. Cell. Physiol.* 234, 17839–17853. doi: 10.1002/jcp.28410

Zhang, Q., Huang, C., Yang, Q., Gao, L., Liu, H. C., Tang, J., et al. (2016). MicroRNA-30c modulates type I IFN responses to facilitate porcine reproductive and respiratory syndrome virus infection by targeting JAK1. *J. Immunol.* 196, 2272–2282. doi: 10.4049/jimmunol.1502006

Zhang, Q., Ke, H., Blikslager, A., Fujita, T., and Yoo, D. (2018). Type III interferon restriction by porcine epidemic diarrhea virus and the role of viral protein nsp1 in IRF1 Signaling. *J. Virol.* 92:e01677-17. doi: 10.1128/JVI.01677-17

Zhang, Q., and Yoo, D. (2016). Immune evasion of porcine enteric coronaviruses and viral modulation of antiviral innate signaling. *Virus Res.* 226, 128–141. doi: 10.1016/j.virusres.2016.05.015

Zhu, X., He, Z., Hu, Y., Wen, W., Lin, C., Yu, J., et al. (2014). MicroRNA-30e* suppresses dengue virus replication by promoting NF-kappaB-dependent IFN production. *PLoS Negl. Trop Dis.* 8:e3088. doi: 10.1371/journal.pntd.0003088

Zou, Y. F., Liao, W. T., Fu, Z. J., Zhao, Q., Chen, Y. X., and Zhang, W. (2017). MicroRNA-30c-5p ameliorates hypoxia-reoxygenation-induced tubular epithelial cell injury via HIF1alpha stabilization by targeting SOCS3. *Oncotarget* 8, 92801–92814. doi: 10.18632/oncotarget.21582

Conflict of Interest: The authors declare that the research was conducted in the absence of any commercial or financial relationships that could be construed as a potential conflict of interest.

Copyright © 2020 Wang, Shan, Qu, Xue, Wang, Fu, Wang, Wang, Feng, Xu and Liu. This is an open-access article distributed under the terms of the Creative Commons Attribution License (CC BY). The use, distribution or reproduction in other forums is permitted, provided the original author(s) and the copyright owner(s) are credited and that the original publication in this journal is cited, in accordance with accepted academic practice. No use, distribution or reproduction is permitted which does not comply with these terms.

frontiers in Microbiology

REVIEW
published: 28 May 2020
doi: 10.3389/fmicb.2020.00943

Bee Viruses: Routes of Infection in Hymenoptera

Orlando Yañez[1,2], Niels Piot[3], Anne Dalmon[4], Joachim R. de Miranda[5], Panuwan Chantawannakul[6,7], Delphine Panziera[8,9], Esmaeil Amiri[10,11], Guy Smagghe[3], Declan Schroeder[12,13] and Nor Chejanovsky[14]**

[1] Institute of Bee Health, Vetsuisse Faculty, University of Bern, Bern, Switzerland, [2] Agroscope, Swiss Bee Research Centre, Bern, Switzerland, [3] Laboratory of Agrozoology, Department of Plants and Crops, Faculty of Bioscience Engineering, Ghent University, Ghent, Belgium, [4] INRAE, Unité de Recherche Abeilles et Environnement, Avignon, France, [5] Department of Ecology, Swedish University of Agricultural Sciences, Uppsala, Sweden, [6] Environmental Science Research Center, Faculty of Science, Chiang Mai University, Chiang Mai, Thailand, [7] Department of Biology, Faculty of Science, Chiang Mai University, Chiang Mai, Thailand, [8] General Zoology, Institute for Biology, Martin-Luther-University of Halle-Wittenberg, Halle (Saale), Germany, [9] Halle-Jena-Leipzig, German Centre for Integrative Biodiversity Research (iDiv), Leipzig, Germany, [10] Department of Biology, University of North Carolina at Greensboro, Greensboro, NC, United States, [11] Department of Entomology and Plant Pathology, North Carolina State University, Raleigh, NC, United States, [12] Department of Veterinary Population Medicine, College of Veterinary Medicine, University of Minnesota, Saint Paul, MN, United States, [13] School of Biological Sciences, University of Reading, Reading, United Kingdom, [14] Entomology Department, Institute of Plant Protection, The Volcani Center, Rishon LeZion, Israel

OPEN ACCESS

Edited by:
Akio Adachi,
Kansai Medical University, Japan

Reviewed by:
Eugene Ryabov,
United States Department of Agriculture (USDA), United States
Franco Mutinelli,
Istituto Zooprofilattico Sperimentale delle Venezie, Italy
Richou Han,
Guangdong Institute of Applied Biological Resources, China
Jevrosima Stevanovic,
University of Belgrade, Serbia

***Correspondence:**
Orlando Yañez
orlando.yanez@vetsuisse.unibe.ch
Nor Chejanovsky
ninar@volcani.agri.gov.il

Specialty section:
This article was submitted to Virology, a section of the journal Frontiers in Microbiology

Received: *22 February 2020*
Accepted: *20 April 2020*
Published: *28 May 2020*

Citation:
Yañez O, Piot N, Dalmon A, de Miranda JR, Chantawannakul P, Panziera D, Amiri E, Smagghe G, Schroeder D and Chejanovsky N (2020) Bee Viruses: Routes of Infection in Hymenoptera. Front. Microbiol. 11:943. doi: 10.3389/fmicb.2020.00943

Numerous studies have recently reported on the discovery of bee viruses in different arthropod species and their possible transmission routes, vastly increasing our understanding of these viruses and their distribution. Here, we review the current literature on the recent advances in understanding the transmission of viruses, both on the presence of bee viruses in *Apis* and non-*Apis* bee species and on the discovery of previously unknown bee viruses. The natural transmission of bee viruses will be discussed among different bee species and other insects. Finally, the research potential of *in vivo* (host organisms) and *in vitro* (cell lines) serial passages of bee viruses is discussed, from the perspective of the host-virus landscape changes and potential transmission routes for emerging bee virus infections.

Keywords: bee, virus, transmission, *Apis*, non-*Apis*, natural infection, artificial infection

INTRODUCTION

Viruses are omnipresent in practically all life forms, where they pose a potential threat to the health of the organism. This also applies for the viruses found in bees. Most of these viruses were originally discovered in honey bees, either through symptoms or diseases associated with infection. Some honey bee viruses can be propagated in, as well as isolated and purified from honey bee pupae. This enabled the initial characterization of the viruses and the development of diagnostic assays. With these early diagnostic assays, it was shown even then that these "honey bee viruses" could also be detected in other bee species and wasps, although no systematic host-range study has ever been conducted. However, recent studies found that those viruses are much more common and widespread than previously suspected, occurring in numerous other hymenopteran and non-hymenopteran arthropods. Furthermore, there are reports of spillover from and between hymenopteran taxa and non-hymenopteran arthropods. Knowing the different possible virus transmission routes and their potential host-range is key to understanding

prevalence, epidemiology and virulence in different bee species. Numerous studies have recently reported the discovery and transmission routes of viruses in different arthropod species, including many bee species. The aim of this review is to provide an overview of the recent advances of the impact and transmission of viruses found in bees. We have divided this review into two main parts. The first part, 'Natural infections,' summarizes the current knowledge regarding natural infections and the transmission routes of viruses found in honey bees. The second part, 'Artificial infections,' provides an overview of the studies involving controlled experimental virus infections and transmission. The major modes and routes of virus transmission in bees are summarized in **Box 1**.

BOX 1 | Virus transmission routes - Definitions for the present review.

Horizontal transmission is the transmission of infectious agents among individuals of the same generation. Horizontal transmission of viruses in honey bees includes transmission to different bee developmental stages via oral and/or body contact. It includes indirect infections through contaminated food (food-borne transmission) and contact with feces; venereal transmission, where virus is transmitted from drones to queens during the nuptial flights or by artificial insemination, and vector-mediated transmission, where transmission is mediated by other organisms (vectors). This vector can either be a mechanical or biological vector. A mechanical vector is defined as an organism that transmits viruses without being infected itself, while in a biological vector the virus replicates in the vector organism before being transmitted.

Vertical transmission consists of the transmission of viruses to the next generation, which for honey bees is primarily from queens to their eggs. This transmission can be defined as either transovum or transovarial transmission, depending on whether viruses are transmitted on the egg surface or within the egg, respectively. A second form of vertical transmission is transspermal transmission, if the virus is present inside the sperm, which would be the drone equivalent of transovarial transmission. This has so far not been detected in honey bees.

Transmission is defined as the establishment of a new infection in a previously non-infected individual, after acquiring the virus inoculum directly from another infected individual, from a vector or indirectly from the environment. It excludes any passive acquisition or retention of virus inoculum that does not cause infection of the bodily tissues.

PART 1: NATURAL INFECTIONS

Most of our understanding about natural bee virus infections came from studies with honey bees, particularly *Apis mellifera*. A big part of the recent developments in this field allowed for the expansion in knowledge of virus infections in other bee species. Most of these new developments involve bee species that can either be easily reared or are used for commercial pollination services, such as bumble bees (*Bombus* spp.), stingless bees (e.g., *Melipona* spp.), mason bees (e.g., *Osmia* spp.) and leafcutter bees (e.g., *Megachile* spp.). This section is therefore divided into five subsections: transmission of viruses in *Apis mellifera*, distribution of bee viruses in other *Apis* species, recently discovered bee viruses, transmission of bee viruses in non-*Apis* pollinators and transmission of viruses in non-bee insects.

Transmission of Viruses in *Apis mellifera*

Horizontal Transmission

Oral-fecal

This route is arguably the most common route for bee virus transmission, both within honey bee colonies and between bee species (Figueroa et al., 2019). There are diverse and abundant evidence that supports this route of transmission for most viruses found in honey bees. Most bee viruses are shed in copious amounts into the feces, from where they are released into the environment and can be picked up by other bees, through floral networks (Figueroa et al., 2019). Feces are also sometimes shed within bee colonies, particularly when the weather (cold, rain, wind) prevents cleansing flights or when the bees suffer from diarrhea, usually due to indigestible compounds in honey or pollen, or for suffering from nosemosis, a disease caused by *Nosema* sp. Bees complete the transmission when attempting to remove these feces as part of their cleaning activities.

Trophallaxis

A foodborne transmission pathway involving trophallaxis (mouth-to-mouth sharing of food between colony members) was proposed to exist for Israeli acute paralysis virus (IAPV; Chen et al., 2014). Laboratory experiments showed that IAPV can indeed be acquired through trophallaxis (Amiri et al., 2019), but it is not known if this transmission also leads to infection.

Hypopharyngeal glands and larval food

The hypopharyngeal glands are paired tubular secretory organs in the frontal region of the worker bee head (Snodgrass, 1956). They secrete a proteinaceous substance, royal jelly, which is the principal component of larval food. Several viruses have been detected from worker bees hypopharyngeal glands and larval food indicating a potential virus transmission route. Acute bee paralysis virus (ABPV) is frequently detected in the hypopharyngeal glands of ABPV-symptomatic adults (Bailey and Milne, 1969). IAPV, a closely related virus of ABPV (de Miranda et al., 2010a), was also found at relatively high levels in hypopharyngeal glands (Chen et al., 2014). Deformed wing virus (DWV) has also been detected in the glandular secretions of nurse bees (Fievet et al., 2006) and in larval food (Yue and Genersch, 2005). Kashmir bee virus (KBV) and Sacbrood virus (SBV) have been detected in larval food (Shen et al., 2005a). The large amounts of Cloudy wing virus (CWV) in sealed brood suggest an oral transmission route, i.e., that nurse bees infected with CWV can transmit the virus to larva via the larval food (Carreck et al., 2010).

Other food sources

The detection of viruses in food sources (i.e., brood food, honey, pollen) also suggests an oral transmission route. KBV and SBV have been detected in honey, pollen, and royal jelly (Bailey and Fernando, 1972; Singh et al., 2010). *Apis mellifera* filamentous virus (AmFV) has been detected in honey and pollen (Gauthier et al., 2015). IAPV was found in pollen (Chen et al., 2014) while Black queen cell virus (BQCV), Lake Sinai virus (LSV), DWV, and SBV have been detected in pollen pellets (Singh et al., 2010; Ravoet et al., 2015a).

Detection in gut tissues and feces

Black queen cell virus was detected in queen gut tissues and feces, suggesting possible transmission through feces (Chen et al., 2006). However, BQCV seems to be partially dependent on *Nosema apis* for infection of adult bees by ingestion (Bailey et al., 1983a). Several other viruses have been detected in the feces of infected bees such as ABPV (Bailey and Gibbs, 1964), Chronic bee paralysis virus (CBPV; Bailey, 1965), DWV (Chen et al., 2006), KBV (Hung, 2000), IAPV (Chen et al., 2014), and CBPV contaminated feces have recently been proven to provoke CBPV infection and overt disease in naive bees placed in cages previously occupied with contaminated individuals (Ribière et al., 2007).

Topical or body contact

Chronic bee paralysis virus can be transmitted by topical application on newly denuded honey bee cuticula (Bailey et al., 1983b) and it is transmitted from contaminated bees to non-infected bees reared in the same cages (Amiri et al., 2014; Coulon et al., 2018). Similarly, IAPV can be transmitted by topical application to honey bee workers and subsequent physical contact between infected workers and queens that leads to highly infected queens, suggesting that IAPV can also spread through close bodily contact (Amiri et al., 2019).

Vector-mediated transmission

Virus transmission via another organism (a 'vector') is also considered a form of horizontal transmission, since it still concerns transmission between individuals of the same generation. The close interaction between honey bees with obligate parasites such as endo- and ectoparasitic mites create a scenario where such mites can act as either mechanical vectors (i.e., exclusively the physical transfer of the acquired virus to a new host) or even biological vectors (where the virus also replicates inside the vector) for viruses (Chantawannakul et al., 2006; Forsgren et al., 2009). Picorna-like virus particle aggregations were found in lysed cells from the body cavity of the tracheal mite, ***Acarapis woodi*** (Liu, 1991) which is an endoparasitic mite that lives inside the tracheae and air sacs of adult honey bees (Sammataro et al., 2000). Although the identity of the virus was not established, the particle sizes and shapes are one of the most common ones among insect viruses. The role of *A. woodi* as a vector for picorna-like viruses is still unclear, mostly because very little dedicated research has been conducted on the possible role of *A. woodi* as a vector of virus diseases, in part because in the past it has never been linked to any viral disease.

By contrast, there is abundant evidence for vectored virus transmission by the ectoparasitic mite ***Varroa destructor*** (Santillán-Galicia et al., 2010; Möckel et al., 2011; Martin et al., 2012; Gisder et al., 2018; Posada-Florez et al., 2019; Ryabov et al., 2019), which is the reason why this mite is currently the most damaging parasite of the honey bees (Rosenkranz et al., 2010). ABPV, KBV, and IAPV are part of a complex of related viruses (Chen and Siede, 2007; de Miranda et al., 2010b), sometimes referred to as the "AKI complex." These viruses have been associated with honey bee colony losses, particularly when colonies are co-infected with *V. destructor* (Cox-Foster et al., 2007; de Miranda et al., 2010a; Dainat et al., 2012). As yet, there has not been any direct evidence of ABPV replication within varroa mites (Ball, 1983, 1985; de Miranda et al., 2010b). However, high levels of ABPV have been detected in individual varroa-parasitized bees, as well as in entire honey bee colonies, indicating that the mite functions as a mechanical vector of ABPV (Bakonyi et al., 2002; D'Alvise et al., 2019). Effective transmission by *V. destructor* mites to a new host occurs after 36 h of acquiring the virus. DWV is widely detected in colonies infested by *V. destructor*. The mites function as a mechanical vector of DWV as they can transmit DWV during feeding activities (Ball, 1989; Bowen-Walker et al., 1999; Nordström, 2003; Shen et al., 2005b). Moreover, *V. destructor* has been described as a biological vector of DWV since the virus multiplies inside the vector, which is linked to the subsequent appearance of overt DWV infections in emerging bees (Gisder et al., 2009). DWV is a quasispecies made up of a cloud of variants. These variants can be divided into three master variants, DWV-A, -B, and -C (Mordecai et al., 2016c). The latest evidence suggests that DWV-B replicates inside *V. destructor* (Ongus et al., 2004; Campbell et al., 2016; Posada-Florez et al., 2019). DWV-B was originally named Varroa destructor virus 1 that was shown to be virulent when injected in high-titers into pupae or adult bees in cage experiments (Ryabov et al., 2014, 2019; McMahon et al., 2016; Gisder et al., 2018) but had surprisingly protective features when dominant in a colony despite the presence of *V. destructor* (Mordecai et al., 2016a). Interestingly, a positive correlation of DWV-B with bees dying over the winter period in stationary colonies were observed (Natsopoulou et al., 2017), however, these colonies nonetheless survived the overwintering period and did not collapse the following spring. This was not the case when colonies with high-titers of DWV-A and possibly DWV-C resulted in unexpected colony losses over the same overwintering period (Kevill et al., 2017). DWV-A is proposed to be mechanically vectored by *V. destructor* as it could only be transferred in lab-based experiments in a non-propagative manner (Posada-Florez et al., 2019).

Israeli acute paralysis virus is also widely detected in colonies infested by *V. destructor* mites. Evidence shows that *V. destructor* mites serve as an effective mechanical and biological vector of IAPV (Di Prisco et al., 2011). The detection of KBV in *V. destructor* mites and their salivary secretions (Hung and Shimanuki, 1999; Hung, 2000; Shen et al., 2005b) suggests that the parasite may act as a vector of KBV. CBPV was also detected in *V. destructor*, and the mite was involved in CBPV infection within the hive (Celle et al., 2008). *V. destructor* was also proven to acquire Slow bee paralysis virus (SBPV) by feeding on infected pupae and subsequently transmitting the virus to new parasitized pupae (Santillán-Galicia et al., 2010). *V. destructor* was proposed to be a biological vector for Apis rhabdovirus-1/Bee rhabdovirus-1 (ARV-1/BRV-1). Although replication of intermediate forms for these viruses were detected in varroa mites (Levin et al., 2017), the fact that much of the *V. destructor* gut contents, including nucleic acids and possible virus replication intermediate forms, are derived from their bee hosts (Cornman, 2017; Posada-Florez et al., 2019), means that such evidence is not necessarily conclusive for biological vector status of the mite

(see also de Miranda et al., 2015). Nevertheless, Remnant et al. (2017) proposed that *V. destructor* is a genuine host for ARV-1 and -2 because the ssRNA (small RNA) profile of these viruses found in mites were different from those found in honey bees. *V. destructor*-mediated transmission of LSV is also suspected, as the virus is readily detected in the mite, although no causal association has been shown thus far (Daughenbaugh et al., 2015; Ravoet et al., 2015a). Bee Macula-like virus (BeeMLV) is also strongly correlated with the presence of *V. destructor*. It was shown to replicate in bees, and thus accumulate replication intermediates in mites (de Miranda et al., 2015). More conclusive evidence is needed to elucidate the precise role of mites in the transmission of this virus (de Miranda et al., 2015). Similarly, there is no conclusive evidence that SBV is directly transmitted by *V. destructor*, although it is frequently associated with varroa-related damage (Dubois et al., 2020), host-virus molecular interactions (Di Prisco et al., 2016; Ryabov et al., 2016; Remnant et al., 2019) and tolerance (Thaduri et al., 2018) as well as in *V. destructor* behavior (Giuffre et al., 2019). For BQCV, there is no evidence that it replicates in or is transmitted by *V. destructor*.

As in the case of the *V. destructor – Apis mellifera* relationship, Tropilaelaps mites are also ectoparasitic mites that are native to Asia and naturally parasitise *Apis dorsata*. Two species of Tropilaelaps mites (*Tropilaelaps mercedesae* and *T. clareae*) are also able to parasitise *Apis mellifera*. Compared with *V. destructor,* ***T. mercedesae*** is much more dependent on the continuous availability of honey bee brood for feeding and reproduction (Chantawannakul et al., 2016). *T. mercedesae* was also shown to transmit DWV in honey bees (Dainat et al., 2009; Forsgren et al., 2009; Khongphinitbunjong et al., 2016; Wu et al., 2017) and was associated with clinical DWV symptoms, such as reduced longevity, reduced weight at emergence and crippled wings (Khongphinitbunjong et al., 2016). ABPV, another common honey bee virus, has also been detected in *T. mercedesae*, with phylogenetic analyses implying that ABPV might have moved from *T. mercedesae* to *A. mellifera* (Chanpanitkitchote et al., 2018).

Aethina tumida, the small hive beetle (SHB), is a scavenger of honey bee colonies, whose larvae feed on honey, pollen and detritus. It has been shown that SHB can acquire DWV by feeding on DWV-infected brood and bees, by topical contact with DWV-contaminated wax and by exploiting trophallaxis between bees. The occurrence of high DWV titers in SHB suggests that it could be a true host, and possible biological reservoir, for DWV. Since SHB consumes bees, the detection of DWV replication intermediates (negative-strand RNA) is by itself not conclusive evidence for biological-vector status, similar as for varroa, but supports the evidence of quantitative increase in DWV titers (Eyer et al., 2009).

Venereal transmission

Venereal transmission is also considered a form of horizontal transmission, since it involves individuals from the same generation. Because of the challenges in experimentally controlling the natural mating process of honey bee queens and drones, much of the evidence for venereal infection is based on experiments with artificial insemination (Yue et al., 2006; de Miranda and Fries, 2008) the detection of viral particles in the reproductive organs, tissues and secretions of drones and queens (e.g., endophallus, semen, ovaries, spermatheca). That is the case for the detection of ABPV (Yue et al., 2006; Prodělalová et al., 2019), BQCV (Prodělalová et al., 2019), SBV (Prodělalová et al., 2019), AmFV (Gauthier et al., 2015; Prodělalová et al., 2019), IAPV (Chen et al., 2014), and DWV (Fievet et al., 2006; Yue et al., 2006; de Miranda and Fries, 2008; Yañez et al., 2012a; Prodělalová et al., 2019) in semen, which first identified the potential for sexual transmission. Similarly, the occurrence of viruses in the spermatheca of mated queens such as DWV (Chen et al., 2006; de Miranda and Fries, 2008; Francis et al., 2013) and IAPV (Chen et al., 2014) suggests the potential for virus found in sperm to cause infection in the queen tissues; confirming the possibility for sexual transmission through artificial insemination (Yue et al., 2007; de Miranda and Fries, 2008). However, the question whether venereal transmission also occurs naturally remains unresolved. The detection of high titers of DWV in the endophalluses of drones sampled from drone congregation areas (Yañez et al., 2012a), where they can potentially mate with queens during nuptial flights, as well as in the mating signs collected from returning queens (Amiri et al., 2016), showed that there were no functional consequences of high DWV loads in reproductive drones for natural venereal virus transmission. Furthermore, high viral titers were detected in some of the endophallic remains that were left inside mating organs of returning mated queens by the last mating drone (Amiri et al., 2016), again showing that such high-titers were no hinder to successful mating. Similarly, high DWV titers were found in the spermathecae and in the sperm contained in these for several of the tested queens (Amiri et al., 2016). These results provide evidence that DWV can be transmitted through both artificial and natural mating, confirming the earlier indirect evidence from artificial insemination (Chen et al., 2006; Yue et al., 2006, 2007; de Miranda and Fries, 2008).

Vertical Transmission

For honey bees, vertical transmission involves the transfer of viruses from queens or drones (either directly through sperm or indirectly through prior venereal infection of the queen) to their offspring. Several studies reported detection correlated distribution of viruses in queens and their eggs, which implies vertical transmission. For instance, BQCV and DWV were detected in all analyzed queens ($N = 10$) and in all pools of 50 eggs from these queens (Chen et al., 2006). Other indirect evidence relevant for vertical transmission is the presence of viruses in the queen's reproductive organs. BQCV was detected in 70% of queen ovaries while DWV was detected in the ovaries of all analyzed queens (Chen et al., 2006). Francis et al. (2013) also showed the high prevalence of DWV in queen's ovaries with 80% ($N = 86$) testing DWV positive. Moreover, Fievet et al. (2006) showed that the ovaries were the organs with the highest DWV titers in their tested queens. de Miranda and Fries (2008) traced DWV through the entire venereal-vertical infection process, from artificial insemination through infection of the spermatheca and queen's ovaries to the resulting offspring, while Amiri et al. (2016) showed that ovaries can be infected with DWV after natural

mating with DWV-positive drones and the virus can afterward be passed on to the eggs laid by these queens (Amiri et al., 2018). Not all the offspring from DWV-infected queens are DWV positive, nor do all DWV-infected queens also transmit vertically (Yue et al., 2007; de Miranda and Fries, 2008), so barriers to vertical transmission do exist, but in general terms the accumulated evidence indicates that DWV uses vertical transmission as a natural route for dissemination.

Regarding other viruses, the detection of CBPV (Chen et al., 2005, 2006; Blanchard et al., 2007; Ravoet et al., 2015b), IAPV (Chen et al., 2014), KBV (Chen et al., 2005; Shen et al., 2005a), SBV (Chen et al., 2005, 2006; Ravoet et al., 2015b), ABPV (Ravoet et al., 2015b), LSV (Ravoet et al., 2015b), Aphid lethal paralysis virus (ALPV, Ravoet et al., 2015b), and AmFV (Gauthier et al., 2015) in queens, their ovaries or in eggs, implies potential vertical transmission for these viruses as well. Additionally, the detection of BQCV, DWV, CBPV, KBV, and SBV in surface-sterilized eggs (Chen et al., 2006), strongly suggest transovarial transmission of these viruses, a pathway that involves the acquisition of the virus during oogenesis (however, see Amiri et al., 2018).

No information is available for vertical transmission of some less studied viruses, such as CWV, LSV, Moku virus (MV), BeeMLV, and/or ARV-1/BRV-1.

The present knowledge about which bee viruses are transmitted through various transmission routes is summarized in **Table 1**.

TABLE 1 | Routes of infection of viruses associated with honey bees. Overview of their horizontal and vertical transmission routes.

Virus	Transmission					
	Horizontal					Vertical
	Oral*	Fecal	Body Contact	Venereal	Vector-mediated	Queen to eggs
IAPV	+	+	+	Ve.S.	+ (Vd)	+
ABPV	+	+	BC.S	Ve.S.	Vd.S., Tm.S.	+
KBV	+	+	BC.S	–	+ (Vd)	+
BQCV	+	+	?	Ve.S.	–	+
DWV	+	+	–	+	+ (Vd, Tm, At.S.)	+
SBV	+	–	–	Ve.S.	–	+
SBPV	+	?	?	?	+ (Vd)	?
CWV	O.S.	?	?	?	–	?
CBPV	+	+	+	–	Vd.S	+
LSV	+	?	?	–	Vd.S.	+
BeeMLV	?	?	?	?	Vd.S.	?
AmFV	+	?	?	Ve.S.	–	+
ALPV	?	?	?	?	?	+
ARV-1/BRV-1	?	?	?	?	Vd.S.	?
ARV-2/BRV-2	?	?	?	?	Vd.S.	?
ABV-1	?	?	?	?	?	?
ABV-2	?	?	?	?	?	?
ArkBV	?	?	?	?	?	?
BerkBPV	?	?	?	?	?	?
BSRV	?	?	?	–	?	?
C/TSBV	+	?	?	?	?	?
BVX	+	?	?	?	?	?
BVY	+	?	?	?	?	?
VTLV	?	?	?	?	Vd.S.	?
AIV	?	?	?	?	?	?
MV	?	?	?	?	?	?
VDV-2	?	?	?	?	?	?
VDV-3	?	?	?	?	?	?
VOV-1	?	?	?	?	?	?
AFV	?	?	?	?	?	?
ANV	?	?	?	?	?	?
ADV	?	?	?	?	?	?

*ABPV, Acute bee paralysis virus; ABV-1, Apis bunyavirus-1; ABV-2, Apis bunyavirus-2; AmFV, Apis mellifera filamentous virus; ADV, Apis dicistrovirus; AIV, Apis iridescent virus (Bailey et al., 1979); ArkBV and BerkBPV, Arkansas bee virus and Berkeley bee virus (Bailey and Woods, 1974); AFV, Apis mellifera flavivirus; ANV, Apis Nora virus; ARV-1/BRV-1, Apis/Bee rhabdovirus-1; ARV-2/BRV-2, Apis/Bee rhabdovirus-2; BeeMLV, Bee Macula-like virus; BVX and BVY, Bee virus X and Y (Bailey et al., 1983a); BSRV, Big Sioux river virus (Runckel et al., 2011); BQCV, Black queen cell virus; IAPV, Israeli acute paralysis virus; C/TSBV, Chinese/Thai sacbrood virus; CWV, Cloudy wing virus; CBPV, Chronic bee paralysis virus; DWV, Deformed wing virus; KBV, Kashmir bee virus; LSV, Lake Sinai virus; MV, Moku virus; SBV, Sacbrood virus; SBPV, Slow bee paralysis virus; VDV-2 and VDV-3, Varroa destructor virus-2 and -3 (Levin et al., 2016); VOV-1, Varroa orthomyxovirus-1 (Levin et al., 2019); VTLV, Varroa Tymo-like virus (de Miranda et al., 2015). *, including trophallaxis, gut content and contaminated food; +, transmission confirmed; –, non-demonstrated transmission; ?, unknown; O.S., suggested oral transmission by presence in sealed brood; BC.S, suggested transmission by body contact; Ve.S., suggested venereal transmission by presence in semen and/or spermatheca; Vd, transmission confirmed by Varroa destructor; Vd.S., suggested vector-mediated transmission by Varroa destructor; Tm, transmission confirmed by Tropilaelaps mercedesae; Tm.S., suggested vector-mediated transmission by Tropilaelaps mercedesae; At.S., suggested vector-mediated transmission by Aethina tumida.*

Distribution of Bee Viruses in Other *Apis* Species

Bee viruses are capable of infecting multiple host species and horizontal transmission seems to play a crucial role in the global viral distribution patterns in different species of social honey bees (*Apis* spp.), which share ecological habitats and geographic ranges, particularly in south-east Asia. The most prevalent viruses in *Apis* species are DWV and BQCV, which for historical reasons were first described in the European honey bee, *A. mellifera* (Chen and Siede, 2007; Zhang et al., 2012), but have since also been detected in other honey bee species. DWV has been detected in four honey bee species *(A. mellifera*, *A. dorsata, A. florea* and *A. cerana*) (Chantawannakul et al., 2006; Berényi et al., 2007; Sanpa and Chantawannakul, 2009; Kojima et al., 2011; Ai et al., 2012b; Li et al., 2012; Forsgren et al., 2015; Yañez et al., 2016). Nevertheless, DWV occurs less frequently in wild honey bees (i.e., *A. florea* and *A. dorsata*) than BQCV (Zhang et al., 2012; Mookhploy et al., 2015). BQCV and the AKI viruses are also multi-host pathogens that can infect all honey bee species, as well as numerous non-*Apis* species. Since BQCV can be transmitted via contaminated food sources such as honey and pollen, this may be a route of transmission for honey bees residing in close proximity by sharing food sources.

The presence of KBV in *A. cerana* was first shown in bees from India (Bailey and Woods, 1977) and later also in South Korea (Choe et al., 2012). IAPV has also been detected in *A. cerana* (Kojima et al., 2011; Ai et al., 2012b; Yañez et al., 2016).

Sacbrood virus has been detected in several *Apis* species (Allen and Ball, 1996). It is especially prominent and damaging

in *A. cerana* (Shah and Shah, 1988; Grabensteiner et al., 2001; Sanpa and Chantawannakul, 2009; Yoo and Yoon, 2009; Choi et al., 2010; Kojima et al., 2011; Ai et al., 2012a; Forsgren et al., 2015; Yañez et al., 2016). Thai sacbrood virus (TSBV, also known as Chinese sacbrood virus) was the first virus discovered in *A. cerana* from Thailand in 1976 (Bailey and Collins, 1982). TSBV also caused the death of more than 90% of domesticated *A. cerana* populations in Kashmir (Abrol and Bhat, 1990), and was found in *A. dorsata* and *A. florea* in India (Allen and Ball, 1996).

Multiple viral infections in individual bees or whole colonies have been reported in both managed and feral colonies of *Apis* species. This emphasizes the importance of virus–virus and bee–virus interactions (Takahashi et al., 2007; Choi et al., 2008; Sanpa and Chantawannakul, 2009; Ai et al., 2012a; Choe et al., 2012; Li et al., 2012; Ra et al., 2012; Reddy et al., 2013; Forsgren et al., 2015; Mookhploy et al., 2015).

During bee virus surveys in Asia, where both *A. cerana* and *A. mellifera* are cultivated, phylogenetic analysis of the capsid-protein gene of BQCV isolates from Thailand, China, South Korea, and Japan revealed a strong geographic clustering within Asia, distinct from South African and European isolates. No clustering were, however, observed according to the *Apis* host species that the isolates came from Mookhploy et al. (2015). BQCV isolated from Korea and Japan also showed similar levels of regional genetic variation, with high levels of similarity between isolates from the same country or continent (Kojima et al., 2011; Noh et al., 2013). That could be due to local transmission of viruses or spillover of BQCV from managed *A. mellifera* colonies to wild bees, as was the case for DWV spillover to local bumble bees (Fürst et al., 2014; Tehel et al., 2016). Another interesting point is that there appears to be no host-specific genetic adaptation by the virus when it is transmitted between bee species within the same geographic region (Fürst et al., 2014). It has been also suggested that in a two-host system, parasites may either evolve to be generalists, showing low levels of virulence, or specialists, displaying high virulence to each host species (Regoes et al., 2000). These studies highlight the complexity of bee virus disease ecology and transmission between their *Apis* and non-*Apis* hosts.

New, Recently Discovered Bee Viruses

Many new bee viruses have been discovered recently through high throughput sequencing (HTS) technologies (reviewed in Beaurepaire et al., 2020). Most of these have only been characterized taxonomically, through phylogenetic analyses of their genomic sequences, without any information about their biological properties, including, crucially, whether the bee they were found in is actually a true host or not. This includes recently described viruses such as Moku virus (Mordecai et al., 2016b); Apis Nora virus (ANV), Apis bunya virus-1,2 (ABV-1, ABV-2), Apis dicistrovirus (ADV) and Apis flavivirus (AFV) (Remnant et al., 2017), AmFV (Gauthier et al., 2015), Apis rhabdovirus-1,2 (ARV-1,-2)/Bee rhabdovirus-1,2 (BRV-1,-2) (Levin et al., 2017; Remnant et al., 2017), as well as new viruses from the families *Iflaviridae*, *Tymoviridae*, *Nudiviridae,* and *Parvoviridae* (Schoonvaere et al., 2018) and new Tymo-, Seco-, Partiti-, Noda-, Dicistro-, Circo-, Nege-, Sobemo-, and Toti-like viruses (Galbraith et al., 2018; Schoonvaere et al., 2018); and the many picorna-like viruses identified in Australian honey bees (Roberts et al., 2018). Investigating the biological properties of these genetically characterized viruses is the next logical challenge, since just their geographic origin or distribution is not sufficient to infer the putative danger these new viruses represent for honey bees.

Transmission of Bee Viruses in Non-*Apis* Pollinators

Most viruses that were first described in *Apis* sp. have also been detected in other bee species. Below we will give a short overview of the viruses detected in non-*Apis* species (for a more extensive review, we refer to Ravoet et al., 2014; Tehel et al., 2016; Gisder and Genersch, 2017).

Bumble bees are by far the most investigated non-*Apis* species with regard to viral infections and the presence of other pathogens (McMahon et al., 2015). Members of the DWV masters variants have been found in several *Bombus* sp. across different continents (Gisder and Genersch, 2017). Active replication of DWV in *Bombus* sp. has been confirmed in several Bombus species (Levitt et al., 2013; Fürst et al., 2014). Similarly for ABPV, IAPV and KBV infection in *B. terrestris* (Meeus et al., 2014), indicating that *Bombus* spp. are within the true host range of these viruses. Different viruses have different prevalences and titers in different bumble bee species (McMahon et al., 2015), which may reflect distinct susceptibilities, tolerances or transmission networks (Tehel et al., 2016; Figueroa et al., 2019). DWV infections have also been found in species of the genus *Augochlora*, *Ceratina*, *Xylocopa*, *Andrena*, *Heriades*, *Osmia*, *Melipona*, and *Scaptotrigona* (Singh et al., 2010; Guzman-Novoa et al., 2015; Tehel et al., 2016) and species belonging to Halictidae family (Evison et al., 2012; Levitt et al., 2013). Active DWV replication has been detected in *Osmia cornuta*. DWV titers in *M. subnitida* are similar to those found in honey bees. Both results suggest that DWV is capable of infecting and multiplying in at least *Osmia* spp. and *Melipona* spp. (Mazzei et al., 2014; de Souza et al., 2019). BQCV has been detected in several *Bombus* species as well as in *Melipona* and solitary bees of the genera *Xylocopa*, *Osmia*, *Andrena* and *Heriades* (Singh et al., 2010; Ravoet et al., 2014). Active replication of the virus has only been reported for *Bombus* spp. (Peng et al., 2011). The AKI virus complex has been detected in the genera *Bombus*, *Augochlora*, *Andrena*, *Heriades, Xylocopa* and *Melipona*, but active replication has only been shown in *Bombus* spp. (Singh et al., 2010; Levitt et al., 2013; Niu et al., 2016; Tehel et al., 2016; Alvarez et al., 2018) and bees from the Halictidae family (Levitt et al., 2013). So far infections with CBPV and SBPV have only been identified in *Bombus* sp., where active virus replication was verified only for SBPV (Niu et al., 2016).

Sacbrood virus was detected in *Bombus*, *Andrena, Ceratina*, and *Xylocopa* species (Singh et al., 2010; Levitt et al., 2013) and the Halictidae family (Levitt et al., 2013). Viruses of the LSV complex have been identified in *Bombus*, *Osmia*, and *Andrena* species,

but virus replication has only been reported for *Bombus* sp. and *Osmia* sp. The species *Halictus scabiosae*, *Halictus sexcinctus*, and *Halictus simplex* were screened for viruses by Bigot et al. (2017), where the *Halictus scabiosae* Adlikon virus (HsAV) was described and identified as a virus closely related to LSV. ARV-1/BRV-1 was found in *Bombus* sp. (Levin et al., 2017). As apparent from this short overview, most of these viruses are detected in many different genera of bees. Therefore, it would be difficult to pinpoint the true host range of most viruses and our current knowledge is far from a clear understanding of the presence and replication of viruses in non-*Apis* and non-*Bombus* bee species. It is impossible to tell which bee species is the primary host, or even whether this question is relevant in the complicated context of bee virus transmission. Unraveling the directionality of virus transmission is therefore difficult from the current knowledge, based largely on natural surveys, but may benefit from systematic experimental approaches (e.g., Fürst et al., 2014; Meeus et al., 2014; Figueroa et al., 2019). That said, we will now break down the transmission routes into intra-species and inter-species transmission for non-*Apis* bee species.

Inter-Species Virus Transmission

Natural inter-species virus transmission can occur via several different routes (**Figure 1**). Oral-fecal transmission is most likely the main route of inter-species virus transmission. Several viruses such as CBPV, KBV, DWV, BQCV, and IAPV have been identified in the feces of honey bees (Hung, 2000; Chen et al., 2006; Ribière et al., 2007; Chen et al., 2014). Although no study to date has reported the presence of viruses in the feces of non-*Apis* species, one could expect that virus particles are shed via the feces, similar to how this happens in honey bees. Several studies have directly identified the role of shared flowers in the transmission of a number of bee pathogens, including viruses (Singh et al., 2010; Graystock et al., 2015; Adler et al., 2018; Alger et al., 2019). Therefore, infected bees visiting flowers can contaminate the flower surface, nectar and pollen with virus particles they shed via their feces. Studies have identified the potential of indirect virus transmission via shared flowers (Singh et al., 2010; Bodden et al., 2019).

Analysis of the corbicular pollen from foraging honey bees showed the presence of SBV, BQCV and DWV in the pollen. DWV was also found in pollen collected by non-*Apis* bees. As infected pollen could be found on non-infected bees and *vice versa* (Singh et al., 2010), one can conclude that corbicular pollen is not primarily contaminated by the bee itself, e.g., through salivary excretions, but rather by previous visits from infected bees (Singh et al., 2010; Figueroa et al., 2019). The viability of the DWV present on the pollen has been demonstrated by injection into honey bees and *Osmia* spp. (Mazzei et al., 2014), although this does not of course mean a similar viability for oral infection. Oral transmission requires many orders of magnitude greater quantities of virus (de Miranda et al., 2013). DWV is naturally notoriously unstable outside the cell (de Miranda et al., 2013), and other pathogens are also known to lose viability rapidly on flower petals (Figueroa et al., 2019).

Apart from shared flowers, which is most likely the main route of inter-species transmission, there are other interactions between bee species that could promote the transmission of viruses between bee species. Robbing is one such interaction, where a bee steals stored resources from another nest, whether from the same or from a different species. Robbing is a well-known phenomenon between honey bee colonies and occurs primarily during a dearth of floral resources (Kuszewska and Woyciechowski, 2014). Robbing of honey bee colonies by bumble bees (Genersch et al., 2006) and wasps has also been documented, but is more individual rather than systematic and usually toward the end of summer when both wasp and bumble bee colonies are in natural decline. Viruses can certainly be detected in honey (Milićević et al., 2018), so that robbing honey does expose robbing bees and wasps to potential infection (Genersch et al., 2006), but direct evidence for virus transmission through honey is so far absent, for honey bees or bumble bees.

Some social and solitary bees suffer from brood parasitism. This is when a different, parasitic bee species invades the nest of its host species and uses the host's resources to its own reproductive benefit (Lhomme and Hines, 2018). Such intrusion also involves exposure to potentially infectious viruses present in the host bees and brood or on the nest structures, enabling inter-species transmission from the nest of the host to the brood parasites.

Although rare, there are reports of bumble bee species reusing old nests (Taylor and Cameron, 2003). As viral particles can build up in the nest during the development, reusing an old nest will expose the new colony to these viruses. However, viral particles present in the old nest are exposed to environmental conditions (e.g., humidity and heat) and can deteriorate, losing their infectivity. The environmental stability of viruses found in honey bees seems to be highly dependent on the virus, where some viruses deteriorate faster compared to others (Chen et al., 2007; Dainat et al., 2011; Forsgren et al., 2017). Forsgren et al. (2017) showed that BQCV remains detectable up to 4 days in dead bees stored at 4°C, whereas DWV degrades faster. One side note on these studies is that they do not assess the infectability of the virus. Because the environmental stability of the virus and the loss of its infectability likely differ between viruses present in a dead host and viruses that are outside their host, yet further research is still needed here.

The reuse of nesting sites is more common in solitary bees, which often re-occupy nesting sites used in previous years (Krunicì and Stanisavljevicì, 2006). As for bumble bees, old nest sites of solitary bees (i.e., hollow cavities in sand, stone, wood, or straw) can contain virus particles that were present on the pollen brought in by solitary bees the previous year. If these viruses are still contagious they could infect the adult female or the larvae of the next generation.

Intra-Species Transmission

The intra-specific transmission of viruses in non-*Apis* bees should also be highlighted. The very different lifestyles and social structures of non-*Apis* bee species will greatly affect how effectively, different bee viruses are transmitted.

Eusocial non-*Apis* species belong to the tribes *Meliponini* (stingless bees) and *Bombini* (bumble bees). Both tribes have a social structure similar to honey bees, with a single reproductive

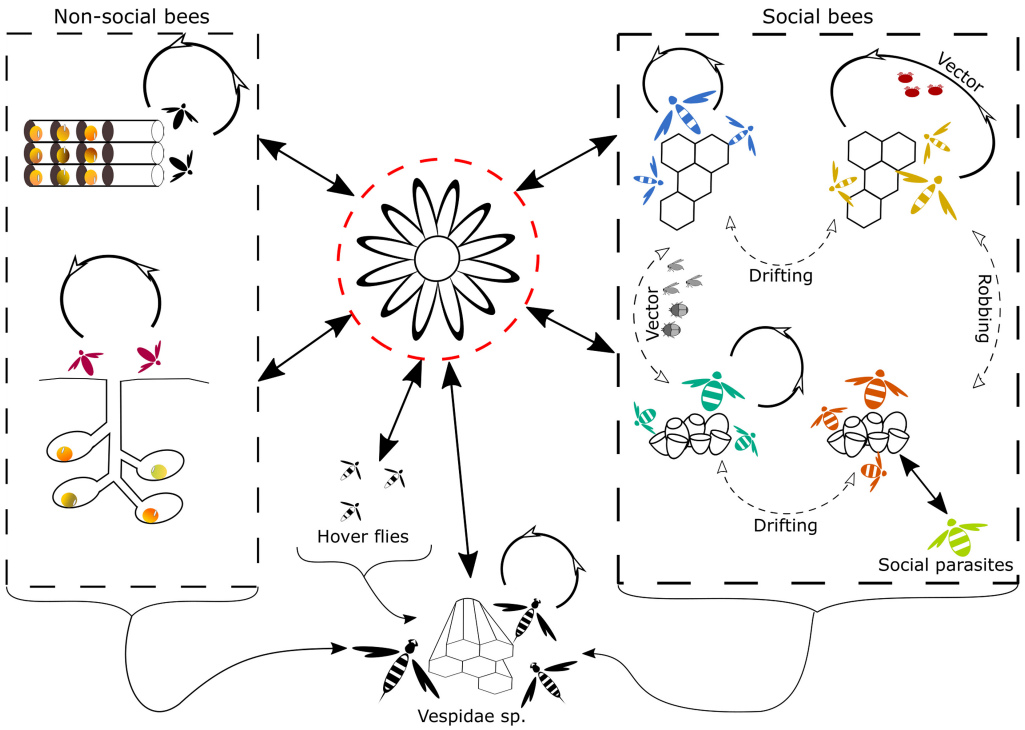

FIGURE 1 | Graphical representation of the natural routes of inter- and intra-species transmission of viruses found in Hymenoptera. Transmission routes that are more likely to occur are represented by solid arrows, transmission routes that are less likely or less frequently observed are represented by dotted arrows. The most likely route of inter-species transmission is through the use of shared flowers (Singh et al., 2010; Alger et al., 2019), depicted in the middle surrounded by a red dotted line. Inter- and intra-species transmission in non-social bees, depicted on the left side can occur through contact at nest aggregations or the reuse of virus-contaminated old nest cavities (Krunicì and Stanisavljevicì, 2006). In social bees, depicted on the right side, the main intra-species transmission route is likely, via intense contact in the nest. Social behavior such as trophallaxis and body contact could mediate transmission (Amiri et al., 2014, 2019; Chen et al., 2014; Coulon et al., 2018 and others, see main text). Further intra-species transmission can also occur via vectors, for honey bees this is a very important transmission route for several viruses, mediated by *V. destructor* (Santillán-Galicia et al., 2010; Möckel et al., 2011; Gisder et al., 2018; Posada-Florez et al., 2019; Ryabov et al., 2019 and others, see main text). Intra-and inter-species transmission via vectors, other than *V. destructor* [e.g., the small hive beetle, phorid flies (Eyer et al., 2009; Core et al., 2012; Menail et al., 2016)] are less frequent. Robbing and drifting are also two potential routes of inter- and intra-species transmission, respectively, described in social bees. Yet their role in virus transmission is likely to be minor compared to other transmission routes. Lastly, social parasitism creates a high contact between individuals from different species and hence is likely to facilitate virus transmission, in social bees. Inter-species transmission in *Vespidae* sp. can occur through feeding on infected Hymenoptera, or other insects that are infected with a virus or contain the virus on their exterior (Loope et al., 2019). Another potential transmission route for wasps is the use of shared contaminated flowers (Mordecai et al., 2016b). Intra-species transmission in social *Vespidae* sp. is also likely to occur via intense contact within the nest.

queen and non-reproductive worker bees attending the brood and foraging. A social nest structure creates a high contact between nest mates which facilitates virus transmission. Bees of the family *Halictidae* are widely distributed. This family displays a plasticity of social behaviors ranging from solitary to communal, semi-social and primitively eusocial (Danforth, 2002), allowing for different levels of horizontal transmission. Strictly solitary species on the other hand have very little contact with other individuals from the same species, apart from mating. Intra-species transmission here is most likely via the use of shared flowers or potential contact in large nest aggregations.

Drifting is a term used for bees with faulty orientation and homing, when bees enter a non-natal colony from the same species. This phenomenon is well described for honey bees (Pfeiffer and Crailsheim, 1998), but it also occurs in other bee species, e.g., *Halictus ligatus* (Packer, 1986), *Melipona scutellaris* (Alves et al., 2009) and *Bombus* sp. (Lopez-Vaamonde et al., 2004). Drifting exposes the intruding individual to the nest structures or pollen provisions of other individuals from the same species and may thus facilitate viral transmission.

Vector-Mediated Transmission

Another possible transmission route between non-*Apis* bees are parasitoids, parasites and commensals living in, on or with the host bee or its nest structures. Neither *V. destructor*, the highly potent vector of honey bee viruses in *A. mellifera* (Traynor et al., 2020) nor similar virus-transmitting mites parasitizing *Apis* bees in Asia (Forsgren et al., 2009, etc. see above in section "Vector-Mediated Transmission" in: Transmission of Viruses in *Apis mellifera*) parasitize non-*Apis* bees. However, non-*Apis* bees are host to a plethora of other parasites, ranging from ecto-parasites to parasitoids, that could potentially vector viruses. DWV has been identified in several species of parasitoid phorid flies, i.e., *Megaselia scalaris* and *Apocephalus borealis*, with evidence of

replicating virus in the larvae of *Megaselia scalaris* (Core et al., 2012; Menail et al., 2016). *A. borealis* is a known parasitoid of bumble bees, which was also detected in honey bees. *M. scalaris* on the other hand is a broad host parasitoid, known to affect different insect species (Robinson, 1975; Mongiardino et al., 2013) and has also been suggested to be a parasitoid of Melipona colonies (Macieira et al., 1983). Even though DWV has been identified in these phorid flies, further research is still needed to establish the true potential of these species as an intra-specific and potentially inter-specific vector of bee viruses. The geographic expansion of the invasive SHB to temperate climatic zones means that it can now also encounter various bumble bee species, whose colonies it is able to invade (Hoffmann et al., 2008). Not least, it has been recently shown that SHBs can also complete an entire life cycle in association with nests of solitary bees *Megachile rotundata* (Gonthier et al., 2019). Since SHB is a replicative host or biological vector for DWV (Eyer et al., 2009), such invasion may result in the transmission of viruses among bee species.

Transmission of Viruses in Non-bee Insects

Hymenoptera

Many species of the *Vespidae* family prey on bees and/or share nectar resources with Apoidea, this exposes them to bee-associated viruses. Several of these viruses have been detected in wasps of the *Vespidae* family. DWV has been reported in several species of the *Vespula* genus such as *V. vulgaris, V. pensylvanica, V. crabro, V. velutina,* and other *Vespula* spp. (Singh et al., 2010; Evison et al., 2012; Levitt et al., 2013; Forzan et al., 2017; Mazzei et al., 2018). Furthermore, DWV has also been detected in other genera of the *Vespidae* family such as *Polistes* spp. and *Bembix* spp. (Singh et al., 2010; Santamaria et al., 2018) the latter genus is mostly known to hunt flies (Evans, 2002), but is also described as a predator of stingless bees (Evans and O'Neill, 2007). Besides DWV other viruses have also been detected in wasp species, such as IAPV (Yañez et al., 2012b), Moku virus (Garigliany et al., 2017) ALPV, KBV, and BQCV (Mazzei et al., 2019; Yang et al., 2019). An RNAseq analysis of different tissues of Asian hornets, *V. velutina,* recently identified 18 virus species and added ABPV, BeeMLV and DWV-C to the list of bee associated viruses found in wasp species (Dalmon et al., 2019). Furthermore, the same study showed the presence of DWV, BQCV, and ABPV in tissues other than the gut, which suggests that these viruses cause a real infection in *V. velutina*. Similarly, the detection of virus replication of DWV, IAPV, KBV, and BQCV strongly suggests these viruses truly infect wasp species (Yañez et al., 2012b; Forzan et al., 2017; Mazzei et al., 2018, 2019).

Interestingly, a study in Hawaii by Loope et al. (2019) showed that the presence of *V. destructor* in *A. mellifera* has a cascade effect on the DWV variants found in *Vespula pensylvanica*. The arrival of *V. destructor* reduced the DWV variant diversity in honey bees as well as *V. pensylvanica*. These results further underline that predation of bees by wasps is a potential route of virus transmission. Furthermore, Mordecai et al. (2016b) showed that Moku virus is predominantly present in *V. pensylvanica* but is also found in honey bees and varroa in the same locations. Their data suggest that *V. pensylvanica* is likely the primary host of Moku virus, based on high viral loads and full genome recovery of the virus in the wasp. However, as they found the virus also in honey bees and *V. destructor*, it is also transmitted from wasps to bees and subsequently to varroa, the most likely route here is transmission via the use of shared flowers (Mordecai et al., 2016b).

The Moku virus, also highlights that for several viruses found in honey bees, the honey bees themselves may not be the primary host, yet they acquire the virus from other species. This has also been shown by de Souza et al. (2019), who found that DWV-C was more dominant in *Melipona subnitida* compared to *A. mellifera* in Brazilian colonies. Although the honey bee is often the focal host of studies, the detection and identification of honey bees as a potent host species for a virus does not directly imply that the honey bee is the primary host for this virus. Further research is still needed to untangle the role of different host species for most viruses found in honey bees.

The ants *Camponotus vagus* and *Formica rufa* feed on honeydew but also honey bee cadavers. Both species, when collected near apiaries, have been shown to carry CBPV which they could have acquired either through feeding on dead infected bees, or by sharing the same source of honeydew (Celle et al., 2008). Larvae and adult *Lasius platythorax* ants collected from honey bee colonies have been shown to carry ABPV, DWV-A, and DWV-B (Schläppi et al., 2020). Replicative strands of the CBPV and ABPV genomes were detected in *C. vagus* and in *L. platythorax,* respectively, suggesting possible viral replication and true host status for these ant and wasp species. However, as with *V. destructor*, such results should be interpreted with caution, since the virus (and its replication intermediates) may have come with the bee cadaver, rather than from the wasp/ant host tissues. Similarly, replicative strands of the DWV genome were detected in *Myrmica rubra* (Schläppi et al., 2019), an invasive species of ant in North America (Groden et al., 2005), and in the Argentine ant *Linepithema humile* (Sébastien et al., 2015), also one of the most widespread and abundant invasive ant species (Holway et al., 2002). Specific strains of LSV were detected in *Messor* ant species, which were thought to be genuine infections rather than the result of inter-species transmission (Bigot et al., 2017).

Coleoptera

The SHB, *Aethina tumida*, is a scavenger/parasite of honey bee colonies that was native in Africa, but has recently become invasive on several continents. Adult beetles enter honey bee and bumble bee colonies where they mate and reproduce. SHB feeds on the pollen, honey and honey bee brood and is therefore exposed to any virus found in these hive products (Neumann and Elzen, 2004). Additionally, the SHB can exploit trophallaxis and be fed directly by bees. Furthermore, replicative strands of the DWV genome have been detected in *A. tumida* (Eyer et al., 2009), although these can be either acquired passively through feeding or indicate active virus replication in SHB. BQCV, DWV, IAPV, KBV, and SBV, have been detected in *A. tumida* as well (Levitt

et al., 2013). Additionally, DWV has been detected in individuals of the *Coccinellidae* and *Tenebrionidae* families (Levitt et al., 2013). However, further research is still needed to confirm the host status of Coleoptera for these viruses.

Diptera

The adults of some species of hoverfly (*Syrphidae, Diptera*) are considered to be Batesian mimics of adult honey bees. They feed on flowers, effectively imitate honey bee behavior (Golding and Edmunds, 2000) and share many floral resources with bees as adults (Power and Stout, 2011). It has been shown that some species of the genus *Eristalis* carry BQCV, SBV, and DWV-B, most likely acquired through horizontal transmission (Bailes et al., 2018). Levitt et al. (2013) reported the presence of DWV in samples of the *Calliphoridae* and the *Muscidae* families of flies.

Other Insects

Levitt et al. (2013) collected a large number of insects in the proximity of apiaries and screened them for the presence of five bee-associated viruses. In addition to the detection of bee viruses in various species of Hymenoptera, Coleoptera, and Diptera (as mentioned above), BQCV, DWV, IAPV, KBV, and SBV were all also detected in species of *Blattodea*, Dermaptera, and Lepidoptera, while only DWV was detected in a specimen of Pentatomidae. None of these viruses were detected in specimens of Odonata or Orthoptera, although only very few specimens of these orders were analyzed.

Other Arthropods

Several bee-associated viruses, BQCV, DWV, IAPV, and SBV, were detected in Arachnids sampled near apiaries. As with other parasites, parasitoids and commensals, it is unclear if these viruses represent true infections (and thus host status) or were acquired passively through feeding on infected bees or contaminated material (Levitt et al., 2013).

PART 2: ARTIFICIAL INFECTIONS

This section deals with the deliberate, experimental infection of bees with controlled amounts of virus, using a variety of inoculation techniques, trying to mimic a natural transmission route. This requires a source of relatively pure virus and, ideally, uninfected experimental bees. The success of the infection procedure is tested either through molecular evidence of replication of the inoculated virus, or more commonly a significant quantitative increase in post-inoculation virus titer that can only be attributed to the inoculum. A number of negative control inoculations are therefore also required, to rule out alternative sources of infection or virus titer increase.

Sources of Virus Inoculum

The primary requirement for controlled inoculation is a source of relatively pure virus. There are two main approaches to achieving this: through the *in vivo* (bees) or *in vitro* (cell cultures) propagation of natural virus isolates (de Miranda et al., 2013; Genersch et al., 2013), or through reverse genetics, where the entire virus genome is transcribed synthetically from plasmid clones or PCR products and introduced into bees as full-length infectious RNA (Benjeddou et al., 2002; de Miranda et al., 2013; Lamp et al., 2016; Ryabov et al., 2019). Most studies on artificial inoculation of bee viruses thus far have been conducted with virus material propagated *in vivo*, in honey bee pupae, and enriched and purified through differential centrifugation (de Miranda et al., 2013). Because multiple virus infections are common in the bee colonies and most bee viruses have similar physico-chemical properties, making it impossible to separate them by differential centrifugation, these studies normally involved semi-pure virus inocula containing varying amounts of contaminating viruses (Bailey and Ball, 1991; Carrillo-Tripp et al., 2015; Remnant et al., 2019; Thaduri et al., 2019). Covert virus infections (virus present at very low levels) in either the propagating pupae, for preparing inoculum, or in the experimental bees can easily be co-amplified and interfere with the virus under study (Carrillo-Tripp et al., 2015; Remnant et al., 2019). Moreover, crude bee preparations also contain host cellular material that can independently or in synergy with either the inoculated or resident background viruses to influence the virus infection dynamics. An alternative approach would be to synthesize the virus of interest *in vitro* (Lamp et al., 2016; Ryabov et al., 2019; Seitz et al., 2019; Jin et al., 2020; Yang et al., 2020) thereby ensuring the highest level of purity. Both cell cultures and reverse genetics also allow virus to be produced that is free of contaminants, while reverse genetics also has the option of introducing specific genetic changes to the virus genome (Lamp et al., 2016; Ryabov et al., 2019; Jin et al., 2020). The combination of reverse genetics and cell culture propagation is particularly powerful for obtaining large amounts of pure infectious virus particles. However, despite persistent attempts during the last several decades, it was not until recently that cell culture systems and infection methods were optimized for honey bee virus infection and propagation (Genersch et al., 2013; Carrillo-Tripp et al., 2015) and full-length infectious plasmid clones of several honey bee viruses were developed (Yang et al., 2013; Lamp et al., 2016; Ryabov et al., 2019; Seitz et al., 2019). Recently, a molecular clone of CBPV was shown to cause typical clinical symptoms mimicking naturally CBPV-infected honey bees (Seitz et al., 2019). Similarly, SBV and DWV clones have been synthetized to express the enhanced green fluorescent protein (EGFP; Jin et al., 2020; Ryabov et al., 2020). Besides creating a clone that produces typical symptoms, it adds the advantage of a reporter gene for protein expression studies (Jin et al., 2020). One valid criticism of the reverse genetics approach is that it usually involves a single pure genetic clone, while viruses exist naturally as quasispecies – a collection of interrelated major variants, point mutants, recombinants and defective genomes (Dolan et al., 2018). Experiments with pure single genome viruses therefore lack the functional and genetic complexity of natural virus isolates. The obvious solution to this is to create a diverse set of infectious cDNA clones representing the genetic diversity of the original population (e.g., Ryabov et al., 2019).

Multiple positive and negative controls for all the steps of the inoculation process, from the manipulation of the individuals, incubation conditions, mode of inoculation, etc., are required

to ensure that the infection is due to the target virus in the inoculum, and not due to contaminants in either the inoculum or the recipient host. The quality and quantity of the virus in the original inoculum as well as in the inoculated bees can be evaluated by qualitative and quantitative real-time PCR and by sequencing. The methods for virus propagation and virus infectivity assays have been described in detail in the Beebook (de Miranda et al., 2013). Here, we focus on summarizing the results of virus infectivity assays conducted during the last years.

Artificial infection experiments in honey bees primarily involve two forms of inoculation: by direct injection of micro volumes of virus into the honey bee using a fine needle, mimicking the vectored transmission by varroa, or by feeding, mimicking the oral-fecal transmission route. Very occasionally topical application is used, mimicking transmission by contact. Inoculation by injection allows absolute control over the amount of virus each bee receives, but not necessarily of the subsequent progression of the infection. This is because injection directly by-passes the main physical and physiological antiviral defenses, leaving the infection subject to only molecular controls. This is in contrast to oral inoculation, which often requires much higher amounts of virus (between 10^6 and 10^{11} particles, depending on the virus; Bailey and Gibbs, 1964; Bailey and Ball, 1991; de Miranda et al., 2013) to initiate infection, due to these natural physical and physiological barriers, but whose subsequent progression is much more measured and predictable. The precise conditions for artificial inoculation vary greatly among viruses. Some of them have been studied widely while for others this information is largely unknown.

Oral Inoculation and Injections

DWV

Oral inoculation of adult bees with DWV does not induce overt DWV infections, even when using large titers of the virus (10^8 genome equivalents), and the virus was restricted to the abdominal organs (Möckel et al., 2011). Artificial oral inoculation of DWV seems to be rather ineffective (Iqbal and Mueller, 2007), much of which can be attributed to the extreme instability of DWV in isolation (de Miranda et al., 2013). However, when feeding 2 days-old larvae with 2 μl of serial dilutions of DWV, Khongphinitbunjong et al. (2015) observed significant higher viral titers in the resulting adults than in sucrose-fed controls, suggesting that both the developmental stage used for oral infection and the virus quantity were significant for establishing infection. Similar results were obtained by Thaduri et al. (2019) for oral inoculation of larvae with a single dose of freshly prepared crude DWV extracts containing 10^8–10^9 DWV genome equivalents, although the majority of this would have been unpackaged cytoplasmic RNA and only a fraction from virus particles. The results for adult bees were equivocal due to the high background levels of DWV in newly emerged adult bees (Thaduri et al., 2019). Artificially reared newly hatched larvae orally inoculated with high doses of DWV (about 10^{10} virus genome equivalents) established high levels of DWV infection (Ryabov et al., 2016). Sequential experimental oral infections with DWV and *Nosema ceranae* in 2 days old workers resulted in lower DWV loads when *N. ceranae* was inoculated before DWV, suggesting competitive interference between pathogens (Doublet et al., 2015).

Overt DWV infections could only be obtained through injecting the virus into young pupae (Möckel et al., 2011; Natsopoulou et al., 2017; Dubois et al., 2020; Yañez et al., 2020), even with as little as 80 virus particles, but never through feeding (Möckel et al., 2011). Injection has been used frequently to mimic natural inoculation by varroa while feeding on nymphs or adult bees. Worker pupae at the white eye stage (12–13 days old) micro-injected with10^6 copies of DWV exhibited virus replication and significant immune-gene expression modulations 5 days post injection (Ryabov et al., 2016), and injection of 10^7 copies of either clone-derived DWV isolates or wild DWV isolates reached about 10^{10} to 10^{11} genome copies per bee after only 24 h post-injection (Ryabov et al., 2019). Similar results were obtained by Yañez et al. (2020) when serially injecting DWV into pink-eye pupae. When young adults were injected with 10^4 to 10^6 copies of DWV into the thorax or abdomen no acute mortality was observed but the bees' lifespan decreased and flight behavior was affected (Mazzei et al., 2016; Bigot et al., 2017; Coulon et al., 2020). Both Natsopoulou et al. (2017) and Dubois et al. (2020) showed that DWV-A and DWV-B were equally capable of causing DWV symptoms, after injecting white-eye pupae and letting the pupae complete development *in vitro*. Mortality was significantly higher for adult honey bees injected with 10^7 copies of DWV-B compared to bees injected with the same amount of DWV-A (McMahon et al., 2016). Gisder et al. (2018) showed that a DWV-B dominant isolate from mites changed genetic character to a DWV-A dominant derived isolate after a single passage in bee pupae, most likely through a simple quantitative shift in the relative levels of DWV-A and DWV-B genomes after passaging. The original DWV-B dominant isolate was more virulent than the evolved DWV-A dominant isolate when considering pupal mortality and adult bee cognitive behavior, but not for adult bee mortality. The elevated virulence of the DWV-B dominant isolate could be attributed to more efficient replication in pupae and wider dissemination in adult bee neurological tissues. The consensus sequences of matching source and passaged isolates with different virulence properties clustered differently with either DWV-A or DWV-B, depending on which region of the genome was analyzed, which allowed the elevated virulence to be mapped to the DWV-B RNA-dependent RNA polymerase (RdRp) region of the DWV genome (Gisder et al., 2018). Such differential phylogenetic affiliation across the DWV genome is most easily explained by a significant presence of recombinant viruses in the quasispecies, enough to change the genetic character of the consensus sequence of the whole isolate (Dolan et al., 2018). Such DWV-A/DWV-B recombinants are readily generated naturally in mixed infections (Moore et al., 2011; Zioni et al., 2011; Ryabov et al., 2014, 2019; Cornman, 2017; Dalmon et al., 2017) and have been used to map other differential traits of DWV-A and DWV-B as well (Moore et al., 2011; Ryabov et al., 2014, 2019).

SBV

Bailey et al. (1981) preferred injection to pupae up to 24 h old rather than injection in adult bees when infecting bees with

BQCV, SBV, and SBPV. Early reports indicate that SBV extracted from larval or adult tissues (by grinding them in a 4:1 mixture of water and carbon tetrachloride followed by clarifying the extracts by centrifugation) were infectious to *A. mellifera*. Mature adult worker bees were infected by injection; newly emerged adult workers and larvae were infected by feeding (Bailey, 1969). Extrapolation from Bailey's data indicates that about 10^7-10^8 viral particles fed to larvae resulted in above 90% mortality (Bailey, 1969; Bailey and Fernando, 1972). Electron microscope counts of the of virus particles from extracts of the heads of drones 5 days after injection indicated that about 7×10^{11} particles per drone-head, at least 100 times the number in an infected adult worker bee head (Bailey, 1969). Liu et al. (2010) reported that second instar *A. cerana* larva were fed with 5 μl SBV (Chinese SBV) solution or PBS (7.8×10^5 genome copies/μl). Over 90% larval mortality was achieved by 96 h post infection. When comparing transmission for both DWV and SBV, Ryabov et al. (2016) used an inoculum of a mixture of approximately 10^{10} SBV and 10^{10} DWV genome equivalents for young larvae (oral infection), and 10^6 SBV and 10^6 DWV genome equivalents for pupae (injection).

BQCV

Oral inoculation was successfully used to inoculate pre-pupa (7 days) or 2 days old workers (respectively, 1.4×10^7 BQCV genome equivalents per larva and 1.4×10^9 genome equivalents per bee) to look for interactions between pathogens (BQCV and *N. ceranae*) and between the virus and pesticides (Doublet et al., 2015). Dose-dependent inoculation assays showed that only the high titers of BQCV (1.4×10^9) caused higher mortalities of the larvae but no impact on adult worker survival was observed (Doublet et al., 2015).

ABPV, IAPV, KBV

Bailey et al. (1963) challenged adult honey bees with ABPV in three different ways: by feeding, spraying, and artificial injection of an ABPV suspension. The LD_{50} (number of ABPV particles per bee that would have killed half of the bees in a group after 6 days) was equivalent to about 10^2 virus particles per bee when preparations were injected into the haemocoel compared to more than 10^{11} virus particles per bee for feeding and 10^8 to 10^9 particles per bee for spraying, illustrating the high virulence of ABPV upon injection.

Boncristiani et al. (2013) described that *in vitro* injection of honey bee pupae with 10^4 viral genome equivalents of an IAPV-enriched extract resulted in symptomatic infection.

Oral infections with IAPV can be achieved by feeding IAPV-sucrose solution to honey bees in cage experiments and in honey bee colonies (Maori et al., 2007, 2009; Singh et al., 2010). Approximately $5–7 \times 10^9$ IAPV genome equivalents in 30 ml sucrose were used to obtain colony infections) (Singh et al., 2010). IAPV-enriched sucrose solutions caused high mortality of recently emerged adult bees (concentrations above 10^8 genomic copies per microliter, NC, unpublished).

An inoculum containing a mixture of viruses, enriched for SBV and IAPV with low levels of BQCV and DWV was able to produce high levels of mortality within 3 days of oral infection in newly emerged honey bees. Further investigation concluded that the bees died from the extremely high titers of IAPV, and not from other viruses (Carrillo-Tripp et al., 2016; Dolezal et al., 2016).

SBPV

Adult bees injected with preparations of SBPV and antisera to neutralize all the other known bee viruses died after about 12 days at 30 or 35°C. They suffer a paralysis of the legs a few days before death and contained about 10^{12} viral particles (Bailey and Woods, 1974).

CBPV

Blanchard et al. (2007) reported infection of adult bees after topical application of 1.8×10^8 CBPV genome equivalents on the thorax of the bees. Trembling and weakening symptoms were observed 7–8 days post-application and all bees died 8–9 days post-contact (Blanchard et al., 2007). Queens can be infected by topical application of CBPV or following their exposure to CBPV-infected adults. The disease's symptoms include trembling of the legs, spread and disjunct wings and sometimes bloated abdomens (Amiri et al., 2014). Coulon et al. (2018) set up contact transmission experiments, mimicking the natural transmission route in the hive that avoids the stress of shaving and topical application. Tagged bees previously injected (4 days earlier) into the thorax with 4×10^4 CBPV genome equivalents were reared in the same cage with 9-day-old bees. Many of the bees that received the inoculum died after 1–3 days, but 69% of the bees that were in contact with them were still alive after 10 days despite the high titers of CBPV (about 10^8 CBPV genome equivalents, Coulon et al., 2018).

Infection by Mites

After 6 days the larvae that was fed with larval food provided by nurse bees, which was naturally infected with DWV, showed lower DWV titers (about 10^6 genome equivalents/larvae) than larvae exposed to *V. destructor* (Ryabov et al., 2014). Pupae artificially infested with one mite resulted in higher prevalence of DWV in adults than adults from non-infested pupae and DWV titers reached up to 10^{10} genome equivalents per bee even if the distribution of DWV titers across bees were highly varied

Santillán-Galicia et al. (2014) investigated the ability of *V. destructor* to transmit SBPV. *A. mellifera* and mites were fed on SBPV-infected pupae for either 5 or 10 days. Using Probit analysis, they estimated doses necessary to cause 50% (LD_{50}) and 99% (LD_{99}) mortality in bees was 362 and 2266 virus particles, respectively. A time course of SBPV replication in pupae showed that the virus was first detected 42 h after injection. No significant differences were found in the overall proportion of pupae that became infected when mites were introduced over a period of 5 or 10 days, irrespective of the season (July or September). The proportion of pupae infected with SBPV declined significantly with each mite transfer over time, with the majority of pupae becoming infected after the first few mite transfers. These experiments suggest that transmission of SBPV does occur during mite feeding. Furthermore, they conclude that because SBPV is highly virulent as it kills the bees before any dramatic increase in virus titer. This results explains why low SBPV titers exist in honey bee colonies even in the presence of *V. destructor* (Santillán-Galicia et al., 2014).

Cross-Infection Between Bee Species

Apis Species

Only a few studies have been conducted on artificially cross-infection of bee viruses between different *Apis* species, mostly due to the lack of *in vitro* brood rearing techniques for *Apis* species other than *A. mellifera*. Kashmir bee virus was originally found in Eastern honey bees, *A. cerana* in Kashmir (Bailey and Woods, 1977) and later found in *A. mellifera* in Australia (Bailey et al., 1979). Experimental work has shown that the virus could multiply very effectively in *A. mellifera* pupae. Inoculation with 1×10^{-8} ng of purified virus was sufficient to cause infection in some pupae, and at doses of 1×10^{-5} ng of purified virus every inoculated individual became infected. Virus multiplication occurred in cytoplasmic membrane-bound vesicles and caused significant changes in the hemolymph osmolality of infected pupae (Dall, 1987). Bailey also found that infected *A. mellifera* adult bees died within 3 days after either injecting or rubbing KBV on their bodies (Bailey et al., 1981).

Chinese sacbrood virus (CSBV) originating from *A. cerana* could readily establish SBV infections in *A. mellifera* larvae and adults, through both natural and artificial infection (Gong et al., 2016; Sun et al., 2017). Although CSBV was shown to replicate in *A. mellifera* adult bees and larvae, no obvious signs of sacbrood disease was observed (Gong et al., 2016).

Bombus Species

Many studies have shown that viruses first identified in honey bees could also be detected in *Bombus* and other pollinator species (e.g., Singh et al., 2010; Fürst et al., 2014; Gusachenko et al., 2019; see Gisder and Genersch, 2017 for an extensive overview). Several studies also report the active replication of these viruses in *Bombus* spp., indicating that these non-*Apis* bee species are also true hosts for these viruses. However, merely establishing that a virus can replicate in a bee species says nothing about either the pathology or the intra-species transmission of the virus. This additional biological information is crucial for evaluating the ecological consequences of virus prevalence in non-*Apis* pollinators. Establishing the pathology of bee viruses in non-*Apis* pollinators is often difficult, since the contact history of wild-caught bees is not known. Moreover, wild specimens often have multiple infections with several viruses and/or other pathogens have not yet been developed. Artificial infections allow the study of a certain virus in a controlled environment. They also provide insight on the transmission ability of viruses between species. Artificial (cross-species) infections can be performed either by direct injection of the virus in the bee, or through oral administration. In the following sections, we provide a short overview on the application of different infection techniques to look at cross species infection potential.

Micro-Injection

The micro-injection procedure used in bumble bees is similar to that used in honey bees. Firstly, bees are anaesthetized by putting them in the freezer for 10–20 min, subsequently bees are injected using a micro-capillary in the soft tissue between the first pair of sternites (Niu et al., 2016). Niu et al. (2014) showed that injection with as low as 20 virus particles of IAPV originating from honey bees results in infection in *B. terrestris*. Similarly, Wang et al. (2017) showed that injection of 500 virus particles of IAPV from honey bees results in an acute infection inducing rapid mortality in *B. terrestris*. The injection of SBPV particles, on the other hand, has a much less lethal effect on *B. terrestris*. Niu et al. (2016) showed that injecting up to 200,000 virus particles resulted in a moderately increased mortality compared to the control. Interestingly, both IAPV and SBPV inocula originating from white eyed honey bee pupae, reach a similar amount of viral genome copies in the bumble bee, yet IAPV appears much more lethal compared to SBPV (Niu et al., 2016). While the presence of DWV is documented in field samples of several *Bombus* species, published experimental work is still scarce. Graystock et al. (2015) showed that injections of DWV in *B. terrestris* result in an infection and lead to 50% mortality 10 days after injection.

Other than bumble bees, *Osmia* sp. have been used to test cross-species infectivity of DWV through injection. Mazzei et al. (2014) injected *O. cornuta* with extracts DWV infected honey bees. The bees were injected into the thorax, and later replicating DWV could be detected in the abdomen of the infected bees but not in their heads.

Feeding

Feeding virus particles to bee species other than honey bees, more closely resembles the natural transmission process, as vectors injecting virus are not described for non-*Apis* bees. In nature cross-species infection most likely occur due to feeding on flowers contaminated with fecal matter containing virus particles (*vide supra* for transmission pathways).

Establishing an infection via feeding requires much more viral particles compared to injection, as not all administered virus is able to penetrate the gut tissue and enter the haemocoel. Meeus et al. (2014) reported successful oral infection of *B. terrestris* with KBV and IAPV using 1×10^7 and 0.5×10^7 virus particles, respectively. Similar orders of magnitude were reported for oral infection of *B. terrestris* with IAPV in other studies (Piot et al., 2015; Wang et al., 2019). Both feeding and injection of IAPV highly increase mortality of *B. terrestris*, yet injection is far more lethal compared to feeding (Wang et al., 2019). Similarly, feeding bumble bees with DWV particles is less efficient at triggering an infection compared to injection. *B. terrestris* fed with 1×10^9 of DWV particles show a significant infection in less than half of the individuals (Fürst et al., 2014). However, compared to honey bees, bumble bees can be housed alone without an increased mortality, when they have access to *ad libitum* sugar water.

Schläppi et al. (2020) reported oral transmission of ABPV to the black garden ant *Lasius niger* when feeding on highly infected honey bee pupae (2×10^{11} virus particles), which led to symptoms at colony (fewer emerging workers) and individual level (impaired locomotion and movement speed).

Serial Transmission of Viruses in Honey Bees

Historically, starting with the work of Louis Pasteur on rabies in the 19th century, serial passage of viruses in alternative hosts has been used for attenuating their virulence, in order to develop low-virulence virus strains for use as live vaccines. The principle is

that after the serial passage of a virus to another host species, a loss of virulence is experienced when inoculated again into the original host as the virus becomes adapted to the alternative host and less to the original host. However, serial passaging has also been used to select strains with increased virulence (e.g., HIV-2 in baboons, Locher et al., 2003) and as an experimental technique to study genetic adaptation in virus populations resulting in new viral population-level traits, such as the adaptation to new hosts.

Serial passaging of viruses from honey bees has thus far largely involved *in vivo* serial passaging in pupae and adult bees. This is mostly because immortal honey bee cell lines, a logical pristine environment for pure virus propagation, have not been available until recently (see the section "Cell Line in Honey Bees"). Serial passaging of bee viruses was initially used to identify the infectious agent associated with different disease symptoms in honey bees, most commonly paralysis, and subsequently also to maintain infective virus stocks for experimentation and raising diagnostic antisera. This work started in 1945 with single passages of extracts from paralytic bees (Burnside, 1945) and was developed more thoroughly during the 1960s–1970s, leading to the discovery and initial characterization of the most common and important bee viruses we know today (Bailey and Ball, 1991). For instance, in Bailey et al. (1963), stocks of ABPV and CBPV were maintained by serially injecting those viruses in adult bees. In the case of ABPV, the virus infectivity has been maintained by serial transmission for over two years. While CBPV has been maintained in a similar way for several months.

As mentioned above, serial passaging can be used to either decrease or increase virulence. Mussen and Furgala (1977) compared the virulence of several SBV extracts, including one obtained from symptomatic larvae and another from SBV serially transmitted through adult bees. Both extracts were then inoculated by injection into 1-day-old adult bees, with higher mortality observed with the extracts from adult bees (100% mortality at 14 days after inoculation for adult-derived SBV, compared to 75% from symptomatic larvae). Similar experiments have recently also been conducted with the two master variants of DWV, comparing the relative virulence in honey bee pupae of DWV-A, the original honey bee specific strain (Lanzi et al., 2006; Posada-Florez et al., 2019), and DWV-B, a strain adapted to and capable of replicating in the parasitic mite and virus vector *V. destructor* (Ongus et al., 2004; Ryabov et al., 2019). In one study, no differences were observed in virus titers, development of symptoms or mortality between bees infected by DWV-A and DWV-B separately or infected by the mixture of both, through a single passage in white-eyed pupae (Tehel et al., 2019). In a different study, a single passage in pupae of a DWV isolate from a crippled bee significantly attenuated its virulence when injected into pupae (mortality) and in adult bees (neurotropism and cognitive ability), with attendant genetic changes in the virus linking higher virulence to sequence signatures from the DWV-B genotype, particularly the RNA-dependent RNA polymerase region (Gisder et al., 2018). As discussed above, this change in virulence could also be due to the presence of recombinants in a mixed infection. Virulence attenuation has also been demonstrated for varroa-mediated serial transmission, with reduced pupal DWV-A titers in pupae after just three varroa-mediated passages (Posada-Florez et al., 2019). These experiments demonstrate that artificial injection is useful for the transmission and propagation of viruses but may not reflect the natural interactions between each component within the three-way interactions between DWV, varroa and honey bees.

Serial passages were also used to evaluate viral species interaction during co-infection of the same host (Ryabov et al., 2016; Remnant et al., 2019). Virus isolates propagated *in vivo* in natural pupae inevitably include other common co-purifying viruses, such as SBV and BQCV, especially when propagating DWV (de Miranda et al., 2013) due to its innate instability in isolation (Lanzi et al., 2006). This will naturally also affect the replication and virulence characteristics associated with the propagated inoculum. From the first passages onward, DWV-A was outcompeted by SBV and BQCV (Remnant et al., 2019) both of which replicate very efficiently upon injection (Bailey and Ball, 1991). These unique virus-specific differences revealed by competition between co-replicating viruses are also reflected in both common and virus-specific host molecular responses to co-infection with competing viruses (Ryabov et al., 2016).

Serial transmissions have also been used to test different transmission routes. For instance, Bailey and Gibbs (1964) tested the infectivity of ABPV through serial passages of bee feces. A hundred bees were each fed with 10^6 ABPV particles. After 1 week, fifty bees were fed with syrup containing feces from the first group. The subsequent week, a serial transmission continued using another fifty bees fed with the feces from the second bee group. Those third group bees showed no symptoms of ABPV, nor was there any increase of virus or sign of disease during two further serial transfers. From these results, the author speculates that "when bees ingest feces while cleaning the hive, they become infected, but will be unlikely to receive enough virus to become acutely paralyzed."

Serial passages have been also used to elucidate the behavior of viral quasispecies during and after transmission. Yañez et al. (2020) followed the changes in the DWV-A quasispecies shape upon serial injection into honey bee pupae. The results suggested that DWV-A quasispecies undergoes a rapid, extensive and random expansion of its sequence space, followed by very strong negative selection toward a uniform, common shape by the time the pupae have completed their development, with no particular signature between symptomatic and asymptomatic adults.

Serial passages of viruses have been a useful tool to preserve the viability of virus and to understand the different routes of transmission during the early virology research on the honey bees. In recent years, a few studies used this technique to characterize the complex interactions between co-infecting viruses, *V. destructor* and the honey bee host.

Cell Line in Honey Bees

Following the initial attempts of creating *in vitro* insect cell cultures, the first primary cell line of continuously dividing insect cells was achieved in the 1960s (Grace, 1962), and since then, the field has grown to routinely cultivate primary cells and now immortalized or permanent insect cell lines (Lynn, 1999; van Oers and Lynn, 2010). According to the ExPASY Cellosaurus, thus far, around 1000 insect-derived cell lines have

been established from several different tissue sources of many insect species, majority derived from the families Lepidopteran, Dipteran and Hemipteran (Lynn, 1999). Although there has been less success in the family Hymenoptera (wasps, ants, and bees) (Lynn, 2001), recent attempts have led to the first honey bee immortal cell line, AmE-711 (Goblirsch et al., 2013).

Honey bee primary cell cultures grow relatively slowly compared to other insect or animal cell cultures, regardless of the tissues used to initiate the cell culture (Genersch et al., 2013). Thus far, many attempts have resulted in several honey bee cell culture methods. These methods are highly varied as they use different target tissues, growth media and isolation methods (Bergem et al., 2006; Hunter, 2010; Ju and Ghil, 2015). Honey bee primary cell cultures have been established using different life stages from egg to adult bees and various isolated tissues including neural cells, antennae, fat body, hemocyte, and embryos (Kreissl and Bicker, 1992; Gascuel et al., 1994; Goldberg et al., 1999; Sorescu et al., 2003; Barbara et al., 2008; Ju and Ghil, 2015). Even transfection using human c-myc proto-oncogene into embryonic honey bee cells has generated a cell culture that remained viable for periods up to 8 months (Kitagishi et al., 2011). This cell line was considered as "of honey bee character" despite the expression of a central transcription factor being of human origin which is known to change the entire cellular program by un-regulating the expression of many genes (Nasi et al., 2001; Adhikary and Eilers, 2005). A major breakthrough in the development of a stable honey bee cell line came from the use of honey bee embryonic tissue (Goblirsch et al., 2013; Ju and Ghil, 2015), however, this and likely other primary honey bee cell cultures are plagued with persistent DWV infection, a condition afflicting honey bees worldwide (Martin and Brettell, 2019).

Insect-derived cell cultures have advanced our understanding of insect physiology, development biology, pathology, and molecular biology (Lynn, 1999; van Oers and Lynn, 2010). With their genetic uniformity, they are now used by scientists as a convenient tool to eliminate environmental variables with more consistent results that are impossible to control when working at the organismal or colony levels (Hunter et al., 2003; van Oers and Lynn, 2010). Cell cultures are desirable for detection, identification and isolation of many viruses and intracellular parasites in animals (Leland and Ginocchio, 2007; Hematian et al., 2016). They are especially valuable for rapid characterization of virus–virus, virus–host cellular interactions and their impact on cell survival, which could be commercially important (Carrillo-Tripp et al., 2015). That said, isolation of viruses from naturally infected bees and pupae, or artificially infected individuals in the laboratory (de Miranda et al., 2013), is still the preferred route for virus characterization studies because it is well known that immortalized cell cultures don't reflect the true evolutionary pressure presented to a virus cultivated *in situ* or *in vivo*. Thus far, honey bee virus studies have provided valuable information on the response of hosts to viruses at the population and physiological levels but immortalized driven honey bee cell lines will provide a stable supply of material to a nascent field of honey bee cellular virology (de Miranda et al., 2013; Genersch et al., 2013; Martin and Brettell, 2019). It will also lead to better understanding of honey bee antiviral defense mechanisms (Carrillo-Tripp et al., 2016). Recently, primary cell cultures derived from of both Asian and European honey bees embryonic tissues were used to investigated cellular responses to virus infection (Goblirsch et al., 2013; Xia et al., 2014; Ju and Ghil, 2015). A monolayer of the primary cell culture from embryonic tissues of *A. cerana* was used to study early infection process of CSBV during replication (Xia et al., 2014). The results from this study suggest that after viral adsorption and entry into the host cell, CSBV replicated and assembled progeny virions in the cytoplasm until 48 hpi, after which CSBV particles might be released from the host cell by lysis. An investigation of viral co-infection in the immortal cell culture from embryonic tissues of *A. mellifera* (AmE-711) revealed a similar virus dynamic as individual honey bee (Carrillo-Tripp et al., 2016). These results indicated that different mechanisms of virus-host interaction affect virus infection dynamics, including virus–virus interactions, superinfections, specific virus saturation limits in cells and virus specialization for different cell types (Carrillo-Tripp et al., 2016).

CONCLUSION

Although much is known about both the natural transmission routes and the artificial propagation of bee and bee-related viruses, much more still needs to be clarified. Most of our knowledge about bee virus transmission and infection has been derived from the most common honey bee viruses, i.e., those that also cause disease. The challenge is to elucidate the infection and transmission strategies of the much larger number of apparently non-pathogenic newly discovered viruses, as well as their biological and ecological importance to their hosts. Many of them will probably also use the most common transmission routes identified for the disease-causing viruses. The developmental stage and tissues targeted by these viruses will be important for both their transmission strategy and their effects on the host. Mechanical and biological virus vectors can breach the anatomical and physiological host barriers to virus transmission, with potentially drastic consequences for host health, virus virulence evolution, and applied vector-virus virulence management (Traynor et al., 2020). Also important in virus transmission, as recently reported by Wang et al. (2020) using a metabolomics-based approach, is the occurrence of diametrically opposite changes during virus infection of cells of different species origin, and we believe this phenomenon is possibly related to the type of infection (acute or persistent) that is triggered by the virus. Indeed Santos et al. (2019) and Wang et al. (2019) reported that virions/virus in insect species of three different orders (Lepidoptera, Hymenoptera, and Orthoptera) did not trigger pathogenic infections, while in Dipteran cells there were strong toxic effects (Wang et al., 2020), which can impact transmission among species in nature when sharing food resources. Indeed, Piot et al. (2019) demonstrated the impact of food hot spots on pathogens transmission within altered flower-networks that could negatively impact hosts experiencing an increased exposure. Finally, techniques revised here as inoculation methods, virus serial passaging and cell culture are

all important tools for understanding virus quasispecies behavior, transmission, pathogenicity and virulence or its attenuation in different host bee species.

AUTHOR CONTRIBUTIONS

OY, AD, and NC conceptualized the study. OY, NP, AD, JM, DP, and NC investigated the study. OY, NP, AD, and NC contributed to methodology. OY, NP, AD, JM, PC, DP, EA, GS, DS, and NC wrote the original draft. OY, NP, AD, JM, PC, DP, EA, GS, and NC reviewed and edited the manuscript. OY, NP, AD, JM, PC, DP, EA, GS, DS, and NC approved the final version of manuscript to be published.

ACKNOWLEDGMENTS

We wish to express our sincere gratitude to the honey bee research association "COLOSS" (https://coloss.org), for providing opportunity for the conception of this project and its development and funds towards the publication fee of this article. COLOSS Association is supported by the Ricola Foundation – Nature and Culture and Véto-pharma. Appreciation is addressed to Lars Straub for language revision on earlier versions of the manuscript. OY would like to acknowledge the Vinetum Foundation and the Open Access Publication Fund from the University of Bern. JM wishes to acknowledge the financial support from FORMAS grant 2013-1225 and EU Horizon 2020 R&I grant 773921. PC would like to acknowledge Chiang Mai University.

REFERENCES

Abrol, D. P., and Bhat, A. A. (1990). Studies on 'Thai sac brood virus' affecting indigenous honeybee *Apis cerana* indica Fab. colonies – Prospects and future strategies – I. *J. Anim. Morphol. Physiol.* 37, 101–108.

Adhikary, S., and Eilers, M. (2005). Transcriptional regulation and transformation by Myc proteins. *Nat. Rev. Mol. Cell Biol.* 6, 635–645. doi: 10.1038/nrm1703

Adler, L. S., Michaud, K. M., Ellner, S. P., McArt, S. H., Stevenson, P. C., and Irwin, R. E. (2018). Disease where you dine: plant species and floral traits associated with pathogen transmission in bumble bees. *Ecology* 99, 2535–2545. doi: 10.1002/ecy.2503

Ai, H., Yan, X., and Han, R. (2012a). Complete genome sequence of a Chinese isolate of the Israel acute paralysis virus. *Sociobiology* 58, 49–66.

Ai, H., Yan, X., and Han, R. (2012b). Occurrence and prevalence of seven bee viruses in *Apis mellifera* and *Apis cerana* apiaries in China. *J. Invertebr. Pathol.* 1091, 160–164. doi: 10.1016/j.jip.2011.10.006

Alger, S. A., Burnham, P. A., and Brody, A. K. (2019). Flowers as viral hot spots: honey bees (*Apis Mellifera*) unevenly deposit viruses across plant species. *PLoS One* 14:e0221800. doi: 10.1371/journal.pone.0221800

Allen, M., and Ball, B. (1996). The incidence and world distribution of honey bee viruses. *Bee World* 77, 141–146.

Alvarez, L. J., Reynaldi, F. J., Ramello, P. J., Garcia, M. L., Sguazza, G. G. H., Abrahamovich, A. H., et al. (2018). Detection of honey bee viruses in Argentinian stingless bees (Hymenoptera: Apidae). *Insectes Soc.* 65, 191–197.

Alves, D. A., Imperatriz-Fonseca, V. L., Francoy, T. M., Santos-Filho, P. S., Nogueira-Neto, P., Billen, J., et al. (2009). The queen is dead - long live the workers: intraspecific parasitism by workers in the stingless bee *Melipona scutellaris*. *Mol. Ecol.* 18, 4102–4111. doi: 10.1111/j.1365-294X.2009.04323.x

Amiri, E., Kryger, P., Meixner, M. K., Strand, M. D., Tarpy, D. R., and Rueppell, O. (2018). Quantitative patterns of vertical transmission of deformed wing virus in honey bees. *PLoS One* 13:e0195283. doi: 10.1371/journal.pone.0195283

Amiri, E., Meixner, M., Büchler, R., and Kryger, P. (2014). Chronic Bee paralysis virus in honeybee queens: evaluating susceptibility and infection routes. *Viruses* 6, 1188–1201. doi: 10.3390/v6031188

Amiri, E., Meixner, M. D., and Kryger, P. (2016). Deformed wing virus can be transmitted during natural mating in honey bees and infect the queens. *Sci. Rep.* 6:33065. doi: 10.1038/srep33065

Amiri, E., Seddon, G., Zuluaga Smith, W., Strand, M. K., Tarpy, D. R., and Rueppell, O. (2019). Israeli acute paralysis virus: honey bee queen–worker interaction and potential virus transmission pathways. *Insects* 10:9. doi: 10.3390/insects10050123

Bailes, E. J., Deutsch, K. R., Bagi, J., Rondissone, L., Brown, M. J. F., and Lewis, O. T. (2018). First detection of bee viruses in hoverfly (syrphid) pollinators. *Biol. Lett.* 14:20180001. doi: 10.1098/rsbl.2018.0001

Bailey, L. (1965). The occurrence of chronic and acute bee paralysis viruses in bees outside Britain. *J. Invertebr. Pathol.* 7, 167–169. doi: 10.1016/0022-2011(65)90031-5

Bailey, L. (1969). The multiplication and spread of sacbrood virus of bees. *Ann. Appl. Biol.* 63, 483–491. doi: 10.1111/j.1744-7348.1969.tb02844.x

Bailey, L., and Ball, B. V. (1991). *Honey Bee Pathology*, 2nd Edn. London: Academic Press.

Bailey, L., Ball, B. V., and Perry, J. N. (1981). The prevalence of viruses of honey bees in Britain. *Ann. Appl. Biol.* 97, 109–118. doi: 10.1111/j.1744-7348.1981.tb02999.x

Bailey, L., Ball, B. V., and Perry, J. N. (1983a). Association of viruses with two protozoal pathogens of the honey bee. *Ann. Appl. Biol.* 103, 13–20.

Bailey, L., Ball, B. V., and Perry, J. N. (1983b). Honeybee paralysis: its natural spread and its diminished incidence in England and Wales. *J. Apic. Res.* 22, 191–195.

Bailey, L., Carpenter, J. M., and Woods, R. D. (1979). Egypt bee virus and Australian isolates of Kashmir bee virus. *J. Gen. Virol.* 43, 641–647. doi: 10.1099/0022-1317-43-3-641

Bailey, L., and Collins, M. D. (1982). Taxonomic studies on 'Streptococcus pluton'. *J. Appl. Bacteriol.* 53, 209–213.

Bailey, L., and Fernando, E. F. W. (1972). Effects of sacbrood virus on adult honey-bees. *Ann. Appl. Biol.* 72, 27–35. doi: 10.1111/j.1744-7348.1972.tb01268.x

Bailey, L., and Gibbs, A. J. (1964). Acute infection of bees with paralysis virus. *J. Insect Pathol.* 6, 395–407. doi: 10.1371/journal.pone.0073429

Bailey, L., Gibbs, A. J., and Woods, R. D. (1963). Two viruses from adult honey bees (*Apis mellifera* Linnaeus). *Virology* 21, 390–395. doi: 10.1016/0042-6822(63)90200-9

Bailey, L., and Milne, R. G. (1969). The multiplication regions and interaction of acute and chronic bee paralysis viruses in adult honeybees. *J. Gen. Virol.* 4, 9–14.

Bailey, L., and Woods, R. D. (1974). Three previously undescribed viruses from the honey bee. *J. Gen. Virol.* 25, 175–186. doi: 10.1099/0022-1317-25-2-175

Bailey, L., and Woods, R. D. (1977). Two more small RNA viruses from honey bees and further observations on sacbrood and acute bee-paralysis viruses. *J. Gen. Virol.* 37, 175–182.

Bakonyi, T., Farkas, R., Szendroi, A., Dobos-Kovacs, M., and Rusvai, M. (2002). Detection of acute bee paralysis virus by RT-PCR in honey bee and *Varroa destructor* field samples: rapid screening of representative Hungarian apiaries. *Apidologie* 33, 63–74.

Ball, B. V. (1983). The association of *Varroa jacobsoni* with virus diseases of honey bees. *Exp. Appl. Acarol.* 19, 607–613.

Ball, B. V. (1985). Acute paralysis virus isolates from honeybee colonies infected with *Varroa jacobsoni*. *J. Apic. Res.* 24, 115–119.

Ball, B. V. (1989). "*Varroa jacobsoni* as a virus vector," in *Present Status of Varroatosis in Europe and Progress in the Varroa Mite Control*, ed. R. Cavalloro, (Luxemburg: EC-Experts Group).

Barbara, G. S., Grünewald, B., Paute, S., Gauthier, M., and Raymond-Delpech, V. (2008). Study of nicotinic acetylcholine receptors on cultured antennal lobe

neurones from adult honeybee brains. *Invertebr. Neurosci.* 8, 19–29. doi: 10.1007/s10158-007-0062-2

Beaurepaire, A., Piot, N., Doublet, V., Antuñez, K., Campbell, E., Chantawannakul, P., et al. (2020). Diversity and global distribution of viruses of the western honey bee, *Apis mellifera*. *Insects* 11:239. doi: 10.3390/insects11040239

Benjeddou, M., Leat, N., Allsopp, M., and Davison, S. (2002). Development of infectious transcripts and genome manipulation of Black queen-cell virus of honey bees. *J. Gen. Virol.* 83, 3139–3146. doi: 10.1099/0022-1317-83-12-3139

Berényi, O., Bakonyi, T., Derakhshifar, I., Köglber, H., Topolska, G., Ritter, W., et al. (2007). Phylogenetic analysis of deformed wing virus genotypes from diverse geographic origins indicates recent global distribution of the virus. *Appl. Environ. Microbiol.* 73, 3605–3611. doi: 10.1128/AEM.00696-07

Bergem, M., Norberg, K., and Aamodt, R. M. (2006). Long-term maintenance of *in vitro* cultured honeybee (*Apis mellifera*) embryonic cells. *BMC Dev. Biol.* 6:17. doi: 10.1186/1471-213X-6-17

Bigot, D., Dalmon, A., Roy, B., Hou, C., Germain, M., Romary, M., et al. (2017). The discovery of Halictivirus resolves the *Sinaivirus* phylogeny. *J. Gen. Virol.* 98, 2864–2875. doi: 10.1099/jgv.0.000957

Blanchard, P., Ribière, M., Celle, O., Lallemand, P., Schurr, F., Olivier, V., et al. (2007). Evaluation of a real-time two-step RT-PCR assay for quantitation of Chronic bee paralysis virus (CBPV) genome in experimentally-infected bee tissues and in life stages of a symptomatic colony. *J. Virol. Methods* 141, 7–13. doi: 10.1016/j.jviromet.2006.11.021

Bodden, J. M., Jenny, A., Hazlehurst, E., Erin, M., and Wilson, R. (2019). Floral traits predict frequency of defecation on flowers by foraging bumble bees. *J. Insect Sci.* 19, 4–6. doi: 10.1093/jisesa/iez091

Boncristiani, H. F., Evans, J. D., Chen, Y., Pettis, J., Murphy, C., Lopez, D. L., et al. (2013). *In vitro* infection of pupae with Israeli acute paralysis virus suggests disturbance of transcriptional homeostasis in honey bees (*Apis mellifera*). *PLoS One* 8:e73429. doi: 10.1371/journal.pone.0073429

Bowen-Walker, P. L., Martin, S. J., and Gunn, A. (1999). The transmission of deformed wing virus between honeybees (*Apis mellifera* L.) by the ectoparasitic mite varroa jacobsoni Oud. *J. Invertebr. Pathol.* 73, 101–106. doi: 10.1006/jipa.1998.4807

Burnside, C. E. (1945). The cause of paralysis of honeybees. *Am. Bee J.* 85, 354–363.

Campbell, E. M., Budge, G. E., Watkins, M., and Bowman, A. S. (2016). Transcriptome analysis of the synganglion from the honey bee mite, *Varroa destructor* and RNAi knockdown of neural peptide targets. *Insect Biochem. Mol. Biol.* 70, 116–126. doi: 10.1016/j.ibmb.2015.12.007

Carreck, N. L., Ball, B. V., and Martin, S. J. (2010). The epidemiology of cloudy wing virus infections in honey bee colonies in the UK. *J. Apic. Res.* 49, 66–71.

Carrillo-Tripp, J., Bonning, B. C., and Miller, W. A. (2015). Challenges associated with research on RNA viruses of insects. *Curr. Opin. Insect Sci.* 8, 62–68. doi: 10.1016/j.cois.2014.11.002

Carrillo-Tripp, J., Dolezal, A. G., Goblirsch, M. J., Miller, W. A., Toth, A. L., and Bonning, B. C. (2016). *In vivo* and *in vitro* infection dynamics of honey bee viruses. *Sci. Rep.* 6:22265. doi: 10.1038/srep22265

Celle, O., Blanchard, P., Olivier, V., Schurr, F., Cougoule, N., Faucon, J.-P., et al. (2008). Detection of Chronic bee paralysis virus (CBPV) genome and its replicative RNA form in various hosts and possible ways of spread. *Virus Res.* 133, 280–284. doi: 10.1016/j.virusres.2007.12.011

Chanpanitkitchote, P., Chen, Y., Evans, J. D., Li, W., Li, J., Hamilton, M., et al. (2018). Acute bee paralysis virus occurs in the Asian honey bee *Apis cerana* and parasitic mite *Tropilaelaps mercedesae*. *J. Invertebr. Pathol.* 151, 131–136. doi: 10.1016/j.jip.2017.11.009

Chantawannakul, P., de Guzman, L. I., Li, J., and Williams, G. R. (2016). Parasites, pathogens, and pests of honeybees in Asia. *Apidologie* 47, 301–324.

Chantawannakul, P., Ward, L., Boonham, N., and Brown, M. (2006). A scientific note on the detection of honeybee viruses using real-time PCR (TagMan) in Varroa mites collected from a Thai honeybee (*Apis mellifera*) apiary. *J. Invertebr. Pathol.* 91, 69–73. doi: 10.1016/j.jip.2005.11.001

Chen, Y., Evans, J., Hamilton, M., and Feldlaufer, M. (2007). The influence of RNA integrity on the detection of honey bee viruses: molecular assessment of different sample storage methods. *J. Apic. Res.* 46, 81–87.

Chen, Y., Pettis, J. S., and Feldlaufer, M. F. (2005). Detection of multiple viruses in queens of the honey bee *Apis mellifera* L. *J. Invertebr. Pathol.* 90, 118–121. doi: 10.1016/j.jip.2005.08.005

Chen, Y. P., Pettis, J. S., Collins, A., and Feldlaufer, M. F. (2006). Prevalence and transmission of honeybee viruses. *Appl. Environ. Microbiol.* 72, 606–611.

Chen, Y. P., Pettis, J. S., Corona, M., Chen, W. P., Li, C. J., Spivak, M., et al. (2014). Israeli acute paralysis virus: epidemiology, pathogenesis and implications for honey bee health. *PLoS Pathog.* 10:e1004261. doi: 10.1371/journal.ppat.1004261

Chen, Y. P., and Siede, R. (2007). Honey bee viruses. *Adv. Virus Res.* 70, 33–80.

Choe, S. E., Nguyen, L. T. K., Noh, J. H., Koh, H. B., Jean, Y. H., Kweon, C. H., et al. (2012). Prevalence and distribution of six bee viruses in Korean *Apis cerana* populations. *J. Invertebr. Pathol.* 109, 330–333. doi: 10.1016/j.jip.2012.01.003

Choi, Y. S., Lee, M. L., Lee, M. Y., and Lee, K. (2008). Occurrence of seven honeybee viruses and research of disease occurrence in Korean apiaries. *Korean J. Apic.* 23, 153–159.

Choi, Y. S., Lee, M. Y., Hong, I. P., Kim, N. S., Kim, H. K., Lee, K. G., et al. (2010). Occurrence of sacbrood virus in Korean apiaries from *Apis cerana* (Hymenoptra: Apidae). *Korean J. Apic.* 25, 187–191.

Core, A., Runckel, C., Ivers, J., Quock, C., Siapno, T., DeNault, S., et al. (2012). A new threat to honey bees, the parasitic phorid fly *Apocephalus borealis*. *PLoS One* 7:e29639. doi: 10.1371/journal.pone.0029639

Cornman, R. S. (2017). Relative abundance of deformed wing virus, *Varroa destructor* virus 1, and their recombinants in honey bees (*Apis mellifera*) assessed by kmer analysis of public RNA-Seq data. *J. Invertebr. Pathol.* 149, 44–50. doi: 10.1016/j.jip.2017.07.005

Coulon, M., Dalmon, A., Di Prisco, G., Prado, A., Arban, F., Dubois, E., et al. (2020). Interactions between thiamethoxam and *Deformed wing virus* can drastically impair flight behavior of honey bees. *Front. Microbiol.* 11:766. doi: 10.3389/fmicb.2020.00766

Coulon, M., Schurr, F., Martel, A. C., Cougoule, N., Bégaud, A., Mangoni, P., et al. (2018). Metabolisation of thiamethoxam (a neonicotinoid pesticide) and interaction with the Chronic bee paralysis virus in honeybees. *Pestic. Biochem. Physiol.* 144, 10–18. doi: 10.1016/j.pestbp.2017.10.009

Cox-Foster, D. L., Conlan, S., Holmes, E. C., Palacios, G., Evans, J. D., Moran, N. A., et al. (2007). A metagenomic survey of microbes in honey bee colony collapse disorder. *Science* 318, 283–287. doi: 10.1126/science.1146498

Dainat, B., Evans, J. D., Chen, Y. P., Gauthier, L., and Neumann, P. (2012). Predictive markers of honey bee colony collapse. *PLoS One* 7:e32151. doi: 10.1371/journal.pone.0032151

Dainat, B., Evans, J. D., Chen, Y. P., and Neumann, P. (2011). Sampling and RNA quality for diagnosis of honey bee viruses using quantitative PCR. *J. Virol. Methods* 174, 150–152. doi: 10.1016/j.jviromet.2011.03.029

Dainat, B., Ken, T., Berthoud, H., and Neumann, P. (2009). The ectoparasitic mite *Tropilaelaps mercedesae* (Acari, Laelapidae) as a vector of honeybee viruses. *Insectes Soc.* 56, 40–43.

Dall, J. (1987). Intracellular structures associated with the multiplication of sacbrood virus. *J. Invertebr. Pathol.* 50, 261–268.

Dalmon, A., Desbiez, C., Coulon, M., Thomasson, M., Le Conte, Y., Alaux, C., et al. (2017). Evidence for positive selection and recombination hotspots in Deformed wing virus (DWV). *Sci. Rep.* 7:41045. doi: 10.1038/srep41045

Dalmon, A., Gayral, P., Decante, D., Klopp, C., Bigot, D., Thomasson, M., et al. (2019). Viruses in the invasive hornet *Vespa velutina*. *Viruses* 11:1041. doi: 10.3390/v11111041

D'Alvise, P., Seeburger, V., Gihring, K., Kieboom, M., and Hasselmann, M. (2019). Seasonal dynamics and co-occurrence patterns of honey bee pathogens revealed by high-throughput RT-qPCR analysis. *Ecol. Evol.* 9, 10241–10252. doi: 10.1002/ece3.5544

Danforth, B. N. (2002). Evolution of sociality in a primitively eusocial lineage of bees. *Proc. Natl. Acad. Sci. U.S.A.* 99, 286–290. doi: 10.1073/pnas.012387999

Daughenbaugh, K. F., Martin, M., Brutscher, L. M., Cavigli, I., Garcia, E., Lavin, M., et al. (2015). Honey bee infecting Lake Sinai viruses. *Viruses* 7, 3285–3309. doi: 10.3390/v7062772

de Miranda, J. R., Bailey, L., Ball, B. V., Blanchard, P., Budge, G. E., Chejanovsky, N., et al. (2013). Standard methods for virus research in *Apis mellifera*. *J. Apic. Res.* 52, 1–56. doi: 10.3896/ibra.1.52.4.22

de Miranda, J. R., Cornman, R. S., Evans, J. D., Semberg, E., Haddad, N., Neumann, P., et al. (2015). Genome characterization, prevalence and distribution of a macula-like virus from *Apis mellifera* and *Varroa destructor*. *Viruses* 7, 3586–3602. doi: 10.3390/v7072789

de Miranda, J. R., Dainat, B., Locke, B., Cordoni, G., Berthoud, H., Gauthier, L., et al. (2010a). Genetic characterization of slow bee paralysis virus of the honeybee (*Apis mellifera* L.). *J. Gen. Virol.* 91, 2524–2530. doi: 10.1099/vir.0.022434-0

de Miranda, J. R., Cordoni, G., and Budge, G. (2010b). The Acute bee paralysis virus-Kashmir bee virus-Israeli acute paralysis virus complex. *J Invertebr. Pathol.* 103(Suppl. 1), S30–S47. doi: 10.1016/j.jip.2009.06.014

de Miranda, J. R., and Fries, I. (2008). Venereal and vertical transmission of deformed wing virus in honeybees (*Apis mellifera* L.). *J. Invertebr. Pathol.* 98, 184–189. doi: 10.1016/j.jip.2008.02.004

de Souza, F. S., Kevill, J. L., Correia-Oliveira, M. E., de Carvalho, C. A. L., and Martin, S. J. (2019). Occurrence of deformed wing virus variants in the stingless bee melipona subnitida and honey bee *Apis mellifera* populations in Brazil. *J. Gen. Virol.* 100, 289–294. doi: 10.1099/jgv.0.001206

Di Prisco, G., Annoscia, D., Margiotta, M., Ferrara, R., Varricchio, P., Zanni, V., et al. (2016). Mutualistic symbiosis between a parasitic mite and a pathogenic virus undermines honey bee immunity and health. *Proc. Natl. Acad. Sci. U.S.A.* 113, 3203–3208. doi: 10.1073/pnas.1523515113

Di Prisco, G., Pennacchio, F., Caprio, E., Boncristiani, H. F., Evans, J. D., and Chen, Y. (2011). *Varroa destructor* is an effective vector of Israeli acute paralysis virus in the honeybee, *Apis mellifera*. *J. Gen. Virol.* 92, 151–155. doi: 10.1099/vir.0.023853-0

Dolan, P. T., Whitfield, Z. J., and Andino, R. (2018). Mechanisms and concepts in RNA virus population dynamics and evolution. *Annu. Rev. Virol.* 5, 69–92. doi: 10.1146/annurev-virology-101416-041718

Dolezal, A. G., Hendrix, S. D., Scavo, N. A., Carrillo-Tripp, J., Harris, M. A., Wheelock, M. J., et al. (2016). Honey bee viruses in wild bees: viral prevalence, loads, and experimental inoculation. *PLoS One* 11:e166190. doi: 10.1371/journal.pone.0166190

Doublet, V., Natsopoulou, M. E., Zschiesche, L., and Paxton, R. J. (2015). Within-host competition among the honey bees pathogens *Nosema ceranae* and Deformed wing virus is asymmetric and to the disadvantage of the virus. *J. Invertebr. Pathol.* 124, 31–34. doi: 10.1016/j.jip.2014.10.007

Dubois, E., Dardouri, M., Schurr, F., Cougoule, N., Sircoulomb, F., and Thiéry, R. (2020). Outcomes of honeybee pupae inoculated with deformed wing virus genotypes A and B. *Apidologie* 51, 18–34. doi: 10.1007/s13592-019-00701-z

Evans, H. E. (2002). A review of prey choice in bembicine sand wasps (Hymenoptera: phecidae). *Neotrop. Entomol.* 31, 1–11.

Evans, H. E., and O'Neill, K. M. (2007). *The Sand Wasps*. Cambridge, MA: Harvard University Press. doi: 10.4159/9780674036611

Evison, S. E. F., Roberts, K. E., Laurenson, L., Pietravalle, S., Hui, J., Biesmeijer, J. C., et al. (2012). Pervasiveness of parasites in pollinators. *PLoS One* 7:e30641. doi: 10.1371/journal.pone.0030641

Eyer, M., Chen, Y., Schäfer, M., Pettis, J., and Neumann, P. (2009). Small hive beetle, *Aethina tumida*, as a potential biological vector of honeybee viruses. *Apidologie* 40, 419–428.

Fievet, J., Tentcheva, D., Gauthier, L., de Miranda, J., Cousserans, F., Colin, M. E., et al. (2006). Localization of deformed wing virus infection in queen and drone *Apis mellifera* L. *Virol J.* 3:16. doi: 10.1186/1743-422X-3-16

Figueroa, L. L., Blinder, M., Grincavitch, C., Jelinek, A., Mann, E. K., Merva, L. A., et al. (2019). Bee pathogen transmission dynamics: deposition,persistence and acquisition on flowers. *Proc. R. Soc. B* 286:e20190603. doi: 10.1098/rspb.2019.0603

Forsgren, E., de Miranda, J. R., Isaksson, M., Wei, S., and Fries, I. (2009). Deformed wing virus associated with *Tropilaelaps mercedesae* infesting European honey bees (*Apis mellifera*). *Exp. Appl. Acarol.* 47, 87–97. doi: 10.1007/s10493-008-9204-4

Forsgren, E., Locke, B., Semberg, E., Laugen, A. T., and de Miranda, J. R. (2017). Sample preservation, transport and processing strategies for honeybee RNA extraction: influence on RNA yield, quality, target quantification and data normalization. *J. Virol. Methods* 246, 81–89. doi: 10.1016/j.jviromet.2017.04.010

Forsgren, E., Wei, S., Guiling, D., Zhiguang, L., Van Tran, T., Tang, P. T., et al. (2015). Preliminary observations on possible pathogen spill-over from *Apis mellifera* to *Apis cerana*. *Apidologie* 46, 265–275.

Forzan, M., Sagona, S., Mazzei, M., and Felicioli, A. (2017). Detection of deformed wing virus in *Vespa crabro*. *Bull. Insectol.* 70, 261–265.

Francis, R. M., Nielsen, S. L., and Kryger, P. (2013). Patterns of viral infection in honey bee queens. *J. Gen. Virol.* 94, 668–676. doi: 10.1099/vir.0.047019-0

Fürst, M., McMahon, D. P., Osborne, J. L., Paxton, R. J., and Brown, M. J. F. (2014). Disease associations between honeybees and bumblebees as a threat to wild pollinators. *Nature* 506, 364–366. doi: 10.1038/nature12977

Galbraith, D. A., Fuller, Z. L., Ray, A. M., Brockmann, A., Frazier, M., Gikungu, M. W., et al. (2018). Investigating the viral ecology of global bee communities with high-throughput metagenomics. *Sci. Rep.* 8:8879. doi: 10.1038/s41598-018-27164-z

Garigliany, M., Taminiau, B., El Agrebi, N., Cadar, D., Gilliaux, G., Hue, M., et al. (2017). Moku virus in invasive Asian Hornets, Belgium, 2016. *Emerg. Infect. Dis.* 23, 2109–2112. doi: 10.3201/eid2312.171080

Gascuel, J., Masson, C., Bermudez, I., and Beadle, D. J. (1994). Morphological analysis of honeybee antennal cells growing in primary cultures. *Tissue Cell* 26, 551–558. doi: 10.1016/0040-8166(94)90007-8

Gauthier, L., Cornman, S., Hartmann, U., Cousserans, F., Evans, J. D., de Miranda, J. R., et al. (2015). The *Apis mellifera* filamentous virus genome. *Viruses* 7, 3798–3815. doi: 10.3390/v7072798

Genersch, E., Gisder, S., Hedtke, K., Hunter, W. B., Möckel, N., and Müller, U. (2013). Standard methods for cell cultures in *Apis mellifera* research. *J. Apic. Res.* 52, 1–8. doi: 10.3896/IBRA.1.52.1.02

Genersch, E., Yue, C., Fries, I., and de Miranda, J. R. (2006). Detection of deformed wing virus, a honey bee viral pathogen, in bumble bees (*Bombus terrestris* and *Bombus pascuorum*) with Wing Deformities. *J. Invertebr. Pathol.* 91, 61–63. doi: 10.1016/j.jip.2005.10.002

Gisder, S., Aumeier, P., and Genersch, E. (2009). Deformed wing virus: replication and viral load in mites (*Varroa destructor*). *J. Gen. Virol.* 90, 463–467. doi: 10.1099/vir.0.005579-0

Gisder, S., and Genersch, E. (2017). Viruses of commercialized insect pollinators. *J. Invertebr. Pathol.* 147, 51–59. doi: 10.1016/j.jip.2016.07.010

Gisder, S., Möckel, N., Eisenhardt, D., and Genersch, E. (2018). *In vivo* evolution of viral virulence: switching of deformed wing virus between hosts results in virulence changes and sequence shifts. *Environ. Microbiol.* 20, 4612–4628. doi: 10.1111/1462-2920.14481

Giuffre, C., Lubkin, S. R., and Tarpy, D. (2019). Does viral loads alter behaviour of the bee parasite *Varroa destructor*? *PLoS One* 14:e0217975. doi: 10.1371/journal.pone.0217975

Goblirsch, M. J., Spivak, M. S., and Kurtti, T. J. (2013). A cell line resource derived from honey bee (*Apis mellifera*) embryonic tissues. *PLoS One* 8:e69831. doi: 10.1371/journal.pone.0069831

Goldberg, F., Grünewald, B., Rosenboom, H., and Menzel, R. (1999). Nicotinic acetylcholine currents of cultured Kenyon cells from the mushroom bodies of the honey bee *Apis mellifera*. *J. Physiol.* 514, 759–768. doi: 10.1111/j.1469-7793.1999.759ad.x

Golding, Y. C., and Edmunds, M. (2000). Behavioural mimicry of honeybees (*Apis mellifera*) by droneflies (Diptera: Syrphidae: *Eristalis* spp.). *Proc. Biol. Sci.* 267, 903–909. doi: 10.1098/rspb.2000.1088

Gong, H.-R., Chen, X.-X., Chen, Y. P., Hu, F.-L., Zhang, J.-L., Lin, Z.-G., et al. (2016). Evidence of *Apis cerana* Sacbrood virus Infection in *Apis mellifera*. *Appl. Environm. Microbiol.* 82:2256.

Gonthier, J., Papach, A., Straub, L., Campbell, J., Williams, G. R., and Neumann, P. (2019). Bees and flowers: how to feed an invasive beetle species. *Ecol. Evol.* 9, 6422–6432. doi: 10.1002/ece3.5217

Grabensteiner, E., Ritter, W., Carter, M. J., Davison, S., Pechhacker, H., Kolodziejek, J., et al. (2001). Sacbrood virus of the honeybee (*Apis mellifera*): rapid indentification and phylogenetic analysis using reverse transcription-PCR. *Clin. Diagn. Lab. Immunol.* 8, 93–104. doi: 10.1128/CDLI.8.1.93-104.2001

Grace, T. D. C. (1962). Establishment of four strains of cells from insect tissues grown *in vitro*. *Nature* 195, 788–789. doi: 10.1038/195788a0

Graystock, P., Goulson, D., and Hughes, W. O. H. (2015). Parasites in bloom: flowers aid dispersal and transmission of pollinator parasites within and between bee species. *Proc R. Soc. B Biol. Sci.* 282:20151371. doi: 10.1098/rspb.2015.1371

Groden, E., Drummond, F. A., Garnas, J., and Francoeur, A. (2005). Distribution of an invasive ant, *Myrmica rubra* (Hymenoptera: Formicidae), in Maine. *J. Econ. Entomol.* 98, 1774–1784. doi: 10.1093/jee/98.6.1774

Gusachenko, O. N., Woodford, L., Balbirnie-Cumming, K., Ryabov, E. V., and Evans, D. J. (2019). Deformed Wing Virus spillover from honey bees to bumble bees: a reverse genetic study. *bioRxiv* [Preprint]. doi: 10.1101/2019.12.18.880559

Guzman-Novoa, E., Md. Hamiduzzaman, M., Anguiano-Baez, R., Correa-Benítez, A., Castañeda-Cervantes, E., and Arnold, N. I. (2015). First detection of honey bee viruses in stingless bees in North America. *J. Apic. Res* 55, 185–186. doi: 10.1080/00218839.2015.1100154

Hematian, A., Sadeghifard, N., Mohebi, R., Taherikalani, M., Nasrolahi, A., Amraei, M., et al. (2016). Traditional and modern cell culture in virus diagnosis. *Osong Public Health Res. Perspect.* 7, 77–82. doi: 10.1016/j.phrp.2015.11.011

Hoffmann, D., Pettis, J. S., and Neumann, P. (2008). Potential host shift of the small hive beetle (*Aethina tumida*) to bumblebee colonies (*Bombus impatiens*). *Insect Soc.* 55, 153–162.

Holway, D. A., Lach, L., Suarez, A. V., Tsutsui, N. D., and Case, T. J. (2002). The causes and consequences of ant invasions. *Annu. Rev. Ecol. Syst.* 33, 181–223. doi: 10.1146/annurev.ecolsys.33.010802.150444

Hung, A., and Shimanuki, H. (1999). A scientific note on the detection of kashmir bee virus in individual honeybees and *Varroa jacobsoni* mites. *Apidologie* 30, 353–354.

Hung, A. C. F. (2000). PCR detection of Kashmir bee virus in honey bee excreta. *J. Apic. Res.* 39, 103–106.

Hunter, W. B. (2010). Medium for development of bee cell cultures (*Apis mellifera*: Hymenoptera: Apidae). *In Vitro Cell. Dev. Biol. Anim.* 46, 83–86. doi: 10.1007/s11626-009-9246-x

Hunter, W. B., Ikonomou, L., Schneider, Y.-J., and Agathos, S. N. (2003). Insect cell culture for industrial production of recombinant proteins. *Appl. Microbiol. Biotechnol.* 62, 1–20. doi: 10.1007/s00253-003-1223-9

Iqbal, J., and Mueller, U. (2007). Virus infection causes specific learning deficits in honeybee foragers. *Proc. R. Soc. B Biol. Sci.* 274, 1517–1521. doi: 10.1098/rspb.2007.0022

Jin, L., Mehmood, S., Zhang, G., Song, Y., Su, S., Huang, S., et al. (2020). Visualizing Sacbrood virus of honey bees via transformation and coupling with enhanced green fluorescent protein. *Viruses* 12:224. doi: 10.3390/v12020224

Ju, H., and Ghil, S. (2015). Primary cell culture method for the honeybee *Apis mellifera*. *In Vitro Cell. Dev. Biol. Anim.* 51, 890–893. doi: 10.1007/s11626-015-9924-9

Kevill, J. L., Highfield, A., Mordecai, G. J., Martin, S. J., and Schroeder, D. C. (2017). ABC Assay: method development and application to quantify the role of three DWV mater variants in overawinter colony losses of European honey bees. *Viruses* 9:314. doi: 10.3390/v9110314

Khongphinitbunjong, K., de Guzman, L. I., Tarver, M. R., Rinderer, T. E., Chen, Y. P., and Chantawannakul, P. (2015). Differential viral levels and immune gene expression in three stocks of *Apis mellifera* induced by different numbers of *Varroa destructor*. *J. Insect Physiol.* 72, 28–34. doi: 10.1016/j.jinsphys.2014.11.005

Khongphinitbunjong, K., Neumann, P., Chantawannakul, P., and Williams, G. R. (2016). The ectoparasitic mite *Tropilaelaps mercedesae* reduces western honey bee, *Apis mellifera*, longevity and emergence weight, and promotes Deformed wing virus infections. *J. Invertebr. Pathol.* 137, 38–42. doi: 10.1016/j.jip.2016.04.006

Kitagishi, Y., Okumura, N., Yoshida, H., Nishimura, Y., Takahashi, J.-I., and Matsuda, S. (2011). Long-term cultivation of *in vitro Apis mellifera* cells by gene transfer of human c-myc proto-oncogene. *In Vitro Cell Dev. Biol. Anim.* 47, 451–453. doi: 10.1007/s11626-011-9431-6

Kojima, Y., Toki, T., Morimoto, T., Yoshiyama, M., Kimura, K., and Kadowaki, T. (2011). Infestation of Japanese native honey bees by tracheal mite and virus from non-native European honey bees in Japan. *Microb. Ecol.* 62, 895–906. doi: 10.1007/s00248-011-9947-z

Kreissl, S., and Bicker, G. (1992). Dissociated neurons of the pupal honeybee brain in cell culture. *J. Neurocytol.* 21, 545–556. doi: 10.1007/bf01187116

Krunicì, M. D., and Stanisavljevicì, L. Z. (2006). *The Biology of European Orchard Bee Osmia Cornuta (Latr.) (Hymenoptera: Megachilidae)*. Belgrade: University of Belgrade.

Kuszewska, K., and Woyciechowski, M. (2014). Risky robbing is a job for short-lived and infected worker honeybees. *Apidologie* 45, 537–544.

Lamp, B., Url, A., Seitz, K., Eichhorn, J., Riedel, C., Sinn, L. J., et al. (2016). Construction and rescue of a molecular clone of deformed wing virus (DWV). *PLoS One* 11:e0164639. doi: 10.1371/journal.pone.0164639

Lanzi, G., de Miranda, J. R., Boniotti, M. B., Cameron, C. E., Lavazza, A., Capucci, L., et al. (2006). Molecular and biological characterization of deformed wing virus of honeybees (*Apis mellifera* L). *J. Virol.* 80, 4998–5009. doi: 10.1128/JVI.80.10.4998-5009.2006

Leland, D. S., and Ginocchio, C. C. (2007). Role of cell culture for virus detection in the age of technology. *Clin. Microb. Rev.* 20, 49–78. doi: 10.1128/CMR.00002-06

Levin, S., Galbraith, D. A., Sela, N., Erez, T., Grozinger, C. M., and Chejanovsky, N. (2017). Presence of apisrhabdovirus-1 in populations of pollinators and their parasites from two continents. *Front. Microbiol.* 8:2482. doi: 10.3389/fmicb.2017.02482

Levin, S., Sela, N., and Chejanovsky, N. (2016). Two novel viruses associated with the *Apis mellifera* pathogenic mite *Varroa destructor*. *Sci. Rep.* 6:37710. doi: 10.1038/srep37710

Levin, S., Sela, N., Erez, T., Nestel, D., Pettis, J., Neumann, P., et al. (2019). New viruses from the ectoparasite mite *Varroa destructor* Infesting *Apis mellifera* and *Apis cerana*. *Viruses* 11:94. doi: 10.3390/v11020094

Levitt, A. L., Singh, R., Cox-Foster, D. L., Rajotte, E., Hoover, K., Ostiguy, N., et al. (2013). Cross-species transmission of honey bee viruses in associated arthropods. *Virus Res.* 176, 232–240. doi: 10.1016/j.virusres.2013.06.013

Lhomme, P., and Hines, H. M. (2018). Ecology and evolution of cuckoo bumble bees. *Ann. Entomol. Soc. Am.* 112, 122–140.

Li, J., Qin, H., Wu, J., Sadd, B. M., Wang, X., Evans, J. D., et al. (2012). The prevalence of parasites and pathogens in Asian honeybees *Apis cerana* in China. *PLoS One* 7:e47955. doi: 10.1371/journal.pone.0047955

Liu, T. P. (1991). Virus-like particles in the tracheal mite, *Acarapis woodi* (Rennie). *Apidologie* 22, 213–219.

Liu, X., Zhang, Y., Yan, X., and Han, R. (2010). Prevention of Chinese sacbrood virus infection in *Apis cerana* using RNA interference. *Curr. Microbiol.* 61, 422–428. doi: 10.1007/s00284-010-9633-2

Locher, C. P., Witt, S. A., Herndier, B. G., Abbey, N. W., Tenner-Racz, K., Racz, P., et al. (2003). Increased virus replication and virulence after serial passage of human immunodeficiency virus type 2 in baboons. *J. Virol.* 77, 77–83. doi: 10.1128/jvi.77.1.77-83.2003

Loope, K. J., Baty, J. W., Lester, P. J., and Wilson Rankin, E. E. (2019). Pathogen shifts in a honeybee predator following the arrival of the Varroa mite. *Proc. R. Soc. B Biol. Sci.* 286:20182499. doi: 10.1098/rspb.2018.2499

Lopez-Vaamonde, C., Koning, J. W., Brown, R. M., Jordan, W. C., and Bourke, A. F. (2004). Social parasitism by male-producing reproductive workers in a eusocial insect. *Nature* 430, 557–560. doi: 10.1038/nature02769

Lynn, D. E. (1999). Development of insect cell lines: virus susceptibility and applicability to prawn cell culture. *Method Cell Sci.* 21, 173–181. doi: 10.1023/a:1009824207045

Lynn, D. E. (2001). Novel techniques to establish new insect cell lines. *In Vitro Cell. Dev. Biol. Anim.* 37, 319–321. doi: 10.1007/bf02577564

Macieira, O. J. D., Chaud-Netto, J., and Zanon, A. M. (1983). Oviposition rate and relative viability of descendants from couples of *Megaselia scalaris* (Diptera: Phoridae) reared in different experimental conditions. *Rev. Bras. Biol.* 43, 223–228.

Maori, E., Lavi, S., Mozes-Koch, R., Gantman, Y., Peretz, Y., Edelbaum, O., et al. (2007). Isolation and characterization of Israeli acute paralysis virus, a dicistrovirus affecting honeybees in Israel: evidence for diversity due to intra- and inter-species recombination. *J. Gen. Virol.* 18, 3428–3438. doi: 10.1099/vir.0.83284-0

Maori, E., Paldi, N., Shafir, S., Kalev, H., Tsur, E., Glick, E., et al. (2009). IAPV, a bee-affecting virus associated with colony collapse disorder can be silenced by dsRNA ingestion. *Insect Mol. Biol.* 18, 55–60. doi: 10.1111/j.1365-2583.2009.00847.x

Martin, S. J., and Brettell, L. E. (2019). Deformed wing virus in honeybees and other insects. *Annu. Rev. Virol* 6, 49–69. doi: 10.1146/annurev-virology-092818-015700

Martin, S. J., Highfield, A. C., Brettell, L., Villalobos, E. M., Budge, G. E., Powell, M., et al. (2012). Global honey bee viralandscape altered by a parasitic mite. *Science* 336, 1304–1306. doi: 10.1126/science.1220941

Mazzei, M., Carrozza, M. L., Luisi, E., Forzan, M., Giusti, M. S., Sagona, S., et al. (2014). Infectivity of DWV associated to flower pollen: experimental evidence of a horizontal transmission route. *PLoS One* 9:e113448. doi: 10.1371/journal.pone.0113448

Mazzei, M., Cilia, G., Forzan, M., Lavazza, A., Mutinelli, F., and Felicioli, A. (2019). Detection of replicative Kashmir bee virus and black queen cell virus in Asian hornet *Vespa velutina* (Lepelieter 1836) in Italy. *Sci. Rep.* 9:10091. doi: 10.1038/s41598-019-46565-2

Mazzei, M., Forzan, M., Cilia, G., Sagona, S., Bortolotti, L., and Felicioli, A. (2018). First detection of replicative deformed wing virus (DWV) in *Vespa Velutina* Nigrithorax. *Bull. Insectol.* 71, 211–216.

Mazzei, M., Fronte, B., Sagona, S., Carrozza, M. L., Forzan, M., Pizzurro, F., et al. (2016). Effect of 1,3-1,6 β-Glucan on natural and experimental deformed wing virus infection in newly emerged honeybees (*Apis mellifera* ligustica). *PLoS One* 11:e0166297. doi: 10.1371/journal.pone.0166297

McMahon, D. P., Fürst, M. A., Caspar, J., Panagiotis, T., Brown, M. J. F., and Paxton, R. J. (2015). A sting in the spit: widespread cross-infection of multiple RNA viruses across wild and managed bees. *J. Anim. Ecol.* 84, 615–624. doi: 10.1111/1365-2656.12345

McMahon, D. P., Natsopoulou, M. E., Doublet, V., Fürst, M., Weging, S., Brown, M. J. F., et al. (2016). Elevated virulence of an emerging viral genotype as a driver of honeybee loss. *Proc. Biol. Sci.* 283:20160811. doi: 10.1098/rspb.2016.0811

Meeus, I., de Miranda, J. R., de Graaf, D. C., Wäckers, F., and Smagghe, G. (2014). Effect of oral infection with Kashmir bee virus and Israeli acute paralysis virus on bumblebee (*Bombus terrestris*) reproductive success. *J. Invertebr. Pathol.* 121, 64–69. doi: 10.1016/j.jip.2014.06.011

Menail, A. H., Piot, N., Meeus, I., Smagghe, G., and Loucif-Ayad, W. (2016). large pathogen screening reveals first report of *Megaselia Scalaris* (Diptera: Phoridae) Parasitizing *Apis Mellifera* Intermissa (Hymenoptera: Apidae). *J. Invertebr. Pathol.* 137, 33–37. doi: 10.1016/j.jip.2016.04.007

Milićević, V., Radojièić, S., Kureljušić, J., Šekler, M., Nešić, K., Veljović, L., et al. (2018). Molecular detection of black queen cell virus and Kashmir bee virus in honey. *AMB Express* 8:128. doi: 10.1186/s13568-018-0655-7

Möckel, N., Gisder, S., and Genersch, E. (2011). Horizontal transmission of deformed wing virus: pathological consequences in adult bees (*Apis mellifera*) depend on the transmission route. *J. Gen. Virol.* 92, 370–377. doi: 10.1099/vir.0.025940-0

Mongiardino, K. N. P., Fontanarrosa, J., Padró, I. M., and Soto, R. (2013). First Record of *Megaselia Scalaris* (Loew) (Diptera: Phoridae) Infesting Laboratory Stocks of Mantids (Parastagmatoptera Tessellata, Saussure). *Arthropods* 2, 1–6.

Mookhploy, W., Kimura, K., Disayathanoowat, T., Yoshiyama, M., Hondo, K., and Chantawannakul, P. (2015). Capsid gene divergence of black queen cell virus isolates in Thailand and Japan honey bee species. *J. Econ. Entomol.* 108, 1460–1464. doi: 10.1093/jee/tov102

Moore, J., Jironkin, A., Chandler, D., Burroughs, N., Evans, D. J., and Ryabov, E. V. (2011). Recombinants between Deformed wing virus and *Varroa destructor* virus-1 may prevail in *Varroa destructor*-infested honeybee colonies. *J. Gen. Virol.* 92, 156–161. doi: 10.1099/vir.0.025965-0

Mordecai, G. J., Brettell, L. E., Martin, S. J., Dixon, D., Jones, I. M., and Schroeder, D. C. (2016a). Superinfection exclusion and the long-term survival of honey bees in Varroa-infested colonies. *ISME J.* 10, 1182–1191. doi: 10.1038/ismej.2015.186

Mordecai, G. J., Brettell, L. E., Pachori, P., Villalobos, E., Martin, M. S. J., Jones, I. M., et al. (2016b). Moku virus; a new *Iflavirus* found in wasps, honey bees and Varroa. *Sci. Rep.* 6:34983. doi: 10.1038/srep34983

Mordecai, G. J., Wilfert, L., Martin, S. J., Jones, I. M., and Schroeder, D. C. (2016c). Diversity in a honey bee pathogen: first report of a third master variant of deformed wing virus quasispecies. *ISME J.* 10, 1264–1273. doi: 10.1038/ismej.2015.178

Mussen, E. C., and Furgala, B. (1977). Replication of sacbrood virus in larval and adult honeybees, *Apis mellifera*. *J. Invertebr. Pathol.* 30, 20–34.

Nasi, S., Ciarapica, R., Jucker, R., Rosati, J., and Soucek, L. (2001). Making decisions through Myc. *FEBS Lett.* 49o, 153–162. doi: 10.1016/S0014-5793(01)02118-4

Natsopoulou, M. E., McMahon, D. P., Doublet, V., Frey, E., Rosenkranz, P., and Paxton, R. J. (2017). The virulent, emerging genotype B of Deformed wing virus is closely linked to overwinter honeybee worker loss. *Sci. Rep.* 7:5242. doi: 10.1038/s41598-017-05596-3

Neumann, P., and Elzen, P. J. (2004). The Biology of the Small Hive Beetle (*Aethina Tumida*, Coleoptera: Nitidulidae): gaps in Our Knowledge of an Invasive Species. *Apidologie* 35, 229–247. doi: 10.1051/apido:2004010

Niu, J., Cappelle, K., de Miranda, J. R., Smagghe, G., and Meeus, I. (2014). Analysis of reference gene stability after israeli acute paralysis virus infection in bumblebees *Bombus terrestris*. *J. Invertebr. Pathol.* 115, 76–79. doi: 10.1016/j.jip.2013.10.011

Niu, J., Smagghe, G., De Coninck, D. I. M., Van Nieuwerburgh, F., Deforce, D., and Meeus, I. (2016). *In Vivo* Study of Dicer-2-mediated immune response of the small interfering RNA pathway upon systemic infections of virulent and avirulent viruses in *Bombus Terrestris*. *Insect Biochem. Mol. Biol.* 70, 127–137. doi: 10.1016/j.ibmb.2015.12.006

Noh, J. H., Reddy, K. E., Choe, S. E., Yoo, M. S., Doan, H. T. T., Kweon, C. H., et al. (2013). Phylogenetic analysis of black queen cell virus genotypes in South Korea. *Virus Genes* 46, 362–368. doi: 10.1007/s11262-012-0859-x

Nordström, S. (2003). Distribution of deformed wing virus within honey bee (*Apis mellifera*) brood cells infested with the ectoparasitic mite *Varroa destructor*. *Exp. Appl. Acarol.* 29, 293–302. doi: 10.1023/a:1025853731214

Ongus, J. R., Peters, D., Bonmatin, J.-M., Bengsch, E., Vlak, J. M., and van Oers, M. M. (2004). Complete sequence of a picornalike virus of the genus Iflavirus replicating in the mite *Varroa destructor*. *J. Gen. Virol.* 85, 3747–3755. doi: 10.1099/vir.0.80470-0

Packer, L. (1986). The biology of a subtropical population of *Halictus ligatus* say (Hymenoptera: Halictidae). *Ethology* 72, 287–298.

Peng, W., Li, J., Boncristiani, H., Strange, J. P., Hamilton, M., and Chen, Y. (2011). Host range expansion of honey bee black queen cell virus in the bumble bee, *Bombus huntii*. *Apidologie* 42, 650–658.

Pfeiffer, K. J., and Crailsheim, K. (1998). Drifting of honeybees. *Insects Soc.* 45, 151–167. doi: 10.1007/s000400050076

Piot, N., Meeus, I., Kleijn, D., Scheper, J., Linders, T., and Smagghe, G. (2019). Establishment of wildflower fields in poor quality landscapes enhances micro-parasite prevalence in wild bumble bees. *Oecologia* 189, 149–158. doi: 10.1007/s00442-018-4296-y

Piot, N., Snoeck, S., Vanlede, M., Smagghe, G., and Meeus, I. (2015). The Effect of Oral Administration of DsRNA on Viral Replication and Mortality in *Bombus terrestris*. *Viruses* 7, 3172–3185. doi: 10.3390/v7062765

Posada-Florez, F., Childers, A. K., Heerman, M. C., Egekwu, N. I., Cook, S. C., Chen, Y., et al. (2019). Deformed wing virus type A, a major honey bee pathogen, is vectored by the mite *Varroa destructor* in a non-propagative manner. *Sci. Rep.* 9:12445. doi: 10.1038/s41598-019-47447-3

Power, E. F., and Stout, J. C. (2011). Organic dairy farming: impacts on insect-flower interaction networks and pollination. *J. Appl. Ecol.* 48, 561–569. doi: 10.1111/j.1365-2664.2010.01949.x

Prodělalová, J., Moutelíková, R., and Titěra, D. (2019). Multiple virus infections in western honeybee (*Apis mellifera* L.) ejaculate used for instrumental insemination. *Viruses* 11:306. doi: 10.3390/v11040306

Ra, D. K., Jeong, C., Lee, J. H., Lee, Y. M., Kim, K. H., Han, T. H., et al. (2012). Prevalence of honeybee diseases in Incheon area in 2011. *Korean J. Vet. Serv.* 35, 111–117.

Ravoet, J., De Smet, L., Meeus, I., Smagghe, G., Wenseleers, T., and de Graaf, D. C. (2014). Widespread occurrence of honey bee pathogens in solitary bees. *J. Invertebr. Pathol.* 122, 55–58. doi: 10.1016/j.jip.2014.08.007

Ravoet, J., De Smet, L., Wenseleers, T., and de Graaf, D. C. (2015a). Genome sequence heterogeneity of Lake Sinai Virus found in honey bees and Orf1/RdRP-based polymorphisms in a single host. *Virus Res.* 201, 67–72. doi: 10.1016/j.virusres.2015.02.019

Ravoet, J., De Smet, L., Wenseleers, T., and de Graaf, D. C. (2015b). Vertical transmission of honey bee viruses in a Belgian queen breeding program. *BMC Vet. Res.* 11:61. doi: 10.1186/s12917-015-0386-9

Reddy, K. E., Noh, J. H., Kim, Y. H., Yoo, M. S., Doan, H. T. T., Ramya, M., et al. (2013). Analysis of the nonstructural and structural polyprotein regions, and complete genome sequences of Israel acute paralysis viruses identified from honeybees (*Apis mellifera*) in Korea. *Virology* 444, 211–217. doi: 10.1016/j.virol.2013.06.012

Regoes, R. R., Nowak, M. A., and Bonhoeffer, S. (2000). Evolution of virulence in a heterogeneous host population. *Evolution* 54, 64–71. doi: 10.1111/j.0014-3820.2000.tb00008.x

Remnant, E. J., Mather, N., Gillard, T. L., Yagound, B., and Beekman, M. (2019). Direct transmission by injection affects competition among RNA viruses in honeybees. *Proc. R. Soc. Lond. B Biol. Sci.* 286:e20182452. doi: 10.1098/rspb.2018.2452

Remnant, E. J., Shi, M., Buchmann, G., Blacquière, T., Holmes, E. C., Beekman, M., et al. (2017). A diverse range of novel RNA viruses in geographically distinct honey bee populations. *J. Virol.* 91:e00158-17. doi: 10.1128/JVI.00158-17

Ribière, M., Lallemand, P., Iscache, A.-L., Schurr, F., Celle, O., Blanchard, P., et al. (2007). Spread of infectious chronic bee paralysis virus by honeybee (*Apis mellifera* L.) Feces. *Appl. Environ. Microbiol.* 73, 7711–7716. doi: 10.1128/AEM.01053-07

Roberts, J. M. K., Anderson, D. L., and Durr, P. A. (2018). Metagenomic analysis of Varroa-free Australian honey bees (*Apis mellifera*) shows a diverse Picornavirales virome. *J. Gen. Virol.* 99, 818–826. doi: 10.1099/jgv.0.001073

Robinson, W. H. (1975). *Megaselia Scalaris* (Diptera: Phoridae) associated with laboratory cockroach colonies. *Proc. Entomol. Soc. Wash.* 77, 384–390.

Rosenkranz, P., Aumeier, P., and Ziegelmann, B. (2010). Biology and control of *Varroa destructor*. *J. Invertebr. Pathol.* 103, S96–S119. doi: 10.1016/j.jip.2009.07.016

Runckel, C., Flenniken, M. L., Engel, J. C., Ruby, J. G., Ganem, D., Andino, R., et al. (2011). Temporal analysis of the honey bee microbiome reveals four novel viruses and seasonal prevalence of known viruses, *Nosema*, and *Crithidia*. *PLoS One* 6:e20656. doi: 10.1371/journal.pone.0020656

Ryabov, E. V., Childers, A. K., Lopez, D., Grubbs, K., Posada-Florez, F., Weaver, D., et al. (2019). Dynamic evolution in the key honey bee pathogen deformed wing virus: novel insights into virulence and competition using reverse genetics. *PLoS Biol.* 17:e3000502. doi: 10.1371/journal.pbio.3000502

Ryabov, E. V., Christmon, K., Heerman, C. M., Posada-Florez, F., Harrison, L. R., Chen, Y., et al. (2020). Development of a honey bee RNA virus vector based on the genome of a deformed wing virus. *Viruses* 12:374. doi: 10.3390/v12040374

Ryabov, E. V., Fannon, J. M., Moore, J. D., Wood, G. R., and Evans, D. J. (2016). The Iflaviruses Sacbrood virus and deformed wing virus evoke different transcriptional responses in the honeybee which may facilitate their horizontal or vertical transmission. *Peer J.* 4:e1591. doi: 10.7717/peerj.1591

Ryabov, E. V., Wood, G. R., Fannon, J. M., Moore, J. D., Bull, J. C., Chandler, D., et al. (2014). A virulent strain of deformed wing virus (DWV) of honeybees (*Apis mellifera*) prevails after *Varroa destructor*-mediated, or *in vitro*, transmission. *PLoS Pathog.* 10:e1004230. doi: 10.1371/journal.ppat.1004230

Sammataro, D., Gerson, U., and Needham, G. (2000). Parasitic mites of honey bees: life history, implications, and impact. *Annu. Rev. Entomol.* 45, 519–548. doi: 10.1146/annurev.ento.45.1.519

Sanpa, S., and Chantawannakul, P. (2009). Survey of six bee viruses using RT-PCR in northern Thailand. *J. Invertebr. Pathol.* 100, 116–119. doi: 10.1016/j.jip.2008.11.010

Santamaria, J., Villalobos, E. M., Brettell, L. E., Nikaido, S., Graham, J. R., and Martin, S. J. (2018). Evidence of Varroa-mediated deformed wing virus spillover in Hawaii. *J. Invertebr. Pathol.* 151, 126–130. doi: 10.1016/j.jip.2017.11.008

Santillán-Galicia, M. T., Ball, B. V., Clark, S. J., and Alderson, P. G. (2010). Transmission of deformed wing virus and slow paralysis virus to adult bees (*Apis mellifera* L.) by *Varroa destructor*. *J. Apic. Res.* 49, 141–148.

Santillán-Galicia, M. T., Ball, B. V., Clark, S. J., and Alderson, P. G. (2014). Slow bee paralysis virus and its transmission in honey bee pupae by *Varroa destructor*. *J. Apic. Res.* 53, 146–154. doi: 10.3896/IBRA.1.53.1.16

Santos, D., Mingels, L., Vogel, E., Wang, L., Christiaens, O., Cappelle, K., et al. (2019). Generation of virus- and dsRNA-derived siRNAs with species-dependent length in insects. *Viruses* 11:738. doi: 10.3390/v11080738

Schläppi, D., Chejanovsky, N., Yañez, O., and Neumann, P. (2020). Foodborne transmission and clinical symptoms of honey bee viruses in ants Lasius spp. *Viruses* 12:321. doi: 10.3390/v12030321

Schläppi, D., Lattrell, P., Yañez, O., Chejanovsky, N., and Neumann, P. (2019). Foodborne transmission of deformed wing virus to ants (*Myrmica rubra*). *Insects* 10:394. doi: 10.3390/insects10110394

Schoonvaere, K., Smagghe, G., Francis, F., and de Graaf, D. C. (2018). Study of the metatranscriptome of eight social and solitary wild bee species reveals novel viruses and bee parasites. *Front. Microbiol.* 9:177. doi: 10.3389/fmicb.2018.00177

Sébastien, A., Lester, P. J., Hall, R. J., Wang, J., Moore, N. E., and Gruber, M. A. M. M. (2015). Invasive ants carry novel viruses in their new range and form reservoirs for a honeybee pathogen. *Biol. Lett.* 11:20150610. doi: 10.1098/rsbl.2015.0610

Seitz, K., Buczolich, K., Dikunová, A., Plevka, P., Power, K., Rümenapf, T., et al. (2019). A molecular clone of Chronic Bee Paralysis Virus (CBPV) causes mortality in honey bee pupae (*Apis mellifera*). *Sci. Rep.* 9:16274. doi: 10.1038/s41598-019-52822-1

Shah, F. A., and Shah, T. A. (1988). Thai Sacbrood disease of *Apis cerana* indica. *Indian Bee J.* 50, 110–112.

Shen, M., Cui, L. W., Ostiguy, N., and Cox-Foster, D. (2005a). Intricate transmission routes and interactions between picorna-like viruses (Kashmir bee virus and sacbrood virus) with the honeybee host and the parasitic varroa mite. *J. Gen. Virol.* 86, 2281–2289. doi: 10.1099/vir.0.80824-0

Shen, M., Yang, X., Cox-Foster, D., and Cui, L. (2005b). The role of varroa mites in infections of Kashmir bee virus (KBV) and deformed wing virus (DWV) in honey bees. *Virology* 342, 141–149. doi: 10.1016/j.virol.2005.07.012

Singh, R., Levitt, A. L., Rajotte, E. G., Holmes, E. C., Ostiguy, N., Vanengelsdorp, D., et al. (2010). RNA viruses in hymenopteran pollinators: evidence of inter-taxa virus transmission via pollen and potential impact on Non-*Apis* Hymenopteran Species. *PLoS One* 5:e14357. doi: 10.1371/journal.pone.0014357

Snodgrass, R. E. (1956). *Anatomy of the Honey Bee*. New York, NY: Comstock.

Sorescu, I., Tansa, R., Gheorghe, L., Mardare, A., and Chioveanu, G. (2003). Attempts to *in vitro* cultivate honey bee (*Apis mellifera* L.) haemocytes. *Stud. Res. Vet. Med.* 9, 123–131.

Sun, L., Li, M., Fei, D., Hu, Y., and Ma, M. (2017). Chinese sacbrood virus infection in *Apis mellifera*, Shandong, China, 2016. *Virus Res.* 242, 96–99. doi: 10.1016/j.virusres.2017.09.014

Takahashi, J., Yoshida, T., Takagi, T., Akimoto, S., Woo, K. S., Deowanish, S., et al. (2007). Geographic variation in the Japanese islands of *Apis cerana japonica* and in *A. cerana* populations bordering its geographic range. *Apidologie* 38, 335–340.

Taylor, O. M., and Cameron, S. A. (2003). Nest construction and architecture of the amazonian bumble bee (Hymenoptera: Apidae). *Apidologie* 34, 321–331.

Tehel, A., Brown, M. J. F., and Paxton, R. J. (2016). Impact of managed honey bee viruses on wild bees. *Curr. Opin. Virol.* 19, 16–22. doi: 10.1016/j.coviro.2016.06.006

Tehel, A., Vu, Q., Bigot, D., Gogol-Döring, A., Koch, P., Jenkins, C., et al. (2019). The two prevalent genotypes of an emerging infectious disease, deformed wing virus, cause equally low pupal mortality and equally high wing deformities in host honey bees. *Viruses* 11:e114. doi: 10.3390/v11020114

Thaduri, S., Locke, B., Granberg, F., and de Miranda, J. R. (2018). Temporal changes in the viromes of Swedish Varroa-resistant and Varroa-susceptible honeybee populations. *PLoS One* 13:e0206938. doi: 10.1371/journal.pone.0206938

Thaduri, S., Stephan, J. G., de Miranda, J. R., and Locke, B. (2019). Disentangling host-parasite-pathogen interactions in a Varroa-resistant honeybee population reveals virus tolerance as an independent, naturally adapted survival mechanism. *Sci. Rep.* 9:6221. doi: 10.1038/s41598-019-42741-6

Traynor, K. S., Mondet, F., de Miranda, J. R., Techer, M., Kowallik, V., Oddie, M., et al. (2020). *Varroa destructor*: a complex parasite, crippling bees worldwide. *Trends Parasitol.* 36, 5–19. doi: 10.20944/preprints202002.0374.v1

van Oers, M. M., and Lynn, D. E. (2010). "Insect cell culture," in *Encyclopedia of Life Sciences*, eds John Wiley & Sons Ltd. (Chichester: ELS Language Centers). doi: 10.1002/9780470015902.a0002574.pub2

Wang, H., Meeus, I., Piot, N., and Smagghe, G. (2017). Systemic Israeli acute paralysis virus (IAPV) infection in bumblebees (*Bombus terrestris*) through feeding and injection. *J. Invertebr. Pathol.* 151, 158–164. doi: 10.1016/j.jip.2017.11.015

Wang, L., Swevers, L., Rombouts, C., Meeus, I., Van Meulebroeck, L., Vanhaecke, L., et al. (2019). A metabolomics approach to unravel Cricket Paralysis virus infection in silkworm Bm5 Cells. *Viruses* 11:861. doi: 10.3390/v11090861

Wang, L.-L., Swevers, L., Van Meulebroeck, L., Meeus, I., Vanhaecke, L., and Smagghe, G. (2020). A metabolomic analysis of Cricket Paralysis virus infection in Drosophila S2 cells reveals divergent effects on central carbon metabolism as compared with silkworm Bm5 Cells. *Viruses* 12:393. doi: 10.3390/v12040393

Wu, Y., Dong, X., and Kadowaki, T. (2017). Characterization of the copy number and variants of deformed wing virus (DWV) in the pairs of honey bee pupa and infesting *Varroa destructor* or *Tropilaelaps mercedesae*. *Front. Microbiol.* 8:1558. doi: 10.3389/fmicb.2017.01558

Xia, X., Mao, Q., Wang, H., Zhou, B., and Wei, T. (2014). Replication of Chinese sacbrood virus in primary cell cultures of Asian honeybee (*Apis cerana*). *Arch. Virol.* 159, 3435–3438. doi: 10.1007/s00705-014-2183-3

Yañez, O., Chávez-Galarza, J., Tellgren-Roth, C., Pinto, M. A., Neumann, P., and de Miranda, J. R. (2020). The honeybee (*Apis mellifera*) developmental state shapes

the genetic composition of the deformed wing virus-A quasispecies during serial transmission. *Sci. Rep.* 10:e5956. doi: 10.1038/s41598-020-62673-w

Yañez, O., Jaffé, R., Jarosch, A., Fries, I., Moritz, R. A., Paxton, R., et al. (2012a). Deformed wing virus and drone mating flights in the honey bee (*Apis mellifera*): implications for sexual transmission of a major honey bee virus. *Apidologie* 43, 17–30.

Yañez, O., Zheng, H. Q., Hu, F. L., Neuman, P., and Dietemann, V. (2012b). A scientific note on Israeli acute paralysis virus infection of Eastern honeybee *Apis cerana* and vespine predator *Vespa velutina*. *Apidologie* 43, 587–589.

Yañez, O., Zheng, H. Q., Su, X. L., Hu, F. L., Neumann, P., and Dietemann, V. (2016). Potential for virus transfer between the honey bees *Apis mellifera* and *Apis cerana*. *J. Apic. Res.* 54, 179–191.

Yang, B., Peng, G., Li, T., and Kadowaki, T. (2013). Molecular and phylogenetic characterization of honey bee viruses, *Nosema* microsporidia, protozoan parasites, and parasitic mites in China. *Ecol. Evol.* 3, 298–311. doi: 10.1002/ece3.464

Yang, D., Zhao, H., Shi, J., Xu, X., Wu, Y., Guo, R., et al. (2019). Discovery of Aphid Lethal Paralysis Virus in *Vespa velutina* and *Apis cerana* in China. *Insects* 10:157. doi: 10.3390/insects10060157

Yang, S., Zhao, H., Deng, Y., Deng, S., Wang, X., Diao, Q., et al. (2020). A reverse genetics system for the Israeli acute paralysis virus and chronic bee paralysis virus. *Int. J. Mol. Sci.* 21:1742. doi: 10.3390/ijms21051742

Yoo, M. S., and Yoon, B. S. (2009). Incidence on honey bee disease in Korea 2009. *Korean J. Apic.* 24, 273–278.

Yue, C., and Genersch, E. (2005). RT-PCR analysis of Deformed wing virus in honeybees (*Apis mellifera*) and mites (*Varroa destructor*). *J. Gen. Virol.* 86, 3419–3424. doi: 10.1099/vir.0.81401-0

Yue, C., Schröder, M., Bienefeld, K., and Genersch, E. (2006). Detection of viral sequences in semen of honeybees (*Apis mellifera*): evidence for vertical transmission of viruses through drones. *J. Invertebr. Pathol.* 92, 105–108. doi: 10.1016/j.jip.2006.03.001

Yue, C., Schröder, M., Gisder, S., and Genersch, E. (2007). Vertical-transmission routes for deformed wing virus of honeybees (*Apis mellifera*). *J. Gen. Virol.* 88, 2329–2336. doi: 10.1099/vir.0.83101-0

Zhang, X., He, S. Y., Evans, J. D., Pettis, J. S., Yin, G. F., and Chen, Y. P. (2012). New evidence that deformed wing virus and black queen cell virus are multi-host pathogens. *J. Invertebr. Pathol.* 109, 156–159. doi: 10.1016/j.jip.2011.09.010

Zioni, N., Soroker, V., and Chejanovsky, N. (2011). Replication of *Varroa destructor* virus 1 (VDV-1) and a *Varroa destructor* virus 1-deformed wing virus recombinant (VDV-1-DWV) in the head of the honey bee. *Virology* 417, 106–112. doi: 10.1016/j.virol.2011.05.009

Conflict of Interest: The authors declare that the research was conducted in the absence of any commercial or financial relationships that could be construed as a potential conflict of interest.

Copyright © 2020 Yañez, Piot, Dalmon, de Miranda, Chantawannakul, Panziera, Amiri, Smagghe, Schroeder and Chejanovsky. This is an open-access article distributed under the terms of the Creative Commons Attribution License (CC BY). The use, distribution or reproduction in other forums is permitted, provided the original author(s) and the copyright owner(s) are credited and that the original publication in this journal is cited, in accordance with accepted academic practice. No use, distribution or reproduction is permitted which does not comply with these terms.

frontiers in Microbiology

ORIGINAL RESEARCH
published: 04 June 2020
doi: 10.3389/fmicb.2020.00897

Modulation of Gut Microbiota, Short-Chain Fatty Acid Production, and Inflammatory Cytokine Expression in the Cecum of Porcine Deltacoronavirus-Infected Chicks

*Hai-yan Li[1], Hong-lei Zhang[1,2], Fu-jie zhao[1,2], Shi-qiong Wang[1], Zhi-xiang Wang[1] and Zhan-yong Wei[1,2]**

[1] College of Animal Science and Veterinary Medicine, Henan Agricultural University, Zhengzhou, China, [2] Key Laboratory for Animal-Derived Food Safety of Henan Province, Henan Agricultural University, Zhengzhou, China

Porcine deltacoronavirus (PDCoV) is a novel swine enteropathogenic coronavirus that causes watery diarrhea and induces proinflammatory cytokine responses in piglets. Our previous research showed that the specific-pathogen-free (SPF) chicks exhibited mild diarrhea and low fecal viral shedding, along with cecum lesions after PDCoV infection. Disturbances in the homeostasis of the gut microbiota have been associated with various diseases. We aimed to explore the effects of PDCoV infection on chick gut microbiota, short-chain fatty acid (SCFAs) production, and inflammatory cytokine expression in chicks, and also to investigate the relationship between gut microbiota and SCFAs or inflammatory cytokine expression of the PDCoV-infected chicks. Results obtained using 16S rRNA sequencing showed that infection with PDCoV strain HNZK-02 significantly altered the composition of chick gut microbiota, with the reduced abundance of *Eisenbergiella* and *Anaerotruncus* genera at 5 days post-inoculation (dpi) ($P < 0.05$), and an increased abundance of *Alistipes* genus at 17 dpi ($P < 0.05$). The production of SCFAs in the cecum of PDCoV HNZK-02–infected chicks, including acetic acid, propionic acid, and butyric acid, decreased in all cases. The expression of inflammatory cytokines (interferon-γ, tumor necrosis factor-α, and interleukin-10) was increased in the cecum tissue and serum of the PDCoV HNZK-02–infected chicks when detected by quantitative real-time polymerase chain reaction and enzyme-linked immunosorbent assay, respectively. Further analysis showed significant correlation between bacterial genera and SCFAs or inflammatory cytokines expression in cecum of the PDCoV infected chicks. These findings might provide new insight into the pathology and physiology of PDCoV in chicks.

Keywords: Porcine deltacoronavirus (PDCoV), SPF chick, intestinal microbiota, inflammatory cytokines, short-chain fatty acids

OPEN ACCESS

Edited by:
Ahmed Sayed Abdel-Moneim, Taif University, Saudi Arabia

Reviewed by:
Salama Shany, Beni-Suef University, Egypt
Samy Kasem, Kafrelsheikh University, Egypt

***Correspondence:**
Zhan-yong Wei
weizhanyong@henau.edu.cn

Specialty section:
This article was submitted to Virology, a section of the journal Frontiers in Microbiology

Received: *21 December 2019*
Accepted: *16 April 2020*
Published: *04 June 2020*

Citation:
Li H, Zhang H, zhao F, Wang S, Wang Z and Wei Z (2020) Modulation of Gut Microbiota, Short-Chain Fatty Acid Production, and Inflammatory Cytokine Expression in the Cecum of Porcine Deltacoronavirus-Infected Chicks. Front. Microbiol. 11:897. doi: 10.3389/fmicb.2020.00897

Abbreviations: AA, acetic acid; BA, butyric acid; dpi, days post inoculation; ELISA, enzyme-linked immunosorbent assay; GC, gas chromatography; Gn, gnotobiotic; IBD, infectious bursal disease; IFN-γ, interferon gamma; IL-10, interleukin 10; LDA, linear discriminant analysis; LEFSe, linear discriminant analysis effect size; LLC-PK, LLC-porcine kidney; OTUs, operational taxonomic units; PA, propionic acid; PDCoV, porcine deltacoronavirus; PCoA, principal coordinate analysis; SPF, the specific pathogen free; SCFAs, short-chain fatty acid; TNF-α, tumor necrosis factor alpha.

INTRODUCTION

Porcine deltacoronavirus (PDCoV) is an enveloped, positive-sense single-stranded RNA virus, with a genome length of approximately 25 kb (Zhang, 2016). This virus was originally found in Hong Kong in 2012 (Woo et al., 2012), and the first outbreak of PDCoV-related diarrhea in swine herds was reported in the United States in 2014 (Wang et al., 2014). As an important enteropathogen in pigs, PDCoV can cause acute diarrhea, vomiting, and dehydration in neonatal piglets (Chen et al., 2014; Hu et al., 2016). Moreover, the infected pigs are characterized by thin and transparent intestinal walls and accumulation of large amounts of yellow fluid in the intestinal lumen (Jung et al., 2015; Li et al., 2019). Further, PDCoV-infected piglets show signs of proinflammatory cytokine responses during acute infection (Jung et al., 2018). PDCoV has caused huge economic losses for the pig industries. Apart from infection of gnotobiotic (Gn) and conventional pigs, PDCoV was also reported to have limited ability to infect Gn calves (Jung et al., 2017). Recent studies showed the susceptibility of specific-pathogen-free (SPF) chicks to PDCoV infection, with the clinical syndrome of mild diarrhea and slight lesions in cecum, which was weaker than that of piglets infected with PDCoV (Liang et al., 2019; Boley et al., 2020). However, the reason why PDCoV infection can cause intestinal damage is still unknown.

The chicken gastrointestinal tract is an important site for immune cell development, which not only regulates gut microbiota, but also maintains extraintestinal immunity. Intestinal commensal microbes play a crucial role in gut homeostasis through mutually beneficial interactions with the host immune system (Deriu et al., 2016). Once the intestinal mucosal barrier and microbiota are destroyed, intestinal inflammation will occur. In turn, the host's inflammatory response will elicit changes in the microbial community structure (Deriu et al., 2016). The gut microbiota produces various metabolites, including short-chain fatty acids (SCFAs), which can regulate the host antiviral immune response (Budden et al., 2017). Propionate and butyrate have also been reported to induce differentiation of T-regulatory cells, assisting in control of intestinal inflammation (Donohoe et al., 2014; Louis et al., 2014).

In chicks, recent studies have emphasized the key roles of intestinal microbiota in shaping immunity against viral diseases, including avian influenza, Marek's disease, Newcastle disease (ND), and infectious bursal disease (IBD). These studies not only reflected connections between gut microbiota and distal organs in regulatory functions, but also emphasized the interaction between intestinal microbiota and viral infections and their impacts on immune regulations (Lillehoj and Trout, 1996; Balamurugan and Kataria, 2006; Li, 2007; Chen et al., 2017; Yitbarek et al., 2018). It was reported that different commensal bacteria had their own unique role against viral infection by modulating diverse immune mechanisms (Abt et al., 2012). In the H9N2 avian influenza virus infected chicks, increased levels of interferon gamma (IFN-γ). tumor necrosis factor alpha (TNF-α), and interleukin-17A (IL-17A) led to intestinal microflora dysbiosis (Li H. et al., 2018). However, there are no studies emphasizing how PDCoV affects the gut microbiota in chicks. Thus, in the current study we aimed to observe the intestinal microbiota, SCFAs, and inflammation responses to PDCoV infection in chicks and elucidate the potential associations among them, which will provide the theoretical basis for investigation of the etiology and pathogenesis of PDCoV.

MATERIALS AND METHODS

Virus

The virulent PDCoV strain-HNZK-02 (GenBank accession number MH708123) was isolated and identified by our laboratory and propagated in LLC-porcine kidney (LLC-PK) cells. Passage 5 of this strain was used in current study. Virus propagation and virus titers were performed as described previously (Liang et al., 2019).

Experimental Infection of SPF Chicks With PDCoV Strain-HNZK-02

The SPF chicks were purchased from Jinan SIPAFAS Poultry Co. Ltd. in Jinan, China. Twenty-four-day-old SPF chicks with similar body weight (about 50 g/chick) were randomly divided into two groups, the control (mock) and PDCoV HNZK-02–infected groups. All chicks were housed in the same facility but in different rooms under biosafety conditions and allowed free access to water and feed during the experiment. Feed was formulated to meet or exceed the National Research Council nutrient requirements for chicks (National Research Council [NRC], 1994; **Table 1**). Each chick was intragastrically inoculated with PDCoV strain HNZK-02 or Eagle's Minimum Essential Medium (MEM) with 300 μL/chick (10.5 log10 GE/chick) (n = 10/per group).

Sample and Tissue Collection

Based on our previous study (Liang et al., 2019), three chicks in each group were selected randomly for necropsy at 5 and 17 dpi, respectively. The cecal contents were collected for analysis of

TABLE 1 | The composition and nutrients of the basal diet.

Ingredient	Content (%)	Chemical composition	Content
Corn	55	CP,%	20.6
Soybean meal	31	ME, Mcal/kg	3
Wheat shorts	3.3	Calcium,%	1
Fish meal	3	Total P,%	0.65
Soybean oil	3.5	Available P,%	0.45
dl-Methionine	0.27	Methionine + cysteine,%	0.9
NaCl	0.27	Lysine,%	1.05
Limestone	1.33	–	–
Calcium phosphate	1.33	–	–
Vitamin-mineral premix[a]	1	–	–

[a]*Supplied per kilogram of diet: vitamin A (retinyl acetate), 1,600 IU; cholecalciferol, 300 IU; vitamin E (DL-α-tocopheryl acetate), 10 IU; riboflavin, 3.8 mg; pantothenic acid, 11 mg; niacin, 30 mg; cobalamin, 11 μg; choline chloride, 1,000 mg; biotin, 0.16 mg; folic acid, 0.45 mg; thiamine 1.5 mg; pyridoxine 3.0 mg; Fe, 68 mg; Zn, 50 mg; Mn, 60 mg; I, 0.2 mg; Cu, 8 mg; Se, 0.16 mg.*

gut microbiota and SCFAs. The cecum tissue was collected for inflammatory cytokine mRNA measurements. The serum was collected for inflammatory cytokine detection by enzyme-linked immunosorbent assay (ELISA).

Viral RNA Extraction and Quantitative Real-Time Polymerase Chain Reaction

Viral RNA was extracted from cecal content suspensions using the TRizol™ method (Invitrogen, Carlsbad, CA, United States) according to the manufacturer's instructions. The viral RNA was further reverse transcribed into cDNA. Viral RNA titers were determined using quantitative real-time polymerase chain reaction (qRT-PCR) as reported previously (Liang et al., 2019). The detection limit of the qRT-PCR was 4.6 log10 GE/mL.

DNA Extraction From the Cecal Content and 16S rRNA Sequencing

Total genomic DNA was extracted from 0.5 g of colonic contents using the FastDNA® SPIN Kit (MP Bio, Santa Ana, CA, United States) following the manufacturer's guidelines, with the additional glass-bead beating steps on a FastPrep 24 homogenizer (MP Biomedicals, Santa Ana, CA, United States). The final DNA concentration was quantified on a NanoDrop 2000 UV-vis spectrophotometer (Thermo Scientific, Wilmington, DE, United States). The integrity and size of genomic DNA was checked by 1.0% agarose gel electrophoresis. The DNA extracts were sequenced for 16S rRNA using Illumina MiSeq (Illumina, San Diego, CA, United States), targeting the V3–V4 region with barcoded 338F (5′-ACTCCTACGGGAGGCAGCAG-3′) and 806R (5′-GGACTACHVGGGTWTCTAAT-3′) universal primers (Mori et al., 2013), and sequences were processed according to the standard protocols by Majorbio Bio-Pharm Technology Co. Ltd. (Shanghai, China).

Determination of SCFAs

The SCFAs in cecum were determined using gas chromatography (GC) according to a previously described method (Stewart et al., 2010). The samples were placed on a DB-WAX column (30 m long × 0.53 mm diameter and 1.00 μm film thickness) and were separated by using a TRACE™ 1300 GC with flame ionization detector (FID). The temperature program was 100°C for 0.5 min, then raised to 170°C at 8°C/min and held for 1 min, then raised to 200°C at 40°C/min and held for 2 min. Samples were run with a 30:1 split ratio and a 5.0 mL/min column flow. High-purity hydrogen was used as the carrier gas. The temperatures of the injector and detector were 250 and 270°C, respectively.

Detection of Inflammatory Cytokine Expression

The levels of expression of the inflammatory cytokines (IFN-γ, TNF-α, and IL-10) in the cecum of SPF chicks were quantified by qRT-PCR. Cecum tissue samples were homogenized by the TISSUELYSER-24 (Jingxin, Shanghai, China). Total RNAs were extracted from the supernatant of the cecum tissue lysate by TRizol™ Reagent Kit (Invitrogen, Carlsbad, CA, United States) and were quantified by NanoDrop 2000 spectrophotometer (Thermo Fisher Scientific, Waltham, MA, United States), then further reverse transcribed into cDNA. The total reaction volume of 20 μL contained 2.0 μL of DNA, 10.0 μL of SYBR Green qPCR Mix (Takara Bio Inc., Tokyo, Japan), 7 μL of H_2O, and 0.5 μL of each specific primer. Primers were synthesized according to previous reports (Emami et al., 2019) and are shown in **Table 2**. Reactions were performed under the following conditions: one cycle of preincubated samples at 95°C for 1 min and 39 cycles of amplification samples at 95°C for 5 s, 60°C for 30 s, 72°C for 30 s. Target gene expression of each sample was normalized using glyceraldehyde 3-phosphate dehydrogenase (GAPDH). The relative expression of the target gene for each sample was calculated using the $2^{-\Delta\Delta Ct}$ method (Livak and Schmittgen, 2001).

The expression levels of the IFN-γ, TNF-α and IL-10 in serum were detected using ELISA Kit from Nanjing Jian cheng Biological Institute (Nanjing, China). Serum samples were obtained and measured as previously described (Huang et al., 2015). Absorbance was read at 450 nm using a microplate spectrophotometer. The inflammatory cytokine concentrations were calculated according to a best-fit standard curve.

Data Processing and Statistical Analysis

Raw fastq files were demultiplexed, quality-filtered by Trimmomatic, and merged by FLASH (Magoč and Salzberg, 2011). Sequences with ambiguous bases, shorter than 200 bp, and sequences with an average mass less than 25 were removed. The high-quality reads were clustered into operational taxonomic units (OTUs) with 97% similarity cutoff using UPARSE (version 7.11) and used for further analysis of the Venn diagram, alpha diversity indices (Shannon and Simpson), and richness estimators (ACE and Chao). Beta diversity measures were based on weighted-uniFrac distance analysis and shown by principal coordinate analysis (PCoA), which was conducted to assess the relationships among the different groups. LEfSe was applied to recognize which bacterial taxa contribute to the differences between the two groups (Segata et al., 2011), and the minimal threshold of linear discriminant analysis (LDA) was set at 3.5. The difference between specific taxa was analyzed using one-way analysis of variance (ANOVA) followed by *post hoc* *t*-tests. Data analysis of inflammatory cytokines and SCFAs was performed using GraphPad Prism (version 6.01, La Jolla, CA, United States). A $P < 0.05$ or 0.01 was considered statistically significant or highly significant, which is indicated as follows: $^{*}P < 0.05$, $^{**}P < 0.01$.

RESULTS

Apparent Clinical Characteristics of SPF Chicks Infected With PDCoV

SPF chicks, intragastrically inoculated with PDCoV HNZK-02 at 4 days old, showed mild diarrhea at 5 dpi. PDCoV RNA was detected in the intestinal contents by qRT-PCR at 5 and 17 dpi while non-infected control chicks appeared normal throughout the course of the experiments. PDCoV HNZK-02 infection had

TABLE 2 | The sequences of primers used in this study for real-time RT-PCR.

Genes	Forward primer (5′ to 3′)	Reverse primer (5′ to 3′)	Amplified size (bp)
IFN-γ	GCTCCCGATGAACGACTTGA	TGTAAGATGCTGAAGAGTTCATTCG	63
TNF-α	CCCATCCCTGGTCCGTAAC	ATACGAAGTAAAGGCCGTCCC	77
IL-10	CGCTGTCACCGCTTCTTCA	CGTCTCCTTGATCTGCTTGATG	63
GAPDH	CCTAGGATACACAGAGGACCAGGTT	GGTGGAGGAATGGCTGTCA	64

From Emami et al. (2019).

TABLE 3 | Comparison of phylotype coverage and diversity estimation of the 16S rRNA gene libraries at 97% similarity from the pyrosequencing analysis.

Group	No. of reads	No. of OTUs	Coverage (%)	Richness estimator		Diversity index	
				ACE (mean ± SE)	Chao (mean ± SE)	Shannon (mean ± SE)	Simpson (mean ± SE)
Mock_5d	179,564	277	99.95	226.37 ± 2.67^{c}	231.41 ± 5.95^{b}	3.58 ± 0.16	0.057 ± 0.13
PDCoV HNZK_02_5d	160,137	325	99.93	282.33 ± 0.51^{b}	293.29 ± 2.87^{a}	3.53 ± 0.11	0.072 ± 0.15
Mock_17d	168,425	341	99.95	$303.29 \pm 13.75^{a,b}$	302.96 ± 16.46^{a}	3.82 ± 0.06	0.054 ± 0.09
PDCoV HNZK_02_17d	155,610	351	99.93	311.57 ± 7.58^{a}	318.37 ± 9.47^{a}	3.62 ± 0.06	0.077 ± 0.08

The operational taxonomic units (OTUs) were defined at a 97% similarity level. The coverage percentage (Good's) and richness estimators (ACE and Chao) and diversity indices (Shannon and Simpson) were calculated using Good's method and the mothur program, respectively. In the same column, values with the same superscript letter are not significantly different ($P > 0.05$); those with different superscript letters differ significantly ($P < 0.05$).

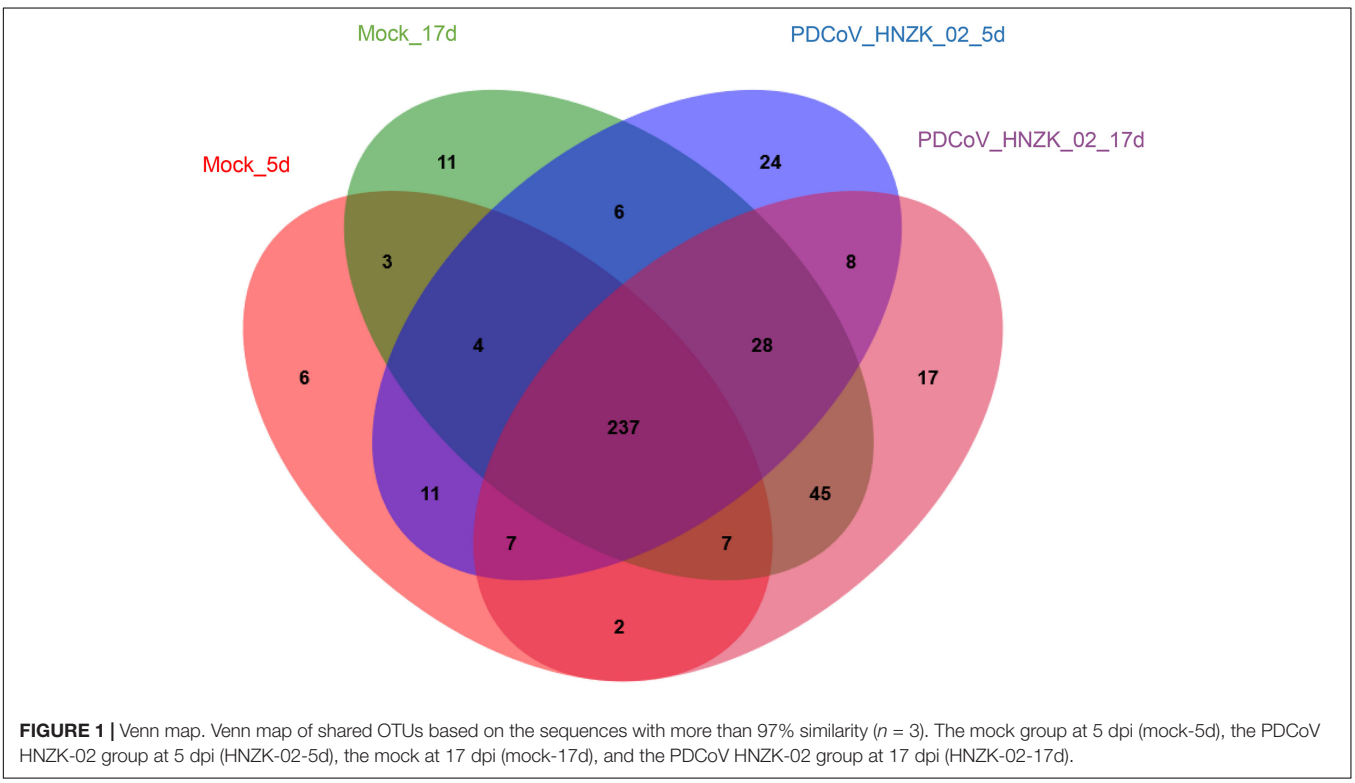

FIGURE 1 | Venn map. Venn map of shared OTUs based on the sequences with more than 97% similarity ($n = 3$). The mock group at 5 dpi (mock-5d), the PDCoV HNZK-02 group at 5 dpi (HNZK-02-5d), the mock at 17 dpi (mock-17d), and the PDCoV HNZK-02 group at 17 dpi (HNZK-02-17d).

no effect on feed consumption compared to controls during the whole experimental period.

Characteristics of Pyrosequencing Results

A total of 12 cecal concent samples, the control chicks ($n = 3$), and PDCoV HNZK-02 groups ($n = 3$) at 5 and 17 dpi, respectively, were evaluated using 16S rRNA gene sequencing. A total of 663,736 sequences with a median read length of 429 bp (range from 274 to 494 bp) were collected. The total number of unique sequences from the four groups was 416. The sequence and species-level OTUs of each group are shown in **Table 3**. The Venn diagram showed that 237 OTUs of the total gut microbial richness (416) were shared among all the sequenced samples. Two hundred and fifty-nine OTUs were shared between the samples

of the mock and PDCoVHNZK-02 groups with a total of 343 at 5 dpi. Three hundred and seventeen OTUs of the total gut microbial richness (375) were shared between the samples of mock and PDCoV HNZK-02 groups at 17 dpi (**Figure 1**).

Alpha and Beta Diversity Analyses

Alpha diversity estimators of community are shown in **Table 3**. Gut microbial richness, according to the Ace and Chao indexes, was significantly increased in the PDCoV HNZK-02 group when compared with that of the mock group at 5 dpi ($P < 0.05$), while there was no significant difference between the two groups at 17 dpi ($P > 0.05$). In Shannon and Simpson alpha diversity indexes, the differences between the PDCoV HNZK-02 and the mock groups at 5 and 17 dpi did not reach statistical significance ($P > 0.05$).

Beta diversity analysis showed that there were some similarities in the microbial composition between the mock and the PDCoV HNZK-02 groups at 5 dpi. However, the microbial composition from chicks with PDCoV inoculation and the controls could be divided into two different clusters at 17 dpi, indicating that the cecal microbial community structure and composition in the control group were significantly different from those in the PDCoV HNZK-02 group at 17 dpi (**Figure 2**).

Difference in Specific Taxa Between PDCoV HNZK-02-Infected Chicks and Controls

To further investigate whether PDCoV HNZK-02 infected chicks experienced any significant alteration in gut microbiota, we analyzed the relative abundance of microbiota at the phylum, family, and genus levels. At 5 dpi, genus level analysis showed the taxonomic abundance was altered in the PDCoV HNZK-02 group, which was characterized by lower abundance of *Eisenbergiella* and *Anaerotruncus* ($P < 0.05$). There were no significant differences at the levels of phylum and family between the mock and the PDCoV HNZk-02 groups (**Figure 3A**). At 17 dpi, the ratio of Firmicutes to Bacteroidetes in the PDCoV HNZk-02 group was lower than that of the mock group. At the family level, the proportion of Rikenellaceae in the chicks inoculated with PDCoV HNZK-02 significantly increased ($P < 0.05$). At the genus level, *Alistipes* and the unclassified f-Ruminococcaceae were significantly increased ($P < 0.05$), whereas the proportion of Ruminococcaceae-UGG-014 was significantly decreased in the PDCoV HNZK-02 group when compared to that of the mock group at 17 dpi ($P < 0.01$) (**Figure 3B**).

The characteristics of bacterial taxonomic abundant in the collected samples were further analyzed using LEfSe algorithm (**Figure 4**). LEfSe analysis revealed that there existed main 8 and 33 discriminative features from phylum to genus (LDA score >3) between the mock and the PDCoV HNZK-02-inoculated chicks at 5 and 17 dpi (**Figures 4A,B**), respectively. More specifically, *Eisenbergiella* and *Anaerotruncus* were the most differential microbiota in the mock at 5 dpi. Moraxellaceae, *Acinetobacter*, Pseudomonadates, *Eubacterium*, and *norank-f Lachnospiraceae* in the PDCoV HNZK-02 group increased when compared to that in the mock group. At 17 dpi, we identified 10 microbial biomarkers from the PDCoV HNZK-02 group, including Rikenellaceae, Bacteroidia, Bacteroidetes, Bacteroidales, *Alistipes*, unclassified-f-Ruminococcaceae, Sphingomonadaceae, *Novosphingobium*, and *Lachnoclostridium*,

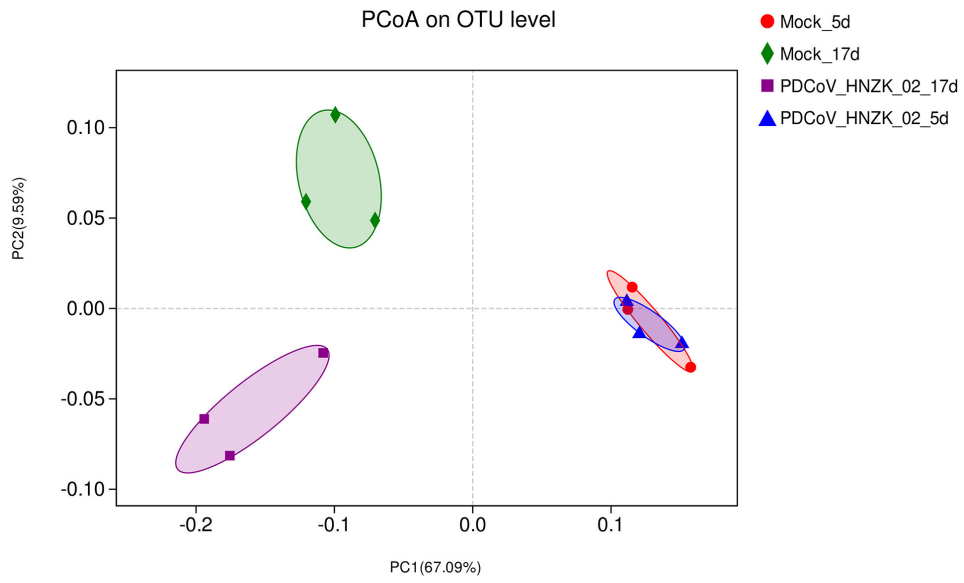

FIGURE 2 | Beta diversity measures in cecal microbiota of chickens ($n = 3$). The scatterplot of the principal coordinate analysis (PCoA) scores shows four different clusters (weighted-uniFrac distance), the blue represents the PDCoV HNZK-02 group at 5 dpi (HNZK-02-5d), the red represents the mock group at 5 dpi (mock-5d), the purple represents the PDCoV HNZK-02 group at 17 dpi (HNZK-02-17d), and the green represents the mock group at 17 dpi (mock-17d).

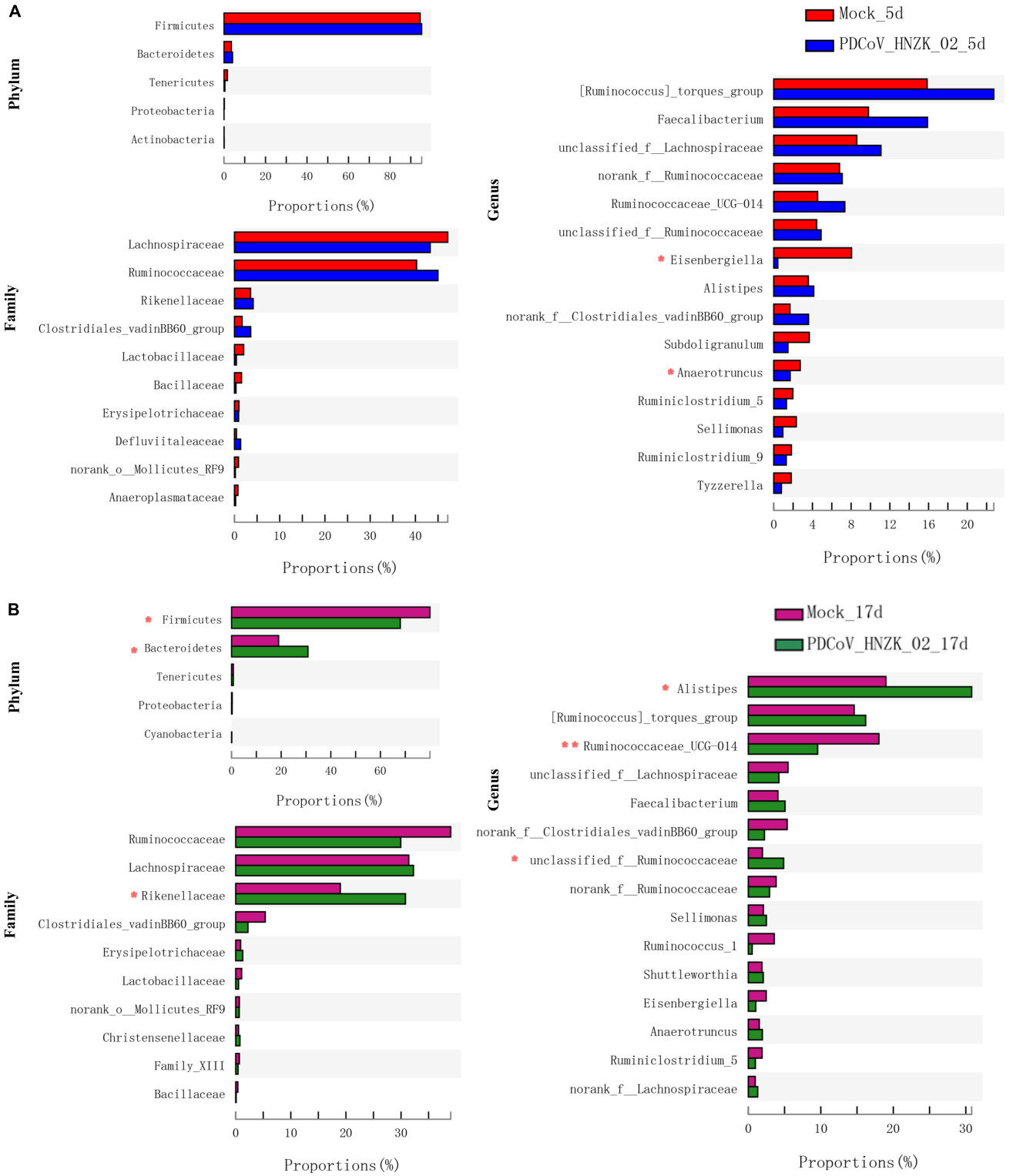

FIGURE 3 | Significant differences analysis in cecal microbiota of chickens. **(A)** Statistical comparison of the relative microbial abundance from phylum to genus between the mock and the PDCoV HNZK-02 groups at 5 dpi (n = 3). **(B)** Statistical comparison of the relative microbial abundance from phylum to genus between the mock and the PDCoV HNZK-02 groups at 17 dpi (n = 3). $^{**}P < 0.01$; $^{*}P < 0.05$.

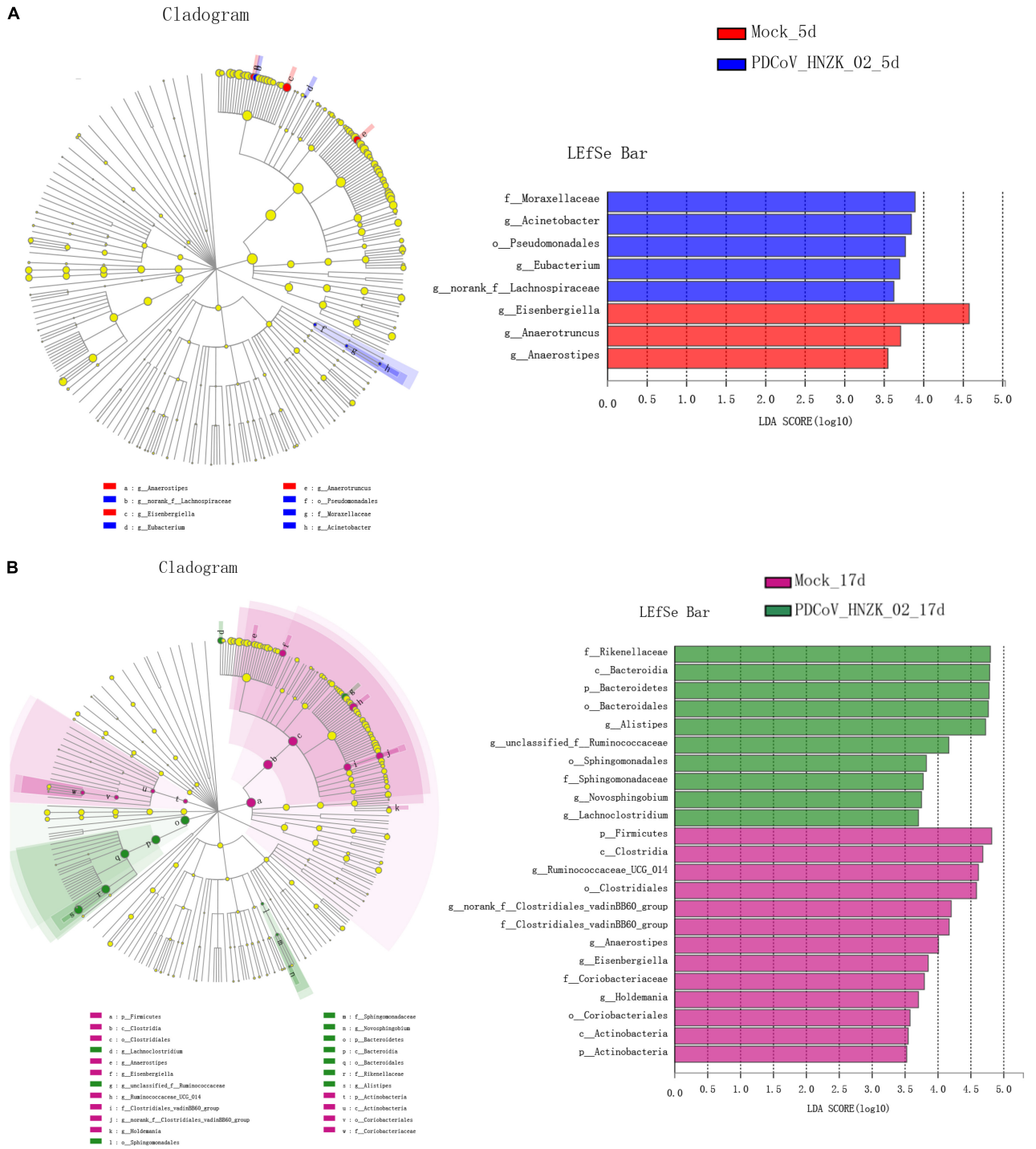

FIGURE 4 | LEfSe analysis in cecal microbiota of chickens. **(A)** LEfSe identifies the taxa with the greatest differences in abundance from phylum to genus between the mock and the PDCoV HNZK-02 groups at 5 dpi (n = 3). **(B)** LEfSe identifies the taxa with the greatest differences in abundance from phylum to genus between the mock and the PDCoV HNZK-02 groups at 17 dpi (n = 3). Linear discriminant analysis (LDA) effect size (LefSe) analysis showing those abundance from phylum to genus between groups; only taxa of an LDA significant threshold of 3.0 are shown.

which could be distinguished from the mock group. 13 clades were more abundant in the mock group than that in the PDCoV HNZK-02 group, including Firmicutes, Clostridia, *Ruminococcaceae-UCG-014*, Clostridia, *norank-f-Clostridiales-vadinBB60-group*, Clostridiales-vadinBB60-group, *Anaerostipe*, *Eisenbergiella*, Coriobacteriaceae,

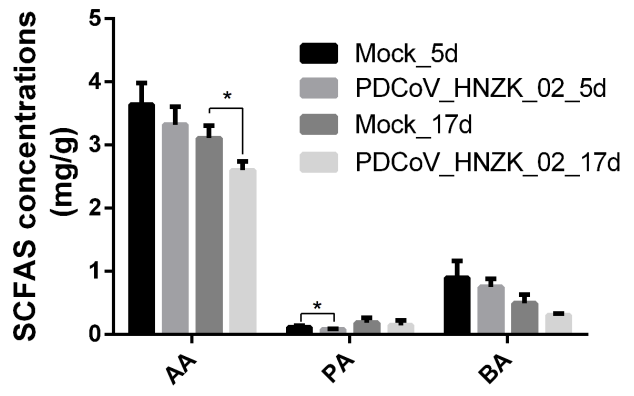

FIGURE 5 | Effects of PDCoV HNZK-02 infection on SCFAs in the cecum of chickens. The SCFAs level of the cecal content among the mock and the PDCoV HNZK-02 groups at 5 and 17 dpi (n = 3). AA, acetic acid; dpi, days post inoculation; BA, butyric acid; PA, propionic acid.

Holdemania, Coriobacteriales, Actinobacteria, and Actinobacteria. There were bigger differences on microbiota compositions between the early and later stages of PDCoV infection (at 5 and 17 dpi, respectively).

SCFA Concentration in Cecal Content of Chicks Inoculated With PDCoV

Compared to the control, there was a decreasing trend in the amounts of acetic acid (AA), propionic acid (PA), and butyric acid (BA) in the PDCoV HNZK-02 group at 5 and 17 dpi. Furthermore, PA and AA levels in the PDCoV HNZK-02 group were greatly decreased at 5 and 17 dpi, respectively ($P < 0.05$) (**Figure 5**).

PDCoV HNZK-02 Infection Promotes the Expression of Inflammatory Cytokines in Chicks

As shown in **Figure 6**, the expression of IFN-γ ($P < 0.01$), TNF-α ($P < 0.05$) and IL-10 ($P < 0.01$) was significantly upregulated at 5 dpi compared with that in the mock chicks (**Figures 6A–C**). Furthermore, IFN-γ expression was significantly upregulated (**Figure 6A**) at 17 dpi ($P < 0.01$).

To evaluate if PDCoV infection could affect IFN-γ, TFN-α, and IL-10 secretion in serum, the concentrations of IFN-γ, TFN-α, and IL-10 in serum were tested with ELISA kits. Our results showed that the changes of the inflammatory cytokines in serum were similar with those in the cecum tissue. The levels of IFN-γ and TNF-α were approximately two and three times as high as in the PDCoV HNZK-02 group when compared to that of the mock group at 5 dpi ($P < 0.01$). The level of IL-10 in the PDCoV infection group was also increased at 5 dpi ($P < 0.05$). The serum levels of IFN-γ in the PDCoV-infected chicks were higher than in the mock group at 17 dpi ($P < 0.01$), and no significant differences were observed for the secretion of TNF-α and IL-10 between the mock and the PDCoV HNZK-02 groups at 17 dpi (**Figures 7A–C**).

Relationship Between Microbial Signatures and the Levels of SCFAs or the Expression of Inflammatory Cytokines in Chicks Infected With PDCoV

Spearman's correlation analysis was conducted between the top 15 bacterial genera and the environmental factors (SCFAs, proinflammatory cytokines), and was directly reflected by a heatmap (**Figure 8**). The threshold $|R| > 0.8$ was considered as having a correlation. The results indicated that *Eisenbergiella* was negatively correlated with TNF-α ($P < 0.05$) and IFN-γ ($P < 0.01$) expression levels, and was positively correlated with PA ($P < 0.01$) at 5 dpi (**Figure 8A**). The *Ruminiclostridium_9* also showed a positively correlation with the IL-10 expression ($P < 0.05$), while Norank_f_ Ruminococcaceae was negatively correlated with BA ($P < 0.001$). At 17 dpi (**Figure 8B**), *Alistipes* and unclassified_f_ Ruminococcaceae showed an extremely significant positive correlation with IFN-γ secretion ($P < 0.05$), but Eisenbergiella and Norank_f_Clostridiales_vadinbb60_group were negatively correlated with it ($P < 0.05$). The level of PA was associated with the increase in the abundance of Ruminiclostridium_5 ($P < 0.05$). *Ruminococcus* and *Eisenbergiella* were positively correlated with AA ($P < 0.05$), while *Alistipes* showed a negative relationship with it ($P < 0.05$). Eisenbergiella, unclassified_f_Lachnospiraceae, Ruminococcaceae_UCG-014, Norank_f_Clostridiales_vadinbb60_group, and Ruminiclostr idium_5 were positively correlated with BA.

DISCUSSION

Gut microflora play an important role in shaping immunity against viral diseases in host. Disruption of microbial homeostasis is associated with a variety of pathological states, which helps the establishment of acute viral infections in chickens (Abaidullah et al., 2019). In this study, the infection model of PDCoV was developed on SPF chicks. Our results demonstrated similar clinical diseases, and the dynamics of the virus shedding in cecum were observed in all SPF chicks inoculated with the PDCoV HNZK-02 strains when compared with our previous experiment (Liang et al., 2019). The influence of PDCoV infection on cecum microbiota of SPF chicken was evaluated, PDCoV HNZK-02 infection significantly altered the gut microbiota composition and decreased SCFAs products in chicks' cecum. Simultaneously, the expression levels of inflammatory cytokines (IFN-γ, IL-10, and TNF-α) in serum and cecum tissue were significantly increased, resulting in the inflammatory response in the chicken. The analysis showed a significant correlation between bacterial genera and SCFAs or inflammatory cytokines.

The diversity of indigenous intestinal microbiota is one of the key factors in resisting the colonization of invading pathogens (Keesing et al., 2010). Several studies have reported that the diarrhea-relating coronaviruses could influence the intestinal microbiota diversity in pigs (Liu et al., 2015; Song et al., 2017;

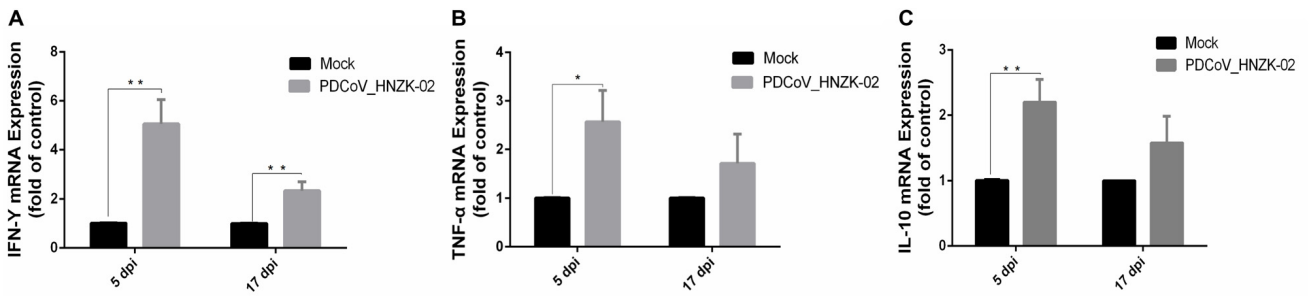

FIGURE 6 | PDCoV HNZK-02 infection promotes inflammatory factors (IFN-γ, TNF-α and IL-10) expression in mRNA levels in the cecum of SPF chickens (n = 3). **(A)** IFN-γ expression in cecum at 5 and 17 dpi. **(B)** TNF-α expression in cecum at 5 and 17 dpi. **(C)** IL-10 expression in cecum at 5 and 17 dpi. $^{**}P < 0.01$; $^{*}P < 0.05$. dpi, days post inoculation; IFN-γ, interferon gamma; IL-10, interleukin 10;TNF-α, tumor necrosis factor alpha.

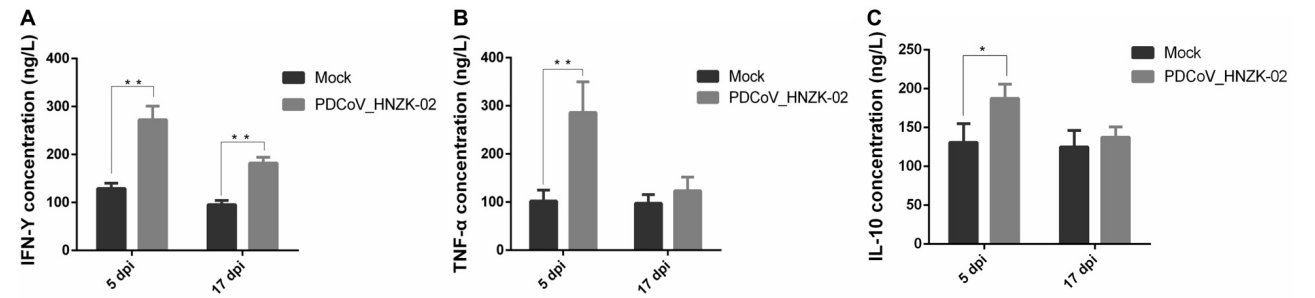

FIGURE 7 | PDCoV HNZK-02 infection increases the expression of inflammatory factors (IFN-γ, TNF-α, and IL-10) in the serum of chickens. **(A)** IFN-γ expression in serum at 5 and 17 dpi (n = 3). **(B)** TNF-α expression in serum at 5 and 17 dpi. **(C)** IL-10 expression in serum at 5 and 17 dpi. $^{**}P < 0.01$, $^{*}P < 0.05$. dpi, days post inoculation; IFN-γ, interferon gamma; IL-10, interleukin 10; TNF-α, tumor necrosis factor alpha.

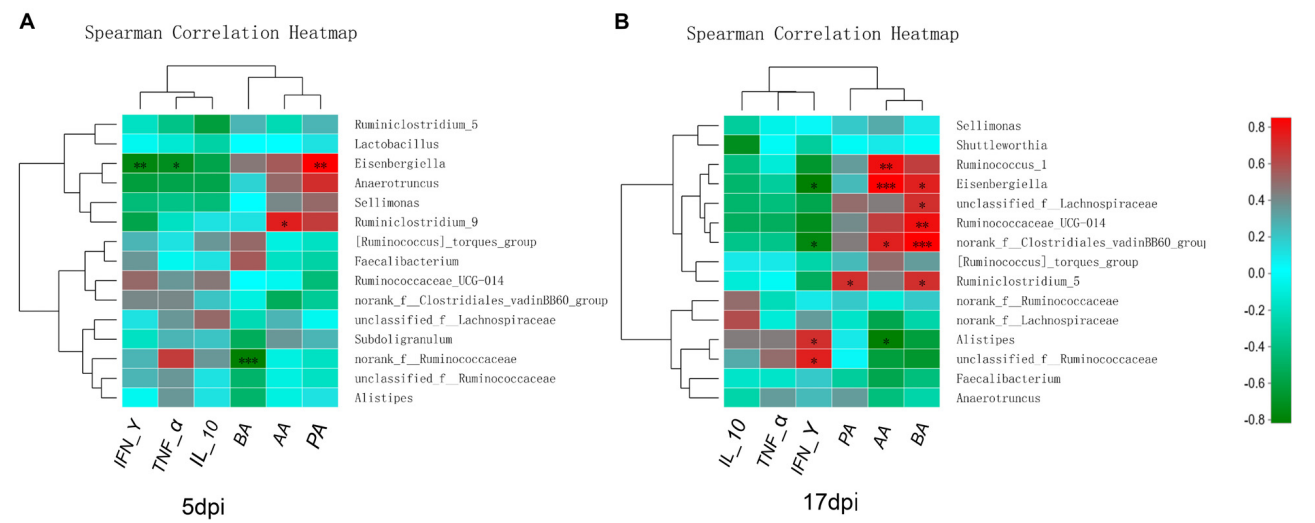

FIGURE 8 | Relationships between bacterial composition and SCFAs or inflammatory factors in cecum. Heatmap of the correlation analysis was conducted between the top 15 bacterial genera and the environmental factors. **(A)** Correlation heatmap at 5 dpi. **(B)** Correlation heatmap at 17 dpi. Red indicates a positive correlation, while green indicates a negative correlation. The deeper color means the greater correlation. $^{*}0.01 < P \leq 0.05$, $^{**}0.001 < P \leq 0.01$, $^{***}P \leq 0.001$. AA, acetic acid; BA, butyric acid; IFN-γ, interferon gamma; IL-10, interleukin 10; PA, propionic acid; TNF-α, tumor necrosis factor alpha.

Huang et al., 2018; Tan et al., 2019). Indeed, many viral agents have been shown to alter the intestinal microbiota in chickens, such as AIV (Yitbarek et al., 2018), Marek's disease virus (MDV) (Lillehoj and Trout, 1996), NDV (Li, 2007), and IBDV (Li L. et al., 2018). In PDCoV-infected chicks, the species richness indices were increased at 5 dpi, and

there were no significant changes in the overall α-diversity of cecal microbiota at 17 dpi. It is possible that the reduced immune response may account for the change of microbial diversity. From the PCoA results, microbiota structure in the PDCoV infected group was clearly distinguished from that of the mock group at 17 dpi, which also reflected SPF chicks' resistance to PDCoV.

From microbial community profiling, the difference between the groups was analyzed at the phylum, family, and genus level. *Eisenbergiella* and *Anaerotruncus* genera were significantly decreased in the PDCoV HNZK-02 at 5 dpi, indicating that PDCoV HNZK-02 infection had a marked influence on chicks' cecal microbiota. According to previous studies, the decrease of the ratio of Firmicutes-to-Bacteroidetes was observed in mice with diabetes (Wen et al., 2008) and in some patients with Crohn's disease and ulcerative colitis (Frank et al., 2007). In our results, a decreased ratio of Firmicutes-to-Bacteroidetes occurred in the PDCoV HNZK-02 group at 17 dpi. More remarkably, the *Alistipes*, considered an opportunistic pathogen (Pandit et al., 2018; Zhang et al., 2018), was significantly increased in the PDCoV HNZK-02 group at 17 dpi. We used linear discriminant analysis (LDA) of effect size (LEfSe) to confirm the taxa that most likely explains the differences between the PDCoV HNZK-02 and mock groups. These findings provide compelling evidence that PDCoV HNZK-02 induced microbiota imbalance and showed that recovery was difficult in a short time period after PDCoV HNZK-02 infection.

Production of SCFAs, as the end products of protein and carbohydrate fermentation (Cummings and Macfarlane, 1991), can easily be affected by the status of the gut microbiota (Lloyd-Price et al., 2019). Studies have shown that *Lactobacillus salivarius* and *L. agilis* could increase propionate and butyrate contents in cecum of chicks (Meimandipour et al., 2010). The changes in butyrate and propionate can influence intestinal physiology and immune function, while acetate can alter lipid metabolism (Macfarlane and Macfarlane, 2011). Our data showed that the changes of gut microbiota composition contributed to the decreased SCFAs, which reduced this protective effect of SCFA in the cecum. However, the interaction of gut microbiota with SCFAs to respond to PDCoV infection needs further studies.

Inflammatory immune responses in the gut can alter the gut luminal environment in a way that favors dysbiosis (Winter et al., 2013). Chicks with dysbiosis are more prone to acute viral infection (Abaidullah et al., 2019), which may in turn further affect the pathogen infectivity. *Eisenbergiella* is strongly correlated with increased levels of TNF-α and IFN-γ, which help in modulating the functional activities of the cells of the immune system (Liu et al., 2010), and to block virus replication and prevent clinical disease (Bradley, 2008; Praveena et al., 2010). This may be the reason that *Eisenbergiella* was decreased in the PDCoV HNZK-02 group at 5 dpi. Moreover, the observation is similar to the increased proinflammatory (TNF-α) cytokine responses of 10-day-old Gn pigs to acute PDCoV infection (Jung et al., 2018). *Alistipes* was strong positively correlated with IFN-γ levels, and the numbers of Ruminococcaceae_UCG-014 were strong negatively correlated with IFN-γ levels, indicating that these bacteria can be tolerated, with IFN-γ responses benefiting for those genera of bacteria. The anti−inflammation activity could be explained in the study regarding to the administration of Norank_f_Lachnospiraceae in gut, and was related to the IL−10 cytokine (Olszak et al., 2014). The results showed the change of microbiota in the cecum was related to intestinal inflammation (directly or indirectly, positively or negatively).

CONCLUSION

In conclusion, the present study revealed that obvious changes were found in the microbial community of chicks infected with PDCoV HNZK-02. PDCoV-inoculated chicks showed a decrease in *Eisenbergiella* and *Anaerotruncus* populations at 5 dpi and an increase in pathogenetic *Alistipes* at 17 dpi with a reduction in SCFAs production. The changes in the microbial community may be related to changes in inflammatory cytokine expression. These results provide new insights into the pathophysiology of chicks infected with PDCoV.

DATA AVAILABILITY STATEMENT

The obtained raw sequencing reads have been added to the NCBI SRA page (Accession Number: PRJNA558384). Other data generated during the study are included in this article.

ETHICS STATEMENT

The experimental procedures were approved by the Laboratory Animals Ethics Committee at Hennan Qixiang Biological Technology Co. Ltd. (HNQX-2018-06), and all husbandry practices and euthanasia were performed with full consideration of animal welfare.

AUTHOR CONTRIBUTIONS

HL and HZ performed the experiments. HL, FZ, and SW performed statistical analyses and wrote the manuscript. Z-xW and Z-yW designed the study and revised the manuscript. All authors read and approved the final manuscript.

FUNDING

This work was supported by the National Key R&D Program (2018YFD0500102) and the National Natural Science Foundation of China (U1704231).

ACKNOWLEDGMENTS

The authors thank Dr. Hui Hu from Henan Agricultural University for designing the study and revising the manuscript.

REFERENCES

Abaidullah, M., Peng, S., Kamran, M., Song, X., and Yin, Z. (2019). Current findings on gut microbiota mediated immune modulation against viral diseases in chicken. *Viruses* 11:681. doi: 10.3390/v11080681

Abt, M. C., Osborne, L. C., Monticelli, L. A., Doering, T. A., Alenghat, T., Sonnenberg, G. F., et al. (2012). Commensal bacteria calibrate the activation threshold of innate antiviral immunity. *Immunity* 37, 158–170. doi: 10.1016/j.immuni.2012.04.011

Balamurugan, V., and Kataria, J. (2006). Economically important non-oncogenic immunosuppressive viral diseases of chicken—current status. *Vet. Res. Commun.* 30, 541–566.

Boley, P. A., Alhamo, M. A., Lossie, G., Yadav, K. K., Vasquez-Lee, M., Saif, L. J., et al. (2020). Porcine deltacoronavirus infection and transmission in poultry, United States. *Emerg. Infect. Dis.* 26, 255–265. doi: 10.3201/eid2602.190346

Bradley, J. (2008). TNF-mediated inflammatory disease. *J. Pathol.* 214, 149–160.

Budden, K. F., Gellatly, S. L., Wood, D. L., Cooper, M. A., Morrison, M., Hugenholtz, P., et al. (2017). Emerging pathogenic links between microbiota and the gut-lung axis. *Nat. Rev. Microbiol.* 15, 55–63.

Chen, C.-J., Wu, G.-H., Kuo, R.-L., and Shih, S.-R. (2017). Role of the intestinal microbiota in the immunomodulation of influenza virus infection. *Microbes Infect.* 19, 570–579. doi: 10.1016/j.micinf.2017.09.002

Chen, Q., Li, G., Stasko, J., Thomas, J. T., Stensland, W. R., Pillatzki, A. E., et al. (2014). Isolation and characterization of porcine epidemic diarrhea viruses associated with the 2013 disease outbreak among swine in the United States. *J. Clin. Microbiol.* 52, 234–243.

Cummings, J., and Macfarlane, G. (1991). The control and consequences of bacterial fermentation in the human colon. *J. Appl. Bacteriol.* 70, 443–459.

Deriu, E., Boxx, G. M., He, X., Pan, C., Benavidez, S. D., Cen, L., et al. (2016). Influenza virus affects intestinal microbiota and secondary *salmonella* infection in the gut through type I interferons. *PLoS Pathog.* 12:e1005572. doi: 10.1371/journal.ppat.1005572

Donohoe, D. R., Holley, D., Collins, L. B., Montgomery, S. A., Whitmore, A. C., Hillhouse, A., et al. (2014). A gnotobiotic mouse model demonstrates that dietary fiber protects against colorectal tumorigenesis in a microbiota-and butyrate-dependent manner. *Cancer Discov.* 4, 1387–1397. doi: 10.1158/2159-8290.CD-14-0501

Emami, N. K., Calik, A., White, M. B., Young, M., and Dalloul, R. A. (2019). Necrotic enteritis in broiler chickens: the role of tight junctions and mucosal immune responses in alleviating the effect of the disease. *Microorganisms* 7:231. doi: 10.3390/microorganisms7080231

Frank, D. N., Amand, A. L. S., Feldman, R. A., Boedeker, E. C., Harpaz, N., and Pace, N. R. (2007). Molecular-phylogenetic characterization of microbial community imbalances in human inflammatory bowel diseases. *Proc. Natl. Acad. Sci. U.S.A.* 104, 13780–13785.

Hu, H., Jung, K., Vlasova, A., and Saif, L. (2016). Experimental infection of gnotobiotic pigs with the cell-culture-adapted porcine deltacoronavirus strain OH-FD22. *Arch. Virol.* 161, 1–14.

Huang, J., Zhang, Z., Li, M., Song, X., Yan, R., Xu, L., et al. (2015). *Eimeria maxima* microneme protein 2 delivered as DNA vaccine and recombinant protein induces immunity against experimental homogenous challenge. *Parasitol. Int.* 64, 408–416. doi: 10.1016/j.parint.2015.06.002

Huang, M.-Z., Wang, S.-Y., Wang, H., Cui, D.-A., Yang, Y.-J., Liu, X.-W., et al. (2018). Differences in the intestinal microbiota between uninfected piglets and piglets infected with porcine epidemic diarrhea virus. *PLoS One* 13:e0192992. doi: 10.1371/journal.pone.0192992

Jung, K., Hu, H., Eyerly, B., Lu, Z., Chepngeno, J., and Saif, L. J. (2015). Pathogenicity of 2 porcine deltacoronavirus strains in gnotobiotic pigs. *Emerg. Infect. Dis.* 21, 650–654. doi: 10.3201/eid2104.141859

Jung, K., Hu, H., and Saif, L. J. (2017). Calves are susceptible to infection with the newly emerged porcine deltacoronavirus, but not with the swine enteric alphacoronavirus, porcine epidemic diarrhea virus. *Arch. Virol.* 162, 2357–2362. doi: 10.1007/s00705-017-3351-z

Jung, K., Miyazaki, A., Hu, H., and Saif, L. J. (2018). Susceptibility of porcine IPEC-J2 intestinal epithelial cells to infection with porcine deltacoronavirus (PDCoV) and serum cytokine responses of gnotobiotic pigs to acute infection with IPEC-J2 cell culture-passaged PDCoV. *Vet. Microbiol.* 221, 49–58. doi: 10.1016/j.vetmic.2018.05.019

Keesing, F., Belden, L. K., Daszak, P., Dobson, A., Harvell, C. D., Holt, R. D., et al. (2010). Impacts of biodiversity on the emergence and transmission of infectious diseases. *Nature* 468, 647–652. doi: 10.1038/nature09575

Li, B., Zheng, L., Li, H., Ding, Q., Wang, Y., and Wei, Z. (2019). Porcine deltacoronavirus causes diarrhea in various ages of field-infected pigs in China. *Biosci. Rep.* 39:BSR20190676. doi: 10.1042/BSR20190676

Li, H., Liu, X., Chen, F., Zuo, K., Wu, C., Yan, Y., et al. (2018). Avian influenza virus subtype H9N2 affects intestinal microbiota, barrier structure injury, and inflammatory intestinal disease in the chicken ileum. *Viruses* 10:270. doi: 10.3390/v10050270

Li, L., Kubasova, T., Rychlik, I., Hoerr, F. J., and Rautenschlein, S. (2018). Infectious bursal disease virus infection leads to changes in the gut associated-lymphoid tissue and the microbiota composition. *PLoS One* 13:e0192066. doi: 10.1371/journal.pone.0192066

Li, Y. (2007). *ERIC-PCR Based Fingerprint to Analyze the Structural Features of Intestinal Microbial Communities of Chicks Infected with Salmonella gallinarum, Newcastle Disease Virus and the Healthy Chicks*. Ph. D. thesis, Sichuan Agricultural University, Sichuan.

Liang, Q., Zhang, H., Li, B., Ding, Q., Wang, Y., Gao, W., et al. (2019). Susceptibility of chickens to porcine deltacoronavirus infection. *Viruses* 11:573.

Lillehoj, H. S., and Trout, J. M. (1996). Avian gut-associated lymphoid tissues and intestinal immune responses to Eimeria parasites. *Clin. Microbiol. Rev.* 9, 349–360.

Liu, H., Zhang, M., Han, H., Yuan, J., and Li, Z. (2010). Comparison of the expression of cytokine genes in the bursal tissues of the chickens following challenge with infectious bursal disease viruses of varying virulence. *Virol. J.* 7:364. doi: 10.1186/1743-422X-7-364

Liu, S., Zhao, L., Zhai, Z., Zhao, W., Ding, J., Dai, R., et al. (2015). Porcine epidemic diarrhea virus infection induced the unbalance of gut microbiota in piglets. *Curr. Microbiol.* 71, 643–649. doi: 10.1007/s00284-015-0895-6

Livak, K. J., and Schmittgen, T. D. (2001). Analysis of relative gene expression data using real-time quantitative PCR and the 2- $\Delta\Delta$CT method. *Methods* 25, 402–408.

Lloyd-Price, J., Arze, C., Ananthakrishnan, A. N., Schirmer, M., Avila-Pacheco, J., Poon, T. W., et al. (2019). Multi-omics of the gut microbial ecosystem in inflammatory bowel diseases. *Nature* 569, 655–662. doi: 10.1038/s41586-019-1237-9

Louis, P., Hold, G. L., and Flint, H. J. (2014). The gut microbiota, bacterial metabolites and colorectal cancer. *Nat. Rev. Microbiol.* 12, 661–672. doi: 10.1038/nrmicro3344

Macfarlane, G. T., and Macfarlane, S. (2011). Fermentation in the human large intestine: its physiologic consequences and the potential contribution of prebiotics. *J. Clin. Gastroenterol.* 45, S120–S127. doi: 10.1097/MCG.0b013e31822fecfe

Magoč, T., and Salzberg, S. L. (2011). FLASH: fast length adjustment of short reads to improve genome assemblies. *Bioinformatics* 27, 2957–2963. doi: 10.1093/bioinformatics/btr507

Meimandipour, A., Hair-Bejo, M., Shuhaimi, M., Azhar, K., Soleimani, A., Rasti, B., et al. (2010). Gastrointestinal tract morphological alteration by unpleasant physical treatment and modulating role of Lactobacillus in broilers. *Br. Poult. Sci.* 51, 52–59. doi: 10.1080/00071660903394455

Mori, H., Maruyama, F., Kato, H., Toyoda, A., Dozono, A., Ohtsubo, Y., et al. (2013). Design and experimental application of a novel non-degenerate universal primer set that amplifies prokaryotic 16S rRNA genes with a low possibility to amplify eukaryotic rRNA genes. *DNA Res.* 21, 217–227. doi: 10.1093/dnares/dst052

National Research Council [NRC] (1994). *Nutritional Requirements of Poultry. 9th Rev*. Washington, DC: National Academy Press.

Olszak, T., Neves, J. F., Dowds, C. M., Baker, K., Glickman, J., Davidson, N. O., et al. (2014). Protective mucosal immunity mediated by epithelial CD1d and IL-10. *Nature* 509, 497–502. doi: 10.1038/nature13150

Pandit, R. J., Hinsu, A. T., Patel, N. V., Koringa, P. G., Jakhesara, S. J., Thakkar, J. R., et al. (2018). Microbial diversity and community composition of caecal microbiota in commercial and indigenous Indian chickens determined using 16s rDNA amplicon sequencing. *Microbiome* 6:115. doi: 10.1186/s40168-018-0501-9

Praveena, P. E., Periasamy, S., Kumar, A., and Singh, N. (2010). Cytokine profiles, apoptosis and pathology of experimental *Pasteurella multocida* serotype A1 infection in mice. *Res. Vet. Sci.* 89, 332–339. doi: 10.1016/j.rvsc.2010.04.012

Segata, N., Izard, J., Waldron, L., Gevers, D., Miropolsky, L., Garrett, W. S., et al. (2011). Metagenomic biomarker discovery and explanation. *Genome Biol.* 12:R60. doi: 10.1186/gb-2011-12-6-r60

Song, D., Peng, Q., Chen, Y., Zhou, X., Zhang, F., Li, A., et al. (2017). Altered gut microbiota profiles in sows and neonatal piglets associated with porcine epidemic diarrhea virus infection. *Sci. Rep.* 7:17439. doi: 10.1038/s41598-017-17830-z

Stewart, M. L., Nikhanj, S. D., Timm, D. A., Thomas, W., and Slavin, J. L. (2010). Evaluation of the effect of four fibers on laxation, gastrointestinal tolerance and serum markers in healthy humans. *Ann. Nutr. Metab.* 56, 91–98. doi: 10.1159/000275962

Tan, Z., Dong, W., Ding, Y., Ding, X., Zhang, Q., and Jiang, L. (2019). Changes in cecal microbiota community of suckling piglets infected with porcine epidemic diarrhea virus. *PLoS One* 14:e0219868. doi: 10.1371/journal.pone.0219868

Wang, L., Byrum, B., and Zhang, Y. (2014). Detection and genetic characterization of deltacoronavirus in pigs, Ohio, USA, 2014. *Emerg. Infect. Dis.* 20, 1227–1230. doi: 10.3201/eid2007.140296

Wen, L., Ley, R. E., Volchkov, P. Y., Stranges, P. B., Avanesyan, L., Stonebraker, A. C., et al. (2008). Innate immunity and intestinal microbiota in the development of Type 1 diabetes. *Nature* 455, 1109–1113. doi: 10.1038/nature07336

Winter, S. E., Lopez, C. A., and Bäumler, A. J. (2013). The dynamics of gut-associated microbial communities during inflammation. *EMBO Rep.* 14, 319–327. doi: 10.1038/embor.2013.27

Woo, P. C., Lau, S. K., Lam, C. S., Lau, C. C., Tsang, A. K., Lau, J. H., et al. (2012). Discovery of seven novel Mammalian and avian coronaviruses in the genus deltacoronavirus supports bat coronaviruses as the gene source of alphacoronavirus and betacoronavirus and avian coronaviruses as the gene source of gammacoronavirus and deltacoronavirus. *J. Virol.* 86, 3995–4008. doi: 10.1128/JVI.06540-11

Yitbarek, A., Taha-Abdelaziz, K., Hodgins, D. C., Read, L., Nagy, É., Weese, J. S., et al. (2018). Gut microbiota-mediated protection against influenza virus subtype H9N2 in chickens is associated with modulation of the innate responses. *Sci. Rep.* 8:16367. doi: 10.1038/s41598-018-34065-8

Zhang, J. (2016). Porcine deltacoronavirus: overview of infection dynamics, diagnostic methods, prevalence and genetic evolution. *Virus Res.* 226, 71–84. doi: 10.1016/j.virusres.2016.05.028

Zhang, W., Jiao, L., Liu, R., Zhang, Y., Ji, Q., Zhang, H., et al. (2018). The effect of exposure to high altitude and low oxygen on intestinal microbial communities in mice. *PLoS One* 13:e0203701. doi: 10.1371/journal.pone.0203701

Conflict of Interest: The authors declare that the research was conducted in the absence of any commercial or financial relationships that could be construed as a potential conflict of interest.

Copyright © 2020 Li, Zhang, zhao, Wang, Wang and Wei. This is an open-access article distributed under the terms of the Creative Commons Attribution License (CC BY). The use, distribution or reproduction in other forums is permitted, provided the original author(s) and the copyright owner(s) are credited and that the original publication in this journal is cited, in accordance with accepted academic practice. No use, distribution or reproduction is permitted which does not comply with these terms.

frontiers in Microbiology

ORIGINAL RESEARCH
published: 12 June 2020
doi: 10.3389/fmicb.2020.00901

Temperature Dramatically Shapes Mosquito Gene Expression With Consequences for Mosquito–Zika Virus Interactions

Priscila Gonçalves Ferreira[1], Blanka Tesla[2], Elvira Cynthia Alves Horácio[3,4], Laila Alves Nahum[3,4,5], Melinda Ann Brindley[2,6,7], Tiago Antônio de Oliveira Mendes[1]* and Courtney Cuinn Murdock[2,7,8,9,10,11,12]**

[1] Department of Biochemistry and Molecular Biology, Universidade Federal de Viçosa, Viçosa, Brazil, [2] Department of Infectious Diseases, College of Veterinary Medicine, University of Georgia, Athens, GA, United States, [3] René Rachou Institute, Oswaldo Cruz Foundation, Belo Horizonte, Brazil, [4] Department of Genetics, Ecology and Evolution, Institute of Biological Sciences, Federal University of Minas Gerais, Belo Horizonte, Brazil, [5] Promove College of Technology, Belo Horizonte, Brazil, [6] Department of Population Health, College of Veterinary Medicine, University of Georgia, Athens, GA, United States, [7] Center for Vaccines and Immunology, University of Georgia, Athens, GA, United States, [8] Odum School of Ecology, University of Georgia, Athens, GA, United States, [9] Center for the Ecology of Infectious Diseases, University of Georgia, Athens, GA, United States, [10] Center for Emerging and Global Tropical Diseases, University of Georgia, Athens, GA, United States, [11] River Basin Center, University of Georgia, Athens, GA, United States, [12] Department of Entomology, College of Agriculture and Life Sciences, Cornell University, Ithaca, NY, United States

OPEN ACCESS

Edited by:
Declan C. Schroeder, University of Minnesota, United States

Reviewed by:
Tadahisa Teramoto, Georgetown University, United States
Anna-Bella Failloux, Institut Pasteur, France

***Correspondence:**
Melinda Ann Brindley
mbrindle@uga.edu
Tiago Antônio de Oliveira Mendes
tiagoaomendes@ufv.br
Courtney Cuinn Murdock
ccm256@cornell.edu

Specialty section:
This article was submitted to Virology, a section of the journal Frontiers in Microbiology

Received: *27 September 2019*
Accepted: *16 April 2020*
Published: *12 June 2020*

Citation:
Ferreira PG, Tesla B, Horácio ECA, Nahum LA, Brindley MA, de Oliveira Mendes TA and Murdock CC (2020) Temperature Dramatically Shapes Mosquito Gene Expression With Consequences for Mosquito–Zika Virus Interactions. Front. Microbiol. 11:901. doi: 10.3389/fmicb.2020.00901

Vector-borne flaviviruses are emerging threats to human health. For successful transmission, the virus needs to efficiently enter mosquito cells and replicate within and escape several tissue barriers while mosquitoes elicit major transcriptional responses to flavivirus infection. This process will be affected not only by the specific mosquito-pathogen pairing but also by variation in key environmental variables such as temperature. Thus far, few studies have examined the molecular responses triggered by temperature and how these responses modify infection outcomes, despite substantial evidence showing strong relationships between temperature and transmission in a diversity of systems. To define the host transcriptional changes associated with temperature variation during the early infection process, we compared the transcriptome of mosquito midgut samples from mosquitoes exposed to Zika virus (ZIKV) and non-exposed mosquitoes housed at three different temperatures (20, 28, and 36°C). While the high-temperature samples did not show significant changes from those with standard rearing conditions (28°C) 48 h post-exposure, the transcriptome profile of mosquitoes housed at 20°C was dramatically different. The expression of genes most altered by the cooler temperature involved aspects of blood-meal digestion, ROS metabolism, and mosquito innate immunity. Further, we did not find significant differences in the viral RNA copy number between 24 and 48 h post-exposure at 20°C, suggesting that ZIKV replication is limited by cold-induced changes to the mosquito midgut environment. In ZIKV-exposed mosquitoes, vitellogenin, a lipid carrier protein, was most up-regulated at 20°C. Our results provide a deeper understanding of the temperature-triggered transcriptional changes in *Aedes aegypti* and can be used to further define the molecular mechanisms driven by environmental temperature variation.

Keywords: temperature, *Aedes aegypti*, Zika virus, RNA-seq, transcriptome, immune response

INTRODUCTION

Over the past three decades, there have been significant advances in our understanding of the physiological and molecular interactions between pathogens and mosquito vectors (Bartholomay and Michel, 2018; Kumar et al., 2018; Simões et al., 2018). Research has provided substantial insights into the immune genes and pathways that shape resistance to vector-borne pathogens and has revealed many promising targets for genetic manipulation (Wilke and Marrelli, 2015; Yen et al., 2018; Shaw and Catteruccia, 2019). However, we are only just beginning to understand the complexity underlying mosquito–pathogen interactions. The response mosquitoes mount toward a given pathogen is a dynamic phenotype that is dependent upon both the specific mosquito–pathogen pairing (Lambrechts et al., 2013; Zouache et al., 2014; Duggal et al., 2015; Chouin-Carneiro et al., 2016) and the variation in key environmental factors (Okech et al., 2007; Alto et al., 2008; Parham and Michael, 2010; Parham et al., 2015; Cohen et al., 2016; Gloria-Soria et al., 2017; Murdock et al., 2017; Shragai et al., 2017; Siraj et al., 2018). Knowledge of how vectors respond to environmental variation is especially relevant for understanding how vector-borne pathogens emerge, defining the biological constraints on transmission, and anticipating the robustness of novel vector-control approaches (that manipulate mosquito physiological and immunological mechanisms to limit virus infection) in field settings.

Vector-borne flaviviruses are emerging threats to human health. Yellow fever virus (YFV), dengue virus (DENV), West Nile virus (WNV), and most recently, Zika virus (ZIKV) can be found throughout tropical and subtropical zones. For successful transmission, flaviviruses are taken up through the bite of a mosquito vector when it takes a blood meal from an infectious host. To complete infection within the mosquito vector, the virus needs to efficiently enter, replicate within, and escape several tissue barriers, primarily the midgut and salivary glands (Franz et al., 2015; Kumar et al., 2018). A number of studies have demonstrated that mosquitoes elicit major transcriptional changes in response to flavivirus infection, which could play an important role in limiting infection (Xi et al., 2008; Sim and Dimopoulos, 2010; Colpitts et al., 2011; Bonizzoni et al., 2012; Chauhan et al., 2012; Angleró-Rodríguez et al., 2017; Etebari et al., 2017; Saldaña et al., 2017a). These include differential regulation of genes involved in RNA interference (RNAi), classical immune pathways (e.g., JAK-STAT, Toll), production and transport of energy, and metabolism, as well as the production of non-coding RNAs (small and long) and microRNAs that could be involved in targeted gene regulation. Currently, it is unclear how conserved these responses to infection are across different mosquito–flavivirus combinations (Etebari et al., 2017) and how relevant environmental variation shapes the nature, magnitude, and timing of these responses (Murdock et al., 2012b, 2014; Adelman et al., 2013).

One of the major environmental variables that influence mosquito–pathogen interactions, as well as vector-borne transmission, is variation in environmental temperature. Mosquitoes are small ectothermic organisms, and many studies have already demonstrated that temperature can markedly affect diverse aspects of mosquito physiology, ecology, and pathogen replication. This, in turn, will shape the proportion of mosquitoes that become infected and infectious, the overall transmission potential of mosquito populations (Christofferson and Mores, 2016; Murdock et al., 2017; Tesla et al., 2018a; Mordecai et al., 2019), and how the distributions of mosquito vectors and vector-borne pathogens will shift in response to climate change (Siraj et al., 2014; Campbell et al., 2015; Ryan et al., 2015, 2018; Misslin et al., 2016). The extent to which temperature shapes transmission directly, through effects on pathogen biology, or indirectly, through effects on mosquito immunity and physiology, remains largely unexplored (Murdock et al., 2012a).

In previous work (Tesla et al., 2018a), we have demonstrated that ZIKV transmission by *Aedes aegypti* is optimized at a mean temperature of 29°C and has a thermal range from 22.7 to 34.7°C. Further, we observed constraints on ZIKV transmission at cool and warm temperatures to be mediated by different factors. To overcome the midgut barrier, a minimal viral load is necessary (Vazeille et al., 2019). Cool temperatures inhibited ZIKV transmission due to slow virus replication and escape from the midgut, resulting in a decrease in metrics of vector competence (e.g., the proportion of mosquitoes that became infected, disseminated infection, and became infectious) and lengthening the extrinsic incubation period (e.g., the interval of time before ZIKV can be detected in the saliva and mosquitoes become infectious [Tesla et al., 2018a; see **Figures 1**, **2**)]. In contrast, increased mosquito mortality at hotter temperatures constrained transmission despite efficient ZIKV infection and rapid dissemination.

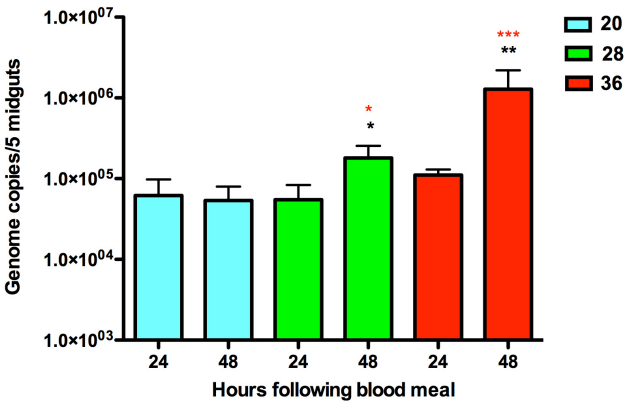

FIGURE 1 | Quantification of ZIKV RNA in infected *Aedes aegypti* mosquitoes housed at 20, 28, and 36°C at two time points, 24 and 48 h. The average number of ZIKV genome copies present in pools of five midgut samples and standard error are shown. The *y*-axis is log-transformed. Black asterisks represent *p*-value < 0.05 calculated by *T*-test between the time points of 24 and 48 h post-infection for the same temperature. Red asterisks represent *p*-value < 0.05 calculated by ANOVA with Tukey correction for multiple hypotheses between the three different temperatures for the same time point after blood meal.

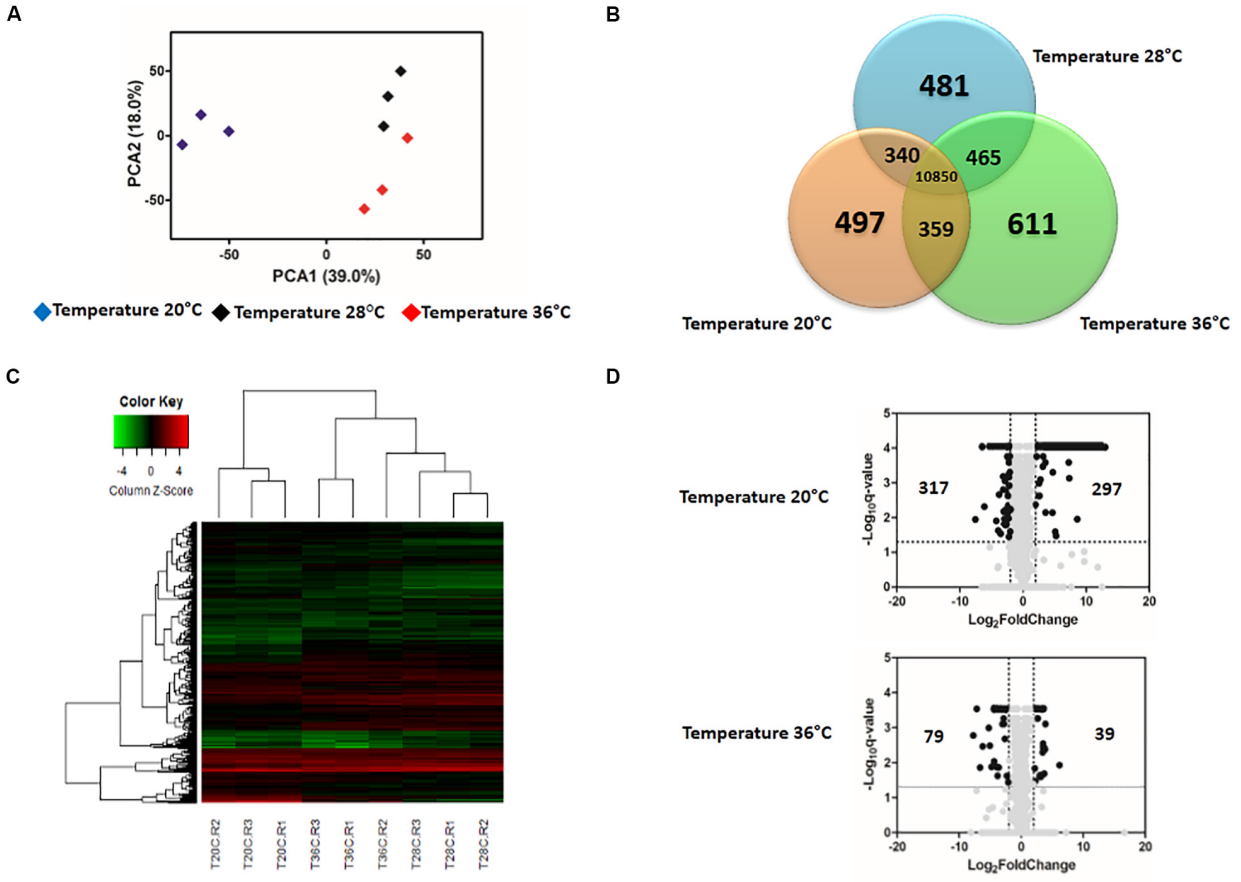

FIGURE 2 | Effect of temperature in the expression profile of uninfected blood-fed *Aedes aegypti.* **(A)** Principal Component Analysis (PCA) plot showing the global gene expression profiles. **(B)** Venn Diagram reporting the number of specific and shared genes. **(C)** Heatmap plot showing local differences (naming scheme: TC20R1 = replicate 1 for the temperature 20°C). **(D)** Volcano plot representing the differential gene expression in RNAseq samples from *Ae. aegypti* exposed to three different constant temperatures (20, 28, and 36°C) at 48 h.

These temperature constraints on infection are likely regulated through different mechanisms. Temperature variation in general could profoundly impact arbovirus infection and replication early in infection due to shifts in the balance and dynamics of the midgut environment, the first host environment encountered. This environment is fairly complex, as arboviruses encounter oxidative and nitration stress associated with digestion of the blood meal (Luckhart et al., 1998; Graça-Souza et al., 2006; Xi et al., 2008), the presence [e.g., *Wolbachia* (Bian et al., 2010)] and proliferation of microbial flora (Xi et al., 2008; Carissimo et al., 2014; Hegde et al., 2015; Saraiva et al., 2016; Barletta et al., 2017; Saldaña et al., 2017b), and key immune factors (Campbell et al., 2008; Xi et al., 2008; Cirimotich et al., 2009; Sánchez-Vargas et al., 2009; Souza-Neto et al., 2009). To better understand the effects of temperature on the ZIKV-mosquito interaction, we used RNA sequencing to describe the transcriptional response of *Ae. aegypti* midguts to ZIKV during the early infection process at three different temperatures (20, 28, and 36°C) previously shown to impact ZIKV infection, dissemination, and transmission rates (Tesla et al., 2018a).

MATERIALS AND METHODS

Ethics Statement

All mosquito infection work with ZIKV was approved by the University of Georgia, Athens Institutional Biosafety Committee (reference number 2015-0039).

Virus Production

Zika virus MEX1-44 was isolated from *Ae. aegypti* mosquitoes from Tapachula, Chiapas, Mexico in January 2016, kindly provided by the University of Texas Medical Branch Arbovirus Reference Collection. ZIKV stocks were propagated in Vero cells cultured in DMEM (Dulbeco's Modified Eagle Medium), 5% fetal bovine serum (FBS) at 37°C and 5% CO_2. Four days following inoculation, when cells showed visible cytopathic effect (>90%), supernatant containing virus was collected, cell debris was cleared by centrifugation (3,500 × *g* for 5 min), and virus was aliquoted and frozen at −80°C. The stock was titrated using standard plaque assays on Vero cells (Willard et al., 2017) and expressed in plaque-forming units per milliliter (PFU/mL).

Mosquito Husbandry

Aedes aegypti eggs collected in Chiapas, Mexico, were hatched in ddH_2O under reduced pressure in a vacuum desiccator. Larvae were grown in trays, with 200 larvae in 1L ddH_2O and four fish food pellets (Hikari Cichlid Cod Fish Pellets). Emerging adults were kept in rearing cages and fed with 10% sucrose solution *ad libitum*. Colonies were maintained on O-positive human blood (Interstate Blood Bank, male donors between 30 and 35 year). Both larvae and adults were maintained under the standard insectary conditions (27°C ± 0.5°C, 80% ± 5% relative humidity, and a 12:12 light: dark diurnal cycle) (Percival Scientific) that replicate rearing and experimental conditions used in Tesla et al. (2018a).

Experimental Mosquito Infection

Briefly, 3 to 4-day-old female mosquitoes (F5 generation; $n = 600$) were separated using a vacuum aspirator, transferred to an arthropod containment level three (ACL-3) facility at the University of Georgia and housed at 28°C ± 0.5°C, 80% ± 5% relative humidity, 12 h:12 h light:dark cycle (Percival Scientific). Mosquitoes were fed with a non-infectious or ZIKV-containing blood-meal (10^6 PFU/mL) after a 12-h period of starvation in a manner previously described (Tesla et al., 2018b). After the feed, engorged ZIKV-exposed ($n = 120$) and unexposed mosquitoes ($n = 120$) were randomly allocated across 12 paper cups (six with ZIKV-exposed and six with ZIKV-unexposed mosquitoes, $n = 20$ mosquitoes per cup). Forty engorged females that fed on either infectious blood or non-infectious blood were randomly distributed across one of three temperature treatments, 20°C, 28°C, and 36°C (±0.5°C) at 80% ± 5% relative humidity and with a 12 h:12 h light:dark cycle. Mosquitoes were provided 10% sucrose *ad libitum* throughout the duration of the experiment (48 h), and three full biological replicates were performed.

Viral Genome Quantification

Viral genomes were detected as previously described (Willard et al., 2019). Briefly, dissected mosquito midguts were collected in pools of five, and viral RNA was isolated using the Zymo Quick-RNA Viral Kit (Zymo, Irvine, CA, United States). Viral RNA samples were reverse-transcribed (RT) to cDNA (High Capacity RNA-to-cDNA Kit, Applied Biosystems, Foster City, CA, United States). The F5 generation was used to maintain genetic proximity with field populations of *Ae. aegypti*. To quantify the number of ZIKV genomes, we used the cDNA in a quantitative PCR (qPCR) reaction assay using TaqMan Gene Expression Master Mix (Applied Biosystems, ThermoFisher, Waltham, MA, United States), primers, and probes (F: ZIKV 1086, R: ZIKV 1162c, ZIKV 1107-FAM; TaqMan MGB Probe; Invitrogen Custom Primers) (Lanciotti et al., 2008). Each sample was analyzed in duplicate, and each plate contained a DNA plasmid standard curve (ZIKV molecular clone), no template, and no primer controls. ZIKV copy numbers were extrapolated from the generated standard curve using the Applied Biosystems protocol. The limit of detection was experimentally established to be 30 copies. Final copy numbers were adjusted by back-calculations to the total RNA and cDNA volume and expressed as copies per five-midgut pool. Outliers were identified by Grubbs test, implemented in Graphpad QuickCalcs[1], and removed. The results were analyzed in GraphPad Prism 5.0. An unpaired *T*-test was applied to compare the two different times (24 and 48) post-infection for the same temperature. ANOVA with Tukey as the multiple hypothesis correction was used to compare the data from the three different temperatures (20, 28, and 36) at the same time points. A *p*-value below 0.05 was considered statistically significant.

Midgut Dissection and RNA Isolation

Mosquito responses to blood meal digestion, midgut microbial proliferation, and arbovirus midgut infection contribute significantly to viral bottlenecks during infection, and these processes could dynamically differ with temperature (Xi et al., 2008; Bonizzoni et al., 2011; Oliveira et al., 2011; Ramirez et al., 2012). Further, these responses likely occur early on during the infection process (<3 days post-infection) at optimal temperatures for ZIKV transmission (e.g., 29°C), as the proportion of mosquitoes with ZIKV-infected midguts plateaus by day three post-infection at temperatures above 28°C (Tesla et al., 2018a). To capture gene expression changes in the mosquito midgut early during the infection process, we isolated total RNA from midgut tissues. Fifteen ZIKV-exposed and 15 non-exposed mosquitoes were removed from each temperature at 24 and 48 h post-infection for RNA sequencing. The mosquitoes were killed with cold ethanol and washed in cold PBS containing 0.2% RNase inhibitor (Sigma-Aldrich) and 0.1% DEPC (Amresco). Midguts were carefully dissected and stored immediately in RNAlater (Invitrogen) at 4°C for 24 h, after which they were transferred to −80°C conditions. Total RNA was isolated from pools of 15 midguts using the Qiagen RNeasy Mini Kit as per the manufacturer's instructions.

Library Preparation and Sequencing

Extracted RNA was sent to the University of Georgia Genomics Core for cDNA library preparation and RNA sequencing. The quality of the total RNA was analyzed using an Agilent Bioanalyzer RNA 6000 Pico Kit (Agilent Technologies). Poly(A) mRNA from total RNA was captured by magnetic oligo-dT beads and fragmented by heating (94°C, 6 min) in the presence of divalent cations (Mg^{2+}) using the KAPA Stranded mRNA-Seq Kit for Illumina®. Fragmented poly(A) mRNA samples were converted to cDNA using random priming. After second-strand synthesis, an adenine residue was added to 3′-end of dscDNA fragments, and Illumina TruSeqLT adapter ligation to 3′-dAMP library fragments was performed. Adapter-ligated DNA was amplified by PCR using the KAPA Library Amplification Primer Mix. After creating the library of DNA templates, the fragment size distribution of these libraries was confirmed by electrophoresis and the library concentration was determined by qPCR. Sequencing was completed on an Illumina NextSeq 500 using the PE75bp (75 bp sequencing reads) settings on a High-Output 150-cycle kit using Illumina standard protocols for loading. Raw sequencing files were demultiplexed using the

[1]https://www.graphpad.com/quickcalcs/Grubbs1.cfm

Illumina BaseSpace cloud platform demultiplexing pipeline. Four technical replicates were run per sample.

RNA Sequence Analysis in Response to Temperature and Zika Virus Exposure

The Tuxedo suite of tools was used to analyze the RNA-seq data (Trapnell et al., 2013). At each stage of the analysis pipeline, we were careful to identify and correct possible sources of bias in the study (Conesa et al., 2016). Read quality was assessed using FastQC (Andrews, 2010). Poor quality reads (quality score below 20), short reads (less than 25 bases), and adapter sequences (Bolger et al., 2014) were removed using Trimmomatic (v 0.36).

We aligned and mapped clean reads up to two different loci to the *Ae. aegypti* genome (NCBI ID: GCA_002204515.1) obtained from NCBI[2] using TopHat (v 2.1.1) (Trapnell et al., 2009). We then performed differential gene expression analysis on RNAseq reads using Cuffdiff (Trapnell et al., 2013), which calculates expression levels in response to experimental treatments of interest (e.g., temperature and ZIKV-exposure) and determines whether observed variations in expression levels across groups are significantly different. The *Ae. aegypti* genome and its annotation file (NCBI ID: GCA_002204515.1) were used to run bias detection and determine the transcripts examined for differential expression, respectively. The relative expression levels were produced as fragments per kilobase of transcript per million fragments mapped (FPKM values), which normalized read count based on gene length and the total number of mapped reads. After quantification and normalization of expression values, differential expression analysis was carried out on the experimental data from 24 and 48 h following the blood meal. To characterize changes in the RNA transcriptome in response to temperature, we compared the RNA expression profiles of unexposed mosquitoes maintained at standard conditions and near the predicted thermal optimum for ZIKV transmission (28°C) to those of mosquitoes housed under cool (20°C) and hot (36°C) conditions. To determine whether temperature modified global RNA expression in ZIKV-exposed individuals, we compared whether the variation in expression profiles of ZIKV-exposed individuals across temperature treatments was similar to that of their unexposed counterparts. Finally, to evaluate the effects of ZIKV infection on global RNA expression, we compared RNA expression between unexposed and ZIKV-exposed mosquitoes within a given temperature treatment. The data quality assessment from the RNAseq analysis was performed using R package (v 3.4.4) (R Development Core Team, 2008) and plotted using GraphPad Prism (version 5.01 for Windows, GraphPad Software, San Diego, CA, United States)[3]. Perl scripts were written to extract specific information from RNAseq analysis output files necessary for each assessment of the results obtained. Principal-component analysis (PCA) was employed to examine the quality of replicates and the overall differences between samples and to determine the proximity among the experimental groups.

[2]https://www.ncbi.nlm.nih.gov/

[3]www.graphpad.com

Gene Ontology (GO) Analysis

We employed BiNGO (v 3.0.3) (Maere et al., 2005) to determine which GO terms were significantly over-represented in a set of genes. First, the FASTA sequences of all differentially expressed genes were recovered using the protein database on the NCBI's Batch Entrez[4]. The sequences were inputted into STRING (v 10.5) (Szklarczyk et al., 2017) to predict protein–protein interactions. GO functional annotations were provided by AgBase-Goanna (v 2.00) (Mccarthy et al., 2006), using the *Ae. aegypti* protein sequences in FASTA format from the STRING database as an input file. The similarity search for GO annotations was performed by Blastp using the UniProt Database with *E*-value: $10e^{-5}$, Matrix: BLOSUM62, and word size: 3. This file annotation was employed as a reference set for enrichment analysis. We used the default mode, employing Hypergeometric tests for assessing the enrichment of a GO term in the test set, and *p*-values were corrected by Benjamini and Hochberg False Discovery Rate (FDR) correction to control for type I error. Corrected *p*-values less than 0.05 were considered significant.

RESULTS

From a total of 36 RNA samples that were sequenced using the Illumina platform, the number of clean paired reads varied between 2,063,917 and 3,028,305 for each library. All libraries resulted in a concordant pair alignment rate higher than 70%.

Cool Temperatures Restrict ZIKV Replication in the Mosquito Midgut

Viral RNA quantification of exposed mosquitoes revealed levels of ZIKV RNA in midgut samples from mosquitoes that imbibed a blood meal containing ZIKV (**Figure 1**). ZIKV replication was evident in mosquitoes housed at 28°C and 36°C, with increases in mosquito RNA copy number between 24 and 48 h post-feed (hpf). Further, the efficiency of ZIKV replication was maximized at the warmest temperature, with mosquitoes housed at 36°C having higher ZIKV RNA levels in their midguts than those housed at 28°C. Although the presence of ZIKV RNA was observed 24 and 48 h following the infectious blood meal in mosquitoes housed in the cool environment (20°C), we did not find significant increases in the viral copy number (**Figure 1**). This result suggests that cooler temperatures constrain ZIKV replication in the midgut.

The Effect of Temperature on Gene Expression in Unexposed Mosquitoes

Gene-expression patterns were influenced by both temperature and time post-blood feed. In general, the principal component analysis (PCA) plot showed a high degree of reproducibility among the replicate samples within each temperature treatment. At 24 hpf, temperature clearly distinguished gene expression profiles (**Supplementary Figure S1A**). However, by 48 hpf, mosquitoes housed at 28°C and 36°C had gene expression

[4]https://www.ncbi.nlm.nih.gov/sites/batchentrez

profiles that were more similar to each other than to mosquitoes housed at 20°C (**Figure 2A**). According to the Venn diagram, the vast majority of genes expressed in the midgut were similar for mosquitoes housed across the three temperature treatments (10,459 at 24 hpf, **Supplementary Figure S1B**; 10,850 at 48 hpf, **Figure 2B**). When concentrating on the differentially expressed genes, Euclidean distance heatmap analysis demonstrated that samples at 24 hpf were separated by temperature treatment in three distinct groups (**Supplementary Figure S1C**), while for samples at 48 hpf, 28 and 36°C samples cluster more closely with one another than with the 20°C (**Figure 2C**). This is the same profile as was seen in the PCA analysis, which employed all transcriptome data. Among these genes, 1665 differentially expressed genes (q-value < 0.05) were seen between mosquitoes held at 20 and 28°C for 24 h, and 3634 were seen by 48 h (**Supplementary Table S1**). In contrast, when comparing mosquitoes held at 36 and 28°C, we identified 1697 and 1695 differentially expressed genes after 24 and 48 h, respectively (**Supplementary Table S2**). In order to perform a more stringent analysis, we produced a volcano plot, which indicated a total of 70 and 297 upregulated genes [$\log_2$(Fold Change) >2 and q-value < 0.05] in mosquitoes housed at 20°C for 24 and 48 h, respectively, compared to those housed at 28°C. For downregulated genes [$\log_2$(Fold Change) <-2 and q-value < 0.05], we found 53 and 317 after 24 and 48 h, respectively (**Supplementary Figure S1D** and **Figure 2D**). We did not find as strong an effect of exposure time when mosquitoes were housed at 36°C, with only 19 and 39 genes up-regulated and 89 and 79 genes down-regulated after 24 and 48 h, respectively (**Supplementary Figure S1D** and **Figure 2D**).

To further define the effect of temperature on mosquito cellular and physiological responses, we sorted the top 20 up- or down-regulated genes at both the cool and hot temperatures, using mosquitoes maintained at 28°C as our standard (**Table 1**). The cool temperature produced a larger response, up-regulating genes hundreds of times compared to standard conditions, whereas the 36°C treatment had a more moderate effect. The transcript with the highest enrichment at 20°C was protein-G12 (1459-fold), whereas a serine protease easter was the most down-regulated (187-fold). For mosquitoes housed at 36°C, heat shock protein 70 (HSP 70) was the transcript most enriched (71-fold) relative to 28°C, while facilitated trehalose transporter Tret1 was the most down-regulated gene (212-fold). Surprisingly, both cool and warm temperature treatments induced some of the same genes to be differentially regulated. Six genes (protein G12, serine protease SP24D, and chymotrypsin-2) were up-regulated in mosquitoes housed at both 20°C and 36°C when compared to those at 28°C, while six genes (serine protease easter, facilitated trehalose transporter Tret1, venom protease, solute carrier family 2 facilitated glucose transporter member 3, and tryptase) were down-regulated.

All differentially expressed genes in the midgut at 48 hpf were submitted for gene ontology (GO) analysis to identify cellular processes that were most perturbed in response to temperature treatment, as revealed by the transcriptome profile. GO analysis of the enriched and depleted transcripts from mosquitoes housed at 20°C revealed that 20 enriched GO terms were related to oxidation–reduction processes and 111 depleted GO terms were involved in gene expression, RNA processing, metabolic processes, and generation of energy (**Figure 3**). Mosquitoes housed at 36°C displayed up-regulated expression related to amine metabolism and cell redox homeostasis processes and down-regulated expression of genes associated with metabolic processes, cellular respiration, and energy derivation by oxidation of organic compounds (**Figure 3**).

The Effect of Temperature on Gene Expression in ZIKV-Exposed Mosquitoes

The gene expression profiles in ZIKV-exposed mosquitoes were also significantly affected by environmental temperature and time post-blood feed. In general, the effect of temperature on differential gene expression was similar to patterns observed in non-ZIKV-exposed blood-fed control mosquitoes outlined above. For example, PCA and heatmap analyses on differential gene expression from mosquito midguts at 24 hpf illustrated three distinct groups separated by temperature treatment (**Supplementary Figures S2A,C**). At 48 hpf, gene expression in mosquitoes housed at 20°C was more distinct than those housed at 28 and 36°C (**Figures 4A,C**). Further, Venn diagrams demonstrate that 1,416 and 10,786 genes were expressed across all temperatures at 24 hpf (**Supplementary Figure S2B**) and 48 hpf (**Figure 4B**), respectively, with the highest overlap in gene expression occurring in mosquitoes housed at 28°C and 36°C at both time points (**Supplementary Figure S2B** and **Figure 4B**). Finally, as seen in the absence of ZIKV infection, at 24 hpf, only 1669 and 1797 genes were differentially expressed in mosquitoes housed at 20 and 36°C, respectively, relative to those housed at 28°C. By 48 hpf, we observed a general increase in the number of genes differentially expressed at 20°C (3056, **Supplementary Table S3**) and a general decrease at 36°C (1518, **Supplementary Table S4**) relative to mosquitoes housed at 28°C. When we evaluated differential expression through a volcano plot, the profile was similar to that of mosquitoes that were not exposed to ZIKV (**Supplementary Figure S2D** and **Figure 4D**).

Several genes that strongly increased at 20°C remained among the top 20 differentially expressed after ZIKV exposure. Lysosomal alpha-mannosidase (XP_021703511.1), two vitellogenins (XP_001660818.2 and XP_001657509.1), phosphoenolpyruvate carboxykinase (XP_001647937.2), protein G12 isoforms (XP_021712126.1, XP_021701760.1, XP_001660827.1, XP_021701761.1, XP_001656377.1, and XP_001656375.1), beta-galactosidase (XP_021705369.1), alpha-N-acetylgalactosaminidase (XP_001650490.2), serine protease SP24D (XP_001659962.1), and chymotrypsin-2 (XP_021698904.1) are some of the genes that remained among the top 20 genes changed by cold temperature in the ZIKV-infection condition. We also saw that although glutamine synthetase (XP_001654186.1) and trypsin (XP_001663002.1) were not listed among the 20 most differentially expressed, they showed enrichment of 50- and 74-fold, respectively. Further, facilitated trehalose transporter Tret1, found to be the most down-regulated in unexposed mosquitoes kept at 36°C, was also the most down-regulated (25-fold) in ZIKV-exposed mosquitoes

TABLE 1 | Top 20 up- and down-regulated genes of uninfected *Aedes aegypti* in response to low (20°C) and to high (36°C) temperature for 48 h post-blood-feeding (relative to standard rearing temperature of 28°C).

GENES UP-REGULATED		TEMPERATURE 20°C		TEMPERATURE 36°C	
Gene ID	**Gene Description**	**Fold Change**	***q*-value**	**Fold Change**	***q*-value**
XP_021701760.1	Protein G12	1459.541989	0.0000886602	11.11657146	0.000290131
XP_021698904.1	Chymotrypsin-2	857.284352	0.0000886602		
XP_001660827.1	Protein G12	603.3619885	0.0000886602	7.4143488679	0.000290131
XP_001650490.2	Alpha-N-acetylgalactosaminidase	548.7746389	0.0000886602		
XP_001659962.1	Serine protease SP24D	473.2635493	0.0000886602	11.29286782	0.000290131
XP_021712126.1	Protein G12-like	442.0421098	0.0000886602		
XP_021701761.1	Protein G12	402.0329675	0.0000886602	6.3523041907	0.000548702
XP_001663002.1	Trypsin 3A1-like	384.5293743	0.0110252		
XP_021705369.1	Beta-galactosidase	315.6714553	0.0000886602		
XP_001656375.1	Protein G12	245.4048583	0.0000886602		
XP_001656377.1	Protein G12 isoform X2	221.8114454	0.0000886602	5.0806039301	0.000290131
XP_021703511.1	Lysosomal alpha-mannosidase isoform X2	217.023882	0.0000886602		
XP_001647937.2	Phosphoenolpyruvate carboxykinase [GTP]	180.2043466	0.0000886602		
XP_001659796.1	Beta-1,3-glucan-binding protein	159.2092116	0.000730421		
XP_021712858.1	Protein G12 isoform X2	149.8743826	0.000256108		
XP_001657509.1	Vitellogenin-A1-like	138.4047839	0.0000886602		
XP_001659961.1	Chymotrypsin-2	110.7367288	0.0000886602	8.596677982	0.000290131
XP_001652194.1	Protein singed wings 2	84.66536466	0.0000886602		
XP_001660818.2	Vitellogenin-A1	67.79655212	0.0000886602		
XP_001654186.1	Glutamine synthetase 1 mitochondrial	65.69082595	0.0000886602		
XP_021693649.1	Heat shock protein 70 A1			71.53314665	0.0118095
XP_001660673.2	Trypsin 5G1-like			14.98866514	0.0007852
XP_001663776.1	Protein G12			14.35856831	0.00416417
XP_001658359.2	Brachyurin			12.24869336	0.000290131
XP_021701762.1	Protein G12-like			12.07440339	0.00379042
XP_001663895.2	Trypsin 5G1			11.04851064	0.00505811
XP_001658471.2	Mite group 2 allergen Gly			10.38200486	0,000290131
XP_011493274.2	Extensin			9.222769233	0.000290131
XP_001659492.2	Serine protease SP24D			7.5082672369	0.000290131
XP_001661186.2	Protein G2			6.9220050786	0.000290131
XP_001651623.2	Surface antigen CRP170			6.151678044	0.000290131
XP-021712126.1	Protein G12-like			5.6022641153	0.000548702
XP_001660908.1	Maltase 1			5.3506716535	0.000290131
XP_011492940.1	Peptidoglycan-recognition protein SC-2			5.030075309	0.000290131
GENES DOWN-REGULATED		**TEMPERATURE 20°C**		**TEMPERATURE 36°C**	
Gene ID	**Gene Description**	**Fold Change**	***q*-value**	**Fold Change**	***q*-value**
XP_001652078.2	Serine protease easter	187.8360285	0.0112238	33.06859855	0.0032544
XP_001658147.1	Facilitated trehalose transporter Tret1	39.72595509	0.0000886602	212.5163457	0.00166701
XP_001652075.2	Venom protease	31.87315659	0.0000886602	21.42212957	0.000290131
XP_001663064.2	UDP-glucuronosyltransferase 2B18	28.70798168	0.0000886602		
XP_001652079.1	Serine protease easter	18.68203877	0.0124204	15.08894466	0.0134155
XP_001655069.1	Queuine tRNA-ribosyltransferase accessory subunit 2	15.34875785	0.0000886602		
XP_001656516.2	Xaa-Pro aminopeptidase ApepP	15.23840501	0.0000886602		
XP_001649987.2	Synaptic vesicle glycoprotein 2B	13.81630566	0.00215644		
XP_021706766.1	Glycerol-3-phosphate dehydrogenase mitochondrial isoform X1	13.39803945	0.0000886602		
XP_021699787.1	Solute carrier family 2 facilitated glucose transporter member 3	13.34678167	0.0000886602	99.27028299	0.0138613
XP_001655305.2	Protein MAK16 homolog A	12.43254717	0.0000886602		
XP_001649768.1	Exosome complex component RRP43	11.98593043	0.0000886602		
XP_001653029.1	Protein takeout	11.66609644	0.0000886602		

(Continued)

TABLE 1 | Continued

GENES DOWN-REGULATED		TEMPERATURE 20°C		TEMPERATURE 36°C	
Gene ID	**Gene Description**	**Fold Change**	***q*-value**	**Fold Change**	***q*-value**
XP_021698953.1	CAD protein	11.58599466	0.0291848		
XP_001656680.1	NHP2-like protein 1 homolog	10.79948043	0.0000886602		
XP_001655729.2	Tryptase	10.69882162	0.0000886602	13.05191869	0.000290131
XP_001662512.1	Nucleoside diphosphate kinase	10.5849313	0.0000886602		
XP_001663497.1	Protein lethal(2)essential for life	10.23543137	0.0000886602		
XP_001655105.1	Sorbitol dehydrogenase	10.21211653	0.0000886602		
XP_021699336.1	Nucleoside diphosphate kinase-like	10.07585248	0.0000886602		
XP_001652056.2	Vitellogenic carboxypeptidase			37.57757336	0.00101347
XP_001655104.1	Sorbitol dehydrogenase			27.67324652	0.013266
XP_001663173.2	Solute carrier family 22 member 8			19.16072174	0.000290131
XP_021702456.1	Sodium-coupled monocarboxylate transporter 1 isoform X1			18.47599301	0.000290131
XP_001651077.2	Synaptic vesicle glycoprotein 2B			17.7140231	0.000290131
XP_001656519.2	Solute carrier family 22 member 21 isoform X2			14.01519585	0.000290131
XP_001662495.2	Lipase 1			13.73780875	0.000290131
XP_021706833.1	Sodium-coupled monocarboxylate transporter 1 isoform X2			13.50049126	0.000290131
XP_021698236.1	Solute carrier organic anion transporter family member 2A1			11.93072658	0.000290131
XP_021702682.1	Acidic amino acid decarboxylase GADL1 isoform X3			11.91023521	0.000290131
XP_001649855.2	Sodium/potassium/calcium exchanger 4			11.67450924	0.000290131
XP_021710339.1	Synaptic vesicle glycoprotein 2C			10.26811889	0.000290131
XP_001662720.1	Putative transporter SVOPL			10.08241963	0.000290131
XP_021713275.1	Synaptic vesicle glycoprotein 2A			8.744949179	0.000290131

kept at the same temperature. Finally, serine protease SP24D (XP_001659962.1) and some G12 proteins (XP_021701760.1, XP_021701761.1, XP_001660827.1, and XP_001656377.1) that were enriched at both cool and warm temperatures remained enriched at these temperatures in ZIKV-exposed mosquitoes (**Table 2**).

Despite these similarities, we did note some key differences between the top 20 genes most differentially expressed in unexposed (**Table 1**) and ZIKV-exposed mosquitoes (**Table 2**), with the greatest change in expression reflected in mosquitoes housed at 20°C and 36°C at 48 h relative to those housed at 28°C. In unexposed mosquitoes kept at 20°C, vitellogenin-A1-like (XP_001657509.1) and vitellogenin-A1 (XP_001660818.2) were up-regulated, yet ZIKV exposure amplified the enrichment from 138- and 68-fold to 3748- and 2644-fold (**Tables 1**, **2**). Surprisingly, in ZIKV-exposed mosquitoes, we did not detect a large up-regulation of Hsp70 at 36°C like we did in the unexposed population.

The GO analysis of differentially expressed genes at 48 hpf in ZIKV-exposed mosquitoes demonstrated distinct effects of cool and warm temperatures on cellular and metabolic function relative to mosquitoes housed at 28°C (**Figure 5**). Further, the functions of these differentially expressed genes were, in part, different from those in unexposed mosquitoes housed at these temperatures (**Figure 3**). For example, when maintained at 20°C, oxidative-reduction processes were no longer enriched, as was seen in unexposed mosquitoes. Instead, ZIKV-exposed mosquitoes housed at 20°C had significant enrichment of the Toll signaling pathway, a known anti-dengue pathway in *Ae. aegypti* (Tchankouo-Nguetcheu et al., 2010). Additionally, endosome transport, Ras protein signal transduction, actin cytoskeleton organization, epithelial tube morphogenesis, pH reduction, and proteolysis were enriched. In contrast, nuclear transport, regulation of viral reproduction, "*de novo*" protein folding, generation of energy, gene expression, RNA processing, and metabolic processes were down-regulated in addition to the expression associated with gene expression, RNA processing, and metabolic processes observed in unexposed counterparts at this temperature (**Figure 5**). ZIKV-exposed mosquitoes housed at 36°C no longer had significant enrichment in genes associated with cellular amine processes and had significant depletion in genes associated with hexose and phosphate metabolic processes and with the generation of precursor metabolites and energy (**Figure 5**).

Effects of Temperature on Oxidative Stress and Innate Immune Mechanisms

To further explore the effects of temperature on uninfected and ZIKV-exposed mosquitoes, we highlight differences in those genes involved in managing oxidative stress, innate immunity, and apoptosis at both 20 and 36°C compared to 28°C at 48 hpf (**Supplementary Tables S5**, **S6** and **Supplementary Figures S3**, **S4**). Virus infection has previously been shown to be modified by complex responses related to detoxification of the blood meal, metabolism, immunity, and apoptosis in some systems (Sanders et al., 2005; Girard et al., 2010; Tchankouo-Nguetcheu et al., 2010; Colpitts et al., 2011; Wang et al., 2012; Neill et al., 2015; Eng et al., 2016). Further, these responses need not respond

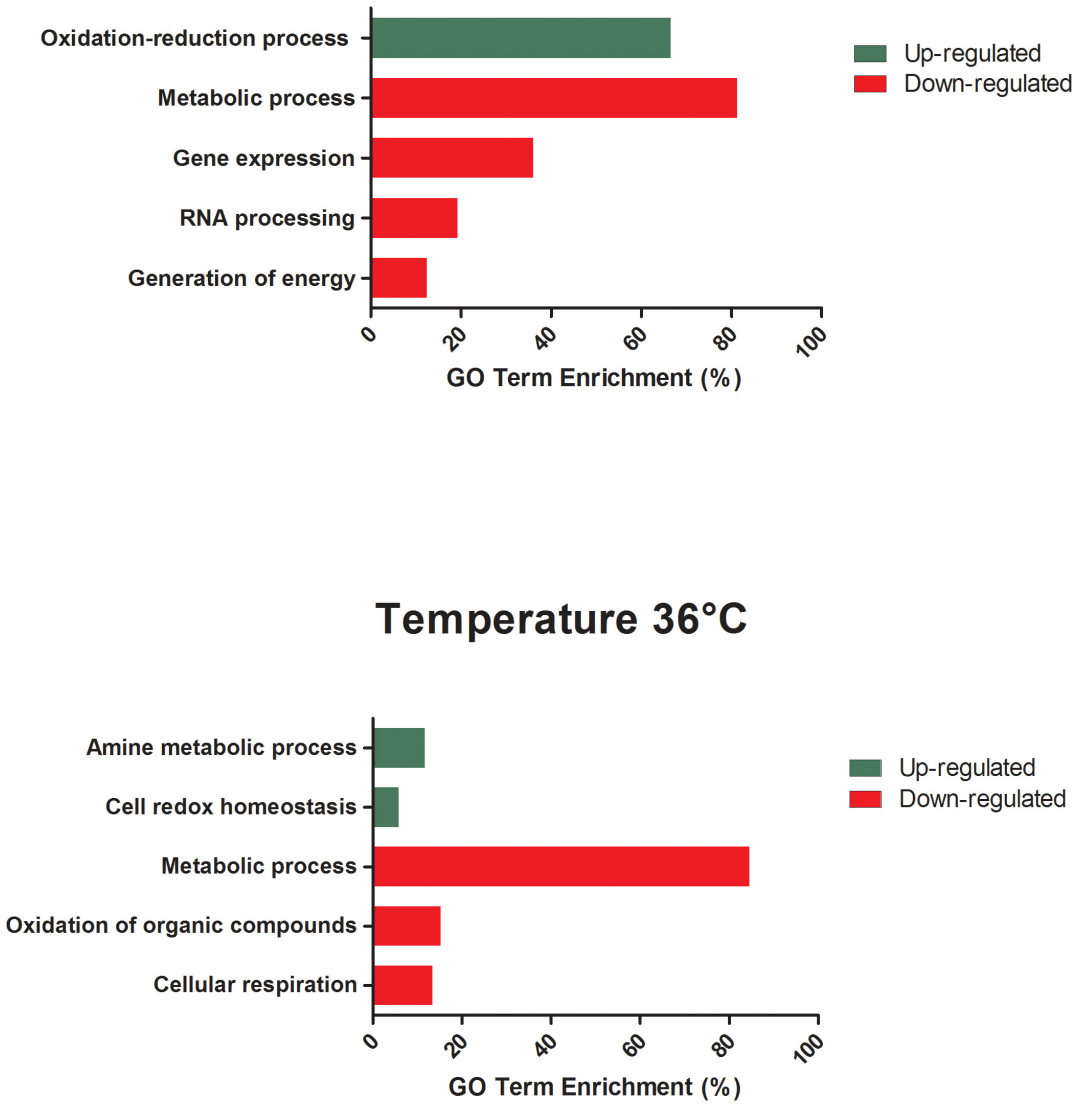

FIGURE 3 | GO term enrichment analysis of differentially expressed genes of unexposed *Aedes aegypti* kept under the lowest (20°C) and the highest (36°C) temperature conditions in the category of biological processes for up- and down-regulated genes at 48 h.

equivalently to temperature variation, as shown in previous work, which demonstrated that mosquito immune responses differed qualitatively and quantitatively across a range of environmental temperatures (Murdock et al., 2012b). The majority of genes involved in managing oxidative stress, innate immunity, and apoptosis exhibited qualitatively different patterns in gene expression in response to cool and warm temperatures in uninfected and ZIKV-exposed mosquitoes. However, while significant, the majority of these differences were very subtle (<2.0-fold; **Supplementary Figures S3**, **S4**). We did observe components of the melanization and Toll pathways to be modestly expressed (>2.0 fold; **Supplementary Figures S3**, **S4**) in response to temperature. An isoform of phenoloxidase (XP_021699380.1), a c-type lectin (XP_001661643.1), and the Toll receptor 6 (TLR6) (XP_021712805.1) were significantly enriched in both uninfected and ZIKV-exposed mosquitoes housed at 20°C.

Mosquito Responses to ZIKV Infection Are Remarkably Modulated by Environmental Temperature

To investigate the effects of ZIKV-exposure on global gene-expression patterns from mosquito midguts early on in the

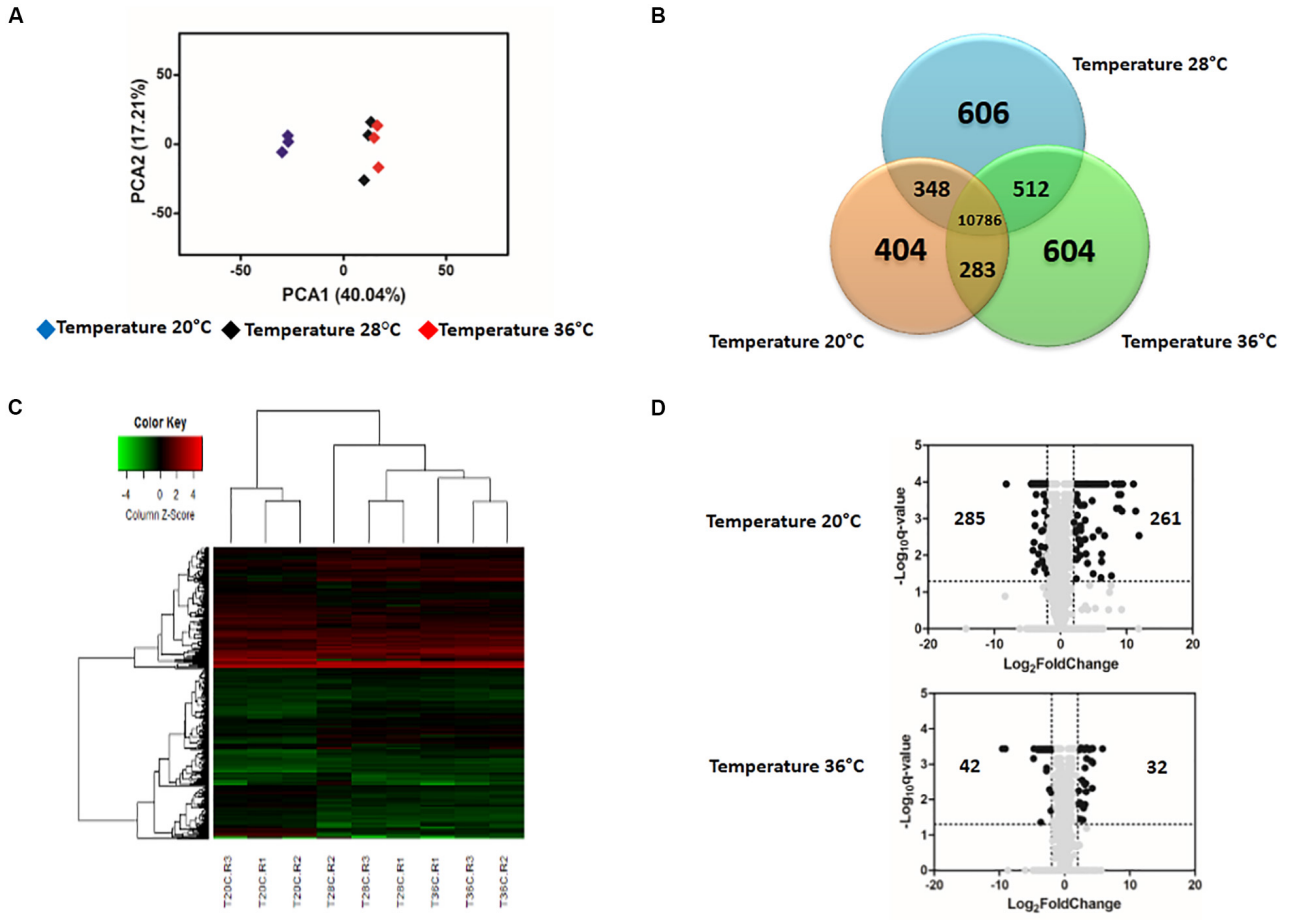

FIGURE 4 | Effect of temperature on the expression profile of Zika-exposed *Aedes aegypti.* **(A)** Principal Component Analysis (PCA) plot showing the global gene expression profiles. **(B)** Venn Diagram reporting the number of specific and shared genes. **(C)** Heatmap plot showing local differences (naming scheme: TC20R1 = replicate 1 for the temperature 20°C). **(D)** Volcano plot representing the differential gene expression in RNAseq samples from infected *Ae. aegypti* exposed to three different constant temperatures (20, 28, and 36°C) at 48 h.

infection process, we compared gene expression between ZIKV-exposed and unexposed mosquitoes within each temperature treatment. The PCA plots demonstrate that ZIKV exposure does not alter mosquito transcription at 24 hpf (**Supplementary Figure S5**) within a given temperature treatment. However, 48-hpf ZIKV-exposed and unexposed samples under the cold temperature condition were distributed in two distinct groups, although one of the ZIKV-exposed biological replicates was relatively close to the control group (**Figure 6A**). Also, the overall number of differentially expressed genes between ZIKV-exposed and unexposed mosquitoes varied across temperature treatments. For example, at 24 hpf, we observed a total of 225, 154, and 161 genes differentially expressed between ZIKV-exposed and unexposed mosquitoes at 20°C, 28°C, and 36°C, respectively (**Supplementary Tables S7–S9**). We identified only two proteins – a sodium/potassium/calcium exchanger 4 (XP_001649855.2) and an uncharacterized protein (XP_001654261.2) – that were up-regulated in ZIKV-exposed mosquitoes at all temperatures (**Supplementary Figure S6A**) and one protein – chymotrypsin-2 (XP_021698609.1) that was down-regulated (**Supplementary Figure S6B**). At 48 hpf, we observed more genes to be differentially expressed (1188 genes) in mosquitoes housed at 20°C between ZIKV-exposed and unexposed mosquitoes, versus only 180 and 50 genes at 28 and 36°C, respectively (**Supplementary Tables S7–S9**). Only one uncharacterized protein (XP_001658660.2) was up-regulated in the ZIKV-exposed mosquitoes at all temperatures (**Figures 7A,B**) at this sampling time point. These results indicate that while the physiological responses of mosquito midguts to ZIKV exposure early in the infection process are similar within a given temperature treatment, these responses are significantly distinct across different environmental temperatures.

When concentrating on the top 10 most differentially expressed genes between ZIKV-exposed and unexposed mosquitoes at each temperature treatment at 48 hpf (**Table 3**), only at 20°C did we observe genes with altered expression (enrichment or depletion) of 10-fold or more. GO analysis

TABLE 2 | Top 20 up- and down-regulated genes of Zika-exposed *Aedes aegypti* in response to low (20°C) and to high (36°C) temperature for 48 h post-blood-feeding relative to standard insectary conditions (28°C).

GENES UP-REGULATED		TEMPERATURE 20°C		TEMPERATURE 36°C	
Gene ID	**Gene Description**	**Fold Change**	***q*-value**	**Fold Change**	***q*-value**
XP_001657509.1	Vitellogenin-A1-like	3748.76585	0.00288439		
XP_001660818.2	Vitellogenin-A1	2644.35472	0.000624083		
XP_021701760.1	Protein G12	2081.92156	0.000113659	18.9560964	0.00036736
XP_001660827.1	Protein G12	668.331471	0.000113659	9.8533206	0.00036736
XP_021701762.1	Protein G12-like	626.881959	0.000624083	9.79462325	0.00599791
XP_021712126.1	Protein G12-like	580.732514	0.000113659	8.68875819	0.00126501
XP_001663776.1	Protein G12	519.780968	0.000113659	10.3753637	0.000690526
XP_021701761.1	Protein G12	498.942585	0.000113659	9.76777521	0.00036736
XP_021698904.1	Chymotrypsin-2	476.004037	0.000113659		
XP_001657506.2	Vitellogenin-A1-like	467.414928	0.000526591		
XP_001656377.1	Protein G12 isoform X2	400.561513	0.000113659	8.94238711	0.00036736
XP_021702099.1	Probable nuclear hormone receptor HR3 isoform X5	356.184271	0.000526591		
XP_001656375.1	Protein G12	315.925373	0.000113659		
XP_001659962.1	Serine protease SP24D	315.50958	0.000113659	8.63508273	0.00036736
XP_021705369.1	Beta-galactosidase	310.614205	0.000113659		
XP_001650490.2	Alpha-N-acetylgalactosaminidase	292.584595	0.000113659		
XP_001652055.1	Vitellogenic carboxypeptidase-like	206.875645	0.0359751		
XP_001652056.2	Vitellogenic carboxypeptidase	123.386436	0.000113659		
XP_001647937.2	Phosphoenolpyruvate carboxykinase [GTP]	106.495599	0.000113659		
XP_021703511.1	Lysosomal alpha-mannosidase isoform X2	103.072096	0.000113659		
XP_001652358.2	Peritrophin-1			55.8211523	0.00036736
XP_021697715.1	Peritrophin-1-like			16.3831402	0.00036736
XP_001658471.2	Mite group 2 allergen Gly d 2.01			15.940003	0.00036736
XP_001663895.2	Trypsin 5G1			9.16859073	0.00365688
XP_001660673.2	Trypsin 5G1-like			8.69411995	0.0136618
XP_001661186.2	Protein G12			7.2863687	0.00036736
XP_001663102.2	Malate synthase			6.86576273	0.00036736
XP_001663439.2	Collagenase			6.39130263	0.00279659
XP_021707618.1	Probable chitinase 2			6.27684681	0.00036736
XP_001651623.2	Surface antigen CRP170			5.38042449	0.00036736
XP_001653091.2	Trypsin alpha-3			5.26940475	0.00036736
XP_001659961.1	Chymotrypsin-2			5.00475692	0.00036736
GENES DOWN-REGULATED		**TEMPERATURE 20°C**		**TEMPERATURE 36°C**	
	Gene Description	**Fold Change**	***q*-value**	**Fold Change**	***q*-value**
XP_001663064.2	UDP-glucuronosyltransferase 2B18	22.0442425	0.000113659	5.62311675	0.00036736
XP_011493503.2	H/ACA ribonucleoprotein complex subunit 1	20.5197322	0.000113659		
XP_001654398.2	rRNA 2'-O-methyltransferase fibrillarin	19.1980783	0.000113659		
XP_001659197.1	DNA-directed RNA polymerase III subunit RPC10	18.0109204	0.00732014		
XP_001658147.1	Facilitated trehalose transporter Tret1	17.354405	0.000113659	25.7984056	0.00036736
XP_001663005.2	Periodic tryptophan protein 1 homolog	16.363733	0.000113659		
XP_021698953.1	CAD protein	16.0097625	0.00443189		
XP_001655305.2	Protein MAK16 homolog A	15.3024421	0.000113659		
XP_001656228.2	COX assembly mitochondrial protein 2 homolog	14.7057657	0.000721477		
XP_021706766.1	Glycerol-3-phosphate dehydrogenase mitochondrial isoform X1	14.6844772	0.000113659		
XP_001649209.1	RRP15-like protein isoform X2	14.5214136	0.00156177		
XP_001652303.1	mRNA turnover protein 4 homolog	14.3570755	0.000113659		
XP_001662723.2	Titin homolog	14.3017521	0.000113659		

(Continued)

TABLE 2 | Continued

GENES DOWN-REGULATED		TEMPERATURE 20°C		TEMPERATURE 36°C	
	Gene Description	**Fold Change**	***q*-value**	**Fold Change**	***q*-value**
XP_021699084.1	Proton-coupled amino acid transporter 1-like	14.2666035	0.000113659		
XP_001658562.1	Activator of basal transcription 1	13.971742	0.000113659		
XP_021695012.1	46 kDa FK506-binding nuclear protein	13.8346093	0.000113659		
XP_001660583.2	Glutamate-rich WD repeat-containing protein 1	13.2594589	0.000113659		
XP_021703839.1	Protein Notchless	13.0245353	0.000113659		
XP_001656680.1	NHP2-like protein 1 homolog	12.0716418	0.000113659		
XP_001655996.2	H/ACA ribonucleoprotein complex non-core subunit NAF1	11.9572191	0.000113659		
XP_001662495.2	Lipase 1			16.3418567	0.00036736
XP_021698905.1	Chymotrypsin-2			13.9310298	0.00036736
XP_001649987.2	Synaptic vesicle glycoprotein 2B			12.6667105	0.0434966
XP_021702682.1	Acidic amino acid decarboxylase GADL1 isoform X3			11.6866538	0.00036736
XP_001649098.2	Probable cytochrome P450 9f2			8.68297843	0.00036736
XP_021699787.1	Solute carrier family 2 facilitated glucose transporter member 3			7.85777033	0.00036736
XP_001652075.2	Venom protease			6.9627634	0.00153067
XP_021702456.1	Sodium-coupled monocarboxylate transporter 1 isoform X1			6.31621377	0.00036736
XP_001651954.2	Trypsin			6.12067175	0.00036736
XP_001649855.2	Sodium/potassium/calcium exchanger 4			5.8573577	0.00036736
XP_021704942.1	Excitatory amino acid transporter 1			5.56974007	0.00036736
XP_021708608.1	Putative helicase MOV-10			5.4055447	0.00036736
XP_001656046.1	Alanine–glyoxylate aminotransferase 2-like			5.35883724	0.00036736
XP_021698609.1	Chymotrypsin-2			5.27740974	0.00036736
XP_001661015.2	Putative alpha-L-fucosidase			5.02108797	0.00036736
XP_001658000.3	Glutathione S-transferase 1			5.0085396	0.00517339
XP_021704288.1	Phosphotriesterase-related protein			4.96319797	0.00036736
XP_001661388.1	Chymotrypsin-1			4.7758913	0.00036736

demonstrated that functions associated with these genes included metallopeptidases (angiotensin-converting enzyme and vitellogenic carboxypeptidase), ammonia/nitrogen metabolism (argininosuccinate lyase and alanine aminotransferase 1), and iron ion binding (a member of the cytochrome P450 family, 4g15).

Interestingly, two vitellogenins (XP_001660818.2 and XP_001657509.1) that were strongly up-regulated in ZIKV-exposed and unexposed mosquitoes housed at 20°C relative to those housed at 28°C were the genes most enriched by ZIKV exposure at the cold temperature (**Table 3**). The expression of these genes did not change in response to ZIKV exposure at 28°C (**Supplementary Table S8**) and 36°C (**Supplementary Table S9**), suggesting that cold stress alters the midgut vitellogenin expression and may be more significant during a viral infection. ZIKV exposure induced a depletion of beta-1,3-glucan-binding protein (GNBP), which binds to β−1,3-glucan and lipopolysaccharide on the surface of pathogens (Dimopoulos et al., 1997), when mosquitoes were maintained at 20°C. Finally, among the most down-regulated genes in ZIKV-exposed mosquitoes at 28°C, solute carrier family 22 (XP_001656519.2), synaptic vesicle glycoprotein (XP_001651077.2), and vitellogenic carboxypeptidase (XP_001652056.2) (**Table 3**) were also among the most down-regulated genes in unexposed mosquitoes housed at 36°C relative to 28°C (**Table 1**).

DISCUSSION

The dynamics and distribution of vector-borne diseases depend on the interplay between the pathogen, the mosquito, and the environment. Temperature is a strong driver of vector-borne disease transmission (Kilpatrick et al., 2008; Lambrechts et al., 2011; Carrington et al., 2013a,b; Mordecai et al., 2013, 2017; Johnson et al., 2015; Shocket et al., 2018; Tesla et al., 2018a). Despite the strong effects of temperature on mosquito-borne pathogens, little is known about the underlying mechanisms involved (Adelman et al., 2013). In this study, RNA sequencing of *Ae. aegypti* midguts unexposed or exposed to ZIKV, taken early in the infection process, revealed different transcriptional responses to variation in environmental temperature, with ZIKV infection modifying these responses to temperature.

Previously, we found that temperature significantly affected the efficiency of the establishment of ZIKV infection in *Ae. aegypti* midguts, with cool temperatures limiting ZIKV transmission primarily due to poor midgut infection, slow replication, and poor dissemination, while high mosquito mortality at warmer temperatures inhibited ZIKV transmission despite efficient ZIKV infection (Tesla et al., 2018a). Similar to our previous study, we were unable to detect ZIKV replication when mosquitoes were housed in cool conditions (**Figure 1**), which is similar to findings for other flavivirus systems in

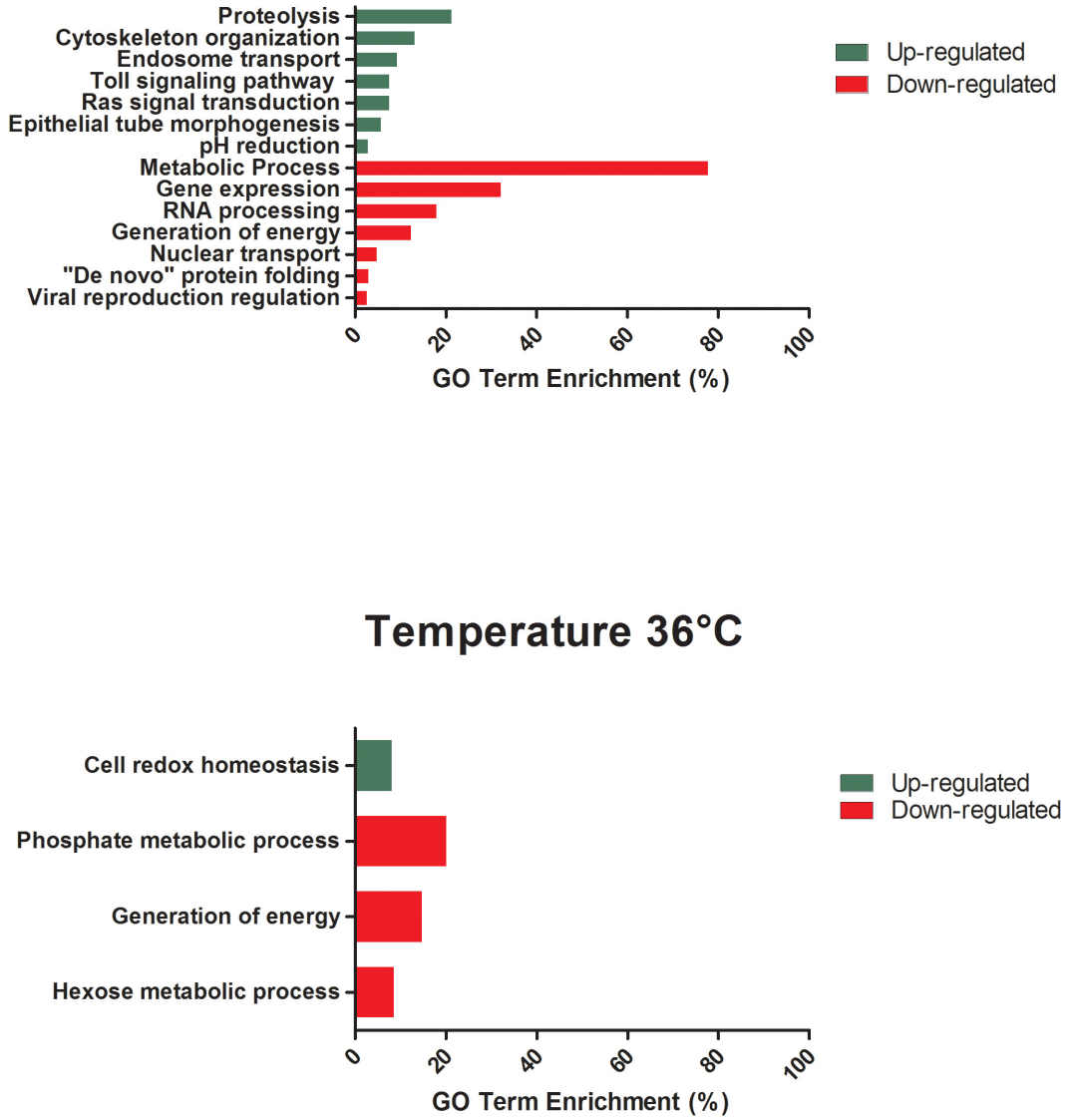

FIGURE 5 | GO term enrichment analysis of differentially expressed genes of *Aedes aegypti* exposed to Zika virus under the lowest (20°C) and in the highest (36°C) temperature conditions in the category of biological processes for up- and down-regulated genes at 48 h.

which infection rates were measured across different constant temperatures (Watts et al., 1987; Kilpatrick et al., 2008; Johansson et al., 2012; Xiao et al., 2014). There was no significant difference in the viral RNA levels quantified from the three temperatures at 24 hpf, reflecting the initial concentration of viral RNA ingested in the blood meal (**Figure 1**). Therefore, we can confirm that while all treatment groups obtained ZIKV in the blood meal, only the mosquitoes housed at standard (28°C) or warm (36°C) temperatures were actively replicating virus by 48 hpf.

We found that variation in temperature elicited strong expression responses in unexposed and ZIKV-exposed mosquitoes. We observed that mosquitoes housed at a cold temperature (20°C) had more genes differentially expressed at 48 hpf relative to mosquitoes housed in standard (28°C) and warm environments (36°C), which exhibited more similar patterns in gene expression (**Figures 2A**, **4A**). This is not entirely surprising, as metabolic theory predicts that low body temperatures will inevitably depress the rates of biochemical reactions (Angilletta et al., 2010). Our data support this hypothesis, as many of the genes drastically altered at 20°C participate in blood meal digestion, peritrophic membrane (PM) formation, metabolism, and managing oxidative stress associated

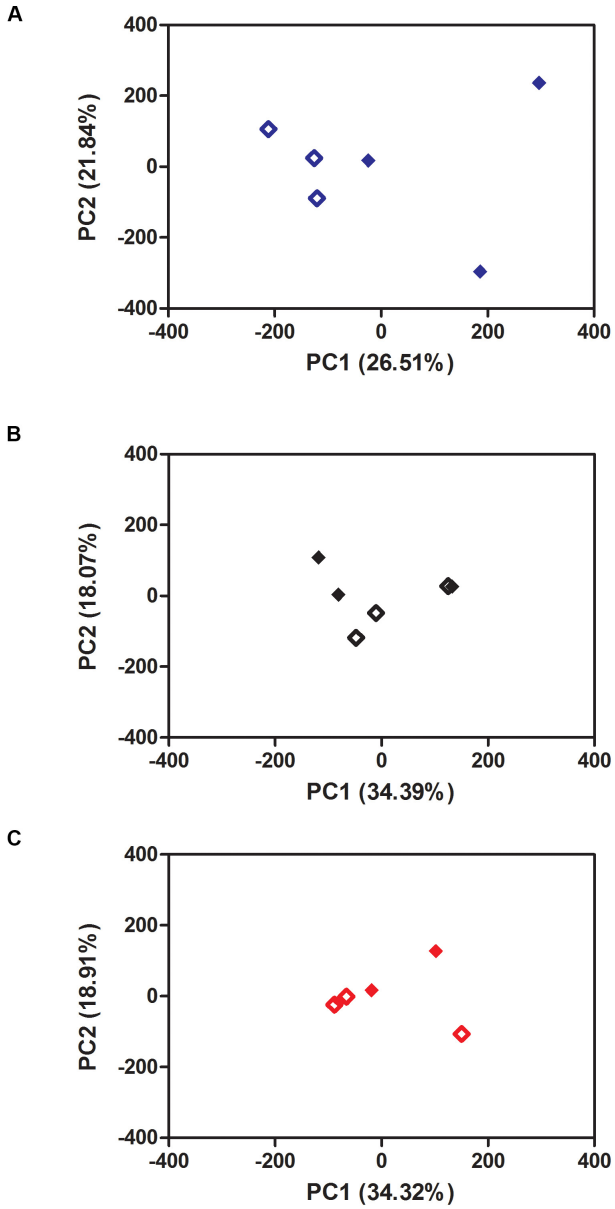

FIGURE 6 | Principal Component Analysis (PCA) of the effect of Zika exposure on *Aedes aegypti* gene expression at three different constant temperatures: **(A)** 20°C, **(B)** 28°C, **(C)** 36°C at 48 h. Open diamond: non-exposed mosquitoes. Closed diamond: Zika-exposed mosquitoes.

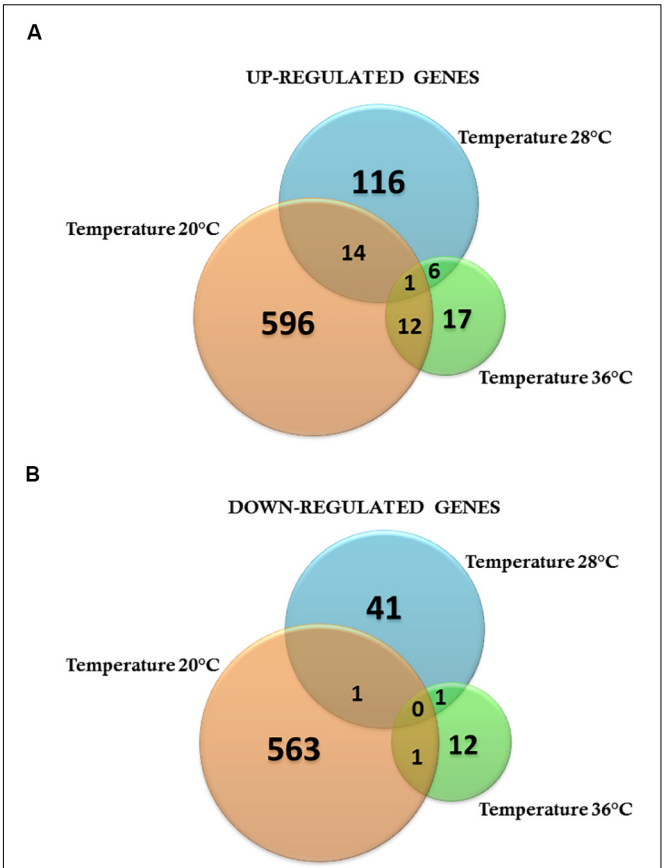

FIGURE 7 | Venn diagram representing the number of specific differentially expressed genes for Zika-infected *Aedes aegypti* exposed to three different constant temperatures (20, 28, and 36°C). **(A)** Up-regulated genes. **(B)** Down-regulated genes at 48 h.

with the breakdown of hemoglobin into heme, a cytotoxic product (**Tables 1**, **2**). Phosphoenolpyruvate carboxykinase and trypsin are upregulated in *Ae. aegypti* midgut during the first few hours after ingestion of a blood meal (Sanders et al., 2003) but were extraordinarily up-regulated in mosquitoes 48 hpf when housed in a cool environment in our study. Additionally, protein G12, which has previously been associated with blood meal digestion and nitrile-specific detoxification (Morlais et al., 2003; Fischer et al., 2008; Bonizzoni et al., 2011), was one of the most enriched transcripts. Further, two digestive proteases involved in glycoside hydrolysis, beta-galactosidase and alpha-N-acetylgalactosaminidase (Santamaría et al., 2015), were highly induced at 48 hpf. Glutamine synthetase, an enzyme that contributes to PM formation, was also highly induced, further demonstrating that cool temperatures delay blood meal digestion (**Supplementary Tables S1**, **S3**). Although the PM is semi-permeable, it is thought to form a barrier and protect the midgut from pathogens [e.g., viruses (Wang and Granados, 2000), bacteria (Kuraishi et al., 2011; Jin et al., 2019), malaria (Rodgers et al., 2017), and protozoa (Weiss et al., 2014)] and other harmful substances present in the insect gut after a blood meal (Wang et al., 2004; Shibata et al., 2015).

We also observed several genes involved in the innate immune response to be modestly upregulated in response to 20°C relative to their levels under warmer temperature conditions in both unexposed and ZIKV-exposed mosquitoes. Melanization is a major effector mechanism of the mosquito immune response and has been implicated in the defense against a diversity of pathogens [e.g., bacteria (Hillyer et al., 2003a,b), malaria (Kumar et al., 2003; Jaramillo-Gutierrez et al., 2009), filarial worms (Christensen et al., 2005; Huang et al., 2005), and viruses (Rodriguez-Andres et al., 2012)]. Phenoloxidase, a key enzyme

TABLE 3 | Top 10 up- and down-regulated genes of Zika-exposed *Aedes aegypti* relative to uninfected mosquitoes kept at low (20°C), standard (28°C), and high (36°C) temperatures 48 h post-blood-feeding.

GENES UP-REGULATED		TEMPERATURE 20°C		TEMPERATURE 28°C		TEMPERATURE 36°C	
Gene ID	**Gene Description**	**Fold Change**	***q*-value**	**Fold Change**	***q*-value**	**Fold Change**	***q*-value**
XP_011493087.1	Angiotensin-converting enzyme	14.1809276	0.000429978				
XP_001652055.1	Vitellogenic carboxypeptidase-like	13.75772483	0.000429978				
XP_001657506.2	Vitellogenin-A1-like	11.96534425	0.000429978				
XP_001657509.1	Vitellogenin-A1-like	11.70010847	0.000429978				
XP_001660818.2	Vitellogenin-A1	10.9320344	0.000429978				
XP_001652056.2	Vitellogenic carboxypeptidase	10.74370729	0.000429978				
XP_001660472.2	Alanine aminotransferase 1	10.39479931	0.000429978				
XP_001656695.1	Argininosuccinate lyase	10.17572724	0.000429978				
XP_001648376.1	Cytochrome P450 4g15	10.00001321	0.000429978				
XP_001659164.1	Leucine-rich repeat transmembrane neuronal protein 3	9.612555348	0.000429978				
XP_001649098.2	Probable cytochrome P450 9f2			4.118816919	0.0027631		
XP_001659492.2	Serine protease SP24D			3.289321443	0.0027631		
XP_021698905.1	Chymotrypsin-2			3.165229262	0.0027631		
XP_001661721.2	Solute carrier family 45 member 4			3.060526797	0.0027631		
XP_001654886.2	Zinc carboxypeptidase A 1			2.871948741	0.0027631		
XP_001661388.1	Chymotrypsin-1			2.816727502	0.0027631		
XP_021698904.1	Chymotrypsin-2			2.669611858	0.0027631		
XP_021707253.1	Lipase member H			2.612389473	0.0027631		
XP_021697282.1	Multiple inositol polyphosphate phosphatase 1			2.446636883	0.0027631		
XP_001658491.2	Trypsin 5G1-like			2.279646301	0.0027631		
XP_001652358.2	Peritrophin-1					8.437408782	0.00630758
XP_001648381.1	UNC93-like protein					7.430915686	0.00630758
XP_021710339.1	Synaptic vesicle glycoprotein 2C					5.329166839	0.00630758
XP_021697715.1	Peritrophin-1-like					4.823164447	0.00630758
XP_011493129.2	Flocculation protein FLO11					2.282808753	0.00630758
XP_021706761.1	Cysteine sulfinic acid decarboxylase					2.236697262	0.00630758
XP_021707618.1	Probable chitinase 2					2.214805485	0.00630758
XP_001658086.2	Peptidoglycan recognition protein 1					2.009494011	0.00630758
XP_001649855.2	Sodium/potassium/calcium exchanger 4					1.947834362	0.00630758
XP_021709756.1	ATP-binding cassette sub-family A member 3 isoform X1					1.930421649	0.00630758

(Continued)

TABLE 3 | Continued

GENES DOWN-REGULATED		TEMPERATURE 20°C		TEMPERATURE 28°C		TEMPERATURE 36°C	
Gene ID	**Gene Description**	**Fold Change**	**q-value**	**Fold Change**	***q*-value**	**Fold Change**	***q*-value**
XP_001659797.2	Beta-1.3-glucan-binding protein	8.48073909	0.000429978				
XP_001657206.1	Cytochrome P450 9e2	4.355565374	0.000429978				
XP_001652358.2	Peritrophin-1	2.847448995	0.000429978				
XP_021699084.1	Proton-coupled amino acid transporter 1-like	2.551861447	0.000429978				
XP_001659796.1	Beta-1.3-glucan-binding protein	2.517270058	0.000429978				
XP_001649098.2	Probable cytochrome P450 9f2	2.415932254	0.000429978				
XP_001649745.1	Very long-chain specific acyl-CoA dehydrogenase mitochondrial	2.281021429	0.000429978				
XP_001654398.2	rRNA 2'-O-methyltransferase fibrillarin	2.204742243	0.000429978				
XP_001661250.1	Peroxiredoxin-6	1.971170346	0.000429978				
XP_001649797.1	Peptide methionine sulfoxide reductase	1.965683434	0.000429978				
XP_001652056.2	Vitellogenic carboxypeptidase			6.420385839	0.0027631		
XP_001655729.2	Tryptase			5.300762859	0.0027631		
XP_001647719.2	Transferrin			4.298907297	0.0027631		
XP_001655031.2	Carbonic anhydrase 2			3.707662693	0.0027631		
XP_011493147.1	Glycine-rich protein 5			3.626857343	0.0027631		
XP_001651077.2	Synaptic vesicle glycoprotein 2B			3.02148965	0.0027631		
XP_001659383.2	Angiopoietin-related protein 1			2.46044625	0.0027631		
XP_001651411.2	Lysosomal alpha-mannosidase			2.427598779	0.0027631		
XP_001656519.2	Solute carrier family 22 member 21 isoform X2			2.425681278	0.0027631		
XP_011493149.1	Hyphally-regulated protein			2.384835903	0.0049383		
XP_021696806.1	Pupal cuticle protein Edg-78E					18.1975207	0.00630758
XP_011493274.2	Extensin					3.699473591	0.00630758
XP_001661011.1	Protein lethal(2)essential for life					3.215359388	0.00630758
XP_001658359.2	Brachyurin					2.357013464	0.00630758
XP_001649783.1	Maltase 1					1.680632876	0.0148679
XP_001647586.2	Asparagine synthetase [glutamine-hydrolyzing] 1					1.637484216	0.00630758
XP_021694990.1	Myrosinase 1-like					1.626761779	0.00630758
XP_021693649.1	Heat shock protein 70 A1					1.55902061	0.02715
XP_001651895.1	Acyl-CoA:lysophosphatidylglycerol acyltransferase 1					1.523434001	0.00630758
XP_001649752.1	Heat shock protein 83					1.48484568	0.00630758

in the melanization pathway, was up-regulated in mosquito midguts at 20°C (**Supplementary Figures S3B**, **S4B**). Studies in both butterflies and *Anopheles stephensi* demonstrated that phenoloxidase activity was higher at cool temperatures and becomes less efficient at warmer temperatures (Suwanchaichinda and Paskewitz, 1998; Murdock et al., 2012b). The production of melanin is also essential for other physiological processes such as cold acclimatization in insects (Crill et al., 1996; Kutch et al., 2014), the formation of the hard protective layer around eggs, and wound healing (Lai et al., 2009). Our data also reveal that c-type lectin, reported to participate in the activation of the melanization cascade (Yu and Kanost, 2000; Christensen et al., 2005), was also up-regulated. Therefore, our results suggest that cold stress triggers numerous molecular changes in the mosquito, including modest changes in the levels of important immune effectors that could have important consequences for arboviral infection.

Contrary to what we observed at the cool temperature, exposure to hot conditions (36°C) does not trigger pronounced up- or down-regulation of genes relative to standard conditions (28°C). The heat shock protein 70 (HSP 70) transcript was most enriched in response to the hot environment (**Table 1**). The upregulation of HSP 70 is associated with reduced lifespans in other insect systems (Feder and Krebs, 1998; Feder, 1999), which may explain the rapid mosquito mortality we observed at this temperature in previous work (Tesla et al., 2018a). HSP70 has also been suggested to facilitate arbovirus infection in mosquitoes in terms of viral entry, viral RNA synthesis, and virion production (Kuadkitkan et al., 2010; Taguwa et al., 2015).

Zika virus exposure induced very modest effects when comparing ZIKV-exposed and unexposed mosquitoes reared at 28 and 36°C, while those that experienced the cool temperature exhibited a larger alteration in gene expression at 48 hpf (**Figure 6** and **Supplementary Figure S5**). This may not be entirely surprising, as ZIKV-induced transcriptional changes under standard rearing conditions (28°C) have previously been shown to be subtle 48 h post-infection (Murdock et al., 2012a) and ZIKV was only observed to be actively replicating at 28 and 36°C. When concentrating on differentially expressed genes between ZIKV-exposed and unexposed mosquitoes at each temperature treatment (**Table 3**), only at 20°C do we observe changes of 10-fold or more. Therefore, the presence of ZIKV in the blood meal did alter the response of mosquitoes to temperature variation, with the most pronounced differences occurring in mosquitoes housed at the cool temperature. In particular, the midguts of ZIKV-exposed mosquitoes experienced enhanced signal transduction processes, pH modification, midgut epithelial morphogenesis, and Toll pathway activation relative to ZIKV-exposed mosquitoes at 28°C (**Figure 5**), and this pattern was qualitatively different to a similar comparison in unexposed mosquitoes (**Figure 3**). These changes could be reflective of patterns observed in other studies demonstrating that mosquitoes infected with blood-borne pathogens actively modify ROS metabolism in midgut cells to control levels of hydrogen peroxide (H_2O_2), which in turn is an important modulator of downstream innate immune responses (e.g., Toll pathway), antimicrobial peptide production, and pathogen infection (Molina-Cruz et al., 2008; Herrera-Ortiz et al., 2011; Oliveira et al., 2011, 2012). Furthermore, the presence and abundance of particular microbial flora [e.g., *Wolbachia* (Pan et al., 2012)] and the proliferation of the midgut flora due to ingestion of the blood meal (Carissimo et al., 2014; Saraiva et al., 2016; Barletta et al., 2017) can also trigger ROS production, with temperature variation modifying these effects.

Additionally, vitellogenin proteins (Vg) were highly upregulated (>3000 fold) when ZIKV-exposed mosquitoes were housed at cool temperatures relative to ZIKV-exposed mosquitoes at 28°C (**Table 2**) and unexposed mosquitoes at 20°C (**Table 3**). Vg is a precursor egg-yolk protein but may also function by shielding cells from the negative effects of inflammation and infection (Corona et al., 2007; Azevedo et al., 2011). Work with honey bees suggests that Vg-incubated insect cells display enhanced tolerance against H_2O_2-induced oxidative stress (Fluri et al., 1977; Seehuus et al., 2006). Vg also binds to dying cells, suggesting that it may play a role in recognizing damaged cells and shielding healthy cells from toxic by-products (Havukainen et al., 2013). Both caspase dronc [an inhibitor caspase (Cooper et al., 2007)] and an effector caspase (Bryant et al., 2008), which are important components of the apoptotic pathway controlling mechanisms of cell death, were enriched in mosquitoes housed at 20°C (**Supplementary Figures S3E**, **S4E**). Thus, elevated Vg expression may combat cellular damage resulting from elevated heme toxicity and oxidative stress (Havukainen et al., 2013) associated with the delayed breakdown of hemoglobin in the blood meal (Bottino-Rojas et al., 2015) in mosquitoes housed at cool temperatures. There may also be a direct effect of Vg on ZIKV, as it has been associated with antiviral effects in some fish species (Garcia et al., 2010). Entry of ZIKV into mammalian cells is associated with apoptotic mimicry, with viral lipids interacting with phosphatidylserine receptors on cells gaining entry in a pathway similar to clearance of apoptotic cells (Hamel et al., 2015). Honey bee Vg binds to dying cells through interactions with lipids (Havukainen et al., 2013). Although the receptors ZIKV uses to interact and enter mosquito cells have not been identified, if Vg protein coats viral particles, it may impede normal cellular interaction and entry. Alternatively, ZIKV infection could be limited at the cooler temperature if infected mosquitoes balance ROS metabolism toward a higher state of oxidative stress, as shown in other systems (Molina-Cruz et al., 2008; Herrera-Ortiz et al., 2011; Pan et al., 2012; Bottino-Rojas et al., 2015; Wong et al., 2015), facilitating downstream innate immune mechanisms and virus killing. Whether overexpressions of Vg lipoproteins have direct effects on ZIKV infection or reflect a response to buffer ZIKV-exposed mosquitoes to a higher state of oxidative stress in the midgut remain open questions that will be explored in future experiments.

Finally, in ZIKV-exposed mosquitoes at 36°C, we observed peritrophin, one of the components of the peritrophic matrix, to be highly up-regulated relative to ZIKV-exposed mosquitoes housed at 28°C (**Table 2**) and unexposed mosquitoes housed at 36°C (**Table 3**). Although PM formation is highly induced 3–24 hpf, peritrophin can undergo positive modulation by pathogens in other vector-borne disease systems (e.g., *Le. major*) (Coutinho-Abreu et al., 2013). While we cannot confirm whether HSP70 or modulation of peritrophin play a role in ZIKV

infection, these could be potential mechanisms explaining why we detect higher viral RNA levels at 36°C in this study (**Figure 1**) and efficient viral dissemination and salivary gland invasion in previous work (Tesla et al., 2018a).

Although we estimated the effects of mean constant temperatures on the immune-physiological profiles of *Ae. aegypti* in response to ZIKV infection to maintain experimental tractability, mosquitoes and their pathogens live in a variable world where temperatures fluctuate daily and seasonally (easily encompassing the range of temperatures explored here). Both mosquito immunity and virus transmission have previously been shown to differ in fluctuating environments relative to constant temperature environments (Lambrechts et al., 2011; Carrington et al., 2013a,b; Murdock et al., 2013). There is also a substantial body of work demonstrating carry-over effects of environmental variation in the larval environment on adult mosquito phenotypes, fitness, and metrics of transmission (Muturi and Alto, 2011; Muturi et al., 2011a,b; Alto and Bettinardi, 2013; Buckner et al., 2016; Evans et al., 2018). While outside the scope of this study, future work should investigate how both fluctuating environmental conditions and the larval environment modify the physiological and immunological responses of adult mosquitoes to arbovirus infection and temperature variation in the adult environment. Finally, while there is currently limited evidence demonstrating that mosquitoes select microhabitats to optimize internal body temperatures for metabolic demands (Blanford et al., 2009), as in other ectothermic organisms (Huey, 1991; Hertz et al., 1994; Gvoždík, 2002; Dillon et al., 2009), if this did occur in the field, it would modify the range of field-relevant temperatures mosquitoes effectively experience.

In this study, we demonstrate profound effects of temperature on ZIKV viral replication and the transcriptional responses of mosquitoes. Temperature variation may alter the ZIKV infection process either through modifying the response of mosquitoes to ZIKV infection, altering the efficiencies of viral-specific processes, or, more likely, both. Our study focused on midgut responses early in the infection process. However, disentangling these effects will require the sampling of other immunological tissues and at later time points where high levels of ZIKV RNA can be detected. While further work is needed to determine the precise mechanisms at play, our results indicate that temperature shifts the balance and dynamics of the midgut environment, which could result in direct and indirect consequences for the ZIKV-infection process. These results do reinforce the assertion that the conventional approach of studying the mechanisms underpinning mosquito–pathogen interactions under a narrow set of laboratory conditions or across canonical innate immune pathways is likely missing important biological complexity. To move forward, we need to begin framing our mechanistic understanding of this dynamic phenotype in the ecologically variable world in which mosquitoes and pathogens associate. This study represents a key advance toward this objective.

DATA AVAILABILITY STATEMENT

The fast raw data were deposited in the NCBI SRA database under accession number PRJNA615972. This Sequence Read Archive (SRA) submission will be released on 2020–10–20 or upon publication, whichever is first.

ETHICS STATEMENT

All mosquito infection work with ZIKV was approved by the University of Georgia, Athens Institutional Biosafety Committee (reference number 2015-0039).

AUTHOR CONTRIBUTIONS

BT performed the experiments. PF and TO analyzed the RNAseq data. CM, MB, TO, and LN designed the experiments, acquired the funding, and supervised the project. All authors wrote the manuscript.

FUNDING

This work was supported by co-funding from Brazilian Fundação de Amparo à Pesquisa do Estado de Minas Gerais (FAPEMIG) (APQ-04765-16), the University of Georgia's Office for Research (OVPR, grant 302070035), and an NSF-RAPID award 1640780. The funders had no role in study design, data collection and interpretation, and decision to submit the work for publication.

ACKNOWLEDGMENTS

We thank the University of Texas Medical Branch Arbovirus Reference Collection for providing the virus and Dr. Americo Rodriguez from the Instituto Nacional de Salud Publica for providing mosquito eggs. We also thank the Universidade Federal de Viçosa and the University of Georgia for the use of the facilities in which this work was carried out. The bioinformatics analyses were performed in the UFV Cluster.

SUPPLEMENTARY MATERIAL

The Supplementary Material for this article can be found online at: https://www.frontiersin.org/articles/10.3389/fmicb.2020.00901/full#supplementary-material

REFERENCES

Adelman, Z. N., Anderson, M. A. E., Wiley, M. R., Murreddu, M. G., Samuel, G. H., Morazzani, E. M., et al. (2013). Cooler temperatures destabilize RNA interference and increase susceptibility of disease vector mosquitoes to viral infection. *PLoS Negl. Trop. Dis.* 7:e2239. doi: 10.1371/journal.pntd.0002239

Alto, B. W., and Bettinardi, D. (2013). Temperature and dengue virus infection in mosquitoes: independent effects on the immature and adult stages. *Am. J. Trop. Med. Hyg.* 88, 497–505. doi: 10.4269/ajtmh.12-0421

Alto, B. W., Lounibos, L. P., Mores, C. N., and Reiskind, M. H. (2008). Larval competition alters susceptibility of adult Aedes mosquitoes to dengue infection. *Proc. R. Soc. B Biol. Sci.* 275, 463–471. doi: 10.1098/rspb.2007.1497

Andrews, S. (2010). *FastQC: A Quality Control Tool for High Throughput Sequence Data*. Available online at: http://www.bioinformatics.babraham.ac.uk/projects/fastqc (accessed March 11, 2018).

Angilletta, M. J., Huey, R. B., and Frazier, M. R. (2010). Thermodynamic effects on organismal performance: is hotter better? *Physiol. Biochem. Zool.* 83, 197–206. doi: 10.1086/648567

Angleró-Rodríguez, Y. I., MacLeod, H. J., Kang, S., Carlson, J. S., and Dimopoulos, N. J. G. (2017). *Aedes aegypti* molecular responses to Zika Virus: modulation of infection by the toll and Jak/Stat immune pathways and virus host factors. *Front. Microbiol.* 8:2050. doi: 10.3389/fmicb.2017.02050

Azevedo, D. O., Zanuncio, J. C., Delabie, J. H. C., and Serrão, J. E. (2011). Temporal variation of vitellogenin synthesis in *Ectatomma tuberculatum* (Formicidae: Ectatomminae) workers. *J. Insect Physiol.* 57, 972–977. doi: 10.1016/j.jinsphys.2011.04.015

Barletta, A. B. F., Nascimento-Silva, M. C. L., Talyuli, O. A. C., Oliveira, J. H. M., Pereira, L. O. R., Oliveira, P. L., et al. (2017). Microbiota activates IMD pathway and limits Sindbis infection in *Aedes aegypti*. *Parasit. Vectors* 10:103. doi: 10.1186/s13071-017-2040-2049

Bartholomay, L. C., and Michel, K. (2018). Mosquito immunobiology: the intersection of vector health and vector competence. *Annu. Rev. Entomol.* 63, 145–167. doi: 10.1146/annurev-ento-010715-023530

Bian, G., Xu, Y., Lu, P., Xie, Y., and Xi, Z. (2010). The endosymbiotic bacterium Wolbachia induces resistance to dengue virus in *Aedes aegypti*. *PLoS Pathog.* 6:e833. doi: 10.1371/journal.ppat.1000833

Blanford, S., Read, A. F., and Thomas, M. B. (2009). Thermal behaviour of *Anopheles stephensi* in response to infection with malaria and fungal entomopathogens. *Malar. J.* 8, 1–9. doi: 10.1186/1475-2875-8-72

Bolger, A. M., Lohse, M., and Usadel, B. (2014). Trimmomatic: a flexible trimmer for Illumina sequence data. *Bioinformatics* 30, 2114–2120. doi: 10.1093/bioinformatics/btu170

Bonizzoni, M., Dunn, W. A., Campbell, C. L., Olson, K. E., Dimon, M. T., Marinotti, O., et al. (2011). RNA-seq analyses of blood-induced changes in gene expression in the mosquito vector species, *Aedes aegypti*. *BMC Genomics* 12:82. doi: 10.1186/1471-2164-12-82

Bonizzoni, M., Dunn, W. A., Campbell, C. L., Olson, K. E., Marinotti, O., and James, A. A. (2012). Complex modulation of the *Aedes aegypti* transcriptome in response to dengue virus infection. *PLoS One* 7:e50512. doi: 10.1371/journal.pone.0050512

Bottino-Rojas, V., Talyuli, O. A. C., Jupatanakul, N., Sim, S., Dimopoulos, G., Venancio, T. M., et al. (2015). Heme signaling impacts global gene expression, immunity and dengue virus infectivity in *Aedes aegypti*. *PLoS One* 10:e0135985. doi: 10.1371/journal.pone.0135985

Bryant, B., Blair, C. D., Olson, K. E., and Clem, R. J. (2008). Annotation and expression profiling of apoptosis-related genes in the yellow fever mosquito *Aedes aegypti*. *Insect Biochem. Mol. Biol.* 38, 331–345. doi: 10.1016/j.ibmb.2007.11.012

Buckner, E. A., Alto, B. W., and Lounibos, L. P. (2016). Larval temperature-food effects on adult mosquito infection and vertical transmission of dengue-1 virus. *J. Med. Entomol.* 53, 91–98. doi: 10.1093/jme/tjv145

Campbell, C. L., Keene, K. M., Brackney, D. E., Olson, K. E., Blair, C. D., Wilusz, J., et al. (2008). *Aedes aegypti* uses RNA interference in defense against Sindbis virus infection. *BMC Microbiol.* 8:47. doi: 10.1186/1471-2180-8-47

Campbell, L. P., Luther, C., Moo-Llanes, D., Ramsey, J. M., Danis-Lozano, R., and Peterson, A. T. (2015). Climate change influences on global distributions of dengue and chikungunya virus vectors. *Philos. Trans. R. Soc. B Biol. Sci.* 370:20140135. doi: 10.1098/rstb.2014.0135

Carissimo, G., Pondeville, E., McFarlane, M., Dietrich, I., Mitri, C., Bischoff, E., et al. (2014). Antiviral immunity of Anopheles gambiae is highly compartmentalized, with distinct roles for RNA interference and gut microbiota. *Proc. Natl. Acad. Sci. U.S.A.* 112, E176–E185. doi: 10.1073/pnas.1412984112

Carrington, L. B., Armijos, M. V., Lambrechts, L., and Scott, T. W. (2013a). Fluctuations at a low mean temperature accelerate dengue virus transmission by *Aedes aegypti*. *PLoS Negl. Trop. Dis.* 7:e2190. doi: 10.1371/journal.pntd.0002190

Carrington, L. B., Seifert, S. N., Armijos, M. V., Lambrechts, L., and Scott, T. W. (2013b). Reduction of *Aedes aegypti* vector competence for dengue virus under large temperature fluctuations. *Am. J. Trop. Med. Hyg.* 88, 689–697. doi: 10.4269/ajtmh.12-0488

Chauhan, C., Behura, S. K., DeBruyn, B., Lovin, D. D., Harker, B. W., Gomez-Machorro, C., et al. (2012). Comparative expression profiles of midgut genes in dengue virus refractory and susceptible *Aedes aegypti* across critical period for virus infection. *PLoS One* 7:e47350. doi: 10.1371/journal.pone.0047350

Chouin-Carneiro, T., Vega-Rua, A., Vazeille, M., Yebakima, A., Girod, R., Goindin, D., et al. (2016). Differential susceptibilities of *Aedes aegypti* and *Aedes albopictus* from the Americas to Zika Virus. *PLoS Negl. Trop. Dis.* 10:1–11. doi: 10.1371/journal.pntd.0004543

Christensen, B. M., Li, J., Chen, C. C., and Nappi, A. J. (2005). Melanization immune responses in mosquito vectors. *Trends Parasitol.* 21, 192–199. doi: 10.1016/j.pt.2005.02.007

Christofferson, R. C., and Mores, C. N. (2016). Potential for extrinsic incubation temperature to alter interplay between transmission potential and mortality of dengue-infected *Aedes aegypti*. *Environ. Health Insights* 10, 119–123. doi: 10.4137/ehi.s38345

Cirimotich, C. M., Scott, J. C., Phillips, A. T., Geiss, B. J., and Olson, K. E. (2009). Suppression of RNA interference increases alphavirus replication and virus-associated mortality in *Aedes aegypti* mosquitoes. *BMC Microbiol.* 9:49. doi: 10.1186/1471-2180-9-49

Cohen, J. M., Civitello, D. J., Brace, A. J., Feichtinger, E. M., Ortega, C. N., Richardson, J. C., et al. (2016). Spatial scale modulates the strength of ecological processes driving disease distributions. *Proc. Natl. Acad. Sci. U.S.A.* 113, E3359–E3364. doi: 10.1073/pnas.1521657113

Colpitts, T. M., Cox, J., Vanlandingham, D. L., Feitosa, F. M., Cheng, G., Kurscheid, S., et al. (2011). Alterations in the *Aedes aegypti* transcriptome during infection with west nile, dengue and yellow fever viruses. *PLoS Pathog.* 7:e1002189. doi: 10.1371/journal.ppat.1002189

Conesa, A., Madrigal, P., Tarazona, S., Gomez-Cabrero, D., Cervera, A., McPherson, A., et al. (2016). A survey of best practices for RNA-seq data analysis. *Genome Biol.* 17:13. doi: 10.1186/s13059-016-0881-888

Cooper, D. M., Thi, E. P., Chamberlain, C. M., Pio, F., and Lowenberger, C. (2007). Aedes Dronc: a novel ecdysone-inducible caspase in the yellow fever mosquito. *Aedes aegypti*. *Insect Mol. Biol.* 16, 563–572. doi: 10.1111/j.1365-2583.2007.00758.x

Corona, M., Velarde, R. A., Remolina, S., Moran-Lauter, A., Wang, Y., Hughes, K. A., et al. (2007). Vitellogenin, juvenile hormone, insulin signaling, and queen honey bee longevity. *Proc. Natl. Acad. Sci. U.S.A.* 104, 7128–7133. doi: 10.1073/pnas.0701909104

Coutinho-Abreu, I. V., Sharma, N. K., Robles-Murguia, M., and Ramalho-Ortigao, M. (2013). Characterization of Phlebotomus papatasi Peritrophins, and the Role of PpPer1 in Leishmania major Survival in its Natural Vector. *PLoS Negl. Trop. Dis.* 7:e2132. doi: 10.1371/journal.pntd.0002132

Crill, W. D., Huey, R. B., and Gilchrist, G. W. (1996). Within- and Between-Generation Effects of Temperature on the Morphology and Physiology of Drosophila melanogaster. *Evolution.* 50, 1205–1218. doi: 10.2307/2410661

Dillon, M. E., Wang, G., Garrity, P. A., and Huey, R. B. (2009). Review: thermal preference in Drosophila. *J. Therm. Biol.* 34, 109–119. doi: 10.1016/j.jtherbio.2008.11.007

Dimopoulos, G., Richman, A., Müller, H. M., and Kafatos, F. C. (1997). Molecular immune responses of the mosquito Anopheles gambiae to bacteria and malaria parasites. *Proc. Natl. Acad. Sci. U.S.A.* 94, 11508–11513. doi: 10.1073/pnas.94.21.11508

Duggal, N. K., Reisen, W. K., Fang, Y., Newman, R. M., Yang, X., Ebel, G. D., et al. (2015). Genotype-specific variation in West Nile virus dispersal in California. *Virology* 485, 79–85. doi: 10.1016/j.virol.2015.07.004

Eng, M. W., van Zuylen, M. N., and Severson, D. W. (2016). Apoptosis-related genes control autophagy and influence DENV-2 infection in the mosquito vector, *Aedes aegypti*. *Insect Biochem. Mol. Biol.* 76, 70–83. doi: 10.1016/j.ibmb.2016.07.004

Etebari, K., Hegde, S., Saldaña, M. A., Widen, S. G., Wood, T. G., Asgari, S., et al. (2017). Global transcriptome analysis of *Aedes aegypti* mosquitoes in response to Zika Virus Infection. *mSphere* 2:e00456-17. doi: 10.1128/mSphere.00456-417

Evans, M. V., Shiau, J. C., Solano, N., Brindley, M. A., Drake, J. M., and Murdock, C. C. (2018). Carry-over effects of urban larval environments on the transmission potential of dengue-2 virus. *Parasit. Vectors* 11:426. doi: 10.1186/s13071-018-3013-3013

Feder, M. E. (1999). Engineering candidate genes in studies of adaptation: the heat-shock protein Hsp70 in Drosophila melanogaster. *Am. Nat.* 154, S55–S66.

Feder, M. E., and Krebs, R. A. (1998). Natural and genetic engineering of the heat-shock protein Hsp70 in drosophila melanogaster: consequences for thermotolerance. *Am. Zool.* 38, 503–517.

Fischer, H. M., Wheat, C. W., Heckel, D. G., and Vogel, H. (2008). Evolutionary origins of a novel host plant detoxification gene in butterflies. *Mol. Biol. Evol.* 25, 809–820. doi: 10.1093/molbev/msn014

Fluri, P., Wille, H., Gerig, L., and Liischer, M. (1977). Juvenile hormone, vitellogenin and haemocyte composition in winter worker honeybees (Apis mellifera). *Experientia* 33, 1240–1241. doi: 10.1007/BF01922354

Franz, A. W. E., Kantor, A. M., Passarelli, A. L., and Clem, R. J. (2015). Tissue barriers to arbovirus infection in mosquitoes. *Viruses* 7, 3741–3767. doi: 10.3390/v7072795

Garcia, J., Munro, E. S., Monte, M. M., Fourrier, M. C. S., Whitelaw, J., Smail, D. A., et al. (2010). Atlantic salmon (Salmo salar L.) serum vitellogenin neutralises infectivity of infectious pancreatic necrosis virus (IPNV). *Fish Shellfish Immunol.* 29, 293–297. doi: 10.1016/j.fsi.2010.04.010

Girard, Y. A., Mayhew, G. F., Fuchs, J. F., Li, H., Schneider, B. S., McGee, C. E., et al. (2010). Transcriptome Changes in *Culex quinquefasciatus* (Diptera: Culicidae) salivary glands during west nile virus infection. *J. Med. Entomol.* 47, 421–435. doi: 10.1603/me09249

Gloria-Soria, A., Armstrong, P. M., Turner, P. E., and Turner, P. E. (2017). Infection rate of *Aedes aegypti* mosquitoes with dengue virus depends on the interaction between temperature and mosquito genotype. *Proc. R. Soc. B Biol. Sci.* 284:20171506. doi: 10.1098/rspb.2017.1506

Graça-Souza, A. V., Maya-Monteiro, C., Paiva-Silva, G. O., Braz, G. R. C., Paes, M. C., Sorgine, M. H. F., et al. (2006). Adaptations against heme toxicity in blood-feeding arthropods. *Insect Biochem. Mol. Biol.* 36, 322–335. doi: 10.1016/j.ibmb.2006.01.009

Gvoždík, L. (2002). To heat or to save time? Thermoregulation in the lizard *Zootoca vivipara* (Squamata: Lacertidae) in different thermal environments along an altitudinal gradient. *Can. J. Zool.* 80, 479–492. doi: 10.1139/z02-015

Hamel, R., Dejarnac, O., Wichit, S., Ekchariyawat, P., Neyret, A., Luplertlop, N., et al. (2015). Biology of Zika virus infection in human skin cells. *J. Virol.* 89, 8880–8896. doi: 10.1128/jvi.00354-315

Havukainen, H., Münch, D., Baumann, A., Zhong, S., Halskau, Ø, Krogsgaard, M., et al. (2013). Vitellogenin recognizes cell damage through membrane binding and shields living cells from reactive oxygen species. *J. Biol. Chem.* 288, 28369–28381. doi: 10.1074/jbc.M113.465021

Hegde, S., Rasgon, J. L., and Hughes, G. L. (2015). The microbiome modulates arbovirus transmission in mosquitoes. *Curr. Opin. Virol.* 15, 97–102. doi: 10.1016/j.coviro.2015.08.011

Herrera-Ortiz, A., Martínez-Barnetche, J., Smit, N., Rodriguez, M. H., and Lanz-Mendoza, H. (2011). The effect of nitric oxide and hydrogen peroxide in the activation of the systemic immune response of *Anopheles albimanus* infected with *Plasmodium berghei*. *Dev. Comp. Immunol.* 35, 44–50. doi: 10.1016/j.dci.2010.08.004

Hertz, P. E., Fleishman, L. J., and Armsby, C. (1994). The influence of light intensity and temperature on microhabitat selection in two anolis lizards. *Funct. Ecol.* 8, 720–729. doi: 10.2307/2390231

Hillyer, J. F., Schmidt, S. L., and Christensen, B. M. (2003a). Hemocyte-mediated phagocytosis and melanization in the mosquito *Armigeres subalbatus* following immune challenge by bacteria. *Cell Tissue Res.* 313, 117–127. doi: 10.1007/s00441-003-0744-y

Hillyer, J. F., Schmidt, S. L., and Christensen, B. M. (2003b). Rapid phagocytosis and melanization of bacteria and plasmodium sporozoites by hemocytes of the mosquito *Aedes aegypti*. *J. Parasitol.* 89, 62–69.

Huang, C. Y., Christensen, B. M., and Chen, C. C. (2005). Role of dopachrome conversion enzyme in the melanization of filarial worms in mosquitoes. *Insect Mol. Biol.* 14, 675–682. doi: 10.1111/j.1365-2583.2005.00597.x

Huey, R. B. (1991). Physiological consequences of habitat selection. *Am. Nat.* 137, 91–115.

Jaramillo-Gutierrez, G., Rodrigues, J., Ndikuyeze, G., Povelones, M., Molina-Cruz, A., and Barillas-Mury, C. (2009). Mosquito immune responses and compatibility between *Plasmodium parasites* and anopheline mosquitoes. *BMC Microbiol.* 9:154. doi: 10.1186/1471-2180-9-154

Jin, M., Liao, C., Chakrabarty, S., Wu, K., and Xiao, Y. (2019). Comparative proteomics of peritrophic matrix provides an insight into its role in Cry1Ac resistance of cotton bollworm helicoverpa armigera. *Toxins* 11:92. doi: 10.3390/toxins11020092

Johansson, M. A., Arana-Vizcarrondo, N., Biggerstaff, B. J., Gallagher, N., Marano, N., and Staples, J. E. (2012). Assessing the risk of international spread of yellow fever virus: a mathematical analysis of an urban outbreak in Asunción, 2008. *Am. J. Trop. Med. Hyg.* 86, 349–358. doi: 10.4269/ajtmh.2012.11-0432

Johnson, L. R., Ben-Horin, T., Lafferty, K. D., McNally, A., Mordecai, E., Paaijmans, K. P., et al. (2015). Understanding uncertainty in temperature effects on vector-borne disease: a Bayesian approach. *Ecology* 96, 203–213. doi: 10.1890/13-1964.1

Kilpatrick, A. M., Meola, M. A., Moudy, R. M., and Kramer, L. D. (2008). Temperature, viral genetics, and the transmission of West Nile virus by *Culex pipiens* mosquitoes. *PLoS Pathog.* 4:e1000092. doi: 10.1371/journal.ppat.1000092

Kuadkitkan, A., Wikan, N., Fongsaran, C., and Smith, D. R. (2010). Identification and characterization of prohibitin as a receptor protein mediating DENV-2 entry into insect cells. *Virology* 406, 149–161. doi: 10.1016/j.virol.2010.07.015

Kumar, A., Srivastava, P., Sirisena, P. D. N. N., Dubey, S. K., Kumar, R., Shrinet, J., et al. (2018). Mosquito innate immunity. *Insects* 9:E95. doi: 10.3390/insects9030095

Kumar, S., Christophides, G. K., Cantera, R., Charles, B., Han, Y. S., Meister, S., et al. (2003). The role of reactive oxygen species on *Plasmodium melanotic* encapsulation in *Anopheles gambiae*. *Proc. Natl. Acad. Sci. U.S.A.* 100, 14139–14144. doi: 10.1073/pnas.2036262100

Kuraishi, T., Binggeli, O., Opota, O., Buchon, N., and Lemaitre, B. (2011). Genetic evidence for a protective role of the peritrophic matrix against intestinal bacterial infection in *Drosophila melanogaster*. *Proc. Natl. Acad. Sci. U.S.A.* 108, 15966–15971. doi: 10.1073/pnas.1105994108

Kutch, I. C., Sevgili, H., Wittman, T., and Fedorka, K. M. (2014). Thermoregulatory strategy may shape immune investment in *Drosophila melanogaster*. *J. Exp. Biol.* 217, 3664–3669. doi: 10.1242/jeb.106294

Lai, S.-C., Chen, C.-C., and Hou, R. F. (2009). Immunolocalization of prophenoloxidase in the process of wound healing in the mosquito *Armigeres subalbatus* (Diptera: Culicidae). *J. Med. Entomol.* 39, 266–274. doi: 10.1603/0022-2585-39.2.266

Lambrechts, L., Paaijmans, K. P., Fansiri, T., Carrington, L. B., Kramer, L. D., Thomas, M. B., et al. (2011). Impact of daily temperature fluctuations on dengue virus transmission by *Aedes aegypti*. *Proc. Natl. Acad. Sci. U.S.A.* 108, 7460–7465. doi: 10.1073/pnas.1101377108

Lambrechts, L., Quillery, E., Noël, V., Richardson, J. H., Jarman, R. G., Scott, T. W., et al. (2013). Specificity of resistance to dengue virus isolates is associated with genotypes of the mosquito antiviral gene Dicer-2. *Proc. R. Soc. B Biol. Sci.* 280:20122437. doi: 10.1098/rspb.2012.2437

Lanciotti, R. S., Kosoy, O. L., Laven, J. J., Velez, J. O., Lambert, A. J., Johnson, A. J., et al. (2008). Genetic and serologic properties of Zika virus associated with an epidemic. Yap State, Micronesia, 2007. *Emerg. Infect. Dis.* 14, 1232–1239. doi: 10.3201/eid1408.080287

Luckhart, S., Vodovotz, Y., Cui, L., and Rosenberg, R. (1998). The mosquito Anopheles stephensi limits malaria parasite development with inducible synthesis of nitric oxide. *Proc. Natl. Acad. Sci. U.S.A.* 95, 5700–5705.

Maere, S., Heymans, K., and Kuiper, M. (2005). BiNGO: a Cytoscape plugin to assess overrepresentation of Gene Ontology categories in Biological Networks. *Bioinformatics* 21, 3448–3449. doi: 10.1093/bioinformatics/bti551

Mccarthy, F. M., Wang, N., Magee, G. B., Nanduri, B., Lawrence, M. L., Camon, E. B., et al. (2006). AgBase: a functional genomics resource for agriculture. *BMC Genomics* 7:229. doi: 10.1186/1471-2164-7-229

Misslin, R., Telle, O., Daudé, E., Vaguet, A., and Paul, R. E. (2016). Urban climate versus global climate change—what makes the difference for dengue? *Ann. N. Y. Acad. Sci.* 1382, 56–72. doi: 10.1111/nyas.13084

Molina-Cruz, A., DeJong, R. J., Charles, B., Gupta, L., Kumar, S., Jaramillo-Gutierrez, G., et al. (2008). Reactive oxygen species modulate Anopheles gambiae immunity against bacteria and Plasmodium. *J. Biol. Chem.* 283, 3217–3223. doi: 10.1074/jbc.M705873200

Mordecai, E. A., Caldwell, J. M., Grossman, M. K., Lippi, C. A., Johnson, L. R., Neira, M., et al. (2019). Thermal biology of mosquito-borne disease. *Ecol. Lett.* 22, 1690–1708. doi: 10.1111/ele.13335

Mordecai, E. A., Cohen, J. M., Evans, M. V., Gudapati, P., Johnson, L. R., Lippi, C. A., et al. (2017). Detecting the impact of temperature on transmission of Zika, dengue, and chikungunya using mechanistic models. *PLoS Negl. Trop. Dis.* 11:e0005568. doi: 10.1371/journal.pntd.0005568

Mordecai, E. A., Paaijmans, K. P., Johnson, L. R., Balzer, C., Ben-Horin, T., de Moor, E., et al. (2013). Optimal temperature for malaria transmission is dramatically lower than previously predicted. *Ecol. Lett.* 16, 22–30. doi: 10.1111/ele.12015

Morlais, I., Mori, A., Schneider, J. R., and Severson, D. W. (2003). A targeted approach to the identification of candidate genes determining susceptibility to Plasmodium gallinaceum in *Aedes aegypti*. *Mol. Genet. Genomics* 269, 753–764. doi: 10.1007/s00438-003-0882-887

Murdock, C. C., Blanford, S., Hughes, G. L., Rasgon, J. L., and Thomas, M. B. (2014). Temperature alters Plasmodium blocking by Wolbachia. *Sci. Rep.* 4:3932. doi: 10.1038/srep03932

Murdock, C. C., Cox-foster, D., Read, A. F., and Thomas, M. B. (2012a). Rethinking vector immunology: the role of environmental temperature in shaping resistance. *Nat. Rev. Microbiol.* 10, 869–876. doi: 10.1038/nrmicro2900

Murdock, C. C., Paaijmans, K. P., Bells, A. S., King, J. G., Hillyer, J. F., Read, A. F., et al. (2012b). Complex effects of temperature on mosquito immune function. *Proc. R. Soc. B Biol. Sci.* 279, 3357–3366. doi: 10.1098/rspb.2012.0638

Murdock, C. C., Evans, M. V., McClanahan, T. D., Miazgowicz, K. L., and Tesla, B. (2017). Fine-scale variation in microclimate across an urban landscape shapes variation in mosquito population dynamics and the potential of *Aedes albopictus* to transmit arboviral disease. *PLoS Negl. Trop. Dis.* 11:e5640. doi: 10.1371/journal.pntd.0005640

Murdock, C. C., Moller-Jacobs, L. L., and Thomas, M. B. (2013). Complex environmental drivers of immunity and resistance in malaria mosquitoes. *Proc. R. Soc. B* 280:20132030. doi: 10.1098/rspb.2013.2030

Muturi, E. J., and Alto, B. W. (2011). Larval environmental temperature and insecticide exposure alter *Aedes aegypti* competence for arboviruses. *Vector-Borne Zoonotic Dis.* 11, 1157–1163. doi: 10.1089/vbz.2010.0209

Muturi, E. J., Kim, C. H., Alto, B. W., Berenbaum, M. R., and Schuler, M. A. (2011a). Larval environmental stress alters *Aedes aegypti* competence for Sindbis virus. *Trop. Med. Int. Heal.* 16, 955–964. doi: 10.1111/j.1365-3156.2011.02796.x

Muturi, E. J., Lampman, R., Costanzo, K., and Alto, B. W. (2011b). Effect of temperature and insecticide stress on life-history traits of *Culex restuans* and *Aedes albopictus* (Diptera: Culicidae). *J. Med. Entomol.* 48, 243–250. doi: 10.1603/me10017

Neill, K. O., Huang, N., Unis, D., and Clem, R. J. (2015). Rapid selection against arbovirus-induced apoptosis during infection of a mosquito vector. *Proc. Natl. Acad. Sci. U.S.A.* 112, E1152–E1161. doi: 10.1073/pnas.1424469112

Okech, B. A., Gouagna, L. C., Yan, G., Githure, J. I., and Beier, J. C. (2007). Larval habitats of *Anopheles gambiae* s.s. (Diptera: Culicidae) influences vector competence to *Plasmodium falciparum* parasites. *Malar. J.* 6:50. doi: 10.1186/1475-2875-6-50

Oliveira, G., de, A., Lieberman, J., and Barillas-Mury, C. (2012). Epithelial Nitration by a Peroxidase/NOX5 System Mediates Mosquito Antiplasmodial Immunity. *Science* 335, 856–859. doi: 10.1126/science.1209678

Oliveira, J. H. M., Gonçalves, R. L. S., Lara, F. A., Dias, F. A., Gandara, A. C. P., Menna-Barreto, R. F. S., et al. (2011). Blood meal-derived heme decreases ROS levels in the midgut of *Aedes aegypti* and allows proliferation of intestinal microbiota. *PLoS Pathog.* 7:e1001320. doi: 10.1371/journal.ppat.1001320

Pan, X., Zhou, G., Wu, J., Bian, G., Lu, P., Raikhel, A. S., et al. (2012). Wolbachia induces reactive oxygen species (ROS)-dependent activation of the Toll pathway to control dengue virus in the mosquito *Aedes aegypti*. *Proc. Natl. Acad. Sci. U.S.A.* 109, E23–E31. doi: 10.1073/pnas.1116932108

Parham, P. E., and Michael, E. (2010). Modeling the effects of weather and climate change on malaria transmission. *Environ. Health Perspect.* 118, 620–626. doi: 10.1289/ehp.0901256

Parham, P. E., Waldock, J., Christophides, G. K., Hemming, D., Agusto, F., Evans, K. J., et al. (2015). Climate, environmental and socio-economic change: weighing up the balance in vector-borne disease transmission. *Philos. Trans. R. Soc. B Biol. Sci.* 370:20130551. doi: 10.1098/rstb.2013.0551

Ramirez, J. L., Souza-Neto, J., Cosme, R. T., Rovira, J., Ortiz, A., Pascale, J. M., et al. (2012). Reciprocal tripartite interactions between the *Aedes aegypti* midgut microbiota, innate immune system and dengue virus influences vector competence. *PLoS Negl. Trop. Dis.* 6:e1561. doi: 10.1371/journal.pntd.0001561

Rodgers, F. H., Gendrin, M., Wyer, C. A. S., and Christophides, G. K. (2017). Microbiota-induced peritrophic matrix regulates midgut homeostasis and prevents systemic infection of malaria vector mosquitoes. *PLoS Pathog.* 13:e1006391. doi: 10.1371/journal.ppat.1006391

Rodriguez-Andres, J., Rani, S., Varjak, M., Chase-Topping, M. E., Beck, M. H., Ferguson, M. C., et al. (2012). Phenoloxidase activity acts as a mosquito innate immune response against infection with semliki Forest Virus. *PLoS Pathog.* 8:e1002977. doi: 10.1371/journal.ppat.1002977

Ryan, S. J., Carlson, C. J., Mordecai, E. A., and Johnson, L. R. (2018). Global expansion and redistribution of Aedes-borne virus transmission risk with climate change. *PLoS Negl. Trop. Dis.* 13:e7213. doi: 10.1371/journal.pntd.0007213

Ryan, S. J., Mcnally, A., Johnson, L. R., Mordecai, E. A., Ben-Horin, T., Paaijmans, K., et al. (2015). Mapping physiological suitability limits for malaria in Africa under climate change. *Vector-Borne Zoonotic Dis.* 15, 718–725. doi: 10.1089/vbz.2015.1822

Saldaña, M. A., Etebari, K., Hart, C. E., Widen, S. G., Wood, T. G., Thangamani, S., et al. (2017a). Zika virus alters the microRNA expression profile and elicits an RNAi response in *Aedes aegypti* mosquitoes. *PLoS Negl. Trop. Dis.* 11:e0005760. doi: 10.1371/journal.pntd.0005760

Saldaña, M. A., Hegde, S., and Hughes, G. L. (2017b). Microbial control of arthropod-borne disease. *Mem. Inst. Oswaldo Cruz* 112, 81–93. doi: 10.1590/0074-02760160373

Sánchez-Vargas, I., Scott, J. C., Poole-Smith, B. K., Franz, A. W. E., Barbosa-Solomieu, V., Wilusz, J., et al. (2009). Dengue virus type 2 infections of *Aedes aegypti* are modulated by the mosquito's RNA interference pathway. *PLoS Pathog.* 5:e1000299. doi: 10.1371/journal.ppat.1000299

Sanders, H. R., Evans, A. M., Ross, L. S., and Gill, S. S. (2003). Blood meal induces global changes in midgut gene expression in the disease vector, *Aedes aegypti*. *Insect Biochem. Mol. Biol.* 33, 1105–1122. doi: 10.1016/S0965-1748(03)00124-3

Sanders, H. R., Foy, B. D., Evans, A. M., Ross, L. S., Beaty, B. J., Olson, K. E., et al. (2005). Sindbis virus induces transport processes and alters expression of innate immunity pathway genes in the midgut of the disease vector, *Aedes aegypti*. *Insect Biochem. Mol. Biol.* 35, 1293–1307. doi: 10.1016/j.ibmb.2005.07.006

Santamaría, M. E., González-Cabrera, J., Martínez, M., Grbic, V., Castañera, P., Díaz, I., et al. (2015). Digestive proteases in bodies and faeces of the two-spotted spider mite, *Tetranychus urticae*. *J. Insect Physiol.* 78, 69–77. doi: 10.1016/j.jinsphys.2015.05.002

Saraiva, R. G., Kang, S., Simões, M. L., Angleró-Rodríguez, Y. I., and Dimopoulos, G. (2016). Mosquito gut antiparasitic and antiviral immunity. *Dev. Comp. Immunol.* 64, 53–64. doi: 10.1016/j.dci.2016.01.015

Seehuus, S.-C., Norberg, K., Gimsa, U., Krekling, T., and Amdam, G. V. (2006). Reproductive protein protects functionally sterile honey bee workers from oxidative stress. *PNAS* 103, 962–967. doi: 10.1073/pnas.0502681103

Shaw, W. R., and Catteruccia, F. (2019). Vector biology meets disease control: using basic research to fight vector-borne diseases. *Nat. Microbiol.* 4, 20–34. doi: 10.1038/s41564-018-0214-7

Shibata, T., Maki, K., Hadano, J., Fujikawa, T., Kitazaki, K., Koshiba, T., et al. (2015). Crosslinking of a peritrophic matrix protein protects gut epithelia from bacterial exotoxins. *PLoS Pathog.* 11:e5244. doi: 10.1371/journal.ppat.1005244

Shocket, M. S., Ryan, S. J., and Mordecai, E. A. (2018). Temperature explains broad patterns of Ross River virus transmission. *eLife* 7:e37762. doi: 10.7554/eLife.37762

Shragai, T., Tesla, B., Murdock, C., and Harrington, L. C. (2017). Zika and chikungunya: mosquito-borne viruses in a changing

world. *Ann. N. Y. Acad. Sci.* 1399, 61–77. doi: 10.1111/nyas.13306

Sim, S., and Dimopoulos, G. (2010). Dengue virus inhibits immune responses in *Aedes aegypti* cells. *PLoS One* 5:e10678. doi: 10.1371/journal.pone.0010678

Simões, M. L., Caragata, E. P., and Dimopoulos, G. (2018). Diverse host and restriction factors regulate mosquito–pathogen interactions. *Trends Parasitol.* 34, 603–616. doi: 10.1016/j.pt.2018.04.011

Siraj, A. S., Rodriguez-Barraquer, I., Barker, C. M., Tejedor-Garavito, N., Harding, D., Lorton, C., et al. (2018). Spatiotemporal incidence of Zika and associated environmental drivers for the 2015-2016 epidemic in Colombia Amir. *Sci. Data.* 5:180073. doi: 10.1038/sdata.2018.73

Siraj, A. S., Santos-Vega, M., Bouma, M. J., Yadeta, D., Ruiz Carrascal, D., and Pascual, M. (2014). Altitudinal changes in malaria incidence in highlands of Ethiopia and Colombia. *Science* 343, 1154–1158. doi: 10.1126/science.1244325

Souza-Neto, J. A., Sim, S., and Dimopoulos, G. (2009). An evolutionary conserved function of the JAK-STAT pathway in anti-dengue defense. *Proc. Natl. Acad. Sci. U.S.A.* 106, 17841–17846. doi: 10.1073/pnas.0905006106

Suwanchaichinda, C., and Paskewitz, S. M. (1998). Effects of larval nutrition, adult body size, and adult temperature on the ability of *Anopheles gambiae* (Diptera: Culicidae) to Melanize Sephadex beads. *J. Med. Entomol.* 35, 157–161.

Szklarczyk, D., Morris, J. H., Cook, H., Kuhn, M., Wyder, S., Simonovic, M., et al. (2017). The STRING database in 2017: quality-controlled protein – protein association networks, made broadly accessible. *Nucleic Acids Res.* 45, 362–368. doi: 10.1093/nar/gkw937

Taguwa, S., Maringer, K., Li, X., Bernal-Rubio, D., Rauch, J. N., Gestwicki, J. E., et al. (2015). Defining Hsp70 subnetworks in dengue virus replication reveals key vulnerability in flavivirus infection. *Cell* 163, 1108–1123. doi: 10.1016/j.cell.2015.10.046

Tchankouo-Nguetcheu, S., Khun, H., Pincet, L., Roux, P., Bahut, M., Huerre, M., et al. (2010). Differential protein modulation in midguts of *Aedes aegypti* infected with chikungunya and dengue 2 viruses. *PLoS One* 5:e13149. doi: 10.1371/journal.pone.0013149

R Development Core Team (2008). *R: A Language and Environment for Statistical Computing*. Vienna: R Foundation Statics Computing, doi: 10.1007/978-3-540-74686-7

Tesla, B., Demakovsky, L. R., Mordecai, E. A., Ryan, S. J., Bonds, M. H., Ngonghala, C. N., et al. (2018a). Temperature drives Zika virus transmission: evidence from empirical and mathematical models. *Proc. R. Soc. B Biol. Sci.* 285:20180795. doi: 10.1098/rspb.2018.0795

Tesla, B., Demakovsky, L. R., Packiam, H. S., Mordecai, E. A., Rodríguez, A. D., Bonds, M. H., et al. (2018b). Estimating the effects of variation in viremia on mosquito susceptibility, infectiousness, and R0 of Zika in *Aedes aegypti*. *PLoS Negl. Trop. Dis.* 12:e0006733. doi: 10.1371/journal.pntd.0006733

Trapnell, C., Pachter, L., and Salzberg, S. L. (2009). TopHat: discovering splice junctions with RNA-Seq. *Bioinformatics* 25, 1105–1111. doi: 10.1093/bioinformatics/btp120

Trapnell, C., Roberts, A., Goff, L., Pertea, G., Kim, D., Kelley, D. R., et al. (2013). Differential gene and transcript expression analysis of RNA-seq experiments with TopHat and Cufflinks. *Nat. Protoc.* 7, 562–578. doi: 10.1038/nprot.2012.016

Vazeille, M., Madec, Y., Mousson, L., Bellone, R., Barré-Cardi, H., Sousa, C. A., et al. (2019). Zika virus threshold determines transmission by European *Aedes albopictus* mosquitoes. *Emerg. Microbes Infect.* 8, 1668–1678. doi: 10.1080/22221751.2019.1689797

Wang, H., Gort, T., Boyle, D. L., and Clem, R. J. (2012). Effects of manipulating apoptosis on sindbis virus infection of *Aedes aegypti* mosquitoes. *J. Virol.* 86, 6546–6554. doi: 10.1128/jvi.00125-12

Wang, P., and Granados, R. R. (2000). Calcofluor disrupts the midgut defense system in insects. *Insect Biochem. Mol. Biol.* 30, 135–143. doi: 10.1016/S0965-1748(99)00108-3

Wang, P., Li, G., and Granados, R. R. (2004). Identification of two new peritrophic membrane proteins from larval *Trichoplusia ni*: structural characteristics and their functions in the protease rich insect gut. *Insect Biochem. Mol. Biol.* 34, 215–227. doi: 10.1016/j.ibmb.2003.10.001

Watts, D. M., Burke, D. S., Harrison, B. A., Whitmire, R. E., and Nisalak, A. (1987). Effect of Temperature on the Vector Efficiency of *Aedes aegypti* for Dengue 2 Virus. *Am. J. Trop. Med. Hyg.* 36, 143–152.

Weiss, B. L., Savage, A. F., Griffith, B. C., Wu, Y., and Aksoy, S. (2014). The peritrophic matrix mediates differential infection outcomes in the tsetse fly gut following challenge with commensal, pathogenic, and parasitic microbes. *J. Immunol.* 193, 773–782. doi: 10.4049/jimmunol.1400163

Wilke, A. B. B., and Marrelli, M. T. (2015). Paratransgenesis: a promising new strategy for mosquito vector control. *Parasit. Vectors* 8:342. doi: 10.1186/s13071-015-0959-2

Willard, K. A., Demakovsky, L., Tesla, B., Goodfellow, F. T., Stice, S. L., Murdock, C. C., et al. (2017). Zika virus exhibits lineage-specific phenotypes in cell culture, in *Aedes aegypti* mosquitoes, and in an embryo model. *Viruses* 9:E383. doi: 10.3390/v9120383

Willard, K. A., Elling, C. L., Stice, S. L., and Brindley, M. A. (2019). The oxysterol 7-ketocholesterol reduces zika virus titers in vero cells and human neurons. *Viruses* 11, 1–17. doi: 10.3390/v11010020

Wong, Z. S., Brownlie, J. C., and Johnson, K. N. (2015). Oxidative stress correlates with Wolbachia-mediated antiviral protection in Wolbachia-Drosophila associations. *Appl. Environ. Microbiol.* 81, 3001–3005. doi: 10.1128/AEM.03847-14

Xi, Z., Ramirez, J. L., and Dimopoulos, G. (2008). The *Aedes aegypti* toll pathway controls dengue virus infection. *PLoS Pathog.* 4:e1000098. doi: 10.1371/journal.ppat.1000098

Xiao, F. Z., Zhang, Y., Deng, Y. Q., He, S., Xie, H. G., Zhou, X. N., et al. (2014). The effect of temperature on the extrinsic incubation period and infection rate of dengue virus serotype 2 infection in *Aedes albopictus*. *Arch. Virol.* 159, 3053–3057. doi: 10.1007/s00705-014-2051-1

Yen, P.-S., James, A., Li, J.-C., Chen, C.-H., and Failloux, A.-B. (2018). Synthetic miRNAs induce dual arboviral-resistance phenotypes in the vector mosquito *Aedes aegypti*. *Commun. Biol.* 1:11. doi: 10.1038/s42003-017-0011-5

Yu, X. Q., and Kanost, M. R. (2000). Immulectin-2, a lipopolysaccharide-specific lectin from an insect, *Manduca sexta*, is induced in response to Gram-negative bacteria. *J. Biol. Chem.* 275, 37373–37381. doi: 10.1074/jbc.M003021200

Zouache, K., Fontaine, A., Vega-Rua, A., Mousson, L., Thiberge, J. M., Lourenco-De-Oliveira, R., et al. (2014). Three-way interactions between mosquito population, viral strain and temperature underlying chikungunya virus transmission potential. *Proc. R. Soc. B Biol. Sci.* 281:20141078. doi: 10.1098/rspb.2014.1078

Conflict of Interest: The authors declare that the research was conducted in the absence of any commercial or financial relationships that could be construed as a potential conflict of interest.

Copyright © 2020 Ferreira, Tesla, Horácio, Nahum, Brindley, de Oliveira Mendes and Murdock. This is an open-access article distributed under the terms of the Creative Commons Attribution License (CC BY). The use, distribution or reproduction in other forums is permitted, provided the original author(s) and the copyright owner(s) are credited and that the original publication in this journal is cited, in accordance with accepted academic practice. No use, distribution or reproduction is permitted which does not comply with these terms.

frontiers in Microbiology

REVIEW
published: 26 June 2020
doi: 10.3389/fmicb.2020.01297

Chikungunya Virus: An Emergent Arbovirus to the South American Continent and a Continuous Threat to the World

*Marcela S. Cunha†, Pedro A. G. Costa†, Isadora Alonso Correa, Marcos R. M. de Souza, Pedro Teles Calil, Gustavo P. Duarte da Silva, Sara Mesquita Costa, Vinícius Wakoff P. Fonseca and Luciana J. da Costa**

Departamento de Virologia, Instituto de Microbiologia Paulo de Góes, Universidade Federal do Rio de Janeiro, Rio de Janeiro, Brazil

OPEN ACCESS

Edited by:
Akio Adachi, Kansai Medical University, Japan

Reviewed by:
Emi E. Nakayama, Osaka University, Japan
Melinda Ann Brindley, University of Georgia, United States

***Correspondence:**
Luciana J. da Costa
ljcosta@micro.ufrj.br

† These authors have contributed equally to this work

Specialty section:
This article was submitted to Virology, a section of the journal Frontiers in Microbiology

Received: *06 February 2020*
Accepted: *20 May 2020*
Published: *26 June 2020*

Citation:
Cunha MS, Costa PAG, Correa IA, de Souza MRM, Calil PT, da Silva GPD, Costa SM, Fonseca VWP and da Costa LJ (2020) Chikungunya Virus: An Emergent Arbovirus to the South American Continent and a Continuous Threat to the World. Front. Microbiol. 11:1297. doi: 10.3389/fmicb.2020.01297

Chikungunya virus (CHIKV) is an arthropod-borne virus (arbovirus) of epidemic concern, transmitted by *Aedes* ssp. mosquitoes, and is the etiologic agent of a febrile and incapacitating arthritogenic illness responsible for millions of human cases worldwide. After major outbreaks starting in 2004, CHIKV spread to subtropical areas and western hemisphere coming from sub-Saharan Africa, South East Asia, and the Indian subcontinent. Even though CHIKV disease is self-limiting and non-lethal, more than 30% of the infected individuals will develop chronic disease with persistent severe joint pain, tenosynovitis, and incapacitating polyarthralgia that can last for months to years, negatively impacting an individual's quality of life and socioeconomic productivity. The lack of specific drugs or licensed vaccines to treat or prevent CHIKV disease associated with the global presence of the mosquito vector in tropical and temperate areas, representing a possibility for CHIKV to continually spread to different territories, make this virus an agent of public health burden. In South America, where Dengue virus is endemic and Zika virus was recently introduced, the impact of the expansion of CHIKV infections, and co-infection with other arboviruses, still needs to be estimated. In Brazil, the recent spread of the East/Central/South Africa (ECSA) and Asian genotypes of CHIKV was accompanied by a high morbidity rate and acute cases of abnormal disease presentation and severe neuropathies, which is an atypical outcome for this infection. In this review, we will discuss what is currently known about CHIKV epidemics, clinical manifestations of the human disease, the basic concepts and recent findings in the mechanisms underlying virus-host interaction, and CHIKV-induced chronic disease for both *in vitro* and *in vivo* models of infection. We aim to stimulate scientific debate on how the characterization of replication, host-cell interactions, and the pathogenic potential of the new epidemic viral strains can contribute as potential developments in the virology field and shed light on strategies for disease control.

Keywords: Chikungunya virus, emergent arbovirus, virus–cell interaction, pathogenesis, epidemiology

INTRODUCTION

The Chikungunya virus (CHIKV) is an arthropod-borne virus (arbovirus) globally distributed to the tropical areas that has recently spread to subtropical areas and the western hemisphere. CHIKV is an arthritogenic virus belonging to the family *Togaviridae*, genus *Alphavirus*, and is the etiological agent of the acute febrile illness Chikungunya fever (CHIKF) that caused millions of human cases since major outbreaks starting in 2004 (Sharp et al., 2014). This disease was named after the Makonde (Kimakonde) language from the south of Tanzania, which means "to bend over," referring to the posture assumed by individuals that display the most severe forms of the disease with extreme and incapacitating joint pain. Although CHIKV infection is associated with low mortality rates, it imposes severe morbidity to the acute-infected individuals. The debilitating joint pain can persist for several months to years as a clinical outcome known as "post-chikungunya chronic polyarthralgia" (pCHIKV-CPA), which deeply affects the patient's quality of life (Consuegra-Rodríguez et al., 2018). Since 2004, substantial urban outbreaks of CHIKV infection have occurred throughout the tropical and subtropical regions of the world, particularly in geographical areas inhabited by the vectors *Aedes* spp. mosquitoes (Petersen and Powers, 2016). More recently, CHIKV outbreaks occurred in Africa, Asia, Europe, the Americas, and the Pacific islands (Petersen and Powers, 2016). This unprecedented spread of CHIKV infections was accompanied by high morbidity, several cases of neuropathies, and atypical disease presentations, making CHIKV a major global health threat. Facing this scenario, the characterization of the infectious and pathogenic potential of the actual circulating virus isolates will help to understand and, more effectively, control the disease.

The first isolation of CHIKV, and the report of an epidemic, occurred in 1952/53 in Tanganyika Province, actual Tanzania, with the infected individual presenting disabling joint pains, severe fever, and eventually rash (Lumsden, 1955; Ross, 1956). The bite of infected female mosquitoes transmits the virus, and its circulation could be related to two different cycles of transmission: (1) a sylvatic cycle where enzootic transmissions between non-human primates and *Aedes* spp. mosquitoes, such as *Ae.* (Diceromyia) *furcifer*, *Ae.* (Diceromyia) *taylori, Ae.* (Stegomyia) *luteocephalus*, *Ae.* (Stegomyia) *africanus,* and *Ae.* (Stegomyia) *neoafricanus*, which occasionally spilled over to humans; (2) an urban cycle where humans and *Ae. aegypti* and *Ae. albopictus* are involved. The importance of the sylvatic cycle could be highlighted in a recent study that detected the virus in non-human primates from Malaysia and revealed a high similarity between human and non-human primate sequences of CHIKV. Thus, these monkeys maybe both hosts and reservoirs for CHIKV (Suhana et al., 2019). In addition, CHIKV has been detected in other zoophilic mosquitoes *Ae. dalzieli*, *Ae. argenteopunctatus*, *Cx. ethiopicus*, and *An. rufipes* suggesting that other species may participate in a secondary sylvatic cycle (Diallo et al., 1999).

Phylogenetic studies show that CHIKV originated from Africa, although the specific region where the virus evolved could not be pinpointed, and subsequently spread to Asia. These studies also classify viral isolates into three main lineages: the enzootics East/Central/South African (ECSA), West African, and the endemic/epidemic Asian strains. The Asian lineage could be sub-divided into two clades: the Indian clade, which was extinct, and the Southeast Asian lineage that continues to circulate (Powers et al., 2000; Volk et al., 2010). The recent epidemic that affected La Réunion Island and other islands from Indian Ocean revealed a new strain derived from the ECSA group, which was named the India Ocean lineage (IOL) (Njenga et al., 2008). The distribution of CHIKV genotypes worldwide is represented in **Figure 1A**.

Mutations in the viral genome impact at viral propagation and adaptation of these lineages in different vectors. *Ae. aegypti* and *Ae. albopictus* mosquitoes are the main vectors in the urban cycle of CHIKV transmission. Studies showed that genomic differences amongst circulating CHIKV accounted for its transmission from each of these vectors. For instance, the presence of the A226V variant on the envelope (E1) gene of CHIKV was related to an increase in viral infectivity, dissemination, and transmission in *Ae. albopictus*, resulting in the wide spread of the virus (Tsetsarkin et al., 2007). This mutation did not confer any advantage to transmission in *Ae. aegypti*. Followed by the selection of A226V, adaptation substitutions L210Q and K252Q (E2 protein) that arose independently in the IOL strain in India are associated with a greater increase of CHIKV dissemination in *Ae. albobictus* vector (Tsetsarkin and Weaver, 2011; Tsetsarkin et al., 2014). Still, variants K211E, in the E1 gene, and V264A, in the envelope (E2) gene, lead to an increase in viral dissemination and transmission for *Ae. aegypti* but not for *Ae. Albopictus* (Agarwal et al., 2016). Moreover, the T98A variant in E1 enhances the vector-adaptability effect of A226V, since epistatic interactions between E1-98T and E1-A226V are restrictive (Tsetsarkin et al., 2011). In another study, variant G60D in the E2 increased CHIKV infectivity in *Ae. albopictus* in the presence of either alanine or valine at position 226 in E1 protein. This change also increases infectivity in *Ae. aegypti*. The E2 variant, I211T, increases the CHIKV infectivity exclusively for *Ae. albopictus* but only when associated with A226V change. I211T variant could be related to the maintenance of CHIKV in the enzootic Africa cycle since it was detected in most sequences from the ECSA clade obtained before 2005 (Tsetsarkin et al., 2009). Mutations occurring at the 3′-UTR could also contribute to vector adaptability, since a 177 nt duplication found in the Caribbean strain of CHIKV and confirmed in sequences from Mexico, Trinidad, and the Dominican Republic, conferred a growth advantage in insect cell cultures to viruses harboring this duplication over the Asian strain and other Caribbean strains lacking the duplication (Stapleford et al., 2016). The most relevant variants, as well as their impact on each vector and in virus infectivity, are summarized in **Table 1**.

Mainly during the 1960s and 1970, epidemics of CHIKV were restricted to Africa and Southeast Asia, in countries like South Africa, Democratic Republic of Congo, Uganda, Indonesia, Thailand, and India. However, this scenario started to change in 2004 with reports of an outbreak in Lamu, Kenya, beginning in May and reaching its peak in July, with an estimated 75% of the island's population affected (Sergon et al., 2008). The disease then

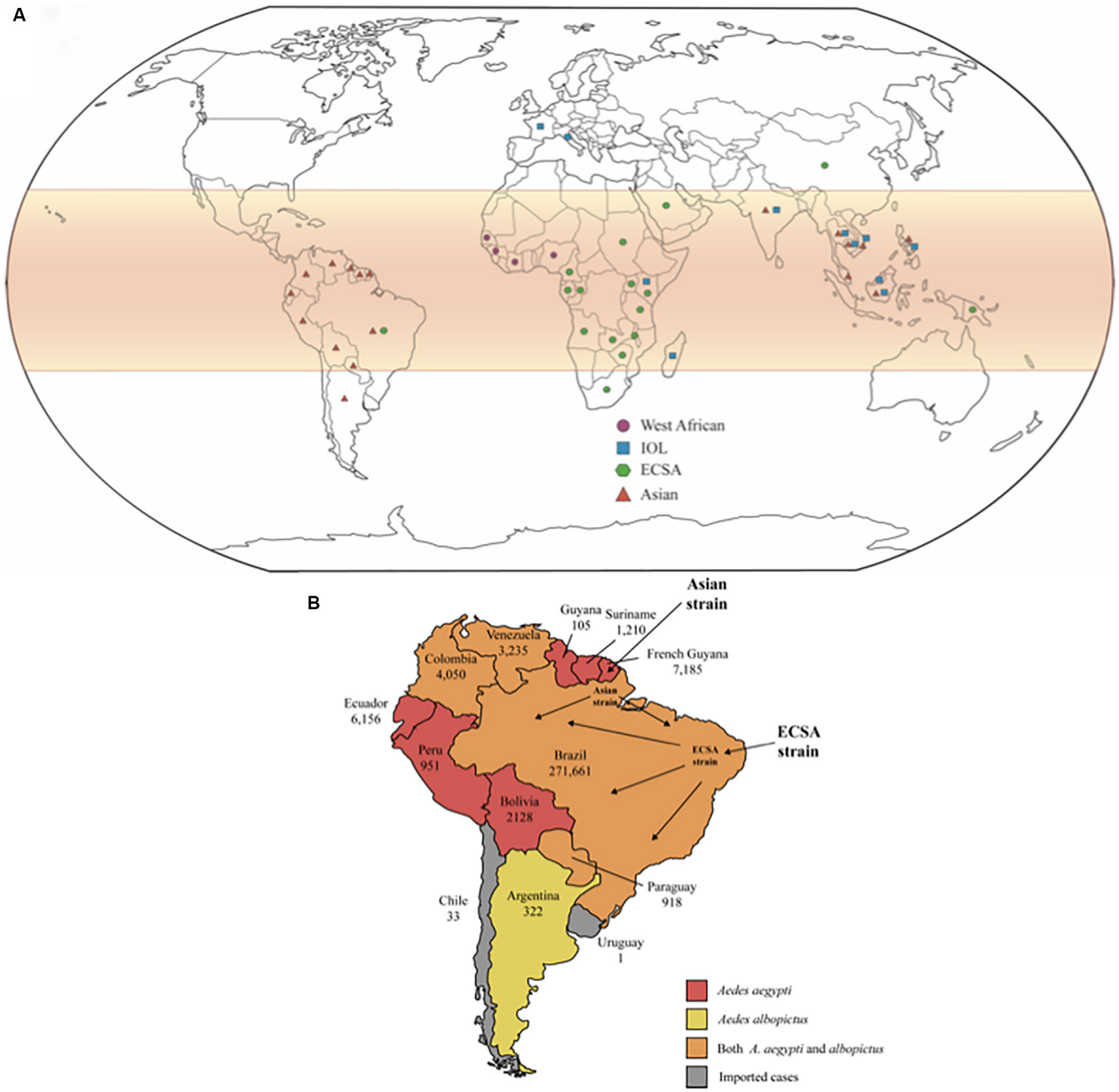

FIGURE 1 | (A) Global distribution of CHIKV lineages. CHIKV infections are more likely to occur in tropical and sub-tropical regions of the globe, highlighted in red on the map. The geometric forms represent the different lineages of CHIKV that are currently in circulation. **(B)** The number of confirmed cases is shown for each country individually. There is not autochthonous transmission reported in Chile and Uruguay, only imported cases. The Asian strain first reached South America by French Guyana, but ECSA strain has arrived by northeast Brazil and got predominated in Brazil. The colors represent the circulation of Aedes aegypti and albopictus in each country, as indicated in the subtitle.

spread through Mombasa and the Comoros islands. Other islands from the Indian Ocean were affected, including La Réunion Islands where, between March 2005 and April 2016, 244,000 cases were reported (Renault et al., 2007).

The variant E1-A226V on the viral envelope glycoprotein was detected for the first time in viruses that circulated during the La Reunion epidemic (Tsetsarkin and Weaver, 2011). This adaptation of CHIKV to *Ae. albopictus* allowed that regions of the planet such as Italy (during July and August 2007) (Fadila and Failloux, 2006; Rezza et al., 2007) and France (during 2010 and 2014) (Grandadam et al., 2011; Delisle et al., 2015), that never had reported CHIKF cases, experienced the occurrence of CHIKV disease.

The CHIKV adaptation to *Aedes albopictus* has constantly been associated to spread of CHIKF to new areas of the globe. In fact, full-length viral sequences unraveled unique adaptive variants in, at least, three occasions, that conferred selective advantage for CHIKV transmission by *Ae. albopictus*

TABLE 1 | CHIKV variants associated with vector adaptability.

Variant	Gene	Function	References
A226V	E1	Increased infectivity, transmission, and dissemination in *Ae. Albopictus*	Schuffenecker et al., 2006; Tsetsarkin et al., 2007
T98A	E1	Enhanced vector adaptability of A226V	Tsetsarkin et al., 2011
K211E	E1	Epistatic effect – Increased dissemination in *Ae. Aegypti*	Agarwal et al., 2016
V264A	E2		
L210Q	E2	Enhanced disseminated infection in *Ae. albopictus* and fitness increment of A226V variant	Tsetsarkin and Weaver, 2011; Tsetsarkin et al., 2014
K252Q	E2	Enhanced disseminated infection in *Ae. albopictus* and fitness increment of A226V variant	Tsetsarkin and Weaver, 2011; Tsetsarkin et al., 2014
I211T	E2	Increased infectivity in *Ae. albopictus* when associated with A226V	Tsetsarkin et al., 2009
G60D	E2	Increased infectivity in *Ae. aegypti* and *albopictus*	Tsetsarkin et al., 2009
177 nt insertion	3′ UTR	Increased viral replication in insect cell culture	Stapleford et al., 2016

(Tsetsarkin et al., 2007; Beesoon et al., 2008; De Lamballerie et al., 2008; Dubrulle et al., 2009; Severini et al., 2018).

EPIDEMIOLOGY OF CHIKV ON THE SOUTH AMERICAN CONTINENT

In 2013, the American continent reported the first cases of autochthonous transmission of CHIKV on the island of Saint Martin and Martinique Islands. In January 2014, CHIKV transmissions occurred in several Caribbean islands, including Dominica, Anguilla, British Virgin Islands, Saint Barthelemy, Guadeloupe, the Federation of St. Kitts and Nevis, Dominican Republic; and Saint Vincent and the Grenadines. The number of infected people overcame 30,000 cases in 4 months. It is interesting to note that at these sites, only *Ae. aegypti* mosquitoes were the circulating vectors (Nasci, 2014; Leparc-Goffart et al., 2014), indicating that different from the explosion of CHIKV infections in La Reunion related to viral adaptation to another mosquitoes vector, other factors contributed to the introduction and spread of CHIKV in the American continent. Lanciotti and Valadere demonstrated that the strain of CHIKV circulating in the Caribbean Islands belongs to Asian genotype and is closely related to strains circulating in Indonesia (2007), China (2012), Yap Islands (2013), and Philippines (2013) (Lanciotti and Valadere, 2014).

In February 2014, CHIKV had already reached continental territory, when autochthonous infections were observed in French Guiana, the first country in South America to declare CHIKV infection. At this point, the dispersion of CHIKV to other American countries was only a matter of time. From 2014 to 2015, more than 16,000 individuals were infected in French Guiana. Importantly, infections presented several atypical cases, such as neurological disorders, cardio-respiratory failure, acute hepatitis, acute pancreatitis, renal disorders, and muscular impairment. Only two deaths associated with CHIKF during this period were documented (Bonifay et al., 2018; **Figure 1B**).

CHIKV cases arose in Venezuela in June 2014, from recent travelers from the Dominican Republic or Haiti, and in July 2014, autochthonous transmissions were reported. Phylogenetic analysis showed that the CHIKV circulating in Venezuela clustered to the Asian genotype (Caribbean clade) and did not harbor the main substitutions associated with *Ae. albopictus* viral adaptation (Camacho et al., 2017).

Ecuador was another country that early confirmed community transmission of CHIKV. Berry et al. (2020) showed that CHIKV was introduced into Ecuador at multiple time points in 2013–2014, and these introductions were all associated with the Caribbean islands, despite the increasing influx of Venezuelan citizens. From 2014 to 2017, Ecuador reported 35,714 CHIKF cases. The transmission for two or more years after the 2015 epidemic peak suggests that CHIKV has become endemic in this country. The CHIKF outbreaks in Ecuador were associated with the Asian strain which harbors the E1:A98T and E1:K211E amino acid changes. Since *Ae. aegypti* is the main mosquito vector in Ecuador this data indicates that CHIKV had not acquired all the adaptative substitutions necessary to increase viral fitness within this vector (Berry et al., 2020).

CHIKV autochthonous cases were confirmed in Colombia in September 2014, and during the epidemics (2014–2015) more than 460,000 cases diagnosed of CHIKF by clinical features were reported, with the majority of them occurring in women, with 12 fatal cases reported. The rate of new infections is decreasing over time, although Colombia is the country with the third-highest number of infections, according to the Pan American Health Organization (PAHO). The characterization of Colombian CHIKV genomes determined that it belongs to the Asian strain and clustered with three distinct Asian strain branches: Panama (Caribbean Colombia, Huila); Nicaragua (Cauca and Risaralda); and St. Barts (Bogotá, D.C), which may be the result of three independent introductions. Each subclade showed non-synonymous mutations (nsP2-A153V, Y543H, G720A; nsP3-L458P; and Capsid R78Q), and that may impact on CHIKV fitness and pathogenesis (Rico-Mendoza et al., 2019; Villero-Wolf et al., 2019; **Figure 1B**).

Records of CHIKV infection cases in Bolivia are extremely scarce. However, CHIKV circulated in this country since March 2015, when 204 cases were reported (Carbajo and Vezzani, 2015). In 2017, 3,367 cases were reported across the country (including clinically diagnosed only) (Escalera-Antezana et al., 2018; **Figure 1B**).

Since 2014, Peru has reported 27 confirmed cases of CHIKV, all of them imported from neighboring countries such as Venezuela and Colombia (Ministerio de Salud, Dirección General de Epidemiología, 2015). This country

has the circulation of *Aedes aegypti* vector in 18 territories and co-circulation of other arboviruses such and ZIKV and Dengue. The first case of autochthonous transmission of CHIKV was reported in 2015 and since then, 951 cases of autochthonous transmission were confirmed in the country according to PAHO. Different regions of Peru present divergent rates of CHIKV infection, varying from 4.6 to 9.4% of all cases of febrile illness (Alva-Urcia et al., 2017; Sánchez-Carbonel et al., 2018), demonstrating that several factors could impact on the epidemiology of CHIKV infection, including the molecular diagnostics, which, in addition to being poorly established and accessible in the country, and the environmental factors, such as natural climatic events, that can increase the frequency of infections.

Some South American countries situated mostly under the Tropic of Capricorn present temperate climate, with warm summers and low temperatures in the winter season, which impair the establishment of a considerable mosquito's population and, consequently, the transmission of arboviruses is negatively impacted. The first CHIKV imported case in Chile was described in 2014, from the Dominican Republic. Since then, all cases reported in Chile were imported, mainly from travelers returning from the Caribbean islands. Argentina, however, presented autochthonous CHIKV transmissions in 2016, and more than 320 lab-confirmed cases were reported, according to PAHO (Perret et al., 2018; **Figure 1B**).

In 2017, 123,087 autochthonous cases were confirmed in the American continent (Pan American Health Organization, 2020). In Brazil, unprecedented dissemination of CHIKV infections has been occurring since 2015, with an accumulated of 712,990 confirmed cases notified over a 4-year period. This outbreak had its major incidence in the Southeast and Northeast regions of the Brazilian territory, corresponding to two-thirds of all confirmed Brazilian cases mainly in periurban and highly populated urban areas of the country.

The first local transmission of the CHIKV in Brazil that occurred in September 2014, at the city of Oiapoque, state of Amapá, localized in the Northern region of Brazil was related to the Asian lineage. Soon after this first autochthonous detection, CHIKV infections from the ECSA genotype were notified in the city of Feira de Santana, Bahia state, the north-eastern region of Brazil. Asian and ECSA genotypes co-circulate in the North and Northeast regions of Brazil (Nunes et al., 2015). However, CHIKV ECSA strain spread to other northeastern states, such as Paraíba, Sergipe, Pernambuco, and Alagoas. In 2017 this strain reached the Amazon region. Interestingly, while the north and southeast regions of Brazil had the majority of CHIKV cases in 2016, Roraima, for instance, the northernmost state of Brazil located in the Amazon basin, only had its exponential increase of cases in 2017. All strains analyzed from this outbreak in Roraima were of the ESCA strain. An extended analysis demonstrated that most cases circulating in Roraima and Amapa since 2015 were of the CHIKV ECSA origin (Naveca et al., 2019). The CHIKV Asian strain was first identified in Roraima in 2014, representing people returning from Venezuela, but the infection did not spread from these two cases. This data demonstrates the high potential of CHIKV ECSA spread in the Brazilian territory.

CHIKV ECSA also reached the southeast region of Brazil, causing large outbreaks. Increasing evidence indicates that the ECSA genotype has predominated in the Southern region, especially in Rio de Janeiro. Xavier et al. (2019) sequenced 11 near-complete CHIKV genomes from clinical samples of patients from Rio de Janeiro, and together with the whole sequencing of 2 CHIKV genomes from positive individuals by Cunha et al. (2017), during the 2016 outbreak, and 10 partially sequenced samples (CHIKV E1 gene) by Souza et al. (2017), the phylogenetic reconstructions confirmed that in Rio de Janeiro the ECSA strain is the driving force of the epidemics (**Figure 1B**).

Phylogenetic analysis also demonstrated that the origin of ECSA strain in Rio de Janeiro was from the north-eastern region of Brazil. Xavier et al. (2019) also showed that there is high human mobility between the two regions and the epidemic waves from the north-eastern region and Rio de Janeiro state had synchronicity during late 2015 to the early months of 2016. Moreover, they estimated that CHIKV was circulating unnoticed for at least 5 months before the first reports of autochthonous transmissions in Rio de Janeiro (Xavier et al., 2019). Another work has estimated an even earlier ECSA genotype introduction in the Rio de Janeiro state. The time-scaled phylogenetic tree estimated the introduction as early as 2014 (Souza et al., 2019).

Corroborating data from Cunha et al. (2017), the genomes of the CHIVK circulating ECSA strain did not carry the E1-A226V and E2-L210Q *Ae. albopictus* adaptive changes. In fact, in Brazil, *Ae. aegypti* is the main circulating mosquito strain (Cunha et al., 2017; Souza et al., 2019; Xavier et al., 2019). Thus, it is expected that mutations that confer high viral fitness in *Ae. albopictus* have not been fixed at these locals.

Although the Brazilian ECSA CHIKV did not harbor the E1-A226V and E2-(L210Q, V264A), which were also related to CHIKV-vector adaptability (Tsetsarkin and Weaver, 2011), unique mutations such as E1-K211T, E1-N335D, E1-A377V, and E1-M407L are present together with E2-A103T (Cunha et al., 2017; Souza et al., 2017). The impact of these mutations on CHIKV adaptability to *Aedes ssp*. vectors still needs to be addressed, but as for the polymorphic E1-211K, the E1-K211E mutation has been implicated in better viral transmission for *Ae. aegypti* but not for *Ae. albopictus* (Agarwal et al., 2016). Importantly, the unprecedented spread of the ECSA strain in Brazil, which substituted the Asian strain in the north part of the country, suggests a greater potential of transmission of this strain.

The dynamics of CHIKV disease in South America, its spread, and the outcome expected can be influenced by several complex factors. The climate patterns, like pluviosity, humidity, ocean-atmosphere climate phenomenon, such as El Niño–Southern Oscillation (ENSO), as well as other parameters, as vector habitat availability, adaptability of the virus into a new vector species, cocirculation of other arboviruses, heterogeneity of health systems in each country, country's economy and the Human Development Index, mobility of individuals (by traveling, exodus, among other reasons), the efficiency in combating disease vectors, the capacity of surveillance and epidemiological vigilance, with the proper actions to stop the outbreaks. All the previous parameters are related to viral vector biology and adaptability. In any case, the biological behavior of

each CHIKV strain cannot be ruled out and the characterization of different CHIKV strains in terms of replication, virus-cell interaction, and pathogenesis urge to be determined.

Virus Particle, Genomic Structure, and the Replication Cycle

The CHIKV viral particle carries the 11.8 Kb, single-stranded positive genomic RNA, which is arranged in two modules: the 5′ two-thirds codes for the non-structural protein (nsPs1-4) and the 3′ one-third codes for the structural proteins (CP, E3, E2, 6K, E1) (Knipe et al., 2001); additionally the 3′ one-third can be translated as a truncated polyprotein composed of CP, E3, E2, C-terminal 6K fused with a Transframe or TF peptide (Firth et al., 2008; Snyder et al., 2013). The 5′ terminus is capped with a 7-methylguanosine and the 3′ terminus is polyadenylated. The genomic RNA is enclosed by a capsid formed by 240 copies of a single Capsid (CP) protein arranged as icosahedrons with T4 symmetry. This nucleocapsid is delimited by the external phospholipid envelope formed essentially by cholesterol and sphingolipid derived from the host cell plasma membrane containing the virus glycoproteins E1 and E2. Each CP interacts with the cytosolic domain of E2. The glycoproteins are arranged as trimeric spikes composed of heterodimers of E1 and E2, and each viral particle contains 80 spikes which lead to the incorporation of 240 copies of E1 and E2 (reviewed in Knipe et al., 2001; Jin and Simmons, 2019). Glycoproteins E1 and E2 mediate CHIKV infection of susceptible cells, where E2 is responsible for receptor binding while E1 plays a role in viral-host membranes fusion.

Until recently, the cellular receptor used by CHIKV, and other arthritogenic alphaviruses, was not known, but several pieces of evidence pointed out to CHIKV use of glycosaminoglycans (Smit et al., 2002; Gardner et al., 2014; Weber et al., 2017; and reviewed in Solignat et al., 2009), T-cell immunoglobulin and mucin 1 (TIM-1) (Moller-Tank et al., 2013), and other PtdSer-binding proteins, such as Axl and TIM-4 (Jemielity et al., 2013) and prohibitin (Wintachai et al., 2012) as adsorption factors. However, Zhang et al. (2018) demonstrated that CHIKV and other arthritogenic alphaviruses, such as Ross River Virus (RRV) and Mayaro Virus (MAYV), use Mxra8 (also known as DICAM, ASP, or Limitrin) as a cell receptor for virus entry. Mxra8 is an adhesion molecule of epithelial, myeloid, and mesenchymal cells with homology to the junctional adhesion molecule that serves as the receptor for reoviruses. The immunoglobulin domains A and B of CHIKV E2 bind to Mxra8 and this binding was necessary for CHIKV mouse infection. Interestingly, infection with the CHIKV ECSA strain La Réunion did not show any requirement to use Mxra8 for viral entry, which indicates that other unknown molecules can function as CHIKV receptors. In addition, this observation demonstrates that different genotypes of CHIKV can adapt differently to the host, thus possibly indicating divergent outcomes of CHIKV disease.

Even though several studies pointed out that E2 acts on CHIKV binding to surface cell receptors, while E1 is the main protein factor involved in the intracellular process of virus entry, there is evidence that points to shared participation of the two proteins at the viral entry and its subsequent events. First, like other alphaviruses, CHIKV can use endocytosis to enter a cell, in a pH-dependent process in clathrin-coated vesicles via receptor-mediated interaction (DeTulleo and Kirchhausen, 1998; Smith and Helenius, 2004; Kielian et al., 2010). In this scenario, after CHIKV enter cells via receptor-mediated endocytosis, the acidic endosomal environment results in glycoproteins irreversible conformational changes followed by E2-E1 heterodimers dissociation and E1 rearrangement into fusogenic homotrimers that induce fusion of viral and endosomal membrane, allowing the release of the nucleocapsid into the cytosol (Voss et al., 2010). But the *Old-World Alphavirus* title (Weaver et al., 1994) makes something very clear about CHIKV: the virus, its vectors, and its final hosts have been coevolving for a long time. Therefore, other pathways did not take long to be elucidated, like the clathrin-independent, epidermal growth factor receptor substrate15 (Eps15)-dependent pathway (Bernard et al., 2010), which also takes the virus particle into the endosome. A third pathway exploited by the virus to get into an acidic cell compartment is the macropinocytosis, recently attributed to CHIKV (Lee et al., 2019), but an already well-established mechanism for other enveloped viruses, such as Ebola virus (EBOV), and non-enveloped viruses, such as adenoviruses; the Rab GTPases- and phosphoinositide-dependent maturation of the macropinosome induces its fusion to endosomal compartments (Egami et al., 2014). The low pH of acid milieu creates the proper microenvironment required to induce conformational changes in the viral envelope, dissociating E1-E2 heterodimers and forming E1 homotrimers, allowing CHIKV fusion to the endosome membrane and the release of the nucleocapsid into the target cell's cytosol where, as it was demonstrated to the Sindbis Virus (SINV), the uncoating of the viral genomic RNA is carried out by the association of the CP and the ribosomes (Singh and Helenius, 1992).

Like other togaviruses and due to the particular arrangement of alphavirus genomic RNA, following uncoating, the CHIKV non-structural (ns) proteins are translated as polyproteins P123 and P1234, with 1,857 amino acids and 2,475 amino acids, respectively. A well-conserved opal (UGA) stop codon is present at the C-terminus of nsP3 and determines the translation of P123, which contains the nsP1, nsP2 and, nsP3 proteins. The readthrough of the opal stop codon leads to the translation of the full-length P1234, that contains the nsP4 protein, the viral RNA-dependent RNA polymerase (RdRp), in addition to the nsP1-nsP3 proteins. The readthrough frequency of the opal stop codon, determined for the SINV, is about 5–20% of the genomic mRNA translation. Therefore, the stoichiometric concentration of nsP4 is 1/20 to 1/5 of the other non-structural proteins (Shirako and Strauss, 1994).

Interestingly, some isolates of alphaviruses code an amino acid residue at the place of the opal stop codon. For instance, a SINV isolate presenting severe morbidity and mortality in mice codes for cysteine at the opal stop codon position (Suthar et al., 2005), while in ONNV both arginine and the opal stop codon are present, and a viral fitness advantage and higher infectivity in the *Anopheles gambiae* mosquito vector is related to the presence of the opal stop codon (Myles et al., 2006). Analyses by deep-sequencing of a Caribbean isolate of CHIKV

(ECSA-derived IOL linage) demonstrated the presence of both the opal stop codon and arginine at the end of nsP3 coding region. The moderate disease was observed in mice infected with a Sri Lanka CHIKV isolate harboring an opal stop codon to arginine change. Sri Lanka isolate shares high similarity with the Caribbean isolate, and the opal stop codon to arginine change did not alter viral replication kinetics (Jones et al., 2017). Collectively, these data suggest that the identification of viral determinants will contribute to a better understanding of CHIKV disease severity and prognostics, and the epidemic potential of different viral strains.

The full-length P1234 is autocatalytically cleaved into nsP4 and P123, the premature cleavage of nsP4 has a simple biological explanation: the cycle's continuity depends on fast replication of the viral genetic material. The nsP1-4 are part of the replication complex (RC), which will determine the replication of the viral genomic RNA and the transcription of the genomic and the subgenomic (26S RNA) viral RNAs. The initial RC complex is formed by the uncleaved P123 plus nsP4 (P123-nsP4), which is targeted and anchored to the plasma membrane by the association of the nsP1alpha-helical peptide and palmitoylated amino acids within the P123. The association of the nsP1 membrane-binding domain with the plasma membrane will induce bulb-shaped invaginations, called spherule, where viral RNA synthesis takes place (**Figure 2**). The negative-strand RNA bears the subgenomic promoter, a sequence of 21 nucleotides, complementary to the nucleotides of the junction region, 19 of the upstream and two downstream of the replication's initiation point. The subgenomic 26S RNA is identical in sequence to the one-third of the genomic RNA 3′ terminus and serves as a template to structural proteins synthesis. Like genomic RNA, the subgenomic RNA is also capped and polyadenylated (Knipe et al., 2001). As P123 is cleaved into the final nsP1, nsP2, and nsP3 proteins, its association with nsP4 in a specific quaternary structure convert the RC into a positive-strand RNA replicase, which will synthesize the viral genomic and subgenomic RNA.

The nsP1 is an initiation factor for negative-strand RNA synthesis and RNA capping via its guanine-7-methyltransferase and guanylyltransferase enzymatic activities.

The nsP2 works as an RNA helicase, a nsPolyprotein protease, and recognizes the subgenomic RNA promoter.

The nsP3 acts as a replicase unit and also as an accessory protein involved in RNA synthesis by recruiting several host-cell factors that participate and optimize viral replication. The nsP3 hypervariable domain (HVD), at the C-terminus, binds the Ras-GHP SH3 domain (G3BP) protein family to promote replication for several alphaviruses. This biding is particularly critical for CHIKV and is, in part, related to the capacity of the virus to inhibit stress granule formation (Kim et al., 2016; Meshram et al., 2018). In this sense, nsP3 VHD binding to the fragile X syndrome (FXR) family members also plays a role in alphavirus replication. Beyond a role in avoiding the formation of stress granules, binding of nsP3 to these proteins is also important to promote viral RNA synthesis by facilitating the assembly of the RC complexes. Different studies have shown that for several alphaviruses the nsP3 binding to these family members is virus-specific and also cell type-specific, presenting a high level of redundancy. However, for CHIKV the binding of host factors from different families is not redundant (Kim et al., 2016; Meshram et al., 2018), pointing out to a critical role of this replication step for the CHIKV–host coevolution.

More recently, two other cellular factors binding to the HVD of nsP3 were implicated in promoting virus replication and permissiveness of CHIKV infection. The host DHX9 DEXH-box helicase is a DNA/RNA helicase that has been demonstrated to participate in the replication of diverse RNA positive viruses (*Picornaviridae*, *Arteriviridae*, *Flaviviridae* – Pestivirus genus, and *Retroviridae* – HIV-1). Matkovic et al. (2019) showed that the nsP3 HVD binds DHX9, redirects this protein from the nucleus to the cytoplasm at discrete puncta structures to increase CHIKV genomic RNA translation early at the viral infectious cycle. Further, they demonstrated that CHIKV nsP2 also binds to DHX9 and targets it to the proteasomal for its degradation. This step is critical to the switch of genomic RNA translation to replication (Matkovic et al., 2019).

Four and a half highly conserved LIM1 domain (FHL1) is a cellular protein that recently has been implicated as a cellular factor promoting CHIKV tropism. This protein has three distinct spliced isoforms in human cells (1A, 1B, and 1C). 1A is abundantly expressed in skeletal muscles and fibroblasts, while 1B and 1C are present in muscle, brain, and testis. Meertens et al. (2019) demonstrated that FHL1 binds to the nsP3 HVD and promotes CHIKV replication. This host factor was also important to the ONNV Old World alphavirus, while it had no impact on the replication of the New World alphaviruses MAYV, SINV, and Semliki Forest Virus (SFV). Primary cells from patients with FHL1 deficiency were resistant to CHIKV infection, highlighting the importance of this cellular factor in promoting skeletal muscle and fibroblast tropism of CHIKV and viral pathogenesis. Strikingly, the dependence of this factor was demonstrated for all CHIKV strains, except the Western African linage, reinforcing the hypothesis that the success of emergent and re-emergent CHIKV strains to spread and establish in the human population and on mosquito vectors will be determined by the interaction of different host factors and the viral proteins.

Collectively, these new findings help to expand the model of CHIKV replication: after the release of viral capsid in the target cell cytoplasm, uncoating of genomic RNA is followed by the translation of P123 and P1234 non-structural precursors, facilitated by the host DHX9 helicase. The initial RC complex formed by P123 and nsP4 then associates with the incoming genomic RNA and the complex is targeted to the plasma membrane by the nsP1 portion of P123. G3BP and FXR factors associates with the RC complex at this very early stage to avoid genomic RNA degradation. DHX9 degradation by the viral nsP2 is critical to the switch from translation to viral replication. Once the first double-stranded RNA replication intermediates are synthesized, they are isolated into the membrane spherule leading to the amplification of these processes. The new synthesized positive-stranded genomic RNAs exit the membrane spherules and are translated in close proximity of the plasma membrane, forming new RC complexes, which by binding of G3BP, FXR, and possibly FHL1, oligomerize and increase the formation of new RCs to amplify the amount of viral genomic RNA within

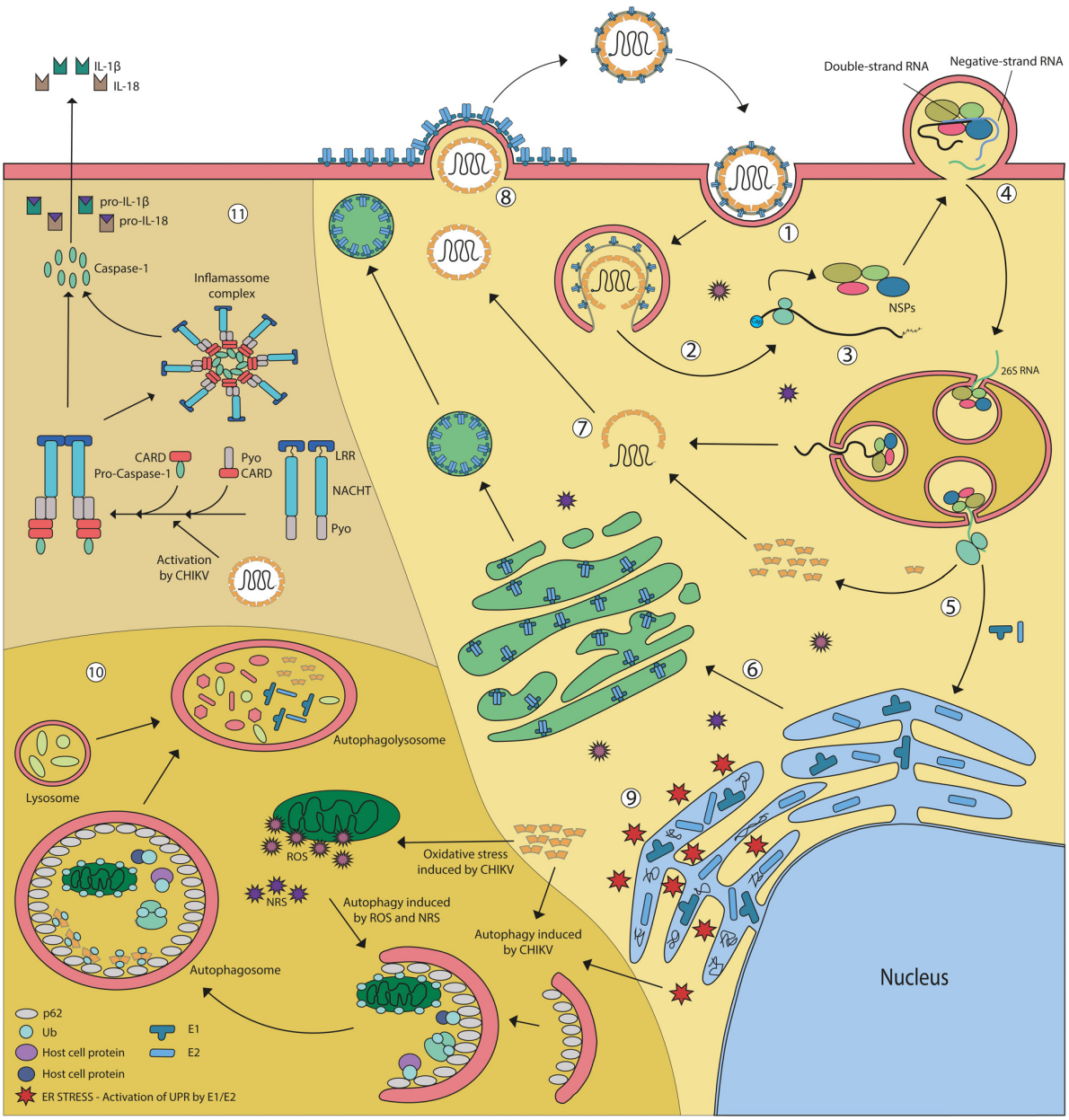

FIGURE 2 | CHIKV life cycle in mammalian infected cells. **(1)** CHIKV cell binding occurs through the interaction of virus E2 protein and a still unknown cellular receptor. Like other alphaviruses, it can enter the cell by clathrin-dependent and independent endocytosis. **(2)** Once inside the endosome, the acidic environment leads to conformational rearrangement of glycoproteins followed by dissociation of E2-E1 heterodimers and E1 rearrangement into fusogenic homotrimers that induce fusion of viral and endosomal membrane, allowing the release of nucleocapsid into the cytosol. **(3)** Following uncoating and genomic RNA release, the non-structural proteins are translated as polyproteins denominated P123 and P1234. **(4)** A replicative complex (RC) formed by uncleaved P123 plus nsP4, the genomic RNA, and several host factors is targeted and anchored at the plasma membrane inducing bulb-shaped invaginations, known as spherules, where RNA synthesis will occur. dsRNA indicates the viral replicative intermediate. nsP1-3 associates with nsP4 in a specific quaternary structure converts the RC into a positive-strand RNA replicase, which synthesizes the viral genomic and subgenomic RNAs. Spherules are internalizate and shape functional large cytopathic vacuoles that bear multiple spherules. **(5)** Subgenomic RNA (26S) is translated, producing the structural polyprotein **(6)** E1and E2-E3 (pE2) are translocated into the ER and go through the post-translational process of maturation and glycosylation. **(7)** Capsid autoproteolysis releases free capsid into the cytoplasm that interacts with genomic RNA, giving origin to the nucleocapsid. **(8)** The viruses bud out of infected cells through the cell membrane in a pH and temperature-dependent process. **(9)** CHIKV replication induces ER stress and activates the Unfolded Protein Response (UPR). By non-elucidated mechanisms CHIKV infection also results in oxidative stress, generating Reactive Oxygen Species (ROS) and Reactive Nitrogen Species (NRS). **(10)** Both ER and oxidative stress can trigger autophagy, a pro-survival signal, in an attempt to preserve cell viability. When CHIKV capsid is produced in the cytoplasm, it can be ubiquitinated and sequestered by adaptor protein SQMT1/p62 into the autophagosomes, leading to capsid degradation in the autophagolisosome. **(11)** CHIKV is able to trigger NLRP3 inflammasome, starting a signaling cascade that culminates in the activation of the caspase 1, that turns able to cleaves of pro IL-1β and pro IL-18, generating mature cytokines, that will elicit adaptive responses, but also can contribute to pathological inflammatory events such as edema and arthritic disease symptoms.

the infected cell early on the infection. Studies from SINV and SFV suggest a high dynamics of spherule internalization through a Phosphatidylinositol-3 kinase (PI3K) activated endocytosis, actin and myosin-dependent transport, and fusion with late endosomes (Spuul et al., 2010), leading to the formation of the so-called large cytopathic vacuoles (CPV-1) (**Figure 2**).

Subgenomic viral RNAs exiting from CPV-1 are immediately translated in close proximity to the Endoplasmic Reticulum (ER) to produce the viral structural polyprotein. At the C-terminal of the CP, a peptide signal leads to the translocation of the polyprotein across the ER membrane. Whereas, through proteolytic processing, it will give rise to intermediate proteins CP, p62, 6K or 6k/TF and E1. From a new stage of proteolysis, hijacking cellular proteases, the final structural proteins will appear: CP, E2, E3, 6K, or 6K/TF and E1 (Aliperti and Schlesinger, 1978; Kääriäinen and Ahola, 2002; Melton et al., 2002; Ramsey and Mukhopadhyay, 2017). Alphavirus capsid proteins are multifunctional and have an intrinsic protease activity. Thus, CP is autocleaved out of the structural precursor protein by its Serine-protease activity. In CHIKV the CP N-terminal is unstructured and has the RNA-binding domain, whereas the C-terminal globular domain harbor the Serine-Histidine-Aspartic acid protease domain. CP will remain in the cytosol for the formation of the viral nucleocapsid.

The glycoprotein E1 has only one transmembrane domain, while E2 has two transmembrane domains. They go through a post-translational process of maturation and glycosylation and are exported in vesicles, hijacking the cellular secretory machinery, up to the cell's plasma membrane.

The glycoprotein E3 is translated right after the capsid protein; it aids with cellular chaperones in the proper folding of E2 and E1, and has a specified signal sequence that addresses the remainder of the polyprotein to the ER membranes. It remains associated with E2, which is why both are called pE2 at this stage, until the moment it reaches the *trans*-Golgi, where the cellular Furin protease is responsible for the cleavage of pE2 in E2 and E3, making the "spike" now functional.

The 6K protein is a hydrophobic small protein that joins the E2 and E1 parts of the polyprotein, allowing for proper envelope processing. It also participates in membrane permeabilization, virus assembly, and budding. An additional protein, which is an extension of the 6K N-terminus, is also synthesized during alphavirus infection. This protein results from a −1 frameshift event 40 nucleotides before the beginning of E1 glycoprotein and leads to the formation of a truncated structural precursor, as described above (Firth et al., 2008; Snyder et al., 2013). This frameshift occurs in a 10–18% frequency during the subgenomic RNA translation. The resulting protein is an 8 kDa TF that is incorporated into viral particles and probably participates in viral assembly.

The newly formed virus particles bud out from infected cells through the cell membrane in a pH and temperature-dependent process, which requires that the temperature is close to physiological (∼36°C) and that the pH is neutral or slightly alkaline (Lu and Kielian, 2000). There are some other mandatory requirements for exporting viral particles, such as the connection between the capsid and E2 (Suomalainen et al., 1992), the heterodimerization between E1 and E2 (Sjöberg and Garoff, 2003), and the interaction between virus' structures and host-cell factors: Arf1 and Rac1 assisting the stabilization of E2/E1-containing cytopathic vacuole type II, trafficked by actin filaments—that E2 apparently induces the accumulation and the elongation—by a mechanism involving Rac1, Arp3, and PIP5K1, all constitutive cellular factors (Radoshitzky et al., 2016). **Figure 2** summarizes the major features of the CHIKV replication cycle.

VIRUS–CELL INTERACTION

CHIKV Infection and Host and Virus Transcriptional and Translational Regulation

Transcriptional shutoff during CHIKV infection impairs the cellular response to viral replication and avoid the establishment of an antiviral state. The CHIKV nsP2 mediate degradation of RBP1, the catalytic subunit of cellular RNA polymerase II, resulting in transcriptional shutoff, cytopathic effect, and reduced IFN-β production. Thus, nsP2 expression is cytotoxic and suppresses both cytokine production and activation of interferon-stimulated genes (ISGs) in infected cells (Akhrymuk et al., 2019).

CHIKV infection also results in the shutoff of host cell protein synthesis, whereas viral proteins continue to be synthesized. The host cell shutoff is a result of Eukaryotic Translation Initiation Factor 2 α (eIF2α) phosphorylation (White et al., 2011). Phosphorylation of eIF2α disables the ternary complex, essential for cap-dependent translation initiation. How CHIKV infection results in eIF2α phosphorylation remain unclear. Although infection increases the double-stranded RNA-dependent protein kinase (PKR) activation, eIF2α phosphorylation also occurs independently of PKR (White et al., 2011).

Moreover, CHIKV modulates protein synthesis by interfering with mTOR activation. Joubert et al. (2015) demonstrated that during the first 24 h of infection, mTOR and S6K phosphorylation is reduced, which directly impacts on host cell protein synthesis. mTORC1 low activity is associated with AMP phosphorylation kinase (p-AMPK), an energy-sensing enzyme, followed by TSC2 activation, which acts as an inhibitor of mTOR phosphorylation (Joubert et al., 2012). Inhibition of the mTOR complex 1 (mTORC1) increases CHIKV production and this effect is independent of IFN-I production and autophagy induction. To bypass the deleterious effect of mTORC1 inhibition for cap-dependent mRNA translation, CHIKV protein synthesis is mediated via Mnk/eIF4E pathway (Joubert et al., 2015). Interestingly, mTORC1 inhibition also increases SINV infection, but had no effect on influenza A infection (a member of the *Orthomyxoviridae* family), suggesting that different viruses developed singular strategies to modulate mTORC1 activity (Joubert et al., 2015).

The PI3K-AKT-mTOR pathway is the major pathway that mTOR is involved in. Thaa et al. (2015) demonstrated that CHIKV infection induces AKT serine 473 phosphorylation but had no effect on S6 phosphorylation, one of the downstream

targets of the PI3K-AKT-mTOR pathway. AKT phosphorylation by CHIKV is lower compared with other alphaviruses like SFV. SFV nsP3 triggers strong AKT activation, which is associated with the RC internalization. On the other hand, replication complexes were broadly localized at the cell periphery in CHIKV infection (Thaa et al., 2015). However, it remains to be elucidated how different CHIKV strains will impact on both AKT activation and mTOR modulation. Different alphaviruses modulate the PI3K-AKT-mTOR pathway in specific manners associated with particular virus replication features.

CHIKV, Autophagy, and Oxidative Stress

Macroautophagy, referred herein as autophagy, is a homeostatic process conserved in eukaryotes that recycle cargo proteins and organelles through lysosomal degradation by their selective sequestration inside double-membrane vesicles, known as autophagosome (Yang and Klionsky, 2010). It is also described as a cytoprotective process with important roles in immunity response against sterile and infection-associated inflammation, including viral infection (Deretic and Levine, 2018).

Despite its relevance to the immune response against infections, autophagy may play a role in both anti and pro-viral replication. For instance, some viruses are able to subjugate the autophagy machinery in its own advantage. This process has been investigated for alphaviruses (Liang et al., 1998; Orvedahl et al., 2007, 2010; Eng et al., 2012; Joubert et al., 2012). The role of autophagy during CHIKV infection is still controversial and can be divergent according to the cell type used to replicate CHIKV.

First reports showed that CHIKV infection of human embryonic kidney 293 cells (HEK-293T) leads to an increased number of the microtubule-associated protein 1A/1B light-chain 3 (LC3) puncta and augmentation of membrane-bound vacuoles, suggesting that CHIKV infection triggers an autophagic response (Krejbich-Trotot et al., 2011). Accordingly, CHIKV replication was dramatically reduced when autophagy was blocked biochemically or by RNA interference (Krejbich-Trotot et al., 2011).

Oxidative stress is an important mechanism to fight back pathogens. It occurs due to a dysregulation of redox control, caused by increased levels of reactive oxygen species (ROS) and reactive nitrogen species (RNS) and/or a reduction in the antioxidant defense system (Jones, 2006; Cataldi, 2010). Free oxidative species are able to initiate autophagy and can also lead to cell death during strong and prolonged stimulation (Djavaheri-Mergny et al., 2007; Filomeni et al., 2010). Joubert et al. (2015) assessed CHIKV capacity to induce ROS and RNS. They observed, in murine fibroblast cells (MEF), that CHIKV infection led to increased production of both ROS and NO. In addition, they demonstrated that CHIKV-induced autophagy on these cells was mediated by the independent induction of endoplasmatic reticulum (ER) and oxidative stress pathways, delaying cell death by apoptosis through induction of IRE1a-XBP-1 pathway at the same time as ROS-mediated AMPK activation and mTOR inhibition. Consequently, the treatment with *N*-acetyl-l-cysteine, a potent antioxidant, reduces CHIKV-induced autophagy, observed by the decrease in LC3 puncta on these cells (Joubert et al., 2012). Therefore, it was demonstrated that CHIKV infection can induce endoplasmic reticulum and oxidative stress at the early stages of infection to trigger autophagy (**Figure 2**).

Interestingly, during the late stages of viral replication in MEF cells, autophagy is suppressed concomitantly with enhanced cell death by apoptosis, favoring viral release and spread (Joubert et al., 2012), showing a time-dependent pattern of autophagy regulation by CHIKV infection.

In human epithelial adenocarcinoma cells (HeLa), CHIKV infection can regulate autophagy through the interaction between viral proteins and the autophagic receptors sequestosome 1/p62 (SQSTM1/p62) and calcium-binding and coiled-coil domain-containing protein 2/nuclear dot 10 protein 52, known as NDP52. Both proteins are able to interact with both cargo proteins and LC3, directing autophagy targets to autophagosomes (Judith et al., 2013). It was shown that SQSTM1/p62 can protect CHIKV infected human cells from death by binding ubiquitinated viral capsid and targeting it to lysosomal degradation (**Figure 2**). Moreover, CHIKV infection in certain cell types leads to robust SQSTM1/p62 degradation. Differently, it is being described that NDP52, but not its murine ortholog, interacts with the viral protein nsP2 promoting viral replication (Judith et al., 2013). Therefore, during CHIKV infection, autophagy can be regulated in different ways playing both pro- or anti-viral roles according to the time of the replication cycle and to the cell type and this can be crucial for the infection progression and virus spread.

CHIKV and the Endoplasmic Reticulum Stress

The ER is an essential cellular membrane organelle, with a dynamic structure that plays important roles in many cellular processes, including protein synthesis, folding and secretion, calcium homeostasis, lipid production, and the transport of cellular components. ER plays an essential role in the replication process of several viruses, including viral entry, assembly, protein synthesis, and genome replication. The massive viral replication can cause disturbances on the protein folding machinery, disrupting ER homeostasis, which culminates in ER stress (Liu and Kaufman, 2003; He, 2006; Inoue and Tsai, 2013; Jheng et al., 2014). The ER stress activates an evolutionarily conserved prosurvival pathway, termed the unfolded protein response (UPR), that acts for maintenance of ER homeostasis. UPR has three main mechanisms to restore the adequate ER function: (1) inhibition of protein synthesis, (2) induction of genes of chaperone family, necessary for the folding protein processes, (3) eliminating the amount of misfolded or unfolded proteins by activation of the ER-associated protein degradation (ERAD) pathway (Malhotra and Kaufman, 2007; Hetz et al., 2011).

In mammalian cells, the three main branches of the UPR are the protein kinase-like ER-resident kinase (PERK), the activating transcription factor 6 (ATF6), and the inositol-requiring enzyme 1 (IRE1). These proteins are associated with the ER chaperone BiP/Grp78. When unproperly folded proteins accumulate in the ER lumen, BiP/Grp78 dissociates from these three transmembrane signaling proteins, resulting in activation and initiation of the UPR pathway. Then, activated

PERK phosphorylates eIF2α at Ser51, decreasing the load of proteins entering into the ER lumen by blocking general protein translation. Activated ATF6 is a transcription factor that increases the transcription of a number of ER chaperones, the X box-binding protein 1 (XBP1), and other transcription factors. Activation of IRE1 results in the IRE1 mediated splicing of the XBP1 mRNA, which activates the expression of downstream genes like chaperones and other proteins involved in protein degradation (Yoshida et al., 2001; Harding et al., 2002; Vattem and Wek, 2004; Jheng et al., 2014).

Beyond triggering ER stress and UPR, viruses have evolved different strategies to subvert these cellular responses for their own benefit, e.g., enhancing replication, persisting in infected cells, and evading immune responses, as described for several viral families, such as *Flav* i-, *Herpes*-, and *Togaviridae* (reviewed by Ambrose and Mackenzie, 2011; Green et al., 2014; Li et al., 2015).

CHIKV infection results in the activation of the UPR pathway in different cell lines. However, results from different groups are discordant and may reflect the cell-specificity for UPR activation. Fros et al. (2015) showed that in Vero cells, the expression of CHIKV envelope proteins alone can induce UPR by the upregulation of ATF4 and GRP78/Bip. Additionally, CHIKV-infected Vero and an adult WT mouse model of CHIKV arthritis only partially induced by XBP1. Furthermore, the authors demonstrated that individual expression of CHIKV non-structural protein nsP2 protein was sufficient to inhibit the UPR pathway (Fros et al., 2015). Whereas, CHIKV infection of HEK293 cells activated the ATF6-UPR branch, but not IRE1 or PERK pathways. In these cells, CHIKV infection blocked eIF2α phosphorylation even in the presence of pharmacological activation of UPR by Thapsigargin and Tunicamycin. The authors demonstrated that nsP4 was sufficient to inhibit phosphorylation of eIF2α (Rathore et al., 2013).

ER stress, autophagy, and apoptosis in response to CHIKV infection were also investigated in HeLa and HepG2 cells and showed distinct results. In HeLa cells, CHIKV infection activated the PERK branch of UPR, with consequent eIF2α phosphorylation (Khongwichit et al., 2016). Diversely, Joubert et al. (2012) observed activation of UPR in HeLa through the splicing of XBP1 by IRE1 during CHIKV infection. The ATF6 branch was also activated in these cells. Whereas in HepG2 IRE1 activation was strong, the activation of PERK and ATF6 was less pronounced and only a low level of eIF2α phosphorylation was observed. For both cells, the downstream protein CHOP, which is involved in apoptosis signaling, was also upregulated (Khongwichit et al., 2016).

Moreover, the silencing of IRE1 during CHIKV infection of HeLa leads to fewer CHIKV-induced autophagosomes. Apparently, CHIKV-induced autophagy is dependent on both triggering of oxidative stress and UPR pathways. These data reinforce the idea that the ER could serve as a subcellular platform for autophagy initiation. Signaling of UPR and autophagy are interconnected, and these two pathways crosstalk to modulate the cell survival or dead by apoptosis (Bernales et al., 2006; Axe et al., 2008; Joubert et al., 2012).

Data regarding ER stress and UPR during CHIKV infection, although apparently conflicting, indicate that CHIKV infection can elicit distinct interactions with cell machinery depending on the cell type and possibly the viral strain analyzed. These data raise the necessity to further investigate the role of UPR on cell lines with close similarity to the cells naturally infected by CHIKV, as epithelial cells, skin fibroblasts, muscular, and endothelial cells. Furthermore, the use of mouse models of infection can also contribute to determining the relevance of the UPR signaling to CHIKV replication and pathogenesis.

CHIKV and the Inflammasome

Inflammasomes are cytosolic molecular complexes that initiate inflammatory responses upon the detection of pathogens, cellular damage, or environmental irritants by the pattern recognition receptors (PRRs). Upon activation, inflammasome is assembled and activates caspase-1, which cleaves proinflammatory cytokines prointerleukin-1β (proIL-1β) and prointerleukin-18 (pro IL-18) resulting in proteolytic maturation and secretion of active forms of these cytokines (IL1- β and IL-18, respectively). All these signaling cascades lead to a type of programmed cell death known as pyroptosis that is inherently inflammatory and characterized by caspase 1-dependent formation of plasma membrane pores leading to ion fluxes, that culminates with the cytoplasmic membrane rupture and subsequent release of intracellular content in order to control microbial infections (Martinon et al., 2002; Bergsbaken et al., 2009; Conforti-Andreoni et al., 2011; **Figure 2**).

In a scenario of viral infections, inflammasome can amplify the sensing of viral nucleic acids (RNA or DNA). Although inflammasome signaling and activity is supposed to resolve the infection and promote homeostasis, high levels of inflammasome-triggered proinflammatory cytokines have been associated with inflammation and pathogenesis of several viral, bacterial, autoimmune diseases, and cancer (Davis et al., 2011; McAuley et al., 2013; Negash et al., 2013; Wikan et al., 2014; Olcum et al., 2020).

The role of inflammasome on CHIKV replication and pathogenesis has been poorly explored. One study, from Ekchariyawat et al. (2015), demonstrated that CHIKV infection could generate inflammasome signaling in human dermal fibroblasts cells, culminating in activation of caspase 1 and increase IL1 β expression and maturation, as well as induction of the expression of the inflammasome sensor AIM2, although AIM2 has been implicated in recognition of dsDNA only. In the absence of inflammasome assembly (through caspase 1 silencing), CHIKV replication rates were enhanced (Ekchariyawat et al., 2015). Moreover, ASC2 and NLRP3 expression, as well as IFN- β and some ISGs, were upregulated in CHIKV-infected fibroblasts.

More recently, Chen and colleagues showed that NLRP3 inflammasome is activated in humans and mice. Expression of NLRP3, ASC, and caspase 1 was100-fold enhanced in PBMCs from a cohort of CHIKV-infected patients. Also, IL18 and IL1 β mRNA levels were increased in these patients in the acute phase of CHIKF (Chen et al., 2017). In a mouse model of CHIKV-induced inflammation, subcutaneous inoculation of ECSA CHIKV strain isolated from La Réunion (LR2006-OPY1), a microarray gene analysis revealed increased expression of NLRP3, NLRP1, NLRC4, IL-1β - and IL-18-binding protein, caspase-1, IL-18 receptor, and IL-18 receptor accessory protein,

with high expression coinciding with the peak of inflammatory arthritic disease symptoms (Chen et al., 2017). Furthermore, using a molecule that inhibits the activation of the NLRP3 inflammasome, the group observed substantial improvement of arthritic symptoms, with a reduction of inflammation, myositis, and osteoclastic bone loss, although the general replication remained at the same levels. Also, in $ASC^{-/-}$ mice the foot swelling after CHIKV infection was less severe, compared to wild type mice. Taken together, these studies reveal the relevance of inflammasome on CHIKV infection, highlighting its role in the pathology of arthritic disease and inflammation. Concisely, the compelling data open the possibility for the development of therapeutic strategies targeting the inflammasome pathway to ameliorate arthritic symptoms.

CHIKV Pathogenesis

Dermal fibroblasts are the primary targets and the main sites of CHIKV replication (Sourisseau et al., 2007; Ekchariyawat et al., 2015), but other skin cells are also susceptible, like keratinocytes and melanocytes (Gasque and Jaffar-Bandjee, 2015). From the skin, the virus migrates via lymphatic circulation, to the nearest lymph node, reaching the bloodstream where it infects mostly monocyte-derived macrophages (Sourisseau et al., 2007). In a non-human primate (NHP) model, CHIKV migration was demonstrated by the presence of $CD68^{+}$ macrophages positive for CHIKV antigen trafficking to lymphoid tissue and the spleen from early timepoint up to 3 months after infection (Labadie et al., 2010). From the blood, the virus reaches joints, muscles, and bones, which are the sites most linked to the chronic symptoms of the disease. Satellite cells of skeletal muscle are permissible for CHIKV infection and can act as a reservoir of mature skeletal fibers precursors, therefore, they have an active and crucial role in maintaining tissue structure (Ozden et al., 2007) and, when infected, can constitute a site of viral persistence. Mature skeletal muscle fibers and primary myoblasts have also been targeted by CHIKV (Couderc et al., 2008; Lohachanakul et al., 2015). In the joints, viral RNA and proteins were found during the acute and chronic phase of the infection; macrophages, primary human chondroblasts, and fibroblasts from synovial tissues are susceptible to CHIKV infection, with synovial macrophages being the main site of viral persistence linked to CHIKV (Hoarau et al., 2010; Zhang et al., 2018). The bones of the regions closest to the joints are also targets of infection since primary human osteoblasts are permissive to CHIKV (Chen et al., 2015). These are the preferred targets of viruses, which are not coincidentally linked to the most commonly observed clinical manifestations. The appearance of unusual clinical manifestations, affecting central nervous, cardiovascular, respiratory, digestive, hematopoietic, and renal systems is due to the presence of cells, vital to local homeostasis, that is also susceptible to the CHIKV infection.

The Immune Response at Acute Phase of Infection

The type I interferon (IFN) response is an early innate immune mechanism that elicits antiviral responses and activates components of the innate and adaptive immune systems. IFNs are quickly induced after recognition of viruses by host pattern recognition receptors (PRRs), mainly by Toll-like receptors (TLRs), cytosolic receptors as retinoic acid-inducible gene-I (RIG-I), and melanoma differentiation-associated gene 5 (MDA5) (Thon-Hon et al., 2012; Jang et al., 2015). After recognition of their respective ligands (double-stranded [ds] RNA for RIG-I and MDA5), the mitochondrial antiviral-signaling protein (MAVS) is activated via Card-card interactions, domains presented both in MAVS and cytosolic receptors. Then, TBK1 is activated by MAVs and phosphorylates the interferon regulatory factor 3 (IRF-3), which dimerizes and translocates into the nucleus. This signaling pathway induces the production of type I IFNs through activation of the IFN-α/β promoter. IFNs are secreted and act in autocrine and paracrine ways, after activation of the interferon-α/β receptor (IFNAR), triggering a signaling cascade of events that culminates in the expression of ISGs that enhance viral recognition and interfere with several steps of the viral cycle (Platanias, 2005; Hu et al., 2018).

The role of IFNs for CHIKV pathogenesis is well known. Viral replication is controlled by IFNs in cells, and mice lacking IFNAR have important viral dissemination, related to high rates of mortality (Schilte et al., 2010; Suhrbier et al., 2012). In cynomolgus macaques, infection with the isolate CHIKV-LR recapitulates common characteristics of the immune response, such as an increase in plasma levels of IFN-α/β, interleukin 6, and monocyte chemoattractant protein 1, correlating with peak levels of viremia (Labadie et al., 2010). Additionally, in fibroblastic cell lines, CHIKV infection induces the expression of antiviral genes, as IFN-α and RIG-I. Moreover, CHIKV is able to interfere with the nuclear translocation of phosphorylated STAT1, a transcription factor that promotes the expression of several ISGs (Thon-Hon et al., 2012).

Cook et al. (2019) recently showed distinct but synergistic roles for IFN-α and β in controlling CHIKV replication and disease. While IFN-α acts in non-hematopoietic cell types, reducing replication and early dissemination of CHIKV, IFN-β has a substantial impact on pathogenesis, since it can limit neutrophil-mediated inflammation at the site of infection (Cook et al., 2019).

Recently, Bae et al. (2019), through a gene screening in HEK293T cells, reported that viral protein nsP2 and envelope glycoproteins E1 and E2 are strong antagonists of the IFN-β signaling pathway. Triggering of IFN response, although a common feature of RNA viruses, can vary in amplitude and intensity depending on the virus species and even different genotypes and/or strains from the same species. The characterization of IFN response during the infection of the CHIKV isolates related to the most recent epidemics in Latin America will allow us to understand the pathogenic potential of these viruses.

Natural killer (NK) cells are at the front line in controlling virus replication via stimulation of IFN-I. Like other viruses, CHIKV is able to induce the activation of a phenotype rarely seen in the NK cells of healthy patients; these cells have the NKG2C1 receptor activated, which makes them highly cytotoxic, leading to the lysis of infected cells (Petitdemange et al., 2011).

Antibodies and $CD8^+$ T cells are key players in adaptive immune responses. It has been shown the activation and multiplication of $CD8^+$ T cells during the first days of infection followed by a switch to $CD4^+$ T-cells, but the exact role of T-cells in CHIKV infection remains uncertain. In mice, $CD8^+$ T cells were recruited to the musculoskeletal tissue in the first week of infection (Teo et al., 2013), which could be one of the reasons for the increased levels of IFN-γ (Wauquier et al., 2011). These cells can also be linked, among other mechanisms described above, with the control of viral replication in the acute phase, since there is an increase in perforins, granzymes, and proteins linked to the degranulation of $CD8^+$ T cells, which would culminate in apoptosis of infected cells (Dias et al., 2018).

Regarding antibodies, anti-CHIKV antibodies are fully capable of offering protection even in the first days of infection, since IgM is detected initially at 2–3 days after the appearance of symptoms (Litzba et al., 2008). Antibody-mediated response suppresses the spread of the virus, either by direct neutralization or by activation of the complement system (Lum et al., 2013). In a study with rhesus macaques comparing the CHIKV strains La Reunion (CHIKV-LR) and Western Africa 37997 (CHIKV-37997), T-cell and antibody responses were more robust in the animals infected with LR compared to 37997 (Messaoudi et al., 2013). A different study showed that 90% of antibody response against CHIKV was mediated by IgM within the first 9 days of infection in cynomolgus macaques inoculated with CHIKV-LR (Kam et al., 2014).

Immune Response at the Chronic Phase of Infection

Chronification of the infection usually leads to continuous inflammation of the joints. This inflammation can be immune-mediated by several elements that, *a priori*, could be allies in fighting infection; it is possible for NK cells to infiltrate synovial tissues and maintain an inflammatory environment conducive to arthralgia, for example. However, NK cells associated with the chronic phase of the disease have reduced expression of cytolytic mechanisms, such as perforin, and increased expression of IFN-γ and TNF-⟨, pro-inflammatory components that can contribute to the establishment of a highly inflamed environment in joints (Thanapati et al., 2017).

The CHIKV-Induced Disease

Usual Clinical Manifestation of CHIKF

Arthritis and arthralgia

CHIKV, among other mosquito-transmitted alphaviruses, like RRV, Barmah Forest Virus (BFV), and MAYV, can cause debilitating pain and inflammation of joints in humans (Staples et al., 2009), leading to the severe and debilitating rheumatic symptoms that are experienced by most infected individuals, that could result in a negative impact on everyday activities (Ross, 1956). For this reason, epidemiological studies established unusually severe joint pain as the distinguishing and most common feature of CHIKV infection (Brighton et al., 1983; Powers and Logue, 2007). The severe pain starts in the acute phase of infection, affecting both peripheral and large joints, and becomes chronic, typically lasting from weeks to months (Queyriaux et al., 2008; Vijayakumar et al., 2011). In 25–42% of infections, inflammatory-related affections, like joint effusions, redness, and warmth, can be observed. These joint symptoms are usually polyarticular, bilateral, symmetrical, and can fluctuate, but the anatomical location does not usually change (Deller and Russell, 1968; Queyriaux et al., 2008; Simon et al., 2011; Vijayakumar et al., 2011).

Fever

One of the most common symptoms of the acute phase of infection is an abrupt onset of fever, coincident with the viremia and polyarthralgia, reaching 40°C in some cases, resulting in chills and rigors (Simon et al., 2011). Fever, in addition to lasting from many days to 2 weeks, are also typically biphasic in nature (with a period of remission of 1–6 days) (Halstead et al., 1969; Thiberville et al., 2013), which means an early elevation in body temperature followed by a later one, caused by a dynamic balance between exogenous and endogenous pyrogens and prostaglandins.

Myalgia

Muscle pain, dissociated from inflammation (myositis), is frequent in 46–59% of cases, mainly affecting arms, thighs, and calves (Zim et al., 2013). It can be a confounding factor, since other arbovirus diseases, such as dengue, can also develop myalgia (Kumar et al., 2017), one of the reasons why some researchers call CHIKV clinical manifestations as a "dengue-like" disease, but with a particular articular tropism.

Dermatologic involvement

The most common cutaneous manifestation of CHIKF is macular or maculopapular rash, distributed mainly in the extremities, trunk, and face, associated with severe pruritus (Shivakumar et al., 2007), observed in up to 50% of cases. In most cases, the lesions follow fever episodes, but they also can occur concomitantly since both depend on viremia. They generally do not produce sequelae, but, in some patients, they induce pigmentary changes, mainly in the malar area of the face, with a predilection for the tip of the nose, but also seen in extremities and trunk, desquamation and xerosis (Prashant et al., 2009). There are other less common dermatological manifestations, which includes erythema and swelling of the pinnae, mimicking erysipelas' Milian ear sign; multiple aphthae, erosions, and cheilitis were also observed in oral mucosa, but they were all no-sequelae self-limited manifestations, except for hyperpigmentation of the hard palate in a few patients; and genital involvement, in the form of ulcers, over the scrotum and base of the penile shaft in men and labia majora in women. The infection can also flare-up of pre-existing psoriasis and lichen planus manifestations.

Other usual manifestations

Pain in the ligaments, headache, fatigue, and severe tiredness, digestive symptoms (diarrhea, vomiting, gastrointestinal bleeding, nausea or abdominal pain), red eyes, conjunctivitis, and lymphadenopathy have also been described, only during the

acute phase of infection (Economopoulou et al., 2009); therefore, the impact on the quality of life of people affected by the infection begins with the first symptoms and extends to the remission of polyarthralgia at the end of the chronic phase.

Unusual Manifestations of CHIKV Infection

Atypical manifestations of the infection, unlike the aforementioned typical manifestations, depend mostly on the underlying disease, already manifested and exacerbated by the infection or only predisposing in the affected individual, and in this case, CHIKV can be a trigger for the onset of its clinical syndrome. Of note, the spread of new epidemic strains has the potential to induce new subsets of clinical manifestations.

Neurological complications

In both adults and children, the most prevalent neurological manifestation is encephalitis, during the acute phase of the infection, usually manifested in less than 24 h after the sudden onset of high fever (Robin et al., 2008; Venkatesan et al., 2013). Although the manifestation of encephalitis, in general, is not related to the age of the patient, the incidence of CHIKV-associated encephalitis shows that individuals younger than 3 years old or older than 65 are more likely to develop the syndrome. Retrospective studies have made it possible to estimate a frequency of 8.6 per 100,000 CHIKV infection cases (Simon et al., 2007). Epileptic seizures, meningoencephalitis, syndrome of meningeal irritation and Guillain-Barré syndrome have also been described, but these are considerably less frequent cases (Robin et al., 2008; Tournebize et al., 2009; Venkatesan et al., 2013; Gérardin et al., 2016); further studies still need to address whether the unprecedented epidemics of CHIKV infection in the South American continent was in fact accompanied by a higher frequency of higher morbidity and atypical clinical manifestations. Some reports, however, had already associated CHIKV infection with diverse neurological complications (Pereira et al., 2017; Mehta et al., 2018).

Cardiovascular manifestations

Heart failure was diagnosed in patients with acute infection during La Réunion (island) outbreak of chikungunya fever, in 2005–2006 (Robin et al., 2008), but approximately 60% of the cases have a previous cardiovascular pathological history, such as valvular or coronary disease. This scenario allows us to jump to two conclusions: (1) 40% of infected patients had a flaw in one of their most vital systems without first manifesting any symptoms that involved it, which makes CHIKV infection a potential cardiovascular risk factor for healthy patients; and (2) the virus has a potentiating character, that is, it can be an unexpected factor in the prognosis of cardiovascular diseases previously diagnosed. Myocarditis after arboviruses infections has been described since 1972 (Menon et al., 2010), which can be the main cause for other registered manifestations, which include ventricular and atrial gallops, tachycardia and tachypnea, blood pressure instability, chest pain, electrocardiograph (ECG) abnormalities, and acute myocardial infarction (Spodick, 1986; Dec et al., 1992; Touret et al., 2006).

Pregnancy risks and vertical transmission

Although there are reports of concomitance between infection and spontaneous abortions in the second trimester (Dreier et al., 2014), studies have failed to establish a direct relationship between prenatal obstetric complications and CHIKV infection. Regarding its symptoms, on the other hand, the management of infected pregnant women needs to be delicate, since classic high fever can lead to neural tube defects, congenital heart defects, and oral clefts when it occurs in the first trimester of pregnancy (Fritel et al., 2010), and when it occurs in the second and third trimesters, it can result in abrupt uterine contractions and abnormalities in the fetal heart rhythm, resulting in premature births or stillborn babies (Torres et al., 2016). When it comes to mother-to-child transmission, there is no evidence to sustain the antepartum or peripartum risk of fetal transplacental infection and infected newborns are linked only to the intrapartum transmission when the parturient has a positive viremia (Solanki et al., 2007; Gérardin et al., 2008; Sissoko et al., 2008).

Renal disorders

An acute pre-renal failure was reported in several cases, of which one-third of the affected patients with previous kidney disease (Robin et al., 2008). The condition is usually controlled by increasing the patient's blood volume by intravenous hydration, and the reported cases seem to have responded well to this therapeutic approach. There's only one case of a nephritic syndrome that emerged during an outbreak of CHIKV in Delhi with full recovery (Lemant et al., 2008).

Deaths

CHIKV was recognized as a non-lethal infection, however during the outbreak in Reunion Island in 2005–2006, the greater number of patients with atypical manifestations of the infection also contributed to the increase in CHIKV-related deaths, with a mortality rate as high as 48% (Renault et al., 2007). Another study points to a significantly lower rate, of approximately 10% (Economopoulou et al., 2009), but it also links all deaths to the aforementioned atypical manifestations. The major concern of analysts is that many deaths during epidemic periods were underreported by health professionals, which would make the infection mortality rate higher than that already estimated for the disease.

As described above, several atypical manifestations of CHIKV were reported upon recent reemergence and emergence of CHIKV worldwide. In La Reunion Island, clinical features that had never been associated with CHIKF were reported, such as pneumonia, diabetes, bullous dermatosis, toxic hepatitis, encephalitis or meningoencephalitis, myocarditis, and cardio-respiratory failure (Economopoulou et al., 2009). During the 2008 outbreak of CHIKF in South India, various cases of cutaneous manifestations, including vesiculobullous eruptions with significant morbidity in infants were associated with CHIKV infections (Inamadar et al., 2008). The authors hypothesized that these novel manifestations could be associated with the IOL circulating strain of CHIKV. In French Guiana, the introduction of the CHIKV Asian strain was associated with severe forms of the disease, including cases of sepsis and a Guillian-Barrè

syndrome (Bonifay et al., 2018). In Brazil, where the ECSA strain predominates, atypical neurological manifestations have been reported (Azevedo et al., 2018). Although it is still early to associate CHIKV infection severity with the introduction of different viral strains in susceptible populations, studies are needed in other to characterize the biological properties of different CHIKV strains.

DISCUSSION

The introduction of CHIKV within the human population is estimated to have occurred at the beginning of the 20th century; still, the highly epidemic potential of this arbovirus was only truly appreciated after the large epidemics occurring from the first decade of the 21st century in Kenya, La Reunion islands, and the Caribbean. Strikingly, the CHIKV genotype responsible for these large epidemics was the ECSA-derived Indian Ocean Lineage. Mutation within the viral envelope glycoproteins that accounted for virus adaptability to *Ae. albopictus* are regarded as an important factor leading to massive virus dissemination in these regions. However, coincident with this unprecedented spread of CHIKV, descriptions of atypical clinical outcomes began to be reported. In Brazil, a CHIKV ECSA genotype, derived from an ancestral ECSA virus from Central Africa, was responsible for the large epidemic that occurred from 2015 to 2018 in several parts of the national territory affecting at least 700,000 individuals. The severity of the symptoms and the morbidity of CHIKF still need to be accounted, but there are reports of atypical cases of meningoencephalitis and other neurological complications in CHIKV-infected patients in Brazil.

Although the factors involved in the unprecedented dissemination of ECSA-derived IOL could be due to viral determinants related to adaptability to the arthropod vector, as already demonstrated, other viral determinants such as increased viral replication capacity, modulation of host IFN response, that has the potential to increase virus pathogenicity cannot be excluded. In fact, as reviewed here, several studies conducted with the La Reunion CHIKV isolate CHIKV-LR, demonstrated its higher capacity to induce disease symptoms and establish infection in immunocompetent murine models of infection when compared to other CHIKV genotypes. Although in the immunocompromised murine model these results were not reproducible and the ECSA-derived IOL was not able to induce higher mortality rates when compared to the other CHIKV genotypes. This data reinforces the importance of continuous studying CHIKV replication properties, host-cell interaction, and pathogenesis to comprehensively address the epidemic potential of different emerging and reemerging CHIKV genotypes.

The South-American ECSA genotype, on the other hand, does not harbor the vector-adapting mutations observed for the ECSA-derived IOL, and studies are urgently needed to understand the role of unique mutations observed throughout its genome for mosquito adaptability, virus replication, and pathogenesis. Characterization of viral determinants of disease severity and virus pathogenicity in this emerging ECSA-related genotype will help to predict the impact of future epidemics. As well as the characterization of different genotypes of CHIKV in terms of replication capacity, virus-host interaction, and pathogenesis will be crucial to the development of the best vaccine strategy.

Nonetheless, a comprehensive analysis of the atypical CHIKF symptoms due to the Brazilian outbreak from 2015 to 2019 is still lacking, since clinical data are scarce in the literature. Nevertheless, the impact of CHIKV in the Brazilian population could account for the introduction of a new pathogen into a naïve population with a higher probability to spread due to the highly populated urban areas and the high density of the mosquito vectors. However, the number of cases of CHIKV infection in Brazil, which were several orders of magnitude higher than in any other country of South America, was accompanied by the introduction of the ECSA strain, which substituted the Asian strain that was first introduced into the country. While in other regions of South America and in Central America, the Asian strain was responsible for the outbreaks. Thus, one cannot rule out the contribution of specific viral factors that allowed for the behavior of the epidemics in Brazil.

It is important to point out that the CHIKV introduction and epidemics in South America, and specifically in Brazil, occurred concomitantly with the epidemic of Zika virus, and the ongoing outbreaks of Dengue virus. Co-infections may promote the onset of serious illness, such as those with neurological symptoms. The number of co-infection cases still need to be fully addressed, but its impact on the clinical outcome of co-infected individual need to be anticipated.

Regarding viral-host interactions, it is clear that plenty of information on cellular processes is still a matter of debate, once depending on the cell type or animal model, some outcomes for the same question/issue can be quite contradictory. The deep comprehension of essential cellular processes that CHIKV can interfere with and alter to its own replication is a crucial task that researchers need to face and investigate. Thereby, results from new researches in the field of host-viral interaction could bring new strategies to combat this threat and to minimize the social, economic, and health burden, improving the life quality from the affected population, alleviating symptoms, avoiding some atypical complications, and interrupting viral persistence establishment.

AUTHOR CONTRIBUTIONS

MC, MS, IC, GS, and SC wrote the review and revised the figures. PAC and VF wrote the review. LC wrote and revised the review and revised the figures. All the authors contributed to the article and approved the submitted version.

FUNDING

This study was financed in part by the Coordenação de Aperfeiçoamento de Pessoal de Nível Superior – Brasil (CAPES) – Finance Code 001. This work was also supported by FINEP, CNPq, and FAPERJ. PAC, IC, SC, and VF are the recipients of a CNPq fellowship. GS is the recipient of a CAPES fellowship.

REFERENCES

Agarwal, A., Sharma, A. K., Sukumaran, D., Parida, M., and Dash, P. K. (2016). Two novel epistatic mutations (E1:K211E and E2:V264A) in structural proteins of Chikungunya virus enhance fitness in *Aedes aegypti*. *Virology* 497, 59–68. doi: 10.1016/j.virol.2016.06.025

Akhrymuk, I., Lukash, T., Frolov, I., and Frolova, E. I. (2019). Novel mutations in nsP2 abolish chikungunya virus-induced transcriptional shutoff and make the virus less cytopathic without affecting its replication rates. *J. Virol.* 93:e02062-18. doi: 10.1128/JVI.02062-2018

Aliperti, G., and Schlesinger, M. J. (1978). Evidence for an autoprotease activity of sindbis virus capsid protein. *Virology* 90, 366–369. doi: 10.1016/0042-6822(78)90321-5

Alva-Urcia, C., Aguilar-Luis, M. A., Palomares-Reyes, C., Silva-Caso, W., Suarez-Ognio, L., Weilg, P., et al. (2017). Emerging and reemerging arboviruses: a new threat in eastern peru. *PLoS One* 12:e0187897. doi: 10.1371/journal.pone.0187897

Ambrose, R. L., and Mackenzie, J. M. (2011). West Nile virus differentially modulates the unfolded protein response to facilitate replication and immune evasion. *J. Virol.* 85, 2723–2732. doi: 10.1128/JVI.02050-2010

Axe, E. L., Walker, S. A., Manifava, M., Chandra, P., Roderick, H. L., Habermann, A., et al. (2008). Autophagosome formation from membrane compartments enriched in phosphatidylinositol 3-phosphate and dynamically connected to the endoplasmic reticulum. *J. Cell Biol.* 182, 685–701. doi: 10.1083/jcb.200803137

Azevedo, M. B. D., Coutinho, M. S. C., Silva, M. A. D., Arduini, D. B., Lima, J. D. V., Monteiro, L., et al. (2018). Neurologic manifestations in emerging arboviral diseases in Rio de Janeiro City, Brazil, 2015-2016. *Rev. Soc. Bras. Med. Trop.* 51, 347–351. doi: 10.1590/0037-8682-0327-2017

Bae, S., Lee, J. Y., and Myoung, J. (2019). Chikungunya virus-encoded nsP2, E2 and E1 strongly antagonize the interferon-β signaling pathway. *J. Microbiol. Biotechnol.* 29, 1852–1859. doi: 10.4014/jmb.1910.10014

Beesoon, S., Funkhouser, E., Kotea, N., Spielman, A., and Robich, R. M. (2008). Chikungunya fever, Mauritius, 2006. *Emerg. Infect. Dis* 14, 337–338. doi: 10.3201/eid1402.071024

Bergsbaken, T., Fink, S. L., and Cookson, B. T. (2009). Pyroptosis: host cell death and inflammation. *Nat. Rev. Microbiol.* 7, 99–109. doi: 10.1038/nrmicro2070

Bernales, S., McDonald, K. L., and Walter, P. (2006). Autophagy counterbalances endoplasmic reticulum expansion during the unfolded protein response. *PLoS Biol.* 4:e423. doi: 10.1371/journal.pbio.0040423

Bernard, E., Solignat, M., Gay, B., Chazal, N., Higgs, S., Devaux, C., et al. (2010). Endocytosis of chikungunya virus into mammalian cells: role of clathrin and early endosomal compartments. *PLoS One* 5:e11479. doi: 10.1371/journal.pone.0011479

Berry, I. M., Rutvisuttinunt, W., Sippy, R., Beltran-Ayala, E., Figueroa, K., Ryan, S., et al. (2020). The origins of dengue and chikungunya viruses in Ecuador following increased migration from Venezuela and Colombia. *BMC Evol. Biol.* 20:31. doi: 10.1186/s12862-020-1596-1598

Bonifay, T., Prince, C., Neyra, C., Demar, M., Rousset, D., Kallel, H., et al. (2018). Atypical and severe manifestations of chikungunya virus infection in French Guiana: a hospital-based study. *PLoS One* 13:e0207406. doi: 10.1371/journal.pone.0207406

Brighton, S. W., Prozesky, O. W., and de la Harpe, A. L. (1983). Chikungunya virus infection. A retrospective study of 107 cases. *S. Afr. Med. J.* 63, 313–315.

Camacho, D., Reyes, J., Negredo, A., Hernández, L., Sánchez-Seco, M., and Comach, G. (2017). Asian genotype of Chikungunya virus circulating in Venezuela during 2014. *Acta Trop.* 174, 88–90. doi: 10.1016/j.actatropica.2017.06.026

Carbajo, A. E., and Vezzani, D. (2015). Waiting for chikungunya fever in Argentina: spatio-temporal risk maps. *Mem. Inst. Oswaldo. Cruz.* 110, 259–262. doi: 10.1590/0074-02760150005

Cataldi, A. (2010). Cell responses to oxidative stressors. *Curr. Pharm. Des.* 16, 1387–1395. doi: 10.2174/138161210791033969

Chen, W., Foo, S. S., Taylor, A., Lulla, A., Merits, A., Hueston, L., et al. (2015). Bindarit, an inhibitor of monocyte chemotactic protein synthesis, protects against bone loss induced by chikungunya virus infection. *J. Virol.* 89, 581–593. doi: 10.1128/JVI.02034-14

Chen, W., Foo, S. S., Zaid, A., Teng, T. S., Herrero, L. J., Wolf, S., et al. (2017). Specific inhibition of NLRP3 in chikungunya disease reveals a role for inflammasomes in alphavirus-induced inflammation. *Nat. Microbiol.* 2, 1435–1445. doi: 10.1038/s41564-017-0015-4

Conforti-Andreoni, C., Ricciardi-Castagnoli, P., and Mortellaro, A. (2011). The inflammasomes in health and disease: from genetics to molecular mechanisms of autoinflammation and beyond. *Cell. Mol. Immunol.* 8, 135–145. doi: 10.1038/cmi.2010.81

Consuegra-Rodríguez, M. P., Hidalgo-Zambrano, D. M., Vásquez-Serna, H., Jimenez-Canizales, C. E., Parra-Valencia, E., and Rodriguez-Morales, A. J. (2018). Post-chikungunya chronic inflammatory rheumatism: follow-up of cases after 1 year of infection in Tolima, Colombia. *Travel Med. Infect. Dis.* 21, 62–68. doi: 10.1016/j.tmaid.2017.11.013

Cook, L. E., Locke, M. C., Young, A. R., Monte, K., Hedberg, M. L., Shimak, R. M., et al. (2019). Distinct roles of interferon alpha and beta in controlling Chikungunya. Virus replication and modulating neutrophil-mediated inflammation. *J. Virol.* 94:19. doi: 10.1128/JVI.00841-19

Couderc, T., Chrétien, F., Schilte, C., Disson, O., Brigitte, M., Guivel-Benhassine, F., et al. (2008). A mouse model for Chikungunya: young age and inefficient type-I interferon signaling are risk factors for severe disease. *PLoS Pathog.* 4:e29. doi: 10.1371/journal.ppat.0040029

Cunha, M. S., Cruz, N. V. G., Schnellrath, L. C., Medaglia, M. L. G., Casotto, M. E., Albano, R. M., et al. (2017). Autochthonous transmission of East/Central/South African Genotype Chikungunya Virus, Brazil. *Emerg. Infect. Dis.* 23, 1737–1739. doi: 10.3201/eid2310.161855

Davis, B. K., Wen, H., and Ting, J. P. (2011). The inflammasome NLRs in immunity, inflammation, and associated diseases. *Annu. Rev. Immunol.* 29, 707–735. doi: 10.1146/annurev-immunol-031210-101405

De Lamballerie, X., Leroy, E., Charrel, R. N., Ttsetsarkin, K., Higgs, S., and Gould, E. A. (2008). Chikungunya virus adapts to tiger mosquito via evolutionary convergence: a sign of things to come? *Virol. J.* 5:33. doi: 10.1186/1743-422X-5-33

Dec, G. W. Jr., Waldman, H., Southern, J., Fallon, J. T., Hutter, A. M. Jr., and Palacios, I. (1992). Viral myocarditis mimicking acute myocardial infarction. *J. Am. Coll. Cardiol.* 20, 85–89. doi: 10.1016/0735-1097(92)90141-9

Delisle, E., Rousseau, C., Broche, B., Leparc-Goffart, I., L'ambert, G., Cochet, A., et al. (2015). Chikungunya outbreak in Montpellier, France, September to October 2014. *Eurosurveillance* 20:21108. doi: 10.2807/1560-7917.ES2015.20.17.21108

Deller, J. J. Jr., and Russell, P. K. (1968). Chikungunya disease. *Am. J. Trop. Med. Hyg.* 17, 107–111. doi: 10.4269/ajtmh.1968.17.107

Deretic, V., and Levine, B. (2018). Autophagy balances inflammation in innate immunity. *Autophagy* 14, 243–251. doi: 10.1080/15548627.2017.1402992

DeTulleo, L., and Kirchhausen, T. (1998). The clathrin endocytic pathway in viral infection. *EMBO J.* 17, 4585–4593. doi: 10.1093/emboj/17.16.4585

Diallo, M., Thonnon, J., Traore-Lamizana, M., and Fontenille, D. (1999). Vectors of chikungunya virus in Senegal: current data and transmission cycles. *Am. J. Trop. Med. Hyg.* 60, 281–286. doi: 10.4269/ajtmh.1999.60.281

Dias, C. N. S., Gois, B. M., Lima, V. S., Guerra-Gomes, I. C., Araújo, J. M. G., Gomes, J. A. S., et al. (2018). Human CD8 T-cell activation in acute and chronic chikungunya infection. *Immunology* 155, 499–504. doi: 10.1111/imm.12992

Djavaheri-Mergny, M., Amelotti, M., Mathieu, J., Besançon, F., Bauvy, C., and Codogno, P. (2007). Regulation of autophagy by NFkappaB transcription factor and reactives oxygen species. *Autophagy* 3, 390–392. doi: 10.4161/auto.4248

Dreier, J. W., Andersen, A. M., and Berg-Beckhoff, G. (2014). Systematic review and meta-analyses: fever in pregnancy and health impacts in the offspring. *Pediatrics* 133, e674–e688. doi: 10.1542/peds.2013-3205

Dubrulle, M., Mousson, L., Moutailler, S., Vazeille, M., and Failloux, A. B. (2009). Chikungunya virus and Aedes mosquitoes: saliva is infectious as soon as two days after oral infection. *PLoS One* 4:e5895. doi: 10.1371/journal.pone.0005895

Economopoulou, A., Dominguez, M., Helynck, B., Sissoko, D., Wichmann, O., Quenel, P., et al. (2009). Atypical Chikungunya virus infections: clinical manifestations, mortality and risk factors for severe disease during the 2005-2006 outbreak on Réunion. *Epidemiol. Infect.* 137, 534–541. doi: 10.1017/S0950268808001167

Egami, Y., Taguchi, T., Maekawa, M., Arai, H., and Araki, N. (2014). Small GTPases and phosphoinositides in the regulatory mechanisms of macropinosome formation and maturation. *Front. Physiol.* 30:374. doi: 10.3389/fphys.2014.00374

Ekchariyawat, P., Hamel, R., Bernard, E., Wichit, S., Surasombatpattana, P., Talignani, L., et al. (2015). Inflammasome signaling pathways exert antiviral effect against Chikungunya virus in human dermal fibroblasts. *Infect. Genet. Evol.* 32, 401–408. doi: 10.1016/j.meegid.2015.03.025

Eng, K. E., Panas, M. D., Murphy, D., Karlsson Hedestam, G. B., and McInerney, G. M. (2012). Accumulation of autophagosomes in semliki forest virus-infected cells is dependent on expression of the viral glycoproteins. *J. Virol.* 86, 5674–5685. doi: 10.1128/JVI.06581-11

Escalera-Antezana, J. P., Murillo-García, D. R., Gómez, C., Unzueta-Quiroga, R. C., and Rodríguez-Morales, A. J. (2018). Chikungunya in bolivia: domestic imported case series in cochabamba. *J. Formos. Med. Assoc.* 117, 1133–1134. doi: 10.1016/j.jfma.2018.10.009

Fadila, A., and Failloux, A. B. (2006). Chikungunya: an unexpected emergence in Europe. *Curr. Opin. Virol.* 21, 146–150. doi: 10.1016/j.coviro.2016.09.014

Filomeni, G., Desideri, E., Cardaci, S., Rotilio, G., and Ciriolo, M. R. (2010). Under the RO thiol network is the principal suspect for autophagy commitment. *Autophagy* 6, 999–1005. doi: 10.4161/auto.6.7.12754

Firth, A. E., Chung, B. Y., Fleeton, M. N., and Atkins, J. F. (2008). Discovery of frameshifting in Alphavirus 6K resolves a 20-year enigma. *Virol. J.* 5:108. doi: 10.1186/1743-422X-5-108

Fritel, X., Rollot, O., Gerardin, P., Gauzere, B. A., Bideault, J., Lagarde, L., et al. (2010). Chikungunya virus infection during pregnancy, Reunion, France, 2006. *Emerg. Infect. Dis* 16, 418–425. doi: 10.3201/eid1603.091403

Fros, J. J., Major, L. D., Scholte, F. E. M., Gardner, J., van Hemert, M. J., Suhrbier, A., et al. (2015). Chikungunya virus non-structural protein 2-mediated host shut-off disables the unfolded protein response. *J. Gen. Virol.* 96(Pt 3), 580–589. doi: 10.1099/vir.0.071845-0

Gardner, C. L., Hritz, J., Sun, C., Vanlandingham, D. L., Song, T. Y., Ghedin, E., et al. (2014). Deliberate attenuation of chikungunya virus by adaptation to heparan sulfate-dependent infectivity: a model for rational arboviral vaccine design. *PLoS Negl. Trop. Dis.* 8:e2719. doi: 10.1371/journal.pntd.0002719

Gasque, P., and Jaffar-Bandjee, M. C. (2015). The immunology and inflammatory responses of human melanocytes in infectious diseases. *J. Infect.* 71, 413–421. doi: 10.1016/j.jinf.2015.06.006

Gérardin, P., Barau, G., Michault, A., Bintner, M., Randrianaivo, H., Choker, G., et al. (2008). Multidisciplinary prospective study of mother-to-child chikungunya virus infections on the island of La Reunion. *PLoS Med.* 5:60. doi: 10.1371/journal.pone.000060

Gérardin, P., Couderc, T., Bintner, M., Tournebize, P., Renouil, M., Lémant, J., et al. (2016). Chikungunya virus-associated encephalitis: a cohort study on La Réunion Island, 2005-2009. *Neurology* 86, 94–102. doi: 10.1212/WNL.0000000000002234

Grandadam, M., Caro, V., Plumet, S., Thiberge, J. M., Souarès, Y., Failloux, A. B., et al. (2011). Chikungunya virus, southeastern France. *Emerg. Infect. Dis.* 17:910. doi: 10.3201/eid1705.101873

Green, A. M., Beatty, P. R., Hadjilaou, A., and Harris, E. (2014). Innate immunity to dengue virus infection and subversion of antiviral responses. *J. Mol. Biol.* 426, 1148–1160. doi: 10.1016/j.jmb.2013.11.023

Halstead, S. B., Udomsakdi, S., Scanlon, J. E., and Rohitayodhin, S. (1969). Dengue and chikungunya virus infection in man in Thailand, 1962-1964. V. Epidemiologic observations outside Bangkok. *Am. J. Trop. Med .Hyg.* 18, 1022–1033. doi: 10.4269/ajtmh.1969.18.1022

Harding, H. P., Calfon, M., Urano, F., Novoa, I., and Ron, D. (2002). Transcriptional and translational control in the Mammalian unfolded protein response. *Annu. Rev. Cell Dev. Biol.* 18, 575–599. doi: 10.1146/annurev.cellbio.18.011402.160624

He, B. (2006). Viruses, endoplasmic reticulum stress, and interferon responses. *Cell Death Differ.* 13, 393–403. doi: 10.1038/sj.cdd.4401833

Hetz, C., Martinon, F., Rodriguez, D., and Glimcher, L. H. (2011). The unfolded protein response: integrating stress signals through the stress sensor IRE1α. *Physiol. Rev.* 91, 1219–1243. doi: 10.1152/physrev.00001.2011

Hoarau, J. J., Jaffar Bandjee, M. C., Krejbich Trotot, P., Das, T., Li-Pat-Yuen, G., Dassa, B., et al. (2010). Persistent chronic inflammation and infection by chikungunya arthritogenic alphavirus in spite of a robust host immune response. *J. Immunol.* 184, 5914–5927. doi: 10.4049/jimmunol.0900255

Hu, Y. W., Zhang, J., Wu, X. M., Cao, L., Nie, P., and Chang, M. X. (2018). TANK-Binding Kinase 1 (TBK1) isoforms negatively regulate type i interferon induction by inhibiting TBK1-IRF3 Interaction and IRF3 phosphorylation. *Front. Immunol.* 9:84. doi: 10.3389/fimmu.2018.00084

Inamadar, A. C., Palit, A., Sampagavi, V. V., Raghunath, S., and Deshmukh, N. S. (2008). Cutaneous manifestations of chikungunya fever: observations made during a recent outbreak in south India. *Int. J. Dermatol.* 47, 154–159. doi: 10.1111/j.1365-4632.2008.03478.x

Inoue, T., and Tsai, B. (2013). How viruses use the endoplasmic reticulum for entry, replication, and assembly. *Cold Spring Harb. Perspect. Biol.* 5:a013250. doi: 10.1101/cshperspect.a013250

Jang, J. H., Shin, H. W., Lee, J. M., Lee, H. W., Kim, E. C., and Park, S. H. (2015). An overview of pathogen recognition receptors for innate immunity in dental pulp. *Med. Inflamm.* 2015:794143. doi: 10.1155/2015/794143

Jemielity, S., Wang, J. J., Chan, Y. K., Ahmed, A. A., Li, W., Monahan, S., et al. (2013). TIM-family proteins promote infection of multiple enveloped viruses through virion-associated phosphatidylserine. *PLoS Pathol.* 9:e1003232. doi: 10.1371/journal.ppat.1003232

Jheng, J. R., Ho, J. Y., and Horng, J. T. (2014). ER stress, autophagy, and RNA viruses. *Front. Microbiol.* 5:388. doi: 10.3389/fmicb.2014.00388

Jin, J., and Simmons, G. (2019). Antiviral functions of monoclonal antibodies against Chikungunya Virus. *Viruses* 11:E305. doi: 10.3390/v11040305

Jones, D. P. (2006). Redefining oxidative stress. *Antioxid. Redox. Signal.* 8, 1865–1879. doi: 10.1089/ars.2006.8.1865

Jones, J. E., Long, K. M., Whitmore, A. C., Sanders, W., Thurlow, L. R., Brown, J. A., et al. (2017). Disruption of the opal stop codon attenuates Chikungunya Virus-induced arthritis and pathology. *mBio* 8:e001456-17. doi: 10.1128/mBio.01456-17

Joubert, P. E., Stapleford, K., Guivel-Benhassine, F., Vignuzzi, M., Schwartz, O., and Albert, M. L. (2015). Inhibition of mTORC1 enhances the translation of chikungunya proteins via the activation of the MnK/eIF4E pathway. *PLoS Pathog.* 11:e1005091. doi: 10.1371/journal.ppat.1005091

Joubert, P. E., Werneke, S. W., de la Calle, C., Guivel-Benhassine, F., Giodini, A., Peduto, L., et al. (2012). Chikungunya virus-induced autophagy delays caspase-dependent cell death. *J. Exp. Med.* 209, 1029–1047. doi: 10.1084/jem.20110996

Judith, D., Mostowy, S., Bourai, M., Gangneux, N., Lelek, M., Lucas-Hourani, M., et al. (2013). Species-specific impact of the autophagy machinery on Chikungunya virus infection. *EMBO Rep.* 14, 534–544. doi: 10.1038/embor.2013.51

Kääriäinen, L., and Ahola, T. (2002). Functions of alphavirus nonstructural proteins in RNA replication. *Prog. Nucleic Acid Res. Mol. Biol.* 71, 187–222. doi: 10.1016/s0079-6603(02)71044-1

Kam, Y. W., Lee, W. W., Simarmata, D., Le Grand, R., Tolou, H., Merits, A., et al. (2014). Unique epitopes recognized by antibodies induced in chikungunya virus-infected non-human primates: implications for the study of immunopathology and vaccine development. *PLoS One* 9:e95647. doi: 10.1371/journal.pone.0095647

Khongwichit, S., Wikan, N., Abere, B., Thepparit, C., Kuadkitkan, A., Ubol, S., et al. (2016). Cell-type specific variation in the induction of ER stress and downstream events in chikungunya virus infection. *Microb. Pathog.* 101, 104–118. doi: 10.1016/j.micpath.2016

Kielian, M., Chanel-Vos, C., and Liao, M. (2010). Alphavirus entry and membrane fusion. *Viruses* 2, 796–825. doi: 10.3390/v2040796

Kim, D. Y., Reynaud, J. M., Rasalouskaya, A., Akhrymuk, I., Mobley, J. A., Frolov, I., et al. (2016). New world and old world alphaviruses have evolved to exploit different components of stress granules, FXR and G3BP proteins, for assembly of viral replication complexes. *PLoS Pathog.* 12:e1005810. doi: 10.1371/journal.ppat.1005810

Knipe, D. M., Howley, P. M., Griffin, D. E., Lamb, R. A., Martin, M. A., Roizman, B., et al. (2001). "Togaviridae: the viruses and their replication," in *Fields - Virology*, eds M. K. David and M. H. Peter (Philadelphia, PA: Lippincott Williams & Wilkins), 746–753.

Krejbich-Trotot, P., Gay, B., Li-Pat-Yuen, G., Hoarau, J. J., Jaffar-Bandjee, M. C., Briant, L., et al. (2011). Chikungunya triggers an autophagic process which promotes viral replication. *Virol J.* 8:432. doi: 10.1186/1743-422X-8-432

Kumar, R., Sharma, M. K., Jain, S. K., Yadav, S. K., and Singhal, A. K. (2017). Cutaneous manifestations of chikungunya fever: observations from an outbreak at a tertiary care hospital in Southeast Rajasthan, India. *Ind. Dermatol. Online J.* 8:336. doi: 10.4103/idoj.IDOJ_429_16

Labadie, K., Larcher, T., Joubert, C., Mannioui, A., Delache, B., Brochard, P., et al. (2010). Chikungunya disease in nonhuman primates involves long-termviral

persistence inmacrophages. *J. Clin. Invest.* 120, 894–906. doi: 10.1172/JCI40104

Lanciotti, R. S., and Valadere, A. M. (2014). Transcontinental movement of Asian genotype chikungunya virus. *Emerg. Infect. Dis.* 20, 1400–1402. doi: 10.3201/eid2008.140268

Lee, C. H. R., Mohamed Hussain, K., and Chu, J. J. H. (2019). Macropinocytosis dependent entry of Chikungunya virus into human muscle cells. *PLoS Negl. Trop. Dis.* 13:e0007610. doi: 10.1371/journal.pntd.0007610

Lemant, J., Boisson, V., Winer, A., Thibault, L., André, H., Tixier, F., et al. (2008). Serious acute chikungunya virus infection requiring intensive care during the Reunion Island outbreak in 2005-2006. *Crit. Care Med.* 36, 2536–2541. doi: 10.1097/CCM.0b013e318183f2d2

Leparc-Goffart, I., Nougairede, A., Cassadou, S., Prat, C., and de Lamballerie, X. (2014). Chikungunya in the Americas. *Lancet* 383:514. doi: 10.1016/S0140-6736(14)60185-9

Li, S., Kong, L., and Yu, X. (2015). The expanding roles of endoplasmic reticulum stress in virus replication and pathogenesis. *Crit. Rev. Microbiol.* 41, 150–164. doi: 10.3109/1040841X.2013.813899

Liang, X. H., Kleeman, L. K., Jiang, H. H., Gordon, G., Goldman, J. E., Berry, G., et al. (1998). Protection against fatal Sindbis virus encephalitis by beclin, a novel Bcl-2-interacting protein. *J. Virol.* 72, 8586–8596. doi: 10.1128/jvi.72.11.8586-8596.1998

Litzba, N., Schuffenecker, I., Zeller, H., Drosten, C., Emmerich, P., Charrel, R., et al. (2008). Evaluation of the first commercial chikungunya virus indirect immunofluorescence test. *J. Virol. Methods* 149, 175–179. doi: 10.1016/j.jviromet.2008.01.004

Liu, C. Y., and Kaufman, R. J. (2003). The unfolded protein response. *J. Cell Sci.* 116(Pt 10), 1861–1862. doi: 10.1242/jcs.00408

Lohachanakul, J., Phuklia, W., Thannagith, M., Thongsakulprasert, T., Smith, D. R., and Ubol, S. (2015). Differences in response of primary human myoblasts to infection with recent epidemic strains of Chikungunya virus isolated from patients with and without myalgia. *J. Med. Virol.* 87, 733–739. doi: 10.1002/jmv.24081

Lu, Y. E., and Kielian, M. (2000). Semliki forest virus budding: assay, mechanisms, and cholesterol requirement. *J. Virol.* 74, 7708–7719. doi: 10.1128/JVI.74.17.7708-7719.2000

Lum, F. M., Teo, T. H., Lee, W. W., Kam, Y. W., Rénia, L., and Ng, L. F. (2013). An essential role of antibodies in the control of Chikungunya virus infection. *J. Immunol.* 190, 6295–6302. doi: 10.4049/jimmunol.1300304

Lumsden, W. H. (1955). An epidemic of virus disease in Southern Province, Tanganyika Territory, in 1952-53. II. General description and epidemiology. *Trans. R. Soc. Trop. Med. Hyg.* 49, 33–57. doi: 10.1016/0035-9203(55)90081-x

Malhotra, J. D., and Kaufman, R. J. (2007). The endoplasmic reticulum and the unfolded protein response. *Semin. Cell Dev. Biol.* 18, 716–731. doi: 10.1016/j.semcdb.2007.09.003

Martinon, F., Burns, K., and Tschopp, J. (2002). The inflammasome: a molecular platform triggering activation of inflammatory caspases and processing of proIL-beta. *Mol. Cell.* 10, 417–426. doi: 10.1016/s1097-2765(02)00599-3

Matkovic, R., Bernard, E., Fontanel, S., Eldin, P., Chazal, O., Hassan Hersi, D., et al. (2019). The Host DHX9 DExH-Box helicase is recruited to Chikungunya Virus replication complexes for optimal genomic RNA translation. *J. Virol.* 93:e01764-18. doi: 10.1128/JVI.01764-18

McAuley, J. L., Tate, M. D., MacKenzie-Kludas, C. J., Pinar, A., Zeng, W., Stutz, A., et al. (2013). Activation of the NLRP3 inflammasome by IAV virulence protein PB1-F2 contributes to severe pathophysiology and disease. *PLoS Pathog.* 9:e1003392. doi: 10.1371/journal.ppat.1003392

Meertens, L., Hafirassou, M. L., Couderc, T., Bonnet-Madin, L., Kril, V., Kümmerer, B. M., et al. (2019). FHL1 is a major host factor for chikungunya virus infection. *Nature* 574, 259–263. doi: 10.1038/s41586-019-1578-4

Mehta, R., Gerardin, P., de Brito, C. A. A., Soares, C. N., Ferreira, M. L. B., and Solomon, T. (2018). The neurological complications of chikungunya virus: a systematic review. *Rev. Med. Virol.* 28:e1978. doi: 10.1002/rmv.1978

Melton, J. V., Ewart, G. D., Weir, R. C., Board, P. G., Lee, E., and Gage, P. W. (2002). Alphavirus 6K proteins form ion channels. *J. Biol. Chem.* 277, 46923–46931. doi: 10.1074/jbc.M207847200

Menon, P. R., Sankar, J., Gopinathan, K. M., and Mohan, G. (2010). A child with serious Chikungunya virus (CHIKV) infection requiring intensive care, after an outbreak. *Indian J. Pediatr.* 77, 1326–1328. doi: 10.1007/s12098-010-0174-2

Meshram, C. D., Agback, P., Shiliaev, N., Urakova, N., Mobley, J. A., Agback, T., et al. (2018). Multiple host factors interact with the hypervariable domain of Chikungunya Virus nsP3 and determine viral replication in cell-specific mode. *J. Virol.* 92:e0838-18. doi: 10.1128/JVI.00838-18

Messaoudi, I., Vomaske, J., Totonchy, T., Kreklywich, C. N., Haberthur, K., Springgay, L., et al. (2013). Chikungunya virus infection results in higher and persistent viral replication in aged rhesus macaques due to defects in anti-viral immunity. *PLoS Negl. Trop. Dis.* 7:e2343. doi: 10.1371/journal.pntd.0002343

Ministerio de Salud, Dirección General de Epidemiología (2015). *Primer Caso Autóctono De Chikungunya Y Riesgo De Transmisión En El Perú Lima: Ministerio De Salud Del Perú*. Available online at: http://www.dge.gob.pe/portal/docs/alertas/2015/AE005.pdf (accessed March 22, 2020).

Moller-Tank, S., Kondratowicz, A. S., Davey, R. A., Rennert, P. D., and Maury, W. (2013). Role of the phosphatidylserine receptor TIM-1 in enveloped-virus entry. *J. Virol.* 87, 8327–8341. doi: 10.1128/JVI.01025-13

Myles, K. M., Kelly, C. L., Ledermann, J. P., and Powers, A. M. (2006). Effects of an opal termination codon preceding the nsP4 gene sequence in the O'Nyong-Nyong virus genome on *Anopheles gambiae* infectivity. *J. Virol.* 80, 4992–4997. doi: 10.1128/JVI.80.10.4992-4997.2006

Nasci, R. S. (2014). Movement of chikungunya virus into the Western hemisphere. *Emerg. Infect. Dis.* 20, 1394–1395. doi: 10.3201/eid2008.140333

Naveca, F. G., Claro, I., Giovanetti, M., de Jesus, J. G., Xavier, J., de Melo Iani, F. C., et al. (2019). Genomic, epidemiological and digital surveillance of Chikungunya virus in the Brazilian Amazon. *PLoS Negl. Trop. Dis.* 13:e0007065. doi: 10.1371/journal.pntd.0007065

Negash, A. A., Ramos, H. J., Crochet, N., Lau, D. T., Doehle, B., Papic, N., et al. (2013). IL-1β production through the NLRP3 inflammasome by hepatic macrophages links hepatitis C virus infection with liver inflammation and disease. *PLoS Pathog.* 9:e1003330. doi: 10.1371/journal.ppat.1003330

Njenga, M. K., Nderitu, L., Ledermann, J. P., Ndirangu, A., Logue, C. H., Kelly, C. H., et al. (2008). Tracking epidemic Chikungunya virus into the Indian Ocean from East Africa. *J. Gen. Virol.* 89(Pt 11), 2754–2760. doi: 10.1099/vir.0.2008/005413-0

Nunes, M. R. T., Faria, N. R., de Vasconcelos, J. M., Golding, N., Kraemer, M. U., de Oliveira, L. F., et al. (2015). Emergence and potential for spread of Chikungunya virus in Brazil. *BMC Med.* 13:102. doi: 10.1186/s12916-015-0348-x

Olcum, M., Tastan, B., Kiser, C., Genc, S., and Genc, K. (2020). Microglial NLRP3 inflammasome activation in multiple sclerosis. *Adv. Protein Chem. Struct. Biol.* 119, 247–308. doi: 10.1016/bs.apcsb.2019.08.007

Orvedahl, A., Alexander, D., Tallóczy, Z., Sun, Q., Wei, Y., Zhang, W., et al. (2007). HSV-1 ICP34.5 confers neurovirulence by targeting the Beclin 1 autophagy protein. *Cell Host Microb.* 1, 23–35. doi: 10.1016/j.chom.2006.12.001

Orvedahl, A., MacPherson, S., Sumpter, R. Jr., Tallóczy, Z., Zou, Z., and Levine, B. (2010). Autophagy protects against Sindbis virus infection of the central nervous system. *Cell Host Microb.* 7, 115–127. doi: 10.1016/j.chom.2010.01.007

Ozden, S., Huerre, M., Riviere, J. P., Coffey, L. L., Afonso, P. V., Mouly, V., et al. (2007). Human muscle satellite cells as targets of Chikungunya virus infection. *PLoS One* 2:e527. doi: 10.1371/journal.pone.0000527

Pan American Health Organization (2020). *Chikungunya*. Available online at: https://www.paho.org/hq/index.php?Itemid=40931&lang=pt (accessed January 2, 2020).

Pereira, L. P., Villas-Bôas, R., Scott, S. S. O., Nóbrega, P. R., Sobreira-Neto, M. A., Castro, J. D. V., et al. (2017). Encephalitis associated with the chikungunya epidemic outbreak in Brazil: report of 2 cases with neuroimaging findings. *Rev. Soc. Bras. Med. Trop.* 50, 413–416. doi: 10.1590/0037-8682-0449-2016

Perret, C., Vizcaya, C., Weitzel, T., Rosas, R., Dabanch, J., and Martinez, C. (2018). Chikungunya, emerging disease in Latin America. Description of the first cases in Chile. *Rev. Chil. Infectol.* 35, 413–419. doi: 10.4067/s0716-10182018000400413

Petersen, L. R., and Powers, A. M. (2016). Chikungunya: epidemiology. *F1000Research* 5:F1000FacultyRev–82. doi: 10.12688/f1000research.7171.1

Petitdemange, C., Becquart, P., Wauquier, N., Béziat, V., Debré, P., Leroy, E. M., et al. (2011). Unconventional repertoire profile is imprinted during acute chikungunya infection for natural killer cells polarization toward cytotoxicity. *PLoS Pathog.* 7:e1002268. doi: 10.1371/journal.ppat

Platanias, L. C. (2005). Mechanisms of type-I- and type-II-interferon-mediated signalling. *Nat. Rev. Immunol.* 5, 375–386. doi: 10.1038/nri1604

Powers, A. M., Brault, A. C., Tesh, R. B., and Weaver, S. C. (2000). Re-emergence of chikungunya and o'nyong-nyong viruses: evidence for distinct geographical lineages and distant evolutionary relationships. *J. Gen. Virol.* 81(Pt 2), 471–479. doi: 10.1099/0022-1317-81-2-471

Powers, A. M., and Logue, C. H. (2007). Changing patterns of chikungunya virus: re-emergence of a zoonotic arbovirus. *J. Gen. Virol.* 8(Pt 9), 2363–2377. doi: 10.1099/vir.0.82858-0

Prashant, S., Kumar, A. S., Basheeruddin, D. D., Chowdhary, T. N., and Madhu, B. (2009). Cutaneous manifestations in patients suspected of chikungunya disease. *Indian J. Dermatol.* 54, 128–131. doi: 10.4103/0019-5154.53186

Queyriaux, B., Simon, F., Grandadam, M., Michel, R., Tolou, H., and Boutin, J. P. (2008). Clinical burden of chikungunya virus infection. *Lancet Infect. Dis.* 8, 2–3. doi: 10.1016/S1473-3099(07)70294-3

Radoshitzky, S. R., Pegoraro, G., Chî, X. O. D., Ng, L., Chiang, C. Y., Jozwick, L., et al. (2016). siRNA screen identifies trafficking host factors that modulate alphavirus infection. *PLoS Pathog.* 12:e1005466. doi: 10.1371/journal.ppat.1005466

Ramsey, J., and Mukhopadhyay, S. (2017). Disentangling the frames, the state of research on the alphavirus 6K and TF proteins. *Viruses* 9:E228. doi: 10.3390/v9080228

Rathore, A. P., Ng, M. L., and Vasudevan, S. G. (2013). Differential unfolded protein response during Chikungunya and Sindbis virus infection: CHIKV nsP4 suppresses eIF2α phosphorylation. *Virol. J.* 10:36. doi: 10.1186/1743-422X-10-36

Renault, P., Solet, J. L., Sissoko, D., Balleydier, E., Larrieu, S., Filleul, L., et al. (2007). A major epidemic of chikungunya virus infection on Reunion Island, France, 2005-2006. *Am. J. Trop. Med. Hyg.* 77, 727–731. doi: 10.4269/ajtmh.2007.77.727

Rezza, G., Nicoletti, L., Angelini, R., Romi, R., Finarelli, A. C., Panning, M., et al. (2007). Infection with chikungunya virus in Italy: an outbreak in a temperate region. *Lancet* 370, 1840–1846. doi: 10.1016/S0140-6736(07)61779-6

Rico-Mendoza, A., Porras-Ramírez, A., Chang, A., Encinales, L., and Lynch, R. (2019). Authors' response to the letter to the editor entitled: co-circulation of dengue, chikungunya, and Zika viruses and cross-protection. *Rev. Panam. Salud Púb.* 43:77. doi: 10.26633/RPSP.2019.77

Robin, S., Ramful, D., Le Seach, F., Jaffar-Bandjee, M. C., Rigou, G., and Alessandri, J. L. (2008). Neurologic manifestations of pediatric chikungunya infection. *J. Child Neurol.* 23, 1028–1035. doi: 10.1177/0883073808314151

Ross, R. W. (1956). The Newala epidemic. III The virus: isolation, pathogenic properties and relationship to the epidemic. *J. Hyg.* 54, 177–191. doi: 10.1017/s0022172400044442

Sánchez-Carbonel, J., Tantaléan-Yépez, D., Aguilar-Luis, M. A., Silva-Caso, W., Weilg, P., Vásquez-Achaya, F., et al. (2018). Identification of infection by Chikungunya, Zika, and Dengue in an area of the Peruvian coast. Molecular diagnosis and clinical characteristics. *BMC Res. Notes* 11:175. doi: 10.1186/s13104-018-3290-0

Schilte, C., Couderc, T., Chretien, F., Sourisseau, M., Gangneux, N., Guivel-Benhassine, F., et al. (2010). Type I IFN controls chikungunya virus via its action on nonhematopoietic cells. *J. Exp. Med.* 207, 429–442. doi: 10.1084/jem.20090851

Schuffenecker, I., Iteman, I., Michault, A., Murri, S., Frangeul, L., Vaney, M. C., et al. (2006). Genome microevolution of chikungunya viruses causing the Indian Ocean outbreak. *PLoS Med.* 3:e263. doi: 10.1371/journal.pmed.0030263

Sergon, K., Njuguna, C., Kalani, R., Ofula, V., Onyango, C., Konongoi, L. S., et al. (2008). Seroprevalence of Chikungunya virus (CHIKV) infection on Lamu Island, Kenya, October 2004. *Am. J. Trop. Med. Hyg.* 78, 333–337. doi: 10.4269/ajtmh.2008.78.333

Severini, F., Boccolini, D., Fortuna, C., Di Luca, M., Toma, L., Amendola, A., et al. (2018). Vector competence of Italian *Aedes albopictus* populations for the chikungunya virus (E1-226V). *PLoS Negl. Trop. Dis.* 12:e0006435. doi: 10.1371/journal.pntd.0006435

Sharp, T. M., Roth, N. M., Torres, J., Ryff, K. R., Pérez Rodríguez, N. M., Mercado, C., et al. (2014). Chikungunya cases identified through passive surveillance and household investigations–Puerto Rico, May 5-August 12, 2014. *MMWR Morb. Mortal. Wkly. Rep.* 63, 1121–1128.

Shirako, Y., and Strauss, J. H. (1994). Regulation of Sindbis virus RNA replication: uncleaved P123 and nsP4 function in minus-strand RNA synthesis, whereas cleaved products from P123 are required for efficient plus-strand RNA synthesis. *J. Virol.* 68, 1874–1885. doi: 10.1128/jvi.68.3.1874-1885.1994

Shivakumar, V., Okade, R., Rajkumar, V., and Rajashekar, T. S. (2007). Unusual facial melanosis in viral fever. *Indian J. Dermatol.* 52, 116–117.

Simon, F., Javelle, E., Oliver, M., Leparc-Goffart, I., and Marimoutou, C. (2011). Chikungunya virus infection. *Curr. Infect. Dis. Rep.* 13:218. doi: 10.1007/s11908-011-0180-1

Simon, F., Parola, P., Grandadam, M., Fourcade, S., Oliver, M., Brouqui, P., et al. (2007). Chikungunya infection: an emerging rheumatism among travelers returned from indian ocean islands. Report of 47 cases. *Medicine* 86, 123–137. doi: 10.1097/MD/0b013e31806010a5

Singh, I., and Helenius, A. (1992). Role of ribosomes in Semliki Forest virus nucleocapsid uncoating. *J. Virol.* 66, 7049–7058. doi: 10.1128/jvi.66.12.7049-7058.1992

Sissoko, D., Malvy, D., Giry, C., Delmas, G., Paquet, C., Gabrie, P., et al. (2008). Outbreak of Chikungunya fever in Mayotte, Comoros archipelago, 2005-2006. *Trans. R. Soc. Trop. Med. Hyg.* 102, 780–786. doi: 10.1016/j.trstmh.2008.02.018

Sjöberg, M., and Garoff, H. (2003). Interactions between the transmembrane segments of the alphavirus E1 and E2 proteins play a role in virus budding and fusion. *J. Virol.* 77, 3441–3450. doi: 10.1128/JVI.77.6.3441-3450.2003

Smit, J. M., Waarts, B. L., Kimata, K., Klimstra, W. B., Bittman, R., and Wilschut, J. (2002). Adaptation of alphaviruses to heparan sulfate: interaction of Sindbis and Semliki forest viruses with liposomes containing lipid-conjugated heparin. *J. Virol.* 76, 10128–10137. doi: 10.1128/JVI.76.20.10128-10137.2002

Smith, A. E., and Helenius, A. (2004). How viruses enter animal cells. *Science* 304, 237–242. doi: 10.1126/science.1094823

Snyder, J. E., Kulcsar, K. A., Schultz, K. L., Riley, C. P., Neary, J. T., Marr, S., et al. (2013). Functional characterization of the alphavirus TF protein. *J Virol.* 87, 8511–8523. doi: 10.1128/JVI.00449-13

Solanki, B. S., Arya, S., and Maheshwari, P. (2007). Chikungunya disease with nephritic presentation. *Int. J. Clin. Pract.* 61:1941. doi: 10.1111/j.1742-1241.2007.01329.x

Solignat, M., Gay, B., Higgs, S., Briant, L., and Devaux, C. (2009). Replication cycle of chikungunya: a re-emerging arbovirus. *Virology* 393, 183–197. doi: 10.1016/j.virol.2009.07.024

Sourisseau, M., Schilte, C., Casartelli, N., Trouillet, C., Guivel-Benhassine, F., Rudnicka, D., et al. (2007). Characterization of reemerging chikungunya virus. *PLoS Pathog.* 3:e89. doi: 10.1371/journal.ppat.0030089

Souza, T. M., Azeredo, E. L., Badolato-Corrêa, J., Damasco, P. V., Santos, C., Petitinga-Paiva, F., et al. (2017). First Report of the East-Central South African Genotype of Chikungunya Virus in Rio de Janeiro, Brazil. *PLoS Curr.* 9:ecurrents.outbreaks.4200119978d62ccaa454599cd2735727. doi: 10.1371/currents.outbreaks.4200119978d62ccaa454599cd2735727

Souza, T. M. L., Vieira, Y. R., Delatorre, E., Barbosa-Lima, G., Luiz, R. L. F., Vizzoni, A., et al. (2019). Emergence of the East-Central-South African genotype of Chikungunya virus in Brazil and the city of Rio de Janeiro may have occurred years before surveillance detection. *Sci. Rep.* 9:2760. doi: 10.1038/s41598-019-39406-9

Spodick, D. H. (1986). Infection and infarction. Acute viral (and other) infection in the onset, pathogenesis, and mimicry of acute myocardial infarction. *Am. J. Med.* 81, 661–668. doi: 10.1016/0002-9343(86)90554-1

Spuul, P., Balistreri, G., Kääriäinen, L., and Ahola, T. (2010). Phosphatidylinositol 3- kinase-, actin-, and microtubule-dependent transport of Semliki Forest Virus replication complexes from the plasma membrane to modified lysosomes. *J. Virol.* 84, 7543–7557. doi: 10.1128/JVI.00477-10

Stapleford, K. A., Moratorio, G., and Henningsson, R. (2016). Whole-genome sequencing analysis from the Chikungunya Virus caribbean outbreak reveals novel evolutionary genomic elements. *PLoS Negl. Trop. Dis.* 10:e0004402. doi: 10.1371/journal.pntd.0004402

Staples, J. E., Breiman, R. F., and Powers, A. M. (2009). Chikungunya fever: an epidemiological review of a re-emerging infectious disease. *Clin. Infect. Dis.* 49, 942–948. doi: 10.1086/605496

Suhana, O., Nazni, W. A., Apandi, Y., Farah, H., Lee, H. L., and Sofian-Azirun, M. (2019). Insight into the origin of chikungunya virus in Malaysian non-human primates via sequence analysis. *Heliyon* 5:e02682. doi: 10.1016/j.heliyon.2019.e02682

Suhrbier, A., Jaffar-Bandjee, M. C., and Gasque, P. (2012). Arthritogenic alphaviruses–an overview. *Nat. Rev. Rheumatol.* 8, 420–429. doi: 10.1038/nrrheum.2012.64

Suomalainen, M., Liljeström, P., and Garoff, H. (1992). Spike protein-nucleocapsid interactions drive the budding of alphaviruses. *J. Virol.* 66, 4737–4747. doi: 10.1128/jvi.66.8.4737-4747.1992

Suthar, M. S., Shabman, R., Madric, K., Lambeth, C., and Heise, M. T. (2005). Identification of adult mouse neurovirulence determinants of the Sindbis virus strain AR86. *J. Virol.* 79, 4219–4228. doi: 10.1128/JVI.79.7.4219-4228.2005

Teo, T. H., Lum, F. M., Claser, C., Lulla, V., Lulla, A., Merits, A., et al. (2013). A pathogenic role for CD4+ T cells during Chikungunya virus infection in mice. *J. Immunol.* 190, 259–269. doi: 10.4049/jimmunol.1202177

Thaa, B., Biasiotto, R., Eng, K., Neuvonen, M., Götte, B., Rheinemann, L., et al. (2015). Differential phosphatidylinositol-3-Kinase-Akt-mTOR activation by semliki forest and Chikungunya Viruses Is dependent on nsP3 and connected to Replication complex internalization. *J. Virol.* 89, 11420–11437. doi: 10.1128/JVI.01579-15

Thanapati, S., Ganu, M., Giri, P., Kulkarni, S., Sharma, M., Babar, P., et al. (2017). Impaired NK cell functionality and increased TNF-α production as biomarkers of chronic chikungunya arthritis and rheumatoid arthritis. *Hum. Immunol.* 78, 370–374. doi: 10.1016/j.humimm.2017.02.006

Thiberville, S. D., Moyen, N., Dupuis-Maguiraga, L., Nougairede, A., Gould, E. A., Roques, P., et al. (2013). Chikungunya fever: epidemiology, clinical syndrome, pathogenesis and therapy. *Antiviral Res.* 99, 345–370. doi: 10.1016/j.antiviral.2013.06.009

Thon-Hon, V. G., Denizot, M., Li-Pat-Yuen, G., Giry, C., Jaffar-Bandjee, M. C., and Gasque, P. (2012). Deciphering the differential response of two human fibroblast cell lines following Chikungunya virus infection. *Virol. J.* 9:213. doi: 10.1186/1743-422X-9-213

Torres, J. R., Falleiros-Arlant, L. H., Dueñas, L., Pleitez-Navarrete, J., Salgado, D. M., and Brea-Del Castillo, J. (2016). Congenital and perinatal complications of chikungunya fever: a Latin American experience. *Int. J. Infect. Dis.* 51, 85–88. doi: 10.1016/j.ijid.2016.09.009

Touret, Y., Randrianaivo, H., Michault, A., Schuffenecker, I., Kauffmann, E., Lenglet, Y., et al. (2006). Early maternal-fetal transmission of the Chikungunya virus. *Presse Med.* 35(11 Pt 1), 1656–1658. doi: 10.1016/S0755-4982(06)74874-6

Tournebize, P., Charlin, C., and Lagrange, M. (2009). Neurological manifestations in Chikungunya: about 23 cases collected in Reunion Island. *Rev. Neurol.* 165, 48–51. doi: 10.1016/j.neurol.2008.06.009

Tsetsarkin, K. A., Chen, R., and Leal, C. (2011). Chikungunya virus emergence is constrained in Asia by lineage-specific adaptive landscapes. *Proc. Natl. Acad. Sci. U.S.A.* 108, 7872–7877. doi: 10.1073/pnas.1018344108

Tsetsarkin, K. A., Chen, R., Yun, R., and Rossi, S. L. (2014). Multi-peaked adaptive landscape for chikungunya virus evolution predicts continued fitness optimization in *Aedes albopictus* mosquitoes. *Nat. Commun.* 5:4084. doi: 10.1038/ncomms5084

Tsetsarkin, K. A., McGee, C. E., Volk, S. M., Vanlandingham, D. L., Weaver, S. C., and Higgs, S. (2009). Epistatic roles of E2 glycoprotein mutations in adaption of chikungunya virus to *Aedes albopictus* and *Ae. aegypti* mosquitoes. *PLoS One* 31:e6835. doi: 10.1371/journal.pone.0006835

Tsetsarkin, K. A., Vanlandingham, D. L., McGee, C. E., and Higgs, S. (2007). A single mutation in chikungunya virus affects vector specificity and epidemic potential. *PLoS Pathog.* 3:e201. doi: 10.1371/journal.ppat.0030201

Tsetsarkin, K. A., and Weaver, S. C. (2011). Sequential adaptive mutations enhance efficient vector switching by Chikungunya virus and its epidemic emergence. *PLoS Pathog.* 7:e1002412. doi: 10.1371/journal.ppat.1002412

Vattem, K. M., and Wek, R. C. (2004). Reinitiation involving upstream ORFs regulates ATF4 mRNA translation in mammalian cells. *Proc. Natl. Acad. Sci. U.S.A.* 101, 11269–11274. doi: 10.1073/pnas.0400541101

Venkatesan, A., Tunkel, A. R., Bloch, K. C., Lauring, A. S., Sejvar, J., Bitnun, A., et al. (2013). Case definitions, diagnostic algorithms, and priorities in encephalitis: consensus statement of the international encephalitis consortium. *Clin. Infect. Dis.* 57, 1114–1128. doi: 10.1093/cid/cit458

Vijayakumar, K. P., Nair Anish, T. S., George, B., Lawrence, T., Muthukkutty, S. C., and Ramachandran, R. (2011). Clinical profile of Chikungunya patients during the epidemic of 2007 in Kerala. *India J. Glob. Infect. Dis.* 3, 221–226. doi: 10.4103/0974-777X.83526

Villero-Wolf, Y., Mattar, S., Puerta-González, A., Arrieta, G., Muskus, C., Hoyos, R., et al. (2019). Genomic epidemiology of Chikungunya virus in Colombia reveals genetic variability of strains and multiple geographic introductions in outbreak, 2014. *Sci. Rep.* 9:9970. doi: 10.1038/s41598-019-45981-8

Volk, S. M., Chen, R., Tsetsarkin, K. A., Adams, A. P., Garcia, T. I., Sall, A. A., et al. (2010). Genome-scale phylogenetic analyses of chikungunya virus reveal independent emergences of recent epidemics and various evolutionary rates. *J. Virol.* 84, 6497–6504. doi: 10.1128/JVI.01603-09

Voss, J. E., Vaney, M. C., Duquerroy, S., Vonrhein, C., Girard-Blanc, C., Crublet, E., et al. (2010). Glycoprotein organization of Chikungunya virus particles revealed by X-ray crystallography. *Nature* 468, 709–712. doi: 10.1038/nature09555

Wauquier, N., Becquart, P., Nkoghe, D., Padilla, C., Ndjoyi-Mbiguino, A., and Leroy, E. M. (2011). The acute phase of Chikungunya virus infection in humans is associated with strong innate immunity and T CD8 cell activation. *J. Infect. Dis.* 204, 115–123. doi: 10.1093/infdis/jiq006

Weaver, S. C., Hagenbaugh, A., Bellew, L. A., Netesov, S. V., Volchkov, V. E., Chang, G. J., et al. (1994). A comparison of the nucleotide sequences of eastern and western equine encephalomyelitis viruses with those of other alphaviruses and related RNA viruses. *Virology* 202:1083. doi: 10.1006/viro.1993.1599

Weber, C., Berberich, E., von Rhein, C., Henß, L., Hildt, E., and Schnierle, B. S. (2017). Identification of functional determinants in the Chikungunya Virus E2 Protein. *PLoS Negl. Trop. Dis.* 11:e0005318. doi: 10.1371/journal.pntd.0005318

White, L. K., Sali, T., Alvarado, D., Gatti, E., Pierre, P., Streblow, D., et al. (2011). Chikungunya virus induces IPS-1-dependent innate immune activation and protein kinase R-independent translational shutoff. *J. Virol.* 85, 606–620. doi: 10.1128/JVI.00767-10

Wikan, N., Khongwichit, S., Phuklia, W., Ubol, S., Thonsakulprasert, T., Thannagith, M., et al. (2014). Comprehensive proteomic analysis of white blood cells from chikungunya fever patients of different severities. *J. Transl. Med.* 12:96. doi: 10.1186/1479-5876-12-96

Wintachai, P., Wikan, N., Kuadkitkan, A., Jaimipuk, T., Ubol, S., Pulmanausahakul, R., et al. (2012). Identification of prohibitin as a Chikungunya virus receptor protein. *J. Med. Virol.* 84, 1757–1770. doi: 10.1002/jmv.23403

Xavier, J., Giovanetti, M., Fonseca, V., Thézé, J., Gräf, T., Fabri, A., et al. (2019). Circulation of chikungunya virus East/Central/South African lineage in Rio de Janeiro, Brazil. *PLoS One* 14:e0217871. doi: 10.1371/journal.pone.0217871

Yang, Z., and Klionsky, D. J. (2010). Eaten alive: a history of macroautophagy. *Nat. Cell Biol.* 12, 814–822. doi: 10.1038/ncb0910-814

Yoshida, H., Matsui, T., Yamamoto, A., Okada, T., and Mori, K. (2001). XBP1 mRNA is induced by ATF6 and spliced by IRE1 in response to ER stress to produce a highly active transcription factor. *Cell* 107, 881–891. doi: 10.1016/S0092-8674(01)00611-0

Zhang, R., Kim, A. S., Fox, J. M., Nair, S., Basore, K., Klimstra, W. B., et al. (2018). Mxra8 is a receptor for multiple arthritogenic alphaviruses. *Nature* 557, 570–574. doi: 10.1038/s41586-018-0121-3

Zim, M. M., Sam, I. C., Omar, S. S., Chan, Y. F., AbuBakar, S., and Kamarulzaman, A. (2013). Chikungunya infection in Malaysia: comparison with dengue infection in adults and predictors of persistent arthralgia. *J. Clin. Virol.* 56, 141–145. doi: 10.1016/j.jcv.2012.10.019

Conflict of Interest: The authors declare that the research was conducted in the absence of any commercial or financial relationships that could be construed as a potential conflict of interest.

Copyright © 2020 Cunha, Costa, Correa, de Souza, Calil, da Silva, Costa, Fonseca and da Costa. This is an open-access article distributed under the terms of the Creative Commons Attribution License (CC BY). The use, distribution or reproduction in other forums is permitted, provided the original author(s) and the copyright owner(s) are credited and that the original publication in this journal is cited, in accordance with accepted academic practice. No use, distribution or reproduction is permitted which does not comply with these terms.

frontiers in Microbiology

ORIGINAL RESEARCH
published: 29 July 2020
doi: 10.3389/fmicb.2020.01807

Sequencing the Genome of Indian Flying Fox, Natural Reservoir of Nipah Virus, Using Hybrid Assembly and Conservative Secondary Scaffolding

Julien Fouret[1,2], Frédéric G. Brunet[3], Martin Binet[1,2], Noémie Aurine[1], Francois Enchéry[1], Séverine Croze[4], Marie Guinier[2], Abdelghafar Goumaidi[2], Doris Preininger[5], Jean-Nicolas Volff[3], Marc Bailly-Bechet[6], Joël Lachuer[7,4], Branka Horvat[1*†] and Catherine Legras-Lachuer[2,8*†]*

[1] CIRI, International Center for Infectiology Research, Team Immunobiology of Viral Infections, Univ Lyon, INSERM U1111, CNRS UMR 5308, Ecole Normale Supérieure de Lyon, Université Claude Bernard Lyon 1, Lyon, France, [2] Viroscan3D, Trévoux, France, [3] Institut de Génomique Fonctionnelle de Lyon, Université de Lyon, CNRS UMR 5242, Ecole Normale Supérieure de Lyon, Université Claude Bernard Lyon 1, Lyon, France, [4] Plateforme Profilexpert, Université Claude Bernard Lyon 1, Lyon, France, [5] Tiergarten Schönbrunn, Vienna, Austria, [6] Université Nice Sophia Antipolis, INRA, CNRS, ISA, Nice, France, [7] Cancer Research Center of Lyon, INSERM 1052/CNRS 5286, Université de Lyon, Lyon, France, [8] Ecologie Microbienne, CNRS UMR 5557, LEM, INRA, VetAgro Sup, Université Claude Bernard Lyon 1, Villeurbanne, France

Indian fruit bats, flying fox *Pteropus medius* was identified as an asymptomatic natural host of recently emerged Nipah virus, which is known to induce a severe infectious disease in humans. The absence of *P. medius* genome sequence presents an important obstacle for further studies of virus–host interactions and better understanding of mechanisms of zoonotic viral emergence. Generation of the high-quality genome sequence is often linked to a considerable effort associated to elevated costs. Although secondary scaffolding methods have reduced sequencing expenses, they imply the development of new tools for the integration of different data sources to achieve more reliable sequencing results. We initially sequenced the *P. medius* genome using the combination of Illumina paired-end and Nanopore sequencing, with a depth of 57.4x and 6.1x, respectively. Then, we introduced the novel scaff2link software to integrate multiple sources of information for secondary scaffolding, allowing to remove the association with discordant information among two sources. Different quality metrics were next produced to validate the benefits from secondary scaffolding. The *P. medius* genome, assembled by this method, has a length of 1,985 Mb and consists of 33,613 contigs and 16,113 scaffolds with an NG50 of 19 Mb. At least 22.5% of the assembled sequences is covered by interspersed repeats already described in other species and 19,823 coding genes are annotated. Phylogenetic analysis demonstrated the clustering of *P. medius* genome with two other *Pteropus* bat species, *P. alecto* and *P. vampyrus*, for which genome sequences are currently available. SARS-CoV entry receptor ACE2 sequence of *P. medius* was 82.7% identical with ACE2 of *Rhinolophus sinicus* bats, thought to be the natural host of SARS-CoV. Altogether, our results confirm that a lower

OPEN ACCESS

Edited by:
Zhengli Shi,
Wuhan Institute of Virology (CAS), China

Reviewed by:
Aaron T. Irving,
Duke-NUS Medical School, Singapore
Xinglou Yang,
Wuhan Institute of Virology (CAS), China

***Correspondence:**
Julien Fouret
julien@fouret.me
Branka Horvat
branka.horvat@inserm.fr
Catherine Legras-Lachuer
catherine.lachuer@univ-lyon1.fr

† These authors have contributed equally to this work

Specialty section:
This article was submitted to Virology, a section of the journal Frontiers in Microbiology

Received: *15 January 2020*
Accepted: *09 July 2020*
Published: *29 July 2020*

Citation:
Fouret J, Brunet FG, Binet M, Aurine N, Enchéry F, Croze S, Guinier M, Goumaidi A, Preininger D, Volff J-N, Bailly-Bechet M, Lachuer J, Horvat B and Legras-Lachuer C (2020) Sequencing the Genome of Indian Flying Fox, Natural Reservoir of Nipah Virus, Using Hybrid Assembly and Conservative Secondary Scaffolding. Front. Microbiol. 11:1807. doi: 10.3389/fmicb.2020.01807

depth of sequencing is enough to obtain a valuable genome sequence, using secondary scaffolding approaches and demonstrate the benefits of the scaff2link application. The genome sequence is now available to the scientific community to (i) proceed with further genomic analysis of *P. medius*, (ii) to characterize the underlying mechanism allowing Nipah virus maintenance and perpetuation in its bat host, and (iii) to monitor their evolutionary pathways toward a better understanding of bats' ability to control viral infections.

Keywords: hybrid genome assembly, Nipah virus, *Pteropus medius*, *Pteropus giganteus*, secondary scaffolding, bats

INTRODUCTION

Bats have been reported to be the natural reservoir of several zoonotic viruses that cause severe human diseases, including Marburg, Ebola, Nipah, Hendra, SARS, and MERS viruses (Wang and Anderson, 2019). *Pteropus medius* (also known as *P. giganteus* and commonly called Indian flying fox (Mlikovsky, 2012) is a frugivorous giant bat, widely distributed in Southeast Asia, and shown to host numerous viral species (Anthony et al., 2013), including Nipah virus (Yadav et al., 2019). Nipah virus is a recently emerged zoonotic *Paramyxovirus*, capturing the attention of both scientific and public health communities due to its high lethality rate, up to 90% in Bangladesh and India epidemics, associated with human-to-human transmission (Mathieu and Horvat, 2015; Arunkumar et al., 2019). Although this virus is highly pathogenic in humans and numerous other mammalian species, it is asymptomatic in its natural host, fruit bats (Enchéry and Horvat, 2017). A better understanding of virus–host interactions requires further studies necessitating the availability of the sequenced genome (Shi, 2010), which has been lacking for *P. medius*. Therefore, our work aims to provide the genome sequence of *P. medius* as a new resource for genomic studies, analysis of molecular basis of bats' unique adaptation and bats' immunovirology and should help in understanding the underlying evolutionary mechanisms used by emerging viruses, like Nipah virus, to cross species barriers and to widespread in the newly introduced host. Moreover, recent outbreaks of numerous pathogenic viruses from bats, including SARS coronavirus (Hu et al., 2015), urge improved comprehension and characterizations of bat species.

Although bats make up more than 20% of existing mammals with 1,400 species (Lazzeroni et al., 2018), only 38 bat genome assemblies are currently available in the NCBI Genbank database. Several different sequencing strategies have been used in the past years to sequence bat genomes, including (i) high coverage long-read sequencing strategy, e.g., 83x of PacBIO *Eonycteris spelaea* (Wen et al., 2018), (ii) Illumina sequencing (e.g., 93x for paired-end libraries and 67x of mate-pair libraries) for *P. alecto* (Zhang et al., 2013) and also (iii) hybrid sequencing, e.g., 145x of Illumina short reads and 24x of PacBio long-reads for *Rousettus aegyptecus* (Pavlovich et al., 2018). Combined technological developments applied to genome assembly, including Hi-C (Ghurye et al., 2018), optical mapping (Jiao et al., 2017) and synthetic long reads (Coombe et al., 2016) provide a possibility for the high quality chromosome-level assembly (Teeling et al., 2018). In contrast to direct sources of evidence used for scaffolding the genome sequence, secondary scaffolding leverages less direct type of information to improve assembly scaffolding. In this report, we focus on a reference-assisted assembly method using Ragout (Kolmogorov et al., 2014) and a gene-based method using AGOUTI (Zhang et al., 2015) that require a reference genome and RNA-Seq data, respectively (Zhang et al., 2013; Pavlovich et al., 2018; Wen et al., 2018).

We used a combination of Illumina paired-end reads and Nanopore long-reads sequencing with coverage of 57.4x and 6.1x, respectively, based on a genome size estimation of 2 Gb. In addition, the sequencing results in this study have benefited from the produced RNA-seq data. Although the sequencing coverage obtained in this study was lower than in some other recent reports, we show here that it has been enough to provide a good quality genome using current computational method. In the first step, we provide an assembly based directly on sequencing evidence (paired-end and long-reads), where assembled fragments are called solid scaffolds. Then, we improve the assembly using secondary scaffolding methods, AGOUTI (gene-based) and Ragout (reference-assisted), using RNA seq data obtained with an Illumina 75 bp paired-end sequencing. Finally, we provide an original tool, called scaff2link, which integrates both sources of secondary scaffolding to keep only non-discordant linkages, hence avoiding potential errors. The development of these methods is essential for a better use of available resources, particularly when the number of the high-quality genome sequences is expected to increase rapidly. To follow the impact of the different methods regarding the quality of the assembly, we next describe metrics for each mentioned step: solid scaffolds, secondary scaffolding and the use of scaff2link. Therefore, in the same order, the metric described in this study contains: (i) fragmentation state of the genome sequence; (ii) benchmark using single-copy orthologs (SCO), and (iii) DNA-Seq realignment consistency. To characterize the nature of the sequence provided as a resource, we performed a k-mer analysis on solid scaffolds, describing the state of ploidy. Based on quality metrics, we show that the best assembly was obtained after integration of both secondary scaffolding methods with scaff2link. Finally, we demonstrate the potential use of the obtained genome assembly by providing annotation of

both coding genes and interspersed repeats and performing the phylogenetic analysis.

This new approach allowed us to assemble the genome of *P. medius* with a length of 1,985 Mb, consisting of 33,613 contigs and 16,113 scaffolds with a NG50 of 19 Mb. Identified repeat elements covered 22.5% of the assembled sequences and 19,823 coding genes were annotated, thus providing the first genome sequence of this bat species and making it available for further studies and better understanding of the mechanisms of Nipah virus emergence.

MATERIALS AND METHODS

Pteropus medius Sampling and Cell Generation

Cell culture from *Pteropus* bat flying fox was generated from a wing-membrane skin biopsy of a female specimen of *P. medius* (known also as Indian flying fox and *P. giganteus*, belonging to *Yinpterochiroptera* suborder) (**Figure 1**), collected in the Tiergarten Schönbrunn (Vienna, Austria), during the regularly veterinary check, as previously described (Gaudino et al., 2020). Briefly, sample was washed with sterile PBS and transferred into freezing medium Cryo-SFM (PromoCell Bioscience) in dry ice, for the shipment from the zoo. To obtain a primary cell culture (Ptgv), samples were thawed and fractioned in a Petri dish, then homogenates were harvested in different media and cultured in DMEM/F-12 medium (Gibco) supplemented with 10% fetal bovine serum, 1% L-glutamine (200 mM), 1,000 U/mL of penicillin, 1,000 U/mL of streptomycin, at 37°C, at 5% CO2. We confirmed that the biological sample belongs to the *P. medius* species by sequencing a mitochondrial region D-loop (Saccone et al., 1987) and nuclear introns ACOX2, COPS7A, BGN, ROGD1, and STAT5A, suggested to be pertinent to distinguish among closely related species (Dool et al., 2016). We compared these sequences with those obtained from several individuals phenotypically identified as *P. medius*, sampled at National Institute of High Security Animal Diseases, Bhopal, India.

FIGURE 1 | Fruit bat *Pteropus medius*. Female specimen of *P. medius*, called Daya, born in 24 March, 2009 in the Tiergarten Schönbrunn, Vienna, Austria. Its wing-membrane skin biopsy was used for the generation of primary cell line and subsequent genome sequencing.

Illumina DNA-Seq

Genomic DNA was purified from a pelleted primary Ptgv cells using NucleoSpin® Tissue kit (MACHEREY-NAGEL, 740952). A paired-end library was constructed with an insert size of 462 bp in average using NEXTFLEX® PCR-Free DNA-Seq Kit (Bioo Scientific) with Bioruptor (Diagenode) for DNA fragmentation step. Paired-end short-reads of 150 bp were generated on Illumina NextSeq 500 platform using a high output flowcell.

Illumina RNA-Seq

Primary cell cultures of Ptgv cells, containing principally fibroblast-like cells, were used as a source of RNA. Three replicates were obtained for each condition 24 h post-infection, either from Nipah virus-infected Ptgv cells at three viral particles/cell or from non-infected cells (incubated with mock preparation). The level of Nipah virus infection was bellow 3% in Ptgv cells. Experiments were done in BSL-4 facility INSERM Jean Mérieux in Lyon. Supplementary samples were obtained from another *Pteropus* bat trachea tissue (Aurine et al., 2019). RNA was extracted using NucleoSpin® RNA (MACHEREY-NAGEL, 740955). Libraries were generated using NEXTFLEX® Rapid Directional RNA-Seq Library Prep Kit according to manufacturer's protocol (Bioo Scientific) using 185 ng of extracted RNA as input material. Libraries were sequenced via Illumina NextSeq 500 in paired-end 75 bp using a Mid-Output Flow Cell.

DNA Extraction for MinION Sequencing

High-molecular-weight DNA was extracted from cell culture using the MagAttract® HMW DNA Kit (Qiagen). Then, genomic DNA was sheared using Covaris g-TUBE as per manufacturer's guidelines to obtain approximately 10 kb fragments without any additional enrichment or purification step.

Quantity and Quality Measurement for DNA MinION Sequencing

DNA concentration was measured using the Quantus™ Fluorimeter with the QuantiFluor® dsDNA Kit (Promega), and purity was evaluated by measuring A260/A280 and A260/A230 ratios using a NanoDrop™ spectrophotometer. The quality of DNA and its size were assessed by electrophoretic migration using Fragment Analyzer with the High Sensitivity Large Fragment 50 Kb Analysis Kit (AATI).

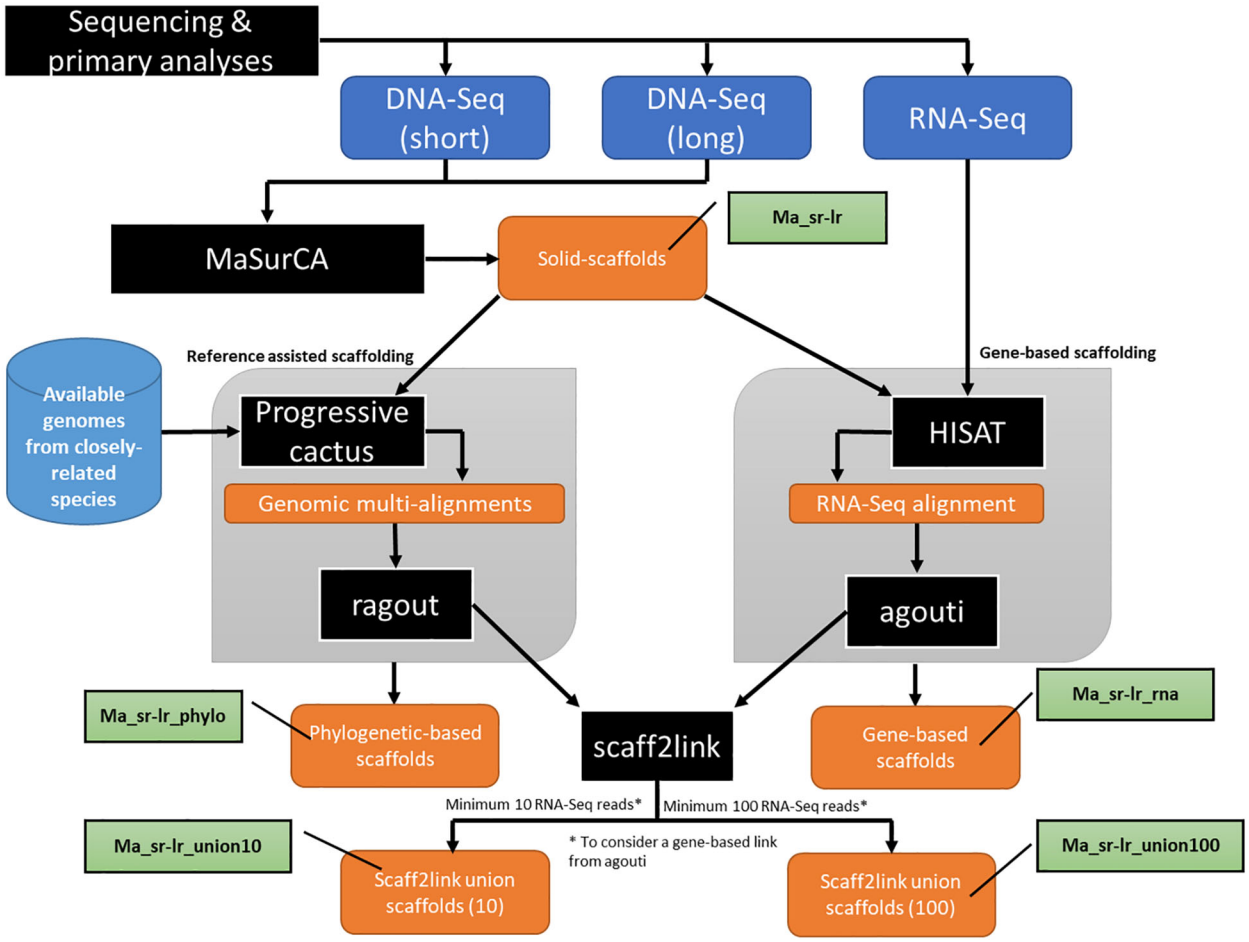

FIGURE 2 | Schematic presentation of the main analytical steps of the assembly workflow of *Pteropus medius* genome. Analytic steps, including the applied software (MaSurCa, HISAT, Progressive cactus AGOUTI and Scaff2link) are marked in black, input data in dark blue, data obtained from databases in light blue, nomenclature used for produced assemblies in green and produced data in orange.

Library Preparation for MinION Sequencing

Sequencing libraries were prepared using the Ligation Sequencing Kit 1D (SQK-LSK108) or the 1D^2 Sequencing Kit (SQK-LSK308) (Oxford Nanopore Technologies). The libraries were then loaded to MinION using a flow cell R9.5 version (FLO-MIN106) (ONT) and the sequencing runs were performed under MinKNOW version 1.7.14 for up to 48 h.

Illumina Primary Analysis

Raw reads were trimmed using cutadapt (version 1.9.1 with options: -q 30 -m 115 for DNA-seq and -q 30 -m 50 for RNA-Seq). For DNA-seq, resulting reads were corrected using lighter (version 1.1.1). Expected genome size has been predicted using kmergenie software (v1.7016).

MinION Primary Analysis

Base calling was done through albacore (v2.1.10). Low quality ends and chimera reads were trimmed using porechop (v0.2.3). Resulting long-reads were filtered using filtlong with short DNA-Seq Illumina reads to estimate quality (v0.2.0 with options: –trim –split 250 –min_length 200 –min_mean_q 85, –length_weight 0 and –window_q_weight 0).

Assembly and Primary Scaffolding

Hybrid assembly using both Illumina short-reads and Nanopore long-reads was achieved using MaSurCA whole genome assembly software (v3.2.4) (Zimin et al., 2013), with a k-mer size of 97. This value was chosen after preliminary tests (described in the **Supplementary Material**). Gap filling was performed on this assembly using gapfiller (v1.10) with 20 iterations.

Secondary Scaffolding

For gene-based scaffolding, RNA-Seq data has been aligned using *hisat2* (v2.1.0) on the assembly. Gene annotation have been predicted using *augustus* (v3.3.1) with human training set. Finally, these data were integrated with AGOUTI (v0.3.2).

For reference-based scaffolding, genome sequences of *P. vampyrus* (pteVam2), *P. alecto* (pteAle1), and *R. aegyptecus*

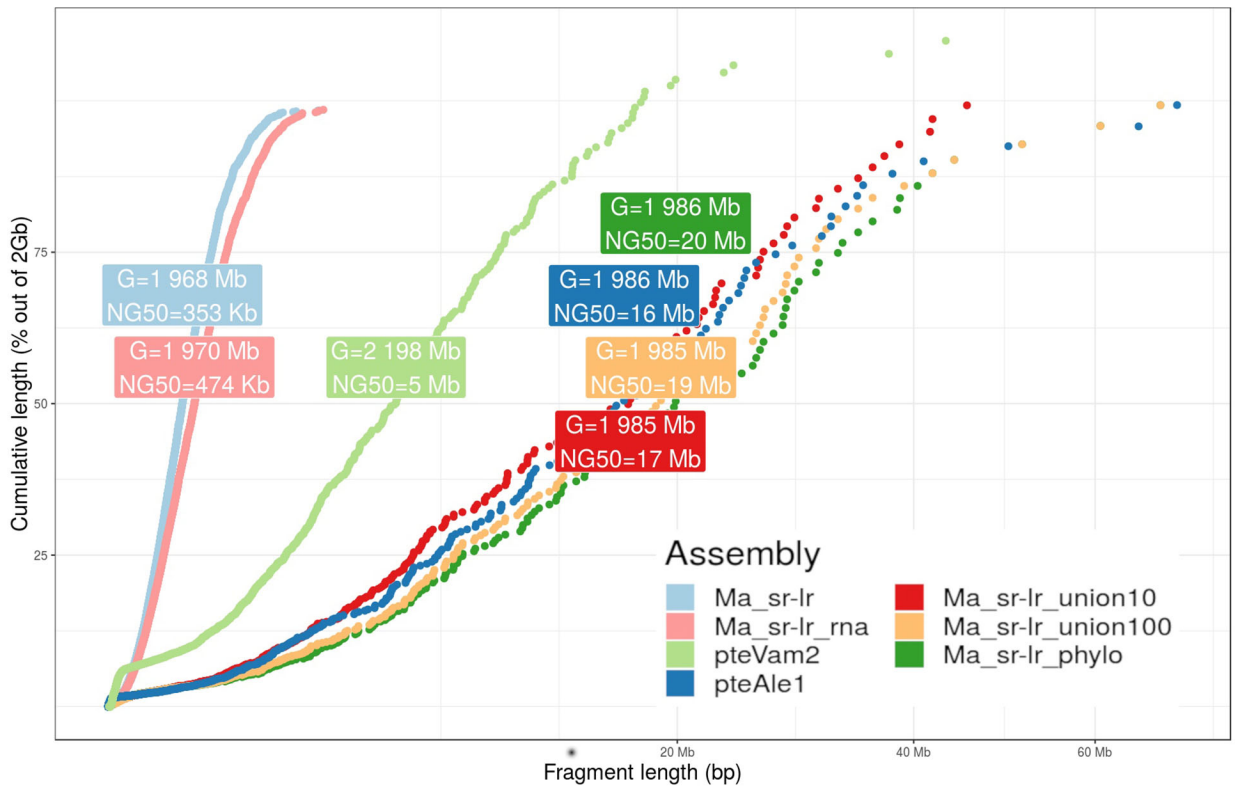

FIGURE 3 | Fragmentation graph for produced assemblies. The graph presents a scatter plot comparing cumulative length (*y*-axis) and the fragment length (*x*-axis) for four different *P. medius* scaffold assemblies, compared with already published *P. vampyrus* (pteVam2) and *P. alecto* (pteAlel). For each assembly, cumulative lengths were computed along sorted fragments, from the smallest to the highest. A label box gives information about the total size of the assembly (G) and the NG50 values, where the genome size has been set to 2 Gb for normalization.

(Raegyp2) were extracted from Genbank database and aligned with the solid-scaffold assembly using progressive Cactus (https://github.com/glennhickey/progressiveCactus). The software Ragout v2.1 performed the scaffolding based on the multi genome alignment using both pteVam2 and pteAle1 assembly sequences as reference, Raegyp2 as outgroup and the solid scaffold assembly as target (Kolmogorov et al., 2018).

Scaff2link Script

We developed an algorithm to integrate, in a conservative way, scaffolding results given by Ragout and AGOUTI (available at: https://github.com/jfouret/scaff2links). Briefly, this algorithm builds a graph with phylogenetic and gene-based linkage information as input for edges, and fasta formatted sequences as input for nodes (**Supplementary Figure S1**). First, linear paths are simplified and then higher level of simplification is added using pattern of directed acyclic graph (DAG) (**Supplementary Figure S2**). The pseudocode of the algorithm is given in **Supplementary Material**.

Assembly Evaluation

NG50 have been computed for all assemblies using a genome size of 2 Gb. K-mer Analysis Toolkit (v2.3.1) have been used to compare 23-mers presence and multiplicity in Illumina reads and in assembly. BUSCO (v3) has been used to control the presence in single copy of SCO shared in *Laurasiatheria* super order. Illumina DNA-Seq reads were mapped with bowtie2 (v 2.2.9) with options to consider an alignment properly paired if fragment size is in range 150 (-I) and 2,000 (-X) and "-very-sensitive" mode. More specifically, metrics were computed using "flagstat" tools of the SAMtools suite (v1.9).

Genome Annotation

Genomes from *P. vampyrus* (pteVam2), *P. alecto* (pteAle1), and *R. aegyptecus* (Raegyp2) and the Ma_sr-lr_union100 assembly were aligned using progressive Cactus (https://github.com/glennhickey/progressiveCactus) (Paten et al., 2011). *R. aegyptecus* was used as outgroup to improve the multiple alignment process and has been chosen because it was a species close to the *Pteropus* genus with a good quality assembly. Gene annotation was performed using the Comparative Annotation Toolkit (CAT) v0.1 (Zhang et al., 2013) automated pipeline with *P. alecto* as reference and *P. medius* as target with a step of *ab initio* gene prediction using Augustus 3.3.1 (Stanke and Waack, 2003). Of note, *R. aegyptecus* genome assembly has been used solely to improve the multiple genome alignment of the three *Pteropus* species genomes, however, *R. aegyptecus* was not used directly to infer *P. medius* genome annotation.

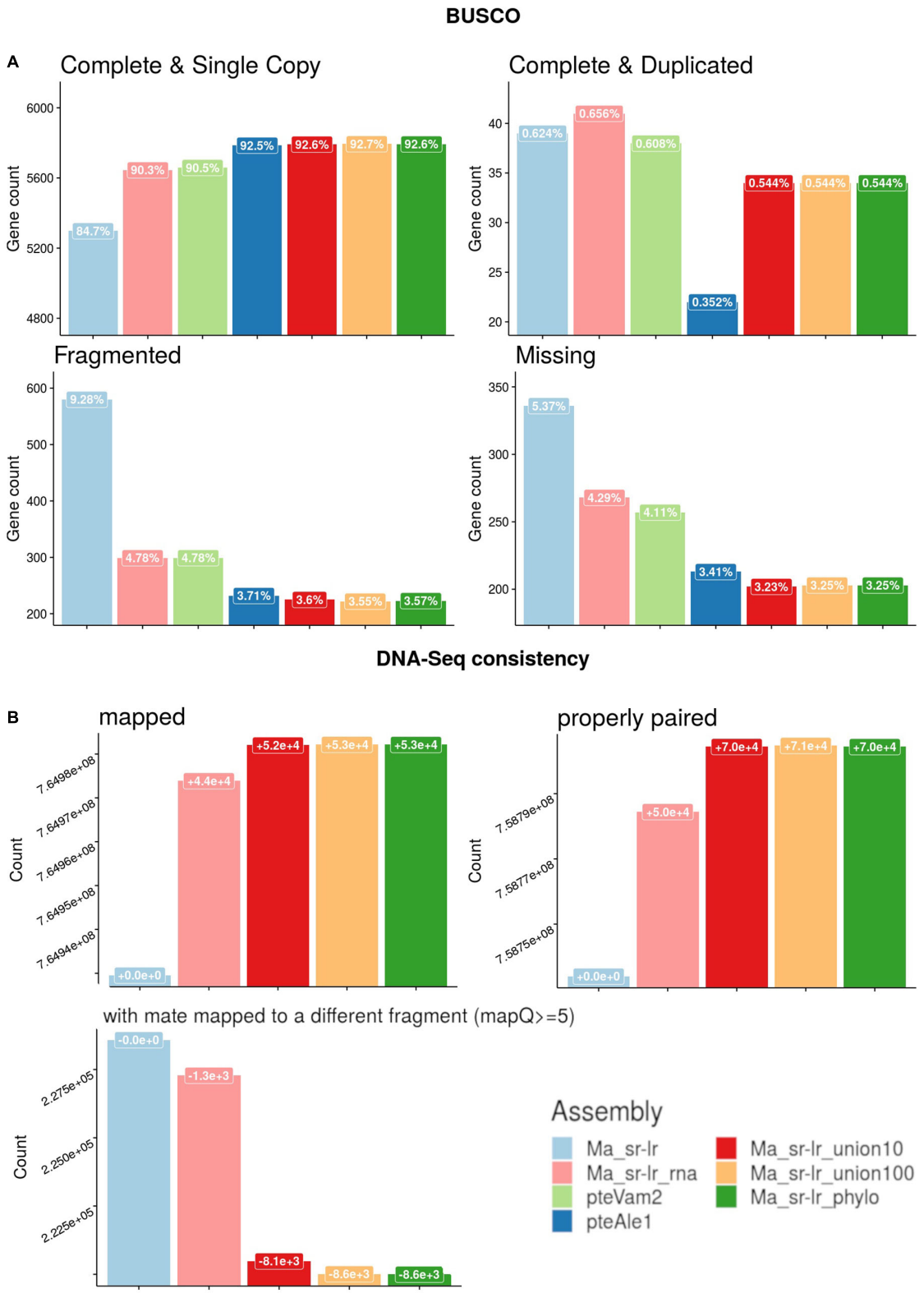

FIGURE 4 | Quality assessments of produced assemblies. **(A)** Benchmark of universal single-copy orthologs (BUSCO) genes for the *Laurasitharia* super order with comparison to already published assemblies of two *Pteropus* species, *P. vampyrus* (pteVam2), and *P. alecto* (pteAlel). **(B)** Short-reads mapping against produced assemblies were analyzed. *Y*-axis is the number of reads that are either (i) mapped (ii) properly paired or (iii) mapped with quality superior to five and with a mate mapped to a different fragment. The label box on top of each bar chart presents the evolution of read counts compared to the solid scaffold assembly (Ma_sr-lr).

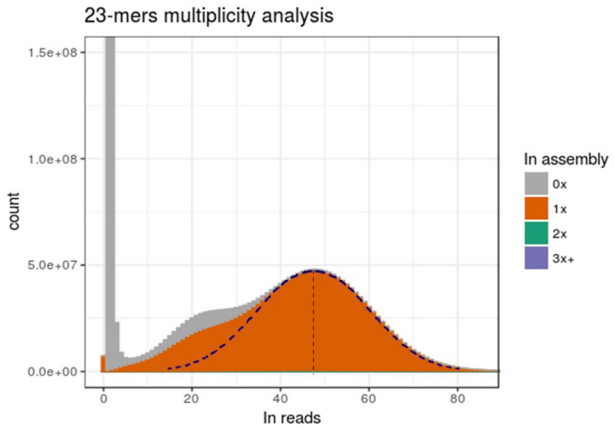

FIGURE 5 | Genome assembly is representative of only one allele. The *x*-axis presents the multiplicity of a k-mers. The *y*-axis is the amount of distinct k-mers present at this multiplicity in reads. Fill colors represent the number of time (0x, 1x, 2x or 3x, and more) a distinct k-mer is present in assembly. The right part of the dotted Gaussian curve has been hand-traced and a symmetry has been applied to get the left part.

CAT is using other dependencies: Hal v1, SAMtools 1.7–2 and BEDtools v2.26.0. Repeated sequences were annotated with *RepeatMasker* (v open-4.0.7) using rmblast (Nucleotide-Nucleotide BLAST with *RepeatMasker* Extensions 2.2.27+) and RepeatMasker Combined Database (Dfam_Consensus-20170127, RepBase-20170127) filtered for mammal species. Additional option for *RepeatMasker* were "-s -nolow -no_is."

Phylogenetic Analysis

Proteomes were retrieved from NCBI for *Miniopterus natalensis* (GCF_001595765.1), *Eptesicus fuscus* (GCF_000308155.1), *Myotis brandtii* (GCF_000412655.1), *M. lucifugus* (GCF_000147115.1), *M. davidii* (GCF_000327345.1), *Rousettus. aegyptiacus* (GCF_001466805.2), *P. alecto* (GCF_000325575.1), *P. vampyrus* (GCF_000151845.1), *Rhinolophus ferrumequinum* (GCF_004115265.1), *Desmodus rotundus* (GCF_002940915.1), *Hipposideros armiger* GCF_001890085.1), and *Phyllostomus discolor* (GCF_004126475.1). More specifically "GCF_*_translated_cds.faa.gz" file was fetched from NCBI RefSeq FTP repository for each species. For *P. medius*, the proteome was translated from the annotation. In case of isoforms, only the longest isoform per gene was kept. SCO were identified thanks to OrthoFinder[1] (Emms and Kelly, 2019) using default parameters. Multiple sequences alignment was conducted separately on each locus using MAFFT v7.123b (Katoh, 2002) with, generalized affine gap score, BLOSSUM80 (–bl) matrix for scores, an open gap penalty of 10 (–op 10) and all other parameters set to default. All positions with at least one gap were removed from the MSA along with surrounding five residues, as gaps may be linked with a missing or incorrect sequence. Of note, the models implemented in the phylogenetic tools used hereafter do not consider gaps in a multiple sequence alignment. Then conserved blocks were extracted from each MSA using Gblocks 0.91b (−b1 = 13, −b2 = 13, −b3 = 2, −b4 = 10) in order to improve the phylogeny (Talavera and Castresana, 2007). MSA were then concatenated. Maximum of 20 likelihood searches have been conducted with respectively 20 distinct starting trees to identify the best tree using RAxML 8.2.9 (Stamatakis, 2014). Separately, bootstrapping was done with 100 iterations. The random seed "12345" was used at all steps with RAxML. The tree was rooted manually. A MSA subset with 500,000 sites was used for estimation of divergence times using soft fossil constraints with PAML v4.9j mcmctree program (Yang, 2007). Configuration files used in PAML are available in the **Supplementary Material**. The procedure has been repeated with another subset with no significant changes in age time and confidence intervals. The minimum age of fossil data, obtained from paleobiodb database[2], were used as lower bound; all values used for the calibration were specified (**Supplementary Figure S3**). An upper constraint was set for the root using the upper value of the 95% confidence interval available for the *Chiroptera* order on Time Tree database[3] (Kumar et al., 2017).

RESULTS

Sequencing Depth

Pteropus medius DNA was extracted from cultured primary bat cells and sequenced using both paired-end Illumina and Nanopore sequencing, generating 114.5 Gb of Illumina DNA-Seq data (after primary analysis; see section "Materials and Methods"). Based on the analysis on distinct k-mer counts in DNA-Seq short-reads, the software kmergenie (Chikhi and Medvedev, 2014) predicted a genome size from 1.92 to 1.98 Gb, corresponding to the range of size of previously published bat genomes (Teeling et al., 2018). Using an alternative method based on the C-value (Smith and Gregory, 2009), the genome size was estimated at 1,994 Gb, with a GC content of about 38% deduced from DNA-Seq data. We then used a genome size of 2 Gb to calculate the depth of sequencing and subsequently normalized assembly metrics. The sequencing depth obtained for Illumina paired-end data was 57.4x. For long-read data, 12.1 Gb of MinION were produced after primary analysis with a mean long-read size of 7 kb, corresponding to a depth of 6.1x. These data altogether were then used for the final assembly. We also isolated the cellular RNA and performed the RNA-Seq analysis using the same biological material, then used the produced data in the secondary scaffolding step.

Solid Scaffold Assembly With Pieces of Evidence Directly Linked to Sequencing

Both Illumina paired-end and MinION long-reads were assembled with the MaSurCA (Zimin et al., 2013) hybrid software and gaps were filled with gapfiller (see section "Materials and Methods"). The workflow of this step is part of the general workflow presented in **Figure 2**, where the

[1] docker://davidemms/orthofindersha256:fbd408ae21ce

[2] https://paleobiodb.org

[3] http://www.timetree.org

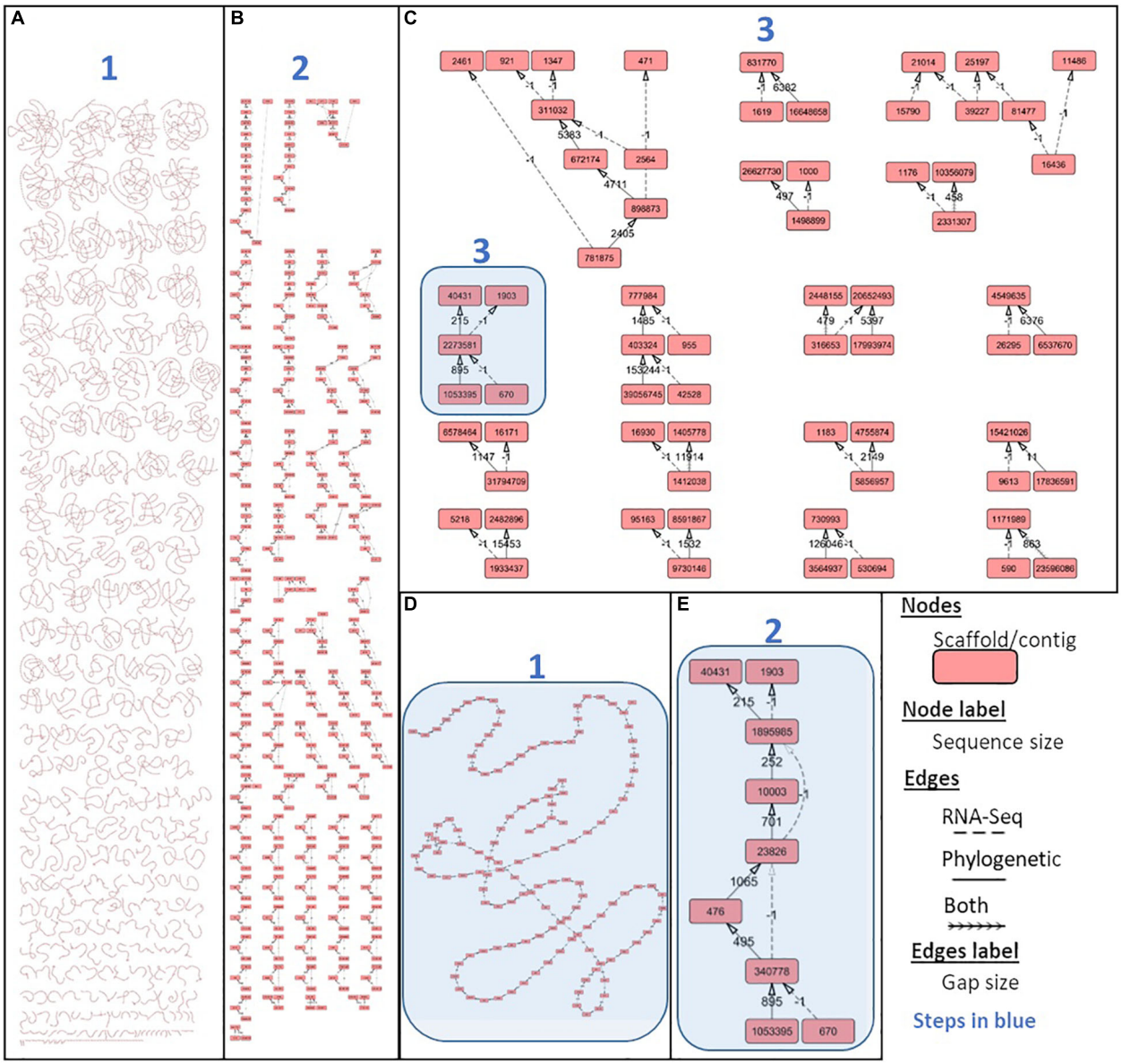

FIGURE 6 | Integrating phylogenetic and gene-based secondary scaffolding with Scaff2links. Scaff2link allows the import of linkages established by both AGOUTI for gene-based scaffolding and Ragout for reference-assisted scaffolding (see section "Materials and Methods"). The results of the process of conservative union from (1) the initial state with links parsed from Ragout and AGOUTI to (2) the linear chain simplification and (3) the directed acyclic graph simplification is respectively shown on **(A)**, **(B)**, and **(C)** were connected components resolved up to a single node are no longer displayed. One connected component at the initial step 1, 2, and 3 are respectively shown on **(D)**, **(E)**, and **(C)** and highlighted in blue. Graph structure and different steps (1–3) are detailed in **Supplementary Material**.

assembly produced is named "Ma_sr-lr" for (Ma: MaSurCa, sr: short-reads, lr: long-reads). Metrics describing this assembly are the fragmentation state of the genome sequence (**Figure 3**), benchmark using SCO (**Figure 4A**) and DNA-Seq realignment consistency (**Figure 4B**).

Previously published *Pteropus* bat genomes from *P. vampyrus* (Lindblad-Toh et al., 2011) and *P. alecto* (Zhang et al., 2013) were used for comparative analysis. For the fragmentation presented on **Figure 3**, the Ma_sr-lr reached an NG50 of 353 kb, with a total length of 1.968 Gb. Ma_sr-lr NG50 metrics was ∼14 and ∼45 times lower compared to *P. vampyrus* (NG50: 5 Mb) and *P. alecto* (NG50: 16 Mb) assemblies, respectively (**Figure 3**). Focusing on the potential use of the genomes for gene annotation, we have used BUSCO (Benchmark of Universal Single Copy Orthologs). This approach attempts a homology-based annotation of a group of genes selected because their orthologs are present in at least 90% of species from *Laurasiatheria* in single copy. For "Ma_sr-lr," only 84.7% of BUSCOs (**Figure 4A**) have been successfully annotated and confirmed to be present as a single copy, even if it has been lower than in *P. vampyrus* (90.5%) or *P. alecto*

(92.5%). The relative difference with other *Pteropus* is lower than the fragmentation of the genomes, indicating that we might have reached a limit of genome contiguity which facilitates gene annotation. Indeed, 353 kb (NG50 of Ma_sr-lr) is in order of magnitude ∼35 times higher than the median gene size among species of the *Pteropus* genus; 11.5 kb for *P. vampyrus* (RefSeq 101) and 10.4 kb for *P. alecto* (RefSeq 102) (NCBI Resource Coordinators, 2017).

k-mers Analysis Describing the State of Ploidy of the Solid Scaffold Assembly

We then focused on comparing the distribution of k-mer multiplicity between DNA-Seq reads and the assembly. As shown in **Figure 5**, large number of k-mers with low multiplicity in Illumina DNA-Seq reads were not present in the assembly (corresponding to the first left peak, close to 0x); this is most probably an artifact from sequencing errors. This peak is followed by a bimodal Gaussian-like distribution, suggesting that those two mixed distributions correspond to the heterozygous k-mers (left curb; mean: ∼24x) and for homozygous k-mers (right curb; mean: ∼48x); we indeed expected homozygous k-mers to be twice more present in sequencing reads. Half of heterozygous k-mers were apparently not integrated in the assembly, while the remaining part was integrated only once (**Figure 5**). This suggests that most heterozygous positions were inserted only once in the genome assembly. On the other side, if two alleles were integrated in the assembly for a consequent number of polymorphic positions, we would expect to see a significant proportion of homozygous k-mers present at a multiplicity of two in the assembly; however, only 1.7% of the total k-mers is found twice in the assembly (not visible in the graph). Therefore, the assembly presented in this report is very likely to be representative of a haplotype.

Secondary Scaffolding Using Reference-Assisted or Gene-Based Methods

The workflow used to perform secondary scaffolding is presented in **Figure 2**. Both methods start with the Ma_sr-lr assembly. The assembly produced after reference-assisted scaffolding is called "Ma_sr-lr_phylo." The number of scaffolds (**Supplementary Table S1**), 29,459 for Ma_sr-lr, was diminished by 2,018 and 13,011 by gene-based scaffolding (Ma_sr-lr_rna) and reference-assisted (Ma_sr-lr_phylo) scaffolding, respectively. Quality was assessed based on different metrics as explained above.

The state of fragmentation of obtained assemblies is presented on **Figure 3**. While reference-assisted scaffolding showed a very high NG50 value of 20 Mb, the value for gene-based scaffolding was limited to 474 Kb (**Figure 3**). Interestingly, the value of NG50 for Ma_sr-lr_phylo assembly outperforms the NG50 of *P. alecto* assembly (16 Mb) (Zhang et al., 2013), while having a smaller number of Ns (any nucleotide according to the IUPAC code) in its sequence (**Supplementary Table S1**). During the scaffolding processes, Ns are produced when resolving a gapped linkage of two fragments.

Annotation metrics of Benchmark of Universal Single-Copy Orthologs (BUSCOs), is presented on the **Figure 4A**. The percentage of complete and single copy BUSCOs annotated raised from 84.7 to 90.3% (+5.6%) and 92.6% (+7.9%) for Ma_sr-lr_rna and Ma_sr-lr_phylo, respectively. It appears that in most cases this difference corresponds to fragmented BUSCOs in the solid-scaffold assembly, which can be annotated on a single fragment in Ma_sr-lr_rna and Ma_sr-lr_phylo assemblies (**Figure 4A**).

Finally, **Figure 4B** presents metrics of DNA-Seq Illumina read realignment. There is a slight increase in mapped reads for both Ma_sr-lr_rna and Ma_sr-lr_phylo assemblies, $+4.4 \cdot 10^4$ and $+5.3 \cdot 10^4$ mapped reads (out of $7.65 \cdot 10^8$), respectively. An increase within the same order of magnitude co-occurs for the number of properly paired reads. Given options to the aligners define proper alignment with the constraint of the fragment size to be between 500 and 2,000, as expected from sequencing. Finally, the number of reads with a mate mapped to different fragments had decreased. All these data together indicate that the most added linkages are consistent with DNA-Seq realignment.

Scaff2links to Integrate Two Types of Linkage Source for Scaffolding

The Scaff2link steps presented on the general workflow (**Figure 2**) combine different pieces of evidence allowing to avoid errors at secondary scaffolding steps (see section "Materials and Methods"). Scaff2link allows conservative integration of both linkage information built by AGOUTI and Ragout. When importing links from AGOUTI based on RNA-Seq data, the minimum number of reads to consider a linkage is an option; this option has been tested with 10 and 100 minimum RNA-Seq reads leading to Ma_sr-lr_union10 and Ma_sr-lr_union100 assemblies, respectively. A general picture of the assembly states during scaff2link processing is shown in **Figure 6**, with intermediary steps presented on **Figures 6A,B** and the final step depicted in **Figure 6C**, corresponding to Ma_sr-lr_union100. In this final step, there were still unresolved links due to contradictory information (potentially linked with scaffolding errors) or fork-like graph structures that are impossible to resolve without introducing potential misassembles. Then, the quality has been assessed with the same metrics as those used before.

First, NG50 values of reference-assisted scaffolding are high with 17 and 19 Mb (**Figure 3**), corresponding to Ma_sr-lr_union10 and Ma_sr-lr_union100, respectively. These values are close to Ma_sr-lr_phylo (20 Mb) and still higher than *P. alecto* (16 Mb).

Second, in terms of quality for gene annotation (**Figure 4A**), results for scaff2link assemblies are very similar to the reference-assisted assembly Ma_sr-lr_phylo. Interestingly, for Ma_sr-lr_union100 compared to Ma_sr-lr_phylo, one more BUSCO annotation is complete (from fragmented) and presents as a single copy, indicating a slightly better scaffolding quality.

Third, regarding DNA-Seq read mapping (**Figure 4B**), results are again very similar to Ma_sr-lr_phylo. More detailed changes in read counts are given in **Table 1**. There are more reads mapped on Ma_sr-lr_union100 assembly than on

TABLE 1 | Details for DNA-Seq consistency for Scaff2links assemblies in comparison to reference-assisted scaffolding.

Features*	Scaffolds «Phylo»	Difference with	
		«union100»	«union10»
Number of mapped[#]	764,982,145	+20	−126
Number of properly paired	758,804,408	+358	+26
Number of Singletons	2,288,435	−26	+94
Number with mate mapped to a different fragment	309,158	−132	+276
Number with mate mapped to a different fragment (mapQ ≥ 5)	219,998	+16	+48

**More detailed view of DNA-Seq consistency within scaffold assemblies after secondary scaffolding. The table focus on differences between union100 and union10 assemblies which differ in the minimum number of reads to support a linkage through mRNA-Seq. DNA-Seq consistency is expressed in terms of short-read alignment statistics. [#]"Mapped" stands for the number of reads mapped. "Properly paired" stands for the number of reads that are properly paired (right strand and insert size range). A Singleton is a read with an unmapped mate. mapQ corresponds to a pared quality score of a read alignment.*

Ma_sr-lr_phylo assembly (+20 reads), there are even more reads mapped properly in pairs (+358). Being slightly better than other assemblies, the Ma_sr-lr_union100 was chosen to perform annotation and the identification of repeats, and for the final upload in ENA.

Genome Annotation

A total of 19,823 coding genes were annotated on Ma_sr-lr_union100 scaffold assembly, as shown in **Table 2** and compared to 19,260 for *P. vampyrus* annotation (PteVam2/RefSeq 101). Therefore, in terms of annotated gene count, both are similar (19.8 k vs 19.3 k). More mRNAs were annotated for *P. medius* (42 k vs 33 k), this type of difference being expected when different annotation methods are used. Finally, as shown in **Table 3**, genes including introns are covering 40.3% of the genome and CDS only (coding sequence) 3.7%. Although the majority of CDSs are complete, some (5 k out of 39 k) miss either a start codon and/or a stop codon. This would require manual inspection for each CDS to elucidate the cause of incompleteness; each non-complete CDS might be the result of the gap presence (bench of Ns), more problematically a mis-assembly or it may be an event of pseudogenization. Using RepeatMasker, 22.5% of the genome was identified as already known interspersed repeats, discovered and annotated in another species and present in the repeat database (repbase), as shown **Table 4**.

TABLE 3 | Coverage of genome annotation.

Statistics*	Value
% of genome covered by genes	40.3
% of genome covered by CDS	3.7
Mean mRNAs per gene	2
Mean exons per mRNA	12
Mean introns per mRNA	11
Overlapping genes	3,344
Contained genes	1,123
CDS: complete	37,076
CDS: start, no stop	684
CDS: stop, no start	1,256
CDS: no stop, no start	3,103

**The table summarizes statistics representing the coverage of the genome annotation for protein-coding genes only, produced with GAG (Genome Annotation Toolkit) software (https://github.com/genomeannotation/GAG).*

Phylogenetic Analysis

To investigate genetic relationships between *P. medius* and the other bat species for which the complete genome sequences are available, we performed the phylogenetic analysis with 12 published bat genomes with RefSeq proteomes available (**Figure 7**). A total of 9,710 SCO were found thanks to OrthoFinder. Following multiple sequence alignment and post-alignment analysis (described in the section "Materials and Methods"), the concatenated MSA contained 3,694,685 positions of which 473,736 were variable in at least one species accounting for 94,420 distinct alignment patterns. All bootstrap analyses (100%) were consistent with the topology of this tree. This analysis strongly supports that *P. medius* is phylogenetically closer to *P. vampyrus* than to *P. alecto*. Our timescale, based on protein alignments, indicates a divergence time of 1.57 MY (0.9–2.57948) between both *P. medius* and *P. vampyrus*, and 2.98 MY (1.97795–4.56922) between them and *P. alecto*. Finally, as angiotensin converting enzyme 2 (ACE2) is considered to be the entry receptor for SARS-CoV-2, the virus responsible for the current pandemic of COVID-19 (Zhou et al., 2020), we compared the sequences of ACE2 (805 amino acids) between *P. medius* and two *Rhinolophus* bat species, *R. ferrumequinum* and *R. sinicus*, thought to be a natural reservoir of coronaviruses (Ge et al., 2013). We observed 82.1% of identity of *P. medius* with both

TABLE 2 | Gene annotation statistics by features, summarized for *P. medius* and *P. vampyrus* genome annotations, considering only protein coding genes.

Features	Number		Total length		Shortest length		Longest length		Mean	
	P. medius	*P. vampyrus*	*P. medius*	*P. vampyrus*	*P. medius*	*P. vampyrus*	*P. medius*	*P. vampyrus*	*P. medius*	*P. vampyrus*
Gene	19,823	19,260	799,771,699	821,869,377	35	132	1,646,990	2,090,425	40,346	42,672
mRNA	42,119	33,311	2,268,593,933	1,611,530,784	35	132	1,646,990	2,090,425	53,862	48,378
Exons	502,353	372,960	130,167,394	94,948,423	1	1	17,601	17,106	259	255
Introns	460,234	339,649	2,139,347,007	1,517,261,659	1	1	863,371	923,485	4,648	4,467
CDS	39,106	33,311	73,655,104	59,627,155	46	96	102,629	102,513	1,883	1,790

TABLE 4 | Interspersed repeats annotated in *P. medius* genome sequence using RepeatMasker.

Class*	Sub-class	Count	Cumulative size (bp)	Percentage in the genome (%)
DNA	–	1,010	191,112	0.01
	PiggyBac	1,954	721,278	0.04
	TcMar-Mariner	648	125,351	0.01
	TcMar-Tc2	1,737	618,278	0.03
	TcMar-Tigger	32,925	11,660,016	0.59
	hAT	824	208,125	0.01
	hAT-Ac	478	217,854	0.01
	hAT-Blackjack	3,968	1,037,449	0.05
	hAT-Charlie	72,918	17,479,065	0.89
	hAT-Tag1	403	144,892	0.01
	hAT-Tip100	12,415	4,240,959	0.22
LINE	CR1	3,663	1,159,469	0.06
	L1	399,046	293,952,163	14.97
	L2	53,043	19,005,727	0.97
	RTE-BovB	1,110	618,176	0.03
	RTE-X	1,646	676,407	0.03
LTR	–	1,631	574,128	0.03
	ERV1	44,596	23,334,633	1.19
	ERVK	5,915	1,601,327	0.08
	ERVL	41,775	22,884,779	1.17
	ERVL-MaLR	75,722	27,922,114	1.42
	Gypsy	1,965	693,212	0.04
RC	Helitron	332	113,660	0.01
SINE	5S	11,447	2,005,503	0.10
	MIR	67,536	9,536,267	0.49
	tRNA	1,887	252,641	0.01
	tRNA-5S	2,413	393,491	0.02
Unknown	–	639	130,749	0.01
Total	Interspersed	844,981	441,707,409	22.50

**Results from RepeatMasker are summarized by repeat class and the repeat class below 0.01% is masked but was taken into account for the total counts.*

Rhinolophus bat species. The percentage of similitude (based on BLOSSUM62 matrix) of *P. medius* sequence is respectively of 90.3 and 89.8% for *R. ferrumequinum* and *R. sinicus* (**Supplementary Figure S4**). Of note, the percentage of similitude between *R. ferrumequinum* and *R. sinicus* is 95.3%.

DISCUSSION

In this study, we sequenced and assembled a solid scaffold for the *P. medius* genome. We obtained NG50 of 353 kb, on which we were able to annotate most of the genes as shown by BUSCO analysis. In addition, we report here that the process of secondary scaffolding is beneficial in terms of assembly quality (6.1x of Nanopore long-reads and 57.4x Illumina paired-end) with sequencing cost that remains relatively moderate, making thus this approach rather attractive. Although it would probably be insufficient to provide a resourceful assembly if closely related species have not been fully sequenced, we show in this study that it is possible to take advantages of published genomes from close species to provide a good quality assembly. In a context where international consortiums provide the scientific community with high quality genome sequences at chromosome level (Genome 10K Community of Scientists, 2009; Teeling et al., 2018), for a genus without available genome sequences, there will be more resources available for reference-assisted scaffolding methods and for sequencing species of interest at lower cost.

Our results suggest that the combination of different sources of information for secondary scaffolding is necessary to limit the introduction of misassembles and improve quality; we thus developed the scaff2link software, which is compatible and reusable with Ragout and AGOUTI. We have shown that the Ma_sr-lr_union100, produced by scaff2link, is slightly better than other assemblies. Indeed, Scaff2links prevents the linkage of fragments within a new scaffold if contradictory information exists between gene-based and synteny-based secondary scaffolding. This is expected to limit the number of scaffolds produced with mis-assemblies. Finally, our results suggest the advantage of the utilization of the Ma_sr-lr_union100 assembly for gene annotation and subsequent analysis of regulatory features including NGS applications, such as RNA-Seq. Ma_sr-lr_union100 assembly could also be used to perform genome-wide comparative studies to identify or compare loci, including coding sequences or regulatory motifs. However, the fact that some contiguities in the genome are based on prediction (from secondary scaffolding), rather than on actual data might be problematic for some analysis. As example, for use as a reference genome for Ragout, it would be preferable to use Ma_sr-lr assembly.

Similarly to the previously sequenced *E. spelaea* bat genome (Wen et al., 2018), the main class of repeats present in *P. medius* genome are LINE (long-interspersed nuclear elements), covering ∼16% of the genome. However, the percentage of total genome coverage for interspersed repeats found in this study was lower than previous reports about closely related bat species (Wen et al., 2018). This difference is linked with the lower sensitivity of the tool used to search similarities between the genome and the repeat database (RMBlast, used in this study). To our current knowledge there is no published work with significant statistical support allowing the resolution of phylogenetic relationship of *P. medius* with *P. alecto* and *P. vampyrus*. Phylogenetic analysis shown the clustering of *P. medius* genome with two other *Pteropus* bat species, *P. alecto* and *P. vampyrus*. The overall tree topology for bats is concordant with other studies (Teeling et al., 2005; Hawkins et al., 2019). Finally, the tree topology is coherent with the geographical distribution of those bats: *P. medius* (Molur et al., 2008) and *P. vampyrus* (Bates et al., 2008), which clustered together, are both present on the Asian continent. On the other hand, phylogenetically more distant species *P. alecto* is mainly located in Australia (Roberts et al., 2017). We estimated in this study the divergence time between *Pteropus* species lower than the minimum ranges reported on Time Tree database. However, some other studies reported divergence times focused on *Pteropus* genus even lower than ours (Almeida et al., 2014); in that study the 95% confidence interval for the divergence time between *P. vampyrus* and *P. medius* (0.5–1.4) overlaps with ours (0.9–2.57948). We conducted our timescale estimation using

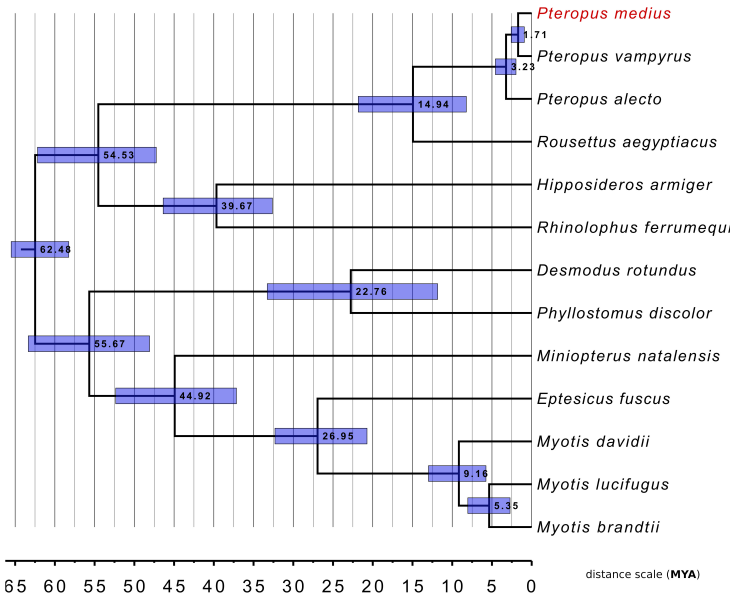

FIGURE 7 | Phylogenetic classification of *P. medius* among other bats and within *Pteropus* species. The distance scale unit is MYA (Million Years Ago). All bootstrap values were 100%. Horizontal blue bars around each node represents the 95% confidence interval relative to this node age.

SCO sequences, where the proportion of site under non-neutral selection may vary among branches. We acknowledge that time divergence estimations on branch with a greater proportion of sites under positive selection might be estimated higher than the real divergence time; inversely time divergence estimations on branches with a higher proportion of sites under negative selection might be estimated lower.

Indian *P. medius* bats have been suggested to host coronaviruses (Anthony et al., 2013; Yadav et al., 2020). To underline the importance of having available an annotated *P. medius* genome, we analyzed the ACE2 gene which is considered to code for the entry receptor for coronavirus SARS-CoV-2, responsible for the current pandemic of COVID-19 (Zhou et al., 2020). Comparison of the sequences of ACE2 between *P. medius* and *R. sinicus*, thought to be a natural reservoir of coronaviruses (Ge et al., 2013) revealed 82.1% of identity and 89.8–90.3% of similarity (**Supplementary Figure S3**). Although this is a preliminary result, it emphasizes the interest of having ready-to-use genomic resources for a maximum of species, for the further in-depth analysis.

Altogether, these results confirm that a lower depth of sequencing is enough to obtain reliable genome sequence using secondary scaffolding approaches and demonstrate the benefits of the scaff2link application, described in this article. The genome sequence is now available to the scientific. In addition, as bats display many unique biological features among mammals (Racey, 2015), growing number of new bat species are expected to be sequenced, some of them within the Bat 1K project for sequencing all bats' species (Teeling et al., 2018). A meta-analysis of bat phylogenetic and positive selection recently suggested a number of genes known to be primarily related to immune responses (Hawkins et al., 2019) and their further functional analysis will allow the understanding of their role in hosting different viruses by bats. Increasing the availability of different bat genomes is indeed essential for a better understanding of the genetic and evolutionary mechanisms that underlie the adaptations specifically to bats, such as their ability to fly which is unique among mammals, their metabolic adaptation, as well as the immuno-virological peculiarities associated to their capacity to both host and transmit Nipah virus as well as the other viruses highly pathogenic to humans.

DATA AVAILABILITY STATEMENT

The datasets generated for this study can be found in the European Nucleotide Archive (ENA), N° PRJEB32728, ERP115442. Some files important for the reproducibility of this work are available at: https://github.com/jfouret/pMed_genomeData.

ETHICS STATEMENT

Ethical approval was not required for this study according to local regulations as tests were performed in the course of regular health checks by veterinarians of the Vienna Zoo.

AUTHOR CONTRIBUTIONS

JF, BH, CL-L, and MB-B conceived, designed, and supervised the study. DP performed the sampling of biological material.

JF, NA, and FE performed the experimental processing of the samples. SC and MG performed, respectively, MinION and Illumina sequencing with inputs from JF for MinION sequencing. JF led the software development and performed the sequence analysis, genome assembly, and gene annotation. MB contributed significantly for genome assembly, evaluation, and genome annotation. AG, JF, and JL brought methodological inputs. FB, JF, and J-NV performed the phylogenic analysis. JF wrote the initial manuscript. FB, AG, BH, CL-L, and JL did the proofreading. All authors read and approved the final manuscript.

ACKNOWLEDGMENTS

The work was supported by LABEX ECOFECT (ANR-11-LABX-0048) at "Université de Lyon," within the program "Investissements d'Avenir" (ANR-11-IDEX-0007) operated by the French National Research Agency (ANR), by Aviesan Sino-French agreement on Nipah virus study and ViroScan3D. JF was supported by the doctoral fellowship CIFRE-Défense operated by the Direction Générale de l'Armement (DGA). We wish to thank A. Weissenbacher and Tiergarten Schönbrunn (Vienna, Austria) for the *Pteropus* bat samples. We are also grateful to Drs. K. Dhondt and M. Roche (Lyon) for the help to initialize and realize this work; to E. Guillot-Combe for the tutorship during the JF Ph.D. thesis work; to A. Raout (Bhopal, India) for sharing sequences from *P. medius* nuclear introns; and to N. Lartillot (LBBE, Lyon) and A. Sadier (UCLA) for advice with our phylogenomic analysis.

SUPPLEMENTARY MATERIAL

The Supplementary Material for this article can be found online at: https://www.frontiersin.org/articles/10.3389/fmicb.2020.01807/full#supplementary-material

REFERENCES

Almeida, F. C., Giannini, N. P., Simmons, N. B., and Helgen, K. M. (2014). Each flying fox on its own branch: a phylogenetic tree for *Pteropus* and related genera (Chiroptera: Pteropodidae). *Mol. Phylogenet. Evol.* 77, 83–95. doi: 10.1016/j.ympev.2014.03.009

Anthony, S. J., Epstein, J. H., Murray, K. A., Navarrete-Macias, I., Zambrana-Torrelio, C. M., Solovyov, A., et al. (2013). A strategy to estimate unknown viral diversity in mammals. *mBio* 4:e598-13. doi: 10.1128/mBio.00598-513

Arunkumar, G., Chandni, R., Mourya, D. T., Singh, S. K., Sadanandan, R., Sudan, P., et al. (2019). Outbreak Investigation of Nipah Virus Disease in Kerala, India, 2018. *J. Infect. Dis.* 219, 1867–1878. doi: 10.1093/infdis/jiy612

Aurine, N., Baquerre, C., Gaudino, M., Jean, C., Dumont, C., Rival-Gervier, S., et al. (2019). Reprogrammed pteropus bat stem cells present distinct immune signature and are highly permissive for *Henipaviruses*. *bioRxiv* [Preprint], doi: 10.1101/846410

Bates, P., Francis, C., Gumal, M., Bumrungsri, S., Walston, J., Heaney, L., et al. (2008). *Pteropus vampyrus*. *IUCN Red List Threat. Spec.* 2008:e.T18766A8593657. doi: 10.2305/IUCN.UK.2008.RLTS.T18766A8593657.en

Chikhi, R., and Medvedev, P. (2014). Informed and automated k-mer size selection for genome assembly. *Bioinformatics* 30, 31–37. doi: 10.1093/bioinformatics/btt310

Coombe, L., Warren, R. L., Jackman, S. D., Yang, C., Vandervalk, B. P., Moore, R. A., et al. (2016). Assembly of the complete sitka spruce chloroplast genome using 10x genomics' gemcode sequencing data. *PLoS One* 11:e0163059. doi: 10.1371/journal.pone.0163059

Dool, S. E., Puechmaille, S. J., Foley, N. M., Allegrini, B., Bastian, A., Mutumi, G. L., et al. (2016). Nuclear introns outperform mitochondrial DNA in inter-specific phylogenetic reconstruction: lessons from horseshoe bats (Rhinolophidae: Chiroptera). *Mol. Phylogenet. Evol.* 97, 196–212. doi: 10.1016/j.ympev.2016.01.003

Emms, D. M., and Kelly, S. (2019). OrthoFinder: phylogenetic orthology inference for comparative genomics. *Genome Biol.* 20:1832. doi: 10.1186/s13059-019-1832-y

Enchéry, F., and Horvat, B. (2017). Understanding the interaction between henipaviruses and their natural host, fruit bats: paving the way toward control of highly lethal infection in humans. *Int. Rev. Immunol.* 36, 108–121. doi: 10.1080/08830185.2016.1255883

Gaudino, M., Aurine, N., Dumont, C., Fouret, J., Ferren, M., Mathieu, C., et al. (2020). High pathogenicity of nipah virus from *Pteropus lylei* Fruit Bats, Cambodia. *Emerg. Infect. Dis.* 26:284. doi: 10.3201/eid2601.191284

Ge, X.-Y., Li, J.-L., Yang, X.-L., Chmura, A. A., Zhu, G., Epstein, J. H., et al. (2013). Isolation and characterization of a bat SARS-like coronavirus that uses the ACE2 receptor. *Nature* 503, 535–538. doi: 10.1038/nature12711

Genome 10K Community of Scientists, (2009). Genome 10K: a proposal to obtain whole-genome sequence for 10 000 vertebrate species. *J. Hered.* 100, 659–674. doi: 10.1093/jhered/esp086

Ghurye, J., Rhie, A., Walenz, B. P., Schmitt, A., Selvaraj, S., Pop, M., et al. (2018). Integrating Hi-C links with assembly graphs for chromosome-scale assembly. *bioRxiv* [Preprint], doi: 10.1101/261149

Hawkins, J. A., Kaczmarek, M. E., Müller, M. A., Drosten, C., Press, W. H., and Sawyer, S. L. (2019). A metaanalysis of bat phylogenetics and positive selection based on genomes and transcriptomes from 18 species. *Proc. Natl. Acad. Sci. U.S.A.* 116, 11351–11360. doi: 10.1073/pnas.1814995116

Hu, B., Ge, X., Wang, L.-F., and Shi, Z. (2015). Bat origin of human coronaviruses. *Virol. J.* 12, 221. doi: 10.1186/s12985-015-0422-421

Jiao, W.-B., Accinelli, G. G., Hartwig, B., Kiefer, C., Baker, D., Severing, E., et al. (2017). Improving and correcting the contiguity of long-read genome assemblies of three plant species using optical mapping and chromosome conformation capture data. *Genome Res.* 27, 778–786. doi: 10.1101/gr.213652.116

Katoh, K. (2002). MAFFT: a novel method for rapid multiple sequence alignment based on fast Fourier transform. *Nucleic Acids Res.* 30, 3059–3066. doi: 10.1093/nar/gkf436

Kolmogorov, M., Armstrong, J., Raney, B. J., Streeter, I., Dunn, M., Yang, F., et al. (2018). Chromosome assembly of large and complex genomes using multiple references. *bioRxiv* [Preprint], doi: 10.1101/088435

Kolmogorov, M., Raney, B., Paten, B., and Pham, S. (2014). Ragout–a reference-assisted assembly tool for bacterial genomes. *Bioinformatics* 30, i302–i309. doi: 10.1093/bioinformatics/btu280

Kumar, S., Stecher, G., Suleski, M., and Hedges, S. B. (2017). TimeTree: a resource for timelines, timetrees, and divergence times. *Mol. Biol. Evol.* 34, 1812–1819. doi: 10.1093/molbev/msx116

Lazzeroni, M. E., Burbrink, F. T., and Simmons, N. B. (2018). Hibernation in bats (Mammalia: Chiroptera) did not evolve through positive selection of leptin. *Ecol. Evol.* 8, 12576–12596. doi: 10.1002/ece3.4674

Lindblad-Toh, K., Garber, M., Zuk, O., Lin, M. F., Parker, B. J., Washietl, S., et al. (2011). A high-resolution map of human evolutionary constraint using 29 mammals. *Nature* 478, 476–482. doi: 10.1038/nature10530

Mathieu, C., and Horvat, B. (2015). Henipavirus pathogenesis and antiviral approaches. *Expert Rev. Anti Infect. Ther.* 13, 343–354. doi: 10.1586/14787210.2015.1001838

Mlikovsky, J. (2012). Correct name for the Indian flying fox (Pteropodidae). *Vespertilio* 16, 202–204.

Molur, S., Srinivasulu, C., Bates, P., and Francis, C. (2008). *Pteropus giganteus*. *IUCN Red List Threat. Spec.* 2008:e.T18725A8511108. doi: 10.2305/IUCN.UK.2008.RLTS.T18725A8511108.en

NCBI Resource Coordinators, (2017). Database resources of the national center for biotechnology information. *Nucleic Acids Res.* 45, D12–D17. doi: 10.1093/nar/gkw1071

Paten, B., Earl, D., Nguyen, N., Diekhans, M., Zerbino, D., and Haussler, D. (2011). Cactus: algorithms for genome multiple sequence alignment. *Genome Res.* 21, 1512–1528. doi: 10.1101/gr.123356.111

Pavlovich, S. S., Lovett, S. P., Koroleva, G., Guito, J. C., Arnold, C. E., Nagle, E. R., et al. (2018). The egyptian rousette genome reveals unexpected features of bat antiviral immunity. *Cell* 173, 1098–1110. doi: 10.1016/j.cell.2018.03.070

Racey, P. A. (2015). "The uniqueness of bats," in *Bats and Viruses*, eds L. F. Wang, and C. Cowled, (Hoboken, NJ: John Wiley & Sons Ltd), 1–22. doi: 10.1002/9781118818824.ch1

Roberts, B., Eby, P., Tsang, S. M., and Sheherazade. (2017). *Pteropus alecto*. The IUCN Red List of Threatened Species 2017. doi: 10.2305/IUCN.UK.2017-2.RLTS.T18715A22080057.en

Saccone, C., Attimonelli, M., and Sbisà, E. (1987). Structural elements highly preserved during the evolution of the D-loop-containing region in vertebrate mitochondrial DNA. *J. Mol. Evol.* 26, 205–211. doi: 10.1007/bf02099853

Shi, Z. (2010). Bat and virus. *Protein Cell* 1, 109–114. doi: 10.1007/s13238-010-0029-27

Smith, J. D. L., and Gregory, T. R. (2009). The genome sizes of megabats (Chiroptera: Pteropodidae) are remarkably constrained. *Biol. Lett.* 5, 347–351. doi: 10.1098/rsbl.2009.0016

Stamatakis, A. (2014). RAxML version 8: a tool for phylogenetic analysis and post-analysis of large phylogenies. *Bioinformatics* 30, 1312–1313. doi: 10.1093/bioinformatics/btu033

Stanke, M., and Waack, S. (2003). Gene prediction with a hidden Markov model and a new intron submodel. *Bioinformatics* 19, ii215–ii225. doi: 10.1093/bioinformatics/btg1080

Talavera, G., and Castresana, J. (2007). Improvement of phylogenies after removing divergent and ambiguously aligned blocks from protein sequence alignments. *Syst. Biol.* 56, 564–577. doi: 10.1080/10635150701472164

Teeling, E. C., Springer, M. S., Madsen, O., Bates, P., O'brien, S. J., and Murphy, W. J. (2005). A molecular phylogeny for bats illuminates biogeography and the fossil record. *Science* 307, 580–584. doi: 10.1126/science.1105113

Teeling, E. C., Vernes, S. C., Dávalos, L. M., Ray, D. A., Gilbert, M. T. P., Myers, E., et al. (2018). Bat Biology, genomes, and the Bat1K project: to generate chromosome-level genomes for all living bat species. *Annu. Rev. Anim. Biosci.* 6, 23–46. doi: 10.1146/annurev-animal-022516-022811

Wang, L.-F., and Anderson, D. E. (2019). Viruses in bats and potential spillover to animals and humans. *Curr. Opin. Virol.* 34, 79–89. doi: 10.1016/j.coviro.2018.12.007

Wen, M., Ng, J. H. J., Zhu, F., Chionh, Y. T., Chia, W. N., Mendenhall, I. H., et al. (2018). Exploring the genome and transcriptome of the cave nectar bat *Eonycteris spelaea* with PacBio long-read sequencing. *Gigascience* 7:giy116. doi: 10.1093/gigascience/giy116

Yadav, P. D., Shete, A. M., Kumar, G. A., Sarkale, P., Sahay, R. R., Radhakrishnan, C., et al. (2019). Nipah virus sequences from humans and bats during nipah outbreak, Kerala, India, 2018. *Emerg. Infect. Dis.* 25, 1003–1006. doi: 10.3201/eid2505.181076

Yadav, P. D., Shete-Aich, A., Nyayanit, D. A., Pardeshi, P., Majumdar, T., Balasubramanian, R., et al. (2020). Detection of coronaviruses in *Pteropus* & *Rousettus* species of bats from different States of India. *Indian J. Med. Res.* 151, 226–235. doi: 10.4103/ijmr.IJMR_795_20

Yang, Z. (2007). PAML 4: phylogenetic analysis by maximum likelihood. *Mol. Biol. Evol.* 24, 1586–1591. doi: 10.1093/molbev/msm088

Zhang, G., Cowled, C., Shi, Z., Huang, Z., Bishop-Lilly, K. A., Fang, X., et al. (2013). Comparative analysis of bat genomes provides insight into the evolution of flight and immunity. *Science* 339, 456–460. doi: 10.1126/science.1230835

Zhang, S. V., Zhuo, L., and Hahn, M. W. (2015). AGOUTI: improving genome assembly and annotation using transcriptome data. *bioRxiv* [Preprint], doi: 10.1101/033019

Zhou, P., Yang, X.-L., Wang, X.-G., Hu, B., Zhang, L., Zhang, W., et al. (2020). A pneumonia outbreak associated with a new coronavirus of probable bat origin. *Nature* 579, 270–273. doi: 10.1038/s41586-020-2012-2017

Zimin, A. V., Marçais, G., Puiu, D., Roberts, M., Salzberg, S. L., and Yorke, J. A. (2013). The MaSuRCA genome assembler. *Bioinform. Oxf. Engl.* 29, 2669–2677. doi: 10.1093/bioinformatics/btt476

Conflict of Interest: JF, MB, MG, AG, and CL-L were employed by the company ViroScan3D.

The remaining authors declare that the research was conducted in the absence of any commercial or financial relationships that could be construed as a potential conflict of interest.

Copyright © 2020 Fouret, Brunet, Binet, Aurine, Enchéry, Croze, Guinier, Goumaidi, Preininger, Volff, Bailly-Bechet, Lachuer, Horvat and Legras-Lachuer. This is an open-access article distributed under the terms of the Creative Commons Attribution License (CC BY). The use, distribution or reproduction in other forums is permitted, provided the original author(s) and the copyright owner(s) are credited and that the original publication in this journal is cited, in accordance with accepted academic practice. No use, distribution or reproduction is permitted which does not comply with these terms.

frontiers in Microbiology

ORIGINAL RESEARCH
published: 30 July 2020
doi: 10.3389/fmicb.2020.01715

Screening and Validation of Reference Genes for RT-qPCR Under Different Honey Bee Viral Infections and dsRNA Treatment

Yanchun Deng[1,2,3†], Hongxia Zhao[4†], Sa Yang[1,2], Li Zhang[1,2], Lina Zhang[1,2] and Chunsheng Hou[1,2]*

[1] Institute of Apicultural Research, Chinese Academy of Agricultural Sciences, Beijing, China, [2] Key laboratory of Pollinating Insect Biology, Ministry of Agriculture and Rural Affairs, Beijing, China, [3] Graduate School of Chinese Academy of Agricultural Sciences, Beijing, China, [4] Guangdong Key Laboratory of Animal Conservation and Resource Utilization, Guangdong Public Laboratory of Wild Animal Conservation and Utilization, Guangdong Institute of Applied Biological Resources, Guangdong Academy of Science, Guangzhou, China

OPEN ACCESS

Edited by:
Declan C. Schroeder,
University of Minnesota, United States

Reviewed by:
Irina V. Safenkova,
Research Center of Biotechnology of the Russian Academy of Sciences, Russia
Eugene Ryabov,
United States Department of Agriculture (USDA), United States

***Correspondence:**
Chunsheng Hou
houchunsheng@caas.cn

[†] These authors have contributed equally to this work

Specialty section:
This article was submitted to Virology, a section of the journal Frontiers in Microbiology

Received: 05 January 2020
Accepted: 30 June 2020
Published: 30 July 2020

Citation:
Deng Y, Zhao H, Yang S, Zhang L, Zhang L and Hou C (2020) Screening and Validation of Reference Genes for RT-qPCR Under Different Honey Bee Viral Infections and dsRNA Treatment. Front. Microbiol. 11:1715. doi: 10.3389/fmicb.2020.01715

Honey bee viruses are one of the most important pathogens that have contributed to the decrease in honey bee colony health. To analyze the infection dynamics of honey bee viruses, quantification of viral gene expression by RT-qPCR is necessary. However, suitable reference genes have not been reported from viral and RNAi studies of honey bee. Here, we evaluated the expression of 11 common reference genes (*ache*2, *rps*18, β-*actin*, *tbp*, *tif*, *rpl*32, *gadph*, *ubc*, α-*tubulin*, *rpl14*, and *rpsa*) from *Apis mellifera* (Am) and *Apis cerana* (Ac) under Israeli acute paralysis virus (IAPV), chronic bee paralysis virus (CBPV), and Chinese sacbrood virus (CSBV) infection as well as dsRNA-PGRP-SA treatment, and we confirmed their validation by evaluating the levels of the *defensin 1* and prophenoloxidase (*ppo*) genes during viral infection. Our results showed that the expression of selected genes varied under different viral infections. *ache*2, *rps*18, β-*actin*, *tbp*, and *tif* can be used to normalize expression levels in *Apis mellifera* under IAPV infection, while the combination of *actin* and *tif* is suitable for CBPV-infected experiments. The combination of *rpl*14, *tif*, *rpsa*, *ubc*, and *ache*2 as well as more reference genes is suitable for CSBV treatment in *Apis cerana*. *Rpl*14, *tif*, *rps*18, *ubc*, and α-*tubulin* were the most stable reference genes under dsRNA treatment in *Apis mellifera*. Furthermore, the geNorm and NormFinder algorithms showed that *tif* was the best suitable reference gene for these four treatments. This study screened and validated suitable reference genes for the quantification of viral levels in honey bee, as well as for RNAi experiments.

Keywords: honey bee, RT-qPCR, reference genes, bee virus, dsRNA treatment

INTRODUCTION

Honey bees provide a significant pollination service for many agricultural crops and wild plants. However, a decline in bee populations has been recently observed in the United States and parts of European countries (Brutscher et al., 2015). Although multiple biotic and abiotic factors contribute to colony decline, several epidemiological and temporal monitoring studies have indicated that

pathogens play an important role in colony loss (Brutscher et al., 2015). Among these pathogens, RNA viruses are the major impacting factors, including two *Apis mellifera* viruses, Israeli acute bee paralysis virus (IAPV) (Maori et al., 2007) and chronic bee paralysis virus (CBPV) (Genersch and Aubert, 2010), as well as one *Apis cerana* virus, namely, Chinese sacbrood virus (CSBV) (Li et al., 2018).

Israeli acute paralysis virus, a positive-sense RNA virus in the family *Dicistroviridae*, has a widespread impact on honey bee health and has been linked with colony losses (Chen et al., 2014; Galbraith et al., 2015). RNA-seq data indicated that IAPV attacks several core genes in insect immune pathways (Toll, JAK-STAT and RNA interference pathways) (Galbraith et al., 2015). Although CBPV has not been classified, its genome, which is made up of two segments of single-stranded RNA in a non-enveloped anisometric capsid, shows homology to the Nodaviridae and Tombusviridae families (Coulon et al., 2017). Exposure of honey bees to CBPV alone promoted downregulation of immune-related genes, such as *dorsal-1a* and *ppo* (Coulon et al., 2017). CSBV, a geographic strain of SBV isolated from *A. cerana* in China, can cause fatal infections to *A. cerana* larvae by decreasing antimicrobial peptide levels (Shan et al., 2017). The quantification of viral and immune gene expression levels is one of the most important aspects when studying host and virus interactions (Marcial-Quino et al., 2016). RNA interference (RNAi) technology is frequently used as a research tool to study the function, transcription and regulation of gene including immune genes (Vyas et al., 2017; Zhu et al., 2019). Introducing exogenous double stranded RNA (dsRNA) into the insect cells activates RNAi pathways that normally function to induce antiviral responses (Dietrich et al., 2017). To analyze the expression differences in immune genes during viral infection and RNAi process, RT-qPCR is used to assess gene expression by normalization with reference genes. Most gene expression studies focused on honey bee select *actin* as an internal control (Chen et al., 2014), though RPS5 (Wheeler et al., 2006) and EIF S8 (Hunt et al., 2007) are also occasionally used. However, the identification of reference genes was not made in advance when these studies assessed viral dynamics and the changes in corresponding target genes.

As summarized by Shakeel et al. (2018), the identification and validation of reference genes for qRT-PCR have been performed in various insect species. For honey bee, the stability of reference genes has been investigated in different developmental stages and tissues (Lourenco et al., 2008; Reim et al., 2013; Moon et al., 2018a), and even after bacterial challenge (Scharlaken et al., 2008). However, suitable candidate reference genes have not been validated during honey bee viral infection. Moreover, most of these genes displayed variable expression levels under different experimental conditions (Thellin et al., 2009).

Thus, we evaluated the expression of 11 reference genes under infection with three different viruses and under experimental RNAi conditions to identify the most suitable reference genes for different conditions. Here, 11 reference genes, including *A. mellifera ribosomal protein L32* (*Amrpl*32), *A. mellifera 40S ribosomal protein S18* (*Amrps*18), *A. mellifera TATA-box-binding protein* (*Amtbp*), *A. mellifera*α*-tubulin alpha-1C chain* (*Am*α*-tubulin*), *A. mellifera glyceraldehyde-3-phosphate dehydrogenase 2* (*Amgadph*), *A. mellifera acetylcholinesterase 2* (*Amache*2), *A. mellifera translation initiation factor eIF-2B subunit delta* (*Amtif*), *A. mellifera ubiquitin-conjugating enzyme E2-22 kDa* (*Amubc*), *A. mellifera actin related protein 1* (*Am*β*-actin*), *Apis cerana 60S ribosomal protein L14* (*Acrpl*14), *Apis cerana 40S ribosomal protein SA* (*Acrpsa*), *Actbp*, *Ac*α*-tubulin*, *Acgadph*, *Acache2*, *Actif*, *Acubc*, and *Ac*β*-actin*, were analyzed in *A. mellifera* under IAPV or CBPV infection as well as RNAi experimental conditions. The corresponding genes from *A. cerana* were also used to determine the most stable reference genes for RT-qPCR under CSBV infection. Five common algorithms, including NormFinder, BestKeeper, Delta-Ct, geNorm, and RefFinder, were used to evaluate reference gene expression. We also tested the reliability of the reference genes by investigating the expression levels of two immune genes, *defensin 1* and prophenoloxidase (*ppo*), under different viral infections. We hope that this report will provide a basis for future studies on gene expression in honey bee under viral infection.

MATERIALS AND METHODS

Collection of Virus-Infected Honey Bees

Israeli acute paralysis virus-infected *A. mellifera* adults with obvious paralysis symptom (Maori et al., 2007) were collected from three different apiaries in Beijing, Miyun, China, while CBPV-infected *A. mellifera* adults with paralysis symptom (Olivier et al., 2008) were collected from three different apiaries in Guangdong Province in China. They were tested by RT-PCR with special primers (Diao et al., 2018). Healthy *A. cerana* larvae were collected from three different apiaries in Guangdong Province in China. CSBV-infected larvae were taken from naturally infected colonies with obvious cystic phenotypes and symptoms. The samples were immediately transported to the laboratory on dry ice to avoid the degradation of the active substances therein.

We collected seemingly healthy bee samples from the experimental apiary at the Institute of Apicultural Research (IAR), Chinese Academy of Agricultural Sciences, Beijing, China. Newly emerged bees (*A. mellifera*) were obtained from brood frames taken from the experimental honey bee hives and maintained in an incubator at 30°C and 60% relative humidity (RH) for approximately 12 h with access to a 50% sucrose solution. Honey bee samples were divided into five groups with three repetitions per group with 30 bees. The first, second, and third groups consisted of bees treated with IAPV, CBPV, and CSBV, respectively; the fourth group consisted of bees treated with dsRNA-pgrpsa; and the fifth group was used to test the reliability of the reference genes. Each group contained a blank control, except for the dsRNA experiment, which had dsRNA-GFP as a control.

To gain reliable samples, PCR detection was performed. Samples in IAPV group were collected every day (24, 48, 72, and 96 h) and followed by PCR using IAPV primers (**Supplementary Table S1**). Similarly, samples in CBPV group were collected every day (0, 24, 48, 72, and 96 h) and followed by PCR using CBPV primers (**Supplementary Table S1**). The naturally CSBV-infected

larvae and the healthy larvae of *A. cerana* were collected from 2th to 6th-instar and followed by PCR using CSBV primers (**Supplementary Table S1**). Samples in dsRNA treatment group were collected every day (24, 48, 72, and 96 h) and followed by PCR using PGRP-SA primers (**Supplementary Table S1**).

Purification and Inoculation of IAPV and CBPV

To purify the viruses, the IAPV (IAPV-BJ, KX421583.1) and CBPV (CBPV-HB, MF175174.1, and MF175173.1) field strains originating from paralyzed bees showing clinical symptoms of viral infection were collected in May 2017 in China. IAPV and CBPV were screened for predominance in the samples, as well as the absence of other common viruses. IAPV was purified as described by Maori et al. (2007). CBPV was purified from the heads of bees by ultracentrifugation in a 10 to 40% (w/v) sucrose gradient as previously described by Olivier et al. (2008). To avoid interference by other viruses, PCR was run to identify whether there was infection by four other common honey bee viruses before virus purification (**Supplementary Table S1**), such as black queen cell virus (BQCV), acute bee paralysis virus (ABPV), deformed wing virus (DWV) and aphid lethal paralysis virus (ALPV) following the method of Diao et al. (2018) and Yang et al. (2019). The purified virus particles were dissolved in sucrose at −80°C and aliquoted until use.

Purified virus particles (5 μl, 1 μg/μl) with about 4.0×10^4 genome equivalent copies was injected into the abdominal intersegment space of 30 individual newly emerged bees taken from a healthy colony. For the IAPV and CBPV infection groups, 5 μg of IAPV and CBPV, respectively, was injected into newly emerged honey bees (*A. mellifera*). The naturally infected CSBV and normal control *A. cerana* larvae were collected from the 2nd to 6th instars. For the dsRNA group, dsRNA-PGRP-SA and dsRNA-GFP (5 μg) were injected into newly emerged honey bees (*A. mellifera*) at 0 and 48 h, respectively. The honey bee samples were detected for six other viruses before they were used for the infection experiments. The infected bees were maintained in an incubator at 30°C, and their mortality was calculated each day. Bees in control group were injected with PBS buffer.

RNA Extraction and RT-qPCR

Total RNA was extracted with the TRIol Kit (Ambion, Life Technologies, United States) following the manufacturer's instructions. A NanoDrop 2000 (Thermo Scientific, United States) was used to check the quality of each RNA sample. RNA samples with A260/280 ratios ranging from 1.8 to 2.2 were used for cDNA synthesis with the PrimeScript RT Reagent Kit with gDNA Eraser (Takara, Dalian, China) according to the manufacturer's instructions. The cDNAs of all samples were stored at −20°C until use.

The specific primers for the reference genes were designed using Primer-BLAST (**Table 1**). The RT-qPCR reaction system consisted of 12.5 μL 2 × SYBR Premix Ex Taq^{TM} II (Takara, Dalian, China), 0.5 μL each of the forward and reverse primers (10 mM), 2 μL cDNA template, and 9.5 μL double-distilled H_2O for a total volume of 25 μL. The RT-qPCR conditions followed the manufacturer's instructions. All reactions were performed using SYBR Green Premix and amplified under the following cycling conditions: an initial cycle at 95°C; 40 cycles of 95°C for denaturation, 25 s at 55°C for annealing and 20 s at 72°C for extension; and the generation of a melting curve consisting of a single peak to rule out non-specific products and primer dimers afterward. The RT-qPCR analysis was performed with three biological replicates for each sample and three technical replicates for each biological replicate and was measured as the mean Ct value. The results were analyzed using the 9600 plus Software.

PCR Detection for Viral and Immune Genes

The primer sequences, orientation and references are provided in **Supplementary Table S1**. The cDNAs of all samples were gained in the above, followed by the PCR cycles. The PCR reaction consisted of a total 20 μL volume containing 10 μL 2 × GoTaq reaction buffer (Promega, United States), 0.5 μL 10 μM of the sense and antisense primers, 1 μL of cDNA, and 8 μL nuclease-free water. The cycling conditions were as follows: 1 min at 95°C; 33 cycles of 30 s at 94°C, 30 s at 55 and 72°C for 1 min; a final extension of 10 min at 72°C; and cooling to 4°C. The PCR amplification products were separated in a 2% agarose gel stained with GV II (BIOMEC, China) and photographed with a FR-200A luminescent and fluorescent biological image analysis system (Furi, China). The product size was determined using a 100-bp molecular size ladder.

dsRNA Synthesis

The specific primers for PGRP-SA and GFP tagged with T7 promoter sequence were designed using Primer-BLAST to amplify the templates for synthesis of dsRNA (**Supplementary Table S2**). Amplification was performed under normal PCR conditions as follows: 30 s at 95°C; followed by 35 cycles of 8 s at 95°C, 30 s at 56°C, and 30 s at 72°C; and a final extension incubation at 72°C for 5 min. The PCR templates were purified using a Qiagen purification kit (Qiagen, Germantown, MD, United States). dsRNA-PGRP-SA and dsRNA-GFP were produced using a T7 RNAi Transcription Kit (Vazyme, China) according to the manufacturer's instructions. The reaction product was subjected to DNase and RNAse digestion, and then incubated at 37°C for 8 h. Subsequently, the samples were dried at 37°C for 10 min and resuspended in 20–40 μL of nuclease-free H_2O. The quality of the dsRNA was checked by electrophoresis and quantified with a spectrophotometer (NanoDrop Technologies, Wilmington, DE, United States). Then, 5 μg each of PGRPSA dsRNA and *GFP* dsRNA was injected into newly emerged *A. mellifera* at 0 and 48 h, respectively.

Stability of Expression of Selected Reference Genes

The stability of expression of the candidate reference genes was evaluated by five statistical algorithms, namely, the delta CT method (Silver et al., 2006), BestKeeper (Pfaffl et al., 2004), geNorm (Vandesompele et al., 2002), NormFinder (Andersen et al., 2004), and the online platform RefFinder (Xie et al., 2012).

TABLE 1 | Primers used for RT-qPCR of the candidate reference genes.

Gene name	Gene symbol	Primer sequence (5′–3′)	Amplicon size (bp)	GenBank accession no.
Apis mellifera ribosomal protein L32	*Amrpl32*	F:CGTCACCAGAGTGATCGTTACA R:CCCCATGAGCAATTTCAGCAC	244	NM_001011587.1
Apis mellifera 40S ribosomal protein S18	*Amrps18*	F:GGTGTTGGTCGTCGTTATGC R:CGCAAACCTCTATGAGCACG	269	XM_625101.6
Apis mellifera TATA-box-binding protein	*Amtbp*	F:GCAACCTCAAACACCGCAAA R:TGCAGAAGCCGGTGTCATAG	121	XM_623085.6
Apis mellifera tubulin alpha-1C chain	*Amα-tubulin*	F:TGAGTCAGACAGTAGTCGGAT R:TACCCATTTGGACACCAGCC	126	XM_006558697.3
Apis mellifera glyceraldehyde-3-phosphate dehydrogenase 2	*Amgadph*	F:TACCGCTTTCTGCCCTTCAA R:GCACCGAACTCAATGGAAGC	142	XM_393605.7
Apis mellifera acetylcholinesterase 2	*Amache2*	F:GACGCGAAGACCATATCCGT R:TCTGTGTCCTTGAAGTCCGC	140	NM_001040230.1
Apis mellifera translation initiation factor eIF-2B subunit delta	*Amtif*	F:TGAAACAAGAGGAACATGTCTAA R:CGTTCTGCTTTTATTTCCTCCC	121	XM_006559190.3
Apis mellifera ubiquitin-conjugating enzyme E2-22 kDa	*Amubc*	F:TCAAAAGGGTGAACACGAGC R:AGTTCGCTGAATGCGTCAAC	208	XM_016917677.1
Apis mellifera actin related protein 1	*Amactin*	F:TTGTATGCCAACACTGTCCTT R:TGGCGCGATGATCTTAATTT	120	NM_001185146.1
Apis cerana 60S ribosomal protein L14	*Acrpl14*	F:TTGCTTCCGGTAAACCATGC R:ATGTTTGCAGCTTCCCATGC	261	XM_017051728.2
Apis cerana 40S ribosomal protein SA	*Acrpsa*	F:TTGGAAGTCTCCTAGTGGCA R:GCTCTTTGTCCAGTTTGTCGG	314	XM_017053220.2
Apis cerana TATA-box-binding protein	*Actbp*	F:AAGTCCGATGACCCCAGCTA R:TAGCTGCAAAACCTAACTTCTGAAT	302	XM_028665297.1
Apis cerana tubulin alpha-1 chain	*Actubulin*	F:GTTCGACTGTGCGTTGTGTG R:TGACCATCAGGTTGGATGCC	211	XM_017057619.2
Apis cerana glyceraldehyde-3-phosphate dehydrogenase 2	*Acgadph*	F:CTGCACAGACCCGAGTGAAT R:GCAACAACCTGAGCACCAAA	120	XM_017062468.2
Apis cerana acetylcholinesterase	*Acache2*	F:CTGGTCTTGGTAAAGGGCCA R:CCTGGACGAAGCCCTAACAC	303	XM_017066417.2
Apis cerana translation initiation factor eIF-2B subunit delta	*Actif*	F:TGGAACTGCTCAAGTTGCCT R:ATCGGCTGGTGTAACATCGT	241	XM_028664590.1
Apis cerana ubiquitin-conjugating enzyme E2-22 kDa	*Acubc*	F:GCTGCTGCCATGACTTTACG R:TAGCGCGTTCCAAATCCCAA	280	XM_017048857.2
Apis cerana actin	*Acacetin*	F:CGAGCACGGTATCATCACCA R:CCAAGTCCAGACGGAGGATG	329	JX899419.1
Apis mellifera defensin 1	*AmDef1*	F:AAGAACGTGCCGACAGACAT R:TCGCAATGACCTCCAGCTTT	121	NM_001011616.2
Apis mellifera phenoloxidase subunit A3	*Amppo*	F:AGATGGCATGCATTTGTTGA R:CCACGCTCGTCTTCTTTAGG	332	NM_001011627.1
Apis cerana defensin 1	*AcDef1*	F: AATTCGAGCCACTTGAGCATCC R: CAATGACCTCCAGCTTTACCCAA	148	XM_017050425.2

geNorm is based on the principle that the expression ratio of two reference genes should be constant in all samples, regardless of the experimental conditions or sampling time (Hellemans et al., 2007). The gene expression stability (M) is defined as the average pairwise variation compared with all other tested candidate genes by geNorm, and the reference genes with the

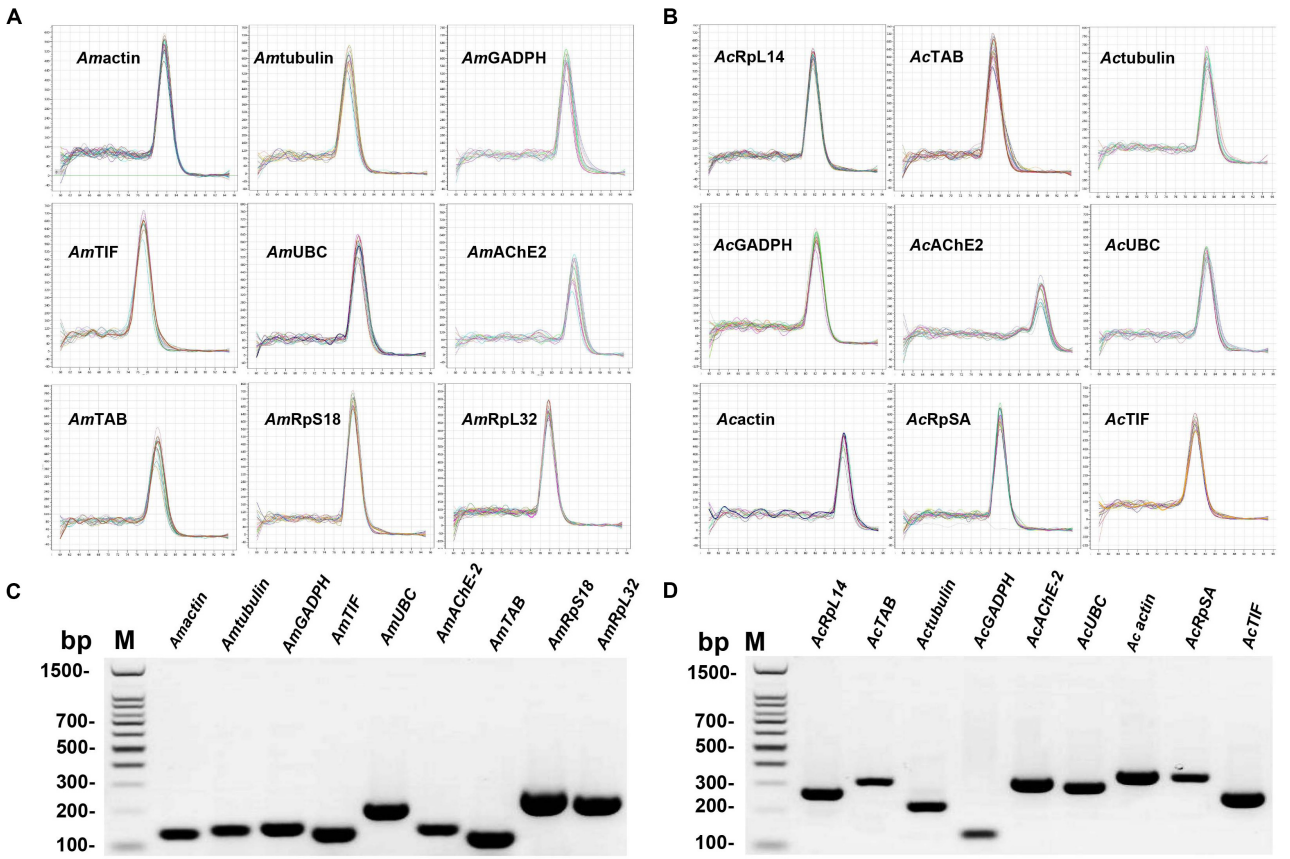

FIGURE 1 | Confirmation of primer specificity and amplicon size. **(A)** Melting curve analysis of the *Apis mellifera* candidate reference genes. All RT-qPCR products had a single melting curve indicating the breakdown of only one PCR product. **(B)** Melting curve analysis of *Apis cerana* candidate reference genes. All RT-qPCR products had a single melting curve indicating only one PCR product. **(C)** Amplification results for *Apis mellifera* candidate genes from cDNA template. **(D)** Amplification results for *Apis cerana* candidate genes from cDNA template. M: DL1500 DNA marker.

lowest *M*-value remained (Vandesompele et al., 2002). Pairwise variation (Vn/Vn + 1) analysis between the normalization factors (NFn and NFn + 1) was performed by geNorm to determine the optimal number of reference genes (Vandesompele et al., 2002). NFn was also calculated by the stepwise inclusion of a less stable gene until the $(n + 1)$th gene had no significant contribution to the newly calculated NFn + 1 (Vandesompele et al., 2002). In particular, if the pairwise variation Vn/n + 1 between the two sequential normalization factors NFn and NFn + 1 was lower than the cut-off value of 0.15, it was considered that NFn + 1 is not required (Peng et al., 2018). NormFinder was used to estimate changes and intra- and intergroup expression variation among the candidate reference genes (Andersen et al., 2004). The most stable gene is the one with the lowest stability value according to the intra- and intergroup variability of each gene (Andersen et al., 2004). BestKeeper determines the most stably expressed genes according to the standard deviation (SD) and coefficient of variation (CV) of all the Ct values for each gene (Pfaffl et al., 2004). When the SD values of genes are <1, they are considered stable (Marcial-Quino et al., 2016). Similarly, the delta-Ct method was used to identify suitable housekeeping genes based on the average SD value of each gene (Silver et al., 2006). To identify the optimal reference genes, RefFinder, a user-friendly web-based comprehensive tool that provides a comprehensive ranking evaluation based on the geometric mean and integrates with other computational algorithms (geNorm, NormFinder, BestKeeper, and the comparative Delta-Ct method), was used to reduce bias or avoid contradictory results caused by using individuals (Peng et al., 2018). Individual genes were assigned an appropriate weight and the geometric mean of their weights was calculated for the overall final ranking based on each program.

Validation of the Selected Reference Genes

The three strategies for expression profile normalization using the reference genes in each treatment are as follows: (1) the optimal reference gene from all the samples, (2) the optimal reference gene from each treatment, and (3) the least stable reference gene from each treatment.

To validate the candidate reference genes, the relative expression levels of two immune genes (*defensin1* and *prophenoloxidase*) were used to evaluate the reference genes by RT-qPCR. The $2^{-\Delta\Delta CT}$ method was employed to validate and

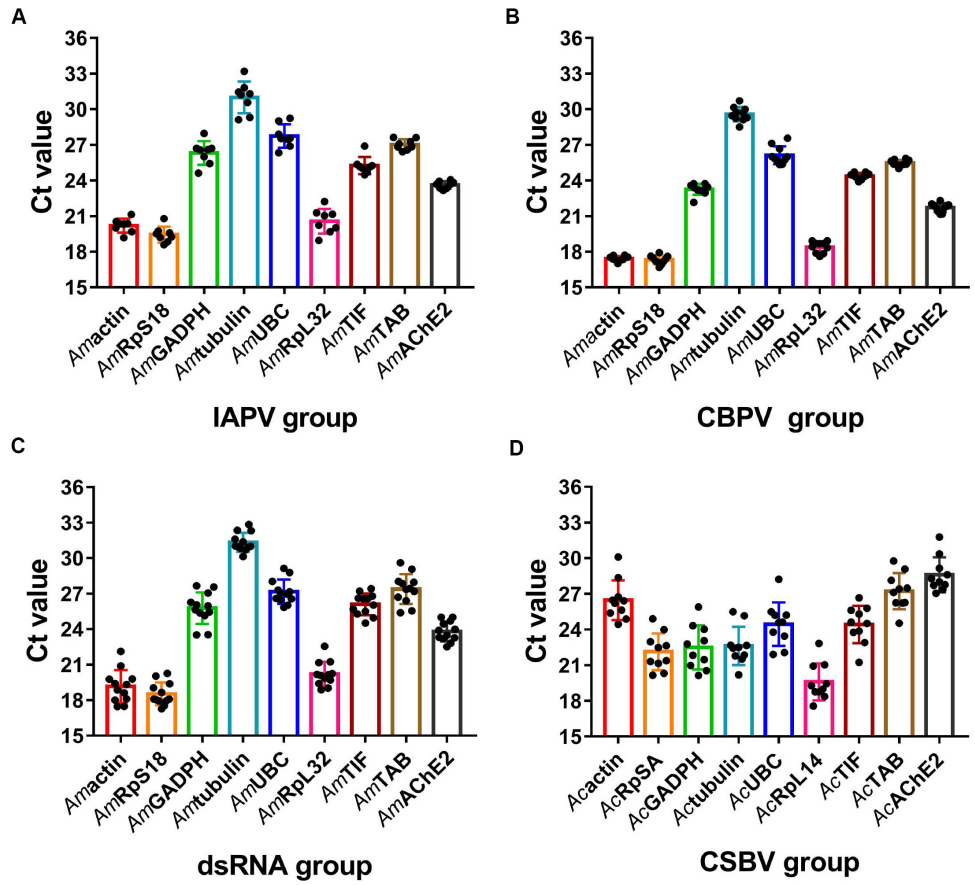

FIGURE 2 | Expression profiles of candidate reference genes in different groups. Scatter plot analysis showing the raw Ct values of the candidate reference genes in **(A)** IAPV-infected honey bee. **(B)** CBPV-infected honey bee. **(C)** honey bee exposed to dsRNA PGRPSA treatment and **(D)** CSBV-infected *A. cerana* larvae.

quantify the expression levels of *def1* and *ppo* after viral infection. One-way ANOVA was used to analyze the significance and the means were compared using Tukey's multiple comparison test ($P < 0.05$) using the GraphPad Prism software.

RESULTS

Identification of Primer Specificity and the Efficiency of the Candidate Reference Genes

The reference gene candidates in this study were selected based on the following two criteria: (a) genes routinely used in honey bees or insects for transcript normalization and (b) genes described as stably expressed under environmental stress. Eleven candidate reference genes were selected for *A. mellifera* and *A. cerana* under different treatments. The amplicon sizes of the target genes were between 100 and 320 bp with primer lengths of 17–25 bp and a 40–60% GC content. Primer specificity for each gene was validated by melting curve analysis during qRT-PCR, and a single peak was observed in each reaction (**Figures 1A,B**). Primer specificity for all genes was further tested using 2.0% agarose gels. A single PCR amplification band of the expected size was observed, suggesting that primer dimers and non-specific amplified products were not generated (**Figures 1C,D**). Additionally, the amplification efficiencies ranged from 92.2 to 107% based on the standard curves for the 18 genes. Moreover, correlation coefficients (R^2) were greater than 0.99, which fit the RT-qPCR requirements (**Supplementary Table S3**).

Characterization of Candidate Reference Genes

To analyze the expression profiles of the candidate reference genes, sample validation was performed by PCR (**Supplementary Table S1**). As shown in **Supplementary Figure S1**, the samples from the IAPV-treated group were positive but the control groups were not (**Supplementary Figure S1A**). Similarly, positive results were also observed for the CBPV and CSBV groups (**Supplementary Figures S1B,C**). The results for the dsRNA treatment groups showed that the expression of PGRP-SA had been markedly downregulated compared to the control group (**Supplementary Figure S1D**).

A reliable reference gene should show constant expressions level under different experimental conditions (Galli et al., 2015).

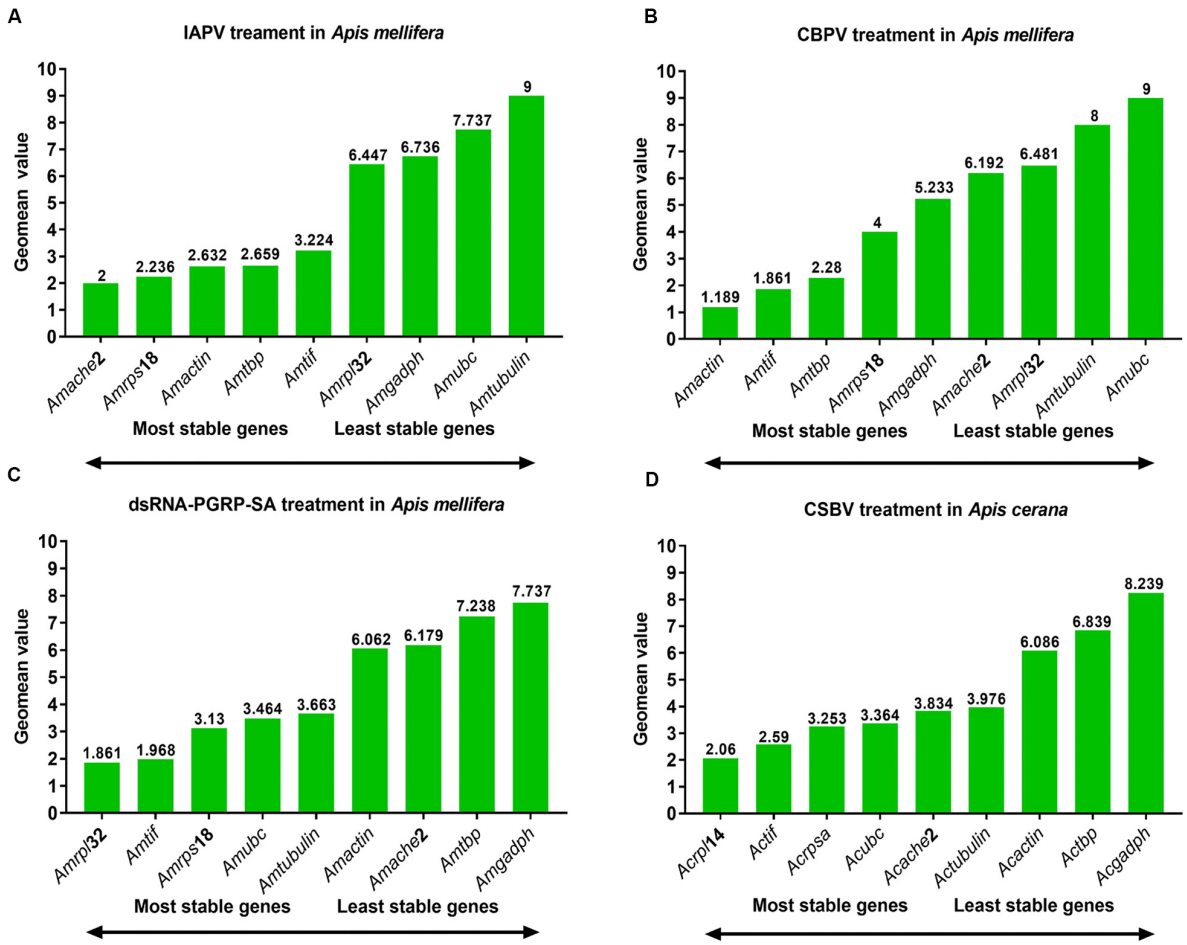

FIGURE 3 | Expression stability of candidate reference genes analyzed by RefFinder. Expression stability of candidate reference genes during **(A)** IAPV infection, **(B)** CBPV infection, and **(C)** CSBV infection in *A. cerana* larvae as well as **(D)** honey bees treated with dsRNA-PGRP-SA.

We next evaluated the expression levels of the candidate reference genes and found that the average Ct values of the reference genes in different samples ranged from 16 to 32 (**Figure 2**). In the *A. mellifera* groups, RPS18 was the most abundant with the lowest mean Ct value at 19.43 ± 0.67 in the IAPV-treated group (**Figure 2A**), 17.31 ± 0.37 in the CBPV-treated group (**Figure 2B**) and 18.52 ± 0.96 in the dsRNA-treated group (**Figure 2C**). In contrast, *Amα-tubulin* transcription showed the lowest level with the highest mean Ct value at 30.99 ± 1.33 in the IAPV-treated group, 29.58 ± 0.62 in the CBPV-treated and 31.33 ± 0.80 in the dsRNA-treated group (**Figure 2**). In the *A. cerana* group, *ache*2 exhibited the smallest SD value (28.6 ± 1.47) but had the lowest expression level (**Figure 2D**). In contrast, *rpl*14 exhibited the smallest Ct value (19.59 ± 1.56) but had a larger SD value. *Tif* was a moderately stable gene with Ct average values at 25.25 ± 0.73 in the IAPV-treated group, 24.38 ± 0.26 in the CBPV-treated group, 26.10 ± 0.9 in the dsRNA-treated group and 24.43 ± 1.57 in the CSBV-infected *A. cerana* groups (**Figure 2**). However, reference genes from the CSBV-infected group exhibited larger SD values, suggesting that studies should carefully consider when only using one gene as an internal reference for the quantification of genes related to CSBV in *A. cerana* (**Figure 2D**).

Stability of the Candidate Reference Genes Under Different Viral Infections and dsRNA Treatment

The rankings for the expression stability of these 11 genes in honey bee under treatment with IAPV, CBPV, CSBV or dsRNA was analyzed using different algorithms (**Table 1** and **Figure 3**). In the IAPV treatment group, *Amrps*18, *Amtif*, and *Amache*2 were considered the most stable genes with the lowest *M* value according to the geNorm and NormFinder analysis (**Table 2**). However, the ranking obtained with BestKeeper and Delta CT showed that *Amache*2, *Amtbp*, and *Amβ-actin* were the top three stable candidate reference genes (**Table 2**). To identify the most suitable reference genes, the results of these four programs were integrated with RefFinder (He et al., 2019), which showed that the stability of these genes in *A. mellifera* treated with IAPV was as follows: *Amache*2, *Amrps*18, *Amactin*, *Amtbp*, *Amtif*, *Amrpl*32, *Amgadph*, *Amubc*, and *Amα-tubulin* (**Figure 3A**). However,

TABLE 2 | Gene expression stability ranked by the geNorm, NormFinder, and BestKeeper algorithms.

Treatments	Gene	GeNorm		NormFinder		BestKeeper			delta-CT	
		M	R	SV	R	CV	SD	R	SD	R
IAPV	*Amβ-actin*	0.749	4	0.02	3	2.14	0.432	3	0.588	3
	*Amrps*18	0.659	1	0.018	2	2.41	0.468	5	0.669	4
	Amgadph	0.820	5	0.077	6	2.77	0.729	6	0.996	7
	Amα-tubulin	1.373	8	0.267	8	3.22	0.999	9	1.332	9
	Amubc	0.839	6	0.101	7	2.66	0.737	7	0.985	6
	*Amrpl*32	0.871	7	0.038	4	4.13	0.850	8	1.041	8
	Amtif	0.697	2	0.014	1	1.73	0.437	4	0.726	5
	Amtbp	0.749	4	0.053	5	1.34	0.363	2	0.446	2
	Amache2	0.742	3	0.018	2	1.08	0.255	1	0.318	1
CBPV	*Amβ-actin*	0.380	1	0.015	2	0.96	0.166	1	0.211	1
	*Amrps*18	0.430	3	0.015	2	1.64	0.285	4	0.669	8
	Amgadph	0.464	4	0.030	4	1.35	0.314	6	0.463	5
	Amα-tubulin	0.640	7	0.096	6	1.59	0.470	8	0.617	7
	Amubc	0.732	8	0.067	5	2.28	0.595	9	0.750	9
	*Amrpl*32	0.488	5	0.030	4	2.07	0.381	7	0.467	6
	Amtif	0.380	1	0.013	1	0.81	0.197	2	0.262	2
	Amtbp	0.407	2	0.030	4	0.85	0.218	3	0.263	3
	Amache2	0.507	6	0.021	3	1.32	0.287	5	0.376	4
dsRNA	*Amβ-actin*	1.023	5	0.033	3	5.55	1.064	8	1.384	9
	*Amrps*18	1.152	7	0.049	4	5.55	1.064	8	0.963	4
	Amgadph	1.032	6	0.063	6	3.85	0.992	7	1.332	8
	Amα-tubulin	1.255	8	0.147	9	2.03	0.636	1	0.617	1
	Amubc	0.895	3	0.058	5	2.82	0.766	4	1.024	5
	*Amrpl*32	0.856	2	0.030	2	3.60	0.727	3	1.030	6
	Amtif	0.806	1	0.014	1	2.94	0.768	5	0.914	3
	Amtbp	1.032	6	0.080	7	3.45	0.946	6	1.263	7
	Amache2	0.925	4	0.082	8	2.97	0.707	2	0.843	2
CSBV	*Acacetin*	1.450	4	0.124	8	4.39	1.161	4	1.676	7
	Acrpsa	2.077	9	0.059	3	5.73	1.267	7	1.550	3
	Acgadph	1.580	6	0.108	7	6.73	1.514	9	1.852	9
	Acα-tubulin	1.490	5	0.077	5	4.85	1.098	2	1.604	6
	Acubc	1.758	7	0.062	4	5.42	1.325	8	1.833	8
	*Acrpl*14	1.435	3	0.037	1	6.13	1.200	6	1.555	4
	Actif	1.371	1	0.053	2	4.86	1.187	5	1.574	5
	Actbp	1.769	8	0.178	9	4.22	1.149	3	1.526	2
	Acache2	1.428	2	0.099	6	3.82	1.093	1	1.467	1

M, gene expression stability; R, ranking; SV, stability value; SD, standard deviation; CV, coefficient of variation.

Amubc and *Amα-tubulin* were ranked as the least stable genes in the IAPV-infected group.

As shown in **Table 2**, *Amtif* and *Amtbp* were the top two stable candidate reference genes in *A. mellifera* infected with CBPV based on the ranking with geNorm, Delta-CT and BestKeeper. However, the ranking obtained with NormFinder was *Amtif*, *Amactin* and *Amrps*18, which was different from that obtained with geNorm. Based on the comprehensive analysis by RefFinder, the stability of these genes in *A. mellifera* treated with CBPV was as follows: *Amβ-actin*, *Amtif*, *Amtbp*, *Amrps*18, *Amgadph*, *Amache2*, *Amrpl*32, *Amubc*, and *Amα-tubulin* (**Figure 3B**). Because *Amubc* and *Amα-tubulin* were ranked as the least stable genes in IAPV-infected and CBPV-infected *A. mellifera,* they were not recommended as reference genes for qRT-PCR analyses in honey bee infected with viruses (**Figures 3A,B**).

For *A. cerana* larvae infected with CSBV, *Actif*, *Acache2*, and *Acrpl*14 were the top three stable candidate reference genes based on the geNorm algorithms (**Table 2**). *Acrpl*14, *Actif*, and *Acrpsa* were the top three stable candidate reference genes according to NormFinder. However, the ranking obtained with BestKeeper showed that *Acache2*, *Acα-tubulin* and *Actbp* were the top three stable candidate reference genes. Furthermore, the ranking obtained with the Delta CT method showed that *Acache2*, *Actbp*, and *Acrpsa* were the top three suitable genes (**Table 2**). The outcome from integration with RefFinder showed that the stability of the genes in *A. cerana* infected with CSBV was as follows: *Acrpl*14, *Actif*, *Acrpsa*, *Acubc*, *Acache2*, *Acα-tubulin*, *Acacetin*, *Actbp*, and *Acgadph* (**Figure 3C**). However, according to their larger *M* values (1.3 to 2.0), none of the reference genes used in CSBV-infected *A. cerana* was stable (**Table 2**).

For *A. mellifera* treated with dsRNA-PGRP-SA and dsRNA-GFP, *Amtif*, *Amrpl*32 and *Amubc* were the top three stable candidate reference genes according to the geNorm algorithms (**Table 2**). *Amtif*, *Amrpl*32 and *Am*actin were the top three stable

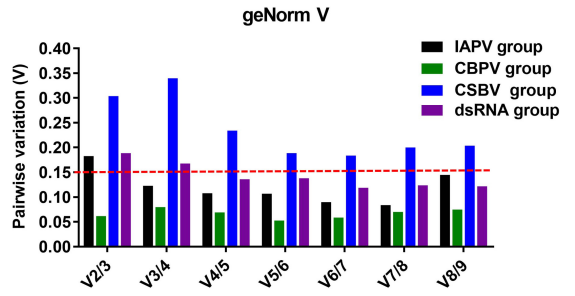

FIGURE 4 | Determination of the optimal number of reference genes for normalization based on the pairwise variation values calculated by geNorm. The value of Vn/Vn + 1 < 0.15 means n should be the optimal number of reference genes selected for RT-qPCR analysis among IAPV-infected (black), CBPV-infected (green), and CSBV-infected (blue) honey bees, as well as honey bees exposed to dsRNA-PGRPSA (purple).

candidate reference genes based on NormFinder. However, the ranking obtained with BestKeeper showed that *Amα-tubulin*, *Amache*2, and *Amrpl*32 were the top three stable candidate reference genes. Moreover, the ranking by the Delta-CT method showed that *Amα*-tubulin, *Amache*2 and *Amtif* were the top three reference genes (**Table 2**). According to the RefFinder results, the stability of the genes in *A. mellifera* treated with dsRNA was as follows: *Amrpl*32, *Amtif*, *Amrps*18, *Amubc*, *Amα*-tubulin, *Amactin*, *Amache*2, *Amtbp*, and *Amgadph* (**Figure 3D**).

Determination of the Optimal Number of Reference Genes

To determine the optimal number of reference genes, we used geNorm to calculate the pairwise variation. In the IAPV treatment group, $V_3/V_4 < 0.15$ indicated that three reference genes was sufficient to accurately normalize RT-qPCR data (**Figure 4**). Therefore, *Amache*2, *Amrps*18 and *Amactin* were considered to be a suitable combination of reference genes for RT-qPCR analyses in honey bee infected with IAPV. In the CBPV treatment group, $V_2/V_3 < 0.15$ indicated that two reference genes was sufficient to normalize RT-qPCR data. Thus, *Amactin* and *Amtif* were considered to be a suitable combination of reference genes for RT-qPCR. In contrast, in the CSBV treatment group, $Vn/Vn + 1 > 0.15$ indicated that more reference genes are required and should be combined for RT-qPCR data normalization. In the dsRNA treatment group, $V_4/V_5 < 0.15$ suggested that *rpl*32, *tif*, *rps*18, and *ubc* were a suitable combination of reference genes for RT-qPCR analyses in honey bee treated with dsRNA (**Figure 4**).

Validation of the Selected Reference Genes

As shown in **Figure 5A**, the relative expression levels of the *defensin 1* and *ppo* genes varied based on the different reference genes. In the IAPV-infected group, the relative expression levels of *defensin 1* were downregulated from 5.1- to 2.9-fold and from 3.2- to 2.6-fold when *Amache*2 and *Amtif* were used as reference genes, respectively, while the expression levels of *defensin 1* were upregulated from 2.5- to 7-fold if *Amα-tubulin* was the reference gene. In the CBPV-infected group, the normalization of *ppo* expression levels to *Amactin* or *Amtif* as reference genes exhibited similar downregulated expression trends for both CBPV-infected and uninfected honey bees (**Figure 5B**). However, the relative expression levels of *ppo* were upregulated to 2.25-fold at 96 h after CBPV infection when *Amα-tubulin* was the reference gene (**Figure 5B**). In the CSBV-infected group, the relative expression levels of *defensin 1* were upregulated from 1.4- to 5.6-fold and from 1.2- to 3.4-fold in 5th and 6th CSBV-infected honey bee larvae when we used *Acrpl*14 and *Actif* as reference genes, respectively, while the relative expression levels of *defensin 1* were upregulated from 7.3- to 15.3-fold when *Acgadph* used as the reference gene (**Figure 5C**). In contrast, when *Acgadph* was used for normalization, the expression levels of *defensin 1* exhibited a significant difference from that of *Acrpl*14 ($P < 0.01$). In the dsRNA treatment group, the relative expression levels of *pgrpsa* were downregulated 0. 16-, 0. 06-, and 0.28-fold after 72 h of dsRNA-*pgrpsa* treatment when *Amrpl*32 (best), *Amgadph* (worst) and *Amtif* (modest) were used as the reference genes (**Figure 5D**), respectively, while the relative expression levels of *pgrpsa* were upregulated 6. 5-, 2. 4-, and 7.2-fold at 72 h after dsRNA-gfp treatment if we used *Amrpl*32, *Amgadph* and *Amtif* as the reference genes, respectively (**Figure 5D**). This result showed that normalization of *pgrpsa* expression using the best (*Amrpl*32) and modest (*Amtif*) reference genes exhibited nearly similar outcomes after dsRNA treatment, though its expression exhibited significant differences ($P < 0.05$ and $P < 0.01$) compared to those of *Amrpl*32 and *Amgadph* as reference genes (**Figure 5D**).

DISCUSSION

RT-qPCR is an important, simple and practical technique for assessing gene expression when compared to other quantitative methods such as Northern blotting, *in situ* hybridization and RNA-seq technology (Peng et al., 2018; Adeyinka et al., 2019; He et al., 2019). The application of accurate reference genes is crucial for the quantification of gene expression in *A. mellifera* and *A. cerana*. In our study, five algorithms were used to identify the stability of reference genes. *Ache*2, *rps*18, *actin*, *tbp*, and *tif* are suitable to normalize the gene expression levels in IAPV-infected *A. mellifera*. The combination of *actin* and *tif* is suitable for CBPV-infected *A. mellifera*, while the combination of *rpl*14, *tif*, *rpsa*, *ubc*, and *ache*2 as well as more reference genes is suitable for CSBV-infected *A. cerana* larvae. This result suggests that further studies should be performed to select candidate reference genes for CSBV infection. Moreover, *rpl*14, *tif*, *rps*18, *ubc*, and *α-tubulin* showed the most stable expression in *A. mellifera* under dsRNA treatment.

Our results showed that reference genes were different under different viral infection conditions. An increasing number of studies have reported that using a single reference gene to normalize RT-qPCR might be insufficient and inaccurate for the quantification of gene expression (Yang et al., 2018). As shown in our four experiments, the number of suitable reference genes was greater than two (**Figure 4**). Additionally,

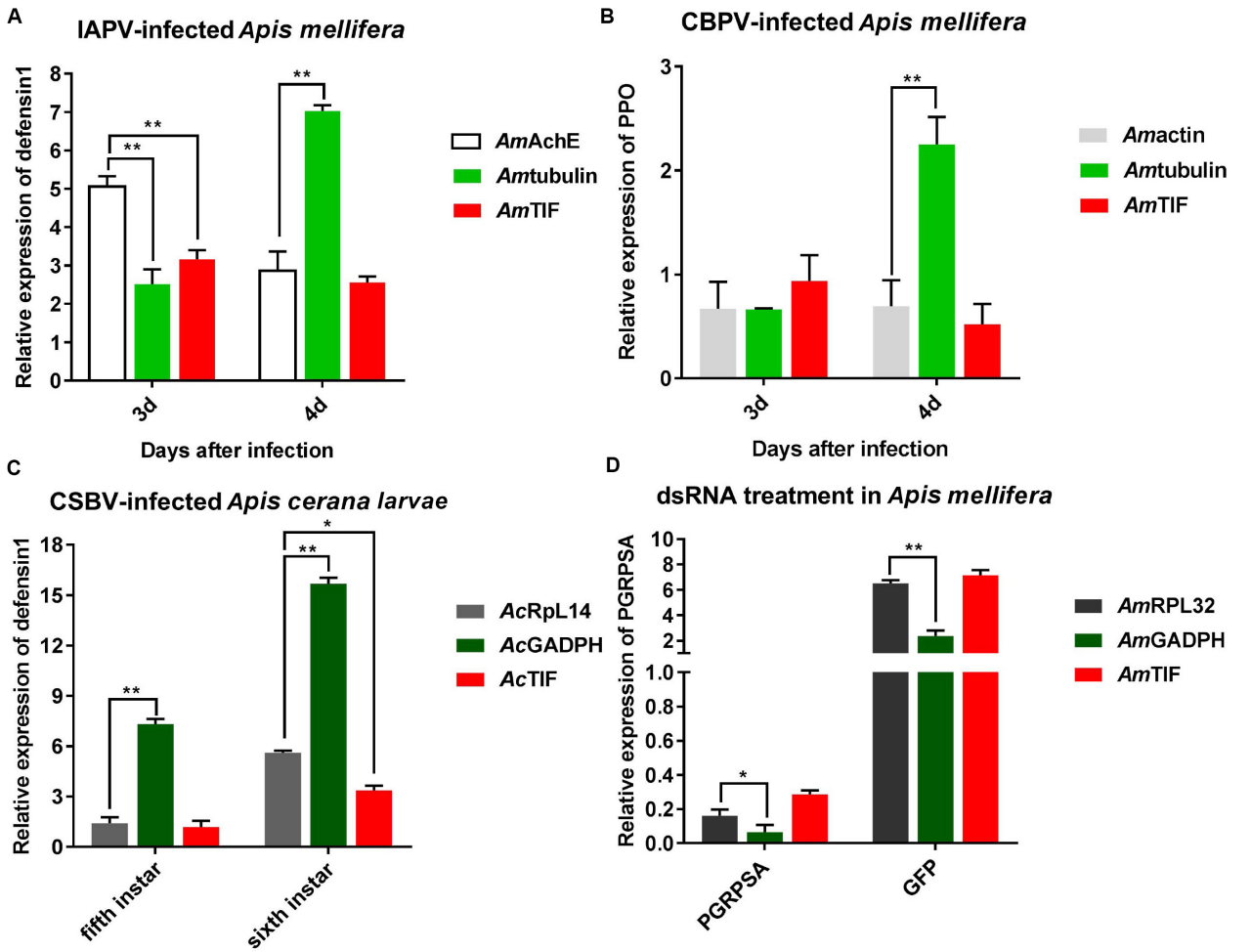

FIGURE 5 | Validation of reference gene stability. **(A)** Relative expression levels of *defensin 1* in IAPV-infected honey bee. **(B)** Relative expression of *ppo* in CBPV-infected honey bee. **(C)** Relative expression of *defensin 1* in CSBV-infected honey bee larvae. **(D)** Relative expression of PGRP-SA in honey bees treated with dsRNA-PGRP-SA. Bars represent the means and standard deviations of three biological replicates. Asterisks indicate significant differences. (*$P < 0.05$ and **$P < 0.01$).

TABLE 3 | Comparison analysis on stability of candidate reference genes in stingless bees, bumblebee, *Apis mellifera* and *Apis cerana*.

Bees	Condition	Most stable reference genes	References
Stingless bees *(Frieseomelitta*	Development	*rpl32*, *rps18*	Freitas et al., 2019
varia, Melipona quadrifasciata,	Sex	*rpl32*, *rps18*, *rps5*, *tbp-af*	Freitas et al., 2019
and Scaptotrigona bipunctata)	Tissues, organs and body parts	*rps18*, *rps5*, *tbp-af*	Freitas et al., 2019
	Bacterial injection	*rps18*, *rpl32*, *tbp-af*	Freitas et al., 2019
	Pesticide exposure	*rps5*, *tbp-af*, *rpl32*, *rps18*	Freitas et al., 2019
Bombus terrestris	IAPV infection	*ppai*, *rpl23*, *ubi*	Niu et al., 2014
Apis mellifera	Abdomens	*rpl32*, *rps18*, *or gapdh*	Moon et al., 2018b
	Head	*rps18*, *gapdh*	Moon et al., 2018a
	Bacterial infection	*actin*, *rpS18*, *gapdh*	Scharlaken et al., 2008
	Development	*gapdh*, *rpl32*, *ef1α-f1*	Reim et al., 2013
	IAPV infection	*ache2*, *rps18*, *actin*, *tbp, tif*	This study
	CBPV infection	*actin*, *tif*, *tbp*, *rps18*	This study
	dsRNA treatment	*rpl32*, *tif*, *rps18*, *ubc*, *tubulin*	This study
Apis cerana	CSBV infection	*rpl14*, *tif*, *rpsa*, *ubc*, *ache2*, *tubulin*	This study

Elongation factor 1 alpha-f1: ef1α-f1, peptidylprolyl isomerase A: ppia, polyubiquitin:UBI.

the stability of these reference genes was different under different experimental conditions. As determined by RefFinder (**Figure 3**), *tif* was a relatively stable reference gene under all of our experimental conditions. Actually, *tif* have been widely used as housekeeping genes for gene expression analysis during Bombyx mori Cytoplasmic Polyhedrosis Virus (BmCPV) and Bombyx mori Bidensovirus (BmBDV) infection (Guo et al., 2016). *Ache*2 was the most stable reference gene under IAPV infection, while β-*actin* was the most stable reference gene under CBPV infection. In contrast, α-*tubulin* exhibited the worst stability under IAPV and CBPV infection. *AcRpl*14 and *Amrpl*32 were the most stable reference genes under CSBV infection and dsRNA treatment, respectively, while *Acgadph* and *Amgadph* exhibited the worst stability under CSBV infection and dsRNA treatment, respectively. However, *gapdh* and *rps*18 were suggested to be the optimal reference genes for RT-qPCR-based under the labor-specific gene expression, bacterial infected and developmental gene expression in Western honey bee as shown in **Table 2** (Scharlaken et al., 2008; Reim et al., 2013; Moon et al., 2018a). Previous studies have shown that some ribosome-associated genes have been used as stable internal reference genes for quantitative analysis (Wang et al., 2019). For instance, Freitas et al. (2019) found that *rpl*32, *rps*5, and *rps*18 were identified as suitable reference genes for the different tissues of stingless bees. Similarly, *rpl23* was identified the reliable reference gene in bumblebees challenged by IAPV (Niu et al., 2014; **Table 3**). Although our study showed that *rpl*32 displayed stable expression in *A. mellifera* under dsRNA treatment, it exhibited the worst stability during IAPV and CBPV infection in *A. mellifera* (**Figure 3**), while *rps*18 was the better reference gene in *A. mellifera* under dsRNA treatment or viral infection (**Table 3**).

Likewise, the stability of the same reference gene varied under different experimental conditions. Although actin is used as an internal control in most gene expression studies during honey bee viral infection, such as IAPV infection (Chen et al., 2014), CSBV infection (Shan et al., 2017), and CBPV infection (Coulon et al., 2017), *actin* exhibited poorer stability during CSBV infection (**Figure 3**). *Gadph*, the other most commonly used reference gene, also showed expression variability from the 2nd to 6th honey bee infected with CSBV infection as well as dsRNA treatment (**Figure 3**). Similarly, α-*tubulin*, another commonly used reference gene, exhibited worse stability under IAPV and CBPV infection. This might result due to interactions between α-tubulin and acetylation, as Zhang et al. (2016) found that acetylated α-*tubulin* will enhance viral titers by promoting fusion with viral inclusion bodies.

This study systematically analyzed 11 reference genes for RT-qPCR under viral infection in *A. mellifera* and *A. cerana*. These results will facilitate future studies in honey bee under different viral infection conditions.

DATA AVAILABILITY STATEMENT

The raw data supporting the conclusions of this manuscript will be made available by the authors, without undue reservation, to any qualified researcher.

AUTHOR CONTRIBUTIONS

CH and YD conceived the manuscript. YD, HZ, SY, LiZ, and LinZ performed the experiments. YD analyzed the data and wrote the manuscript. CH revised the manuscript. All authors contributed to the article and approved the submitted version.

FUNDING

We thank for the support from the National Natural Science Foundation of China (No. 31572471), the Agricultural Science and Technology Innovation Program (CAAS-ASTIP-2019-IAR), the Fundamental Research Funds for CAAS (Y2020PT17), and Young Talent Program of CAAS, GDAS Special Project of Science and Technology Development (2018GDASCX-0107).

SUPPLEMENTARY MATERIAL

The Supplementary Material for this article can be found online at: https://www.frontiersin.org/articles/10.3389/fmicb.2020.01715/full#supplementary-material

FIGURE S1 | Sample collection and validation by RT-PCR. **(A)** IAPV was injected into newly emerged *A. mellifera* after 24, 48, 72, and 96 h. **(B)** CBPV was injected into newly emerged *A. mellifera* after 0, 24, 48, 72, and 96 h. **(C)** The larvae naturally infected with CSBV were validated from the 5th to 9th instar. **(D)** dsRNA-PGRP-SA and dsRNA-GFP were injected into newly emerged *A. mellifera* and validated at 24, 48, 72, and 96 h.

TABLE S1 | Primer used for detection common viruses and PGRP-SA.

TABLE S2 | Primer sequences and amplicon size for dsRNA synthesis of PGRP-SA and GFP.

TABLE S3 | The standard curve for the quantification RT-qPCR of the reference genes.

REFERENCES

Adeyinka, O. S., Tabassum, B., Nasir, I. A., Yousaf, I., and Husnain, T. (2019). Identification and validation of potential reference gene for effective dsrna knockdown analysis in *chilo partellus*. *Sci. Rep.* 9:13629. doi: 10.1038/s41598-019-49810-w

Andersen, C. L., Jensen, J. L., and Ørntof, T. F. (2004). Normalization of real-time quantitative reverse transcription-PCR data: a model-based variance estimation approach to identify genes suited for normalization, applied to bladder and colon cancer data sets. *Cancer Res.* 64, 5245–5250. doi: 10.1158/0008-5472.CAN-04-0496

Brutscher, L. M., Daughenbaugh, K. F., and Flenniken, M. L. (2015). Antiviral defense mechanisms in honey bees. *Curr. Opin. Insect. Sci.* 7, 71–82. doi: 10.1016/j.cois.2015.04.016

Chen, Y. P., Pettis, J. S., Corona, M., Chen, W. P., Li, C. J., and Spivak, M. (2014). Israeli acute paralysis virus: epidemiology, pathogenesis and implications for honey bee health. *PLoS Pathog.* 10:e1004261. doi: 10.1371/journal.ppat.1004261

Coulon, M., Schurr, F., Martel, A. C., Cougoule, N., and Dubois, E. (2017). Metabolisation of thiamethoxam (a neonicotinoid pesticide) and interaction

with the chronic bee paralysis virus in honey bees. *Pestic. Biochem. Phys.* 144, 10–18. doi: 10.1016/j.pestbp.2017.10.009

Diao, Q. Y., Li, B. B., Zhao, H. X., Wu, Y. Y., Guo, R., Dai, P. L., et al. (2018). Enhancement of chronic bee paralysis virus levels in honeybees acute exposed to imidacloprid: a Chinese case study. *Sci. Total Environ.* 630, 487–494. doi: 10.1016/j.scitotenv.2018.02.258

Dietrich, I., Shi, X. H., McFarlane, M., Watson, M., Blomström, A. L., Skelton, J. K., et al. (2017). The antiviral RNAi response in vector and non-vector cells against orthobunyaviruses. *PLoS Neglect. Trop. D.* 1:5. doi: 10.1371/journal pntd.ooo5272

Freitas, F. C. P., Depintor, T. S., Agostini, L. T., Luna-Lucena, D., Nunes, F. M., Bitondi, M. M. G., et al. (2019). Evaluation of reference genes for gene expression analysis by real-time quantitative pcr (qpcr) in three stingless bee species (*hymenoptera*: *apidae*: *meliponini*). *Sci Rep.* 9:17692. doi: 10.1038/s41598-019-53544-0

Galbraith, D. A., Yang, X., Ni, O. E. L., Yi, S., Grozinger, C., and Schneider, D. S. (2015). Parallel epigenomic and transcriptomic responses to viral infection in honey bees (*apis mellifera*). *PLoS Pathog* 11:e1004713. doi: 10.1371/journal.ppat.1004713

Galli, V., Borowski, J. M., Perin, E. C., Messias, R., da, S., Labonde, J., et al. (2015). Validation of reference genes for accurate normalization of gene expression for real time-quantitative PCR in *strawberry fruits* using different cultivars and osmotic stresses. *Gene* 554, 205–214. doi: 10.1016/j.gene.2014.10.049

Genersch, E., and Aubert, M. (2010). Emerging and re-emerging viruses of the honey bee (*apis mellifera* l.). *Vet Res.* 41:54. doi: 10.1051/vetres/2010027

Guo, H., Jiang, L., and Xia, Q. (2016). Selection of reference genes for analysis of stress-responsive genes after challenge with viruses and temperature changes in the *silkwormbombyx mori*. *Mol Genet Genomic*s. 291, 999–1004. doi: 10.1007/s00438-015-1125-4

He, S., An, T. A. R., and Liu, S. (2019). Validation of reliable reference genes for RT-qPCR Studies of Target gene expression in *Colletotrichum camelliae* During spore germination and mycelial growth and interaction with host plants. *Front. Microbiol.* 10:2055. doi: 10.3389/fmicb.2019.02055

Hellemans, J., Mortier, G., De Paepe, A., Speleman, F., and Vandesompele, J. (2007). qBase relative quantification framework and software for management and automated analysis of real-time quantitative PCR data. *Genome Biol.* 8:R19.

Hunt, G. J., Amdam, G. V., Schlipalius, D., Emore, C., Sardesai, N., Williams, C. E., et al. (2007). Behavioral genomics of honey bee foraging and nest defense. *Naturwissenschaften* 94, 247–267. doi: 10.1007/s00114-006-0183-1

Li, S., Ming, L., Dongliang, F., Qingyun, D., Jian, W., Liqin, L., et al. (2018). Preparation and application of egg yolk antibodies against chinese sacbrood virus infection. *Front. Microbiol.* 9:1814. doi: 10.3389/fmicb.2018.01814

Lourenco, A. P., Mackert, A., Cristino, A. D. S., and Simoes, Z. L. P. (2008). Validation of reference genes for gene expression studies in the honey bee, *Apis mellifera*, by quantitative real-time RT-PCR. *Apidologie* 39, 372–385. doi: 10.1051/apido:2008015

Maori, E., Lavi, S., Mozes-Koch, R., Gantman, Y., Peretz, Y., Edelbaum, O., et al. (2007). Isolation and characterization of israeli acute paralysis virus, a dicistrovirus affecting honey bees in *israel*: evidence for diversity due to intra- and inter-species recombination. *J. Gen. Virol.* 88, 3428–3438. doi: 10.1099/vir.0.83284-0

Marcial-Quino, J., Fierro, F., De la Mora-De la Mora, I., Enríquez-Flores, S., Gómez-Manzo, S., Vanoye-Carlo, A., et al. (2016). Validation of housekeeping genes as an internal control for gene expression studies in *Giardia lamblia* using quantitative real-time PCR. *Gene* 581, 21–30. doi: 10.1016/j.gene.2016.01.018

Moon, K., Lee, S. H., and Kim, Y. H. (2018a). Validation of quantitative real-time pcr reference genes for the determination of seasonal and labor-specific gene expression profiles in the head of western honey bee, *apis mellifera*. *PLoS One* 13:e0200369. doi: 10.1371/journal.pone.0200369

Moon, K., Lee, S. H., and Kim, Y. H. (2018b). Evaluation of reference genes for quantitative real-time pcr to investigate seasonal and labor-specific expression profiles of the honey bee abdomen. *J. Asia Pac Entomol.* 21, 1350–1358. doi: 10.1016/j.aspen.2018.10.014

Niu, J. Z., Cappelle, K., Miranda, J. R., Smagghe, G., and Ivan, M. (2014). Analysis of reference gene stability after Israeli acute paralysis virus infection in bumblebees *Bombus terrestris*. *J. Invertebr. Pathol.* 115, 76–79. doi: 10.1016/j.jip.2013.10.011

Olivier, V., Blanchard, P., Chaouch, S., Lallemand, P., Schurr, F., Celle, O., et al. (2008). Molecular characterisation and phylogenetic analysis of chronic bee paralysis virus, a honey bee virus. *Virus Res.* 132, 1–68. doi: 10.1016/j.virusres.2007.10.014

Peng, S., Liu, L., Zhao, H., Wang, H., and Li, H. (2018). Selection and validation of reference genes for quantitative real-time PCR normalization under ethanol stress conditions in *Oenococcus oeni SD-2a*. *Front. Microbiol.* 9:892. doi: 10.3389/fmicb.2018.00892

Pfaffl, M. W., Tichopad, A., Prgomet, C., and Neuvians, T. P. (2004). Determination of stable housekeeping genes, differentially regulated target genes and sample integrity: bestkeeper-excel-based tool using pair-wise correlations. *Biotechnol. Lett.* 26, 509–515. doi: 10.1023/B:BILE.0000019559.84305.47

Reim, T., Thamm, M., Rolke, D., Blenau, W., and Scheiner, R. (2013). Suitability of three common reference genes for quantitative real-time pcr in honey bees. *Apidologie* 44, 342–350. doi: 10.1007/s13592-012-0184-3

Scharlaken, B., de Graaf, D. C., Goossens, K., Brunain, M., Peelman, L. J., and Jacobs, F. J. (2008). Reference gene selection for insect expression studies using quantitative real-time PCR: the head of the honey bee, *Apis mellifera*, after a bacterial challenge. *J. Insect. Sci.* 8:33. doi: 10.1673/031.008.3301

Shakeel, M., Alicia, R., Bin, T. U., and Fengliang, J. (2018). Gene expression studies of reference genes for quantitative real-time pcr: an overview in insects. *Biotechnol Lett.* 40, 227–236. doi: 10.1007/s10529-017-2465-4

Shan, L., Liuhao, W., Jun, G., Yujie, T., Yanping, C., Jie, W., et al. (2017). Chinese sacbrood virus infection in asian honey bees, (*apis cerana cerana*), and host immune responses to the virus infection. *J. Invertebr. Pathol.* 150, 63–69. doi: 10.1016/j.jip.2017.09.006

Silver, N., Best, S., Jiang, J., and Thein, S. (2006). Selection of housekeeping genes for gene expression studies in human reticulocytes using real-time pcr. *BMC Mol. Biol.* 7:33. doi: 10.1186/1471-2199-7-33

Thellin, O., Elmoualij, B., Heinen, E., and Zorzi, W. (2009). A decade of improvements in quantification of gene expression and internal standard selection. *Biotechnol. Adv.* 27, 323–333. doi: 10.1016/j.biotechadv.2009.01.010

Vandesompele, J., De Preter, K., Pattyn, F., Poppe, B., Van Roy, N., De Paepe, A., et al. (2002). Accurate normalization of real-time quantitative rt-pcr data by geometric averaging of multiple internal control genes. *Genome Biol.* 3:research0034. doi: 10.1186/gb-2002-3-7-research0034

Vyas, M., Raza, A., Yousaf Ali, M., Ashraf, M. A., Mansoor, S., Shahid, A. A., et al. (2017). Knock down of whitefly gut gene expression and mortality by orally delivered gut gene-specific dsRNAs. *PLoS One* 1:e0168921. doi: 10.1371/journal.pone.0168921

Wang, Z., Meng, Q., Zhu, X., Sun, S., Gao, S., Gou, Y., et al. (2019). Evaluation and validation of reference genes for quantitative real-time PCR in *Helopeltis theivora Waterhouse* (Hemiptera: Miridae). *Sci. Rep.* 9:13291. doi: 10.1038/s41598-019-49479-1

Wheeler, D. E., Buck, N., and Evans, J. D. (2006). Expression of insulin pathway genes during the period of caste determination in the honey bee, *apis mellifera*. *Insect. Mol. Biol.* 15, 597–602. doi: 10.1111/j.1365-2583.2006.00681.x

Xie, F., Xiao, P., Chen, D., Xu, L., and Zhang, B. (2012). Mirdeepfinder: a mirna analysis tool for deep sequencing of plant small rnas. *Plant Mol. Biol.* 80, 75–84. doi: 10.1007/s11103-012-9885-2

Yang, D. H., Zhao, H. X., Shi, J. M., Xu, X., Wu, Y. Y., Guo, R., et al. (2019). Discovery of aphid lethal paralysis virus in vespa velutina and apis cerana in china. *Insects* 10:157. doi: 10.3390/insects10060157

Yang, X., Pan, H., Yuan, L., and Zhou, X. (2018). Reference gene selection for RT-qPCR analysis in *Harmonia axyridis*, a global invasive lady beetle. *Sci. Rep.* 8:2689. doi: 10.1038/s41598-018-20612-w

Zhang, S., Jiang, Y., Cheng, Q., Yi, Z., and Chen, M. (2016). Inclusion body fusion of human parainfluenza virus type 3 regulated by acetylated α-α-tubulin enhances viral replication. *J. Virol.* 91:e1802-16. doi: 10.1128/JVI.01802-16

Zhu, B., Shan, J., Li, R., Liang, P., and Gao, X. (2019). Identification and RNAi-based function analysis of chitinase family genes in diamondback moth, *plutella xylostella*. *Pest Manag. Sci.* 75, 1951–1961. doi: 10.1002/ps.5308

Conflict of Interest: The authors declare that the research was conducted in the absence of any commercial or financial relationships that could be construed as a potential conflict of interest.

Copyright © 2020 Deng, Zhao, Yang, Zhang, Zhang and Hou. This is an open-access article distributed under the terms of the Creative Commons Attribution License (CC BY). The use, distribution or reproduction in other forums is permitted, provided the original author(s) and the copyright owner(s) are credited and that the original publication in this journal is cited, in accordance with accepted academic practice. No use, distribution or reproduction is permitted which does not comply with these terms.

Advantages of publishing in Frontiers

OPEN ACCESS
Articles are free to read for greatest visibility and readership

FAST PUBLICATION
Around 90 days from submission to decision

HIGH QUALITY PEER-REVIEW
Rigorous, collaborative, and constructive peer-review

TRANSPARENT PEER-REVIEW
Editors and reviewers acknowledged by name on published articles

Frontiers
Avenue du Tribunal-Fédéral 34
1005 Lausanne | Switzerland

Visit us: www.frontiersin.org
Contact us: frontiersin.org/about/contact

REPRODUCIBILITY OF RESEARCH
Support open data and methods to enhance research reproducibility

DIGITAL PUBLISHING
Articles designed for optimal readership across devices

FOLLOW US
@frontiersin

IMPACT METRICS
Advanced article metrics track visibility across digital media

EXTENSIVE PROMOTION
Marketing and promotion of impactful research

LOOP RESEARCH NETWORK
Our network increases your article's readership